



XLIX ZJAZD PTChem i SITPChem

Gdańsk, 18-22 wrzesień 2006



Annals of Polish Chemical Society' 2007



***Roczniki
Polskiego Towarzystwa Chemicznego
2007***

ISBN-978-83-922424-7-5

[Http://www.pg.gda.pl/chem/InneJednostki/PTChem/ptch.htm](http://www.pg.gda.pl/chem/InneJednostki/PTChem/ptch.htm)



KOMITET REDAKCYJNY

dr hab. Tadeusz OSSOWSKI, prof. UG

prof. dr hab. inż. Aleksander KOŁODZIEJCZYK

prof. dr hab. Zygmunt WARNKE

dr hab. inż. Józef HAPONIUK

prof. dr hab. inż. Waclaw GRZYBKOWSKI

dr hab. inż. Aleksander HERMAN

prof. dr hab. inż. Jerzy CIARKOWSKI

prof. dr hab. inż. Waldemar WARDENCKI, prof. nadzw. PG

prof. dr hab. inż. Andrzej KŁONKOWSKI

prof. dr hab. inż. Kazimierz DAROWICKI

prof. dr hab. Romuald PIOSIK

Prof. dr hab. Bogdan SKWARZEC

prof. zw. dr hab. inż. Wiesław WOJNOWSKI

prof. dr hab. inż. Jan HUPKA

prof. dr hab. Piotr SZEFER

dr hab. inż. Barbara BECKER

dr inż. Bożena ZABIEGAŁA

**SULPHUR ANALOGS OF PYRIMIDINE BASES: NEW 2-THIO- 6-
ALKOXYCARBONYLURACILS AND 2-THIO- 6-
HYDROXYAMINOCARBONYLURACILS**

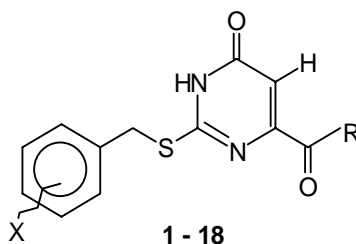
Grażyna Bartkowiak

*Department of Mass Spectrometry, Faculty of Chemistry, Adam Mickiewicz University,
Poznań*

Introduction:

The title compounds (**1-18**) constitute a subclass of derivatives of orotic acid (6-carboxyuracil, vitamin B₁₃), an important representative of pyrimidine compounds, which takes crucial part in metabolic processes in living organisms [1] and exhibits various physiological effects [2]. Its sulphur analog — 2-thioorotic acid — is also of interest because of its biological activity and chelating power with metal cations. The great interest with this compound results in continuous search of its new derivatives, modified both in the position 2 of uracil ring (sulphur atom) and in the position 6 (carboxylic group).

Among derivatives of carboxylic acids on the special attention deserve hydroxamic acids. These compounds possess a wide spectrum of biological activities including antibacterial, anti-inflammatory, antifungal and antitumor properties [3-5] and are also known as stimulators of growth of several plants [6]. Hydroxamates have been identified as selective inhibitors of matrix metalloproteinases [7] and other enzymes, for example 5-lipoxygenase, an enzyme involved in the biosynthesis of mediators of allergic disorders [8]. Wide range of physiological properties of sulphur analogs of pyrimidine bases (2-thiouracil, 2-thioorotic acid) as well as activity of hydroxamic acids encouraged me to obtain (*via* methyl esters) new hydroxamic acids, rooted from substituted 2-benzylthioorotic acids, containing in the phenyl ring chloro, bromo or nitro substituents in the positions *ortho*, *meta* or *para*. The substrates have been synthesized previously in our laboratory [9].



Compound	X	R	Compound	X	R
1	<i>o</i> -Cl	OCH ₃	10	<i>o</i> -Cl	NHOH
2	<i>m</i> -Cl	OCH ₃	11	<i>m</i> -Cl	NHOH
3	<i>p</i> -Cl	OCH ₃	12	<i>p</i> -Cl	NHOH
4	<i>o</i> -Br	OCH ₃	13	<i>o</i> -Br	NHOH
5	<i>m</i> -Br	OCH ₃	14	<i>m</i> -Br	NHOH
6	<i>p</i> -Br	OCH ₃	15	<i>p</i> -Br	NHOH
7	<i>o</i> -NO ₂	OCH ₃	16	<i>o</i> -NO ₂	NHOH
8	<i>m</i> -NO ₂	OCH ₃	17	<i>m</i> -NO ₂	NHOH
9	<i>p</i> -NO ₂	OCH ₃	18	<i>p</i> -NO ₂	NHOH

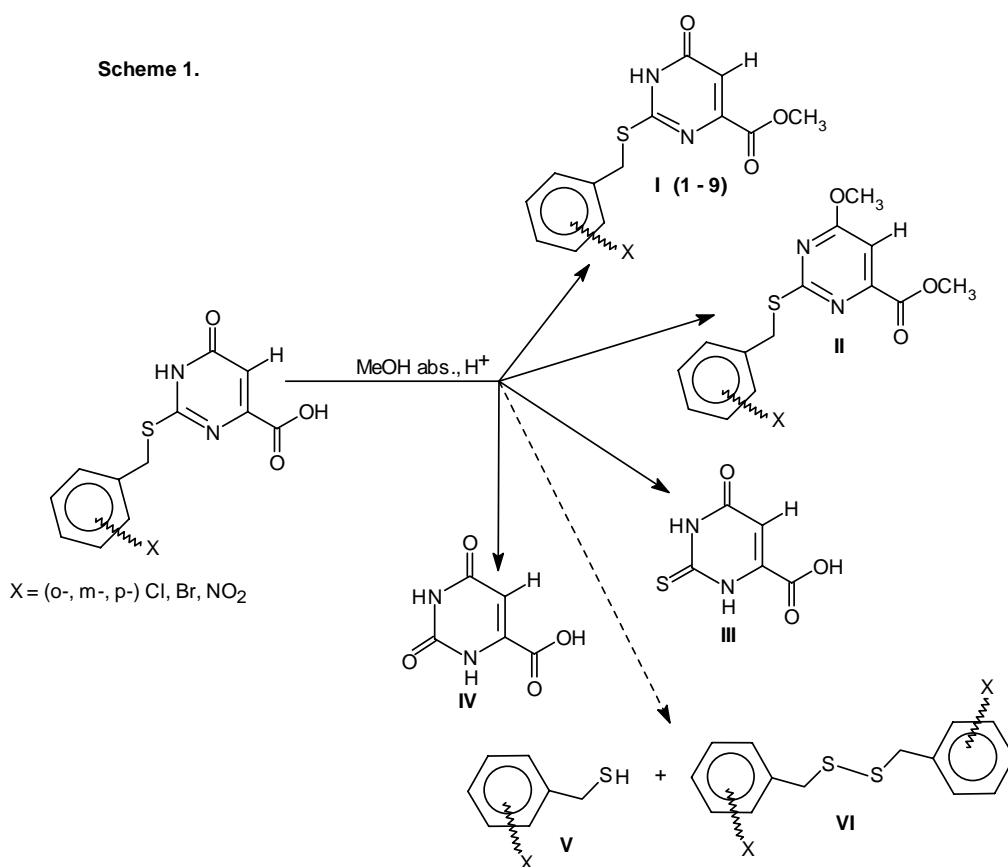
My aim was to examine the reactivity of the above 2-benzylthioorotic acids under the conditions of esterification reaction, to receive X-substituted 2-benzylthio-6-

methoxycarbonyluracils (methyl esters **1 – 9**) and to transform them into corresponding 2-benzylthio-6-hydroxyaminocarbonyluracils (hydroxamic acids **10 – 12**). The research of antimicrobial properties of the compounds studied is being in progress.

Experimental part

At first, a conventional method was elaborated to synthesize methyl esters of 2-(chloro, bromo or nitro) benzylthioorotic acids **1-9**. Starting material was refluxed with boiling absolute methanol and catalytic amount of concentrated sulphuric acid to the entire dissolution of the substrate. The reaction mixture was evaporated on the vacuum rotary evaporator to 1/10 of previous volume. TLC monitoring showed a complicated mixture of products. The obtained mixture was purified and products separated using silica gel column chromatography. The set of products received (**I-VI**) is presented on the **Scheme 1**.

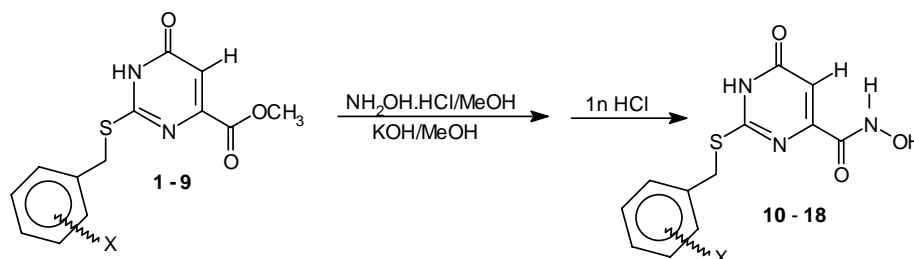
In the second method of esterification 2-*o*-chlorobenzylthioorotic acid was submitted to the action of thionyl chloride in absolute methanol at room temperature. After standing over night only products **I** and **II** were isolated from the reaction mixture. All products were identified using electron ionization mass spectrometry, electrospray MS and ¹H NMR.



The purified esters **1-9** were dissolved (or suspended) in methanol and added to the previously prepared mixture of saturated solutions of hydroxylamine hydrochloride in methanol and potassium hydroxide in methanol (2:1) and then stirred magnetically over three days. After this time the reaction mixture was neutralized with 1n HCl and gave the positive result of the FeCl₃ test (coloured complex) for hydroxamic acids. The neutral or slightly acidic solution containing one of the hydroxamic acids **10 – 18** was

gently evaporated under reduced pressure and cooled in the refrigerator. The precipitated solid was filtered, washed with small amount of cold absolute methanol and dried.

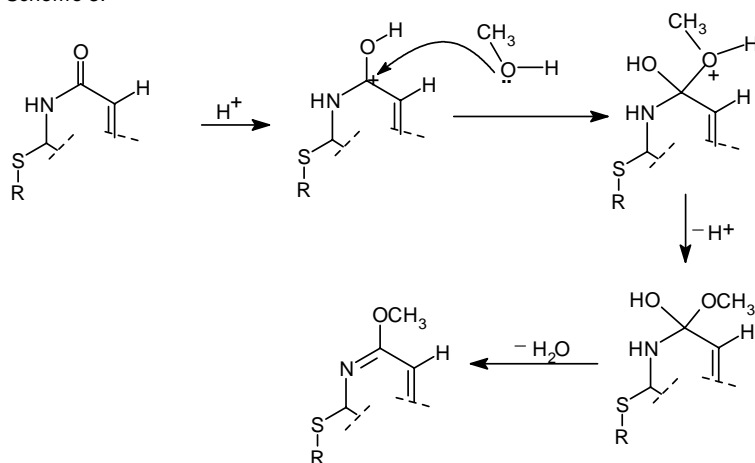
Scheme 2.



Results and discussion

2-benzylthiorotic acids, containing X substituent (X = Cl, Br or NO₂) in the position *ortho*, *meta* or *para* of phenyl ring turned out to be susceptible to decomposition in the conditions of esterification reactions (acidic methanol, temperature 63-64°C). One of the side reactions observed is debenzylation to the 2-thiorotic acid **III** (Scheme 1), the other is hydrolysis of C_{sp2}-S bond of benzylthiorotic acid, which yielded the orotic acid **IV** and was accompanied with formation of appropriate X-benzyl-mercaptane (**V**) and/or di-(X-benzyl)-disulphide (**VI**), substances of unpleasant smell. Surprisingly, 2-(*o*-, *m*- or *p*-)(chloro, bromo or nitro)benzylthio-4-methoxy-6-methoxycarbonylpyrimidines (compounds **II**) are also formed in this reaction. The possible mechanism of creating these compounds (similar to the reaction of the hemiacetal formation) is shown on Scheme 3.

Scheme 3.



As a consequence of side reactions, the laborious separation – silica gel column chromatography – was needed to isolate desirable esters from the reaction mixture and the yield received was about 15 percent. To the quick identification of compounds obtained especially mass spectral methods (EIMS and ESIMS) appeared useful and convenient. Characteristic parameters of the obtained new 2-benzylthio-6-methoxycarbonyluracils **1-9** are collected in Table 1.

The isolated and purified esters **1 – 9** were used further to obtain hydroxamic acids as described earlier. Some characteristics of products **10 – 18** (X substituted 2-benzylthio-6-hydroxyaminocarbonyluracils) are shown in Table 2.

Table 1. Structure, thin layer chromatography (phase A* = BuOH- AcOH-H₂O 5:2:3), melting points and molecular ions (EIMS, m/z) of esters **1 - 9**

Compound	Substituent X	Molecular formula	R _f (TLC) phase A*	m.p. °C	M ⁺ m/z
1	<i>o</i> -Cl	C ₁₃ H ₁₁ N ₂ O ₃ SCl	0,95	240-246	310/312
2	<i>m</i> -Cl		0,96	228-229	
3	<i>p</i> -Cl		0,95	233-237	
4	<i>o</i> -Br	C ₁₃ H ₁₁ N ₂ O ₃ SBr	0,95	243-245	354/356
5	<i>m</i> -Br		0,96	239-240	
6	<i>p</i> -Br		0,95	240-243	
7	<i>o</i> -NO ₂	C ₁₃ H ₁₁ N ₃ O ₅ S	0,95	244-247	321
8	<i>m</i> -NO ₂		0,96	239-241	
9	<i>p</i> -NO ₂		0,96	247-249	

Table 2. Characteristic data for hydroxamic acids **10 - 18**

Compound	Substituent X	Molecular formula	Molecular weight	m.p. °C	Complex with Fe ³⁺ (colour)
10	<i>o</i> -Cl	C ₁₂ H ₁₀ N ₃ O ₃ SCl	311	126-129	violet
11	<i>m</i> -Cl			120-123	
12	<i>p</i> -Cl			116-118	
13	<i>o</i> -Br	C ₁₂ H ₁₀ N ₃ O ₃ SBr	355	128-131	violet
14	<i>m</i> -Br			124-126	
15	<i>p</i> -Br			123-126	
16	<i>o</i> -NO ₂	C ₁₂ H ₁₀ N ₄ O ₅ S	322	128-130	dark red to brown
17	<i>m</i> -NO ₂			125-127	
18	<i>p</i> -NO ₂			132-135	

Summary:

New organic compounds, derivatives of pyrimidine bases, rooted from 2-thioorotic acid and expected to possess significant physiological activity, were received.

The main difficulty in the synthesis of hydroxamic acids appeared the first step, i. e. the esterification of substituted 2-benzylthioorotic acids and proper separation of products. The side reactions took place due to the lability of sulphur-carbon bonds in the applied conditions (presence of strong concentrated acid, raised temperature). Other synthetic routes to the desired esters should be investigated to make this synthesis more selective and efficient. Synthesis of hydroxamic acids proceeds mostly unambiguously, although it requires observing strictly basicity/acidity conditions.

Electrospray ionization mass spectrometry turned out to be convenient to the identification of isolated main and by-products of above-mentioned reaction as well as to evaluate the degree of purity or kind of contaminations of compounds studied (variety of pseudo molecular ions, protonated and deprotonated, are easily detected).

References:

- [1] A. M. Pita, Y. Wakabayashi et al.; *Clinical Nutrition*. 22(1), 2003; 93-8;
- [2] F. Iwańczak, R. Śmigiel; *Gastroenterologia Polska* 11 (4), 2004, 375-383;
- [3] A. Kleeman, J. Engel, B. Kutscher, D. Reichert; *Pharmaceutical Substances, Synthesis, Patents, Applications*, 4rd ed.; Thieme, Stuttgart, 2001;
- [4] W. P. Steward, A. L. Thomas; *Expert Opin. Invest. Drugs* 9, 2000, 2913;
- [5] W. P. Steward; *Cancer Chemother. Pharmacol.* 43, 1999, Suppl. S56-60;
- [6] C. Rentzea, W. Rademacher, A. Harreus; Jung J. Eur. Pat. Appl. EP 350, 693, 1990; *Chem Abstr.* 1977, 87, 201125;
- [7] N. M. Hooper, A. Turner; *J. Biochem. Soc. Trans.* 28, 2000, 441-6;
- [8] T. Kolasa, A. O. Stewart, C. D. Brooks; *Tetrahedron: Asymmetry* 7, 1996, 729-736;
- [9] E. Wyrzykiewicz., G. Bartkowiak; *Pol. J. Chem.* 69, 1995, 566

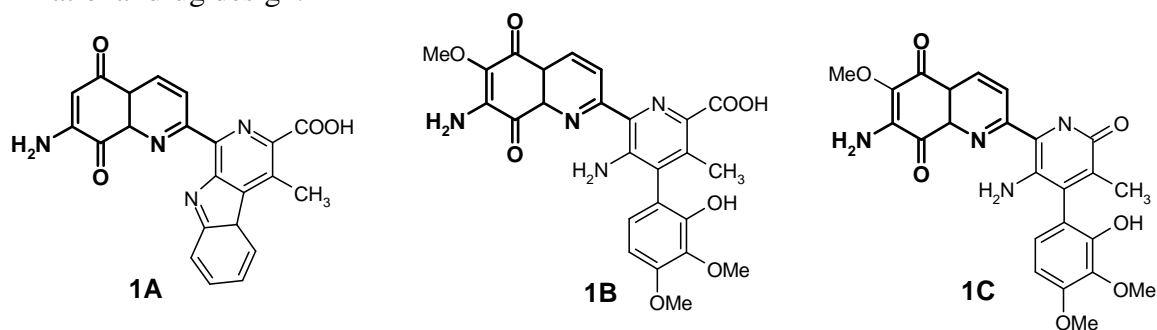
DESIGN AND SYNTHESIS OF POTENTIAL BIOEFFECTORS BASED ON 5,8-QUINOLINEDIONE MOIETY

A. Bestwina B. Podeszwa, J. Finster, R. Musiol*

Instytut Chemii Uniwersytet Śląski, 40-007 Katowice, ul Szkolna 9

Introduction

Quinoline-5,8-dione and its derivatives constitute group of compounds of great biological and pharmaceutical importance. This moiety is present in many antiviral and antibacterial factors [1-3]. Well known are also antitumor, and antimicrobial agents containing quinolinedione substructure [4]. Especially lavendamycin (**1A**), streptonigrin (**1B**) and streptonigrone (**1C**) are potent antitumor agents the activity of which is believed to be determined by presence of quinolinedione moiety [5, 6]. Main obstacle in study on such compounds is their synthetic unavailability. Mentioned bioactive structures (**1A**, **1B**, **1C**) as well as some of their derivatives could be obtained from *Streptomyces* species [7] or by applying biosynthetic procedures [8-14]. However purely synthetic ways are necessary to built more diverse group of derivatives essential in rational drug design.



Scheme 1. Structures of: **1A** lavendamycin, **1B** streptonigrin and **1C** streptonigrone. In bold 7-amino-5,8-quinolinedione moiety is shown.

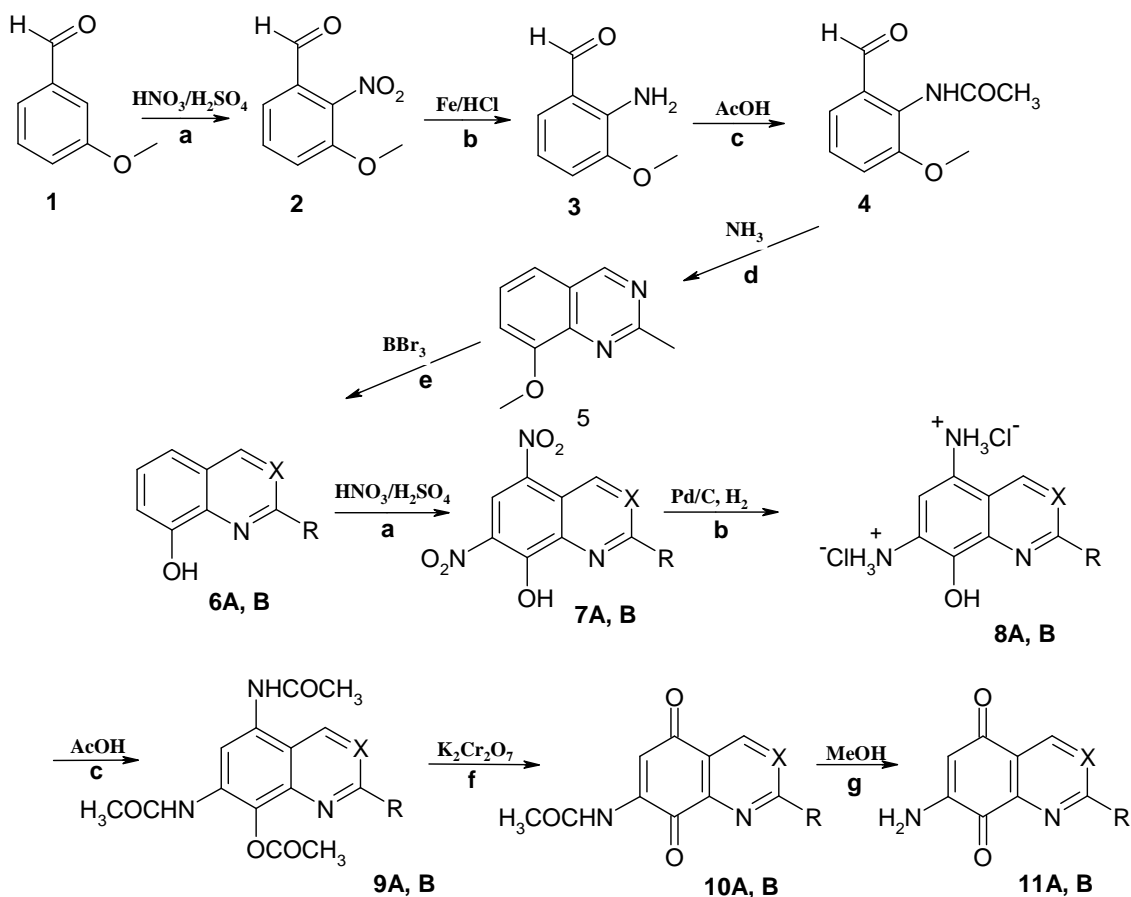
Reported methods for the synthesis of structures based on quinolinediones are quite complex. They consist of many steps and result in low overall yields [15-19]. Furthermore, to the best of our knowledge, there is no applicable protocol leading to quinazoline derivatives. Thus, in our study focused on the synthesis new biologically active structures we have modified known procedure to facilitate obtaining some new interesting structures.

Results and discussion

Formerly, some remarks on quinoline-5,8-dione azaanalogues were made and their value in our understanding of HIV-1 integrase inhibitors chemistry [19]. In this paper we wish to report some findings on design and synthesis of new, quinazoline based analogues of quinoline-5,8-dione and its derivatives that could be of great biological importance. During our works we found out their significant values as bioeffectors, especially fungicides and herbicides [20]. Main problem in quinolinedione chemistry is a multistep, time consuming synthesis that restrains more comprehensive research.

* Corresponding author: rmusiol@us.edu.pl

Scheme 2 shows a procedure that we have successfully applied to obtain known quinolinedione and their, even more interesting, analogues. From easily available 3-methoxybenzaldehyde, through nitration (a), reduction (b), acylation (c), cyclization (d), hydrolysis (e, h) and oxidation (g) we have obtained 8-hydroxy-2-methyl-quinazoline which was further reacted as commercially available 8-hydroxyquininaldine.



Scheme 2. Synthesis of quinoline-5,8-diones and analogues R=H, CH₃ A) X=C, B) X=N.

Experimental

Melting points were recorded on Boetius apparatus and are uncorrected. The ¹H NMR spectra were obtained on Bruker 500MHz. When diffuse, easily exchangeable protons were not listed. Analytical thin-layer chromatography was performed on Merck silica gel 60F₂₅₄ alumina pre-coated plates (0.25mm layer). All liquid chromatography separations were performed using Merck silica gel 50-100 mesh. Solvents as ether, chloroform, ethanol were dried and purified according to common procedures. Chemicals obtained from commercial suppliers (POCh, Merck, Sigma-Aldrich) were used without further purification.

8-hydroxy-2-methyl-quinazoline 6B was obtained as yellow solid mp 160°C (lit. mp 154-158°C [21]) in 90% yield.

8-hydroxy-5,7-dinitro-2-methyl-quinoline 7A, and **8-hydroxy-5,7-dinitro-2-methyl-quinazoline 7B**, was obtained according to known procedure by direct nitration [22].

7A: yellow solid, yield 61%, mp 295°C, lit mp. 290-300°C [22].

7B: yellow solid mp 250°C, yield 85%. ¹HNMR 500 MHz, DMSO-d₆, δ: 2,78 (s, 3H); 9,10 (s, 1H); 10,22 (s, 1H); 11,23 (s, 1H).

8-hydroxy-5,7-diamino-2-methyl-quinoline 8A and **8-hydroxy-5,7-diamino-2-methyl-quinazoline 8B**. Reduction of **7A** or **7B** with gaseous hydrogen in presence of 5% Pd/C afford in respective amine. However free diamine was found very unstable it was immediately further converted to more stable diacetic derivative.

8-acetoxy-5,7-diacetamino-2-methyl-quinoline 9A and **8-acetoxy-5,7-diacetamino-2-methyl-quinazoline 9B**. To the mixture of 1,6 mmol of **7**, 0,13g Pd/C in hydrochloric acid solution (0,66 cm³ of conc. HCl in 6 cm³ H₂O) was hydrogenated until the color changed from yellow to deep red and filtered. The residue was washed with small amount of water. Collected solutions were mixed with 1,33g of sodium acetate 0,66 g sodium sulfate and dropwise 4,5cm³ of acetic anhydride. Mixture was stirring during one hour in room temperature and then during 30 min in ice bath. Resulted white solid was separated washed with cold water and dried in the air to give **9**.

9A: yellow solid, 80% yield, mp 258°C (lit mp 260,5°C [22]).

9B: yellow solid, 50% yield mp 274-276°C (decomp.). ¹HNMR, 500 MHz, DMSO-d₆, δ: 2,16 (s, 3H); 2,34 (s, 3H); 2,42 (s, 3H); 2,62 (s, 3H); 7,88 (s, 1H); 9,47 (s, 1H); 9,57 (s, 1H); 11,40 (s, 1H).

7-acetamino-2-methyl-5,8-quinolinedione 10A and **7-acetamino-2-methyl-5,8-quinazolinedione 10B**. To suspension of 0,47 mmol of **9** in 5,8 cm³ acetic anhydride was added dropwise the solution of 0,42 g potassium dichromate in 5,5 cm³ of water. Mixture was heated gently and stirred during 1,5 hour. The resulted mixture was extracted with dichloromethane (12 times with 2,5 cm³). Combined organic layers were washed with 3% aqueous solution of sodium bicarbonate, dried with magnesium sulfate and then evaporated to dryness. Crude compound **10** was obtained and used in further synthesis without complex purification.

10A: yellow solid mp 210-212°C (lit mp 217°C [22]) yield 67%.

10B: yellow solid mp 210°C (decomp.) in 80% yield ¹HNMR, 500 MHz, CDCl₃, δ: 2,33 (s, 3H); 2,98 (s, 3H); 7,98 (s, 1H); 8,31 (s, 1H); 9,43 (s, 1H).

7-amino-2-methyl-5,8-quinolinedione 11A: red solid mp 240°C (lit mp 240°C [22]), yield 60%.

Conclusions

Knowledge about activity of quinazolines is essential for more rational design of new bioeffectors. Introducing additional nitrogen atom is slight change in structure of quinoline leading to significant changes in chemical behavior. In table 1 some features important for our study are presented.

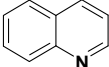
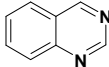
Structure		
pKa [23]	4,75	3,43
Molecular volume [24]	123,8	119,2
LogP [24]	1,94	1,53
Molecular refractivity [25]	42,81	38,80

Table 1. Differences in important molecular properties of quinoline and quinazoline.

Such differences are even more significant in the case of functionalized quinazolines [26]. Knowledge about these relationships would help us to control pharmaceutically important features of potential drugs like membrane permeability or cellular uptake.

Particularly, we hope that quinazoline based analogues of active diones will be deprived of cytotoxicity. Multistep synthesis presented in this paper allows to obtain structurally diverse quinazolines with satisfied yields and excellent purity. Further study will be focused on finding new fungicides and herbicides with the quinazoline moiety.

Literature

- [1] B. S Lindsay, H. C. Christiansen, B. R. Copp *Tetrahedron*, 56 (2000) 497.
- [2] S. Hibino, *Heterocycles*, 6 (1977) 1485.
- [3] B. R. Copp, H. C. Christiansen, B. S Lindsay, S.G. Franzblau, *Bioorg. Med. Chem. Lett.*, 15 (2005) 4097.
- [4] H. J. Park, Y. S. Kim, J. S. Kim, E. J. Lee, Y. J. Yi, H. J. Hwang, M. E. Suh, C. K. Ryu, S. K. Lee, *Bioorg. Med. Chem. Lett.*, 14 (2004) 3385.
- [5] D. L. Boger, M. Yasuda, L. A. Mitscher, S. D. Drake, P. A. Kitos, S. C. Thompson, *J. Med. Chem.*, 30 (1987) 1918.
- [6] I. A. Shaikh, F. Johnson, A. P. Grollman *J. Med. Chem.*, 29 (1986) 1329.
- [7] K. V. Rao, W. P. Cullen, *Antibiot. Annu.*, (1959–1960) 950.
- [8] S. J. Gould, S. M. Weinreb, in: *Progress in the Chemistry of Organic Natural Products*, W. Herz, H. Grisebach, G. W. Kirby, (ed), Vol. 41, Springer, Nowy Jork, 1982, str. 77.
- [9] S. J. Gould, C. C. Chang, *J. Am. Chem. Soc.*, 102 (1980) 1702.
- [10] S. J. Gould, D. E. Cane, *J. Am. Chem. Soc.*, 104 (1982) 343.
- [11] S. J. Gould, C. C. Chang, D. S. Darling, J. D. Roberts, M. Squillacote, *J. Am. Chem. Soc.*, 102 (1980) 1707.
- [12] Y. G. Whittle, S. J. Gould, *J. Am. Chem. Soc.*, 109 (1987) 5043.
- [13] S. J. Gould, C. C. Chang, *J. Am. Chem. Soc.*, 100 (1978) 1624.
- [14] W. J. Gerwick, S. J. Gould, H. Fonouni, *Tetrahedron Lett.*, 24 (1983) 5445.
- [15] D. L. Boger, S. R. Duff, J. S. Panek, M. Yasuda, *J. Org. Chem.*, 50 (1985) 5782.
- [16] T. K. Liao, W. H. Nyberg, C. C. Cheng, *J. Heterocycl. Chem.*, 13 (1976) 1063.
- [17] V. Petrow, B. Sturgeon, *J. Chem. Soc.*, (1954) 570.
- [18] G. Bringmann, Y. Reichert, V. V. Kane, *Tetrahedron*, 60 (2004) 3539.
- [19] K. A. Majerz-Maniecka, R. Musiol, W. Nitek, B. J. Oleksyn, J. Polanski, *Bioorg. Med. Chem. Lett.*, 16 (2005) 1005.
- [20] R. Musiol, J. Jampilek, K. Kralova, D. R. Richardson, D. Kalinowski, B. Podeszwa, J. Finster, H. Niedbala, A. Palka, J. Polanski, *Bioorg. Med. Chem.* (2007) in print.
- [21] H. J. Park, H. Y. Min, S. S. Kim, J. Y. Lee, S. K. Lee, Y. S. Lee, *Arch. Pharm.*, 337 (2004) 20.
- [22] M. Behforouz, J. Haddad, W. Cai, M. B. Arnold, F. Mohammadi, A. C. Sousa, M. A. Horn, *J. Org. Chem.*, 61 (1996) 6552.
- [23] B. Tyman-Szram, R. Musiol, M. Sajewicz, J. Polanski, *J. Planar Chromatogr. Modern TLC*, 18 (2005) 328.
- [24] Tool for calculation properties available at <http://www.molinspiration.com/>.
- [25] M. Saxena, S. Gaur, P. Prathipati, A. K. Saxena, *Bioorg. Med. Chem.*, 24 (2006) 8249.
- [26] R. Musiol, J. Jampilek, B. Podeszwa, J. Finster, D. Tabak, J. Polanski Structure-lipophilicity Relationship in Series of Quinoline Derivatives II-16, 76 in *Proceedings of XVIII IUPAC Conference on Physical Organic Chemistry*, 20-25 August 2006, Warsaw.

INVESTIGATION OF HEAVY METALS MOBILITY IN INDUSTRIAL WASTE POLLUTED SOILS

A. Bielicka*, K. Świerk, I. Bojanowska, M. Lempart

*Department of Environmental Engineering, Faculty of Chemistry, University of Gdansk,
18 J. Sobieskiego St., 80 - 852 Gdańsk, Poland*

**e-mail: albi@chem.univ.gda.pl*

Metals, once emitted, can reside in the environment for hundreds of years or more. They are persistent environmental contaminations. Human activity has drastically changed the biogeochemical cycles and balance of some heavy metals in the environment. Excessive levels of metals in the environment are hazardous to human. During the recent decades considerable attention has been given to problems concerning negative effects of heavy metals on various ecosystems in different environmental compartments. Numerous field observations indicate a significant increase of heavy metals concentrations in soils, especially agricultural and forest ones [1].

Proper evaluation of the effect of heavy metals on the natural environment is possible on the basis of knowledge about their forms and bindings with soil, sediment, sludge or solid waste components found. Sequential extraction could be the source of the above mentioned information, enabling identification and quantitative determination of various forms of the same chemical element. It is therefore widely used as a tool for the study of fate of metals in the environment [2-8].

The loading of ecosystems with chromium and other heavy metals can be due to pollution by waste materials. Landfill leachates are still one of the major sources of heavy metals discharged to the surrounding environment [3].

The aim of this work was to identify the environmental impact of industrial waste disposal and mobility of heavy metals in polluted soils.

A five-step sequential fractionation scheme was used to partition the metals into exchangeable (F I), acid-soluble (F II), reducible (F III), organic matter (F IV) and residual (F V) fractions (Fig.1). The metals forms occurred in fractions F I - F IV can be released to ecosystems under changeable natural conditions. The metals forms occurring in the residual fraction (FV) are permanently immobilized [2-4].

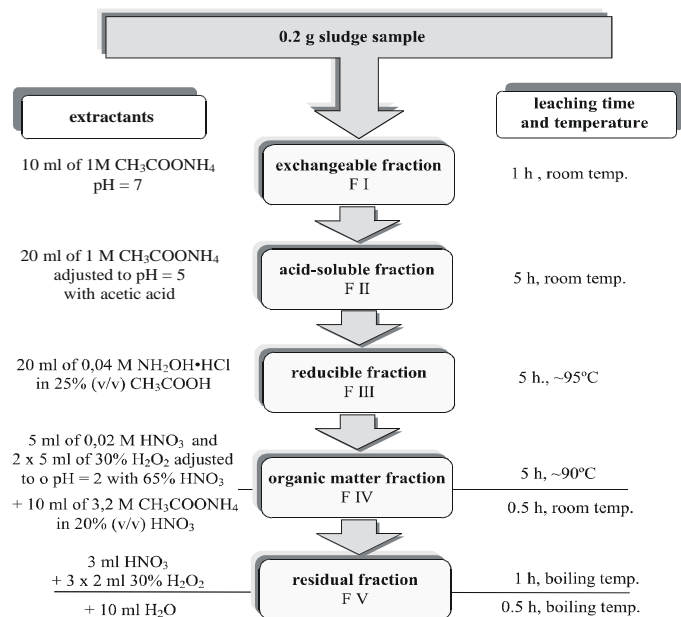


Fig. 1. Schematic diagram of the sequential extraction of metals from galvanic wastewater sludge

Table 1. The metals contents in leachates and particular fractions determined by the sequential extraction

soil/sludge	Sandy soil/galvanic sludge				Agricultural soil/galvanic sludge				Loamy soil/galvanic sludge			
Time	0	1 week	1 month	3 months	0	1 week	1 month	3 months	0	1 week	1 month	3 months
Metal	[mgCu kg⁻¹ d.w.] mean ± S.D., n= 3				[mgCu kg⁻¹ d.w.] mean ± S.D., n= 3				[mgCu kg⁻¹ d.w.] mean ± S.D., n= 3			
Leachate	0.00	0.27±0.10	0.55±0.20	1.23±0.70	0.00	0.32±0.12	0.65±0.24	1.35±0.71	0.00	0.28±0.11	0.56±0.22	1.34±0.59
Fraction I	1.29±1.06	0.57±0.18	0.91±0.35	1.13±0.40	0.68±0.01	0.68±0.01	0.69±0.01	1.65±0.90	0.90±0.39	1.00±0.53	2.40±1.45	3.55±2.49
Fraction II	1.49±0.04	1.12±0.41	2.27±1.33	1.51±0.09	1.91±0.64	1.79±0.44	3.14±0.80	7.49±3.21	7.37±1.10	7.90±3.22	2.43±0.82	21.8±1.50
Fraction III	3.58±3.71	4.65±3.50	1.42±1.23	4.27±2.85	2.96±1.26	2.49±1.77	5.88±0.67	8.08±3.74	7.36±6.94	9.10±4.00	2.38±0.81	12.8±7.20
Fraction IV	1.79±0.08	1.68±0.14	2.76±1.67	2.09±1.18	15.7±1.41	15.0±12.1	23.3±7.20	26.7±10.2	3.64±3.12	3.94±1.65	7.95±1.08	9.80±1.71
Fraction V	2.11±1.44	1.67±0.46	1.74±0.06	2.04±1.17	13.5±1.27	12.9±3.00	15.2±3.70	17.8±5.90	2.32±1.90	2.48±0.84	1.72±0.84	6.43±0.45
Metal	[mgNi kg⁻¹ d.w.] mean ± S.D., n= 3				[mgNi kg⁻¹ d.w.] mean ± S.D., n= 3				[mgNi kg⁻¹ d.w.] mean ± S.D., n= 3			
Leachate	0.00	0.55±0.27	1.03±0.53	2.08±0.9	0.00	0.88±0.14	1.65±0.47	2.80±0.94	0.00	0.97±0.30	2.24±0.98	3.90±1.53
Fraction I	5.54±1.50	8.00±0.97	7.21±3.19	5.18±0.52	2.97±1.88	3.75±0.79	4.11±1.05	4.26±0.65	5.96±0.68	7.35±1.32	6.02±0.84	6.42±1.28
Fraction II	32.8±7.80	27.2±7.30	26.6±13.1	25.9±2.50	30.9±8.90	19.4±8.10	19.0±2.80	33.4±1.50	44.8±1.00	34.0±1.10	33.2±4.90	44.2±1.80
Fraction III	31.7±5.00	32.1±12.7	37.2±8.20	22.1±3.00	73.5±10.4	64.6±9.80	66.7±4.50	60.7±2.30	52.0±15.0	51.6±13.2	55.1±1.90	40.0±1.00
Fraction IV	5.94±3.54	8.58±3.32	11.0±2.99	11.6±0.93	30.0±1.70	27.0±9.10	26.5±1.60	30.1±2.00	16.3±1.20	16.1±1.7	15.3±2.50	17.6±3.80
Fraction V	6.18±2.01	5.65±2.27	6.52±1.36	7.68±0.59	23.0±0.20	19.2±5.70	16.7±0.80	19.1±4.00	16.3±3.30	11.8±2.10	11.1±1.30	13.5±1.90
Metal	[mgFe kg⁻¹ d.w.] mean ± S.D., n= 3				[mgFe kg⁻¹ d.w.] mean ± S.D., n= 3				[mgFe kg⁻¹ d.w.] mean ± S.D., n= 3			
Leachate	0.00	3.10±1.29	7.2±1.57	9.30±1.90	0.00	4.47±0.74	5.07±0.76	6.32±1.47	0.00	3.30±0.29	8.35±1.54	12.2±2.54
Fraction I	70.6±2.80	33.9±2.98	60.5±13.6	41.5±14.7	250±10.4	81.8±7.73	132±52.0	189±18.0	497±22.0	187±15.0	294±19.0	323±29.0
Fraction II	169±51.0	62.1±10.4	53.5±38.3	258±16.2	365±16.0	107±9.00	151±71.0	274±21.0	674±27.0	217±18.0	340±18.0	498±33.0
Fraction III	3454±663	3326±442	3513±821	2637±280	8104±715	9077±300	6185±758	3239±335	6772±539	6493±250	4577±147	5286±119
Fraction IV	444±156	258±83.0	264±85.0	468±160	4066±570	3739±981	2915±339	4204±784	1570±354	1166±187	1031±85.0	1301±361
Fraction V	1071±90.8	1390±131	1320±109	1487±156	18265±1906	19724±5400	15184±2000	13534±1927	9447±539	8136±1662	7543±732	7717±1374
Metal	[mgZn kg⁻¹ d.w.] mean ± S.D., n= 3				[mgZn kg⁻¹ d.w.] mean ± S.D., n= 3				[mgZn kg⁻¹ d.w.] mean ± S.D., n= 3			
Leachate	0.00	2.95±1.65	5.59±1.89	7.23±2.39	0.00	4.78±1.22	6.28±2.43	8.02±3.13	0.00	3.47±1.11	4.96±2.01	7.69±3.78
Fraction I	302±48.0	368±80.0	447±184	438±33.0	227±7.00	262±9.00	236±67.0	270±13.0	304±41.0	375±51.0	354±11.2	428±38.0
Fraction II	680±132	664±105	808±284	794±90.0	818±161	798±146	883±234	1379±43.0	783±153	824±143	915±21.0	1260±67.0
Fraction III	278±67.0	329±51.0	399±82.0	212±29.0	627±159	724±89.0	773±37.0	821±23.0	444±126	469±71.0	534±18.0	438±54.0
Fraction IV	25.9±3.90	26.8±6.10	52.2±37.1	25.4±4.70	159±45.0	134±29.0	154±17.0	142±17.0	65.2±21.4	50.8±9.50	65.3±10.6	43.9±28.2
Fraction V	17.2±1.00	9.50±2.00	19.1±10.3	13.2±1.20	83.7±10.1	61.3±12.0	74.0±6.20	67.0±16.2	45.6±7.00	27.3±3.50	36.2±6.10	34.1±6.90

In experiments dewatered galvanic sludge from electroplating plant and three types of soils: sandy forest, agriculture and loamy, were used. The soil samples were taken from the top 20 cm layer. Investigations were performed for air-dry weight of the sludge and soils samples. Each soil and galvanic sludge were mixed in the ratio of 50 to 1 (10g of soil and 0.2 g of sludge). The experiment was carried out on three parallel soil-sludge samples using 30 ml polypropylene columns. During experiments demineralized water (100 ml/week) was added to each column. The leachates were collected to determine the quantity of leached metals.

Before the start of the experiment and after 1 week, 1 and 3 months, the sequential extraction of metals was carried out according to the schematic diagram presented in Figure 1. In this diagram the optimum experimental ratio of the mass sludge sample to the volume of extractants was also presented.

Metals concentrations were determined using Atomic Absorption Spectroscopy Method, AAS model 30, the Karl Zeiss Jena Company.

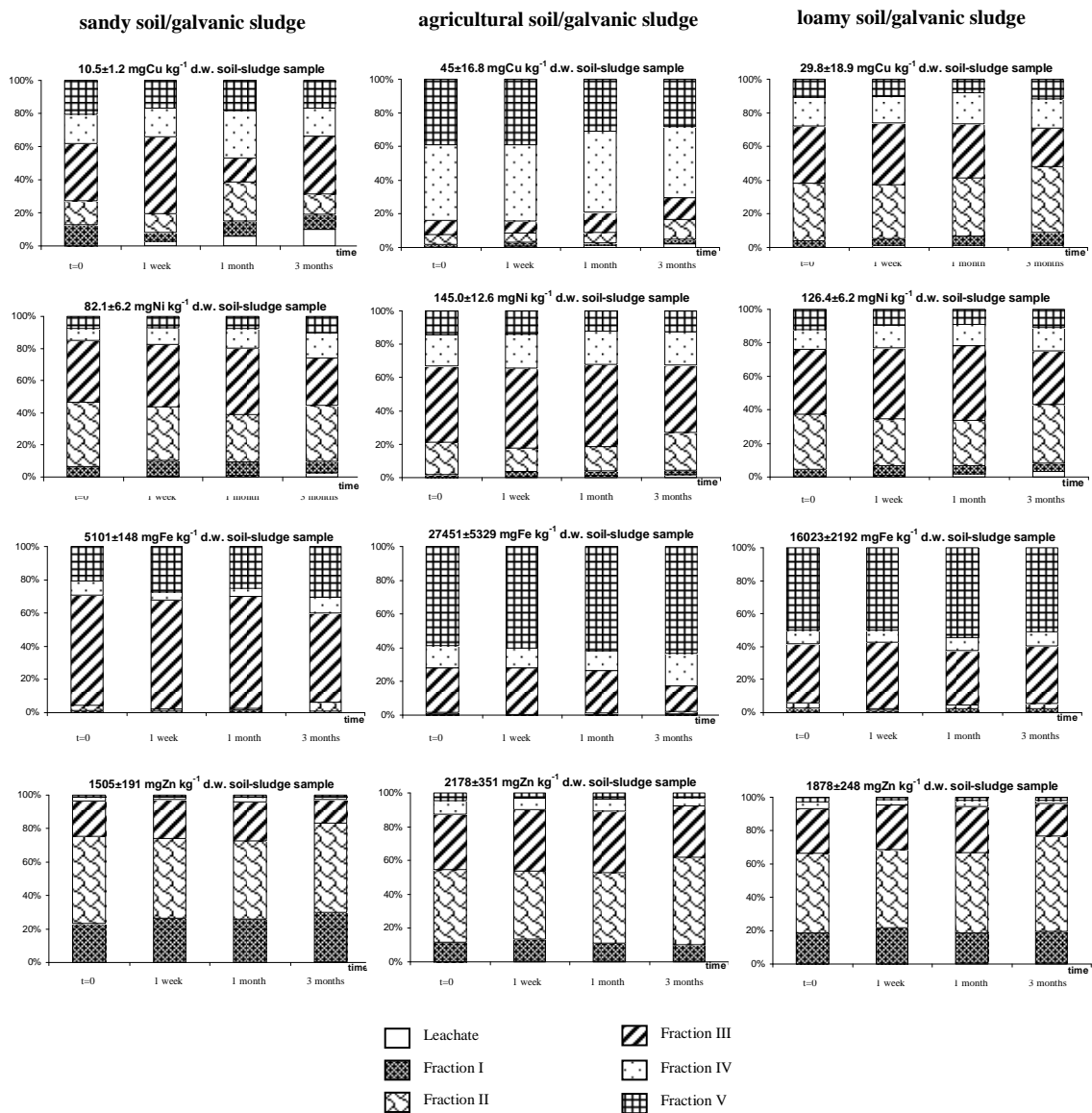


Fig. 2. Percent contribution of selected metals in particular fractions and leachates in the total metal contents

The mean value with standard deviation value of the metals contents in leachates and particular fractions were presented in Table 1.

The quantities of Cu, Ni, Fe and Zn extracted with different extractants, with each metal fraction expressed as percentage of the sum of metal content in F I - F V fractions and leachates are given in Figure 2.

The amounts of metals (Cu, Ni, Fe, Zn) leaching from sludge-soil samples were increasing with contact (Tab. 1, Fig. 2).

The occurrence of Cu, Ni, Fe and Zn in particular fractions of sequential extraction depends on the type of investigated soil (sandy forest, agricultural or loamy).

Contribution of particular fractions of metals present in the sludge-soil samples has not shown significant changes during investigated time (3 months).

Financial support by the University of Gdańsk, projects BW/8000-5-0279-6 and DS/8270-4-0093-6 are gratefully acknowledged.

References:

-
- [1] A. Bielicka, I. Bojanowska, A. Wiśniewski, Polish J. Environ. Stud., 14(1) (2005) 5
 - [2] A. Bielicka, I. Bojanowska, K. Świerk, J. Kowalczyk, Annals of the Polish Chemical Society, Vol II (2005) 114
 - [3] A. Bielicka, I. Bojanowska, A. Wiśniewski, Polish J. Environ. Stud., 14(2) (2005) 151
 - [4] A. Tessier, P.G.C. Campbell, M. Bisson, Anal. Chem., 51(7) (1979) 844
 - [5] A. Bielicka, I. Bojanowska, K. Świerk, Annals of the Polish Chemical Society, Vol. 3, Part 3 (2004) 1183
 - [6] Kalembkiewicz J., Socho, Wiad. Chem. 59(7-8) (2005) 697
 - [7] Kot A., Namieśnik J., Trend. Anal. Chem. 19(2/3) (2000) 69
 - [8] Hauser L., Tandy S., Schulin R., Nowack B., Environ. Sci. Technol., 39 (2005) 6819

SURFACE FUNCTIONALIZATION OF THE SILICA SPHERICAL PARTICLES

Beata Borak¹, Agnieszka Baszczuk², Marek Jasiorski³, Krzysztof Maruszewski^{1,4}

¹*Wrocław University of Technology, Faculty of Mechanics, Institute of Materials Science and Applied Mechanics, Smoluchowskiego 25, 50-370 Wrocław*

²*Institute of Low Temperature and Structures Research, Polish Academic of Science, Okólna 2, 50-950 Wrocław*

³*Wrocław University of Technology, Faculty of Chemistry, Smoluchowskiego 23, 50-372 Wrocław*

⁴*Electrotechnical Institute, Skłodowskiej-Curie 55/61, 50-369 Wrocław*

Abstract

We have used a modified Stöber process to obtain silica particles of a controlled size with narrow size distribution. By including functionalized organosilanes in the synthesis process, we have created particles with functional amine, thiol and vinyl groups on the surface. The effects of reaction conditions and the loading of the functionalized organosilanes on particle size was examined by SEM and TEM.

Introduction

Unmodified silica particles have only hydroxide groups on the surface and are not suitable for the preparation of inorganic-organic composite materials. The bonding force of the hydroxide groups with some typical compounds is usually small. Functionalization of silica particles leads to the presence of active groups on the particles surface and is expected to prepare the active sites to bind other molecules. The most common functional groups are: -NH₂ (amines), -SH (thiols), and -COOH (carboxylic acid). Especially useful are amine groups transformed to aldehyde groups which easily connect to proteins and enzymes via Schiff base linkage [1-3]. The chemical interactions of amine groups with other functional groups are well characterized too. The thiol groups are used for anchoring metal complexes and metal ions [4].

In this work we present results of synthesis functionalized silica particles by the sol-gel method. We have created silica particles with amine, thiol and vinyl groups on the surface by including functionalized organosilanes in synthesis process.

Experimental

All particles have been obtained in the sol-gel process. The basic precursor was tetraethoxysilane (TEOS, Alfa Aesar), as a functionalized organosilanes we used 3-Aminopropyltriethoxysilane (APTES, Aldrich), 3-Mercaptopropyltrimethoxysilane (MPTMS, Alfa Aesar) and Vinyltriethoxysilane (TVOS, Aldrich). The syntheses were a modified Stöber process [5] in which TEOS has been co-hydrolyzed with functionalized organosilanes. Particles with functional amine groups have been obtained by hydrolysis of APTES only without TEOS. The morphology and size of the obtained particles have been examined by scanning electron microscopy (SEM, XL 30 Philips CP) and transmission electron microscopy (TEM, TESLA BS500). The IR measurements were carried out at room temperature with a Bruker IFS-88 FT spectrometer in the region of

400-4000 cm^{-1} . Suspension of the powders in Nujol were placed between KBr wafers and IR spectra were measured.

Results and discussion

Figure 1a presents SEM micrographs of the silica particles with amine groups on the surface. The particles have been obtained by hydrolysis of APTES without TEOS. The obtained particles are spherical in shape with diameters in the range from 0.5 μm to 5 μm .

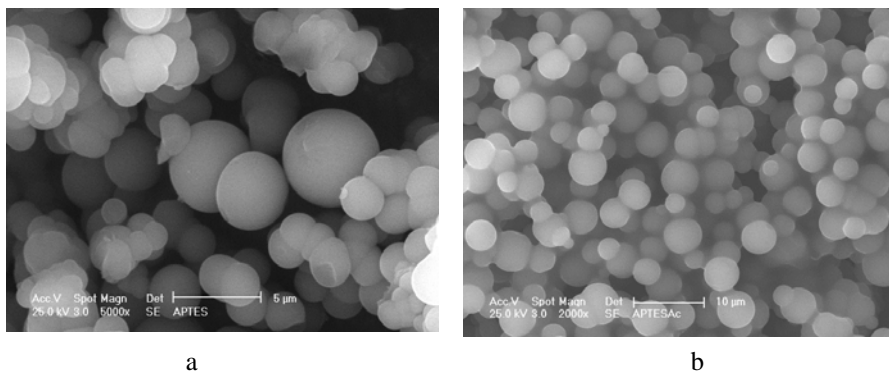


Fig. 1. SEM micrographs of the silica particles with amine groups (a) and the same particles after reaction with acetone (b).

The presence of the amine groups on silica particles surface was confirmed by the FT-IR measurement (Fig 2a). The spectrum shows a very characteristic sharp band at 1610 cm^{-1} assigned to the stretching vibration of NH_2 group [6].

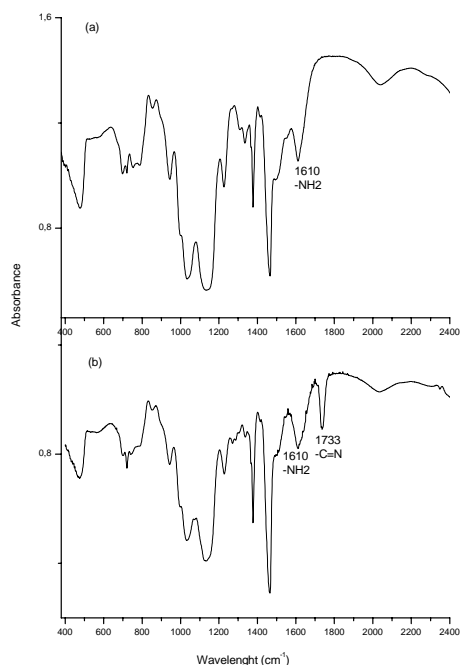


Fig. 2. FT-IR spectra of silica particles obtained from APTES (a) and the same particles after reaction with acetone (b).

Modified silica particles were impregnated in acetone to transform $-NH_2$ groups in reaction with carbonyl groups of the acetone to imino groups (Schiff bases) (Figure 3). The change of powder color from white to yellow after impregnation in acetone was observed. The FT-IR spectra measured for silica particles after impregnation in acetone (Figure 2b) shows new sharp band at 1733 cm^{-1} corresponding to the $C=N$ groups of Schiff bases (imines) [3,7] created in reaction with acetone. One can observe that after impregnation in acetone characteristic band at 1610 cm^{-1} assigned to the NH_2 group doesn't disappear, which means that NH_2 groups on the surface of silica particles are still present. Interesting fact is that the shape of the silica particles after and before the impregnation does not change and the particles are still spherical (Fig. 1b).

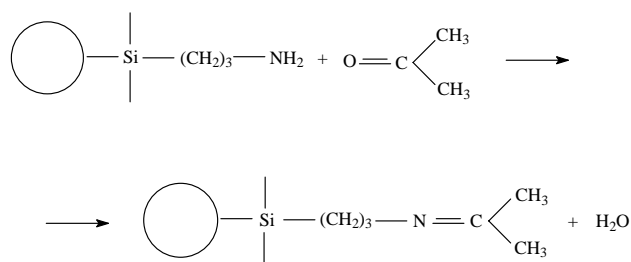


Fig. 3. The procedure of the coupling reaction of silica particles with amine groups and acetone.

After co-hydrolyzation of the TEOS with MPTMS and TEOS with TVOS silica particles with thiol and vinyl groups respectively were obtained. The TEM micrographs of these particles are present on Figure 4. Not all particles are spherical, some of them are irregular. The size of the particles with thiol groups are in the range from 380 to 1300 nm. The particles with vinyl groups are bigger, their diameters are from 2,8 to 3.8 μm .

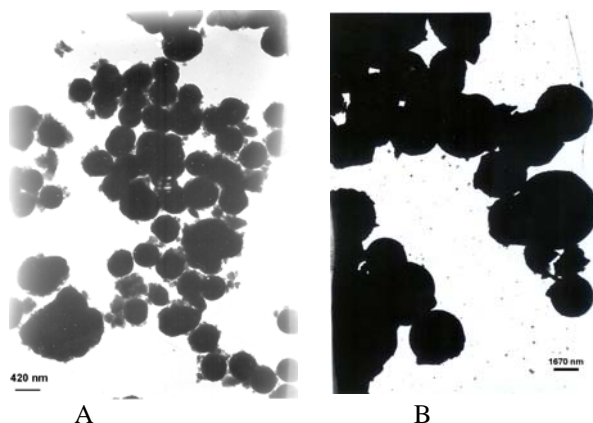


Fig. 4. TEM micrograph of the silica particles with thiol (A) and vinyl (B) groups.

The FT-IR spectra of silica particles before and after the functionalization are presented on the Figure 5a-5c. For silica particles (Fig. 5a) it is possible to see the Si-O-Si symmetric and asymmetric bands located at 798 cm^{-1} and 1098 cm^{-1} , respectively and the band at 949 cm^{-1} corresponding to the Si-O group. In Fig 5b the spectrum shows a band at 693 cm^{-1} corresponding to the Si-C stretching vibration of the functional group containing the thiol. The presence of the thiol groups ($-SH$) is observed in the band at

2550 cm^{-1} . In Fig. 5c the spectrum shows a band at 1645 cm^{-1} associated to the $-\text{C}=\text{C}-$ group of vinyl group.

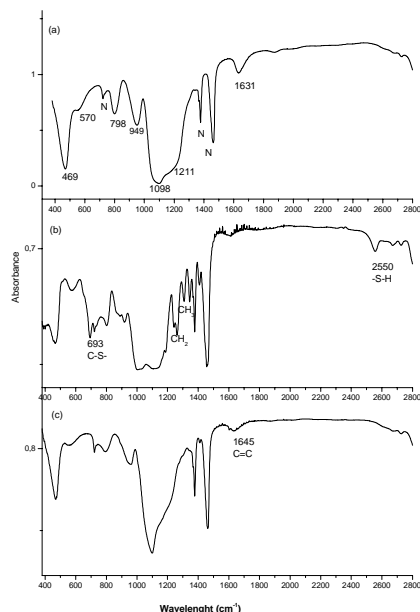


Fig. 5. FT-IR spectra of (a) silica nanoparticles, (b) particles with thiol groups and (c) particles with vinyl groups.

Conclusions

The silica particles with amine, thiol and vinyl groups on the surface have been obtained. Some of the particles have spherical shape and size about a few micrometers. The presence of the functional groups is confirmed by the IR measurements. The amine groups were transformed to the imines in the reaction with acetone. This process doesn't change spherical shape of the particles.

Acknowledgements

The authors thank to Professor Jan Baran from Institute of Low Temperature and Structures Research of Polish Academic of Science for his help in the IR measurements. This study was supported by Polish Scientific Research Committee research grant No. 3 T08D 031 28

Reference

- [1] M. Arroyo-Hernández, R.J. Martín-Palma, J. Pérez-Rigueiro, J.P. García-Ruiz, J.L. García-Fierro, J.M. Martínez-Duart, *Mater. Sci. Eng. C* 23 (2003) 697
- [2] X. Liu, Z. Ma, J. Xing, H. Liu, *J. Magn. Magn. Mater.* 270 (2004) 1
- [3] X.Q. Zhang, W.Y. Yang, X.Z. You, Y. Wei, *Appl. Surf. Sci.* 84 (1995) 267
- [4] G. Hernández, R. Rodríguez, *J. Non-Cryst. Solid* 246 (1999) 209
- [5] W. Stöber, A. Fink, E. Bohn, *J. Colloid Interface Sci.* 26 (1968) 62
- [6] H. Okabayashi, I. Shimizu, E. Nishio, C.J. O'Connor, *Colloid Polym. Sci.* 275 (1997) 293
- [7] N.I. Maliavski, O.V. Dushkin, E.V. Tchekounova, J.V. Markina, G. Scarinci, *J. Sol-Gel Sci. Technol.* 8 (1997) 571

LAPACHOL – SYNTHESIS AND APPLICATION

Zygmunt Boruszczak

*Institute of Technology of Polymers and Dyes, Technical University of Lodz,
12/14, The Stefanowskiego Street, 90-953 Lodz, Poland*

Introduction

Natural dyes, derivatives of 1,4-naphthoquinone, such as lawson, lapachol and juglone, were used in historical times for dyeing of fabrics, as well as in folk medicine and cosmetics. Today, endeavours are made towards broader application of these dyes in medicine, what is, first of all, associated with their microcidal features [1]. A special interest has, for the last decade, been attracted by lapachol (Fig. 1- B), occurring in wood and bark of *Tabebuia avellanedia*, a South-American tree, known under the names of La Pacho, Pou d'Arco and Taheebo [2].

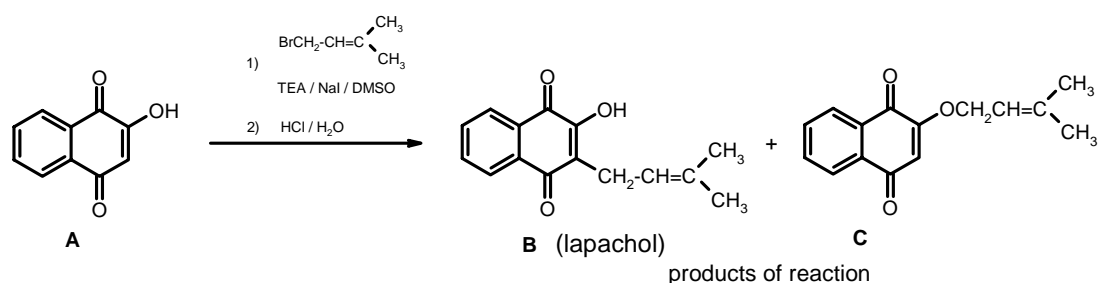


Fig. 1. Reaction of lapachol synthesis

The raw material, obtained from this tree, reveals bactericidal, fungicidal and antimalarial activity. Because of limited resources of the natural raw material, the issue of producing synthetic lapachol becomes more and more important, as well as the determination of its usability for cosmetics and medicine. The application of synthetic lawson in these branches is strictly associated with its potential biocidal activity, regarding various pathogenic microorganisms. The goals of the study included:

- design of lapachol synthesis method,
- evaluation of biocidal activity of lapachol solutions
- assessment of the possibility to obtain biocidal fabric.

Experimental

Lapachol synthesis

The synthesis of lapachol was performed by modified K. Schaffner-Sabb's method [3], acting with prenyl bromide onto lawson solution in DMSO, in the presence of triethylamine (TEA) and NaI (Fig.1). The product of that reaction contained, beside lapachol (B), O-alkyl compound (C) and unreacted lawson. The mixture of those two components was dissolved in toluene and sequentially extracted with NaHCO₃ and NaOH solutions. The extract in soda lye was acidified with hydrochloric acid. The extracted raw lapachol was crystallised with isopropanol, giving a product with melting temperature at 139 – 140°C (lit. [3] 140°C). Lapachol structure was confirmed by ¹H NMR (CDCl₃), δ (ppm): 1,68 (3H, s), 1,79 (3H, d), 3,30 (2H, d), 5,22 (1H, t), 7,33 (1H, s, OH), 7,76 – 8,13 (4H, m, ArH) spectrum.

Bactericidal and fungicidal properties of lapachol and Lawson* solutions

*Naphthoquinone dye applied for comparative purposes

The evaluation was performed by screening method, employing the well technique: wells, hollowed in medium with inoculated microorganisms, were filled with dye solution in acetone (200 µl) at concentration of 10 mg/cm³, then incubated for 24 h in temperature of 37°C (bacteria) and for 5 days in 30°C (fungi). The results have been presented in Table 1 as bactericidal activity rates, determined by the diameter of microorganism growth suppression zone / well diameter ratio.

Table 1. Bactericidal and fungicidal activity of lapachol and lawson

Microorganisms	Studied compounds		
	lapachol	lawson	acetone*
	Bactericidal activity rate		
<i>Corynebacterium xerosis CX</i>	-	1,77	-
<i>Klebsiella pneumoniae KP</i>	1.03	1.69	-
<i>Bacillus licheniformis BL</i>	1.54	2.62	1.08
<i>Micrococcus luteus ML</i>	1.46	2.08	-
<i>Staphylococcus aureus S.A.</i>	1.08	1.54	-
<i>Escherichia coli EC</i>	1.08	1.31	-
<i>Pseudomonas aeruginosa PA</i>	-	1.54	-
	Fungicidal activity rate		
<i>Aspergillus niger AN</i>	1.06	2.70	-

- no growth suppression zone; * applied for control purposes

Dyeing of wool and polyamide fabric and evaluation of their biocidal properties

Synthetic lapachol and lawson were applied for dyeing of wool (W) and polyamide (PA). The dyeing procedure was performed for one hour in a Roaches Engineering Ltd. dyeing machine, with 1:20 liquor ratio, pH=5.5 (acetate buffer), in temperature of 98°C. Dyed samples of the fabrics were submitted to resistance tests in conformity with ISO standards (Table 2). The obtained results confirmed good binding of the dyes, both with wool and polyamide.

The obtained dyeing was submitted to evaluation of biocide activity against bacteria, listed in Table 1 and the following fungi: *Trichophyton mentagrophytes* and *Aspergillus niger*. The applied evaluation method was conformable with AAT CC 147-1998 Standard. The obtained results have been demonstrated in Table 3.

Table 2. Functional qualities of PA and W fabrics, dyed with lapachol and lawson

Dye %*	Fabric type	Rubbing dry / wet	Sublimation 150 °C	Washing	Perspiration alkaline / acid	Water
0.5 lapachol	PA	5/5	4-5/4/5	3/5/5	2/3/3 2/2/2	2/2/2
	W	5/5	-	2/4-5/4-5	3/2/4 3/2/4-5	4/2/4-5
0.5 lawson	PA	5/5	4-5/4-5/5	3/5/5	2/4/4 2/3/3	2/3/2
	W	5/5	-	4/5/5	3/4/4 3/4/4	3/3/4

* with regards to fabric mass

Results and discussion

The performed studies have demonstrated that lapachol and lawson reveal bactericidal properties against most of the tested organisms. The largest growth suppression zones – from 1.69 to 2.7 – were observed around the wells with lawson solution. With regards to lapachol, those values were distinctly lower, not exceeding 1.6, while no growth suppression was observed in case of *Corynebacterium xerosis* and *Pseudomonas aeruginosa*. The studies of fungicide properties, performed only for *Aspergillus niger*, demonstrated strong activity of lawson (2.7) and weaker on of lapachol (1.06).

Similar studies, done for wool fabric, dyed with lapachol and lawson in concentrations from 0.02 to 1%, did not reveal any growth suppression zones for either bacteria or fungi. Those microorganisms grew also under the fabric, in direct contact with its surface. The observed effect is to be associated with the fairly high stability of the keratin-NH₃⁺ O-dye binding, what, in consequence, leads to elimination of free dye.

In the case of the polyamide material, the presence of growth suppression zones was confirmed for only two bacteria: *Micrococcus luteus* and *Staphylococcus aureus*, with lapachol, used for dyeing at concentration of 1%. In all the other concentration ranges, contact activity was observed with regards to the studied bacteria, i.e., no bacterial growth under the fabric.

The results of fungicidal tests, performed with polyamide fabric for *Trichophyton mantagrophytes* and *Aspergillus niger*, have proven that both lapachol and lawson inhibit the development of these fungi. The growth suppression effect was observed under the fabric, in direct contact with its surface, but it was also manifested by presence of a growth suppression zone. It was also found that *Aspergillus niger* was more sensitive and that either lapachol or lawson concentration at 0.04% was satisfactory to inhibit further development of the fungus. The biocidal effect of the polyamide fabric can be explained by weaker binding of either lapachol or lawson with polyamide fibre. The fibre, when compared with wool, has got a much lower number of amine groups, capable for ion binding with OH groups of lapachol and lawson. In result of this feature, in presence of water or humid environment, active biocidal dye particles appear in direct fibre surrounding.

The study was financed from the funds of Research Project No 3T09 B01928.

Table 3. Bactericidal and fungicidal properties of fabrics, dyed with lapachol and lawson

Dye Fabric	% of dye ¹ used for dyeing	Observed effects ²								
		Bacteria							Fungi	
		CX	KP	BL	ML	SA	BC	PA	TM	AN
lapachol/W	0.02 - 1	No effects								
lawson/W	0.02 - 1	No effects								
lapachol PA	0.02	-	-	-	-*	-*	-*	-*	-	-
	0.04	-	-*	-*	-*	-*	-*	-*	-	+
	0.06	-	-*	-*	-*	-*	-*	-*	-	+
	0.08	-	-*	-*	-*	-*	-*	-*	+	+
	0.1	-	-*	-*	-*	-*	-*	-*	+	+
	0.2	-	-*	-*	-*	-*	-*	-*	+	+
	0.3	-	-*	-*	-*	-*	-*	-*	+	+
	0.4	-	-*	-*	-*	-*	-*	-*	+	+
	0.5	-	-*	-*	-*	-*	-*	-*	+	+
	0.6	-	-*	-*	-*	-*	-*	-*	+	+
	0.8	-*	-*	-*	-*	-*	-*	-*	+	+
1	-*	-*	-*	+	+	-*	-*	+	+	
lawson PA	0.02	-*	-*	-*	-*	-*	-*	-*	-	-
	0.04	-*	-*	-*	-*	-*	-*	-*	-	+
	0.06	-*	-*	-*	-*	-*	-*	-*	+	+
	0.08	-*	-*	-*	-*	-*	-*	-*	+	+
	0.1	-*	-*	-*	-*	-*	-*	-*	+	+
	0.2	-*	-*	-*	-*	-*	-*	-*	+	+
	0.3	-*	-*	-*	-*	-*	-*	-*	+	+
	0.4	-*	-*	-*	-*	-*	-*	-*	+	+
	0.5	-*	-*	-*	-*	-*	-*	-*	+	+
	0.6	-*	-*	-*	-*	-*	-*	-*	+	+
	0.8	-*	-*	-*	-*	-*	-*	-*	+	+
1	-*	-*	-*	-*	-*	-*	-*	+	+	

¹ vs. fabric mass

² + the presence of growth suppression zone; - no growth suppression zone;

* growth suppression under the fabric

Literature

- [1] L. B. Dama et al. J. Ecotoxicol. Environ. Monit., 8(3) (1998) 213-215.
- [2] A. Ravelo et al., in: Studies in Natural Products Chemistry, Elsevier B.V. 2003, Vol. 29, 719-760.
- [3] K. Schaffner-Sabba et al. J. Med. Chem., 27 (1984) 990-994.

LAWSONE AND LAPACHOL APPLIED FOR POLYAMIDE DYING IN LIQUID AND SUPERCRITICAL CARBON DIOXIDE

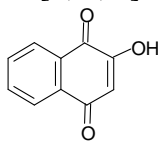
Zygmunt Boruszcak, Anna Kosmalska, Paweł Wawrzyniak*,
Marian Zaborski

Technical University of Lodz, Institute of Polymer & Dye Technology, Stefanowskiego
12/16, 90-924 Łódź, Poland (Corresponding author: akosmalska@poczta.onet.pl)

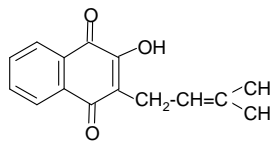
* Technical University of Lodz, Faculty of Process and Environmental Engineering,
Wólczańska 213, 93-005 Łódź, Poland

Introduction

A development of synthetic dyes caused a considerable decrease of natural dyes application in textile industry in the end of 19th century. Nowadays, there is a strong tendency to apply the synthetic dyes on a big scale for dyeing of textiles that could exhibit antibacterial or antifungal activity against common pathogens [1, 2]. The most popular and easy technologies of such textiles production are based on employing dyes that show a maximum zone of microbial inhibition in dyeing process of fibres [3]. The naphthoquinone compounds (lawsone and lapachol – Fig. 1) have an interesting position among such dyes [4, 5, 6].



lawsone (C.J. Natural Orange 6)



lapachol (Natural Yellow 16)

Fig. 1. The chemical structure of lawsone and lapachol.

The aim of the present study was to determine a possibility of polyamide (PA6) dyeing with synthetic lawsone and lapachol in liquid and supercritical carbon dioxide. Techniques of textile dyeing using supercritical fluids as a solvent are relatively new and still under study; the majority of papers appeared in the last decade [7, 8, 9]. Different kinds of disperse dyes and fibres were investigated but mostly it was not possible to dye fibres in this medium with good fastness properties and to acceptable colour depth. The results obtained were usually worse than in the traditional aqueous dyeing procedure. Nevertheless, it is believed that carbon dioxide, especially in supercritical state, can be very useful for dyeing because of more in-depth penetration into the structure of the materials. The major requirement for this process to proceed successfully is a supply of suitable and low-molecular weight dyes which are sufficiently soluble in liquid carbon dioxide. Both lawsone and lapachol comply with these requirements.

Experimental

Lawsone used in the study was synthesized according to the method described by Fieser [10] in which 4-amino-3-hydroxynaphthalene-1-sulfonic acid was used as a starting material. Lapachol was obtained according to the method described by Schaffner-Sabba [11].

The object for dyeing was a knitwear of polyamide PA6 fibres (thickness: 67 dtex, degree of crystallinity: 0.49). Weight of the samples was in the range from 2.0 to 3.0 g. The amount of reactive dye used was 0.5 ÷ 1.0% owf (on weight of fabric).

Traditional water-based dyeing was carried out with a dye apparatus, purchased from Roadies Engineering Ltd., at the following parameters: the liquor ratio 1:20, pH = 5.0 (acetate buffer), dyeing time: 1 hour at 98°C.

Dyeing experiments in CO₂ were carried out in a stainless steel autoclave of 100 cm³ volume equipped with a thermostat, temperature controller and pressure indicator. To increase the solubility of the dye ethanol or acetone were used as co-solvents. The fabric and dye solution in the co-solvent (2 cm³) put into a small glass tube were placed at the bottom of the autoclave and closed. When the autoclave was filling up with the liquid CO₂ (c.a. 70% of the vessel volume) and the dye dissolved in the medium the desired temperature and pressure was set. The dyeing processes were conducted for 15 to 90 minutes. The parameters of dyeing experiments are shown in Table 1.

Table 1. Parameters of polyamide (PA) dyeing with synthetic lawsone and lapachol

Lawsone				
Sample	System	Temp [°C]	Pressure [bar]	Time [min]
PA-1	H ₂ O (pH=5,0)1% owf dye	98	–	60
PA-2	CO ₂ (“sub-critical”)1% owf dye	25	61	15
PA-3			90	
PA-4*			90 *	
PA-5	CO ₂ (supercritical)1% owf dye	45	90	15
Lapachol				
PA-6	H ₂ O (pH=5.0)1% owf dye	98	–	60
PA-7	H ₂ O (pH=5.0) 0.5% owf dye	98	–	60
PA-8	CO ₂ (“sub-critical”)0.5% owf dye	25	90	30
PA-9	CO ₂ (supercritical)0.5% owf dye	50	96	30
PA-10	CO ₂ (supercritical) 1% owf dye	50	95	90

* refers to a fabric sample which was first padded in a dye solution in ethanol, dried and then subjected to dyeing in CO₂

The evaluation of colours obtained was determined on the basis of spectrophotometric investigation using UV-VIS Spectrophotometer CM-3600d (KONICA MINOLTA Co., Ltd.). The colour parameters were determined in the CIELab system with the use of *L**, *a**, *b** parameters.

Fastness properties of the dyed samples were examined according to ISO standards (ISO 105-E04 and ISO 105-C06/25).

Results

The results obtained revealed that synthetic lawsone is a useful dye for polyamide fabric dyeing in sub- and super-critical carbon dioxide. All the experiments carried out showed colouristic effect which can be defined as orange. The results of dyeing carried out in CO₂ were compared with those obtained using traditional water-based procedure and the study showed almost the same dyeing results. Spectrophotometric measurements revealed very small differences related to intensity and tint of the colour obtained. The results are summarized in Table 2. The values of *dE** were in the range from 9.87 to 20.72. The lowest *dE** value was observed for the samples PA-4* and PA-5 which indicates a very slight difference of colours obtained using CO₂ in comparison with the sample dyed in water; PA-1. The higher temperature and pressure of CO₂ supplied to the autoclave the better results of dyeings were observed.

Table 2. The effect of techniques applied for PA dyeing with synthetic lawsone on colour strength (symbols of the samples – explained in Table 1)

Lawsone					
Sample	Colour obtained	L*	a*	b*	dE*
PA-1	orange	63.28	32.24	35.18	–
PA-2	orange	77.35	26.17	35.14	15.82
PA-3	orange	79.60	22.58	31.95	20.72
PA-4*	orange	68.98	36.02	43.40	9.87
PA-5	orange	63.71	38.77	47.07	12.95

L* - the lightness coordinate, a* - the red/green coordinate (with +a* indicating red, and –a* indicating green), b* - the yellow/blue coordinate (with +b* indicating yellow, and –b* indicating blue), dE* - the colour difference between the samples dyed in CO₂ and polyamide dyed in water which was the reference sample

From analysis of the brightness parameter (L^*) it followed that its values were almost identical for PA-1 and PA-5 samples, dyed respectively: in water (60 min at 98°C) and in supercritical CO₂ (15 min at 45°C). Insignificantly greater difference of the L^* value was observed for PA-4* sample which was first padded in the solution of lawsone in ethanol and then subjected to the treatment with “sub-critical” CO₂ (T = 25°C, p = 90 bar). The other dyeing experiments (samples PA-2 and PA-3) carried out with the use of CO₂ should be estimated favourably although differences of colours were greater.

The effectiveness of polyamide fabric dyeing in CO₂ was varified by fastness tests. The results showed that colour fastness of fibres dyed in carbon dioxide was very similar to that of fibres dyed in water. In general, the differences did not exceed a unit in the five-degree scale; where 4-5 corresponds to an excellent fastness. The best results were observed for rubbfastness (4-5) which can fulfil the requirements of most users. The other fastness properties were estimated as good or satisfactory.

Additional spectral measurement was also done in order to test the effectiveness of dye-fiber interaction. The test consisted in measurement of light beam reflected from the sample dyed in sub-critical CO₂ and the same sample after washing in 1% solution of a commercial wool detergent. The measurements done before and after washing showed that the colour parameters of the examined sample changed very slightly. The loss of colour was inconsiderable and it was equal 6.09 of CIELab units. It can be concluded therefore, that a small change of the spectral value before ($dE^* = 58.58$) and after washing ($dE = 52.49$) indicates a high degree of bonding between lawsone and polyamide fiber. This bond is of ionic nature, to a great extent, and results from interactions between amino groups of polyamide -NH₂ and –OH groups in lawsone. The presence of such a bond was proved in a wool-lawsone system [12].

Much worse results of dyeing with the use of CO₂ were observed when lapachol was applied as a dye. Dyeings obtained were characterized by low colour intensity and were far from the results gained with a typical aqueous dyeing procedure. The results are summarized in Table 3. Colour difference between the PA-8 sample dyed in CO₂, applied in near subcritical state, was $dE^* = 37.49$ and for PA-9 sample dyed in supercritical CO₂, $dE^* = 20.53$ of CIELab units. Increase of the dye concentration to 1% owf and dyeing time to 90 minutes caused a decrease of the dE^* value to 14.71.

All the experiments carried out with the use of CO₂ led to a pale pink colours. They were convergent with dyeings obtained in water, what suggests that lapachol is present in ionized form which is characterized by the colour of rosy. Yellow dyeings are typical of a non-ionized form.

Table 3. The effect of techniques applied for PA dyeing with synthetic lapachol on colour strength

Lapachol					
Sample	Colour obtained	L*	a*	b*	dE*
PA-6	pink	53,19	25,01	10,64	–
PA-7	pink	56,46	26,91	8,06	–
PA-8	pale pink	86,94	5,46	3,80	37,49
PA-9	pale pink	72,04	17,30	7,89	20,53
PA-10	pale pink	62,91	22,34	4,11	14,71

symbols of the samples – like in Table 1; symbols L*, a*, b*, dE* - like in Table 2

Samples dyed with lapachol were investigated in the fastness test; the same as in the case of samples dyed with lawsone. From the results analysis it followed that colours obtained with lapachol had average fastness and the results were typical of dyes that are linked with fibres according to ionic mechanism. The fastness examined were slightly worse, except rubbfastness, in comparison with dyeings obtained with the use of lawsone as a dye. It indicates a weak bonding between lapachol and polyamide.

Conclusion

Process of polyamide dyeing with lawsone in carbon dioxide (applied in supercritical and “sub-critical” state) proceeded readily and very quickly and it was possible to obtain almost the same dyeing results using carbon dioxide within 15 minutes and typical aqueous dyeing procedure (60 min at 98°C). The use of lapachol led to the worse results. The dyeings obtained were characterized by lower intensity compared with a typical aqueous dyeing technique. The unfavourable results are connected with lower ability of lapachol to undergo ionization in unpolar medium of CO₂. In consequence this influences lapachol-polyamide bonding unfavourably.

Acknowledgements

This work was supported by the Polish State Committee for Scientific Research (Grant No 3T09B01928).

References

- [1] TB. Machado, et al., *Int. J. Antimicrob. Agents*, 21 (2003) 279
- [2] R. Singh, et al., *Dyes and Pigments*, 66 (2005) 99
- [3] L. B. Dama, et al., *J. Exotical Environ. Monit.*, 8(3) (1998) 213
- [4] F. Malekzadeh, *Appl. Microbiology*, 16 (4) (1968) 663
- [5] A.G. Ravelo et al., in: *Studies in Natural Products Chemistry*, Atta-ur-Rahman (ed), vol. 29, Elsevier, 2003, str.719
- [6] D.Lemordant, J.P. Forestier, *Journ. d' Agric. Trad. et de Bota. Appl.*, XXX, 1 (1983) 69
- [7] E. Schollmeyer, D. Knittel, et al., DE 39 06 724 A1, D 06 P 1/00; Germany: 13.09.1990
- [8] W. Saus, D. Knittel, E. Schollmeyer, *Text. Res. J.*, 63 (1992)135
- [9] E. Bach, et al., *Melliand Int.*,3 (1998) 192
- [10] L.F. Fieser, et al., *Organic Synthesis*, 21 (1941) 56
- [11] K. Schaffner-Saaba, et al., *J. Med. Chem.*, 27 (1984) 990
- [12] K.C James, et al., *J. Soc. Cosmet. Chem.*, 37(5) (1986) 35

RESIDENTIAL COURSE

– NEW PROPOSAL FOR ACADEMIC TEACHERS TRAINING

Malgorzata Brindell¹, Iwona Maciejowska¹, Joanna Mania², Renata Wietecha-Posluszny¹, Michał Woźniakiewicz¹, Paul Yates³

¹ *Faculty of Chemistry, Jagiellonian University, Krakow, Poland*

² *PLIVA Kraków, Zakłady Farmaceutyczne SA, 31-546 Kraków, ul. Mogilska 80*

³ *Keele University, United Kingdom, ECTN*

Introduction

The Faculty wishes to meet the teaching quality guidelines set for the European Higher Education Area (EHEA) by the ENQA (European Network for Quality Assurance), which stipulate that: “teaching staff should be given opportunities to develop and extend their teaching capacity (...) Institutions should provide poor teachers with opportunities to improve their skills to an acceptable level.” [1].

Academic teachers at the Faculty of Chemistry Jagiellonian University have the annual workload of 210 teaching hours at the BSc or MSc level, and doctoral students are obliged to teach 90 hours per year. In 2001, the Faculty started a course for PhD students and new teaching staff, which dealt with “Selected Problems in the Methodology of Teaching Chemistry at University Level.” [2]. Each year it was becoming increasingly difficult to decide on a meeting time that would be convenient for the entire staff, all of whom had also other commitments. To solve that problem a residential course for new staff of Faculty of Chemistry at JU was organized in June 2005.

In 2003, the ECTN (European Chemistry Thematic Network) created the Newly Appointed University Chemistry Teaching Staff (NAUCTS) group, whose main objective was to organize a pilot summer school aimed at improving the teaching skills. The establishment of the NAUCTS group was greeted with an enthusiasm at many faculties, as South and Eastern European universities had provided little in-service training for their teaching staff, and opportunities to exchange experiences was scarce as a result. Jagiellonian University then became the venue for the first working meeting in January 2005.

Comparison

Those two residential courses have many things in common:

The objectives: to disseminate best practice and to facilitate the networking of staff.

- Some topics: PBL, image of chemistry, presentation skills, assessment and evaluation, tutorial
- Methods: work in group, workshops, evening sessions of discussions etc.
- Both schools received very positive evaluation from participants.

The difference is e.g. that while during the ECTN school emphasis was laid on the European dimension of chemical study, the Polish school highlighted rather the possibilities of solving local problems.

Organisation

One of the objectives of the ECTN Summer School was to facilitate the networking of staff from different countries. Given the need to bring people together over large distances a residential summer school was the only feasible way of achieving this. Malta was selected as the venue as it was reasonably accessible from most of Europe, the cost of accommodation was reasonable, and it was felt that somewhere with an established reputation as a holiday destination might attract the young staff we wished to attend.

The main organisational problem was that of attracting enough delegates to apply. Publicity was done throughout the ECTN, but the response was generally disappointing. Despite the fact that all costs of delegates, including travel, were covered it seemed that the opportunity to attend such a meeting on teaching was far less attractive than it would have been for a research conference. A detailed procedure for evaluating applications had been developed, but in the end did not need to be used. However, after some time we did manage to recruit around thirty suitable delegates.

In advance of the meeting an electronic discussion group was set up on Yahoo. This proved invaluable in allowing delegates to introduce each other, and in providing written documentation in advance of the meeting. It was also used after the meeting to facilitate initial networking.

The Jagiellonian course has contained three parts:

- Preparation for the meeting: course organisation, presentation of main teacher's aids – posters, models, overheads, literature, computer programs, the Internet resources etc. – items which may cause problems in transportation
- 3 day residential course (Zakopane)
- Summary meeting: presentation of plots of new classes, impact of the residential course on subsequent teaching methods and ideas arising from the course presented in conferences [3-5]

Input from industry

In the informal atmosphere of the residential course in Zakopane there was also a chance to look at the higher education from the broader perspective, confront the academic knowledge with actual requirements of a potential employer. How and what students are taught, what the university graduates know and what kind of professional experience they have, finally effects their chances to find a better job. Based on the example of the pharmaceutical industry (which is one of the major employers of chemistry graduates in Krakow) the importance of the proper documentation of the conducted experiments was emphasized – “Anything not documented (properly) means not done” (OECD Principles on Good Laboratory Practise). Contemporary industry (chemical, pharmaceutical, any) is govern by rules of Good Manufacturing Practice (GMP), modern chemical laboratories are obligated to follow Good Laboratory Practice (GLP). The teacher should not only try to make his/her course more attractive for students, by showing students that knowledge they gain at the course is not purely theoretical but can be used in “real life” certainly attracts, but also needs to be responsible for preparing their students/graduates to be competitive at the global job market. Substantial feature expected from new employees is independence and ability of critical thinking. Unfortunately those aspects are traditionally considered as deficits of Eastern European and Asian students. Young participants of Zakopane residential course had dynamically discussed the possibilities of changes in daily routine of their own courses to encourage their students to act more independently and ask more critical questions.

Evaluation

The ECTN Summer School generally ran with few problems. Detailed evaluation [6] was collected at the end; this was overwhelmingly positive but there were some useful suggestions for improvement. The networking aspect was also successful, but it did prove necessary to modify the programme in order to allow delegates more free time. Informal feedback suggested that this did facilitate the networking process.

One problem did emerge afterwards, which was the dominance of native English speakers in discussion groups. This may have been exacerbated by the fact that such speakers also dominated the list of presenters. In the debriefing meeting a number of suggestions were made in order to address this in a subsequent Summer School.

The evaluation of the residential school in Zakopane resulted in different suggestions [7]. According to opinions of participants, they appreciated the opportunity to exchange the experience and ideas among themselves. Moreover, they found constructive criticism of presented oral presentations and teaching&learning chemistry beneficial in a wider context. In the evaluation questionnaire participants also listed as useful, valuable and important: adjusting program to the needs of participants, introduction of formal regulations, unknown from previous experience (e.g. new organisation of studies according to Bologna Declaration), increased self-awareness etc.

It was also evaluated that during the course some difficulties appeared. Especially self-evaluation, looking at their own teaching from the students' point of view seemed to have been the most problematic tasks.

Results and conclusions:

Major problems that may occur during the residential course are presented in table 1. Possible solutions were also proposed, as they are recommended both by participants and the teaching staff.

Table 1

Problems	Suggested solutions
× Making off-topics	√ Professional moderator
× Long discussion	
× Overcrowded programme	√ Interactive forms, diversity in classes,
× Reduced leisure time	√ Outdoor activities
× Problems in absence of home for mothers/fathers with young children	√ Planning events long time in advance
× Need of financial support higher than by other forms of training	√ Sponsors, grants, reducing costs (e.g. sleeping in dormitories)

It was showed that residential training of academic staff has many unique advantages:

- The participants focus on the subject of the course since there are no other classes or duties during that time

- The discussion is almost unlimited since the time can be adjusted to the needs of participants.
- There is an opportunity for a better meeting with other participants during informal situations (e.g. meals, excursions, travelling) which leads to the integration of the young academic teachers and networking.

The proceedings of the ECTN Summer School, which are available in the Internet [8] were written by the delegates themselves. In order to do this, groups of two or three were asked to report on specific sessions. Each group consisted of delegates drawn from different countries so as to facilitate collaborations between different countries after the event had ended.

This year the training at the Faculty of Chemistry is to be continued; the ECTN training will be held in the year 2007 again on Malta.

References:

- [1] Standards and Guidelines for Quality Assurance in the European Higher Education Area www.enqa.net/files/BergenReport210205.pdf , p.17;
- [2] I.Maciejowska, PhD Students as Academic Teachers. How We Can Help Them?, Variety in Chemistry Education, Dublin, 31.08-02.09.2003;
- [3] A.Białaś, I. Maciejowska, Design of a catalyst for air protection, Variety in Chemistry Education, Keele, 30.08-01.09.2006;
- [4] M. Woźniakiewicz, M.Herman, M.Kochanowski, J.Milczarek, M.Wieczorek, A.Skulska, A.Zakrzewska, J.Dobrowolska, S.Walas, I.Maciejowska, P. Kościelniak, Modelowy regulamin zajęć laboratoryjnych - anatomia sukcesu, Annual Meeting of Polish Chemical Society, Gdańsk 18-22.09.2006; Book of Abstracts p.272
- [5] J. Milczarek, I. Maciejowska, S. Walas „...Przychodzi farmaceuta do chemika...” czyli ćwiczenie laboratoryjne z fabułą, Annual Meeting of Polish Chemical Society, Gdańsk 18-22.09.2006; Book of Abstracts p.272
- [6] ECTN Newly Appointed University Chemistry Teaching Staff Summer School, Results of Evaluation Questionnaire;
- [7] I.Maciejowska, M. Brindell, R. Wietecha-Posluszny, Residential Summer School – efficacious way of academic teachers’ training, 8th ECRICE, Budapest, 31.08 - 01.09. 2006, Book of abstract p. 153-154
- [8] European Chemistry Thematic Network, Newly Appointed University Chemistry Teaching Staff, Summer School Malta 22-27 June 2005, Proceedings, http://www.cpe.fr/ectn-assoc//network/wgws_naucts/ssm_index.htm

TRITIUM KINETIC ISOTOPE EFFECTS ON ENZYMATIC DECOMPOSITION OF 5'-HYDROXY-L-TRYPTOPHAN

Elżbieta Boroda, Marianna Kańska

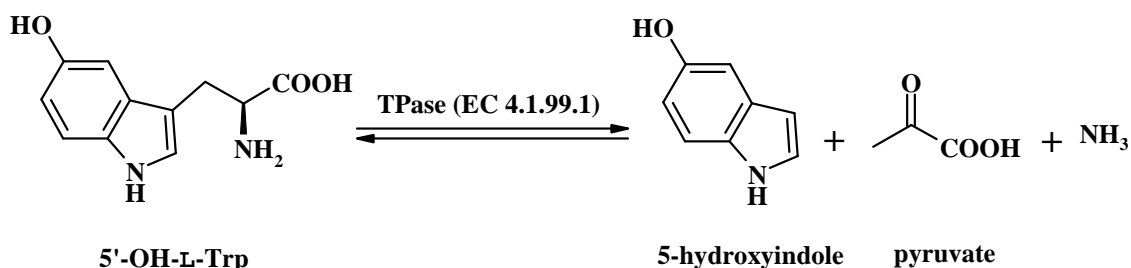
Department of Chemistry, University of Warsaw Pasteur 1 Str., 02-093 Warsaw, Poland

Abstract

The tritium kinetic isotope effect on position 2 has been determined in the reaction of decomposition of 5'-hydroxy-L-tryptophan, 5'-OH-L-Trp, catalysed by enzyme TPase, (EC. 4.1.99.1). The numerical values of isotope effects in the course of reaction were obtained by competitive method using 5'-hydroxy-[1-¹⁴C]-L-tryptophan as internal radiometric standard.

Introduction

The enzyme tryptophanase (L-Tryptophan indole lyase EC 4.1.99.1), TPase, catalyses the decomposition of 5'-OH-L-Trp to the corresponding 5-hydroxyindole, pyruvic acid, and ammonia [1]. (Scheme 1).



Scheme 1. The reversible reaction catalyzed by the enzyme TPase

Under certain conditions, there is a possibility of the reverse reaction, leading to formation of L-tryptophan. This enzyme also decomposes L-serine, L-cysteine, S-methyl-L-cysteine, and is often used in synthesis of 5'-hydroxy-L-tryptophan [2]. In the literature, the mechanism of TPase catalysis are well documented [3, 4]. One technique often used in studying such kind of reaction mechanisms is kinetic isotopic effect method (KIE). In the course of KIE study the ratios of reaction rates for lighter and heavier isotopes should be determined since numerical values of KIE's will be used to find rate determining step.

Aforementioned studies require the synthesis of isotopomer of 5'-OH-L-Trp labeled with isotopes of hydrogen in 2-position of side chain and isotopomer of this compound specifically labeled with ¹⁴C in carboxylic group. For measuring reliable values of KIE we applied internal radioactive standard method. It assumes using doubly labeled substrate for KIE determination. The substrate, in our case 5'-OH-L-Trp, should bear one label (¹⁴C) in position non-involved in course of reaction, and second label

(tritium) is bonded to 2-position. In this method KIE is determined from changing the value of ratio $^{14}\text{C}/^3\text{H}$ in course of reaction.

For this studies we have used the following isotopomers: 5'-OH-[2- ^3H]-L-Trp and 5'-OH-[1- ^{14}C]-L-Trp. The ^{14}C -labelled compounds were used as internal radiometric standards for precise determination of numerical values of KIE.

The synthesis of abovementioned isotopomers of tryptophan have been described by us earlier [5, 6].

Results and discussion

Tritium kinetic isotope effects ($^1\text{H}/^3\text{H}$) of hydrogen bonded to α -carbon position of 5'-OH-L-Trp in course of decomposition have been measured in water in room temperature. The values of tritium kinetic isotope effects in mentioned above reaction are given in Table 1.

Table 1. Tritium KIE for enzymatic decomposition of 5'-OH-[2- ^3H]-L-Trp

Degree of conversion [f]	KIE
0,022	4,09
0,061	4,99
0,063	4,62
0,100	4,48
0,107	4,87
0,142	4,49
0,142	5,00
0,163	4,56
0,180	4,79
0,220	4,43
	Avg. 4,63 \pm 0,16

These effects were determined using internal radiometric standard ([1- ^{14}C]-5'-OH-L-Trp) and Yankwich-Tong equation (1) to calculate KIE values [7]. Internal radioactive standard method assumes using $^3\text{H}/^{14}\text{C}$ ratio instead of specific activity of ^3H -labeled 5'-OH-L-Trp, therefore, the determination of KIE is much more precise. The experimental error was accessed by Student t-test with 95% of confidence.

$$\alpha = \frac{\ln\left[1 - f \frac{(1-f)R_0}{R_f}\right]}{\ln(1-f)} \quad (1)$$

where:

- α - $^1\text{H}/^3\text{H}$ kinetic isotope effect,
- R_0 - $^3\text{H}/^{14}\text{C}$ radioactivity ratio in 5'-OH-L-Trp at the start of reaction,
- R_f - $^3\text{H}/^{14}\text{C}$ radioactivity ratio in 5'-OH-L-Trp after f degree of conversion,
- f - degree of conversion.

Considerably large KIE of tritium implies that its value is typical to primary KIE, and therefore, the hydrogen atom in position 2 plays a significant role in transformation of the enzyme-substrate complex into enzyme-product complex. In this study, the kinetic isotope effect of enzymatic decomposition of 5'-OH-L-Trp was determined for the first time using the radioactive isotopes. While, KIE for this reaction has been previously investigated, it was relied upon the stable isotopes, specifically determining the solvent isotope effects. The magnitude of KIE for tritium indicates that hydrogen atom bonded with α -carbon of 5'-OH-L-Trp is involved in a proton transfer during the decomposition of a tryptophan.

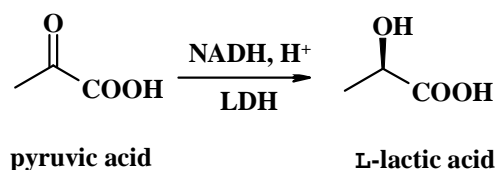
Experimental

Materials

All chemicals were from Aldrich. Enzymes TPase (EC 4.1.99.1) from *Escherichia coli*, LDH (EC 1.1.1.27) from rabbit muscle, cofactor PLP, and NADH were from Sigma. The scintillation cocktail was from Rotiszint (Germany).

Methods

The concentration of pyruvic acid was determined spectrophotometrically using Shimadzu UV-102 CE-LV spectrometer. This indirect procedure consists of conversion of pyruvic acid to L-lactic acid by enzyme LDH and coenzyme NADH (Scheme 2) and determining the concentration changes of NADH by measuring the absorbance at 340 nm [8, 9].



Scheme 2. Conversion of pyruvic acid into L-lactic acid by enzyme LDH

The radioactivity of all samples was determined using an automatic liquid scintillation counter (LISA LSC PW470 – Raytest, Germany).

KIE assays

KIE assays were carried out at room temperature. In catalysed reaction by TPase the LDH/NADH couple allows indirectly determine the concentration of pyruvic acid [11] (scheme 2), and degree of decomposition of 5'-OH-L-Trp.

For each kinetic run the assayed sample of [2-³H]-, and [1-¹⁴C]-5'-OH-L-Trp was placed in encapped vial and dissolved in 4.5 ml of 0.1 M phosphate buffer, pH 8. Radioactivity of ³H-isotopomer was 3-7 fold higher than ¹⁴C-one. To this the following reagents were added in turn:

1. 90 mg of KCl;
2. 9,5 mg D, L-dithiothreitol (HSCH₂(OH)CH₂(OH)CH₂SH 1,4-dithiobutan-2,3-diol,);
3. 300 μ l of 1mM 5'-pyridoxal phosphate, PLP, (cofactor);
4. 600 μ l of the enzyme L-lactic dehydrogenase of activity 270 U/ml;
5. 300 μ l of 2 mM NADH;
6. 300 μ l of enzyme TPase (0.13 U/ml).

In the preset time of the course of reaction the 1 ml of volume samples were taken, and degree of conversion was determined spectrophotometrically. Next, reaction was quenched by acidifying the reaction mixture to pH 5 with glacial acetic acid. The non reacted 5'-OH-L-Trp and L-lactic acid were separated on ion exchange column (Amberlite IR 120 H⁺ form, 60 \times 5 mm) by elution with 0.3 M NH₃(aq) and their radioactivities were measured on LSC. Additionally the degree of conversion was checked using radioactivity of the product and substrate.

Contract/grant sponsor: this work was supported by grants BST-1121-12000023 and 120000-501/68-BW-172102.

References

- [1] Y. Morino, E. E. Snell, *Methods of Enzymology*, 17a, (1993), 439
- [2] Y. Morino, E. E. Snell, *J Biol Chem*, 12, 242, (1967), 2793
- [3] R. S. Philips, B. Sundarareju, N. G. Faleev, *J. Am. Chem. Soc*, 122, (2000), 1008
- [4] F. Cook, in: *Enzyme mechanism from isotope effects*. CRS Press, Boca Raton, FL, USA, (1991), p. 37
- [5] E. Boroda, R. Kański, M. Kańska, *J Label Compd Radiopharm*, 46, (2003), 441
- [6] E. Boroda, S. Rakowska, R. Kański, M. Kańska, *J Label Compd Radiopharm*, 46, (2003), 691
- [7] J. Y. Tong, P. E. Yankwich, *J Phys Chem*, 61, (1957), 540
- [8] R. S. Philips, M. Lee, *Bioorg Med Chem*, 3, (1995), 195
- [9] T. Wanatabe, R. S. Philips, *J Biochem*, 83, (1977), 733

COMPUTATIONAL EXERCISES IN ELEMENTARY CHEMISTRY FOR NON-CHEMISTRY STUDENTS

Paweł Broś^{1,2}, Zofia Kluz¹,
Anna Migdał-Mikuli¹, Małgorzata Włodarczyk¹
¹*The Department of Chemical Education of Jagiellonian University*
²*Gymnasium No. 41 in Kraków*

In the academic year 2003/2004 the Faculty of Biotechnology and the Faculty of Physics, Astronomy, and Applied Computer Science of Jagiellonian University introduced Biophysics as a new interdisciplinary (interdepartmental) subject. Teaching is conducted by staff from these faculties and from JU's Faculty of Chemistry.

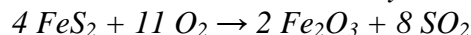
Students taking this course have 150 timetabled hours on chemistry consisting of lectures, seminars and exercises on General Chemistry with elements of Physical Chemistry (90 hours) and Organic Chemistry (60 hours).

In the academic year 2005/2006 thirty-three students enrolled on the course. These were graduates of secondary schools with varying study profiles: Biology/Chemistry, Mathematics/Physics, Mathematics/Computer Science, Mathematics/Physics/Computer Science, Mathematics/Biology/Chemistry, general, Computer and Natural Sciences, and Mathematics.

Nineteen students had passed the extended version of the 'matura' school graduation exam in Chemistry. This shows that the level of knowledge of Chemistry possessed by first year students of Biophysics is extremely varied. This is confirmed by the results of a test carried out during the first lecture of the academic year 2005/2006 which consisted of 13 questions on elementary material from the secondary school curriculum. The average number of points scored by the students was 17.21 out of a maximum 29 (59.34%). These results show that students are ill-prepared to take on the new, often challenging material included in the course.

It was especially surprising that they had difficulty solving this problem:

Sulphur(IV) oxide can be produced on an industrial scale by burning pyrite (FeS₂):



Calculate what volume of Sulphur(IV) oxide, measured in normal conditions, would be produced as a result of burning 30 g of pyrite.

As many as 21 (63.63%) of the students left this question unanswered, which required nothing more than calculation of the molar mass of FeS₂, knowledge of the molar volume of gases (22.4 dm³), and the ability to express a single proportion:

$$\begin{array}{ccc} 4 \cdot 120 \text{ g FeS}_2 & \xrightarrow{\text{produces}} & 8 \cdot 22.4 \text{ dm}^3 \text{ SO}_2 \\ 30 \text{ g FeS}_2 & \xrightarrow{\text{produces}} & x \text{ dm}^3 \text{ SO}_2 \\ & & x = 11.2 \text{ dm}^3 \text{ SO}_2 \end{array}$$

Please note that this question did not require that students be able to solve chemical reaction equations.

Another question which caused the students great difficulty was:

Formalin is an aqueous solution of methanal (formaldehyde) with a concentration of around 40%. Design an experiment allowing the identification of methanal (formaldehyde) in formalin. Draw a diagram for the experiment and specify the expected results. Write an equation for the reaction that takes place.

The difficulty factor of this question was only 0.21. This seems to suggest that in many schools no chemical experiments are performed at all. This was confirmed by the results of a questionnaire in which 28% of students reported that they had never seen or carried out a chemical experiment.

It is little wonder therefore that first year Biophysics students have difficulty coping with lectures in elementary Chemistry with elements of Physical Chemistry. Their inability to handle the material was confirmed by the results of the final exam for this part of the course.

In order to even out the students' level as well as prepare them to take on new material the Department of Chemical Education of Jagiellonian University has prepared support materials to be used as an independent study aid by students preparing for exercises or attending lectures. The materials have been recorded on CD-ROM and will be made available to all Biophysics students starting from the academic year 2006/2007.

In the "You should be able to..." section the CD contains all the material from the secondary school curriculum which students need to know to be able to keep up with the new material introduced as the course progresses. For example, before a lecture on chemical bonds (from the point of view of quantum mechanics) the students can use the CD to update their knowledge of doublet/octet rules and the formation of ionic and covalent bonds.

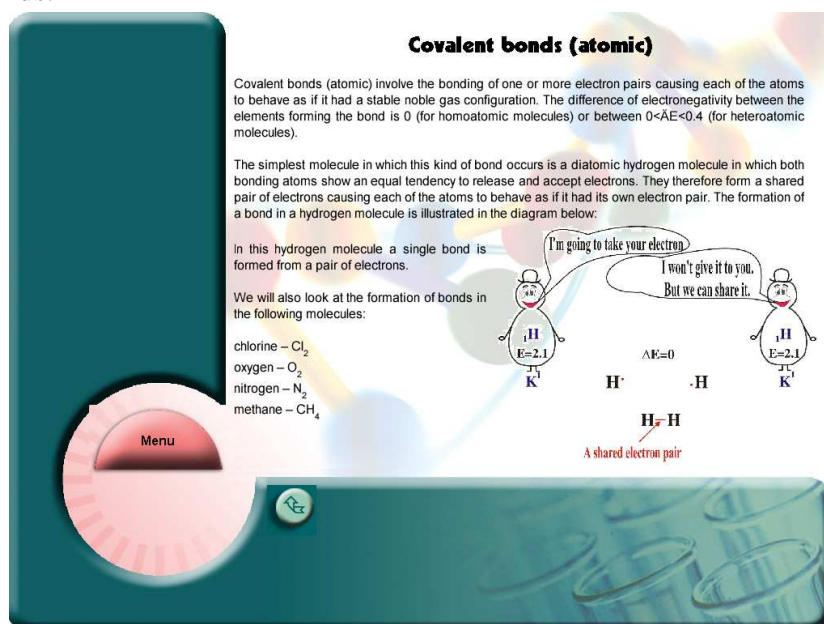


Fig. 1. A screenshot of the page on the formation of covalent bonds.

Particular emphasis has been placed on providing support material for computational exercises. The fifteen teaching hours on this subject cover a wide range of topics from the following areas:

1. Elementary chemical calculations – stoichiometry;
2. Solutions and concentrations of solutions;
3. Reactions in aqueous solutions (electrolytic dissociation, the hydrogen ion concentration exponent, hydrolysis – hydrolysis constant and degree of hydrolysis, solubility and the solubility product);
4. Oxidisation and reduction reactions;
5. Electrochemistry;
6. Thermochemistry;
7. Chemical kinetics.

Students are required to thoroughly recap material from the secondary school syllabus and also apply themselves during the semester.

The material on the CD is divided into two parts: “You should be able to...” and “Check your knowledge”. Part I contains a compendium of elementary secondary school material presented as follows: at the beginning of each section there is a glossary explaining the concepts needed to complete the exercises (fig. 2). This is followed by about 10 example exercises with step-by-step solutions and a full commentary (fig. 3). Below are some examples of material from the first section of Introduction to Chemical Calculations – Stoichiometry.

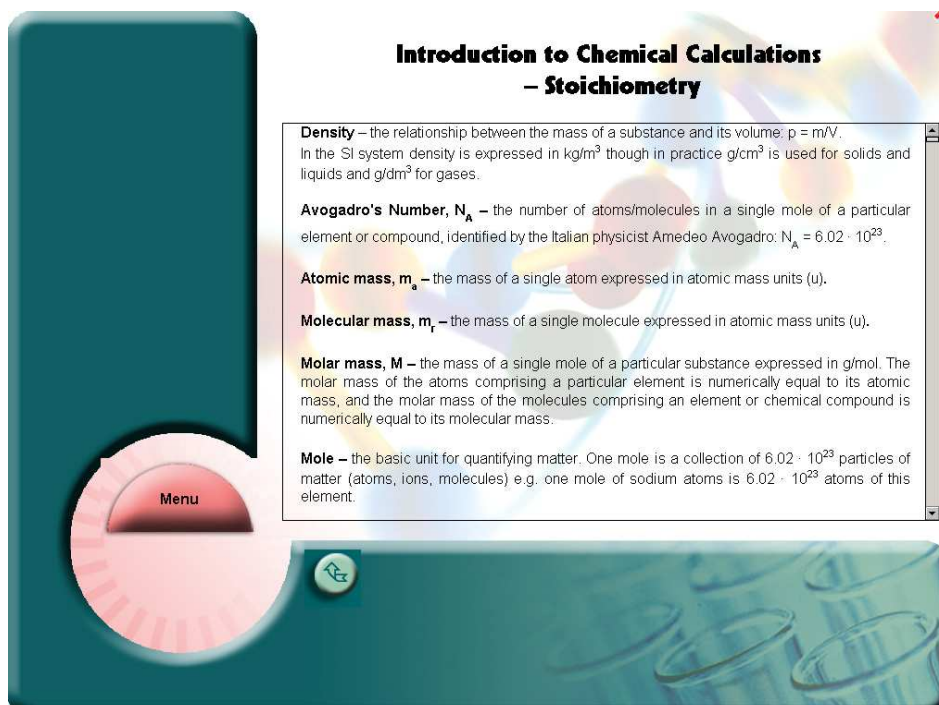


Fig. 2

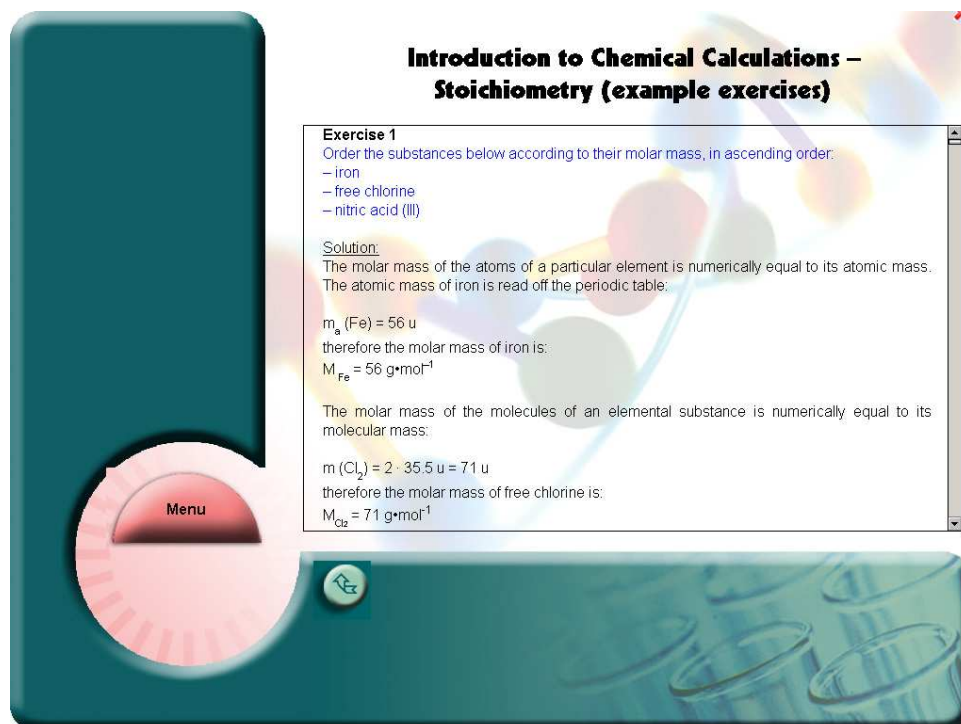


Fig. 3

The second part of the CD – “Check your knowledge” is designed to help students recap material for the oral examination (kolokwium) i.e. the more difficult topics. The glossary section includes explanations of the concepts of reaction yield and the ideal gas equation of state. The programme then presents about 10 solved problems with full commentary, about 10 problems with answers, and 10 test questions.

The authors of the support material hope that providing students with this 'legal cheat sheet' will encourage and motivate them to independently prepare themselves for lectures and computational exercises.

FEMTOSECOND PRIMARY EVENTS IN BACTERIORHODOPSIN PHOTOCYCLE

B. Brożek-Płuska, M. Kurczewska, K. Kurczewski, H. Abramczyk,
*Technical University, Department of Chemistry, Laboratory of Molecular Laser
Spectroscopy at IARC, Wroblewskiego 15 Street, 93-590 Lodz, Poland*
email:brozek@mitr.p.lodz.pl

Abstract

Ultrafast time resolved electronic spectra of the primary intermediates induced in the BR photocycle are measured by the femtosecond pump-probe spectroscopy. The primary events in bacteriorhodopsin (BR) occurring within the first 3.5 ps are discussed on the basis of the two-state, many-mode model proposed recently in our laboratory.

1. Introduction

Femtosecond pump-probe electronic absorption [1-5], pump-probe IR absorption [6], pump-probe resonance Raman and CARS methods [7-8] as well as transient fluorescence decays [9] or fluorescence up-conversion [10] make possible to study photophysical and photochemical events initiated by the absorption of a photon. Bacteriorhodopsin (BR) belongs to the broad group of retinal proteins, which are responsible for very important biological functions, such as vision, photosynthesis and phototaxis or proton pumping [11, 12]. Bacteriorhodopsin photocycle induced by light absorption in the retinal chromophore results in the transfer of proton from the cytoplasmic to the extracellular surface of the bacterium cell. The BR photocycle is initiated by absorption of a photon from the visible range because BR in the all-trans configuration (BR₅₆₈) has a maximum absorption for the S₀→S₁ transition at 568nm.

Although the photophysical and photochemical processes of BR have been topic researches for over 30 years the primary events in the native BR and its retinal modified analogs occurring within the first 3.5ps have still remained the subject of debate and cover the focused areas of frontier research. Specifically, the main questions that need to be answered are: a) what is the precise timescale on which C₁₃=C₁₄ isomerization in BR₅₆₈ occurs [4, 6, 8]? b) what is the physical nature of the J₆₂₅ intermediate?. Has it all-trans or 13-cis configuration? Does it represent the excited S₁ or the ground S₀ state? c) what is the origin of discrepancy between the stimulated emission monitored at around 900nm for the early intermediates and the spontaneous fluorescence at 730nm? To explain the experimental results on the ultrafast dynamics in BR and its retinal modified analogs many theoretical models have been proposed. They can be roughly divided into two groups: two-state models, and three-state models. The current status on these models and their later modifications is presented in a recent overview [13].

Recently a new model (called two-state, many-mode model) has been proposed [13]. The model revises most of the commonly accepted interpretations of electronic spectra of the transient intermediates in the BR photocycle. The main idea of the two-state, many-mode model is: first, the model assumes that the primary events reflected by the initial sequence of transient electronic spectra within the first 3.5ps are not associated with a substantial C₁₃=C torsional motion. In contrast to the previous models, the model assumes that the femtosecond transient spectra evolution are related to the intermolecular energy relaxation and intramolecular energy exchange due to the coupling between the electronic degrees of freedom and the vibrational normal modes

of the retinal. The theoretical details of the model are presented in our recent paper [13]. We have shown [13] that the two-state, many-mode model is able to rationalize the complex pattern of behavior for the primary events in BR₅₆₈ and the artificial pigments such as BR5.13, BR5.12, BR6.11, BR6.9. The goal of this paper is to present new femtosecond pump-probe experimental results performed in our laboratory.

2. Experimental

The femtosecond pump-probe experiments have been performed with a set-up described in our recent paper [13]. The lyophilized BR has been purchased from Munich Innovative Biomaterials. The purity of BR (as purple membranes) is > 99.9% (referring to proteins). The lyophilized BR was re-suspended in water. The aqueous suspension of purple membrane has an optical density OD of 2.

3. Results and discussion

In contrast to the previous experiments we used the excitation at 396nm, corresponding to the longer wavelengths of the $S_1 \rightarrow S_n$ transition. The upper excited state S_n is deactivated rapidly to the lower excited state S_1 where the photocycle of BR₅₆₈ starts. Fig. 1 shows the transient transmission changes $\Delta T/T_0$ as a function of delay time between the pump and the probe pulses for several characteristic wavelengths where $\Delta T = T - T_0$, T corresponds to the transmission of BR₅₆₈ in water solution when the both the pump and the probe pulses are employed, T_0 corresponds to the transmission without the pump pulse. At zero delay (point A in Fig.1) we observe the bleaching of the ground state S_0 of BR₅₆₈ due to depletion that corresponds to the positive $\Delta T/T_0$ signal at 568nm. At the same time the $\Delta T/T_0$ signal at 710nm becomes negative which has been assigned to the excited state absorption (ESA) from the vibrationally hot Franck-Condon states $S_1(B_u) \rightarrow S_n$ and indicates that the relaxation of the S_n state excited by the pump pulse occurs within the time resolution of the experiment. Fig. 2 enlarges the horizontal scale to see more details for very short time delays. One can notice that the bleach recovery at 568nm goes beyond the zero with the decay time of 217 fs and the signal becomes negative between 250-1500fs delay. It indicates that both the bleach and transient absorption contribute to the signal at 568nm. The transient transmission minimum is observed at 1000 fs followed by a recovery to zero with the rise time of 147 fs. In contrast to the signal at 568 nm, the $\Delta T/T_0$ signal at 710nm is negative at zero delay with minimum at 500 fs and the decay time of 884 fs followed by recovery to zero between 500-1500fs. At 1500 fs the transient transmission $\Delta T/T_0$ begins decreasing again with the decay time of 849 fs and reaches minimum at around 3 ps. At around 10 ps the signal at 710 nm begins to increase again with the time constant of 8.3 ps (Fig.1). This behaviour corresponds very well to the features predicted by the two-state, many-mode model. According to the model the transient absorption at 710 nm (negative $\Delta T/T_0$ signal in Fig. 2) corresponds to the ESA from the vibrationally hot Franck-Condon states of the C=C stretching for the electronic transition $S_1(B_u) \rightarrow S_n$ with maximum at 682 nm. The maximum of the transient absorption (minimum of the $\Delta T/T_0$ signal) at 568 nm delayed by 500 fs with respect that at 710 nm (see Fig. 2) corresponds to the ESA and is related to the coupling with the relaxed CH₃ rock vibrations (maximum at 528 nm) and the relaxed HOOP vibrations with the maximum at 586 nm due the intramolecular energy transfer between the high frequency modes (C=C stretching) and the CH₃ rock as well as HOOP motions.

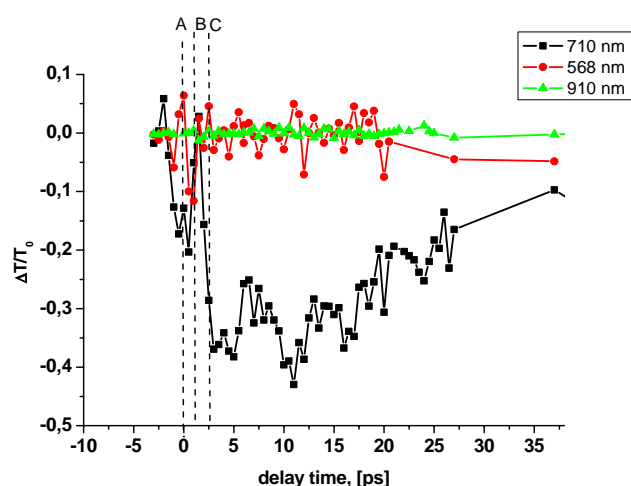


Fig.1 $\Delta T/T_0$ as a function of delay time for several characteristic wavelengths at 568 nm, 710 nm, 910 nm.

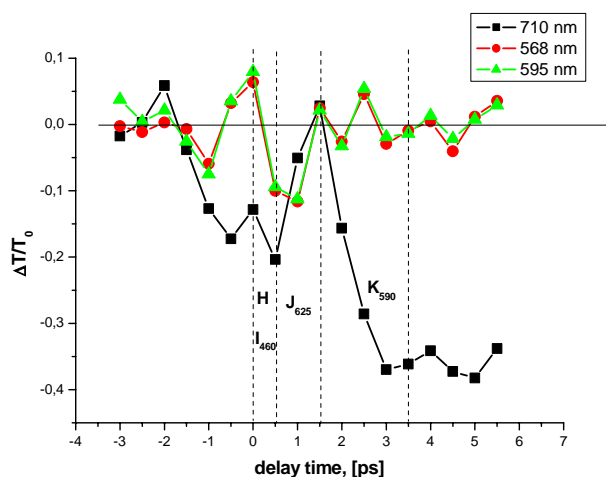


Fig.2 $\Delta T/T_0$ as a function of delay time for a few characteristic wavelengths: 710nm, 568 nm, 595 nm.

At around 500 fs for 710 nm and at 1000 fs for 568 nm the $\Delta T/T_0$ signals begin to increase which is related to the next step in the ultrafast dynamics. The process results in the stimulated emission (SE_{torsion}) increase (maximum at 730 nm) and the recovery to zero at 710 nm, and the state absorption ESA decrease in the region 586–682 nm and the recovery to zero at 568 nm (1500 fs in Fig.2). This process corresponds to the intramolecular energy transfer from the HOOP vibrations to the torsional motion (at 300cm^{-1}) around $C_{13}=C_{14}$ bond and results in the most important process of the BR photocycle - all-trans \rightarrow 13-cis photoisomerization. When the electronic state $S_1(B_u)$ becomes coupled with the torsional mode the all-trans \rightarrow 13-cis photoisomerization occurs leading to the generation of the K_{590} photoproduct in the ground state. This process is illustrated in Fig. 2 by drastic decrease of the transient transmission at 710nm between 1500–3000 fs. At around 10 ps the recovery becomes dominant for $\Delta T/T_0$ signal at 710nm (Fig.1). The recovery has the lifetime of 8.3 ps and corresponds to the repopulation of the ground state S_0 through the non-reactive channel. In contrast to the

transient transmission changes $\Delta T/T_0$ observed for 568 nm and 710 nm the signal at the zero delay in the region of near IR is close to zero. The $\Delta T/T_0$ signal becomes positive with the rise time of 643 fs and we have assigned it to the stimulated emission SE_{C=C} due to the coupling with the primary accepting high frequency vibrations. The positive signal reaches its maximum at 1000 fs delay time and goes beyond zero to reach its minimum at 1500 fs where the signals at 568 nm and 710 nm are recovered to zero (see Fig. 2). The time delay of 1500 fs corresponds to three important events: a) coupling with the torsional motion, b) all-trans-13-cis isomerization of the retinal, c) generation of the K₅₉₀ photoproduct. The negative transient transmission signal in near IR can be assigned to two processes: a) the transient absorption of BR₅₆₈ molecules coupled to the C=C stretching vibrations that have returned to the ground state (non-reactive path), b) the transient absorption of the K₅₉₀ photoproduct coupled to the C=C stretching vibration (reactive path of the photocycle).

4. Conclusions

The results obtained in this paper clearly demonstrate the dominant role played by the intermolecular energy relaxation and the intramolecular resonance energy exchange processes between the vibrational modes on the femtosecond electronic dynamics in BR photocycle. The high frequency C=C stretching mode is the primary reaction coordinate upon excitation, not the torsional coordinate. This conclusion is consistent with that obtained in earlier experimental and computational studies, in which bond-stretching dominates the motions at the early times [8-9, 14-15]. The coupling between S₁(B_u) and the torsional coordinate leading to the photoisomerization is achieved at the end of the sequence of the intramolecular energy exchange events within the first 3.5 ps upon excitation.

Acknowledgements

The author gratefully acknowledges the support of this work through KBN grant 3 T09A 139 26. The author would like to express her sincere thanks to prof. G. H. Atkinson and dr A. Terentis for fruitful discussion and many valuable suggestions.

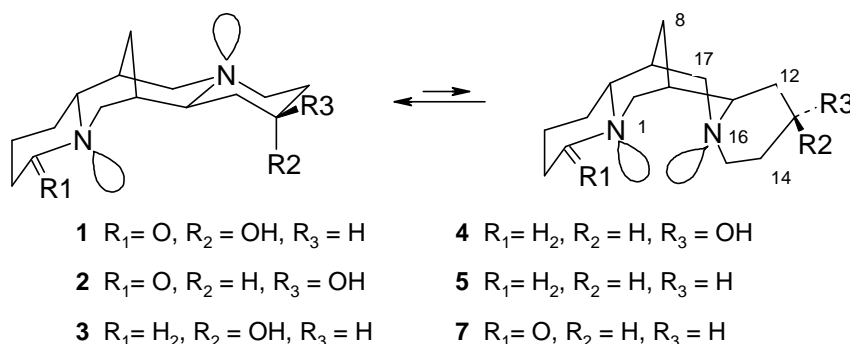
References

1. R.A. Mathies, C.H. Brito Cruz, W.T. Pollard, C.H.V. Shank, *Science* **240** (1988) 777
2. J.W. Petrich, J. Brenton, J.L. Martin, A. Antonetti, *Chem. Phys. Lett.* **137** (1987) 369
3. J. Dobler, W. Znith, W. Kaiser, D. Oesterhelt, *Chem. Phys. Lett.* **144** (1988) 215
4. T. Ye, N. Friedman, Y. Gat, G.H. Atkinson, M. Sheves, M. Ottolenghi, S. Ruhman, *J. Phys. Chem. B* **103** (1999) 5122
5. A. Aroni, B. Hou, N. Friedman, M. Ottolenghi, I. Russo, S. Ruhman, M. Sheves, T. Ye, Q. Zhong, *Biochemistry*, **66** (2001) 1210-1219
6. J. Herbst, K. Heyne, R. Diller, *Science* **297** (2002) 822
7. G.H. Atkinson, L. Ujj, Y. Zhou, *J. Phys. Chem. A* **104** (2000) 4130
8. A.C. Terentis, L. Ujj, H. Abramczyk, L. Ujj, G.H. Atkinson, *Chem. Phys.* **313** (2005) 51-62
9. B. Schmidt, C. Sobotta, B. Heinz, S. Laimgruber, M. Braun, P. Gilch, *Biochimica et Biophysica Acta*, **1706** (2005) 165-173
10. M. Du, G.R Fleming, *Biophysical Chemistry* **48** (1993) 101
11. T.G. Ebrey, in *Thermodynamics of membranes, receptors and channels*, New York, CRC Press, 1993, p. 353
12. J.K. Lanyi, *J. Phys. Chem. B* **104** (2000) 11441
13. H. Abramczyk, *J. Phys. Chem.* **120** (2004) 11120
14. A.B. Myers, R.A. Harris, R.A. Mathies, *J. Chem. Phys.* **79** (1983) 603
15. S.O. Smith, M.S. Braiman, A.B. Myers, J.A. Pardo, J.M.L. Courtin, Ch. Winkel, J. Lugtenburg, R.A. Mathies, *J. Am. Chem. Soc.* **109** (1987) 3108

NMR SPECTRA AND CONFORMATION OF 13-HYDROXY-SPARTEINE AND 13-HYDROXYLUPANINE EPIMERS

Tadeusz Brukwicki, Jacek Włodarczyk and Waleria Wysocka,
Adam Mickiewicz University, Faculty of Chemistry, Laboratory of Chemistry of
Heterocyclic Compounds, Grunwaldzka 6, 60-780 Poznań

Most bis-quinolizidine alkaloids of sparteine type assume in the solid state the conformation with ring C a boat. Two of the three known up till now alkaloids which have untypical conformation with ring C a chair are 13 α -hydroxylupanine (**1**) and 13 β -hydroxylupanine (**2**) [1]. But most bis-quinolizidine alkaloids of sparteine type occur in conformational equilibrium in solution. We have proposed a method allowing estimation of the fraction of the two main conformers in the mixture [2]. Recently, we have published new NMR and IR studies of the solution conformation of **1** and **2** [1]. We have found that the equilibrium is shifted towards the domination of the boat form, and at the equilibrium its fraction amounts to ca. 85 % in CDCl₃ solution. The determination was made on the basis of the coupling constant $J_{H7-H17\beta}$ for both 13-hydroxylupanine epimers and the chemical shifts of C(12) and C(14) atoms for the epimer α on the assumption that the effect of 13 α -hydroxy group in lupanine system is the same as in sparteine system, i.e. the conformation of 13 α -hydroxysparteine is the same as that of sparteine.



This paper presents the ¹³C NMR and ¹H NMR spectra of 13 α -hydroxysparteine (**3**) and 13 β -hydroxysparteine (**4**) (Tables 1 and 2, respectively). The main aim of this investigation is to check if the presence of the 13 α or 13 β hydroxy group causes a shift of the conformational equilibrium in a sparteine system or not (and if our previous assumption on which we determined the equilibrium in 13-hydroxylupanine epimers is true) as well as to determine the conformational equilibrium in **1** and **2** with better accuracy.

The signals in the spectra were assigned by means of 2D NMR techniques (¹H-¹H COSY, ¹³C-¹H HSQC and ¹H-¹H NOESY). The spectra are as expected for **3** and **4** in the conformation with ring C a boat assumed in ca. 100 %. The signals of H17 β both in **3** and **4** are triplets with the coupling constants amounting to 10.9 Hz. The geminal coupling constant determined from the signal of H17 α is 11.1 Hz both in **3** and **4**. As the sum of the coupling constants is equal to the difference in the frequencies of the first and the last line of the signal, we can assume that $J_{H7-H17\beta}$ is ca. 10.7 Hz. This is almost the same value (the same in the limits of error) as that determined for H17 β proton in sparteine (10.8 Hz). It means that the assumption upon which the method of determination of the fraction of conformers in 13 α -hydroxylupanine (**1**) [1,2] is based, is true. Moreover, we have now determined the effect of the hydroxy group (difference in the chemical shifts of the appropriate carbon atom in the hydroxy derivative and the chemical shift of the same carbon atom in sparteine) to a greater accuracy than before for 13 α -OH group and for 13 β -

OH group for the first time. These values can be used as correction in the determination of the fraction of conformers both in 13 α -hydroxylupanine (**1**) and in 13 β -hydroxylupanine (**2**) using chemical shifts of C(12) and C(14) carbon atoms.

Table 1. ^{13}C NMR chemical shifts of 13 α -hydroxysparteine (**3**), 13 β -hydroxysparteine (**4**), 13 α -hydroxylupanine (**1**) and 13 β -hydroxylupanine (**2**), (CDCl_3 , ppm from TMS)

C atom	13 α -hydroxy-sparteine (3)	$\Delta = \delta_3 - \delta_5$	13 α -hydroxy-lupanine (1)	13 β -hydroxy-sparteine (4)	$\Delta' = \delta_4 - \delta_5$	13 β -hydroxy-lupanine (2)	Sparteine (5)
2	56.12	-0.16	171.19	56.27	-0.01	171.25	56.28
3	25.77	-0.19	33.09	25.92	-0.04	32.42	25.96
4	24.69	-0.11	19.78	24.75	-0.05	19.50	24.80
5	29.28	-0.13	27.46	29.40	-0.01	27.31	29.41
6	66.41	-0.14	60.86	66.45	-0.10	60.57	66.55
7	32.98	-0.22	32.40	33.12	-0.08	32.24	33.20
8	27.43	-0.31	26.62	27.48	-0.26	26.62	27.74
9	35.48	-0.75	34.30	35.81	-0.42	34.35	36.23
10	61.63	-0.38	46.75	61.66	-0.35	46.71	62.01
11	57.25	-7.21	57.11	61.86	-2.60	61.17	64.46
12	41.54	6.76	40.17	43.57	8.79	41.56	34.78
13	65.01	40.06	64.46	69.34	44.39	68.97	24.95
14	32.76	6.70	31.73	35.24	9.18	33.84	26.06
15	49.13	-6.31	49.16	52.83	-2.66	52.78	55.44
17	53.18	-0.47	52.43	52.61	-1.04	51.49	53.65

We use the handbook equation [2]

$$F_C = \frac{\delta_{\text{exp}} - \delta_C}{\delta_B - \delta_C}$$

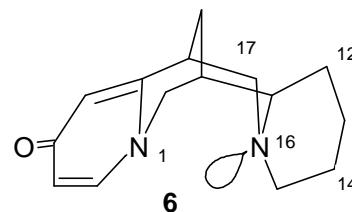
where

F_C is the fraction of the chair conformer

δ_{exp} is experimental chemical shift of the appropriate C atom (or coupling constant)

δ_B is chemical shift of this atom in the boat conformer (or model comp. **5**)

δ_C is chemical shift of this atom in the chair conformer (or model comp. **6**)



The results are shown in Table 3.

There is a discrepancy in the results determined according to different criteria. The less accurate are those derived from the coupling constants but the calculation using ^{13}C chemical shifts can also be imprecise because of the accumulation of possible errors of corrections determined by comparison of two experimental values. However, the tendency is clear: 13 α -hydroxylupanine (**1**) occurs in the equilibrium with about 11 – 14 % of the chair conformer while its epimer **2** – with ca. 16 – 23 % of this conformer.

We must answer the following two questions:

- 1) why the 13-hydroxy derivatives of sparteine occur in the boat conformation almost exclusively, while those of lupanine have the equilibrium shifted towards the presence of small but detectable amount of the chair conformer and

- 2) why is there a larger amount of chair conformer in 13 β -hydroxylupanine than in its 13 α epimer.

Table 2. ¹H NMR chemical shifts of 13 α -hydroxysparteine (**3**), 13 β -hydroxysparteine (**4**), 13 α -hydroxylupanine (**1**) and 13 β -hydroxylupanine (**2**), (CDCl₃, ppm from TMS)

H atoms	13 α -hydroxysparteine (3)	13 α -hydroxylupanine (1)	13 β -hydroxysparteine (4)	13 β -hydroxylupanine (2)	sparteine (5)	
					[6]	with corr. ^a
2 α eq	2.67		2.69		2.53	2.67
2 β ax	1.93		1.95		1.79	1.93
3 α ax	1.50	2.32	1.55	2.30	1.38	1.52
3 β eq	1.54	2.46	1.52	2.46	1.38	1.52
4 α eq	1.70	1.84	1.71	1.82	1.55	1.69
4 β ax	1.20	1.60	1.21	1.62	1.08	1.22
5 α ax	1.38	1.58	1.37	1.56	1.24	1.38
5 β eq	1.24	1.76	1.25	1.77	1.12	1.26
6	1.74	3.30	1.75	3.32	1.58	1.72
7	1.85	2.06	1.85	2.02	1.69	1.83
8 α eq	2.06	2.17	2.05	2.15	1.91	1.05
8 β ax	1.08	1.27	1.09	1.30	0.90	1.04
9	1.43	1.60	1.54	1.68	1.32	1.46
10 α eq	2.53	4.48	2.54	4.53	2.38	2.52
10 β ax	2.00	2.53	2.03	2.55	1.84	1.98
11	2.42	2.11	2.09	1.82	1.83	1.97
12 α eq	1.61	1.66	1.84	1.82	1.21	1.35
12 β ax	1.61	1.66	1.37	1.43	1.35	1.49
13 α ax	~1.7 (OH)	2.35 (OH)	3.63	3.59	1.15	1.29
13 β eq	4.08	4.08	~1.65 (OH)	2.21 (OH)	1.55	1.69
14 α eq	1.68	1.65	1.92	1.82	1.43	1.57
14 β ax	1.86	1.78	1.55	1.52	1.43	1.57
15 α ax	2.41	2.37	2.11	2.05	1.86	2.00
15 β eq	2.59	2.54	2.82	2.77	2.63	2.77
17 α ax	2.44	2.02	2.35	2.00	2.20	2.34
17 β eq	2.71	2.85	2.76	2.87	2.54	2.68

^a in the ref. [6] chemical shifts were referred to the signal of CDCl₃.

Ad 1) It is obvious that the hydroxy group introduced to the sparteine system causes very little changes in its conformational equilibrium. The DFT calculations performed by Galasso et al. [3] have conclusively proved that **5** has a strong preference (3.4 kcal/mole, 99.96 %) to conformation with ring C a boat over that with ring C a chair. 2-Oxosparteine (lupanine, **7**) which has the conformation with ring C a boat in the solid [4] occurs in the equilibrium with 90 % dominance of the boat form [2] in chloroform solution and the Galasso calculations show the preference of the boat form diminished to only 1.4 kcal/mole (ca. 91.4 %) [5]. The main factor shifting the equilibrium is the lack of the repulsion of free electron pairs on N1 and N16 nitrogen atoms present in **5** and absent in **7**. Thus a small factor shifting additionally the equilibrium is detectable in lupanine system and not visible in sparteine one.

Table 3. Fraction of conformer with ring C a chair

Compound	C(12)			C(14)			$J_{H7-H17\beta}$	
	Chem. shift		fraction of chair conf. (%)	Chem. shift		fraction of chair conf. (%)	exper. (Hz)	fraction of chair conf. (%)
	exper. (ppm)	with correction		exper. (ppm)	with correction			
1	40.17	33.41	10.9	31.73	25.03	14.3	9.9	11.1
2	41.56	32.77	16.0	33.84	24.66	17.3	8.9	23.5

Ad 2) The chair conformer present exclusively in the solid state of both 13-hydroxylupanine epimers is stabilized by intermolecular hydrogen bond between the OH and C=O groups [1]. In solution, the conformational preference changes and this hydrogen bond is replaced by a system of hydrogen bonds linking the hydroxy groups with N(16) nitrogen atom, lactam group or the solvent (they are seen in IR spectra [1]). The reason why in 13 β -hydroxylupanine the equilibrium is shifted toward a greater amount of the chair epimer could be a better steric accessibility of the hydroxy group in 13 β position.

REFERENCES

- [1] Borowiak T., Wolska I., Wysocka W., Brukwicki T., *J.Mol.Struct.* **753**, 27 (2005)
 [2] Wysocka W., Brukwicki T., *J.Mol.Struct.* **385**, 23 (1996)
 [3] Galasso V., Asaro F., Berti F., Kovač B., Habuš I., Sacchetti A., *Chem. Phys.* **294**, 155 (2003)
 [4] Doucerain H., Chiaroni A., Riche C., *Acta Crystallogr.* **B32**, 3213 (1976)
 [5] Galasso V., Asaro F., Berti F., Habuš I., Kovač B., de Risi C., *Chem. Phys.* **301**, 33 (2004)
 [6] Duddeck H., Skolik J., Majchrzak-Kuczyńska U., *Khim.Geterosikl. Soed.* 1026 (1995)

SYNTHESIS AND SPECTRAL PROPERTIES OF QUATERNARY AMINOALKYLAMMONIUM SALTS

B. Brycki, I. Kowalczyk, M. Krysmann

Laboratory of Microbiocides Chemistry, Faculty of Chemistry, Adam Mickiewicz University, Grunwaldzka 6, 60-780 Poznań

Introduction

Quaternary aminoalkylammonium salts play an important role in the living processes and many functions of prokaryotic and eukaryotic cells have been shown to be alkylammonium salts dependent. These compounds also exhibit an excellent antimicrobial activity, therefore they are used as antiseptics, bactericides and fungicides, and as therapeutic agents, as well.

In general, ammonium salts contain alkyl chain lengths in the range C₈ to C₁₆ as these show good antimicrobial activities. For the use as softeners and hair conditioning agents chain lengths between C₁₆ to C₁₈ are used [1,2].

The use of microbiocide of the same type for a long time may cause an increase of resistance, which is a very serious problem. Antimicrobial resistance in bacteria comprises a wide variety of biochemical mechanisms and processes that allow microorganisms to grow in the presence of microbiocides. To avoid this problem, microbiocides have to be continuously changed [3-5].

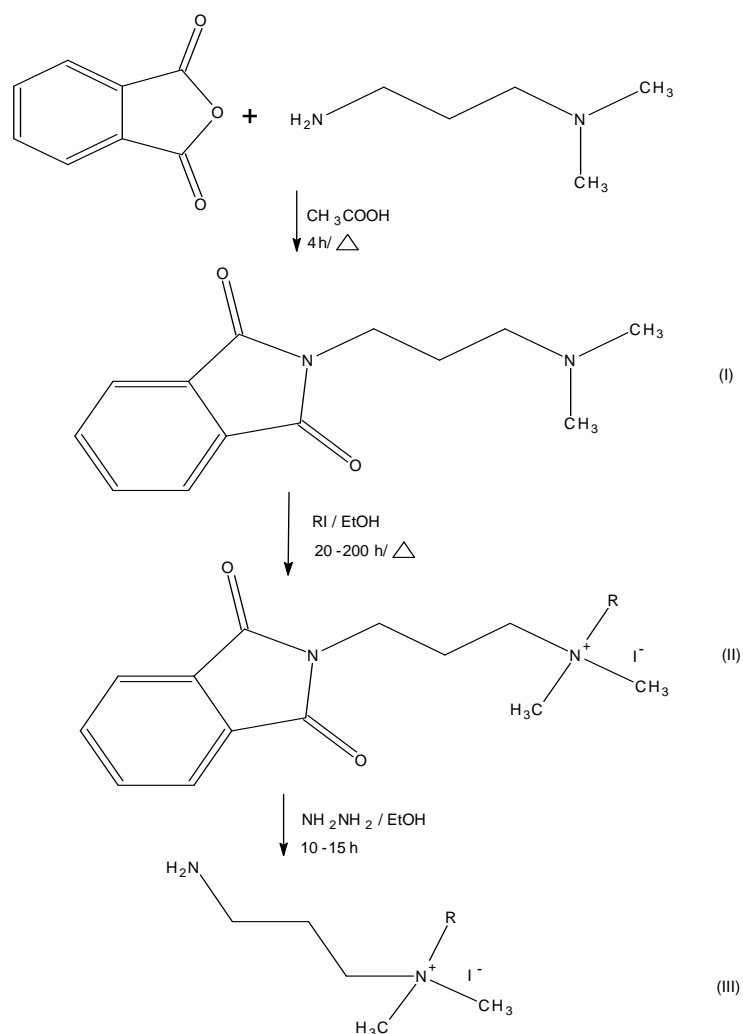
In this paper we present an efficient method of synthesis and spectroscopic analysis (FTIR, ES-MS, ¹H NMR, ¹³C NMR, 2D NMR) of novel quaternary ammonium compounds containing two methyl groups, one amino group and alkyl chain. The sequence of synthesis of quaternary alkylammonium salts is shown in Scheme 1.

Experimental section

N,N-dimethyl-3-phthalimidopropylamine (I) was obtained by the reaction of a commercially available *N,N*-dimethylpropyl-1,3-diamine with phthalic anhydride in acetic acid. The reaction mixture was heated under reflux for 4 h. At the next stage *N,N*-dimethyl-3-phthalimidopropylamine (I) was refluxed with an excess of alkyl iodide in ethanol for 20-200 h. The obtained *N*-alkyl-*N,N*-dimethyl-3-phthalimidopropylammonium iodides (II) were purified by crystallization from anhydrous ethanol (Table 1).

The final *N*-alkyl-*N,N*-dimethyl-3-aminopropylammonium iodides (III) were prepared by reaction of *N*-alkyl-*N,N*-dimethyl-3-phthalimidopropylammonium iodides (II) with monohydrate hydrazine in ethanol at room temperature for 10-15 h. Crude *N*-alkyl-*N,N*-dimethyl-3-aminopropylammonium iodides (III) were purified by crystallization from anhydrous ethanol (Table 2).

The NMR spectra of all obtained compounds were measured in CDCl₃ with a Varian Gemini 300VT spectrometer, operating at 300,07 Hz and 75,46 Hz for ¹H and ¹³C, respectively. Infrared spectra were recorded using a FTIR Bruker IFS 113v and IFS 66v/S spectrometers, in KBr pellets. MS spectra were measured in water solution on Waters Micromass ZQ spectrometer.



Scheme 1. Synthesis of *N*-alkyl-*N,N*-dimethyl-3-aminopropylammonium iodides (III)

Table 1. Characterization of *N*-alkyl-*N,N*-dimethyl-3-phthalimidopropylammonium iodides (II)

R	Formula	Molecular mass[g/mol]	ES MS [g/mol]	M.p. [°C]	Reaction time [h]	Yield [%]
C ₂ H ₅	C ₁₅ H ₂₁ N ₂ O ₂	388.24	261.34	240-241	20	63
C ₄ H ₉	C ₁₇ H ₂₅ N ₂ O ₂	416.30	289.39	159-161	70	55
C ₆ H ₁₃	C ₁₉ H ₂₉ N ₂ O ₂	444.35	317.44	137-139	90	51
C ₈ H ₁₇	C ₂₁ H ₃₃ N ₂ O ₂	472.40	345.50	123-125	100	56
C ₁₀ H ₂₁	C ₂₃ H ₃₇ N ₂ O ₂	500.46	373.55	113-115	120	62
C ₁₂ H ₂₅	C ₂₅ H ₄₁ N ₂ O ₂	528.51	401.60	113-114	140	68
C ₁₆ H ₃₃	C ₂₉ H ₄₉ N ₂ O ₂	584.62	457.71	125-126	180	56
C ₁₈ H ₃₇	C ₃₁ H ₅₃ N ₂ O ₂	612.67	485.76	132-133	200	79

Table 2. Characterization of *N*-alkyl-*N,N*-dimethyl-3-aminopropylamonium iodides (III)

R	Formula	Molecular mass[g/mol]	ES MS [g/mol]	M.p. [°C]	Reaction time [h]	Yield [%]
C ₂ H ₅	C ₇ H ₁₉ N ₂	258.14	131.24	123-124	10	72
C ₆ H ₁₃	C ₁₁ H ₂₇ N ₂	314.25	187.34	164-165	10	71
C ₈ H ₁₇	C ₁₃ H ₃₁ N ₂	342.30	215.40	166-167	15	75
C ₁₀ H ₂₁	C ₁₅ H ₃₅ N ₂	370.36	243.45	168-169	15	69
C ₁₆ H ₃₃	C ₂₁ H ₄₇ N ₂	454.52	327.61	181-183	15	63
C ₁₈ H ₃₇	C ₂₃ H ₅₁ N ₂	482.57	355.66	183-184	15	67

Results and discussion

Synthesis of *N*-alkyl-*N,N*-dimethyl-3-aminopropylamonium iodides (III) were carried out in a relatively mild conditions according to a general procedure described in the experimental part. The solid products were purified by a crystallization to give *N*-alkyl-*N,N*-dimethyl-3-aminopropylamonium iodides with good yields.

The structure of synthesized compounds have been confirmed by molecular spectroscopy FTIR, ES-MS, ¹H and ¹³C NMR.

FTIR spectra of *N,N*-dimethyl-3-phthalimidopropylamine (1), *N*-ethyl-*N,N*-dimethyl-3-phthalimidopropylamonium iodide (2) and *N*-ethyl-*N,N*-dimethyl-3-aminopropylamonium iodide (3) are shown in Fig. 1

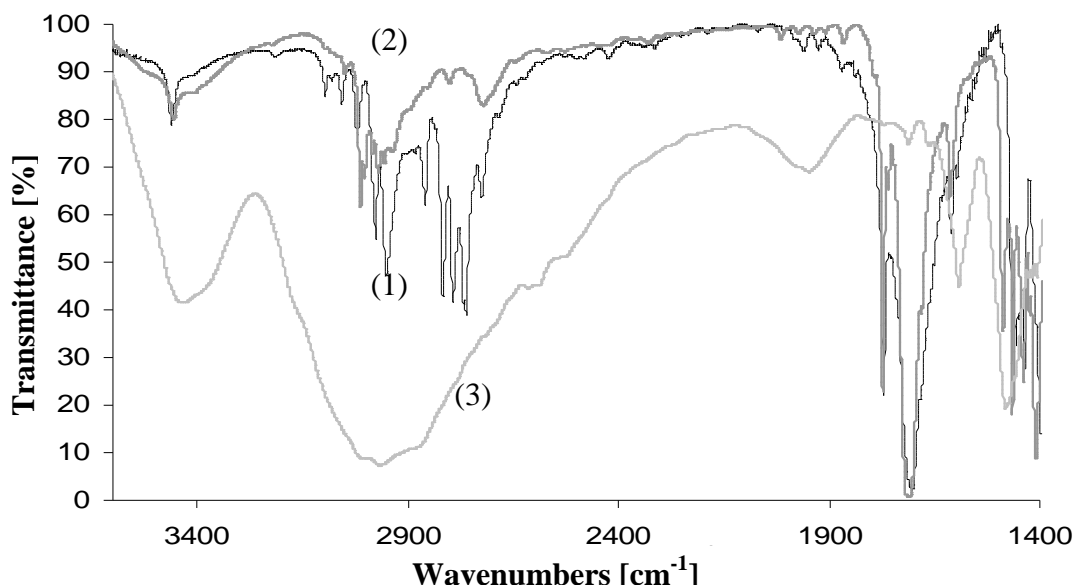


Fig. 1. FTIR spectra of *N,N*-dimethyl-3-phthalimidopropylamine (1), *N*-ethyl-*N,N*-dimethyl-3-phthalimidopropylamonium iodide (2) and *N*-ethyl-*N,N*-dimethyl-3-aminopropylamonium iodide (3).

FTIR spectra of *N*-alkyl-*N,N*-dimethyl-3-phthalimidopropylamonium iodides (II) show a characteristic band in the region 1772-1708 cm⁻¹ which is due to stretching asymmetric and

symmetric vibrations of carbonyl group, $\nu(\text{C}=\text{O})$, in a phthalimide moiety. These bands, both asymmetric and symmetric, of *N*-alkyl-*N,N*-dimethyl-3-phthalimidopropylammonium iodides (II) slightly shift to lower frequencies as the length of alkyl chain increases. No split of the carbonyl bands was observed and that confirms the equivalence of the both carbonyl groups in the phthalimide moiety. The unambiguous assignments of proton and carbon shifts was made by homonuclear and heteronuclear correlated spectra (Fig. 2).

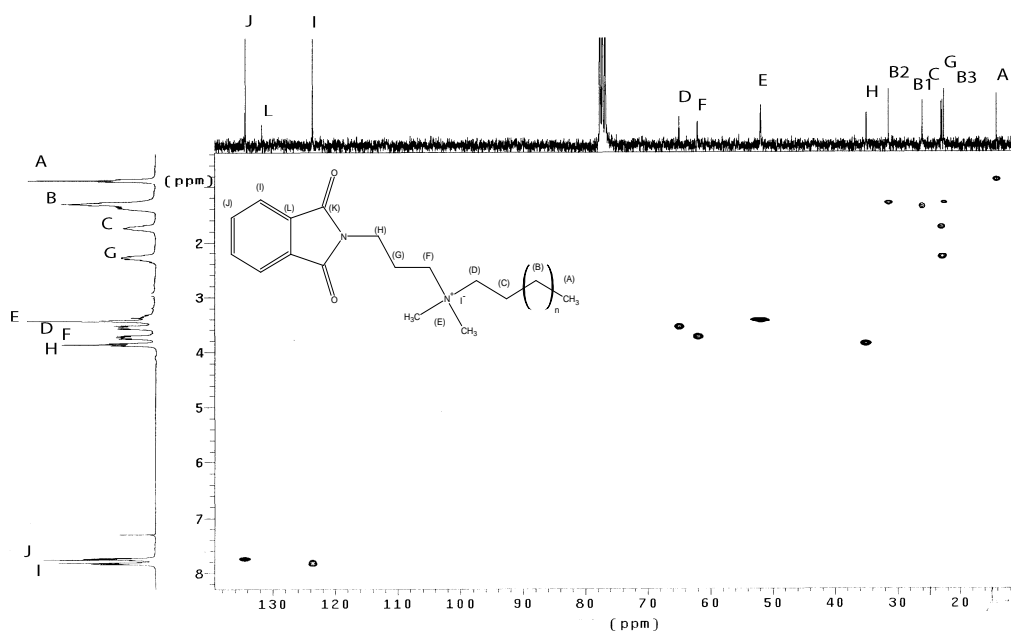


Fig. 2. The assignments of chemical shifts of protons and carbons in *N*-hexyl-*N,N*-dimethyl-3-phthalimidopropylammonium iodide by two-dimensional ^1H - ^{13}C heteronuclear shift correlated spectra.

References

- [1] V. Majtan, L. Majtanova, Chem. Papers 54(1) (2000) 49
- [2] F. Devinsky, L. Masarova, L. Lacko, D. Mlyncik, Coll. Czech. Chem. Commun., 49 (1984) 2819
- [3] B. Brycki, J. Werner, I. Kowalczyk, Czwartorzędowe sole amoniowe i obszary ich zastosowania w gospodarce, ed. R. Zieliński, Instytut Technologii Drewna, Poznań 2005, 57
- [4] B. Brycki, J. Werner, Annals of Polish Chemical Society, 3 (2004) 139
- [5] B. Brycki, J. Werner, I. Kowalczyk, Annals of Polish Chemical Society, 1 (2005) 192

ALKYLAMMONIUM MICROBIOCIDES

Bogumił Brycki

Laboratory of Microbiocides Chemistry, Faculty of Chemistry, Adam Mickiewicz University, Grunwaldzka 6, 60-780 Poznań

Introduction

Microorganisms, the first inhabitants of the biosphere, have the incredible ability to survive and adapt to almost any challenge. They live everywhere, even in extreme conditions, like volcanic craters and the ice of Antarctica. Microorganisms play an important role in a circulation of elements, digestive processes and biotechnology, although, from the other hand they are responsible for diseases, the degradation of food and biodeterioration processes. In order to minimize the negative effects of microorganisms, their populations must be reduced to the safe level by physical, biological or chemical methods.[1,2] In the physical methods, the UV and gamma irradiation, high and low temperatures, high pressure, and magnetic and electric fields of high intensity are used. Some bacteria and their metabolites, as bacteriocines, can be used in biological methods. The physical and biological methods have a limited applications and the most important are chemical methods, where the chemicals with biocidal activity, microbiocides, are applied. In early times, the use of chemicals as sulfur dioxide or salts and oxides of heavy metals, was quite empirical. In more recent times, the modern antimicrobial agents have been used and the mechanisms of their action have been recognized. Currently, most of the microbiocides, belong to the following groups: (1) phenol derivatives, (2) halogen derivatives, (3) oxidizing agents, (4) alcohols, (5) aldehydes, (6) acids and their derivatives, (7) organic derivatives of nitrogen, (8) metals and their organic and inorganic derivatives. These compounds are cell poisons whose lethal action results mainly from their ability to coagulate, precipitate or otherwise denature proteins and enzymes. Phenols, alcohols, acids and halogen-releasing agents provide good examples of microbiocides of this type which are protein-denaturing agents. Any agent which is capable of denaturing proteins has the potential to be used as a disinfectant. Oxidizing agents, such as hydrogen peroxide or magnesium salt of monoperoxyphthalic acid, react rapidly with cell proteins and destroy their molecular structure while metal salts act as protein precipitants. Before any antimicrobial activity can result, such agents must first cross the cell membrane and react with one or more of the cell constituents. Microbiocides may function by inactivating enzymes, disrupting semipermeable membranes or interfering with cell synthesis or division. Among the microbiocides currently used, the widely studied and applied are quaternary ammonium compounds (QAC). The above group mainly consists of alkyltrimethylammonium salts, dialkyldimethylammonium salts and alkyldimethylbenzylammonium salts. The nitrogen atom in QAC can also be included to aromatic or aliphatic rings. The very interesting group of QAC are the gemini surfactants, with two charged nitrogen atoms connected by a spacer. These compounds are intensively studied because of their low CMC value and the high antimicrobial activity. The mechanism of antimicrobial activity of quaternary alkylammonium salts is based on: (1) adsorption of compound on the bacterial cell surface, (2) diffusion through the cell wall, (3) binding to the cytoplasmic membrane, (4) release of potassium cations and other cytoplasmic constituents and (6) precipitation of cell contents and the death of the cell

[2]. The use of QAC is safe, because in the most cases their acute toxicity is low (LD_{50} (oral, rat) > 200 mg/kg). The continuous use of QAC, similarly as other antimicrobial agents, can trigger of the resistance or insusceptibility to microbiocides [3]. The resistance can be intrinsic and acquired. To avoid this effect, the active substances have to be changed.

According to our previous studies on antifungal activity and mechanism of resistance of bis-(3-aminopropyl)dodecylamine, we decided to prepare a novel quaternary ammonium compounds with mono, bis and tris aminopropyl groups, as well as QAC with bisaminopropyl groups and monohydroxyethyl group to increase of adhesive forces [4].

Results and discussion

Synthesis of N-3-aminopropyl-N,N-dimethyl-N-alkylammonium iodides (**I**), N,N-bis-(3-aminopropyl)-N,N-dialkylammonium iodides (**II**), N,N,N-tris-(3-aminopropyl)-N-alkylammonium iodides (**III**) and N,N-bis-(3-aminopropyl)-N-(2-hydroxyethyl)-N-alkylammonium iodides (**IV**) were carried out by reaction of 3-(dimethylamine)-propylamine and bis-(3-aminopropyl)amine with phthalic anhydride (Fig.) [5-7]. The phthalimide derivatives were alkylated and quaternized by corresponding alkyl iodides. The hydroxyethyl derivative was obtained by reaction with ethylene oxide. Phthalimide moieties were removed by use of hydrate of hydrazine. Most of the alkylammonium iodides were obtained with good yields and purified by crystallization from ethanol or acetonitrile. Alkylammonium iodides with long hydrocarbon chains, were difficult to crystallize because of their surface active properties. One analog of the title compounds, N-decyl-N,N-dimethyl-N-(3-aminopropyl)ammonium bromide has been previously obtained by alkylation of N,N-dimethyl-N-3-ethoxycarbonylpropylamine [8].

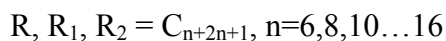
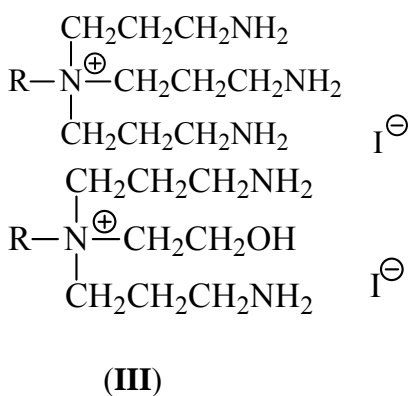
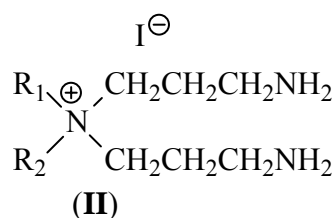
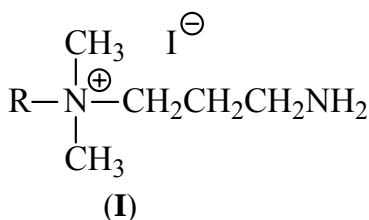


Fig. Structures of N-hydroxyethyl (IV) and mono (I), bis (II) and tris (III) N-(3-aminopropyl)-N-alkylammonium iodides.

The structures of iodides were confirmed by FTIR, UV, ^1H NMR, ^{13}C NMR and 2D NMR spectroscopy. For N,N-bis(phthalimidopropyl)-N-propylamine X-ray studies and B3LYP and DFT calculations have been carried out [9]. The molecular structure of this compound presents the first case of a folded conformation which is stabilized by an intramolecular hydrogen bond C-H...O. Also the supramolecular structure is stabilized by weak C-H...O and C-H... π hydrogen bonds. The antimicrobial activity was determined, using bacteria strains, *Staphylococcus aureus* and *Escherichia coli*, and fungi strains, *Candida albicans* and *Aspergillus niger*. The biocidal activity is very good and strongly depends on the structure of the examined alkylammonium iodides. As previously studies showed, the length of alkyl chain play the dominant role in the biocidal effects [1]. For N,N-bis(3-aminopropyl)-N,N-dialkyl ammonium iodides, the relationship of the biocidal activity of N-dodecyl-N-propyl-N,N-(3-aminopropyl)ammonium iodide to N-butyl-N-propyl-N,N-bis-(3-aminopropyl)ammonium iodide against *Staphylococcus aureus* is 40. Similar relationship value for the above iodides, i.e. 35, is for *Escherichia coli*. It means that the longer alkyl chain the better antibacterial activity is observed. However, it is important to note, that alkyl chains longer than C-14 lower the biocidal effectiveness. The fungicidal activity of obtained iodides is slightly different in comparison to the bactericidal effects. The most effective against fungi, *Candida albicans* and *Aspergillus niger*, are compounds with two long alkyl chains. Relationship of fungicidal activity of N,N-bis-(dodecyl)-N,N-bis-(3-aminopropyl)ammonium iodide to N-dodecyl-N-butyl-N,N-bis-(3-aminopropyl)ammonium iodide against *Candida albicans* is 10; for *Aspergillus niger* the relationship $C_{12}C_{12}/C_{12}C_4$ is 5.

Summary

A novel quaternary alkylammonium iodides, with aminopropyl and hydroxyethyl groups, have been synthesized and characterized by FTIR, UV and NMR spectroscopy. The new QAC, containing additional functional groups, show an excellent antimicrobial activity, which depends on the length of alkyl chain.

References

- [1] Russell, Hugo & Ayliffe's Principles and Practice of Disinfection, Preservation and Sterilization", ed A. P. Fraiese, P.A. Lambert and J-Y. Maillard, Blackwell Publishing, Birmingham, 2004.
- [2] „Disinfection, Sterilization, and Preservation”, ed. Block S.S., Lippincott Williams & Wilkins, 5th ed, 2001.
- [3] “Understanding Antibacterial Action and Resistance”, Russell A.D., Chopra I., Ellis Horwood, 2nd ed., 1996.
- [4] A. Koziróg, A.S. Kuberski, Z. Żakowska, B. Brycki, Pol. J. Microbiology, 54 (2005) 271.
- [5] B. Brycki, J. Werner, I. Kowalczyk, Annals of Polish Chemical Society, 1 (2005) 192.
- [6] B. Brycki, I. Kowalczyk, M. Krysmann, Annals of Polish Chemical Society (2006) in press.

- [7] B. Brycki, A. Szwajca, W. Jerzykiewicz, *Annals of Polish Chemical Society*, (2006) in press.
- [8] Ch. Rav-Acha, I. Ringel, S. Sarel, J. Katzhendler, *Tetrahedron*, 44 (18) (1988) 5879.
- [9] B. Brycki, I. Kowalczyk, J. Werner, T. Borowiak and I. Wolska, *J. Mol. Struct.*, 791 (2006) 137-143.

SYNTHESIS AND SPECTROSCOPIC PROPERTIES OF QUATERNARY HYDROXYALKYLAMMONIUM SALTS

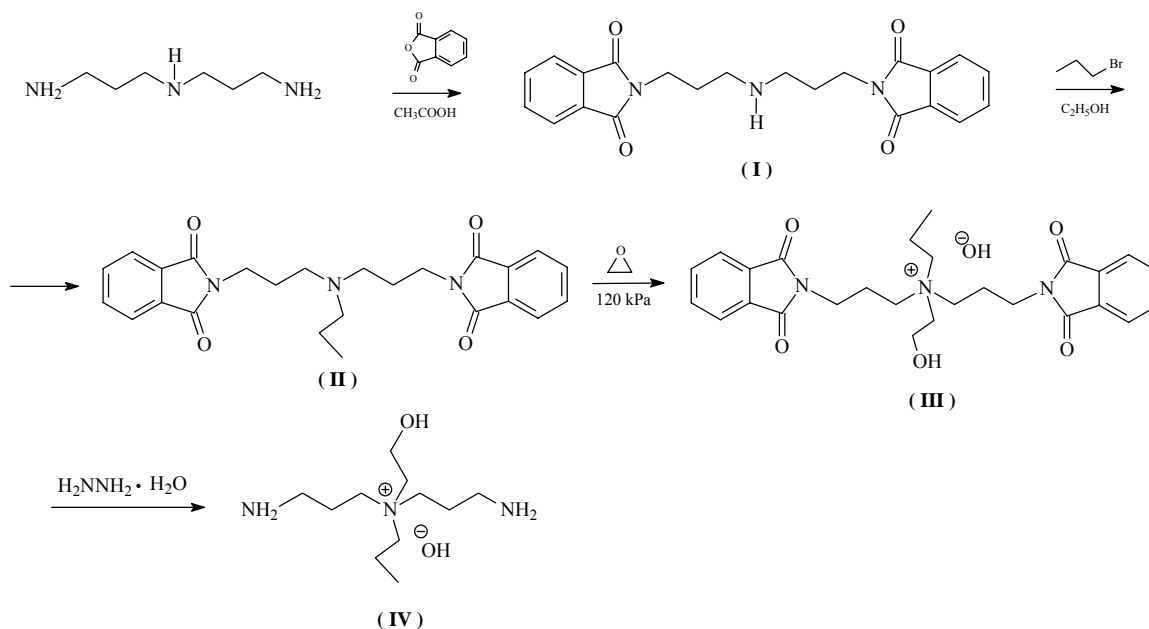
B. Brycki, A. Szwajca, W. Jerzykiewicz*

Laboratory of Microbiocides Chemistry, Faculty of Chemistry,
Adam Mickiewicz University, Grunwaldzka 6, 60-780 Poznań
* Institute of Heavy Organic Synthesis "Blachownia",
Energetyków 9, 47-225 Kędzierzyn-Koźle

Introduction

Quaternary ammonium compounds having two alkyl chains and two hydrophilic groups in a molecule have been reported to show unexpected physicochemical properties in comparison with quaternary ammonium compounds having one alkyl chain and one hydrophilic group [1]. They show a good water solubility, much lower critical micelle concentration values (cmc), lower surface tension of aqueous solutions, very good foaming properties and high viscosity of their aqueous solutions.

In our studies of antimicrobial agents, we have designed and prepared so far new quaternary ammonium salts with two hydrophobic alkyl chains and two hydrophilic groups [2]. In this paper we present an efficient method of synthesis of novel quaternary ammonium compounds in which a hydroxyl group is connected to alkyl chain (Scheme 1). The spectroscopic properties (FTIR, ESI-MS, ^1H NMR, ^{13}C NMR) of these compounds have been investigated and compared to spectra of quaternary ammonium salts previously obtained.



Scheme 1. Synthesis of *N,N*-bis-(3-aminopropyl)-*N*-(2-hydroxyethyl)-*N*-propylammonium hydroxide.

Experimental section

The reagents and solvents were used of commercially available reagent quality. Preparation of *N,N*-bis-(3-phthalimidopropyl)amine (I) and *N,N*-bis-(3-phthalimidopropyl)-*N*-propylamine (II) were described in the last papers [2,3]. *N,N*-bis-(3-phthalimidopropyl)-*N*-(2-hydroxyethyl)-*N*-propylammonium hydroxide (III) were obtained by a reaction of *N,N*-bis-(3-phthalimidopropyl)-*N*-propylamine (II) with ethylene oxide in water-methanol mixture. The epoxidation reactions were performed in a steel reactor at 70°C under pressure 100-120 kPa. The ethylene oxide consumption was precisely measured and recorded by a computer. After evaporation of the solvents, the highly viscous liquid was obtained (III). The crude product was used for the synthesis of compound (IV) with monohydrate hydrazine in ethanol at room temperature for 24 h. After this time, the precipitate, 2,3-dihydrophthalazine-1,4-dione, was filtered out and the residue was evaporated under vacuum to give yellow, highly viscous oil. The TLC analysis have shown that quaternary ammonium salt (IV) was obtained almost quantitatively. To get the crystals of (III), the *N,N*-bis-(3-phthalimidopropyl)-*N*-(2-hydroxyethyl)-*N*-propylammonium picrate (V) was prepared by a reaction of *N,N*-bis-(3-phthalimidopropyl)-*N*-(2-hydroxyethyl)-*N*-propylammonium hydroxide (III) with 2,4,6-trinitrophenol in water at room temperature for 48 h. Crude *N,N*-bis-(3-phthalimidopropyl)-*N*-(2-hydroxyethyl)-*N*-propylammonium picrate was purified by a crystallization from acetonitrile (m.p.144°C).

The structures of the prepared compounds were confirmed by molecular spectroscopy. The NMR spectra were measured with a Varian Gemini 300VT spectrometer, operating at 300,07 Hz and 75,46 Hz for ¹H and ¹³C, respectively. Infrared spectra were recorded using a FTIR Bruker IFS 113v and IFS 66v/S spectrometers, in nujol and fluorolube. The ESI (electrospray) mass spectra were recorded on a Waters/Micromass (Manchester, UK) ZQ mass spectrometer equipped with a Harvard Apparatus syringe pump. The sample solutions were prepared in methanol at a concentration of approximately 10⁻⁵M. The standard ESI mass spectra were recorded at the cone voltage 30V (50V, 80V).

Results and discussion

Quaternary ammonium salts having one or three nitrogen atoms and one hydroxyl group in alkyl chains were prepared by reactions shown in Scheme 1. Compounds (I) and (II) were obtained with very high yields due to the high reactivity of the primary and secondary alkylamine towards phthalic anhydride and alkyl halide, respectively. The ethylene oxide has been found to be an effective agent for preparing quaternary ammonium salts. The yield of the reaction with ethylene oxide under chosen conditions was over 70%.

The structures of synthesized compounds have been confirmed by FTIR, ESI-MS, ¹H and ¹³C NMR spectroscopy.

FTIR spectra of *N,N*-bis-(3-phthalimidopropyl)-*N*-(2-hydroxyethyl)-*N*-propylammonium picrate is shown in Fig. 1.

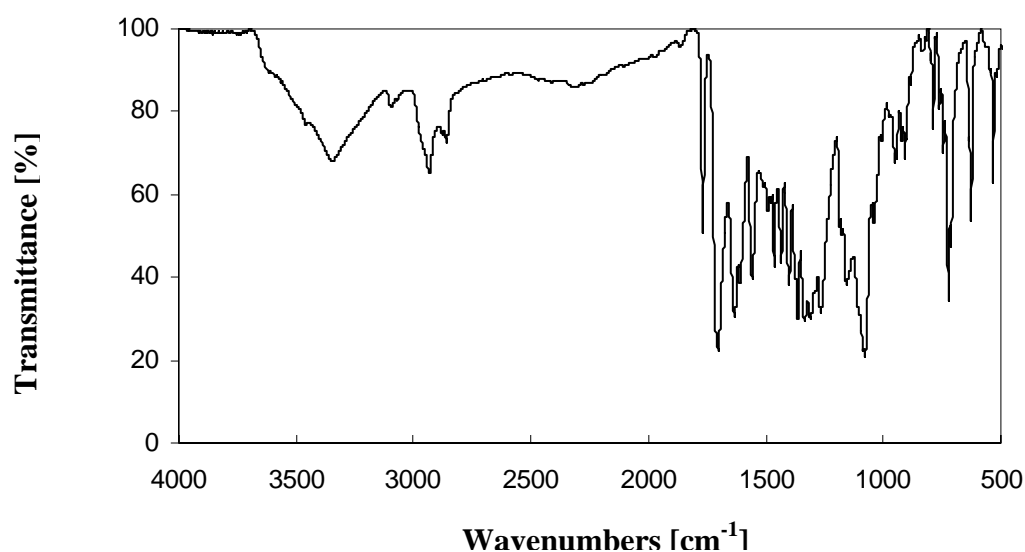


Fig. 1. FTIR spectra of *N,N*-bis-(3-phthalimidopropyl)-*N*-(2-hydroxyethyl)-*N*-propylammonium picrate.

The FTIR spectrum shows a characteristic band in the region 1768-1702 cm^{-1} which is due to stretching, asymmetric and symmetric, vibrations of carbonyl group, $\nu(\text{C}=\text{O})$, in a phthalimide moiety. No split of the carbonyl bands was observed what confirms the equivalence of the all carbonyl groups in the molecule. The broad band with a center about 3450 cm^{-1} corresponds to the stretching vibrations of OH group.

In the ^1H NMR spectra of *N,N*-bis-(3-phthalimidopropyl)-*N*-(2-hydroxyethyl)-*N*-propylammonium picrate the protons of methylene groups are observed as triplets and multiplets in the range 1,8 – 3,7 ppm [1,87 (2H, m), 2,31 (4H,m), 3,53 (2H, m), 3,79 (6H, m)], methyl group at 1,92 ppm (3H, t) and ArH at 7,83 (8H, m).

In the ^{13}C NMR spectra of *N,N*-bis-(3-phthalimidopropyl)-*N*-(2-hydroxyethyl)-*N*-propylammonium picrate the signals of carbon atoms of methylene groups are observed in the range 16,0 – 61,6 ppm and the peak of methyl group lies at 10,7 ppm. Aromatic carbon atoms resonate in the range 123,6 – 134,8 ppm. The signal of carbonyl group is observed at 168,5 ppm.

In the ESI spectrum of the *N,N*-bis-(3-phthalimidopropyl)-*N*-(2-hydroxyethyl)-*N*-propylammonium picrate the most characteristic signal is at m/z 478. With increasing cone voltage the intensity of peak at m/z 478 decreases and the intensity of the signals at m/z 188 and m/z 160 increases. The most likely fragmentation pathway of these fragments of ammonium salt is shown in Figure 2. The ESI-MS spectra of *N,N*-bis-(3-phthalimidopropyl)-*N*-(2-hydroxyethyl)-*N*-propylammonium hydroxide show peaks corresponding to the fragmentation pieces including $\text{C}_{27}\text{H}_{32}\text{N}_3\text{O}_5$ (m/z 478), $\text{C}_{27}\text{H}_{32}\text{N}_3\text{O}_5 \cdot \text{H}_2\text{O}$ (m/z 496) and $\text{C}_{27}\text{H}_{32}\text{N}_3\text{O}_5 \cdot 2\text{H}_2\text{O}$ (m/z 514). The obtained results indicate that the physicochemical properties of ammonium salts depend on the counter anion.

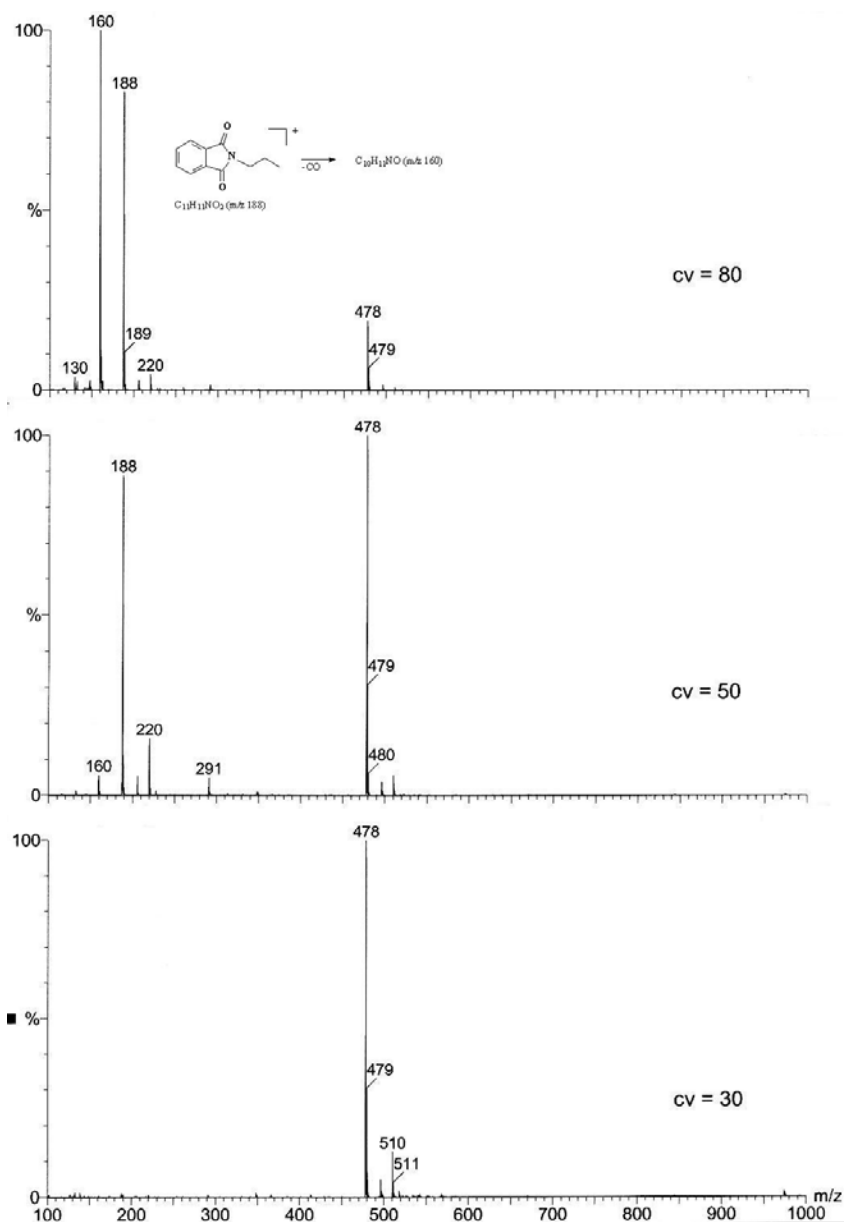


Fig. 2. The ESI-MS spectra of *N,N*-bis-(3-phthalimidopropyl)-*N*-(2-hydroxyethyl)-*N*-propylammonium picrate.

References

- [1] Tae-Seong Kim, Toshiyuki Kida, Yohji Nakatsuji, and Isao Ikeda, *Langmuir*, 12 (1996) 6304
- [2] B. Brycki, J. Werner, *Annals of Polish Chemical Society*, 3 (2004) 139
- [3] B. Brycki, J. Werner, I. Kowalczyk, *Czwartorzędowe sole amoniowe i obszary ich zastosowania w gospodarce*, ed. R. Zieliński, Instytut Technologii Drewna, Poznań 2005, 57
- [4] B. Brycki, J. Werner, I. Kowalczyk, *Annals of Polish Chemical Society*, 1 (2005) 192

SYNTHESIS AND SPECTROSCOPIC PROPERTIES OF *N,N*-BIS-(1,8-NAPHTHALIMIDOPROPYL)-*N*-ALKYLAMINE INTERCALATORS

B. Brycki, W. Grzesiak

*Laboratory of Microbiocides Chemistry, Faculty of Chemistry, Adam Mickiewicz University,
Grunwaldzka 6, 60-780 Poznań*

Introduction

The new compounds with antitumoral activity have become one of the most important goals in a medicinal chemistry. The especially interesting group of chemicals used in cancer therapy are molecules which interact with DNA. On the basis of the type of interaction with DNA these drugs may be classified into three groups; (a) alkylating agents, (b) agents that cause nicking of the helix and (c) intercalators. During the last decade a special attention has been paid to intercalators, because of their high potential anticancer activity [1,2]. Intercalators are molecules that bind reversible to the double-helical DNA. They usually have a flat, π -deficient aromatic or heteroaromatic, ring. These molecules bind to DNA double helical structures by intercalating between stacked base pairs, thereby distorting the DNA backbone conformation and interfering with DNA-protein interaction. Among the intercalators, naphthalimides represent a promising group of DNA-targeted anticancer agents [1-6]. The first naphthalimides as potential antitumour agents were synthesized in the 1970's. As a result of these studies, two compounds, *mitonafide* and *amonafide*, have been developed. Moreover, the studies have also shown that bis-intercalating agents have generally a greater affinity to DNA than corresponding, mono-intercalating agents. Some of them, for example DMP 8408 or LU 795539, are very promising drugs for anticancer therapy.

In this paper we present a synthesis of novel bisnaphthalimide intercalators and their spectroscopic analysis (FT-IR, ^1H NMR, ^{13}C NMR). Scheme of synthesis of *N,N*-bis-(1,8-naphthalimidopropyl)-*N*-alkylamines is shown in Fig. 1.

Experimental section

N,N-bis-(1,8-naphthalimidopropyl)-*N*-alkylamines were synthesized by acylating of appropriate amines with 1,8-naphthalic anhydride. *N,N*-bis-(3-aminopropyl)-*N*-alkylamine in ethanol was added dropwise by 10 minutes to a suspension of 1,8-naphthalic anhydride in ethanol. The mixture was stirred at room temperature for 24h. After that the precipitate was filtered, washed with ether, dried and crystallized with organic solvents. The product with *N*-dodecyl substituent is very hygroscopic.

The NMR spectra were measured with a Varian Gemini 300VT spectrometer in CDCl_3 . Infrared spectra were recorded in KBr pellets using a FT-IR Bruker IFS 113v spectrometer.

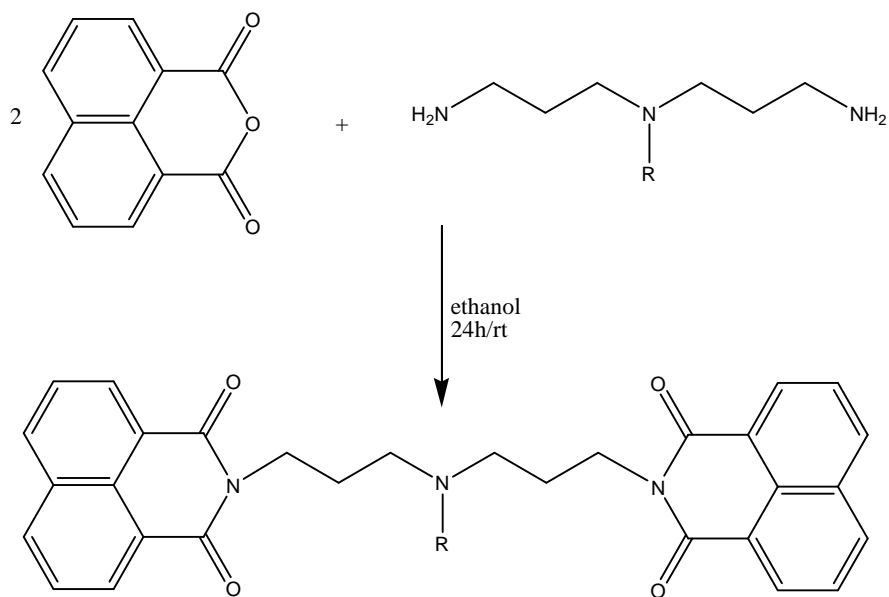


Fig. 1. Preparation of *N,N*-bis-(1,8-naphthalimidopropyl)-*N*-alkylamines.

Results and discussion

Synthesis of *N,N*-bis-(1,8-naphthalimidopropyl)-*N*-alkylamines were carried out in a relatively mild conditions according to a general procedure described in the experimental part. The solid products were purified by a crystallization from acetonitrile to give *N,N*-bis-(1,8-naphthalimidopropyl)-*N*-alkylamines with good yields.

The structure of synthesized compounds have been confirmed by a molecular spectroscopy FT-IR, ^1H NMR and ^{13}C NMR. FT-IR spectrum of *N,N*-bis-(1,8-naphthalimidopropyl)-*N*-propylamine is shown in Fig. 1.

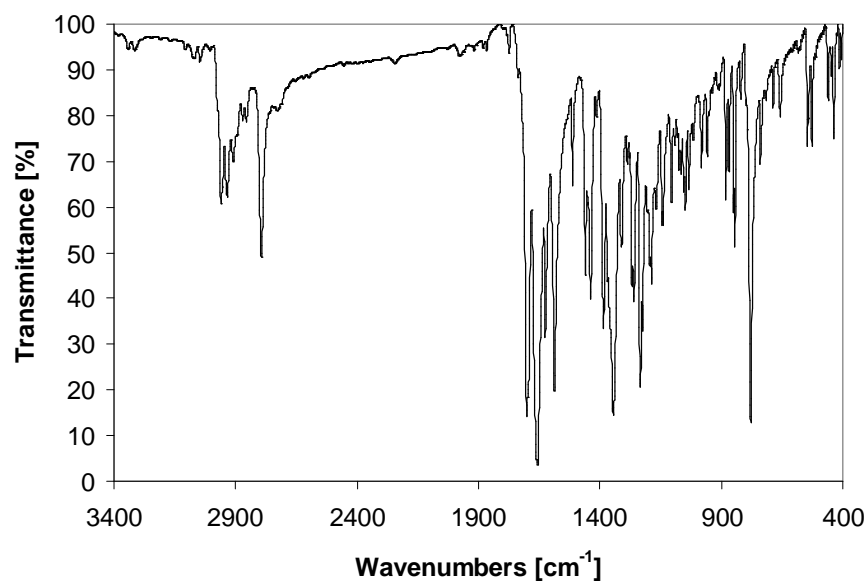


Fig. 1. FT-IR spectrum of *N,N*-bis-(1,8-naphthalimidopropyl)-*N*-propylamine.

FT-IR spectrum of *N,N*-bis-(1,8-naphthalimidopropyl)-*N*-propylamine show a characteristic band in region 1690-1740 cm^{-1} which is due to stretching, asymmetric and symmetric, vibrations of carbonyl group, $\nu(\text{C}=\text{O})$, in a naphthalimide moiety. No split of the carbonyl bands was observed and that confirms the equivalence of the both carbonyl groups in the naphthalimide molecule.

^1H NMR and ^{13}C NMR spectra of *N,N*-bis-(1,8-naphthalimidopropyl)-*N*-propylamine and *N,N*-bis-(1,8-naphthalimidopropyl)-*N*-dodecylamine are shown in Fig. 2. and Fig. 3, respectively.

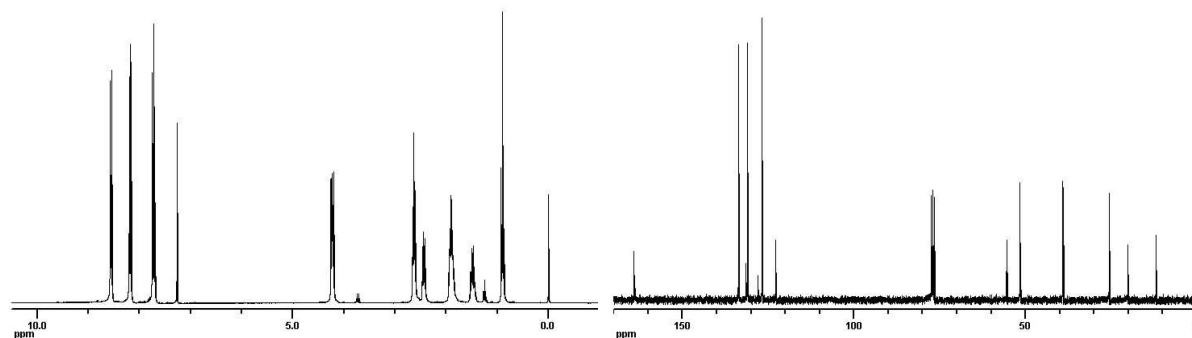


Fig. 2. ^1H NMR and ^{13}C NMR spectra of *N,N*-bis-(1,8-naphthalimidopropyl)-*N*-propylamine.

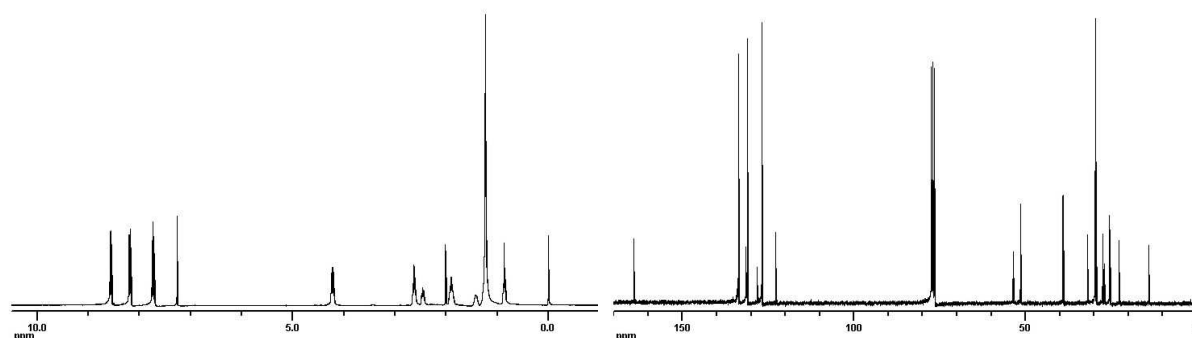


Fig. 3. ^1H NMR and ^{13}C NMR spectra of *N,N*-bis-(1,8-naphthalimidopropyl)-*N*-dodecylamine.

In the ^1H NMR spectra of *N,N*-bis-(1,8-naphthalimidopropyl)-*N*-propylamine the protons of methylene groups are observed as triplets and multiplets in the range 1.48 – 4.22 ppm [1.48 (2H, m), 1.9 (4H, m), 2.45 (2H, t), 2.65 (4H, t), 4.22 (4H, t)], methyl group at 0.9 ppm (3H, t) and ArH in the range 7.70 – 8.57 ppm (12H, m). Similarly, for *N,N*-bis-(1,8-naphthalimidopropyl)-*N*-dodecylamine. the protons of methylene groups are observed as triplets and multiplets in the range 1.21 – 4.22 ppm [1.21 (18H, m), 1.40 (2H, m), 1.90 (4H, m), 2.46 (2H, t), 2.63 (4H, t), 4.22 (4H, t)], methyl group at 0.86 ppm (3H, t) and ArH in the range 7.72 – 8.56 (12H, m).

In the ^{13}C NMR spectra of *N,N*-bis-(1,8-naphthalimidopropyl)-*N*-propylamine the signals of carbon atoms of methylene groups are observed in the range 20.2 – 55.5 ppm (20.2, 25.5, 39.1, 51.6, 55.5) and the peak of methyl group lies at 11.9 ppm. Aromatic carbon atoms

resonate in the range 122.7 – 133.7 ppm. The signal of carbonyl group is observed at 164.1 ppm. For *N,N*-bis-(1,8-naphthalimidopropyl)-*N*-dodecylamine, the signals of carbon atoms of methylene groups are observed in the range 22.7 – 53.6 ppm and the peak of methyl group lies at 14.1 ppm. Aromatic carbon atoms resonate in the range 122.8 – 133.7 ppm. The signal of carbonyl group is observed at 164.1 ppm.

References

- [1] R. Martinez and L. Chacón-García, *Current Medicinal Chemistry*, 12 (2005) 127.
- [2] M. F. Braña, M. Cacho, A. Gradillas, B. de Pascual-Teresa and A. Ramos, *Current Pharmaceutical Design*, 7 (2001) 1745.
- [3] M. F. Braña and A. Ramos, *Current Medicinal Chemistry - Anti-Cancer Agents*, 1 (2001) 237.
- [4] V. Pavlov, Paul Kong Thoo Lin, V. Rodilla, *Chemico-Biological Interactions*, 137 (2001) 15.
- [5] P. Kong Thoo Lin, A. M. Dance, C. Bestwick and L. Milne, *Biochemical Society Transactions*, 31 (2003) 407.
- [6] M. F. Braña, J. M. Castellano, M. Morán, M. J. Pérez de Vega, X. D. Qian, C. A. Romerdahl, G. Keilhauer, *Eur. J. Med. Chem.*, 30 (1995) 235.

WHAT COMPUTER TOOLS CAN BE USED IN CHEMISTRY BLENDED TEACHING?

Andrzej Burewicz Piotr Jagodziński Robert Wolski

*Department of Chemical Education, Faculty of Chemistry, Adam Mickiewicz University, Grunwaldzka 6, 60-780 Poznań
tel. no.: +48 618291375, burewicz@amu.edu.pl, wola@amu.edu.pl*

Teaching is a process that constantly changes. This can be ascribed to the progress in pedagogy (subject didactics) and those fields that seem to have nothing in common with the teaching process. Importantly, one of them is computer science. As technology develops, teaching methods and techniques change as well. At present, progress is being made in methods and techniques based on computer networks, and, in particular, on the Internet. Moreover, attention should be paid to the learner since the way s/he assimilates knowledge depends on many factors. The most important of them are: learner personality traits, the nature of the teaching process, evaluation criteria of knowledge assimilation, nature of the material taught, and the teacher's personality [1].

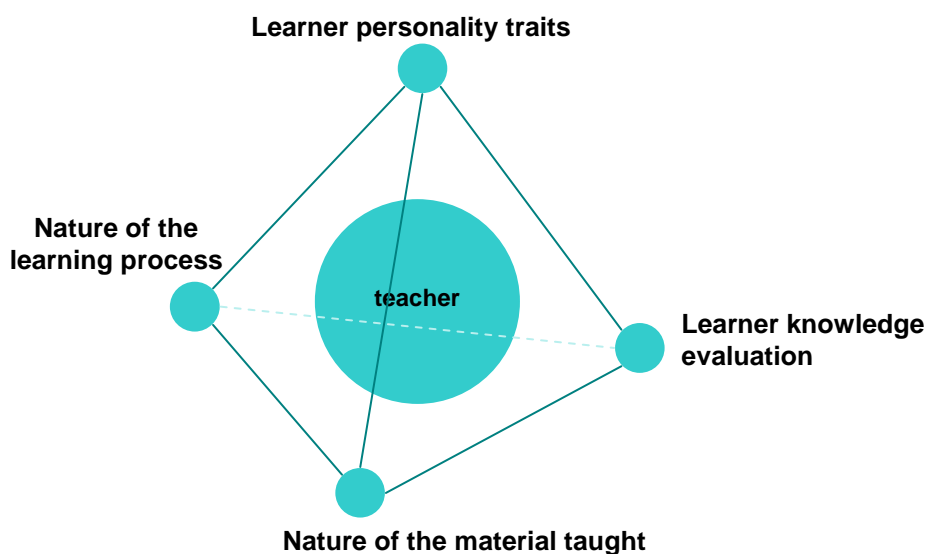


Fig. 1. Variables determining the learning process

The problem lies in the combination of the timetabling system applied in Polish schools with teaching use of the Internet. The possible solution is to implement e-learning in teaching. To fully understand how to implement the technique, the concept of e-learning should first be clarified.

It is very difficult to define the idea of e-learning. The term is variously understood. E-learning, according to the general definition, is a teaching technique based on data communications technologies used to transmit information. The following ways of implementing courses can be distinguished:

- individual work with training materials available through the computer network or on CDs or DVDs.
- Internet lectures delivered in synchronous mode or at the learner's request.
- group training using technology that enables group work
- video conferences held using appropriate equipment
- sending information by email
- using discussion lists to exchange information and experience
- using communicators to exchange information

It has to be mentioned that e-learning is not a computer system. The only role of computer systems is to support and enable information distribution.

The diagram below specifies the role of e-learning in teaching and learning. [2].

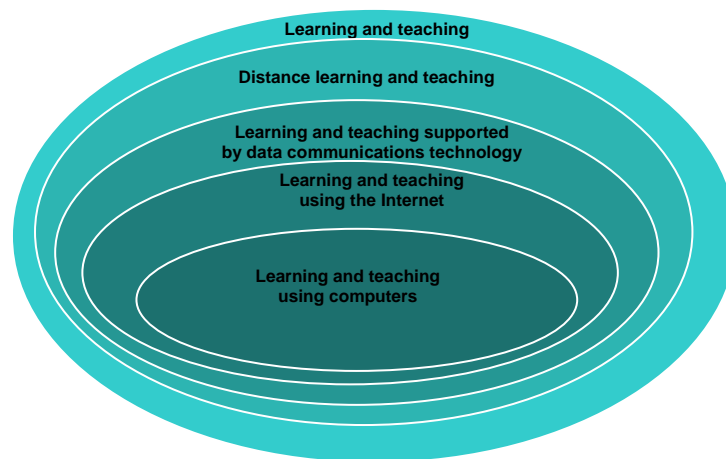


Fig. 2. Diagram showing the role of e-learning in the processes of learning and teaching

Before implementing e-learning in the teaching process, it is necessary to become familiar with its strengths and weaknesses. This will enable correct implementation of the method in the teaching process, and prevent irregularities in the implementation.

The strengths of e-learning are:

- teaching process centralization
- information standardization
- easy information modification and the possibility of its immediate distribution
- convenience of training
- individualization of teaching
- interactive training
- flexible selection of material to be taught

The weaknesses of e-learning are:

- expenses related to system implementation
- possible poor preparation of the material to be taught

- material to be taught is fragmented, thus attention can be shifted away from the main subject
- students have to possess appropriate computer equipment

As I mentioned, the teaching programme in Poland is supported by the timetabling system: students and their teachers meet in classrooms where classes are conducted.

How can traditional teaching be combined with e-learning? The solution is blended learning. The Polish equivalent of the term is "nauczanie mieszane".

What is blended learning? It is an extension and elaboration of the present teaching system. This type of teaching is directed towards an individualized education style. It enables combining modern teaching methods in traditional classes with technology-based teaching using computer networks. Thus, blended learning consists of:

- multimedia technologies,
- texts, animations, and film sequences available on the Internet,
- electronic mail, conferences, and video conferences,
- traditional lessons.

This means combining traditional classroom forms of education with individual student work with a personal tutor, i.e. the computer, at home [3, 4].

What is needed to implement blended learning in chemistry teaching?

There are four stages of blended learning implementation:

- preparing the server,
- selection of appropriate software,
- preparation of a "lesson",
- verifying the educational effectiveness of the prepared material.

The Server preparation constitutes the first stage of blended learning implementation. Computer equipment to function as server is necessary. It should suit the requirements: the number of users and the Internet connection capacity. To start up the server, an operating system is necessary. There are two options to choose from: Microsoft Windows XP/Microsoft Windows 2000, and Linux. Usually a newly bought computer is equipped with Microsoft Windows XP or Microsoft Windows 2000 operating systems. Otherwise, Linux operating system can be used. This is a system for servers. Its installation procedure does not differ from that of Windows. There are a few distributions to choose from:

- Free Mandriva Linux 2007
- SUSE Linux 10.1
- Gentoo
- Fedora Core
- Ubuntu

Appropriate distributions can be downloaded from the following web sites: www.mandriva.pl, www.susek.info, www.fedora.pl.

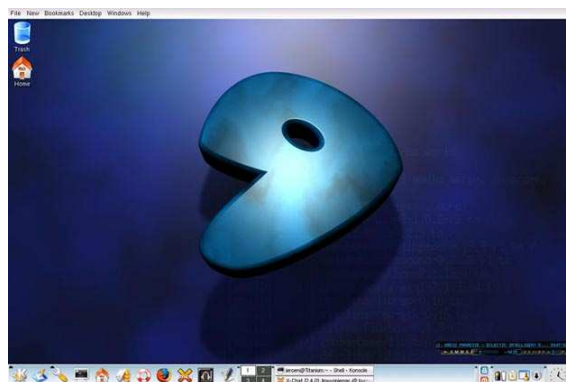


Fig.3 Linux desktop

Apache HTTP Server is the essential software. This software enables access to the previously prepared web sites on the Internet. The software is available for virtually all operating systems. It is fast and easy to use. It is not difficult to install the server, and installation instructions can be found in computer magazines, and on the Internet. Additionally, MySQL and PHP should be installed. These software packages are essential for some server programmes to operate, e.g. phpBB2 internet forum, or LMS systems [5, 6].

The next step is to select software, and prepare the “lesson”. ToolBook and Authorware are authoring programmes that can be used to prepare courses. They enable comprehensive course preparation. Any tool generating a file in the form of HTML code can be used to create texts for Internet lessons, e.g.: Dreamweaver, FrontPage, GoLive, NetObjects Fusion. Courses ought to appeal to the user. They should combine sound, animations, or films into one interactive whole. When creating interactive courses, one can use: Director, Flash, LiveMotion. Integral to the course preparation, the design should be prepared carefully. Special attention should be paid to colour selection. The design can be prepared in the following programmes: FreeHand, Fireworks, Illustrator, Photoshop, Paint Shop Pro, Gimp. Sound effects (Audacity, Cool Edit Pro), and film sequences (Movie Maker, Pinnacle Studio, Premiere, Video Studio) can additionally attract the user. [7]

- [1]. Burewicz A. Gulińska H., *Chemistry Didactics*, UAM, Poznań 2002 [*Dydaktyka Chemii*]
- [2]. Hyla M., *E-learning Guide*, Oficyna Ekonomiczna, Kraków 2005 [*Przewodnik po e-learningu*]
- [3]. Throne K., *Blended Learning: How to Integrate Online and traditional Learning*, Kogan Page Limited, Sterling VA 2003
- [4]. Mantyla K., *Blending E-learning*, The American Society for Training & Development, Alexandria 2003, USA
- [5]. EasyLinux, Linux New Media Polska, Warszawa 2005 (2 2005)
- [6]. Meloni J.C., *PHP, MySQL, and Apache for everybody* Second Edition, Helion, Gliwice 2005 [PHP, MySQL i Apache dla każdego].
- [7]. Harton W., Harton K., *E-Learning tools and Technologies*, Wiley Publishing Inc., Indianapolis 2003

EDUCATIONAL EFFECTIVENESS OF THE FILMS OF THE BRANCHED STRUCTURE IN TEACHING CHEMISTRY

Andrzej Burewicz Piotr Jagodziński Robert Wolski

*Department of Chemical Education, Faculty of Chemistry, Adam Mickiewicz University, Grunwaldzka 6, 60-780 Poznań
tel: +48 618291375, burewicz@amu.edu.pl, wola@amu.edu.pl*

Instructive film as a didactic means has many advantageous features [1]. The use of images in combination with acoustic effects it affects not only the intellect but also the imagination and emotions of the viewer, which helps remember the contents. It is the most comprehensive from among the audiovisual means.

The most important element in teaching chemistry that helps absorbing knowledge, develop the ability of observation and drawing conclusions is the chemical experiment. It can be used at the stage of introduction, research, illustration, modelling as well as for the purpose of recollection, verification or control of what has been taught. In teaching chemistry the use of an instructive film permits closer visualisation of chemical phenomena, shows a proper way of organisation and performance of the experiment and gives an idea of correct approach to interpretation of future chemical experiments performed by the students themselves [2].

At the Department of Chemical Education, Adam Mickiewicz University, a number of educational films have been made on chemical experiments illustrating the high school syllabus. The film sequences have been edited on a computer using the program Adobe Premiere Pro 1,5. The nonlinear edition was applied with some attractive transition effects added between film sequences. The same program Adobe Premiere Pro 1,5 also permitted addition of graphic elements and sound edition.

The films were made in three variants, the first variant presented the correct performance of the chemical experiment. The films are used in teaching chemistry in the scope of the syllabus in the and are addressed to those who are learning chemistry. Watching the films the students learn about the chemical reagents and apparatus or laboratory instruments needed for the correct performance of the experiment [3].

Tollens test

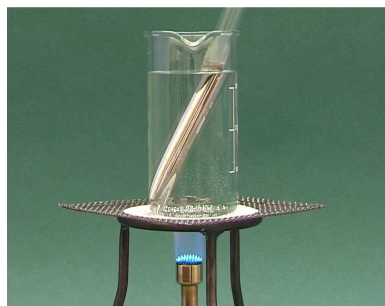


Fig. 1a. The correct course of the chemical reaction, the silver mirror..

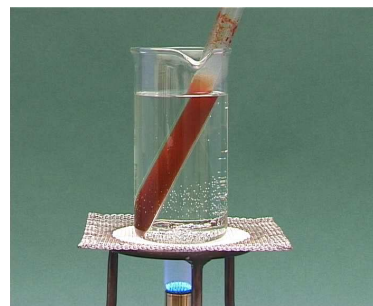


Fig. 1b, c. Testing the students knowledge, incorrect variants of the Tollens test.

The second and third variants of the film present the course of the experiment with incorrectly chosen substrates or incorrect performance of the experiment. These versions, with reference to the first one, are addressed to those who wish to check their knowledge after having finished working on a certain part of the syllabus [4].

Film was chosen as a didactic means taking into account its advantages over other means, which can be listed as follows: generation of engagement and interest in the contents of the lesson, generation of certain intellectual responses, facilitation of perception of the contents to be taught (the information given in the verbal form accompanied with image is better memorised). Moreover, the use of film permits overcoming the restriction of teaching at a certain place and time, the films can be shown at even moderately equipped schooling centres, they provide insight into these fragments of reality that are inaccessible to direct observation, provide truthful presentation of the reality, permit speeding up or slowing down the course of phenomena to help grasp the contents of the events.

Chemical reaction of benzene nitrogeneration



Fig. 2a. The correct course of the reaction leading to nitrobenzene as its product.



Fig. 2b, c. Incorrect variants of the reaction of benzene nitrogeneration shown to test the students' knowledge.

The study

The educational effectiveness of the films was tested on general high school students. The total number of students taking part in the test was 186, divided into the experimental and the control groups of 92 and 94 students, respectively. The control group of 94 students worked with conventional printed instructions to perform a given chemical experiment, and they repeated their knowledge using the notes. The experimental group of 92 students worked with films and repeated their knowledge using the 3 variants of a given film. Prior to the educational experiment the students were asked to take the preliminary test to estimate their level of knowledge in particular field. At the next step the students were asked to carry out the target chemical experiments using conventional printed instructions or using the information from the films. Having performed the experiments the students were asked to sit a final test in order to assess the increase in the level of their knowledge in a given field of chemistry. The increase in the level of knowledge and the education effectiveness of the films were assessed for the four taxonomic categories of the didactic aims: memorisation of

information, understanding of information, use of the information in typical situations and use of the information in solving new problems [5].

Results

The results of the educational experiment has shown that in the control group the increase in the level of knowledge in the four taxonomic categories of the aims of teaching was 28% in memorisation of information, 27% in understanding of information, 25% in the use of the information in typical situations and 36% in the use of the information in solving new problems. In the experimental group the corresponding values were 56%, 49%, 65% and 73%, respectively (Fig. 3).

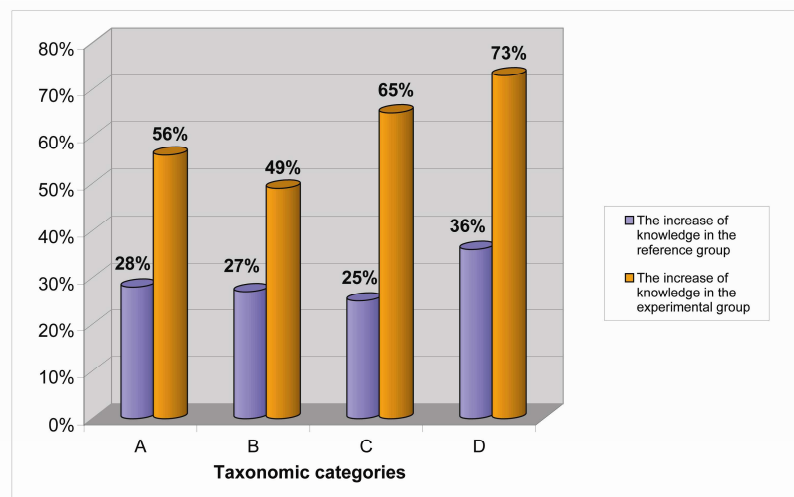


Fig. 3. The increase in the level of knowledge of students from the experimental and control groups in the four categories of the aims of teaching: A – memorisation, B – understanding, C – use in typical situation, D – use in solving new problems.

According to these results the educational effectiveness of the films presented in particular taxonomic categories of the education aims was A – 28%, B – 22%, C – 40%, D – 37%, respectively.

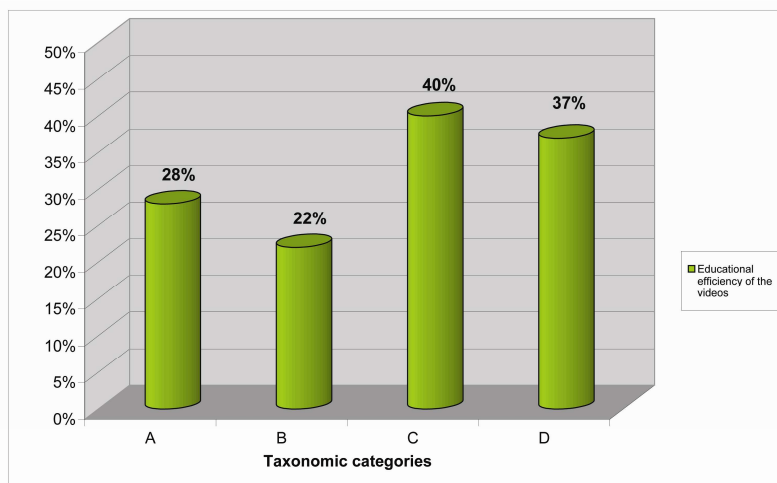


Fig. 4. The educational effectiveness of films as didactic means for the four categories of the aims of teaching: A, B, C, D.

The results definitely show the greater educational benefit in the experimental group to which the information was presented by the films. Exposition to films had a particularly good educational effect in the categories C (application in a typical situation) and D (application in solving new problems) (Fig. 4)

List of references:

- [1]. Stryjowski W., Wstęp do teorii filmu dydaktycznego, UAM Poznań 1997
- [2]. Skrzypczak J., Film dydaktyczny w szkole wyższej, PWN Warszawa 1985
- [3]. Burewicz A., Jagodziński P., Eksperyment laboratoryjny w nauczaniu chemii, ZDCh UAM Poznań 2005.
- [4]. Burewicz A., Jagodziński P., Ćwiczenia laboratoryjne z dydaktyki chemii. Eksperyment w liceum, UAM Poznań 2002
- [5]. Niemierko B., Ocenianie szkolne bez tajemnic, WSiP SA Warszawa 2002

ADSORPTION OF SODIUM DODECYLBENZENESULFONATE TO TiO₂.

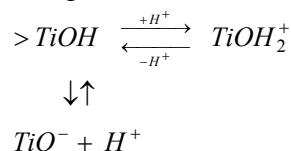
S. Bzdon, J. Perkowski, M. Szadkowska-Nicze

*Międzyresortowy Instytut Techniki Radiacyjnej, Politechnika Łódzka,
93-590 Łódź ul. Wróblewskiego 15*

Abstract: The adsorption of sodium dodecylbenzenesulfonate (SDBS) to TiO₂ studies were performed at acidic, base and natural pH of SDBS solutions at concentrations below the CMC of SDBS. The results were interpreted in terms of Langmuir adsorption model. The Langmuir constants estimated for adsorption of SDBS to TiO₂ at natural pH and in HNO₃ and NaOH electrolytes solutions were equal to ca. $4 \times 10^3 \text{ M}^{-1}$. A larger Langmuir adsorption constant, $K = 17.28 \times 10^3 \text{ M}^{-1}$ obtained in H₂SO₄ solution suggests the stronger adsorption binding in the presence of SO₄²⁻ ions in solutions. The results of investigations have indicated that both electrostatic forces substrate-adsorbate and ionic interactions in solution are important in the adsorption of anionic surfactant to TiO₂.

Introduction

Surfactants are widely employed in the domestic and industrial sectors. They cause serious ecological problems, since surfactants don't undergo natural decomposition. The advanced oxidation processes (AOP) have a great concern in chemical methods of surfactants destruction in the last years. The photodegradation of surfactants using semiconductor particles as catalyst represents an efficient kind of AOP methods. Titanium dioxide (TiO₂) in the anatase form appears to be the most photoactive and practical among semiconductors for widespread environmental application such as water purification, wastewater treatment, hazardous waste control and water disinfection [1]. Photocatalytic destruction of surfactants on TiO₂ surface mediated in water is heterogeneous process which can be divided into five steps: surfactant diffusion from solution to catalyst surface; adsorption of surfactant on the TiO₂ surface; chemical reaction on the catalyst surface; desorption of products from substrate and diffusion of products into solution. Adsorption of detergents on TiO₂ surface is one of the most important step in photocatalytic oxidation processes. Titanium dioxide particles suspended in water are known to be amphoteric. In TiO₂, the principal amphoteric surface functionality is the "titanol" moiety, >TiOH [2]. The hydroxyl groups on the TiO₂ surface undergo the acid-base equilibrium according to scheme :



At sufficiently low pH an oxide surface is expected to be protonated giving a positive surface charge. At high pH the surface will be deprotonated with a negative charge. At some intermediate pH the surface has net zero charge. The isoelectric point at pH \approx 5 was determined for TiO₂ gel film derived from TiCl₄ [3]. In the case of TiO₂ P25 Degussa, the pH of zero point of charge, (pH_{zpc}), was equal to 6.25 [4]. In the present work, we have studied the adsorption from non-micellar aqueous solutions of the anionic surfactant to TiO₂ particles depending on pH of the systems.

The value pH_{zpc} for TiO_2 implies that interactions with anionic surfactants should be favored at low pH under conditions in which $\text{pH} < \text{pH}_{\text{zpc}}$. We used the typical anionic surfactant such as sodium dodecylbenzenesulfonate (SDBS) which is widely used in the manufacturing of toothpastes, bath soaps, wash powders, car shampoos, and in a variety of other industrial detergents owing to its advanced foaming ability even in hard waters. We investigated the adsorption of SDBS on TiO_2 at acidic, base and natural pH of SDBS solutions i.e. below, above and in the pH_{zpc} range, respectively.

Experimental

Titanium dioxide powder, TiO_2 P25 Degussa was used as adsorbent. Dodecylbenzenesulfonic acid sodium salt (SDBS), (Fluka) was used as adsorbate. The absorption maximum for aqueous solutions of SDBS was observed at 224 nm ($\epsilon = 9485 \text{ mol}^{-1} \text{ dm}^3 \text{ cm}^{-1}$). The critical micellization concentration (CMC) of SDBS equal to $1,5 \times 10^{-3} \text{ mol dm}^{-3}$ (M) was determined by conductometric method. All experiments were carried out at concentrations below the CMC of SDBS. The pH of SDBS solutions was adjusted using NaOH (Przedsiębiorstwo Chemiczne "Odczynniki" Lublin, p.a.), HNO_3 (POCh, Gliwice, p.a.) and H_2SO_4 (Chempur, p.a.). A fixed amount of substrate (0.2 g) was suspended in 200 cm^3 of aqueous solutions of SDBS with various initial concentrations. The suspensions of TiO_2 powders in surfactant solutions were allowed to equilibrate for 2 hours (although the adsorption reach saturation in 1 h) in the dark at room temperature under constant stirring. The amount of SDBS adsorbed on the TiO_2 surface was calculated from the absorption spectra of equilibrated solutions. The TiO_2 powder was removed by centrifugation and filtration using $0.45 \mu\text{m}$ Sartorius filters.

Results and discussion

The adsorption curves of SDBS to TiO_2 (Fig.1) were obtained from $2,9 \times 10^{-4}$ – $1,4 \times 10^{-3}$ M SDBS solutions at pH 1,9 (H_2SO_4 adjusted), 2,1 (HNO_3 adjusted), 5,7-6,9 (natural pH of SDBS solutions in concentration range under consideration) and 11,5 (NaOH adjusted).

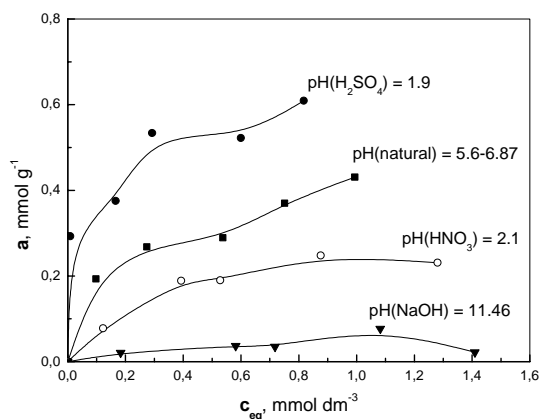


Fig.1. The influence of pH on adsorption of SDBS to TiO_2 .

The adsorption of SDBS to TiO_2 particles can be discussed in terms of a simple Langmuir adsorption isotherm:

$$\Theta = \frac{K \cdot c_{eq}}{1 + K \cdot c_{eq}} \quad (1)$$

where Θ is the fractional coverage of TiO_2 by SDBS molecules, c_{eq} is the equilibrium concentration of the SDBS solution (M), and K is the Langmuir constant for adsorption-desorption equilibrium (M^{-1}).

Assuming that a is the amount of adsorbed SDBS to 1 g TiO_2 (mol g^{-1}), and a_m is the maximum amount of adsorbed SDBS for monolayer coverage of TiO_2 (mol g^{-1}), one can obtain $\Theta = a / a_m$, and linear relationship (2) can be derived:

$$\frac{c_{eq}}{a} = \frac{1}{a_m \cdot K} + \frac{c_{eq}}{a_m} \quad (2)$$

The results of SDBS adsorption to TiO_2 for different pH conditions were fitted to Langmuir expression (2) as plotted in Figure 2.

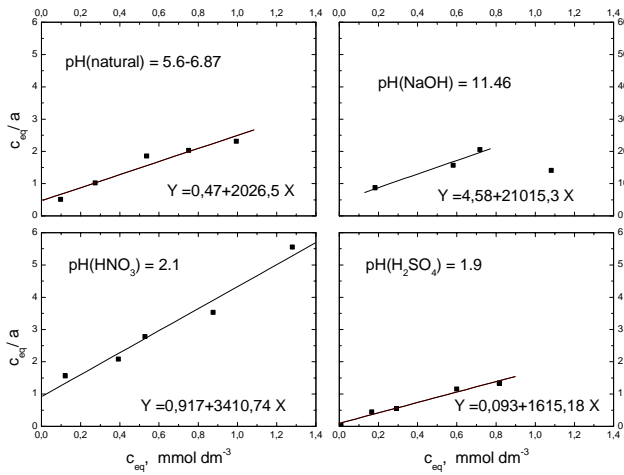


Figure 2. The adsorption of SDBS to TiO_2 depending on pH of solutions in terms of Langmuir model

The values of a_m and K obtained from Figure 2 are given in Table 1.

Table 1.

Langmuir adsorption constant data for adsorption of SDBS to TiO_2

pH	a_m (mol g^{-1})	$K \times 10^{-3}$ (M^{-1})	Number of SDBS molecules covered 1nm^2 of TiO_2	Area of TiO_2 occupied by SDBS molecule (\AA^2)
5.6 – 6.87 (natural)	4.93×10^{-4}	4.31	5.94	16.95
1.9 (H_2SO_4)	6.19×10^{-4}	17.28	7.46	13.41
2.1 (HNO_3)	2.93×10^{-4}	3.73	3.53	28.34
11.46 (NaOH)	4.75×10^{-5}	4.59	0.57	174.82

Using the surface area of the TiO_2 P25 equal to $50 \text{ m}^2 \text{ g}^{-1}$ and a_m values (Table 1) we have calculated the number of SDBS molecules covered 1nm^2 of TiO_2 particle surface and the TiO_2 area occupied by one molecule of SDBS.

The Langmuir constants ($K \approx 4 \times 10^3 \text{ M}^{-1}$) calculated for adsorption of SDBS to TiO_2 at natural pH and in HNO_3 and NaOH electrolytes solutions are similar in order of

magnitude to those obtained for adsorption of sodium dodecylsulfate to TiO_2 at $\text{pH}=3.0$ ($K=8 \times 10^3 \text{ M}^{-1}$) [5] and for lysine adsorption to TiO_2 ($K=3 \times 10^3 \text{ M}^{-1}$) [6].

A considerably larger Langmuir adsorption constant ($K = 17.28 \times 10^3 \text{ M}^{-1}$) obtained in H_2SO_4 solution suggests the stronger adsorption binding in the presence of SO_4^{2-} in solution.

The results summary shown in Table 1 clearly indicate that electrostatic interactions are involved in the adsorption of SDBS to TiO_2 surfaces. The low amount of adsorbed SDBS in alkaline system ($4.75 \times 10^{-5} \text{ mol g}^{-1}$) can be explained by electrostatic repulsion of anionic sulfonate head groups. The hydrophobic chain can be easier adsorbed on the negative TiO_2 surface than the negative sulfonate moiety in alkaline solution. One can suppose that the SDBS ions could lie transversely on the TiO_2 surface. Hidaka and Zhao [7] suggested that under alkaline condition, only single-layer adsorption can take place on the TiO_2 particles owing to electrostatic effects.

The positive charged TiO_2 surface has a strong tendency to adsorb the negative sulfonate moiety of SDBS at lower pH value. The amounts of adsorbed SDBS in acidic solutions are one magnitude of order higher comparing to alkaline medium.

If we assume that the SDBS molecule is lying flat on the TiO_2 surface, it should occupy ca. 62 \AA^2 . The areas of TiO_2 occupied by one molecule of SDBS in acidic solutions (Table 1) indicate that the sulfonate head group appears to interact directly with the TiO_2 surface. The area of the triangle formed by the sulfonate oxygen atoms is approximately equal to $7\text{-}8 \text{ \AA}^2$. [8]. One can suggest that sulfonate group hold the rest of the SDBS molecule nearly perpendicular to the TiO_2 surface, especially in the presence of SO_4^{2-} ions in the solution.

The electrolytes used to pH adjusting have changed the ionic strength of SDBS solutions as it is shown in Figure 3.

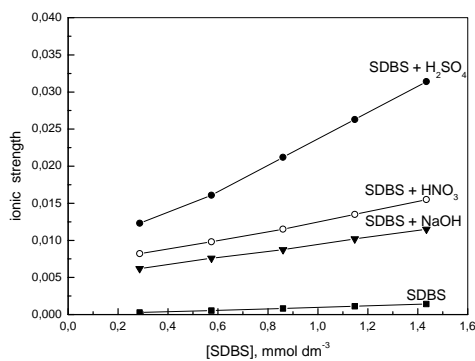


Figure 3. The ionic strength dependence of electrolyte solutions on concentration of SDBS.

A considerably increase of ionic strength of SDBS solutions occur in the presence of H_2SO_4 electrolyte. One can suggest that molecules of anionic surfactants are push out from the solutions and the enhancement of SDBS adsorption to TiO_2 take place in such conditions.

Conclusions

Our results indicate that both electrostatic forces substrate-adsorbate and ionic interactions in solution are important in the adsorption of anionic surfactant to TiO_2 .

SDBS adsorption to TiO_2 from aqueous solutions was not only pH- dependent, but electrolyte species in solution have affected SDBS adsorption to TiO_2 too.

References

- [1] A. Zalewska, J. Hupka, in: Zaawansowane techniki utleniania w ochronie środowiska, R. Zarzycki (ed), Polska Akademia Nauk, Łódź, 2002, chap.7, Fotokataliza z wykorzystaniem TiO₂. pp.174-204.
- [2] M.R. Hoffmann, S.T. Martin, W. Choi, and D.W. Bahnemann, Chem.Rev.,95 (1995)69-96.
- [3] K.D. Dobson, P.A. Connor, and A.J. McQuillan, Langmuir, 13 (1997) 2614-2616.
- [4] C. Kormann, D.W. Bahnemann, M.R. Hoffman, Environ.Sci.Technol. 25 (1991) 494-500.
- [5] K.D. Dobson, A.D. Roddick-Lanzilotta, A.J. McQuillan, Vibrational Spectroscopy 24 (2000) 287-295.
- [6] A.D. Roddick-Lanzilotta, P.A. Connor, A.J. McQuillan, Langmuir 14 (1998) 6479-6484
- [7] H. Hidaka, J.Zhao, Colloids and Surfaces, 67 (1992), 165-182.
- [8] S. Dube, N.N. Rao, J. Photochem. Photobiol. A: Chem. 93 (1996) 71-77.

COPOLYMERIZATION OF *O*-METHACRYLOIL-*O*'-METHYL BISPHENOL-A WITH METHYL METHACRYLATE AND DETERMINATION OF REACTIVITY RATIOS

Władysław Charmas, Małgorzata Topyła, Janina Nowak

Department of Organic Chemistry and Technology, Maria Curie-Skłodowska University, ul. Gliniana 33, 20-614 Lublin, Poland

Most of the synthetic polymeric materials are produced by the free radical polymerization. Methacrylate copolymers have found important applications. Copolymerizations of functional methacrylates with other monomers provide simple routes for synthesis of biologically active materials and coating formulations [1]. Copolymers from methyl methacrylate (MMA) are used in the formation of biologically active films and production of materials for optical telecommunication applications [2,3].

The reactivity ratios are among the most important parameters for the composition equations of copolymers, which can offer information such as the relative reactivity of monomer pairs and determine the copolymer composition.

This paper presents the synthesis, characterization and determination of reactivity ratios for the comonomers, *O*-methacryloilo-*O*'-methyl bisphenol A (MMO-D) and methyl methacrylate (MMA).

Copolymerization

Copolymerization was carried out in tetrahydrofuran (THF) solution at 65°C using 2,2'-azobisisobutyronitrile (AIBN) as a free radical initiator (Fig. 1). Predetermined quantities of MMO-D [4], MMA and THF were mixed in the reaction tube and degassed with nitrogen. After the sealed tube had been kept at the required temperature, the contents were poured into a large excess of methanol. The precipitated copolymer was filtered, off washed with methanol and purified by repeated precipitation with methanol from a solution of DMF and finally dried under vacuum. The copolymerization was stopped at low conversions (<15% wt).

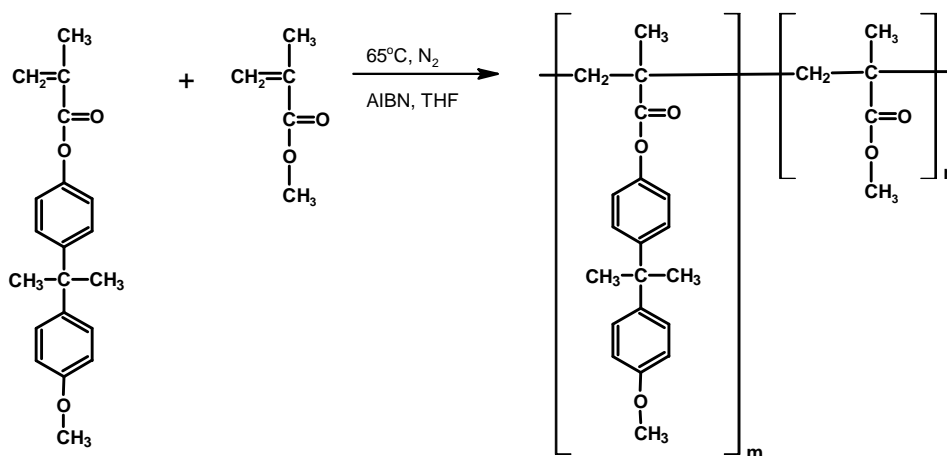


Figure 1

Copolymer Compositons

Since the chemical structure of copolymers can be presented as in Fig. 1, the average compositions of copolymer samples were determined from the corresponding $^1\text{H-NMR}$ spectra. The assignment of the resonance peaks in the $^1\text{H-NMR}$ spectrum allows for the accurate evaluation of the content of both kinds of monomeric unit in the copolymer. The $^1\text{H-NMR}$ spectrum of the copolymer, poly(MMO-D-*co*-MMA) (0.5:0.5) is shown in Fig. 2. The aromatic protons show signals between 7.26 and 6.75 ppm. The signals at 1.03-3.79 ppm are due to the aliphatic protons.

Thus, the mole fraction of MMO-D in the copolymer chains was calculated from the integrated intensities of aromatic protons of MMO-D and aliphatic protons of MMO-D and MMA units.

The following expression is used to determine the composition of copolymers. Let m_1 be the mole fraction of MMO-D and $(1-m_1)$ be that of MMA. There are 8 aromatic protons in MMO-D and 14 aliphatic protons. MMA unit has 8 aliphatic protons.

$$C = \frac{\text{Intensities of aromatic protons}}{\text{Intensities of aliphatic protons}} = \frac{8m_1}{14m_1 + 8(1-m_1)} \quad (1)$$

which after simplification gives:

$$m_1 = \frac{-8C}{6C - 8} \quad (2)$$

The copolymer compositions and the values of C are presented in Table 1. The relationship between the molar percentage of MMO-D (M_1) incorporated into the copolymer and the comonomer feed ratio is shown in Fig. 3. It indicates that the distribution of monomeric units is statistical with an azeotropic composition when the mole fraction of MMO-D in the feed is 0.66.

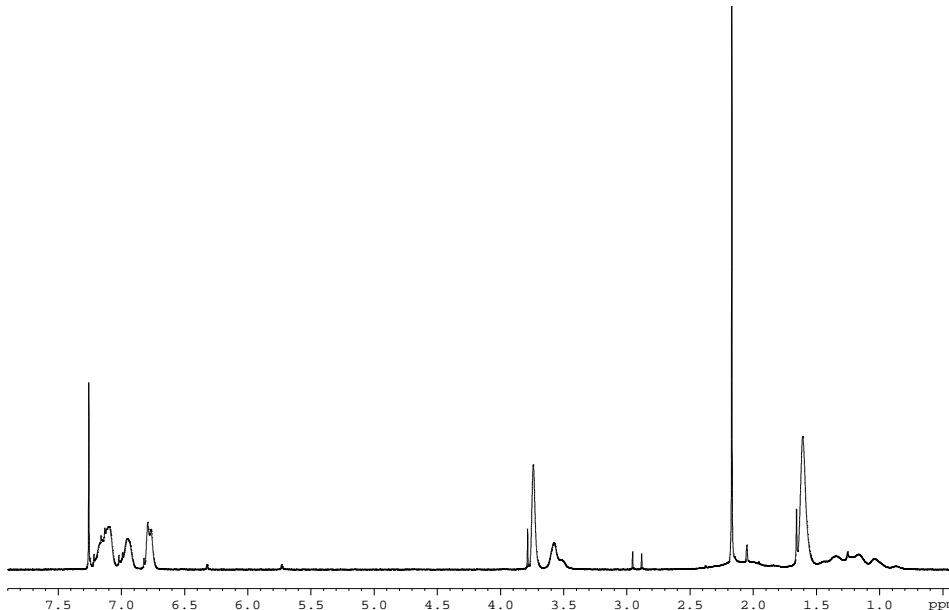


Fig. 2. $^1\text{H-NMR}$ spectrum of poly(MMO-D-*co*-MMA) (0.5:0.5)

Tab. 1. Composition Data of Free Radical Copolymerization of MMO-D with MMA in the THF Solution at 65°C

No	Feed Composition		Conversion [%]	Intensity of Protons		C	Copolymer Composition	
	M ₁	M ₂		(I _{Ar})	(I _{Al})		m ₁	m ₂
1.	0.75	0.25	11.43	4.7357	10.0992	0.4689	0.7233	0.2767
2.	0.50	0.50	11.70	8.4718	21.3334	0.3971	0.5656	0.4344
3.	0.40	0.60	7.12	10.2287	28.5149	0.3587	0.4907	0.5093
4.	0.25	0.75	7.27	4.5867	15.5365	0.2952	0.3792	0.6208

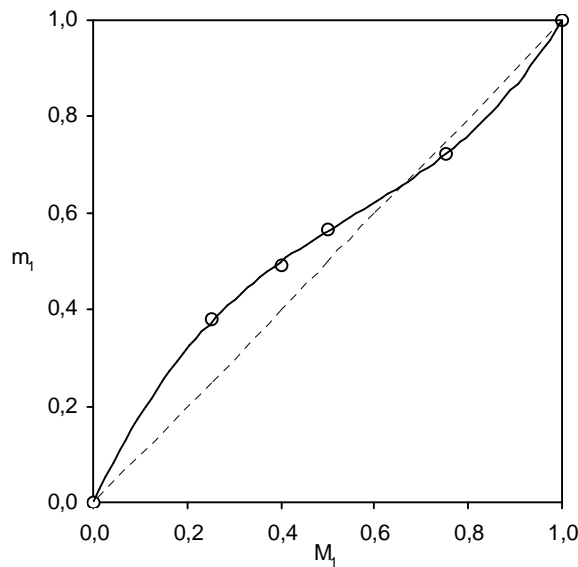


Fig. 3. Copolymer composition diagram of poly(MMO-D-co-MMA) system.

Reactivity Ratios

The knowledge of reactivity ratio is essential for the preparation of any copolymers having a definite composition. The reactivity ratios of MMO-D and MMA were evaluated from the monomer feed ratios and the copolymer composition by the application of the Fineman-Ross (F-R) [5], Kelen-Tüdös (K-T) [6] and extended Kelen-Tüdös (extended K-T) [7] methods. The reactivity ratio related to monomer 1 (MMO-D) is r_1 , and that of monomer 2 (MMA) is r_2 . The values of r_1 and r_2 from the F-R, K-T and extended K-T methods are presented in Table 2. According to C. Hagiopol [8] since the r_1 and r_2 values are less than 1, this system gives rise to azeotropic polymerization at a particular composition of the monomers which is calculated using the equation

$$N_1 = \frac{(1-r_2)}{(2-r_1-r_2)} = 0.66$$

when the mole fraction of monomer MMO-D in the feed is 0.66, the copolymer formed will have the same composition as that of the feed. When the mole fraction of the feed is less than 0.66 with respect to MMO-D, the copolymer is relatively richer in this monomer unit than the feed. When the mole fraction of the monomer MMO-D in the feed is above 0.66, the copolymer is relatively richer in the MMA unit than in the feed.

Tab. 2. Comparison of Reactivity Ratios by Various Methods for Poly(MMO-D-co-MMA)

Methods	r_1	r_2	r_1r_2
F-R	0.6272	0.2995	0.1878
K-T	0.6482	0.3175	0.2058
Extended K-T	0.6396	0.3046	0.1948

Conclusions

Copolymers of poly(MMO-D-co-MMA) were synthesized by free radical solution polymerization. The copolymer compositions were found by the $^1\text{H-NMR}$ analysis of the polymers. The reactivity ratios were determined by the F-R, K-T and extended K-T methods giving values in good agreement. The values of r_1 and r_2 are less than unity indicating that the system gives rise to an azeotropic polymerization.

References:

- [1] T. Gendy, Y. Barakat, A. Mohammad, A. Youssef, *Polym Int*, 24 (1991) 234
- [2] S. C. Pandeya, N. Rather, A. Singh, *J Polym Materials*, 16 (1999) 253
- [3] M. Jöhnck, L. Müller, A. Neyer and J. W. Hofstraat, *Eur Polym J*, 36 (2000) 1251
- [4] W. Charnas, M. Topyła, J. Nowak, *Zgłoszenie patentowe P-370-046* (2004)
- [5] M. Fineman, S. D. Ross, *J Polym Sci*, 5 (1950) 259
- [6] T. Kelen, F. Tüdös, *J Macromol Sci Chem*, A9 (1975) 1
- [7] T. Kelen, F. Tüdös, B. Turcsunyi, J. P. Kennedy, *J Polym Sci*, A15 (1977) 3047
- [8] C. Hagiopol, *Copolymerization*, Kluwer Academic / Plenum Publishers, 1999.

APPLICATION OF PIG LIVER ESTERASE IN THE HYDROLYSIS OF 3,5-DIACETOXYCYCLOPENTENES

Małgorzata Chernik, Alicja Filipowicz-Szymańska,
Joanna Głowczyk-Zubek, Ryszard Ostaszewski

Faculty of Chemistry, Warsaw University of Technology, Noakowskiego 3,
00-664 Warsaw

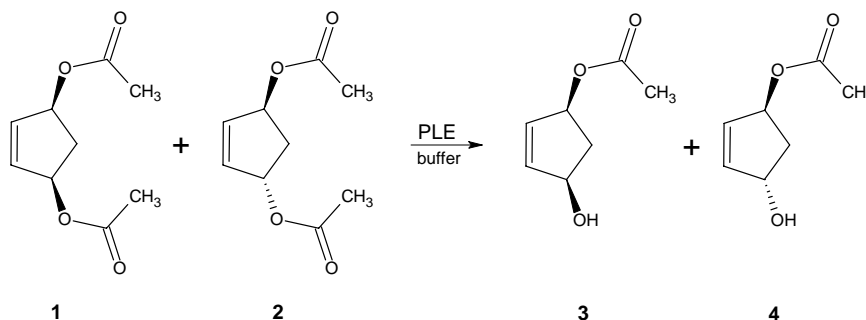
Abstract Enzymatic hydrolysis of a mixture of *cis*- (**1**) and *trans*-3,5-diacetoxycyclopentene (**2**) was carried out in the presence of crude and purified pig liver esterase (PLE). Significant differences in reactivity and enantioselectivity of various biocatalyst fractions (obtained in the salting out process and after its immobilization on talc) were observed.

Introduction

Cis-3-acetoxy-5-hydroxycyclopentene (**3**) is an useful starting material for synthesis of prostaglandins and other biologically active compounds. Stereoselective and enantioselective desymmetrisation of *cis*- (**1**) and *trans*-3,5-diacetoxycyclopentene (**2**) mixture is an important step in prostaglandins synthesis. It is well known, that enantioselective hydrolysis of diesters **1** and **2** is catalyzed by lipases: *pig pancreatic lipase*, *wheat germ lipase*, *Aspergillus niger lipase* and some esterases. There are stereoselective reactions in which isomer *cis* **1** reacted faster [1,2]. The *cis*-3,5-diacetoxycyclopentene hydrolysis (**1**) by *pig liver esterase* (PLE), giving (-)-(5*S*,3*R*)-3-acetoxy-5-hydroxycyclopentene, has been also described [3].

Results

The object of our research was the hydrolysis of the *cis*- and *trans*-3,5-diacetoxycyclopentene (**1** and **2**) mixture catalyzed by PLE (Scheme1). The course of model reaction was monitored by gas chromatography. *Cis*- and *trans*-3-acetoxy-5-hydroxycyclopentene (**3** and **4**) and starting esters **1** and **2** were observed in the reaction mixture.



Scheme 1. The hydrolysis of *cis*- and *trans*-3,5-diacetoxycyclopentene mixture

PLE was obtained from pig liver using a modification of a method reported in literature [4, 5]. It allowed to reduce the research cost. In the presence of crude enzymatic preparation both stereoisomers **1** and **2** were hydrolysed with similar rate. Then the crude enzymatic preparation was purified by ammonium sulphate(VI) outsalting to 60% saturation (P0-60). It turned out, that using this purified enzymatic protein increases the rate of *trans*-3,5-diacetoxycyclopentene (**2**) hydrolysis (Table 1).

Table 1. Course of model hydrolysis catalysed with PLE and P0-60 enzymatic preparations

Enzyme	Time [hours]	Conversion (GC)*	Isomer <i>cis</i> (3)	Isomer <i>trans</i> (4)	Difference in isomers amount
PLE	26	45,7 %	22,6 %	23,1 %	0,5 %
P0-60	26	49,1 %	19,5 %	29,6 %	10,1 %

*the sum of amount of isomer *cis* (3) and *trans* (4) in the reaction mixture

The fractionation of crude enzyme PLE was performed by salting out with ammonium sulphate(VI) to 20%, 40%, 60% and 80 % of saturation. In the range of salting to 20% no precipitate has been obtained. Three next enzymatic preparations have been marked as P0-40, P40-60 and P60-80. The first of them (P0-40) was inactive as hydrolysis biocatalyst.

As a result two enzymatic preparations P40-60 and P60-80 were used in the next experiments and the starting enzyme PLE was compared with them.

Table 2. Composition [%] of model reaction mixture containing esters 1, 2, 3 and 4.

hours	PLE					P40-60					P60-80				
	1	2	3	4	de 4*	1	2	3	4	de 4*	1	2	3	4	de 4*
23	51	38	4	7	27	50	32	7	11	22	56	32	4	8	33
46	46	31	10	13	13	40	15	17	28	24	40	13	19	29	21

*diastereomeric excess of 4

In Table 2 there are listed compositions of reaction mixtures containing compounds 1, 2, 3 and 4 after 23 and 46 hours. Under the influence of both purified enzymes P40-60 and P60-80 *trans*-3,5-diacetoxycyclopentene (2) reacted faster producing *trans*-3-acetoxy-5-hydroxycyclopentene excess (4) as a result.

The influence of immobilization of all obtained biocatalysts on its activity was checked. The immobilisation of P0-60 enzyme was carried out in sol-gel system, on talc and on the celite. The enzyme reactivity was checked in colour reaction with *p*-nitrophenyl acetate and in model hydrolysis of 3,5-diacetoxycyclopentenes. It was found that immobilization in sol-gel system inactivates PLE. Hydrolysis reactions with enzymes adsorbed on the talc and the celite run much slower (Table 3).

Table 3. The comparison of 3,5-diacetoxycyclopentenes hydrolysis results

Enzymatic preparation	The protein mass used in reaction (Lowry method)	Time [hours]	Conversion [%]
P0-60	376 µg	44	85
P0-60 on celite	Not measured*	44	13
P0-60 on talc	376 µg	44	18
Blind assay	Lack of catalyst	44	2

* Celite impurities interfered with the Lowry assay

After the immobilization on celite the stereoselectivity of hydrolysis of 3,5-diacetoxycyclopentenes decreased. On the other hand, after immobilization on the talc

hydrolysis took place with higher stereoselectivity in comparison with native P0-60 enzyme reaction. (Table 1 and 4.).

Table 4. Comparison of stereoselectivity of the P0-60 immobilized preparations

Enzyme	Conversion (GC)	Isomer <i>cis</i> (3)	Isomer <i>trans</i> (4)	Difference in isomers amount
P0-60 on celite	48,2 %	20,2 %	28,0%	7.8 %
P0-60 on talk	53,%	20,8 %	32,9 %	12,1 %

In further investigations, enzymes immobilized on talc were used: TPLE, TP40-60 and TP60-80. An enzymatic preparation TP60-80, adsorbed on talc, lost his activity completely. Reactions with enzyme TPLE and TP40-60 run more slowly than previously. The TPLE preparation had higher stereoselectivity, however in the reaction with TP40-60 higher diastereoisomeric excess of *trans*-3-acetoxy-5-hydroxycyclopentene (4) was obtained than previously (Table 5).

Table 5. Hydrolysis of 3,5-diacetoxycyclopentenes catalyzed by enzymes immobilized on talc

hours	TPLE					TP40-60				
	1	2	3	4	de 4	1	2	3	4	de 4
26	51	41	3	4	14	47	27	8	18	39
46	44	31	11	14	12	42	20	28	28	36
68	38	24	16	22	16	38	18	29	29	29

After the reactions were stopped, the mixtures were separated by liquid column chromatography. Enantiomeric ratio of (-) and (+) *cis*-3-acetoxy-5-hydroxycyclopentene (3) isolated from all reactions was analyzed by means of HPLC with chiral column (Whelk SS). All results are listed in the Table 6. The obtained *trans*-3-acetoxy-5-hydroxycyclopentene was optically inactive.

Table 6. Enantiomeric ratio of (-) and (+) *cis*-3-acetoxy-5-hydroxycyclopentene (3)

Enzyme	<i>cis</i> -3-acetoxy-5-hydroxycyclopentene	
	3(-) / 3(+)	[α]
PLE	34 / 66	24,56°
P40-60	77 / 23	-31,74°
P60-80	77 / 23	
TPLE	26 / 74	
TP40-60	73 / 27	

Conclusions

In our research application of *pig liver esterase* to the stereoselective hydrolysis of 3,5-diacetoxycyclopentenes (1 and 2) was showed. The obtained preparations: P40-60, P60-80 as well as TPLE and TP40-60 hydrolysed faster stereoisomer *trans* (2) that might be

used in enzymatic separation of esters **1** and **2**. Catalytic properties of pig liver esterase could be modified by purification and immobilization in a simple way on talc. The hydrolysis catalyzed by PLE lead to excess of (-)-*cis*-3-acetoxy-5-hydroxycyclopentene, while during hydrolysis with purified preparations P40-60 and P60-80 (+)-*cis*-3-acetoxy-5-hydroxycyclopentene was obtained. Enzyme immobilization has great influence on its catalytic activity.

Experimental part

Preparation of crude pig liver esterase: pieces of fresh pig liver and acetone (300 ml) were homogenized in blender. Precipitate was homogenized again in acetone (150 ml) and then with methylene chloride (150 ml). Obtained precipitate was crumbled and dried under vacuum.

Immobilization of enzymatic preparations on talc (PLE, P40-60, P60-80): Enzymatic preparation (250 mg) was dissolved in phosphate buffer pH 7.00 (5ml). To the solution talc Luzenac was added (1.0 g) and dispersion was shaken in 1.5 hour. Next the mixture was centrifuged. Obtained precipitate was dried under vacuum. Amounts of immobilized proteins were determined by Lowry's method.

Hydrolysis of 3,5-diacetoxycyclopentene (1, 2): Acetone (2 ml), 3,5-diacetoxycyclopentene (0.5 g; 2.7 mmol) and enzymatic preparation were placed into phosphate buffer pH 7.00 (50 ml) The mixture was stirred at 30°C. Reaction run was monitored by GC. After the completion of reaction, the enzyme was filtered off. Mixture was extracted with diethyl ether. The organic phase was dried and ether was evaporated. Products and substrates were separated by column liquid chromatography (Kieselgel 60, 230-430 mesh, eluent – changing from CH₂Cl₂ to CHCl₃).

Literature:

- [1] S. Miura, S. Kurozumi, T. Toru, T. Tanaka, M. Kobayashi, S. Matsubara, S. Ishimoto, Tetrahedron., 32 (1976) 1893
- [2] T. Sugai, K. Mori, Synthesis., 1988 (1988) 19
- [3] K. Laumen, M. Schneider, Tetrahedron Lett., 25 (1984) 5875
- [4] D. Seebach, M. Eberle, Chimia., 40 (1986) 315
- [5] W. M. Connors, A. Pihl, A. Dounce, E. Stotz, J. Biol. Chem., 184 (1950) 29

THE REACTION OF SELENOPHOSPHORIC ACIDS WITH O-ACYLATED HYDROXYLOAMINE.

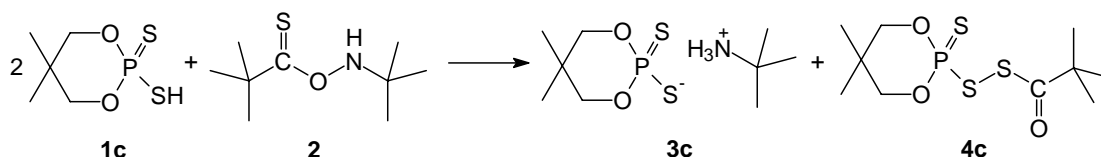
Grzegorz Cholewiński, Dariusz Witt, Radosław Majewski*, Tadeusz Ossowski* and Janusz Rachoń

Gdansk University of Technology, Chemical Faculty, Department of Organic Chemistry,
ul. G. Narutowicza 11/12, 80-952 Gdansk

* University of Gdansk, Chemical Faculty, Department of Supramolecular Chemistry,
ul. Sobieskiego 18/19, 80-852 Gdansk

Introduction

The new reaction of dithiophosphoric acid **1c** with O-thioacylhydroxylamines **2**, which proceeds via N-O bond cleavage and lead to ammonium dithiophosphates **3c**, acyl thiophosphoryl disulphates **4c** has been recently described [1] (Scheme 1).



Scheme 1 The reaction of two equivalents of dithiophosphoric acid **1c** with O-thioacylhydroxylamines **2**.

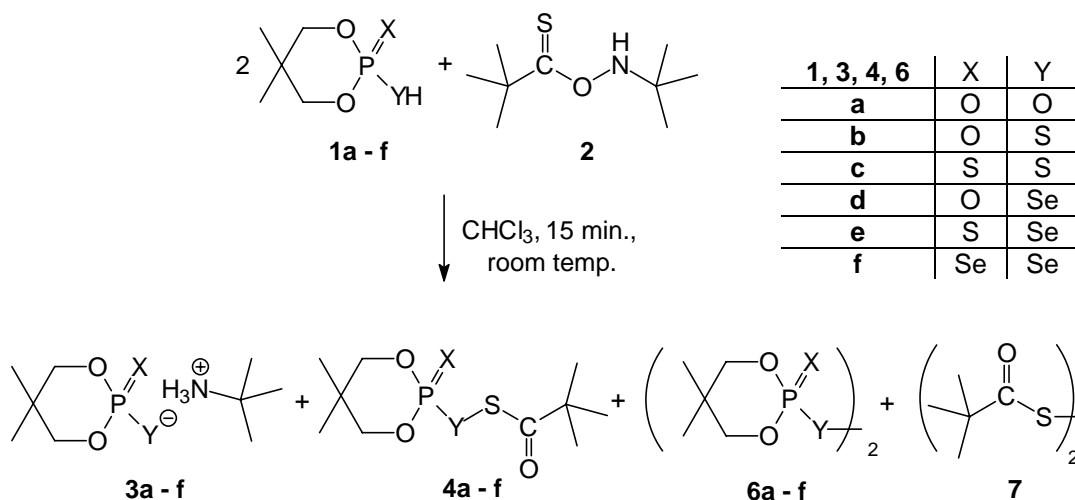
The influence of radical traps and light on the reaction strongly suggested the radical mechanism of the process. Moreover, considerable ability of dithiophosphate anions to one electron oxidation [2] implied involvement of a single electron transfer process (SET) with dithiophosphate anion $>P(S)S^-$ as SET donor and radical scavenger as well [3].

On the other hand, it is known very well, that selenoles participate in the $S_{RN}1$ reaction as a SET donors [4]. Taking above facts into account we decided to examine reactivity of selenophosphoric acid derivatives towards O-thioacylhydroxylamine and compare them with thiophosphoric and phosphoric acids ones. We also expected to find correlation between course of the reaction and oxidation potentials of phosphate anions **5** (see Table 2) under investigation.

Results and discussion

In the first series of experiments O-thiopivaloyl-N-tert-butylhydroxylamine **2** was treated with two equivalents of phosphoric acid derivatives **1** (Scheme 2) in standard conditions (15min., room temperature, $CHCl_3$ as a solvent). Thus, in the case of phosphoric acid **1a** (X, Y = O) the reaction did not occur and starting materials **1a**, **2** were quantitatively recovered (Table 1). However, monothiophosphoric acid **1b** (X = O, Y = S) gave, analogically to dithiophosphoric acid **1c** [1,3], ammonium monothiophosphate **3b** (^{31}P NMR, $\delta = 53,8$ ppm) and monothiophosphoric-acyl disulfide **4b** (^{31}P NMR, $\delta = 13,9$ ppm). On the other hand, monoselenophosphoric acid **1d** (X = O, Y = Se) produced, apart from expected tert-butylammonium monoselenophosphate **3d** (^{31}P NMR, $\delta = 44,6$ ppm, $^1J_{P-Se} = 745,3$ Hz), symmetric bis-(2-oxo-5,5-dimethyl-1,3,2-dioxaphosphorinan-2-yl) diselenide **6d** (^{31}P NMR, $\delta = 3,96$ ppm, $^1J_{P-Se} = 488,9$ Hz) and pivaloyl disulfide **7**. Similarly, selenothiophosphoric acid **1e** (X = S, Y = Se) lead to tert-butylammonium selenophosphate **3e** (^{31}P NMR, $\delta = 98,5$

ppm, $^1J_{P-Se} = 739,1$ Hz) and bis-(2-thiono-5,5-dimethyl-1,3,2-dioxaphosphorinan-2-yl) diselenide (^{31}P NMR, $\delta = 67,2$ ppm, $^1J_{P-Se} = 471,3$ Hz) **6e** and pivaloyl disulphide **7**.



Scheme 2 The reaction of two equivalents of phosphoric acid derivatives **1** with O-thiopivaloyl-N-tert-butylhydroxylamine **2**

Table 1. Products of reaction of phosphoric acids **1** with O-thiopivaloyl-N-tert-butylhydroxylamine **2**.

	X	Y	Yield %			
			3	4	6	7
a	O	O	0	0	0	0
b	O	S	100	81	0	0
c	S	S	99 ³	92 ³	0	0
d	O	Se	100	0	49	70
e	S	Se	100	0	83	84
f	Se	Se	100	0	0	38

The question arose: is it the same reaction like in the case of mono – and dithiophosphoric acids **1b**, **1c**? The first product should be (2-oxo-5,5-dimethyl-1,3,2-dioxaphosphorinan-2-yl)-S-pivaloyl selenosulfide **4d** or (2-thiono-5,5-dimethyl-1,3,2-dioxaphosphorinan-2-yl)-S-pivaloyl selenosulfide **4e** which could symmetrize to diselenide **6d,e** and pivaloyl disulphide **7** respectively.

To prove this hypothesis the reaction of monoselenophosphoric acid **1d** was monitored with ^{31}P NMR technique (room temperature, $CDCl_3$ as a solvent). The tert-butylammonium monoselenophosphate **3d** precipitated from the reaction mixture after several seconds. After filtration the ^{31}P NMR spectrum was recorded immediately. There was one resonance signal: $\delta = 6,63$ ppm, $^1J_{P-Se} = 485,8$ Hz observed and identified as bis-(2-thiono-5,5-dimethyl-1,3,2-dioxaphosphorinan-2-yl) diselenide **6d**. The ^{31}P NMR repeated after 24h, 48h did not indicate any further changes. It could mean that symmetrization of (2-oxo-5,5-dimethyl-1,3,2-dioxaphosphorinan-2-yl)-S-pivaloyl selenosulfide **4d** to bis-(2-thiono-5,5-dimethyl-1,3,2-dioxaphosphorinan-2-yl) diselenide **6d** was very fast or **4d** was not obtained at all. Subsequently, we examined reaction of selenothiophosphoric acid **1e** with O-thiopivaloyl-N-tert-butylhydroxylamine **2** in NMR tube. Tert-butylammonium selenothiophosphate **3e** was

filtered off and filtrate analyzed with ^{31}P NMR technique. The only signal was $\delta = 72,2$ ppm, $^1J_{\text{P-Se}} = 467,1$ Hz (adequate for a compound with single P-Se bond) which could be assigned to (2-thiono-5,5-dimethyl-1,3,2-dioxaphosphorinan-2-yl)-S-pivaloyl selenosulfide **4e**. On the spectrum performed after 24h the signal $\delta = 72,2$ ppm, $^1J_{\text{P-Se}} = 467,1$ Hz decreased and the new one appeared: $\delta = 68,2$ ppm, $^1J_{\text{P-Se}} = 478,7$ Hz and assigned as bis-(2-thiono-5,5-dimethyl-1,3,2-dioxaphosphorinan-2-yl) diselenide **6e** ($\delta = 67,2$ ppm, $^1J_{\text{P-Se}} = 471,3$ Hz). Moreover, intensity of this new signal increased after 48h and 96h. The compound with $\delta = 72,2$ ppm, $^1J_{\text{P-Se}} = 467,1$ Hz was isolated from the reaction mixture and fully characterized by ^1H NMR, ^{13}C NMR, IR, MALDI-TOF-MS. All above data confirmed formation of (2-thiono-5,5-dimethyl-1,3,2-dioxaphosphorinan-2-yl)-S-pivaloyl selenosulphide **4e**. Furthermore, the conversion of **4e** to **6e** was observed in the same time and conditions as in the crude reaction mixture of **1e** and **2**.

These observations supported hypothesis where final products **6d,e** and **7** are formed as the result of symmetrization of intermediate **4d** or **4e**.

We also investigated reaction of two equivalents of diselenophosphoric acid **1f** with O-thiopivaloyl-N-tert-butyl-hydroxylamine **2**. Tert-butylammonium diselenophosphate **3f** (^{31}P NMR $\delta = 84,8$ ppm, $^1J_{\text{P-Se}} = 749,5$ Hz) was filtered off and on the ^{31}P NMR spectrum the one resonance signal was observed: $\delta = 70,6$ ppm, $^1J_{\text{P-Se}} = 485,8$ Hz, $^1J_{\text{P-Se}} = 956,0$ Hz, which could be assigned as the most likely structures: (2-seleno-5,5-dimethyl-1,3,2-dioxaphosphorinan-2-yl)-S-pivaloyl selenosulfide **4f** or bis-(2-thiono-5,5-dimethyl-1,3,2-dioxaphosphorinan-2-yl) diselenide **6f**.

The sample of this reaction mixture was kept at room temperature 24 h and ^{31}P NMR analysis indicated, apart from $\delta = 70,6$ ppm, $^1J_{\text{P-Se}} = 485,8$ Hz, $^1J_{\text{P-Se}} = 956,0$ Hz, numerous others signals. Since bis-(O,O-dialkylselenophosphoric) diselenides ($>\text{P}(\text{Se})\text{-Se-}$)₂ are described as a relatively stable compounds [5] we concluded, that signal $\delta = 70,6$ ppm, $^1J_{\text{P-Se}} = 485,8$ Hz, $^1J_{\text{P-Se}} = 956,0$ Hz is from (2-seleno-5,5-dimethyl-1,3,2-dioxaphosphorinan-2-yl)-S-pivaloyl selenosulfide **6f** which is not stable and undergoes decomposition.

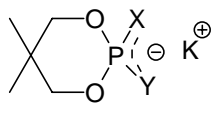
In the next set of experiments the radical mechanism of the reaction was examined. Thiophenols are known to be free radical traps [3]. Hence, to proof the hypothesis that SET process is involved, we performed the reactions of two equivalents of i) monothiophosphoric acid **1b** and ii) selenothiophosphoric acid **1e** with O-thiopivaloyl-N-tert-butyl-hydroxylamine **2** in the presence of one equivalent of 2,6-dimethylthiophenol.

After 30 min. the reaction mixtures were quenched with triethylamine [3] and analyzed with ^{31}P NMR. The only products were: triethylammonium monothiophosphate (^{31}P NMR $\delta = 54,4$ ppm) and triethylammonium selenothiophosphate (^{31}P NMR $\delta = 97,7$ ppm, $^1J_{\text{P-Se}} = 740,1$ Hz) respectively. These experiments showed, that 2,6-dimethylthiophenol prevents the formation of monothiophosphoric-acyl disulfide **4b** or (2-thiono-5,5-dimethyl-1,3,2-dioxaphosphorinan-2-yl)-S-pivaloyl selenosulfide **4e** in the above reaction mixtures.

The fact, that phosphoric acid **1a** did not react with O-thiopivaloyl-N-tert-butylhydroxylamine **2** in contrast to its sulfur and selenium analogs **1b-f**, which underwent reaction of the N-O bond cleavage in hydroxylamine, required rational explanation. The results of our experiments strongly suggested, that SET process is involved in the mechanism of the reaction under discussion. Thus, the first stage is single electron transfer process from phosphate anion to protonated O-acylated

hydroxylamine [3]. In other words, the course of the reaction should depend on oxidation potentials of phosphate anion and its sulfur and selenium analogs **5**. To verify this hypothesis we measured oxidation potentials of phosphate anions **5** by cyclic voltamperometry technique. The results are summarized in Table 2.

Table 2. Redox potentials of phosphate anions **5**.

 5a - f			
	X	Y	E [V] 5
a	O	O	above 2.0
b	O	S	0.8
c	S	S	0.56
d	O	Se	0.42
e	S	Se	0.23
f	Se	Se	0.24

The all measurements were performed for potassium salts of **5a-f** (0.001 M) in the solution of 0.1 M TBAP (tetrabutylammonium perchlorate) in acetonitrile. Working electrode; glassy carbon (3 mm diameter), counter electrode was a platinum wire, and as a reference electrode was used a saturated calomel electrode (SCE). All measurements were made on Autolab 30 electroanalytical system.

Data presented in the Table 2 show, that oxidation potentials of phosphate anions **5** decrease with increasing of the atomic mass of chalcogen X, Y dramatically. The electrochemical measurements indicated, that replacement of at least one oxygen atom for sulfur or selenium in phosphoric acid **1** molecule decreased the oxidation potential of anions **5** and improved their ability as a SET donor.

Conclusions

Sulfur and selenium analogs of phosphoric acids **1b-f** reacted with O-acylated hydroxylamine **2** with N-O bond cleavage. The course and products of the reaction depended on structure of used phosphoric acid derivatives. Monothiophosphate anion **5b** possesses low enough oxidation potential and can participate in the reaction as a SET donor, analogically to dithiophosphoric acid **1c** [1,3]. They lead to tert-butylammonium thiophosphates **3b,c** and disulfides **4b,c**. Additionally, in the case of selenothiophosphoric **1e** acid subsequent conversion of selenosulfide **4e** to symmetric diselenide **6e** and pivaloyl disulfide **7** was observed.

Literature

- [1] L. Doszczak, W. Przychodzen, D. Witt, J. Rachon, Phosphorus, Sulfur and Silicon, 177 (2002) 1851.
- [2] G. Brunton, B. C. Gilbert and R. J. Mawby, J. Chem. Soc. Perkin Trans. 2, (1976) 650.
- [3] L. Doszczak, W. Przychodzen, D. Witt, J. Rachon, J. Chem. Soc., Perkin Trans. 2 (2002) 1747.
- [4] A. B. Peňňory, A. B. Pierini, R. A. Rossi, J. Org. Chem., 49 (1984) 3834.
- [5] R. D. Gorak, N. I. Zemlanski, Zh. Obsch. Khim., 41 (1970) 1994.

SYNTHESIS AND INITIAL PHYSICO-CHEMICAL
INVESTIGATIONS OF HETERONUCLEAR Cu(II)-Nd(III)
COMPOUND

B. Cristóvão^{1*}, W. Ferenc¹ and J. Sarzyński²

¹*Faculty of Chemistry, Maria Curie-Skłodowska University, Pl 20-031, Lublin, Poland*

²*Institute of Physics, Maria Curie-Skłodowska University, Pl 20-031, Lublin, Poland*

**Author for correspondence: e-mail: cristovao@poczta.onet.pl*

ABSTRACT

The heteronuclear copper(II)-neodymium(III) compound having formula $[\text{Nd}(\text{H}_2\text{O})_5(\text{CuL})_2][\text{CuL}] \cdot 8\text{H}_2\text{O}$ was obtained by reacting $\text{Na}[\text{CuL}]$ (where L = Schiff base) with NdCl_3 . The complex was characterized by elemental analysis, thermogravimetric studies, ASA and magnetic measurements. Magnetic susceptibility measurements were carried out in the range of 76 – 303 K. The magnetic susceptibility data change with temperature according to the Curie-Weiss law with $\Theta = -35$ K. The magnetic moment decreases from $5,00\mu_B$ at 303 K to $4,38\mu_B$ at 76 K.

INTRODUCTION

Heteronuclear compounds are the subject of the investigations for the reason of their particular physical and chemical properties. Besides they can be treated as models for investigation of magnetic exchange involving *d* and *f* electrons and because of their potential applications in production of high temperature superconductors and magnetic materials [1-7]. In this paper we have described synthesis and magnetic properties of $[\text{Nd}(\text{H}_2\text{O})_5(\text{CuL})_2][\text{CuL}] \cdot 8\text{H}_2\text{O}$.

EXPERIMENTAL

The violet crystals of $[\text{Nd}(\text{H}_2\text{O})_5(\text{CuL})_2][\text{CuL}] \cdot 8\text{H}_2\text{O}$ were prepared in the following way: glycylglycine (5mmol), 5-bromosalicylaldehyde (5 mmol) and NaOH (10 mmol) were dissolved and stirred in hot EtOH/H₂O (v : v = 1 : 1). $\text{CuCl}_2 \cdot 2\text{H}_2\text{O}$ (5mmol) was then added to the solution and the resulting solution was adjusted to pH ~ 9. Last excess of NdCl_3 (8 mmol) was added. The solution was filtered and the filtrate was allowed to evaporate slowly at room temperature.

The contents of carbon, hydrogen and nitrogen in the obtained compound were determined by elemental analysis using a CHN 2400 Perkin Elmer analyser. The contents of metals were established by ASA method using ASA 880 spectrophotometer (Varian).

Anal. Calcd. for $\text{C}_{33}\text{H}_{48}\text{O}_{24}\text{N}_6\text{Br}_3\text{Cu}_3\text{Nd}$: C, 26.6 %; H, 3.2 %; N, 5.7 %; Cu, 12.8 %; Nd, 9.7 %. Found: C, 27.8 %; H, 2.7 %; N, 5.5 %; Cu, 12.2 %; Nd, 10.3 %.

The dehydration process of Cu(II)–Nd(III) complex was studied in air using a Setsys 16/18 TG, DTA instrument. The experiment was carried out under air flow in the

temperature range of 297–773 K. The sample (4.86 mg) of compound was heated in Al₂O₃ crucibles.

The magnetic susceptibility values of the Cu(II)-Nd(III) complex were determined by Gouy method in the temperature range of 76 – 303 K. The calibrant employed was Hg[Co(SCN)₂] for which the magnetic susceptibility of 1.644·10⁻⁵ cm³g⁻¹ was taken. Correction for diamagnetism of the constituent atoms was calculated by the use of Pascal's constants [8]. The effective magnetic moment values were calculated from the equations:

$$\mu_{\text{eff}} = 2.83 (\chi_M \cdot T)^{1/2} \quad (1)$$

$$\mu_{\text{eff}} = 2.83 [\chi_M (T - \Theta)]^{1/2} \quad (2)$$

RESULTS AND DISCUSSION

The new heteronuclear copper(II)–neodymium(III) compound was synthesised and next on the basis of elemental analysis, thermal analysis, ASA and the literature of subject its formula [Nd(H₂O)₅(CuL)₂][CuL]·8H₂O (where L = Schiff base derived from 5-bromosalicylaldehyde and glycyglycine) was established. The dehydration process of the obtained complex was studied in air atmosphere in the temperature range of 297–773 K. The Cu(II)–Nd(III) complex is stable up to 323 K. Next at 323 – 473 K it dehydrates in one step losing all molecules of lattice water. The mass loss calculated from TG curve being equal to 10.6% corresponds to the loss of 8 molecules of water (theoretical values is 9.7 %). The dehydration process is connected with an endothermic effect seen on DTA curve.

Experimental magnetic data plotted as magnetic susceptibility χ_g , $1/\chi_g$ and magnetic moment μ_{eff} versus temperature are presented in Table 1 and Figs. 1, 2 and 3.

Table 1. The magnetic data of [Nd(H₂O)₅(CuL)₂][CuL]·8H₂O

[Nd(H ₂ O) ₅ (CuL) ₂][CuL]·8H ₂ O					
T (K)	$\chi_g \cdot 10^6$ (cm ³ /g)	μ_{eff} (μ_B)	T (K)	$\chi_g \cdot 10^6$ (cm ³ /g)	μ_{eff} (μ_B)
76	20.697	4.38	213	8.731	4.83
123	14.870	4.74	223	8.364	4.85
133	12.041	4.46	233	8.005	4.85
143	11.617	4.54	243	7.732	4.88
153	10.957	4.57	253	7.468	4.89
163	10.910	4.70	263	7.232	4.92
173	10.532	4.76	273	7.015	4.94
183	10.052	4.79	283	6.846	4.97
193	9.505	4.79	293	6.619	4.98
203	9.146	4.83	303	6.440	5.00

The magnetic susceptibility changes with temperature according to the Curie-Weiss law with $\Theta = -35$ K indicating the weak antiferromagnetic interaction in this complex (Table 1, Figs. 1, 2).

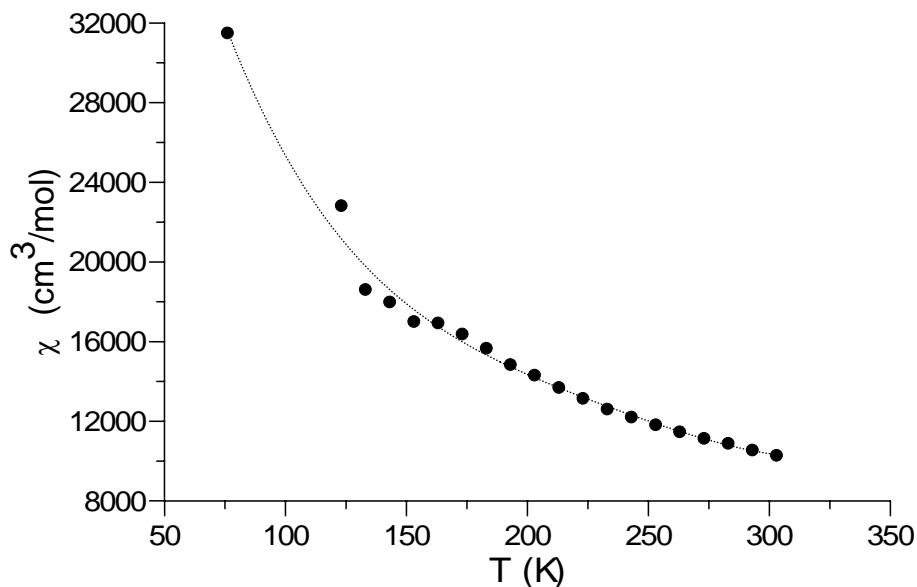


Fig. 1. Experimental magnetic data plotted as magnetic susceptibility χ_g versus temperature

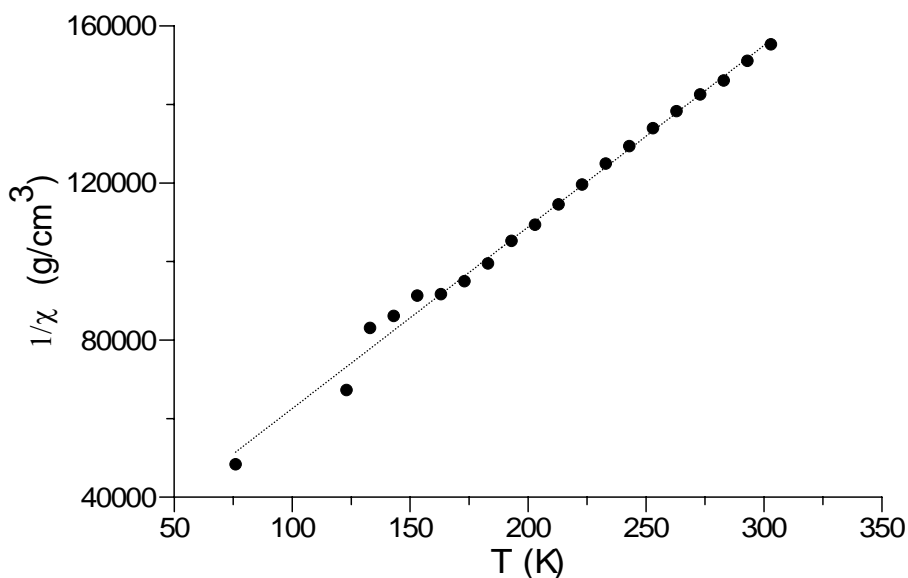


Fig. 2. Experimental magnetic data plotted as $1/\chi_g$ versus temperature

The magnetic moment values decrease from $5,00\mu_B$ at 303 K to $4,38\mu_B$ at 76 K (Table 1, Fig. 3). This decrease could be also caused by crystal-field effects as well as a cooperative antiferromagnetic interaction of metal ions [1, 2, 9, 10].

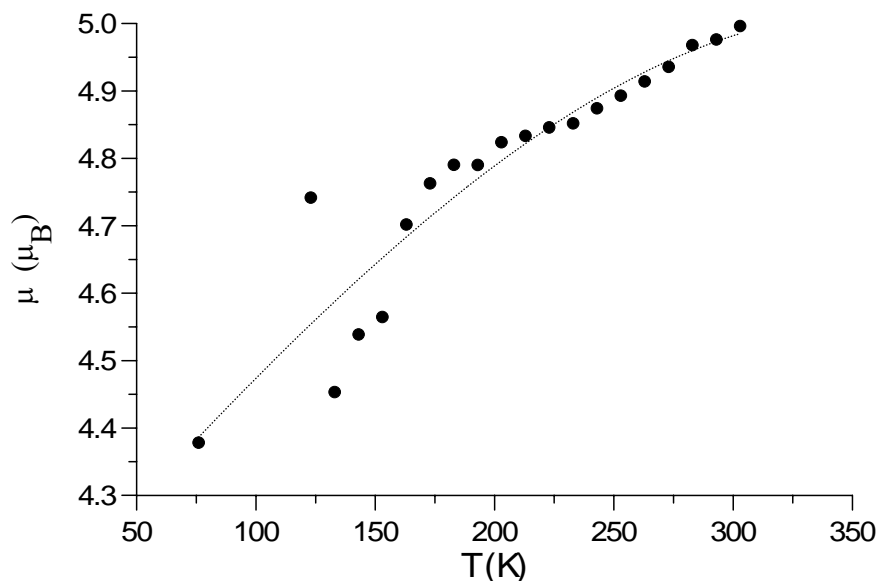


Fig. 3. Experimental magnetic data plotted as magnetic moment μ_{eff} versus temperature

The magnetic measurements of $[\text{Nd}(\text{H}_2\text{O})_5(\text{CuL})_2][\text{CuL}] \cdot 8\text{H}_2\text{O}$ in the temperature range of 1.7 – 76 K and the mechanism of the $d-f$ system interaction in this heteronuclear compound will be the subject of future studies.

CONCLUSIONS

A novel heteronuclear compound $[\text{Nd}(\text{H}_2\text{O})_5(\text{CuL})_2][\text{CuL}] \cdot 8\text{H}_2\text{O}$ has been prepared. Its magnetic moment and magnetic susceptibility values decrease with temperature which can be due to crystal field effect and antiferromagnetic interactions of pairs of metal ions.

REFERENCES

- [1] Y. Zou, W.-L. Liu, S. Gao, C.-S. Lu, D.-B. Dang, Q.-J. Meng, *Polyhedron*, 23 (2004) 2253.
- [2] B. Wu, W. Lu, X. Zheng, *Trans. Met. Chem.*, 28 (2003) 323.
- [3] M. Andruh, I. Ramade, E. Codjovi, O. Guillou, O. Kahn, J. C. Trombe, *J. Am. Chem. Soc.*, 115 (1993) 1822.
- [4] Q. Y. Chen, Q. H. Luo, Z. L. Wang, J. T. Chen, *J. Chem. Soc. Chem. Commun.*, (2000) 1033.
- [5] X. M. Chen, M. S. J. Aubin, Y. L. Wu, Y. S. Yang, T. C. W. Mark, D. N. Hendrickson, *J. Am. Chem. Soc.*, 117 (1995) 9600.
- [6] S. Wang, Z. Pang, D. L. Smith, *Inorg. Chem.*, 32 (1993) 4992.
- [7] E. K. Brechin, S. G. Harris, S. Parson, R. E. Winpenny, *J. Chem. Soc., Dalton Trans.*, (1997) 1665.
- [8] E. König, *Magnetic Properties of Coordination and Organometallic Transition Metal Compounds*, Springer Verlag, Berlin 1966.
- [9] E. Huskowska, J. Legendziewicz, *J. Alloys Comp.* 300-301 (2000) 303.
- [10] G. Oczko, J. Legendziewicz, J. Mroziński, G. Meyer, *J. Alloys Comp.* 275-277 (1998) 219.

ANALYSIS OF USEFULNESS OF THEORETICAL AND EMPIRICAL GARFINKLE EQUATIONS FOR COMPARISONS WITH LINEAR NONEQUILIBRIUM THERMODYNAMIC PHENOMENOLOGICAL EQUATION FOR CHEMICAL REACTION

Andrzej S. Cukrowski, Anna Kolbus

*Institute of Chemistry, Faculty of Mathematical and Natural Sciences,
Swietokrzyska Academy,*

Checinska 5, 25-020 Kielce, Poland

*Institute of Physical Chemistry, Polish Academy of Sciences,
Kasprzaka 44/52, 01-224 Warsaw, Poland*

After having read our paper [1] Garfinkle informed us that the papers [2,3] could be interesting for us. As we have found the results presented in these and other papers of this author (see, e.g. [4,5]) not trivial we have decided to analyze some of those results.

To write equations in a shorter form we introduce reduced dimensionless affinity α

$$\alpha = A / RT \quad (1)$$

where A , R and T denote the affinity, the universal gas constant and temperature, respectively. Using fundamental definitions for the rate of chemical reaction and dependence of chemical potential on concentration Garfinkle [4] derived the following theoretical equation

$$d\alpha / dt = -\nu \sum (v_i^2 / c_i) \quad (2)$$

where t , ν , v_i , c_i are the time, the reaction rate, stoichiometric coefficients, and concentrations, respectively. Analyzing the affinity decay for numerous experimental data for chemical reactions Garfinkle obtained the following experimental relation

$$d\alpha / dt = A_r [1/t - 1/t_k] \quad (3)$$

where A_r is the affinity rate constant and t_k is the expected (most probable) time to attain the equilibrium. Hjelmfelt et al [6] have shown that eq. (3) can be treated as an approximate expression only and t_k which should be infinite can be treated as an artifact of that representation only. So, one could conclude that t_k can not be treated as a useful quantity. However, Garfinkle emphasized that his natural path approach was developed to bridge the gap between the mass action and nonequilibrium thermodynamic approaches. We decided to check if Garfinkle equations can be useful for an analysis of the range in which the formalism of linear nonequilibrium thermodynamics can be used.

We present the analysis of two simple reactions only.

I. The reaction $A \leftrightarrow B$ with concentrations $c_A + c_B = c_0 = \text{const}$ and starting from $c_B = 0$. We can obtain

$$c_A = c_0 k_r / (k_f + k_r) + [c_0 k_f / (k_f + k_r)] \cdot \exp[-(k_f + k_r)t] \quad (4)$$

where k_f and k_r are the rate constants for the forward and reverse reactions,

$$\nu = -dc_A / dt = c_0 k_f \exp[-(k_f + k_r)t] \quad (5)$$

$$d\alpha / dt = -(k_f + k_r)^2 / \{k_f [1 - \exp[-(k_f + k_r)t]] - k_r [1 - \exp[(k_f + k_r)t]]\} \quad (6)$$

$$\lim_{t \rightarrow \infty} d\alpha / dt = [(k_f + k_r) / (k_f k_r c_0)] d\nu / dt \quad (7)$$

We can rewrite this equation as

$$dv/dt = L \lim_{t \rightarrow \infty} d\alpha/dt \quad (8)$$

where

$$L' = k_f k_r c_0 / (k_f + k_r) = k_f c_A^{eq} \quad (9)$$

where the index *eq* denotes the chemical equilibrium.

We can also assume that if only *t* is sufficiently large (*v* and α are sufficiently small) we can rewrite eqs. (8) and (9) in a form

$$v = L' \alpha = (L'/RT)A = LA \quad (10)$$

$$L = k_f c_A^{eq} / RT \quad (11)$$

So, we can see that if the time is large enough we can derive from the theoretical Garfinkle equation the phenomenological coefficient *L* in the same form as that derived in [1] which is also in agreement with the result of Baranowski [7] obtained in a different way.

In order to analyze the experimental Garfinkle equation we consider a simplified case of the reaction $A \leftrightarrow B$ for which

$$k_f = k_r = k \quad (12)$$

In this case eq. (6) simplifies to

$$d\alpha/d\tau = -2/\sinh 2\tau \quad (13)$$

where τ is a dimensionless quantity

$$\tau = kt \quad (14)$$

It is convenient to introduce

$$\xi = 1/\tau \quad (15)$$

and to analyze the derivative $d\alpha/d\tau$ as a function of ξ in the following form

$$-d(d\alpha/d\tau)/d\xi = D(\xi) \quad (16)$$

We can see that the derivative $D(\xi)$ have the following properties:

1. $\lim_{\xi \rightarrow 0} D(\xi) = 0$ (17)

2. For small ξ the derivative $D(\xi)$ is an increasing function of ξ

3. For $\xi = 1.245$ the maximum value

$$D(1.245) = 1.169 \quad (18)$$

corresponding to an inflection point of the function

$$f(\xi) = d\alpha/d\tau \quad (19)$$

is obtained

4. For ξ larger than 1.245 the derivative $D(\xi)$ is a decreasing function of ξ

5. After taking into account that $\lim_{\tau \rightarrow 0} \sinh 2\tau = 2\tau$ from eqs. (13) and (16) we see that

$$\lim_{\xi \rightarrow \infty} D(\xi) = 1 \quad (20)$$

That is why (in some ranges of ξ) $f(\xi)$ can be treated as nearly a straight line. Usually experimental points for reaction are obtained for the appropriate range of *t* in which concentrations of product can be accurately measured. This range of *t* corresponds to some ranges of τ and ξ . One can draw a straight line through experimental points. If the range of ξ is not too large the curve $f(\xi)$ can be approximated by $y(\xi)$ which is a tangent (straight) line. The intercept of $y(\xi)$ with the axis ξ can be obtained in a form

$$\xi_k = \xi - y/(dy/d\xi) \quad (21)$$

If the experimental points are in the range of ξ corresponding to the maximum magnitude of $D(\xi)$ we get the maximum value of the intercept of ξ_k equal to $\xi_k(\max)$

$$\xi_k(\max) = 0.535 \quad (22)$$

$$0 < \xi_k < 0.535 \quad (23)$$

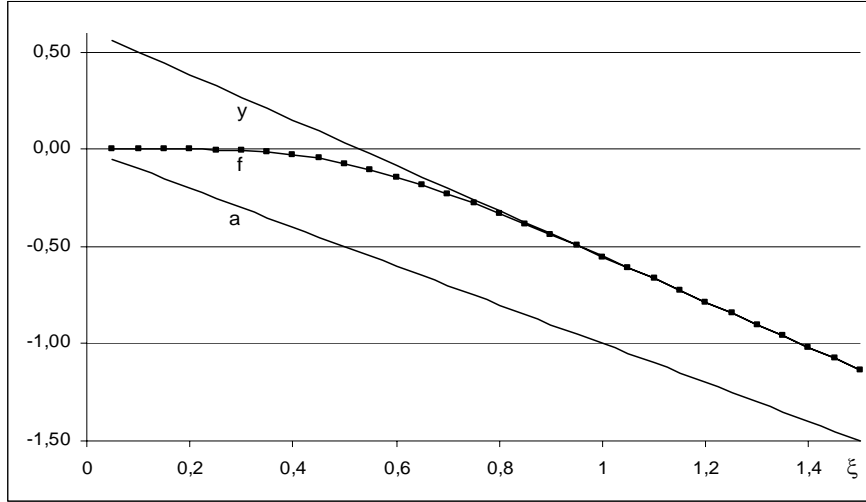


Fig. 1

In Fig. 1 we show $f(\xi)$ (see eq. (19)) as a function of ξ (see eqs. (13) and (15)) and additionally present the straight tangent line for $f(1.245)$ giving the intercept for $\xi = \xi_k(\max) = 0.535$ and the asymptote $f(\xi) = -\xi$ (denoted by f, y, a, respectively).

We can also write

$$\tau_k(\min) = 1/\xi_k(\max) \quad (24)$$

$$1/0.535 < \tau_k < \infty \quad (25)$$

$$1/0.535k < t_k < \infty \quad (26)$$

For example if $D(\xi) = 1$ one gets $\xi_k = 0$ which would correspond to the very early stages of chemical reaction when the concentration of product is nearly equal to 0. However, from eqs (4), (12), (14) and (15) it follows that for $\xi = 1.245$, i.e., for the inflection point, the molar fraction of product $x_B = 0.400$ and $\xi_k(\max)$ calculated from eq. (21) is equal to 0.535 and $\tau_k(\min) = 1/0.535$. For larger magnitudes of ξ , e.g. $\xi = 2$ ($\tau = 1/2$) we have $x_B = 0.316$ and $\xi_k = 0.477$ ($\tau_k = 1/0.477$). Naturally, in this case the experiments would be performed for a shorter time than those performed near to the inflection point. From Fig. 5 in Ref. [1] we see that the linear nonequilibrium thermodynamic phenomenological equation (for which the chemical reaction rate is proportional to the affinity) can be used for $0.3 < x_B < 0.5$. It means that those ranges of x_B are obtained if only τ_k does not differ much from $\tau_k(\max)$. The same conclusion can be drawn if t_k (see eqs. (14) and (24)-(26)) is analyzed. It should be emphasized that t_k is the quantity introduced by Garfinkle in eq. (3).

II. The second reaction analyzed by us is $A + A \leftrightarrow B + B$ in the simplified case when $k_f = k_r = k$ and for the concentrations $c_A + c_B = c_0 = \text{const}$ and starting from $c_B = 0$. We can obtain

$$c_A = (1/2)c_0[1 + \exp(-4c_0kt)] \quad (27)$$

$$v = (-1/2)dc_A/dt = -c_0^2k \exp(-4c_0kt) \quad (28)$$

$$d\alpha/dt = -8c_0k/[\exp(4c_0kt) - \exp(-4c_0kt)] \quad (29)$$

In the same way as for the reaction $A \leftrightarrow B$ we can derive

$$L' = (c_0^2 / 4)k = k(c_A^{eq})^2 \quad (30)$$

$$L = k(c_A^{eq})^2 / RT \quad (31)$$

It is worthwhile to observe that recently we have shown that the generally known following relation between ν_A and A/RT [8,9]

$$\nu_A = \nu_{Af} [1 - \exp(-\alpha)] \quad (32)$$

where ν_{Af} is the forward reaction rate, can be written in a form [1,10,11]

$$\nu_A = L'[(1 + \sqrt{K})/(\sqrt{K} + \exp \alpha)]^2 [1 - \exp(-\alpha)] \quad (33)$$

which is convenient in an analysis of the range of molar fraction of product for which the linear phenomenological nonequilibrium thermodynamic equation is a sufficient approximation (K is the thermodynamic equilibrium constant).

We can also write eq. (29) in the form

$$d\alpha / d\tau' = -2 / \sinh 2\tau' \quad (34)$$

introducing

$$\tau' = 2c_0 kt \quad (35)$$

$$\xi' = 1 / \tau' \quad (36)$$

we could also introduce $D(\xi')$, $f(\xi')$, $y(\xi')$, $\xi'_k(\max)$, $\tau'_k(\min)$ in the same way as we have done for the reaction $A \leftrightarrow B$. We would obtain the time t_k introduced by Garfinkle

$$1/1.070kc_0 < t_k < \infty \quad (37)$$

If we introduce $\tau'_k(\min) = 1/0.535$ to eq. (27) we can get $x_B = 0.400$. We can compare this result with the range $0.35 < x_B < 0.5$ (see Fig. 3 in Ref. [1]) and draw similar conclusions as those for reaction $A \leftrightarrow B$. The only difference is that in eq. (34) the concentration c_0 appears.

Just to summarize: 1. for very simple chemical reactions such as $A \leftrightarrow B$ and $A + A \leftrightarrow B + B$ we have shown that the time t_k introduced by Garfinkle can be useful. If only t_k does not differ much from $t_k(\min)$ the linear relation between the reaction rate and the affinity (used within the formalism of linear nonequilibrium thermodynamics) can be treated as a sufficient approximation. 2. We have also shown that the expression for the phenomenological coefficient L (see eqs. (11) and (31)) can be derived from the Garfinkle theoretical equation (for a large time) in the same form as that derived in Refs. [1] and [7].

References

1. A.S. Cukrowski, A. Kolbus, Acta Phys. Polon. B 36 (2005) 1485.
2. M. Garfinkle, Discrete Dynamics Nature Society, 4 (2000) 145.
3. M. Garfinkle, J. Phys. Chem. A 106 (2002) 490.
4. M. Garfinkle, J. Phys. Chem. 79 (1983) 2779.
5. M. Garfinkle, J. Phys. Chem. 93 (1989) 2158.
6. A. Hjelmfelt, J.L. Brauman, J. Ross, J. Chem. Phys., 92 (1990) 3569.
7. B. Baranowski "Termodynamika nierównowagowa w chemii fizycznej", PWN, Warszawa 1974 (in Polish).
8. J. Ross, P. Mazur, J. Chem. Phys. 35 (1961) 19.
9. P. Glansdorf, I. Prigogine, Thermodynamic Theory of Structure, Stability and Fluctuations, Wiley, London 1971.
10. A. Kolbus, A.S. Cukrowski, Annals Polish Chem. Soc. 2/III (2003) 1048.
11. A.S. Cukrowski, A. Kolbus, Annals Polish Chem. Soc. 3/3 (2004) 1274.

QUALITATIVE AND QUANTATIVE DETERMINATION OF Cu(II) CONTENT IN STRAWBERRIES - STUDENT EXERCISE AT THE ACADEMY OF AGRICULTURE IN WARSAW

Beata Dasiewicz, Katarzyna Dobrosz-Teperek
SGGW, Katedra Chemii WTŻ, ul. Nowoursynowska 159c, 02-776 Warszawa

Introduction

The dynamic development of science and technology calls for new ways of educating students. The classical XIX century chemical analysis undoubtedly teaches the basics of chemistry and helps in comprehending the learning material. However, in the process of educating students who are going to enter their professional careers in the near future and will face various challenges, it would not be advisable to leave out the present-day methods of analysis. Having this in mind the authors of this article decided to design an exercise which would combine the elements of both classical and modern analysis.

The experiment

The research material is strawberries. The student exercise consists of two parts.

I. The classical qualitative determination of copper ion (II) content.

Description of the experiment:

Equipment: chromatographic plate covered with silica gel, mortar, 100 cm³ beaker, test-tube, chromatographic chamber or beaker with a closely fitting glass lid, atomizer or wash bottle, capillary tube, filter paper, UV lamp.

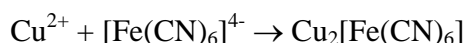
Reagents: 2-3 strawberries, copper(II) chloride solution of approximately 10%, ethanol, concentrated hydrochloric acid, potassium hexacyanoferrate (II) solution of approximately 6%.

Execution:

- 1 Grind the strawberries in the mortar, put them into the beaker and add 20 cm³ of distilled water. Heat up and keep the content of the beaker boiling for about 5 minutes.
- 2 Trickle the content of the beaker into the test-tube. Place a specimen quantity of the obtained solution on the chromatographic plate using the capillary tube. Next to it place the solution of copper (II) chloride, which will serve as a reference standard. Dry the plate.
- 3 Pour the solvent mixture into the chromatographic chamber. Its layer should not exceed 0,5 cm. The solvent mixture consists of ethanol, concentrated hydrochloric acid and water in the voluminal ratio of 20:5:5.
- 4 Place the dried plate in the previously prepared chromatographic chamber at the angle

of approximately 15°. Cover the chamber tightly. After about 20-25 minutes, when the front of the solvent situates itself 1cm from the edge of the plate, take the plate out and dry it.

- 5 Examine the plate in UV light. Notice the darker spots located in the same point in the strawberry extract and the reference standard solution.
- 6 Spray the plate with potassium hexacyanoferrate (II) solution. Notice some brown spots in the point examined in UV light (Fig.1). The spots originate from the complex created by the ion of copper and the ions of hexacyanoferrate (II):



The appearance of the colored complex and the spots visible in UV light undoubtedly prove the presence of ions of copper (II) in the examined fruit [1].

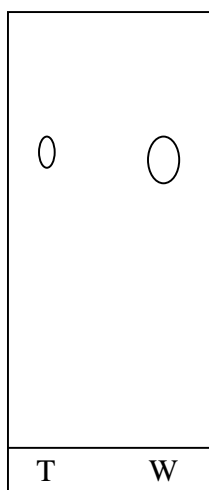


Fig. 1. Chromatographic plate. T – the strawberry extract, W - the reference standard solution

II. The quantitative determination of copper content.

This part of the experiment cannot be conducted by the students by their own means. The material for determination should be examined by a laboratory that specializes in instrumental analysis.

- 1 The students get to know the method and aim of mineralization in theory. It is a modern method that includes the use of a microwave device. It differs from the older methods in the quickness of specimen preparation (only 30 minutes), in the lack of loss of specimen and the highly volatile components it contains (because the whole mineralization process takes place in the same closed container) and in the elimination of the outside pollution. The dry matter of the solid specimen should weigh around 2 g. The effect of the microwave mineralization is that the organic material is destroyed and the specimen becomes a water solution, which later undergoes further examination.

- 2 The subsequent analysis of the mineralized specimens is conducted by means of Atomic Absorption Spectroscopy (AAS). The atoms demonstrate the ability to absorb the radiation, which is a characteristic of the particular chemical elements [2,3]. The induction of the absorption effect requires atomization of the specimen, i.e. (that is) its evaporation and dissociation of the molecules into atoms. The AAS is a very sensitive analytic method that renders the specific determination of the content of various elements possible. The lower limit of the determination of copper content is 0,03 mg/l
- 3 The AAS spectrophotometer consists of a source of characteristic radiation, an atomizer for creating atomic gas, a monochromator (for example a diffraction grating) and a detector (photomultiplier). The source of radiation very often consists of special lamps containing atoms induced to emit radiation. The specimen (in the form of water solution) undergoes atomization in a special acetylene blowpipe or a graphite furnace that is electrically heated up to a very high temperature[3,4].

Results

The qualitative determination of copper content in strawberries is immediate and does not create any difficulties for the students.

The results of the quantitative determination, which the students receive in the form of figures, call for further interpretation. The content of copper in the specimen after mineralization oscillates between 0,032-0,075 mg/l. The students convert the acquired results to the copper content per one kilogram of the examined material. They assess whether the determined quantity falls within the permissible limits. A low content of copper can in particular be the evidence of deficiency of this element in the soil, which has an influence on the crop yield. Among the pomicultural plants, strawberries are particularly susceptible to copper deficiency. This deficiency is capable of causing the appearance of white spots on the plant's leaves and can even suppress the plant's growth.

The exercise is of particular importance to the students of pomiculture because it provides them with directions on how to make good use of modern chemical analysis in the production of healthy, ecological food in the future.

References (in Polish):

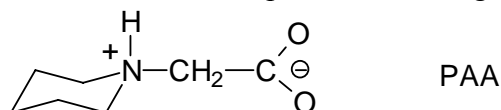
- [1] Z. Matysikowa, R. Piosik, Z. Warnke, *Doświadczenia chemiczne dla szkół średnich*, WSiP, Warszawa 1987.
- [2] J. Minczewski, Z. Marczenko, *Chemia analityczna t.2*, Wydawnictwo Naukowe PWN, Warszawa 2005.
- [3] W. Szczepaniak, *Metody instrumentalne w analizie chemicznej*, Wydawnictwo Naukowe PWN, Warszawa 1996.
- [4] B. Weltz, *Atomic Absorption Spectrometry*, VCH Weinheim 1985.

STRUCTURE OF THE COMPLEX OF PIPERIDINEACETIC ACID WITH *p*-HYDROXYBENZOIC ACID AND RELATED COMPOUNDS

Z. Dega-Szafran, G. Dutkiewicz, Z. Kosturkiewicz, M. Szafran

Faculty of Chemistry, Adam Mickiewicz University, Grunwaldzka 6, 60-780 Poznań, Poland

1-Piperidineacetic acid (PAA) can be treated as a synthetic aminoacid in which the amino group is involved in an alicyclic ring. PAA, like typical aminoacids, exists in a zwitterion form in the solid [1] and in aqueous solution [2], but in the isolated molecule appears in the neutral form [1]. Because of its amphoteric character PAA forms complexes with acid in the 1:1 and 2:1 stoichiometry. The aim of this work is a comparison of eight structures of PAA complexes with inorganic acids and phenols.



The 1:1 complexes of PAA with HCl [3], HClO₄ [4], 2,6-dichloro-4-nitrophenol (DCNP) [5] and 2,4-dinitrophenol (24DNP) [6], solved by X-ray diffraction, have three different type structures.

In PAAH·Cl, the PAA is protonated and engaged in the intermolecular COOH...Cl⁻ hydrogen bond with chlorine anion. Each of the chlorine anions is involved in the COOH...Cl and N⁺-H...Cl hydrogen bonds. The structure in the crystals is organized in the sandwich like infinite two-dimensional layers (Fig. 1a, Table 1) [1].

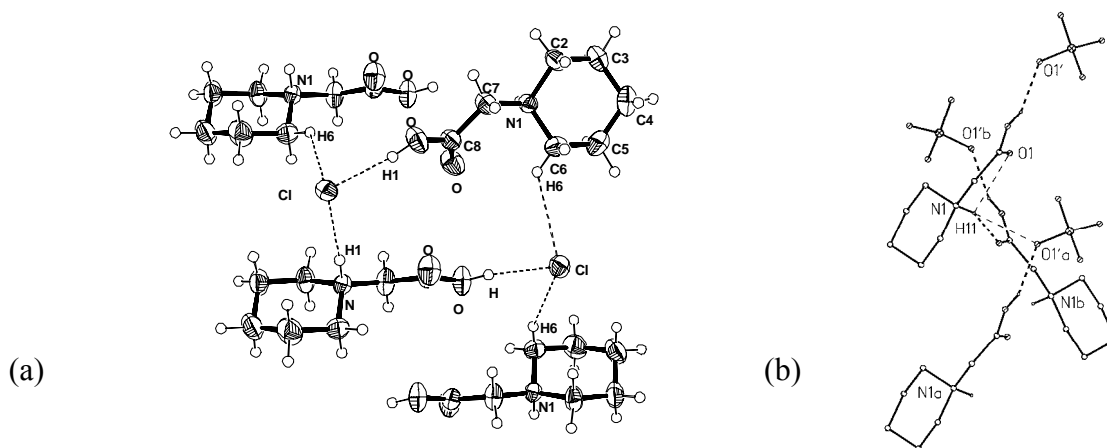


Fig. 1. Molecular structure and hydrogen bonds in the crystals of (a) 1-piperidiniumacetic acid chloride and (b) 1-piperidiniumacetic acid perchlorate

In PAAH·ClO₄ the COOH group is involved in two hydrogen bonds, with ClO₄⁻ anion and with N⁺-H atom of a neighboring molecule, related by the twofold screw axis parallel to *x*. The N⁺H atom forms trifurcated hydrogen bond, the intermolecular with OClO₃⁻ and COOH, and intramolecular with the C=O group. (Fig. 1b, Table 1) [4].

Table 1
Geometrical parameters of the hydrogen bonded complexes of 1-piperidineacetic acid (PAA) with acids (AH)

AH	Crystal system	Space group	COO \cdots donor	N ⁺ -H \cdots acceptor	Ref
1:1 complexes					
HCl	Monoclinic	P2 ₁ /c	2.964(1)	3.062(1) ^a	3
HClO ₄	Orthorhombic	P2 ₁ 2 ₁ 2 ₁	2.664(1)	2.957(1) ^b	4
DCNP	Triclinic	P $\bar{1}$	2.469(2)	2.869(2) ^c	5
24DNP	Triclinic	P $\bar{1}$	2.500(3) A 2.431(3) B	2.875(3) ^c A 2.797(3) ^c B	6
2:1 complexes					
HCl	Triclinic	P $\bar{1}$	2.463(3) ^d A 2.462(3) ^d B	2.755(2) ^c B 3.167(2) ^a A 2.717(2) ^c B	7
HClO ₄	Monoclinic	C2/c	2.441(3) ^d	2.766(2) ^c	8
TNP	Monoclinic	P2 ₁ /c	2.472(5) ^d	2.735(5) ^c 2.747(5) ^e	9
HBA	Monoclinic	C2	2.589(2) ^f 2.519(2) ^d	2.773(3) ^c 2.820(3) ^c	This work

Types of hydrogen bonds:

a) N⁺-H \cdots Cl; b) N⁺-H \cdots OCIO₃; c) N⁺-H \cdots O=C; d) COO \cdots HOOC; e) N⁺-H \cdots OPh; f) O-H \cdots OOC

In the crystal structure of the 1:1 complex of PAA with 2,6-dichloro-4-nitrophenol (DCNP) PAA is linked with DCNP through the O \cdots H-O hydrogen bond. Two such complexes form a centrosymmetric dimer, (PAA·DCNP)₂, in which PAA moieties, as zwitterions, are joined by two N⁺-H \cdots O hydrogen bonds, around the symmetry center (Fig. 2a, Table 1) [5].

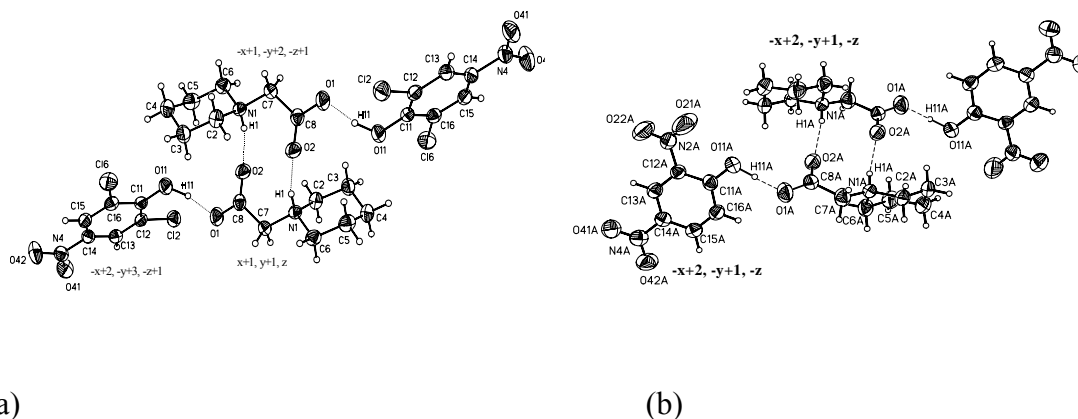


Fig. 2. Molecular arrangement of the complex of 1-piperidineacetic acid with DCNP (a) and 24DNP (dimer A) (b).

A similar structure as in $(\text{PAA}\cdot\text{DCNP})_2$ has the 1:1 complex of PAA with 2,4-dinitrophenol (24DNP). PAA forms with 24DNP two non-equivalent centrosymmetric dimers, denoted as A and B, through $\text{O}\cdots\text{H}\cdots\text{O}$ hydrogen bonds of different lengths, in which two PAA moieties are joined by two $\text{N}^+\text{-H}\cdots\text{O}$ hydrogen bonds, around two different symmetry centers. The difference between A and B is explained by a participation of B in a greater number of the intermolecular $\text{C}\cdots\text{H}\cdots\text{O}$ hydrogen bonds (Fig. 2b, Table 1) [6].

In the 2:1 complexes of PAA with HCl and HClO_4 homoconjugated cations with short symmetric hydrogen bonds are formed.

The crystals of $(\text{PAA})_2\text{H}\cdot\text{Cl}$ belong to the triclinic system with two symmetrically independent hydrogen bonded complexes (A and B) at two different inversion centers. Four 1-piperidiniumacetates, as zwitterions, are held together by a network of hydrogen bonds of the types $\text{O}\cdots\text{H}\cdots\text{O}$, $\text{N}^+\text{-H}\cdots\text{O}=\text{C}$ and $\text{N}^+\text{-H}\cdots\text{Cl}$. Two carboxylate groups are bridged by linear and centrosymmetric $\text{O}\cdots\text{H}\cdots\text{O}$ hydrogen bonds. Two complexes play different roles in the crystals. In complex A both N-H atoms interact with chlorine anions by two $\text{N}^+\text{-H}\cdots\text{Cl}$ hydrogen bonds, while in complex B the $\text{N}^+\text{-H}$ atoms participate only in intra and inter-molecular hydrogen bonds with the COO^- groups (Fig. 3a. Table 1) [7].

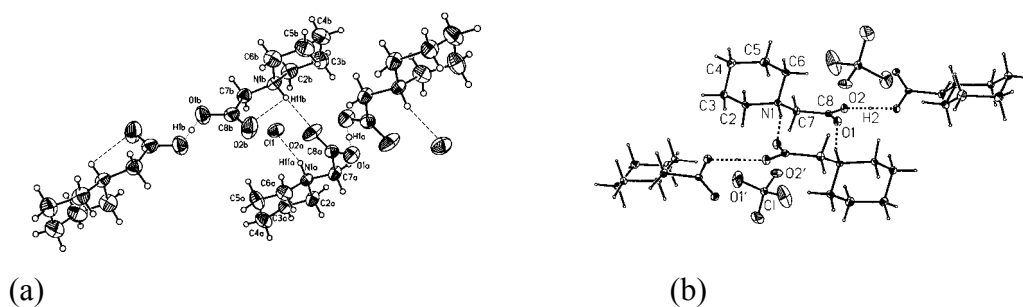


Fig. 3. Molecular structure and hydrogen bonds in the crystals of the 2:1 complexes of (a) 1-piperidineacetic acid with HCl and (b) with HClO_4 .

In the crystals of $(\text{PAA})_2\text{H}\cdot\text{ClO}_4$ two 1-piperidiniumacetate, as zwitterions, form a homoconjugated cation connected by the short and symmetrical $\text{O}\cdots\text{H}\cdots\text{O}$ hydrogen bond. These cations are related by the symmetry centre and are connected by the $\text{N}^+\text{-H}\cdots\text{O}=\text{C}$ hydrogen bonds. The ClO_4^- anion is not engaged in the hydrogen bonds, but interacts via Coulombic attraction with the positively charged nitrogen atoms (Fig. 3b Table 1) [8].

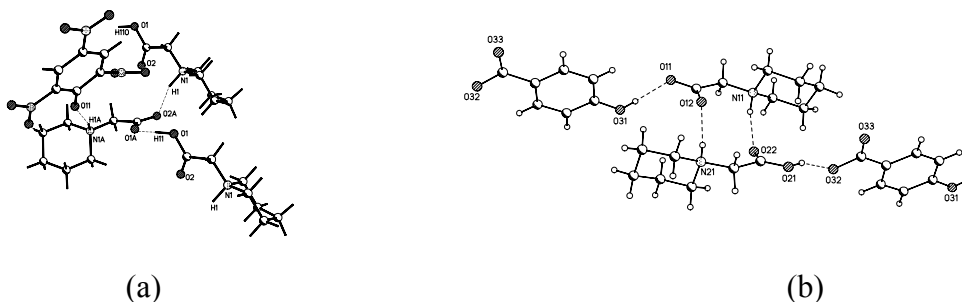


Fig. 4. Projection of the 2:1 complex of 1-piperidineacetic acid with TNP (a) and HBA (b).

The unusual 2:1 complex is formed by PAA with picric acid (TNP). In the crystals there are three kinds of molecules: 1-piperidiniumacetates, 1-piperidineacetic acid and picric anion. The molecules are joined together by two $N^+-H\cdots O$ and one $O-H\cdots O$ hydrogen bonds. The 1-piperidinium acetate molecules are linked with 1-piperidineacetic acid cations into infinite chain through the $O\cdots H-O$ hydrogen bonds. The N^+-H atom of the zwitterion interacts with phenolate oxygen atom by the $N-H\cdots O$ hydrogen bond (Fig. 4a, Table 1) [9]

In this work, a new 2:1 complex of PAA with p-hydroxybenzoic acid (HBA) has been synthesized. HBA has two donor groups, COOH and OH, hence we expected another hydrogen-bonded system in the complex investigated. Similarly as in $(PAA)_2TNP$, there are three kinds of molecules in the crystals: 1-piperidiniumacetate, 1-piperidineacetic acid and p-hydroxybenzoate anion, but the orientation of molecules in crystals are different. 1-Piperidiniumacetate and 1-piperidineacetic acid form the non-symmetrical cyclic dimer through two non-equivalent $N^+-H\cdots O=C$ hydrogen bonds. The p-hydroxybenzoate anion are linked with such dimer through the $O-H\cdots OOC$ hydrogen bond between the hydroxyl group of HBA and the carboxylate group of 1-piperidiniumacetate and with 1-piperidineacetic acid through $COO\cdots HOOC$ hydrogen bond, between the protonated cation and the benzoate anion (Fig. 4b, Table 1).

CONCLUSIONS

In all the complexes investigated the piperidine ring adopts a chair conformation with the CH_2COO substituent in the equatorial position.

In the 1:1 complexes of PAA with inorganic acids a proton is transferred from acid to PAA, while in the complexes with phenols two molecules of PAA, as zwitterions, form a cyclic dimer, which further interacts with organic molecules.

In the 2:1 complexes of PAA with HCl and $HClO_4$ two homoconjugated cations interact with each other by the $N-H\cdots O-C$ hydrogen bonds. The effect of the anion is different. The Cl^- anion is engaged in the $N-H\cdots Cl$ hydrogen bond, while the ClO_4^- anion interacts electrostatically with the positively charged nitrogen atom. In the 2:1 complexes of PAA with TNP and HBA, the PAA molecules form a linear or cyclic dimer, respectively, in which one molecule of PAA is protonated. The dimer is engaged in the $O-H-O$ hydrogen bonds with TNP^- and HBA^- anions.

In summary, the eight complexes investigated represent seven different structures. The hydrogen-bonded system depends more on the number of donor groups than on their acidity, however the determination of the role of the components in the hydrogen-bonded complexes of PAA with acids on their structures needs further investigation.

References

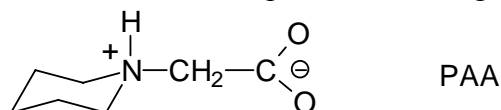
- [1] Z. Dega-Szafran, Z. Kosturkiewicz, E. Nowak, M. Petryna, M. Szafran, *J. Mol. Struct.*, 613 (2002) 37
- [2] P. Barczyński, Z. Dega-Szafran, E. Dulewicz, M. Petryna, M. Szafran, *Polish J. Chem.*, 74 (2000) 1149
- [3] Z. Dega-Szafran, G. Dutkiewicz, Z. Kosturkiewicz, M. Petryna, M. Szafran, *J. Mol. Struct.*, 690 (2004) 1
- [4] Z. Dega-Szafran, M. Petryna, E. Tykarska, M. Szafran, *J. Mol. Struct.*, 643 (2002) 69
- [5] Z. Dega-Szafran, G. Dutkiewicz, Z. Kosturkiewicz, M. Petryna, *J. Mol. Struct.*, 741 (2005) 115
- [6] Z. Dega-Szafran, G. Dutkiewicz, Z. Kosturkiewicz, M. Petryna, *J. Mol. Struct.*, 697 (2004) 151
- [7] Z. Dega-Szafran, M. Petryna, G. Dutkiewicz, Z. Kosturkiewicz, *Polish J. Chem.*, 77 (2003) 1501
- [8] Z. Dega-Szafran, M. Petryna, M. Szafran, E. Tykarska, *J. Mol. Struct.*, 688 (2004) 121
- [9] Z. Dega-Szafran, G. Dutkiewicz, Z. Kosturkiewicz, M. Petryna, *J. Mol. Struct.*, 708 (2004) 15

STRUCTURE OF THE COMPLEX OF PIPERIDINEACETIC ACID WITH *p*-HYDROXYBENZOIC ACID AND RELATED COMPOUNDS

Z. Dega-Szafran, G. Dutkiewicz, Z. Kosturkiewicz, M. Szafran

Faculty of Chemistry, Adam Mickiewicz University, Grunwaldzka 6, 60-780 Poznań, Poland

1-Piperidineacetic acid (PAA) can be treated as a synthetic aminoacid in which the amino group is involved in an alicyclic ring. PAA, like typical aminoacids, exists in a zwitterion form in the solid [1] and in aqueous solution [2], but in the isolated molecule appears in the neutral form [1]. Because of its amphoteric character PAA forms complexes with acid in the 1:1 and 2:1 stoichiometry. The aim of this work is a comparison of eight structures of PAA complexes with inorganic acids and phenols.



The 1:1 complexes of PAA with HCl [3], HClO₄ [4], 2,6-dichloro-4-nitrophenol (DCNP) [5] and 2,4-dinitrophenol (24DNP) [6], solved by X-ray diffraction, have three different type structures.

In PAAH·Cl, the PAA is protonated and engaged in the intermolecular COOH···Cl⁻ hydrogen bond with chlorine anion. Each of the chlorine anions is involved in the COOH···Cl and N⁺-H···Cl hydrogen bonds. The structure in the crystals is organized in the sandwich like infinite two-dimensional layers (Fig. 1a, Table 1) [1].

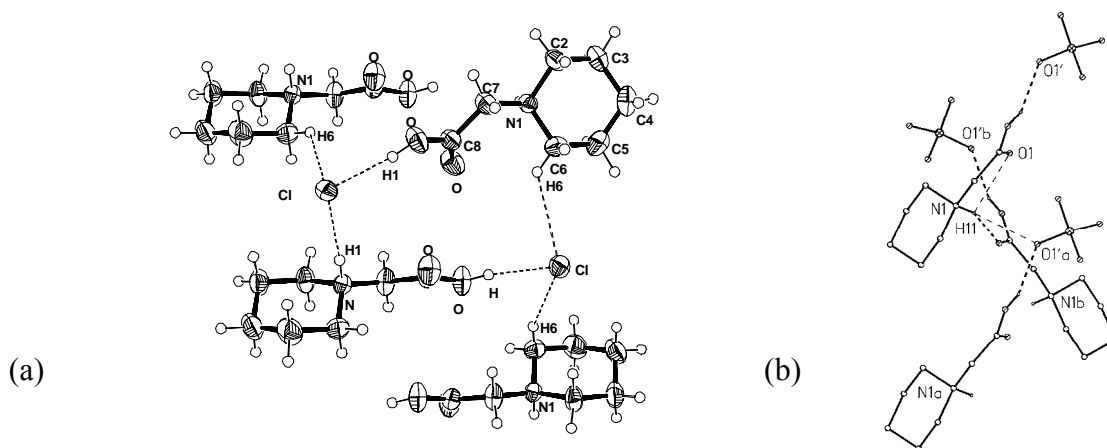


Fig. 1. Molecular structure and hydrogen bonds in the crystals of (a) 1-piperidiniumacetic acid chloride and (b) 1-piperidiniumacetic acid perchlorate

In PAAH·ClO₄ the COOH group is involved in two hydrogen bonds, with ClO₄⁻ anion and with N⁺-H atom of a neighboring molecule, related by the twofold screw axis parallel to *x*. The N⁺H atom forms trifurcated hydrogen bond, the intermolecular with OClO₃⁻ and COOH, and intramolecular with the C=O group. (Fig. 1b, Table 1) [4].

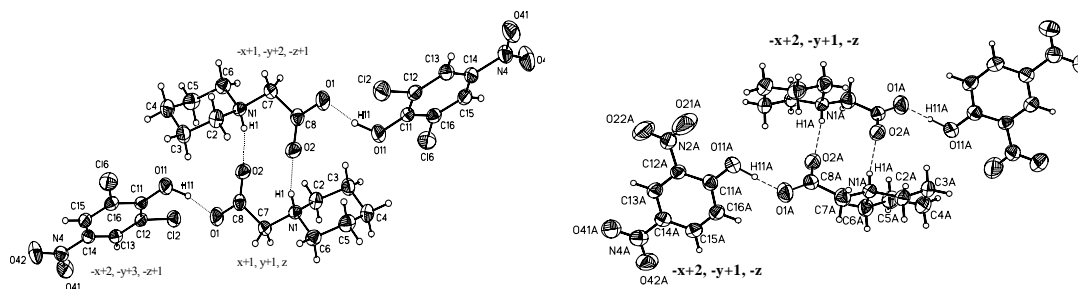
Table 1
Geometrical parameters of the hydrogen bonded complexes of 1-piperidineacetic acid (PAA) with acids (AH)

AH	Crystal system	Space group	COO \cdots donor	N ⁺ -H \cdots acceptor	Ref
1:1 complexes					
HCl	Monoclinic	P2 ₁ /c	2.964(1)	3.062(1) ^a	3
HClO ₄	Orthorhombic	P2 ₁ 2 ₁ 2 ₁	2.664(1)	2.957(1) ^b	4
DCNP	Triclinic	P $\bar{1}$	2.469(2)	2.869(2) ^c	5
24DNP	Triclinic	P $\bar{1}$	2.500(3) A 2.431(3) B	2.875(3) ^c A 2.797(3) ^c B	6
2:1 complexes					
HCl	Triclinic	P $\bar{1}$	2.463(3) ^d A 2.462(3) ^d B	2.755(2) ^c B 3.167(2) ^a A 2.717(2) ^c B	7
HClO ₄	Monoclinic	C2/c	2.441(3) ^d	2.766(2) ^c	8
TNP	Monoclinic	P2 ₁ /c	2.472(5) ^d	2.735(5) ^c 2.747(5) ^e	9
HBA	Monoclinic	C2	2.589(2) ^f 2.519(2) ^d	2.773(3) ^c 2.820(3) ^c	This work

Types of hydrogen bonds:

a) N⁺-H \cdots Cl; b) N⁺-H \cdots OCIO₃; c) N⁺-H \cdots O=C; d) COO \cdots HOOC; e) N⁺-H \cdots OPh; f) O-H \cdots OOC

In the crystal structure of the 1:1 complex of PAA with 2,6-dichloro-4-nitrophenol (DCNP) PAA is linked with DCNP through the O \cdots H-O hydrogen bond. Two such complexes form a centrosymmetric dimer, (PAA·DCNP)₂, in which PAA moieties, as zwitterions, are joined by two N⁺-H \cdots O hydrogen bonds, around the symmetry center (Fig. 2a, Table 1) [5].



(a)

(b)

Fig. 2. Molecular arrangement of the complex of 1-piperidineacetic acid with DCNP (a) and 24DNP (dimer A) (b).

A similar structure as in $(\text{PAA}\cdot\text{DCNP})_2$ has the 1:1 complex of PAA with 2,4-dinitrophenol (24DNP). PAA forms with 24DNP two non-equivalent centrosymmetric dimers, denoted as A and B, through $\text{O}\cdots\text{H}\cdots\text{O}$ hydrogen bonds of different lengths, in which two PAA moieties are joined by two $\text{N}^+\text{-H}\cdots\text{O}$ hydrogen bonds, around two different symmetry centers. The difference between A and B is explained by a participation of B in a greater number of the intermolecular $\text{C}\cdots\text{H}\cdots\text{O}$ hydrogen bonds (Fig. 2b, Table 1) [6].

In the 2:1 complexes of PAA with HCl and HClO_4 homoconjugated cations with short symmetric hydrogen bonds are formed.

The crystals of $(\text{PAA})_2\text{H}\cdot\text{Cl}$ belong to the triclinic system with two symmetrically independent hydrogen bonded complexes (A and B) at two different inversion centers. Four 1-piperidiniumacetates, as zwitterions, are held together by a network of hydrogen bonds of the types $\text{O}\cdots\text{H}\cdots\text{O}$, $\text{N}^+\text{-H}\cdots\text{O}=\text{C}$ and $\text{N}^+\text{-H}\cdots\text{Cl}$. Two carboxylate groups are bridged by linear and centrosymmetric $\text{O}\cdots\text{H}\cdots\text{O}$ hydrogen bonds. Two complexes play different roles in the crystals. In complex A both N-H atoms interact with chlorine anions by two $\text{N}^+\text{-H}\cdots\text{Cl}$ hydrogen bonds, while in complex B the $\text{N}^+\text{-H}$ atoms participate only in intra and inter-molecular hydrogen bonds with the COO^- groups (Fig. 3a. Table 1) [7].

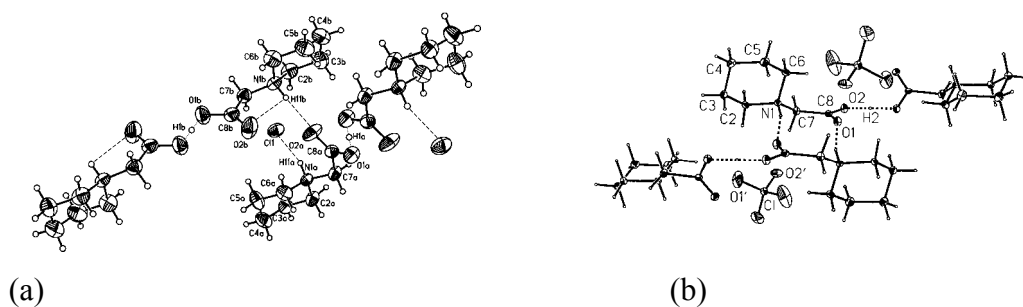


Fig. 3. Molecular structure and hydrogen bonds in the crystals of the 2:1 complexes of (a) 1-piperidineacetic acid with HCl and (b) with HClO_4 .

In the crystals of $(\text{PAA})_2\text{H}\cdot\text{ClO}_4$ two 1-piperidiniumacetate, as zwitterions, form a homoconjugated cation connected by the short and symmetrical $\text{O}\cdots\text{H}\cdots\text{O}$ hydrogen bond. These cations are related by the symmetry centre and are connected by the $\text{N}^+\text{-H}\cdots\text{O}=\text{C}$ hydrogen bonds. The ClO_4^- anion is not engaged in the hydrogen bonds, but interacts via Coulombic attraction with the positively charged nitrogen atoms (Fig. 3b Table 1) [8].

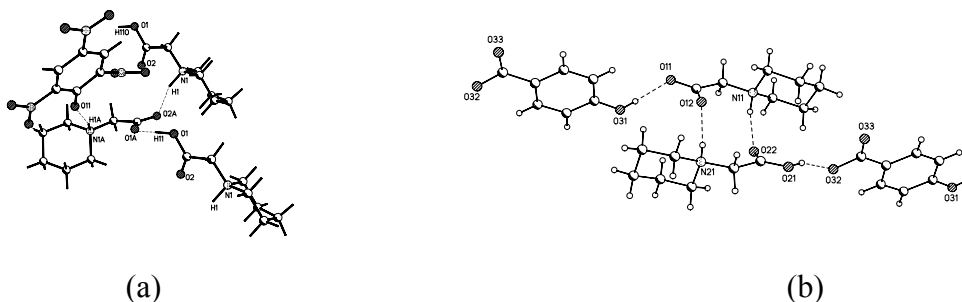


Fig. 4. Projection of the 2:1 complex of 1-piperidineacetic acid with TNP (a) and HBA (b).

The unusual 2:1 complex is formed by PAA with picric acid (TNP). In the crystals there are three kinds of molecules: 1-piperidiniumacetates, 1-piperidineacetic acid and picric anion. The molecules are joined together by two $N^+-H\cdots O$ and one $O-H\cdots O$ hydrogen bonds. The 1-piperidinium acetate molecules are linked with 1-piperidineacetic acid cations into infinite chain through the $O\cdots H-O$ hydrogen bonds. The N^+-H atom of the zwitterion interacts with phenolate oxygen atom by the $N-H\cdots O$ hydrogen bond (Fig. 4a, Table 1) [9]

In this work, a new 2:1 complex of PAA with p-hydroxybenzoic acid (HBA) has been synthesized. HBA has two donor groups, COOH and OH, hence we expected another hydrogen-bonded system in the complex investigated. Similarly as in $(PAA)_2TNP$, there are three kinds of molecules in the crystals: 1-piperidiniumacetate, 1-piperidineacetic acid and p-hydroxybenzoate anion, but the orientation of molecules in crystals are different. 1-Piperidiniumacetate and 1-piperidineacetic acid form the non-symmetrical cyclic dimer through two non-equivalent $N^+-H\cdots O=C$ hydrogen bonds. The p-hydroxybenzoate anion are linked with such dimer through the $O-H\cdots OOC$ hydrogen bond between the hydroxyl group of HBA and the carboxylate group of 1-piperidiniumacetate and with 1-piperidineacetic acid through $COO\cdots HOOC$ hydrogen bond, between the protonated cation and the benzoate anion (Fig. 4b, Table 1).

CONCLUSIONS

In all the complexes investigated the piperidine ring adopts a chair conformation with the CH_2COO substituent in the equatorial position.

In the 1:1 complexes of PAA with inorganic acids a proton is transferred from acid to PAA, while in the complexes with phenols two molecules of PAA, as zwitterions, form a cyclic dimer, which further interacts with organic molecules.

In the 2:1 complexes of PAA with HCl and $HClO_4$ two homoconjugated cations interact with each other by the $N-H\cdots O-C$ hydrogen bonds. The effect of the anion is different. The Cl^- anion is engaged in the $N-H\cdots Cl$ hydrogen bond, while the ClO_4^- anion interacts electrostatically with the positively charged nitrogen atom. In the 2:1 complexes of PAA with TNP and HBA, the PAA molecules form a linear or cyclic dimer, respectively, in which one molecule of PAA is protonated. The dimer is engaged in the $O-H-O$ hydrogen bonds with TNP^- and HBA^- anions.

In summary, the eight complexes investigated represent seven different structures. The hydrogen-bonded system depends more on the number of donor groups than on their acidity, however the determination of the role of the components in the hydrogen-bonded complexes of PAA with acids on their structures needs further investigation.

References

- [1] Z. Dega-Szafran, Z. Kosturkiewicz, E. Nowak, M. Petryna, M. Szafran, *J. Mol. Struct.*, 613 (2002) 37
- [2] P. Barczyński, Z. Dega-Szafran, E. Dulewicz, M. Petryna, M. Szafran, *Polish J. Chem.*, 74 (2000) 1149
- [3] Z. Dega-Szafran, G. Dutkiewicz, Z. Kosturkiewicz, M. Petryna, M. Szafran, *J. Mol. Struct.*, 690 (2004) 1
- [4] Z. Dega-Szafran, M. Petryna, E. Tykarska, M. Szafran, *J. Mol. Struct.*, 643 (2002) 69
- [5] Z. Dega-Szafran, G. Dutkiewicz, Z. Kosturkiewicz, M. Petryna, *J. Mol. Struct.*, 741 (2005) 115
- [6] Z. Dega-Szafran, G. Dutkiewicz, Z. Kosturkiewicz, M. Petryna, *J. Mol. Struct.*, 697 (2004) 151
- [7] Z. Dega-Szafran, M. Petryna, G. Dutkiewicz, Z. Kosturkiewicz, *Polish J. Chem.*, 77 (2003) 1501
- [8] Z. Dega-Szafran, M. Petryna, M. Szafran, E. Tykarska, *J. Mol. Struct.*, 688 (2004) 121
- [9] Z. Dega-Szafran, G. Dutkiewicz, Z. Kosturkiewicz, M. Petryna, *J. Mol. Struct.*, 708 (2004) 15

PERFECTING TEACHING METHODS AT THE WARSAW AGRICULTURAL UNIVERSITY: APPLYING THE METHOD OF SYMBOLIC ANALOGY IN THE PROCESS OF MEMORISING CHEMICAL CONCEPTS

Katarzyna Dobrosz-Teperek

*Warsaw Agricultural University, Faculty of Food Technology,
Department of Chemistry, Nowoursynowska Str. 159c, 02-776 Warsaw, Poland*

Introduction

The graduate of a modern school should possess broad general knowledge and the basic subjects should be modernised by being made more interdisciplinary. For this reason, the teaching programmes for the sciences such as chemistry should be enriched with elements of creative thinking.

With these theses in mind, the author of this article would like to encourage chemistry teachers to introduce into their lessons activating teaching methods aimed at the all-round development of the young.

The method of symbolic analogy is one of the synectic methods developed by William J. J. Gordon and is meant to teach students how to apply a creative approach to solving problems [1-4].

The analogies that are developed may be presented in any form, including as pictures. In that case, this type of analogy is sometimes called the doodle method [5].

Experimental

• Method

Initial studies were carried out to evaluate the possibility of applying the abovementioned activating method in the process of teaching chemical concepts to full-time year students (during the first semester of the 2005/2006 academic year) of the Faculty of Horticulture and Landscape Architecture at the Warsaw Agricultural University. 150 students took part in the studies. After they completed the inorganic chemistry lessons, an appropriate review topic – catalysis – was selected before the exam, and review lectures were planned to use the activating teaching method. The students received from the lecturer a word – catalyst – for which they were to individually draw a picture.

The aim of the lessons was to:

- use the activating teaching method to review chemical concepts with the example of the catalyst
- give students the opportunity to express themselves on the particular topic in chemistry in a way consistent with their artistic abilities
- developing students' creativity
- presenting to the students a nonverbal method, i.e. a symbolic analogy method used to develop specialists in a range of areas of science and life

• Plan of lectures

Topic: Catalysis

Method: Symbolic analogy (doodle method)

Type of activity: Individual work

- **Comments**

The effects of these lessons exceeded all expectations. The students really like the form of lesson, working energetically and not requiring any encouragement. Original ideas were developed. The students had the opportunity to show their own creativity. After the lesson, the work done by the individual participants was evaluated together with the students. Then, in a secret ballot, the student chose three pictures that they liked the most. These situation illustrations have been shown in Figures 1-3.

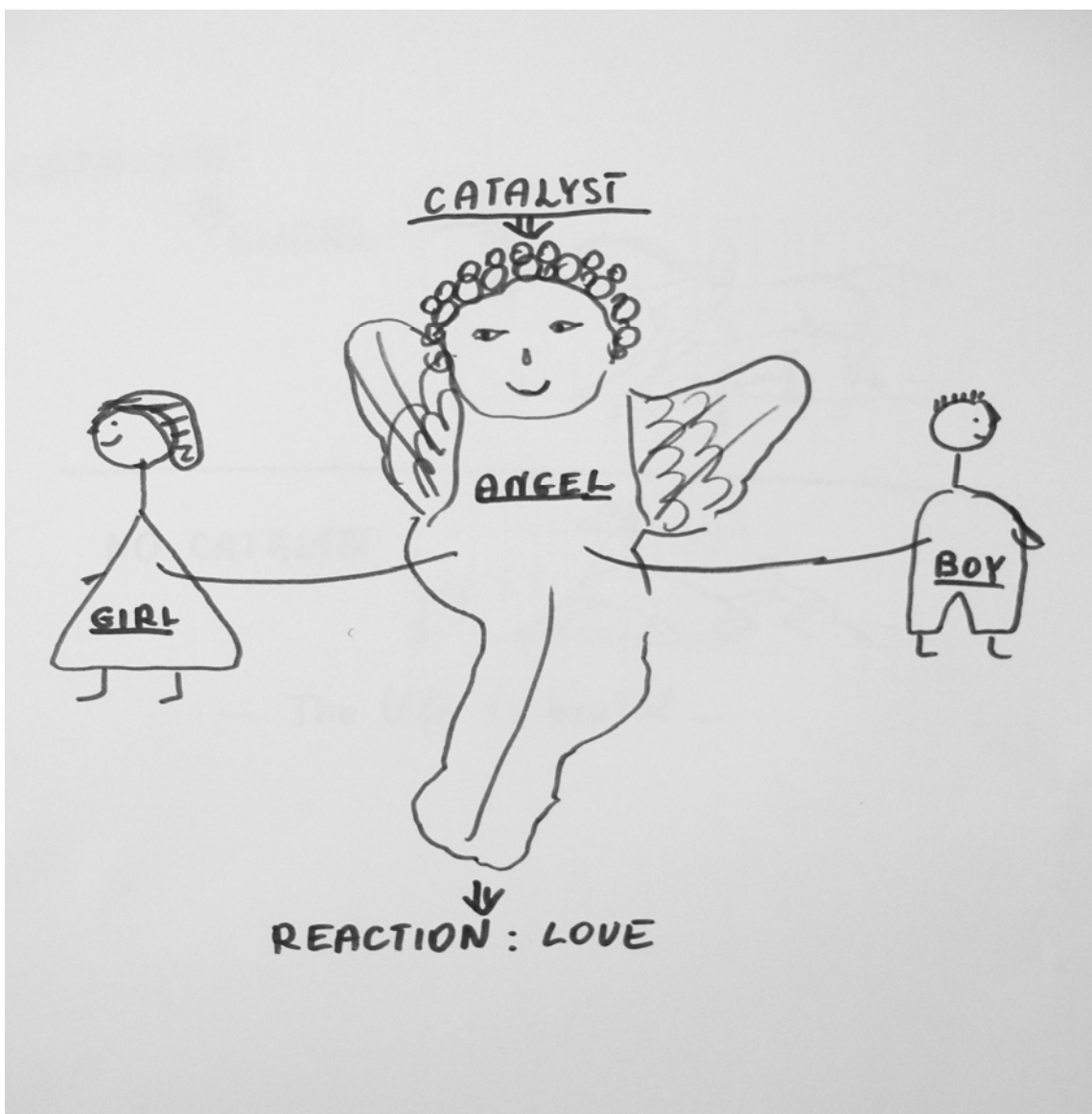


Fig. 1. Proposal I.

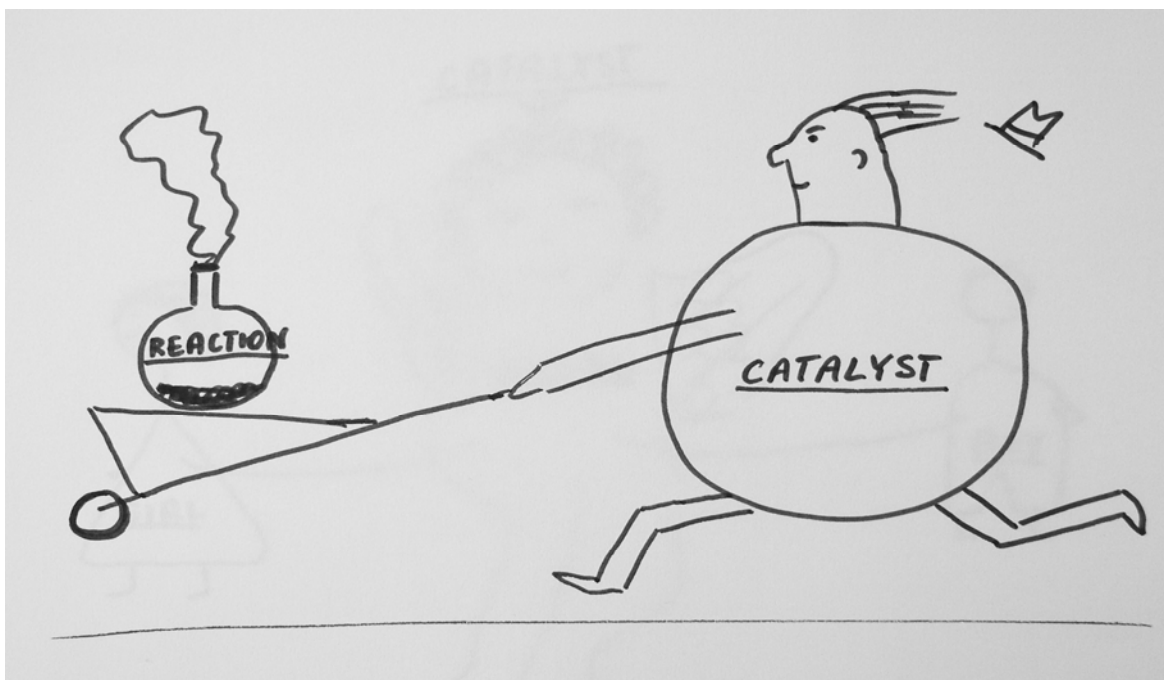


Fig. 2. Proposal II.

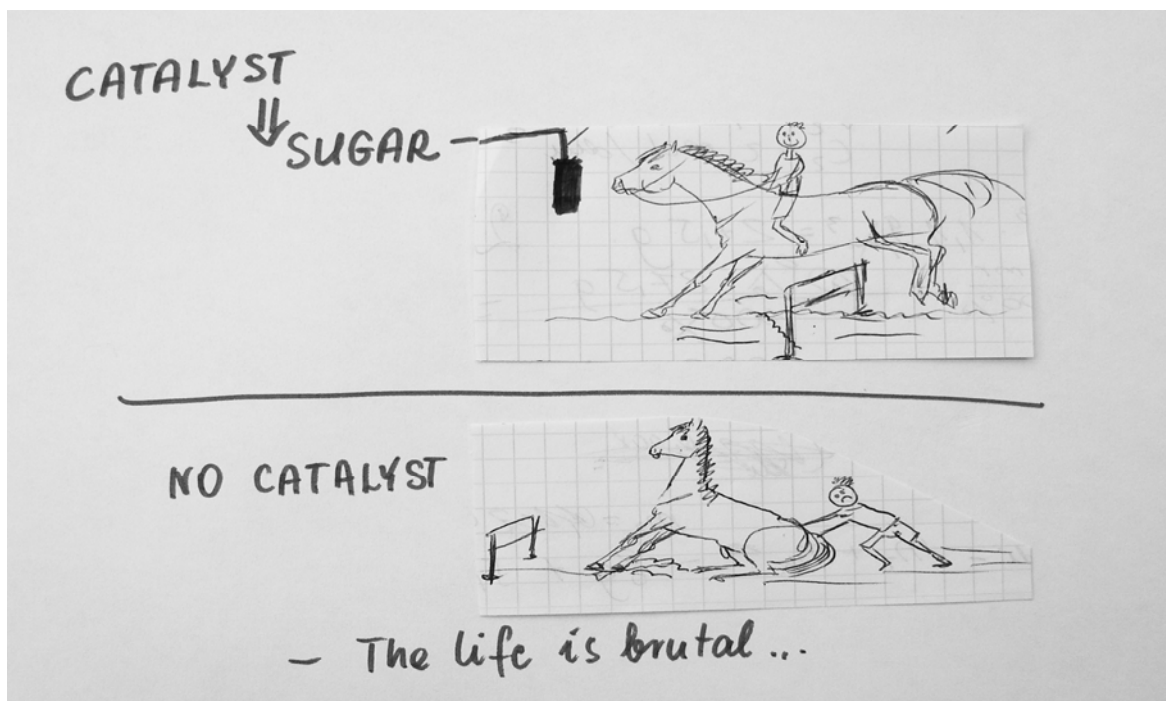


Fig. 3. Proposal III.

Results and discussion

The attractiveness of the method use was studied using a questionnaire [6] filled out after the experimental lesson.

The results of the questionnaire suggest that the students evaluated positively what was, to them, a new teaching method. More than 70% of the 150 participants thought that the lessons were educational and motivated them to think unconventionally.

The students stressed that how gladly they took part in the work during such lessons. The form of play brings out in students their spontaneity and power of association, making the lessons a pleasure.

Conclusion

The aim of the work was to show that school capable of helping to develop among its students the ability to think creatively. What is more, that it is capable of doing this not only in teaching the humanities but also the sciences, such as chemistry. Developing and stimulating the creativity of students should be one of the aims of any given teaching plan. For this reason it is important to take advantage of all opportunities to organise teaching in this respect. One such opportunity is to make use of the natural interest that the young have for various areas of life.

The author had hoped the method of teaching used would encourage students to learn, especially those of them who had little interest in chemistry.

References (in Polish):

- [1] M. I. Łojewska „Twórcze myślenie współczesnego inżyniera”, Zeszyty Naukowe Ośrodka Nauk Społecznych Politechniki Warszawskiej, z.2/1994, str. 125.
- [2] A. Galska-Krajewska „Kształtowanie umiejętności twórczego myślenia w nauczaniu chemii”, Chemia w Szkole, nr 4/2003, str.205.
- [3] A. Galska-Krajewska „Wykorzystanie metody synektycznej w nauczaniu chemii”, Chemia w Szkole, nr 3/1988, str.162.
- [4] J. Paśko „Synektyka aktywna w nauczaniu chemii”, Chemia w Szkole, nr 2/1991, str.115.
- [5] E. Brudnik, A. Muszyńska, B. Owczarska, Ja i mój uczeń pracujemy aktywnie. Przewodnik po metodach aktywizujących, Wyd. OWN, Kielce 2003, str. 27.

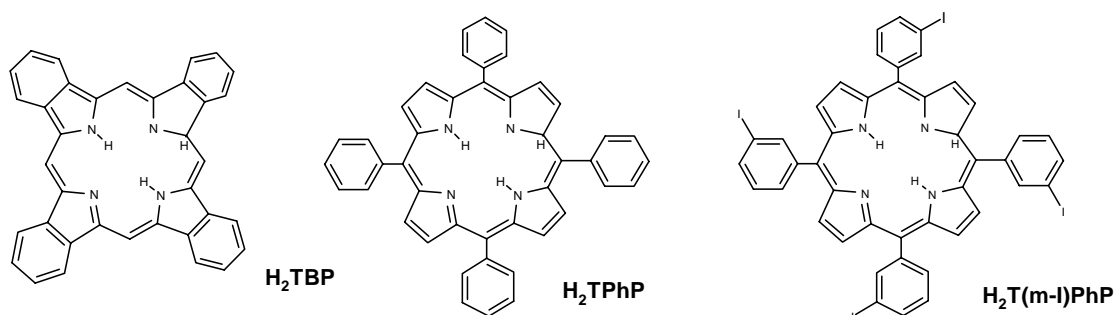
ELECTROCHEMICAL CHARACTERISTICS OF PLATINUM MODIFIED WITH IRON COMPLEXES OF PORPHYRINS IMMOBILIZED IN NAFION FILM

Sławomir Domagała, Józef Dziegieć

*University of Łódź, Department of General and Inorganic Chemistry, 90-136 Łódź,
ul. Narutowicza 68, e-mail: domagala@chemul.uni.lodz.pl*

Immobilization of metalloporphyrins into polymer coated electrodes has been developed intensively over the past years due to the fact that these materials are efficient electrocatalysts for chemical applications. It has been shown that such chemically modified electrodes can be used as tools in fundamental electrochemical investigations as chemical sensors, energy-producing or electrochromic devices and they can be used for investigation of electrocatalytical properties. Some metalloporphyrins after immobilization in a polymer film on electrode can act as red-ox mediators for oxidation of organic compounds. Iron complexes of porphyrins can be effective mediators for oxidation of some phenol and hydroquinone derivatives [1-8].

The aim of this work was to investigate properties of platinum modified with three porphyrins (Scheme 1) and their iron complexes immobilized in Nafion[®] film as well as determination of catalytic activity of such modified conducting phase in electrochemical oxidation of 4-aminophenol and some hydroquinone derivatives.



EXPERIMENTAL

All reagents were purchased from Aldrich. The cyclic voltammetry measurements were done under an Ar atmosphere on AUTOLAB (Eco Chemie BV) in three electrode system, where the working and modified electrode was platinum (Pt), $\phi=2$ mm, the reference electrode was saturated calomel electrode (SCE), and the counter electrode was the cylindrical platinum gauze. For the preparative electrolysis in potentiostatic conditions a Pt plate (5.0 cm^2) was used. The electrolysis was carried out under potentiostatic conditions in a glass cell (50 ml) at $25 \text{ }^\circ\text{C}$. The products were extracted with CH_2Cl_2 and CHCl_3 from the electrolyte solution and then identified by UV-Vis, IR, NMR and melting points.

RESULTS AND DISCUSSION

In order to determine properties of platinum modified with three porphyrins and their complexes with Fe(II) ions immobilized in Nafion[®] film the cyclic voltammetry in three electrode system was done. The working electrode was platinum or platinum modified with iron porphyrins immobilized in Nafion film coated on. The reference was saturated calomel electrode (SCE), and counter electrode was cylindrical platinum gauze. Figure 1a, (plot a) shows typical voltammograms of iron tetraphenylporphyrin immobilized in Nafion[®] film (Pt/Nafion[®]/FePorphyrin) measured in 0.1 M HClO₄.

Voltammograms gave a steady state form on Pt/Nafion[®]/FePorphyrin even after repeated potential scanning which proves that porphyrins and their iron complexes are effectively immobilized in Nafion[®] film coated on Pt.

Linear dependence of the anodic and cathodic current (i_{pa} , i_{pc}) on square root of scan rate ($v^{1/2}$) shows that within scan rate range 5-100 mV/s the red-ox process as well as in the solution as in the Nafion[®] film is diffusion limited (fig. 1b).

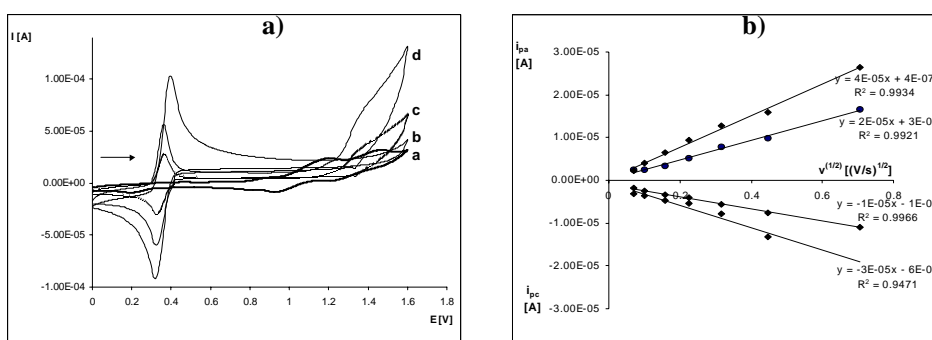


Figure 1. Cyclic voltammograms **a)** a) iron complex of tetraphenylporphyrin (FeTPhP) immobilized in Nafion[®] film on Pt, in 0.1 M HClO₄ (Pt/Nafion[®]/FeTPhP), 0.1 V/s; b) 1,4-hydroquinone (10⁻³ M) in 0.1 M HClO₄ on Pt, 0.1 V/s; c) 1,4-hydroquinone (10⁻³ M) with FeTPhP(10⁻³ M) in solution of 0.1 M HClO₄ on Pt, 0.1 V/s; d) 1,4-hydroquinone (10⁻³ M) in 0.1 M HClO₄ on Pt/Nafion[®]/FeTPhP, 0.1 V/s; **b)** dependence of i_{pa} , $i_{pc}=f(v^{1/2})$ for iron complex of tetraphenylporphyrin (FeTPhP) immobilized in Nafion[®] film on Pt, in 0.1 M HClO₄ (Pt/Nafion[®]/FeTPhP), 0.1 V/s; T=298 K.

Due to determine changes of porphyrins and their iron complexes amount (Γ) immobilized in Nafion[®] film coated on Pt, the 20 voltammetric cycles were done in each case within scan rate range 10-100 mV/s in 0.1 HClO₄. It was calculated from $\Gamma=Q/nFA$, (Q- charge [C], A- area of electrode surface [cm²], F- Faraday's constant, and n- number of electrons). The amount of porphyrins and their iron complexes immobilized in Nafion[®] film has not been changed significantly after repeated scanning.

The apparent diffusion coefficient and constants of electrode process rate of investigated porphyrins and their iron complexes in solution and in Nafion[®] film were calculated and summarized in table 1.

To investigate mediatory properties of iron porphyrin complexes immobilized in Nafion film the cyclic voltammetry was performed in solutions containing 1,4-hydroquinone, 2,3,5,6-tetrafluoro-1,4-hydroquinone, 2,3,5,6-tetrabromo-1,4-hydroquinone and 4-aminophenol on bare Pt (fig.1a, plot b), on bare Pt with iron porphyrins in solution (Pt + FePorphyrin in solution) (fig.1a, plot c), and on Pt coated with Nafion[®] film and iron porphyrin immobilized in (Pt/Nafion[®]/FePorphyrin) (fig. 1, plot d).

The best results were obtained for modified electrode, *i.e.* with iron porphyrins immobilized in Nafion[®] film coated on Pt (Pt/Nafion[®]/FePorphyrin) (fig. 1, plot d). In this case the greater currents of anodic and cathodic peaks of organic compounds oxidation and reduction were obtained than in the others. The considerable increase of anodic and cathodic current values as well as decrease of cathodic and anodic peak potential differences ΔE_p , observed on the voltammograms of oxidized organic compounds performed on Pt/Nafion[®]/FePorphyrin compared to other cases, point to catalytic activity of new conducting phase. In the other hand, the diminution of the porphyrin complexes reduction cathodic peak on Pt/Nafion/FePorphyrin when the organic compound is present in solution can point to mediatory activity of iron porphyrins immobilized in Nafion[®] film coated Pt during oxidation of organic substrates. Taking into account the results of preparative electrolysis in potentiostatic conditions, we have observed decrease of electrolysis time on Pt/Nafion/FePorphyrin compared to bare Pt with iron porphyrins present in solution. The longest electrolysis time was observed in case when oxidation has been carried out on bare Pt and without iron porphyrins in solution.

Table 1. The final products and yield of oxidation process; $E_{\text{substr.}}$: 0.372 V for 1,4-hydroquinone, 0.416 V for 2,3,5,6-tetrafluoro-1,4-hydroquinone, 0.425 V for 2,3,5,6-tetrabromo--1,4-hydroquinone, 0.451 V for 4-aminophenol; $E_{\text{med.}}$: 1.584 for FeTBP, 1.475 for FeTPhP, 1.475 for FeT(m-I)PhP; vs SCE.

COMPOUND	ELECTRODE	FINAL PRODUCTS	
1,4-hydroquinone	Pt at $E_{\text{substr.}}$	1,4-benzoquinone	94%
	Pt + FeTBP in solution at E_{med}	1,4-benzoquinone	96%
	Pt + FeTPhP in solution at E_{med}	1,4-benzoquinone	97%
	Pt + FeT(m-I)PhP in solution at E_{med}	1,4-benzoquinone	95%
	Pt/Nafion [®] /FeTBP at E_{med}	1,4-benzoquinone	95%
	Pt/Nafion [®] /FeTPhP at E_{med}	1,4-benzoquinone	96%
	Pt/Nafion [®] /FeT(m-I)PhP at E_{med}	1,4-benzoquinone	97%
2,3,5,6-tetrafluoro-1,4-hydroquinone	Pt at $E_{\text{substr.}}$	2,3,5,6-tetrafluoro-1,4-benzoquinone	95%
	Pt + FeTBP in solution at E_{med}	2,3,5,6-tetrafluoro-1,4-benzoquinone	97%
	Pt + FeTPhP in solution at E_{med}	2,3,5,6-tetrafluoro-1,4-benzoquinone	96%
	Pt + FeT(m-I)PhP in solution at E_{med}	2,3,5,6-tetrafluoro-1,4-benzoquinone	97%
	Pt/Nafion [®] /FeTBP at E_{med}	2,3,5,6-tetrafluoro-1,4-benzoquinone	97%
	Pt/Nafion [®] /FeTPhP at E_{med}	2,3,5,6-tetrafluoro-1,4-benzoquinone	98%
	Pt/Nafion [®] /FeT(m-I)PhP at E_{med}	2,3,5,6-tetrafluoro-1,4-benzoquinone	96%
2,3,5,6-tetrabromo-1,4-hydroquinone	Pt at $E_{\text{substr.}}$	2,3,5,6-tetrabromo-1,4-benzoquinone	93%
	Pt + FeTBP in solution at E_{med}	2,3,5,6-tetrabromo-1,4-benzoquinone	95%
	Pt + FeTPhP in solution at E_{med}	2,3,5,6-tetrabromo-1,4-benzoquinone	96%
	Pt + FeT(m-I)PhP in solution at E_{med}	2,3,5,6-tetrabromo-1,4-benzoquinone	94%
	Pt/Nafion [®] /FeTBP at E_{med}	2,3,5,6-tetrabromo-1,4-benzoquinone	97%
	Pt/Nafion [®] /FeTPhP at E_{med}	2,3,5,6-tetrabromo-1,4-benzoquinone	97%
	Pt/Nafion [®] /FeT(m-I)PhP at E_{med}	2,3,5,6-tetrabromo-1,4-benzoquinone	98%
4-aminophenol	Pt at $E_{\text{substr.}}$	1,4-benzoquinone	89%
	Pt + FeTBP in solution at E_{med}	1,4-benzoquinone	91%
	Pt + FeTPhP in solution at E_{med}	1,4-benzoquinone	92%
	Pt + FeT(m-I)PhP in solution at E_{med}	1,4-benzoquinone	94%
	Pt/Nafion [®] /FeTBP at E_{med}	1,4-benzoquinone	95%
	Pt/Nafion [®] /FeTPhP at E_{med}	1,4-benzoquinone	94%
	Pt/Nafion [®] /FeT(m-I)PhP at E_{med}	1,4-benzoquinone	95%

Table 2. The diffusion coefficients and the standard rate constant of electrode processes.

PORPHYRIN	MEDIUM	$D_{anod.1}$	$D_{anod.2}$	$D_{cat.1}$	$D_{cat.2}$	$k_{s\ anod1}$	$k_{s\ anod2}$	$k_{s\ cat.1}$	$k_{s\ cat.2}$
H ₂ TBP	solution	4.72×10^{-5}	1.64×10^{-5}	8.17×10^{-6}	3.48×10^{-6}	8.33×10^{-3}	8.33×10^{-2}	4.34×10^{-1}	1.59×10^{-1}
H ₂ TPhP	0.1 M	7.10×10^{-5}	1.08×10^{-5}	4.07×10^{-6}	1.45×10^{-5}	2.34×10^{-3}	3.57×10^{-1}	1.21×10^{-1}	2.69×10^{-2}
H ₂ T(m-I)PhP	NaClO ₄	2.32×10^{-5}	2.44×10^{-5}	1.04×10^{-6}	9.66×10^{-6}	2.16×10^{-3}	8.55×10^{-1}	1.71×10^{-1}	1.22×10^{-2}
H ₂ TBP	Nafion [®] film	7.25×10^{-8}	3.56×10^{-8}	3.56×10^{-9}	4.01×10^{-9}	3.30×10^{-4}	4.32×10^{-3}	3.78×10^{-2}	2.34×10^{-3}
H ₂ TPhP		5.03×10^{-8}	2.11×10^{-8}	2.34×10^{-9}	3.41×10^{-9}	3.45×10^{-4}	5.19×10^{-2}	4.01×10^{-2}	4.12×10^{-3}
H ₂ T(m-I)PhP		4.42×10^{-8}	4.09×10^{-8}	3.22×10^{-9}	4.21×10^{-9}	4.23×10^{-4}	4.67×10^{-2}	2.17×10^{-2}	2.34×10^{-3}
FeTBP	solution	2.56×10^{-5}	5.39×10^{-6}	5.34×10^{-6}	2.67×10^{-6}	5.62×10^{-3}	6.23×10^{-2}	3.02×10^{-1}	8.58×10^{-2}
FeTPhP	0.1 M	3.59×10^{-5}	6.55×10^{-6}	2.75×10^{-6}	1.02×10^{-5}	1.45×10^{-3}	1.78×10^{-1}	8.34×10^{-2}	1.06×10^{-2}
FeT(m-I)PhP	NaClO ₄	1.04×10^{-5}	1.13×10^{-5}	7.27×10^{-7}	6.92×10^{-6}	1.34×10^{-3}	5.12×10^{-1}	7.45×10^{-2}	6.39×10^{-3}
FeTBP	Nafion [®] film	5.02×10^{-8}	2.03×10^{-8}	2.47×10^{-9}	2.98×10^{-9}	2.34×10^{-4}	3.11×10^{-3}	2.08×10^{-2}	1.56×10^{-3}
FeTPhP		3.40×10^{-8}	1.26×10^{-8}	1.67×10^{-9}	2.31×10^{-9}	1.96×10^{-4}	3.78×10^{-2}	3.04×10^{-2}	2.79×10^{-3}
FeT(m-I)PhP		3.12×10^{-8}	2.89×10^{-8}	1.98×10^{-9}	3.05×10^{-9}	3.07×10^{-4}	2.98×10^{-2}	1.34×10^{-2}	1.67×10^{-3}

CONCLUSIONS

Character of voltammograms and value of anodic and cathodic currents are comparable even after several cycles, which proves the effective (stable) immobilization of investigated porphyrins and their iron complexes in Nafion[®] layer.

Linear dependence of i_{pa} , $i_{pk} = f(v^{1/2})$ within the scan range 5-100 mV/s indicates that transport of the substance to electrode surface within Nafion[®] film is linear diffusion limited.

In case of the modified electrode (Pt/Nafion[®]/FePorphyrin) the increase of anodic peaks on voltammograms during oxidation of organic compounds is observed, and drastic decrease of cathodic peak related to iron porphyrin reduction, which seems to point out to the mediatory activity of these complexes and modified electrode surface.

Currents of oxidation observed during preparative electrolyses proves the catalytic properties of the modified conducting phase. The preparative electrooxidation of the investigated compounds showed that conversion of substrate occur in the shortest time on platinum modified with porphyrin complexes immobilized in Nafion[®] film.

REFERENCES

- [1] R.W. Murray, in Chemically Modified Electrodes, Electroanalytical Chemistry, Vol. 13, A.J. Bard, ed., Marcel Dekker Inc., 1984, NY
- [2] R.P. Buck, in Theory and Principles of Membrane Electrodes, Chapt. 1, Ion-Selective Electrodes in Analytical Chemistry, Vol. 1, H. Freiser, ed., Plenum Press, 1978, NY
- [3] J.W. Ross, J.H. Riseman, J.A. Krueger, Pure Appl. Chem., 36 4 (1973) 473
- [4] L.C. Clark, Trans. Am. Soc. Artif. Int. Organs., 2 (1956) 41
- [5] R. Guiladd, K.M. Kadish, Chem.Rev., (1988) 88 1121-1146
- [6] G. Peychal-Heiling, G.S. Wilson, Anal. Chem., (1971) 4, 43
- [7] A. Deronizer, J.C. Moutet, Coord. Chem. Rev., 147 (1996) 339
- [8] F. Bedioui, S.Trevin, J.Devynck, Electroanalysis, 8 (1996) 1085

Pd-POLYANILINE(SiO₂) COMPOSITE – CATALYTIC PROPERTIES

A. Waksmundzka-Góra¹, A. Drelinkiewicz^{1,2}, W. Makowski², J.W. Sobczak³, J. Stejskal⁴

¹*Institute of Catalysis and Surface Chemistry, Polish Academy of Sciences, 30-239 Kraków, Niezapominajek 8, Poland*

²*Faculty of Chemistry, Jagiellonian University, 30-060 Krakow, Ingardena 3, Poland*

³*Institute of Physical Chemistry, Polish Academy of Sciences, 01-224 Warszawa, Kasprzaka 44, Poland*

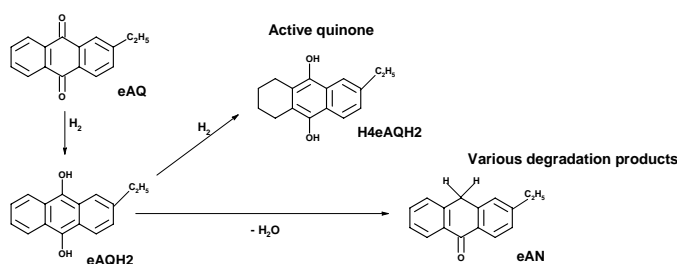
²*Institute of Macromolecular Chemistry, Academy of Sciences of the Czech Republic, Heyrovsky Sq. 2, 162 06 Prague, Czech Republic*

Abstract

A novel palladium catalysts supported on SiO₂ coated with film of polyaniline (PANI) were studied in the hydrogenation of 2-ethylanthraquinone (eAQ). This reaction is a key stage of anthraquinone method of H₂O₂ production. Two series of catalysts TP and MD, differing in ordering of PANI macromolecules in the film were used. Much better performance of PANI film-containing TP and MD catalysts than that of typical Pd/SiO₂ was ascribed to advantageous modification of environment surrounding the Pd centres due to hydrophobic character of PANI. The influence of polymer was especially attractive in TP-based catalysts with “brush-like ordering” of PANI macromolecules in the film covering supporting SiO₂ grains.

Introduction

Introductory study of eAQ hydrogenation showed very promising properties of polyaniline film-containing 2%Pd/PANI(SiO₂) (24.4 wt % PANI) catalyst [1, 2]. To a better knowledge of the PANI role, in the present work the TP and MD supports differing in the organization of PANI macromolecules in the film covering supporting SiO₂ grains were used. Their activity was tested in the hydrogenation of 2-ethylanthraquinone (eAQ), key reaction in the anthraquinone method of H₂O₂ production [3-5]. Al₂O₃, SiO₂ or silica-alumina supported Pd catalysts are commonly used in this process. The hydrogenation of quinone system in eAQ produced 2-ethylanthrahydroquinone (eAQH₂) (Scheme 1) and its oxidation by air leads to H₂O₂ and regeneration of the starting eAQ. Undesired processes accompanying desired eAQ to eAQH₂ reduction and leading to lowering of selectivity are hydrogenation of aromatic rings and hydrogenolytic cleavage of C-O in the hydroquinone eAQH₂. H₄eAQH₂ (2-ethyl-5,6,7,8-tetrahydroanthrahydroquinone),



Scheme 1 Reaction pattern of eAQ hydrogenation

formed by phenyl ring saturation is the only desired product because its oxidation leads to H₂O₂. Other by-products, not capable to H₂O₂ formation (2-ethylanthrone, 2-ethyloxanthrone, 2-ethylanthracene, dimers) present degradation products. To improve the selectivity of quinone-hydroquinone stage the use of lipophilic-resin based Pd catalysts has been considered [6]. The desired product, eAQH₂ is more polar than the starting eAQ, and an increase in the lipophilic character of the environment surrounding the Pd centres could facilitate the removal of the polar eAQH₂ from the vicinity of the catalytic surface thus lowering probability of undesired reactions [6]. Results obtained in this work on catalysts containing hydrophobic polymer, PANI (Fig. 1) confirmed very well this hypothetical supposition.

Experimental

An overlayer of PANI was introduced onto supporting SiO₂ via the oxidative polymerization of aniline hydrochloride in the presence of (NH₂)S₂O₈ at 0-2^oC. Two polymerization procedures TP and MD, resulting in different organization of PANI macromolecules in the film were used. Their preparation and characterization has already been reported [7-9]. In TP procedure, PANI films are produced on silica before the polymerization of aniline in the reaction mixture has started giving a “brush-like” ordering of PANI-macromolecules in the TP film (Fig. 1 a). In MD procedure the polymerization was performed in the presence of water soluble polymer, poly(N-vinylpyrrolidone) (stabiliser). The initiation of polymerization started then at the stabilizer chains and colloidal particles of PANI generated in aqueous phase adhered to the SiO₂ grains producing less ordered and more dense film (Fig. 1 b).

Catalysts (0.5 wt %Pd) were prepared by reacting the PANI(SiO₂) – TP and MD supports with aqueous PdCl₂ solutions (PdCl₂ 2.3 x 10⁻³ mol/dm³) of molar ratio NaCl : PdCl₂ = 2.5 (TP-aq and MD-aq catalysts) and NaCl : PdCl₂ = 12 : 1 (TP-Cl and MD-Cl catalysts). The suspension was stirred up to complete disappearance of Pd²⁺ in the solution (24 h), filtered, washed with water until the Cl⁻ ions were removed and dried (4h at 60^oC). The reduction of catalysts was performed in the reactor (“in situ”, 30 min at 62^oC). Characterization of catalysts was performed with XPS and TEM techniques.

Hydrogenation of eAQ was carried out in agitated glass reactor at atmospheric pressure of hydrogen, temperature 62^oC, a mixture 2-octanol-xylene (1:1) as the solvent, (eAQ 20 g/dm³). The course of hydrogenation was followed by measuring hydrogen uptake against reaction time. Product analysis was performed with HPLC and GC-MS.

Results and discussion

Deposition of PANI only slightly reduced the specific surface area from 156.4 m²g⁻¹ in pristine SiO₂ to 150.3 m²g⁻¹ and 141.1 m²/g in the TP and MD respectively. XPS analysis found C, N, Si, O elements within the surface of TP, MD supports. The C/N ratios (ca. 6) obtained from the XPS and elemental analysis are very close to the (C₆H₄N) formula of PANI. Not complete covering of supporting SiO₂ grains by PANI is evidenced by the XPS signal of Si. The content of PANI in the MD sample (10.3 wt %) is ca. two times higher that that in TP (5.6 wt %). However, 4-times higher N/Si and C/Si ratios in MD catalysts show higher content of PANI within the surface of MD support. Hence MD procedure resulted in preferential deposition of PANI onto the outer surface of SiO₂

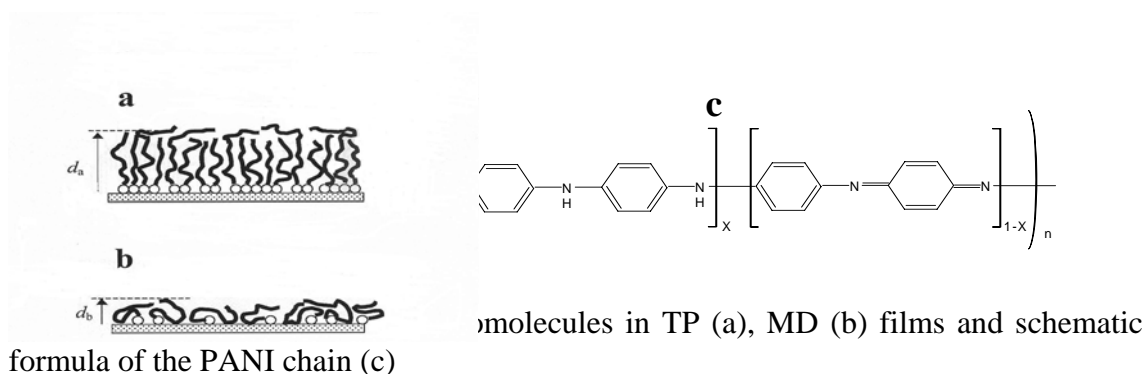


Table 1 Properties of catalysts and surface composition (in at %) characterized by XPS

Sample	PANI wt %	Surface area m ² /g	C	N	Si	O	Pd	Cl	C/Si	N/Si
SiO ₂		156.4								
TP	5.6	150.3	8.83	1.23	37.69	52.15			0.23	0.033
TP-aq		152.5	7.06	0.94	32.38	58.98	0.15	0.30	0.22	0.029
TP-Cl		122	7.82	0.92	32.26	58.55	0.16	0.29	0.24	0.028
MD	10.3	141.1	27.57	3.5	24.76	44.16			1.11	0.141
MD-aq		137	22.34	3.39	26.75	46.94	0.16	0.31	0.83	0.127
MD-Cl		144	19.81	3.14	27.85	48.85	0.11	0.19	0.71	0.113

grains and formation of more dense polymer film (Fig. 1b). The content of Pd is very similar (0.15 – 0.16 at %) at the surface of all catalysts. SEM studies showed very uniform distribution of Pd in hydrogen-activated catalysts. From TEM images the size of Pd particles within 2 – 6 nm was estimated (Fig. 2) in all the catalysts.

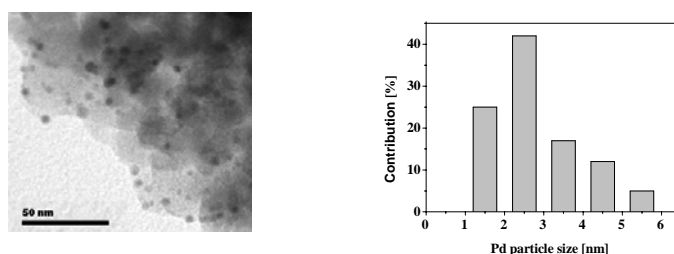


Fig. 2 TEM micrographs of TP-aq catalyst and diagram of Pd-particles size contribution

The role of PANI was studied in the first quinone-hydroquinone stage and in further hydrogenation of eAQH₂ (Scheme 1) giving H₄eAQ (active quinone) and degradation products. In the quinone-hydroquinone reduction, much better performance in terms of activity and selectivity exhibited MD-based catalysts with more dense PANI film (Table 2). Fig. 3 presents the consumption of hydroquinone form, eAQH₂ over 0.5%Pd/SiO₂ and TP-aq and MD-aq catalysts. The highest reactivity in the over-all process of eAQH₂ consumption exhibited typical 0.5%Pd/SiO₂ catalysts. Evidently lower reactivity in this undesired process is offered by the PANI film-containing TP and MD catalysts. Over both TP-aq and MD-aq catalysts only very low content of degradation products is observed, evidently lower than that observed on 0.5%Pd/SiO₂ (Fig. 3 b, c). This effect proves significant decrease in reactivity of PANI film-containing catalysts to the hydrogenolytic cleavage of C-O in eAQH₂. On both PANI containing catalysts as a dominating reaction the saturation of phenyl ring in eAQH₂

yielding H₄eAQ (active quinone) proceeded. This domination is especially high on TP catalyst with “brush-like ordering” of PANI chains. The observed, attractive role of PANI can be related with influence of polymer on the geometry of eAQH₂ molecule adsorption, which is a deterministic factor for its hydrogenation. Owing to hydrophobic properties, adsorption via aromatic ring is preferred thus facilitating the formation of H₄eAQH₂.

Table 2 Data obtained in quinone-hydroquinone stage

Catalyst	TP-aq	TP-Cl	MD-aq	MD-Cl
Rate [mol H ₂ /min] x 10 ⁻⁵	1.72	1.09	2.11	1.33
Selectivity [%]	67.3	68.5	86	91

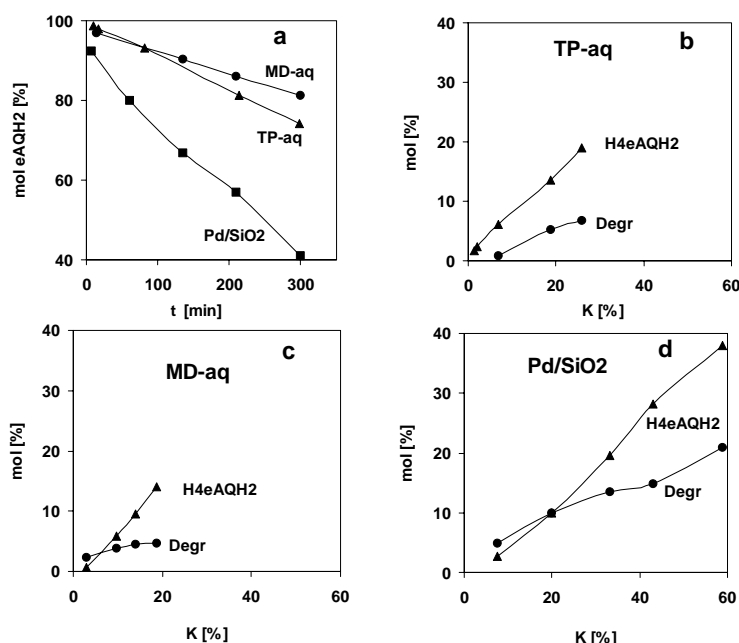


Fig. 3 Hydrogenation of hydroquinone form, eAQH₂ on Pd/SiO₂, TP-aq and MD-aq

References

- [1] A. Drelinkiewicz, A. Waksmundzka-Góra, W. Makowski, J. Stejskal, Catal. Comm. 6 (2005) 347
- [2] J. Stejskal, J. Quadrat, I. Sapurina, J. Zemek, A. Drelinkiewicz, I. Krivka, J. Prokes, Eur. Polym. J. 38 (2002) 631
- [3] Ulmann's Encyclopedia of Industrial Chemistry, Vol. 13 A (VCH, Weinheim, 1989) p. 443
- [4] E. Santacesaria, M. Di Serio, R. Velotti, U Leone, J. Mol. Catal. 94 (1994) 37
- [5] J. Petr, L. Kurc, Z. Belohlav, L. Cerveny, Chem. Eng. Process, 43 (2004) 887
- [6] A. Biffis, R. Ricoveri, S. Campestrini, M. Kralik, B. Corain, Chem. Eur. J. 8 (2002) 2962
- [7] I. Sapurina, A.Yu. Osadchev, B.Z. Volchek, M. Trchova, A. Riede, J. Stejskal, Synth. Met., 129 (2002) 29
- [8] A. Riede, J. Stejskal, M. Helmstedt, Synth. Met., 121 (2001) 1365
- [9] A. Reide, M. Helmstedt, I. Sapurina, J. Stejskal, J. Coll. Inter. Sci., 248 (2002) 413

Composite solid electrolytes in the CaO-ZrO₂-Al₂O₃ system: preparation, properties, and application to the solid galvanic cells

Magdalena Dudek, Grzegorz Róg, Władysław Bogusz^(*),
Mirosław Bućko, Anna Kozłowska –Róg

AGH – University of Science and Technology, Faculty of Materials Science and Ceramics,
al. Mickiewicza 30, 30-059 Kraków, potoczek@uci.agh.edu.pl

^(*)Faculty of Physics, Warsaw University of Technology, ul. Koszykowa 75, 00-662 Warszawa

Abstract

Relatively low oxygen ion conductivity of a pure CaZrO₃ amounting about 10⁻⁶ S·cm⁻¹ at the temperature of 1273K limits its practical use as a solid electrolyte in solid-state galvanic cells. Calcium zirconate based composites containing 1 to 10 %mol Ca₃Al₂O₆ as a disperse phase were prepared. The electrical conductivity values for the samples were significantly higher than those of pure CaZrO₃. The maximum conductivity values were observed for 2 % mol Ca₃Al₂O₆ content. The (CaZrO₃ + Ca₃Al₂O₆) composites appeared to be purely oxygen-ion conductors. The materials prepared were applied as electrolytes in solid galvanic cells. In this way the Gibbs free energy of formation of NiCr₂O₄ at the temperature of 1273K was determined. The possibility of application of CaZrO₃-based composite materials as electrolytes in electrochemical oxygen sensors in the temperature range 873K – 1273K was also demonstrated.

1. Introduction

Calcium zirconate, CaZrO₃ being the most stable compound existing in the quasi-binary ZrO₂-CaO system appeared to be a good oxygen ion-conductor at higher temperatures [1]. High chemical stability, good thermal shock resistance at temperatures exceeding 1000°C at a very low oxygen activity makes CaZrO₃ a more suitable solid electrolyte for the determination of oxygen in molten metals than the zirconia solid solutions [2,3]. In order to lower the operating temperature of CaZrO₃, a disperse heterophase can be introduced in it. Composites consisting of a solid ion-conductor matrix and a disperse Al₂O₃ phase were shown to have electrical conductivity significantly higher compared to the pure matrix phase [3,4]. As it resulted from thermodynamic considerations, a pure Al₂O₃ was not stable phase in contact with CaZrO₃ [5]. Therefore, tricalcium aluminate, (Ca₃Al₂O₆) which was suggested to be chemically inert in respect with CaZrO₃, was chosen as a heterophase.

The purpose of our investigations was to examine how the presence of Ca₃Al₂O₆ heterophase in CaZrO₃ matrix influenced electrical and electrochemical properties of the composite prepared. However, the practical purpose of this research was to obtain composite materials based on CaZrO₃, which could be applied as electrolytes in solid galvanic cells in the temperature range 873-1273 K

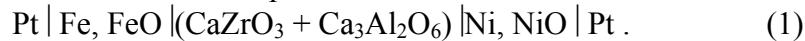
2. Experimental

CaZrO₃ and Ca₃Al₂O₆ powders were prepared by a citrate method. The details of experimental procedure of preparation of the powders were described in our previous work [6]. The powders of CaZrO₃ and Ca₃Al₂O₆ to which some ethanol was added, were mixed for 30 min., in a rotary-vibratory mill with yttria stabilized zirconia

ceramics as a grinding medium. As a lubricant served oleic acid. In this way, homogenous mixtures containing up to 10 % mol $\text{Ca}_3\text{Al}_2\text{O}_6$ were obtained. Then, the mixtures were dried in a room temperature, granulated and cold isostatically pressed under a pressure of 200 MPa. Thus obtained pellets were heated, first to the temperature of 723K, kept there for 30 min., and then sintered at 1723 K in air, for 4 h.

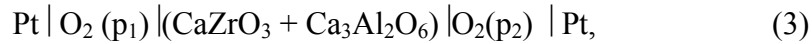
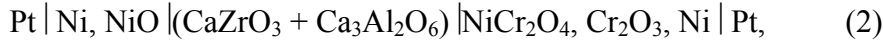
The samples were X-ray analysed, and its phase composition was determined in this way. Density of the samples was measured by the Archimedes method. To determine their electrical properties, the a.c. impedance spectroscopy method was used. The measurements were performed in the temperature range 473 -117K.

The transference oxygen partial number in all samples prepared was estimated from EMF measurements in the temperature range of 823 – 1273K. To this purpose the following galvanic cell was set up.



Two-phase mixtures, (Fe, Fe_xO) and (Ni, NiO) with known equilibrium oxygen partial pressure were used as half-cells.

Knowing the transference oxygen number, the samples were tested as electrolytes in the galvanic cells, according to the following schemes.



The measurements were performed at the temperature of 1273 K (cell 2) and in the temperature range 873-1273K (cell 3). Details of the experimental procedure were similar to those described in reference [7]. The cell (3) operated as an oxygen gas sensor. Pt/air was applied as a reference electrode (p_1). The test gas mixture (p_2) containing 0.1 % O_2 in argon, was used as a second electrode.

3. Results and discussion

In all the samples prepared, only the CaZrO_3 and $\text{Ca}_3\text{Al}_2\text{O}_6$ phases were found in X-ray diffraction patterns.

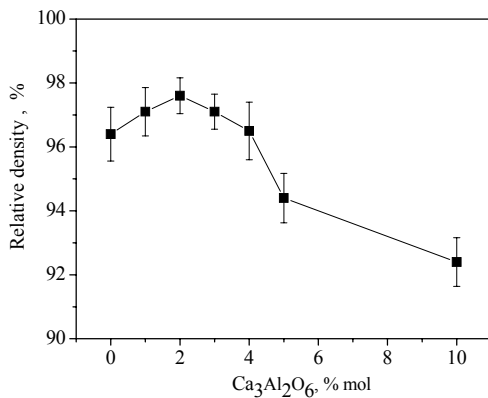


Fig.1 Compositional dependence of relative density of the sintered materials

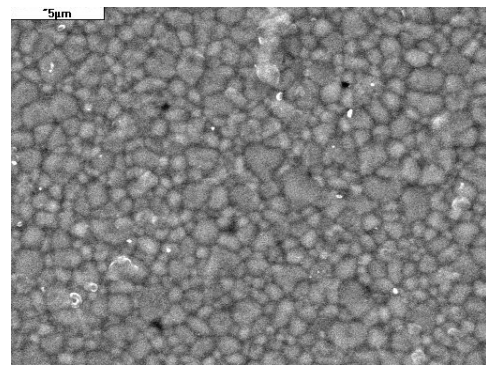


Fig 2. Microstructure of the $(\text{CaZrO}_3+\text{Ca}_3\text{Al}_2\text{O}_6)$ composite containing 2 % mol $\text{Ca}_3\text{Al}_2\text{O}_6$

Fig.1 shows, how the $\text{Ca}_3\text{Al}_2\text{O}_6$ inclusions influences density of the samples. An increase of $\text{Ca}_3\text{Al}_2\text{O}_6$ inclusions up to content of 4 % mol, caused a deterioration in a

sinterability of the powders. It resulted from shrinkage incompatibilities of the matrix and inclusions in the course of densification. Only gas-tight composite samples should be applied as electrolytes in solid-state galvanic cells. Fig 2. presents typical microstructure of the CaZrO_3 containing 2 % mol $\text{Ca}_3\text{Al}_2\text{O}_6$ with small and close porosity, and with isometric grains of 1-2 μm in size.

Impedance spectroscopy enabled the determination of the bulk (σ_b) and grain boundary ionic (σ_{gb}) conductivities of the composite samples sintered. Respective values of the conductivities at the temperature of 873 K are given in table 1. The values of the activation energy (E_a), calculated in the temperature range 473-1173K are also given.

Tab.1 Electrical conductivity at 873K of the composite $\text{CaZrO}_3\text{-Ca}_3\text{Al}_2\text{O}_6$ samples prepared

x	$\sigma(\text{S/cm}), 873\text{K}$		E_a, eV
	Bulk	grain boundary	
0	$6.81 \cdot 10^{-9}$	-----	2.31 (b)
1	$4.15 \cdot 10^{-5}$	$8.74 \cdot 10^{-6}$	1.09 (b) 1.23 (gb)
2	$6.82 \cdot 10^{-5}$	$7.11 \cdot 10^{-5}$	0.89 (b) 1.06 (gb)
3	$5.72 \cdot 10^{-5}$	$7.28 \cdot 10^{-5}$	0.92 (b) 0.95 (gb)
4	$4.41 \cdot 10^{-5}$	$5.11 \cdot 10^{-5}$	0.98 (b) 1.12 (gb)
5	$3.82 \cdot 10^{-5}$	$3.12 \cdot 10^{-5}$	1.11 (b) 1.16 (gb)
10	$3.27 \cdot 10^{-5}$	$2.81 \cdot 10^{-5}$	1.14 (b) 1.21 (gb)

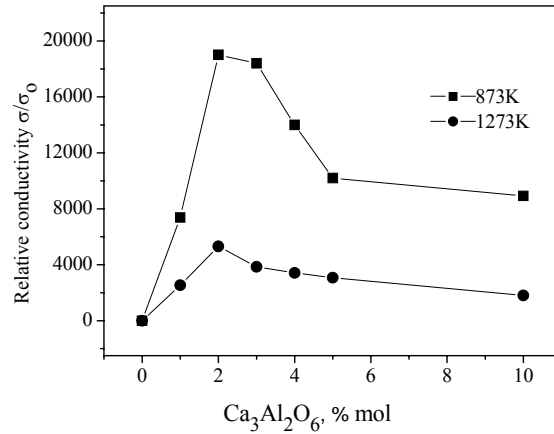


Fig 2. Changes of the relative total conductivity (σ/σ_0) of the ($\text{CaZrO}_3\text{+Ca}_3\text{Al}_2\text{O}_6$)composites at 873K and 1273K respectively

As seen from table 1, the bulk and grain boundary conductivity of the composite samples increased up to 3 % mol $\text{Ca}_3\text{Al}_2\text{O}_6$ content, and then fell towards smaller values. In contrary, opposite changes in activation energy values were observed. To visualize an influence of a presence of $\text{Ca}_3\text{Al}_2\text{O}_6$ phase on conduction properties of the composite, the relative total conductivity (σ/σ_0), where σ_0 being the conductivity of pure CaZrO_3 at the temperatures of 873 K and 1273 K is plotted against the $\text{Ca}_3\text{Al}_2\text{O}_6$ content in fig. 2. The inclusion of 2 % mol $\text{Ca}_3\text{Al}_2\text{O}_6$ caused the enhancement in the conductivity by factor ranging from 19987 to 5310, depending on the temperature at which conductivity was measured. The EMF values of cell (1), measured at temperatures from 823K to 1273K, were compared to the respective EMF, measured with the cell involving as a reference electrolyte fully calcia stabilized zirconia. The electrodes in this cell were identical as in the cell (1). The calculated oxygen transference number in the composite samples was found to vary from 0.97 to 0.99 what indicated on their practically pure oxygen ion conduction.

As a solid electrolyte in the cells (2) and (3), a sample containing 2 % mol $\text{Ca}_3\text{Al}_2\text{O}_6$ was applied. The overall cell (2) reaction is the reaction of formation of NiCr_2O_4 , from oxides. On the basis of the EMF of the cell (2), the standard Gibbs free energy of nickel chromite formation (from oxides), $\Delta_f G^\circ (\text{NiCr}_2\text{O}_4)$ could be calculated according to the equation

$$\Delta_f G^\circ (\text{NiCr}_2\text{O}_4) = -2 FE \quad (4)$$

The determined $\Delta_f G^\circ(\text{NiCr}_2\text{O}_4)$ values at the temperature of 1273K are presented in table 2 along with some data existing in literature. As is seen, the results agree well each other. In this way, the usefulness of CaZrO_3 -based composite containing 2 % mol dispersed $\text{Ca}_3\text{Al}_2\text{O}_6$ for thermodynamic investigations was demonstrated.

Tab.2 The standard Gibbs free energies of formation (from oxides) $\Delta_f G^\circ(\text{NiCr}_2\text{O}_4)$ at =1273K

Reference	$\Delta_f G^\circ$ for NiCr_2O_4 [kJ/mol]
this work	-25.60
7	-26.50
8	-26.59
9	-25.33

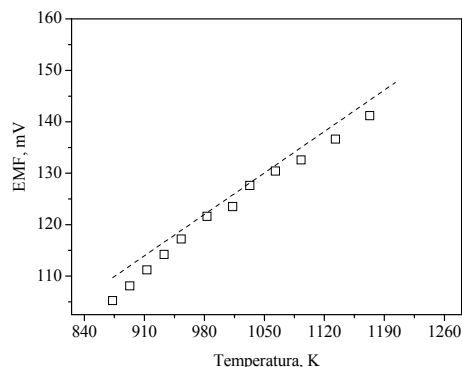


Fig 3. EMF of the cell (3) calculated from Nernst's equation (---) and obtained (□) by our measurements

The EMF values of the cell (3), calculated from the Nernst's equation and obtained from our measurements are shown in Fig. 3. The difference between the calculated and observed values did not exceed 3 mV. Thus, the composite investigated seems to be promising electrolyte also for oxygen sensing.

References

1. V.S.Stubican. In: Science and Technology of Zirconia III. Advances in Ceramics, vol.24. Editors: S.Somiya, Y.Yamamoto, H.Yanagida. American Ceramic Society: Columbus, OH. 1988, pp.71-82.
2. D. Janke, Metallurgical Transactions 13B (1982), 227-235.
3. C. Wang, X.Xu, Yu.H.Wen, K.Zhao. Solid State Ionics 28/30(1988), 542-545.
4. R.C Agrawal, Gupta R.K, J.Mater.Sci. 34 (1999), 1131-1162.
5. M.Bannister, J.Australian Ceram.Soc. 22(1982), 16-25.
6. M. Dudek, G.Róg, W. Bogusz, A. Kozłowska-Róg, Kompozyty 4 (2005), 14-19.
7. A. Kozłowska-Róg, G.Róg, Thermodynamics of Nickel Chromite. Roczniki Chemii 47(1973), 869-870.
8. H.Schmalzried, Yu.D.Tret'yakov. Ber.Bunsenges.physik.Chem. 69(1965), 396-399.
9. M.Dudek, M.Bučko, G.Róg. Inżynieria Materiałowa 23/24(2001), 294-295.

Acknowledgement

This work was financially supported by the AGH - University of Science and Technology in Cracow under contract No. 11.11.160.110.

SELENOORGANIC COMPOUNDS AS OXIDATION REACTION CATALYSTS

M. Giurg*, E. Kowal and H. Muchalski

Wrocław University of Technology, Faculty of Chemistry, Department
of Organic Chemistry, Wybrzeże Wyspiańskiego 27, 50-370 Wrocław, Poland

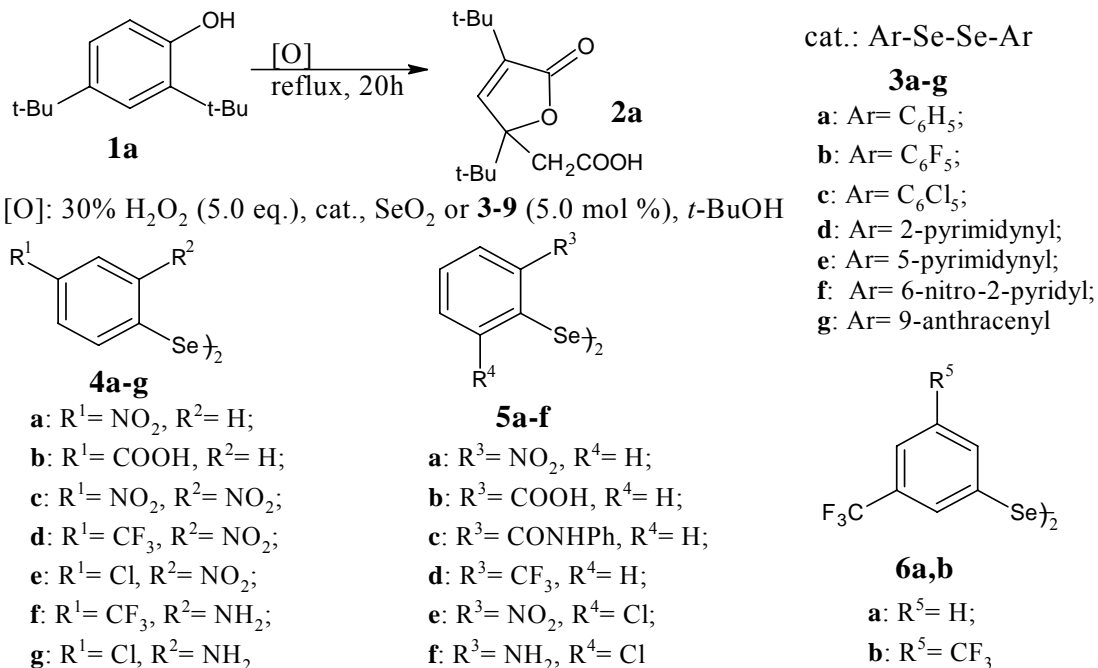
E-mail; mirosław.giurg@pwr.wroc.pl

Introduction

The Sharpless and Reich reported benzeneseleninic acids and its anhydride as good oxidation catalysts in combination with hydroperoxides [1]. Since that time selenoorganic catalysts play an important role in organic chemistry. A further improvement in selenium catalyzed oxidations came with the introduction of electron-withdrawing nitro or trifluoromethyl substituents in the aromatic ring making the catalysts more selective. More recently we selected 2-phenylbenziselenazol-3(2H)-one (ebselen) and polymeric diselenides such as PADS and PPDS as high active oxygen transfer catalysts [2]. The mechanism of their action involves formation of the active intermediates that have selenoxy radical or hydroperoxy groups at the selenium atom [3]. Although several works on the oxidative transformations of various functional groups with these reagents have been published recently, only a few of them report oxidative transformations of the arene ring [4].

Results and Discussion

Here we report that hydrogen peroxide in the presence of selenium catalysts is a good reagent for oxidative degradation of arenes to 1,4-benzo- and naphthoquinones to ring-cleaved products such as carboxylic acids and lactones. The catalytic effectiveness of various selenium compounds was evaluated in the model oxidation of di-*tert*-butylphenol **1a** to 5-carboxymethyl-2(5*H*)-furanone **2a** as is shown in Scheme 1.



Scheme 1

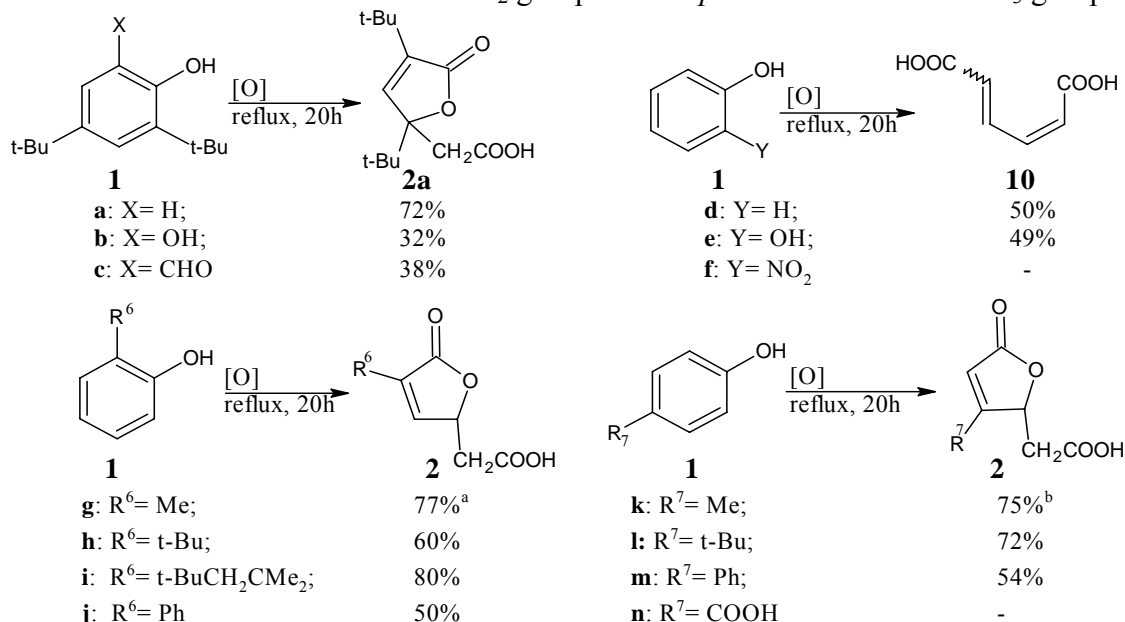
Hydrogen peroxide was used in stoichiometric amounts and the SeO₂, organic diselenides **3–6**, polymeric diselenides PADS (**7**) and PPDS (**8**), or ebselen (**9**) was used in 5% molar ratio. The reaction was carried out in *tert*-butanol at gentle reflux for 20 h. Reaction did not proceed when hydrogen peroxide was used without catalyst. In the presence of SeO₂ the desired 5-carboxymethyl-3,5-di-*tert*-butyl-2(5*H*)-furanone (**2a**) was formed in 25% yield. When organic diselenides **3f**, **3g**, **4c-g**, **5a**, **5b**, **5d** and PADS were used as catalysts, the yields of lactone **2a** were higher. In the presence of the bis-(2-nitro-4-trifluoromethylphenyl) diselenide (**4d**) the substrate was converted almost quantitatively and desired 5-carboxymethylfuranone **2a** was isolated in the highest 72% yield as colourless solid melt at 132-133°C (lit. [5] 132-133°C), Table 1.

Table 1: Oxidation of 2,4-di-*tert*-butylphenol (**1a**) to 5-carboxymethylfuranone **2a**

Catalyst	Yield 2a (%) ^a	Catalyst	Yield 2a (%) ^a	Catalyst	Yield 2a (%) ^a
none	— ^b	4a	3.2	5c	18
SeO ₂	25	4b	7.6	5d	53
3a	7	4c	67	5e	2.0
3b	14	4d	72	5f	1.5
3c	17	4e	60	6a	17
3d	22	4f	28	6b	19
3e	12	4g	50	PADS (7)	31
3f	52	5a	63	PPDS (8)	11
3g	45	5b	45	Ebselen (9)	14

^a Preparative yield. ^b Unreacted substrate was isolated in almost quantitative yield.

These results support our earlier hypothesis that active catalyst intermediate, peroxyselemonic acid is stabilized by *ortho* substituent interacting by resonance and through intramolecular hydrogen bond. This effect can be enhanced by introduction of the additional electron-withdrawing group to the *para* position. In the presented reaction the most effective *ortho* substituent was the NO₂ group and the *para* substituent was CF₃ group.



^a) Mixture with 2-methylmuconic acids isomers in ratio 7 : 3 was formed.

^b) Mixture with 3-methylmuconic acids isomers in ratio 2 : 3 was formed.

Scheme 2

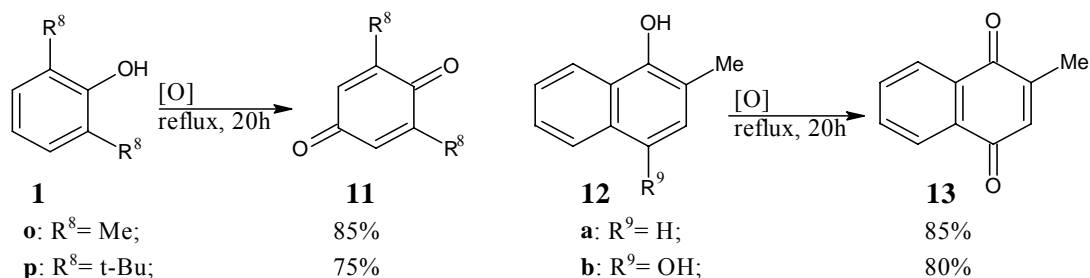
Moreover, it should be noted that catalyst of choice **4d** is easy to obtain by one step selenenylation of commercially available 2-nitro-4-trifluoromethylchlorobenzene with dilithium diselenide according to the procedure elaborated in our laboratory [6].

The reagent, hydrogen peroxide/**4d** was successfully applied for preparative oxidative degradation of different hydroxyarenes to corresponding lactones **2** and muconic acid (**10**) (Scheme 2), 1,4-benzoquinones **11** and menadione (**13**) (Scheme 3), cinnamic acids **16** and benzofuranones **18** (Scheme 4).

In preparative scale, the carboxymethylfuranone **2a** having bulky *tert*-butyl substituents was formed by oxidation of *tert*-butylphenol **1a** and its *ortho* substituted hydroxy **1b** or formyl **1c** derivatives. Unsubstituted phenol (**1d**) and its *ortho* hydroxy substituted derivative **1e** underwent oxidative rearrangement to isomeric muconic acid (**10**) and lactonization did not take place. Muconic acids were recently identified in the effluents from the bleaching of wood pulps [7].

Other alkyl and aryl monosubstituted phenoles **1g-m** having free one or both *ortho* positions, underwent oxidative ring rearrangements to 3- and 4-substituted 5-carboxymethylfuran-2(5H)-ones form **2g-j** and **2k-m**. It has been found that phenol having strong electron-withdrawing nitro **1f** or carboxy **1n** group are resistant toward oxidation, Scheme 2. If both *ortho* positions are substituted by alkyl groups in **1o,p**, only 1,4-benzoquinones **11o,p** were formed. Similarly, from 1-hydroxy-2-methylnaphthalenes **12a,b**, menadione (**13**) was formed in good yield, Scheme 3.

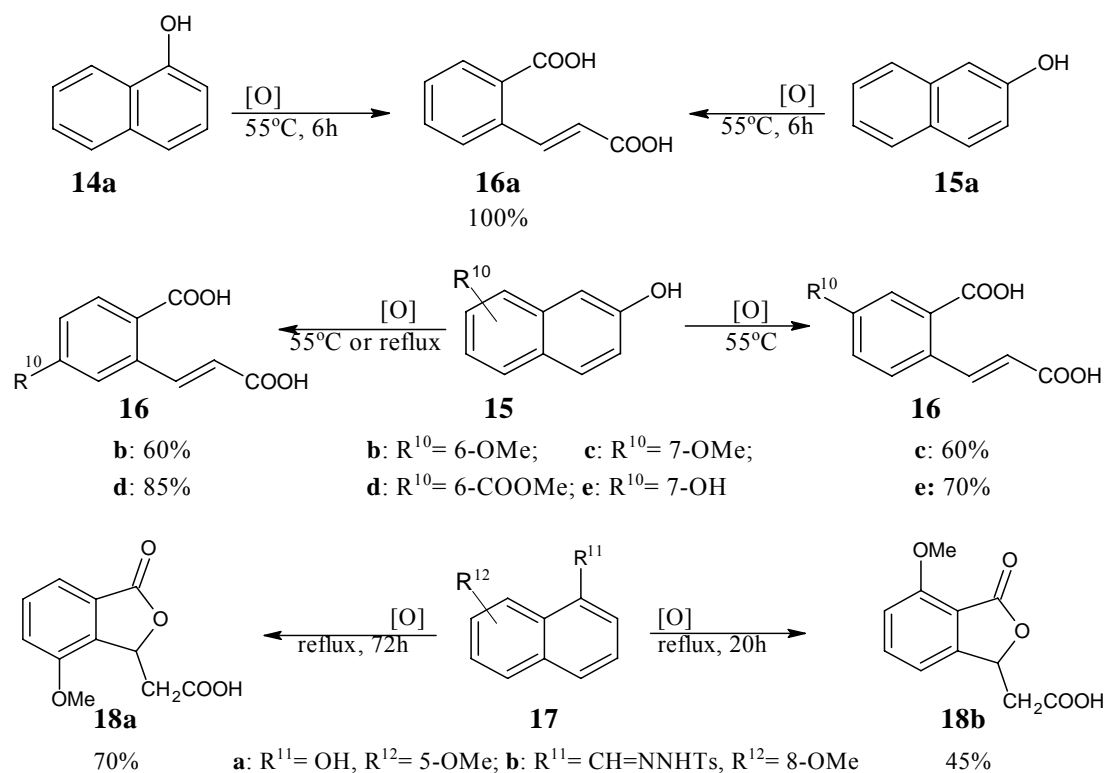
The above results give evidence that first step of reaction is selective *ortho* hydroxylation of electron rich arene ring [7] by strong electrophilic selenium intermediate.



Scheme 3

It is known that H₂O₂/PADS system oxidation of 1- and 2-hydroxynaphthalenes in reflux give *E*-2-carboxycinnamic acid with almost quantitative yield. Oxidation both hydroxynaphthalenes **14a** and **15a** with H₂O₂/**4d** system at mild reaction condition gives quantitatively the same product **16a**. Similar results were observed when 6- or 7-methoxy-2-hydroxynaphthalenes **15b,c** were oxidized at 55°C for 20 or 60h respectively. *E*-2-Carboxycinnamic acids **16b,c** substituted at remote ring carbon atom were formed in 60% yield. Oxidation of 6-carboxymethyl- or 7-hydroxy-2-naphtholes **15d,e** gives better results, but carboxymethyl derivatives require high temperature, excess of oxidant (10 eq.) and 72 h reaction time. On the contrary, oxidation of 5-methoxy-1-hydroxynaphthalene (**17a**) and 8-methoxy-1-naphthaldehyde tosylhydrazone (**17b**) with H₂O₂/**4d** system using excess of oxidant (10 eq.) give lactones, (1-oxo-1,3-dihydroisobenzofuran-1-yl) acetic acid **18a** and **18b** respectively, having methoxy substituents at the vicinity to the condensed heterocyclic ring, Scheme 4.

The above reaction has a practical value, because ring substituted cinnamic acids could find both, research and industrial application [8]. Chemoselective oxidative degradation of hydroxybenzenes to functionalized products such as lactones [7], is of current interest in medicinal chemistry [9].



Scheme 4

References

- [1] (a) T. Hori, K. B. Sharpless, *J. Org. Chem.*, 43 (1978) 1689; (b) K. J. Reich, F. Chow, S. L. Peake, *Synthesis* 1978, 299.
- [2] (a) J. Młochowski, M. Brząszcz, M. Giurg, J. Palus, H. Wójtowicz. *Eur. J. Org. Chem.*, 2003, 4329; (b) J. Młochowski, M. Brząszcz, M. Chojnacka, M. Giurg, H. Wójtowicz, *ARKIVOC* (iii) (2004) 226, and references cited therein.
- [3] (a) L. Syper, J. Młochowski, *Tetrahedron*, 43 (1987) 207; (b) H. Wójtowicz, M. Brząszcz, K. Kloc, J. Młochowski, *Tetrahedron* 57 (2001) 9743; (c) M. Giurg, E. Wiech, K. Piekalska, M. Gębała, J. Młochowski, M. Wolański, B. Ditkowski, W. Peczyńska-Czoch, *Polish J. Chem.*, 80 (2006) 297.
- [4] (a) N. Sonoda, S. Tsutsumi, *Techno. Rept. Osaka Univ.*, 14 (1965) 977; *Chem. Abstr.*, 62 (1965) 16178; (b) M. Giurg, L. Syper, J. Młochowski, *Polish J. Chem.*, 78 (2004) 231; (c) E. Kowal, H. Muchalski, A. Skrzętnicka, M. Giurg, L. Syper, J. Młochowski, *Annals of the Polish Chem. Soc.*, 4 (2004) 1282.
- [5] D. G. Brown, L. Beckmann, C. H. Ashby, *Tetrahedron Lett.*, (1977) 1363.
- [6] M. Giurg, J. Młochowski, *Synthetic Commun.*, 29 (1999) 2281.
- [7] L. N. Mander, C. M. Williams, *Tetrahedron*, 59 (2003) 1105.
- [8] D. G. Harmatan, R.G. Holzinger, *Ullman's Encyclopedia of Industrial Chemistry*, WILEY-VCH, Weinheim, 8 (2003) 6119.
- [9] (a) Y. S. Rao, *Chem. Rev.* 76 (1976) 625; (b) G. Pattenden, *Fortschn. Chem. Org. Naturst.* 35 (1978) 133.

RENEWABLE ENERGY IN POMORSKIE PROVINCE.

Piotr Glamowski, Anna Januszewska, Ewa Maria Siedlecka
Department of Environmental Engineering, Faculty of Chemistry,
University of Gdansk
Sobieskiego 18, 80-952 Gdańsk, piotr@hydrolab.pl

This paper is to present different kinds of renewable energies and their merits as well as their faults that are used in Pomorskie province. The issues described in the paper concern influence of production, storage, transportation, reforming and exploitation the energy in environmental protection. Analyzed methods of energy exploitation from the renewable sources allow to limit air, water and soil pollution. We also try to present possibilities to exploit the unconventional energy in Pomorskie province.

The analysis of the last decades has indicated that the energy consumption and environmental pollution with the products of combustion is exponential in its character. Although it is true that the natural sources of conventional energy (such as coal, petrol and natural gas) are sufficient to fulfill the needs of a few next generations, it is also the fact that by-products and wastes of combustion (dusts, oxides of nitrogen, sulfur and carbon) are not absorbable for natural environment. In the last years appeared the possibility to improve the situation. Many institutions and private persons have tried to reconstruct primeval state and stop natural environment degradation. Publicity campaigns, toughening regulations and punishments for environmental pollution as well as stricter their execution have already given first results, which are observable also in Poland. The amount of pollutions introduced to environment became significantly lower in comparison with previous years, while the acreage of national, landscapes parks, nature reserves and so on increased. In the campaign all accessible achievements of natural sciences were used. On the basis of different researches multistage and broad strategies of improvement of the environment were taken. Natural fuels that are after all running out should be eliminated and replaced with the new, unconventional and renewable sources of energy. Taken into account present development of technology, alternative sources of energy cannot be the main source of energy. These alternative sources of energy because of their specificity, such as dependence on weather, season, a time of the day, geographical placement, require the aid of traditional sources of energy. Both kinds of sources should be treated complementary.

Renewable energy in Pomorskie province

The conditions of insolation in Poland, the country placed in temperate climate, are typical for most middle European countries. Average sums of insolation in one year in Poland depend on the region and amount to from 1300 to 1900 hours. Average year sum on insolation for Pomorskie province equals to 1600 hours, that is 18,2 % of the period of one whole year.

Advantageous insolation is the one of the positive aspects that can be useful for production of thermal and electrical energy. There is the possibility to obtain solar

energy at rural areas of Baltic seaside, as well as large fields that are not used economically.

The surface area of Pomorskie province and its advantageous seaside placement create favourable conditions for localization of wind power plants. The reserves of wind energy are stable source of energy: 75% of acreage of Poland belongs to the regions of good wind conditions, and 5% of this acreage are the regions of extremely good wind conditions. And the Pomorskie province belongs to the last.

But the most serious source of renewable energy in Pomorskie province is biomass. Currently, in this region act a few heating systems using straw as fuel. Durability of stoves fueled with straw is much bigger than the stoves fueled with coal, because straw contains less sulfur than coal. There is also installed a few heating systems fueled with timber wastes. The interest in using wood and timber wastes as a energy fuel arose due to easiness of its acquiring and low maintenance costs. The supply of wood biomass increase and will be increasing. We have information that every year over 7 mln m³ unused timber waste is left in forests and about the growing of agricultural areas that are not used. We can also anticipate increase supply of straw accordingly to development of production liquid of bio-fuel.

There are also installations using bio-gas as fuel in Pomorskie province as well as electric generators and boilers at wastewater plants and at garbage dumps.

The province is placed in the range of river basin of Wisła and seaside rivers. The main rivers are: Wisła, Wda, Wierzyca, Brda, Motława with Radunia and the rivers flowing immediately into the sea i.e. Leba, Reda, Łupawa, Słupia. There is many lakes (about 1,5 thousand of over 1ha surface area): Wdzyckie, Żarnowieckie, Charzykowskie, Raduńskie. The biges are Łebsko and Gardno. Waterway network is very thick, complicated and diverse. This is why at the area of Pomorskie province act over 20 hydroelectric power stations of different powers.

Conclusions

After consideration of many aspects of using renewable energy in Pomorskie province it can be said that the way in which we use natural sources of energy influences ecological development of the region. In Pomorskie province renewable sources of energy are exploited very scanty. But we have note here geographical situation of Pomorskie province and limited financial potential of industry as well as individual persons.

Renewable sources of energy can take essential part in energy balance of the indyvidual districts of our province. They can have positive impact on energy safety of the region, especially on the parts of the province that are underdeveloped in the regard of energy supply. Potentially the main consumers of energy from renewable sources are agriculture, transport and the housing industry. Especially in the regions that are afflicted with unemployment the renewable sources of energy can create many new places of employment. And agricultural areas which cannot be used for food production because of soil contamination can still be used for energy crops.

There is there is general agreement that development of power production based at renewable sources can contribute to find a solution of many ecological problems generated by power industry.

Reference.

- [1]. Lewandowski W.M., (2001), Proekologiczne źródła energii odnawialnej, Wydawnictwa Naukowo–Techniczne,
- [2]. Ciechanowicz W., (1997), Energia, środowisko i ekonomia, Instytut Badań Systemowych PAN,.
- [3]. Praca zbiorowa pod redakcją Flejterskiego S., Lewandowskiego P., Nowaka W., (2003), Energia odnawialna na Pomorzu Zachodnim, I Regionalna Konferencja i Wystawa,
- [4]. Informacje wewnętrzne Wydziału Środowiska i Rolnictwa Pomorskiego Urzędu Wojewódzkiego w Gdańsku.
- [5]. Bochliński J., Zawadzki J., (1999), Polska – nowy podział terytorialny, Świat Książki, strony: 241, 246.

STRUVITE PRECIPITATION AS EA METHOD FOR PHOSPHATES REDUCTION.

Piotr Glamowski, Anna Januszewska, Ewa Maria Siedlecka
Department of Environmental Engineering, Faculty of Chemistry,
University of Gdansk

Ul. Sobieskiego 18, 80-952 Gdańsk, piotr@hydrolab.pl

Introduction

„Struvite” is a commonly used name of magnesium ammonium phosphate. It occurs in the form of crystals in natural conditions as well as in technical objects, most frequently wastewater plants.

In 1939 the presence of struvite was observed in wastewater plants for the first time. However the first documented exploitation problems come from 1960 from wastewater plant *Hyperion* in Los Angeles, where the diameter of fermented sludge pipes substantially decreased because of precipitated struvite.

The aim of this job is to determine optimal conditions for removing of magnesium ammonium phosphate from wastewater. Controlled precipitation of struvite in wide range of pH and magnesium ions concentration was performed. And then was found out the optimal range of the parameters for the best phosphates reduction.

Conditions of the performed research

In the investigations were used the samples of supernatant from fermented wastewater sludge centrifuges. The effective precipitation of struvite depends on concentration of ions, that it is built of, and the value of pH. The range of pH applied in investigations was taken from previously performed investigation of controlled precipitation of struvite in prepared wastewater. Optimal pH fluctuated from 8,5 to 9,6. And such the range was used in the investigation. The doses of magnesium ions was chosen on the basis of molar proportions of particular ions present in raw wastewater and equaled: 24, 30, 35, 40, 45 and 50 mg Mg^{2+}/dm^3 . The source of magnesium ions was solution $MgCl_2$, where the concentration of Mg^{2+} ions amounted to 10 000 mg/dm³. [1,2,3].

The performance of the experiment

The appropriate quantity of $MgCl_2$ solution was added To 100 cm³ wastewater. And then pH of the wastewater was adjusted to proper level by the means of 1mol/dm³ NaOH solution. Then the wastewater was mixed by using magnetic stirrer. The samples for analysis were taken after 10, 20 and 30 minutes, then permeated. After this concentration of phosphate, ammonium and magnesium ions were determined.

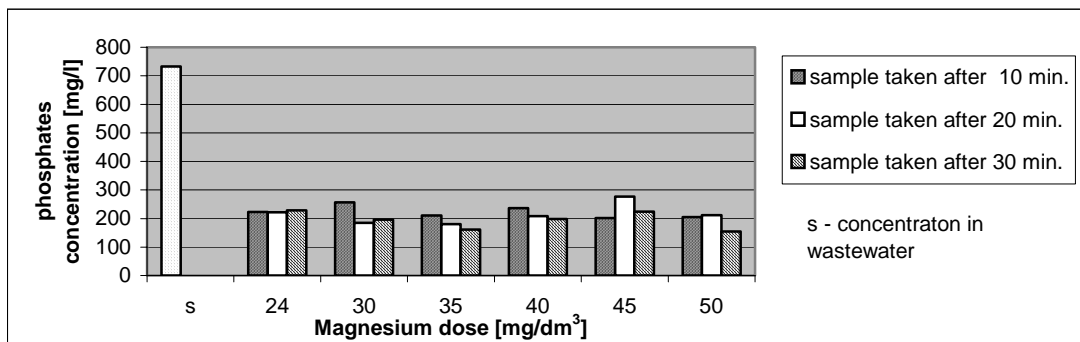
Results

The results of experimental works are given in Tab. 1

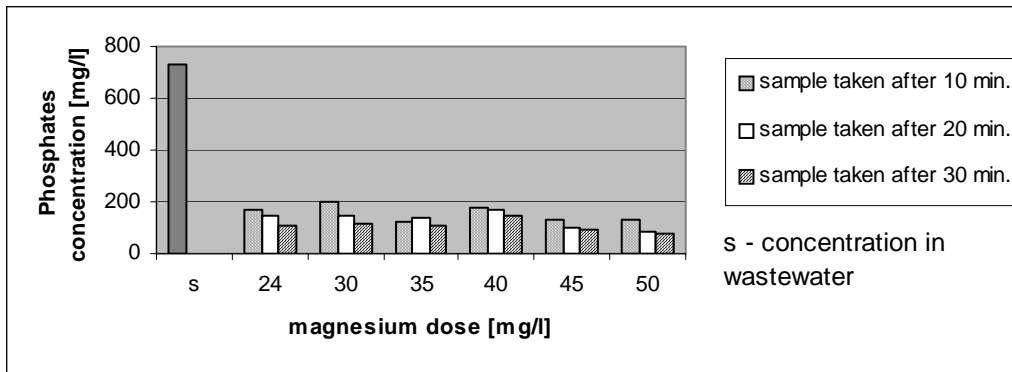
Tab 1. Concentration of phosphates after struvite precipitation in various conditions.

pH	t (min.)	Magnesium dose [$\text{mg Mg}^{2+} / \text{dm}^3$]					
		24	30	35	40	45	50
8,5	10	223,17	256,99	210,67	236,72	201,76	204,88
	20	221,31	184,64	180,4	208,7	277,26	211,33
	30	228,72	196,06	161,48	197,82	224,49	155,01
8,8	10	209,9	181,48	296,26	163,56	185,31	102,08
	20	387,79	153,96	140,66	127,37	167,76	97,77
	30	177,66	190,8	109,21	118,81	94,15	73,42
9,0	10	166,98	199,1	125,14	176,32	132,48	131,69
	20	145,01	149,61	139,63	167,63	99,52	85,79
	30	108,81	117,63	106,43	142,98	89,63	77,98
9,2	10	124,87	129,45	119,21	109,74	96,43	98,08
	20	192,9	101,45	96,98	86,85	76,94	65,4
	30	85,42	81,96	73,63	72,45	51,84	21,32
9,4	10	108,44	113,96	111,24	98,79	119,74	77,63
	20	101,99	99,61	98,34	83,98	56,43	69,08
	30	95,02	52,27	75,26	69,08	53,51	24,87
9,6	10	125,02	131,21	141,45	111,45	110,32	81,45
	20	111,97	116,19	95,83	92,9	78,26	73,82
	30	127,8	94,43	107,63	83,65	69,67	68,26

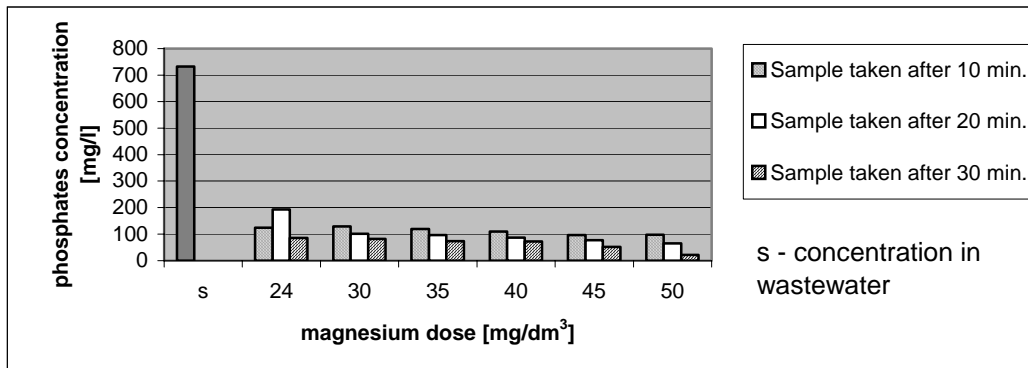
The graphs at the pictures 1-5 shows the how the phosphate concentration changed during the struvite precipitation after 10,20 and 30 minutes after the beginning the process.



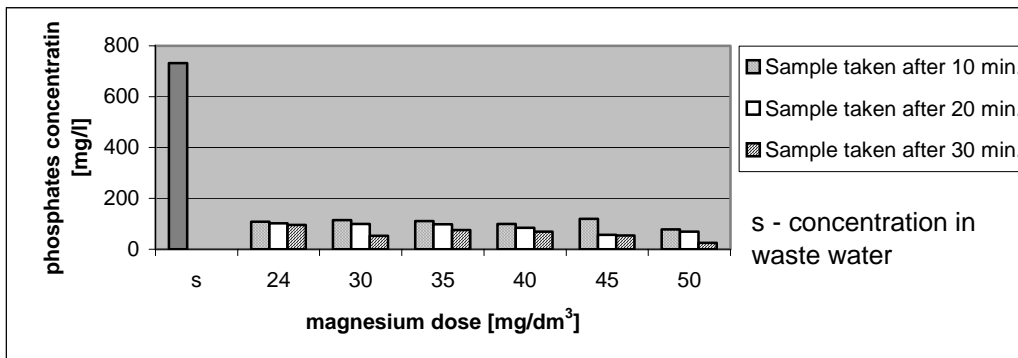
Picture. 1. Phosphates concentration in pH = 8,5.



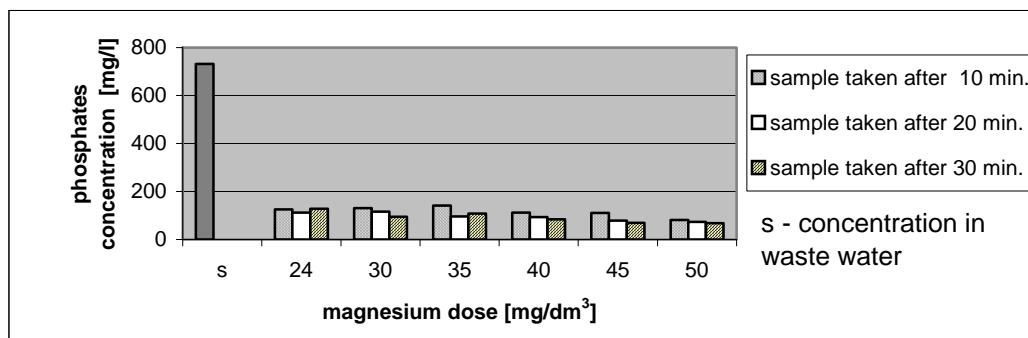
Picture. 2. Phosphates concentration in pH = 9.



Picture. 3. Phosphates concentration in pH = 9,2



Picture. 4. Phosphates concentration in pH = 9,4



Picture. 5. Phosphates concentration in pH = 9,6

There is a significant reduction of concentration of phosphates during the precipitation of struvite. In tested pH range, the lowest value of concentration reduction was reached in pH = 8,5, where it was between 70 and 84%, dependently on used magnesium dose. The increase of the reduction followed the increase of pH, and accordingly in pH=9 the reduction amounted to from 80 to 92%. In higher pH (9,2-9,4) the reduction of phosphates concentration stabilized at the level 90-95%. In the higher range of pH (9,6) the reduction minimally decreased.

In accordance with the magnesium dose the reduction of phosphates concentration increased and mostly it reached the maximum at the dose 45 mg/dm³.

Because of time of precipitation in majority cases the highest reduction was reached in 30 minutes after the beginning of the process.

Conclusions

The results of the investigations prove that controlled struvite precipitation is a good method of phosphate removing from wastewater. Obtained data show that optimal conditions of precipitation are in pH between 9,2-9,4 and magnesium dose 45mg/dm³. By such the parameters the reduction of phosphate concentration is from 90 to 95 %.

As it was shown in experiments, effectiveness of phosphate removing from wastewater during controlled struvite precipitation equals over 90%. In spite the fact that the method is quite new and not popular, the process can be competitive for another methods of phosphates reduction, although it requires rebuilding of technological line. The other advantage of the method is that formed struvite can be used in different industrial domains, as e.g. good fertilizer for plants. It eliminates problems of overproduction of wastes that rises when another method are applied.

Acknowledgements

We are very grateful Ms Agnieszka Kamińska and Mr Michał Kołodziejczyk for their help in lab works. The investigations were financed by DS./8270-4-0093-6.

Literature

- [1] Tabernacki K., Struwit w miejskich oczyszczalniach ścieków. Gaz, woda i technika sanitarna nr12/2002, SIGMA-NO, Warszawa 2002
- [2] Stratful I., Scrimshaw D.M., Conditions influencing the precipitation of magnesium ammonium phosphate. Water Research.Vol.35, No.17, Elsevier Science Ltd. 2001
- [3] Munch V.E., Barr K., Controlled struvite crystallisation for removing phosphorus for anaerobic digester sidestreams. Water Research.Vol.35, No.1, Elsevier Science Ltd. 2001

PREPARATION OF CHROMIUM VANADATE BY HIGH-ENERGY BALL MILLING AND SOL-GEL METHODS

A. Gomulczak, J. Najman

*Faculty of Chemical Engineering and Technology, Cracow University of Technology,
Warszawska 24, 31-155 Cracow, Poland*

INTRODUCTION

Properties of synthesized materials often depend on the synthesis method. In this study the chromium vanadate formation was considered using mechanical treatment of metal oxides and sol-gel method. The compounds from V_2O_5 - Cr_2O_3 system [1] exhibit magnetic and catalytic properties [2-3].

Chromium(III) metavanadate(V) can be obtained through high-temperature reaction of oxides in solid state at atmospheric pressure [2,4], at high pressure [5] and using wet methods [6,7]. There were also made attempts using mechanochemical methods [8].

EXPERIMENTAL

A. Mechanochemical synthesis

Materials: Cr_2O_3 (Fluka) and V_2O_5 (Aldrich) mixture with mol ratio of 1:1 (V-Cr-O)

Mechanical treatment: planetary ball mill *Pulverisette 6* (Fritsch GmbH), BPR=10:1; rpm=550; dry conditions: Ar; time of milling: up to 60 h (V-Cr-O/60). The samples for analyses were taken off after 4.5h (V-Cr-O/4.5) and 30h (V-Cr-O/30).

B. Sol-gel method

Materials: $Cr(NO_3)_3 \cdot 9H_2O$, NH_4VO_3 and $C_6H_8O_7 \cdot H_2O$ (POCh Gliwice).

Procedure: precipitated citrates of both metals after evaporation were heated for 5 hours at 350°C and 450°C, respectively.

C. Samples characterization techniques

The solid compounds were characterized using conventional methods: powder X-ray diffraction (XRD) using Philips X'Pert diffractometer (CuK_{α}), thermal analysis (TA) using SDT TA Instrument and infrared spectroscopy (FTIR) using Spectrofotometer TS 2000 Scimitar Series.

RESULTS AND DISCUSSION

A. Tojo *et al.* [8] show that synthesis of $CrVO_4$ by milling for 3 hours occurs when hydrated chromium oxide was used. However, in the case of anhydrous chromium oxide using the synthesis did not succeed.

Our preliminary study shows that mechanochemical synthesis of $CrVO_4$ using metal oxides as precursors takes place but it requires longer time of milling.

The kinetics of formation of $CrVO_4$ phase during milling has been estimated by the effects of melting of V_2O_5 and/or $CrVO_4$ (DTA curves in Fig.1), as well as XRD patterns shown in Fig.2.

Chromium vanadate appeared in samples after 4.5 hrs of milling. Its quantity increases with time (see: effect of melting at ca. 920°C in Fig. 1 b-d). However, the presence of chromium vanadate as a crystalline phase is observable after 30hrs of milling because of its small amount in the sample (Fig. 2d).

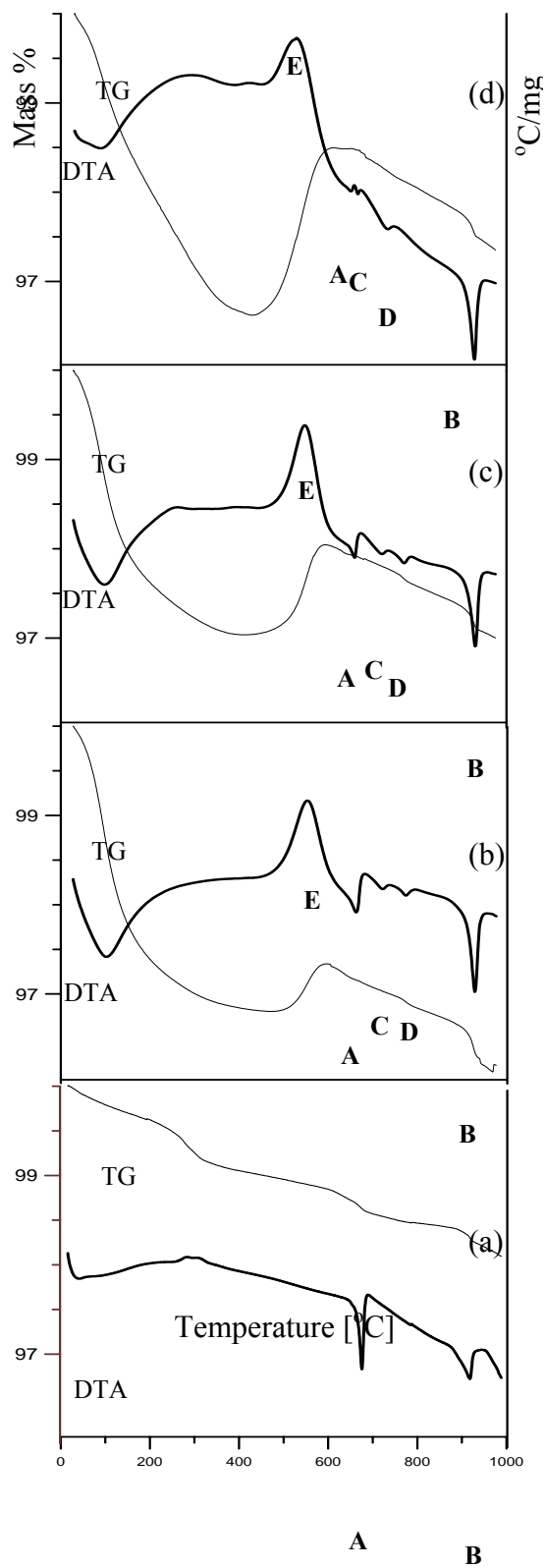


Fig.1 TA results of non-milled (a) and milled for 4.5h (b), 30h (c) and 60h (d) samples. (A-melting of V_2O_5 , B-melting of $CrVO_4$, C-decomposition and D-melting of $Cr_2V_4O_{13}$, E -oxidation of WC).

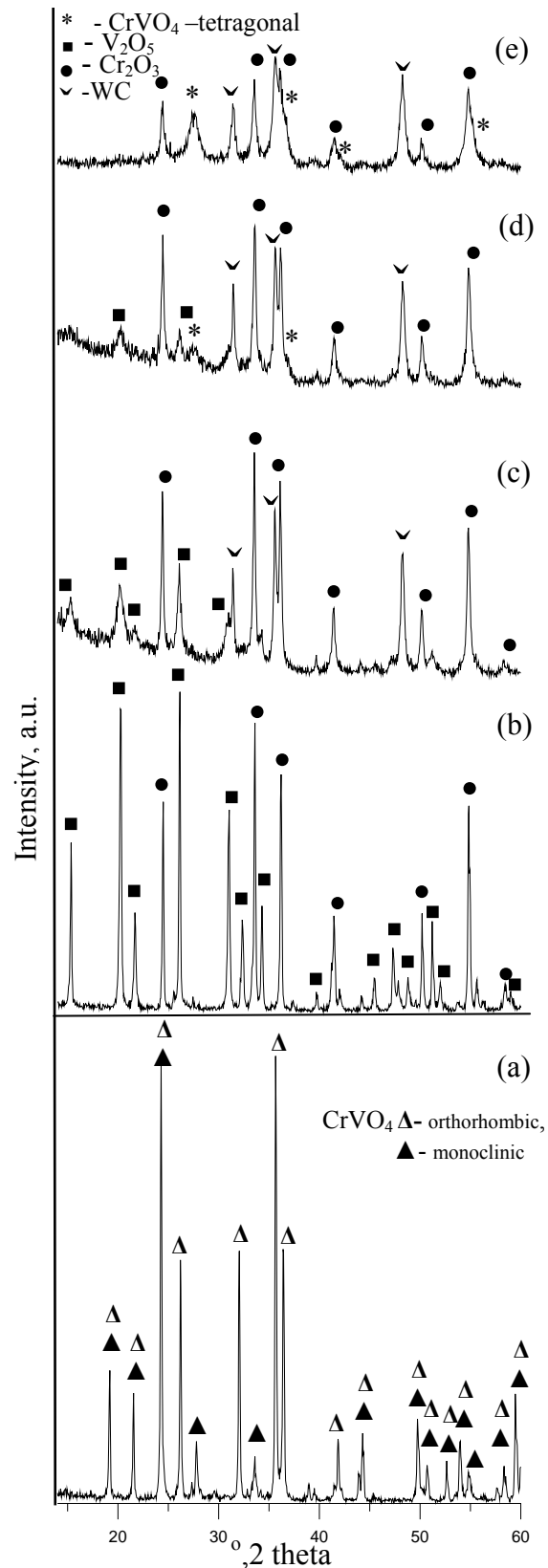


Fig.2 XRD results: of $CrVO_4$ - sol-gel (a), non-milled (b) and milled for 4.5h (c), 30h (d) and 60h (e) samples. (WC- contamination)

Chromium vanadate appeared in samples after 4.5 hrs of milling. Its quantity increases with time (see: effect of melting at ca. 920°C in Fig. 1 b-d). However, the presence of chromium vanadate as a crystalline phase is observable after 30hrs of milling because of its small amount in the sample (Fig. 2d).

Unfortunately, even 60 hrs milling did not lead to total conversion of substrates. Therefore, peaks of Cr₂O₃ are still present. Intensities of V₂O₅ peaks decline in XRD spectra after 30 h of milling because of its amorphization, not its absent in the sample.

The effect of V₂O₅ melting registered at 670°C indicates the presence of this oxide in the samples.

Besides CrVO₄ and non-reacted metal oxides, Cr₂V₄O₁₃ appears in the samples, which is confirmed by a sequence of two endothermic effects on DTA curve, at ca. 720 and 770°C. It necessary to noticed that the first can be attributed to decomposition of Cr₂V₄O₁₃ to CrVO₄ and V₂O₅, and the second one to melting of non-decomposed Cr₂V₄O₁₃. These effects are small and do not increase with time of milling, also the lack of reflexes corresponding to this phase in XRD spectra confirms its small content. The exoeffect on DTA curve at 530°C (Fig. 1 b-d) combined with mass increase on TG curve is caused by oxidation of WC – the material of the vial that was introduced into the sample during milling as a contamination.

Due to multiphase composition of this system interpretation of IR spectra is difficult and non-unequivocal.

Chromium metavanadate obtained by this way has tetragonal structure. Such form is known as a result of high-pressure — high-temperature synthesis [8].

B. Using sol-gel method leads to formation the chromium vanadate, as a mixture of monoclinic and orthorhombic forms (Fig.2a).

Similar to tetragonal CrVO₄ (from the mechanochemical treatment), these two forms melt at ca. 920°C (results of these tests are not included in this paper). Lack of other thermal effects confirms total conversion of reactants.

FTIR absorption spectra complete and confirm above conclusion. All bands in the range of 1000-400 cm⁻¹ are characteristic for CrVO₄, V₂O₅ and Cr₂O₃ (Fig.3). Bands at ca 950 and 880 cm⁻¹ correspond to stretching vibrations of V-O bonds in CrVO₄, bands at ca. 730, 650 and 425 cm⁻¹ correspond to stretching vibrations Cr-O in CrVO₄ (Fig.3c). Stretching vibrations of V-O-V bridges are connected with 540 cm⁻¹ band.

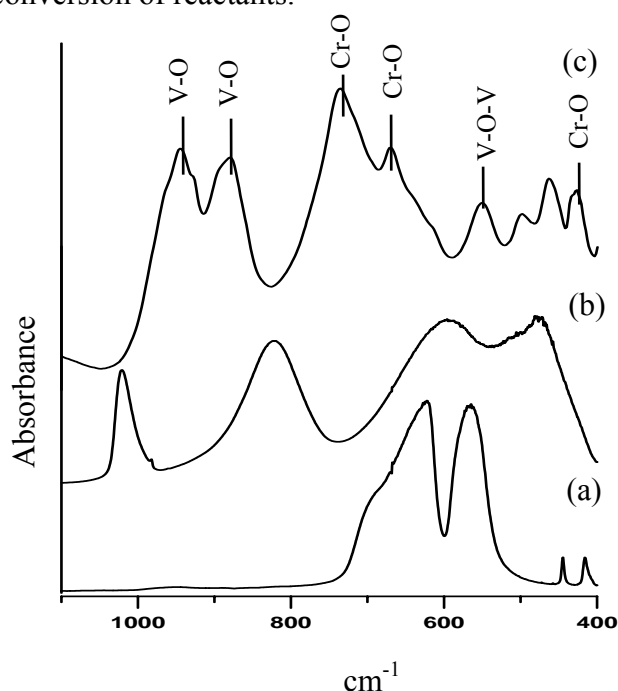


Fig. 3 IR of Cr₂O₃ – (a); V₂O₅ – (b); and CrVO₄ – (c) (method sol-gel)

4. CONCLUSIONS

It was shown that the chromium metavanadate using high energy ball milling as well as sol-gel method can be obtained. By mechanical treatment of chromium and vanadium oxides, metavanadate forms in tetragonal form. In the latter case, CrVO₄ forms as the only product of reaction being a mixture of monoclinic and orthorhombic forms of metavanadate.

The products obtained by two ways have different catalytic properties depending on the used method of synthesis. Their catalytic activity was tested in oxidative dehydrogenation of propane and oxidation of carbon monoxide reactions. This is a subject of another study.

Acknowledgment

This study was supported by the Science and Education Ministry, Poland
Projects No: C-1/BW/06 and C-1/DS/06.

References:

- [1] R. C. Kerby, J. R. Wilson, *Can. J. Chem.* 51 (1973) 1032
- [2] M. J. Isasi, R. Sáez-Puche, M. L. Veiga *et al.*, *Mat. Res. Bull.*, 23 (1988) 595
- [3] A. M. Youssef, A. I. Ahmed, S. E. Samra *et al.*, *Adsorption Sci. Technol.*, 18 (2000) 777
- [4] J. Walczak, E. Filipek, *J. Therm. Anal. Cal.*, 35 (1989) 69.
- [5] J. Baran, J.C. Mulle, J. Joubert, *J. Solid State Chem.*, 14 (1975) 8
- [6] P. Soudan, J.P. Pereira-Ramos, J. Farcy, G. Grégoire, *et al.*, *Solid State Ionics*, 135 (2000) 291
- [7] M. Touboul, K. Melghit, *J. Mater. Chem.*, 5 (1995) 147
- [8] T. Tojo, Q. Zhang, F. Saito, *J. Solid State Chem.*, 179 (2006) 433

ELECTROCHEMICAL FORMATION AND PROPERTIES OF TWO-COMPONENT FILMS OF TRANSITION METAL COMPLEXES AND [C₆₀]FULLERENE OR [C₇₀]FULLERENE

Joanna Grabowska and Krzysztof Winkler

Institute of Chemistry, University of Białystok, Hurtowa 1, 15-399 Białystok

1. Introduction

The new electrochemically active materials have been of considerable interest in recent years due to their potential application as electroactive materials in batteries [1], supercapacitors [2], sensors [3,4] or electrochromic devices [5].

Recently, we have focused on the development of novel electroactive polymers based on fullerenes [6-12]. The electrochemical reduction of fullerene epoxides, C₆₀O and C₇₀O, results in deposition of polymeric films onto electrode surfaces [6,7]. The two-component films of fullerenes or their derivatives and transition metal complexes are formed on the electrode during reduction carried out in solution containing fullerenes and complexes of such transition metals as palladium [8-11], platinum [12,13], rhodium [8] or iridium [8]. In the resulting films, the fullerene moieties are believed to be bonded to the metal centers in η^2 fashion to form a polymeric network. Polymers of C₆₀ and transition metal complexes, C₆₀/M, exhibit electrochemical activity in the negative potential range due to the reduction of the fullerene moieties present. The process of film reduction is accompanied by the transport of cations from the supporting electrolyte into the film [9]. Therefore, these films exhibit *n*-doped properties. Redox-active films of transition metals and fullerene derivatives containing electron-donating groups, 2'-ferrocenylpyrrolidino-[3',4';1,2][C₆₀]fullerene and C₆₀ with a covalently linked zinc *meso*-tetraphenylporphyrin, can be also synthesized under electrochemical conditions [10,11]. These films can undergo both *p*- and *n*-doping. At negative potentials, reduction of fullerene moieties occurs. In positive potential range, the processes of ferrocene or zinc *meso*-tetraphenylporphyrin oxidation take place.

So far, most of the work was focused on the study of formation and properties of [C₆₀]fullerene based electroactive materials. In this paper, the processes of electropolymerization of two component films of transition metal complexes and [C₆₀]fullerene, C₆₀/M, and [C₇₀]fullerene, C₇₀/M, are compared. The electrochemical properties of these films are also investigated.

2. Experimental

Palladium(II) acetate, Pd(ac)₂, (Alfa), and C₆₀ (Southern Chemical Group) were used without additional purification. Supporting electrolytes: tetra(ethyl)ammonium perchlorate, (Et₄N)ClO₄ (Aldrich), tetra(*n*-butyl)ammonium perchlorate, (*n*-Bu₄N)ClO₄ (Sigma), and tetra(*n*-hexyl)ammonium perchlorate, (*n*-Hx₄N)ClO₄ (Fluka) were used as received. Anhydrous acetonitrile (99.9 %, Aldrich) was used as received from. Toluene (Aldrich) was purified by distillation over sodium under argon atmosphere.

Voltammetric experiments were performed on a PAR potentiostat with a three-electrode cell. A 1.5 mm diameter Au disk electrode (Bioanalytical Systems, Inc.) was used as the working electrode. For imaging by scanning electron microscopy, SEM, films were deposited electrochemically on Au foil (Goodfellow Metals, Ltd., Cambridge, UK). Prior to the experiment, the Au foil was annealed in a Bunsen flame. A silver wire immersed in a mixture of 0.01 M AgClO₄ and 0.09 M (*n*-Bu₄N)ClO₄ in acetonitrile and separated from the

working electrode by a "thirsty glass" tip (Bioanalytical Systems, Inc.) served as the reference electrode. For this reference electrode, the ferrocene/ferrocenium formal redox potential was +161 mV. A Pt tab with a surface area of about 0.5 cm² served as the counter electrode.

Secondary electron scanning electron microscopy images were obtained with the use of an SEM FEI XL30s instrument of FEG (Oregon, USA). The accelerating voltage for the electron beam was 10 and 20 keV and the average working distance was 5 mm.

3. Results and discussion

The C₆₀/M and C₇₀/M (M = Pd, Rh, and Ir) films were prepared through electroreduction of an acetonitrile/toluene (1:4, v:v) solution that contained both fullerene and transition metal complex and the supporting electrolyte, 0.1 M (*n*-Bu₄N)ClO₄. Films were grown under cyclic voltammetry conditions at a sweep rate of 100 mV/s. Figure 1 shows the multicyclic voltammograms of C₆₀/Rh and C₇₀/Rh films formation. Upon repeated scanning of the potential between 100 and -1450 mV, an increase of the current in the potential range for fullerene moiety reduction is seen for two systems. The comparison of voltammograms obtained in solutions containing C₆₀ and C₇₀ indicates for slightly higher efficiency of C₆₀/Rh formation than yield of C₇₀/Rh deposition. Higher differences in mass of polymer deposited on the electrode surface were detected by electrochemical quartz crystal microbalance (EQCM) studies. Results of EQCM experiments allow estimation of C₆₀/Rh and C₇₀/Rh film thickness. Assuming that C₆₀/Rh and C₇₀/Rh layers have structures proposed by Nagashima *et al.* [14] for C₆₀/Rh polymer, the mass of the undoped monolayer calculated to be 1,17·10⁻⁷ g/cm² and 1,22·10⁻⁷ g/cm² for C₆₀/Rh and C₇₀/Rh, respectively. Results of EQCM studies shows that during one voltametric cycle about 15 monolayers of C₆₀/Rh and about 7 monolayers of C₇₀/Rh were deposited at the electrode surface. Difference in yields of films formation obtained by EQCM is much higher that suggested by results of cyclic voltammograms. This effect is probably related to the fact that only the thin surface layer of the polymers are involved in the reduction/reoxidation processes.

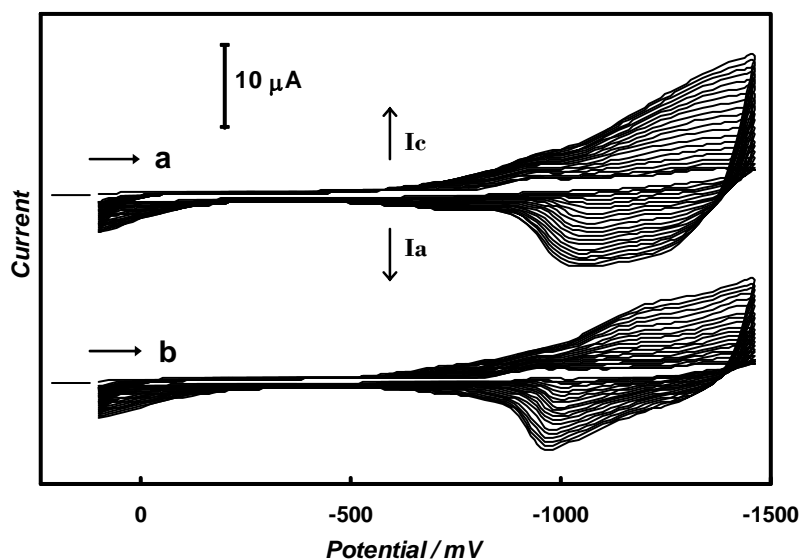


Figure 1. Multicyclic voltammogram (20 cycles) obtained in acetonitrile/toluene (1:4, v:v) solution containing 0.1 M (*n*-Bu₄N)ClO₄, 0.85 mM (CF₃CO₂)₄Rh₂, and 0.25 mM C₆₀ (a) or 0.25 mM C₇₀ (b). The sweep rate was 100 mV/s.

The electrode covered with the C₆₀/Rh or C₇₀/Rh films was transferred to the solution of acetonitrile containing only the supporting electrolyte and the cyclic voltammograms were

recorded. Relevant data obtained for C_{60}/Rh or C_{70}/Rh are shown in Figure 2 and 3, respectively. Films are electrochemically active in negative potential range due to the reduction of fullerene cage. Switching between oxidation states at negative potentials involves cation transport between the film and the solution. Therefore, the voltammetric response of the film is strongly affected by the nature of the cation of supporting electrolyte.

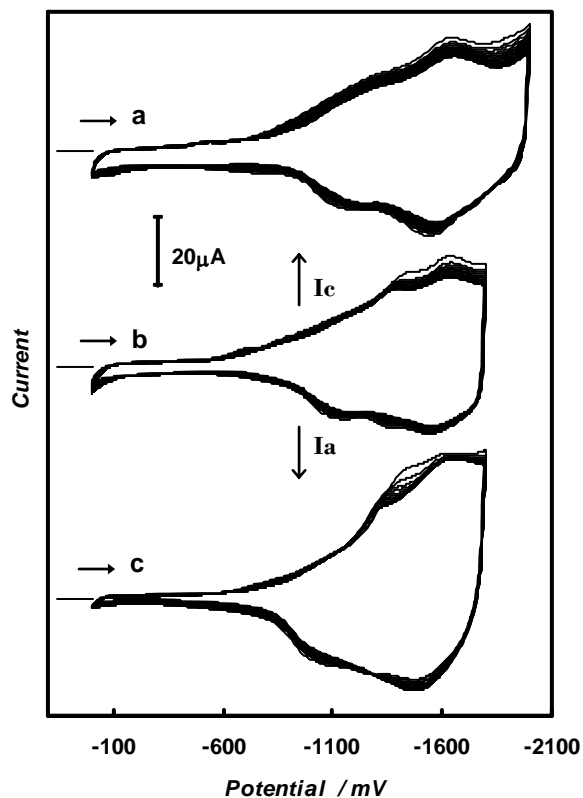


Figure 2. Multicyclic voltammograms of C_{60}/Rh film in acetonitrile containing (a) 0.1 M $(Et_4N)_4ClO_4$, (b) 0.1 M $(n-Bu_4N)ClO_4$, and (c) 0.1 M $(n-Hx_4N)ClO_4$.

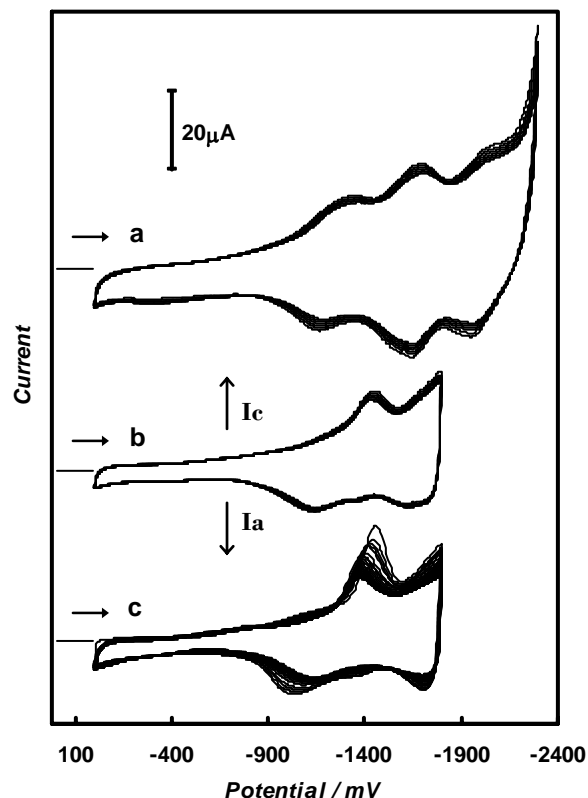


Figure 3. Multicyclic voltammograms of C_{70}/Rh film in acetonitrile containing (a) 0.1 M $(Et_4N)_4ClO_4$, (b) 0.1 M $(n-Bu_4N)ClO_4$, and (c) 0.1 M $(n-Hx_4N)ClO_4$.

The voltammetric responses of C_{60}/Rh and C_{70}/Rh films in acetonitrile containing the same supporting electrolyte are significantly different. The C_{70}/Rh film shows much more reversible electrochemical behavior at negative potentials. In solution containing relatively small tetra(ethyl)ammonium cations, C_{70}/Rh film exhibit remarkable stability and reversibility of the film reduction processes. Three reduction steps corresponding to the processes of fullerene moieties reduction are observed. Moreover, the film exhibit good stability in the wide potential range. However, a small decrease of the current during potential cycling beyond the third oxidation process is observed. Similar studies were done for solution containing fullerenes and palladium and iridium complexes. Also in these cases, films containing C_{70} exhibit higher reversibility upon potential cycling.

It was reported that the rate of C_{60}/Pd film reduction is limited by the transport of cations of supporting electrolyte from the solution to the film [9]. The rate of this process depends on the structure of the film. The morphology of the C_{60}/Rh and C_{70}/Rh films are shown in Figure 4. The C_{70}/Rh film is less uniform and exhibits higher porosity. This effect is particularly well seen for thicker films (Fig. 4d). The porous structure allows the solvent swelling and the supporting electrolyte counter-ions migrate more easily through the film.

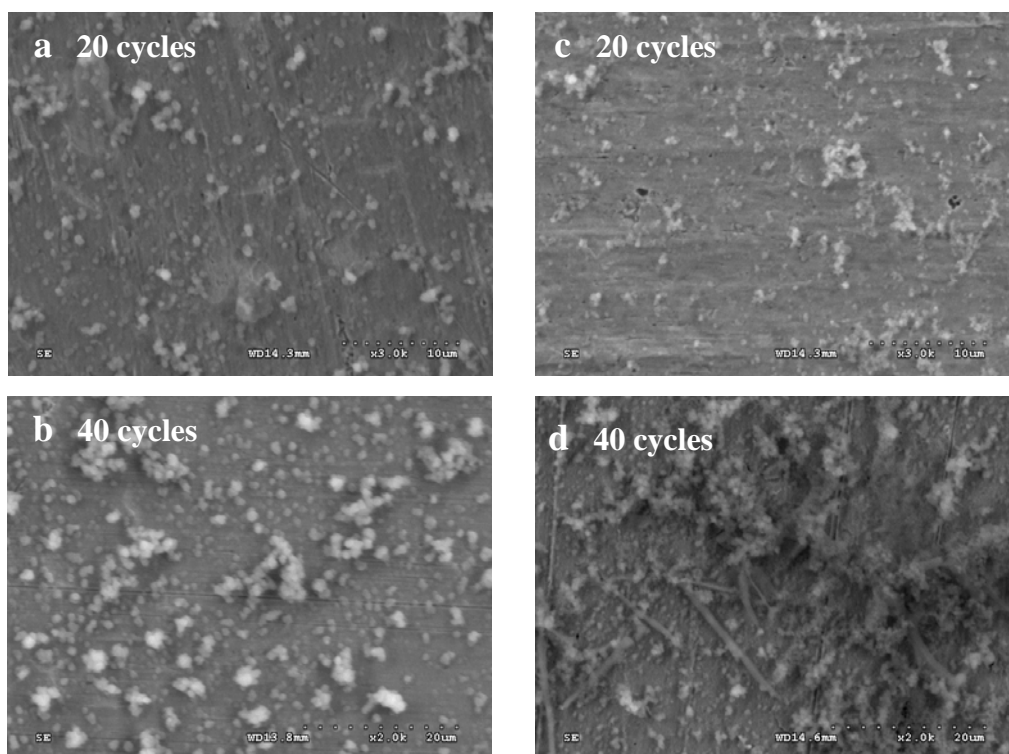


Figure 4. SEM images of (a, b) C_{60}/Rh and (c, d) C_{70}/Rh films electropolymerized on a gold foil surface under cyclic voltammetry conditions from acetonitrile/toluene (1:4, v:v) solution containing 0.1 M $(n-BuN)_4ClO_4$, 0.85 mM $(CF_3CO_2)_4Rh_2$, and 0.25 mM C_{60} (a) or 0.25 mM C_{70} .

4. Conclusions

Both, C_{60} and C_{70} fullerenes form electrochemically active solid films on the electrode surface during reduction carried out in acetonitrile/toluene mixture containing fullerene and selected transition metal complexes. The efficiency of film formation obtained for C_{60} is higher than the yield of C_{70}/Rh deposition. Films formed in the presence of $[C_{70}]$ fullerene exhibit higher porosity.

References

- [1] P. Novak, K. Muller, K.S.V. Santhanam, O. Haas, *Chem. Rev.*, 97 (1997) 207
- [2] A. Burke, *J. Power Sources*, 91 (2000) 37
- [3] M.S. Wrighton, *Science*, 231 (1986) 32
- [4] G. Fortier, E. Brassard, D. Belanger, *Biosens. Bioelectron.*, 5 (1990) 473
- [5] H. Yoshima, M. Kobayashi, K.B. Lee, D. Chung, A.J. Heeger, F. Wudl, *J. Electrochem. Soc.*, 134 (1987) 46
- [6] K. Winkler, D.A. Costa, A.L. Balch, W.R. Fawcett, *J. Phys. Chem.*, 99 (1995) 17431
- [7] K. Winkler, D.A. Costa, W.R. Fawcett, A.L. Balch, *Adv. Mater.*, 9 (1997) 153
- [8] A.L. Balch, D.A. Costa, K. Winkler, *J. Am. Chem. Soc.*, 120 (1998) 9614
- [9] K. Winkler, A. de Bettencourt-Diaz, A.L. Balch, *Chem. Mater.*, 11 (1999) 2265
- [10] M.E. Plonska, A. de Bettencourt-Diaz, A.L. Balch, K. Winkler, *Chem. Mater.*, 15 (2003) 4122
- [11] M.E. Plonska, K. Winkler, S. Gadce, F. D'Souza, A.L. Balch, *Electroanalysis*, 18 (2006) 841
- [12] A. Hayashi, A. de Bettencourt-Diaz, K. Winkler, A.L. Balch, *J. Mater. Chem.*, 12 (2002) 1386
- [13] M.E. Plonska, A. Makar, K. Winkler, A.L. Balch, *Polish J. Chem.*, 78 (2004) 1431
- [14] H. Nagashima, A. Nakaka, Y. Saio, M. Kato, T. Kawanishi, K. Itoh, *J. Chem. Soc., Chem. Commun.*, (1992) 377

PHASE TRANSITION IN $[\text{Cu}(\text{NH}_3)_5](\text{BF}_4)_2$ STUDIED WITH NEUTRON SCATTERING METHODS

Ł. Hetmańczyk^a, E. Mikuli^a, I. Natkaniec^{b,c}

^a *Department of Chemical Physics, Faculty of Chemistry, Jagiellonian University, Ingardena 3, 30-060 Kraków, Poland*

^b *Frank Laboratory of Neutron Physics, JINR, Dubna 141980, Russia*

^c *H. Niewodniczański Institute of Nuclear Physics, PAS, Radzikowskiego 152, Kraków 31-342, Poland*

Abstract

Quasielastic and inelastic incoherent neutron scattering (QENS and IINS) data for $[\text{Cu}(\text{NH}_3)_5](\text{BF}_4)_2$ are reported. Neutron scattering elastic peak, registered at 70 K and also at higher temperatures, shows distinct broadening, which is typical for dynamically, orientationally disordered crystals (ODIC). Fast reorientational motion of NH_3 ligands in $[\text{Cu}(\text{NH}_3)_5]^{2+}$ can be pretty good described by a simple model of 120° instantaneous jumps around 3-fold axis on a picoseconds correlation time scale. The NH_3 ligands do not suddenly change neither the velocity nor the character of their reorientational motion at detected previously phase transition. The dynamical, orientational disorder is also confirmed by very much diffused spectra of the phonon density of states $G(\omega)$ for all temperatures higher than 70 K.

Introduction

According to Tomlinson and Hathaway [1], the compound being studied has a regular structure at room temperature (space group: No. 225 = $\text{Fm}\bar{3}\text{m} = \text{O}_h^5$), with a lattice parameter of $a = 11.10 \text{ \AA}$ and with four molecules in the unit cell. The high symmetry of the crystal lattice is possible because the NH_3 groups perform fast reorientational motions (measurable in picoseconds) around their threefold axis. The complex cation $[\text{Cu}(\text{NH}_3)_5]^{2+}$ has square-based pyramid configuration (C_{4v}) or a trigonal bi-pyramidal configuration (D_{3h}) [2]. In our previous paper [3] we have performed quantum chemical calculations for both these possible complex cation structures, in order to decide which cation structure is preferred by the crystal structure. The conclusions from our calculations are as follows: firstly, both complex cation structures have almost the same energy at equilibrium geometry, and secondly, the energy barrier between them is very low. Thus the dynamic transition between both these complex cation structures is possible and very probable.

The phase transitions in $[\text{Cu}(\text{NH}_3)_5](\text{BF}_4)_2$, at $T_c^h = 147.9 \text{ K}$ - while heating and at $T_c^c = 141.7 \text{ K}$ - while cooling were determined by us by means of differential scanning calorimetry (DSC) in the temperature range of 90–300 K [4]. The presence of ca. 6 K hysteresis at the phase transition temperature suggests that the detected phase transition is of the first order type. A large transition entropy ($\Delta S \approx 25.1 \text{ J}\cdot\text{mol}^{-1}\cdot\text{K}^{-1}$) indicates considerable configurational disordering in the high temperature phase (so-called ODIC crystals).

Experimental

Both synthesis and chemical analysis (certifying proper composition and purity of the investigated compound) were described in our previous paper [4]. The IINS spectra were measured simultaneously using the time-of-flight method in the NERA spectrometer [5] in the high flux pulsed reactor IBR-2 in Dubna (Russia). The sample was mounted into a thin-wall aluminum container which was placed in a top-loaded cryostat cooled with a helium refrigerator. The temperature of the sample could be changed within the range 20-300 K and stabilized with ± 0.5 K accuracy. The energy resolution of the spectrometer amounts to ca. 3 % for the IINS spectra in the range 100-1000 cm^{-1} . The spectral width of the elastic peak at 4.2 Å equals to ca. 3.5 cm^{-1} . The IINS measurements were made for several scattering angles. The final IINS spectra were obtained by summing up the data taken from all 15 detectors, which cover scattering angles from 20° to 160°. Each spectrum was registered with good statistic (exposition time was approximately 10 hours per spectrum).

Results and Discussion

The quasielastic neutron scattering data were analyzed in terms of simple 120° jump model. It is commonly known that in hexamine and tetrammine compounds NH_3 molecules perform fast stochastic reorientations around 3-fold symmetry axis. For an instantaneous jump model around n-axis the scattering law $S(Q, \omega)$ for powder sample consists of two components and can be expressed by the following formula:

$$S(Q, \omega) = y_0 + N \cdot [\text{EISF}(Q) \cdot \delta(\omega) + (1 - \text{EISF}(Q)) \cdot L(\omega, \Gamma)], \quad (1)$$

where: y_0 is the linear background, N is the normalization factor, $\delta(\omega)$ represents elastic part and $L(\omega, \Gamma)$ is the Lorentzian function representing quasielastic broadening. The EISF (elastic incoherent structure factor) gives information on geometry of the motion, especially of those parts of molecules which contain the hydrogen atoms due to high incoherent scattering cross section. Moreover, the EISF parameter calculated for chosen momentum transfer $Q = \frac{4\pi}{\lambda} \sin(\theta)$ value is temperature independent (assuming that during lowering of temperature and especially after the phase transitions the distance of proton to axis rotation does not change).

The $\Gamma = \text{HWHM}$ (half width at half maximum) has two major properties: firstly it is inversionally proportional to the mean time τ between instantaneous jumps and secondly it is independent of the scattering vector Q . The equation (1) convoluted with instrumental resolution function (Gaussian function with energy of incoming neutrons ≈ 4.2 Å and the energy resolution of the TOF spectrometer = 0.418 meV) was fitted to the experimental data. The parameters y_0 , N , EISF and Γ were determined by best fit using least square method. The spectrum registered at the lowest temperature (20 K) was taken as a resolution function because no broadening was observed.

Fig. 1a shows quality of the fit (solid line) together with linear background (dashed line) quasielastic component (dotted line) and resolution function (dashed dotted line). The theoretical EISF for 120° jumps model of all NH_3 is given by:

$$\text{EISF}(Q) = \frac{1}{3} \cdot \left[1 + \frac{2 \cdot \sin(Q \cdot r \cdot \sqrt{3})}{Q \cdot r \cdot \sqrt{3}} \right]. \quad (2)$$

The r parameter denotes proton distance to the 3-fold rotation axis. One can see quite good agreement between calculated according to equation (2) ($r = 0.76$ Å, EISF =

0.421) and experimentally (1) determined elastic incoherent structure factor (EISF = 0.426). Thus one can conclude that motion of NH₃ groups in [Cu(NH₃)₅](BF₄)₂ can be pretty good described by a simple model of 120° jumps of all protons between their equivalent sites.

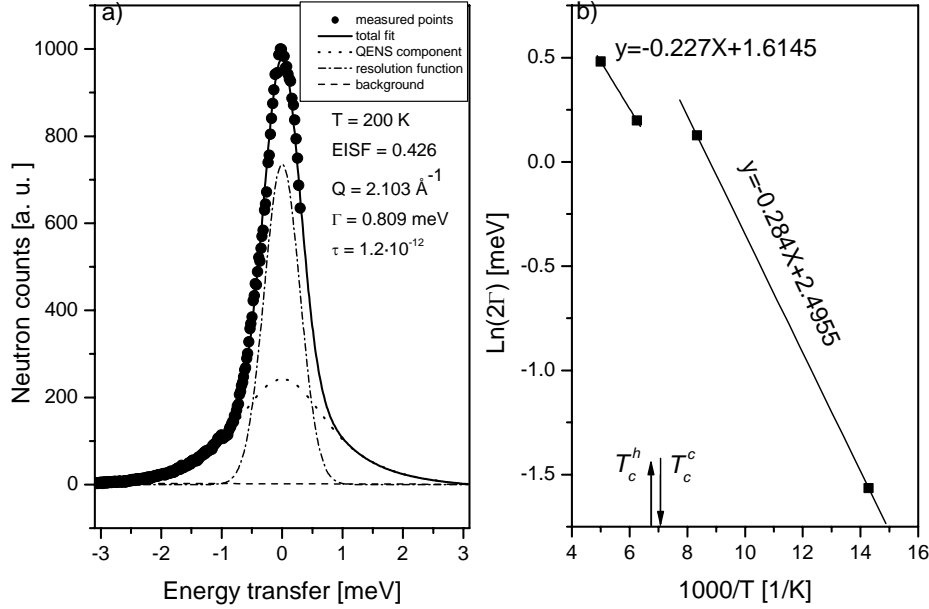


Fig. 1. Example of fitting the 120° jumps model to the QENS experimental spectra for T = 200 K (a) and Arrhenius plot of the determined FWHM of the QENS component, 2Γ vs. $1000/T$ (b).

The QENS spectra were measured with NERA time of flight spectrometer at the following temperatures: 20, 70, 120, 160 and 200 K. The data for polycrystalline sample were registered for different scattering angles but we choose to analysis the data obtained after summing up data from all 15 detectors. The mean scattering angle equals to 88° (2θ) which corresponds to the neutron momentum transfer equal to 2.103 \AA^{-1} . The energy of incoming neutrons was equal to ca 4.75 meV (neutrons were monochromatized using Bragg scattering from pyrolitic graphite). The final spectrum was corrected for the sample holder (Al) scattering and also corrected for diffraction. The data were not corrected for multi scattering because of thickens of the sample. The registered QENS spectra show an asymmetry on the right side due to beryllium filters cut-off edge that is way the fitting was performed only to part of the spectrum see Fig. 1a. Determination of QENS width (Lorentzian part, Γ) allows one to calculate the energy activation for rotations of NH₃ molecules. This is thermally activated process and can be well described by Arrhenius law:

$$\Gamma(T) = A \exp\left(\frac{-E_a}{RT}\right). \quad (3)$$

Fig. 1b shows an Arrhenius plot 2Γ vs. $1000/T$. The estimated activation energy equals to 19.6 meV ($1.9 \text{ kJ}\cdot\text{mol}^{-1}$) for high temperature phase and 24.5 meV ($2.4 \text{ kJ}\cdot\text{mol}^{-1}$) for the low temperature phase. The arrows indicate phase transitions temperatures determined by DSC method. The mean time τ between jumps, calculated according to the following relation: $\tau = \frac{3\hbar}{2\Gamma}$ increases with temperature increasing. It

changes from around $9.5 \cdot 10^{-12}$ s at 70 K to $1.2 \cdot 10^{-12}$ s at 200 K. The elastic peak, registered at 70 K and also at higher temperatures, shows distinct broadening, which is typical for dynamically, orientationally disordered crystals (ODIC).

Fig. 2a shows the inelastic incoherent neutron spectra (IINS) and Fig. 2b shows the generalized proton-weighted phonon density of states $G(\omega)$ calculated from IINS spectra in one phonon harmonic approximation. We can see that the $G(\omega)$ spectra obtained for all temperatures higher than 70 K are much diffused and broadened. It is due to great disorder connected with fast molecular motions, especially to the disorder of hydrogen atoms. Just the $G(\omega)$ spectra obtained for the low-temperature phase at temperature 20 K show some peaks characteristic for ordered phase.

Concluding the NH_3 groups perform fast stochastic reorientation in the temperature range of 70 – 200 K. Motion of NH_3 groups in $[\text{Cu}(\text{NH}_3)_5](\text{BF}_4)_2$ can be pretty good described by a simple model of 120° jumps around 3-fold axis within picoseconds time scale. This motion is not affected by detected by means of DSC method phase transitions. Phases above 70 K are dynamically orientationally disordered. One can see broadening of the QENS spectra as well as broadening and diffused character of the peaks in the $G(\omega)$ phonon density of states function.

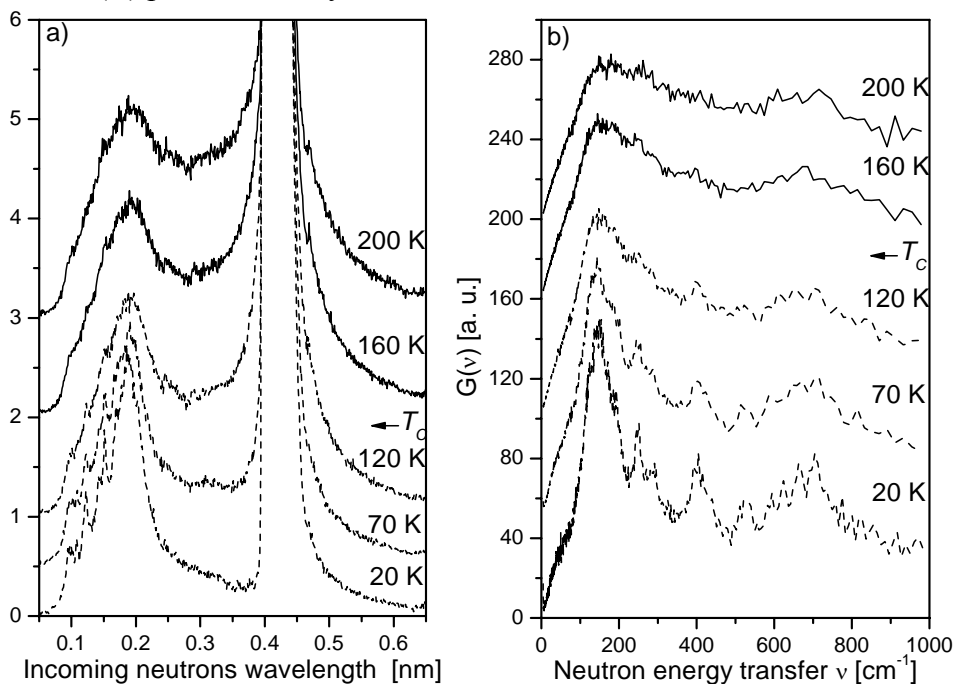


Fig. 2. The temperature dependence of the IINS spectra of $[\text{Cu}(\text{NH}_3)_5](\text{BF}_4)_2$ (a) and of the phonon density function $G(\omega)$ (b).

References

- [1] A.A.G Tomlinson, B.J.J Hathaway, Chem. Soc., A (1968) 1905
- [2] J. Stankowski, J. Mol. Struct., 597 (2001) 109
- [3] A. Migdał-Mikuli, E. Mikuli, M. Barańska, Ł. Hetmańczyk, Chem. Phys. Lett., 381 (2003) 329
- [4] A. Migdał-Mikuli, E. Mikuli, Ł. Hetmańczyk, E. Ściesińska, J. Ściesiński, J. Mol. Struct., 792-793 (2006) 157
- [5] I. Natkaniec, S.I. Bragin, J. Brańkowski, J. Mayer, in: Proceedings of the ICANS XII Meeting, Abington, 1993, RAL Report 94-025, Vol. I, 1994, pp. 89–96

SPECIATION OF NITROGEN FUNCTIONAL GROUPS FORMED ON THE SURFACE OF ORGANIC MATERIALS MODIFIED BY DIFFERENT AGENTS

Magdalena Hofman, Leszek Wachowski, Agata Woźniak, Monika Musiał

Adam Mickiewicz University, Faculty of Chemistry, Grunwaldzka 6, 60-780 Poznań, Poland

Introduction

The properties of active carbon are known to depend on the type of organic material used for its production, the presence of mineral components and heteroatoms (e.g. nitrogen, oxygen, sulphur and phosphorus) and the conditions of carbonisation and activation [1,2]. It has been established that preliminary modification, either thermal or chemical, of the materials used as the catalyst support also leads to improvement in the active carbon texture, number and type of the surface functional groups [3-5]. Heteroatoms, occurring on the surface of the catalyst material or a support of the active component, generate formation of active centres of certain type [6]. In view of the growing practical possibilities of applications of active carbons enriched in nitrogen in removal of H_2S , SO_2 , COCl_2 , as electrode material in supercapacitors, as catalysts or catalyst support [6,7] this type of material enjoys great interest. Modification of the active carbon precursor by a treatment with nitrogen has been found to lead to significant changes in the texture and an increase in the nucleophilic character of the active carbon surface [6].

The enrichment of the active carbon precursor in nitrogen is performed by a treatment with ammonia and its derivatives [2,4-7] or nitrogen (II) oxide [8,9]. From the catalytic point of view, of greatest concern is the type of surface functional groups acting as active centres in a given catalytic reaction.

Experimental

The measurements were performed on samples characterized by different degrees of coalification, i.e.: waste plum stones, Polish brown coal from the Konin colliery and Polish sub-bituminous coal from the Sośnica colliery. The starting raw samples were crushed and sieved, then carbon samples were subjected to demineralisation by hydrochloric and hydrofluoric acids, according to the Radmacher and Mohrhauer method [10]. The samples were divided into two parts. The first part of the samples was exposed to nitrogen (II) oxide at two different temperatures, e.g. 270°C and 300°C for 2h [9], whereas the second part was

ammonoxidised. Ammoxidation was carried out using a mixture of ammonia and air at a volume ratio of 1:3 (250/750 cm³/min.) in a flow reactor at 300°C or 350°C, for 5 h [2,4-6]. The chemical composition of the samples investigated was performed by an Elementar Vario ELIII microanalyser. The FT-IR/PAS spectra of the active carbon samples were recorded on a Bio-Rad Excalibur 3000MX spectrometer equipped with a photoacoustic detector MTEC 300 (in the helium atmosphere in a detector) over the 4000-400 cm⁻¹ range at the resolution of 4 cm⁻¹ and a maximum source aperture. XPS spectra were recorded using VG Scientific ESCALAB-210 System. Measurements were made using X-ray radiation Al K α . The depth of the analyzed layer was ca. 3.5-4 nm.

Results and discussions:

According to elemental analysis results, the amount of nitrogen introduced into samples studied depends on the temperature of the modification process but also on the degree of coalification [2,5]. Results of the elemental analysis of the selected samples prior to and after introduction of nitrogen are given in Table 1 and 2.

Table 1. The influence of ammoxidation on elemental composition of the samples studied (wt.%)

Sample code	C		H		N			(O+S)		
	E	F	E	F	E	F, T ₁	E	F, T ₂	E	F
P	48.8	72.3	6.1	5.0	0.1	5.3	-	-	45.0	17.4
P	48.8	69.9	6.1	4.0	-	-	0.1	10.8	45.0	15.3
SD	77.8	68.4	5.2	3.0	0.9	12.4	-	-	16.1	16.2
SD	77.8	69.1	5.2	2.9	-	-	0.9	13.1	16.1	14.9

S- subbituminous coal, D – material demineralised, T₁ – ammoxidation in lower temp, T₂ – ammoxidation in higher temp., E – before ammoxidation, F – after ammoxidation

As follows from these data, after modification the samples reveal significant differences in the content of nitrogen. Ammoxidation leads to introduction of much more nitrogen than nitrogenization in analogous samples (e.g.: SD). The above fact can be explained by the kind of modification agent. In the case of ammoxidation it is a mixture of NH₃/air, which is also a simultaneously oxidizing agent which facilitates the introduction of nitrogen, whereas in nitrogenization the only modifying agent is NO. The increase in the nitrogen content is accompanied by a decrease in the content of carbon as a result of changing proportions of the elements in the sample.

Table 2. The influence of nitrogenization on elemental composition of the samples studied (wt.%)

Sample code	C		H		N			(O+S)		
	X	Y	X	Y	X	Y, T ₁	X	Y, T ₂	X	Y
BD	62.3	76.3	5.4	4.6	0.6	3.6	-	-	31.7	15.5
BD	62.3	78.2	5.4	4.3	-	-	0.6	3.9	31.7	13.6
SD	77.8	82.1	5.2	4.1	0.9	3.2	-	-	16.1	10.6
SD	77.8	81.4	5.2	3.7	-	-	0.9	3.6	16.1	11.0

B –brown coal, S –subbituminous coal, D –after demineralization, T₁ –nitrogenization at 270°C, T₂ –nitrogenization at 300°C, X- before nitrogenization, Y- after nitrogenization

As follows from the XPS analysis of raw plum stones (P), the greatest amount of carbon occurs in them in the form hydroxyl and ether, carboxyl and carbonyl groups [11]. Nitrogen occurs mainly in pyrrolic and pyridinium groups and in a low amount in pyridine structures. The sample ammoxidised at a higher temperature (PN₂) was characterised by a greater content of carbon. The majority of carbon occurred in the form of C-OH, C-N (in different configuration) and carboxyle groups. The dominant nitrogen species (Fig.1) were the pyrrolic and pyridinium as well as quaternary nitrogen groups (N-Q) and N-X forms, but also there are also imine, amine and imide species [4,11].

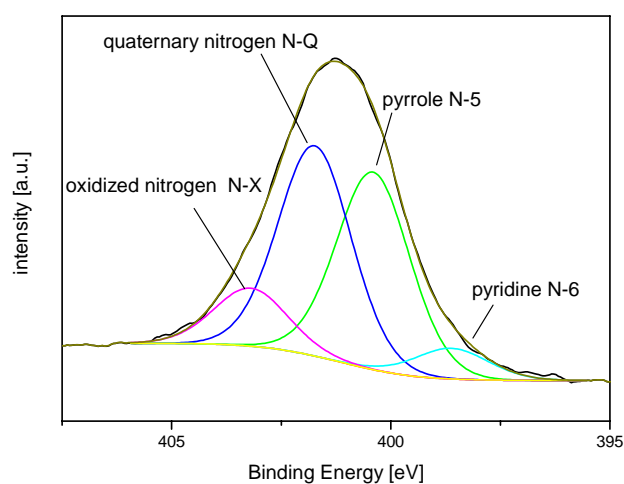


Fig. 1. The N 1s spectrum of PN₂ sample

Nitrogenization of previously demineralised coal samples leads to formation of the group –NCO giving in the FT-IR/ PAS spectra a band with a maximum at about 2225 cm⁻¹. The spectra of these samples show also a band at about 1700 cm⁻¹, which can be assigned to amide groups, and a band near 1605 cm⁻¹, which most probably is the so-called carbon band. Moreover, the band at about 830-820 cm⁻¹ is most probably the evidence of the presence of

-O-NO₂ and NO₃⁻ groups, while a broad band in the range 870-750 cm⁻¹ suggests the presence of aromatic hydrocarbons [9].

Conclusions

Modification of carbonaceous materials by nitrogen(II) oxide or ammoxidation leads to an increased content of carbon and nitrogen and a decreased content of hydrogen and total content of oxygen and sulphur. The increasing temperature of the above processes results in the increase of nitrogen introduced onto their surfaces.

The N 1s XPS spectra show the presence of different nitrogen functionalities in the samples, such as: pyrrole, pyridine, pyridone, amine and chemisorbed nitrogen oxides. The first two mentioned are characterised by the highest thermal stability.

The FTIR-PAS spectra of demineralised and later nitrogenized samples show a maximum at 2225 cm⁻¹ assigned to the group -NCO and at about 1700 cm⁻¹ assigned to amide groups, indicating the presence of these groups on the surface of the samples.

Acknowledgement

We are gratefully acknowledge the financial support given by the Polish State Committee for Scientific Research, Project No 1275/T09/2005/29.

References:

- [1] Jankowska H., Świątkowski A., Choma J., *Węgiel aktywny*, WNT Warszawa 1985.
- [2] Wachowski L., Hofman M., *Thermochim. Acta*, **437(1-2)**: 82 (2005).
- [3] Puri B.R., *Chemistry and Physics of Carbons*, Ed. P. Walker Jr., wyd. Marcel Dekker, New York 1970 t.6, p.191.
- [4] Wachowski L., Ryczkowski J., Hofman M., Pasiieczna S., *J. Phys. IV France*, **129** 225 (2005).
- [5] Wachowski L., Hofman M., *J. Therm. Anal. Cal.*, **83** 379 (2006).
- [6] Wachowski L., Skupiński W., Hofman M., *Appl. Catal. A: General*, **303(2)** 230 (2006).
- [7] Skupińska J., Karpińska M., Wachowski L., Hofman M., *React. Kinet. Catal. Lett.*, **82** 311 (2004).
- [8] Garcia F., Espinal J.F., Martonez de Lecea C.S., Mondragon F., *Carbon*, **42** 1507 (2004).
- [9] Wachowski L., Ryczkowski J., Hofman M., Pasiieczna S., *J. Phys. IV France* (in press).
- [10] Radmacher W., Mohrhauer P., *Bernst. Chem.*, **37** (1956) 353.
- [11] Wachowski L., Sobczak J.W., Hofman M., *Appl. Surf. Sci.* (submitted).

INFLUENCE OF HYDROCHLORIC ACID CONCENTRATION ON Pd(II) MICROQUANTITIES SORPTION FROM THE 2.0 M NaCl – 0.5 ÷ 2.0 M HCl SYSTEMS ON DIFFERENT ION-EXCHANGERS

Z. Hubicki, M. Leszczyńska

*Department of Inorganic Chemistry, Faculty of Chemistry,
Maria Curie – Skłodowska University, 20-031 Lublin, Poland*

INTRODUCTION

The introduction of catalytic converters of automobiles containing platinum, palladium and rhodium (platinum group elements, PGEs) for reducing emission of gaseous pollutants, such as carbon monoxide, nitrogen oxides and hydrocarbons, has resulted in increasing concentration of PGEs in environmental matrices, especially in roadside dust, soil and plants. Therefore concerns have arisen with respect to the health risks generated by the possible inhalation of dust and contamination through food and water. Various technological methods have been developed to control the pollution of surface and ground waters as well as soil. Ion exchange chromatography is one of the most common concentration techniques used in noble metal chemistry.

The aim of the present work is selective removal of Pd(II) ions from the 2.0 M NaCl – 0.5 ÷ 2.0 M HCl solutions on the chelating ion-exchange resins of polyamine (Diaion CR-20), aminophosphonic (Chelite P), thiourea (Lewatit TP-214) and thiol (Chelite S) functional groups as well as on the anion exchangers of various basicity (Duolite A-368 and Lewatit MP-64). The ion exchange capacities (C_r) as well as the recovery factors of Pd(II) ions (%R) were determined for these ion exchangers.

Choice of model systems used in the studies of Pd(II) ion sorption follows from the fact that solutions of similar chemical composition are frequently used in hydrometallurgical processes of noble metals recovery on a commercial scale e.g. Mathhey Rustenberg Refiners (MMR).

EXPERIMENTAL

Determination of the recovery factors of Pd(II)

The samples of 0.5 g dry resin were shaken mechanically with 50 cm³ of the Pd(II) solution from 1 to 240 minutes at 298 K. After equilibrium was reached, the ion exchanger was filtered off in order to determine the content of Pd(II) ions in the raffinate.

The recovery factor (%R) of Pd(II) was calculated from the equation (1):

$$\%R = \frac{g_o}{g_w} \times 100\% \quad (1)$$

The amount of metal adsorbed (g_o) was calculated by the difference between the initial (g_w) concentration in the aqueous solution and that after sorption. From these experiments, time dependence of %R of palladium(II) was obtained.

Determination of the distribution coefficients and resin capacities

The dynamic procedures were applied. The one-centimetre diameter columns were filled with swollen ion exchangers in the amount of 10 cm³. Then Pd(II) solutions of the initial concentration 100 µg/cm³ were passed through the ion exchanger bed at the rate of 0.35 cm/min.. The eluate was collected in the fractions and the palladium(II) content was determined.

The weight (D_w) and bed (D_b) distribution coefficients of Pd(II) as well as the working ion exchange capacities (C_w) were calculated from the breakthrough curves according to the equations (2 – 3):

$$D_w = \frac{U - U_o - V}{m_j} \quad (2)$$

where: U is the effluent volume at $C = C_o/2$ [cm³], U_o is the dead volume in the column (liquid volume in the column between the bottom edge of ion-exchanger bed and the outlet) [cm³], V is the void (inter-particle) ion exchanger bed volume (which amounts to ca. 0.4 of the bed volume) [cm³], m_j is the dry ion exchanger weight [g].

$$D_b = D_w \times d_z \quad (3)$$

where: d_z is the bed density [g/cm³] [1].

The working ion exchange capacities (C_w) are expressed in g of Pd(II) per cm³ of swollen anion exchanger.

Palladium(II) concentrations in the raffinate and eluate were determined using the spectrophotometric iodide method which is based on formation of the red-brown PdI₄²⁻ complex in the presence of excess of potassium iodides. It is necessary to use the reducing agent (usually ascorbic acid) in order to avoid oxidation of iodides [2,3].

RESULTS AND DISCUSSION

As follows from the research results, the working ion exchange capacities (C_r [g/cm³]), the weight (D_w) and bed (D_b) distribution coefficients of Pd(II) ions (Table 1) calculated from the breakthrough curves (Fig. 1) depend on hydrochloric acid concentration in the 2.0 M NaCl – 0.5 ÷ 2.0 M HCl solutions as well as on the ion exchanger used.

The values of working ion exchange capacities in the above systems allowed the ion exchangers studied to be placed in the following sequence as far as their application for removal of Pd(II) was concerned:

- 0.5 M HCl – 2.0 M NaCl – 100 µg/cm³ Pd (II)
Lewatit TP-214 > Chelite S > Lewatit MP-64 > Duolite A-368 > Diaion CR-20
- 1.0 M HCl – 2.0 M NaCl – 100 µg/cm³ Pd (II)
Chelite S > Lewatit TP-214 > Lewatit MP-64 > Duolite A-368 > Diaion CR-20
- 2.0 M HCl – 2.0 M NaCl – 100 µg/cm³ Pd (II)
Chelite S > Lewatit TP-214 > Lewatit MP-64 > Duolite A-368 > Diaion CR-20.

Hard and soft acid and base theory (HSAB) confirms that the selective resins of the functional groups containing N or S donor atoms i.g. Chelite S and Lewatit TP-214 interact strongly with soft acids like precious metals. The sorption mechanism on these ion exchangers can be anion-exchanging, coordinating or both.

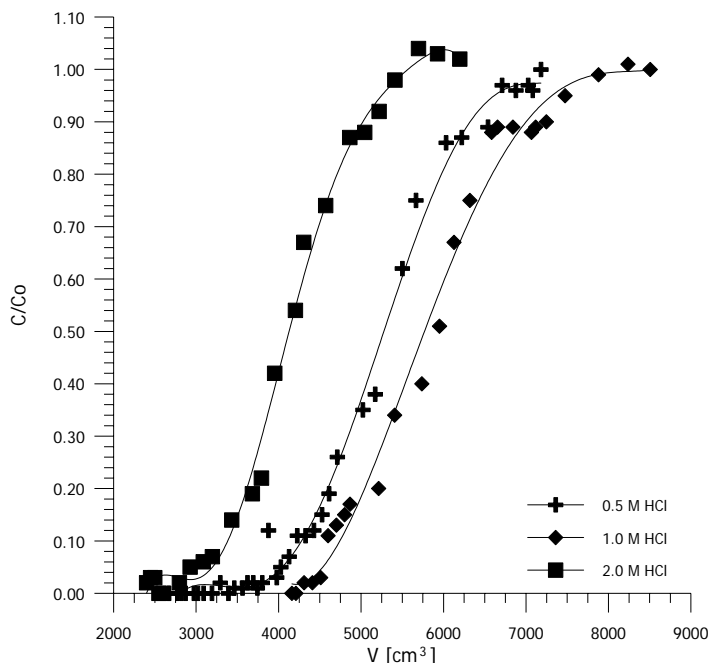


Fig.1. Breakthrough curves of Pd(II) on Chelite S in the 2.0 M NaCl – 0.5 ÷ 2.0 M HCl – 100 µg/cm³ Pd(II) solutions.

Table 1. Values of weight distribution coefficients in the 2.0 M NaCl – 0.5 ÷ 2.0 M HCl solutions on the ion exchangers under consideration.

Ion exchanger	Weight distribution coefficients (D_w)		
	2.0 M NaCl – 0.5 M HCl	2.0 M NaCl – 1.0 M HCl	2.0 M NaCl – 2.0 M HCl
Duolite A-368	145.6	115.5	91.7
Lewatit TP-214	701.5	710.6	653.9
Chelite P	5.3	5.5	4.5
Chelite S	527.7	577.8	411.2
Lewatit MP-64	154.4	129.4	93.2

The values of Pd(II) recovery factors determined for the ion exchangers under investigation assumed almost 100% values in the hydrochloric acid solutions of a concentration 0.5 M, decrease evidently with the increasing acidity of the system and when sorption equilibrium occurred at the ion exchanger – solution phase contact time – 120 min. The observed decrease in the above mentioned values with the increasing HCl

concentration can be explained by formation of HCl_2^- anion which exhibits higher affinity for the ion exchangers than the Pd(II) chloride complexes. This dependence refers to all ion exchangers in question (Fig. 2).

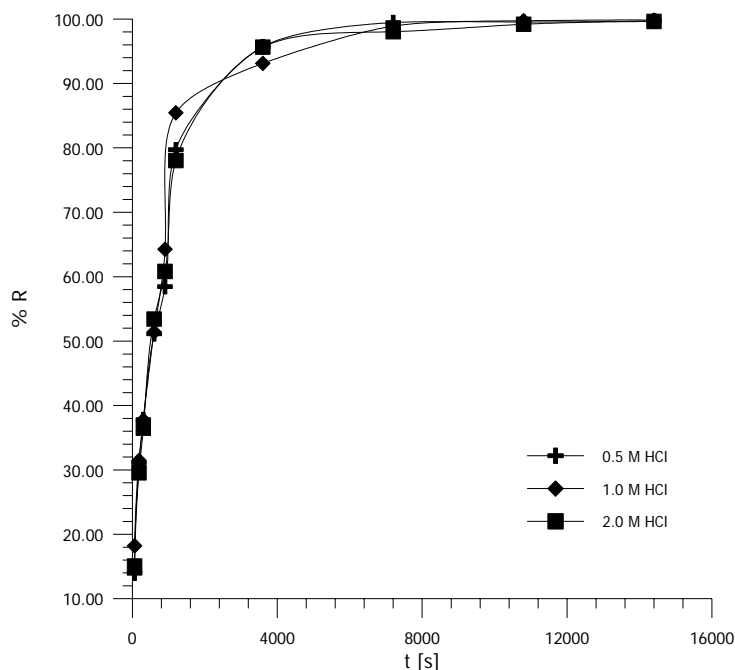


Fig. 2. Influence of phase contact time on recovery factors of Pd(II) in the 2.0 M NaCl – 0.5 ÷ 2.0 M HCl – $100 \mu\text{g}/\text{cm}^3$ Pd(II) solutions on Chelite S.

The ion exchanger of the functional aminophosphonic groups Chelite P can not be used in recovery of Pd(II) chloride complexes due to lack of selectivity towards Pd(II) ions.

CONCLUSIONS

As follows from the static and dynamic investigations both chelating ion exchangers of styrene – divinylbenzene matrices – Lewatit TP-214 and Chelite S and medium and weakly basic anion exchangers Lewatit MP-64 and Duolite A-368 can be extensively applied in technologies of palladium recovery from anodic slimes originating from copper and nickel electrorefining as well as used up automobile converters.

REFERENCES

- [1] J. Minczewski, J. Chwastowska, R. Dybczyński, Separation and preconcentration methods in inorganic trace analysis, John Wiley & Sons, New York, 1982.
- [2] Z. Marczenko, M. Balcerzak, Spektrofotometryczne metody w analizie nieorganicznej, PWN, Warszawa 1998.
- [3] Z. Marczenko, A.P. Ramsza, *Chem. Anal.* 23 (1978) 23.

THE POSSIBILITIES OF OBTAINING BIOGAS FOR MOTORIZATION PURPOSES IN KUJAWSKO-POMORSKIE VOIVODSHIP

A. Iglińska*, R. Buczkowski, M. Cichosz

* *Faculty of Environmental Protection, University of Humanities and Economics,
ul. Okrzei 94, 87-800 Włocławek*

*Section of Chemical Proecological Processes, Faculty of Chemistry,
Nicolaus Copernicus University, ul. Gagarina 7, 87-100 Toruń*

Introduction

Considerable interest in renewable energy sources was a result of a rapid increase in energy demand caused by the industrial revolution. The fuel crisis of the 1970-ties brought to the world's attention that natural resources are limited [1].

Additionally, a great threat to the humankind was posed by the global climate warming, which was brought about by the carbon dioxide emission to the atmosphere resulting from the combustion of conventional energy sources.

Biogas is created as a result of anaerobic fermentation of organic waste, during which methanogenic bacteria decompose organic substances into simple compounds.

During the process of anaerobic fermentation, up to 60% of organic substance is transformed into biogas. Biogas is composed of many chemical compounds, the most important of which are:

- methane (40-80%)
- carbon dioxide (20-60%)
- hydrogen sulfide (0.1-5.5%) and
- trace amounts of hydrogen, carbon monoxide, nitrogen, oxygen and other gases [2,3].

Biogas containing more than 40% of methane can be used in order to produce heat or electricity, and its calorific value is between 4 and 8 kWh/m³.

Biogas potential

This paper focuses on biogas obtained from animal farms. The potential for biogas production was estimated basing on the collected information on stock population in 2005 (The Agency for Restructuring and Modernization of Agriculture in Toruń, The Voivodship Veterinary Inspectorate in Bydgoszcz).

In order to convert physical units into big units SD, the following mean indicators were adopted: cattle 0.8 SD, pigs 0.2 SD, poultry 0.004 SD. It was based on converting coefficients presented in MOŚ, ZN i L ordinance (MOŚ, ZNiL – The Ministry for Environmental Protection, Natural Resources and Forestry).

The technical potential for biogas production was calculated according to the formula:

$$P_t = SD \times W_{smo} \times M \quad (1)$$

where:

SD – the number of big units (big animal units of weight of 500 kg)

W_{smo} – the indicator of dry organic mass production in relation to SD

M – methane production per dry organic mass unit

The biogas production potential was calculated according to the formula:

$$P_p = SD \times W_{smo} \times B \quad (2)$$

where:

SD – the number of big units (big animal units of weight of 500 kg)

W_{smo} – the indicator of dry organic mass production in relation to SD

M – biogas production per dry organic mass unit

Calculations were based on the data presented in Table 1.

Table 1. Empirical data for biogas production from animal waste

Specification		Cattle		Pigs		Poultry
		dung	Fermented liquid manure	dung	Fermented liquid manure	Fermented liquid manure
Dry mass	Ton of dry mass/ton of waste	0.23	0.1	0.2	0.07	0.15
Content of dry organic mass in dry mass	Ton of dry organic mass/ ton of dry mass	0.80	0.8	0.9	0.82	0.76
Production of dry organic mass (W_{smo})	kg of dry organic mass./ SD/day	3.0 – 5.4 on average – 4.2		2.5 – 4.0 on average – 3.3		5.5 – 10 on average- 7.78
Biogas production (B)	m ³ /ton of dry organic mass	175 – 520 on average – 347		220 – 637 on average – 428		327 - 722 on average – 524
Methane production (M)	m ³ /ton of dry organic mass	On average – 218		On average – 269		On average– 330

In the area of kujawsko-pomorskie voidvodship there are 125 farms in which the average livestock density is more than 20.000 heads of poultry, 110 farms where there are more than 2000 heads of pigs and 106 farms where there are more than 200 heads of cattle.

The number of stock in these farms is 127,300 of heads of poultry, (31,800 of SD), 100,200 heads of pigs (50,100 of SD) and 19,300 heads of cattle (24.100 of SD). The greatest number of animals kept on farms can be found in the following counties:

- poultry – toruński inowrocławski, bydgoski, aleksandrowski counties,

- pigs – żniński, bydgoski, golubsko-dobrzyński, rypiński, brodnicki counties,
- cattle – inowrocławski, nakielski, żniński, bydgoski counties.

The biogas production potential that can be obtained from poultry farms in kujawsko-pomorskie voidvodship is about 47.4 million m³/year, the technical potential is about 29.8 million m³/year.

The biogas production potential that can be obtained from pig farms in kujawsko-pomorskie voidvodship is about 25.8 million m³/year, the technical potential is about 16.2 million m³/year.

The biogas production potential that can be obtained from cattle farms in kujawsko-pomorskie voidvodship is about 12.8 million m³/year, the technical potential is about 8 million m³/year.

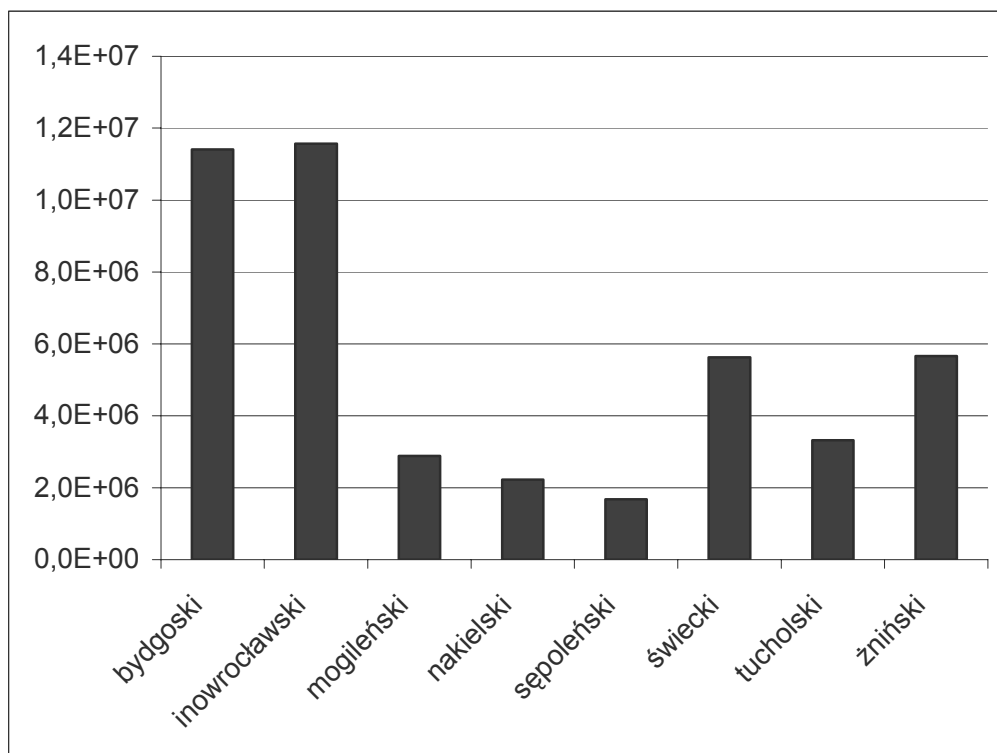


Fig. 1. The possibility of biogas production in bydgoski subregion [m³/year]

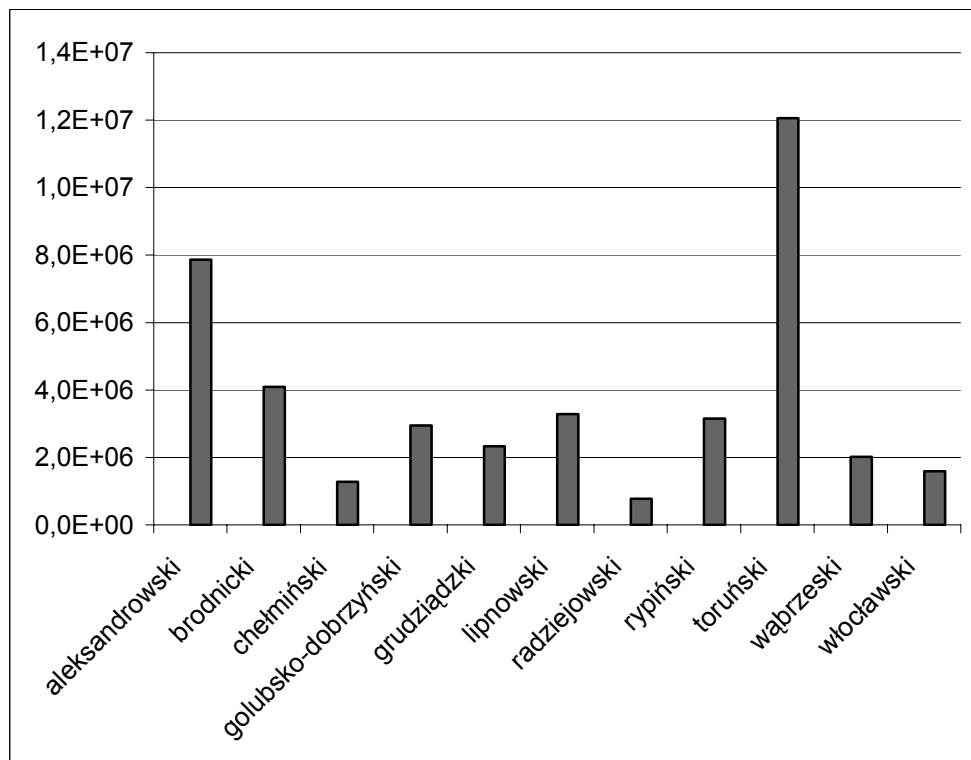


Fig. 2. The possibility of biogas production in toruńsko-włocławski subregion [m³/year]

Summary

The biogas production potential that can be obtained from all poultry, pig, and cattle farms in kujawsko-pomorskie voidvodship is about 458.5 million m³/year, the technical potential is about 54.1 million m³/year.

References

- [1] G. Lastella, *Energy Conversion and Management*, **43**, 63-75, 2002.
- [2] H. Maeng, H. Lund H., F. Hvelplund F., *Applied Energy*, **64**, 195-206, 1999.
- [3] S.S. Kapdi, V.K. Vijay, S.K. Rajesh, *Renewable Energy*, **30**, 1195-1202, 2005.

THE EFFICIENCY OF CITRIC ACID PRODUCTION IN THE PROCESS OF ELECTRODIALYSIS WITH SELECTED MEMBRANES

B. Igliński, R. Buczkowski, S. Koter*

Section of Chemical Proecological Processes,

**Department of Physical Chemistry*

Faculty of Chemistry, Nicolaus Copernicus University,

Gagarina 7, 87-100 Toruń

Introduction

Due to its buffering and complex-forming properties as well as its pleasant sour flavor and low toxicity, citric acid is widely used in the production of food, alcoholic and non-alcoholic beverages and in oil manufacture, pharmaceutical, metallurgical, chemical, cosmetics, textile, tobacco, plastics, plating industries and many others [1,2].

Citric acid is mainly obtained from saccharose or molasses by means of microbiological fermentation by the selected moulds *Aspergillus niger*. In order to recover acid from the fermentation broth, calcium citrate is precipitated with lime milk, and thus obtained precipitate is treated with sulfuric acid. Apart from the main product - citric acid, calcium sulfate is also produced. This waste, is produced at the ratio of 2.5 tons of gypsum per 1 ton of anhydrous citric acid [3].

In order to decrease the amount of wastes and sewage, the attempts are made to find environmentally-friendly technologies, that will not produce harmful wastes stored at waste dumps. One of such methods is the electrodialysis with bipolar membrane - an alternative to the conventional method of obtaining citric acid [4,5].

Experimental

The investigations on sodium citrate conversion to citric acid and sodium hydroxide were carried out using the laboratory electrodialyser TS001 by FumaTech GmbH, Germany. The electrodialyser consisted of four independent liquid circuits: acid, salt and electrode solutions. Each circuit of electrolyte comprised a thermostated tank of solution, a pump, and a flowmeter. The stack was made of polypropylene and was equipped with platinized titanium electrodes. The process was carried out galvanostatically using a constant current power supply (Sorensen 9B2M2, AG Technology, USA).

Electrodialysis was conducted using the following membranes:

- cation-exchange Neosepta CMX, Tokuyama Corp., Japan,
- anion-exchange Neosepta ACM, Tokuyama Corp., Japan,
- bipolar Neosepta BP, Tokuyama Corp., Japan,
- cation-exchange fumasep® FKB, Fumatech GmbH, Germany,
- anion-exchange fumasep® FAB, Fumatech GmbH, Germany,
- bipolar fumasep® FBM, Fumatech GmbH, Germany.

The effective surface of a single membrane was constant and was 52 cm², whilst the distance between membranes was 8 mm.

Membrane sheets were kept in 5% solution of NaCl with addition of NaN₃ (≈100 ppm) – this stopped the development of microorganisms.

Results and discussion

The mean concentration current efficiency $\overline{CE}_{a,c}$ was calculated using the following formula:

$$\overline{CE}_{a,c} = |z| \frac{\Delta c_a V_{a,0}}{n_F} = |z| \frac{(c_{a,t} - c_{a,0})}{n_F} V_{a,0} \quad (1)$$

where: z – anion charge ($z_a = -3$),

Δc_a – increase in acid concentration,

$c_{a,t}$ – acid concentration in time t ,

$c_{a,0}$ – initial acid concentration,

$V_{a,0}$ – initial acid volume ($=0.1 \text{ mol/dm}^3$),

n_F – transmitted charge calculated according to the following formula:

$$n_F = \frac{It}{F} \quad (2)$$

where: I – current intensity [A] (mean reading),

t – time of process [s],

F – Faraday constant 96 487 [C/mol].

In the formula (1) charge $z = -3$, since in the solutions of Na_3A there are virtually only A^{3-} ions.

In the terms of salt concentrations that were used, basing on literature data giving dissociation constants: $K_1 = 8,2 \cdot 10^{-4}$, $K_2 = 1,8 \cdot 10^{-5}$, $K_3 = 4 \cdot 10^{-7}$, it was found that more than 99% is taken by form A^{3-} .

Using concentrations, due to changes in solutions' volumes (here it is mainly electroosmosis and anion A^{3-} migration), lowers $\overline{CE}_{a,c}$ efficiency. Because of this, the authors considered the number of moles instead of concentrations when calculating the efficiency. Thus, we receive mean mole current efficiency $\overline{CE}_{a,n}$.

$$\overline{CE}_{a,n} = |z| \frac{\Delta n_a}{n_F} = |z| \frac{(c_{a,t} V_{a,t})_{obs} + \sum_{i=1}^n C_{i,pr} V_{i,pr} - c_{a,0} V_{a,0}}{n_F} \quad (3)$$

where: $(c_{a,t} V_{a,t})_{obs}$ – the number of moles calculated from experimental data,

$C_{i,pr}$ – acid concentration at the moment of taking a sample V_{pr} ,

n – the number of samples taken during the whole experiment.

Table 1. Electrodialysis efficiencies, T – Tokuyama membranes, F – Fumatech membranes.

No of ED	Membrane type	I [A]	t [h]	$C_{s,0}$	$\overline{CE}_{a,c}$	$\overline{CE}_{a,n}$
1	F	3,9	8	0,5	0,780	0,967
2	T	3,9	8	0,5	0,776	0,846
3	F	3,9	20	0,5	0,781	0,939
4	T	3,9	20	0,5	0,484	0,684
5	F	5,2	8	0,5	0,715	0,899
6	T	5,2	8	0,5	0,445	0,670
7	F	5,2	8	1,0	0,758	0,913
8	T	5,2	8	1,0	0,716	0,858

Basing on the data in Table 1, it can be found that the efficiencies $\overline{CE}_{a,n}$ are higher than the concentration efficiencies $\overline{CE}_{a,c}$. When comparing membranes, it is found that efficiencies of citric acid production are higher for Fumatech membranes. The efficiencies for Fumatech membranes are comparable although electrodialysis was conducted in various process conditions. The prolongation of electrodialysis duration as well as increase in current intensity adversely influences efficiency in case of Tokuyama membranes.

Tokuyama Corp. Membranes were bought in the mid 90-ties and were considerably more susceptible to damage during the process of electrodialysis than FumaTech GmbH membranes used in 2005. This proves the great technological progress that takes place during membrane formation.

Summary:

In this paper the comparison between two commercial sets of membranes proved the superiority of those produced by Fumatech GmbH – higher efficiency $\overline{CE}_{a,n}$ as well as mechanical durability.

Acknowledgements

This work was financially supported by the Polish State Committee for Scientific Research (project No 3T09B12128).

References

- [1] H.S. Grewal, K.L. Kalra, *Biotechn. Adv.* **13** (2), 209-234, 1995.
- [2] B. Igliński, R. Buczkowski, A. Warszawski, B. Dejevska, *Pol. J. Appl. Chem.*, **27** (3-4), 83-91 (2004).
- [3] B. Igliński, E. Lemanowska, R. Buczkowski, *Ann. Pol. Chem. Soc.*, **3**, 1329-1332, (2004).
- [4] T. Xu, W. Yang, *Chem. Eng. Process*, **41**, 519-524, 2002.
- [5] T. Xu, W. Yang, *J. Membrane Sci.*, **203**, 145-153, 2002.

MANAGEMENT OF SODIUM CITRATE ELECTRODIALYSIS BY-PRODUCTS

B. Igliński, R. Buczkowski,
*Section of Chemical Proecological Processes,
Faculty of Chemistry, Nicolaus Copernicus University,
Gagarina 7, 87-100 Toruń*

Introduction

Electrodialysis (ED) is an electrochemical separation process by which ionic (electrically charged) species are transported from one solution to another by crossing one or more selective permeability membranes, under the influence of electrical current [1].

Electrodialysis is an electrochemical process mainly used in industry for solution demineralization. A new type of membrane, the bipolar membrane (BP), allows the electrodisociation of water [2,3]. Bipolar membrane water splitting technology provides an attractive complement to the microbiological fermentation technology [4]. As an added advantage the produced acid is usually at a relatively high concentration so that the subsequent purification via crystallization or other techniques is relatively inexpensive.

Production of citric acid from sodium citrate was carried out by electrodialysis [5,6]. The by-products of sodium citrate electrodialysis are: sodium base and gases created during electrode reactions: hydrogen and oxygen.

Sodium base is one of the essential chemical substances and has applications in almost every branch of industry. There are many ways of producing base, but at an industrial level it is mainly obtained from sodium chloride electrodialysis.

Experimental

Ionite reclamation

The reclamation of tap water demineralization set used in the Section of Chemical Proecological Processes was conducted. Tap water flows in series through: volume gauge, four ionic columns, measuring tank with conductivity and temperature sensor – into the treated water tank.

The columns are made of polyvinyl chloride. Table 1 contains more precise data concerning presently used ionites, packing height, volume and total exchange capacity of particular columns.

Ionite reclamation was started by washing out suspension from the ion exchange bed using tap water. The basic reclamation was conducted in the reverse direction (that is, from top to bottom) in relation to the direction of water flow during the work cycle of the set.

For cation exchanger reclamation 10% solution of pure hydrochloric acid was used, whilst for anion exchanger 8% solution of sodium base from the electrodialysis was used. The process was conducted as long as analytical solution concentration at the inlet and outlet was the same – it was potentiometrically determined using the apparatus Titrino 736 GP.

Table 1. Characterization of water demineralization columns

Parameter	Column 1	Column 2	Columns 3 and 4
Ionite type	Wofatit KPS (slightly acid cation exchanger Kt-COOH)	Wofatit KPS (highly acid cation exchanger Kt-SO ₃ H)	Wofatit SBW (highly alkaline anion exchanger An-N(CH ₃) ₃ OH)
Packing height [cm]	30	22	30
Ionic capacity [cm ³]	2355	1725	2355
Exchange capacity [mval/cm ³]	0,8	1,43	0,9
Total exchange capacity [mval]	1880	2470	2120

After the reclamation, columns were rinsed with deionized water as long as no reclamation solution could be found at their outlet.

Table 2 contains control parameters – 8 weeks since the reclamation, when (according to water meter 320 dm³ of water had flown through the set. Such an amount of deionized water was used in April and May 2003 for didactics and research purposes in the Section of Chemical Proecological Processes.

Table 2. Control parameters after 8 weeks since the reclamation

Control parameters	Units	inlet	Water after the column			
		0	1	2	3	4
Exchange capacity	mval		1880	2470	2120	2120
pH		7,6	6,5	3,4	4,5	4,7
Acid consumption (up to pH=4,3)	mmol/dm ³	4,56	0,46	0	0	0
Base consumption (up to pH=8,3)	mmol/dm ³	0,20	4,30	5,28	0	0
Total hardness	mval/dm ³	5,08	0,98	0	0	0
chlorides	mmol/dm ³	0,91	0,91	0,91	0,08	0
silica	mg SiO ₂ /dm ³	20	15	15	5	1
conductivity	μS/cm	523	550	670	18	3

In Table 2 the number “0” stands for concentration lower than analysis sensitivity.

The lack of hardness traces in deionized water and conductivity values similar to values of distilled water prove that the set worked correctly.

Basing on the anion content, it can be estimated that from 1 dm³ of water (4,56 + 0,91) = 5,47 mval of ions is taken away. Assuming the mean exchange capacity of the set to be 4300 mval, it should still last for demineralization of 790 dm³ of water, that is, about 470 dm³ should still be expected to be obtained.

In practice, the next reclamation was conducted in October 2005, after receiving 800 dm³ of demineralized water. In addition, no differences in water quality were found when comparing the reclamation conducted with analytically pure sodium base with one obtained from electro dialysis.

Carbonization of NaOH solution

Figure 1 represents the efficiency of the process of NaOH solution carbonization (a mixture of NaHCO₃ and Na₂CO₃ is created) as well as calcination (Na₂CO₃ is obtained), according to reaction 1 equation, depending on NaOH initial concentration and the temperature the process was conducted at. Carbonization time, which was 90 minutes – was long enough to find sediment in each case (non-zero efficiency).

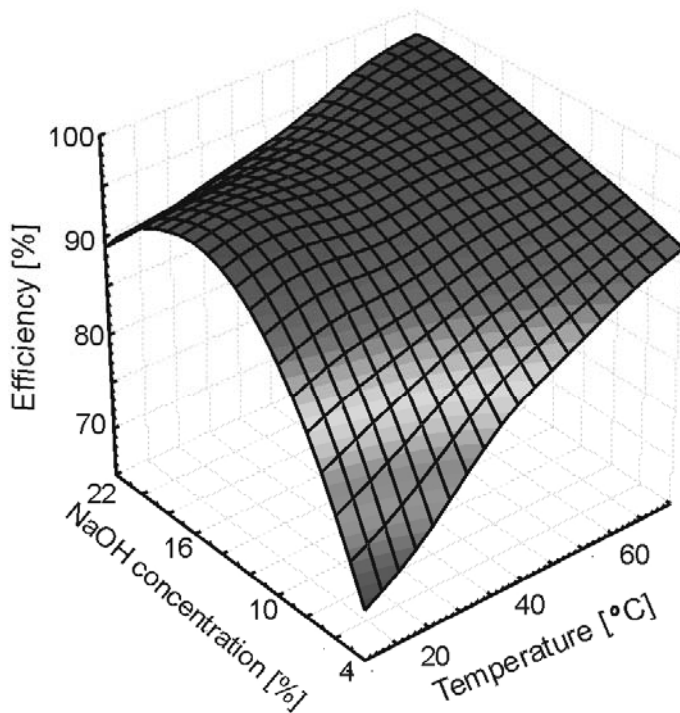


Fig. 1. Efficiency of obtaining Na₂CO₃

Basing on the obtained graph, it is found that at low initial NaOH concentration, efficiency highly depends on carbonization process temperature.

At high NaOH concentrations and lower temperature, efficiency slightly decreases due to losses.

Management of gaseous products

Hydrogen and oxygen are produced in electrode compartments (water electro dialysis) as a result of electrode reactions: oxidation at the cathode and reduction at the anode. These products have many applications. Hydrogen (by itself or together with oxygen) can be used as a non-conventional (alternative) energy source.

According to experts' estimates, after oil supplies (and later on coal as well) have run out, it is hydrogen that will become one of the basic energy sources.

The fuel crisis of the 1970-ties brought to the world's attention that natural resources are limited. At present, attention is often drawn to a more real danger of

trespassing the ecological barrier, particularly if the issues of the environmental protection will not be treated seriously.

Acknowledgments

This work was financially supported by the Polish State Committee for Scientific Research (project No 3T09B12128).

References

- [1] B. Igliński, R. Buczkowski, A. Warszawski, B. Dejewski, *Pol. J. Appl. Chem.*, **27** (3-4), 83-91 (2004).
- [2] T. Xu, W. Yang, *Chem. Eng. Process*, **41**, 519-524, 2002.
- [3] T. Xu, W. Yang, *J. Membrane Sci.*, **203**, 145-153, 2002.
- [4] T. Xu, *J. Membrane Sci.*, **37**, 1-22, 2002.
- [5] B. Igliński, E. Lemanowska, R. Buczkowski, *Annals of Polish Chemical Society*, **3**, 1329-1332, 2004.
- [6] B. Igliński, S. Koter, R. Buczkowski, M. Lis, *Pol. J. Env. Stud.*, **15(3)**, 409-415, 2006.

SYNTHESIS OF CHIRAL SELECTORS BASED ON SULPHOACRYLATE AND TRANS –(R,R)-CYCLOHEXYL-1,2- DIAMINE

Teresa Jabłońska-Pikus, Władysław Majewski, Władysław Charmas

Faculty of Chemistry, MCS University, pl. M. Curie-Skłodowskiej 3, 20-031 Lublin, Poland

Introduction

Many drugs and physiologically important compounds contain a stereogenic centre or in general are chiral molecules. The resolution of racemic compounds can be achieved by means of either an intra or intermolecular approach.

The intramolecular method is based on preparation of diastereoisomers, then on their separation by crystallization or chromatography on nonchiral columns and finally on chemical regeneration of pure enantiomers. The intermolecular method involves a chiral medium which, in HPLC, can be either the mobile phase or the stationary phase.

The chiral stationary phase is usually prepared by the immobilization of chiral molecules on siliceous support with appropriate alkyl spacers [1].

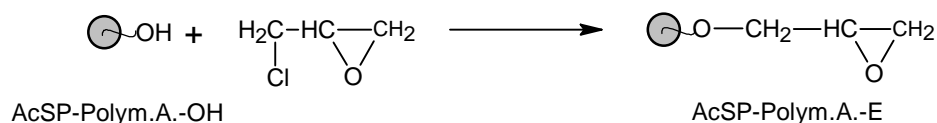
The main drawback of these materials is associated with the presence of unreacted silanol groups on their surface.

In the present paper the preparation and characterization of the new chiral stationary phase based on synthetic copolymer and trans (R,R)1,2-diaminocyclohexane is illustrated.

Experimental

Synthesis of porous copolymer of mono- and diacrylate esters of bisphenol-S and divinylbenzene [AcSP-Polym.A-OH] containing the hydroxyl functional groups on their surface was published earlier [2]. In experiments the beads of diameter 5-10 μm were used.

The reactive hydroxyl groups were subjected to a reaction with epichlorohydrin and transferred into glycidyl groups after the removal of hydrogen chloride. In the second step the modified beads (AcSP-Polym.A.-E) have been functionalized with selector trans (R,R)-1,2-diaminocyclohexane. The anchored selector has been later derivatized with different aryl chlorides in order to obtain a broader spectrum of CSP.



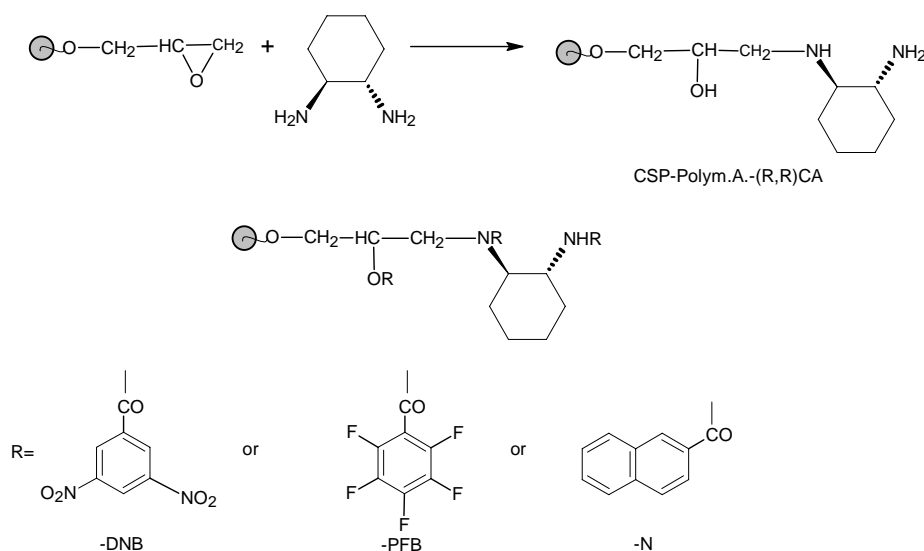


Fig.1. Synthesis of the polymeric chiral stationary phases.

The C,H,N analysis was performed on a Perkin Elmer CHN 2400 analyzer, whereas the IR spectra were obtained on a Perkin Elmer 1700 FTIR spectrometer with KBr pallets. Parameters such as the specific surface areas, pore volumes, pore size distributions and average pore diameters were determined by the method of nitrogen adsorption on the surface of studied stationary phase in a dry state. The swellability coefficient (B) was determined from equilibrium swelling in acetone, methanol, 1,4-dioxane, dichloromethane, 2-propanol and heptane with the centrifugation method [3].

B can be expressed as follows:

$$\%B = \frac{V_s - V_0}{V_0} \cdot 100\%$$

where V_s is the volume of the copolymer after swelling and V_0 of the dry copolymer. The beads were examined with atomic force microscopy (AFM Nanoscope III, Digital Instruments, United States) in the contact mode.

Results and discussion

The syntheses of the new chiral stationary phases are presented in Figure 1. All phases have been characterized in different steps in the working process by FTIR and elemental analysis.

The FTIR spectrum of AcSP-Polym.A.-E shows the adsorption line at 908 cm^{-1} which is attributed to the oxirane ring. The disappearance of this line and additionally bands at 2860 cm^{-1} and 1670 cm^{-1} in the spectrum of CSP-Polym.A.-(R,R)CA indicates opening of the oxirane ring.

The FTIR spectrum of CSP-Polym.A.-(R,R)CA-DNB shows bands at 1544 cm^{-1} characteristic of asymmetric vibration and 1345 cm^{-1} symmetric vibration of the bond C-NO₂. In the

spectrum of CSP-Polym.A.-(R,R)CS-N the strong adsorption band at 993 cm^{-1} characteristic of naphthalene ring and in the spectrum of CSP-Polym.A.-(R,R)CA-PFB the bands at 478 cm^{-1} characteristic of the band $C_{Ar}-F$ and 777 and 761 cm^{-1} characteristic of substitution 1,2,3 in the benzene ring are visible.

Characterization of the porous structure of the modified achiral and chiral polymeric stationary phases for chromatography is presented in Table 1.

Table 1. The structure of porous polymeric achiral and chiral phases.

Polymeric phase	Specific surface area [m^2/g]	Pore volume [cm^3/g]	Average pore radius [\AA]
AcSP-Polym.A.-OH	159.7	0.65	72
AcSP-Polym.A.-E	130.7	0.53	74
CSP-Polym.A.-(R,R)CA	114.6	0.51	84
CSP-Polym.A.-(R,R)CA-DNB	99.1	0.39	73
CSP-Polym.A.-(R,R)CA-PFB	109.8	0.49	85
CSP-Polym.A.-(R,R)CA-N	99.3	0.42	79

The results confirm that chemical modification of the surface of polymeric matrix change not only the chemical character phases but also their porous structure. The specific surface area and pore volume of the chiral phase are smaller than those of the matrix. The shape and developed surface of CSP-Polym.A.-(R,R)CA are presented in Figure 2.

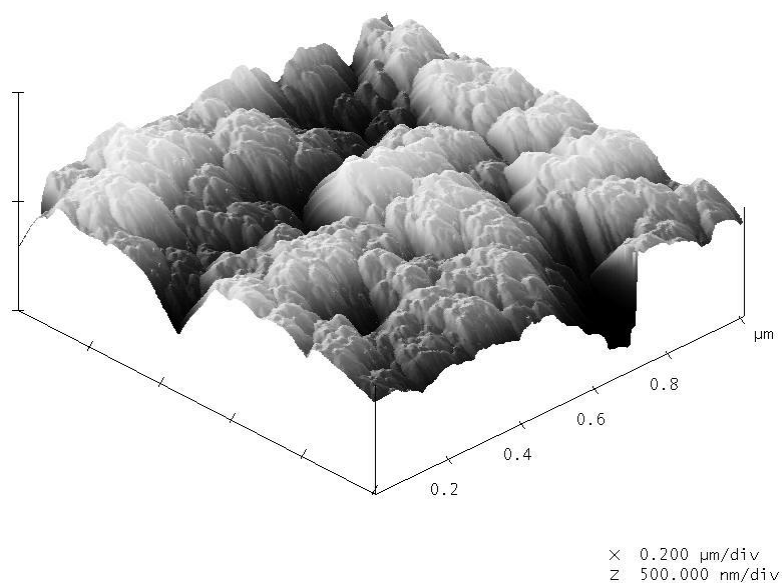


Fig. 2a. AFM micrograph of CSP-Polym.A.-(R,R)CA

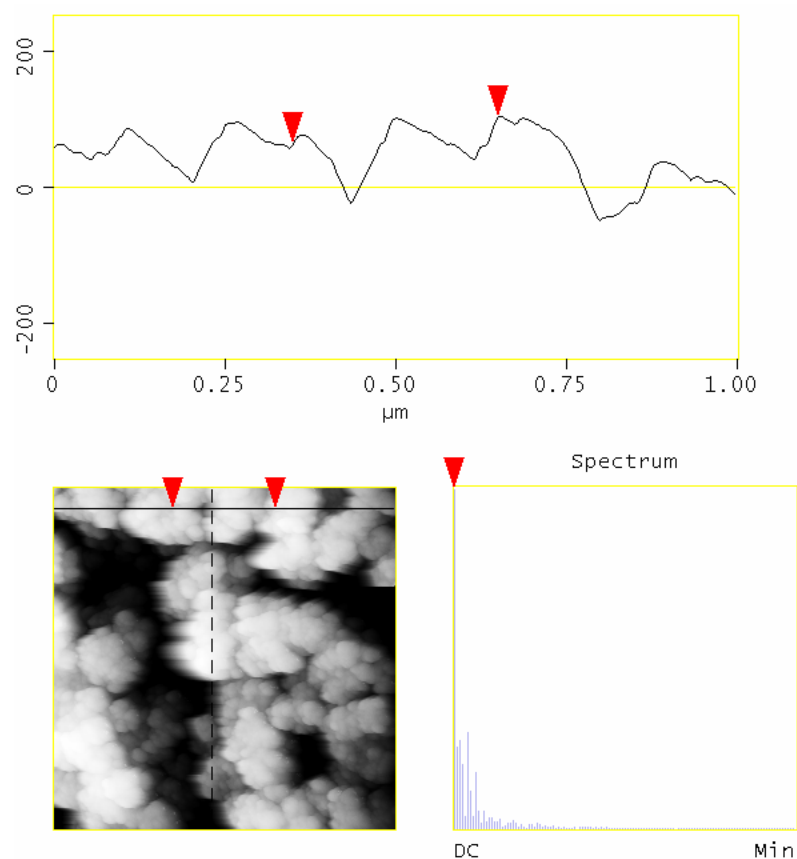


Fig. 2b. Section Analysis of CSP-Polym.A.-(R,R)CA

In Table 2 the swellability coefficients of chiral phases are presented. From the data, we can see that all new chiral stationary phases swell similarly. In acetone and methanol the B values are rather large and in nonpolar n-hexane very small.

The properties of the presented chiral packing materials suggest that they can be applied to HPLC separation.

Table 2. Swelling of polymeric achiral and chiral phases

Phase	B [%]					
	A	M	D	H	P	CM
AcSP-Polym.A.OH	16.7	15.9	14.2	1.0	4.8	9.2
CSP-Polym.A.-(R,R)CA	16.7	15.9	14.2	1.0	4.8	9.2
CSP-Polym.A.-(R,R)CA-N	17.5	10.5	10.7	0.4	4.4	9.8
CSP-Polym.A.-(R,R)CA-DNB	14.5	11.4	8.0	0.4	4.7	8.6
CSP-Polym.A.-(R,R)CA-PFB	13.4	7.4	4.8	0.6	3.1	7.9

A – acetone, M – methanol, D – 1,4-dioxane, H – hexane, P – propan-2-ol, CM - dichloromethane

References

- [1] Ihara T., Sugimoto Y., Asada M., Nakagama T., Hobo T., *J. Chromatogr., A* 694 (1995) 49.
- [2] Majewski W., Jabłońska-Pikus T., Charmas W., *Annals Pol.Chem.Soc.*, (2005) 367
- [3] Tunel A., Piskin E., *J.Appl.Polym.Sci.*, 62 (1996) 789.

MONO-, DI-, AND TRI-TERTBUTYL ETHERS OF GLYCEROL. AN ANALYTICAL STUDY.

Małgorzata E. Jamróz^{1,*}, Małgorzata Jarosz¹,
Janina Witowska-Jarosz², Elżbieta T. Bednarek², Witold Tęcza¹,
Michał H. Jamróz¹, Jan Cz. Dobrowolski^{1,2,*}, Jacek Kijęński^{1,3}

¹ Industrial Chemistry Research Institute, 8 Rydygiera Street, 01-793 Warsaw
E-mail: Małgorzata.Jamroz@ichp.pl; Phone: +(22) 568 2021

² National Institute of Public Health, 30/34 Chelmska Street, 00-725 Warsaw

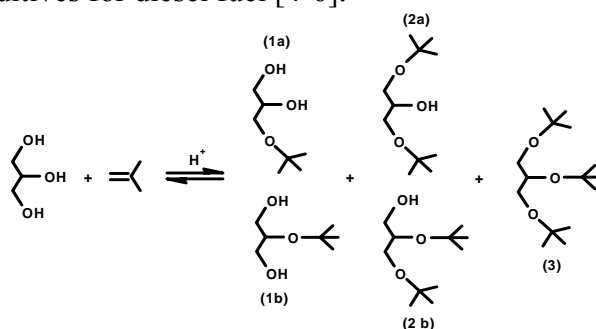
³ Warsaw University of Technology, 3 Noakowskiego Street, 00-664 Warsaw

Abstract:

This paper presents the analytical efforts accompanied by developing synthesis of tert-butyl glycerol ethers for biodiesel reformulation. GC, GC-MS, IR, Raman, NMR, and computational studies were performed to facilitate the identification and characterization glycerol tert-butyl ethers. GC and selective ion monitoring as well as chemical ionization GC-MS methods were used to control and to optimize the synthesis. Electron impact MS, NMR, IR and Raman molecular spectroscopy techniques were applied to characterize the main reaction products isolated in a pure form: 3-tert-butoxy-propane-1,2-diol, 1,3-di-tert-butoxy-propan-2-ol, and 1,2,3-tri-tert-butoxy-propane. Computational DFT studies were performed to support and rationalize both vibrational spectroscopy analysis and the isomer ratio.

Introduction

Biodiesel is one of the leading alternatives to fossil fuels in transportation. The main products of the biodiesel manufacturing are methyl esters of fatty acids (FAME) and glycerol formed as a byproduct [1-3]. Therefore, new methods of glycerol utilization are desirable. One of the methods is glycerol ethers synthesis. The ethers are excellent oxygen additives for diesel fuel [4-6].



Scheme 1

Recently, we developed a procedure of catalytic synthesis of high value glycerol ethers (primarily di- and tri-tert-butyl), obtained directly from glycerol and isobutene from the cracking derived fraction [7] (Scheme 1). Several products were obtained in this reaction; the desired ones being: 1,3-di-tert-butoxy-propan-2-ol (**2a**), 2,3-di-tert-butoxy-propan-1-ol (**2b**), 1,2,3-tri-tert-butoxy-propane (**3**). However, 3-tert-butoxy-propane-1,2-diol (**1a**) and 2-tert-butoxy-propane-1,3-diol (**1b**) were always present in

the mixture. Also, dimers and trimers of isobutene were always formed as undesired byproducts. Efficacy of **2a**, **2b**, and **3** for biodiesel fuel results from their decrease of emission of particulate matter, viscosity, cold filter plugging point, and cloud point. **1a** and **1b** are undesired because of their insolubility in hydrocarbons and introduction of excess water into the fuel. The aim of this paper is to describe analytical efforts accompanying development of our technology. In particular, we have shown that the GC, GC-MS, IR, Raman, NMR, and computational studies enable identification and characterization of the tert-butyl ethers of glycerol.

Results and Discussion

GC: For the determination of all components (Fig. 1) the multicomponent calibration method was used. Glycerol was determined by standard addition method with 1-butanol as a standard.

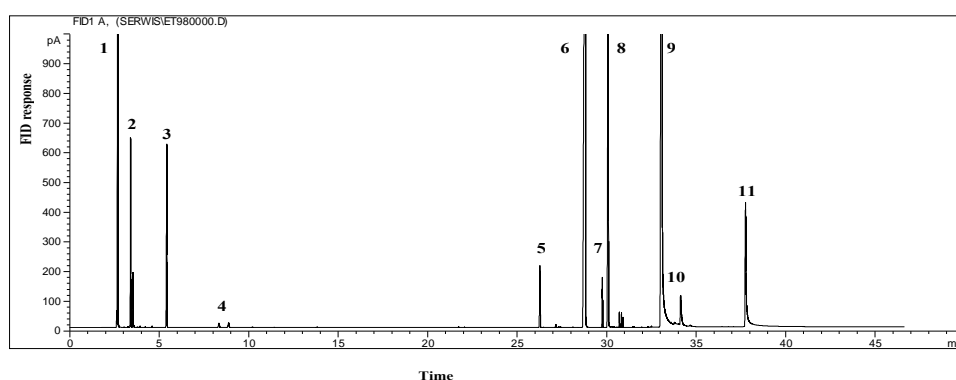


Fig. 1. Exemplary GC analysis of products of glycerol reaction with isobutene fraction. **1**- C₄; **2**-isobutene dimers; **3**-tert-butyl alcohol; **4**-isobutene trimers; **5**-1,2,3-tri-tert-butoxy-propane; **6**-1,3-di-tert-butoxy-propan-2-ol; **7**, **8**-isomers of di-butoxy-propan-ol; **8**-3-tert-butoxy-propane-1,2-diol; **9**, **10**-isomers of butoxy-propane-diol; **11**-glycerol.

GC-MS: In the standard EI mass spectra the mixture components were very similar to each other. Thus, the chemical ionization (CI) technique was used. The selective ion monitoring SIM and CI MS techniques enabled to assign the GC peaks and to interpret the EI MS spectra of pure 1,3-di-tert-butoxy-propan-2-ol (**2a**) and 1,2,3-tri-tert-butoxy-propane (**3**) inaccessible in data bases.

NMR: Most assignments at ¹H and ¹³C NMR resonances in the isolated ethers were done using standard procedures. In ambiguous cases, the ¹H{¹³C} GHMQC spectra were used as a final and unequivocal tool for specific assignments. For example, this type of spectra was used to distinguish the C1H₂ and C3H₂ resonances in compounds **1a**.

FT-IR and FT-Raman: The most striking difference in the IR spectra upon successive tert-butyl etherification of glycerol is the decrease in intensity of the ν(OH) stretching band localized at ca. 3400 cm⁻¹ for **1a**, at 3450 cm⁻¹ for **2a**, and absent for **3** (Fig. 2). This analogous decrease is observed in intensity and frequency of the broad γ(OH) out-of-plane vibration band at ca. 600 cm⁻¹. Changes of the δ(OH) bending vibrations band can be observed only as a decrease of the backgrounds at ca 1400 cm⁻¹.

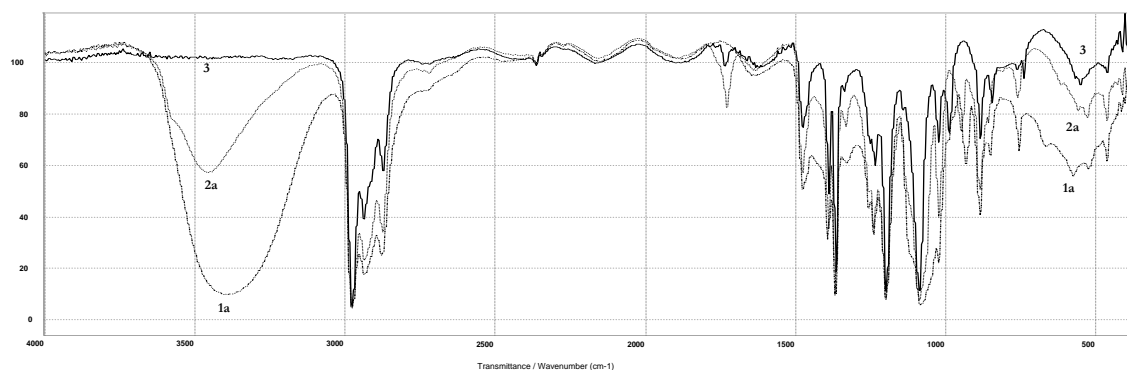


Fig. 2. The full mid IR range of liquid films of 3-tert-butoxy-propane-1,2-diol (**1a**), 1,3-di-tert-butoxy-propan-2-ol (**2a**), and 1,2,3-tri-tert-butoxy-propane (**3**)

The 1150- 900 cm^{-1} range is very informative (Fig. 3). The IR spectrum of (**3**), exhibits three main bands in the region: an intense band at ca. 1085 cm^{-1} , and two medium intensity bands at 1020 cm^{-1} and 985 cm^{-1} . The former is due to asymmetric $\nu^{\text{as}}(\text{C-O}+\text{C}_\text{P}-\text{C}_\text{P})$ stretching vibrations, where P denotes skeleton. The next is due to $\rho(\text{CH}_3)$ rocking vibrations, while the latter corresponds to the $\rho(\text{CH}_2)$ rocking vibrations. The other bands of the region were also assigned by using detailed PED analysis [8].

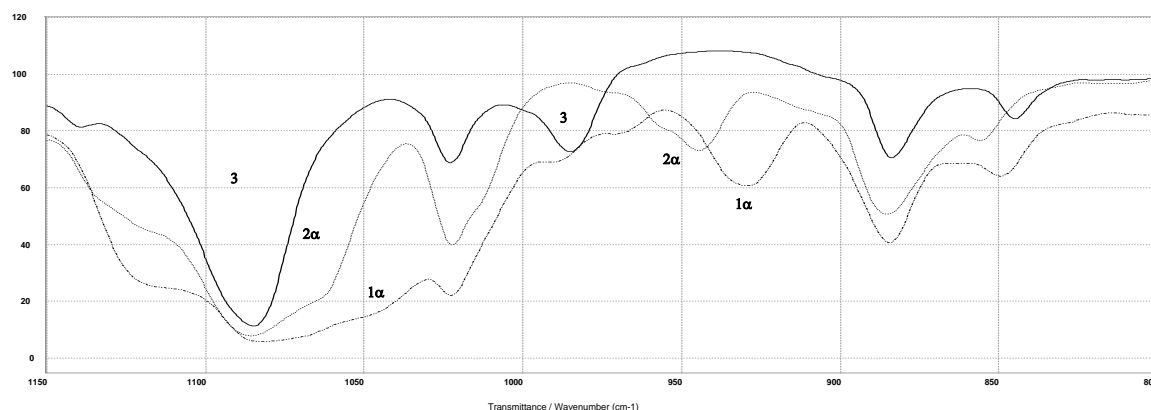


Fig. 3. The FTIR spectra of liquid films of 3-tert-butoxy-propane-1,2-diol (**1a**), 1,3-di-tert-butoxy-propan-2-ol (**2a**), and 1,2,3-tri-tert-butoxy-propane (**3**): (a) finger-print range, (b) stretching ether C-O vibrations range.

The IR spectrum of **2a**, bands at ca. 1085, 1020, 885, and 850 cm^{-1} are the same as in the IR spectrum of **3**. A new band at ca. 1120 cm^{-1} is due to the $\nu(\text{C-O(H)})$ stretching vibrations and band at ca. 1060 cm^{-1} and at ca. 950 cm^{-1} correspond to the ether C-O asymmetric stretching modes engaged into intermolecular C-O...H-O hydrogen bonds and to the rocking $\rho(\text{CH}_2)$ vibrations, respectively.

Again, the IR spectrum of **1a** is similar to that of **2a** (Fig. 3), and the bands at ca. 1120, 1085, 1060, 1020, 885, and 850 cm^{-1} can be interpreted as in the previous case. A new band at 1040 cm^{-1} can be assigned to the alcoholic C-O asymmetric stretching vibrators engaged in the intermolecular hydrogen bonds. The other band can be found at

ca. 935 cm^{-1} and can be assigned to the rocking $\rho(\text{CH})$ vibrations with a contribution of the $\rho(\text{CH}_2)$ rocking vibrations.

The changes in Raman spectra with successive tert-butyl etherification of glycerol are less obvious. The $\nu(\text{OH})$ and $\nu(\text{C-O})$ bands are not intense and the only changes worth of mentioning are those in the 950 and 700 cm^{-1} range. As a result, the variations in the Raman spectra do not permit ether differentiating in the mixture.

Calculations: Glycerol exhibits at least 100 conformers [10]. Introduction of tert-butyl increases noticeably number of conformers. To estimate energy difference between the isomers **1a** vs. **1b**; and **2a** vs. **2b** hundreds of conformers were calculated at the AM1 level and the most stable conformers were reoptimized by the B3LYP/6-31G** method. The ΔG estimated have shown that **1a** is more stable than **1b** by 3.5 kcal/mol and **2a** is more stable than **2b** by 3.3 kcal/mol .

Conclusions

GC technique and GC-MS, ^1H and ^{13}C NMR, $^1\text{H}\{^{13}\text{C}\}$ GHSQC, FT-IR, and Raman molecular spectroscopy methods were used in analyses and characterization of (**1a**) 3-tert-butoxy-propane-1,2-diol, (**2a**) 1,3-ditert-butoxy-propan-2-ol, and (**3**) 1,2,3-tri-tert-butoxy-propane which can be of interest in the chemical industry as oxygen additives for diesel fuel. Except EI MS spectra of **1a**, the other MS characteristics have not been reported. The CI MS measurements were necessary to observe the molecular ions. The $^1\text{H}\{^{13}\text{C}\}$ GHMQC spectra were used as an unequivocal tool for the NMR assignments. The IR spectra range between 1150 and 900 cm^{-1} was interpreted in details based on both comparison of the experimental and the theoretical B3LYP/6-31G** spectra and PED analysis. The calculations were used also to establish that **1a** and **2a** are more stable than their isomers by 3.5 kcal/mol and 3.3 kcal/mol , respectively.

Acknowledgements

This work was supported by the KBN Grant No. 3 T09B 058 29. The computational Grant G19-4 from the Interdisciplinary Center of Mathematical and Computer Modeling (ICM) at Warsaw University is gratefully acknowledged.

References

- [1] Natl. Renew. Ener. Lab., <http://www.nrel.gov/docs/legosti/fy98/24089.pdf>
- [2] Chemical Market Reporter, February 7, (2005)12.
- [3] S. Ritter, Gasoline, Chem. Eng. News, 83 (2005) 37.
- [4] D. Lipkin, U.S. Pat. No. 2,221,839, 1940.
- [5] G. A. Olah, U.S. Pat. No. 5,520,710, 1996.
- [6] H. Nouredini, US Pat. 6,174,501, 2001.
- [7] J. Kijeński, M. E. Jamróz, W. Tęcza, M. Jarosz, Appl. Pol. Pat., P-371 959 (2004).
- [8] M. H. Jamróz, Vibrat. Ener. Distrib. Anal.: VEDA 4 program, Warsaw 2004.
- [9] Wiley Registry of Mass Spectral Data, 8th Edition, John Wiley & Sons, Inc. 2006.
- [10] R. Chelli, F. L. Gervasio, C. Gellini, P. Procacci, G. Cardini, V. Schettino, J. Phys. Chem. A, 104 (2000) 11220-11222.

COMPARISON OF THE INFLUENCE OF SELECTED ORGANIC SOLVENTS ON THE GROWTH OF *CHLORELLA VULGARIS* ALGAL CULTURES

G. Janikowska

Division of Analytical Chemistry, Faculty of Pharmacy, Medical University of Silesia, Jagiellońska 4, 41-200 Sosnowiec

INTRODUCTION

The organic solvents fall to surrounding us to water environment with industrial sewages or other, in result of different activities of man (usage of pesticides, environmental pollution) [1]. It can make way a lipid soluble chemicals to interiors of microorganisms by multidirectional biochemical interaction [2]. The direct effect of solvents on aquatic plants can be observed as increase or decrease in total cell count or total cell volume of microorganisms.

The algas *Chlorella* are recommended by OECD (Organization of Economic Cooperation Development) and other world agencies (EPA, ISO) to investigations of influence of chemical matter on aquatic environment, as also estimation of cleanness of waters [3]. Algal tests permit to rate influence of examined chemicals in aquatic environment, one from links of trophic chain. Serve to estimations of biological activity of chemical substances. Aim of the present work was comparison of influence of selected organic solvents on growth of alga *Chlorella vulgaris* cultures.

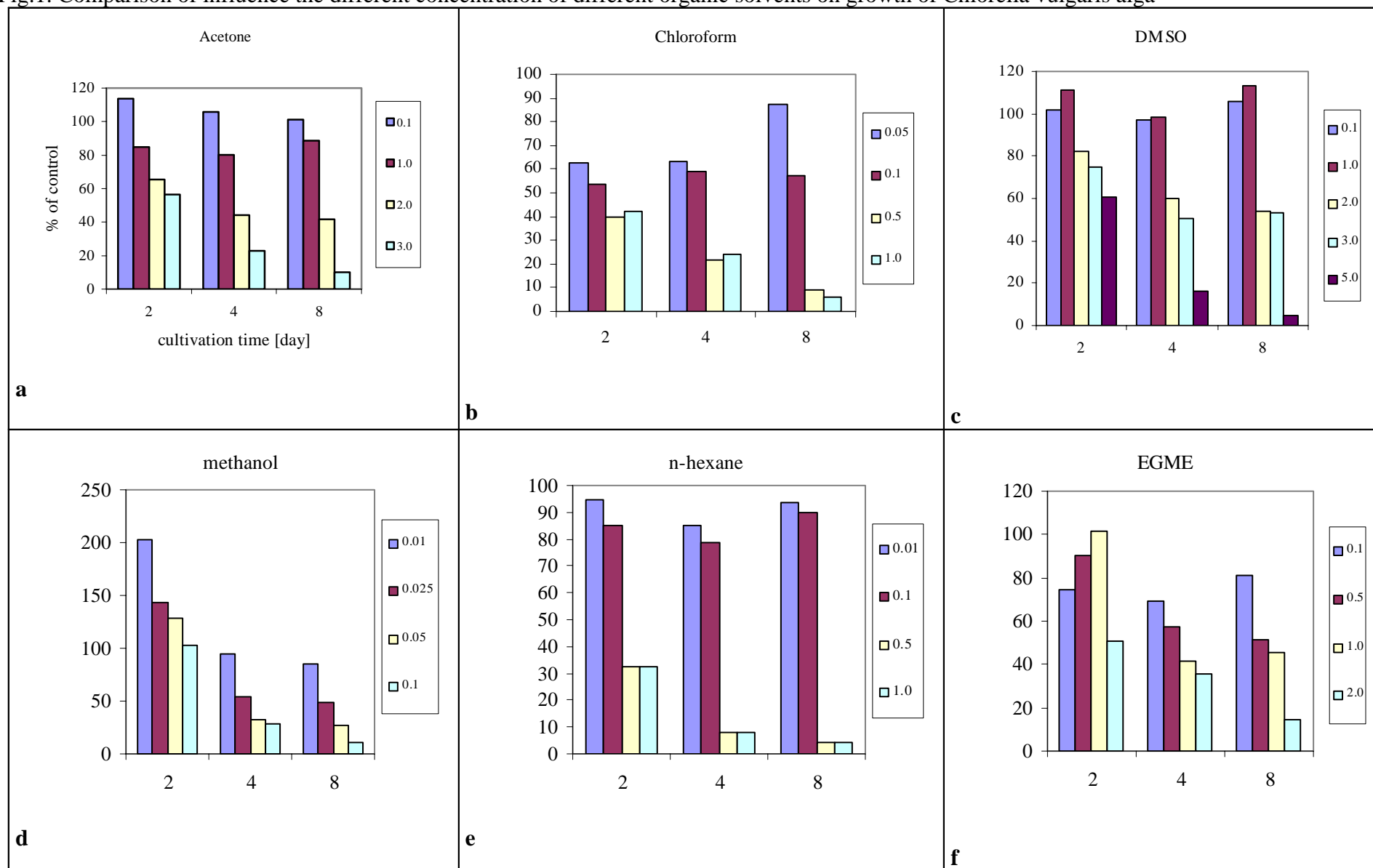
MATERIALS AND METHODS

The cultures of alga *Chlorella vulgaris* Beijerinck 1890 strain A-8 carried out in 200 ml Erlenmayer flasks, in liquid medium Kühl-Lorenzen [4] modified by Borns and others [5], in conditions of continuous lighting with mercury-glow lamp (4800 lx) and continuous mixings with magnetical stirrers. Both cultures, controls cultures and cultures with addition of suitable quantities of selected solvents as acetone, chloroform, dimethyl sulphoxide (DMSO), methanol, hexane and ethyl glycol monoether (EGME) were carried out simultaneously in these same conditions and in five repetitions. In investigations are used initial density of cultures about 300 thousand of cells in 1cm³ of culture. Initial concentrations of each solvent were situated in borders from 0.01 to 5.0 % v/v. Estimation of cultures growth were carried out by Bürker heamocytometer under light - microscope every day.

RESULTS AND DISCUSSION

On base of effected investigations were marked the growth curve of alga cultures, which were used to calculations the relationship of a values of cells number to each days in control cultures and investigated cultures, i.e. cultures with each solvents. Results of these dependences for all examined solvents and all their concentrations are presented in fig. 1. However the effects of influence this same quantities of solvents on different chemical construction are introduced in fig. 2. For these comparisons the analysed course of culture growth in select time, and namely in 2, 4 and 8 day of culture that three different phases of growth are presented. Greatest relationship dose-answer we can see in relation to following days of culture duration in case of acetone (of figs 1a), instead in relation to differences in dose of solvent (0.01 - 1.0 % v/v) in case of n-hexane in all introduced days of cultivation (of figs.1e) but in case of chloroform only for 8 day of culture duration (of figs.1b).

Fig.1. Comparison of influence the different concentration of different organic solvents on growth of *Chlorella vulgaris* alga



In case of methanol the toxic effect deepened together with increase of concentration and in following days of culture duration (figs. 1d). Such effect for DMSO we can observe only for highest concentrations (of figs. 1c). At highest concentration of EGME observed effect is not so strong (figs. 1f).

The inhibition effects observed in course of growth of examined *Chlorella* cultures were differed into dependence on kind of investigated solvent. Differences are referred both the inhibition and the moment of occurrence of this effect during the time of cultures (fig. 1). In every investigated chance the effect of growth inhibition was increasing with initial concentration of solvent in cultures medium.

It can be suppose that observed different effects of investigated solvents caused are not only their immediate toxicity, but also their metabolite toxicity which are coming into lively cell and time of their exposition and biodegradation.

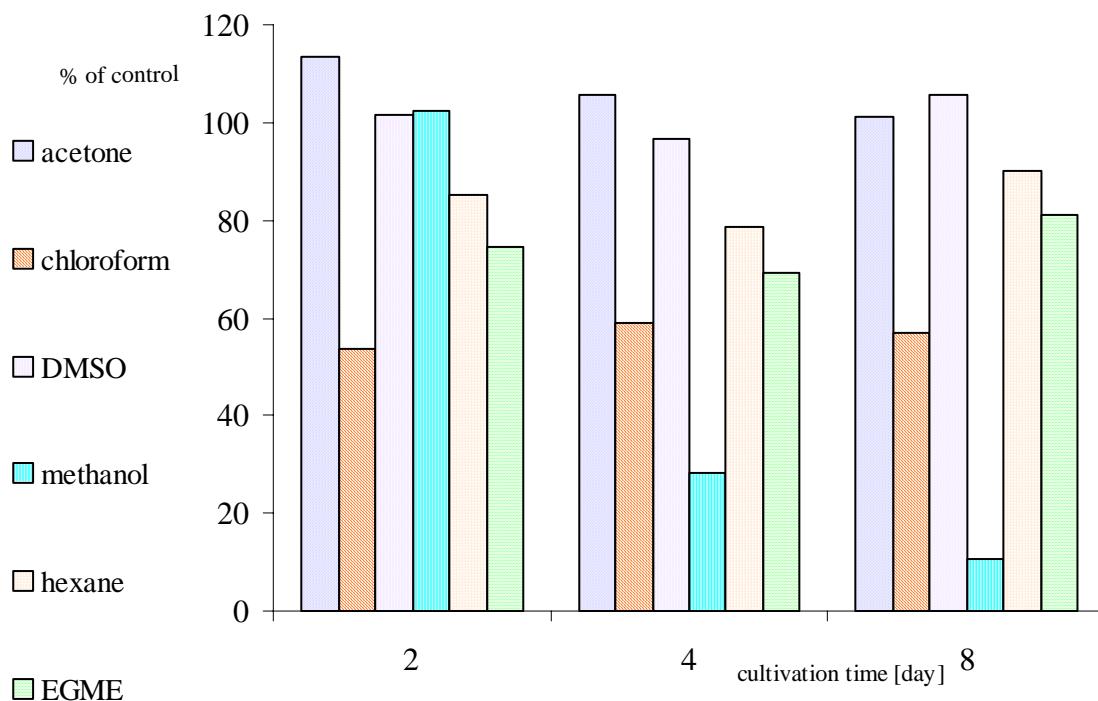


Fig. 2. Comparison of influence this same concentration (0.1% v/v) of different organic solvents on growth *Chlorella vulgaris* alga

Fig. 2. shows mechanism of multidirectional influences of solvent concentration during the time of growth of alga, such as a late toxic activity of methanol and immediate of chloroform. And also lack of influence of acetone and DMSO in this same concentration (0.1% v/v) on growth of cultures. In case of methanol probably only metabolites called out the cascade of stimulant processes in cell with trend to inhibition of proliferation that inhibit a cell life (apoptosis). Instead in case of chloroform we observe the effect of holding the inhibition of growth on this same level by following days of observation.

Reports of literature in influence of organic solvents on aquatic environment from one side confirm passed analysis in this work and from second show a little other dependences. Most recognized in respect of toxicities is acetone [1, 2, 6-8]. Introduced investigations confirm the

results of Stratton, who in paper with bluegreen algae showed that DMSO and acetone are least toxic solvents [7]. Instead El Jay ascertained that DMSO is most proper solvent to usages in bioassays [8]. Toxicity of chemical compound not only depends from their chemical construction but also depends on species of microorganism which test of toxicity became passed. Different sensitivity of the alga species to the organic solvents causes slight and sometimes a large differences in values of toxic concentrations [1, 9]. On base of knowledge about toxicity of solvents in aquatic environment and recognising the scientific and regulatory need for testing relatively hydrophobic or 'difficult substances', the OECD currently recommends that selected organic solvents may be used in aquatic toxicity testing in order to help achieve more effective dispersion of the toxicant. The OECD recommends a maximum solvent concentration exactly given for each solvents [10]. These data determine the guidelines to usages of maximum quantities of solvents in aquatic environment.

CONCLUSION

Observed changes in biological activity of investigated solvents came to light in growth of alga *Chlorella vulgaris* cells.

Investigated solvents in heterogeneous manner acts on alga cells.

Ascertained changes show univocally that investigated substances disturb equilibrium in growth of *Chlorella* cells in relation to growth of control cultures. Effect of their activities is different and decide of them the quantities and chemical construction and time after exposition.

REFERENCES

- [1] G. Stratton, T. Smith, Bull. Environ. Contam. Toxicol. 40 (1988) 736
- [2] A. El Jay, Bull. Environ. Contam. Toxicol. 57 (1996) 191
- [3] OECD Guidelines for the testing of chemicals, Paris (1993)
- [4] A. Kühl, H. Lorenzen, Methods in cell physiology, 1 (1964) 159
- [5] Borns E., Böhm H., Schultze D.: Wiss. Hefte d. Päd. Inst. Köthen. 2 (1973) 55
- [6] G. LeBlanc, D. Surprenant, Arch Environ Contam Toxicol. 12 (1983) 305
- [7] G. Stratton, Bull. Environ. Contam. Toxicol. 38 (1987) 1012
- [8] A. El Jay, Arch Environ Contam Toxicol. 31 (1996) 84
- [9] M. Tadros, J. Philips, H. Patel, V. Pandiripally, Bull. Environ. Contam. Toxicol. 52 (1994) 333
- [10] T. Hutchinson, N. Shillabeer, M. Winter, D. Pickford, Aquat Toxicol. 76 (2006) 69

THE INFLUENCE OF POLYHEDRAL OLIGOSILSESQUIOXANES (POSS) ON THERMAL PROPERTIES OF SEGMENTED POLYURETHANE ELASTOMERS

B. Janowski, K. Pielichowski

*Department of Chemistry and Technology of Polymers
Cracow University of Technology, ul. Warszawska 24,
31-155 Kraków, Poland*

Introduction

Segmented polyurethane (PU) based elastomers have versatile mechanical and thermophysical properties due to the formation of microphase separation from the thermodynamic incompatibility (immiscibility) of solid-like hard segments and rubbery soft segment sequences. The hard segments usually involve interchain interactions by means of van der Waals' forces and hydrogen bonding, which determine the strength of the hard segment and thus macroscopic properties [1]. Incorporating into polymers inorganic or organometallic segments, such as polyhedral oligomeric silsesquioxanes (POSS) to afford improved properties continues to be a driving force for the development of new hybrid organic/inorganic materials [2]. These hybrid polymers display improved properties such as higher T_g , increased oxygen permeability, reduced flammability and enhanced mechanical strength [3-5]. The POSS molecule contains a polyhedral silicon-oxygen nanostructured skeleton with intermittent siloxane chains (general formula $(\text{SiO}_{3/2})_n$). In this work, we report the synthesis and characterization of polyurethane networks incorporating POSS.

Materials

For synthesis of polyurethane/POSS nanohybrid elastomers 4,4'-diphenylmethane diisocyanate (MDI) (Aldrich), polytetramethylene glycol (PTMG, $M=1400$) (Terathane® 1400, Invista), 1,4-butanediol (BD) (Aldrich), and 1-(1-(2,3-dihydroxypropoxy)butyl)-3,5,7,9,11,15-isobutylpentacyclo-[9.5.1.1.(3,9).1(5,5).1(7,13)] octasiloxane (PHIPOSS) (Hybrid Plastics) were used. PHIPOSS was used to replace part of chain extender (1,4-butanediol) and thus the POSS cages act as pendant groups. The chosen POSS molecule has $n = 8$ (pseudo-cubic), with the corner isobutyl group. This has approximately 14 Å in molecular axis, with an inner Si-Si diameter of 5.5 Å.

Preparation of Polyurethane/POSS Nanohybrid Elastomers

MDI was charged into a 100 ml three-necked round bottomed flask, equipped with a mechanical stirrer and nitrogen inlet. It was melted at 70°C and PHIPOSS solution in PTMG was then added in one portion. Previously the PHIPOSS mixture in PTMG was heated to 120°C to dissolve the POSS cage into the polyol and then cooled to 60°C. The reaction was performed under a nitrogen atmosphere at 80°C for 2 h to form a polyurethane prepolymer. The NCO groups content was then determined and prepolymer was mixed with suitable amount of 1,4-butanediol. Mixture was poured out on Petri dish and cured at 110°C for 2 h and post-cured at 80°C in 16 h. The obtained polyurethane elastomers contained 40 wt. % of soft segments and 2, 4, 6, 8, 10 wt. % of PHIPOSS.

Techniques

Thermogravimetry (TG): dynamic mode at a heating rate of 10 deg/min in temperature range of 25 to 600°C, in argon atmosphere, open α -Al₂O₃ pan, sample mass - ~4 mg;

Differential scanning calorimetry (DSC): dynamic mode at heating rate of 10 deg/min, sealed aluminium pan, all samples were heated from -100 to 190°C, sample mass - ~5 mg;

Wide angle X-ray diffraction (WAXD): wavelength - 1,54 Å (Cu K α), scan range of 2θ from 3 to 50° with step interval of 0,05°.

Attenuated total reflectance Fourier spectroscopy (ATR-FTIR): spectral range from 3500 to 600 cm⁻¹, ZnSe crystal, incident angle of 30°.

Results

Thermogravimetric Analysis (TG).

TG curves of the PU elastomers are shown in Fig. 1. Within the experimental temperature range, all the polymers displayed similar degradation profiles. It can be seen that amount of solid residue for samples containing 2 and 4 wt. % of PHIPOSS was lower (and decreasing) than for PU; then, for samples with 6-10 wt. % of PHIPOSS an increasing trend was observed (Tab. 1). One can explain this effect in such a way that relatively large POSS cages can increase interchain PU distance which results in an easier diffusion of volatile products out of material, lowering thus the amount of solid residue. On the other hand, after exceeding of 4 wt. % of PHIPOSS barrier effect of POSS moieties becomes dominant and the amount of solid residue gradually increases.

Differential Scanning Calorimetry (DSC).

DSC profiles displayed for all elastomers single glass transition temperature (T_g) in the experimental temperature range. It can be seen that the composites containing 2

POSS content (wt.%)	$T_{5\%}$ (°C)	Solid residue (%)
0	294,9	11,0
2	299,8	7,8
4	299,7	5,8
6	298,2	6,2
8	296,6	7,5
10	290,3	9,3
PHIPOSS	240.0	21.5

Tab. 1. The temperatures of the 5 wt. % mass loss ($T_{5\%}$) and amount of solid residue of PU/POSS polymers

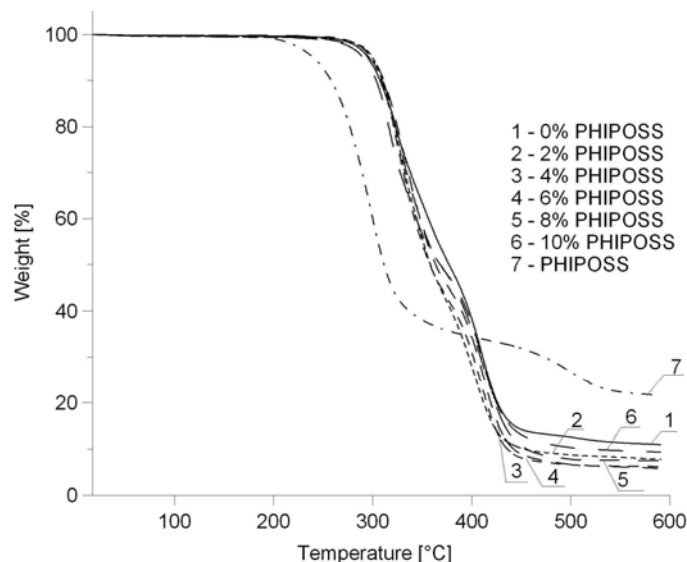


Fig. 1. TG profiles of PU/POSS polymers.

and 4 wt. % of PHIPOSS displayed lower T_g of soft segments (-58°C and -63°C, respectively) in comparison with the control PU elastomer (-50°C), while the hybrids

POSS content (wt.%)	Glass transition temperature (°C)
0	-50
2	-58
4	-63
6	-49
8	-51
10	-52

Tab. 2. Glass transition temperature of PU/POSS polymers

containing 6, 8 and 10 wt. % of PHIPOSS showed the comparable T_g to the control PU (Tab. 2).

It is proposed that in POSS-modified polymers there could be the two competitive factors influencing the glass transition temperatures. On the one hand, POSS cages on the segmental level could restrict the motion of macromolecular chains and stabilize T_g 's on the level comparable to T_g of the pristine PU. On the other hand, the presence of the bulky POSS cages could act as the internal plasticizer resulted in decreased values of T_g .

Wide Angle X-ray Diffraction (WAXD).

When PHIPOSS is incorporated in the polyurethane, the amorphous fraction becomes so large that some of the peaks are quite weak. The major peak in the PHIPOSS ($2\theta = 8.2^\circ$) can be clearly identified in polyurethane (Fig 2.), which suggests that the POSS molecules are probably aggregated and form nanoscale crystals. According to the Scherrer equation, the mean dimension of the crystallites can be estimated from the breadth of the reflection peak (Tab. 3).

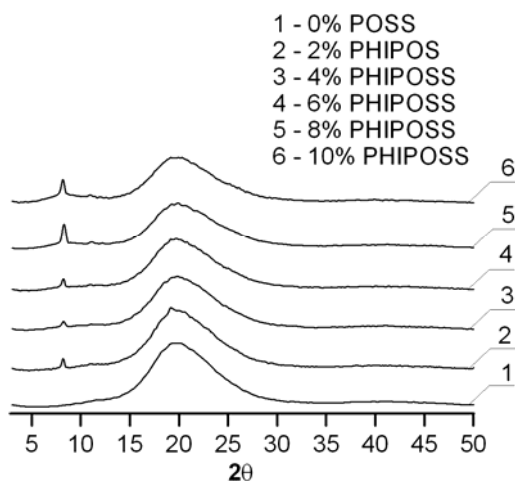


Fig. 2. WAXD diffractograms of PU/POSS polymers

PHIPOSS content (% m/m)	B (deg)	t (nm)
2	0.2	40
4	0.4	20
6	0.15	53
8	0.3	27
10	0.4	20

Tab. 3. Breadths of the X-ray peaks (B) and the mean dimensions (t) of the POSS crystallites

Attenuated Total Reflectance Fourier Spectroscopy (ATR-FTIR).

The results of ATR-FTIR (Fig. 4) showed two absorption bands for all elastomers at 1079 cm^{-1} (hydrogen-bonded ether groups) and at 1105 cm^{-1} (non-bonded ether groups), assigned to the soft polyether segment. After incorporation of PHIPOSS into the polyurethane chains the intensity of the band from the hydrogen-bonded ether groups decreased. It means that incorporation of the POSS molecules into polyurethane matrix resulted in decreased amount of the hydrogen bonds in the soft segment's phase.

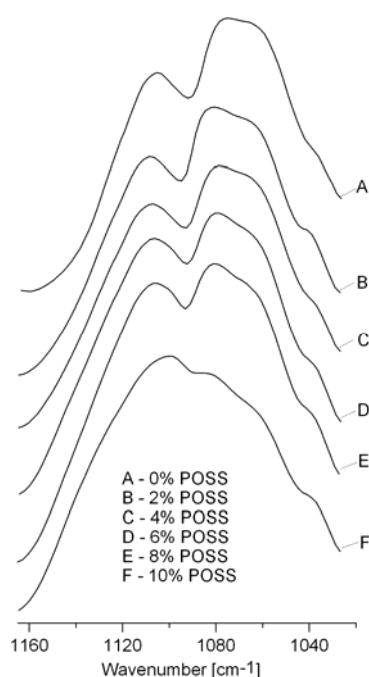


Fig. 4. The bands of the ether bonds stretching vibrations in the PU/POSS polymers.

Conclusions

A series of segmented polyurethane elastomers (PU) incorporating POSS was obtained. TG and DSC were employed to thermally characterize the POSS-reinforced polyurethanes. The results of DSC showed that the glass transition temperatures of the POSS-containing nanocomposites are dependent on the content of POSS. When the contents of POSS are less than 6 wt. %, the nanocomposites displayed the decreased glass transition temperatures in comparison with pristine PU. TG showed that for the samples containing PHIPOSS 5% mass loss temperatures are shifted toward higher values except of sample containing 10 wt. % of POSS. WAXD showed that the peak of PHIPOSS can be clearly identified in nanocomposites, which suggests that the POSS molecules are probably aggregated and form nanoscale crystals. IR analysis revealed that after incorporation of PHIPOSS into the polyurethane chains the intensity of the bands of the hydrogen-bonded ether groups were decreased. Incorporation of the POSS molecules into polyurethane chains resulted in decreased amount of the hydrogen bonds in the soft segment's phase.

References:

- [1] H. Liu, S. Zheng, *Macromol. Rapid. Commun.*, 26 (2005) 196.
- [2] K. Pielichowski, J. Njuguna, B. Janowski, J. Pielichowski, *Adv. Polym. Sci.* 201 (2006) 225.
- [3] R.Y. Kannan, H.J. Salacinski, M. Odlyha, P.E. Butler, A.M. Seifalian, *Biomaterials* 27 (2006) 1971.
- [4] Y. Liu, H. Zheng, *J. Appl. Polym. Sci. Part A*, 44 (2006) 1168.
- [5] B.X. Fu, B.S. Hsiao, S. Pagola, P. Stephens, H. White, M. Rafailovich, J. Sokolov, P.T. Mather, H.G. Jeon, S. Phillips, J. Lichtenhan, J. Schwab, *Polymer*, 42 (2001) 599.

Functionalization of Poly(2-Hydroxyethyl Methacrylate) with Chloroacetate Groups: Immobilization of Bioactive 1-Naphthylacetic Acid

Roman Jantas, Zbigniew Draczyński, Dawid Stawski

Department of Physical Chemistry of Polymers, Technical University of Łódź, 90-924 Łódź, Poland

In recent years, much attention has been directed to speciality polymers [1]. Poly(vinyl alcohol) or polysaccharides are good examples of macromolecular carriers for bioactive agents immobilization [2-4]. In most cases these polymers have been previously transformed into suitable reactive derivatives, in order to achieve the attachment of bioactive compound as well as to introduce a spacer between the carrier and the bioactive compounds. A gradual release of the bioactive agent can be achieved by hydrolytic or enzymatic cleavage of the linking bond. In this context, poly(2-hydroxyethyl methacrylate) (PHEMA) containing reactive hydroxyl groups, may be used for coupling of bioactive compounds.

In this paper, we report the applicability of pendant chloroacetate groups previously linked to PHEMA in coupling of bioactive carboxylic acid (1-naphthylacetic acid) by reaction with its potassium salt. A study of the hydrolysis of resulting adduct in the heterogeneous phase was also made in order to evaluate the release of the bioactive acid.

EXPERIMENTAL

Materials

2-Hydroxyethyl methacrylate (HEMA) was dried and distilled under reduced pressure. N,N-dimethylacetamide (DMAc), dimethylsulfoxide (DMSO), lithium chloride (LiCl), chloroacetyl chloride, pyridine and potassium 1-naphthylacetate (KNA) were obtained from Aldrich. All reagents were used without purification. PHEMA was prepared by the procedure described in reference [5]. The number average molecular weight of PHEMA was $M_n=23.600$ g/mol, and $M_w/M_n=1.93$.

Esterification of PHEMA with chloroacetyl chloride

Esterification of PHEMA with chloroacetyl chloride was carried out in DMAc/5% LiCl as a solvent and in the presence of pyridine as catalyst at 30 °C [6].

Reaction of chloroacetylated PHEMA with the potassium 1-naphthylacetate

The chloroacetylated PHEMA was dissolved in DMSO at room temperature. The calculated amount of potassium salt of 1-naphthylacetic acid was added while stirring. All the reactions were performed at 30 °C. After 5 h the product was isolated by precipitation with distilled water. All samples were purified by reprecipitation, using DMSO as solvent and ethanol as precipitant and then dried under reduced pressure at 60 °C to constant weight.

Study of heterogeneous hydrolysis of PHEMA-1-naphthylacetic acid adduct

The approximately 0.1 g of PHEMA-1-naphthylacetic acid adduct powder-form samples were compressed at high pressure to form disks with diameter of 12 mm. The resulting disks were placed in conical flasks with 100 cm³ of NaOH solution (pH = 12.7 ÷ 13.7). Flasks were put into water bath heated to the 25 °C. At fixed intervals, solution

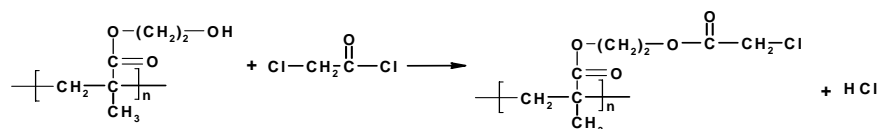
specimens were taken from the liquid above the padded of tables samples. The released bioactive agent in the homogeneous solution, was quantitatively determined by UV spectroscopy at the absorption wavelength of 1-naphthylacetic acid (NAA) at $\lambda=281$ nm using calibration curves (aqueous solution of sodium hydroxide as solvent). Tests were performed for different hydrophilic character of adducts and various pH values of reaction environment.

Measurements

Infrared spectra were recorded using Perkin-Elmer 2000 (FTIR) instrument. $^1\text{H-NMR}$ and $^{13}\text{C-NMR}$ spectra were obtained using Bruker DPX 250 MHz spectrometer. The UV-VIS spectra were obtained using Perkin Elmer UV/VIS Lambda 2 spectrometer. The degree of the esterification of the PHEMA was determined from the elemental analysis of chloride. The values of number average molecular weight (M_n), average molecular weight (M_w) and the polydispersity (M_w/M_n) of the PHEMA were determined by gel permeation chromatography.

RESULTS AND DISCUSSION

PHEMA modified with chloroacetate groups (mPHEMA) to different degrees of substitution were synthesized in a homogenous medium by using the method described for chloroacetylation of poly(vinyl alcohol) [7]. The following scheme shows the reaction:

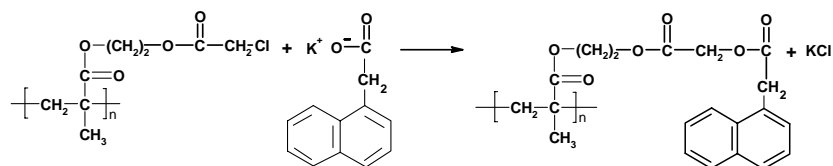


The effect of component ratio on the degree of substitution is summarized in Table 1. As follows from the data in Table 1, the extent of substitution increases with an increase in the ratio of chloroacetyl chloride to PHEMA. For example, the degree of substitution increases from 13.4 to 98.1 mol % as chloroacetyl chloride/hydroxy groups of PHEMA increases from 0.4 to 1.2.

Table 1. Effect of component ratio on the degree of substitution for the esterification of PHEMA with chloroacetyl chloride at 25°C

Sample	ClCH ₂ COCl /-OH	Cl	Degree of
	mole/mole	in mPHEMA wt %	substitution mol %
1	0.4	3.32	13.4
2	1.0	14.89	80.5
3	1.2	16.95	98.1

The coupling of bioactive carboxylic acid to PHEMA functionalized, was carried out by using the KNA according to the following scheme:



In this way mPHEMA-1-NAA adduct was obtained. The elemental analysis of the products obtained from mPHEMA and KNA showed the absence of chlorine, which allowed to assume that the substitution degree in the adduct was the same as for corresponding of mPHEMA.

The FTIR spectrum of mPHEMA (no shown) has a new absorption band at 1760 cm^{-1} of carbonyl groups in $-\text{COO}-\text{CH}_2-\text{Cl}$, which is superimposed on the spectrum of $>\text{C}=\text{O}$ band of ester groups of PHEMA. There is also visible an absorption peak of $-\text{CH}_2\text{Cl}$ groups at 760 cm^{-1} . Moreover in spectrum of the adduct mPHEMA-1-NAA absorption band appears at 1560 , 1513 and 790 cm^{-1} , which results from scissoring vibrations bands $>\text{C}=\text{C}<$ and C-H in the naphthyl ring [8].

The $^1\text{H-NMR}$ spectrum of the same mPHEMA (Fig. 1a) shows a characteristic band of protons of chloroacetate groups at 4.2 ppm , which is superimposed on one of the signals of $-\text{OCH}_2\text{CH}_2\text{O}-$ groups. There are also visible bands of $-\text{CH}_2-$ in the main chain at $1.31 - 2.41\text{ ppm}$, a signal of $\alpha-\text{CH}_3$ groups at $0.63 - 1.31\text{ ppm}$. The spectrum of mPHEMA-1-NAA adduct (Fig. 1b) shows additional signals of naphthyl ring at $7.3 - 8.2\text{ ppm}$.

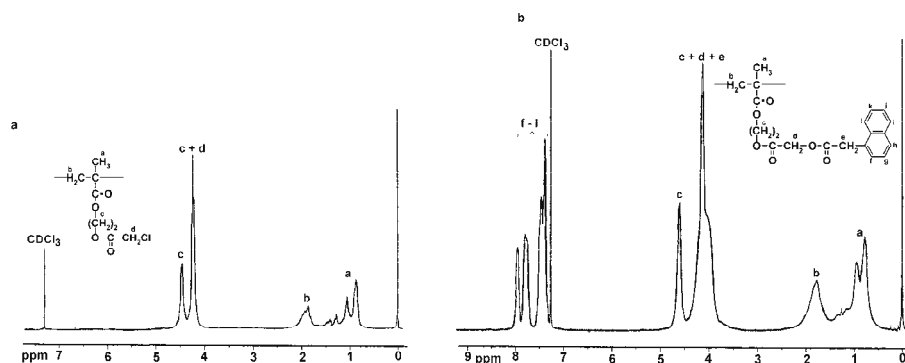


Fig. 1. Spectra $^1\text{H-NMR}$ of: a - chloroacetylated PHEMA (98.1 mol% of chloroacetate groups), b - adduct of PHEMA-1-naphthylacetic acid (98.1 mol% of 1-naphthylacetate groups)

The $^{13}\text{C-NMR}$ spectrum of mPHEMA (Fig. 2a) is characterized by chemical shifts at 41.6 and 167.7 ppm , which correspond to chloromethyl and carbonyl carbon atoms of chloroacetate groups, respectively.

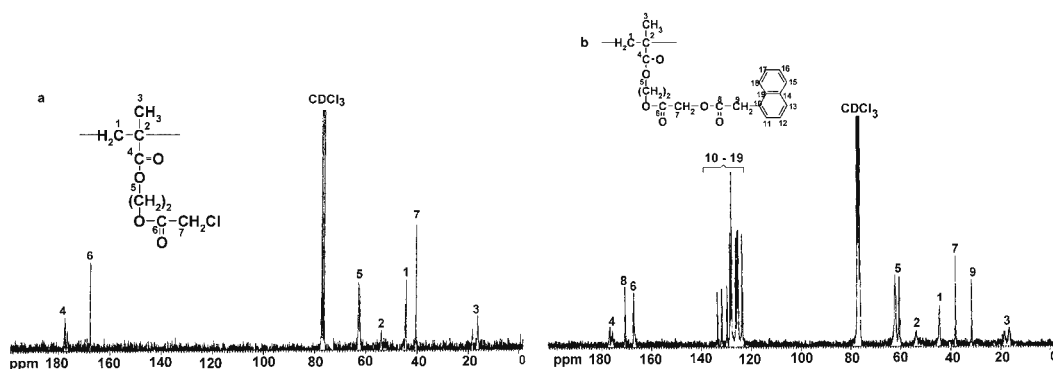


Fig. 2. Spectra $^{13}\text{C-NMR}$ of: a - chloroacetylated PHEMA (98.1 mol% of chloroacetate groups), b - adduct of PHEMA-1-naphthylacetic acid (98.1 mol% of 1-naphthylacetate groups)

The spectrum of the mPHEMA-1-NAA adduct (Fig. 2b) shows additional peaks between 121.5 and 135.0 ppm, which due to the resonance of carbon atoms in the naphthyl ring and the signals at 170.9 ppm can be assigned to the C₁₀H₇-CH₂-CO-groups.

All these spectroscopic results confirm the presence of chloroacetate and naphthylacetate groups in modified PHEMA.

Fig. 3 shows the release behavior of naphthylacetic acid (at 25 °C and pH=12.7) from three mPHEMA-1-NAA adducts, (containing naphthylacetate groups from 13.4 to 98.1 mol%). From the course of kinetic curves it follows that the release of the active compound is the quickest in the case of the adduct with the lowest content of naphthylacetate groups. This seems to be connected with interaction between the polymer and water. The decreased content of naphthylacetate groups makes the polymer more hydrophilic and consequently facilitates the penetration of hydroxyl ions to active sites in the tablet, effectively increasing the relative of hydrolysis.

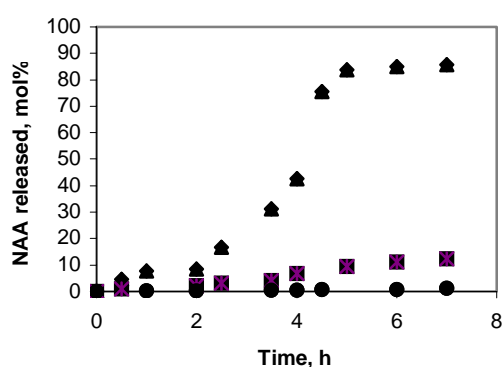


Fig. 3. The release of the bioactive compound (NAA) from mPHEMA-1-NAA adducts of 3 different composition (pH = 12.7 at 25 °C):

(▲) 13.4 mol% 1-naphthylacetate groups; (■) 80.5 mol% 1-naphthylacetate groups; (●) 98.1 mol% 1-naphthylacetate groups

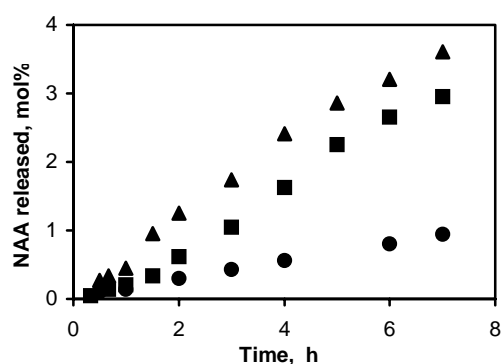


Fig. 4. The release of the bioactive compound (NAA) from mPHEMA-1-NAA adduct at 3 different pH value:

(●) pH = 12.7, (■) pH = 13.0 and (▲) pH = 13.7 (98.1 mol% 1-naphthylacetate groups, at 25 °C)

Fig. 4 shows a typical course of the heterogeneous hydrolysis of mPHEMA-1-NAA adduct (containing 98.1 mol% of naphthylacetate groups) in alkaline medium at 25 °C from pH=12.7 to 13.7. The presented results clearly indicate the increase in the release of bioactive carboxylic acid with the increase in the alkalinity of reaction medium. The hydrolysis rate of adduct is the lowest at pH = 12.7. This is consistent with the results obtained by Arranz *et al.* [7] for the poly(vinyl alcohol)-1-naphthylacetic acid adduct.

Reference

- [1] M. Senuma, T. Tashiro, M. Iwakura, *J. Appl. Polym. Sci.*, 37 (1989) 2837
- [2] E.R. Kenawy, D.C. Sherrington, A. Akelah, *Eur. Polym. J.*, 28 (1992) 841
- [3] E. H. Schacht, G. Desmaretz, E. Goethals, T. St. Piere, *Macromol.*, 16 (1983) 291
- [4] M. Sanchez-Chaves, F. Arranz, C. Diaz, *Macromol. Chem.*, 190 (1989) 2391
- [5] R. Jantas, H. Szocik, *Polymer Bulletin*, 48 (2002) 105
- [6] R. Jantas, B. Delczyk, *Fibres & Textiles in Eastern Europe*, 13 (2005) 60
- [7] F. Arranz, E. Bejarano, M. Sanchez-Chaves, *Makromol. Chem. Phys.* 195(1994) 3789
- [8] X. Liu, L. Gong, M. Xin, J. Liu, *J. Macromol. Catalysis A: Chemical*, 147 (1999) 37

DETERMINATION OF OIL CONTENT IN RAPESEEDS USING TWO METHODS – SOXHLET EXTRACTION AND PULSED NUCLEAR MAGNETIC RESONANCE SPECTROMETRY

Anna Januszewska, Ewa Maria Siedlecka, Piotr Glamowski,
Izabela Tomasiak

*University of Gdansk, Department of Environmental Engineering, Faculty of Chemistry,
ul. Sobieskiego 18, 80–952 Gdansk 6, Poland tel. (0 58) 53 25 437*

Introduction

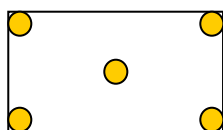
After cereals, oil crops are the second most important source of edible calories for human societies. They are also sources of many industrial products, and have the potential to provide raw materials for many more. The four major global traded oil crops are soybean, oil palm, rapeseed and sunflower, respectively. Together, these four crops account for 72% of worldwide vegetable-oil production [1]. Therefore an accurate and fast determination of oil content is important to breeders, growers and buyers.

The traditional method of oil determination in oilseeds is based on solvent extraction (Soxhlet). This method is laborious, time consuming and uses large volumes of organic solvents, moreover results depends on operator attention. Currently, the alternative techniques to solvent extraction are supercritical fluid extraction [2], NIR spectroscopy [3] and pulsed nuclear magnetic resonance spectrometry [4].

In this article the Soxhlet method was compared with the pulsed nuclear magnetic resonance spectrometry (pulsed NMR).

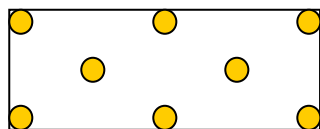
Materials and methods

Samples of rapeseeds were taken in accordance with current international methods of sampling described in ISO standards: PN-EN ISO 542:1997 [5] and PN-EN ISO 664:1997 [6]. In the first instance increment samples were taken from tracks. The number of sampling points, where the increment samples are taken, was defined according to lot size. The sampling points should have been uniformly distributed throughout the lot volume, according to the principles described in PN-EN ISO 542:1997 (Fig. 1) [5].



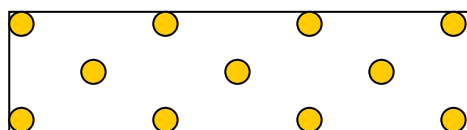
Lot size: > 15 tonnes

Number of incremental samples:
5 sampling points



Lot size: 15 – 30 tonnes

Number of incremental samples:
8 sampling points



Lot size: 30 – 50 tonnes

Number of incremental samples:
11 sampling points

Fig. 1. The number of sampling points [5].

The increment samples were combined and mixed thoroughly to form bulk samples, which were used to create laboratory samples. Part of laboratory samples were collected and combined together. The final analytical samples were selected from this mixture [6].

In this paper the analytical samples were marked 1, 2, 3, 4, 5, 6. The total oil content in rapeseeds was determined in the test samples (5 g), which were obtained from representative and homogenous analytical samples. Four test samples were taken from each analytical samples.

The rapeseeds used in the study were acquired from different growers in Poland.

Soxhlet extraction. The solvent extraction was conducted according to official methods PN-EN ISO 659:1999 [7] and PN-73/R-66164 [8] with petroleum ether (boiling point 40-60°C) as the extraction solvent. The oil was extracted from 5 g samples in Soxhlet apparatus. These samples were prepared by drying rapeseed at $103 \pm 2^\circ\text{C}$. The water contents in all seeds should have been less than 10 % (*m/m*). For each test sample it was necessary to carry out three extraction cycles (4 + 2 + 2 hours) to achieve complete oil recovery from seeds. The oil extraction was repeated for each test sample three times to ensure full oil recovery. After each extraction cycle seeds were grounded carefully in the mortar.

The oil percentage of the collected oil in the seeds was determined gravimetrically and expressed as a weight percent relative to initial weight of the raw oilseeds.

Pulsed nuclear magnetic resonance spectrometry. The total oil content was analyzed directly on Bruker minispec Pulsed NMR analyzer (operating at 10 MHz) in accordance with international standard PN-EN ISO 10565:1999 [9]. Five grams of rapeseed were used for each test. Oilseeds shouldn't have been cleaned and prepared in any way. The water contents of all seeds should have been less than 10 % (*m/m*).

The calibration prior to each series of measurements was checked using three verification samples of known oil contents [9].

Four analysis were carried out on test samples taken from the same homogenous analytical sample.

Statistical analysis. In this study standard deviation (S_R) was estimated by range (R) and coefficient k_n according to the following formula [10]:

$$S_R = k_n \cdot R$$

The range is the largest value minus the smallest value in a data set. This formula can be used when the number of determinations (n) is less than 7 [10].

All extraction and analyses were carried out four times. In this paper $k_n = 0,4857$ where $n = 4$ [10].

Results and Discussion

The oil content in rapeseed was determined using two methods Soxhlet extraction and pulsed NMR and results are listed in Table 1.

The NMR results are not comparable with Soxhlet solvent extraction data. The mean values of oil content determined by this method (~ 42,5 %) were lower then the the Soxhlet extraction (~ 45,7 %).

Table 1. Determination of oil content in rapeseed using two methods – Soxhlet extraction and pulsed nuclear magnetic resonance spectrometry.

Number of analytical samples	Soxhlet method				pulsed NMR method			
	C	C _M	SD _R	RDS	C	C _M	SD _R	RDS
1	45,69 46,21 46,18 46,09	46,04	0,25	0,54	35,90 39,40 41,00 50,00	41,60	6,90	16,60
2	45,66 46,07 46,06 46,03	45,95	0,19	0,41	48,80 43,00 35,90 38,00	41,50	5,20	12,50
3	44,59 44,59 44,60 44,59	44,59	0,01	0,02	31,10 52,60 40,20 50,20	43,50	10,40	23,90
4	45,80 45,78 45,79 45,80	45,79	0,01	0,02	39,40 40,00 37,00 35,40	38,00	2,30	6,00
5	46,69 45,88 45,90 46,08	46,13	0,39	0,85	48,00 44,90 49,30 45,40	46,90	2,10	4,40
6	45,20 46,00 45,01 45,70	45,47	0,48	0,01	42,30 50,10 44,30 37,60	43,70	6,10	13,90

C – the oil content in test samples, which were taken from the same homogenous analytical sample [% of dry mass],

C_M – mean value of the oil content in test samples [% of dry mass],

SD_R – Standard deviation [10],

RDS – Relative standard deviation [%].

The Soxhlet system is repeatable technique for determination of oil content in rapeseed. The values of standard deviation varied from 0,01 to 0,48. For comparison, SD and RSD values obtained for NMR analysis are higher and range between 2,10-10,40 and 4,40-23,90 %, respectively. The Soxhlet method has excellent precision with less than 1% relative standard deviation.

In the case of NMR, data distribution was very high and some statistical errors occurred.

The calibrate procedure cannot be ignored when using this methods. Pulsary NMR is difficult to calibrate. The calibration curve shall be obtained by measuring the signal from the three calibration samples with known oil content (Procedure A) [7] or the one standard of known oil content (Procedure B) [7]. In this study the working calibration curve was obtained according to Procedure A. The series of standards was prepared in a concentration range near to the expected unknown concetration (test sample). All samples were measured in the working range of calibration curve. The correlation coefficient for this linear regression is high (0,98). It means that the calibration model works properly. There could be other couses that could affect final results (sample presentation, water content, different nature of calibration standards then samples, slope of the curve).

In conclusion, the proposed pulsary NMR method is relatively simple, convenient, rapid and non-destructive, without sample preparation. This technique offers considerable savings of solvent disposal costs and analysis time (time of measurments is not more then 2 min.) also eliminates the exposure of laboratory staff to toxic and flammable solvents. The results in Table 1 suggest that the pulsed NMR tehniqe can be used for estimation of oil assay in rapeseed. The best results, in respect of precision are obtained using the conventional Soxhlet extraction. Therefore this method can be useful for the determination of oil content in rapeseed.

Acknowledgements

This study was supported by University of Gdansk (DS/8270-4-0093-6). The authors would like to thank Ms Izabela Tomasiak for her help with experimental work and Elstar Oils S.A. for giving us an opportunity to use NMR analyser.

References

- [1] Murphy D. J., TIBTECH, 14 (1996) 206
- [2] Taylor S. L., King J. W., List G. R., J. Am. Oil Chem. Soc, 70 (4) (1993) 437
- [3] Robertson J. R., Barton F.E. Ibid, 61(1984) 543
- [4] Gambhir P. N., Ararwala A. K., Ibid, 62 (1985) 103
- [5] PN-EN ISO 542:1997, Oilseeds – Sampling, PKN, Warsaw, 1997
- [6] PN-EN ISO 664:1997, Oilseeds – Reduction of laboratory sample to test sample, PKN, Warsaw 1997
- [7] PN-EN ISO 659:1999, Oilseeds – Determiation of oil content (Reference method), PKN, Warsaw 1999
- [8] PN-73/R-66164, Determiation of the oil contents in the oilseeds and oil seed extraction meals, PKN, Warsaw 1973
- [9] PN-EN ISO 10565:1999, Oilseeds – Simultaneous determiation of oil and water contents – Method using pulsed nuclear magnetic resonance spectrometry, PKN, Warsaw 1999
- [10] Eckschlager K., in: Errors in Chemical Analysis, PWN, Warsaw 1974, 138

APPLICATION OF ESI-MS AND FAB/LSIMS-MS IN THE ANALYSIS OF BIS-QUINOLIZIDINE ALKALOIDS

Beata Jasiewicz^{*}, Władysław Boczoń, Elżbieta Wyrzykiewicz
Faculty of Chemistry, A. Mickiewicz University, Grunwaldzka 6, 60-780 Poznań,

1. Introduction

The bis-quinolizidine alkaloids have interested chemists for several decades. Interesting examples of stereoisomeric effects on EI mass spectra of this important group of alkaloids can be found in the literature [1]. Recently growing interest in the study of this type of alkaloids by various mass spectrometric methods has been stimulated by the evidence of their suitability for distinction of stereoisomers, metamers and positional isomers [2-4]. As a continuation of our previous studies of EI-mass fragmentation of the derivatives of sparteine and lupanine [2-4] it seemed reasonable to extend our investigation to ESI and FAB/LSIMS mass spectra of these compounds. The purpose of this study was to investigate the ESI and FAB/LSIMS mass spectra of: 2-phenyl-2,3-didehydrosparteine (**1**), 15-phenyl-14,15-didehydrosparteine (**2**), 2-cyano-2-methylsparteine (**3**), 17-cyanolupanine (**4**), 17-methylsparteine (**5**), 2,17-dimethylsparteine (**6**) and 2-methyl-17-oxosparteine (**7**) (see Figure 1). We wished to determine the cleavage reactions in the processes of the mass fragmentation in the ESI and FAB/LSIMS conditions of **1-7** and to establish whether it would be possible to distinguish the positional isomers (**1**, **2**; **5**, **7**) and metamers (**3**, **4**; **5**, **6**, **7**) on the basis of differences in the values of μ ; μ defined as the ratio of the intensity of the selected fragment ion peak to that of the parent ion peak.

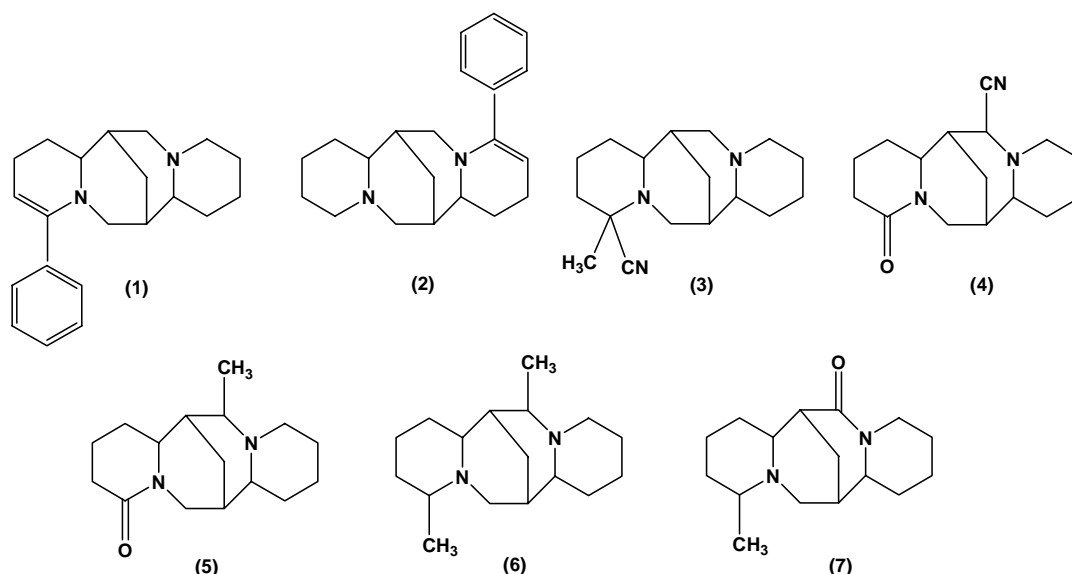


Figure 1

^{*} Corresponding autor: Tel.: +48-61-829-1354; fax: +48-61-865-8008. E-mail address: beatakoz@amu.edu.pl (B. Jasiewicz)

The investigated derivatives of sparteine (**1-3**, **6**) and lupanine (**4**) have A/B trans fused rings with double chair conformations and C/D trans fused rings with boat/chair conformations. In contrast 17-methyllypanine (**5**) has A/B trans fused rings with sofa/chair conformations, as well as 2-methyl-17-oxosparteine (**7**) has A/B trans fused rings with double chair conformations and C/D trans fused rings with sofa/chair conformations.

2. Experimental

The compounds **1-7** were obtained and their structures confirmed according to the literature methods [5-11].

The ESI mass spectra were recorded on a Waters-micromass Manchester UK/ZQ mass spectrometer equipped with a Harvard Apparatus syringe pump. The sample solutions were prepared in methanol. The ESI source potentials were 3kV and cone voltage 30V. The source and desolvation temperatures were 120° and 300°, respectively. Nitrogen was used as neutralizing and desolvation gas. The FAB spectra were produced by LSIMS ionization (Cs⁺ ion bombardment) using 3-nitrobenzyl alcohol (NBA) as ligand matrix. These spectra were recorded on an AMD-Intectra GmbH-Harpstedt D-27243 Model 402 two-sector spectrometer.

3. Results and conclusions

We found that the compounds **1-4** and **7** gave strong positive-ion ESI mass spectra but in the positive-ion mass spectra of **5** and **6** only M+H⁺ (**A**) even-electron fragment ions were observed (Table 1). In the processes of ESI mass fragmentation of M+H⁺ ions of **1** and **2** simple cleavages of Csp³-Csp³ bonds of ring B (for **1**) and ring A (for **2**) gave even-electron B⁺ ions [i.e. (C₁₂H₂₅N+H)⁺ - 1 and (C₁₇H₁₈N₂+H) ± 2]. In the cases of the ESI fragmentation of M+H⁺ ions of **3** and **4** the eliminations of HCN neutral molecules have been observed (ions **B**: C₁₆H₂₆N₂+H⁺ for **3** and C₁₅H₂₂N₂O+H⁺ for **4**, respectively). The cleavages of Csp³-Csp³ bonds of ring B gave C₇H₁₃N+H⁺ even-electron fragment ion **C** (for **3**), as well as the cleavages of Csp³-Csp³ and Csp²-N bonds of ring C gave C₉H₉NO+H⁺ **C** ion for **4**. In the case of ESI mass fragmentation of M+H⁺ ion of **7**, the elimination of neutral molecule of CH₂ has been observed (ion **B**: C₁₅H₂₄N₂O+H⁺). These differences in the mass fragmentations, as well as relative abundances of the ions (Table 1) may be sufficient to differentiate among the isomeric derivatives of sparteines and lupanines (**1-2**; **3-4**; **5-7**, respectively).

The FAB-LSIMS spectra of **1-7** produced in the positive mode by LSIMS ionization (Cs⁺ ions bombardment) show strong fragmentation (Table 2). The relative abundances of M+NBA⁺ (ion **A**), M+H⁺ (**B** even-electron ions), as well as **C**⁺ ions which have been obtained by the cleavages of Csp³-Csp³ bonds of ring B (**1**, **2**) or eliminations of •CN (**3**, **4**) or •CH₃ and •H radicals (**5**, **6**, **7**) clearly differ between the sets of isomers (**1-2**; **3-4**; **5-7**, respectively). The same differences are seen in the cases of ions **D**⁺ of **1**, **2** and **5-7**. These ions have been obtained by the cleavages of Csp³-Csp³ bonds of ring B (**1**, **7**) ring A (**2**) and ring C (**5**, **6**). Generally speaking the main fragment ions compositions correspond to those formed under ESI-MS and EI-MS conditions [2-4].

These ions which have been seen in the positive-ion ESI and positive-ion FAB/LSIMS mass spectra of **1-7** may be useful in the mass fragmentography.

Table 1. Relative abundances of characteristic ion peaks in the positive-ion ESI mass spectra of **1-7**.

Compound	M+H ⁺ (A) Elemental composition m/z (%)	(B) Elemental composition m/z (%)	(C) Elemental composition m/z (%)
1	C ₂₁ H ₂₈ N ₂ +H ⁺ 309 (100)	C ₁₂ H ₁₅ N+H ⁺ 174 (39)	-
2	C ₂₁ H ₂₈ N ₂ +H ⁺ 309 (100)	C ₁₇ H ₁₈ N ₂ +H ⁺ 251 (5)	-
3	C ₁₇ H ₂₇ N ₃ +H ⁺ 274 (100)	C ₁₆ H ₂₆ N ₂ +H ⁺ 247 (99)	C ₇ H ₁₃ N+H ⁺ 112 (20)
4	C ₁₆ H ₂₃ N ₃ O+H ⁺ 274 (0)	C ₁₅ H ₂₂ N ₂ O+H ⁺ 247 (100)	C ₉ H ₁₀ NO+H ⁺ 148 (71)
5	C ₁₆ H ₂₆ N ₂ O+H ⁺ 263 (100)	-	-
6	C ₁₇ H ₃₀ N ₂ +H ⁺ 263 (100)	-	-
7	C ₁₆ H ₂₆ N ₂ O+H ⁺ 263 (57)	C ₁₅ H ₂₄ N ₂ O+H ⁺ 249 (100)	-

Table 2. Relative abundances of characteristic ion peaks in the positive-ion FAB/LSIMS mass spectra of **1-7**.

Compound	M+NBA ⁺ (A) Elemental composition m/z (%)	M+H ⁺ (B) Elemental composition m/z (%)	(C) Elemental composition m/z (%)	(D) Elemental composition m/z (%)	(E) Elemental composition m/z (%)
1	C ₂₁ H ₂₈ N ₂ +C ₇ H ₇ NO ₃ ⁺ 461 (10)	C ₂₁ H ₂₈ N ₂ +H ⁺ 309 (30)	C ₉ H ₁₄ N+C ₇ H ₇ NO ₃ ⁺ 289 (13)	C ₁₂ H ₁₅ N+H ⁺ 174 (8)	C ₇ H ₇ NO ₃ +H ⁺ 154 (100)
2	C ₂₁ H ₂₈ N ₂ +C ₇ H ₇ NO ₃ ⁺ 461 (4)	C ₂₁ H ₂₈ N ₂ +H ⁺ 309 (6)	C ₉ H ₁₄ N+C ₇ H ₇ NO ₃ ⁺ 289 (12)	C ₁₂ H ₁₉ N ₂ +H ⁺ 192 (68)	C ₇ H ₇ NO ₃ +H ⁺ 154 (100)
3	-	C ₁₇ H ₂₇ N ₃ +H ⁺ 274 (100)	C ₁₆ H ₂₆ N ₂ +H ⁺ 247 (28)	-	C ₇ H ₇ NO ₃ +H ⁺ 154 (7)
4	-	C ₁₆ H ₂₃ N ₃ O+H ⁺ 274 (18)	C ₁₅ H ₂₂ N ₂ O+H ⁺ 247 (100)	-	C ₇ H ₇ NO ₃ +H ⁺ 154 (32)
5	-	C ₁₆ H ₂₆ N ₂ O+H ⁺ 263 (100)	C ₁₅ H ₂₂ N ₂ O+H ⁺ 247 (15)	C ₇ H ₁₃ N+H ⁺ 112 (10)	C ₇ H ₇ NO ₃ +H ⁺ 154 (10)
6	-	C ₁₇ H ₃₀ N ₂ +H ⁺ 263 (100)	C ₁₆ H ₂₆ N ₂ +H ⁺ 247 (5)	C ₇ H ₁₃ N+H ⁺ 112 (36)	C ₇ H ₇ NO ₃ +H ⁺ 154 (5)
7	-	C ₁₆ H ₂₆ N ₂ O+H ⁺ 263 (73)	C ₁₅ H ₂₂ N ₂ O+H ⁺ 247 (38)	C ₇ H ₁₃ N+H ⁺ 112 (47)	C ₇ H ₇ NO ₃ +H ⁺ 154 (24)

References

- [1] J. Tamas, in: *Applications of Mass Spectrometry to Organic Stereochemistry*, J. S. Splitter, F. Turecek (ed), VCH New York, 1994, 626
- [2] E. Wyrzykiewicz, W. Boczoń, B. Koziół, *J. Mass. Spectrom.*, 33 (1998) 971
- [3] E. Wyrzykiewicz, W. Boczoń, B. Koziół, *J. Mass. Spectrom.*, 35 (2000) 1271
- [4] B. Jasiewicz, W. Boczoń, E. Wyrzykiewicz, *J. Mass. Spectrom.*, 39 (2004) 541
- [5] W. Boczoń, *J. Mol. Struct.*, 158 (1987) 127
- [6] W. Boczoń, *Bull. Pol. Acad. Sci. Chem.*, 36 (1988) 37
- [7] W. Boczoń, *Bull. Pol. Acad. Sci. Chem.*, 36 (1988) 45
- [8] J. Skolik, Wł. Stopa, *Zesz. Nauk. WSE, Ser. I. Zeszyt 46* (1972) 193
- [9] M. Wiewiórowski, G. Pieczonka, J. Skolik, *J. Mol. Struct.*, 40 (1977) 233
- [10] W. Boczoń, B. Jasiewicz, *Collect. Czech. Chem. Commun.*, 68 (2003) 696
- [11] B. Jasiewicz, W. Boczoń, *J. Mol. Struct.*, (2006) In press

APPLICATION OF SPECTROSCOPIC METHOD TO INVESTIGATION OF α -ISOSPARTEINE COMPLEXES WITH Zn(II) AND Cu(II) ACETATE SALTS

Beata Jasiewicz^{*}, Katarzyna Walczak, Władysław Boczoń
Faculty of Chemistry, A. Mickiewicz University, Grunwaldzka 6, 60-780 Poznań,
Poland

1. Introduction

Lupine alkaloids, also called quinolizidines, constitute a large class of naturally occurring compounds widely distributed among various plant families, such as the *Leguminosae*. Some of these structures have been attracting growing attention as chiral chelating bases [1-5], as can be seen by the broad use of the tetracyclic (-)-sparteine in asymmetric reactions [6-10]. Another chiral bidentate ligand, which can be used in stereoselective synthesis is an α -isosparteine (see Figure 1).

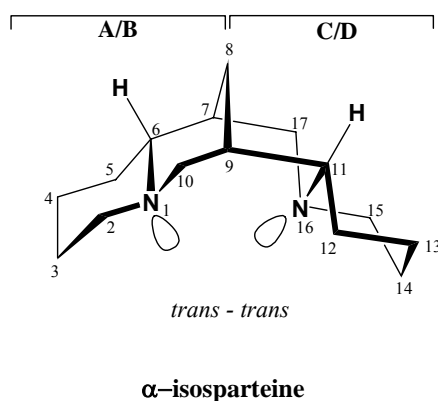


Figure 1. Conformation and atom numbering in α -isosparteine.

It is well known that Zn(II) complexes of sparteine are used as a diluting agents for measuring the hyperfine coupling by EPR on powdered samples whereas Cu(II) sparteine complexes are used as model compounds for the type I copper(II) site of blue copper protein. Over the past decades, several studies on copper(II) complexes of this alkaloid have been reported [11-14] and the copper(II) centers in these complexes are always found to have a distorted tetrahedral geometry. Owing to our interest in the zinc and copper sparteine and α -isosparteine complexes, we have undertaken the research project aimed at characterising the spectral and analytical properties of α -isosparteine complexes with zinc and copper(II) acetate salts. The complexes have been characterised by NMR, UV-Vis, IR and mass spectroscopy and also by elemental analysis.

^{*} Corresponding autor: Tel.: +48-61-829-1354; fax: +48-61-865-8008. E-mail address: beatakoz@amu.edu.pl (B. Jasiewicz)

2. Experimental

2.1. General techniques

The ^{13}C NMR, ^1H NMR, ^1H - ^1H COSY, ^1H - ^{13}C COSY spectra were measured on a Varian Gemini 300 spectrometer at 300 MHz and at ambient temperature, using ~0.5 M solutions in CDCl_3 , TMS as internal reference. The IR spectra were recorded by means of a FT-IR Bruker 113v spectrometer (KBr pellets). Electronic spectra were measured on a JASCO V-550 spectrophotometer, in methanol solution. ESI mass spectra were obtained on a Waters/Micromass (Manchester, UK) ZQ mass spectrometer. The sample solutions were prepared in methanol. Elemental analysis was carried out by means of a Perkin-Elmer 2400 CHN automatic device. α -Isosparteine was obtained according to method described previously [15].

2.2 Synthesis of complexes

The complexes were prepared by the direct reaction of metal(II) acetates with a stoichiometric amount of an alkaloid in a methanol solution. The resulting precipitate was filtered off and recrystallized from methanol.

2.2.1. $[\text{Zn}(\text{CH}_3\text{COO})_2(\alpha\text{-isosparteine})]$ (1)

Yield: 64%. Mp >250 °C (with decomposition). Anal. Calcd. for $\text{C}_{19}\text{H}_{32}\text{N}_2\text{ZnO}_4$: C, 54.68; H, 7.67; N, 6.71. Found: C, 54.73; H, 7.56; N, 6.65. MS (ESI-mass) $m/z = 359$ $[\text{Zn}(\text{C}_{15}\text{H}_{26}\text{N}_2)(\text{CH}_3\text{COO}) + \text{H}]^+$, 300 $[\text{Zn}(\text{C}_{15}\text{H}_{26}\text{N}_2) + \text{H}]^+$, 235 $(\text{C}_{15}\text{H}_{26}\text{N}_2\text{H}) + \text{H}]^+$.

2.2.2. $[\text{Cu}(\text{CH}_3\text{COO})_2(\alpha\text{-isosparteine})]$ (2)

Yield: 60%. Mp 190 °C. Anal. Calcd. for $\text{C}_{19}\text{H}_{32}\text{N}_2\text{CuO}_4$: C, 54.81; H, 7.69; N, 6.74. Found: C, 54.53; H, 7.79; N, 6.70. MS (ESI-mass) $m/z = 358$ $[\text{Cu}(\text{C}_{15}\text{H}_{26}\text{N}_2)(\text{CH}_3\text{COO}) + \text{H}]^+$, 299 $[\text{Cu}(\text{C}_{15}\text{H}_{26}\text{N}_2) + \text{H}]^+$, 235 $(\text{C}_{15}\text{H}_{26}\text{N}_2\text{H}) + \text{H}]^+$.

3. Results and discussion

Newly obtained complexes exhibit the 1:1 stoichiometry as shown by the results of elemental analysis. This is in agreement with fact that conformation of the rings in α -isosparteine is rigid, the same in the free base and in mono- and disalts, namely *trans-trans* all- chair.

The IR absorption in the spectra of quinolizidine and its derivatives in the 2840-2600 cm^{-1} region (the so-called Bohlmann *trans-band*) is assigned to the stretching vibrations of one or more axially oriented $\text{C}_\alpha\text{-H}$ bonds. The intensity and shape of the band depend on the number of the above bands and their steric environment in the molecule. In the band complex covering the range 2840-2600 cm^{-1} in the spectrum of α -isosparteine there are three peaks at 2793, 2758 and 2735 cm^{-1} [16]. The attachment of a metal atom to N atoms results in the disappearance of the *trans-band*. The absence of this band in the spectra of the complexes suggests that both of the nitrogen atoms are involved in coordination. The spectra of both complexes show additional bands: at 1590-1630 cm^{-1} $\nu(\text{C}=\text{O})$. The metal-nitrogen stretching oscillations are observed at about 430-470 cm^{-1} .

In the electronic absorption spectra studied in methanol α -isosparteine display a single intense transitions UV region with the maximum at about 200 nm. The UV-vis

spectrum of **2** shows band ligand-to-metal charge transfer transitions at 305 nm ($\epsilon = 2743$), and the characteristic band of d-d transitions at 675 nm ($\epsilon = 144$).

Complexation of α -isosparteine with zinc(II) and copper(II) acetate gives symmetric complexes. As a consequence, in ^{13}C -NMR spectrum of **1**, only 8 signals are observed. The chemical shifts of the carbon atoms of complex **1** are similar to those reported for α -isosparteine (see Table 1). Additional signals assigned to the $-\text{CH}_3$ and the carbonyl groups are observed at 17.7 and 177.0 ppm, respectively. The position of a bridge carbon signal C-8 is diagnostic of the conformation of the two fused B/C rings in the sparteine skeleton. The theoretical value (35.4 ppm) [17] is in agreement with the value obtained for α -isosparteine and its complex with zinc acetate salt (36.4 and 36.9 ppm, respectively). On the basis of a comparison of the NMR spectra of the complex studied and the free base it was possible to calculate the complexation effect. The complexation-induced ^{13}C shifts are highly dependent on the orientation of nitrogen lone-electron pairs and on the conformation of the intervening carbon skeleton. Therefore, a study of this effects appears to be most relevant in the case of α -isosparteine because the complexation does not change the conformation of the free base.

Table 1. ^{13}C NMR chemical shifts of α -isosparteine and its complex with $\text{Zn}(\text{CH}_3\text{COO})_2$ in CDCl_3 ; δ in ppm

Carbon atom	α - Isosparteine (δ'_c)	α - Isosparteine x $\text{Zn}(\text{CH}_3\text{COO})_2$ (δ_c)	Complexation effect ($\delta_c - \delta'_c$)
2	57.2	59.2	+ 2,0
3	25.3	24.0	- 1.3
4	24.9	23.8	- 1.1
5	30.0	28.2	- 1.8
6	66.3	69.8	+ 3.5
7	35.6	34.9	- 0.7
8	36.4	36.9	+ 0.5
9	35.6	34.9	- 0.7
10	55.8	57.2	+ 1.4
11	66.3	69.8	+ 3.5
12	30.0	28.2	- 1.8
13	24.9	23.8	- 1.1
14	25.3	24.0	- 1.3
15	57.2	59.2	+ 2.0
17	55.8	57.2	+ 1.4
$-\text{COO}^-$	-	177.0	-
$-\text{CH}_3^-$	-	17.7	-

4. Conclusions

New complexes with α -isosparteine, prepared by the reaction of alkaloid with zinc(II) and Cu(II) acetate salts were characterized by IR, UV-Vis and MS methods. The structures of α -isosparteine complexes indicate that α -isosparteine remains structurally unchanged upon complexation. It acts as a symmetrical bidentate chiral ligand with a privileged binding site for tetrahedral coordination and a tendency to

utilize its two-fold symmetry in the crystal. It binds metal centers strongly and predictably.

References

- [1] Y-M Lee, Y-K Kim, H-Ch Jung, Y-I Kim and S-N Choi, *Bull. Korean Chem. Soc.*, 23 (2002) 404
- [2] C. Strohmann, T. Seibel, K. Strohfeldt, *Angew. Chem. Int. Ed.*, 42 (2003) 4531
- [3] C. Strohmann, K. Strohfeldt, D. Schildbach, *J. Am. Chem. Soc.*, 125 (2003) 13672
- [4] J. L. Alcántra-Flores, D. Ramirez-Rosales, S. Bernes, J. Guadalupe, P. Ramirez, A. Duran-Hernandez, R. Gutierrez Perez, R. Zamorano-Ulloa, Y. Reyes-Ortega, *J. Mol. Struct.*, 693 (2004) 125
- [5] B-J Kim, Y-M Lee, E. H. Kim, S. K. Kang and S-N Choi, *Acta Cryst.*, C58 (2002) m361
- [6] F. Marr, R. Fröhlich, D. Hoppe, *Tetrahedron Asymm.*, 13 (2002) 2587
- [7] J. A. Wilkinson, S. B. Rossington, J. Leonard, N. Hussein, *Tetrahedron Lett.*, 45 (2004) 1191
- [8] L. Liu, *Synthesis*, 11 (2003) 1705
- [9] D. M Hodgson, I. D. Cameron, M. Christlieb, R. Green, TG. P. Lee, L. A. Robinson, *J. Chem. Soc., Perkin Trans.*, 1 (2001) 2161
- [10] J. G. Peters, M. Seppi, R. Fröhlich, B. Wibbeling, D. Hoppe, *Synthesis*, 3 (2002) 381
- [11] E. Boschmann, L. M. Weinstock, M. Carmack, *Inorg. Chem.*, 13 (1974) 1297
- [12] S. Lopez, I. Muravyov, S. R. Pulley, S. W. Keller, *Acta Cryst.*, C54 (1998) 355
- [13] Y.-M. Lee, G. Chung, M.-A. Kwon, S.-N. Choi, *Acta Cryst.*, C56 (2000) 67
- [14] S. K. Kang, Y-M Lee, Y-I Kim, Y. Kim, K. Seff, S-N Choi, *Inorg. Chim. Acta*, 357 (2004) 2602
- [15] N. J. Leonard, P. D. Thomas, P. D. Gash, *J. Amer. Chem. Soc.*, 77 (1955) 1552
- [16] J. Skolik, P. J. Krueger, M. Wiewiórowski, *Tetrahedron*, 24 (1968) 5439
- [17] V. Galasso, F. Asaro, F. Berti, B. Kovač, I. Habuš, A. Sacchetti, *Chem. Phys.*, 294 (2003) 155

INFLUENCE OF CHEMICAL STRUCTURE ON PROPERTIES OF CROSS-LINKED POLY(ESTER URETHANE)S

Lidia Jasińska, Adolf Balas, Józef T. Haponiuk
Gdańsk University of Technology
Chemical Faculty, Department of Polymer Technology
80-952 Gdańsk, G. Narutowicza 11/12 Str.

In the last time one could observe new trends in the research concerning synthesis and properties of unsaturated polymers. The presence of double bonds, which come from oligomers [1-3] or low molecular weight chain extenders [4,5] allows to obtain cross-linked polymers using radical technique.

Synthesis of unsaturated polyurethanes allows for improving of physico-chemical properties in comparison to cross-linked polyesters. The use of unsaturated substrates [6-12] in the synthesis of polyurethanes allows for obtaining chemical and thermal stability polymers.

In the present paper results of recent studies on synthesis and physical-chemical properties of oligo(alkyleneester)diols (OAE) and cross-linked poly(ester urethane)s (PEU) are presented. The synthesis of these polymers was conducted in two steps. In the first one prepolymers were obtained via reaction of OAE with 4,4'-diphenylmethane diisocyanate (MDI). After that prepolymers were cross-linked with styrene (St) or methyl methacrylate (MMA) of concentrations of 30wt% in the presence of 1 wt% of methyl ethyl peroxide and 0.003 wt% of cobalt (II) 2-ethylhexanoate.

The unsaturated oligo(alkyleneester)diol was synthesized by polycondensation of ethylene glycol (2.4 mol) with adipic acid (1 mol), phthalic anhydride (0.5mol), and maleic anhydride (0.5 mol). The reaction was carried out under nitrogen atmosphere at the temperature of 190°C. Oligo(alkyleneester)diol was characterized by elemental analysis (Tab. 1).

Tab.1. C, H, O contents in oligo(alkyleneester)diol revealed in elemental analysis.

Elemental analysis						
	C ^a	H ^a	O ^a	C ^b	H ^b	O ^b
OAE	[%]			[%]		
	55,42	5,92	38,16	55,42	5,88	38,69

^a found value, ^b calculated value

The results confirmed the glycol addition to double bonds of OAE and therefore creation of non-linear products. Moreover, the presence of functional groups in OAE was confirmed by the FT-IR spectra analysis (Fig. 1).

The presence of the absorption bands at 1730cm⁻¹ and 1141cm⁻¹, which are characteristic for -C=O and -C-O groups, indicate on the existence of esters groups in the structure of OAE. Furthermore, the absorption bands at 1644 cm⁻¹ and 969 cm⁻¹, corresponding to stretching vibrations of C=C and C=C-C-H groups, affirm that the phthalic and fumaric acids are present in the structure of OAE.

Moreover, the absorption band at 3535cm^{-1} shows that oligo(alkyleneester)diols contain the OH end-groups. This fact was also confirmed by measurements of the acid number of OAE.

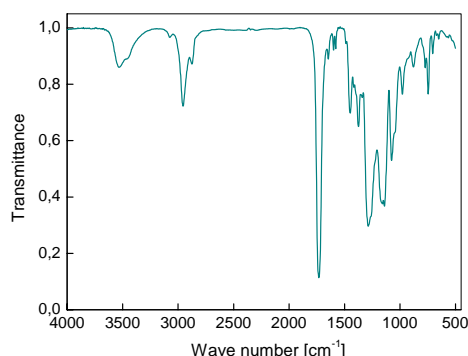


Fig. 1. FT-IR spectrum of oligo(alkyleneester)diol.

Oligo(alkyleneester)diol and 4,4'-diphenylmethane diisocyanate (MDI) were used as substrates in the syntheses of urethane prepolymers (NPU) and poly(ester urethane)s (PEU). Then the prepolymers synthesized with the [NCO/OH] molar ratio 2/1, 1.5/1, 1.2/1, 1/1 and 1/1.5 were used in the synthesis of the following poly(ester urethane)s: PEU[NCO/OH]2/1, PEU[NCO/OH]1.5/1, PEU[NCO/OH]1.2/1, PEU[NCO/OH]1/1, PEU[NCO/OH]1/1.5, respectively. Subsequently, the obtained poly(ester urethane)s were dissolved in styrene or methyl methacrylate used as a cross-linking monomers of concentrations of 30 wt%.

In order to confirm the chemical structure of poly(ester urethane)s we used the Fourier transform infrared spectroscopy (FTIR). The results are presented in Figure 2. The peak located at 3348cm^{-1} , characteristic for $-\text{NH}$ absorption bands, indicates on the presence of the urethane groups. Moreover, the existence of the ester groups were affirmed by the bands at about 1720 , 1145 and 1070cm^{-1} , which are characterized for the $\text{C}=\text{O}$ and $\text{C}-\text{O}-\text{C}$ groups, respectively. The absorption bands at 1640cm^{-1} and 980cm^{-1} ($\nu\text{C}=\text{C}$ and $\gamma\text{C}=\text{C}-\text{H}$) gives information about the presence of double bonds in cross-linked poly(ester urethane)s. This fact suggests that not all double bonds of PEU were involved in the cross-linking reaction with styrene or methyl methacrylate.

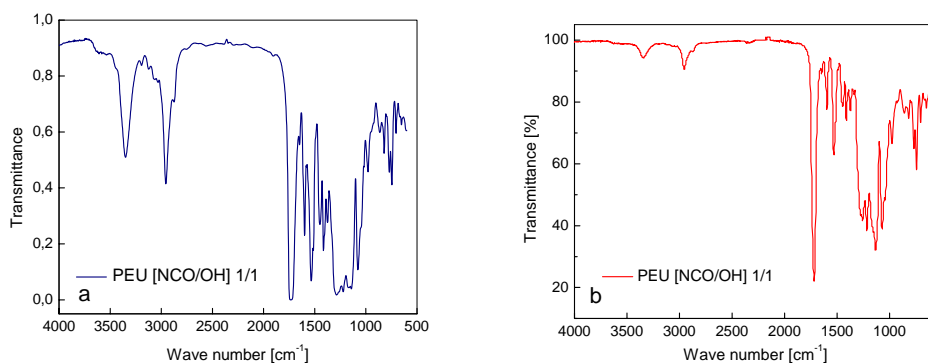


Fig. 2. FT-IR spectra of PEU[NCO/OH]1/1 cross-linked by styrene (a) and methyl methacrylate (b).

The studies of the stress-strain properties of PEU presented in Fig. 3, show that tensile strength of cross-linked poly(ester urethane)s strongly depends on their chemical structure as well as the type of cross-linking agent (Fig. 3a, b). Poly(ester urethane)s synthesized from prepolymers with [NCO] groups molar excess and cross-linked by styrene (PEU/St) have higher tensile strength than their analogues obtained from prepolymers with [OH] groups molar excess and polymers cross-linked by methyl methacrylate. Indeed, Fig. 3 shows that the tensile strength of PEU/St changes from 50 to nearly 75 MPa whereas tensile strength of PEU/MMA change from 10 to 30 MPa. This fact can be explained by the presence of cross-linking allophanate groups and higher cross-linking density of polymers synthesized using styrene as cross-linking agent.

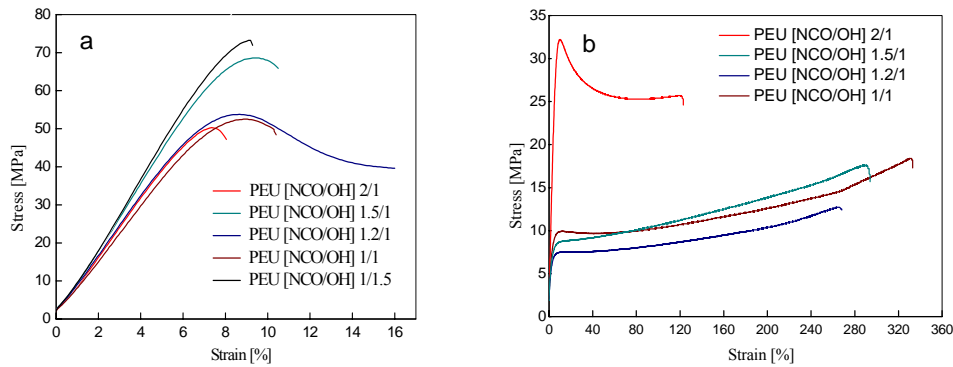


Fig.3. Stress-strain curves of the PEUs cross-linked by styrene (a) and PEU cross-linked by methyl methacrylate (b).

Dynamic mechanical thermal analysis (DMTA) proved the dependence of the chemical structure of poly(ester urethane)s on their dynamic storage moduli (G'), loss moduli (G''), and loss tangents ($\tan\delta$). The plots of G'' vs. temperature show clear of two phase behaviour (Fig. 4). The maxima present on the curves may appear because of the presence of pendant polystyrene side chains in cross-linked PEU. The glass transition temperatures (T_g), defined as maxima of $\tan\delta(T)$ curve, were found at: 46°C, 65°C, 56°C, 57°C, and 60°C for PEU [NCO/OH] 2/1, PEU [NCO/OH] 1.5/1, PEU [NCO/OH] 1.2/1, PEU [NCO/OH] 1/1, and PEU [NCO/OH] 1/1.5, respectively.

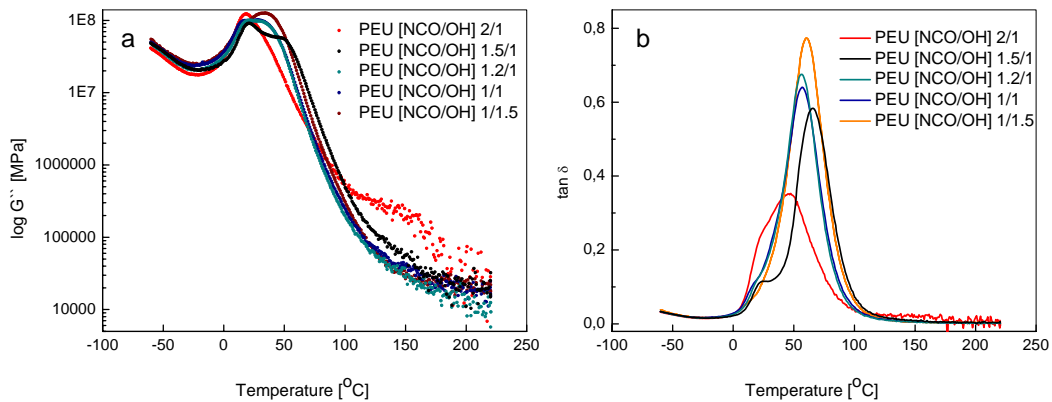


Fig. 4. Variations of the dynamic loss modulus (G'') (a) and the loss tangent ($\tan\delta$) (b) with temperature for PEUs cross-linked by styrene.

Dynamic mechanical thermal analysis of poly(ester urethane)s cross-linked by methyl methacrylate indicates, as in the case of PEU cross-linked by styrene, on the dependence of dynamic-mechanical properties on their chemical structure. The absence of the second maximum on Fig. 5a, indicate on the polymers do not undergo phase separation. Furthermore, the glass transition temperatures of PEU cross-linked by methyl methacrylate were found at: 38°C, 30°C, 56°C, and 32°C for PEU [NCO/OH] 2/1, PEU [NCO/OH] 1.5/1, PEU [NCO/OH] 1.2/1, and PEU [NCO/OH] 1/1, respectively.

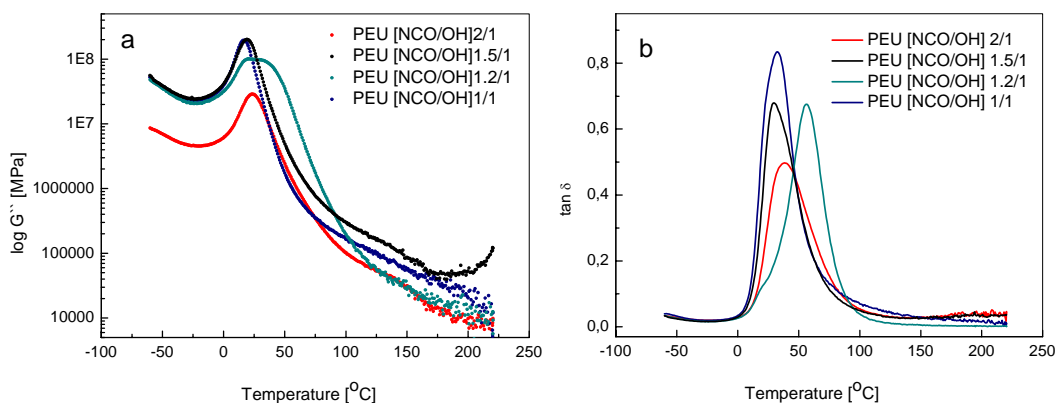


Fig. 5. Variations of the dynamic loss modulus (G'') (a) and the loss tangent ($\tan \delta$) (b) with temperature for PEUs cross-linked by methyl methacrylate.

Conclusions

The mechanical and dynamic-mechanical properties of new cross-linked poly(ester urethane)s have been investigated. The obtained results show the dependence of the mentioned properties on their chemical structure and a kind of cross-linking agent. One can observe that poly(ester urethane)s cross-linked by styrene have higher tensile strength than their analogues obtained using methyl methacrylate as a cross-linking monomer. Moreover DMTA analysis shows very clearly that the maxima on the $G''(T)$ and $\tan \delta(T)$ curves of PEU are strongly chemical composition dependent.

References

- [1] M. X. Xu, W. G. Liu, *Die Angewandte Makromolekulare Chemie*, 240 (1996) 163.
- [2] J. Zhang, M. O. W. Richardson, *Polymer*, 41 (2000) 6843.
- [3] B. Gawdzik, T. Matynia, J. Osypiuk, *J. Appl. Polym. Sci.*, 79 (2001) 1201.
- [4] A. Balas, G. Pałka, B. Płomińska, M. Rutkowska, *Acta Polym.*, 31 (1980) 673.
- [5] S. H. O. Egboh, *J. Macromol. Sci-Chem.*, A19 (1983) 1041.
- [6] A. Szelest – Lewandowska, B. Masiulanis, A. Klocke, B. Glasmacher, *J. Biomat. Appl.*, 17 (2003) 221.
- [7] S. Oprea, S. Vlad, A. Stanciu, *Polymer*, 42 (2001) 7257.
- [8] S. Oprea, S. Vlad, A. Stanciu, C. Ciobanu, M. Macoveanu, *Europ. Polym. J.*, 35 (1999) 1269.
- [9] S. Oprea, S. Vlad, A. Stanciu, *Europ. Polym. J.*, 36 (2000) 2409.
- [10] S. Oprea, *Polym. Degrad. And Stab.*, 75 (2002) 9.
- [11] J. Ledru, B. J. M. Youssef, Saiter, J. Grenet, *J. Therm. Anal. Cal.*, 68 (2002) 767.
- [12] T. Yilmaz, O. Ozarslan, E. Yildiz, A. Kuyulu, E. Ekinci, A. Gungor, *J. Appl. Polym. Sci.*, 69 (1998) 1837.

SYNTHESIS AND CHARACTERISATION OF NEW CHIRAL CALIX[4]ARENE-BONDED SILICA GEL STATIONARY PHASE FOR HIGH PERFORMANCE LIQUID CHROMATOGRAPHY.

Katarzyna Jaszczolt, Magdalena Śliwka-Kaszyńska, Janusz Rachoń

Department of Organic Chemistry, Gdansk University of Technology,

Narutowicza 11/12, 80-952 Gdańsk, Poland,

e-mail: kasiajaszczolt@wp.pl

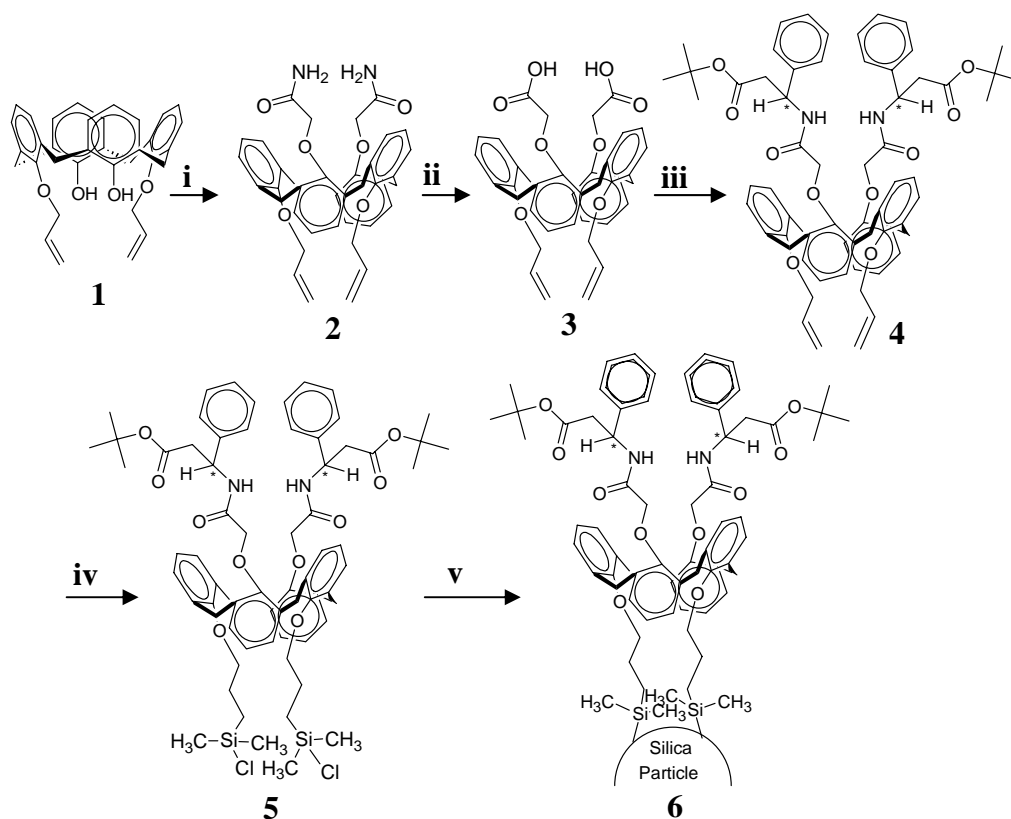
INTRODUCTION

Calixarenes are macrocyclic compounds obtained in the base-induced condensation reaction of *para* substituted phenols and formaldehyde. They possess ability to form reversible host-guest complexes with ions as well as neutral species [1]. A parent tetrahydroxycalix[4]arene does not have chiral recognition ability. However, chirality can be introduced by appropriate chemical modification. There are two different approaches to produce chiral calixarenes. The first one is an attachment of independent chiral substituents at the upper or lower rim of calixarene molecule [2-4]. The second approach is synthesis of 'inherently' chiral calixarenes, built up of nonchiral subunits but chiral on account of non-planar nature of the calixarene structure [5]. Two synthetic pathways have been used for synthesis of inherently chiral calixarenes: a) fragment condensation leading to asymmetric calixarenes build up of three or four different phenol units or b) regio- and stereoselective functionalization of calixarene structure at the lower rim. In 1998 Healy et al. [6] reported synthesis of a new type of chiral silica-bonded calix[4]arene stationary phase in a cone conformation by functionalization of the lower rim of triethoxysilyl-calix[4]arene with L-(-)-ephedrine units. Enantiomeric separation of R(-) and S(+)-1-phenyl-2,2,2-trifluoroethanol on this phase was reported. In 2004 [7] Krawinkler and coworkers synthesized two novel cinchona-calixarene hybrid type receptors by interlinking 9-amino(9-deoxy)-quinine or 9-amino(9-deoxy)-epiquinine and calix[4]arene via urea functional units. They immobilized this receptors onto silica gel to obtain chiral stationary phases, which revealed chiral recognition ability for N-protected amino acids. Both mentioned stationary phases have been blocked in *cone* conformation. Our research group prepared a new chiral stationary phase on the basis of calixarene in *1,3-alternate* conformation.

RESULTS AND DISCUSSION

The silica gel-linked chiral calix[4]arene was synthesized according to the scheme 1. Tetrahydroxycalix[4]arene, used as the starting material for further modifications, was prepared by the modified literature procedures [8, 9]. The synthetic strategy of a novel chiral calix[4]arene-silica-bonded stationary phase involved functionalization of the calix[4]arene structure at the lower rim via the formation of an amide bond between the calixarene **3** and the optically active β -L-(+)-phenylalanine t-butyl ester. To prepare diacid of calix[4]arene **3** we decided to hydrolyze the diamide, because the yields of synthesis of diesters are low (25%) and the isolation of the product is complicated [10]. Therefore we synthesized 25,27-diallyloxy-26,28-diacetamidoxycalix[4]arene **2** in *1,3-alternate* conformation. This compound was obtained in reaction of 25,27-diallyloxy-

26,28-dihydroxycalix[4]arene **1** with iodoacetamide in the presence of catalytic amount of potassium iodide and cesium carbonate as a base. ^1H NMR and ^{13}C NMR analyses confirmed the presence of **2** in *1,3-alternate* conformation (singlet at δ 37.74 ppm for ArCH_2Ar carbons on the ^{13}C NMR spectrum and two doublets at δ 3.84 and 3.72 ppm, $J=15.62$ Hz at the ^1H NMR spectrum). The allylic units were introduced to enable chemical bonding of the calixarene moieties to the silica gel. Product **3** was hydrolyzed with KOH in EtOH/ H_2O in the presence of catalytic amount of H_2O_2 to diacid of the calix[4]arene **3** which was transformed into the activated ester derivative in the reaction with dicyclohexylcarbodiimide (DCC) and N-hydroxysuccinimide (NHS) in dry CHCl_3 and then without isolation of the product (reaction was controlled by TLC) allowed to react with optically active β -L-(+)-phenylalanine t-butyl ester to give chiral calix[4]arene **4** with high yield. The presence of two singlets at δ 36.26 and 36.91 ppm for ArCH_2Ar groups at the ^{13}C NMR spectra and double doublets at δ 3.63 and 3.60 ppm ($J_1=1.95$ Hz, $J_2=14.16$ Hz) for $\text{OCH}_2\text{C}(\text{O})\text{NH}$ at the ^1H NMR spectra evidenced *1,3-alternate* conformation and the optical activity of the product **4**. Rotatory power $[\alpha]_{\text{D}}^{25} = -18.6^\circ$ ($c=0.8$, CHCl_3).



Scheme 1. Synthesis of chiral calix[4]arene stationary phase: **i**) $\text{ICH}_2\text{C}(\text{O})\text{NH}_2$, Cs_2CO_3 , CH_3CN dry, 72h, RT; **ii**) KOH, H_2O_2 cat., $\text{MeOH}/\text{H}_2\text{O}$ (3:2); reflux 24h; **iii**) DCC, NHS, $\text{HCl}\cdot\text{H}_2\text{NCH}(\text{Ph})\text{CH}_2\text{COOC}(\text{CH}_3)_3$, $(i\text{Pr})_2\text{NEt}$, CHCl_3 dry, 24h, RT; **iv**) $(\text{CH}_3)_2\text{SiHCl}$, H_2PtCl_6 , $i\text{PrOH}$, CH_2Cl_2 , reflux 4h; **v**) SiO_2 , dry toluene, Pyridine cat., shaking 5 days, RT.

Hydrosilylation of **4** with chlorodimethylsilane was performed to create calix[4]arene **5**. The hexachloroplatinic acid was used as the catalyst. The crude product was obtained after evaporation of excess of CH₂Cl₂ and chlorodimethylsilane. Analysis of ¹H NMR spectrum of crude product confirmed the complete addition of the silane to the double bond (absence of vinylic protons). Product **5** was chemically bonded to the surface of silica gel Lichrosorb Si-100 (5 μm), which was activated before the reaction by heating for 4 hours with 2 N hydrochloric acid to remove metal ions and maximize the number of silanol groups on the surface and then dried overnight at 150⁰C. The reaction was performed in dry toluene. The solution of crude product **5** and catalytic amount of dry pyridine was added to suspension of silica gel and the mixture was shaken at room temperature for 5 days under nitrogen atmosphere. After that time the modified gel was filtered and washed with toluene, iPrOH, MeOH, CH₂Cl₂, acetone and diethyl ether, respectively. Surface coverage of modified silica calculated from elemental analysis was found to be 275 μmol/g. This relatively low coverage density was probably a consequence of large size of calixarene structure. Chromatographic performance of novel chiral calix[4]arene phase is in progress

EXPERIMENTAL

¹H NMR and ¹³C NMR spectra were recorded on Gemini 500 MHz spectrometer (Varian). Elemental analysis was obtained on analyzer Perkin-Elmer (PE 240). Optical activity was measured on Rudolph Research Autopol II polarimeter. Melting points were determined with an electrothermal melting point apparatus. Reactions were monitored by TLC on pre-coated silica gel plates (SiO₂, Merck, 60F₂₅₄). Flash column chromatography was performed on silica gel 60 (SiO₂, Merck, 230-400 mesh).

2 *1,3-Alternate* (42%), mp=234-235⁰C, 500 MHz ¹H NMR (CDCl₃): δ 7.10 (d, 4H, J=7.3 Hz, ArH); 7.04 (d, 4H, J=7.3 Hz, ArH); 6.86 (t, 2H, J=7.3 Hz, ArH); 6.80 (t, 2H, J=7.3 Hz, ArH); 5.85 (br s, 2H, NH₂); 5.77-5.69 (m, 2H, CH₂CH=CH₂); 5.07 (d, 2H, J=10.7 Hz, CH₂CH=CH₂); 4.87 (d, 2H, J=17.5 Hz, CH₂CH=CH₂); 4.16 (d, 4H, OCH₂CH=CH₂, J=3.9 Hz); 3.87 (br s, 4H, OCH₂C(O)NH₂); 3.84 (d, 4H, ArCH₂Ar, J=15.6 Hz); 3.72 (d, 4H, ArCH₂Ar, J=15.6 Hz). 500 MHz ¹³C NMR (CDCl₃): δ 37.74 (s, ArCH₂Ar, *1,3-alternate*); 172.06 (C=O); 156.50; 153.59; 135.01; 133.62; 133.26; 131.52; 130.21; 123.78; 123.38; 116.42; 71.04; 68.91. Expected and observed fourteen signals.

3 *1,3-Alternate* (81%), mp=230-233⁰C (MeOH), 500 MHz ¹H NMR (CDCl₃): δ 7.07-7.04 (m, 8H, ArH); 6.93 (t, 2H, ArH, J=7.3 Hz); 6.87 (t, 2H, ArH, J=7.3 Hz); 5.66-5.60 (m, 2H, OCH₂CH=CH₂); 4.97 (d, 2H, J=10.2 Hz, OCH₂CH=CH₂); 4.77 (d, 2H, J=17.1 Hz, OCH₂CH=CH₂); 4.13 (s, 4H, OCH₂CH=CH₂); 4.06 (s, 4H, OCH₂COOH); 3.89 (d, 4H, ArCH₂Ar, J=15.8 Hz); 3.75 (d, 4H, ArCH₂Ar, J=15.8 Hz). 500 MHz ¹³C NMR (CDCl₃): δ 37.78 (s, ArCH₂Ar, *1,3-alternate*); 169.08 (s, C=O); 156.30; 153.17; 134.44; 133.70; 133.10; 131.09; 129.75; 124.52; 124.49; 116.27; 70.96; 67.47. Expected and observed fourteen signals.

4 *1,3-Alternate* (86%), mp=123-125⁰C, 500 MHz ¹H NMR (CDCl₃): δ 7.37-7.36 (m, 8H, ArH); 7.31-7.26 (m, 4H, ArH); 7.02 (d, 4H, J=7.3 Hz, ArH); 6.91 (d, 2H, J=7.3 Hz, ArH); 6.81 (d, 2H, J=7.3 Hz, ArH); 6.70 (t, 2H, J=7.3 Hz, ArH); 6.55 (t, 2H, J=7.3 Hz, ArH); 6.02-5.95 (m, 2H, CH₂=CHCH₂O); 5.27 (dd, 2H, J=1.5 Hz, J=10.7 Hz, CH₂=CHCH₂O); 5.22 (dd, 2H, J=1.5 Hz, J=17.1 Hz, CH₂=CHCH₂O); 4.85 (q, 2H,

J=7.8 Hz, C*H); 4.28 (d, 4H, CH₂=CHCH₂O, J=4.4 Hz); 3.61 (dd, 4H, J= 1.9 Hz, J=14.2 Hz, OCH₂C(O)NH); 3.49 (dd, 4H, 4H-CH*CH₂O, J=8.3 Hz, J=14.2 Hz); 3.35-3.29 (m, 8H, ArCH₂Ar); 1.48 (s, 18H, C(CH₃)₃); 500 MHz ¹³C NMR (CDCl₃): δ 36.26 and 36.91 (2s, ArCH₂Ar, *1,3-alternate*); 169.04 (s, C=O); 170.83 (s, C=O); 156.65; 153.84; 137.70; 134.77; 134.64; 133.78; 133.30; 133.27; 132.51; 132.48; 130.89; 130.71; 129.54; 128.69; 127.06; 123.44; 122.64; 116.74; 81.95; 72.35; 70.82; 54.12; 28.28. Expected and observed twenty seven signals. $[\alpha]_D^{25} = -18.6^0$ (c=0.8, CHCl₃).

5 ¹H NMR spectrum of the crude product of hydrosilation addition reaction did not contain signals descended from vinylic protons.

6 Elemental analysis found C 16.5, H 2.6, N 0.7. Estimated coverage density 275 μmol/g.

CONCLUSIONS.

In this study the synthesis of new chiral calix[4]arene silica-bonded stationary phase has been demonstrated. We have designed this new material for application in enantioselective high performance liquid chromatography. The retention power of the column and its selectivity will be examined under reversed phase conditions with the use of various chromatographic conditions and racemic mixtures as analytes.

Acknowledgements

The authors gratefully acknowledge financial support for this work from the State Committee for Scientific Research (KBN 3 T09 A, Project No. 13829).

REFERENCES

- [1] Z. Asfari, V. Böhmer, J. Harrowfield, J. Vicens (Eds.), Calixarenes 2001, Kluwer Academic Publishers, Dordrecht, 2001
- [2] K. Iwamoto, K. Araki, S. Shinkai, J. Org. Chem., 113 (1991) 2385
- [3] C. D. Gutsche, K. C. Nam, J. Am. Chem. Soc., 110 (1988) 6153;
- [4] R. J. Muthukrishnan, C. D. Gutsche, J. Org. Chem., 44 (1979) 3962
- [5] G. Ferguson, J. F. Gallagher, L. Giunta, P. Neri, S. Pappalardo, M. Parisi, J. Org. Chem. 59 (1994) 42
- [6] L. O. Healy, M. M. McEnery, D. G. McCarthy, S. J. Harris, J. D. Glennon, Analytical Letters, 31, 9 (1998) 1543
- [7] K. H. Krawinkler, N. M. Maier, E. Sajovic, W. Lindner, J. Chromatogr. A, 1055, 1 (2004) 119
- [8] C. D. Gutsche, M. Iqbal, D. Stewart, J. Org. Chem., 51 (1986) 742
- [9] C. D. Gutsche, J. A. Levine, J. Am. Chem. Soc. 104, (1982) 2657
- [10] M. Pitarch, J. K. Browne, M. McKervey, Tetrahedron, 30 (1997) 10503

SYNTHESIS AND CYTOSTATIC ACTIVITY STUDIES OF 5'-DIFLUOROMETHYLPHOSPHONATES OF 3'-AZIDO-3'-DEOXYTHYMIDINE (AZT)

Lech Celewicz^{1*}, Agnieszka Jóźwiak¹, Krzysztof Ciszewski¹, Małgorzata Pietkiewicz¹,
Piotr Ruszkowski² and Bogusław Hładon²

¹*Adam Mickiewicz University, Faculty of Chemistry, Grunwaldzka 6,
60-780 Poznań, Poland*

²*Karol Marcinkowski University of Medical Sciences, Department of Pharmacology,
Rokietnicka 5a, 60-806 Poznań, Poland*

Introduction

Some nucleoside analogues have an important role as anticancer and antiviral therapeutics [1,2]. For example, 3'-azido-3'-deoxythymidine (AZT) has been developed as an anti-HIV drug for treatment of acquired immunodeficiency syndrome (AIDS) [2]. In addition, there are some examples of application of AZT as an antineoplastic agent in combination with either cisplatin, methotrexate or 5-fluorouracil in the therapy of advanced colon cancer [3]. Recently, Wagner and coworkers reported on the potent growth inhibitory activity of AZT on cultured human breast cancer cells [4]. It is assumed that the mechanism of anticancer action of AZT involves its intracellular conversion to 5'-triphosphate (via mono- and diphosphate), which function as competitive inhibitor of DNA polymerases and chain terminator of growing DNA strand [3]. Consequently, the development of AZT prodrugs (pronucleotides) which can easily penetrate the lipid-rich cell membranes and then can undergo hydrolysis to 5'-monophosphates or their analogues has become an area of increasing interest [5,6].

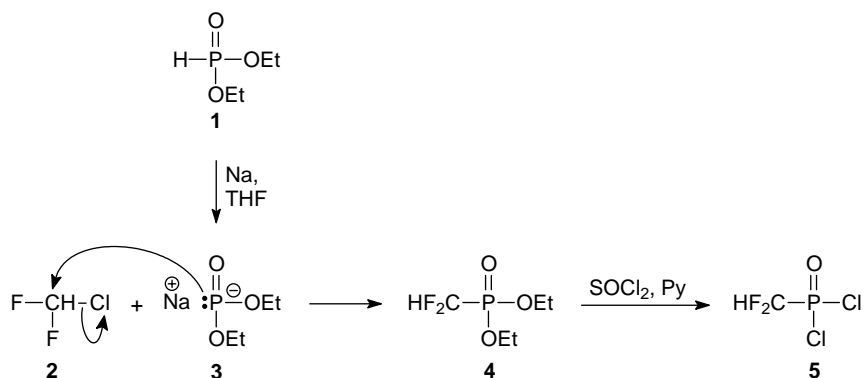
It is known that incorporation of fluorine in drug molecules often increases therapeutic efficacy [7]. Introduction of fluorine into organic compounds dramatically changes their properties mainly due to the strong electron-withdrawing inductive effect of fluorine. Carbon-fluorine bonds substantially increase the lipophilicity of molecules, thereby enhancing the rate of transport of drugs across cell membranes. It is interesting to note that difluoromethyl group closely resembles a hydroxyl group in polarity [8].

In this paper we report the method of the synthesis of 5'-difluoromethylphosphonates of 3'-azido-3'-deoxythymidine (AZT) (**9-13**) and their cytostatic activity.

Results and Discussion

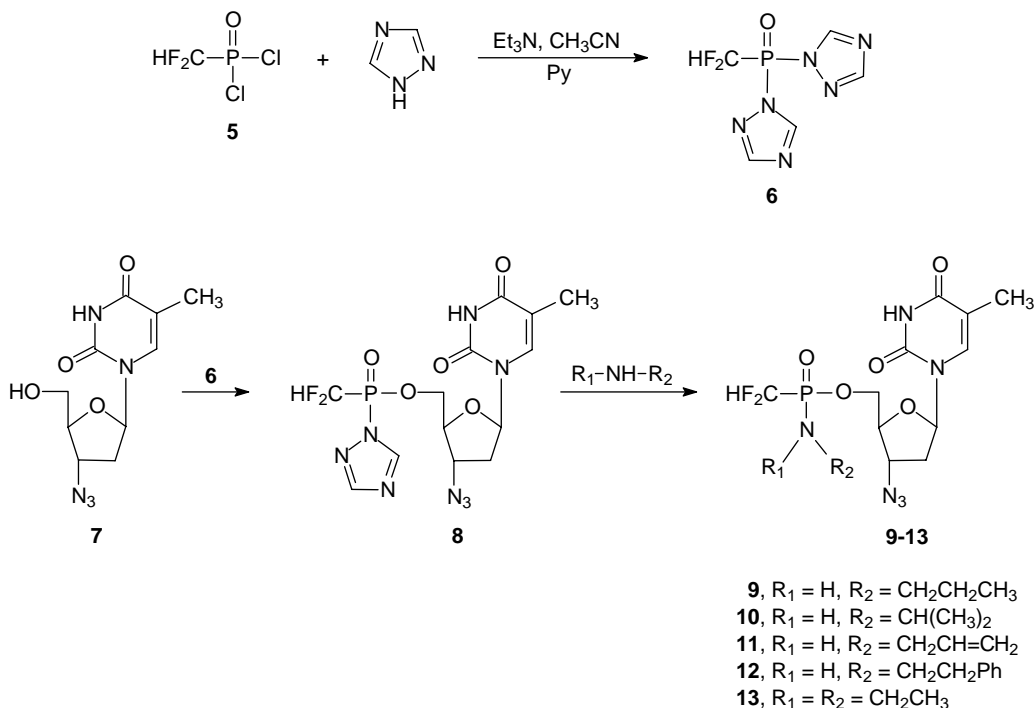
A series of novel phosphoramidates **9-13** was synthesized by phosphorylation of 3'-azido-3'-deoxythymidine (**7**) with difluoromethylphosphonic ditriazolide (**6**) according to the procedure outlined in Scheme 2. 2- and 4-chlorophenyl phosphoroditriazolides were used as phosphorylating agents of 5'-protected nucleosides in the phosphotriester synthesis of oligonucleosides and provided an example for development of our method [9-11]. Difluoromethylphosphonic ditriazolide (**6**) was prepared by the reaction of difluoromethylphosphonic dichloride (**5**) with 1,2,4-triazole in the presence of triethylamine (Scheme 2). Synthesis of difluoromethylphosphonic dichloride (**5**) was achieved by the reaction of diethyl phosphite (**1**) first with metallic

sodium to generate diethyl phosphite sodium salt (**3**) which was then reacted with chlorodifluoromethane (**2**) to give diethyl difluoromethylphosphonate (**4**). Compound **4** was subsequently treated with thionyl chloride to yield desired **5** (Scheme 1) [8]. Reaction of **6** with 3'-azido-3'-deoxythymidine (**7**) in the presence of pyridine afforded reactive intermediate **8**, which was reacted *in situ* with the appropriate amine to give products **9-13** in 65-80% yield. When difluoromethylphosphonic dichloride (**5**) was used as the phosphonylating agent of 3'-azido-3'-deoxythymidine **7** considerable amounts of symmetrical (5'-5')dinucleoside phosphonates were formed.



Scheme 1

The identity of products **9-13** was established on the basis of spectroscopic data (^1H , ^{19}F , ^{13}C , ^{31}P NMR and MS).



Scheme 2

The *in vitro* cytotoxic activity of the phosphoramidates **9-13** was studied in human KB (*nasopharynx carcinoma*) tumor tissue culture (Table 1) [12]. All of investigated compounds showed some activity. The most active compound in the series was N,N-diethyl(difluoromethyl)phosphoramidate of AZT (**13**). The other compounds in the series exhibited moderate activity. The findings indicate that the nature of N-alkyl substituent of phosphoramidates plays an important role as a determinant of their cytotoxic activity.

Table 1. Cytotoxic activity of phosphoramidates **9-13** against KB human cancer cells

Compound	ED ₅₀ ^a	
	µg/ml	µmol/l
9 , R ₁ = H, R ₂ = CH ₂ CH ₂ CH ₃	14.6	34.6
10 , R ₁ = H, R ₂ = CH(CH ₃) ₂	13.7	32.4
11 , R ₁ = H, R ₂ = CH ₂ CH=CH ₂	23	54.7
12 , R ₁ = H, R ₂ = CH ₂ CH ₂ Ph	8.2	16.9
13 , R ₁ = R ₂ = CH ₂ CH ₃	2.2	5.0
Cytosine arabinoside (standard)	0.99	3.5

^aED₅₀ is the concentration of a compound inhibiting by 50% protein biosynthesis in the cell population.

Experimental Section

¹H, ¹⁹F, ¹³C, and ³¹P NMR spectra were recorded on a Varian-Gemini 300 MHz spectrometer. Chemical shifts (δ) are reported in ppm relative to the tetramethylsilane (TMS) peak. Mass spectra were measured on a Waters Micromass ZQ electrospray (ES) mass spectrometer. Thin layer chromatography (TLC) was performed on silica gel 60 F₂₅₄ precoated (0.2 mm) plates and column chromatography on silica gel 60 H (5-40 µm) purchased from Merck. Chemical reagents were purchased from Aldrich. 3'-Azido-3'-deoxythymidine was prepared based on the literature procedure [13] with some our modifications.

General procedure for the synthesis of difluoromethylphosphoramidates **9-13**

To a solution of difluoromethylphosphonic dichloride (0.1 ml, 0.914 mmol) in acetonitrile (1.8 ml) was added 1,2,4-triazole (165 mg, 2.38 mmol) followed by triethylamine (0.260 ml, 190 mg, 1.86 mmol) and the reactants were stirred for 25 min. Then to the mixture 3'-azido-3'-deoxythymidine (0.1 mg, 0.37 mmol) and pyridine (2.3 ml) were added. The reaction mixture was stirred at room temperature for 1.5 h and appropriate amine (4.57 mmol) was added. After 3 h, the reaction mixture was evaporated under reduced pressure. To the residue was added saturated aqueous sodium bicarbonate (15 ml) and the mixture was extracted with chloroform (3 x 7 ml). The combined chloroform extracts were washed with water, dried with anhydrous magnesium sulfate and evaporated to dryness. The residue was purified by silica gel column chromatography using chloroform – methanol (50 : 1 v/v) as eluent to give pure products **9-13**.

Representative spectral data

Compound **10**:

¹H-NMR (CDCl₃) δ: 1.22, 1.23 (d, 6H, J = 5.5 Hz, N-C(CH₃)₂), 1.91, 1.92 (d, 3H, J = 1.1 Hz, 5-CH₃), 2.40 (m, 2H, H-2'', H-2'), 3.48 (m, 2H, H-3', N-CH-(C)₂), 4.05 (m, 1H, H-4'), 4.36 (m, 3H, H-5'', H-5', NH-C-(C)₂), 5.83, 5.99 (dd, 1H, J_{HF} = 30.0 Hz, J_{HP} = 12.0 Hz, CHF₂), 6.12, 6.25 (t, 1H, J = 7.0 Hz, H-1'), 7.24, 7.34 (d, 1H, J = 1.2 Hz, H-6), 9.85 (s, 1H, OC-NH-CO).

¹³C-NMR (CDCl₃) δ: 12.28, 25.68, 25.74, 25.77, 25.83, 37.06, 37.12, 44.17, 44.24, 60.30, 60.38, 63.52, 63.60, 64.15, 64.24, 82.03, 82.10, 84.85, 85.68, 107.71, 110.22, 110.28, 111.09, 111.46, 111.77, 113.66, 114.58, 117.08, 117.14, 135.05, 135.65, 150.16, 150.25, 163.55, 163.66.

¹⁹F-NMR (CDCl₃) δ: -136.75, -135.52 (ddd, 1F, J_{HF} = 30.0 Hz, J_{PF} = 85.0 Hz, J_{FF} = 346.4 Hz, F'), -134.44, -133.22 (ddd, 1F, J_{HF} = 30.0 Hz, J_{PF} = 85.0 Hz, J_{FF} = 346.4 Hz, F'').

³¹P-NMR (CDCl₃) δ: 10.88, 11.60 (dd, 1P, J_{HP} = 12.0 Hz, J_{PF} = 85.0 Hz).

MS-ES m/z (M-H⁻) 421.

Acknowledgments

Research support from Ministry of Science and Higher Education (Grant *No 1 T09A 014 30*) is gratefully acknowledged.

References

1. L. L. Brunton, J. S. Lazo and K. L. Parker (Editors), Goodman & Gilman's The Pharmacological Basis of Therapeutics, McGraw-Hill, New York 2005
2. E. De Clercq, J. Clin. Virol., 30 (2004) 115
3. J. W. Darnowski and F. A. Goulette, Biochem. Pharmacol., 48 (1994) 1797
4. C. R. Wagner, G. Ballato, A. O. Akanni, E. J. McIntee, R. S. Larson, S. L. Chang and Y. J. Abulhajj, Cancer Res., 57 (1997) 2341
5. C. R. Wagner, V. V. Iyer and E. J. McIntee, Med. Res. Rev., 20 (2000) 417
6. S. Peyrottes, G. Coussot, I. Lefebvre, J.-L. Imbach, G. Gosselin, A.-M. Aubertin and C. Perigaud, J. Med. Chem., 46 (2003) 782
7. J. Mann, Chem. Soc. Rev., 16 (1987) 381
8. D. E. Bergstrom and P. W. Shum, J. Org. Chem., 53 (1988) 3953
9. J. Stawinski, T. Hozumi, S. A. Narang, C. P. Bahl and R. Wu, Nucleic Acids Res., 4 (1977) 353
10. K. L. Agarwal and F. Riftina, Nucleic Acids Res., 5 (1978) 2809
11. J. B. Chattopadhyaya and C. B. Reese, Tetrahedron Lett., (1979) 5059
12. B. Hładoń, T. Gośliński, H. Laskowska, D. Baranowski, T. Ostrowski, J. Zeidler, P. Ruszkowski and B. Golankiewicz, Pol. J. Pharmacol., 54 (2002) 45
13. S. Czernecki and J. M. Valery, Synthesis, 239 (1990)

MOBILITY AND BIOAVAILABILITY OF MANGANESE IN INDUSTRIAL ASH AND SOIL

Jan Kalembkiewicz, Elżbieta Sitarz-Palczak

Department of Inorganic and Analytical Chemistry, Faculty of Chemistry

Rzeszów University of Technology

Al. Powstańców Warszawy 6, 35-959 Rzeszów, Poland

ABSTRACT

In this work the chemical forms of Mn in ash and soil were investigated by the method of sequential extraction, properly according to BCR scheme for ash and Tessier scheme for soil.

It was stated, that the used sequential extraction methods characterize respectively: 98.9% total content of Mn in ash and 99.4% total content of Mn in soil.

The determination of manganese in the different extraction solutions has been made by flame atomic absorption spectrometry (FAAS). This work describes a study of the amount of manganese extracted at each stage in a sequential leaching scheme from coal fly ash and soil samples. The interdependencies among the chemical forms of Mn in ash and soil were defined from point of view of the chemical speciation of this element. The quantitative estimation of mobility and bioavailability of the chemical forms of Mn were determined in the examined objects.

Keywords: manganese, sequential extraction, FAAS, fly ash, soil.

1. INTRODUCTION

The levels of heavy metals circulating in the environment have seriously increased during the last few decades due to human activity.

Manganese is an essential trace element known to be related particularly to reproductive function. Its deficiency could lead to negative symptoms such as skeletal abnormalities, brain damage, teratogenicity and abnormal metabolism of carbohydrates and lipids [1].

The behaviour of the elements in the environment (e.g., bioavailability, toxicity and distribution) cannot be reliably predicted on the basis of their total concentration [2,3].

Chemical speciation can be defined as the process of determining and identifying specific chemical species or binding forms; it allows to know the availability and mobility of the metals in order to understand their chemical behaviour and fate; so useful environmental guidelines for potential toxic hazards can be developed [4].

The basic chemical forms of trace metals contained in the environmental samples can be described by using sequential extraction method [5]. The BCR procedure (proposed in 1993 by the European Community's Bureau of References – now Standards, Measurements and Testing Program) [6] and the method proposed by Tessier et al. [7] are most often used for this purpose.

2. EXPERIMENTAL

2.1. Apparatus

A Perkin-Elmer Model 3100 air/acetylene flame atomic absorption spectrometer (Perkin-Elmer Instruments, Shelton, CT USA) was used for the analysis of Mn in the extraction solutions (wavelength of 279.5 nm and fuel flow rate of 0.8 – 1.0 dm³·min⁻¹).

A centrifuge tube - test Model WE 1 (Precision Engineering, Poland) was used for the centrifugation of the soil extracts at 3000 rpm.

A universal shaker Model Vibramax 100 (Heidolph Instruments, Germany) and a hot plate Model HP 88720-26 (Barnstead/Thermolyne, USA) were used for the extraction. The pH of extraction solutions was determined with a pH meter Model CPI-551 (Elmetron, Poland).

2.2. Reagents

All reagents were from POCH, Gliwice, Poland of analytical grade or higher purity. Standard manganese solutions were prepared from standard solutions for atomic absorption (manganese concentration $1.000 \mu\text{g}\cdot\text{cm}^{-3}$ in 1 % of HNO_3 , Aldrich).

2.3. Samples

Coal fly ash samples were collected from the electrostatic precipitator from power-plant Rzeszów S.A (Rzeszów, Poland). The 0.5 kg sample was prepared from overall air-dried 10 kg sample by “quarterning” method - according to procedure BN-81/0623-01 [8]. Next the air-dried ash was sieved initially through a laboratory sieve of 1 mm diameter, and then milled in agate mortar to fine powder ($\varphi \leq 100 \mu\text{m}$) – according to PN-77/G-04528/00 [9].

The soil samples (depth: 0-15 cm) were collected from the area of the University of Technology, Rzeszów, Poland. After sieving through a stainless-steel sieve, with mesh apertures of 2 cm diameter, to remove stones and plant debris as well as to homogenize the bulk soil, a 10-kg amount was air-dried in open racks in the laboratory conditions for two weeks. The 0.5 kg sample was prepared from overall air-dried 10 kg sample by “quarterning” method - according to Namieśnik et al. [5]. The dried soil was sieved again through a steel sieve with mesh apertures of 1 mm, milled in agate mortar to fine powder ($\varphi \leq 100 \mu\text{m}$).

1g of sample was dried at 105°C to constant weight in order to obtain the amount of manganese per g of dry sample in reported values.

The collected soil samples characteristics: the low carbonates and sulphur content account for the slightly alkaline character.

2.4. Total manganese determination

The total content of Mn in fly ash samples after total mineralization with mixture of 8 cm^3 65 % HNO_3 , 4 cm^3 40 % HF, 2 cm^3 37 % HCl and 10 cm^3 H_2O was described in the work [10]. The total content of Mn in soil samples after total mineralization with concentrated acids HF and HClO_4 was described in reference [11]. The concentration of Mn in solutions after mineralization were determined by FAAS method in the conditions described in the earlier work [12].

2.5. Sequential extraction procedures

The four-step protocol proposed by the Measurements and Testing Programme, modified and described in the work [10], was followed for the sequential extraction of Mn from fly ash. The five-step protocol proposed by Tessier et al., described in the work [11], was followed for the sequential extraction of Mn from soil samples. After extraction sample solutions were first centrifuged at 3000 rpm for 15 min and filtered through a filter paper for quantitative analysis MN 616 (Macherey-Nagel GmbH & Co. KG, Germany). The supernatant was used for analysis of Mn by the FAAS method in the conditions described in the work [12]. Remains of ash were washed with 10 cm^3 of double-distilled water and this second supernatant was discarded. Blank samples were prepared according to the proposed procedures and concentrations of the extracts were corrected by the corresponding blank solutions.

3. RESULT AND DISCUSSION

The sequential extraction of Mn from fly ash according to four-stepped BCR method gave the four fraction of manganese: F(I) –acid soluble, F(II) – reducible, F(III) – oxidizable, F(IV) – „residual". The scheme of Tessier et al. thus uses five - steps, suitable fractions of manganese in soil were described as: F(I) exchangeable; F(II) carbonate; F(III) Fe/Mn oxides; F(IV) organic; and F(V) residual.

In Table 1, the distribution of manganese in the four fractions for the fly ash samples and in the five fractions for the soil samples are represented. The contents of manganese associated with acid soluble sample fraction, exchangeable and carbonate represented the availability of this metal, susceptible to pH or ionic composition changes in the environment. Manganese associated with reducible and oxidizable fraction can be released under redox reactions. Soil has a higher content of this metal in fractions F(III) than coal fly ash, since an important proportion of main soil constituents can be altered by redox changes and the associated Mn can be released. On the other hand, coal fly ash samples are generated by an aggressive process like combustion; therefore are low contents of reducible fraction and a lower content of Mn in those fractions. Finally, concentrations of manganese in the residual fractions are considerable for the two kinds of samples. The metal is strongly bound to minerals and resistant components, and does not represent environmental risks. In the examined objects the total concentration of Mn is 325 (± 27) mg·kg⁻¹ dry mass of ash and 348 (± 19) mg·kg⁻¹ dry mass of soil. It was stated, that the used sequential extraction methods characterize respectively: 98.9% the total content of Mn in ash and 99.4% the total content of Mn in soil.

Table 1. Distribution of manganese in fly ash and soil obtained after sequential extraction procedures by BCR (fly ash) and Tessier et al. (soil); n = 6, p = 95%.

BCR procedure		Tessier scheme	
Fractions of Mn in fly ash	Content of Mn [mg·kg ⁻¹ dry mass]		Fractions of Mn in soil
-	-	6.1 (± 3.1)	F(I) exchangeable
F(I) acid soluble	120.0 (± 4.3)	18.6 (± 3.2)	F(II) carbonate
F(II) reducible	85.0 (± 2.5)	162.5 (± 6.6)	F(III) Fe/Mn oxides
F(III) oxidisable	62.5 (± 1.9)	24.4 (± 4.3)	F(IV) organic
F(IV) „residual”	57.5 (± 1.7)	125.6 (± 11.6)	F(V) „residual”
Σ [Mn] _{fraction} *	325.0 (± 26)	337.2 (± 32)	Σ [Mn] _{fraction} *
[Mn] _{total} **	325.0 (± 27)	348.0 (± 19)	[Mn] _{total} **

* Σ [Mn]_{fraction} – sum of the content of Mn in particular fraction ash/soil samples F(I) – F(V).

**[Mn]_{total} – the total content of Mn in ash/soil samples obtained after total mineralization ash/soil.

The important aspect of investigations connected with the distribution of element between individual chemical fractions in different environmental objects is arrangement „degree of lability". He is defined as: sum of concentrations of individual fraction of the metal to the exclusion of last fraction („residual") with reference to total contents of element received as sum of all fractions [13]. It is generally assumed that the greater the „degree of lability" (labile percentage) the greater the potential for bioaccumulation. The „degree of lability" of Mn in fly industrial ash was received on level 83.3%, „residual" to get appropriately 17.7%. For soil the „degree of lability" was carried out on the level 62.8%, and „residual" to state appropriately 37.2%. The received values of „degree of lability" of manganese in fly ash and soil samples, provide about higher abilities of manganese to phase and interfacial migration and to his higher bioaccumulation in fly industrial ash in relation to soil.

The essential problem, from the point of view of ecological toxicity is estimation of the physicochemical conditions with reference to the natural conditions for „leaching" of trace elements are contained in environmental materials. The executed investigations of relating the sequential extraction of Mn from fly industrial ash permit on ascertainment, that:

- manganese is present in surface layer of fly industrial ash in concentration of 325 (± 27) $\text{mg}\cdot\text{kg}^{-1}$ dry mass of ash;
- manganese shows effect immediate of washing from surfacel layer by means of suitable solutions; at use of sequential extraction – BCR method;
- his „leaching" from fly industrial ash in the acid soluble fraction (at $\text{pH} \approx 5$) is average; carries out 37% total content of Mn in ash.

With reference to soil, the „leaching" manganese in environmental conditions is contained first of all in the fractions: exchangeable and carbonate. The quantity of „leaching" manganese in soil amounted to 7% his total content in soil.

REFERENCES

- [1] Shun-Xing L., Feng-Ying Z., Xian-Li L., Wen-Lian C., *Phytochem. Anal.*, **16**, 405 (2005)
- [2] Cukrowski I., *Anal. Chim. Acta*, **336**, 23 (1996)
- [3] Holm P.E., Christensen T.H., Tjell J.C., McGrath S.P., *J. Environ. Qual.*, **24**, 183 (1995)
- [4] Davidson C.M., Thomas R.P., McVey S.E., Perala R., Littejohn D., Ure A.M., *Anal. Chim. Acta*, **291**, 277 (1994)
- [5] Namieśnik J. (ed.), *The preparation of environmental samples for analysis*, WNT, Warszawa, 2002, 80 (in Polish)
- [6] Sahuquillo A., Lopez-Sanchez J.F., Rubio F., Rauren G., Thomas R.P., Davidson C.M., Ure A.M., *Anal. Chim. Acta*, **382**, 317 (1999)
- [7] Tessier A., Campbell P. G. C., Bisson H., *Anal. Chem.*, **51**(7), 844 (1979)
- [8] Branch Norm BN-81/0623-01. Fly ashes and slags from kettles heated with hard and brown coal. Sampling and preparation of samples.
- [9] Polish Norm PN-77/G-04528/00. Solid fuels. Determination of chemical composition of ash. Preparation of ash sample and solution for testing.
- [10] Kalemekiewicz J., Sitarz-Palczak E., *Polish J. Environ Stud.*, **14**(1), 41 (2005)
- [11] Kalemekiewicz J., Sitarz-Palczak E., *Polish J. of Soil Science*, **35**(2), 74 (2002)
- [12] Kalemekiewicz J., Sitarz-Palczak E., *Atomic Spectrosc.*, **22**, 433 (2001).
- [13] Sutherland R.A., Tack F.M.G., *Anal. Chim. Acta*, **454**, 249 (2002).

PREPARATION OF NAFION H SOLUTIONS.

J. Kijeński, M. E. Jamróz, A. R. Migdał, O. Osawaru,
E. Śmigiera, W. Tęcza

*Instytut Chemii Przemysłowej im. prof. Ignacego Mościckiego,
ul. Rydygiera 8, 01-793 Warszawa, Antoni.Migdal@ichp.pl*

INTRODUCTION

Nafion NR50 (in a H form) is a very strong acid with value of the Hammett acidity function (H_0) from (-11) to about (-13) – comparable or lower to 100% sulfonic acid. This classifies the Nafion resin to the group of superacids. The superacidity is attributed to the electron-withdrawing ability of the perfluorocarbon core from the terminate sulfonic acid groups. Simplifying, we can say that Nafion structure consists of a throughout homogeneous hydrophobic semicrystalline perfluorocarbon matrix with randomly clusters of superacidic trifluoromethane sulfonic (triflic) groups. These acidic groups are sites of very high hydrophilicity and hence Nafion must be stored in dry place under nitrogen - otherwise undergoes hydration. The capacity of the triflic groups presented in a bulk of Nafion is $0.8 \div 0.9 \text{ mmol} \cdot \text{g}^{-1}_{(\text{resin})}$. Nafion H resin is both chemically and thermally stable up to 550K, at which temp. the sulfonic groups beginning to decompose.[1]

There are two major drawbacks of this material. The first one is its very low surface area ($<0.02 \text{ m}^2 \cdot \text{g}^{-1}$ of commercial pellets) and the second – burying the majority of triflic active groups in the bulk of polyperfluoroethylene matrix – making them inaccessible to a number of reagents.[2] A method resulting in open up a number of exposed triflic group and in consequence an increase of catalytic activity of Nafion H consists in impregnation of Nafion H on solid support from its solution followed by solvent evaporation. [3]

Influence of the solvent on properties of support/ BCl_3 catalytic systems obtained in similar way from solutions differing in solvent basicity were studied by Marczewski et al..[4] Authors postulate a simple correlation between solvent basicity and activity of such prepared catalytic system. The less basic is the solvent used, the higher is the strength of the acid. The influence of solvent type on the catalytic properties of Nafion H/support composite has not been studied up to date. This might be caused by limited availability of Nafion H solutions in solvents. Nowadays the Nafion H solutions, which are available on the commercial (chemical) market, are mixtures of 5, 10 or 20wt% of resin in lower aliphatic alcohols (mainly methanol) and water. The aim of this work is to present a method of preparation of Nafion H solutions in pure, well-defined solvents.

EXPERIMENTAL & RESULTS

The presented Nafion H dissolving process is based on literature pressurized conventional and microwave (mw) assisted methods of obtaining Nafion H solutions.[5,6] A mixture of twice distilled demineralized water and Nafion NR50 pellets was irradiated in Ertec 02-04 microwave reactor for 2 h at temperature up to 513K (near critical water conditions). The temperature during dissolving was automatically controlled by the flow rate of cooling water in a water jacket and power density. The pressure in the reaction chamber partially generated by solvent evaporation was controlled by power density and by the volume of irradiated mixture. The

maximum mw density was set at $8 \text{ W}\cdot\text{g}^{-1}$. Fig. 1 presents the behavior of process parameters during mw irradiation.

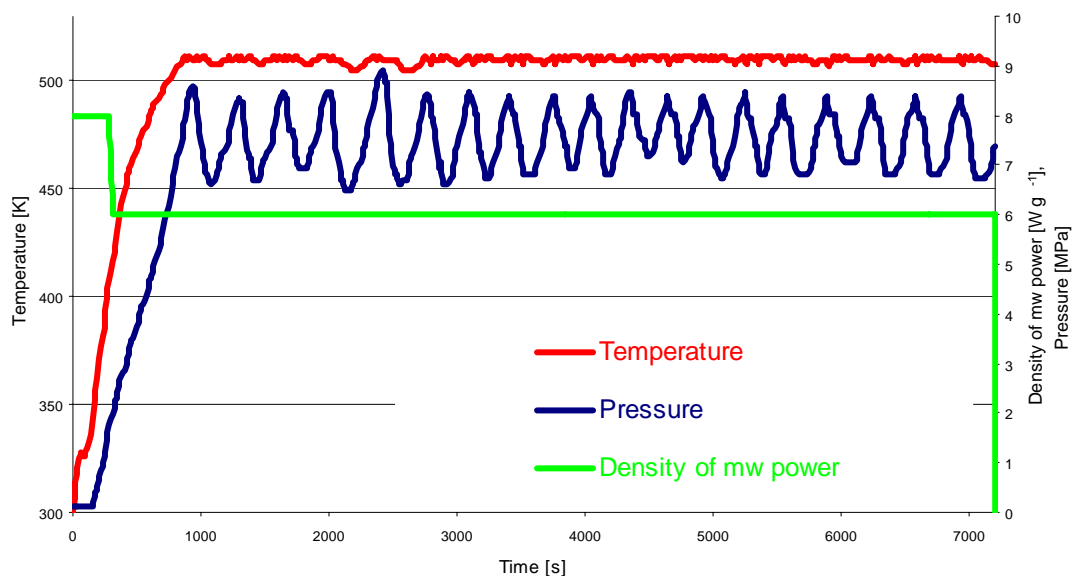


Fig. 1. Conditions of the process of Nafion H dissolving in water.

The obtained Nafion H - water mixture was inhomogeneous and contained Nafion dissolved in water and gel – water swelled Nafion pellets. Process goes through a gelation stage. The domination one of these two forms (gel or solution) in mixture was dependent on process conditions. The obtained Nafion H - water mixture was filtered through a Filtrak 388 filter. The homogeneity of the filtrates was measured by Malvern ZETAMASTER apparatus. Every filtrate from the process was homogeneous Nafion – water solution. The effectiveness parameter of the dissolving process was calculated on the basis of the weight of Nafion H found in the filtrate (equivalent to the weight of residue from filtrate high vacuum evaporation) in reference to the initial weight of Nafion H used. For the process pressure set at 6.5MPa and above the effectiveness of the process was close to 95% and dramatically decreased when the pressure was set below 6.5MPa.

Table 1. Properties of two Nafion H forms.

Form:	Surface area [$\text{m}^2\cdot\text{g}^{-1}$]	Porosity:	Acid capacity: [$\text{mmol}\cdot\text{g}^{-1}$]	Thermal stability [K]
Commercial (pellets)	0,02	Non-porous	0,8	553
Lyophilized ("spongy")	Not detectable	Porous	0,7	collapse above 350

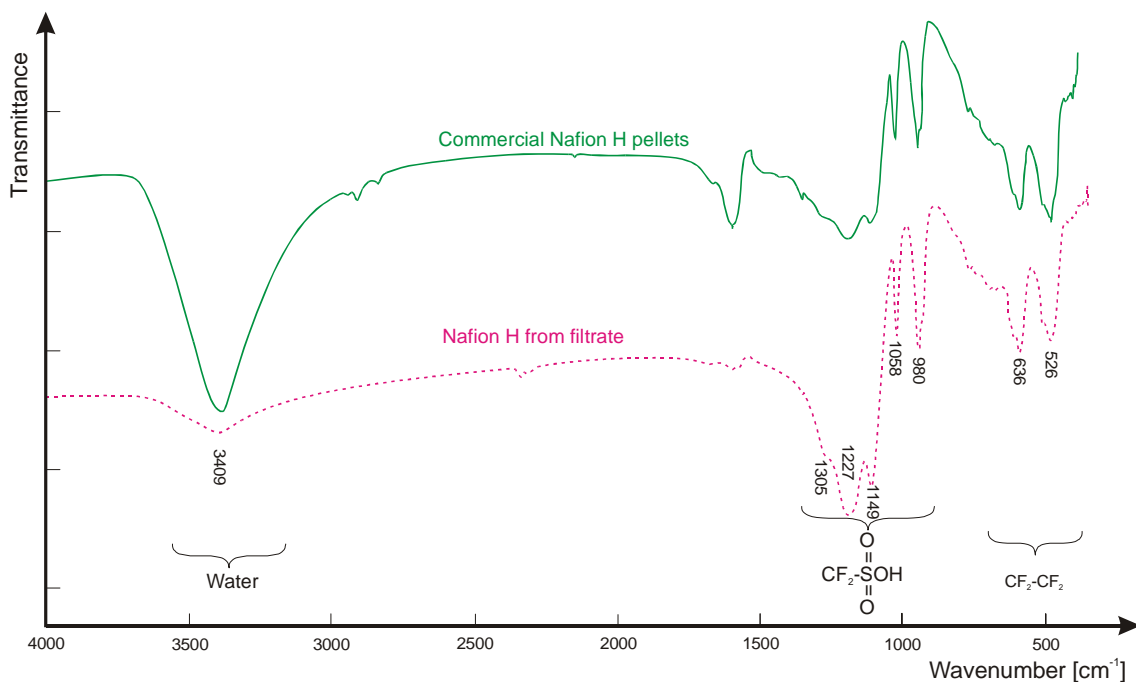


Fig. 2. IR spectra of two Nafion H forms.

The residue from filtrate dried at 243K and under vacuum (<2Pa) for 5 days using Christ GAMMA 2-20 freeze-drier was a white “spongy” structure, form of Nafion H. The IR spectra of commercial Nafion H pellets and a “spongy” structure are presented on fig. 2. The presented spectra indicate that both samples consist of the same substance containing $\text{-CF}_2\text{-}$ groups (oscillation bands at 526 and 636cm^{-1}) and $\text{-SO}_3\text{H}$ groups (oscillation bands at: 980, 1058 and wide band with maximum at $1220\div 1230\text{cm}^{-1}$). A considerable increase of intensity of the band at 3409cm^{-1} wavenumber in commercial Nafion NR50 pellets spectrum indicate the presence of the traces of water in commercial pellets. The presence of sulfonic acid groups in the structure obtained from filtrate was identified in reaction of “spongy” Nafion in water with barium nitrate. The opacity of solution confirmed the presence of sulfonic groups in the structure.

The acid capacity of “spongy” Nafion H, determined on the basis of sodium hydroxide titration of the residue from filtrate high vacuum evaporation, was consistent with ones given for commercial Nafion NR50, which indicates the sulfonic groups don't decompose during dissolving in water or freeze-drying, or that sulfonic groups decomposition is negligible under the presented conditions. Table 1 presents a comparison of properties of two Nafion H form.

This new “spongy” form has some drawbacks, e.g. occurs at limited temp. range – decays with a partial reconstruction of pellets form when warmed to about 350 K. The “spongy” Nafion H structure must be stored under nitrogen in dark place. When stored under air undergoes contamination resulting in pinkish coloration.

The white “spongy” structure of Nafion H, obtained from filtrate (dried at 243K and under vacuum <2Pa for 5 days using freeze-drier) appeared to be easily soluble in many solvents at room temperature. This property enables the preparation of highly concentrated Nafion H solutions of water, methanol, ethanol, butanol, acetonitrile and acetic anhydride – solvents with well-defined properties. The above-mentioned solvents, except water, are unstable in solution and have a limited operating time. Those

solutions must be quickly used otherwise are being contaminated by the product of their decomposition catalyzed by Nafion H. High acidity of Nafion is the main reason for limited validity of such solutions. The “spongy” form of Nafion has a very low solubility in acetic acid or methylene chloride and is almost insoluble in light hydrocarbons.

CONCLUSIONS

Microwave assisted pressure method allows for quick dissolving of Nafion H pellets in water. Synthesized from water solution, new “spongy” form of Nafion H, is easy soluble in many solvents at room temperature. The “spongy” structure of Nafion occurs at limited temperature range – collapses when heated to above 350K.

The stability of Nafion H solutions in organic solvents is limited, mainly due to a high acidity of Nafion and it’s interaction with solvents.

REFERENCES:

- [1] S.R. Saamms, S. Wasmus, R.F. Savinell, *J. Electrochem. Soc.*, 143 (1996), 1498
- [2] Harmer, A. M., Farneth, W. E., Sun, Q., *J. Am. Chem. Soc.*, **1996**, 118, 7708
- [3] Pálinkó, I., Török, B., Prakash, G. K. S., Olah, G. A. *Appl. Catal. A:*, **1998**, 174, 147
- [4] Marczewski, M. Migdał, A., Marczewska, H., *Phys. Chem. Chem. Phys.*, **2003**, 5, 423
- [5] Soczka–Guth, T., et al. US Pat. 6 348 516 B1 (**2002**)
- [6] Grott, W., G., and Ford, Ch., US. Pat. 4 433 082 (**1984**)

STUDIES OF SORPTION AND SEPARATION OF RARE EARTH(III) COMPLEXES WITH EDTA ON MONODISPERSE STRONGLY BASIC ANION EXCHANGERS

Dorota Kołodyńska, Halina Hubicka

*Department of Inorganic Chemistry, Faculty of Chemistry,
Maria Curie-Skłodowska University, 20-032 Lublin, Poland*

Technological progress in recent years has increased the requirements for rare earth elements. Lanthanides of high purity as well as yttrium, its compounds and isotopes find diverse applications in advanced technology. Principal uses are in phosphors for color televisions and computer monitors, trichromatic fluorescent lights, temperature sensors, and X-ray intensifying screens. As oxide, yttrium is also used as a stabilizer in zirconia (YSZ), wear and corrosion resistant cutting tools, seals and bearings, jet engine coatings, oxygen sensors in automobile engines, simulant gemstones. In electronics, yttrium-iron-garnets (YFG) are components in microwave radar to control high frequency signals. Yttrium is an important component in yttrium-aluminum-garnet (YAG) laser crystals used in industrial cutting and welding, medical and dental surgical procedures, temperature and distance sensing, photoluminescence, photochemistry, digital communications, and nonlinear optics. Yttrium is also used in high-temperature superconductors [1-4]. In these applications yttrium was consumed primarily in the form of high purity compounds, especially its oxide and nitrate.

Recent publications dealing with anion exchange of rare earth elements(III) with chelating ligands indicate that their separations on anion exchangers depend not only on the types of formed complexes, but also on the types of anion exchangers.

Dybczyński [5,6] initiated an investigation of the anion exchange elution behaviour of lanthanide isotopes in the ethylenediaminetetraacetic acid (EDTA) and *trans*-1,2-diaminocyclohexane-N,N,N',N'-tetraacetic acid (DCTA) systems. He found that rare earth element complexes with these complexing agents exhibit atypical affinity for anion exchangers. An unusual affinity series was also obtained by Hubicka et al. [7-9] for rare earth element complexes with iminodiacetic acid (IMDA) – $Dy(III) > Ho(III) > Gd(III) > Eu(III) > Er(III) > Y(III) > Sm(III) > Tm(III) > Nd(III) > Pr(III) \gg La(III)$ and N'-(2-hydroxyethyl)ethylenediamine-N,N,N'-triacetic acid (HEDTA) – $Dy(III) > Ho(III) > Er(III) > Y(III) \approx Gd(III) > Tm(III) > Tb(III) > Eu(III) > Sm(III) > Yb(III) > Nd(III) > Pr(III) > La(III)$. The determined affinity series provide possibilities of separation of these pairs (of the largest difference in affinity) whose separation by other methods is time consuming and requires great amounts of complexing agent and frequently does not give satisfactory results.

In the presented paper investigations into the use of monodisperse anion exchangers for the sorption and separation of rare earth element(III) complexes with EDTA were carried out. The studies of separation by frontal analysis were made for $[Y(EDTA)]^-$ and $[Nd(EDTA)]^-$ complexes.

EXPERIMENTAL

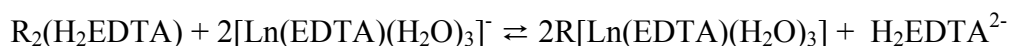
In the studies strongly basic gel monodisperse anion exchangers Lewatit MonoPlus M 500 (type 1) and Lewatit MonoPlus M 600 (type 2) as well as the strongly

basic macroporous anion exchanger Lewatit MonoPlus MP 500 were used. Methanol, 1-propanol and acetone of analytical reagent grade were supplied from POCH S.A.

The breakthrough curves of yttrium(III) and neodymium(III) were determined using the solutions of complexed rare earth elements (with suitable polar organic solvent addition) at a concentration 0.004 M. Solutions of a concentration about 1.5g Ln₂O₃/dm³ at pH 4.6 were used for separation of Y(III) from Nd(III). The frontal analysis process was carried out in glass columns of a diameter 2.0 cm filled with the anion exchanger keeping the flow rate at 0.2 cm³/cm²·min. The percentage of neodymium(III) in yttrium(III) was determined by UV-Visible spectrophotometric analysis using a SPECORD M 42 produced by Carl Zeiss Jena, Germany. The detection limit of neodymium(III) in yttrium(III) was 0.005%.

RESULTS AND DISCUSSION

EDTA, acting as a multidentate chelating ligand, forms strong complexes with most divalent and trivalent metal ions so the ion exchange sorption process of lanthanide complexes with EDTA on the anion exchanger in the H₂EDTA²⁻ form can be presented as follows:



where:

R- the ion exchange skeleton with a functional group.

Addition of organic solvent to the aqueous solution of metal salt in the presence of a complexing agent can cause not only modification of formed complexes stability but also, in the case of many successive complexes formation of the same element, change of their interrelations. On one hand, it results from a specific interaction of the added organic solvent on bond strength and on the other hand, from the influence of dielectric constant value. Literature lacks the data about explanation of lanthanide(III) ions behaviour in the presence of complexing agents in the mixed and nonaqueous systems. Due to this fact, the effect of polar organic solvent addition on effectiveness of Y(III) purification from Nd(III) in the macro-micro system was studied.

From the breakthrough curves of Y(III) and Nd(III) complexes with EDTA in the aqueous solution as well as with 10% (v/v) and 20% (v/v) addition of polar organic solvents on Lewatit MonoPlus M 500, Lewatit MonoPlus M 600 and Lewatit MonoPlus MP 500 in the H₂EDTA²⁻ form, the weight (D_g) and bed (D_v) distribution coefficients and the working ion exchange capacities (C_w) were determined. The total ion exchange capacities (C_t) were calculated by integration along the curve. The differences in the values of calculated the weight (D_g) and bed (D_v) distribution coefficients between Y(III) and Nd(III) complexes with EDTA are presented in Figs.1-3.

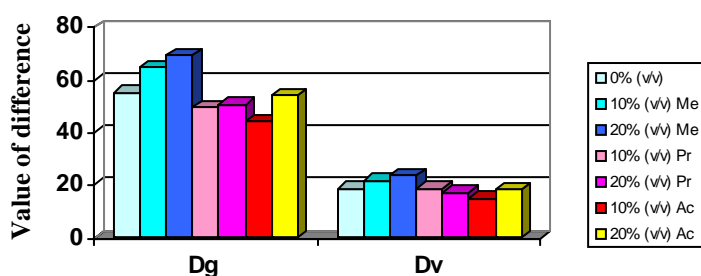


Fig.1. The differences in the values of the weight (D_g) and bed (D_v) distribution coefficients between Y(III) and Nd(III) complexes with EDTA and polar organic solvents (Me-methanol, Pr-1-propanol, Ac-acetone) on Lewatit MonoPlus M 500.

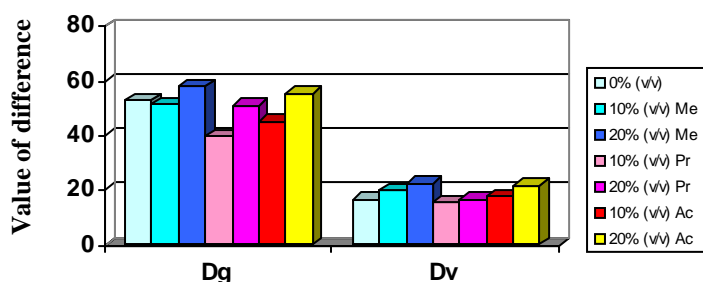


Fig.2. The differences in the values of the weight (D_g) and bed (D_v) distribution coefficients between Y(III) and Nd(III) complexes with EDTA and polar organic solvents (Me-methanol, Pr-1-propanol, Ac-acetone) on Lewatit MonoPlus M 600.

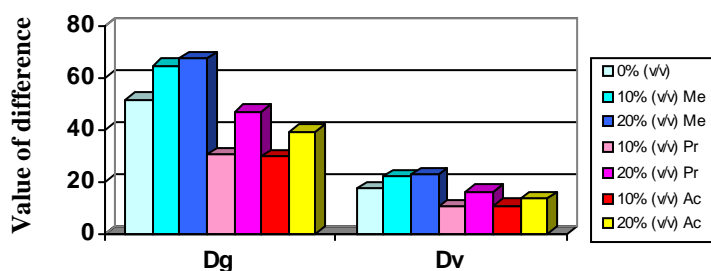


Fig.3. The differences in the values of the weight (D_g) and bed (D_v) distribution coefficients between Y(III) and Nd(III) complexes with EDTA and polar organic solvents (Me-methanol, Pr-1-propanol, Ac-acetone) on Lewatit MonoPlus MP 500.

The highest difference in the values of the distribution coefficients of Y(III) and Nd(III) complexes with EDTA in the aqueous and H₂O-polar organic solvent systems (Figs.1-3) was found in the case of methanol addition. It increases with the increase of percentage contents of methanol and depends on the kind of anion exchanger. The difference in the values of the distribution coefficients of these complexes on Lewatit MonoPlus M 500 (type 1 - the functional groups of $-\text{N}^+(\text{CH}_3)_3$) are higher than those on Lewatit MonoPlus M 600 (type 2 - the functional groups of $-\text{N}^+(\text{CH}_3)_2\text{C}_2\text{H}_4\text{OH}$). For the strongly basic gel anion exchanger Lewatit MonoPlus M 500 and the macroporous anion exchanger of this type – Lewatit MonoPlus MP 500 the difference in the values of the distribution coefficients is similar. In the case of 1-propanol and acetone addition, for the above mentioned anion exchangers the difference of the distribution coefficient values is lower.

The determined working and total ion exchange capacities for the Y(III) and Nd(III) complexes with EDTA indicate that the studied monodisperse anion exchangers achieve larger effective sorption capacity towards Nd(III) than Y(III) complexes.

Taking into account the above statements, separations of Y(III) from Nd(III) complexes with EDTA in the aqueous and H₂O-organic polar solvents medium on monodisperse gel and macroporous anion exchangers were studied using the frontal analysis technique.

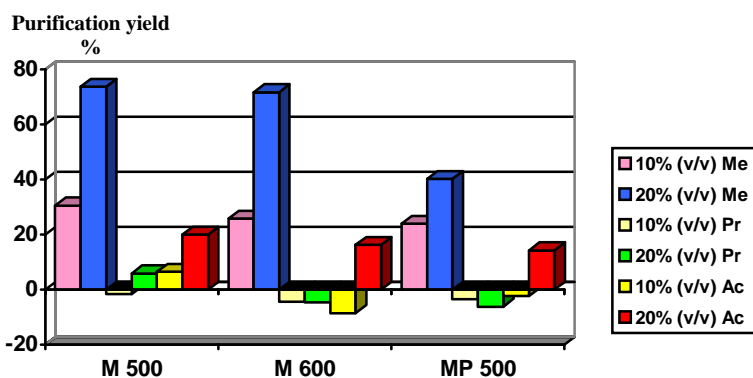


Fig.4. The purification yield of Y_2O_3 in the H₂O-polar organic solvent systems (Me-methanol, Pr-1-propanol, Ac-acetone) on Lewatit MonoPlus M 500 (M 500), Lewatit MonoPlus M 600 (M 600) and Lewatit Mono Plus MP 500 (MP 500) in the H₂EDTA²⁻ form.

The results of separation of Y(III) from Nd(III) (Nd_2O_3 0.35%) with respect to the aqueous solution on Lewatit MonoPlus M 500, Lewatit MonoPlus M 600 and Lewatit MonoPlus MP 500 in the $\text{H}_2\text{EDTA}^{2-}$ form are presented in Fig.4. Taking into consideration the effect of the addition of polar organic solvent on the effectiveness of separations of rare earth element(III) complexes with EDTA on the above mentioned anion exchangers the best results of Y(III) from Nd(III) purification are obtained in the 20% (v/v) methanol system on Lewatit MonoPlus M 500. The yttrium oxide yield obtained in this process is about 74% higher than that obtained in the aqueous solution. For the anion exchanger Lewatit MonoPlus M 600 (type 2) the obtained separation results are almost similar to those obtained on Lewatit MonoPlus M 500 (type 1). In the case of the monodisperse macroporous anion exchanger Lewatit MonoPlus MP 500 the obtained separation results of Y(III) from Nd(III) in the H_2O -10% (v/v) CH_3OH and H_2O -20% (v/v) CH_3OH systems are lower than those on the gel anion exchanger of this type (Lewatit MonoPlus M 500). The yield obtained in this process is 24% and 40% higher in comparison with aqueous solution.

Analogous studies on the separation of Y(III)-Nd(III) complexes with EDTA were carried out in the presence of 1-propanol and acetone (Fig.4). As found in the studies only in the case of 20% (v/v) addition of acetone the effectiveness of separation process increases in comparison with the aqueous solution. However, the yield obtained in this process is only about 20%, 16% and 14% higher compared with the aqueous one.

CONCLUSIONS

1. The addition of polar organic solvent – methanol affects separation of rare earth element(III) complexes with EDTA. This effect probably caused differentiation of structure of lanthanide complexes due to the change of solvation degree or the exchange of water molecules in the primary coordination sphere into polar organic solvent molecules, which can be responsible for their different affinity for anion exchanger [10].

2. In purification of Y(III) from Nd(III) in the aqueous-methanol solutions, monodisperse gel anion exchangers proved to be very effective which confirms that ion exchange structure plays a significant role in separation of rare earth elements(III). Controversial opinions found in literature about the effect of polar organic solvent addition on sorption and separation of elements on ion exchangers seem to be justified as this effect is different which follows from the above studies.

REFERENCES

1. P.L. Goering, B.R. Fisher, B.A. Fowler, *Metals and Their Compounds in the Environment*. The Lanthanides, VCH, Weinheim: New York, Cambridge, 1991, pp.959-970.
2. J. Chegwidde, D.J. Kingsnorth, *Industrial Minerals*, 4 (2002) 52.
3. M. O'Driscoll, *Industrial Minerals*, 5 (2003) 24.
4. Ch. Yuli, G. Gongyi, *Ceramics International*, 23 (1997) 267.
5. R. Dybczyński, *J. Chromatogr.*, 50 (1970) 487.
6. L. Wódkiewicz, R. Dybczyński, *Chem. Anal.*, 14 (1969) 437.
7. H. Hubicka, D. Drobek, *Hydrometallurgy*, 47 (1997) 127.
8. H. Hubicka, D. Drobek, *Hydrometallurgy*, 50 (1999) 51.
9. H. Hubicka, D. Kołodyńska, *Adsorp. Sci. Technol.*, 18 (2000) 719.
10. R. Choppin, *J. Alloys Comp.*, 225 (1995) 242.

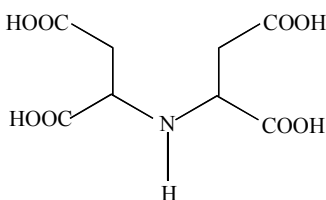
INVESTIGATIONS INTO THE USE OF MONODISPERSE POLYSTYRENE ANION EXCHANGERS FOR THE SEPARATION OF Cu(II), Fe(III), Co(II) AND Ni(II) COMPLEXES WITH IDS

Dorota Kołodyńska, Halina Hubicka, Zbigniew Hubicki

*Department of Inorganic Chemistry, Faculty of Chemistry,
Maria Curie-Skłodowska University, 20-032 Lublin, Poland*

Aminopolycarboxylic acids such as ethylenediaminetetraacetate (EDTA), iminodiacetate (IDA), nitrilotriacetate (NTA), diethylenetriaminepentaacetate (DTPA) and others are used for a wide range of different applications. These synthetic chelating agents are almost resistant to biodegradation [1]. Therefore their concentrations have increased in some aquatic systems often to non-acceptable levels. In the environment, chelating agents have some undesired features such as the remobilization of radionuclides and toxic heavy metals from sediments and soils.

Iminodisuccinate (IDS), commercialized since 1998 by the Bayer AG (Leverkusen, Germany), is a synthetic compound, readily biodegradable, which is produced from the maleic anhydride, ammonia and sodium hydroxide solution. In water equal amounts of the four possible stereoisomers: two identical meso forms RS'-IDS and SR'-IDS (because of an intramolecular mirror plane) and two forms RR'-IDS, SS'-IDS are found [2-4]. The structure of IDS can be described as follows:



It is characterized by low remobilization of heavy metal ions and is superior to conventional complexing agents because of its excellent ability to complex iron(II), copper(II) and calcium ions.

Iminodisuccinic acid Na salt is used in oxidative cotton bleaching for the stabilization of H₂O₂ by complexation of iron and copper ions and to improve the dispersion of pigment particles in the production of paper, decorator's paints and other products. It is used in detergents for dishwashing machines. IDS is applied mainly as a substitute for NTA, in certain cases it can also be utilized as a substitute for EDTA. In membrane-cleaning processes good results are obtained when IDS is combined with sodium polyasparaginate [5].

For IDS no consumption data exist for Europe at present. But as follows from of the Federal Office of Environment Protection data in Germany in the mid 2001 there were registered 69 washing and cleaning products containing IDS and an approximate amount of IDS used in washing and cleaning agents in Germany was 55 t/a.

The aim of this paper is to investigate sorption of copper(II), iron(III), cobalt(II) and nickel(II) complexes with iminodisuccinic acid on strongly basic polystyrene anion exchangers. To this end the monodisperse anion exchangers - Lewatit Mono Plus M 500 and Lewatit Mono Plus MP 500 were used.

Contrary to heterodisperse anion exchangers, monodisperse polystyrene anion exchangers are characterized by good mechanical stability as well as high diffusion coefficients. Owing to properly modified polymer structure and homogeneity in grain

size, the anion exchangers exhibit very good kinetic properties. This allows for significant decrease in anion exchanger contact with the solution. Additionally these properties contribute to better exploitation of ion exchanger functional groups compared with the traditional heterodisperse anion exchangers. Taking economical aspects into account, their large ion exchanger capacity is of significant importance.

EXPERIMENTAL

In our investigations the following metal ions were selected - copper(II), iron(III), cobalt(II) and nickel(II) which represent the toxic trace metals. The initial concentration of metals ions was 10^{-3} M, which is located within the level of real effluents such as electroless copper plating rinse water.

The solutions of metal complexes with IDS were prepared by dissolving equimolar amounts of metal chloride in the IDS solution. The behaviour of copper(II), iron(III), cobalt(II) and nickel(II) was investigated at pH values without adjustment.

In order to measure affinity of Cu(II)-IDS, Fe(III)-IDS, Co(II)-IDS and Ni(II)-IDS complexes, the breakthrough curves were determined using the above mentioned anion exchangers in the Cl⁻, acetate or IDS form. The exemplary breakthrough curves of Cu(II), Fe(III), Co(II) and Ni(II) complexes with IDS on the strongly basic gel monodisperse anion exchanger Lewatit Mono Plus M 500 are presented in Fig. 1. From these breakthrough curves the weight (D_g) and bed (D_v) distribution coefficients as well as the working ion exchange capacities (C_w) of M(II)/M(III) were calculated. The total ion exchange capacities (C_t) were calculated by integration along the curve. The recovery factors (%R) were also determined by means of the static method.

RESULTS AND DISCUSSION

As follows from the research results presented in Tables 1 and 2, the weight (D_g) and bed (D_v) distribution coefficients as well as the working (C_w) and total (C_t) ion exchange capacities of metal(II)/(III) ions for anion exchangers are differentiated.

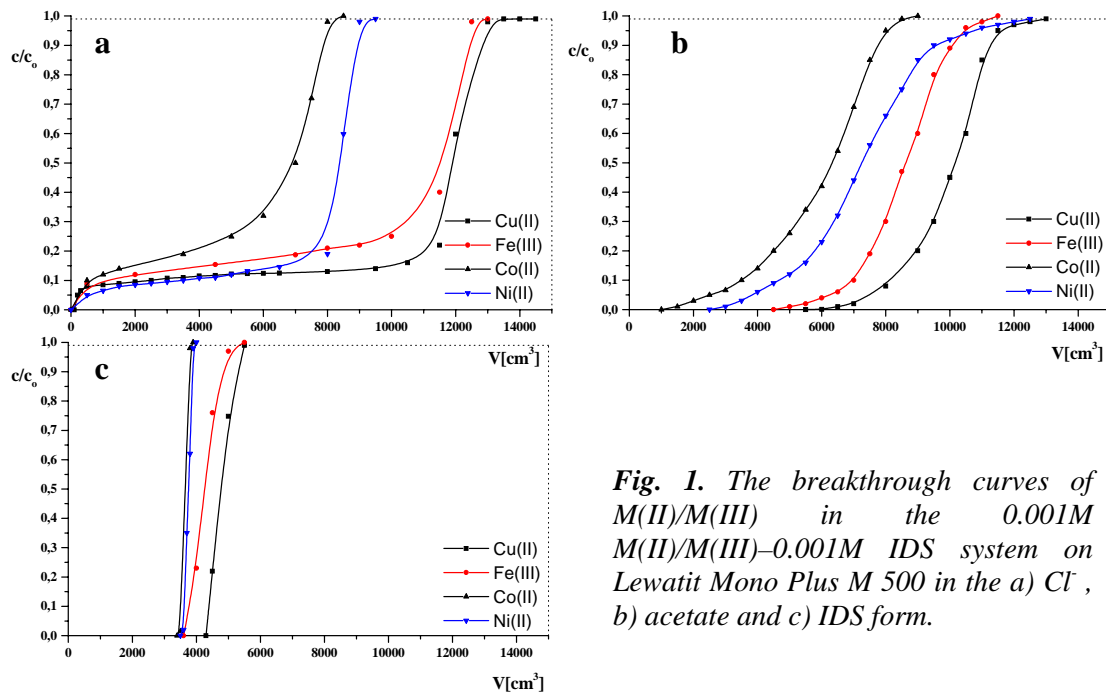


Fig. 1. The breakthrough curves of M(II)/M(III) in the 0.001M M(II)/M(III)–0.001M IDS system on Lewatit Mono Plus M 500 in the a) Cl⁻, b) acetate and c) IDS form.

Tab.1. The values of the weight (D_g) and bed (D_v) distribution coefficients, the working (C_w) and total (C_t) ion exchange capacities for Cu(II), Fe(III), Co(II) and Ni(II) in the 0.001M M(II)/(III)-0.001M IDS system on Lewatit Mono Plus M 500.

Anion exchanger	M(II)/M(III)	D_g	D_v	C_w	C_t
Lewatit Mono Plus M 500 in the Cl ⁻ form	Cu	3635.66	1190.41	0.0019	0.0672
	Fe	3506.65	1148.16	0.0012	0.0664
	Co	2103.38	688.70	0.0005	0.0388
	Ni	2557.91	837.52	0.0006	0.0494
Lewatit Mono Plus M 500 in the acetate form	Cu	2755.99	846.64	0.0291	0.0532
	Fe	2337.65	718.13	0.0238	0.0452
	Co	1714.49	526.69	0.0049	0.0291
	Ni	1965.06	603.67	0.0122	0.0356
Lewatit Mono Plus M 500 in the IDS form	Cu	1237.06	423.32	0.0243	0.0271
	Fe	1103.55	377.63	0.0198	0.0223
	Co	949.14	324.80	0.0178	0.0196
	Ni	974.17	333.36	0.0187	0.0212

Tab.2. The values of the weight (D_g) and bed (D_v) distribution coefficients, the working (C_w) and total (C_t) ion exchange capacities for Cu(II), Fe(III), Co(II) and Ni(II) in the 0.001M M(II)/(III)-0.001M IDS system on Lewatit Mono Plus MP 500.

Anion exchanger	M(II)/M(III)	D_g	D_v	C_w	C_t
Lewatit Mono Plus MP 500 in the Cl ⁻ form	Cu	1945.10	485.93	0.0127	0.0308
	Fe	1925.82	481.11	0.0058	0.0282
	Co	2115.51	528.50	0.0006	0.0340
	Ni	2099.01	524.48	0.0032	0.0348
Lewatit Mono Plus MP 500 in the acetate form	Cu	2341.59	532.05	0.0106	0.0387
	Fe	2029.33	461.10	0.0073	0.0292
	Co	1272.25	289.08	0.0025	0.0180
	Ni	1387.14	315.18	0.0053	0.0230
Lewatit Mono Plus MP 500 in the IDS form	Cu	1380.62	358.47	0.0116	0.0231
	Fe	1293.45	335.84	0.0106	0.0210
	Co	1113.46	289.10	0.0075	0.0170
	Ni	1270.95	330.00	0.0087	0.0202

As follows from the determined breakthrough curves and comparison of calculated weight (D_g) and bed (D_v) values of distribution coefficients as well as working (C_w) and total (C_t) values of ion exchange capacities, the gel anion exchanger Lewatit Mono Plus M 500 was more effective in sorption of above mentioned complexes than the macroporous anion exchanger of this type - Lewatit Mono Plus MP 500.

The research results showed the effect of form of the anion exchanger under investigation on effectiveness of individual element ions sorption. The chloride form (commercial one) of the applied anion exchangers seems to be the most effective owing to the purification yield (high values of distribution coefficients). However, the first

fraction of the purified solution should be redirected on the column for their further purification (Fig. 1a), as complexes of smaller affinity for the anion exchanger are formed in the first stage of the process. The Cl^- form is economically advantageous, as besides preliminary preparation of the ion exchanger, it does not require additional stages of anion exchanger treatment.

The distribution coefficients for the acetate and IDS forms are lower compared to those for the Cl^- form. In the case of IDS form (Fig. 1c) from the beginning of the process complete sorption of the Cu(II) , Fe(III) , Co(II) and Ni(II) complexes is found but the purification yield is lower than for the chloride form.

In the 0.001M M(II)/M(III) -0.001M IDS system the highest affinity for the anion exchanger Lewatit Mono Plus M 500 in the Cl^- form is exhibited by both Cu(II) and Fe(III) , which creates possibility of selective separation of these elements from Co(II) and Ni(II) (Fig. 1a). The obtained results are confirmed by the research carried out by means of the static method depending on the phase contact time for 0.001M M(II)/M(III) -0.001M IDS system (Fig.2).

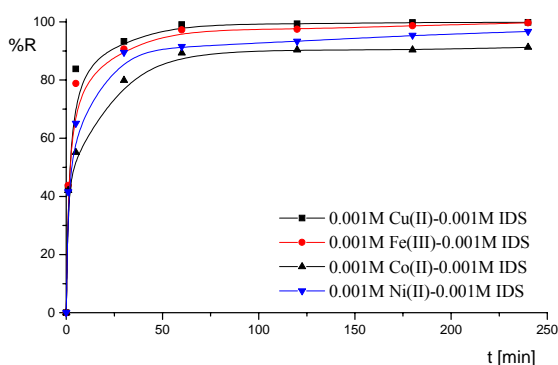


Fig. 2. Comparison of recovery factor (% R) values for Cu(II) , Fe(III) , Co(II) and Ni(II) complexes with IDS on Lewatit MonoPlus M 500 in the Cl^- form.

CONCLUSIONS

Due to common exploitation of complexing both non-biodegradable and more biodegradable (such as IDS) agents, it is essential to search for effective and economical methods for removal of anion complexes of heavy metals with these agents from waters and wastewaters.

The research results indicate possible application of Lewatit Mono Plus M 500 in technologies of heavy metals removal from waste water streams. The presented method is simple and quick. Its another advantage is easy regeneration of an anion exchanger by means of 1M sodium chloride solution.

REFERENCES

- [1]. B. Nörtemann, Appl. Microbiol. Biotechnol., 51 (1999) 751.
- [2]. O. Abollino, M. Aceto, C. Sarzanini, E. Mentasti, Anal. Chim. Acta, 411 (2000) 223.
- [3]. Anonymous IDS Na, Brochure of the company Bayer Chemicals (1998).
- [4]. F. Reinecke, T. Groth, K.P. Heise, W. Joentgen, N. Müller, A. Steinbüchel, FEMS Microbiol. Letters, 188 (2000) 41.
- [5]. T.P. Knepper, Trends Anal. Chem., 22 (2003) 708.

STUDIES OF SORPTION OF HEAVY METAL COMPLEXES WITH EDTA ON GEL AND MACROPOROUS MONODISPERSE ANION EXCHANGERS

Dorota Kołodyńska, Halina Hubicka, Zbigniew Hubicki

*Department of Inorganic Chemistry, Faculty of Chemistry,
Maria Curie-Skłodowska University, 20-032 Lublin, Poland*

Aminopolycarboxylic acids and their salts are variously applied as chelating agents for metal ions in the processes where the concentrations of dissolved, free metal ions have to be controlled. They are used in different industrial applications such as textile, leather, rubber and paper manufacturing as well as nuclear, photography, pharmacy, food industry and in household and agricultural applications. For instance EDTA is used in paper-making and pulp-making to stabilize the action of ozone and hydrogen peroxide on pulp by complexing with metals (especially Fe, Cu and Mn) that catalyse their decomposition [1–3].

On a worldwide scale over 100,000 metric tons of aminopolycarboxylic acids are produced annually. It has been estimated that 65,000 tons of EDTA and DTPA would be realised a year by the pulp and paper industry in the USA [4]. Annual ethylenediaminetetraacetate consumption in West Europe was about 30,000 tons in 1987, but in 1998 this amount was twice as much being 64,000 tons.

Although EDTA is non-toxic to mammals at environmental concentrations, there is same concern about the potential of EDTA to remobilize heavy metals adsorbed onto sediments, so that the elimination of heavy metals in waste water treatment plants (WWTPs) is less efficient. So far attempts to improve chemical and physical methods have not resulted in an economically feasible process. EDTA is difficult to eliminate in conventional biological WWTPs and is hardly adsorbed even onto activated sludge or charcoal. NTA and DTPA present fewer problems with regard to eliminability in WWTPs [2, 4].

Under anaerobic conditions, no degradation could be found for any of the EDTA complexes. One important process for the fate of EDTA in surface waters is the photodegradation of the Fe(III)-EDTA complex [5]. Complexes of EDTA with metals other than Fe(III), such as Zn(II), Cu(II), Ca(II), Mg(II), Ni(II) and Mn(II), are either stable in sunlight or occur at concentrations too low to contribute significantly to the overall degradation of EDTA in surface waters [6].

The aim of this paper was to examine the ion exchange equilibria of metal chelates of EDTA i.e. Cu(II)-EDTA, Fe(III)-EDTA, Co(III)-EDTA, Ni(II)-EDTA with the strongly basic gel and macroporous monodisperse anion exchangers Lewatit Mono Plus M 500 and Lewatit Mono Plus MP 500. All experiments were carried out in an equimolar solution of metal ions and EDTA.

EXPERIMENTAL

The single metal ions aqueous solutions in the presence of EDTA were prepared by dissolving equimolar amounts of appropriate metal chloride in the EDTA solution at pH 4.6. The weight (D_g) and bed (D_v) distribution coefficients as well as the working ion exchange capacities (C_w) of M(II)/M(III) were calculated from the determined breakthrough curves. The total ion exchange capacities (C_t) were calculated by

integration along the curve. For anionic complexes of Cu(II), Fe(III), Co(II) and Ni(II) the recovery factors (%R) were also determined by means of the static method.

RESULTS AND DISCUSSION

The exemplary breakthrough curves of M(II)/M(III) ions in the 0.001M M(II)/M(III)-0.001M EDTA system on the above mentioned polystyrene anion exchangers are presented in Figs 1 and 2.

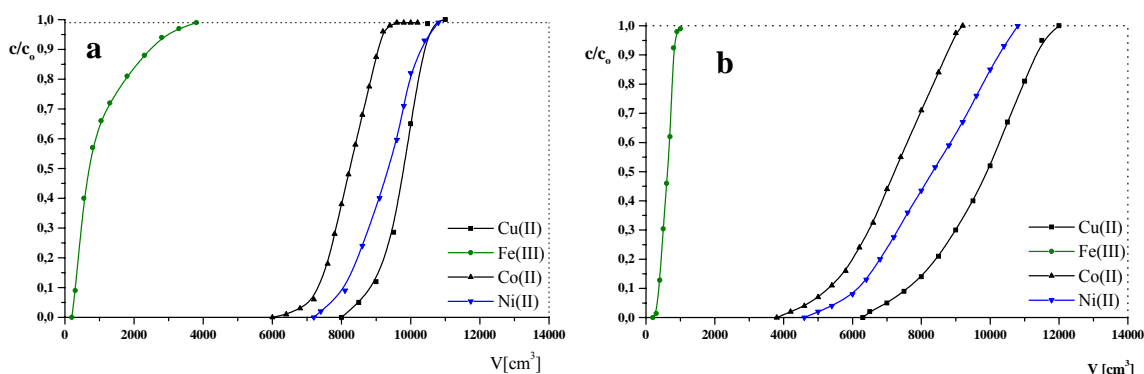


Fig. 1. The breakthrough curves of Cu(II), Fe(III), Co(II) and Ni(II) complexes with EDTA on Lewatit Mono Plus M 500 in the Cl^- (a) and H_2edta^{2-} (b) forms.

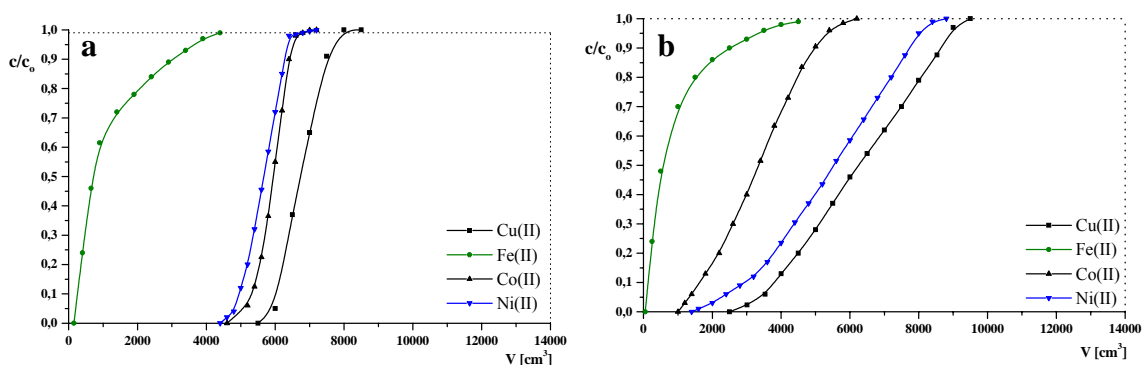


Fig. 2. The breakthrough curves of Cu(II), Fe(III), Co(II) and Ni(II) complexes with EDTA on Lewatit Mono Plus MP 500 in the Cl^- (a) and H_2edta^{2-} (b) forms.

As follows from the research the monodisperse polystyrene anion exchangers, according to their applicability for recovery of anionic complexes of Cu(II), Fe(III), Co(II) i Ni(II) with EDTA in the 0.001M M(II)/(III)-0.001M EDTA system can be put in the order:

Lewatit Mono Plus M 500 in the Cl^- form > Lewatit Mono Plus M 500 in the H_2edta^{2-} form > Lewatit Mono Plus MP 500 in the Cl^- form > Lewatit Mono Plus MP 500 in the H_2edta^{2-} form.

However, taking into account applicability in the sorption processes of $[M(edta)]^{2-}$ and $[M(edta)]^-$ complexes in the 0.001M M(II)/(III)-0.001M EDTA-0.001M÷0.002M NaOH system, the anion exchangers in question can be arranged as follows:

0.001M M(II)/(III) – 0.001M EDTA – 0.001 M NaOH:

Lewatit Mono Plus M 500 in the Cl⁻ form > Lewatit Mono Plus M 500 in the H₂edta²⁻ form > Lewatit Mono Plus MP 500 in the Cl⁻ form > Lewatit Mono Plus MP 500 in the H₂edta²⁻ form;

0.001M M(II)/(III) – 0.001M EDTA – 0.002 M NaOH:

Lewatit Mono Plus M 500 in the Cl⁻ form > Lewatit Mono Plus MP 500 in the Cl⁻ form > Lewatit Mono Plus M 500 in the H₂edta²⁻ form > Lewatit Mono Plus MP 500 in the H₂edta²⁻ form.

As follows from the comparison of sorption of the above mentioned complexes on these anion exchangers, distribution coefficients increase only for the chloride form of monodisperse anion exchangers, with the increasing pH of the model system (Fig. 3). However for the versenian form the distribution coefficients of the above complexes decrease.

The exemplary comparison of the weight (D_g) distribution coefficients of Cu(II) complexes with EDTA on Lewatit Mono Plus M 500 and Lewatit MonoPlus MP 500 in the Cl⁻ and H₂edta²⁻ forms is presented in Fig. 3.

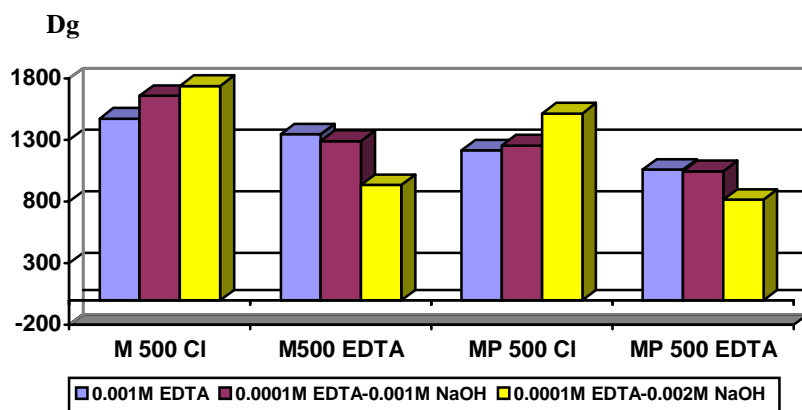


Fig. 3. Comparison of weight (D_g) distribution coefficients of Cu(II) complexes with EDTA on Lewatit Mono Plus M 500 and Lewatit MonoPlus MP 500 in the Cl⁻ and H₂edta²⁻ forms.

The obtained results are also confirmed by the studies of sorption of the Cu(II), Fe(III), Co(II) and Ni(II) complexes with EDTA in the pH range from 2,0 to 6,0 using the static method, at the constant phase contact time which is 24h. With the increasing pH of the starting model solution, the values of recovery factors (%R) of metal ions on the anion exchangers Lewatit Mono Plus M 500 and Lewatit Mono Plus MP 500 in the chloride form increase. Therefore in the next stage, the investigations of sorption by static method depending on the phase contact time were carried out in the 0.001M M(II)/(III)-0.001M EDTA and 0.001M M(II)/(III)-0.001M EDTA-0.001 M÷0.002 M NaOH systems using the above mentioned anion exchangers. The values of recovery factors (%R) of Cu(II) complexes with EDTA in the the 0.001M M(II)/(III)-0.001M EDTA determined for the ion exchangers in question are presented in Fig. 4.

As follows from the comparison of the obtained results in the case of sorption of Cu(II), Co(II) and Ni(II) complexes with EDTA the recovery factors assume almost 100% values in the aqueous solutions as well as with the addition of 0.001M NaOH and 0.002M NaOH for the anion exchangers Lewatit Mono Plus M 500 and Lewatit Mono Plus MP 500 in the chloride form and evidently decrease for the anion exchangers in the versenian form.

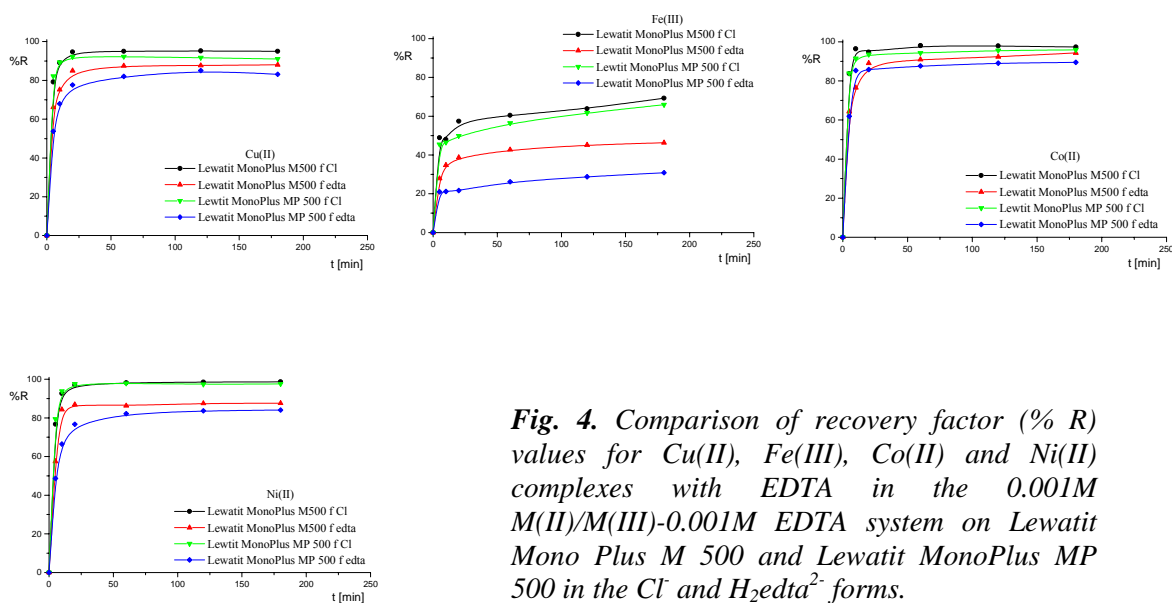


Fig. 4. Comparison of recovery factor (% R) values for Cu(II), Fe(III), Co(II) and Ni(II) complexes with EDTA in the 0.001M M(II)/M(III)-0.001M EDTA system on Lewatit Mono Plus M 500 and Lewatit MonoPlus MP 500 in the Cl⁻ and H₂edta²⁻ forms.

This confirms the competitive sorption of anion complexes of the [M(edta)]²⁻ and [M(Hedta)]⁻ types (formed at pH >3.0) compared with the neutral complexes of the [M(H₂edta)] type. The equilibrium state of sorption for the anion complexes of Cu(II), Co(II) and Ni(II) with EDTA occurs at the ion exchanger solution phase contact time about 60 min. However, the recovery factors of the Fe(III) complexes are lower (values below 70 % at the phase contact time 180 min. for all model systems under investigations).

CONCLUSION

1. The research results indicate high affinity of the anion exchangers Lewatit Mono Plus M 500 and Lewatit Mono Plus MP 500 in the chloride form towards the copper(II) complexes with EDTA. These anion exchangers can be applied in the removal of copper(II) complexes from waters and wastewaters.
2. Differences in affinity of Cu(II) complexes with EDTA for anion exchangers in individual systems are probably due to physicochemical properties of these anion exchangers (porosity of ion exchanger skeleton), kind of form in which it is used as well as to structure of complexes and their stability.

REFERENCES

- [1]. C.G. van Ginkel , K.L. Vandenbroucke , C.A. Stroo, *Bioresource Technology*, 59 (1997) 151.
- [3a]. M. Sillanpää, *Chemosphere*, 33 (1996) 293.
- [3]. M. Sillanpää, M. L. Sihvonen, *Talanta*, 44 (1999) 1487.
- [4]. C. Randt, R. Wittlinger, W. Merz, *Fresenius J Anal. Chem.*, 346 (1993) 728-731.
- [5]. P. Kocot, A. Karocki, Z. Stasicka, *J. Photochem. Photobiol. A: Chem.*, 179 (2006) 176.
- [6]. N. Gschwind, *GWF Wasser Abwasser*, 133 (1992) 546.

PLUTONIUM-241 IN THE ENVIRONMENT - ANALYTICAL PROBLEMS OF DETERMINATION

Andrzej Komosa

Maria Curie-Skłodowska University, Department of Radiochemistry and Colloid Chemistry, Pl. M. C. Skłodowskiej 3, 20-031 Lublin, Poland

Introduction

Plutonium isotopes appeared in the environment as a result of nuclear weapon testing in the atmosphere up to the eighties of past century. Another source of plutonium was Chernobyl disaster in 1986. Occurrence and migration of alpha emitting plutonium isotopes (^{238}Pu , $^{239+240}\text{Pu}$) in various element of the environment was relatively well examined owing to numerous researches on radiochemical methods of plutonium separation and determination using alpha spectrometry with silicon detectors.

However, among plutonium isotopes exists also beta emitting one, ^{241}Pu , which initial introduced activity was ten times higher. Until recently this isotope was not determined frequently because of weak beta radiation emitted. Its presence is important as it decays relatively quickly ($T_{1/2} = 14.4 \text{ y}$) to alpha radiating ^{241}Am . Data of real environment contamination with ^{241}Pu are limited, especially concerning a global fallout. Literature values of activity are diverse and involve mainly local, single immissions of ^{241}Pu . Additionally, as a result of differences in half-live of plutonium isotopes the ratio $^{241}\text{Pu}/^{239+240}\text{Pu}$ is not stable, what makes difficult a comparison between obtained values of activity [1].

Up till now the ^{241}Pu determination was based on alpha radioactivity measurement of ^{241}Am ingrown in the sample [2, 3]. Such methods required two alpha spectrometric measurements in a large time interval. Therefore, it was not useful for quick determination. At present, using ultra low-level spectrometer with liquid scintillator Quantulus (Wallac-Perkin-Elmer), a direct measurement of ^{241}Pu beta radiation is possible. However, it requires proper plutonium separation procedures to be developed. The procedure should enable to introduce a sample directly to liquid scintillation vial for beta radiation measurement [1, 4].

The aim of the paper is to present elaborated procedures for direct ^{241}Pu determination in various samples from environment and their optimization.

Experimental

Three different procedures for separation of plutonium from environmental samples were tested. The purpose was to elaborate optimal procedure for direct determination of ^{241}Pu . Alpha spectrometer Canberra 7401 with PIPS detector was used for alpha plutonium determination and Quantulus (Wallac-Perkin-Elmer) for measurement of total alpha (in channels 600-805) and weak beta radiation of ^{241}Pu (channels 5-265). Standard solution of ^{242}Pu was used for radiochemical yield determination. Alpha spectrometry measurements were usually performed within 600,000 s and these using LS spectrometer within 600 min. LS measurements were performed after 24-hour sample conditioning in a dark and low temperature (inside the spectrometer) to avoid chemiluminescence, which usually occurs in a low-energy region

of a spectrum. Used scintillation vials were made of teflon-coated polyethylene, which ensure a low background and stable conditions during counting.

Results

The best results of plutonium determination were obtained using two-step separation: first one leading to preparation of a source for alpha spectrometry followed by second - chemical treatment and liquid scintillation measurement. Total procedure consists of thermal sample mineralization, hydrochloric acid leaching, two stage co-precipitation (with ferric hydroxide and calcium oxalate) next anion-exchange separation of plutonium and electrodeposition on steel plate. A source prepared in this way was submitted to alpha spectrometric determination of ^{238}Pu and $^{239+240}\text{Pu}$.

The second step of the procedure involved re-dissolution of plutonium from the plate with nitric acid and liquid extraction using TOPO/cyclohexane solution. Organic phase, after neutralization, was introduced to liquid scintillator (Permablend/toluene) and measured by Quantulus spectrometer. Specific activity of ^{241}Pu was calculated on a basis of count rate in beta and alpha channel range of Quantulus, alpha spectrometric count rate of the tracer and amount of ^{242}Pu tracer added before radiochemical treatment. The calculation was performed employing the equation below:

$$A_{\text{Pu-241}} = \frac{N_{\text{LSC}\beta} \cdot N_{\text{SP}\alpha} \cdot A_{242}}{N_{\text{LSC}\alpha} \cdot m \cdot E_{\text{LSC}} \cdot N_{242\text{SP}\alpha}}$$

where:

$N_{\text{LSC}\beta}$ = count rate of beta radiation by LS spectrometer in a channel range 2-265 [cpm];

$N_{\text{LSC}\alpha}$ = count rate of alpha radiation by LS spectrometer in a channel range 600-805 [cpm];

$N_{\text{SP}\alpha}$ = total count rate of alpha radiation as measured by alpha spectrometry with PIPS detector [cps];

E_{LSC} = counting efficiency of ^{241}Pu by LS spectrometer, calculated with tritium standard;

$N_{242\text{SP}\alpha}$ = count rate of alpha radiation of the tracer ^{242}Pu by alpha spectrometry [cps];

m = mass of the sample [g];

A_{242} = tracer ^{242}Pu activity [Bq].

Background was subtracted from all count rate values.

Other examined procedures comprised of thermal mineralization, acid leaching and two-step co-precipitation as before. However, in the next step direct liquid extraction of plutonium was performed. To remove impurities passed together with plutonium to organic phase two steps of purification were applied (acid washing), back-extraction to water phase (with HCl/HI) and next plutonium re-extraction. This procedure was simpler, but knowledge of total alpha emitting plutonium activity (determined from other sample) was necessary.

In third procedure the solution obtained by sample leaching was divided into two parts. First one (smaller volume) is treated for preparation of an alpha plutonium source for spectrometric measurement, and second for LS counting.

All three procedures were tested using soil and waste material samples and also reference material (IAEA-384) of known ^{241}Pu activity (information value).

Table 1 presents range of ^{241}Pu specific activity determined in various materials and isotopic ratios. Calculated activities were referred to a Chernobyl accident (May 1st, 1986) and this of IAEA-384 to reference date Aug. 1st, 1996.

Table 1. Range of ^{241}Pu concentrations [$\text{Bq}\cdot\text{kg}^{-1}$] in various samples

Sample	^{241}Pu [$\text{Bq}\cdot\text{kg}^{-1}$]	$^{241}\text{Pu}/^{239+240}\text{Pu}$
Lublin region, top soil, 0-10cm layer	1 - 7.4	4 - 5
Soil Bragin (Chernobyl), 0-5cm layer	820 - 1480	42 - 60
IAEA-375 (soil Brjansk)	6.8	19
IAEA-384 (sea sediment) measured value	48.5 ± 3.1	0.44
IAEA-384 - information value	66	0.56
IAEA-384 - confidence interval	48 - 188	
Waste of Spanish power plant	14000 - 17000	3.8 - 4

Literature data concerning ^{241}Pu concentration determined in the environment are poor [4, 5]. Therefore it is hard to compare obtained result with other, known data. There is also a lack of suitable reference materials to test and validate our procedures in a good manner.

References

1. A. Komosa, Fizykochemiczne problemy oznaczania i zachowanie się izotopów plutonu w środowisku z uwzględnieniem beta-promieniotwórczego ^{241}Pu . Wyd. Chemii UMCS, Rozprawy Habilitacyjne XL, Lublin 2003, s.178+XII
2. D. I. Strumińska, B. Skwarzec, ^{241}Pu concentration in southern Baltic Sea ecosystem. J. Radioanal.Nuclear Chem. 268 (2006) 59.
3. A. V. Muravitsky, V. F. Razbudey, V. V. Takarevsky, P. N. Vorona, Time-dependent ^{241}Am in the environment from decay of ^{241}Pu released in the Chernobyl accident. Appl. Radiat. Isot. 63 (2005) 487.
4. L. Liong Wee Kwong, J. Gastaud, J. La Rosa, S. H. Lee, P. P. Povinec, E. Wyse, Determination of ^{241}Pu in marine samples using co-precipitation with rare earth fluoride and liquid scintillation spectrometry. J. Radioanal.Nuclear Chem. 261 (2004) 283.
5. J. Moreno, J. J. La Rosa, P. R. Danesi, K. Burns, P. DeRegge, N. Vajda, M. Sinojmeri, Determination of ^{241}Pu by liquid-scintillation counting in the combined procedure for Pu radionuclides, ^{241}Am and ^{90}Sr analysis in environmental samples. Radioactivity and Radiochemistry 9 (1998) 35.

COMPARISON OF PLUTONIUM SEPARATION METHODS IN ORDER TO DETERMINE ITS CONCENTRATION IN ENVIRONMENTAL SAMPLES BY ALPHA SPECTROMETRY

Andrzej Komosa, Sylwia Michalik

Department of Radiochemistry and Colloid Chemistry, Maria Curie-Skłodowska University,
Pl. M. C. Skłodowskiej 3, 20-031 Lublin, Poland.

Introduction

Plutonium isotopes are still present in the environment, despite that their source were nuclear tests, intensively conducted in sixties of past century, and Chernobyl accident as well. They occur in different elements of environment. Because of low specific activity determination of Pu isotopes in environmental samples using alpha spectrometry requires special attention to sample preparation method in order to precisely separate Pu from other components of matrices.

In radiochemical practice a lot of various procedures of Pu separation are known. Most of them include extraction or solubilization of the sample, its concentration by successive co-precipitation with suitable carriers, next separation from carrier and residual contamination using anion exchange or extraction method as well as source preparation in solid, disc form [1, 2].

This paper presents results of determination of various environmental samples (soil, bones, eggshells, reference material) using the alpha spectrometer (Canberra) with PIPS detector. Radiochemical treatment of soil was performed using two different methods. They differed in the stage of sample mineralization (extraction by HCl or solubilization by HF), source preparation (electrodeposition or co-precipitation with NdF_3). On intermediate steps of both procedures also occurred some differences. The possibility of changing some of stages of both procedures and its influence on final result of Pu determination in order to improve the methods was studied.

Experimental and results

The first method of Pu separation was used to radiochemical treatment of soil, bones, eggshell and reference material samples [2]. In the first stage of this procedure a dried and ashed (450-500°C) sample was leached with 6M HCl. From obtained solution trace elements were co-precipitated with ferric hydroxide by 25% NH_4OH addition. The precipitate was dissolved in 6M HCl and then separated from Fe by co-precipitation with calcium oxalate at pH=3. Next, the precipitate was dried, ashed, dissolved in 12M HCl and then second co-precipitation with ferric hydroxide was performed. In the next stage, precipitate was dissolved in 8M HNO_3 , boiled on sand bath with NaNO_2 until nitric oxides disappeared. This stage allows to changing oxidation state of plutonium to the Pu^{4+} form. The solution was introduced on ion-exchange column filled with Dowex 1x8 (50-100 mesh) and equilibrated with 8M HNO_3 in order to exchange of chloride ions into nitrate ions. After sample is passed through the column, following solutions were introduced: 8M HNO_3 , 6M HCl and concentrated HCl in order to eliminate of trace elements (Th, Am) which disturb Pu determination. In final stage Pu was eluted from the column using concentrated HCl with 0,1M NH_4I , which changed plutonium oxidation stage to +3. Obtained solution was evaporated to dryness with aqua regia to

eliminate iodine and ammonium salts. Finally, Pu was electrodeposited onto stainless steel discs from 0,4M ammonium oxalate with 0,3M HCl and measured by alpha spectrometry. This procedure is presented on Figure 1.

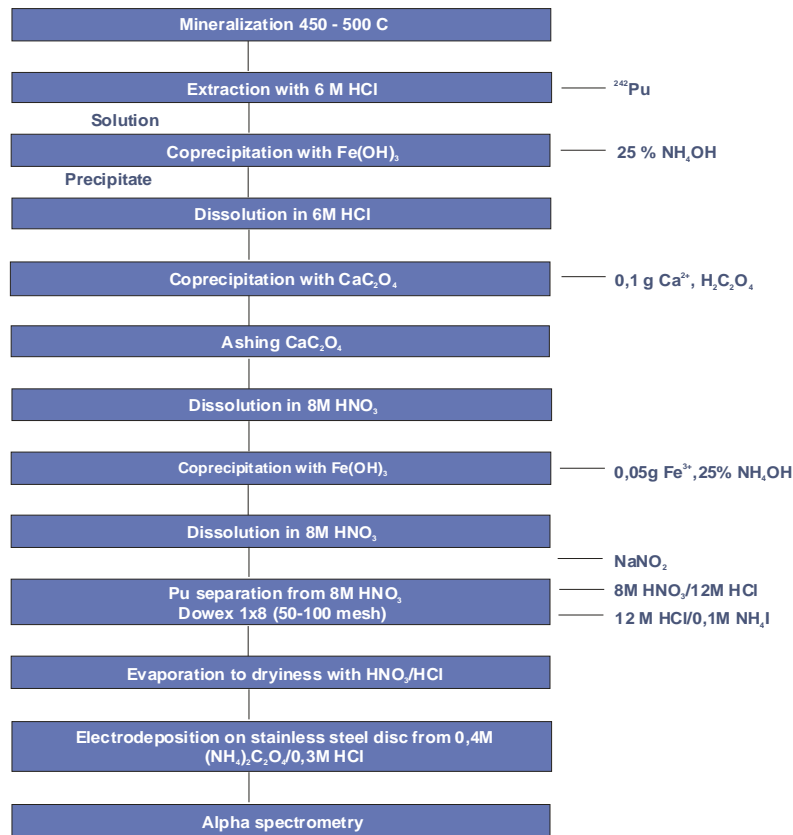


Figure 1. Procedure I of Pu separation from environmental samples

The second method differs generally in mineralization stage and preparation of source for alpha spectrometry [1]. Dried and ashed sample was dissolved in 23M HF, boiled, evaporated to dryness and next thrice dissolved in 14M HNO₃ and evaporated to a form of paste. In the next stage HF was eliminated from the solution using 2M HCl and H₃BO₃ added to the paste. After evaporation 14M HNO₃ was added and evaporated up to 10 ml, diluted to 0,1M HNO₃, bring to boiling and finally chilled. After filtration and before introduction the sample on anion exchange column Pu oxidation state was set. For this purpose hydrazine solution which reduces Fe⁺³ to Fe⁺⁴ was added. Subsequently 12M HCl was added and sample was boiled to decompose of hydrazine. Iron returning to the Fe⁺³ form reduces all Pu species to Pu⁺³ state. Next solution was boiling with NaNO₂ to oxidize Pu to Pu⁺⁴ and HNO₃ was added to 8M concentration. Pu was separated on Dowex 1x8 (50-100 mesh). Firstly 2M HNO₃ was introduced on the column, then 8M HNO₃ and finally the sample was added. Next, column was rinsed as follows: 8M HNO₃ and 10M HCl. Pu was eluted using hydroxylamine hydrochloric in 0.1M HCl. From this solution the source for alpha spectrometry measurement was preparing using co-precipitation with NdF₃ and deposition on membrane filter. Presented method of Pu separation was afterwards modified for treatment of samples of bones and eggshells. Ashed samples of bones and eggshells were dissolved in 14M HNO₃. From obtained solution Pu was co-precipitated with calcium oxalate. Dried and ashed precipitate was dissolved in 14M HNO₃ with addition of small amount of HCl and

evaporated to dryness. Next, sample was again dissolved in 14M HNO₃ and evaporated to 10 ml, whereby solution was complemented to 100 ml and filtrated. After filtration oxidation state of Pu was set. Above procedure is presented on Figure 2.

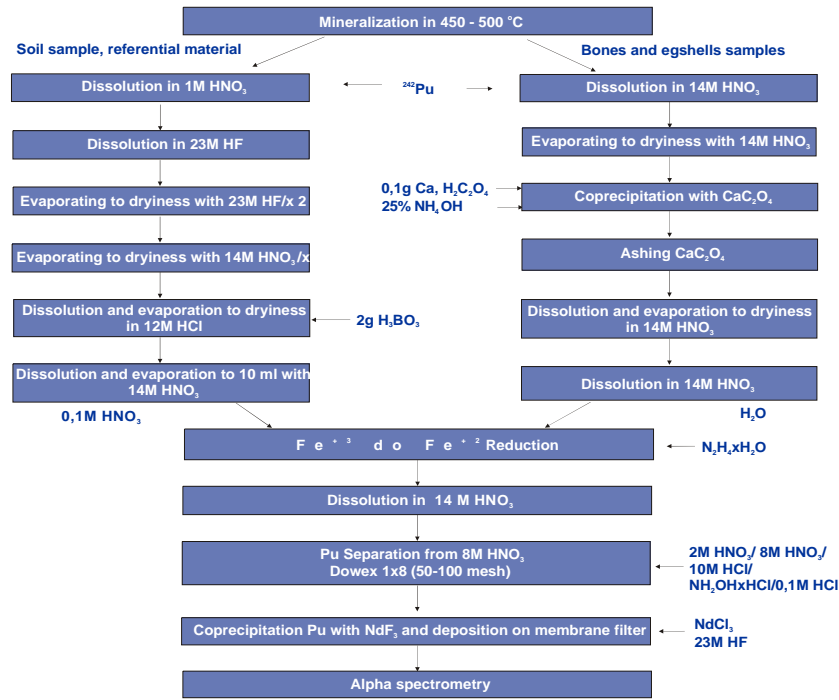


Figure 2. Procedure II of Pu separation from environmental samples

In Table 1 results of determination of ²³⁹⁺²⁴⁰Pu concentration in soil sample IAEA Soil-6 are presented. Sources for alpha spectrometry measurements were prepared by both electrodeposition and co-precipitation methods. Results demonstrate that higher efficiency of separation is observed for source prepared by co-precipitation with NdF₃.

Table 1. ²³⁹⁺²⁴⁰Pu determination in IAEA Soil-6 sample

Method of preparation	Efficiency [%]	²³⁹⁺²⁴⁰ Pu [Bq·kg ⁻¹]	Uncertainty [Bq·kg ⁻¹]	MDA [Bq·kg ⁻¹]
Co-precipitation with NdF ₃	60	1.048	0.084	0.041
Electrodeposition	35	1.116	0.106	0.060
Reference value		1.04	0.96 - 1.11 (confidence interval)	

The most important stage of presented methods was the source preparation for alpha spectrometry. Such sample should characterize by high stability, uniform distribution on the surface and small amount of analyzed material. Proper purification during radiochemical separation is extremely important, as well as high purity of used reagents. In Fig. 3 and 4 spectra of ²⁴²Pu tracer sample, obtained using HF from two different producers, are presented. Presence of alpha peaks of uranium isotopes (²³⁴U, ²³⁵U and ²³⁸U) were clearly visible in Fig. 4.

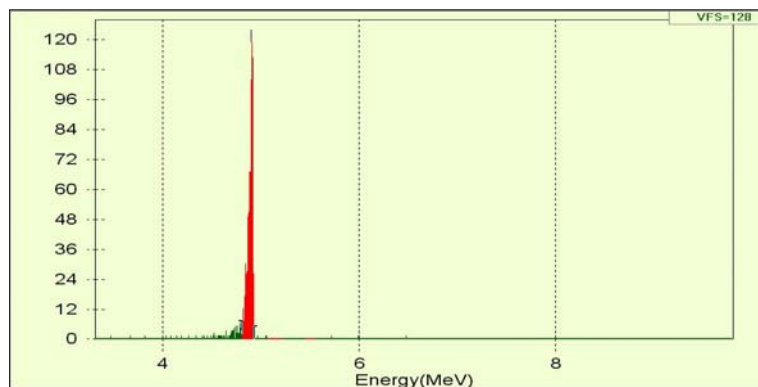


Figure 3. Spectrum of $^{239+240}\text{Pu}$ alpha radiation (test with HF of the first producer) (vertical axis - total counts).

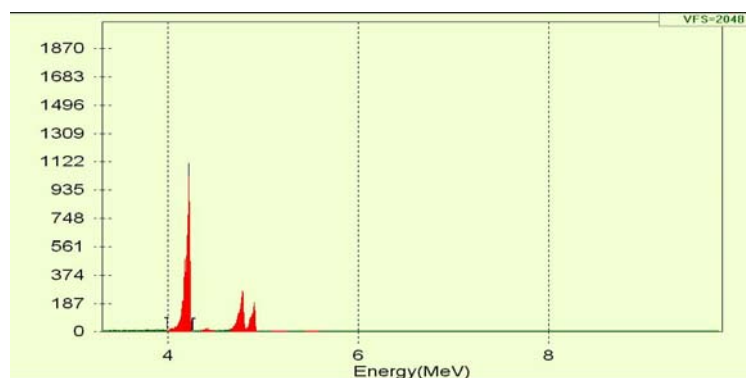


Figure 4. Spectrum of $^{239+240}\text{Pu}$ alpha radiation (test with HF of the second producer) (vertical axis - total counts).

Conclusions

Basing on our study is not possible to point definitely which method of sample preparation for alpha spectrometry is better. Both of them has its limitations and require different reagents and equipment. However, if they are properly and carefully performed both can give valuable results.

References

1. J. W. Mietelski - Nuclear spectrometry in the research of bioavailability of "fuel-like hot particles" in the forest environment. Institute of Nuclear Physics, Report 1921/B, Cracow 2003, pp.154 (in Polish).
2. A. Komosa - Physicochemical problems of plutonium isotope determination and its behavior in the environment including beta-radiated ^{241}Pu . M. Curie-Sklodowska University, Lublin 2003, pp.178 + XII (in Polish).

Acknowledgement

Presented study was supported in part by grant of Polish Ministry of Education and Sciences No. 3T09D 09129.

KIND OF SCINTILLATION COCKTAIL AND VIAL INFLUENCE ON ^{14}C MEASUREMENT PARAMETERS USING ULTRA LOW-LEVEL LIQUID SCINTILLATION SPECTROMETER QUANTULUS

Andrzej Komosa, Katarzyna Ślepecka

Maria Curie-Skłodowska University, Department of Radiochemistry and Colloid Chemistry, Pl. M. C. Skłodowskiej 3, 20-031 Lublin, Poland

Introduction

Modern spectrometers for radiation measurement using liquid scintillation technique are widely applied to beta emitting radionuclide determination, especially that of low energy radiation. Quantulus (Wallac-Perkin-Elmer) spectrometer, owing to sophisticated electronics (amplitude comparator and anticoincidence systems) being an active systems of background reduction, and a passive shielding made of lead enables to measure very low activity of beta radiation. For this purpose it is suitable to determining of beta emitting radioisotopes occurring in the environment [1].

Environmental samples preparation for LS measurements usually requires an application of multi-stage separation procedures for isolation of radionuclide to be determined. Insufficient separation from other contaminants being matrix components causes lowering of scintillation efficiency (so called quenching). For this reason, important factor in determination of specific activity is optimization of measurement conditions [2]. Quenching is the main disadvantageous factor in absolute activity determination. It is influenced by several factors as chemical composition of scintillation cocktail (usually precise composition is not known), its volume taken for measurement or chemical composition of the sample introduced to the cocktail.

Quantulus spectrometer, as scientific device is not equipped with a software containing calibration curves for particular radionuclide and scintillation cocktails. Therefore, it is necessary to perform studies on assessment a proper measurement parameters. Aim of presented research was comparing various scintillation cocktails regarding quenching, cocktail volume and kind of vial during measurements of ^{14}C .

Experimental

Count rate of background and standard solution (n-pentanol marked with ^{14}C) in high energy beta configuration of Quantulus was measured for five commercial scintillation cocktails and two other prepared by dissolution of scintillating substance in suitable solvent. Quenching level was adjusted by addition of CCl_4 to the counting vials (0-0.12 cm^3). Two types of scintillation vials were used: standard low-potassium glass (Packard) and low-diffusion PE (Perkin-Elmer). Volume of cocktail added to the vials varied from 2.5 to 15 cm^3 .

Count rate of ^{14}C was determined in a channel range of 100-600 and measuring time 15 min. Samples were stored inside the apparatus and quenching agent was added successively. Easy View software was used to view spectra and count rate calculation.

Chemical composition of liquid scintillation cocktails used (as specified by producers) is presented in Table 1.

Table 1. Chemical composition of scintillation cocktails (manufacturer's data) [3].

Cocktail	Producer	Solvent (+ emulsifier)	Scintillator
Insta Gel Plus	Packard	1,2,4-trimethylbenzen 55-60% ethoxilated alkylphenol 34-39%	2,5- diphenyloxazole (PPO) up to 1% 1,4-bis(2-methylstyryl)benzene (bis-MSB) up to 1%
Insta Fluor	Packard	o-ksylen 97-99% n-pentanol 1-2%	2,5- diphenyloxazole (PPO) up to 1% 1,4-bis(2-methylstyryl)benzene (bis-MSB) up to 1%
Permablend III*	Packard	Toluene >99%	2,5- diphenyloxazole (PPO) 91% 1,4-bis(2-methylstyryl)benzene (bis-MSB) 9%, 7g/dm ³
Butyl-PBD*	Fluka	Benzene >98%	2,(4-bifenylyl)-5-(4-tert-butylfenyl)-1,3,4-oksadiazol about 15g/dm ³
Ultima Gold AB Ultima Gold LLT	Packard	di-izopropylnaphtalene (DIN) 60-80% ethoxilated alkylphenol 20-40% 2-(2-butoxyethoxy)ethanol 2,5-10% fatty alcohol ethoxylate <2,5%	2,5- diphenyloxazole (PPO) <2,5% 1,4-bis(2-methylstyryl)benzene (bis-MSB) <2,5%
OptiPhase HiSafe3	Perkin-Elmer	di-izopropylnaphtalene (DIN) >60% poly(ethyleneglicol)mono(4-nonylphenyl)ether 25-30% alfa-fenyl-omega-hydroxypoly(oxo-1,2-ethanediyl) phosphate <10%	2,5-diphenyloxazole (PPO) <1% 1,4-bis(2-methylstyryl)benzene (bis-MSB) 0,1%

* - solid substance for preparation of liquid scintillation cocktail

Results

The results are presented as relationship of ¹⁴C standard solution count rate (cpm) versus quench parameter SQP or cocktail volume for two types of vials. It was found that examined scintillation cocktails reveal different susceptibility for quenching agent. For illustration, in Fig. 1 and 2 spectra of ¹⁴C in butyl-PBD and OptiPhase scintillating cocktails (respectively) at various quenching level are shown.

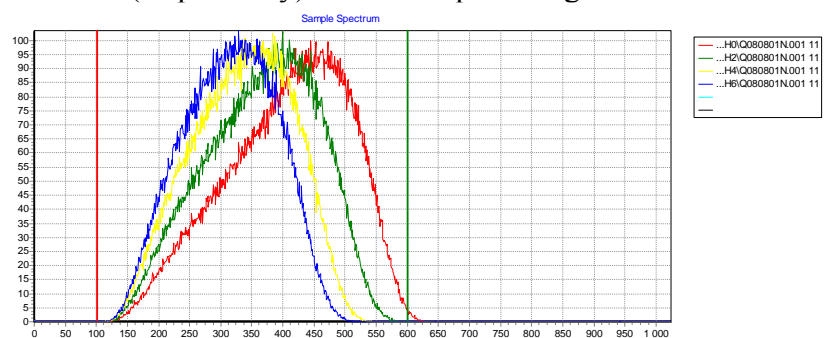


Fig. 1 Spectra of ¹⁴C standard in butyl-PBD with 0, 40, 80 and 120 µl of CCl₄ addition (15 ml, low-potassium glass vial).

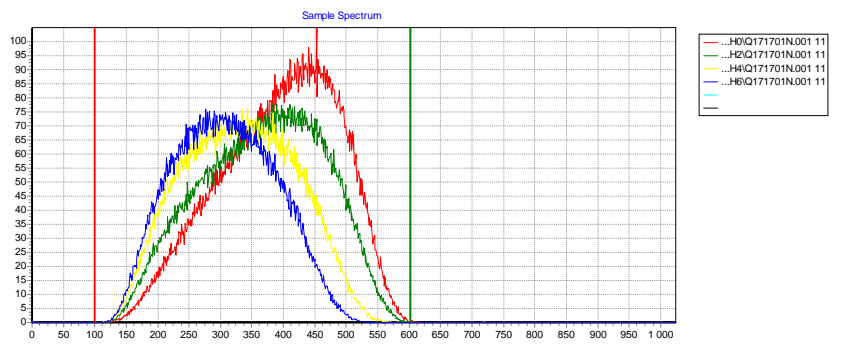


Fig. 2. Spectra of ^{14}C standard in OptiPhase HiSafe 3 with 0, 40, 80 and 120 μl of CCl_4 addition (low-potassium glass vial, 15 ml).

With increasing volume of cocktail quenching effect caused by CCl_4 addition was smaller as a result of smaller quenching agent concentration; however some cocktails are more sensitive for quenching. For example, in Figure 3 and 4 influence of cocktail volume on ^{14}C count rate is presented for Permablend III and butyl-PBD scintillators, respectively. First of them is the most sensitive for quenching with CCl_4 , but second one is the most stable.

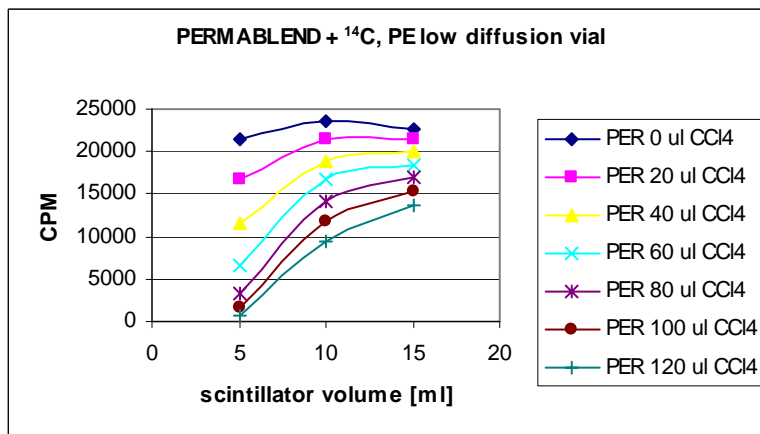


Fig. 3. Count rate of ^{14}C vs. Permablend scintillating cocktail volume.

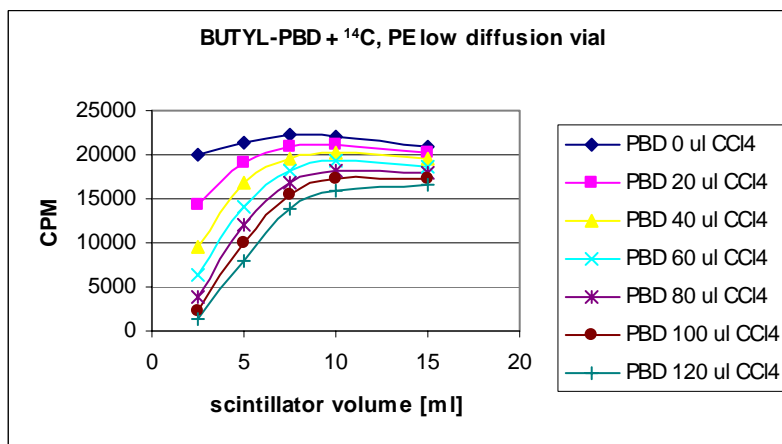


Fig. 4. Count rate of ^{14}C vs. butyl-PBD scintillating cocktail volume.

The scintillating cocktails revealed also different liability for quenching, what is visible in Fig. 5 and 6 in a form of relationship ^{14}C count rate vs. SQP parameter for low (20 μl CCl_4) and high quenching (120 μl CCl_4) at various scintillator volume.

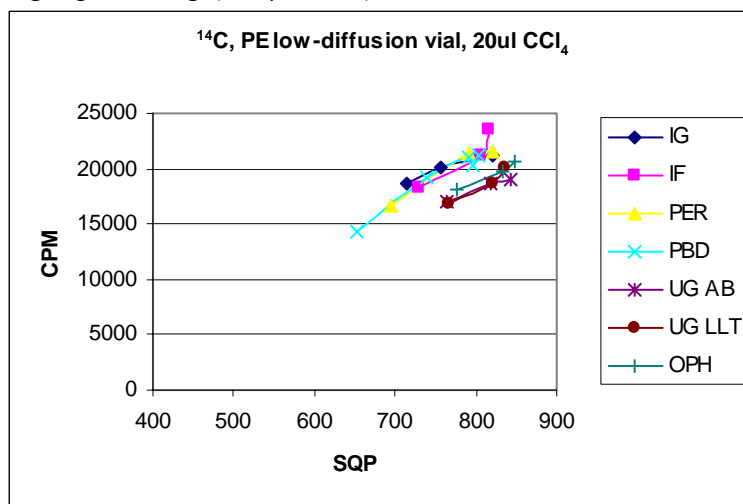


Fig. 5. Count rate of ^{14}C vs. quench level (SQP) with addition of 20 μl CCl_4 .

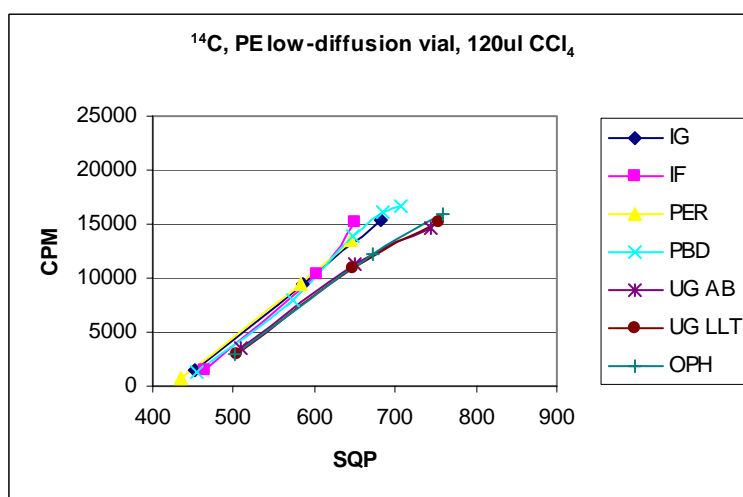


Fig. 6. Count rate of ^{14}C vs. quench level (SQP) with addition of 120 μl of CCl_4 .

Conclusions

Quenching agent addition to scintillator vial has more distinct influence on small cocktail volume, but this relationship is not linear. The most susceptible to quench is Permablend III scintillating cocktail, on the contrary butyl-PBD is the most stable one.

At high quenching level scintillating cocktail sensibility for quench is similar, but InstaFluor, butyl-PBD and Permablend reveal higher resistance.

References

1. <http://las.perkinelmer.com/content/RelatedMaterials/SpecificationSheets>
2. Liquid Scintillation Counting and Organic Scintillators, H. Ross, J. E. Noakes, J. D. Spaulding (Eds.), Lewis Publ., Chelsea, USA 1991.
3. <http://las.perkinelmer.com/Catalog/default.htm?CategoryID=Liquid+Scintillation+Cocktails>

ARYLPIPERAZINYL DERIVATIVES OF CYCLIC IMIDES CONTAINING THE ANTHRACENE SYSTEM AS POTENTIAL AN ANXIOLYTICS

Jerzy Kossakowski, Magdalena Pakosińska-Parys

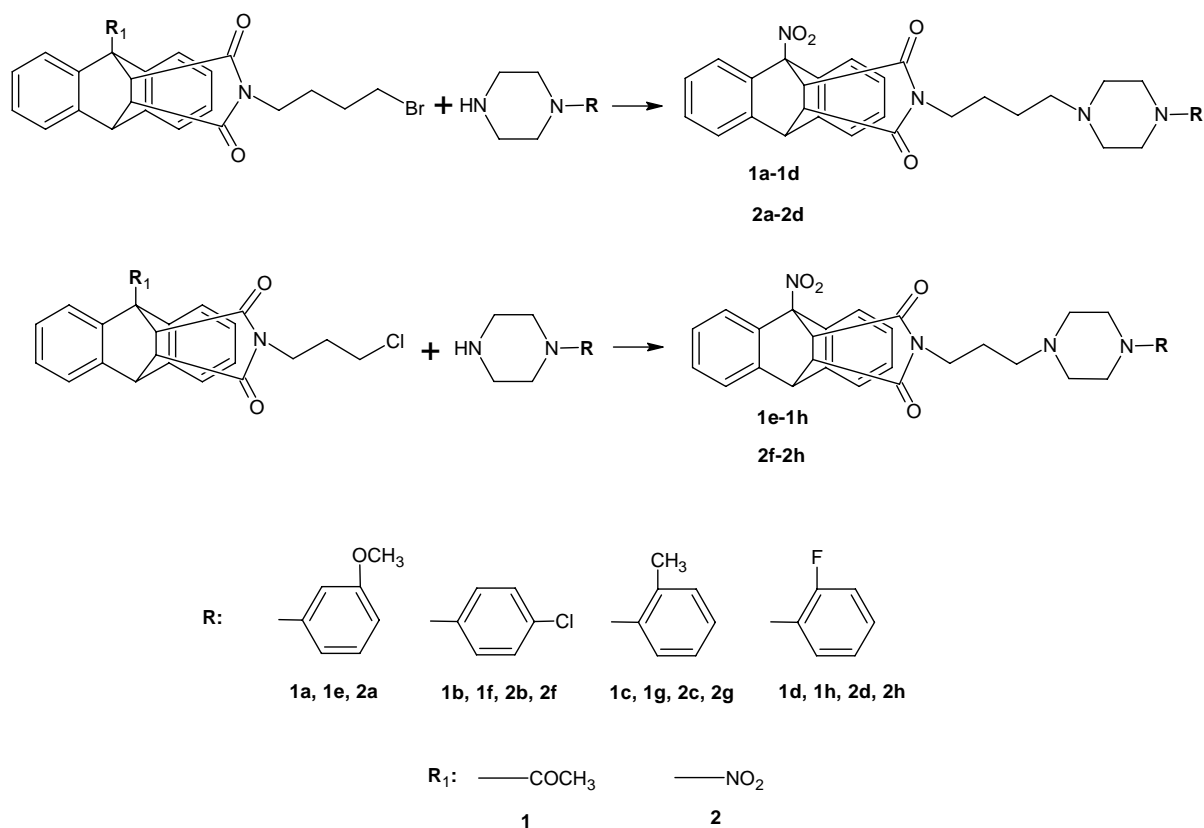
Department of Medical Chemistry, The Medical University of Warsaw, 3 Oczki Street,
02-007 Warsaw, Poland

Introduction

Anxiolytic drugs without side effects are still being sought. New kinds of drugs from this group, without benzodiazepine-related side effects, such as: addiction, drowsiness, convulsion, muscle relaxation, are derivatives of buspirone, which demonstrate efficiency similar to diazepam. During the last years it has been reported that some derivatives of certain isoindole which possess the aryl-1-piperazinealkyl group linked with the imide nitrogen, produce activation of central serotonin system [1] and have anxiolytic or antidepressive activity [2].

Maprotiline and benzoctamine, drugs derived from anthracene, present anxiolytic and antidepressive activity.

Looking for a new group of anxiolytic drugs we decided to link the anthracene system of maprotiline or benzoctamine with aryl-1-piperazinealkyl group to achieve better activity. This group is a part of the buspirone molecule and is considered to be responsible for pharmacological activity [3-6].



Scheme 1. Scheme of the reactions

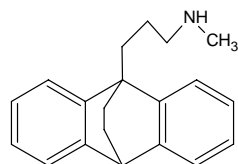


Figure 1. maprotiline

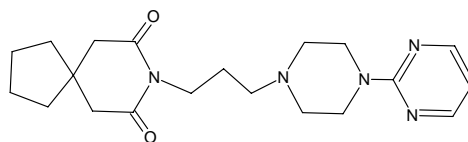


Figure 2. buspirone

EXPERIMENTAL

Chemistry. Melting points were determined in a capillary Kofler's apparatus and are uncorrected. The ^1H NMR spectra were recorded on a Bruker DMX400 spectrometer, operating at 400.13 MHz for ^1H . The chemical shift values, expressed in ppm, were references downfield to TMS at ambient temperature. All values of microanalysis were within $\pm 0.4\%$ of the calculated compositions. Column flash chromatography and TLC were performed on silica gel 60 (Merck) using chloroform or chloroform/methanol (9:1) mixture as eluent.

Physical and ^1H NMR spectral data of compounds 1a-1h and 2a-2h.

1a. Yield 56 %, m.p. 134.1°C ^1H NMR (CDCl_3) δ (ppm): 7.75 (d, $J=7.2\text{Hz}$, 1H, CHarom), 7.42 (d, $J=6.8\text{Hz}$, 1H, CHarom), 7.16 (m, 6H, CHarom), 7.04 (d, $J=7.2\text{Hz}$, 1H, CHarom), 6.53 (d, $J=8\text{Hz}$, 1H, CHarom), 4.75 (s, 1H, CH), 3.88 (m, 1H, CH), 3.84 (s, 3H, OCH_3), 3.33 (m, 7H, CH, CH_2 , CH_2 piperidine), 3.08 (t, $J=6.8\text{Hz}$, 2H, CH_2), 2.88 (s, 3H, CH_3), 2.68 (m, 4H, CH_2 piperidine), 1.28 (m, 2H, CH_2), 0.88 (m, 2H, CH_2). $\text{C}_{35}\text{H}_{37}\text{N}_3\text{O}_4 \cdot \frac{1}{2}\text{H}_2\text{O}$ (590,71): calcd. C 71.16, H 6.79, N 7.11; found C 71.16, H 6.69, N 7.15.

1b. Yield 60 %, m.p. 156.5°C ^1H NMR (CDCl_3) δ (ppm): 7.75 (d, $J=7.2\text{Hz}$, 1H, CHarom), 7.42 (d, $J=7.2\text{Hz}$, 1H, CHarom), 7.18 (m, 7H, CHarom), 7.06 (d, $J=7.2\text{Hz}$, 1H, CHarom), 6.83 (d, $J=8.4\text{Hz}$, 2H, CHarom), 4.75 (m, 1H, CH), 3.84 (d, $J=8.4\text{Hz}$, 1H, CH), 3.31 (m, 5H, CH, CH_2 piperidine), 3.07 (t, $J=7\text{Hz}$, 2H, CH_2), 2.88 (s, 3H, CH_3), 2.67 (m, 4H, CH_2 piperidine), 2.36 (m, 2H, CH_2), 1.26 (m, 2H, CH_2), 0.87 (m, 2H, CH_2). $\text{C}_{34}\text{H}_{35}\text{Cl}_2\text{N}_3\text{O}_3 \cdot \frac{1}{2}\text{H}_2\text{O}$ (613,57): calcd. C 70.76, H 6.11, N 7.28; found C 70.74, H 6.04, N 7.27.

1c. Yield 58 %, m.p. 122.3°C ^1H NMR (CDCl_3) δ (ppm): 7.76 (d, $J=7.2\text{Hz}$, 1H, CHarom), 7.42 (d, $J=7.2\text{Hz}$, 1H, CHarom), 7.2 (m, 7H, CHarom), 7.04 (m, 3H, CHarom), 4.76 (s, 1H, CH), 3.84 (d, $J=8.4\text{Hz}$, 1H, CH), 3.33 (m, 1H, CH), 3.07 (m, 8H, CH_2 , CH_2 piperidine), 2.88 (s, 3H, CH_3), 2.50 (m, 4H, CH_2 piperidine), 2.29 (s, 3H, CH_3), 1.26 (m, 2H, CH_2), 0.87 (m, 2H, CH_2). $\text{C}_{35}\text{H}_{37}\text{N}_3\text{O}_3$ (547,97): calcd. C 76.75, H 6.81, N 7.67; found C 75.01, H 7.19, N 7.48.

1d. Yield 61 %, m.p. 174°C ^1H NMR (CDCl_3) δ (ppm): 7.77 (d, $J=7.2\text{Hz}$, 1H, CHarom), 7.42 (d, $J=6.8\text{Hz}$, 1H, CHarom), 7.18 (m, 10H, CHarom), 4.75 (m, 1H, CH), 3.92 (d, $J=8.4\text{Hz}$, 1H, CH), 3.78 (m, 2H, CH_2), 3.50 (m, 6H, CH_2 , CH_2 piperidine), 3.39 (m, 1H, CH), 3.14 (m, 4H, CH_2 piperidine), 2.88 (s, 3H, CH_3), 1.55 (m, 2H, CH_2), 1.02 (m, 2H, CH_2). $\text{C}_{34}\text{H}_{35}\text{ClFN}_3\text{O}_3 \cdot \frac{1}{2}\text{H}_2\text{O}$ (597,10): calcd. C 68.39, H 6.07, N 7.03; found C 68.57, H 5.95, N 7.03.

1e. Yield 57 %, m.p. 138°C ^1H NMR (CDCl_3) δ (ppm): 7.79 (m, 1H, CHarom), 7.43 (d, $J=7.2\text{Hz}$, 1H, CHarom), 7.26 (m, 9H, CHarom), 7.05 (d, $J=7.2\text{Hz}$, 1H, CHarom), 4.74 (m, 1H, CH), 4.33 (m, 2H, CH_2), 3.90 (d, $J=8\text{Hz}$, 1H, CH), 3.83 (s, 3H, OCH_3), 3.50 (m, 9H, CH, CH_2 piperidine), 2.86 (s, 3H, CH_3), 2.54 (m, 2H, CH_2), 1.57 (m, 2H, CH_2). $\text{C}_{34}\text{H}_{36}\text{ClN}_3\text{O}_4 \cdot 2\frac{1}{2}\text{H}_2\text{O}$ (631,16): calcd. C 64.70, H 6.54, N 6.65; found C 64.75, H 6.13, N 6.85.

1f. Yield 63 %, m.p. 177.2°C ^1H NMR (DMSO) δ (ppm): 7.67 (m, 1H, CHarom), 7.57 (d, $J=7.2\text{Hz}$, 1H, CHarom), 7.19 (m, 7H, CHarom), 7.01 (m, 3H, CHarom), 4.81 (m, 1H, CH), 4.12 (d, $J=8.4\text{Hz}$, 1H, CH), 3.80 (d, $J=12.8\text{Hz}$, 2H, CH_2), 3.40 (m, 1H, CH), 3.30 (m, 2H, CH_2), 3.14 (t, $J=12\text{Hz}$, 2H, CH_2 piperidine), 3.03 (t, $J=6.8\text{Hz}$, 2H, CH_2 piperidine), 2.93 (m,

2H, CH₂ piperidine), 2.82 (s, 3H, CH₃), 2.67 (m, 2H, CH₂ piperidine), 1.82 (m, 2H, CH₂). C₃₃H₃₄Cl₃N₃O₃ · ½H₂O (635,99): calcd. C 62.32, H 5.86, N 6.6; found C 62.18, H 5.46, N 6.69.

1g. Yield 55 %, m.p. 239°C ¹H NMR (DMSO) δ(ppm): 7.71 (m, 1H, CHarom), 7.60 (d, J=7.2Hz, 1H, CHarom), 7.25 (m, 7H, CHarom), 7.00 (m, 3H, CHarom), 4.83 (m, 1H, CH), 4.13 (d, J=8.4Hz, 1H, CH), 3.43 (m, 6H, CH₂ piperidine, CH₂), 3.35 (s, 6H, CH₃), 3.17 (m, 1H, CH), 3.03 (m, 4H, CH₂ piperidine), 2.70 (m, 2H, CH₂), 1.10 (m, 2H, CH₂). C₃₄H₃₆ClN₃O₃ · ½H₂O (588,13): calcd. C 69.40, H 6.70, N 7.11; found C 69.43, H 6.51, N 7.14.

1h. Yield 59 %, m.p. 179.3°C ¹H NMR (CDCl₃) δ(ppm): 7.84 (d, J=7.2Hz, 1H, CHarom), 7.43 (d, J=7.2Hz, 1H, CHarom), 7.23 (m, 10H, CHarom), 4.76 (m, 1H, CH), 3.91 (d, J=8.8Hz, 1H, CH), 3.67 (t, J=12Hz, 2H, CH₂), 3.44 (m, 4H, CH₂ piperidine), 3.38 (m, 1H, CH), 2.88 (s, 3H, CH₃), 2.50 (m, 4H, CH₂ piperidine), 1.89 (m, 2H, CH₂), 1.70 (m, 2H, CH₂). C₃₃H₃₃ClFN₃O₄ · 1 3/4H₂O (605,60): calcd. C 65.44, H 5.78, N 6.94; found C 65.29, H 6.11, N 7.29.

2a. Yield 61 %, m.p. 176.1°C ¹H NMR (CDCl₃) δ(ppm): 7.7 (d, J=7.2Hz, 1H, CHarom), 7.46 (d, J=6.8Hz, 1H, CHarom), 7.30 (m, 5H, CHarom), 7.09 (d, J=7.2Hz, 1H, CHarom), 6.61 (m, 4H, CHarom), 4.82 (m, 1H, CH), 4.34 (d, J=8.8Hz, 1H, CH), 3.8 (s, 3H, CH₃), 3.42 (m, 7H, CH₂ piperidine, CH, CH₂), 3.1 (m, 4H, CH₂ piperidine), 2.9 (m, 2H, CH₂), 1.59 (m, 2H, CH₂), 1.03 (m, 2H, CH₂). C₃₅H₃₇N₃O₄ · 2½H₂O (648,14): calcd. C 60.61, H 6.04, N 8.83; found C 60.87, H 5.84, N 8.69.

2b. Yield 56 %, m.p. 209.8°C ¹H NMR (CDCl₃) δ(ppm): 7.72 (d, J=6.4Hz, 1H, CHarom), 7.46 (d, J=6.8Hz, 1H, CHarom), 7.33 (m, 9H, CHarom), 7.1 (d, J=7.2Hz, 1H, CHarom), 4.8 (s, 1H, CH), 4.36 (d, J=6.8Hz, 1H, CH), 4.1 (m, 2H, CH₂), 3.48 (m, 7H, CH₂ piperidine, CH, CH₂), 3.0 (m, 4H, CH₂ piperidine), 1.56 (m, 2H, CH₂), 1.06 (m, 2H, CH₂). C₃₂H₃₂Cl₂N₄O₄ · 3H₂O (661,56): calcd. C 58.09, H 5.78, N 8.77; found C 57.82, H 5.65, N 9.16.

2c. Yield 60 %, m.p. 218.2°C ¹H NMR (CDCl₃) δ(ppm): 7.7 (d, J=5.6Hz, 1H, CHarom), 7.46 (d, J=6.8Hz, 1H, CHarom), 7.3 (m, 5H, CHarom), 7.2 (m, 2H, CHarom), 7.06 (m, 3H, CHarom), 4.8 (s, 1H, CH), 4.37 (d, J=8.8Hz, 1H, CH), 3.6 (m, 4H, CH₂), 3.47 (d, J=8.8Hz, 1H, CH), 3.08 (m, 8H, CH₂ piperidine), 2.3 (s, 3H, CH₃), 1.6 (m, 2H, CH₂), 1.06 (m, 2H, CH₂). C₃₃H₃₆Cl₂N₄O₄ · 2½H₂O (668,60): calcd. C 59.28, H 6.18, N 8.38; found C 59.07, H 5.66, N 8.07.

2d. Yield 58 %, m.p. 201.7°C ¹H NMR (CDCl₃) δ(ppm): 7.7 (d, J=8Hz, 1H, CHarom), 7.46 (d, J=6.8Hz, 1H, CHarom), 7.29 (m, 5H, CHarom), 7.02 (m, 5H, CHarom), 4.82 (m, 1H, CH), 4.37 (d, J=8.8Hz, 1H, CH), 3.62 (m, 4H, CH₂ piperazine), 3.47 (m, 3H, CH, CH₂), 3.06 (m, 6H, CH₂ piperidine, CH₂), 1.62 (m, 2H, CH₂), 1.04 (m, 2H, CH₂). C₃₂H₃₂ClFN₄O₄ · 3H₂O (645,12): calcd. C 59.57, H 5.93, N 8.68; found C 59.14, H 5.62, N 8.72.

2f. Yield 55 %, m.p. 182°C ¹H NMR (DMSO) δ(ppm): 7.66 (d, J=7.2Hz, 1H, CHarom), 7.60 (m, 1H, CHarom), 7.35 (m, 7H, CHarom), 7.01 (d, J=8.4Hz, 3H, CHarom), 4.99 (m, 1H, CH), 4.36 (d, J=8.8Hz, 1H, CH), 3.80 (d, J=12.8Hz, 2H, CH₂), 3.52 (m, 1H, CH), 3.30 (d, J=11.2Hz, 2H, CH₂ piperidine), 3.16 (t, J=11.6Hz, 2H, CH₂ piperidine), 3.04 (m, 4H, CH₂ piperidine), 2.73 (m, 2H, CH₂), 1.2 (m, 2H, CH₂). C₃₁H₃₀Cl₂N₄O₄ · 3H₂O (647,55): calcd. C 57.50, H 5.60, N 8.65; found C 57.68, H 5.68, N 8.16.

2g. Yield 60 %, m.p. 190°C ¹H NMR (CDCl₃) δ(ppm): 7.75 (d, J=6.8Hz, 1H, CHarom), 7.46 (d, J=7.2Hz, 1H, CHarom), 7.18 (m, 10H, CHarom), 4.82 (m, 1H, CH), 4.30 (d, J=8.8Hz, 1H, CH), 3.39 (m, 1H, CH), 3.19 (t, J=7Hz, 2H, CH₂), 3.04 (m, 4H, CH₂ piperidine), 2.7 (m, 4H, CH₂ piperidine), 2.26 (s, 5H, CH₂, CH₃), 1.25 (m, 2H, CH₂). C₃₂H₃₃ClN₄O₄ · 1 1/4H₂O (595,60): calcd. C 68.73, H 6.21, N 10.02; found C 68.72, H 5.77, N 9.64.

2h. Yield 54 %, m.p. 185.4°C ¹H NMR (CDCl₃) δ(ppm): 7.77 (m, 1H, CHarom), 7.46 (d, J=6.8Hz, 1H, CHarom), 7.34 (m, 5H, CHarom), 7.08 (m, 5H, CHarom), 4.82 (m, 1H, CH),

4.38 (d, J=9.2Hz, 1H, CH), 3.64 (t, J=11.8Hz, 2H, CH₂), 3.46 (m, 2H, CH₂ piperidine, CH), 3.0 (m, 4H, CH₂ piperidine), 2.63 (m, 2H, CH₂), 1.76 (m, 2H, CH₂).
C₃₁H₃₀ClFN₄O₄ · 1H₂O (595,05): calcd. C 62.57, H 5.42, N 9.41; found C 62.60, H 5.28, N 9.18.

Procedure of receipt of relationship compound 1 became published [6].

GENERAL PROCEDURE OF PREPARING N-[4-(4-ARYL-1-PIPERAZINYL)-BUTYL]-1-ACETYLDIBENZO-[e.h]-BICYCLO[2.2.2]-OCTANE-2,3-DICARBOXIMIDE [1a-1d] and N-[4-(4-ARYL-1-PIPERAZINYL)-BUTYL]-1-NITRODIBENZO-[e.h]-BICYCLO[2.2.2]-OCTANE-2,3-DICARBOXIMIDE [2a-2h]

A mixture of the compound **1 or 2** (1.2-1g, 2.94-2.45 mmol), anhydrous K₂CO₃ (1.2-1g, 8.69-7.24 mmol), KI (0.2 g, 1.0 mmol) and the corresponding N-substituted piperazine (0.97-0.44 g, 5.95-2.44 mmol) was refluxed in acetonitrile (30-50 ml) for 50 h. When the reaction was complete by TLC (silica gel, developing system: chloroform:methanol) the mixture was filtered and the solvent was evaporated.

GENERAL PROCEDURE OF PREPARING N-[3-(4-ARYL-1-PIPERAZINYL)PROPYL]-1-ACETYLDIBENZO-[e.h]-BICYCLO[2.2.2]-OCTANE-2,3-DICARBOXIMIDE [1e-1h] and N-[3-(4-ARYL-1-PIPERAZINYL)PROPYL]-1-NITRODIBENZO-[e.h]-BICYCLO[2.2.2]-OCTANE-2,3-DICARBOXIMIDE [2e-2h]

A mixture of the compound **1 or 2** (0.9g, 2.05 mmol), anhydrous K₂CO₃ (0.9g, 6.52 mmol), KI (0.2 g, 1.0 mmol) and the corresponding N-substituted piperazine (0.37-0.72 g, 2.05-4.09 mmol) was refluxed in acetonitrile (50 ml) for 50 h. When the reaction was complete by TLC (silica gel, developing system: chloroform:methanol) the mixture was filtered and the solvent was evaporated.

Results and discussion

In this study we have presented the synthesis of 15 new derivatives of arylpiperazine for potential use in the treatment and anxiety.

Conclusion

Fifteen new N-substituted derivatives of N-[4-(4-aryl-1-piperazinyl)-butyl]-1-acetyldibenzo-[e.h]-bicyclo[2.2.2]-octane-2,3-dicarboximide, N-[4-(4-aryl-1-piperazinyl)-butyl]-1-nitrodibenzo-[e.h]-bicyclo[2.2.2]-octane-2,3-dicarboximide and N-[3-(4-aryl-1-piperazinyl)propyl]-1-acetyldibenzo-[e.h]-bicyclo[2.2.2]-octane-2,3-dicarboximide and N-[3-(4-aryl-1-piperazinyl)propyl]-1-nitrodibenzo-[e.h]-bicyclo[2.2.2]-octane-2,3-dicarboximide was obtained.

References

- [1] Tatarczyńska E., Pawłowski L., Chojnacka-Wójcik E., Maj J., Pol. J. Pharmacol. Pharm. 51 (1989) 41
- [2] Rible L., Taylor D.P., Eison M.S., Stanton H.C.: J. Clin. Psychiatr. 11 (1982) 43
- [3] Kossakowski J., Hejzman E.; Acta Polon. Pharm-Drug Research.: 57 (Suppl.) (2000) 57
- [4] Kossakowski J., Jarocka M.; Acta Polon. Pharm-Drug Research.: 57 (Suppl.)(2000) 60
- [5] Kossakowski J., Zawadowski T., Turło J., Kleps J.; IL Farmaco.: 53 (1998) 169
- [6] Kossakowski J., Szczepek W. and Pakosińska-Parys M., Acta Polon. Pharm. 59 (2002) 6

SYNTHESIS OF ARYL- AND HETEROARYLPIPERAZINYL DERIVATIVES OF AZATRICYCLOUNDECANE SYSTEM AS POTENTIAL 5-HT RECEPTOR LIGANDS

J. Kossakowski, M. Krawiecka, B. Kuran
*Department of Medical Chemistry, Medical University, 3 Oczki St.,
02-007 Warsaw, Poland*

Introduction

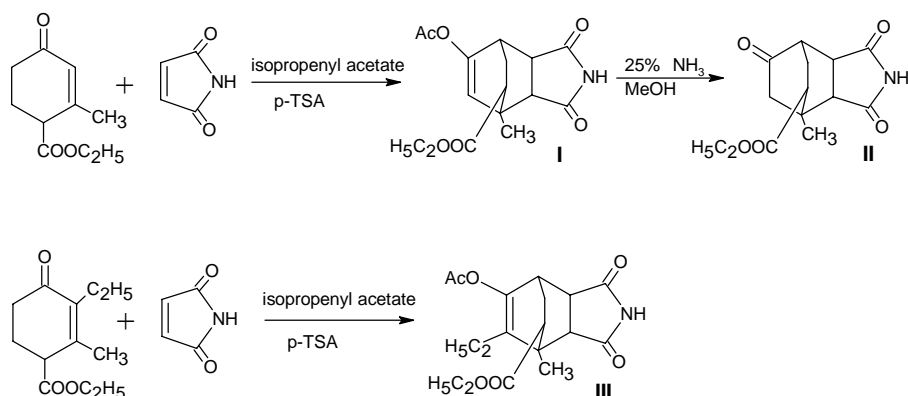
Well-known anxiolytics e.g. buspirone, gepirone, tandospirone display high affinity for the 5-HT_{1A} and D₂ receptor types and therefore are widely used in the treatment of psychotic and neurotic disorders. These drugs possess 4-aryl(heteroaryl)-1-piperazinealkyl group linked with the imide nitrogen [1-4]. Many analogs have been synthesized and have demonstrated anxiolytic and/or antidepressive activity in the pharmacological tests [5-10].

This work is a continuation of our previous studies in search for compounds with anxiolytic and antidepressant activity among a group of long-chain arylpiperazine ligands. Thus the design of the present compound was inspired in the structures of the anxiolytic compounds of new generation and results of our earlier works [10-19].

Results and discussion

The starting imides **I** and **III** were obtained in Diels-Alder's reaction between ethyl 2-methyl-4-oxocyclohex-2-ene-1-carboxylate and ethyl 3-ethyl-2-methyl-4-oxocyclohex-2-ene-1-carboxylate (appropriate) and maleimide, in isopropenyl acetate with catalytic amount of *p*-toluenesulphonic acid (*p*-TSA).

The next step was hydrolysis of compound **I**, using anhydrous ethanol with 25% NH₃ (aq.). The compound **II** was obtained as a result of conducted reaction (Scheme 1).

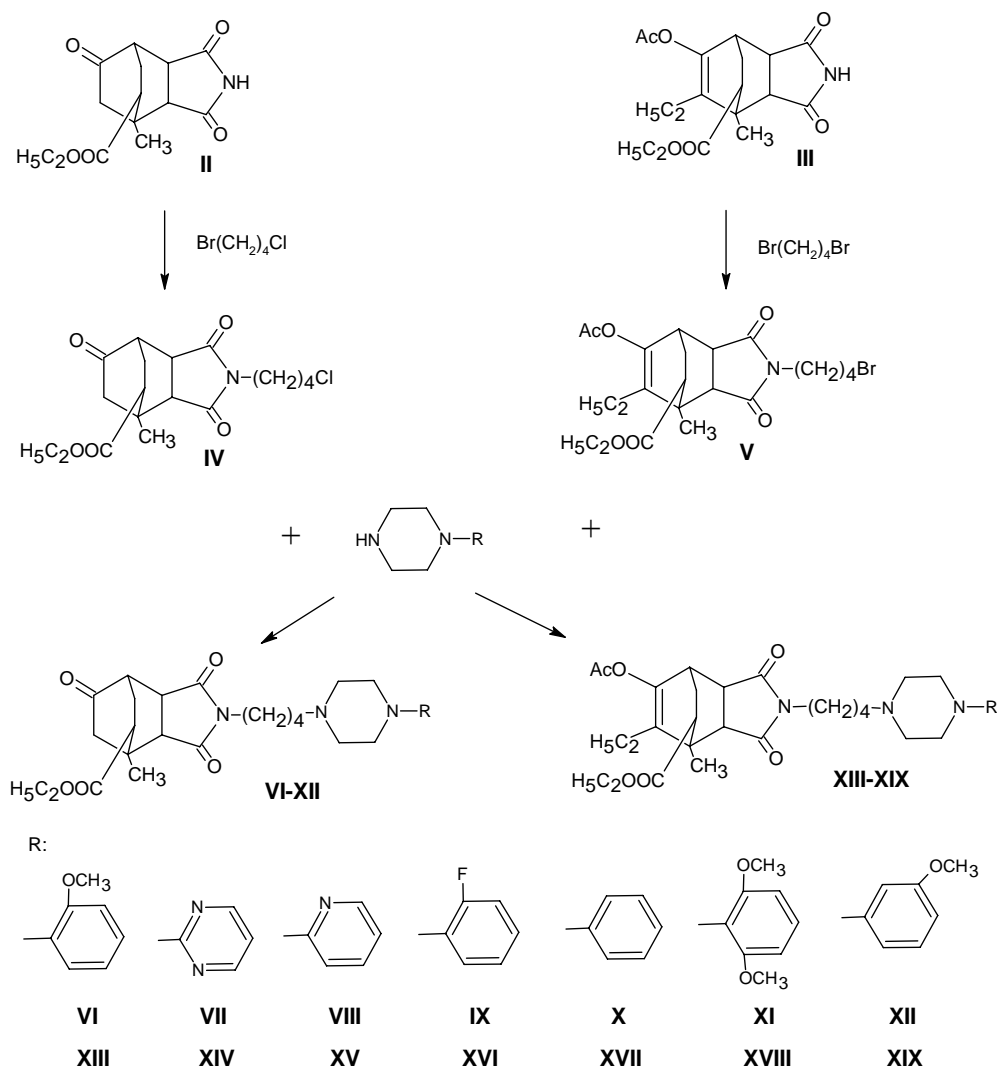


Scheme 1

The imides **II** and **III** were reacted in acetonitrile in the presence of anhydrous K₂CO₃ and KI with the 1-bromo-4-chlorobutane or 1,4-dibromobutane to give derivatives **IV** and **V**, respectively. Finally, the resulting N-substituted imides were condensed with appropriate amines in acetone, again in the presence of anhydrous K₂CO₃ and KI to give derivatives **VI-XIX** (Scheme 2). All new piperazinyl derivatives were converted into their corresponding hydrochlorides. The structures of the all compounds obtained were confirmed by ¹H-NMR spectra and elemental analysis.

Conclusion

In continuation of our research on cyclic imides with potential anxiolytic and antidepressive activity we have obtained fourteen new compounds belonging to the long-chain arylpiperazine ligand class. From the chemical and pharmacological point of view, these compounds are the basis for further research in the field of the potential drugs derived from cyclic imides.



Scheme 2.

Experimental

Melting points were determined in a capillary on an Electrothermal 9100 apparatus and are given uncorrected. $^1\text{H-NMR}$ spectra were recorded in DMSO-d_6 or CDCl_3 on a Bruker AVANCE DMX400 spectrometer operating at 400 MHz. The chemical shift values are expressed in ppm (parts per million) relatively to tetramethylsilane used as an internal standard and coupling constants J are given in Hz. Column chromatography was done using 0.05-0.2 mm Kieselgel (70-325 mesh ASTM, Merck). Reactions were monitored by TLC on 0.2 mm thick Kieselgel G plates with 254 nm fluorescent indicator (Merck), eluted with 9.8:0.2 or 9.5:0.5 chloroform-methanol.

Synthesis of ethyl 10-(acetoxy)-7-methyl-3,5-dioxo-4-azatricyclo [5.2.2.0^{2,6}]undec-10-ene-8-carboxylate (I) and ethyl 10-(acetoxy)-11-ethyl-7-methyl-3,5-dioxo-4-azatricyclo[5.2.2.0^{2,6}]undec-10-ene-8-carboxylate (III)

A mixture of ethyl 2-methyl-4-oxocyclohex-2-ene-1-carboxylate or ethyl 3-ethyl-2-methyl-4-oxocyclohex-2-ene-1-carboxylate (0.01 mol), maleimide (0.01 mol) and a catalytic amount of p-toluenesulphonic acid (p-TSA) was refluxed for 2h in isopropenyl acetate (30 mL). The boiling mixture was filtered and the solvent was evaporated. The residue was crystallized from ethyl acetate.

ethyl 10-(acetoxy)-7-methyl-3,5-dioxo-4-azatricyclo [5.2.2.0^{2,6}]undec-10-ene-8-carboxylate (I) m.p. 196-197 °C, ¹H NMR 400MHz, DMSO δ (ppm): 11.14 (s, 1H, NH), 5.39 (s, 1H, C11-H), 4.01 (m, 2H, O-CH₂-CH₃), 3.33 (s, 1H, C6-H), 2.94 (m, 1H, C2-H), 2.88 (m, 1H, C1-H), 2.71 (d, ³J = 8.0Hz, 1H, C8-H), 2.10 (s, 3H, C10-OAc), 2.06-1.99 (m, 1H, C9-H), 1.81-1.77 (m, 1H, C9-H), 1.44 (s, 3H, C7-CH₃), 1.15 (t, ³J = 7.2Hz, ³J = 6.8Hz, 3H, O-CH₂-CH₃); Anal. Calc. for C₁₆H₁₉NO₆: 60.02 % C, 6.00 % H, 4.33 % N; found: 59.76 % C, 6.09 % H, 4.94 % N.

ethyl 10-(acetoxy)-11-ethyl-7-methyl-3,5-dioxo-4-azatricyclo[5.2.2.0^{2,6}]undec-10-ene-8-carboxylate (III) m.p. 190-191 °C ; ¹H NMR, 400MHz, CDCl₃ δ (ppm): 8.96 (s, 1H, NH), 4.12-4.04 (m, 2H, O-CH₂-CH₃), 3.06 (d, ³J = 2.8Hz, 1H, C8-H), 2.86 (dd, ³J = 2.8Hz, ³J = 8.4Hz, 1H, C2-H), 2.60 (d, ³J = 8.4Hz, 1H, C6-H), 2.45 (m, 1H, C7-H), 2.14 (m, 4H, C10-OAc, C9-H), 2.05-1.87 (m, 3H, C11-CH₂-CH₃, C9-H), 1.62 (s, 3H, C7-CH₃), 1.23 (t, ³J = 7.2Hz, 3H, O-CH₂-CH₃), 0.87 (t, ³J = 7.6Hz, 3H, C11-CH₂-CH₃); Anal. Calc. for C₁₈H₂₃NO₆: 61.89 % C, 6.59 % H, 4.01 % N; found: 61.95 % C, 6.66 % H, 3.977 % N.

Synthesis of ethyl 7-methyl-3,5,10-trioxo-4-azatricyclo[5.2.2.0^{2,6}]undecane-8-carboxylate (II)

The imide I (0,01mol) was dissolved in methanol (30mL) and the 25% solution NH₃ (7mL) was added. The mixture was refluxed for 4h. The boiling mixture was filtered and the solvent was evaporated. The residue was crystallized from ethyl acetate.

ethyl 7-methyl-3,5,10-trioxo-4-azatricyclo[5.2.2.0^{2,6}]undecane-8-carboxylate (II) m.p. 215-216 °C; ¹H NMR 400MHz, DMSO δ (ppm): 11.41 (s, 1H, NH), 4.10 (m, 2H, O-CH₂-CH₃), 3.25 (dd, ³J = 3.2Hz, ³J = 9.2Hz, 1H, C2-H), 2.90 (d, ³J = 9.2Hz, 1H, C6-H), 2.67 (dd, ³J = 6.8Hz, ³J = 10.4Hz, 1H, C1-H), 2.62-2.50 (m, 2H, C8-H, C11-H), 2.23 (m, 1H, C9-H), 1.89-1.78 (m, 2H, C8-H, C9-H), 1.15 (m, 6H, C7-CH₃, O-CH₂-CH₃); Anal. Calc. for C₁₄H₁₇NO₅: 60.02 % C, 6.09 % H, 5.02 % N; found: 60.12 % C, 6.17 % H, 5.04 % N.

General synthesis of N- butyl derivatives of the imides (IV, V)

The appropriate imide (II or III) (0.01 mol) was dissolved in acetone (30 mL), then anhydrous K₂CO₃ (0.01 mol) and 1-bromo-4-chlorobutane or 1,4-dibromobutane (0.02 mol) (respectively)- were added. The mixture was refluxed for 12h. When the reaction was complete, as indicated by TLC, the mixture was filtered and the solvent was evaporated. The residue was purified by flash chromatography (eluent: chloroform-methanol 100:0.2).

ethyl 4-(4-chlorobutyl)-7-methyl-3,5,10-trioxo-4-azatricyclo[5.2.2.0^{2,6}]undecane-8-carboxylate (IV) oil; ¹H NMR 400MHz, CDCl₃ δ (ppm): 4.25-4.13 (m, 2H, O-CH₂-

CH₃), 3.54 (t, ³J = 6.0Hz, 2H, C1'-H), 3.50 (t, ³J = 6.4Hz, 2H, C4'-H), 3.12 (dd, ³J = 3.2Hz, ³J = 9.3Hz, 1H, C2-H), 2.92 (m, 1H, C1-H), 2.85 (d, ³J = 2.0Hz, 1H, C6-H), 2.72 (dd, ³J = 9.3Hz, ⁴J = 2.0Hz, 1H, C11-H), 2.64-2.59 (m, 1H, C8-H), 2.22-2.19 (m, 2H, C9-H), 1.93-1.87 (m, 1H, C11-H), 1.70 (m, 4H, C2'-H, C3'-H), 1.40 (s, 3H, C7-CH₃), 1.29 (t, ³J = 7.2Hz, 3H, O-CH₂-CH₃); Anal. Calc. for C₁₈H₂₄ClNO₅: 58.46 % C, 6.54 % H, 3.79 % N; found: 58.12 % C, 6.54 % H, 3.80 % N.

ethyl 4-(4-bromobutyl)-10-(acetoxo)-11-ethyl-7-methyl-3,5-dioxo-4-azatricyclo[5.2.2.0^{2,6}]undec-10-ene-8-carboxylate (V) oil; ¹H NMR, 400MHz, CDCl₃ δ (ppm): 4.14-4.05 (m, 2H, O-CH₂-CH₃), 3.51-3.38 (m, 4H, C1'-H, C4'-H), 3.08 (m, 1H, C1-H), 2.80 (dd, ³J = 2.4Hz, ³J = 8.0Hz, 1H, C2-H), 2.54 (d, ³J = 8.0Hz, 1H, C6-H), 2.46 (m, 1H, C8-H), 2.17-1.89 (m, 7H, C10-OAc, C11-CH₂-CH₃, C9-H), 1.82 (m, 2H, C2'-H), 1.64 (m, 5H, C1-CH₃, C3'-H), 1.24 (t, ³J = 7.2Hz, 3H, O-CH₂-CH₃), 0.85 (t, ³J = 7.6Hz, 3H, C11-CH₂-CH₃); Anal. Calc. for C₂₂H₃₀BrNO₆: 54.55 % C, 6.24 % H, 2.89 % N; found: 54.24 % C, 6.16 % H, 2.94 % N.

General synthesis of aryl- and heteroarylpiperazinyl derivatives of ethyl 4-(4-chlorobutyl)-7-methyl-3,5,10-trioxo-4-azatricyclo[5.2.2.0^{2,6}]undecane-8-carboxylate (VI-XII) and ethyl 4-(4-bromobutyl)-10-(acetoxo)-11-ethyl-7-methyl-3,5-dioxo-4-azatricyclo[5.2.2.0^{2,6}]undec-10-ene-8-carboxylate (XIII-XIX)

The appropriate piperazine (0.02 mol) was added to a mixture of N-butylimide (0.01 mol), powdered anhydrous K₂CO₃ (0.01 mol), and a catalytic amount of KI in acetone (30 mL). The reaction mixture was refluxed for 24 h. After the reaction completion the inorganic residue was filtered off and the solvent was evaporated. The crude compound obtained was purified by flash chromatography (eluent: chloroform or chloroform-methanol 100:0.2). All new derivatives were converted into their corresponding hydrochlorides with ethereal HCl and recrystallized from methanol.

The results of elemental analysis (C, H, N) of compounds VI-XIX were within ± 0.5% of theoretical values. The values of ¹H NMR chemical shifts of these compounds support the reported structures and are available on request.

References:

- [1] D. L. Nelson, *Pharmacol. Biochem. Behav.* 40 (1991) 1041-1051.
- [2] R. A. Glennon, *Drug. Dev. Res.* 26 (1992) 251-274.
- [3] F. Heiser, Ch. S. Wilcox, *Drugs* 10 (1998) 343-353.
- [4] P. Saurbie, 5HT_{1A} Receptors: a Bridge between Anxiety and Depression, *Behavioral Pharmacology of 5HT_{1A}*, Lawrence Erlbaum Ass. Publ., Hillsdale, NJ (1999) pp. 337-359
- [5] A. J. Bojarski, B. Duszyńska, M. Kołaczkowski, P. Kowalski, T. Kowalska, J. *Bioorg. Med. Chem. Lett.* (2004) 14, 5863-5866
- [6] A. J. Bojarski, M. H. Paluchowska, B. Duszyńska, R. Bugno, A. Kłodzińska, E. Tatarczyńska, E. J. Chojnacka-Wójcik, *Bioorg. Med. Chem.* (2006) 14, 1391-1402
- [7] M. L. López-Rodríguez, M. J. Morcillo, E. Fernandez, E. Porrás, E. Orensanz, M. E. Beneytez, J. Manzanares, J. A. Fuentes, *J. Med. Chem.* (2001) 44, 186-197
- [8] G. Caliendo, F. Fiorino, P. Grieco, E. Perissutti, V. Santagada, B. Severino, G. Bruni, R. Romeo, *Bioorg. Med. Chem.* (2000) 8, 533-538
- [9] A. L. Sabb, R. L. Vogel, M. G. Kelly, Y. Palmer, D. L. Smith, T. H. Andree, L. E. Schechter, *Bioorg. Med. Chem. Lett.* (2001) 11, 1069-1071
- [10] J. Kossakowski, T. K. Sroka, *Acta Polon. Pharm.-Drug Res.* 56(Suppl.) (1999)

89-91.

- [11] J. Kossakowski, J. Kuśmierczyk, *Pharmazie* (2000) 55, 5-8.
- [12] J. Kossakowski, E. Hejchman, *Acta Polon. Pharm.-Drug Res.* 57 (Suppl.) (2000) 57-60.
- [13] J. Kossakowski, M. Jarocka, *Acta Polon. Pharm.-Drug Res.* 57 (Suppl.) (2000) 60-62.
- [14] J. Kossakowski, E. Maleszewska, *Acta Polon. Pharm.-Drug Res.* 57 (Suppl.) (2000) 47-50.
- [15] J. Kossakowski, M. Krawiecka, *Acta Polon. Pharm.-Drug Res.* 57 (Suppl.) (2000) 53-56.
- [16] J. Kossakowski, M. Perliński, *Acta Polon. Pharm.-Drug Res.* 58 (2001) 257-262.
- [17] J. Kossakowski, M. Perliński, *Acta Polon. Pharm.-Drug Res.* 60 (2003) 183-189.
- [18] J. Kossakowski, B. Kuran, *Ann. Pol. Chem. Soc.* (2003) 284-288.
- [19] J. Kossakowski, M. Krawiecka, B. Kuran, *Molecules* (2006) 11, 615-626.

DERIVATIVES OF 2,3-DIHYDRO-5H-[1,4]DITHIINO[2,3-C]PYRROLE-5,7(6H)-DIONE AS POTENTIAL ANXIOLYTICS

Jerzy Kossakowski¹, Anna Wojciechowska¹, Izabela Dybała²

¹Department of Medical Chemistry, The Medical University of Warsaw,
3 Oczki Street, 02-007 Warsaw, Poland

² Faculty of Chemistry, Maria Curie-Skłodowska University, Maria Curie-Skłodowska
Square, 20-031 Lublin, Poland

Introduction

It is known that most anxiolytics and hypnotic-sedative drugs such as benzodiazepines and barbiturates exert their pharmacological actions *via* interactions with a discrete neuronal site on the GABA_A receptor. Suriclone and zopiclone are examples of non benzodiazepine structures binding to this receptor and acting as agonists. Non-benzodiazepine anxiolytics have also been developed that appear to act by modulating the serotonergic, histaminergic and non-aminergic systems [1, 2]. It prompted us to continue our search for potential anxiolytics within arylpiperazine derivatives of 6-(4-bromobutyl)-2,3-dihydro-5H-[1,4]dithiino[2,3-c]pyrrole-5,7(6H)-dione **3** and 6-(3-bromopropyl)-2,3-dihydro-5H-[1,4]dithiino[2,3-c]pyrrole-5,7(6H)-dione **4**, analogues of suriclone. Synthesized compounds possess an alkyl-(*N*-aryl) substituted piperazine moiety, that is the pharmacophore of 5-HT_{1A} receptor and is believed to give high potency in the treatment of anxiety and depression [3, 4].

The structure of all derivatives of compound **2** have been established on the basis of elemental analysis and ¹H NMR spectra. The X-ray crystal structure analysis for one selected compound **3d** was recorded.

The target compounds reported here were synthesized according to the routes outlined in Fig. 1.

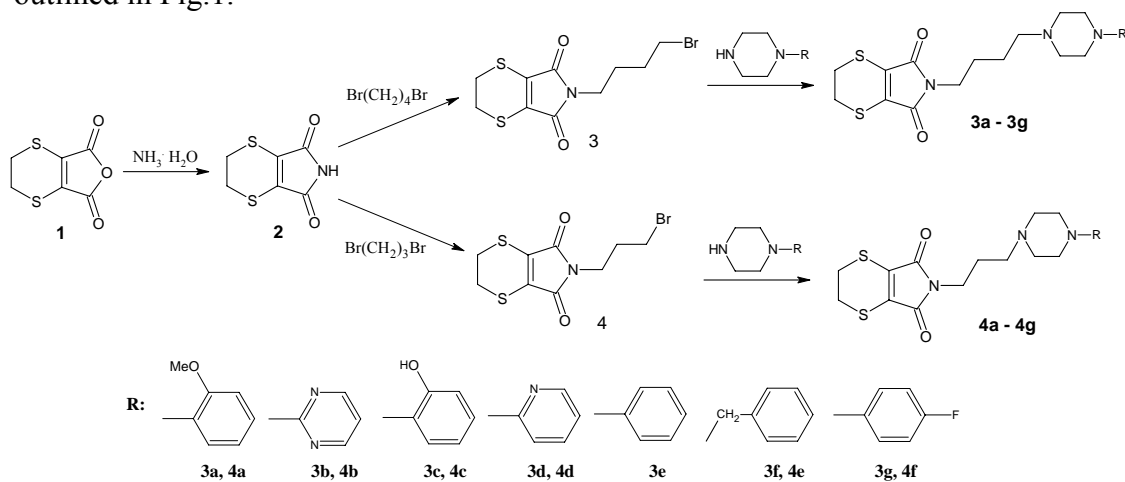


Fig. 1. Method for preparation of compounds **3 a-g** and **4 a-g**.

EXPERIMENTAL

Chemistry

Melting points were determined in a Kofler's apparatus and are uncorrected. The ¹H NMR spectra were recorded on a Bruker AVANCE DMX400 spectrometer, operating at 400.13 MHz. The chemical shift values are expressed in ppm relative to

TMS as an internal standard. Elemental analyses were recorded with a CHN model 2400 Perkin-Elmer.

Synthesis of 2,3-dihydro-5H-[1,4]dithiino[2,3-*c*]pyrrole-5,7(6*H*)-dione 2. The anhydride **1** (4,7 g; 0,025 mole) was dissolved in 25 cm³ 25% NH₃ solution and heated for 1 h. The excess solvent was evaporated. The compound was obtained previously [5].

Synthesis of 6-(4-bromobutyl)-2,3-dihydro-5H-[1,4]dithiino[2,3-*c*]pyrrole-5,7(6*H*)-dione 3 and 6-(3-bromopropyl)-2,3-dihydro-5H-[1,4]dithiino[2,3-*c*]pyrrole-5,7(6*H*)-dione 4. A mixture of dione **2** (2 g; 0,016 mole), 1,4-dibromobutane (7 g; 0,032 mole) or 1,3-dibromopropane (6,42 g; 0,032 mole) and anhydrous K₂CO₃ (2 g, 0,015 mole) was dissolved in 100 cm³ acetone and refluxed for 30 h. The solvent was distilled off, then the oily residue was purified by column chromatography (CHCl₃).

3. Yield 85 %, m.p. 74-76 °C, ¹H NMR (400 MHz, CDCl₃) δ (ppm): 3.58-3.54 (t, J=8 Hz, 2H, N-CH₂), 3.44-3.40 (t, J=8 Hz, 2H, CH₂-Br), 3.32 (s, 4H, CH₂-S), 1.89-1.82 (m, 2H, -CH₂-), 1.79-1.72 (m, 2H, -CH₂-); C₁₀H₁₂BrNO₂S₂ (322.25): calcd. C 37.27, H 3.75, N 4.35; found C 37.51, H 3.75, N 4.35.

4. Yield 40 %, m.p. 70-72 °C, ¹H NMR (400 MHz, CDCl₃) δ (ppm): 3.69-3.66 (t, J=6 Hz, 2H, N-CH₂), 3.38-3.35 (t, J=6 Hz, 2H, CH₂-Br), 3.32 (s, 4H, CH₂-S), 2.20-2.13 (m, 2H, -CH₂-); C₉H₁₀BrNO₂S₂ (308.22): calcd. C 35.07, H 3.27, N 4.55; found C 35.17, H 3.36, N 4.51.

General procedures for the condensation of 4-substituted arylpiperazines with derivatives 3 and 4. A mixture of the derivative **3** (0,5 g; 0,012 mole) or **4** (0,5 g; 0,016 mole), an appropriate amine (0,0024 or 0,0032 mole), anhydrous K₂CO₃ (0,5 g, 0,0038 mole) and catalytic amount of KI was dissolved in 50 cm³ acetone and refluxed for 30 h. The solvent was evaporated, then the residue was purified by column chromatography (CHCl₃: CH₃OH, 99,5:0,5) to give compounds **3a - 3g** and **4a - 4g**, respectively.

3a. Yield 50 %, oil, ¹H NMR (400 MHz, CDCl₃) δ (ppm): 7.02-6.98 (m, 1H, H_αarom), 6.95-6.91 (m, 2H, H_βarom), 6.87-6.85 (m, 1H, H_γarom), 3.86 (s, 3H, OCH₃), 3.58-3.55 (t, J=6 Hz, 2H, N-CH₂), 3.32 (s, 4H, CH₂-S), 3.15 (m, 4H, CH₂-N_{piper}), 2.74 (m, 4H, CH₂-N_{piper}), 2.51 (m, 2H, -CH₂-N), 1.65-1.64 (m, 4H, -CH₂-); C₂₁H₂₈ClN₃O₃S₂ · ½ H₂O · ½ CHCl₃ (511,29): calcd. C 50.50, H 5.82, N 8.22; found C 50.79, H 5.72, N 7.97.

3b. Yield 56 %, m.p. 172-174 °C, ¹H NMR (400 MHz, CDCl₃) δ (ppm): 8.30-8.29 (m, 2H, H_αarom), 6.48 (m, 1H, H_βarom), 3.84 (m, 4H, CH₂-N_{piper}), 3.57-3.54 (t, J=6 Hz, 2H, N-CH₂), 3.32 (s, 4H, CH₂-S), 2.51-2.41 (m, 6H, CH₂-N, CH₂-N_{piper}), 1.65-1.63 (m, 2H, -CH₂-), 1.25 (m, 2H, -CH₂-); C₁₈H₂₃N₅O₂S₂ · ½ H₂O (414.57): calcd. C 52.15, H 5.84, N 16.90; found C 52.29, H 5.70, N 16.61.

3c. Yield 55 %, m.p. 260 °C, ¹H NMR (400 MHz, CDCl₃) δ (ppm): 7.19-6.83 (m, 4H, arom), 3.58-3.55 (t, J=6 Hz, 2H, N-CH₂), 3.32 (s, 4H, CH₂-S), 2.90 (m, 4H, CH₂-N_{piper}), 2.61 (m, 4H, CH₂-N_{piper}), 2.44-2.40 (t, J=8 Hz, 2H, CH₂-N), 1.69-1.62 (m, 2H, -CH₂-), 1.56-1.48 (m, 2H, -CH₂-); C₂₀H₂₇Cl₂N₃O₃S₂ · ½ H₂O (501.51): calcd. C 47.90, H 5.63, N 8.38; found C 48.27, H 5.60, N 8.42.

3d. Yield 55 %, m.p. 115-117 °C, ¹H NMR (400 MHz, CDCl₃) δ (ppm): 8.19-8.18 (d, J=4 Hz, 1H, H_αarom), 7.49-7.45 (t, J=8 Hz, 1H, H_βarom), 6.65-6.60 (m, 2H, H_βarom, H_γarom), 3.58-3.54 (m, 6H, N-CH₂, CH₂-N_{piper}), 3.31 (s, 4H, CH₂-S), 2.58 (m, 4H, CH₂-N_{piper}), 2.43 (s, 2H, CH₂-N), 1.68-1.61 (m, 2H, -CH₂-), 1.57-1.55 (m, 2H, -CH₂-); C₁₉H₂₄N₄O₂S₂ (404.57): calcd. C 56.41, H 5.98, N 13.85; found C 56.19, H 6.00, N 13.46.

3e. Yield 53 %, m.p. 130-132 °C, ¹H NMR (400 MHz, CDCl₃) δ (ppm): 7.28-7.24 (m, 2H, H_αarom), 6.93-6.83 (m, 2H, H_βarom), 6.87-6.83 (m, 1H, H_γarom), 3.58-3.54 (t, J=8 Hz, 2H, N-CH₂), 3.31 (s, 4H, CH₂-S), 3.23 (m, 4H, CH₂-N_{piper}), 2.64 (m, 4H, CH₂-N_{piper}), 2.44 (s, 2H, CH₂-N), 1.68-1.63 (m, 2H, -CH₂-), 1.61-1.55 (m, 2H, -CH₂-); C₂₀H₂₅N₃O₂S₂ (403.58): calcd. C 59.52, H 6.24, N 10.41; found C 59.48, H 6.20, N 10.38.

3f. Yield 56 %, m.p. 95-97 °C, ¹H NMR (400 MHz, CDCl₃) δ (ppm): 7.32-7.31 (m, 5H, arom), 3.55-3.52 (m, 4H, N-CH₂, CH₂-Phe), 3.31 (s, 4H, CH₂-S), 2.61-2.48 (m, 10H, CH₂-N, CH₂-N_{piper}), 1.56-1.48 (m, 4H, -CH₂-); C₂₁H₂₇N₃O₂S₂ (417.61): calcd. C 60.40, H 6.52, N 10.06; found C 60.50, H 6.35, N 9.95.

3g. Yield 50 %, m.p. 135-136.5 °C, ¹H NMR (400 MHz, CDCl₃) δ (ppm): 6.97-6.93 (m, 2H, H_αarom), 6.88-6.85 (m, 2H, H_βarom), 3.57-3.54 (t, J=6 Hz, 2H, N-CH₂), 3.31 (s, 4H, CH₂-S), 3.15 (m, 4H, CH₂-N_{piper}), 2.65 (m, 4H, CH₂-N_{piper}), 2.46 (s, 2H, CH₂-N), 1.66-1.61 (m, 2H, -CH₂-), 1.56 (m, 2H, -CH₂-); C₂₀H₂₄FN₃O₂S₂ (421.57): calcd. C 56.98, H 5.74, N 9.97; found C 56.48, H 5.70, N 9.77.

4a. Yield 50 %, m.p. 140-141.5 °C, ¹H NMR (400 MHz, CDCl₃) δ (ppm): 7.01-6.97 (m, 1H, H_αarom), 6.93-6.88 (m, 2H, H_βarom), 6.86-6.84 (m, 1H, H_γarom), 3.85 (s, 3H, OCH₃), 3.66-3.63 (t, J=6 Hz, 2H, N-CH₂), 3.28 (s, 4H, CH₂-S), 3.08 (m, 4H, CH₂-N_{piper}), 2.60-2.49 (m, 6H, CH₂-N, CH₂-N_{piper}), 1.84 (s, 4H, -CH₂-); C₂₀H₂₅N₃O₃S₂ · ½ H₂O (428.59): calcd. C 56.05, H 6.11, N 9.81; found C 56.42, H 5.90, N 9.70.

4b. Yield 50 %, m.p. 115-117 °C, ¹H NMR (400 MHz, CDCl₃) δ (ppm): 8.30-8.29 (d, J=4 Hz, 2H, H_αarom), 6.48 (s, 1H, H_βarom), 3.79 (s, 4H, CH₂-N_{piper}), 3.66-3.63 (t, J=6 Hz, 2H, N-CH₂), 3.30 (s, 4H, CH₂-S), 2.43 (m, 6H, CH₂-N, CH₂-N_{piper}), 1.83 (s, 2H, -CH₂-); C₁₇H₂₁N₅O₂S₂ (391.53): calcd. C 52.15, H 5.41, N 17.89; found C 52.04, H 5.33, N 17.51.

4c. Yield 55 %, m.p. 111-113.5 °C, ¹H NMR (400 MHz, CDCl₃) δ (ppm): 7.17-6.83 (m, 4H, arom), 3.67-3.63 (t, J=8 Hz, 2H, N-CH₂), 3.33 (s, 4H, CH₂-S), 2.86 (m, 4H, CH₂-N_{piper}), 2.56-2.47 (m, 6H, CH₂-N, CH₂-N_{piper}), 1.82 (m, 2H, -CH₂-); C₁₉H₂₃N₃O₃S₂ (405.55): calcd. C 56.27, H 5.72, N 10.36; found C 56.20, H 5.76, N 10.15.

4d. Yield 51 %, m.p. 166-168 °C, ¹H NMR (400 MHz, CDCl₃) δ (ppm): 8.18-8.09 (s, 1H, H_αarom), 7.50-7.46 (t, J=8 Hz, 1H, H_βarom), 6.64-6.62 (d, J=8 Hz, 2H, H_βarom, H_γarom), 3.66-3.59 (m, 6H, N-CH₂, CH₂-N_{piper}), 3.28 (s, 4H, CH₂-S), 2.56 (m, 6H, CH₂-N_{piper}, CH₂-N), 1.25 (m, 2H, -CH₂-); C₁₈H₂₄Cl₂N₄O₂S₂ · H₂O (481.48): calcd. C 44.90, H 5.65, N 11.64; found C 44.63, H 5.46, N 11.33.

4e. Yield 30 %, oil, ¹H NMR (400 MHz, CDCl₃) δ (ppm): 7.32-7.31 (m, 5H, arom), 3.61-3.57 (t, J=8 Hz, 2H, N-CH₂), 3.53 (s, 2H, CH₂-Phe), 3.31 (s, 4H, CH₂-S), 2.48-2.37 (m, 10H, CH₂-N, CH₂-N_{piper}), 1.79-1.75 (t, J=8 Hz, 2H, -CH₂-); C₂₀H₂₅N₃O₂S₂ (403.56): calcd. C 59.52, H 6.24, N 10.41, found C 59.32, H 6.00, N 10.14

4f. Yield 51 %, m.p. 213-215 °C, ¹H NMR (400 MHz, CDCl₃) δ (ppm): 6.97-6.93 (m, 2H, H_αarom), 6.87-6.84 (m, 2H, H_βarom), 3.66-3.63 (t, J=6 Hz, 2H, N-CH₂), 3.31-3.26 (m, 4H, CH₂-S), 3.13 (m, 4H, CH₂-N_{piper}), 2.62-2.52 (m, 6H, CH₂-N, CH₂-N_{piper}), 1.87 (s, 2H, -CH₂-); C₁₉H₂₄Cl₂FN₃O₂S₂ · 3 ½ H₂O (543.51): calcd. C 41.89, H 5.75, N 7.73; found C 41.94, H 5.90, N 7.60.

X-ray crystallography

Diffraction data for compound **3d** were collected on a KUMA KM4 diffractometer (T = 293K, CuKα: λ = 1.54178 Å). Up to θ_{max} = 72.14°, 3248 reflections

were collected of which 3051 were independent and used in calculations. Crystal structure was solved by direct methods (SHELXS-97 [6]) and refined by full-matrix least-squares on F^2 using the program SHELXL-97 [7]). The non-hydrogen atoms were refined anisotropically. H atoms were positioned geometrically.

Final R indices for reflections with $I > 2\sigma(I)$ are: $R_1 = 0.0455$, $wR_2 = 0.1240$

($R_1 = 0.1485$, $wR_2 = 0.1604$ for all data).

Compound **3d** crystallizes in monoclinic crystal system, space group $P2_1/n$ with unit cell dimensions $a = 14.295(3)$ Å, $b = 9.013(2)$ Å, $c = 16.325(3)$ Å, $\beta = 107.81(3)^\circ$, $V = 2002.5(7)$ Å³, $Z = 4$, $d_c = 1.342$ g cm⁻³.

The view of molecule **3d** and the atom numbering scheme is shown in Fig. 2.

Fig. 2. The molecular structure of **3d** (50% probability ellipsoids) showing the atomic numbering scheme.

The butyl chain present in this molecule adopts expanded *-ap*, *ap*, *-ap* conformation. The piperazine ring has a chair conformation; the pyridine ring is almost parallel to the central plane of the chair.

In the crystal, the molecules of **3d** form layers *via* intermolecular *Cpiperazine*-H...O, *Cpyridine*-H...Npyridine and *Cdithiocyclohexene* -H...S weak hydrogen bonds. Between layers *Cdithiocyclohexene*-H...O interactions are observed.

Results and discussion

In this study we have presented the synthesis of 15 new arylpiperazine derivatives for potential use in the treatment of anxiety.

Conclusion

Fifteen new *N*-substituted derivatives of 2,3-dihydro-5*H*-[1,4]dithiino[2,3-*c*]pyrrole-5,7(6*H*)-dione was obtained. Structure of compound **3d** was confirmed by the X-ray structure analysis.

References

- [1] C.N. Cohen, *Drugs Future*, 10 (1985) 311
- [2] B.E. Leonard, *Hum. Psychopharmacol.*, (1999) 52
- [3] R.A. Glennon, *Drug Dev. Res.*, 26 (1992) 151
- [4] M.L. Lopez-Rodriguez, D. Ayala, B. Benhamu, M. Morcillo, A.Viso, *Curr. Med. Chem.*, 9 (2002) 443
- [5] H.R. Schweizer, *Helv.Chim.Acta*, 52 (1969) 2221
- [6] G.M. Sheldrick: SHELXS-97. Program for the crystal structure solution, University of Göttingen, Germany 1997
- [7] G.M. Sheldrick: SHELXL-97. Program for the refinement of crystal structures from diffraction data, University of Göttingen, Germany 1997

SURFACE PROPERTIES OF POLYSULFONE FILMS MODIFIED BY UV IRRADIATION

J. Kowal¹, B. Czajkowska², M. Gaweda¹

¹ Faculty of Chemistry, Jagiellonian University, ² Collegium Medicum, Jagiellonian University, Krakow Poland,

Polysulfones are frequently used as materials for various medical applications (e.g., membranes for haemodialysis and medical implants of various types) [1]. The hydrophobic character of polysulfone and polyethersulfone surfaces is a consequence of their chemical structures. The hydrophobicity of these polymers is considered to be the reason of membrane fouling with proteins [2] as well as the main parameter determining bacterial adhesion and biofilm formation on medical implants [3]. In this paper we describe the results of our studies on the modification of the surface of polysulfone and polyethersulfone films by means of the irradiation with the UV light absorbed by these polymers (254 and 265 nm). The properties of the polymer surfaces were investigated and the interactions of the cells and bacteria with native and modified polysulfone samples were monitored.

Materials: polysulfone (PSU) (Aldrich, $M_n = 16\ 000$), poly(1,4-phenylene ether-sulfone) (PES) (Aldrich, low mol. weight); the samples were prepared in the form of homogeneous films. **Cells:** human osteoblastic line HFOB 1.19, human fibroblastic line HS-5. The cells were cultured in RPMI 1640 medium (Gibco Lab) supplemented with 10% FCS (Gibco Lab) in an incubator in the atmosphere of air (95%) and CO₂ (5%) at 37°C (fibroblasts) and 34°C (osteoblasts). **Bacteria:** *Staphylococcus epidermidis* (ATCC 35547), (1.5×10^8 cfu/ml), cultured in Tryptic Soy Broth, DIFCO.

Methods: The samples were irradiated with the UV light absorbed by the polymer ($\lambda = 254$ nm) using ASH 400 medium pressure mercury lamp. The absorption spectra of PSU and PES samples in the UV-VIS and IR ranges and ATR IR spectra were recorded for original and irradiated polymer films (8452A Hewlett Packard (UV-VIS), EQUINOX 55, Bruker (FTIR), DIGILAB FTS 60 (ATR) spectrophotometers). Contact angles of water, formamide, ethylene glycol and diiodomethane on the investigated samples were measured using the sessile drop technique (Surftens Universal OEG GmbH Germany). The viability of the cells was determined by the MTS method and the concentrations of collagen type I and osteocalcin - by ELISA tests (DSLabs Inc., USA). In vitro evaluation of the adhesion of fibroblasts and osteoblasts as well as bacteria, *S. epidermidis*, to the investigated samples was done by means of the fluorescence microscope with interference contrast configuration (ECLIPSE TE2000-E, NIKON). The cells were stained with May-Grünwald and Giemsa stain solutions. SEM observation were performed with JSM-5400 Jeol instrument (5kV and 10 kV, 5×10^{-5}). The cells or bacteria attached to investigated films were fixed with glutaraldehyde (2.5% in phosphate buffer), washed with phosphate buffer, dehydrated with ethanol gradient and dried by the CO₂ critical point method.

Results and discussion

Spectral analysis (UV and IR spectra) revealed that the UV irradiation resulted in the degradation of polysulfones as well as in formation of carbonyl and hydroxyl groups.

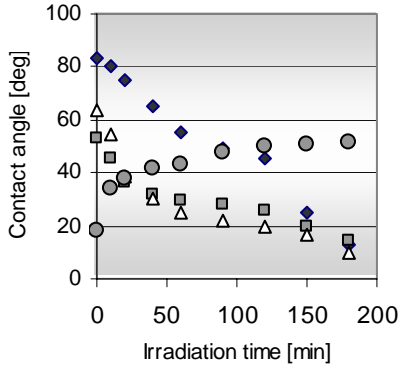


Fig. 1 Contact angles on polysulfone films after various times of irradiation:

◆ water, ■ ethylene glycol, Δ formamide, ● diiodomethane.

The contact angles of water, ethylene glycol and formamide on the investigated samples considerably decreased after UV irradiation while the contact angles of diiodomethane increased with the time of irradiation (see Fig. 1) confirming the increase in hydrophilic character of the both modified polymers.

The changes of polymer surfaces were evaluated in terms of the surface free energy of original and modified samples. According to van Oss, Good and Chaudhury's method [4,5], the surface free energy (see Eq. 1)

$$\gamma^{TOT} = \gamma^{LW} + \gamma^{AB} \quad (1)$$

is expressed as the sum of Lifchitz-van der Waals component and the polar (acid-base) component, defined as

$$\gamma^{AB} = 2\sqrt{\gamma^+ \gamma^-} \quad (2)$$

The Lifchitz-van der Waals, (γ_s^{LW}), the Lewis acid (electron acceptor), (γ_s^+), and Lewis base (electron donor) (γ_s^-), components were calculated for solid PSU and PES films by solving the following equations with contact angles of water, ethylene glycol and diiodomethane:

$$\gamma_L(1 + \cos \theta) = 2\sqrt{\gamma_s^{LW} \gamma_L^{LW}} + 2\sqrt{\gamma_L^+ \gamma_s^-} + 2\sqrt{\gamma_L^- \gamma_s^+} \quad (3)$$

where subscripts S and L refer to the film surface and wetting liquid, respectively and θ is a contact angle.

The acid-base (polar) component ($\gamma_s^{AB} = 2(\gamma_s^+ \gamma_s^-)^{1/2}$) and the total surface energy ($\gamma_s = \gamma_s^{LW} + \gamma_s^{AB}$) were then calculated for original and irradiated polymer films (see Fig. 2).

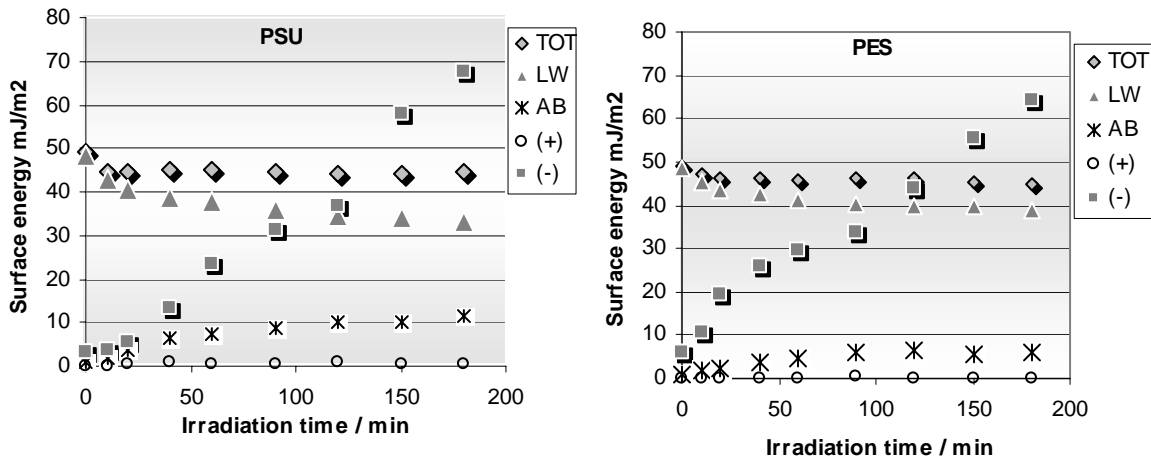


Fig. 2. Polysulfone and polyethersulfone films irradiated with UV light. Total surface-free energy (TOT) and its components: Lifchitz-van der Waals (LW), acid-base (polar), (AB), Lewis acid (electron acceptor), (+), and Lewis base (electron donor) (-), calculated according to van Oss, Good and Chaudhury's method.

Owens, Wendt, Rabel, Kaeble's [6] method is based on the assumption that the surface free energy (Eq. 4) can be considered as composed of two parts: polar, γ^P , and dispersive, γ^D :

$$\gamma^{TOT} = \gamma^P + \gamma^D \quad (4)$$

The interfacial free energy is described as

$$\gamma_{SL} = \gamma_S + \gamma_L - 2(\sqrt{\gamma_S^D \gamma_L^D} + \sqrt{\gamma_S^P \gamma_L^P}) \quad (5)$$

Thus, taking into account the Young's equation we have

$$(1 + \cos \theta) \gamma_L = 2\sqrt{\gamma_S^D \gamma_L^D} + 2\sqrt{\gamma_S^P \gamma_L^P} \quad (6)$$

Experimental contact angles of water, ethylene glycol, formamide and diiodomethane enabled the polar and dispersive components of the solid polymer film to be determined with the use of straight line relation:

$$\frac{(1 + \cos \theta) \gamma_L}{2 \sqrt{\gamma_L^D}} = \sqrt{\gamma_S^P} \cdot \sqrt{\frac{\gamma_L^P}{\gamma_L^D}} + \sqrt{\gamma_S^D} \quad (7)$$

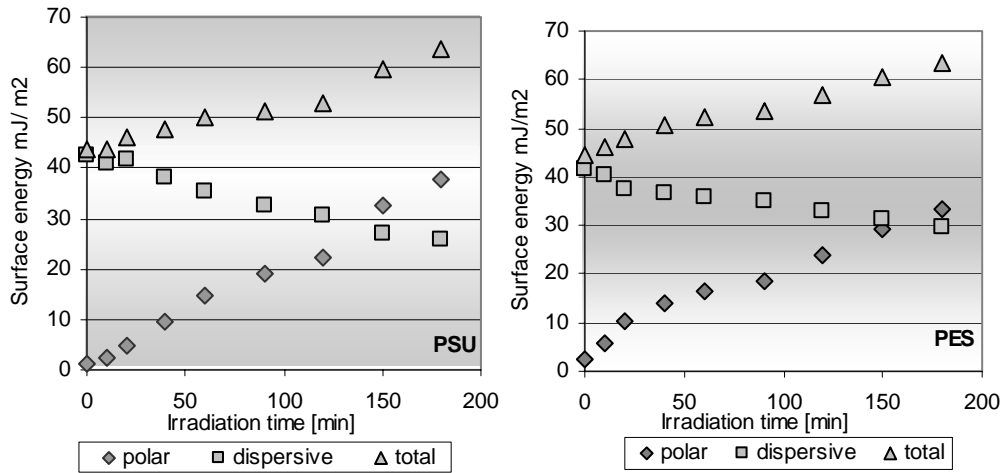


Fig. 3. Polysulfone and polyethersulfone films irradiated with UV light. Total surface-free energy (TOT) and its components: polar and dispersive, calculated according to Owens, Wendt, Rabel, Kaeble's method.

The calculations presented above clearly demonstrate the significant increase in polar component, γ_s^P , of the surface energy, especially the electron donor part, γ_s^+ , with the irradiation time.

The cellular response to the modified polymer samples and biocompatibility of the investigated materials were then estimated.

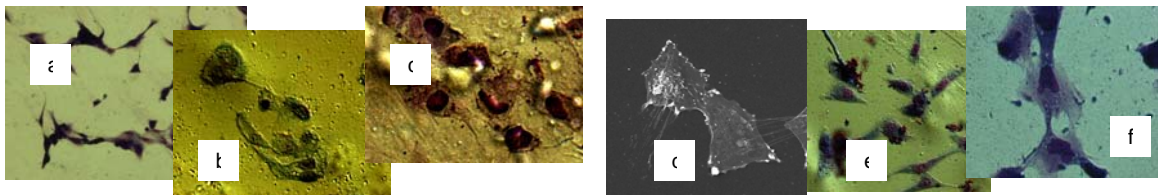


Fig. 4. Microscopic images of the cells: (a), (b) – fibroblasts on original PSU and PES films, (c) - osteoblasts on unmodified PES, (d) – fibroblasts on PES irradiated for 1.5h, (e) - osteoblasts on PES irradiated for 1.5h, (f) - osteoblasts on PSU irradiated for 3h.

The microscopic images of osteoblasts and fibroblasts adhered to the investigated

samples (see Fig. 3) show the flattened cells with filopodial extensions attached to the original and UV treated surfaces, suggesting good biocompatibility, which was confirmed by the determination of the viability of the cells and their ability to secrete collagen (see Table 1).

Table 1. The viability of the cells and the concentration of collagen type I.

Material	Viability %		Concentration of collagen type I secreted by cells [ng/ml]			
	Fibroblasts	Osteoblasts	Fibroblasts		Osteoblasts	
	7 days	7 days	4 days	7 days	4 days	7 days
PSU 0h	65	102	30.2	43.2	27.6	51.7
PSU 1.5h	82	95	26.2	52.0	24.8	39.0
PSU 3h	91	85	24.2	46.6	22.8	37.4
Control	100	100	143	143	24.0	50.4
PES 0h	79	90	27.0	69.9	42.0	59.9
PES 1.5h	68	73	21.6	46.0	27.2	40.9
PES 3h	92	89	21.5	50.7	28.5	52.3
Control	100	100	31.5	143	24.8	62.7

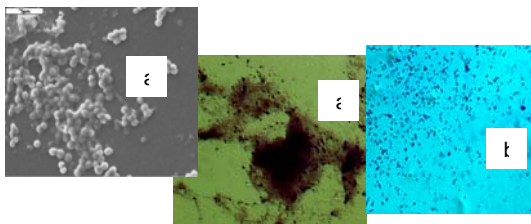


Fig. 5. Microscopic images of *S. epidermidis* adsorbed on the original PSU surface (a) and PSU irradiated for 3h (b).

In vitro evaluation of the adhesion of *Staphylococcus epidermidis* to the investigated samples was done by means of microscopic observations, which showed that the bacteria attachment to the irradiated films is lowered in comparison to that for the original PSU and PES films (see Fig. 5).

Conclusions

Modification of polysulfone and polyethersulfone films by means of UV irradiation leads to the decrease in hydrophobicity of their surfaces. The biocompatibility of modified materials is high; fibroblasts and osteoblasts adhere well to the irradiated samples. The increase of polar component of the surface energy and Lewis base interactions, being the result of UV irradiation in the presence of oxygen, affects the adhesion of *Staphylococcus epidermidis*: bacteria show a tendency to form aggregates and biofilms on original films whereas UV irradiated surfaces are much more resistant to bacteria attachment.

References

- [1] F. Gores, P. Montag, C. Schall, J. Vienken, S. K. Bowry, *Biomaterials* 23 (2002) 3131
- [2] M. Ulbricht, M. Riedel, U. Marx, *J. Membr. Sci.*, 120 (1996) 239
- [3] G. Reid, *International Journal of Antimicrobial Agents* 11 (1999) 223
- [4] C. J. van Oss, R. J. Good, M. K. Chaudhury, *J. Colloid Inter. Sci.*, 111 (1968) 378
- [5] C. J. van Oss, *Colloids and Surfaces B: Biointerfaces* 5 (1995) 91
- [6] D. K. Owens, R. C. Wendt, *J. Appl. Pol. Sci.*, 13 (1969) 1714

STRUCTURAL AND ELECTRONIC PROPERTIES OF HARMANE MONOCATION. THEORETICAL ASPECTS.

Agnieszka Kowalska, Agnieszka Stobiecka and Stanisław Wysocki

*Faculty of Biotechnology and Food Science, Technical University of Łódź
Institute of General Food Chemistry, ul. Stefanowskiego 4/10, 90-924 Łódź, Poland*

1. Introduction

Harmane (1-methyl- β -carboline) belongs to the group of β -carboline alkaloids, which have interesting pharmacological and photophysical properties. In polar, protic solvents and at a low pH range, harmane exists in the monocationic form in which pyridinic N is protonated. Recent studies on β -carbolines proved that theoretical calculations may be useful in the prediction of structural, spectroscopic and acid-base properties of these compounds [1-4]. Angulo and co-workers [4] applied HF/6-31+G(d) method and PCM model to estimate the magnitude of prototropic equilibria of β -carbolines. Semi-empirical methods have also previously been used to predict energies and oscillator strengths for electronic transitions in β -carbolines in the gaseous phase [5,6]. However, there is a lack of theoretical studies on β -carbolines in which solvent effects are included. Therefore, attention in this work has been focused on the use of various theoretical methods to estimate properties of electronic transitions for harmane monocation not only in the gaseous phase but also in the solvent.

2. Methods

All theoretical calculations were carried out using Gaussian 03 suite of programs. Geometry of harmane was optimized using the semi-empirical (AM1 and PM3) as well as Hartree-Fock (HF) and B3LYP (DFT) methods with 6-31G (d) basis set. Additionally, to determine the influence of diffuse functions on the predicted structural and electronic properties of harmane, geometry optimizations with the use of 6-31+G(d,p) basis set were also performed. Electronic transition properties of monocation were estimated using the semi-empirical ZINDO-1 as well as TD B3LYP/6-31+G(d,p) methods with Polarizable Continuum Model (PCM). These calculations were carried out using B3LYP/6-31+G(d,p) optimized geometry of molecule under study. Absorption spectra of harmane (both the neutral and monocationic form) were recorded in a Nicolet Evolution 300 (ThermoElectron Corporation) UV-VIS spectrophotometer at room temperature ($25 \pm 2^\circ\text{C}$). The solutions of β -carboline were prepared by setting the concentration at $\sim 10^{-5}$ M.

3. Results and discussion

3.1. The ground state geometry

From the comparison of experimentally determined [7] and theoretically calculated structural parameters of harmane free base it followed that the semi-empirical methods gave results less consistent with the experimental data. The geometrical parameters obtained using AM1 and PM3 methods had deviations from experimental data $\geq 3^\circ$ for bond angles and $\geq 0.05\text{\AA}$ for bond lengths. On the other hand, HF and B3LYP methods were in reasonably good agreement with the crystallographic data. Differences between theoretically predicted and experimental structural parameters of harmane using the

latter methods were estimated to be less than 0.03 Å and 2° for bond lengths and for bond angles, respectively. As an example, Fig. 1 shows the B3LYP/6-31+G (d,p) optimized geometry of harmane molecule.

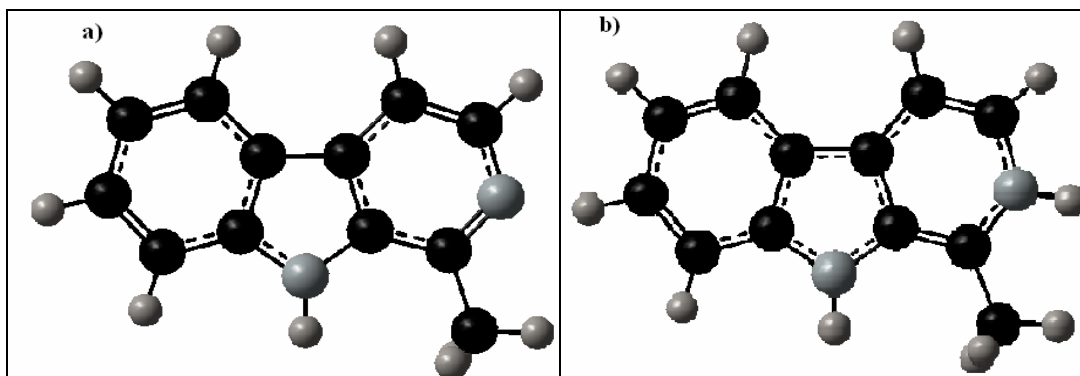


Figure 1. The B3LYP/6-31+G (d,p) optimized structure of neutral (a) and monocationic (b) form of harmane.

3.2. Electronic properties of harmane cation

As can be seen in Fig. 2, four bands may be identified in the absorption spectrum of harmane monocation. The maxima of these bands are situated at ~ 204 nm; I ≈ 250 nm, II ≈ 300 nm and III ≈ 370 nm, respectively. The absorption spectra of neutral form of harmane (for comparison see the spectrum recorded in cyclohexane) are constituted of three bands. Two of them are strong and situated at ~ 240 nm and ~ 286 nm, whereas the third band is weak and consists of two peaks around 330 and 340 nm, respectively. All observed bands result from $\pi \rightarrow \pi^*$ transitions.

The semi-empirical and HF methods overestimated values of HOMO and LUMO energies for both the neutral and monocationic form of harmane due to the negligence of electron correlation. The best results were obtained using the hybrid DFT (B3LYP) method. It should be noted that inclusion of diffuse functions into the B3LYP calculations had little effect on the predicted geometrical parameters but it improved the value of HOMO-LUMO energy gap corresponding to the lowest energy band in the absorption spectra of β -carboline. The theoretically calculated electronic properties of neutral and protonated form of harmane are gathered in Table 1.

Table 1. The calculated values of dipole moment (μ , [D]) and HOMO-LUMO energy gap (ΔE , [eV]) for the neutral and cationic form of harmane.

Calculation method	Free base				Monocation			
	μ [D]	HOMO [eV]	LUMO [eV]	ΔE [eV]	μ [D]	HOMO [eV]	LUMO [eV]	ΔE [eV]
AM1	2.383	-8.550	-0.378	8.172	6.417	-12.272	-5.187	7.085
PM3	2.267	-8.617	-0.557	8.060	6.660	-12.250	-5.339	6.911
HF/6-31G(d)	2.752	-7.725	2.635	10.360	6.355	-11.679	-2.381	9.298
HF/6-31+G(d,p)	2.806	-7.899	1.556	9.455	6.513	-11.727	-2.698	9.029
B3LYP/6-31G(d)	2.792	-5.625	-0.983	4.642	5.803	-9.640	-5.809	3.831
B3LYP/6-31+G(d,p)	2.899	-5.939	-1.386	4.553	5.918	-9.830	-6.020	3.811

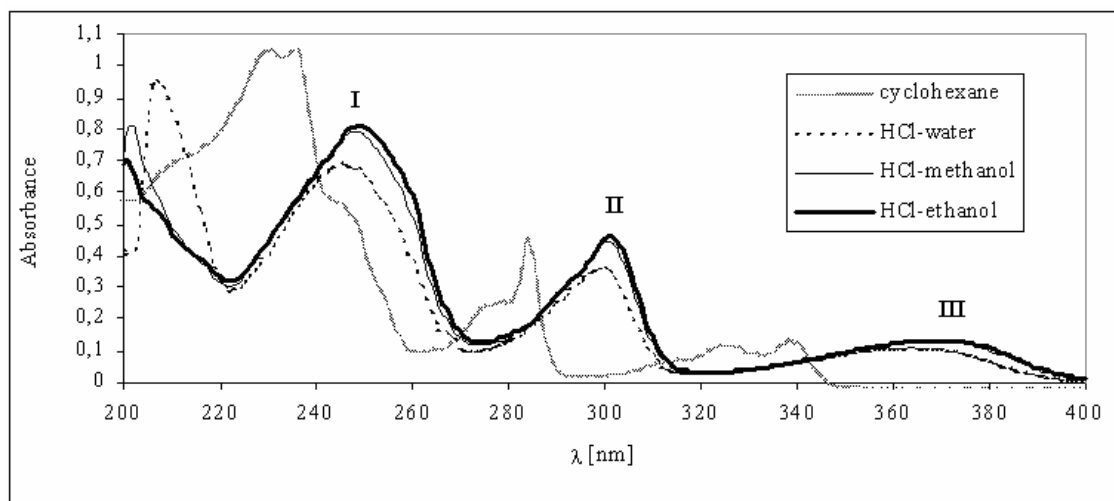


Figure 2. Absorption spectra of harmane dissolved in cyclohexane (----) and in HCl-acidified water (- - -), methanol (—) and in ethanol (—), respectively.

In order to get insight into the singlet electronic transitions in harmane monocation, ZINDO-1 semi-empirical as well as TD B3LYP with PCM methods were applied. The ZINDO-1 predicted excitation energies and oscillator strengths of electronic transitions for harmane monocation were less consistent with the experimental data. The ZINDO-1 calculations suggest that the lowest singlet excited state of harmane cation originated from the two close lying S_1 and S_2 transitions. The S_3 and S_4 transitions might correspond to band II whereas the S_5 and S_6 transitions might originate from band I of the absorption spectra. The results of TD B3LYP calculations indicated that the S_1 state might originate from band III whereas the S_2 transition might be compared with band II of harmane monocation absorption spectra. The S_3 and S_4 states might originate from band I. The S_3 state was expected to be less strong (based on its oscillator strength) making it likely that the peak corresponding to the S_4 would obscure the one arising from the S_3 state. The results of calculations performed on the B3LYP/6-31+G(d,p) optimized geometry of harmane monocation are summarized in Table 2.

4. Conclusions

In order to interpret the absorption spectra of harmane monocation two theoretical approaches were applied, i.e. the semi-empirical ZINDO-1 and the TD B3LYP/6-31+G(d,p) with PCM model, respectively. The former method led to a less consistent description of electronic transitions in harmane monocation when compared to the experimental data. The above inconsistency might result from the fact that no solvent effects were included. Inaccuracy of the method was especially evident in the prediction of two close lying S_1 and S_2 electronic transitions, for which solvent stabilization seems to be crucial. According to the obtained results, the S_2 state has a much larger dipole moment in comparison to the S_1 state, which makes the S_2 state more sensitive to polar environment. Due to solvent stabilization of the S_2 state, it is possible that the S_1 and S_2 states might interchange and the S_2 state would become the lowest-lying excited state. On the other hand, the TD B3LYP/6-31+G(d,p) PCM predicted properties of electronic transitions to the lowest excited singlet states of harmane monocation correlated quite well with the experimental data which may confirm the utility of the latter theoretical approach in the interpretation of the absorption spectra of harmane dissolved in acidified solvents.

Table 2. Transition energies (E), wavelengths (λ) and oscillator strengths (f) of electronic transitions for harmane monocation calculated using ZINDO-1 and TD B3LYP PCM methods.

Transition [†]	ZINDO-1 <i>in vacuo</i>			TD B3LYP/6-31+G(d,p) <i>in water</i>			experimental <i>in water</i>		TD B3LYP/6-31+G(d,p) <i>in methanol</i>			experimental <i>in methanol</i>		TD B3LYP/6-31+G(d,p) <i>in ethanol</i>			experimental <i>in ethanol</i>	
	E [eV]	λ [nm]	f	E [eV]	λ [nm]	f	E [eV]	λ [nm]	E [eV]	λ [nm]	f	E [eV]	λ [nm]	E [eV]	λ [nm]	f	E [eV]	λ [nm]
S ₁	3.245	382	0.1735	3.458	359	0.0735	3.369(III) [‡] f=0.0666	368	3.452	359	0.0724	3.342(III) [‡] f=0.0748	371	3.451	359	0.0738	3.342(III) [‡] f=0.0870	371
S ₂	3.553	349	0.4197	4.145	299	0.2470	4.160(II) [‡] f=0.2072	298	4.138	300	0.2456	4.160(II) [‡] f=0.2912	298	4.135	300	0.2550	4.119(II) [‡] f=0.2028	301
S ₃	4.254	291	0.0216	4.855	252	0.0353	5.034(I) [‡]	246	4.853	256	0.0360	4.999(I) [‡]	248	4.856	255	0.0370	4.959(I) [‡]	250
S ₄	4.670	266	0.7088	4.968	250	0.7858	f=0.9538		4.960	250	0.7787	f=1.0975		4.956	250	0.7787	f=1.0128	
S ₅	4.761	260	0.1460	5.357	232	0.0352			5.352	232	0.0392			5.355	232	0.0422		
S ₆	5.036	246	0.1224	5.428	228	0.0753			5.430	228	0.0732			5.438	228	0.0729		
S ₇	5.151	241	0.1538	5.657	219	0.0014			5.654	219	0.0014			5.651	219	0.0014		
S ₈	5.650	219	10 ⁻⁵	5.780	215	0.1341			5.781	215	0.1361			5.788	214	0.1363		
S ₉	5.773	215	0.4128	6.071	204	0.0656			6.071	204	0.0536			6.076	204	0.0514		
S ₁₀	5.811	213	0.4857	6.092	204	0.0003			6.092	204	0.0008			6.089	204	0.0010		

[†] All transitions were determined to be the $\pi \rightarrow \pi^*$ with the exception of TD B3LYP S₇ and S₁₀ and the ZINDO-1 S₈ which resulted from the $\pi \rightarrow \delta^*$ transition; [‡] numbers corresponding to the bands of absorption spectra of harmane dissolved in HCl-acidified solvents.

References

[1] J. Hidalgo, M. Balón, C. Carmona, M. Muñoz, R.R. Pappalardo, J. Chem. Soc. Perkin Trans. 2 (1990) 65; [2] M. Muñoz, M. Balón, J. Hidalgo, C. Carmona, R.R Pappalardo, E.S Marcos, J. Chem. Soc. Perkin Trans. 2 (1991) 1729; [3] H. Kansch, H. Tylli, J. Gynther, J. Rouvinen, J. Mol. Struct. (TheoChem), 153 (1987) 307; [4] G. Angulo, C. Carmona, R.R Pappalardo, M.A Muñoz, P. Guardado, E.S Marcos, M. Balón, J.Org.Chem., 62 (1997) 5104; [5] A.D.S Marques, H.F Souza, I.C Costa, W.M de Azevedo, J. Mol. Struct. (TheoChem), 520 (2000) 179; [6] A.Dias, A.P Varela, M. da G. Miguel, A.L. Macanita, R.S. Becker, J. Phys.Chem., 96 (1993) 10290; [7] K. El-Sayed, D.M Barnhart, H.L Ammon, G.M Wassel, Acta Cryst., C 42 (1996) 1383

Acknowledgements:

Financial support from the State Committee for Scientific Research, Grant No. 3T08E06327 (Poland) is gratefully acknowledged.

Catalytic and physicochemical properties of Pd-polymethacrylate resins
A. Kozak¹, A. Waksmundzka-Góra¹, J. Noworól², A. Bukowska², W.
Bukowski², A. Drelinkiewicz^{1,3}

¹*Institute of Catalysis and Surface Chemistry, Polish Academy of Sciences, 30-239
Kraków, Niezapominajek 8, Poland*

²*Faculty of Chemistry, Technical University, 35-059 Rzeszów, ul. W. Pola 2*

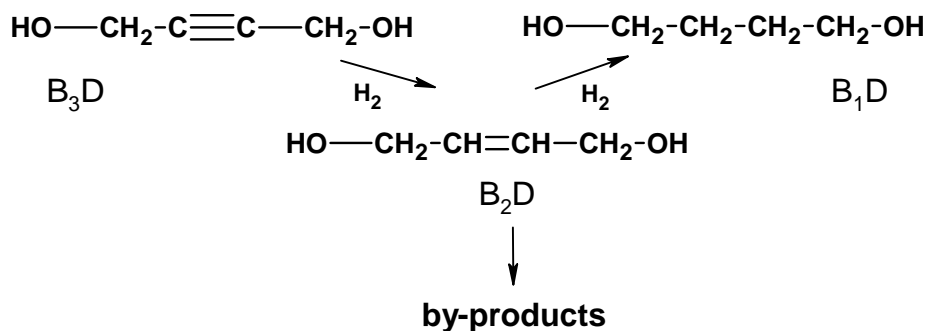
³*Faculty of Chemistry, Jagiellonian University, 30-060 Kraków, Ingardena 3, Poland*

Abstract

Polymethacrylate resin (OFP) supported palladium catalysts were prepared, characterized and used in the hydrogenation of 2-butyne-1,4-diol (B3-D), reaction of industrial relevance. The role of specific properties of Pd/OFP catalysts, like hydrophobic character and swelling ability, in their activity/selectivity behaviour in the hydrogenation of unsaturated triple bonds $C\equiv C$ (B3-D) to $C=C$ (2-butene-1,4-diol, B2-D) and subsequently to the saturated C-C one (butane-1,4-diol, B1-D) was studied. Very advantageous performance of 2%Pd/OFP catalyst in terms of activity and selectivity was observed, especially when the catalysts acted in swollen state induced by medium of low polarity (THF solvent).

Introduction

Currently, the most important catalytic application of organic cross-linked functional polymers (OFP) is acid catalysis, however the use of such material as support for metal nanoparticles is very promising [1, 2, 3]. Catalytic centers formed on functional resins act in the environment of swollen polymer gel, that is in the environment essentially different from the surface of conventional solid (Me-supported) catalysts. One of the most important difference between inorganic solids and OFP is the swelling ability of these organic materials in contact with reaction medium. Swelling of the polymer effectively separates the polymeric chains thus dramatically affecting accessibility of the active centers as well as the selectivity of reaction [1, 3]. The role of such specific properties of Pd-polymethacrylate resins systems in the activity/selectivity behaviour of catalysts is reported in the hydrogenation of 2-butyne-1,4-diol (B3-D), reaction of industrial relevance [4]. Hydrogenation of triple $C\equiv C$ bond in B3-D proceeds via an intermediate olefinic diol B2-D to the fully saturated butyne-1,4-diol (B1-D). B2-D and B1-D, both products are important raw materials for the fine chemical industry (preparation of pharmaceuticals, like endosulfan, pyridoxine (vitamin B₆), insecticides) [1, 2]. On typical catalysts such as Pd/Al₂O₃, Pd/C, Pd/TiO₂, the selectivity to B2-D is frequently reduced due to acid catalyzed reactions yielding by-products (like γ -hydroxybutyraldehyde, n-butyraldehyde, n-butanol, crotyl alcohol) and/or due to the formation of fully saturated B1-D already in the stage of triple bond in B3-D hydrogenation [5, 6]. To selectively produce olefinic diol (B2-D), alkaline additives like KOH, NH₃ are introduced to the hydrogenated solution [6, 7]. Pd/OFP catalysts used in this work exhibited very promising performance in terms of activity and selectivity especially when they acted in swollen state induced by medium of low polarity (THF solvent). Very high activity as well as selective hydrogenation of B3-D to B2-D (95 %) was then observed.



Scheme Hydrogenation of 2-butyne-1,4-diol.

Experimental

The OFP support (3 % crosslinking) containing carboxylic and ester groups was prepared by modification of co-polymer (2-hydroxyethyl methacrylate 20 % mol, styrene 77% mol) with glutaric anhydride (3 % mol). To prepare the catalysts, pristine OFP (spherical grains 75-150 μm) was swollen in THF and appropriate volume of $\text{Pd}(\text{ac})_2$ solution in THF (2.3×10^{-3} PdCl_2 mol/ dm^3) was added. The suspension was gently stirred at room temperature when all of Pd ions reacted (ca. 24 h). To reduce palladium ions, the catalyst was treated with NaBH_4 solution in THF : CH_3OH (9:1) under vigorous stirring, washed with H_2O , THF and dried under vacuum to constant weight (1 h at 50°C). The swollen ability of pristine OFP, as-prepared and reduced catalysts was evaluated by the measurement of the bulk expanded volumes (V_s) in THF, H_2O and THF- H_2O mixtures and expressed as V_s/V_o (V_o –volume of dry sample). Reduced catalysts were also characterized by FTIR, SEM and TEM techniques. Hydrogenation experiments were carried out in agitated batch reactor at atmospheric pressure of H_2 and temperature 22°C ($\text{B}_3\text{D} = 0.05$ mol/ dm^3). The course of reaction was followed by measuring the uptake of hydrogen against time. Samples of solutions were withdrawn from the reactor at appropriate intervals of time and GC analysis was performed (Auto system XL, Perkin Elmer, 30 m PE-5 MS capillary column).

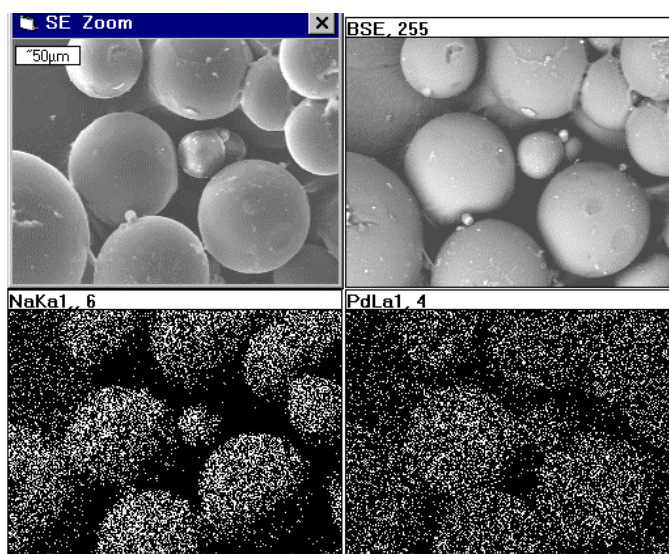


Fig. 1 Scanning electron micrographs (SE, BSE) of reduced 2% Pd/OFP catalyst.

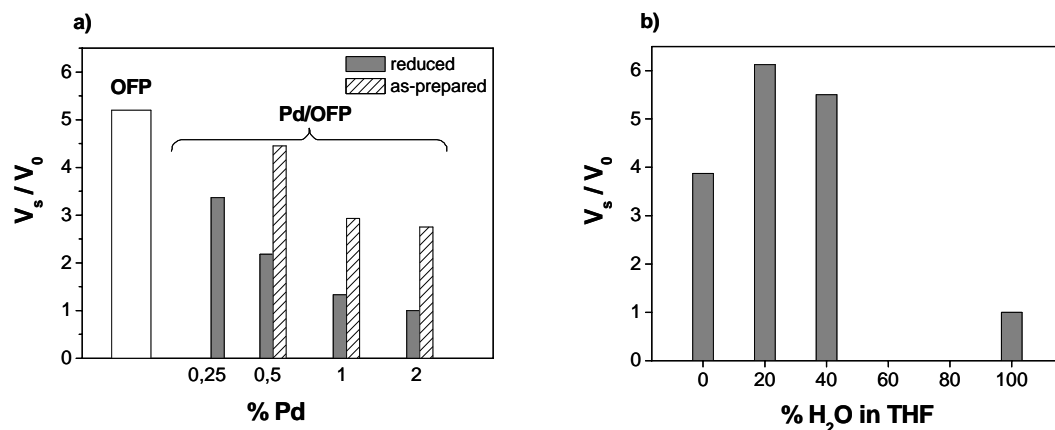


Fig. 2 Swelling efficiency of Pd/OFP catalysts (a) initial OFP and Pd/OFP catalysts, THF medium (b) reduced 2%Pd/OFP in THF-H₂O medium.

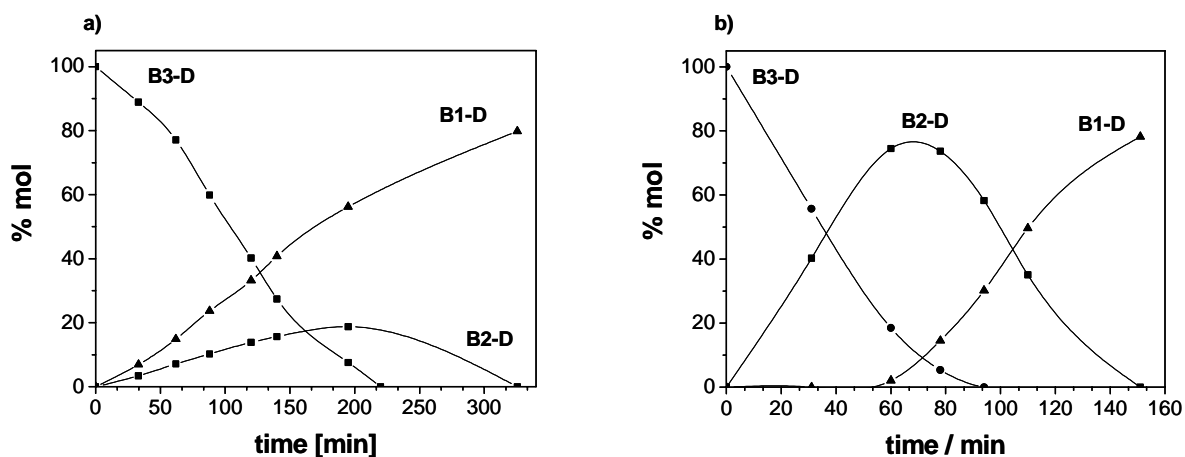


Fig. 3 Products distribution curves, hydrogenation of B3-D in H₂O (a) and THF-H₂O (b) medium.

Results and discussion

From the SEM map (Fig. 1) very homogeneous distribution of Pd through each resin particle of 2%Pd/OFP catalyst can clearly be seen. TEM studies reveal Pd-nanoparticles of nm in size thus indicating that the OFP resin in its swollen state at the stage of catalysts reduction with NaBH₄ prevented Pd particles aggregation. The catalysts were also characterized by bulk expanded volume measurement and results are given in Fig. 2 a, b. Owing to hydrophobic character, no volume expansion of OFP was observed in polar solvent like H₂O, ethanol. The swelling efficiency of OFP as well as Pd-containing samples was very high in THF solvent of low polarity (Fig. 2 a). Although insertion of palladium slowly reduced the swelling ability of pristine OFP, the volume of Pd-containing resins grains was strongly expanded in THF. The swelling ability of as-prepared Pd/OFP (Pd²⁺ ions present) catalysts slowly decreased with a rise in Pd content, however a moderate expansion of catalysts grains was still observed. This can be related to exchange of H⁺ by Pd²⁺ upon reacting Pd(ac)₂ with OFP in acidic form (crosslinking effect). The NaBH₄ reduced 2%Pd/OFP catalyst was also characterized by bulk expanded volume measurements in THF and THF + H₂O mixtures (Fig. 2 b). The

swelling ability slowly increases with a rise in H₂O content in THF and reaches the maximum at 20 % H₂O. The same solvents, H₂O, THF and THF + H₂O mixtures, were used in the hydrogenation of 2-butyne-1,4-diol (B3-D). The change in reagents concentrations (B3-D, B2-D and B1-D) against reaction time in hydrogenation carried out on 2%Pd/OFP catalyst is reported in Fig. 3a and Fig. 3b. In the former case, water was used as the solvent, in the latter, THF-H₂O mixture (20 % H₂O) corresponding to the highest volume expansion of 2% Pd/OFP grains. The data obtained in hydrogenation tests reveal that the catalytic performance of Pd/OFP catalysts, rate of triple bond in B3-D hydrogenation and selectivity to B2-D, both depends critically on their swelling ability. In all system studied, the contribution of reactions producing by-products to the whole hydrogenation process was very low (5-10 mol % of by-products) maybe because most of H⁺ in the OFP was changed by Na⁺ upon the reduction with NaBH₄. In water, solvent in which the polymer does not swell, the catalysts grains can be considered as “closed” because the access of Pd-centers located inside of bulk are rather difficult. Consequently their outer surface mostly participates in the reaction and the rate of B3-D hydrogenation (1.57 mol/min) is the lowest. The rate dramatically increases in THF (3 mol/min) and it becomes especially high (3.5 mol/min) in conditions inducing the highest expansion of catalysts grains (THF + 20 % H₂O). Hence, the catalytic results are in line with the swelling ability of 2%Pd/OFP catalyst. More interesting are the changes in selectivity of B3-D hydrogenation, a consecutive reaction in which the hydrogenation of C≡C (B3-D) to C=C (B2-D) is followed by the hydrogenation of C=C to C-C (B1-D). In aqueous conditions, the formation of fully hydrogenated B1-D proceeds already in the stage of triple bond in B3-D hydrogenation thus resulting in very low yield to B2-D, a desirable olefinic diol. On the other hand, when the grains of catalyst are in expanded state (THF, THF + H₂O) B2-D is selectively formed (95 %). Only the B3-D reacts to B2-D from the initial stage up to 95 % conversion and after that the B2-D undergoes hydrogenation to B1-D. Such selective formation of B2-D was observed in all THF- containing systems. Hence, the swollen state of Pd/OFP catalyst is very advantageous not only in terms of activity but also the selective hydrogenation of starting B3-D to B2-D, a desirable product. Such an effect can be related with the nano-environment surrounding the active centers and their accessibility. The catalysts were quite easily filterable and reusable, without loss of activity for at least three runs. These properties make the Pd/OFP catalysts very promising systems.

References

- [1] B. Corain, M. Zecca, K. Jerabek, *J. Mol. Catal. A; Chemical* 177 (2001) 3
- [2] M. Kralik, V. Kratky, M. De Roso, M. Tonelli, S. Lora, B. Corain, *Chem. Eur. J.*, 9 (2003) 209
- [3] D. Wohrle, A. Pomagailo, „Metal Complexes and Metals in Macromolecules” Wiley-VCH BmbH & Co. KgaA, 2005
- [4] H. Grafje, *Ullmann`s Encyclopedia of Industrial Chemistry*, Weinheim, Germany; Wiley-VGH Verlag GmbH, Vol A4 (1985) 455
- [5] J.M. Winterbottom, H. Marwan, E.H. Stitt, R. Natividad, *Catal. Today*, 79-80 (2003) 391
- [6] M.G. Musolino, C.M.S. Cutrupi, A. Donato, D. Pietropaolo, R. Pietropaolo, *J. Mol. Catal. A; Chemical*, 195 (2003) 147
- [7] M.M. Telkar, C.V. Rode, V.H. Rane, R. V. Chaudhari, *Appl. Catal. A: General*, 216 (2001) 13

ACTIVATING METHODS IN THE TEACHING OF CHEMISTRY IN A SPECIAL SCHOOL*

Wiesław Koźlak

*Warsaw University of Technology, Institute of Chemistry,
09-400 Płock, Łukasiewicza 17*

Introduction

Every human being from his youngest years acquires knowledge which is then in a conscious or spontaneous way used in his daily life. This knowledge helps him to function properly in the surrounding world. Acquisition of definite and systematic knowledge takes place in school in the frames of defined teaching subjects. It is teachers who are transferring the truths about the surrounding world. For the learning process to be interesting, effective and creative, the teachers constantly search for new methods of transferring knowledge which would become the inspiration for the pupils for the independent searching for answers for pervading questions. Activating methods are a promising tool for the didactic work in chemistry lessons. Limited cognitive possibilities of lightly mentally handicapped children require the use of such methods and forms of work that make their own activity higher than the activity of the teacher. It must be pointed out that there is no scientific or quasi-scientific elaborations in this area. There is also lack of text-books for teaching chemistry in special schools. All that chemistry teachers elaborate in their classes, how they introduce pupils into the secrets of chemistry, abstract ideas and the laws that are controlling our world, is innovatory. This work is an attempt to present the methods activating the teaching and learning processes in chemistry lessons including the experiences of teachers working with lightly mentally handicapped pupils.

Specificity of teaching in a special school for lightly mentally handicapped children

Difficult work, requiring lots of patience, devotion and love, correctly fulfilled gives joy and complacency. One has to know the intellectual potential of the child, its cognitive limitations, psychical and emotional maturity in order to properly select the methods of transferring the knowledge and conduct the teaching process. Mental handicap means the lower level of intellectual functioning, occurring with significant limitations in adaptative behavior in the following areas of proficiency: communication, independence, home life, social skills, health and safety, at work and in their free time [1].

Among lightly mentally handicapped children (3%) there are significant differences in the intellectual, emotionally-motivating, orientatively-cognitive and social processes [2-4].

Equally to the attractive didactic methods it is important to aid the intellectual development and emotional sphere through various forms of activity.

Special schools were formed for:

- education and upbringing of children and youths,
- enabling the fulfillment of school duties [5].

Organizational structure of special education system

Six-year primary school

Years 1-3 – first stage of education, years 4-6 – second stage of education

Three-year secondary school – third stage of education

High schools – fourth stage of education

Programme of chemistry teaching in a special secondary school

Programme is limited to the “Chemistry in the surrounding world” area with the elements of environment protection, realized in correlation with physics, biology and geography.

Teaching subjects include: water, air, natural resources, proteins, carbohydrates, organic and mineral acids, lipids, soaps, substances and their transformations, constituents of our planet.

Activating methods for teaching chemistry in a special secondary school

The feature of the activating methods is the dominance of pupils activities over teacher’s actions. The teacher directs the teaching process and pupils almost independently discover the world of chemistry [7,8].

Chemistry as a teaching subject

Chemistry in special schools – after the reform in 1999 in secondary schools.

Primary school – preparation of the pupil for the coexistence with the world.

Secondary school – acquiring the knowledge of the secrets of chemistry, understanding of the world of chemistry as a continuation of the world of nature.

The assumptions of teaching:

- shaping the ability of thinking,
- dealing with the information in an integral way,
- relations with the practice,
- passing the knowledge of basic laws,
- forming proper attitudes (health, environmental protection),
- indication of the importance of chemical knowledge in the daily life.

Teaching of chemistry is realized in connection with the ecological education, covering for instance the areas of “Water” and sources of pollution, methods of water purification and pollution prevention during the excursion to the waste-water purification plant, walk along the river bank, collecting samples of water etc.

Lessons aided with experiments improve the acquisition of knowledge. Additionally didactical games and excursions are employed, as well as work with text-books, movies, problem-oriented methods, micro-teaching.

Activating methods for teaching chemistry in a special school –propositions [9,10]

Method has to correlate with the aim that has to be achieved during the lesson unit.

Improvement of the contact with pupils changes their attitude towards the subject.

Activation means the creation of conditions for the active role in the teaching process through cooperative work, giving pupils special roles, outdoor activities.

Direct observation provides better effect than presentation of the problem during lesson.

Repetitional lessons are chemical mini-competitions, with lottoed questions and tasks, work in teams of 3-4 pupils and estimation of pupils and teams.

Recapitulation lessons use artistic methods such as posters, presentations.

Interesting form of work is making up advertising and warning slogans.

Recapitulation and conclusions

Modern school can not stand aside, it has to participate and help a young human being in his development. Teachers should look for new solutions and methods of work which most effectively will help them in transferring his knowledge.

Changes did not steer clear of special care children and system of special education. The reform in 1999 brought Poland closer to European standards and gave handicapped children equal chances of start adjusted to their capabilities.

The novelty is the third stage of education (secondary school), which introduced chemistry into the teaching programme.

Activating methods in chemistry teaching are: chemical experiment, presentation, work in groups, games and didactical movie.

Chemical experiment allows for full participation in the lesson and obtaining good results without the necessity of longer expressions.

Activating methods allow children to achieve small successes and promote their own activity giving the opportunity of searching for simple solutions of some problems. Activating methods develop creative thinking, children themselves propose simple experiments.

Didactic games is an element of play and lesson is linked with pleasure and achieving successes.

Activating methods are used to diversify the lesson but also form the **new style of work** of teacher and pupil.

Chemical education of lightly mentally handicapped children requires a scientific elaboration, work in the area of didactics of chemistry in which the problems of teaching chemistry in a special school will be discussed.

*Detailed programme of chemical education in a special school, description of activating methods and their practical use (lesson scenarios) were presented in an article sent to the Editor of "Chemia w Szkole" ("Chemistry in School").

Literature:

[1] J. Kostrzewski, Ewolucja poglądów AAMR dotyczących niedorozwoju umysłowego, Roczniki Pedagogiki Specjalnej, 1997

[2] K. Kirejczyk, Upośledzenie umysłowe, Pedagogika, Warszawa 1981

[3] R. Kościelak, Psychologiczne podstawy rewalidacji upośledzonych umysłowo, Warszawa 1989

[4] L. Zegarek, I. Rocznik, Sylwetka Mateusza – charakterystyka ucznia z upośledzeniem w stopniu lekkim, in: Poradnik metodyczny dla nauczycieli kształcących

uczniów z upośledzeniem umysłowym w stopniu lekkim w szkołach ogólnodostępnych i integracyjnych, Warszawa 2001

[5] J. Sowa, Pedagogika specjalna w zarysie, Rzeszów 1998

[6] M. Wiechowska, Chemia. Program nauczania w gimnazjum specjalnym dla uczniów z upośledzeniem umysłowym w stopniu lekkim, DKW – 4014 – 57/00

[7] M. Noskowska, Metody aktywizowania uczniów, Chemia w szkole, 2 (2000)

[8] H. Bielecka, A. Wawrzyniak-Kuczyk, Aktywizujące metody nauczania, Chemia w szkole, 5 (2000)

[9] D. Grabasz, M. Dysz, Fizyka i chemia w kształceniu uczniów z upośledzeniem umysłowym w stopniu lekkim na etapie gimnazjum, in: Poradnik metodyczny dla nauczycieli kształcących uczniów z upośledzeniem umysłowym w stopniu lekkim w szkołach ogólnodostępnych i integracyjnych, Warszawa 2001

ECOLOGICAL ADVANTAGES OF SOLUBLE GLASS

Wiesław Koźlak

*Warsaw University of Technology, Institute of Chemistry,
09-400 Płock, Łukasiewicza 17*

Introduction

From among a large number of chemical compounds, special attention should be paid to sodium soluble glasses, belonging to a group of large tonnage products, having many applications in different branches of industry and economy. It is held that there is not a single area of industry that doesn't utilize soluble glasses. Poland has the basic stock base for the production of soluble glasses (SiO_2 and Na_2CO_3) [1].

Sodium soluble glass was invented about 6000 years ago in Thebes, an ancient city in Upper Egypt. Inhabitants of Thebes owned soda deposits, occurring on the sandy banks of soda lakes, mixed with silica sand. From this mixture, in high temperature smelting crucibles, a transparent solid substance was produced, which after dissolving in water was used for the mummification of bodies. Medieval alchemists knew water glass under the name of oleum silicium. Because there was no application found for this substance it fell into oblivion. Only in 1841 first factory producing water glass was built in France [2].

The first known work regarding the solutions of sodium silicates, describing the changes of their viscosity as a function of concentration and the molar ratio of SiO_2 to Na_2O (which is now called the silicate modulus, M_k^*), was presented in 1926 by Main [3]. In this work it was shown the difference between the physico-chemical properties of silicate solutions and other inorganic substances. This finding did not, however, cause any interest in studying the other properties of water solutions of silicates until the beginning of 1950s. At this time systematic studies on these substances were started in several scientific centres (such as Berlin, Stanford, Wallingford, Mulhouse, Tjumen). In the history of studies on silicate solutions, started by Main, two periods of special interest in this area can be distinguished: 1953-1956 and 1974-2000. Also the literature search from recent years shows that there are only a few centers in the world that undertook the studies on systems containing alkaline metal silicates.

Until now, there is no leading scientific centre in the world working in this area and in Poland the only centre that carries out systematic research of the chemistry of sodium silicates

* $M_k = x_{\text{SiO}_2} / x_{\text{Na}_2\text{O}} \cdot 1.032$, where x_{SiO_2} and $x_{\text{Na}_2\text{O}}$ – weight percent of SiO_2 and Na_2O , 1.032 is the molar mass ratio of both oxides

solutions, mainly manufactured in Poland by Rudniki Chemical Plant, is the Department of Civil Engineering, Mechanics and Petrochemistry of Warsaw University of Technology.

Ecologically friendly sodium soluble glasses

From the ecological point of view, sodium water soluble glasses are safe for the natural environment. They are non-toxic, so they can be added to water, even drinking water, which allows to send cooling waters into a reservoir without purification [4].

Their total non-toxicity and basicity of their aqueous solution (as a result of their hydrolysis) does not cause acidification which only underscores advantages of soluble glasses.

Sodium silicate is not considered as a dangerous material so it is easy to transport in railway and car cisterns and in metal containers.

Among their advantages also the economical profits can be pointed out. Sodium water glasses are cheap and provide the possibility of obtaining large technical and economical benefits.

Soluble silicates inhibit corrosion, prevent deposits formation and are useful also in systems that were already strongly corroded [4,5]. They can be characterized as compounds of low reactivity and relatively high stability, unlimited solubility in water and fire-resistant.

Mentioned friendliness of water glasses for the natural environment allows to make an appeal towards ecologists to consider undertaking of collective actions for the resolution of signalized problems in scientific, experimental and ecological aspects alike.

Studies on the chemistry of aqueous solutions of silicates and selected areas of their applications from the ecological point of view

Soluble glasses form systems especially hard to investigate because of the low stability of silicate ions and various levels of their condensation [6-8]. That is why they are still not sufficiently recognized both in the aspect of their molecular composition and physico-chemical properties.

Till this moment, thanks to the use of most modern methods and techniques of investigation, a huge progress in this area has been made. Many methods for the description of composition and structure of alkaline silicates solutions were proposed, however it is hard to generalize this data because their more detailed analysis shows many divergences [7] which can lead to the statement that the results of investigations probably depend on the method of production of the studied silicate [8,9].

In these investigations the following methods were employed: potentiometric, viscosimetric, spectrophotometric with the use of cationic dyes, method based on the synthesis of b-molybdenosilicic acid, turbidimetric method, ^{29}Si NMR and Poly-Quat.

The analysis of recent literature reports [4] shows the wide spectrum of investigations but because of the large thematic dispersion, the obtained results do not lead to the solution of problems pervading for many years.

Sodium soluble glasses are used for example in such ecologically important areas as communal and industrial water treatment (softening), anti-corrosion protection of water circuit installations, production of moulding masses etc. Extensive catalogue of applications of silicates was presented in an earlier work [4].

In order to underscore the ecological advantages of soluble glasses it was indicated that the most useful method of investigations is turbidimetric method [4,10,11]. It is based on formation of water soluble, colloidal silicate of a studied salt in course of reaction of soluble silicate forms with examined salt and measuring the intensity of radiation scattered by formed silicate. The ability to form the silicate of a studied salt and the course of scattered light intensity changes depend on the chemical composition of silicate solution and its silicate modulus (M_k). Presence of impurities, i.e. alien ions introduced into soluble glass during its production has also significant influence on the course of reaction.

The principles of turbidimetric method, methodology of measurements and testing equipment were described in an earlier work [10,11].

Obtained results in the form of so called turbidity curves have shown that the character of their course is closely related to the type of silicate characterized by its silicate modulus (M_k) and chemical composition of its solutions. In particular it was found that:

- addition of selected salts (of calcium and magnesium in case of evaluation of the possibilities of using water silicates for water treatment and iron salts for the evaluation of anti-corrosion protection of water circuit installations) into solutions of soluble glasses causes the formation of colloidal silicates,
- different courses of turbidity curves indicate that formation of colloidal silicates depends on the type of cation ,
- in order to characterize the nature of interaction between salt and sodium silicates a mathematical model can be used, basing on which average radii of particles and relative sizes of formed colloidal silicate particles were evaluated.

Recapitulation

In the present time it can be said that the knowledge of soluble glasses among researchers belonging to many groups such as chemists, physico-chemists and ecologists is not sufficient. An up-to-date review of the literature of the subject [5] shows that there is only a small number of articles and no text-books at all, which fundamentally discuss the areas of applications of alkali metals silicates and their solutions. That is why an appeal is made to undertake common effort in order to solve pointed out problems, in all aspects: scientific, experimental and ecological.

Fundamental expectations from the ecologists' point of view:

- common research leading to the recognition of action mechanism of silicates in the areas where they are already widely used, with stress put on the problems of natural environment preservation,
- suggestion of expansion of soluble glasses application areas taking into account their ecologically friendly advantages.

This is from where the necessity arises to conduct complex investigations taking into account the influence of the most important parameters on the behavior of silicates. This is a problem of big importance because water glasses from the ecological point of view are very environmentally friendly [6,12].

Literature

- [1] W. Augustyn, N. Grobelny, *Chemik*, 10 (1957) 262
- [2] Informations from the www.fabrykabe.pl/pdfs/system_novalitl.pdf webpage, 27.04.2005.
- [3] V. R. Main, *J. Phys. Chem.*, 30 (1926) 535
- [4] W. Koźlak, *Wiad. Chem.*, 59 (2005) 791; 60 (2006) 379
- [5] W. Koźlak, *Ochrona przed korozją*, in press
- [6] W. Koźlak, *Aura*, submitted for publication
- [7] W. Koźlak, PhD thesis "Studies on selected properties and structure of aqueous solutions of technical silicates", 1980, Politechnika Warszawska
- [8] D. Hoebbel, R. Z. Ebert, *Z. Chem.*, 28 (1988) 41
- [9] W. Koźlak, *Pol. J. Appl. Chem.*, 49 (2005) 227
- [10] W. Koźlak, *Chemik*, 6 (2006) 337
- [11] W. Koźlak, *Ann. Pol. Chem. Soc.*, 3 (2004) 252
- [12] W. Koźlak, *Problemy Ekologii*, in press

DEUTERIUM SOLVENT ISOTOPE EFFECTS IN OXIDATION OF L-TYROSINE CATALYZED BY TYROSINASE

Małgorzata Kozłowska, Marianna Kańska

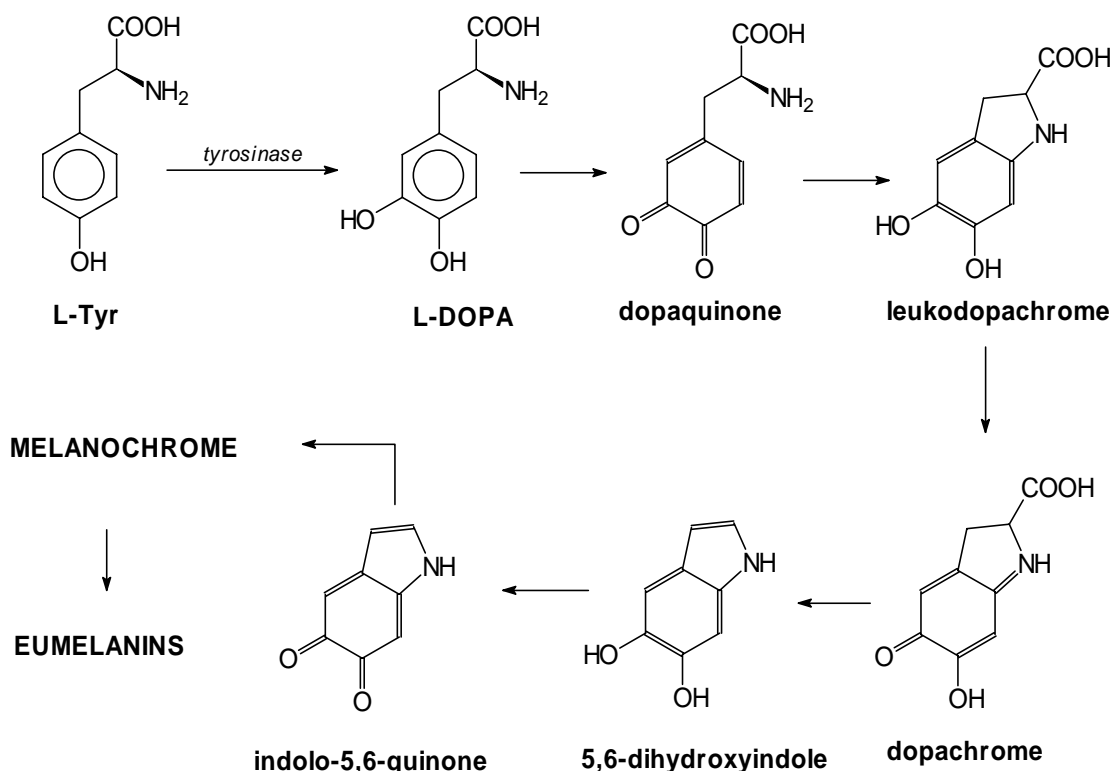
University of Warsaw, Department of Chemistry, Pasteur 1 Str., 02-093 Warsaw

Abstract

The solvent isotope effects on Michaelis, K_m , and maximum reaction rate, V_{max} , in the reaction of hydroxylation of L-tyrosine to L-DOPA catalyzed by enzyme tyrosinase (EC 1.14.18.1) were determined. Solvent isotope effects were obtained by noncompetitive method for L-tyrosine and its two deuteriated isotopomers: $[3',5'\text{-}^2\text{H}_2]$ -, and $[2',6'\text{-}^2\text{H}_2]$ -L-tyrosine.

Introduction

The enzyme tyrosinase (Tyrosinase EC 1.14.18.1) classified to oxyreductases catalyzed two followed (subsequent) oxidation reactions of L-tyrosine to L-DOPA (3',4'-dihydroxyphenylalanine), and next L-DOPA to dopaquinone [1,2]. This *o*-phenol nonenzymatically proceeds to several another unstable intermediates, which polymerize to yield melanins [3], scheme 1.



Scheme 1. Conversion of L-tyrosine into melanins in living cells.

Tyrosinase is widely distributed throughout the nature [4,5]. It plays very important role in browning of vegetable and fruits, it causes also pigmentation in vertebrates, its deficit in mammalian leads to albinism. Exact mechanism of the action of

enzyme tyrosinase is not clear up to now. It would be interesting to study this problem using isotope effect method, particularly investigating the deuterium solvent isotope effects. Kinetics of enzymatic reaction are usually characterized by Michaelis equation:

$$K_m = S \left(\frac{V_{max}}{v} - 1 \right)$$

where v is the reaction rate at substrate concentration S , V_{max} is a maximum reaction rate, and K_m is a Michaelis constant. K_m and V_{max} are interrelated, and approximately speaking K_m is a measure of strength of enzyme-substrate binding, and V_{max} is a measure of the rate of reaction under conditions given. Interpretation of solvent isotope effects may bring new light on the mechanism of reaction studied. In the literature there are many papers concerning using of isotope methods for investigation of mechanism of action of enzyme tyrosinase [6-10]. Some of them report the data of SIE obtained for hydroxylation of L-tyrosine using natural and genetically modified enzymes [11]. The very similar enzyme tyrosine hydroxylase (EC 1.14.16.2), known also as tyrosine 3-monoxygenase or L-tyrosine tetrahydropteridine, was the subject of intensive investigations, and many data concerning isotope effects were obtained using isotope methods [12-14]. This enzyme oxidizes also L-tyrosine to dopachrome *via* L-DOPA, but its structure [15] differs considerably from tyrosinase (EC 1.14.18.1) studied currently by us.

In this work we study the influence of solvent on K_m and V_{max} in the reaction of hydroxylation of L-tyrosine to L-DOPA catalyzed by enzyme tyrosinase. Solvent isotope effects - SIE, were determined for L-tyrosine and its two deuteriated isotopomers, i.e., $[3',5'\text{-}^2\text{H}_2]$ -L-tyrosine, which synthesis was described elsewhere [16] and commercial $[2',6'\text{-}^2\text{H}_2]$ -L-tyrosine. The kinetic of conversion of L-tyrosine into L-DOPA were measured using noncompetitive method, and numerical values of SIE [17] were calculated by dividing kinetics parameters obtained in phosphate buffer by the ones obtained in fully deuteriated buffer. The progress of reaction was monitored indirectly by spectrophotometrical measurements of absorbance of dopachrome (Scheme 1) at $\lambda = 475$ nm (molar extinction coefficient for dopachrome $\epsilon = 3600 \text{ M}^{-1}\text{cm}^{-1}$).

Experimental

Standard mixture contains 0.1M phosphate buffer (pH 7.0), or 0.1M fully deuteriated phosphate buffer (pD 7.0) prepared from 83% $\text{D}_3\text{PO}_4/\text{D}_2\text{O}$, 30% KOD and 99,9% heavy water, L-tyrosine and enzyme Tyrosinase EC 1.14.18.1 (0.02 U/ml). The concentration range of L-tyrosine, $[3',5'\text{-}^2\text{H}_2]$ - L-tyrosine, $[2',6'\text{-}^2\text{H}_2]$ - L-tyrosine was between 2.1 mM and 0.6 mM. The isotopomer $[3',5'\text{-}^2\text{H}_2]$ - L-tyrosine has been synthesised in our laboratory [16] , and $[2',6'\text{-}^2\text{H}_2]$ - L-tyrosine was purchased from Sigma. The total volume of reaction mixture was 2 ml. The progress of reaction was monitored spectrophotometrically by measuring the increasing of absorbance of dopachrome at $\lambda=475$ nm. These kinetic assays were carried out at the room temperature. The maximal velocity (V_{max}) and ratio of Michaelis constant per maximal velocity (K_m/V_{max}) were calculated using computer programme Enzfitter 1.05. The results of solvent kinetic isotope effects concerning of three mentioned above isotopomers of L-tyrosine are shown in Table 1.

Isotopomer of L-tyrosine	SIE on V_{\max}	SIE on V_{\max}/K_m
L-tyrosine	5.71 ± 0.131	9.33 ± 0.37
[3',5'- $^2\text{H}_2$]- L-tyrosine	1.89 ± 0.053	3.66 ± 0.142
[2',6'- $^2\text{H}_2$]- L-tyrosine	4.16 ± 0.036	9.95 ± 2.45

Table 1. Solvent Isotope Effects

Discussion

The oxidation of L-tyrosine in the presence of tyrosinase in phosphate buffer proceeds about 6 times faster than in fully deuteriated medium. Similarly the rates of oxidation for compounds of L-tyrosine labeled with deuterium in aromatic ring are also lower in deuteriated medium. Probably the H/D exchange of labile protons of enzyme causes the conformational changes in active site of enzyme, and this reflects on activity of this biological catalyst slowing considerably its activity.

Acknowledgement

This work was supported by grant KBN 1 T09A 027 30

References

- [1] K. Murano, J. Waite, *Biochim. Biophys. Acta*, 872 (1986) 98
- [2] K. Lerch, *Methods in Enzymology*, Academic Press, New York, 142 (1987) 165
- [3] C. Olivares, C. Jimenez-Carvantes, J. A. Lozano, F. Solano, J. C. Garcia-Borron, *Biochem. J.*, 354 (2001) 131
- [4] J. R. Ros, J. N. Rodríguez López, J. C. Espín, R. Varón, F. Garcia-Cánovas, *Int. J. Biochem. Cell Biol.*, 28 (1996) 917
- [5] J. C. Espín, J. Tudela, F. García-Cánovas, *Anal. Biochem.*, 259 (1998) 118
- [6] A. J. Winder, H. Harris, *Eur. J. Biochem.*, 198 (1991) 317
- [7] L. G. Fenoll, M. J. Panalver, J. N. Rodriguez-Lopez, P. A. Garcia-Ruiz, F. Garcia-Canovas, J. Tudela, *Biochem. J.*, 380 (2004) 643
- [8] J. C. Espin, R. Varon, L. G. Fenoll, M. A. Gilabert, P. A. Garcia-Ruiz, J. Tudela, F. Garcia-Canovas, *Eur. J. Biochem.*, 267 (2000) 1270
- [9] J. N. Rodriguez-Lopez, J. Tudela, R. Varon, F. Garcia-Carmona, F. Garcia-Canovas, *J. Biol. Chem.* 267 (1992) 3801
- [10] J. R. Ross, J. N. Rodriguez-Lopez, F. Garcia-Canovas, *Biochim. Biophys. Acta*. 1204 (1994) 33
- [11] C. Jimenez-Carvantes, J. C. Garcia-Borron, P. Valverde, F. Solano, J. A. Lozano, *Eur. J. Biochem.*, 217 (1993) 549
- [12] P. A. Frantom P. F. Fitzpatric, *JACS* 125 (2003) 16191
- [13] P. J. Hillas, P. F. Fitzpatric, *Biochemistry*, 35 (1996) 6969
- [14] P. F. Fitzpatric, *Biochemistry*, 30 (1991) 3658
- [15] A. W. Tank, N. Weiner, *Methods in Enzymology*, Academic Press, New York, 142 (1987) 71
- [16] M. Kozłowska, R. Kański, M. Kańska, *J. Label. Compd. Radiopharm.*, 48 (2005) 235
- [17] R. L. Schowen, *Prog. Phys. Org. Chem.*, 9 (1972) 275

INFLUENCE OF DANGERS RELATED TO THE USE AND TRANSPORT OF AMMONIA ON THE NATURAL ENVIRONMENT

Wiesław Koźlak, Anna Dorota Klepańska
*Warsaw University of Technology, Institute of Chemistry,
09-400 Płock, Łukasiewicza 17*

Introduction

Civilizational advancement manifesting itself in a dynamic development of particular branches of technology, such as communication, energetics, chemical industry, causes the appearance and increase of several dangers for people, property and natural environment. Also food industry was developed significantly and with its growth increased the need for vegetables and fruits needing freezing and refrigeration. Thanks to that these products are now available on the market all year long. For the process of freezing ammonia is used. Plants that use ammonia in their technological processes (freezing of fruits and vegetables with the use of ammonia installation) create potential dangers for the natural environment and ipso facto danger threatening human life and health.

Dangers caused by ammonia [1]

When analyzing physico-chemical properties of NH_3 , it can be concluded that it creates the dangers of fire and explosion. Direct contact of the worker with this substance may result in a health loss or in extreme instances, death.

Under normal conditions ammonia is a colourless gas having sharp, pungent smell. In industry and commerce it can occur as gaseous ammonia, liquid ammonia or ammoniac water. It can be liquified easily. Because ammonia is almost twice lighter than air, being oxidized it migrates towards upper parts of the room. In air ammonia reacts with water vapour and carbon dioxide forming ammonium carbonate.

Aqueous solutions of ammonia are fire resistant liquids. Ignition is only possible in case of highly concentrated solutions, in high temperature and in presence of highly energetic sources of ignition. Over concentrated solutions, particularly in closed tanks or in case of heating of these solutions, explosive mixtures of ammonia and air can be formed.

Liquified ammonia is a colourless liquid having high heat of vaporization. It dissolves many substances, interacts with copper and its alloys and salts. In contact with such substances as for instance mercury, chlorine, bromine, iodine, hydrofluorine, chlorates (I) etc it self-ignites. In reaction with sodium and calcium ammonia forms explosive products.

Ammonia does not react with steel but it causes the corrosion of zinc, copper and its alloys. High concentration of ammonia is harmful for electrical equipment. In temperatures over 260°C ammonia decomposes to nitrogen and hydrogen. Such temperatures do not occur during normal mode of work of the equipment but can occur for instance during welding when maintenance works are improperly conducted.

Influence of ammonia on human organism. Intoxication prevention

Ammonia is a toxic substance. In gaseous NH_3 form it is harmful for skin, lungs and eyes. Has sharp, pungent smell. Toxic effect of NH_3 is based on formation of ammonium hydroxide in mucous films. Ammonium hydroxide dissolves proteins and because of that leads to deep necrosis changes. Ammonia and ammonium hydroxide directly damage the cells

and cause particularly painful irritation of all mucous films. Inhalant intoxication with ammonia causes swelling, irritation and pneumonia.

Reaction of human organism on ammonia depends on ammonia concentration and time of exposure. Its characteristic sharp smell acts as a warning, protecting from exposure to highly concentrations. That is why severe intoxications with gaseous ammonia occur relatively seldom. At the same time, particularly among people who have contact with gaseous ammonia at work, the receptivity towards the smell of ammonia gradually decreases. The cause of this effect is the gradual paralysis of smelling nerves terminations.

Inhalation of ammonia causes aggravating throat irritations, cough, salivation, nausea, weeping, headache. Slight exposure usually causes irritation of mouth, nose and throat. Cough occurs, elevated body temperature and breath curtailing. In more serious cases a pneumonia can develop, irritation of breathing system, circulation incapacity, which can lead to death. People who survived severe ammonia intoxication have most often irreversible changes in lungs and breathing tracts. Frequent staying in ammonia containing atmosphere can lead to troubles with digestion. High concentrations of ammonia cause burns of I and II degree.

Workers having contact with ammonia should be thoroughly trained in methods of evacuation and use of personal protection equipment such as goggles, respirators, showers, protective clothes etc. All equipment should be constantly controlled in order to prevent accidents. Valves should be precisely marked to avoid accidental dehermetization of the installation [2,3,4].

Proceeding in case of danger of ammonia leak [5,6]

The danger of ammonia leak requires that the crew and other people staying in the area endangered with ammonia equipment failure could evacuate protecting their breathing tracts with masks and half-masks. Failures have to be located and liquidated as fast as possible and that is why it is necessary to maintain rescue forces wherever the danger of areal pollution occurs.

Rescue workers have to be equipped with gas-proof, anti-chemical protective clothes, protecting the whole body from gases, liquids, vapours and dusts.

In case of ammonia leak in a closed room, only especially trained in chemical rescue workers can take part in pollution liquidation. The decision regarding the number of rescue workers, and personal protection equipment is made by a person managing the rescue action. If it is not possible to liquidate the effects of the accident with own forces and measures, the action should be entrusted to outside, specialized rescue forces.

People who take part in a rescue action in area polluted with ammonia should be safeguarded by two additional rescue workers. One person assists inside the polluted room, the other one stays outside and has to be ready to help. Polluted rooms have to be intensively ventilated with fresh air. Before starting any rescue actions, explosimetric measurements and measurements of ammonia concentrations in a polluted atmosphere have to be made. Installations and rooms cleaned from ammonia have to be ventilated with neutral gas and then with air.

The need of starting rescue actions can take place because of a leak of ammonia water to the environment. The methods of rescue crews protection and rescue procedure is similar as in case of gaseous ammonia. The difference is in the fact that spilled ammonia water has to be collected from the ground. Ammonia water can penetrate the sewer system. Polluted areas of sewer systems have to be isolated with barriers. The most effective method is pumping out polluted liquid to asenization cars and transferring it to a dedicated wastewater reservoir. If it is possible, ammonia water has to be diluted as much as possible by pouring as much as possible of clean water into the sewer system. Polluted ground has to be rinsed with water.

First aid [7,8]

Depending on the way that ammonia entered the organism, first aid is based on:

- carrying the affected person out of polluted room into fresh air, taking off polluted clothes, covering with warm blanket and providing calmness,
- maintaining permeability of breathing tracts. In case of dyspnoea oxygen should be given. Artificial respiration should be avoided. Vapors of acetic acid can be given for respiration,
- offering diluted solution of acetic acid (100 grams of vinegar in 1 litre of water), lemon, juice, solution of citric acid. Milk can be given to drink too.
- rinsing burned skin with water.
- rinsing burned eyes with running water for at least 15 minutes. Then eyes should be rinsed many times with 0.9% w/w NaCl solution. Further help of oculist is needed.
- providing medical help to all affected people.

Dangers to natural environment related to the use of NH₃

Danger to the natural environment is related to the change of pH. In strongly alkalized environment fish die because of suffocation caused by damage done to their breathing organs. Polluted water burns into their skin and gills. Spilled ammonia water has to be collected from the ground. Ammonia water can penetrate the sewer system. Polluted areas of sewer systems have to be isolated with barriers. The most effective method is pumping out polluted liquid to aeration tanks and transferring it to a dedicated wastewater reservoir. If it is possible, ammonia water has to be diluted as much as possible by pouring as much as possible of clean water into the sewer system. Polluted areas should be rinsed with water. Large amounts of ammonia solution after diluting it to the concentration of 10-25% can be used as cheap nitrogen fertilizer, very easily assimilated by plants.

In case of an accident during transport outside the production plant it is necessary to remove the car from the inhabited area, remove from the endangered area all people that do not take part in rescue work, inform authorities, wear breathing masks and protective clothes, block all routes leading into the area, remove all sources of ignition, extinguish all open fire, do not use any sparking equipment. In case of release of gaseous ammonia water washing should be used to avoid spreading of a gaseous cloud. In case of accident in the area of a production plant the rescue work has to proceed according to the obliging instructions. The development of ammonia using chemical industry and general chemization of the whole economy causes the increase of potential toxic danger both in the area of the plant and in the surrounding area.

Recapitulation and conclusions

The state of danger related to the use and transport of NH₃ requires an adequate organization of fire protection forces and chemical rescue forces, having necessary rescue equipment and trained crew of professional fire brigade.

Production plants where NH₃ is stored, create huge danger for the environment. It follows the possibility of formation of gaseous mixture around installations and containers caused by leaks and oxidation of vapours, which can not be totally eliminated and that is why it is necessary to mark the explosion danger zones and conduct constant, systematic control and maintenance.

Road transport of NH₃ should meet both technological and fire-protection requirements. Similarly as in the railway transport, auto-cisterns used for ammonia transport

have special protections used to provide adequate conditions for safe transport of dangerous materials.

The development of chemical industry using NH₃ and chemization of the whole economy causes the increase of the potential toxic danger both in the area of the plant using such substances and in the surrounding areas.

Literature:

- [1] Polska Strona Pożarnicza, Ratowniczy Bank Wiedzy
- [2] J. Bednarek, P. Bielicki, in: Podstawy psychologii, pedagogiki i metodyki kształcenia pożarniczego, Warszawa 1997
- [3] P. Bielicki, in: Podstawy taktyki gaszenia pożarów, Kraków 1996
- [4] P. Bielicki, W. Gołębiowski, in: Wybrane zagadnienia z psychologii, pedagogiki oraz organizacja pracy i kierowania, Kraków 1991
- [5] J. Kaczmarczyk, in: Poligon na miarę potrzeb - poligonowe stanowiska ćwiczeń w Centralnej Szkole PSP, Przegląd Pożarniczy, 11 (2001).
- [6] Rozporządzenie Ministra Spraw Wewnętrznych i Administracji z dnia 16 czerwca 2003r. w sprawie ochrony przeciwpożarowej budynków, terenów i innych obiektów budowlanych /Dz. U. 121, poz. 1138/
- [7] E. Burzyński, in: Podejmowanie decyzji w działaniach taktycznych jednostek straży pożarnych, Warszawa 1979
- [8] E. Burzyński, in: Podstawowe działania taktyczne, Warszawa 1975

AN ATTEMPT TO EVALUATE THE POSSIBILITIES OF USING WATER GLASSES FOR THE PURIFICATION OF WATER AND WASTEWATER CONTAINING Pb^{2+} IONS

Wiesław Koźlak

*Warsaw University of Technology, Institute of Chemistry,
09-400 Płock, Łukasiewicza 17*

Introduction

Metals can cause acute poisoning, immediately observable or lingering poisoning. Acute poisoning is caused by such metals as Bi, As, Zn, Cd, Cu, Hg. Lingering poisoning can be caused by for instance As, Zn, Cd, Cr, Cu, Hg, Pb, Sn, Co, Ni, Mn, Se, Tl, Fe and Ag. Lingering poisoning, occurring for an elongated time in a deliquescent form is very dangerous, especially if it causes mutagenic changes or brain damage (lead and mercury poisoning). It is hard to recognize and cure. Lead, mercury and cadmium are among the most toxic metals. These elements are carcinogenic, and when they occur in the environment in concentrations higher than the maximum allowable concentration, i.e. 2 ppm in solid products [mg/kg of food], 0.4 ppm in liquid products [mg/kg of food], 0.1 ppm in water [mg/dm³], 100 ppm in a dry mass of compost [mg/kg], 0.05 ppm in air [mg/kg of food], cause the appearance of tumours. Besides, mercury and lead damage the central neural system and cadmium is the cause of hypertension, being the illness affecting ca. 20% of adult population in civilized countries. Lead, cadmium and nickel are carcinogenic and cause huge desolation in society which allows us to speak of them as of toxic elements.

Toxic properties of Pb [1]

Lead is a soft, grey metal, dissolving in concentrated, hot nitric and sulphuric acids and in acetic acid in the presence of oxygen. It does not dissolve in water. Lead is resistant to corrosion because in humid air produces a layer of hydroxide and carbonate covering its surface. It is a very toxic element. Lead is absorbed through skin and breathing passages [2]. In living organisms it reacts with proteins' thiol groups (-SH) and impedes the incorporation of iron into prosthetic groups of many enzymes and blocking their synthesis. Lead damages central and circumferential nervous systems, being more dangerous for younger organisms. Concentrations of lead in blood as low as 0.2 ppm are dangerous for the nervous system [3]. Lead significantly shortens life expectancy and probably is one of the causes of higher death rate due to the heart illnesses. The symptoms of lead poisoning include excessive excitability, aggression, headaches, insomnia, memory weakening, loss of interest, psychic and mental perturbations. People employed in the production of lead, lead containing batteries, pipes, bullets, alloys, paints and inhabiting the areas near to the highways (up to 0.3 km from the highway) are particularly vulnerable to the poisoning. On average, combustion of 1 litre of gasoline causes the emission of 0.4 to 0.7 g of Pb into the atmosphere. In total, in the northern hemisphere 350000 tons of Pb are emitted from the combustion of gasoline and soils near the highways contain on average from 1000 to 6000 ppm of Pb. There is a correlation between the concentration of Pb in air, soil and water and the level of industrialization of the area. The atmospheric pollution propagates over the whole eco-system of Earth. That is why mostly lead-free gasoline is used. The yield of plants is reduced due to the action of lead in the following way [4]: coniferous trees by

75%, peas by 68%, carrots by 62%, lettuce by 52%. Fuel tanks in airplanes are a subject to corrosion caused by microorganisms because the aviation fuel does not contain tetraethyl lead. A conclusion can be drawn that lead is toxic also for the microorganisms. Beside that, lead poisoning causes the increase of Ca concentration and decrease of Mg concentration in an organism. The deficit of magnesium promotes more severe lead poisoning and the excess of calcium slightly inhibits the poisoning. Oversupply of Mg can be used to reduce the toxicity of lead and simplify its removal from the organism. Mg^{2+} ions also reduce the hemolysis caused by Pb. Drinking water rich with calcium carbonate can act as a certain protection for the organism. Investigations have shown that the use of these waters reduces the deposits of lead in the skeleton by 50%. It is also possible to cure the lead poisoning and remove this metal from the organism by the use of a substance dissolving lead compounds but this kind of treatment is very dangerous and about 2/3 of children with brain damages undergoing that treatment dies.

Experimental

Turbidimetric method, based on the synthesis of water soluble colloidal lead silicate, was used to investigate systems containing sodium water glasses (produced by Eka-Chemicals, Sweden) marked with numbers from 1 to 7 and $Pb(NO_3)_2$. Industrial, concentrated solutions were studied. Table 1 presents the composition of studied water glasses.

Table 1. Composition of studied water glasses

Water glass	Na ₂ O concentration [% w/w]	SiO ₂ concentration [% w/w]	Silicate modulus M_k
1	9.2	29.1	3.264
2	9.6	12.0	12.112
3	9.1	29.0	3.289
4	9.8	31.0	3.264
5	7.0	22.0	3.243
6	7.0	27.2	3.302
7	8.5	28.1	3.412

The method of investigation [5,6]

Turbidimetric method is based on the formation of water soluble, colloidal silicate of the studied salt as a result of reaction of soluble silicate forms with a studied salt of a given element and measurement of the intensity of radiation scattered by the formed silicate. The ability of a silicate of a studied salt to form and the character of changes of scattered radiation intensity depend on the molecular composition of the silicate and silicate modulus. Huge influence on the course of reaction has the presence of impurities i.e. alien ions.

Description of conducted measurements

Into 99.7 cm³ of distilled water 0.3 cm³ of water glass was added. The mixture was stirred for 2 minutes by a magnetic stirrer. Into such solution, after 15 minutes, 33.2 cm³ of the solution of studied salt (8 mmol/dm³ concentration) was introduced while being strongly stirred during 30 seconds. Then the measurement dish was quickly filled with the prepared mixture and the measurements at 455 nm wavelength radiation scattering were carried out. Laboratory turbidimeter Hach 2100 AN was used to measure the changes of turbidity of the mixture. Operating parameters: wavelengths 0 nm, 455 nm, 500 nm, 50 nm, 810 nm, 860

nm; recording time 60 minutes; dish volume 30 ml; sample temperature about 30°C; accuracy: 5% of the readout.

Discussion of the results

The course of dependence, presented in Figures 1a and 1b, describing changes of turbidity in time in the sodium water glass – $Pb(NO_3)_2$ system, shows that turbidity of studied systems increases in time. These so called “turbidity curves” form incrementing functions. It shows that in the function of time, the concentration of colloidal lead silicate increases. Analysis of the experimental results indicates that the presence of lead ions has significant influence on the behavior of silicates regardless of their molecular composition. The values of turbidity fall into range from 299 to 608 NTU. Highest turbidity value after 60 minutes was observed for the water glass No. 5, lowest value – 392 NTU for water glass No. 4. The changes of turbidity during 60 minutes for studied water glasses are as follows: glass No. 1 – 81 NTU, glass No. 2 – 154 NTU, glass No. 3 – 123 NTU, glass No. 4 – 93 NTU, glass No. 5 – 86 NTU, glass No. 6 – 79 NTU, glass No. 7 – 68 NTU, glass No. 8 – 107 NTU.

Fig. 1a.

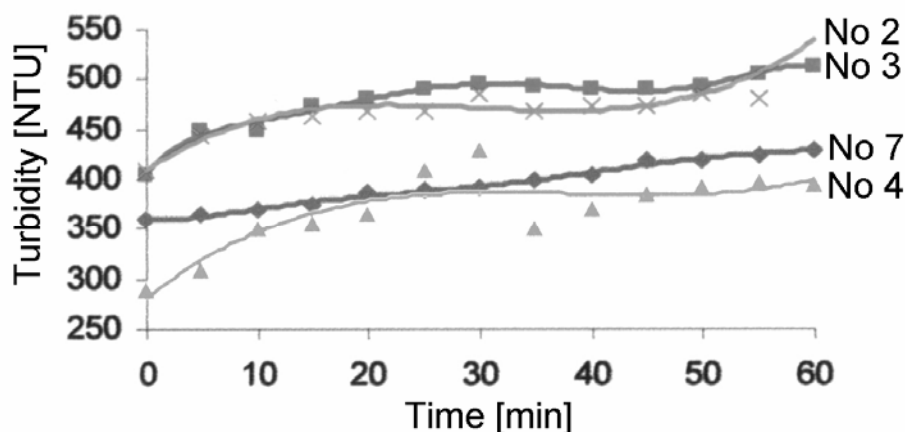
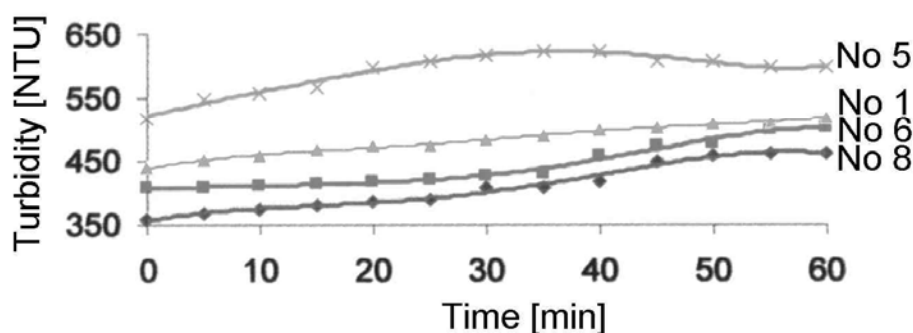


Fig. 1b.



Biggest changes were observed for glass No. 2 and smallest for glass No. 7.

Taking into account the analysis of concentration of particular elements in industrial silicates [5] we can see that water glasses No. 2, 3, and 4 distinguish themselves from the others with the concentration of Al, Fe and Ti. These ions, introduced into water glasses during production have influence on the water glass behavior, parallel to the influence of Pb salt. It confirms earlier hypotheses that the properties of silicate solutions depend on the technology of their production [7]. In the earlier work it was postulated that the behaviour of the silicate is not only influenced by the cations but also by anions of the salt [8]. Basing on this finding and considering the concentrations of particular anions in the studied silicates [5] we can see that the sample No. 2 has much higher than the others concentration of Cl⁻ ions, which probably explains biggest changes of turbidity in time. On the other hand, water glass No. 7, exhibiting lowest value of turbidity changes has highest concentration of SO₄²⁻ ions, compared to other samples.

Relative sizes of colloidal lead silicates' particles were calculated using a spreadsheet [9]. It was prepared basing on the tabular data, formulas and approximations published in a series of "Theoretical investigations on the light scattering of colloidal spheres" articles in "The Journal of Chemical Physics" by W. Heller, H.J. Bhatnagar and M. Nagakaki.

Numerical values were calculated basing on the refraction coefficient values and are presented in Table 2.

Table 2. Calculated values of lead silicate particles, their average radii and the values of refraction coefficients.

Water glass	Relative size of the particle	Average radius of the particle [Å]	Refraction coefficient
1	23.0	10733 - 22513	0.9543
2	23.0	10741 - 22725	0.9549
3	23.0	10733 - 22513	0.9549
4	23.0	10609 - 22449	0.9515
5	23.2	10975 - 23022	0.9674
6	23.0	10779 - 22610	0.9584
7	23.0	10779 - 22610	0.9584

Results of the calculations allow us to conclude that the relative sizes of colloidal lead silicate particles are identical, with the exception of water glass No. 5. Similar finding relates to the average radius of silicate particles. Thus we can conclude that Pb²⁺ ions react with the same silicate forms nevertheless the different molecular composition of their solutions.

Conclusions and recapitulation

- Addition of Pb(NO₃)₂ into the water glass causes the formation of colloidal lead silicates.
- Course of turbidity curves for the water glass – lead (II) nitrate depends on the type of silicate and the concentration of alien ions introduced into the water glass during its production.
- Relative sizes of colloidal silicate particles and their sizes are comparable which means that Pb²⁺ ions react with the same type of silicate anions, regardless of the water glass type.

For the subject of these investigations, which are systems containing alkali metal silicates, being untypical systems, creating many problems, both theoretical and experimental, every new information arising from the studies is a significant contribution for the description of the chemistry of silicate water solutions. Presented works, being a fragment of more complex studies on the structure and properties of water glasses is a significant supplement for the investigations of the influence of salts on the behaviour of silicates. Conducted studies were pioneer ones, the systems containing water glasses and Pb^{2+} salts did not attract any attention in literature nor in experimental works.

References

- [1] N. W. Skinder, *Chemia a ochrona środowiska*, WSiP, Warszawa 1995
- [2] T. Dutkiewicz, *Chemia toksykologiczna*, PZWL, Warszawa 1974
- [3] G. R. Taylor, *Księga przeznaczenia*, PZWL, Warszawa 1975
- [4] A. Hodera, A. Mrozkiewicz, *Uboczne działanie leków*, PZWL, Warszawa 1982
- [5] W. Koźlak, *Annals Pol. Chem. Soc.*, 3 (2004) 252
- [6] W. Koźlak, *Chemik*, 6 (2006) 337
- [7] W. Koźlak, *Pol. J. Appl. Chem.*, 27 (2005) 227
- [8] W. Koźlak, *Chemik*, in press.
- [9] M. Paczuski, E. Kukowska, T. Miałkiewicz, T. Wiśniewski, *Spreadsheet*, Warsaw University of Technology, Płock 2001

MANGANESE(II) SILANETHIOLATES WITH CHALATING HETEROCYCLIC BASES – EXAMINATION OF THEIR INFLUENCE ON PROPERTIES OF NATURAL RUBBER VULCANIZATES ‡

Anna Kropidłowska^{1*}, Aleksandra Makocka², Maciej Miąskowski²,
Józef T. Haponiuk² and Michał Stankowski²

Gdańsk University of Technology, Chemical Faculty, ¹Inorganic Chemistry Department
²Department of Polymer Technology, G. Narutowicza Str. 11/12, 80-952 Gdańsk.

* [Corresponding author. Tel.: +48 58 3472592; fax: +48 58 3472694; E-mail address:
anna@urethan.chem.pg.gda.pl (Anna Kropidłowska)]

‡ *Dedicated to Barbara Becker PhD, D.Sc. for her invaluable inspiration and counsel*

Introduction

Rubber elastomers are still one of the most frequently used materials on a volume basis in industrial and commercial life. They are broadly integrated into today's lifestyle and make a major, irreplaceable contribution to virtually all product areas. Natural rubber is usually vulcanized with sulfur to improve resilience and elasticity [1]. Vulcanization greatly improved the durability and utility of rubber from the 1830s on. The successful development of this process is closely associated with development of the new and efficient additives (accelerating and activating agents) which are components of, so called, vulcanization unit. In this group S-donor complexes, *eg.* dithiocarbamates [2], dithiophosphates [3] and xantates [4] play a very important role, since they can improve vulcanization rate. It was the reason for examining the effect of heteroleptic silanethiolate complexes of manganese(II) with chelating N-donors on properties of natural rubber vulcanizates.

Experimental

Materials: Manganese complexes: [Mn{SSi(OBu^t)₃}₂(2,2'-bipyridine)] and [Mn{SSi(OBu^t)₃}₂(1,10-phenanthroline)] were prepared as reported elsewhere [5]. Other chemicals were obtained from commercial sources and used as received. All samples were obtained using a two-roll mill of 200 mm diameter and 10 mm distance between the rollers. The rubber was mixed (the speed of the roller was 22 rpm) with ingredients according to ASTM (D15-72) and with control of temperature, nip gap and

sequenced addition of ingredients. Vulcanization was carried out a electrically heated auto controlled hydraulic press at 145°C and pressure 5 MPa.

Methods: The strain-stress properties were measured according to ASTM D-412-87 in a Zwick/Roell Universal Testing Machine (model Z020). Test speed was kept at 300 mm/min. The

Table 1. Composition of the samples

Component	phr
NR ^a (ribbed smoked sheets)	100
Stearic acid	3
Stabilizer AR ^b	1.5
Oil	2
Kaolin	30
Sulfur	1.5
ZnO	5
Accelerator T ^c	0.6
[Mn{SSi(O ^t Bu) ₃ } ₂ (N-N)] ^d	x

Abbr.: ^aNR = natural rubber; ^bN-phenyl-β-naphthylamine; ^cN,N,N',N'-tetramethylthiuram disulfide; ^dN-N= phen/bipy

hardness of the samples ($^{\circ}\text{Sh A}$) was measured using Zwick/Roell Hardness Testing Machine model 3130. Elasticity was verified using Schob method on Louis Hepper Leipzig apparatus according to PN-71 C-04255. The density was determined using Radwag set coupled with WPS 510/C/2 balance. The samples were also investigated by FTIR Nicolet 8700, from ThermoElectron Corporation. A diamond ATR accessory (Specac Golden Gate) was employed for ATR FTIR experiments. A 10mm \times 10mm samples were mounted on top of ATR crystal and pressed gently by a pre-mounted sample clamp. ATR effect and atmospheric contributions from carbon dioxide and water vapor were corrected.

Table 2. Samples designation and formulations.

Designation	Composition	Complex content x (phr)	Vulcanization time t [min]
NR	Natural rubber vulcanizate	0	t \in (2, 12)
NR-I/x _(t)	NR with [Mn{SSi(O ^t Bu) ₃ } ₂ (phen)]	x \in (0.5, 3)	t \in (2, 12)
NR-II/x _(t)	NR with [Mn{SSi(O ^t Bu) ₃ } ₂ (bipy)]	x \in (0.5, 3)	t \in (2, 12)

Results and discussion

Rubber processing as well as properties of thus obtained products strongly depend on type of polymer used. Nevertheless these features can be advantageously influenced by the proper ingredients of a rubber blend. Addition of coordination compounds is associated with either chemical or physical interactions between these two and usually rely on the physicochemical characteristic of the substance used as well as the chemical nature of rubber [6]. What more, incorporation of complex compound in elastomers results in a profound effect on mechanical and physical properties of the formed composites.

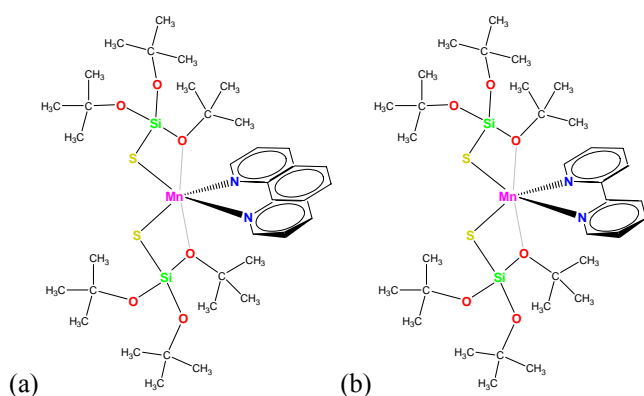


Fig. 1. Schematic structure of [Mn{SSi(O^tBu)₃}₂(N-N)] [5]
(a) N-N=phen, **I**, (b) N-N=bipy, **II**.

The [Mn{SSi(O^tBu)₃}₂(N-N)] species [5] have one property in common – in contrast to many other manganese(II) thiolates they are stable under normal conditions [7]. This enabled us to consider their potential applications and check their effect on properties of natural rubber vulcanizates. For all samples density, hardness, elasticity were determined and mechanical and spectral analysis was performed. The preliminary tests provided a

premise that all examined Mn(II) complexes are well dissolved in natural rubber and their addition influence vulcanization time. The optimal content of the complexes **I-III** was estimated as no more than 3 phr, since greater amount of the compound made the vulcanizates softer and more viscous. Acceleration of rubber ageing using manganese compounds have been previously reported [8] therefore all tests have been repeated after irradiation with UV lamp as well as after 10 months and no deterioration of sample properties was observed.

Table 2. Properties of samples obtained with 8 min vulcanization time.

Sample	Density [g/cm ³]	Hardness [°Sh A]	Sample	Density [g/cm ³]	Hardness [°Sh A]
NR-I	1.10	45.3	NR	1.10	45.3
NR-I/0,5	1.13	45.5	NR-II/0,5	1.11	47.2
NR-I/1	1.12	47.9	NR-II/1	1.11	47.5
NR-I/1,5	1.13	47.8	NR-II/1,5	1.12	48.3
NR-I/2	1.13	49.9	NR-II/2	1.11	48.4
NR-I/3	1.14	48.6	NR-II/3	1.11	48.6

Addition of both complexes I and II influence the mechanical properties of the vulcanizates. NR-I and NR-II possess higher hardness than non-modified NR (Table 2). Also density of

these samples is increased, especially for NR-I, what can suggest higher degree of the cross-linking. Gain of the mechanical properties is particularly well observable also in the case of NR-I (Fig. 2a). Stress at break for this composition vulcanized for 10 minutes (what is the optimal vulcanization time for non-modified rubber) is nearly 2 times greater then for NR. Interestingly it is associated with the improvement of samples elasticity (Fig. 2b) and elongation at break (*ca.* 20%) for NR-I. Addition of manganese(II) silanethiolate into the rubber mixture influenced also the time of the vulcanization. The greater the amount of the compound added - the more vulcanization time can be reduced (Fig. 3a). NR-I/3 samples vulcanized for 2 min. possess greater stress at break comparing to NR. However, since so short time is not always advisable, the optimal time may be estimated as *ca.* 6 min. These vulcanizates are also more elastic comparing with NR (Fig. 3b).

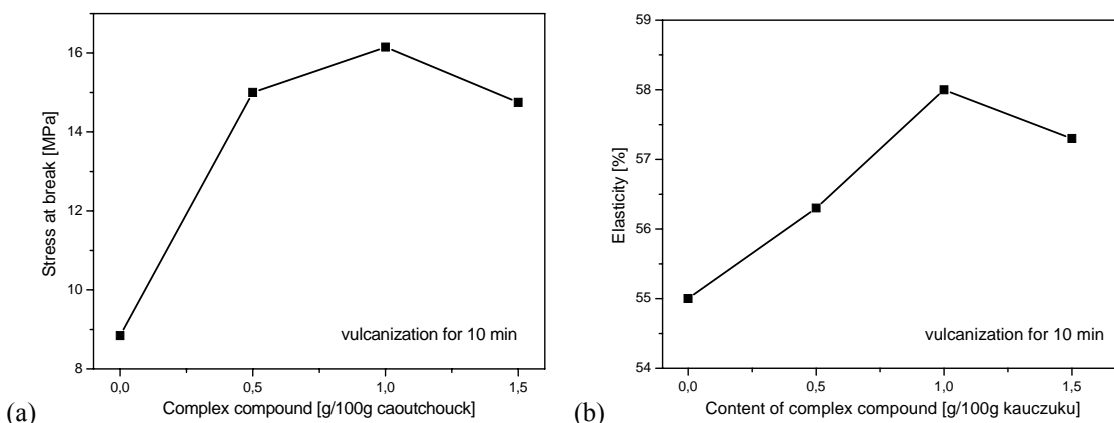


Fig. 2. Properties of samples vulcanized for 10 min (a) stress at break (b) elasticity vs. complex content.

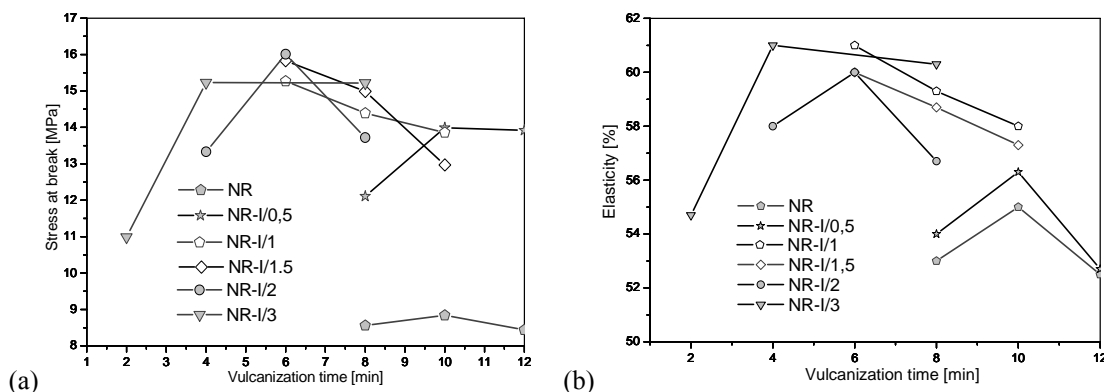


Fig. 3. Properties of vulcanized samples (a) stress at break (b) elasticity vs. vulcanization time.

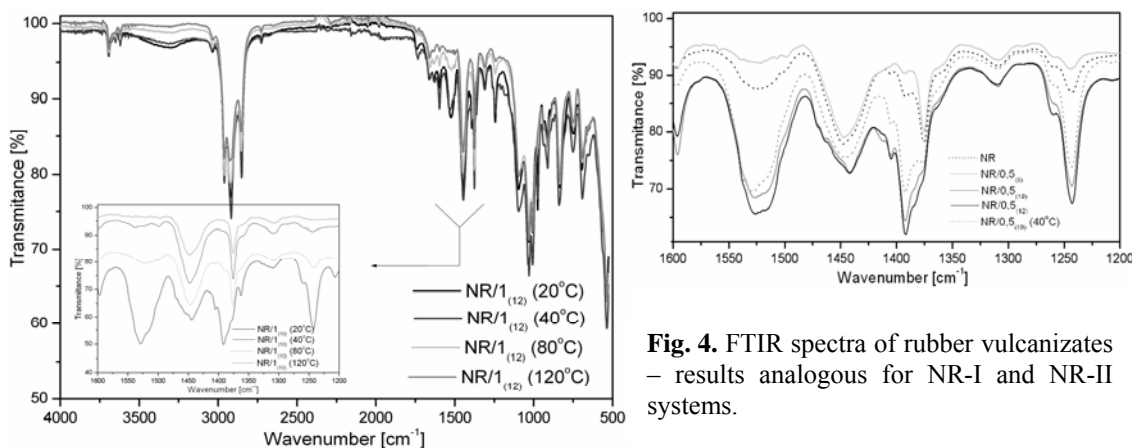


Fig. 4. FTIR spectra of rubber vulcanizates – results analogous for NR-I and NR-II systems.

According to the spectral analysis (Fig. 4) one can assume that some amount of water is absorbed in a blend. Wide band with maximum at about 2207 cm^{-1} (typical for $\nu(\text{OH})$ valence vibrations) decay with the increase of measurement temperature. With the bigger content of the complex, as well as with the rise of temperature the relative intensity of the band at 1375 cm^{-1} is decreasing and simultaneously the intensity of the 1391 cm^{-1} band increases. These are the main changes observable on the recorded spectra. Therefore we can assume that the compositions are stable and do not degrade, even when longer stored at higher temperature.

Conclusions

The modified rubber samples were prepared by sulfur vulcanization with the concentration of manganese complexes in the combination varying from 0.5 to 3.0 phr. It was necessary to define the optimal vulcanization system in order to get the vulcanizates of desired properties. The silanethiolate used do not act as direct accelerators, nevertheless they can be used as vulcanization activating agents. Addition of Mn silanethiolate complex (especially the one with phenanthroline as coligand) improves the mechanical properties (higher elongation and stress at break) and causes decrease of vulcanization time about without deterioration of sample properties.

Acknowledgements

The authors would like to thank Prof. J. Stangret for facilitating FTIR measurements.

References

- [1] J. R. White, S. K. De (ed.), *Rubber Technologist's Handbook*, Rapra Technology (2001) Shrewsbury.
- [2] L. Bateman, C. G. Moore, M. Porter, B. Saville, *The chemistry and physics of rubber-like substances*, Maclaren & Sons Ltd. (1963) London.
- [3] B. H. To, L. H. Davis, R. W. Faulkner, W.W. Paris, *Plast. Rubber Process. Appl.*, **12** (1989) 89-104.
- [4] S. Palaty, R. Joseph, *J. Appl. Polymer Sci.*, **78** (2000) 1769–1775.
- [5] A. Kropidłowska, J. Chojnacki, B. Becker, *Polyhedron* **25** (2006) 2142-2148.
- [6] V.A. Karpinchik, T. V. Koksharova, *Russ. J. Coord. Chem.*, **23** (1997) 136-145.
- [7] A. Kropidłowska, M. Strankowski, B. Becker, *J. Therm. Anal. Cal.*, submitted.
- [8] F. R. Mayo, K. Egger, J. Heller, K. Crawford, *Quarterly Progress Rept.* **3** (1963).

THE ROLE OF SUBJECT COMPETITIONS IN NATURAL SCIENCES TEACHING

Małgorzata Krzeczowska^{1,2}, Ewa Odrowąż^{1,3}, Magdalena Woźniczko⁴
¹*Wydział Chemii UJ*, ²*VI LO w Krakowie*, ³*Gimnazjum nr 52 w Krakowie*, ⁴*Publiczne
Gimnazjum w Bolesławiu*

According to the dictionary definition a competition is an artistic, entertainment or sporting event with a specific procedure allowing the selection by elimination of the best artists, authors etc., who are usually awarded prizes.

So do the subject competitions held in schools fit this definition? Subject competitions are indeed events, albeit of an academic nature, they have specific rules, and they allow the best students to be selected. The students are also awarded prizes though it is not the prizes themselves which they value most but the fact that winning the competition frees them from the obligation to sit the exam at the level in question.

The importance of subject competitions in the work of schools is demonstrated by the fact that there is a government ruling on the subject (the Ruling of the Ministry of National Education and Sport of 29.01.2002 concerning the organisation and conduct of competitions, tournaments and contests). According to the ruling competitions can be:

- 1) interdisciplinary competitions based on the syllabus of various subjects or blocks of subjects,
- 2) subject competitions based on the syllabus of one subject and extending it,
- 3) topical competitions based on a selected subject or subject block.

The ruling also states that:

1. Competitions may also be organised on the provincial or interprovincial level.
2. Competitions on the provincial level are organised by the Chief Education Officer while interprovincial competitions are organised by the appropriate Chief Education Officers on the basis of an agreement.

At the beginning of each school year detailed information on subject competitions can be obtained including precise rules, the theme of particular competitions, and a list of topics and suggested material for preparation.

Having familiarised him/herself with this information the teacher acquires the material specified and presents it to the interested students, discussing how to use it and setting a joint plan of action and schedule for meetings. The teacher then begins to work with the students, stimulating their interest and creating a sense of anticipation in order to motivate them to take creative action.

Each teacher has his/her own way of approaching this task. Usually they have a tried and tested procedure which guarantees that students are provided with the knowledge they need, while also establishing a positive model of discussion as well as reading, writing, note-taking, and listening.

Below I have included a list of selected original questions in Non-organic, Organic and

General Chemistry. They are designed for both gymnasium and secondary school students and differ in their form, content and the methods required for their solution. Each exercise is clear and transparent, and has an answer and commentary concerning its difficulty level and the practicality of the solution. The questions include theoretical and practical (laboratory) questions, and exercises requiring independent analysis rather than simple reproductive learning.

All the proposed questions have been tested in a practical context, with students preparing for the Małopolska Chemistry Competition for Gymnasium Students, the Provincial Chemistry Competition for General Secondary School Students, and the School Chemistry Contest (the so-called 'Olimpiada').

Exercise 1.

1-bromo-3-nitrobenzene can be prepared by: a) bromination of nitrobenzene or b) nitration of bromobenzene. Choose correct answer, and next write the chemical equations to explain your answer.

Exercise 2.

Sodium acetate is widely used in chemical synthesis.

- the laboratory production of the simplest alkane involves the reaction of sodium acetate with sodium hydroxide. Write a balanced equation, and next give orbitals diagram of the simplest alkane molecule. What geometry is expected for this molecule according to the VSEPR model. Comment on a dipole moment of this molecule,
- combustion of 1 mole of this alkane to yield $\text{CO}_2(\text{g})$ and $\text{H}_2\text{O}(\text{g})$ would produce 890,31 kJ; calculate how much heat in kJ is evolved from the reaction of 10 dm^3 of that alkane under the normal-state conditions,
- consider the electrolysis of melted sodium acetate. What are the electrode reactions? How many dm^3 of gas (under the normal-state conditions) - which could be absorbed by limewater - are liberated when 25g of sodium is deposited on the cathode at the same time?

Exercise 3.

Unknown organic compound belongs to hydrocarbons with ring structure and:

- having aromatic character,
- is one of benzenes homologues,
- reacts with chlorine under ultraviolet irradiation,
- during reaction with diluted, strongly alkaline solution of KMnO_4 , the compound is converted into the simplest aromatic carboxylic acid and carbon dioxide.

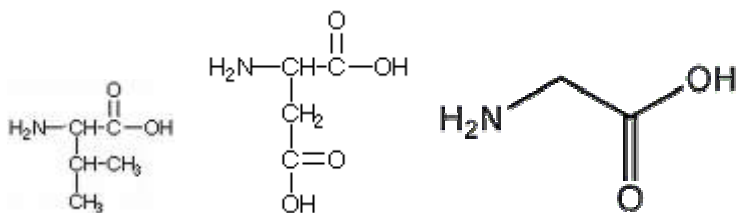
Identify compound using these information.

Exercise 4.

How could you distinguish the following four aqueous solutions of salts: sodium chloride, zinc chloride, aluminium chloride and manganese chloride. You can use only aqueous solution of sodium hydroxide and ammonia. Describe a chemical method for identification of the solutions of NaCl , ZnCl_2 , AlCl_3 and MnCl_2 . Write chemical equations.

Exercise 5.

Look at the structural formulas of selected amino acids:



Using information below give the structural formula and name of the expected peptide:

- firstly, aqueous solution of peptide was titrated with 0.5M NaOH, and next the same volume of aqueous solution of that peptide was titrated with 0.5M HCl; the volume of 0.5M NaOH was twice as much as the volume of 0.5M HCl,
- elementary analysis of that peptide shows percent composition: C 41.4%, and molar mass is equal 261 g/mol.

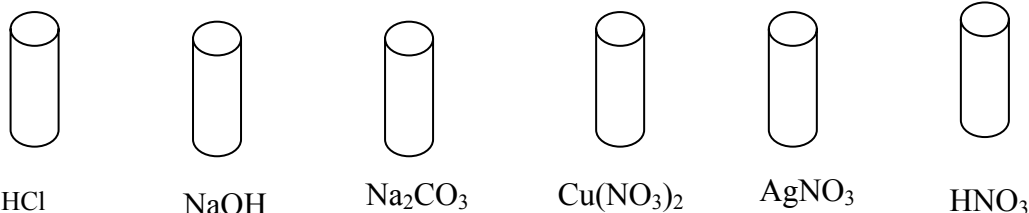
Exercise 6.

There are three isomers of unknown hydroxycarboxylic acid I(1), I(2), I(3); each of them has distinct position of -OH group attached to the linear carbon chain. Information below should be used to provide chemical name and structural formulas of these isomers:

- reaction of two molecules of isomer I(1) results in lactide formation,
- isomer I(2), when heated with a concentrated solution of potassium hydroxide in ethanol, is converted to α,β -unsaturated compound,
- under special conditions, from isomer I(3) γ - lactone is formed,
- each isomer molecule consists of 5 carbon atoms.

Exercise 7.

The following aqueous solutions have been placed in separate test-tubes:



Which of these solutions should be mixed to:

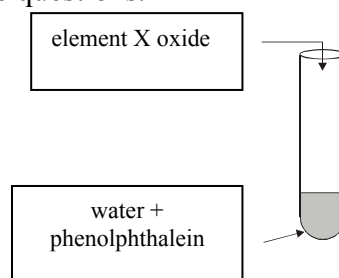
- observe a reaction with gas formation?
- observe formation of a precipitate (blue)
- observe formation of a precipitate (white, darkening under light)
- take place the neutralization reaction

Write the molecular-, ionic-, and the net ionic equations. Suggest experiments to prove your expectations.

Exercise 8.

Read the information below, and write an answer to the questions.

1. Look at the picture:



observation: the color of solution has not been changed.

2. Element X reacts with H_2 to give a gas with characteristic odor.
 3. Element X burns with O_2 to give element X oxide.
 4. Element X oxide reacts with substance Y.
 5. Element Z oxide reacts with water to give substance Y.
 6. Molecular mass of element Z oxide is 62u, and percent composition O 25,8%.
 7. Molecule of element Z oxide consists of 3 atoms.
- a) Write the names of substances X, Y, Z.
 - b) Comment on acid-base behaviour of element Y oxide?
 - c) Write formula of element Z oxide?
 - d) Write chemical equation for reaction: element X oxide reacts with water.
 - e) Write chemical equation for reaction: element X reacts with O_2 . Write name of the formed oxide.
 - f) Write chemical equation for the reaction: element X oxide reacts with substance Y.

The questions are designed to:

- test the students' ability to use solubility tables,
- test the students' ability to apply their knowledge of the properties of d-block elements and their compounds (co-ordination compounds),
- improve the students' laboratory skills,
- give the students practice in writing reaction equations,
- develop the students' ability to predict electrolysis products,
- consolidate the students' knowledge of the construction of energy diagrams for atoms and molecules,
- test the students' ability to interpret information concerning the energy effects of reactions,
- develop the students' ability to draw conclusions from available information,
- teach logical thinking,
- cover the entire gymnasium syllabus for Non-organic Chemistry,
- teach comprehension of texts,
- require more than simple reproductive learning,
- test the students' ability to apply their knowledge of the properties of aromatic hydrocarbons,
- test the students' ability to interpret information concerning the effects of reactions,
- develop the students' ability to select a range of information,
- put the note in a correct order and structure the chemical facts properly.

All exercises have been prepared by Authors based on different chemistry didactic materials for teachers and students.

ELECTROCHEMICAL PROPERTIES OF COMPOSITE MATERIALS ON THE BASE OF COPOLYMERS OF ANILINE WITH ANTHRANILIC ACID.

Paweł KRZYCZMONIK

*Department of General and Inorganic Chemistry, University of Łódź,
ul. Narutowicza 68, 90-136 Łódź, Poland, e-mail pawel@chemul.uni.lodz.pl*

Introduction

Composite (hybrid) materials can be divided according to their chemical properties. Taking into account the type of the compound which forms the matrix of the hybrid and the compound which penetrates into this structure ('guest') hybrid materials are divided into three different types [1].

1. OI – Organic inorganic hybrid materials – The matrix is an organic compound (most often a conductive polymer) with which the particles of an inorganic substance (guest) are connected.
2. IO – Inorganic organic hybrid materials – The matrix is built of an electroactive, inorganic compound while an organic part of the hybrid consist of 'guest' particles.
3. Nanocomposite materials – neither organic nor inorganic form dominates in this structure.

The experiments with electrode composite materials are carried out in different directions. One of the directions is searching for new substances to build organic layers or to modify the already applied compounds. The important feature of organic layers used in composite materials is the presence of function groups with positive and negative charge. It gives the possibility to create anion and cation organic layers which are a very important feature because of the ability to adsorb further constituents on such layers.

The experiments described in this communicate concern the possibility to modify the organic layer formed by polyaniline. The examined modification is based on replacing polyaniline with co-polymer aniline-anthranilic acid or co-polymer aniline-metanilic acid. Dodecamolybdophosphoric acid and Prussian blue were used as inorganic components. Composite materials with heteropolyacid were synthesised in a multistage method by means of depositing successive organic and inorganic layers, (layer by layer) which is described in literature [2,3]

Experimental

The apparatus used in voltammetric measurements consisted of the potentiostat PAR 273 and the microcomputer IBM PC with CorrWare 2.8 and CorrView 2.8 software (Scribner Associates Inc.). The three - electrode measurement cell was used. The working electrodes were disc electrodes of glassy carbon of diameter 0.3 cm and the surface 0.071 cm² and platinum wire of diameter 0.15 cm and the surface 0.96 cm². The counter electrode was platinum mesh. The references electrode was the saturated calomel electrode (SCE).

Composite layers in the research were built of organic and inorganic parts. Polyaniline (PANI) or copolymers aniline-anthranilic acid, aniline-metanilic acid were used as organic structures. They were synthesised by means of cyclic voltammetry from the solutions containing adequate monomers: aniline (AN), anthranilic acid (AA), metanilic acid (MA). Inorganic structures were built of dodecamolybdophosphoric acid H₃PMo₁₂O₄₀ (PMo₁₂) and Prussian blue Fe₄III[FeII(CN)₆]₃.

The synthesis of composite materials consisting of dodecamolybdophosphoric acid and polyaniline or copolymer aniline and anthranilic acid proceeded according to the following procedure:

1. Deposition of PMo_{12} layer by means of immersing the conductive phase of working electrode in the aqueous solution of $\text{H}_3\text{PMo}_{12}\text{O}_{40}$ of concentration 0.002 mol/dm^3 for 10 min.
2. Immersion of the modified surface in the solutions of aniline (or aniline and anthranilic acid) with $0.5 \text{ mol/dm}^3 \text{ H}_2\text{SO}_4$.
3. Electropolymerisation of ultrathin layer of polymer (or copolymer) in the solution $0.5 \text{ mol/dm}^3 \text{ H}_2\text{SO}_4$ within potential range from $E=0.1\text{V}$ to $E=0.85\text{V}$, at $v=50 \text{ mV/s}$, during 3 voltammetric cycles.

The attempts to synthesise composite materials with copolymer of aniline and metanilic acid did not give positive results.

Composite materials consisting of polyaniline or copolymer of aniline with anthranilic acid or metanilic acid and Prussian blue were obtained according to the following procedure. The synthesis was carried out during voltammetric polarisation in the solution of: aniline (or aniline and anthranilic acid or aniline and metanilic acid), $\text{Fe}_2(\text{SO}_4)_3$ 0.001 mol/dm^3 , $\text{K}_3\text{Fe}(\text{CN})_6$ 0.001 mol/dm^3 , H_2SO_4 0.5 mol/dm^3 , KHSO_4 0.5 mol/dm^3 . The process was conducted at sweep potential rate $v=50\text{mV/s}$ within potential range from $E=-0.1\text{V}$ to $E=0.8\text{V}$.

Results and discussion

Figures 1 and 2 present voltammetric curves of composite layers with dodecamolybdophosphoric acid. The measurements were done in supporting electrolyte for the successive thicker layers of the composite. Voltammetric curves for the materials built of phosphomolibden acid and polyaniline or co-polymer aniline-anthranilic acid demonstrate great similarity in the position of respective peaks and the values of peak currents. It is proved by the dependence $i_p=f(v^{1/2})$ for both layers. The slope coefficients of anodic lines equal $8 \cdot 10^{-7}$ (layers with polyaniline) and $\cdot 10^{-6}$ (layers with co-polymer aniline-anthranilic acid) and cathodic lines are $3 \cdot 10^7$ and $5 \cdot 10^{-7}$ respectively. Copolymers of aniline and anthranilic acid reveal the features similar to polyaniline and they can be used to the synthesis of composite materials instead of PANI.

Figures 3, 4 and 5 present voltammetric curves of composite layers with Prussian blue. The diagrams present the measurements done for different sweep potential rates. It results from the comparison of voltammetric curves in figures 3 and 4 that in case of layers with co-polymer aniline-anthranilic acid, the redox system at about 0.2V has better reversibility than in case of layers with polyaniline. The slope coefficient of the lines on the diagram with the dependence $i_p=f(v^{1/2})$ for the layers with co-polymer aniline-anthranilic acid have the same value 0.0002 . The lines are symmetric as in case of reversible processes. On the other hand, the difference of peak potentials is smaller than in case of layers with polyaniline.

Figure 5 presents voltammetric curves of the layers with co-polymer aniline-metanilic acid and Prussian blue. In this case we can observe a clear worsening in the reversibility of electrode processes. The difference of peak potentials increases with the growth of sweep potential rate and the peaks themselves undergo vast extension. It is seen from the diagram of the dependence $i_p=f(v^{1/2})$ that the course of the cathodic line is completely untypical and does not correspond with simple electrode processes.

Conclusions

It results from the research that co-polymer aniline-anthranilic acid can be used in composite materials instead of polyaniline. In connection with phosphomolibden acid it forms the material of properties similar to the material with polyaniline. In the materials with Prussian blue the presence of the same co-polymer increases the reversibility of electrode processes.

On the other hand, co-polymer aniline-metanilic acid cannot be applied in the examined systems. In case of materials with phosphomolibden acid it was not possible to obtain any layers with this co-polymer.

In composite materials with Prussian blue, copolymer of aniline and metanilic acid show worse properties than polyaniline, copolymer of aniline and anthranilic acid. Copolymers containing sulphone groups exhibit better water solubility. It can cause weak immobilisation of inorganic compounds in the layer.

The further research will concern the formation of materials with the application of co-polymer aniline-metanilic acid with other inorganic compounds.

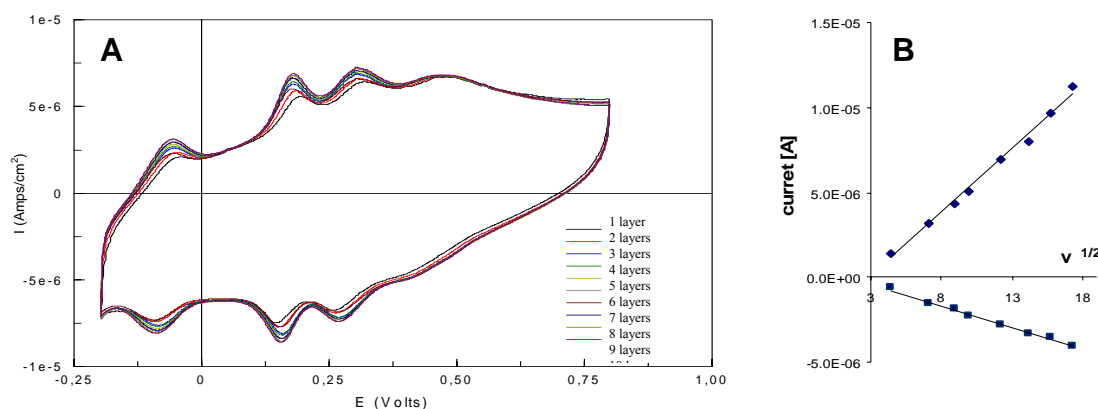


Figure 1. A) Voltammetric curves for the layer of composite PANI-PMo₁₂ in dependence on the number of deposited layers.

B) The dependence of the peak current on the polarisation sweep potential rate.

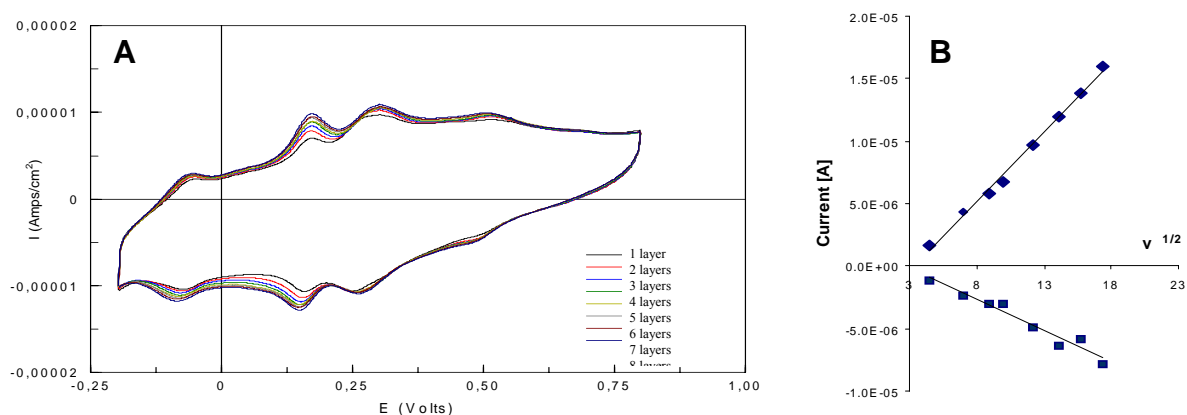


Figure 2. A) Voltammetric curves for the layer of composite PANI-AA-PMo₁₂ in dependence on the number of deposited layers.

B) The dependence of the peak current on the polarisation sweep potential rate.

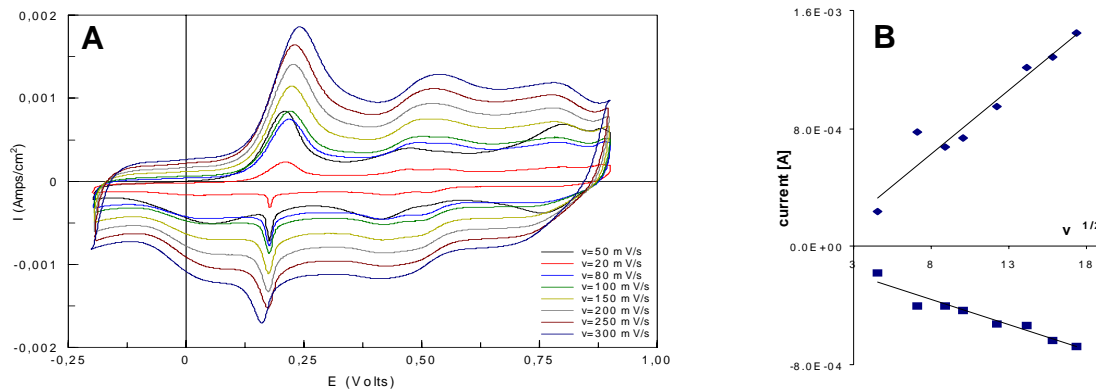


Figure 3. A) Voltammetric curves for the layer of composite PANI-Prussian blue in the solution of supporting electrolyte for different sweep potential rates within the range from 20 to 300mV/S. B) The dependence of the peak current on the polarisation sweep potential rate.

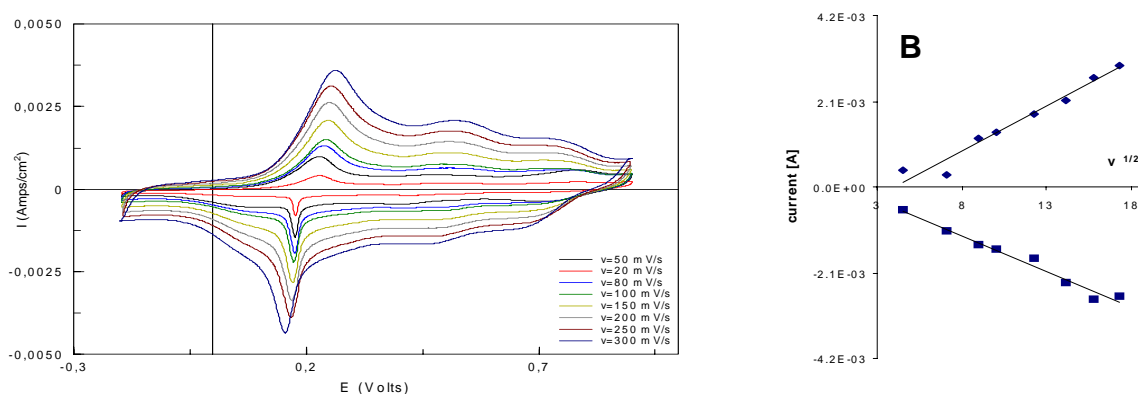


Figure 4. A) Voltammetric curves for the layer of composite PANI-AA Prussian blue in the solution of supporting electrolyte for different sweep potential rates within the range from 20 to 300mV/S. B) The dependence of the peak current on the polarisation sweep potential rate.

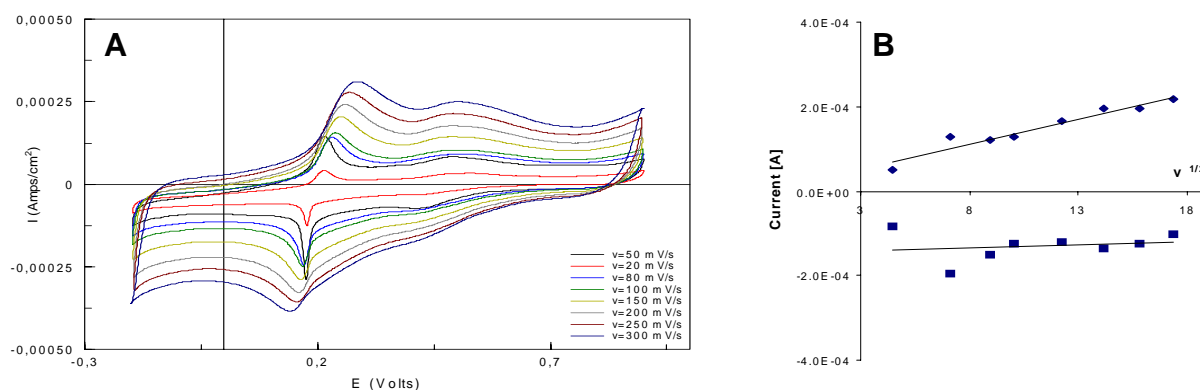


Figure 5. A) Voltammetric curves for the layer of composite PANI-MA Prussian blue in the solution of supporting electrolyte for different sweep potential rates within the range from 20 to 300mV/S. B) The dependence of the peak current on the polarisation sweep potential rate.

References

- [1] Cuentas Gallegos A. K., Doctors thesis Laboratorio de Quimica del Estado Sólido Instituto de Ciencia de Materiales 2003r.
- [2] Kulesza P.J., Chojak M., Miecznikowski K., Lewera A., Malik M.A., Khun A., *Electrochemistry communications* 4, 510-515 (2002)
- [3] Leventis N., Chung Y.C., *J. Electrochem. Soc.* Vol. 137 No 10, 3321 (1990)

SYNTHESIS, STRUCTURE AND PROPERTIES OF POLY(ETHER-ESTER URETHANE)S CROSSLINKED BY VINYL MONOMERS

Kucińska-Lipka Justyna, Janik Helena, Adolf Balas

Chemical Faculty Gdansk University of Technology, Department of Polymer Technology

Narutowicza Street 11/12 80-952 Gdansk

I. Introduction

Classic polyurethanes exhibit a number of advantageous properties, mainly high abrasion resistance, significant hardness and tensile strength. They exhibit also certain drawbacks during synthesis, such as limited lifetime of urethane prepolymers or low resistance of isocyanate groups to humidity. These disadvantages can be eliminated by an introduction of unsaturated bonds to polyurethane structure, what allows additional crosslinking via radical induced polymerization, chemically induced polymerization or radiation induced polymerization.

Numerous papers on polyurethane modifications with unsaturated monomers prove that it is one of the best methods of improvement of these compounds' properties [1,2,3].

There are several groups of unsaturated polyurethanes classified with respect to their properties and structure. The main groups are as follows:

- unsaturated poly(esterurethane)s,
- poly(urethane acrylate)s,
- polyurethanes extended with low molecular weight, unsaturated diols.

The scope of our interest are unsaturated poly(ether-ether urethane)s (PUR-U) synthesized from unsaturated poly(ether-ester)diol (OAEE) and crosslinked by vinyl monomers. OAEE were synthesized with different glycols – ethylene (GE), diethylene (GD) and propylene(GP) ones [Fig. 1]. Synthesis was carried out for 1 hour at 80 °C.

II. Materials

- Poly(ether-ester) OAEE
- 4,4'-diphenylmethane -diisocyanate (MDI)
- Styrene (S)
- Butyl acrylate (AB)
- 2,4,6 triallyloxy-1,3,5 triazine (I)
- methyl ethyl ketone peroxide (MEKPO)
- cobalt 2-ethyl cyclohexanoate (EtHCo)
- urethane prepolymer (QPRE)

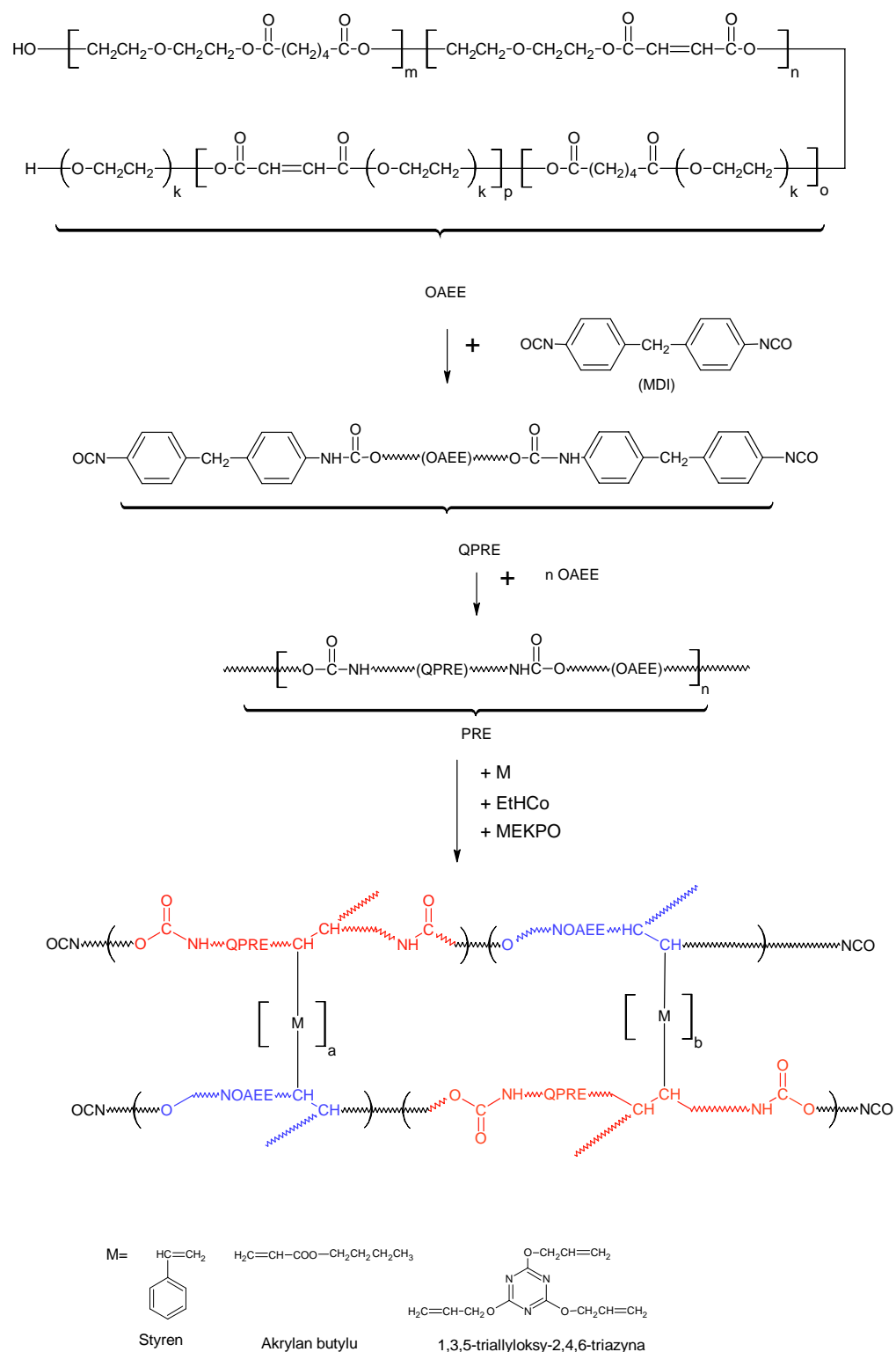


Fig 1. Synthesis of poly(ether-ester urethane)s crosslinked by vinyl monomers

III. Results

On the spectrum of PUR-U [Fig. 2], in the region 3250-3400 cm^{-1} and at 1535 cm^{-1} there are stretching and deformation vibration bands characteristic for urethane groups and corresponding to the secondary amine. The absorption band at 1730 cm^{-1} originates from the stretching vibrations of carbonyl group present in ester and urethane units. Two asymmetric bands in the range 1300 – 1100 cm^{-1} characteristic for ester and ether groups originate from OAEE. The weak band at 2250 cm^{-1} corresponds to free NCO groups. Moreover, there are some additional bands at 3000 cm^{-1} and at about 1600 and 1500 cm^{-1} . They are related to the stretching vibrations of $\text{C}=\text{C}$ and $\text{C}_{\text{Ar}}\text{-H}$ bonds suggesting the presence of aromatic ring, probably originating from MDI and styrene. The peaks at 1630 cm^{-1} correspond to the stretching vibrations of $\text{C}=\text{C}$ group. It suggests that not all double bonds take part in the cross-linking copolymerization reaction. The spectrum exhibits also overlapping bands at 2880 cm^{-1} coming from asymmetric and symmetric stretching vibrations of $-\text{CH}_3$ and $-\text{CH}_2-$ groups as well as the band at 1430 cm^{-1} characteristic for deformation vibrations of (C-H) group of aliphatic hydrocarbon chain.

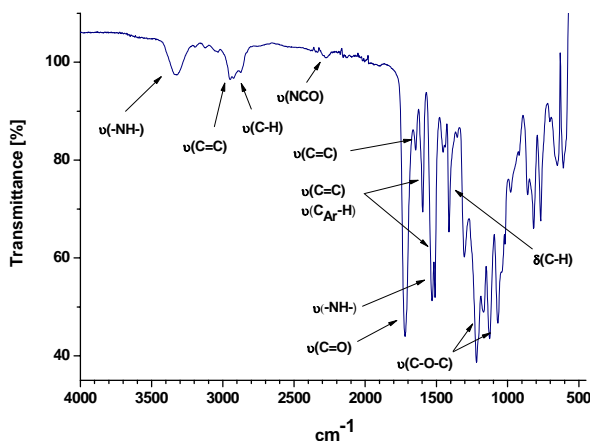
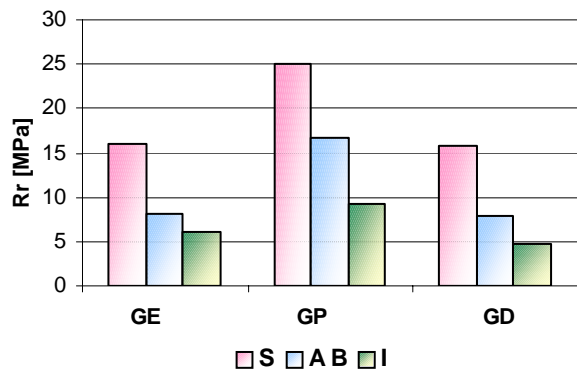


Fig 2. FTIR-ATR spectra of PUR-U

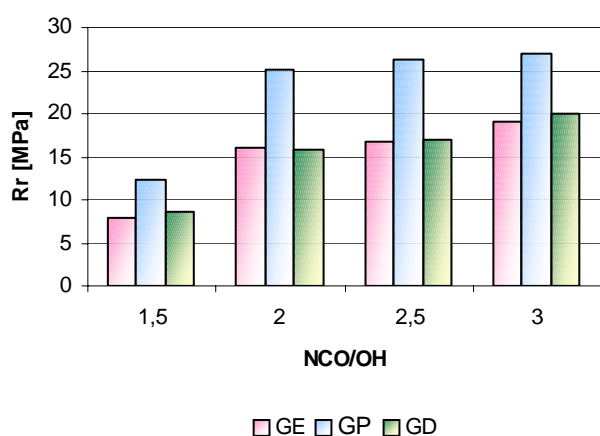
Cross-linked PUR was subjected to the tensile test. It was aimed at evaluation of influence of the type of glycol used during polyurethane synthesis, the content of free NCO groups and the type of crosslinking agent on mechanical properties of obtained polymers.

PUR-U crosslinked with 2,4,6 triallyloxy-1,3,5 triazine (I) exhibit the worst mechanical properties regardless of the type of glycol they had been synthesized from. Poly(ester-ether urethane)s crosslinked by styrene exhibit better mechanical properties than PUR-U crosslinked with the other used monomers.



Crosslinking agent	Rr [MPa]		
	GE	GP	GD
S	16	25,1	15,9
AB	8,2	16,7	7,9
I	6,1	9,2	4,8

Fig 3. Tensile strength of PUR-U containing different crosslinking agents (NCO/OH 2,0:1)



NCO/OH	Rr [MPa]		
	GE	GP	GD
1,5:1	7,8	12,4	8,7
2,0:1	16	25,1	15,9
2,5:1	16,8	26,2	16,9
3,0:1	19	27	20

Fig 4. Tensile strength of PUR-U containing different glycol (PUR-U crosslinked with styrene)

PUR-U with propylene glycol residues in its structure occurred to be the most durable in the tensile test. The higher content of rigid segments makes PUR-U more resistant to tensile deformation. The highest tensile strength was revealed by PEEU of the molar ratio NCO/OH 3,0:1

IV. Conclusions

- Analysis FTIR-ATR spectra confirm the assumed structure of PUR-U
- The increase in molar ratio NCO/OH is accompanied by an improvement in mechanical properties.
- PUR-U crosslinked with styrene and possessing propylene glycol residues in its structure is characterized by superior tensile strength as compared to the remaining polyurethanes.

V. References

1. Oprea S., Vlad'a S., Stanciu S., Polymer 2001, **42**, 7257-7266,
2. Cherian Benny A., Abraham Beena T., Thachil Elby T. Journal of Applied Polymer Science 2006, **100**, 449-456,
3. Aldrighetti C., Tassone P., Ciardelli F. Ruggeri G., Polymer Degradation and Stability 2005, **90**, 346-353.

SYNTHESIS OF MONOACETAL AND POLYMER DERIVATIVES OF METHYL α -D-MANNOPYRANOSIDE

J. Dębiec, S. Kukowka, K. Koziel, W. Turek, J. Maślińska-Solich
Department of Physical Chemistry and Technology of Polymers, Silesian University of Technology, ul. M. Strzody 9, 44-100 Gliwice

Introduction

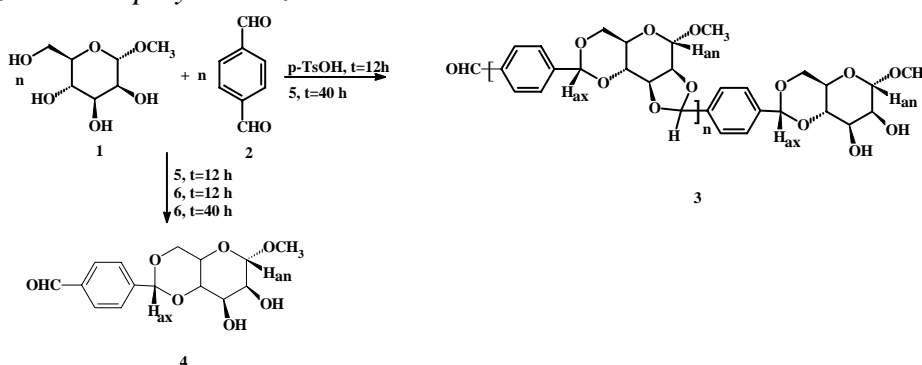
The acetalization reaction is a process that is widely used in organic synthesis to protect the carbonyl of aldehydes and ketones and for the synthesis of enantiomerically pure compounds that find practical application in field of carbohydrate chemistry. This reaction is normally acid catalysed, although the use of transition metal complex as Lewis acid catalysts has been occasionally reported in the literature [1].

Our group is currently working on synthesis of polymer containing carbohydrate units in the main chain by polycondensation of dialdehydes with monosaccharides [2]. The goal of the present research was develop a catalytic process involving selective acetalization of methyl α -D-mannopyranoside with terephthalaldehyde. This paper deals with the heteropolyacids dispersed in the polymer matrix which are applied as acid catalysts in the acetalization of methyl α -D-mannopyranoside. The advantage of this procedure is that it is a single step process without necessity to use hydroxyl protection group chemistry of sugar molecule.

New types of heterogeneous catalysts such as conjugated polymers: polypyrrole (PPy) or poly(N-methylpyrrole) (PMPy) doped with heteropolacids constitute an especially interesting class of catalysts, because their catalytic properties can be precisely tuned via controlled modification of polymer-dopant interactions. The using heteropolyacids such as $H_5PMo_{10}V_2O_{40}$ or $H_4SiW_{12}O_{40}$ have two separated active sites i.e. acid-base (protons) and oxidative-reductive (transition metal ions) [3].

Experimental Part

Acetalization and polyacetalization reactions



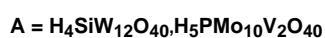
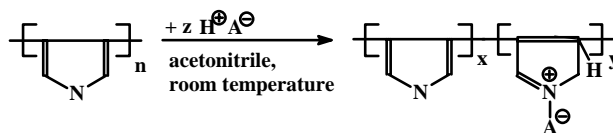
Scheme 1. Polycondensation of methyl α -D-mannopyranoside (1) with terephthalaldehyde (2), catalyzed by PPy($H_5PMo_{10}V_2O_{40}$) (5), PMPy($H_5PMo_{10}V_2O_{40}$) (6)

The reaction between methyl α -D-mannopyranoside (1) and terephthalaldehyde (2) was performed for the molar ratio of the reactants 1:1, in the presence of 0.25 % (w/w) of the catalyst, in benzene-DMSO solution (v/v = 4:1) with azeotropic removal of water. After a certain time (12-40 h) the catalyst was filtered off. The solvents were evaporated

and the residue was washed with 5 % aqueous solution of NaHCO₃ or extracted from chloroform solution with 5 % NaHCO₃. The product was dried under vacuum and analysed (Scheme 1).

Synthesis of catalysts

Polypyrrole and poly(N-methylpyrrole) were synthesized in an one-step polymerization of corresponding monomers (pyrrole or N-methylpyrrole) in presence of hydrogen peroxide (as an oxidative reagent) and heteropolyacid (H₅PMo₁₀V₂O₄₀ or H₄SiW₁₂O₄₀ - as a doping species) in acetonitrile (as a solvent) at room temperature (Scheme 2).



Scheme 2. Reaction of polymerization of pyrrole or N-methylpyrrole with simultaneous incorporation of heteropolyacids H₅PMo₁₀V₂O₄₀ or H₄SiW₁₂O₄₀

Result and discussion

Catalysts: PPy(H₅PMo₁₀V₂O₄₀) (**5**), PMPy(H₅PMo₁₀V₂O₄₀) (**6**), PPy(H₄SiW₁₂O₄₀) (**7**), PMPy(H₄SiW₁₂O₄₀) (**8**), were obtained in one-stage polymerization of a suitable monomer (pyrrole or N-methylpyrrole) in the presence of (H₄SiW₁₂O₄₀ or H₅PMo₁₀V₂O₄₀), which acted as the doping agent.

Polymerization of both matrices was carried out in acetonitrile by oxidizing the monomer with hydrogen peroxide with simultaneous incorporation of heteropolyacids (H₄SiW₁₂O₄₀ or H₅PMo₁₀V₂O₄₀) to the formed polymer.

The composition and structure of the obtained catalysts were studied using IR spectroscopy and X-ray diffraction (XRD). The diffraction pattern of heteropolyacid H₅PMo₁₀V₂O₄₀ is shown in Fig. 1 and the diffraction pattern of polypyrrole doped with this acid is shown in Fig. 2.

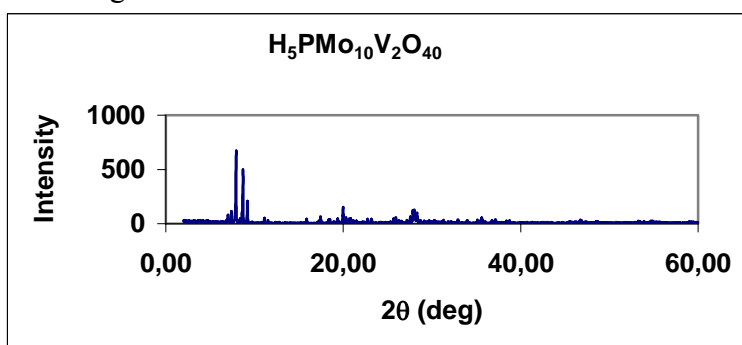


Fig 1. Diffraction pattern of heteropolyacid H₅PMo₁₀V₂O₄₀

The diffraction pattern of H₅PMo₁₀V₂O₄₀ (Fig. 1) confirms the identity of this HPA, which was synthesized in our laboratory, as it is not a commercial product. The diffraction pattern does not contain two most important peaks characteristic of pure MoO₃ (at the angles 2θ = 25.5 ° and 2θ = 39 °). The third peak, which for pure MoO₃ occurs at 2θ = 12.5 ° is shifted. These facts prove that the sample does not contain pure phase of MoO₃.

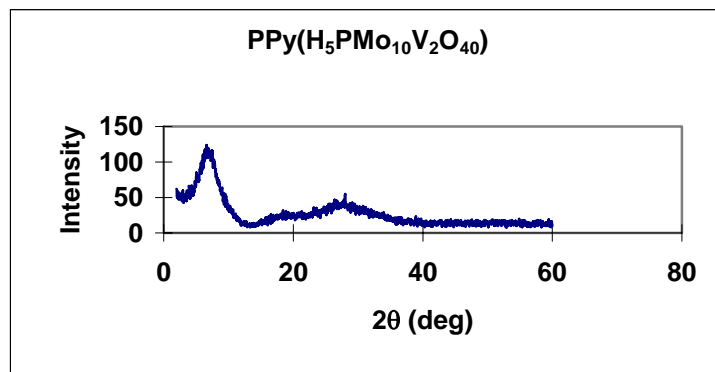


Fig. 2. Diffraction pattern of the catalyst PPy(H₅PMo₁₀V₂O₄₀)

The diffraction pattern of polypyrrole doped with HPA (Fig. 2) does not contain peaks characteristic of pure heteropolyacid. It proves the incorporation of HPA into the polymer matrix, where it is molecularly dispersed. It excludes the possible existence of the heterogenous mixture of the polymer and the crystalline heteropolyacid. The presented diffraction pattern (Fig. 2) is typical of the polymer with a high degree of crystallinity, which contains crystallites of large dimensions.

The heteropolyacids H₅PMo₁₀V₂O₄₀ and H₄SiW₁₂O₄₀ dispersed in the polypyrrole or poly(N-methylpyrrole) matrixes were used in the condensation process methyl α-D-mannopyranoside (**1**) with terephthalaldehyde (**2**).

It was found that the catalytic activity of heteropolyacid H₅PMo₁₀V₂O₄₀ in the poly(N-methylpyrrole) matrix (**6**) is rather low and leads to the condensation product of one molecule of **1** and one molecule **2**, with 60-80 % yield. The structure of the product was determined from analysis of ¹H NMR spectrum (Fig. 3).

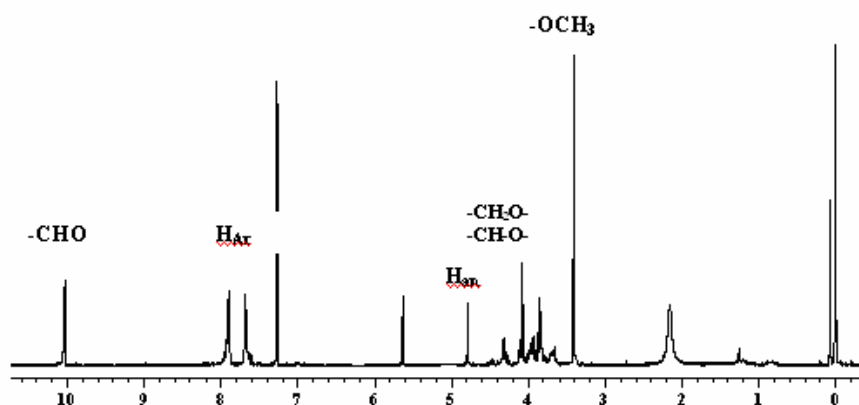


Fig. 3. ¹H NMR (CDCl₃, 300 MHz) spectrum of compound **4**

The characteristic signals due to the acetal proton (5.62 ppm, H_{ax}), anomeric proton (4.76, H_{an}) and aldehyde proton (10.0 ppm) confirmed that the condensation product consists of monoacetal - methyl 4,6-*O*-(1-formyl-4-benzylidene) α-D-mannopyranoside (**4**, Scheme 1). A detailed ¹H NMR analysis of **4** confirmed that the substituent at carbon C-4 and C-6 (in 1,3-dioxane of acetal ring) is in equatorial orientation with respect to the chair-shaped dioxane ring fused to a tetrahydropyran ring. There was no indication of the formation 2,3-*O*-(1-formyl-4-benzylidene) α-D-mannopyranoside substituent at carbon C-2 and C-3 of **1** and polymer products. It seems that the presence

of methyl groups in the structure of the polymer matrix blocks subsequent stages of polycondensation.

However, the $\text{H}_5\text{PMo}_{10}\text{V}_2\text{O}_{40}$ /polypyrrole (**5**) catalyzes of the first stage the condensation **1** with **2** (12 h) and then after prolonged time (40 h) polycondensation process. In this case the macromolecules with 5-membered and 6-membered acetal rings have been obtained (compound **3**, see Scheme 1). The evidence for polymeric materials in polycondensation **1** with **2** has been confirmed by ^1H NMR spectrum (Fig. 4) and ESI-MS spectra.

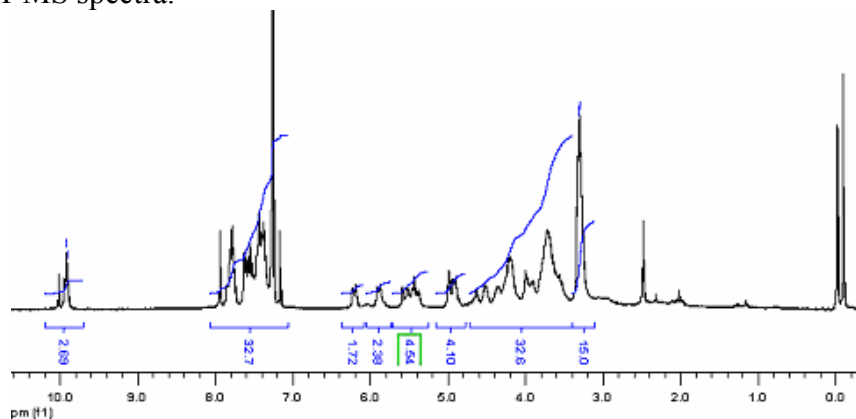


Fig. 4. ^1H NMR (CDCl_3 , 300 MHz) spectrum of compound **3**

The ^1H NMR spectrum of polymer **3** consists of several sets of bands produced by acetal at 6.35–6.28 ppm (H-2 *endo*), 6.0–5.94 ppm (H-2 *exo*), 5.68–5.62 and 5.59–5.47 ppm (4,6-O-terephthylidene) and 5.1–4.9 ppm due to anomeric protons. The relative intensities of *endo*-H and *exo*-H (in 1,3-dioxolane) were 1:1. ESI-MS analysis of the macromolecules suggests, that the product contains all possible terminations of linear macromolecules i.e.: units **1** at both ends, phenylformyl groups at both ends or group **1** at one end and phenylformyl group at the other.

The product of polycondensation of **4** is the polymer with well-defined structure (2,3:4,6). No preferential formation of cyclic diacetals of **1** involving hydroxyl groups at C-2, C-3, C-4 and C-6 was found in the case polyreaction catalyzed by *p*-TsOH.

Conclusions

Polymers doped with heteropolyacids: $\text{PPy}(\text{H}_5\text{PMo}_{10}\text{V}_2\text{O}_{40})$ (**5**) and $\text{PMPy}(\text{H}_5\text{PMo}_{10}\text{V}_2\text{O}_{40})$ (**6**) are active and selective catalysts of acetalization and polyacetalization reactions, which give 4,6-O-(1-formyl-4-benzylidene)- α -D-mannopyranoside. Moreover, $\text{PPy}(\text{H}_5\text{PMo}_{10}\text{V}_2\text{O}_{40})$ at longer reaction times catalyzes the formation of linear macromolecules, probably with well-defined structure (2,3:4,6).

References

- [1] J. Gelas, *Adv. Carbohydr. Chem. Biochem.*, 39 (1981) 71
- [2] J. Maślińska-Solich, *Macromol. Biosci.*, 1 (2001) 312;
J. Maślińska-Solich, S. Kukowka, *Macromol. Biosci.*, 4 (2004) 421;
J. Maślińska-Solich, S. Kukowka, *Macromol. Symp.*, 210 (2004) 67;
J. Maślińska-Solich, E. Gibas, S. Kukowka, *Polimery*, 50 (2005) 509;
J. Maślińska-Solich, S. Kukowka, *Polimery*, 50 (2005) 651
- [3] M. Makoto, *Chem. Commun.*, (2001) 1141

SYNTHESIS AND CHARACTERIZATION OF NEW MDI-BASED THERMOPLASTIC POLYURETHANE ELASTOMERS

Anna Kultys, Magdalena Rogulska, Elżbieta Poździk

Department of Organic Chemistry and Technology, Maria Curie-Skłodowska University, ul. Gliniana 33, 20-614 Lublin, Poland

ABSTRACT

Two series of new thermoplastic segmented polyurethanes (SPUs) were obtained by a one-step melt polymerization from 20–60 mol % poly(tetramethylene oxide) (PTMO) of $\overline{M}_n = 1000$, 4,4'-diphenylmethane diisocyanate (MDI) and 2,2'-[methylenebis(1,4-phenylenemethylenethio)]diethanol (E) or 6,6'-[methylenebis(1,4-phenylene-methylenethio)]dihexan-1-ol (H) as new chain extenders at the NCO/OH molar ratio of 1. We determined physicochemical, thermal and tensile properties as well as Shore A/D hardness of these SPUs. The SPUs containing above 20 mol % PTMO soft segments were elastomers with tensile strengths in the range of about 17–42 MPa. The nonsegmented polyurethanes based on the diol E or H and MDI are also described.

INTRODUCTION

Thermoplastic polyurethane elastomers (TPUs) are segmented block copolymers comprising hard and soft segments. The hard segments (composed of diisocyanates and short-chain diols) particularly affect the modulus, hardness and tear strength, while the soft segments (formed by long-chain diols, mainly polyether and polyester diols) control flexibility and low-temperature resistance [1-4]. TPUs, both poly(ester-urethane)s and poly(ether-urethane)s with excellent tensile strengths are usually obtained from aromatic diisocyanates, mostly 4,4'-diphenylmethane diisocyanate (MDI) and short-aliphatic diols as chain extenders, mostly butane-1,4-diol [1,3]. In particular cases (to obtain TPUs with a high modulus of elasticity or a high thermomechanical resistance) aromatic, aliphatic-aromatic and cycloaliphatic bulky diols are employed as chain extenders, e.g. 2,2'-(1,4-phenylenedioxy)diethanol whether 1,4-cyclohexanediol [3].

The purpose of this paper was to synthesize and characterize new thermoplastic segmented (S) polyurethanes (PUs) based on two newly obtained aliphatic-aromatic chain extenders, i.e. 2,2'-[methylenebis(1,4-phenylenemethylenethio)]diethanol (E) or 6,6'-[methylenebis(1,4-phenylenemethylenethio)]dihexan-1-ol (H), MDI and 20–60 mol % poly(tetramethylene oxide) (PTMO) of $\overline{M}_n = 1000$ as the soft segment. The nonsegmented polyurethanes (NPU) based on the diol E or H and MDI are also described.

EXPERIMENTAL

Materials

The diols E (m.p. = 77–78°C) and H (m.p. = 67–68°C) were obtained by the condensation reaction of (methylenedi-1,4-phenylene)dimethanethiol with 2-chloroethanol or 6-chloroheksan-1-ol, respectively in 10% aqueous solution of sodium hydroxide [5]. PTMO of $\overline{M}_n = 1000$ was purchased from BASF (Ludwigshafen, Germany). Before being used, the PTMO was heated at 120°C *in vacuo* for 1 h. MDI (98%) from Sigma-Aldrich (Steinheim, Germany) and dibutyltin dilaurate (DBTDL) from Merck-Schuchardt (Hohenbrunn, Germany) were used as received. The

polymerization solvent, *N,N*-dimethylformamide (DMF), with a water content of less than 0.02% was purchased from Merck (Darmstadt, Germany) and used as received. The solvent was stored over activated 3 to 4 Å molecular sieves.

Measurements

Reduced viscosities (η_{redS} , dL/g) of 0.5% polymer solution in 1,1,2,2-tetrachloroethane (TChE) were measured in an Ubbelohde viscometer at 25°C. Thermogravimetric analysis (TGA) was performed on a MOM 3 427 derivatograph (Paulik, Paulik and Erdey, Budapest, Hungary) at the heating rate of 10 °C/min in air; measurement relative to Al₂O₃. Differential scanning calorimetry (DSC) thermograms were obtained with a NETZSCH 204 calorimeter at the heating rate of 10 °C/min. Glass-transition temperatures (T_g s) for the polymer samples were taken as the inflection point on the curves of the heat-capacity changes. Melting temperatures (T_m s) were read at endothermic-peak maxima. The hardness of the SPUs was measured by the Shore A/D method at 23°C; values were taken after 15 s. Tensile testing was performed on a Zwick/Roell Z010 (Germany) tensile-testing machine according to Polish Standard PN-81/C-89034 (EN ISO Standard 527-1:1996 and 527-2:1996) at the speed of 100 mm/min at 23°C; the tensile test pieces 1 mm thick and 6 mm wide (for the section measured) were cut from the pressed sheet. Fourier transform infrared (FTIR) spectra were obtained with a Perkin-Elmer 1 725 X FTIR spectrophotometer using thin films or KBr disks. Elemental analysis was performed with a Perkin-Elmer CHN 2400 analyzer.

Polymer Synthesis

(1) **NPU**s (NPUE and NPUH) were prepared by the solution polymerization of an equimolar amount of the diol E or H and MDI (DMF, conc. ~20 wt %), which was carried out under dry nitrogen for 4 h at 85°C in the presence of a catalytic amount of DBTDL. The polymer precipitated and then washed with methanol was dried at 100°C *in vacuo*. The yield was 91-93%.

FTIR (KBr, cm⁻¹): 1704–1703 (bonded C=O stretching), 1528–1524 (N–H bending) and 3402–3390 (N-H stretching) of the urethane group; 1598–1596 (benzene ring); 2923–2915 and 2854–2845 (asymmetric and symmetric C–H stretching of CH₂, respectively).

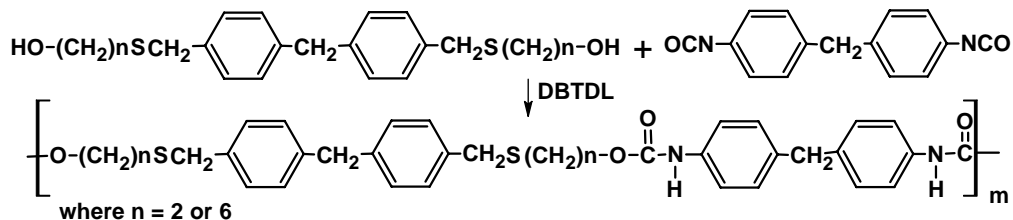
Elem. Anal. NPUE: Calcd. for C₃₄H₃₄N₂O₄S₂: C, 68.18%; H, 5.72%; N, 4.70%. Found: 68.00%; H, 5.64%; N, 5.00. NPUH: Calcd. for C₄₂H₅₀N₂O₄S₂: C, 70.93%; H, 7.09%; N, 3.96. Found: C, 70.70%; H, 6.97%; N, 4.20%.

(2) **SPU**s were prepared by the one-step melt polymerization process from MDI, diol E or H and 20, 40, 50 and 60 mol % PTMO at the NCO/OH molar ratio of 1. MDI was added to melted and mixed dihydroxy compounds at 120°C. The reaction was carried out under dry nitrogen for 2.5 h at 120–140°C.

FTIR (film, cm⁻¹): 1733–1730 and 1708 (v.s., nonbonded and bonded C=O stretching), 1538–1529 (N–H bending), and 3322–3306 (N–H stretching) of the urethane group; 1224–1221 (v.s., C–O stretching of C–O–C); 1599–1598 (benzene ring); 2942–2934 and 2862–2856 (asymmetric and symmetric C–H stretching of CH₂, respectively).

RESULTS AND DISCUSSION

The new hard-segment-type thermoplastic NPUs were synthesized according to the scheme below by step-growth polymerization of aliphatic-aromatic diol E or H with MDI:



Their chemical structures were confirmed by elemental analysis and FTIR. NPUs were colorless, rather brittle materials, insoluble in common organic solvents at room temperature. The thermal characterization of these NPUs is given in Table 2.

The related thermoplastic SPUs were obtained by partial replacement of the diol E or H by 20–60 mol % PTMO. The polymerization reaction was conducted in melt at the NCO/OH molar ratio of 1. Table 1 gives designations, hard-segment contents and η_{red} values. The DSC and TGA data, as well as Shore A/D hardness and tensile properties of the SPUs, can be found in Tables 2 and 3, respectively.

All the SPUs were colorless solids with a partially crystalline structure, as suggested by the presence of endotherms in the DSC thermograms. Generally, a higher ability to crystallize (the higher values of the heat of fusion (ΔH)) was shown by the SPUs derived from the diol H. A relatively good microphase separation was observed for the SPUs with the hard-segment content up to about 46 wt % (from the diol E) and 57 wt % (from the diol H) showed definite T_g s at temperatures -50 to -18°C (the value obtained for pure soft segment was -50°C). The negative definite T_g s, specific for elastomers, were shown by the SPUs containing the hard-segment content of up to about 54 wt % (from the diol E) and 57 wt % (from the diol H), i.e. obtained by using 40–60 mol % PTMO. The characteristics of these TPUs were tensile strengths and elongations at break, respectively in the range of 17.1–42.0 MPa and 660–1730%. All the TPUs were soluble in DMF, *N,N*-dimethylacetamide, *N*-methyl-2-pyrrolidone and TChE at room temperature. Their temperature of 1% weight loss (T_1) ranged from 285 to 305°C. The structures of the SPUs were examined by FTIR.

Tab. 1 Designations, Hard-Segment Contents and η_{red} Values of PUs.

PU	PTMO Content (mol %)	Diol	Hard-Segment Content (wt %)	η_{red} (dL/g)
NPUE	0	E	100.00	insoluble
SPU2E	20	E	72.79	1.18
SPU4E	40	E	53.50	1.13
SPU5E	50	E	45.92	1.47
SPU6E	60	E	39.37	1.06
NPUH	0	H	100.00	0.53
SPU2H	20	H	75.57	2.70
SPU4H	40	H	56.84	2.52
SPU5H	50	H	49.01	2.15
SPU6H	60	H	42.00	1.82

Tab. 2 Thermal Properties of PUs.

PU	DSC				TGA (°C)			
	T_g (°C)		T_m (°C)	ΔH (J/g)	T_1^b	T_{10}^b	T_{50}^b	T_{max}^c
	I ^a	II ^a	I ^a	I ^a				
NPUE		73	130, 153	37.0	215	295	460	350
SPU2E	26	28	111, 159	4.3	275	310	295	410
SPU4E	-2	-4	92	8.3	295	330	400	410
SPU5E	-18	-15	53, 93	12.4	290	345	380	390
SPU6E	-50	-40	67, 85	12.0	285	340	420	440
NPUH	19	45	124	49.5	240	340	390	350
SPU2E	11	11	109	3.5	290	320	395	400
SPU4E	-21	-10	58, 100	25.2	305	340	395	410
SPU5E	-34	-19	60, 98	20.4	300	340	400	400
SPU6E	-48	-41	69, 71	17.9	305	340	390	400

^a I and II – first and second heating scans, respectively.

^b The temperature of 1, 10 and 50% weight loss from the thermogravimetric (TG) curve, respectively.

^c The temperature of the maximum rate of weight loss from the differential TG curve.

Tab. 3 Mechanical Properties of SPUs.

SPU	Hardness (Shore A/D)	Modulus of Elasticity (MPa)	Tensile Strength (MPa)	Elongation at Break (%)	Pressing Temperature (°C)
SPU2E	84/49	81.9	39.1	675	170
SPU4E	76/35	15.3	42.0	945	165
SPU5E	73/29	9.2	30.8	1730	150
SPU6E	66/20	2.6	17.1	1210	145
SPU2H	79/32	19.1	41.3	835	165
SPU4H	77/31	18.7	40.8	790	165
SPU5H	76/30	18.5	40.2	660	165
SPU6H	72/25	2.0	19.7	775	165

REFERENCES

- [1] H. Ulrich in: Encyclopedia of Polymers Science and Technology, H. F. Mark (ed), 3rd ed., John Wiley & Sons, Inc., Hoboken, New Jersey 2003, Vol. 4, p. 26
- [2] C. Hepburn, Polyurethane Elastomers, Applied Science, London 1982, chapt. 9, p. 249
- [3] Z. Wirpsza, Polyurethanes: chemistry, technology and applications, New York 1993: Ellis Horwood
- [4] S. Gogolewski, Colloid Polym. Sci., 267 (1989) 757
- [5] A. Kultys, W. Podkościelny, W. Majewski, J. Polym. Sci. Part. A: Polym. Chem., 38 (2000) 1767

NONSEGMENTED HDI-DERIVATIVE POLYURETHANES CONTAINING BENZOPHENONE UNIT IN THEIR STRUCTURE

Anna Kultys, Piotr Wolski

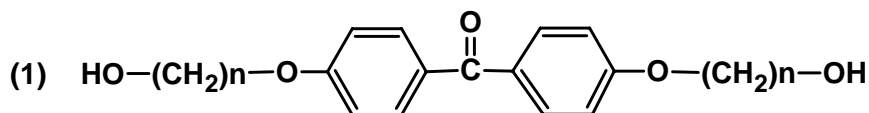
Department of Organic Chemistry and Technology, Maria Curie-Skłodowska University, ul. Gliniana 33, 20-614 Lublin, Poland

ABSTRACT

Two series of thermoplastic nonsegmented polyurethanes (NPU) containing ether or sulfide linkages in the main chain were synthesized from the six aliphatic-aromatic diols and hexane-1,6-diyl diisocyanate (HDI) at the NCO/OH(SH) molar ratio of 1 by solution polyaddition with dibutyltin dilaurate as a catalyst. All these diols were prepared by the condensation reaction of 4,4'-dihydroxybenzophenone (DHB) or 4,4'-dimercaptobenzophenone (DMB) with 2-chloroethanol, 3-chloropropan-1-ol or 6-chlorohexan-1-ol. The structures of all the NPUs were determined by elemental analysis and Fourier transform infrared. Thermal properties of the polymers were examined by differential scanning calorimetry and thermogravimetric analysis. Polarizing microscopy was carried out to examine liquid crystalline properties. Two NPUs with ether linkages showed liquid crystalline properties.

INTRODUCTION

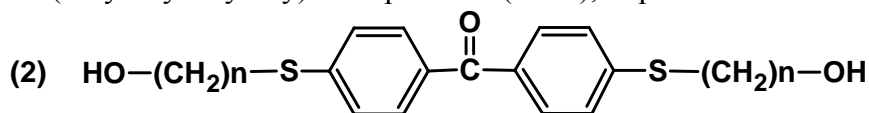
Polyurethanes are mainly prepared by the polyaddition of diols and diisocyanates and are unique polymers with a wide range of applications. Their properties can be readily tailored by the variation of the components, such as monomer type, chemical composition and the synthesis conditions. The present work is aimed at synthesizing, characterizing and comparing the properties of nonsegmented polyurethanes (NPU) with ether or sulfide linkages of the chain. All the NPUs were synthesized from six different benzophenone-derivative aliphatic-aromatic diols of the general formula (1) and (2) and HDI.



n = 2 4,4'-bis(2-hydroxyethoxy)benzophenone (HEB), m.p = 174-175°C

n = 3 4,4'-bis(3-hydroxypropoxy)benzophenone (HPB), m.p. = 163-164°C

n = 6 4,4'-bis(6-hydroxyhexyloxy)benzophenone (HHB), m.p. = 139-140°C



n = 2 4,4'-bis(2-hydroxyethylthio)benzophenone (HETB), m.p = 122-123°C

n = 3 4,4'-bis(3-hydroxypropylthio)benzophenone (HPTB), m.p = 113-114°C

n = 6 4,4'-bis(6-hydroxyhexylthio)benzophenone (HHTB), m.p = 110-111°C

The NPUs derived from sulfur-containing diols (HETB, HPTB and HHTB) and HPB are new polymers, whereas those from diols HEB and HHB have been described in the literature [1,2]. The latter were found to be polymers with liquid crystalline properties. It seemed interesting to us to check if their sulfur analogs also possess such properties.

EXPERIMENTAL

Materials

The diols type (1) and (2) (after recrystallization from benzene or butan-1-ol) were obtained from DHB and DMB by the condensation reaction with suitable monohalogenated alcohols in the mixture of butan-1-ol and aqueous solution of sodium hydroxide. Reagents, including 2-chloroethanol, 3-chloropropan-1-ol and 6-chlorohexan-1-ol from Fluka (Buchs, Switzerland), HDI and dibutyltin dilaurate (DBTDL) from Merck-Schuchardt (Hohenbrunn, Germany) were used as received. The polymerization solvent, *N,N*-dimethylformamide (DMF), with water content of less than 0.02% was purchased from Merck (Hohenbrunn, Germany) and used as received. The solvent was stored over activated 3 to 4 Å molecular sieves.

Measurements

Elemental analysis was performed with a Perkin-Elmer CHN 2400 analyzer. Reduced viscosities (η_{red} , dL/g) of polymer solution in 1,1,2,2-tetrachloroethane (TChE) and phenol/TChE mixture with a weight ratio of 1:3 were measured in an Ubbelohde viscometer (Gliwice, Poland) at 25°C. Thermogravimetric analysis (TGA) was performed on a MOM 3427 derivatograph (Paulik, Paulik and Erday, Budapest, Hungary) at the heating rate of 10°C/min in air, with the measurement relative to Al₂O₃. Differential scanning calorimetry (DSC) thermograms were obtained with a NETZSCH 204 calorimeter at the heating rate of 10°C/min in under nitrogen purge (20 mL/min). Glass-transition temperatures (T_g s) for the polymer samples were taken as the inflection point on the curves of the heat-capacity changes. Melting temperatures (T_m s) were read at endothermic-peak maxima. Polarizing optical microscopic studies were carried out with Alaphote-2 (Nikon) microscope equipped with a Linkam THMS 600 heating stage. Fourier transform infrared (FTIR) spectra were obtained with a Perkin-Elmer 1725 X FTIR spectrophotometer using KBr disks.

NPU Synthesis

All the NSPUs were synthesized by the following method. A solution of diol, HDI and DBTDL in 20 mL of DMF was stirred at 85-90°C under dry nitrogen for 4 hours. In the meantime, as the viscosity of the reaction mixture increased, further solvent (5-10 mL) was added as the reaction proceeded. After the reaction was finished, the viscous mixture obtained was poured into 300 mL of cold methanol, and the precipitated product was filtered, washed twice with 100 mL of boiling methanol and dried at 100°C *in vacuo* up to constant weight [3].

RESULTS AND DISCUSSION

All the NPUs containing ether and sulfide linkages were synthesized according to Scheme 1 by polyaddition of the aliphatic-aromatic diols: HEB, HPB, HHB, HETB, HPTB and HHTB, respectively, with HDI. The reaction was conducted in solution at the NCO/OH(SH) molar ratio of 1 in the presence of DBTDL as a catalyst. DMF was used as the polymerization solvent. Table 1 gives yields and η_{red} values for the all polymers.

Table 1. Yields, η_{red} values and elemental analysis results of the NPUs.

Diol	Yield (%)	η_{red} (dL/g)	Analysis					
			C (%)		H (%)		N (%)	
			Calcd.	Found	Calcd.	Found	Calcd.	Found
HEB	94.6	1.28	63.82	62.74	6.43	6.30	5.95	6.04
HPB	91.4	1.84	65.05	64.58	6.87	5.92	5.64	4.98
HHB	91.7	1.15	68.02	67.66	7.95	7.93	4.81	4.99
HETB	89.7	3.31	59.74	60.90	6.02	6.26	5.57	5.54
HPTB	92.1	1.47	61.12	60.87	6.46	5.91	5.28	5.08
HHTB	92.2	1.63	64.47	63.88	7.54	6.87	4.55	4.19

The NPUs were white (with ether linkages) or yellow (with sulfide linkages) fibers showing high resistance to organic solvents. All the NPUs were soluble in the phenol/TChE mixture (with a weight ratio of 1:3) at room temperature and in DMF, *N,N*-dimethylacetamide and *N*-methyl-2-pyrrolidone at heating (80°C).

The structures of the NPUs obtained were examined by FTIR and elemental analysis. Table 1 presents the results of the elemental analysis of all the polymers. FTIR spectra of all the NPUs showed following absorption: 3479–3328 cm^{-1} , bonded N–H stretching of the urethane group; 2993–2928 and 2881–2856 cm^{-1} , C–H asymmetric and symmetric stretching, respectively, of CH_2 ; 1716–1680 cm^{-1} , bonded C=O stretching of the urethane group; 1643–1641 cm^{-1} , C=O stretching of the aromatic ketone; 1602–1599 cm^{-1} , benzene ring; 1540–1534 cm^{-1} , N–H bending of the urethane group; 852–845 cm^{-1} , bending of the *p*-disubstituted benzene ring.

The thermal behavior of the NPUs was investigated with DSC and TGA, and the numerical data are given in Table 2.

Table 2. Thermal properties of the NPUs.

Diol	DSC					TGA (°C)				
	T_g (°C)		T_m (°C)		ΔH (J/g)		T_5^b	T_{10}^b	T_{50}^b	T_{max}^c
	II ^a	I ^a	II ^a	I ^a	II ^a					
HEB	69	142, 159	142	37.0, 9.4	0.7	340	350	420	360	
HPB	55	107, 127		2.1, 19.9		324	340	410	350	
HHB	31	156	156	53.8	49.2	320	340	410	350	
HETB	44	119		44.3		320	340	410	360	
HPTB	55	117, 166, 186	139, 165	3.4, 31.9	2.3, 3.5	300	320	420	340	
HHTB	54	146, 167, 187	137, 165	3.0, 26.3	2.2, 2.3	310	330	420	310	

^a I and II – first and second heating scans, respectively.

^b The temperature of 5, 10 and 50% weight loss from the thermogravimetric (TG) curve, respectively.

^c The temperature of the maximum rate of weight loss from the differential TG curve.

The NPUs showed relatively good and similar thermal stabilities. Their T_{10} and T_{50} were in the range of 320–350°C and 410–420°C, but the higher T_{10} were observed for polymers containing ether linkages. The T_g s of all the polymers were observed to be in the range of 31–69°C (from second heating scans). For polymers with ether linkages T_g decreased with increase in the number of methylene groups in the diol, but polymers with sulfide linkages showed similar T_g s. The first heating DSC scans of all the NPUs showed, beside glass transitions, the melting transitions (one, two or three endothermic peaks) at temperatures in the range of 107–159°C and 117–187°C for polymers containing ether and sulfide linkages, respectively. The typical DSC thermogram of the chosen NPU is given in Figure 1.

The NPUs derived from sulfur-containing diols as well as HPB were polymers without liquid crystalline properties. This was confirmed by observation by using polarizing optical microscope.

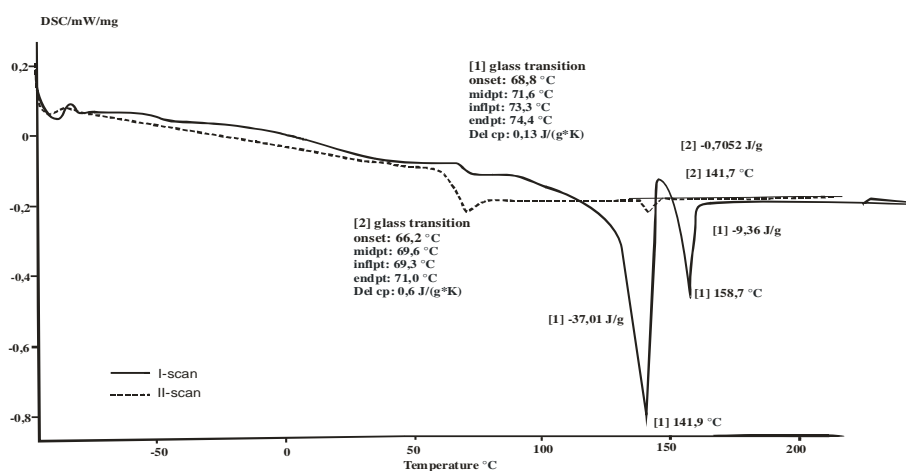
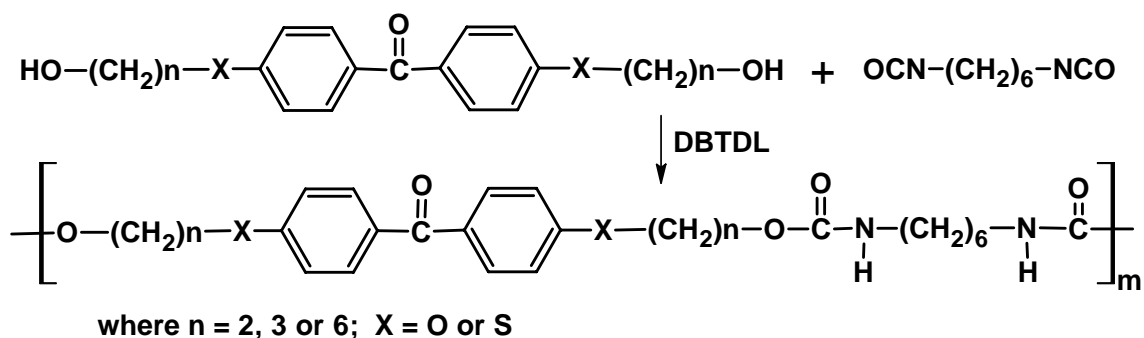


Figure 1. DSC thermogram of the NPU from the diol HEB



Scheme 1

REFERENCES

- [1] Y. Onouchi, S. Inagaki, Cellular Polymers Reprints, 15 (1996) 30
- [2] M. Furukawa, Y. Oda, Cellular Polymers Reprints, 15 (1996) 37
- [3] A. Kultys, W. Podkościelny, W. Majewski, J. Polym. Sci. Part A: Polym Chem., 38, (2000) 1767

VOLTAMMETRIC AND IMPEDANCE CHARACTERISTICS OF ELECTROREDUCTION PROCESSES OF Pd(II)/Pd(0) ONTO HOPG AND POLYCRYSTALLINE GOLD ELECTRODES

A. Leniart, T. Blaszczyk, B. Burnat, H. Scholl

University of Lodz, Department of General and Inorganic Chemistry
ul. Narutowicza 68, 90-136 Lodz, e-mail: leniart@chemul.uni.lodz.pl

INTRODUCTION

Palladium is a metal which plays an important role in various walks of technology. Especially palladium is used as an effective catalyst, precursor for metallization of non-conducting materials [1-3], etc. Moreover palladium is one of the most frequently used metal to study electrochemical processes of hydrogen evolution reactions [4-8]. Interfacial electrochemistry of palladium is widely described by Soriaga *et al.* in monograph edited by Wieckowski [9]. The palladium property was studied by Czerwiński *at al.* [10-11] by means of electrochemical quartz crystal microbalance method. Early studies of the deposition of palladium from solutions containing various concentrations of palladium chloride and hydrochloric acid in perchloric acid solution were made at a palladium rotating disc electrode [12-13]. It was found that the neutral complex PdCl₂ is the electroactive species. It undergoes 2-electron irreversible reduction to Pd(0). The electrochemical deposition of thin palladium layers on Au single crystal substrates was intensively investigated by means of *in situ* scanning tunnelling microscopy and cyclic voltammetry by Kolb's [14-16] and Naohara's groups [17-19]. They reported that the electrochemical deposition of palladium on both Au(111) and Au(100) surfaces proceeds two-dimensionally. Relations between the surface topography, impedance spectroscopy and interface model of the electrolyte solution/electrodeposited Pd layer/matrix electrode were presented by Scholl and co-workers [20]. Additionally they observed spontaneous deposition of palladium onto Highly Oriented Pyrolytic Graphite (HOPG) in 0.01 M HCl + 0.01 M (NH₄)₂PdCl₄ aqueous solution. The aim of this work is to characterize the electroreduction processes of Pd(II)/Pd(0) onto HOPG and polycrystalline gold electrodes and determination of kinetic parameters of these processes in solutions containing palladium ions in supporting electrolyte H₂SO₄ using voltammetry and impedance measurements.

EXPERIMENTAL

Reagents: All the electrolyte solutions were performed from analytical grade chemical reagents H₂SO₄ (POCH, Gliwice), (NH₄)₂PdCl₄ (Ventron GMBH) and triply distilled water. Supporting electrolyte was 0.1 M H₂SO₄. Concentrations of the palladium complex was 0.001M. All solutions were deoxygenated by bubbling pure argon (99.999% - Linde Gas Division, Poland) before each measurement. The electrochemical measurements were carried out at temperature 25.0 ± 0.5 °C (298 ± 0.5 K).

Electrodes: The measurements were conducted using two different working electrodes: the HOPG type ZYB (Advanced Ceramics Corporation, USA) and polycrystalline gold (99.99% - Mint of Poland plc, Warszawa). HOPG was in form of a plate 10 mm x 10 mm and 2-3 mm height. The HOPG surface was cleaned by sticking and detaching of a scotch tape. The polycrystalline gold electrode was prepared in form of a cylinder with 5.25 mm in diameter and ca. 3 mm height. The preparation method of polycrystalline Au surface consisted of initial polishing with SiC abrasive paper up to 2500 grain and next final polishing by cloth with alumina powder, cleaning in ultrasonic cleaner (5 min), rinsing with distilled water and drying with Ar. In the next step samples were cleaned in hot mixture of H₂SO₄ and K₂Cr₂O₇ (5 min), and subsequently cleaned in ultrasonic cleaner, rinsed with distilled water and drayed with Ar. A linear voltammetry with programmed polarization potential in the range 0.4 V → -0.2 V → 1.5 V → 0.4 V at

a potential scan rate of 0.1 V/s was used for electrochemical activation of electrode surface in 0.1 M H₂SO₄ solution. Electrochemical activity was achieved after ca. 50 cycles.

Apparatus: All electrochemical measurements were carried out in three-electrodes cell. The cell was made of a cylinder glass with flat base in which was a hole 0.35 cm in diameter determinative an exposed area of working electrode to 0.096 cm². Volume of this cell was ca. 2 cm³. A specially miniature calomel electrode (Eurosensor, Poland) in saturated NaCl solution (SSCE) was used as reference electrode. This electrode was connected to the cell by means of Luggin capillary. All potentials in this paper are given versus this reference electrode ($E^0 = 0.236$ V vs. NHE). A platinum foil cylinder was used as auxiliary (counter) electrode. Voltammetry measurements were carried out with potentiostat/galvanostat AUTOLAB PGSTAT30 with FRA2 module (EcoChemie, the Netherlands) which allows to measure the electrochemical impedance (EIS).

RESULTS AND DISCUSSION

In Fig. 1 there are presented voltammetric characteristics in 0.1 M H₂SO₄ + 0.001 M (NH₄)₂PdCl₄ solution in the potential range from 0.0 V to 0.9 V for HOPG and from 0.2 V to 0.9 V for polycrystalline gold at a potential scan rate of 0.01 V/s. In both figures there are presented two curves : 1 - 1st and 2 - 10th cycle of the electroreduction-electrooxidation processes. The 10th cycle is finally, repeatable curve.

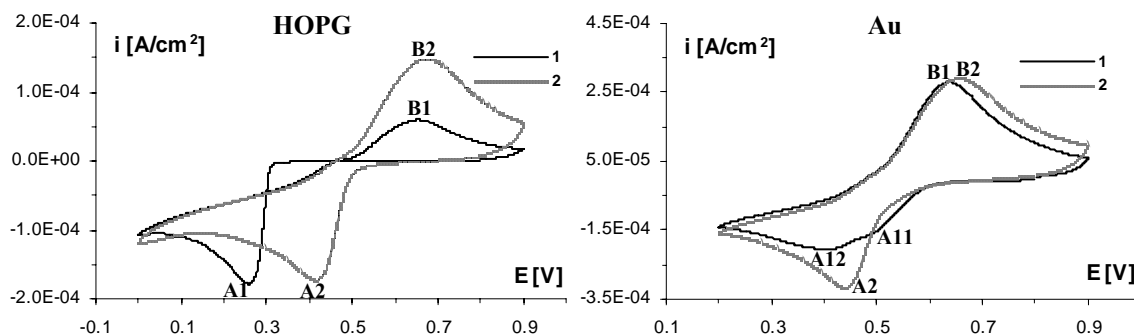


Fig. 1. Voltammetric characteristics for HOPG and polycrystalline gold in aqueous solution of 0.1 M H₂SO₄ with 0.001 M (NH₄)₂PdCl₄; (1 - 1st and 2 - 10th cycle of the electroreduction-electrooxidation processes, $v = 0.01$ V/s, $E_{\text{Ref}} = \text{SSCE}$)

The voltammetric curves for both electrodes show the presence of cathodic and anodic peaks. The peaks B are related to the electrooxidation of deposited palladium. However the peaks A are connected with the electroreduction processes of Pd(II)/Pd(0). For HOPG on the curve 1 cathodic peak at a potential $E_{A1} = 0.260$ V and anodic peak at a potential $E_{B1} = 0.660$ V ($\Delta E_{B1/A1} = 0.400$ V) are observed. The curve 2 is characterised by the peaks at potentials $E_{A2} = 0.410$ V, and $E_{B2} = 0.660$ V ($\Delta E_{B2/A1} = 0.250$ V). For polycrystalline gold on the curve 1 two cathodic peaks at potentials $E_{A11} = 0.490$ V and $E_{A12} = 0.410$ V and one anodic peak at a potential $E_{B1} = 0.660$ V ($\Delta E_{B1/A12} = 0.250$ V) are observed. The peak E_{A11} is observed on the 1st voltammetric curve only. It suggests that the main electroreduction processes of Pd(II)/Pd(0) on the polycrystalline gold are preceded by formation intermetallic alloys of Au_xPd_y. The formation of similar alloys was observed by Nichols *et al.* during Cu electrodeposition onto monocrystalline gold electrode [21]. The curve 2 is characterised by the peaks at potentials $E_{A2} = 0.430$ V, and $E_{B2} = 0.650$ V ($\Delta E_{B2/A1} = 0.220$ V). A large difference between cathodic peak potential and anodic peak potential ($\Delta(E_{pa} - E_{pc}) > 0.220$ V) confirms that the reduction-oxidation processes of Pd(II)/Pd(0) are irreversible. For both electrodes from voltammograms have been determinate cathodic $Q_{(c)}$ and anodic $Q_{(a)}$ charges. Charges for HOPG for curve 1 equal $Q_{(c1)HOPG} = -0.62$ mC, $Q_{(a1)HOPG} = 0.14$ mC and for curve 2 equal $Q_{(c2)HOPG} = -0.83$ mC, $Q_{(a2)HOPG} = 0.40$ mC. Charges for polycrystalline gold for curve 1 equal $Q_{(c1)Au} = -0.82$ mC, $Q_{(a1)Au} = 0.59$ mC and for curve 2 equal

$Q_{(c2)Au} = -0.94$ mC, $Q_{(a2)Au} = 0.71$ mC. These differences between $Q_{(c)}$ and $Q_{(a)}$ for both electrodes suggest that a large part of the electrodeposited palladium atoms remains on the surface electrodes. Consequently these electrodes can be treated as modified electrodes. On the basis of separately executed voltammetric measurements the kinetic parameters of electroreduction processes of Pd(II)/Pd(0) in aqueous solution of 0.1 M H₂SO₄ with 0.001 M (NH₄)₂PdCl₄ at different potential scan rates from 0.005 V/s to 0.2 V/s were calculated. Fig. 2 shows the table with determinate values of the kinetic parameters: the general transfer coefficients of electrode processes αn_{α} , the diffusion coefficients of the Ox form D_{ox} , the formal potentials E_f^0 and the standard rate constants of electroreduction processes of Pd(II)/Pd(0) k_s .

	αn_{α}	D_{ox} [cm ² /s]	E_f^0 [V]	k_s [cm/s]
HOPG	0.854 ± 0.037	$(9.74 \pm 2.72) \cdot 10^{-6}$	0.508 ± 0.003	$(3.19 \pm 0.62) \cdot 10^{-4}$
Au	0.835 ± 0.045	$(8.54 \pm 2.53) \cdot 10^{-6}$	0.511 ± 0.003	$(3.23 \pm 0.61) \cdot 10^{-4}$

Fig. 2. Table with determinate values of kinetic parameters of the electroreduction processes of Pd(II)/Pd(0) in aqueous solution of 0.1 M H₂SO₄ with 0.001 M (NH₄)₂PdCl₄ for HOPG and polycrystalline gold

The determinate values of kinetic parameters are almost the same for both electrodes. We can state that electroreduction processes of Pd(II)/Pd(0) from kinetics point of view proceed identically both for HOPG and for polycrystalline gold electrodes. It is known that four-step dissociation of [PdCl₄]²⁻ complex proceeds in an aqueous solutions. The forming palladium compounds [Pd²⁺] \leftrightarrow [PdCl⁺] \leftrightarrow [PdCl₂] \leftrightarrow [PdCl₃]⁻ \leftrightarrow [PdCl₄]²⁻ in these processes are in equilibrium with each other. Kibler *at al.* [13] calculated that the dominant species in 0.1 M H₂SO₄ + 0.001 M H₂PdCl₄ solution are [PdCl⁺] and [PdCl₂]. Simultaneously they identified that [PdCl₄]²⁻ compounds are adsorbed on the surface of Au(111) and play a crucial role in electrodeposition processes of palladium. It suggests that electroreduction process of Pd(II)/Pd(0) is not simple and perhaps proceed with participation of the various of Pd chloro complexes. Reduction process of Pd(II)/Pd(0) can be described by the following reaction:

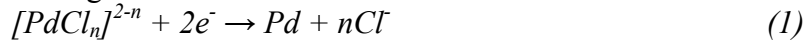


Fig. 3 shows the Nyquist and Bode diagrams of impedance spectra recorded in the frequency range from 10000 Hz to 0.01 Hz with 5 mV sinusoidal perturbation signal at cathodic peak potentials for both electrodes.

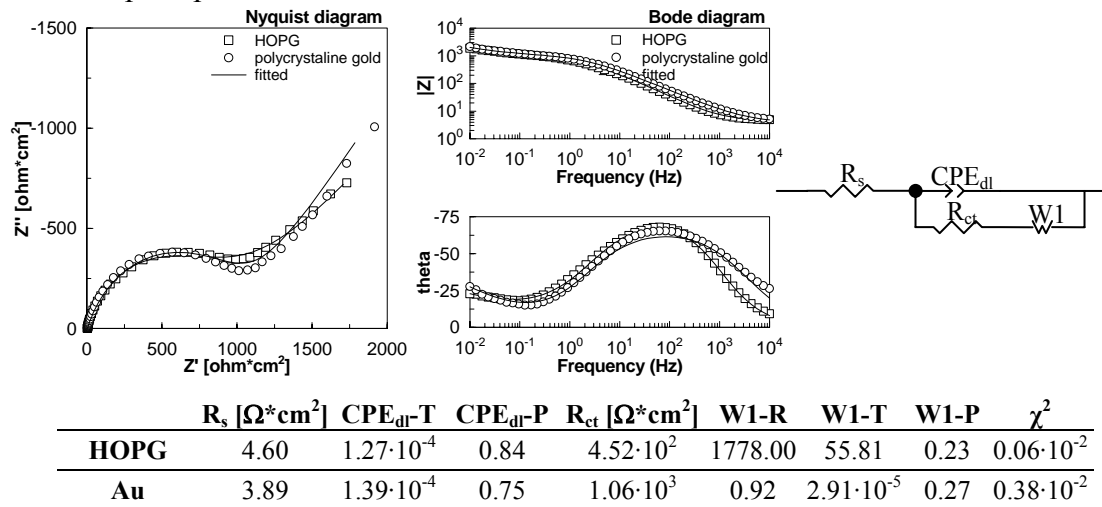


Fig. 3. Impedance spectra at cathodic peak potentials for HOPG and polycrystalline gold in aqueous solution of 0.1 M H₂SO₄ with 0.001 M (NH₄)₂PdCl₄ and equivalent electrical circuit

The impedance data were recalculated on unit geometric area. The impedance spectra obtained for HOPG and polycrystalline gold are typical for quasi-reversible processes with reaction and diffusion control. On the Nyquist diagrams a capacitive loop at high frequencies is visible, which can be connected with double layer capacitance and reduction reaction of Pd(II) ions. Whereas a straight line visible at low frequencies can be associated with semi-infinite linear diffusion of depolarizer to electrode surface. The equivalent electrical circuit (Fig. 3) is the same for HOPG and polycrystalline gold and was fitted the measurements data using Zview2 software (Scribner Associates, Inc.). χ^2 values confirm a goodness of fit. The elements of this circuit can be interpreted as follows: R_s - typical uncompensated solution resistance between working and reference electrodes, CPE_{dl} - constant phase element takes into consideration frequency dispersion and substitutes of double layer capacitance C_{dl} , R_{ct} - the charge transfer resistance of electroreduction processes of Pd(II)/Pd(0) occurring at the solution/surface electrode interface and WI - impedance of mass transfer which is related to diffusion of Pd(II) ions to electrode surface.

SUMMARY

In this paper we present the kinetic parameters of electroreduction processes of Pd(II)/Pd(0), which have been obtained for the first time. From kinetics point of view the electroreduction processes of Pd(II)/Pd(0) proceed identically both for HOPG and for polycrystalline gold. The same impedance spectra for both electrodes are the confirmation of this phenomenon. On the basis of the obtained voltammetric characteristics was found that reduction-oxidation processes of Pd(II)/Pd(0) are irreversible onto both electrodes. On the basis of impedance measurements was found that charge transfer resistances of electroreduction process of Pd(II)/Pd(0) is lower for HOPG than for polycrystalline gold.

ACKNOWLEDGEMENT

This work was supported by grant University of Lodz 505/678.

REFERENCES

- [1] J. Tsuji; *Palladium Reagents and Catalysts: New Perspectives for the 21st Century* Wiley, 2004
- [2] H. Inoue, T. Ito, Ch. Iwakura; *Electrochemical and Solid-State Letters* 2(2)(1999)75
- [3] G. Koziol; Thesis; Faculty of Chemistry, Warsaw University of Technology, Warszawa 1999
- [4] C. Gabrielli, P.P. Grand, A. Lasia, H. Perrot; *J. Electroanal. Chem.* 532(2002)121
- [5] C. Gabrielli, P.P. Grand, A. Lasia, H. Perrot; *Electrochim. Acta* 47(2002)2199
- [6] P. Zoltowski; *Electrochim. Acta* 44(1999)4415
- [7] P. Zoltowski; *Acta Mat.* 51(2003)5489
- [8] A. Czerwinski, I. Kiersztyn, M. Grden; *J. Electroanal. Chem.* 492(2000)128
- [9] M. P. Soriaga, Y-G. Kim, J. E. Soto; *Interfacial chemistry of palladium electrodes*, chapter 15 in monograph edited by A. Więckowski; *Interfacial electrochemistry. Theory, experiment and applications*. Marcel Dekker, Inc., New York 1999, 249-267
- [10] M. Grdeń, J. Kotowski, A. Czerwiński; *Journal of Solid State Electrochemistry* 3(1999)348
- [11] M. Grdeń, J. Kotowski, A. Czerwiński; *Journal of Solid State Electrochemistry* 4(2000)273
- [12] J.A. Harrison, R.P.J. Hill, J. Thompson; *Electroanalytical Chemistry and Interfacial Electrochemistry* 47(1973)431
- [13] W. Davison, J.A. Harrison, J. Thompson; *Faraday Discuss. Chem. Soc.* 56(1973)171
- [14] L.A. Kibler, M. Kleinert, R. Randler, D.M. Kolb; *Surface Science* 443(1999)19
- [15] L.A. Kibler, M. Kleinert, D.M. Kolb; *Surface Science* 461(2000)155/
- [16] L.A. Kibler, M. Kleinert, V. Lazarescu, D.M. Kolb; *Surface Science* 498(2002)175
- [17] H. Naohara, S. Ye, K. Uosaki; *Journal of Physical Chemistry B* 102(1998)4366
- [18] H. Naohara, S. Ye, K. Uosaki; *Colloids and Surfaces A* 154(1999)201
- [19] H. Naohara, S. Ye, K. Uosaki; *Journal of Electroanalytical Chemistry* 473(1999)2
- [20] H. Scholl, T. Błaszczuk, A. Leniart, K. Polański J. *Solid State Electrochem* 8(2004)308
- [21] R. Nichols, W. Beckmann, H. Meyer, N. Batina, D. Kolb; *J. Electroanal. Chem.*, 330(1992)381

SELECTIVE UPTAKE AND RECOVERY OF Cu(II), Co(II), Ni(II) AND Fe(III) BY AMBERLITE IRA-401S MODIFIED WITH ALIZARINE RED S AND SPADNS

M. Leszczyńska, Z. Hubicki

*Department of Inorganic Chemistry, Faculty of Chemistry,
Maria Curie – Skłodowska University, 20-031 Lublin, Poland*

INTRODUCTION

Chelating polymer resins have attracted attention as the metal selective adsorbents in the field of wastewater treatment [1] as well as for the enrichment of trace metal ions prior to the instrumental analysis [2]. The selectivity of a chelating resin for metal ions is mainly attributed to the nature of the ligand immobilized on the polymer matrix. A very simple way of preparation of such sorbents is based on modification of commercial anion exchange resins with chelating reagents containing sulfonic groups or treatment of inert supports with a mixture of liquid anion exchanger [3] and a sulphonated chelating reagent. Aromatic complexing agents (ACA) containing sulfonic acid groups exhibit a high affinity for anion exchangers, as a consequence of their structure, and when retained on the ion exchange resins transform it into a selective ion exchanger. The selectivity depends on the character of functional analytical groups of the ligand. The applicability of sulpho-derivatives of aromatic organic reagents in separation of metal ions has been confirmed by Przeszlakowski [3], Chwastowska [4,5] and Brajter [6].

The research presented here concerns the usefulness of the trisodium salt of 2-sulphophenylazo-chromotropic acid (SPADNS) and sodium salt of 9,10-dihydroxy-9,10-dioxo-2-antracene sulfonic acid (Alizarine Red S) (Fig. 1) in modification of the strongly basic anion exchanger Amberlite IRA-401S.

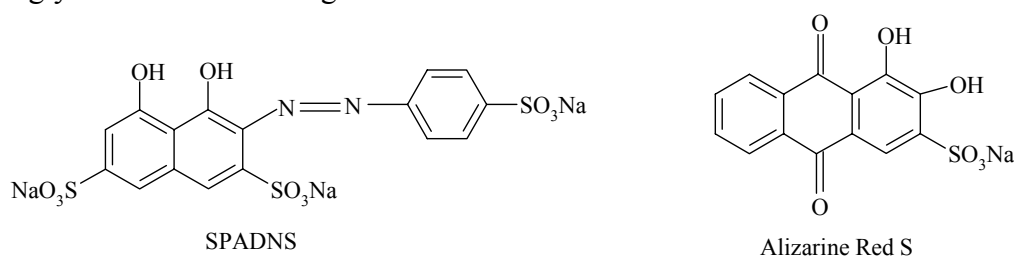


Fig. 1. SPADNS and Alizarine Red S chemical structures.

The modified resin was applied in the uptake and recovery of Fe(III), Cu(II), Ni(II) and Co(II) from 0.001 M chloride solutions as well as from their mixtures of the total concentration 0.0008M.

EXPERIMENTAL

The sorption research of ACA containing sulfonic acid groups on Amberlite IRA-401S (anion exchanger of functional $-\text{N}^+(\text{CH}_3)_3$ groups with the exchange capacity of >1.3 meq/g and particle size 16-50 mesh) as well as Fe(III), Cu(II), Ni(II)

and Co(II) on the modified anion exchanger was carried out by means of static method. The recovery factors of the above mentioned metal ions depending on the ion exchanger – solution contact times and solution composition were determined from Eq. 1:

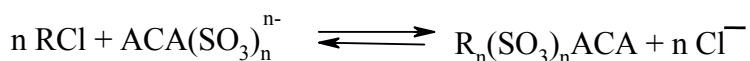
$$R_{\%} = \frac{Q}{Q_0} \times 100\% \quad (1)$$

where: Q – the number of metal ions adsorbed, Q_0 – the initial metal ions concentration in the aqueous solutions.

Metal ions concentration as well as those of SPADNS and Alizarine Red S were determined by the AAS method and spectrophotometrically, respectively.

RESULTS AND DISCUSSION

Aromatic complexing agents (ACA) like SPADNS and Alizarine Red S (ARS) exhibit a high affinity for strongly basic anion exchangers, as a consequence of their aromatic structure and the presence of sulfonic acid groups. Retained on the anion exchange resins they transform them into chelating ion exchangers. The sorption mechanism of sulfo-derivative aromatic complexing agents ($ACA(SO_3)_n^{n-}$) on a strongly basic anion exchanger in the chloride form (RCl) can be described by means of the following reaction:



As follows from the above, $ACA(SO_3)_n^{n-}$ forms a stable ion pair in the anion exchanger phase. SPADNS and ARS can also be retained on Amberlite IRA-401S by means of a molecular mechanism (physical adsorption). The metallic ion (M^{n+}) diffuses into the polystyrene ion exchanger beads and forms coordinate bonds with nitrogen atoms of SPADNS on the anion exchanger. The 2-(p-sulphophenylazo)-1,8-dihydroxy-3,6-naphthalenedisulfonate complex with a metal ion is shown in Fig. 2.

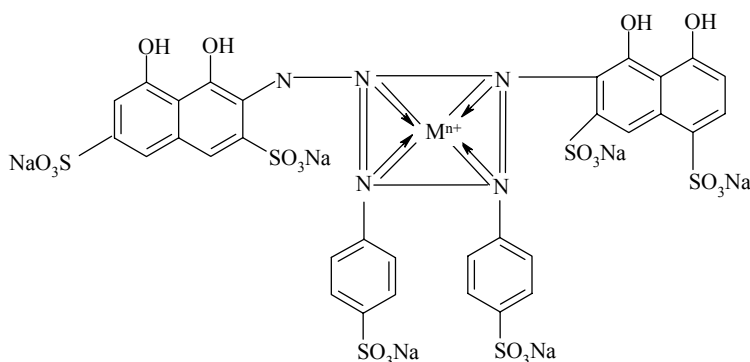


Fig. 2. Metal - 2-(p-sulphophenylazo)-1,8-dihydroxy-3,6-naphthalenedisulfonate complex ion [7].

The effect of phase contact time on sorption (Fig. 3 a-d) shows that copper(II) and cobalt(II) are retained almost quantitatively ($\%R > 90\%$) on Amberlite IRA-401S in the form of SPADNS. The recovery factors of Ni(II) from 0.001 M $NiCl_2$ are smaller than those for the other metal ions in the form of SPADNS, the values do not exceed 60%. It is caused by little affinity of SPADNS ligand for Ni(II). Data of sorption

kinetics for Cu(II), Ni(II) and Co(II) indicate that shaking for 60 min is necessary to attain an equilibrium state. Iron(III) is recovered only in 70% on the modified anion exchanger in both forms.

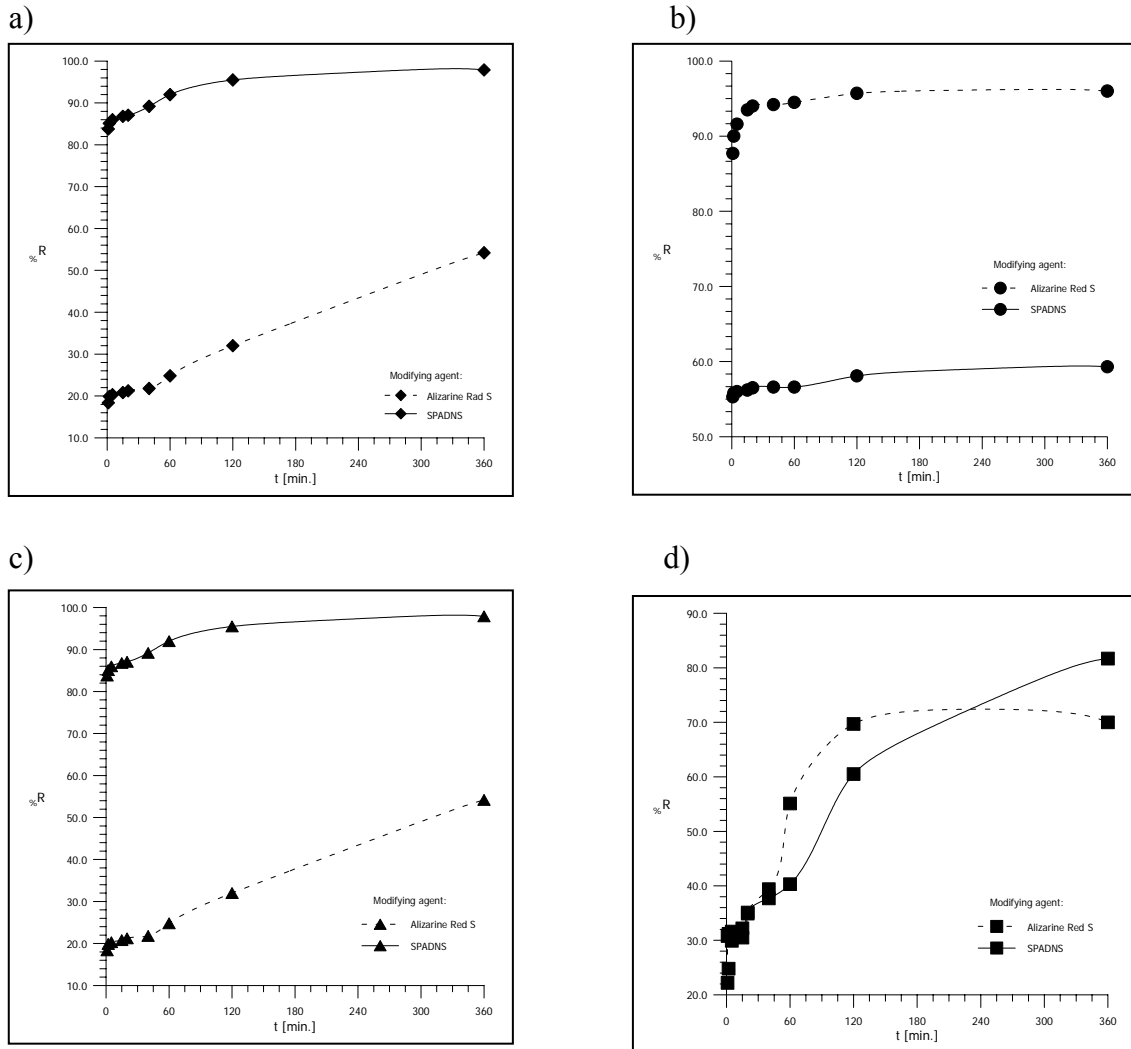
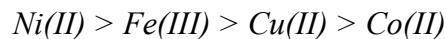
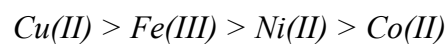


Fig. 2. Influence of phase contact time on the recovery of Cu(II) from 0.001 M CuCl₂ (a), Ni(II) from 0.001 M NiCl₂ (b), Co(II) from 0.001 M CoCl₂ (c), Fe(III) from 0.001 M FeCl₃ (d) on 1 g of modified Amberlite IRA-401S.

There was also studied the influence of phase contact time on Fe(III), Cu(II), Ni(II) and Co(II) sorption from their mixture (Fig. 3). The determined affinity series can be presented as follows:



for the anion exchanger modified by means of ARS and



for Amberlite IRA-401S in the form of SPADNS.

The ion exchange capacities calculated for Cu(II), Ni(II), for Co(II) and Fe(III) expressed in mmol per 1 g of the modified anion exchanger are following: 0.1355, 0.2406, 0.0355, 0.1753 respectively when Alizarine Red S is used as the modifying agent and respectively 0.2410, 0.1483, 0.0864 and 0.2043 respectively for SPADNS.

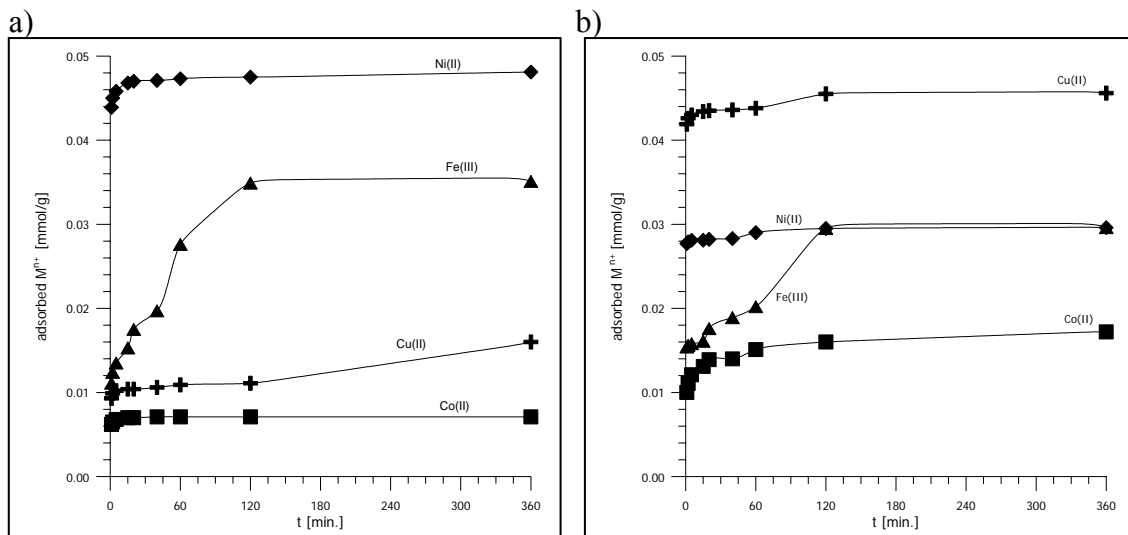


Fig. 3. Influence of phase contact time on the sorption of Cu(II), Ni(II), Co(II) and Fe(III) from their mixture of the total concentration 0.0008 M on 1 g of the modified Amberlite IRA-401S in the form of : a) ARS and b) SPADNS.

CONCLUSION

The strongly basic anion exchanger Amberlite IRA-401S studied in this work can be applied in the modification process in order to obtain a new chelating resin. Aromatic complexing agents (ACA) like SPADNS and Alizarine Red S (ARS) containing sulfonic acid groups transform the commercial anion exchanger into the ion exchanger selective for Cu(II), Ni(II), Co(II) and Fe(III) ions.

The modified resin can be applied in the above mentioned metal ions recovery from waste waters, slimes and solutions originating from used-up catalyst leaching.

REFERENCES

- [1] S.H. Lin, L.S. Lai, H.G. Leu, J. Hazard. Mater., B76 (2000) 139-153.
- [2] A.M. Naghmush, K. Pyrzyńska, M. Trojanowicz, Talanta, 42 (1995) 851-860.
- [3] S. Przeszlakowski, R. Kocjan, I. Cukrowski, Chem. Anal, 31 (1986) 735-741.
- [4] J. Chwastowska, W. Żmijewska, E. Sterlińska, W. Gołębiwska, Chem. Anal., 40 (1995) 879-885.
- [5] J. Chwastowska, Chem. Anal., 32 (1987) 643-649.
- [6] K. Brajter, E. Dąbek-Złotorzyńska, Talanta, 27 (1980) 19-24.
- [7] D.K. Singh, M. Srivastava, Talanta 45 (2005) 1-7.

THE USAGE OF AZO-DYES FOR VOLTAMMETRIC DETERMINATION OF Pt (IV)

H. Levytska, O. Kopot, L. Dubenska, O. Shykula
Ivan Franko Lviv National University, Chemistry Faculty, Lviv, Ukraine

Introduction

The determination of Pt trace-levels in the analysis of biological objects, medical preparations and catalysts of chemical industry and motor-car construction becomes more and more actual in the last years. Platinum compounds are used for the specific oncological treatment. The most known platinum complexes that are used in antitumor treatment are cis-complexes. Despite the wide medical usage of platinum complexes, these substances are toxic and they are able to accumulate in the human body [1]. That is why the determination of its remaining content in the biological objects is considered to be a very actual problem, the solving of which requires the use of sensitive, selective and expressive methods. Investigation of Pt(IV) electrochemical activity in the presence of azodies and creation of new analytical forms is supposed to be the most perspective ones.

Experimental

Reagents and Solutions

The Pt(IV) stock solution (1×10^{-2} M) was prepared by dissolving 0.1951g of metallic platinum in 100,0 ml volumetric flask in concentrated HCl та HNO₃ (3:1).

Arsenazo I (ArI) and tropeoline 0 (Tr0) stock solutions (1×10^{-3} M) were prepared by dissolving a precise amount of azodies in bi-distilled water. All reagents were of analytical grade and all the solutions were prepared with bi-distilled water.

The requisite pH solutions were made with acetic and ammonia buffer solutions, solutions of nitric and hydrochloric acids and tris(hydroxy-metyl)-aminomethane (Tris).

Apparatus

All voltammetric curves were obtained on digital voltammetric equipment which combines a personal computer [2] with mercury dropping working electrode (MDE), a saturated calomel reference electrode and a platinum-wire counter electrode using the polarizing range from 0 to -2 V. The soluble oxygen from electrochemical cell was removed with purified argon. The pH-meter model MV 870 DIGITAL-pH-MESSGERÄT was used for the pH measurements.

Results and Discussion

There are disputed literary data about reducing of Pt(IV) ions on the MDE [3-5]. Therefore first of all we investigated voltammetric behaviour of Pt(IV) depending on pH solution and nature of background electrolyte. Peak ($E = -1,2 \div -1,4$ V) observed in the acidic medium against all examined electrolytes is beyond question. The height of this peak decreases with the increase of pH and as a result peak disappears at pH >6.0. In all literature sources it is interpreted as a peak of catalytic hydrogen evolution [3-5].

The character of Pt(IV) reduction within the limit of potential $0 \div -1$ V depends on background electrolyte and acidity of medium. Against the acetic buffer solution (pH 3,5-6,0) reduction of Pt(IV) ions is not observed. Against Tris+HNO₃+NaNO₃ ($\mu=0,2$) at pH>9,0 within the limit of potential $-0,20 \div -0,28$ V one peak appears (Fig.1). The current of this peak increases to pH 11,0 and remains constant to pH 12,5 (Fig.3).

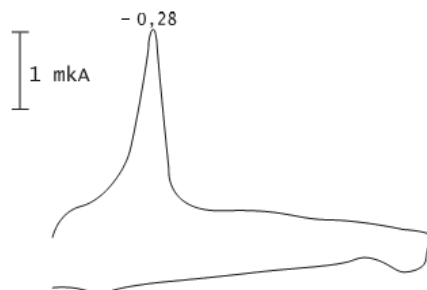


Fig. 1-The voltammogram of Pt(IV) ions $C_{Pt(IV)}=4 \times 10^{-5} M$ on the background of Tris+HNO₃+NaNO₃; $\mu=0,2$; $\nu=0,5$ V/s; pH 11,5; $E_0 = 0V$; $\Delta E = - 1V$.

Under voltammetric investigation of Pt(IV) ions solutions in the wide range of pH (1,2÷9,2) against HCl + NH₄Cl or NH₄OH + NH₄Cl appearance of two peaks P₁ and P₂ at the potential $E_{P1} = -0,35 \div -0,48$ V and $E_{P2} = -0,38 \div -0,49$ V respectively is observed (Fig.2). The height of these peaks practically is independent of medium acidity up to pH 7,0 and decreases sharply within the limit of pH 7,3-9,2 (fig.3).

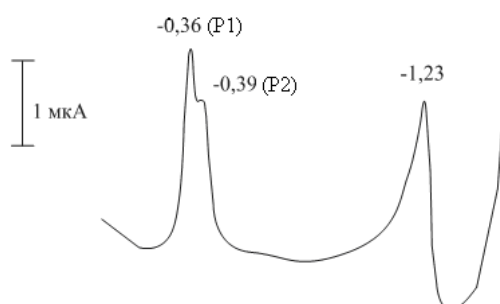


Fig. 2-The voltammogram of Pt(IV) ions $C_{Pt(IV)}=4 \times 10^{-5} M$ on the background of HCl + NH₄Cl; $\mu=1,0$; $\nu=0,5$ V/s; pH 2,5; $E_0 = 0V$; $\Delta E = - 2V$.

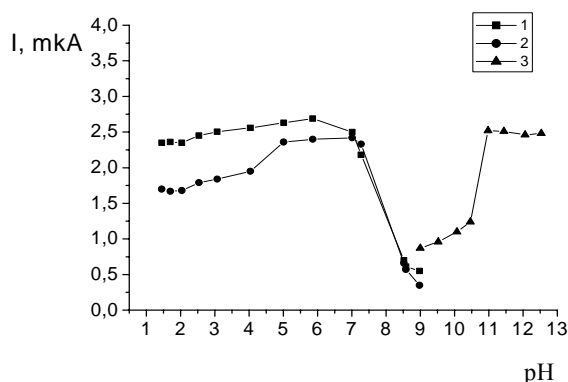


Fig. 3-The current dependence of peaks P₁(1) i P₂(2) on pH against HCl + NH₄Cl and NH₄OH + NH₄Cl and against Tris+HNO₃+NaNO₃ (3); $C_{Pt(IV)}=4 \times 10^{-5} M$; $\nu=0,5$ V/s;

The usage of azodyes allowed to improve analytical characteristic of determination of many metals. In particular TrO was used earlier for successful determination of Pd(II) [6]. Unfortunately, we could not achieve it for Pt(IV), since

Pt(IV)+Tp0 voltammogram is an algebraic sum of individual component voltammograms in the wide range of pH.

ArI is widely used for spectrophotometric and voltammometric determination of a number of metals [7]. Complex compounds of Pt(IV) with ArI are not formed. It is confirmed by absorption spectra. However, on the chloride background in the presence of ArI reduction of free azodye and increase of Pt(IV) peaks is observed in the wide range of pH. But for all that, these peaks increase even at the minor amount of azodye (Fig. 4).

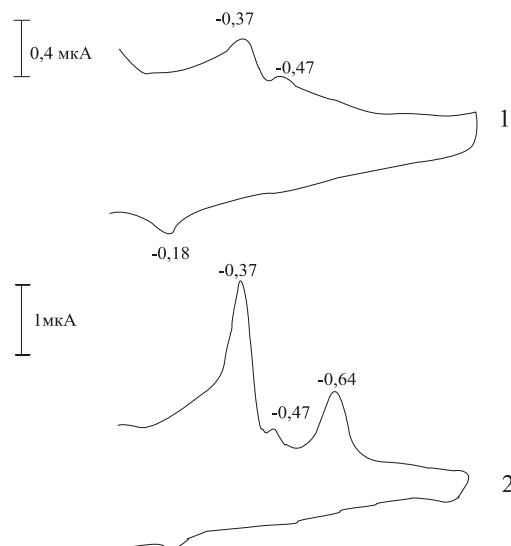


Fig. 4-The voltammogram of Pt(IV) ions in the absence (1) and in the presence (2) of ArI; $C_{Pt(IV)}=1 \times 10^{-4} M$, $C_{ArI}=4 \times 10^{-6} M$; $v=0,5 V/s$; pH 9,5; $E_0 = 0V$; $\Delta E = -1 V$.

The current of peak P1 increases lineary with Pt(IV) concentration over the range $4,0 \times 10^{-6} M$ to $1,2 \times 10^{-4} M$. The linear equation is $I=4,24 \times 10^{-4}-0,01$ with $r=0,9964$. Detection limit was estimated to be $5,8 \times 10^{-6} M$.

It should be noted, that in the absence of azodye at the concentration of platinum $4 \times 10^{-5} M$ and pH 9,5 peaks P1 i P2 are not shown at all.

With the increase of dye concentration up to amount comparable to Pt(IV) ions concentration current increases, then remains constant and at subsequent increase of the concentration of dye decreases (Table 1).

Table 1-The influence of ArI concentration on the current of peaks P₁ i P₂; $C_{Pt(IV)}=4 \times 10^{-5} M$; pH 9,5.

$C_{ArI} \times 10^5, M$	I_{P1}, mA	I_{P2}, mA
0	-	-
0,2	0,55	0,29
0,4	0,90	0,35
1,0	1,41	0,38
2,0	1,76	0,52
4,0	1,72	0,51

To elucidate the nature of Pt(IV) reduction current in the presence of ArI the influence of rate polarizing tension, ionic strength and buffer capacity were studied. The rate criterion was calculated for quantitative estimation the influence (Table 2).

Table 2 –The value of the rate criterion for P₁ and P₂; $v=0,2\div 2,0$ V/s; $\mu=1$.

C _{Pt(IV)} , M	C _{ArI} , M	pH	Peak	lgi/lgv
4×10 ⁻⁵	-	2,0	P ₁	0,60
			P ₂	1,26
	-	3,0	P ₁	0,66
			P ₂	1,28
	-	6,1	P ₁	0,72
			P ₂	1,25
	4×10 ⁻⁶	9,5	P ₁	0,41
			P ₂	1,04
			P ₃	0,72
	4×10 ⁻⁵	9,5	P ₁	0,49
P ₂			1,27	
P ₃			0,81	
1,0×10 ⁻⁴	-	9,5	P ₁	0,29
			P ₂	1,66

The increase of ionic strength causes the peaks P₁ and P₂ shift in the cathode region of potential and increases the current of the peaks. Such dependence is peculiar to kinetic processes. The kinetic nature of the process is also confirmed by the high value of the rate criterion. The surface activity of many organic substances causes some feature of their influence on the electrode processes, *e.g.* noticeable effect of these substances even at the petty concentrations. The height of the reduction peaks of Pt(IV) visibly increases under the adding of ArI even at the concentration in 25 times less. It is, probably, concerned with the presence of unshared pair of electrons (in the N, O, As atoms), which can attach proton. Such protonated substances can react on the cathode by the scheme: $2HB \rightarrow 2B + H_2$, where B – unprotonated molecule of azodye. It is possible, for that reason increase of peaks P₁ and P₂. On the other hand, high surface activity of organic substances result in inhibition of electrochemical processes by the film of adsorbed substance. This inhibition may be caused by the difficulty of depolarizer transmission through the barrier formed by adsorbed substance or the decrease of amount of adsorbed depolarizer as a result of its displacement by particles of the surface active substance [8]. The last effect is typical for electrode kinetic processes with the preceding surface reaction.

The increase of reduction peaks of Pt(IV) in the presence of ArI can be used for voltammetric determination of Pt(IV).

References

- [1] M. Hughes. The Inorganic Chemistry of Biological Processes.-John Wiley & Sons, Ltd., New York, 1981.
- [2] I. Karbovnyck, L. Dubenska, N. Poperechna, Visn. Lviv. Univ., 41 (2002) 125.
- [3] J. Heyrovsky, J. Kuta. Zaklady Polarografie.-Ceskoslov. Akademie Ved., Praha, 1962.
- [4] T. Kryukova, S. Synyakova, T. Aref'eva. Polyarograficheskiy analiz.- M.: Goskhimizdat, 1959.
- [5] Yu. Zolotov, G. Varshal, V. Ivanov. Analiticheskaya khimiya metallov platinovoy gruppy.-M.:KomKniga,2005.
- [6] H. Levytska, S. Tymoshuk, O. Bilyk, Annals, V.3(1) (2004) 326.
- [7] L. Dubenska, H. Levytska, N. Poperechna, Talanta, 54 (2001) 221.
- [8] A. Baranski, J. Dojlido, Z. Galus. Electroanalityczne metody wyznaczenia stałych fizykochemicznych.-PWN, Warszawa, 1979.

NUCLEOPHILIC CLEAVAGE OF CYCLIC SELENENAMIDES

R. Lisiak, J. Palus, J. Młochowski

Institute of Organic Chemistry, Wrocław University of Technology

Wybrzeże Wyspiańskiego 27, 50-370 Wrocław

Introduction

Research into selenoheterocyclic compounds is mainly focused on new ring system synthesis. Only a few works devoted to this problem have been published in last three decades. The most important group of selenoorganic compounds are cyclic selenenamides having Se-N moiety particularly benzenoselenazol-3(2*H*)-ones **1** known as biological response modifiers, reagents, catalysts, photoconducting materials and glutathion peroxidase mimetics [1-4].

There are at least one endocyclic center able to be a target of nucleophilic attack in selenenamides. In case of 1,3,2-benzodiselenazoles **2** these centres are situated on selenium atoms, while in benzenoselenazol-3(2*H*)-ones on selenium and carbonyl carbon atoms. Moreover, side chain can bring an exocyclic function group reactive toward nucleophiles such as carboxyester or amide group.

In this work we reported results of our study on the reactions of hydrolysis and thiolysis of benzenoselenazol-3(2*H*)-ones **1** and their analogues – 1,3,2-benzodiselenazoles **2**. Both hydrolysis and thiolysis proceeds on selenium atom and causes ring opening. Furthermore the side chain groups are unreactive under thiolysis conditions while hydrolysis converts them. Generally, the results depended on used substrate, type of thiol, solvent and pH.

Results and Discussion

Thiolysis of benzenoselenazol-3(2*H*)-ones **1** and 1,3,2-benzodiselenazoles **2**

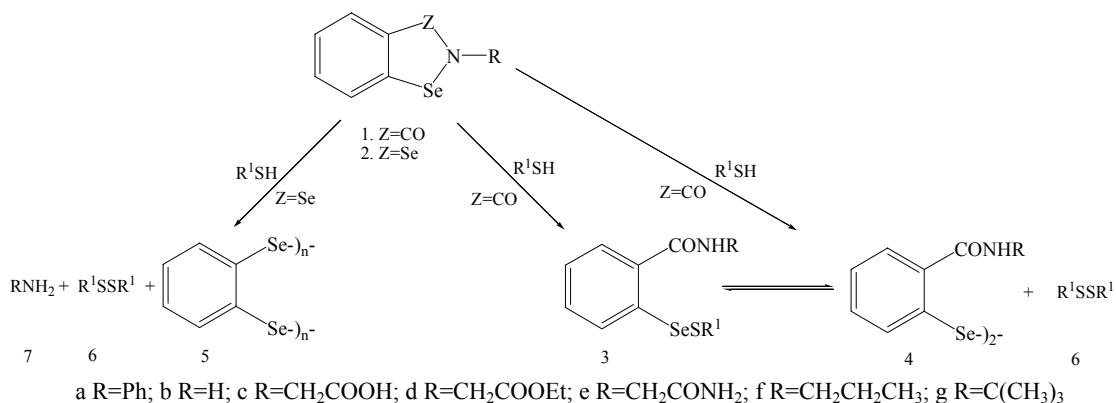
We expected that the products of thiolysis of selenenamides **1** and **2** should be selenosulphides **3** having Se-S moiety, which could undergo further disproportionation to corresponding diselenides **4** and disulphides **6** (Scheme 1).

As the model compounds benzenoselenazol-3(2*H*)-ones having phenyl **1a**, hydrogen **1b** and carboxymethyl group **1c** at nitrogen atom while 1,3,2-benzodiselenazoles having two different substituents at nitrogen: *n*-propyl **2f** and *t*-butyl **2g** were used.

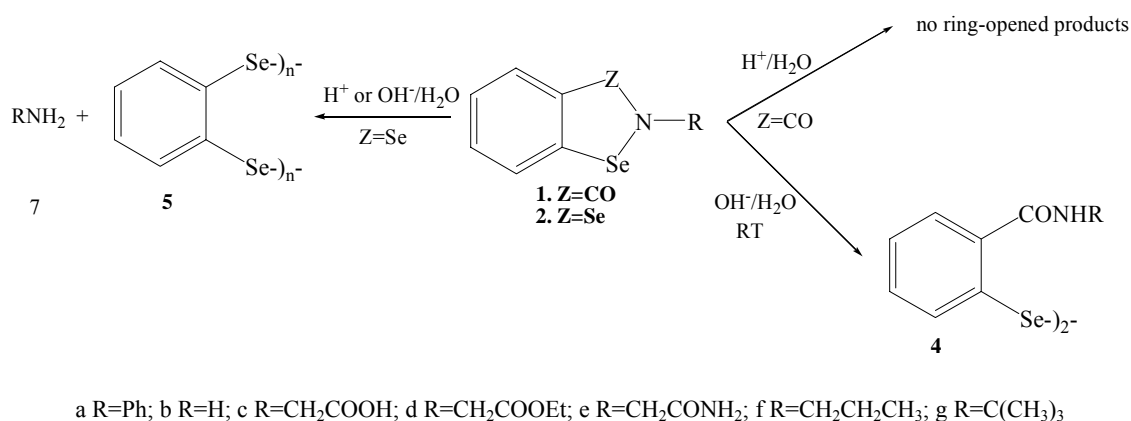
The results of our study on the reaction of compounds **1**, **2** with various thiols depended on selenenamide used, type of thiol and reaction conditions. In the case of reaction **1** with aromatic thiols resulted in formation of stable selenosulphides while aliphatic thiols gave unstable selenosulphides directly converted to diselenides. On the other hand 1,3,2-benzodiselenazoles **2** were converted to polymeric product **5** regardless of thiol, group R or used solvent.

For thiolysis of **1a-c** and **2f-g** commercial available thiols: α -toluenethiol, thiophenol, 2-naphthalenethiol, thioglycolic acid, 2-mercaptoethanol and 1,2-ethanedithiol were used. Our studies were concentrated on the influence of substrate structure and reaction conditions (solvent, pH) on the reaction results.

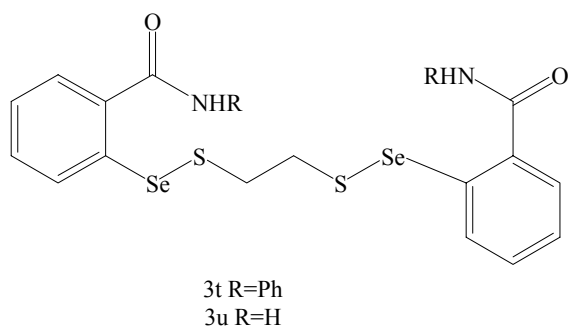
Reactions of **1a-c** with aromatic thiols at 1:1 molar ratio in dichloromethane (room temperature) afforded selenosulphides **3i** – **3q** isolated in 40 – 71% yield.



Scheme 1. Thiolysis of benzisoselenazol-3(2*H*)-ones **1** and 1,3,2-benzodiselenazoles **2**



Scheme 2. Thiolysis of benzisoselenazol-3(2*H*)-ones **1** and 1,3,2-benzodiselenazoles **2**



Scheme 3.

Table. Products of thiolysis **1** and **2**

1 or 2	Substrate		Solvent	Products, yield [%] ^a	
	R	Thiol R ¹		Selenosulphide 3	Diselenide 4 or 5
1a	Ph	PhCH ₂	CH ₂ Cl ₂	3i , 69	-
1a	Ph	PhCH ₂	1,4-dioxane	3i , 54	-
1a	Ph	PhCH ₂	water	3i , 68	-
1b	H	PhCH ₂	CH ₂ Cl ₂	3j , 40	-
1c	CH ₂ COOH	PhCH ₂	CH ₂ Cl ₂	3k , 61	-
1a	Ph	Ph	CH ₂ Cl ₂	3l , 60	-
1b	H	Ph	CH ₂ Cl ₂	3m , 42	-
1c	CH ₂ COOH	Ph	CH ₂ Cl ₂	3n , 68	-
1a	Ph	β-C ₁₀ H ₇	CH ₂ Cl ₂	3o , 66	-
1b	H	β-C ₁₀ H ₇	CH ₂ Cl ₂	3p , 71	-
1c	CH ₂ COOH	β-C ₁₀ H ₇	CH ₂ Cl ₂	3q , 69	-
1a	Ph	CH ₂ COOH	CH ₂ Cl ₂	-	4a , 86
1b	H	CH ₂ COOH	CH ₂ Cl ₂	3r , 40	4b , 57
1b	H	CH ₂ COOH	1,4-dioxane	-	4b , 75
1b	H	CH ₂ COOH	water	-	-
1b	H	CH ₂ COOH	HCl/water	-	4b , trace
1b	H	CH ₂ COOH	NaOH/water	-	4b , 80
1c	CH ₂ COOH	CH ₂ COOH	CH ₂ Cl ₂	-	4c , 70
1a	Ph	CH ₂ CH ₂ OH	CH ₂ Cl ₂	-	4a , 76
1b	H	CH ₂ CH ₂ OH	CH ₂ Cl ₂	-	4b , 81
1c	CH ₂ COOH	CH ₂ CH ₂ OH	CH ₂ Cl ₂	3s , 80	-
1a	Ph	CH ₂ CH ₂ SH	CH ₂ Cl ₂	3t^d , 83	-
1b	H	CH ₂ CH ₂ SH	CH ₂ Cl ₂	3u^d , 67	-
1c	CH ₂ COOH	CH ₂ CH ₂ SH	CH ₂ Cl ₂	-	4c , 75
2g	CH ₂ CH ₂ CH ₃	PhCH ₂ ^b	CH ₂ Cl ₂	-	5^c , 97
2f	C(CH ₃) ₃	PhCH ₂ ^b	CH ₂ Cl ₂	-	5^c , 98

^a isolated yield^b the results the same as for other thiols^c other products: disulphide **6** 70%, amine **7** 64% (as hydrochloride)^d the structures shown at Scheme 3

Most of these products were stable with the exception of **3j**, **3m** and **3p**. The slow decomposition of **3j**, **3m** and **3p** to corresponding diselenides and disulphides was observed after several days storage in refrigerator. Different results were achieved when the aliphatic thiols were used. The thiolysis was carried out under the same conditions as previous one but the major isolated products were diselenides **4a**, **4b** and **4c**. In the case of use **1c** and 2-mercaptoethanol we unexpectedly obtained a stable selenosulphide **3s**. The reaction products **1a** or **1b** with 1,2-ethanedithiol had a structure shown at Scheme 3. Both of them reveal high stability in comparison with **3j**, **3m** and **3p**.

To determine the solvent influence on thiolysis we selected reaction of **1b** with thioglycolic acid because this process in dichloromethane led to mixed products. New reaction was carried out in 1,4-dioxane at 1:1 molar ratio and produced bis[2-(carboxymethylcarbamoyl)phenyl] diselenide **4c** in 75% isolated yield. When this reaction was carried out in water no reaction progress was observed. For comparison, when 1,3,2-benzodiselenazole **2** was treated with α-toluenethiol in 1,4-dioxane and water the results were the same as when dichloromethane was a solvent.

1,2-Benzisoselenazol-3(2*H*)-one **1b** was treated with thioglycolic acid at 1:1 molar ratio in aqueous acidic (hydrochloric acid) or basic medium (sodium hydroxide) and gave bis(2-carbamoylphenyl) diselenide **4b**. In the presence of base the yield of diselenide

lenide was 80% after 1 hour while in the acid condition the product **4b** was formed only in trace amount.

1,3,2-Benzodiselenazoles **2f** and **2g** reacted with mentioned thiols gave poly(bis-1,2-phenylene) diselenide **5** in every reaction conditions. No selenosulphides were detected and isolated. In contrast to thiolysis of benziisoselenazol-3(2*H*)-ones, 1,3,2-benzodiselenazoles gave aside from corresponding diselenide and disulphide also amine **7** (Scheme 1). Alkaline as well as acid medium caused decomposition of **2f-g** to polymeric product **5** before thiol was added.

Hydrolysis of benziisoselenazol-3(2*H*)-ones **1** and 1,3,2-benzodiselenazoles **2**

Selenenamide bond can be cleaved by thiol interaction and hydrolysis as well. There are at least two places susceptible to hydrolysis in benziisoselenazol-3(2*H*)-ones: Se-N and C-N amide bond. We expected that amide group, especially tertiary, is less sensitive to hydrolysis than selenenamide so main products should be diselenides. Alkaline hydrolysis of **1a-f** carried out at room temperature led to corresponding diselenide while both C-N and Se-N bonds remain resistant toward acid hydrolysis. In the case of compounds **1d** and **1e**, where ester or primary amide group was present in side chain, these groups were hydrolysed and gave bis[2-(carboxymethylcarbomoyl)phenyl] diselenide **4c** in alkaline medium and N-carboxymethyl-1,2-benziisoselenazol-3(2*H*)-one **1c** in acid medium (Scheme 2).

In contrast to 1,2-benziisoselenazol-3(2*H*)-ones, 1,3,2-benzodiselenazoles were sensitive to acid. Both **2f** and **2g** were smoothly decomposed by diluted HCl to poly(bis-1,2-phenylene) diselenide **5** and amine (or its hydrochloride) with quantitative yield. Similar effect of the addition **2** to aqueous sodium hydroxide was observed.

Conclusions

Our study confirm covalent interaction of benziisoselenazol-3(2*H*)-ones and their analogues with thiols and potentially with thiol groups of peptides (e.g. glutathione), enzymes etc. It can be reason of biological activity of compounds having Se-N moiety. The results of thiolysis were depended on used selenenamide, type of thiol and reaction conditions.

Selenenamide bond is susceptible to alkaline hydrolysis and corresponding diselenides are the only products. Moreover 1,3,2-benzodiselenazoles can be hydrolysed by acids. Probably it results from low stability of examined 1,3,2-benzodiselenazoles.

This work was supported by Ministry of Education and Science (Grant PBZ-Min-015/P05/2004).

References

- [1] Młochowski, J., Kloc, K., Lisiak, R., Potaczek, P., Wójtowicz, H., *Arkivoc*, (vi), **2007**, 14-46
- [2] Kobayashi, H., Cui, H., Kobayashi, A., *Chem. Rev.*, 104, **2004**, 5265-5288
- [3] Młochowski, J., Brząszcz, M., Giurg, M., Palus, J., Wójtowicz, H., *Eur. J. Org. Chem.*, 22, **2003**, 4329-4339
- [4] Muges, G., du Mont, W.-W., Sies, H., *Chem. Rev.*, 101, **2001**, 2125-2179

SiO₂–TiO₂ THIN FILMS OBTAINED BY THE SOL-GEL METHOD

A. Łukowiak¹, R. Dylewicz², S. Lis², A. Baszczuk³, S. Patela²,
K. Maruszewski^{1,4,*}

¹ *Institute of Materials Science and Applied Mechanics, Wrocław University of Technology, Smoluchowskiego 25, 50-370 Wrocław, Poland*

² *Faculty of Microsystem Electronics and Photonics, Wrocław University of Technology, Janiszewskiego 11/17, 50-372 Wrocław, Poland*

³ *Institute of Low Temperature and Structure Research, Polish Academy of Sciences, Okólna 2, 50-950 Wrocław, Poland*

⁴ *Electrotechnical Institute, Skłodowskiej-Curie 55/61, 50-369 Wrocław, Poland*

* *Corresponding author, e-mail: krzysztof.maruszewski@pwr.wroc.pl*

Abstract

The hybrid silica-titania thin films, with different titania content, were prepared using the sol-gel technique. Their optical properties are presented. Thickness, refractive index and transmission spectra of the film have been measured. The titania precursor was used to increase the refractive index of the material. The more titania precursor for the synthesis has been used, the thinner layer with higher RI has been obtained. The SiO₂–TiO₂ matrix is porous and the dyes' molecules entrapped in it can interact with the surrounding media. Therefore, these thin films can be used as optical sensors. The sol-gel-derived layer has been doped with bromocresol green. The changes in absorption spectrum with increasing pH has been registered.

Keywords: silica-titania thin film, sol-gel method, optical sensor, bromocresol green

1. Introduction

The sol-gel technology allows to prepare glasses and glass-like materials that can be doped with organic compounds. It is very easy to prepare thin films using this method. They are characterized by good thermal and mechanical stabilities, porosity, high surface area, and good optical quality. Such films deposited on silicon substrates can be applied as planar or strip waveguides. Waveguides can be obtained using, for instance, silica-titania hybrids [1]. Control of the refractive index and film thickness is possible by changing starting precursors, solvents and temperature of thermal treatment. Waveguides doped with organic molecules can be used as optical sensors. Some of their applications are pH [2] or humidity sensing [3] and estimating isopropyl alcohol in water [4]. In this work, hybrid silica-titania thin films have been obtained via sol-gel technique. The optical properties of the films before and after thermal treatment are described. The layer was used as a matrix for immobilization of bromocresol green molecules. The changes of absorption spectra with increasing pH are shown.

2. Experimental

The silica (tetraethoxysilane, TEOS) and titania (titanium(IV) n-butoxide, TNBT and titanium(IV) isopropoxide, TIPO) precursors were obtained from Alfa Aesar. All other compounds were purchased from POCH SA. TEOS was mixed with proper amount of alcohol and hydrochloric acid [5] with the molar ratio of 1:8:0.05 for TEOS:ethanol:HCl. The compounds have been stirred on the magnetic stirrer for 30 minutes. Simultaneously, TNBT (or TIPO) was also mixed with alcohols (1:20:20:0.15

for TIPO:ethanol:isopropanol:HCl) [6] but this stage was shorter because of the higher hydrolysis rate of titania precursor [7]. Next, both solution was mixed together and the stirring was continued for one hour. The molar ratio of TEOS to TNBT/TIPO was 3:1, 2:1 or 1:1. The sol was aged for about 20 hours at room temperature. The SiO₂-TiO₂ films were deposited on microscopic glass slides (for transmittance measurements) and silicon wafers with a silica layer (for RI measurements) [5] by a modified dip-coating method [8]. The plates were dried in the air at 60°C or heat-treated in 500°C for one hour. Thin film doped with bromocresol green was also prepared. The dye was added to the sol obtained as previously described and mixed. The film was coated on the glass after a few hours and dried at 60°C to avoid the decomposition of organic dye.

The absorption spectra were recorded using a Varian Cary 2300 spectrophotometer. X-ray powder diffraction diagrams were recorded with Stoe diffractometer equipped with a position sensitive detector (Cu K α radiation). The thicknesses and the refractive indexes of the films were measured at 632.8 nm wavelength ellipsometry.

3. Results and discussion

The sol-gel method was used to prepare transparent silica-titania thin films without cracks. They have good transmission properties in the visible range of the radiation. Figure 1 shows the absorption spectra of the films prepared with different titania content (with the SiO₂ to TiO₂ (TNBT) molar ratios of 3:1, 2:1 or 1:1). For the samples with more titania content, an absorption band with maximum at about 580 or 550 nm can be well seen. The best transmission (from 330 nm) has film with molar ratio of 3:1 after heat treatment. Other plates have higher absorbance after annealing, especially at higher wavelengths. All layers that were only dried at 60°C, have transmittance above 90%. Matrix with low titania content was chosen as material for optical sensors.



Fig. 1. Transmission spectra of thin films dried at 60°C or heat-treated at 500°C.

Sol-gel technology is relatively new method for fabricating passive devices for integrated optics purposes i.e. planar and strip waveguides. Propagation of a laser light in a waveguide can occur only when waveguiding layer has higher refractive index than adjacent layers (optical substrate and optical cladding), where also sufficient thickness for at least one optical mode excitement is needed. Defects in a waveguide structure can disturb the guided mode of light. Imperfections such as porosity, cracks, grain boundaries in polycrystalline film, refractive index inhomogeneity, or surface roughness can scatter light and promote optical losses. However, sol-gel technique allows

achieving good quality films and therefore inexpensive and alternative method for preparing planar waveguides for integrated optics is available [9, 10]. Possibility of fabricating high refractive index glass at low process temperatures as well as feasibility of doping it with almost every material are another advantages of sol-gel technique. Tailoring of refractive index of sol-gel planar waveguide at desirable value is important for passive integrated optics. Since refractive index for silicon dioxide SiO_2 is $n = 1.46$ and for titanium dioxide TiO_2 is $n = 2.7$ (both values given for a laser light wavelength of 632.8 nm) the composition of these two compounds allows to obtain material with refractive index in range from 1.46 to 2.7.

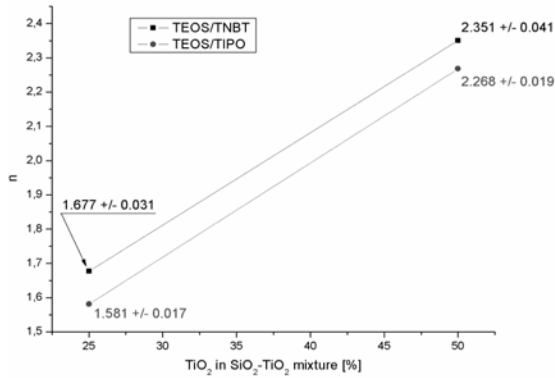


Fig. 2. Refractive index variation of sol-gel layers prepared with TEOS/TNBT and TEOS/TIPO precursors and annealed at 600°C.

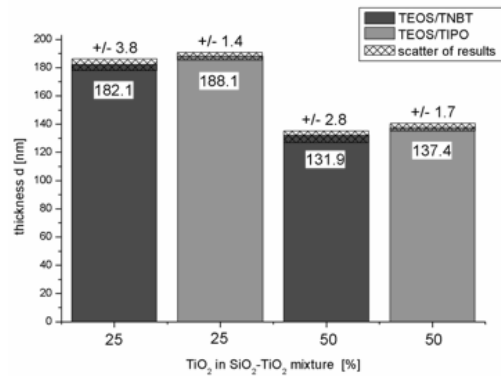


Fig. 3. Measured thickness of sol-gel layers prepared with two different precursors.

Figure 2 shows dependence of refractive index on the quantity of TiO_2 in final SiO_2 - TiO_2 sol-gel layer. Square points represent layers fabricated by TEOS and TNBT precursors. Round points correspond to films prepared by TEOS and TIPO precursors. As can be seen, the refractive index for mixture 50% TiO_2 -50% SiO_2 is clearly higher than for mixture 25% TiO_2 -75% SiO_2 , which is $n=2.35$ and $n=1.67$, respectively. In Figure 3, thickness of four different layers fabricated by different composition of silica to titania in SiO_2 - TiO_2 mixture are presented. The scatter of the results is low, with average value of 2.4 nm, therefore very accurate thickness results were obtained.

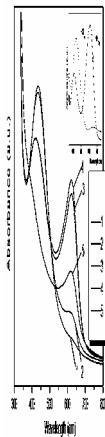


Fig. 4. Absorption spectra of SiO_2 - TiO_2 film after immersing in water solution with different pH. The insert shows the spectra after exposition to gaseous ammonia and hydrochloric acid.

Low deviation of results and high homogeneity of layer thickness was achieved. Despite constant velocity during the withdrawing of layers, thin films which consist of 25% TiO_2 in SiO_2 - TiO_2 mixture have higher thickness than 50% TiO_2 and 50% SiO_2

layers possibly due to lower flow resistant for titania precursors. When precursors were mixed in ratio of 3:1, the thickness was about 185 nm and when the ratio was set as 1:1, thickness was about 134 nm.

The doping of SiO₂-TiO₂ film (with the molar ratio for TEOS:TNBT of 3:1) with bromocresol green resulted in yellow and transparent layer. Its colour changed to blue when the film was immersed in water solution with pH>5. Figure 4 shows that in this case, one absorption band at 435 nm decreases and other band at 620 nm appears. This behavior was also observed when the plate was hold in gaseous ammonia. The changes were fully reversible after exposition to gaseous hydrochloric acid (see insert in Fig. 4). When the plate was placed in the basic solutions (pH>9), the sol-gel matrix started to decompose, the dye was washed and the absorption intensity of the film decreased (line 5 in Fig. 4).

4. Conclusions

The sol-gel method was used to obtain silica-titania thin films with good optical and mechanical properties. The layers have high transmittance in the visible region of the radiation. The addition of titania causes the increase of the refractive index (e.g. 2.35 for film with 50% TiO₂ and 50% SiO₂) thus this material could be used as planar waveguide. The refractive index and thickness of the film depend on the TiO₂ content. Samples with lower silica to titania molar ratio have higher refractive index and are thinner. The film prepared from tetraethoxysilane and titanium n-butoxide can be successfully used as a matrix for molecules of organic dye (bromocresol green). The dye can still change colour with increasing/decreasing pH, even though it is embedded in the sol-gel film. Waveguide obtained by the sol-gel process with molecules of pH indicator entrapped in the SiO₂-TiO₂ matrix could be used as an optical sensor.

Acknowledgements

The authors wish to thank Mrs. T. Morawska-Kowal for absorption measurements and Ministry of Science and Higher Education for financial support of this work (grant No. KBN3T09B04428).

Literature

- [1] G.C. Righini, S. Pelli, *J. Sol-Gel Sci. Technol.*, 8 (1997) 991.
- [2] Y. Kowada, T. Ozeki, T. Minami, *J. Sol-Gel Sci. Technol.*, 33 (2005) 175.
- [3] A. Alvarez-Herrero, G. Ramos, F. del Monte, E. Bernabeu, D. Levy, *Thin Solid Films*, 455-456 (2004) 356.
- [4] P.J. Skrdla, S.B. Mendes, N.R. Armstrong, S.S. Saavedra, *J. Sol-Gel Sci. Technol.*, 24 (2004) 167.
- [5] A. Lukowiak, R. Dylewicz, S. Patela, W. Strek, K. Maruszewski, *Opt. Mater.*, 27 (2005) 1501.
- [6] P. Falaras, A.P. Xagas, *J. Mater. Sci.*, 37 (2002) 3855.
- [7] R.N. Viswanath, A. Chandra Bose, S. Ramasamy, *J. Phys. Chem. Solids*, 62 (2001) 1991.
- [8] H. Dislich, *Thin films from the sol-gel process in: Sol-Gel Technology for Thin Films, Fibers, Performs, Electronics, and Specialty Shapes*, L.C. Klein (ed), Noyes Publications, Park Ridge, New Jersey.
- [9] P. Coudraya, P. Etienneb, Y. Moreaua, *Mater. Sci. Semicon. Proc.*, 3 (2000) 331.
- [10] C. Urlacher, C. Marco De Lucas and J. Mugnier, *Synthetic Metals* 90 (1997) 199.

FIELD TRIPS AS A WAY OF WORKING WITH A CLASS WITH AN EXTENDED CHEMISTRY AND BIOLOGY SYLLABUS

Iwona Maciejowska^{1,2}

¹ *V LO w Krakowie (5th Upper Secondary School)*

² *Department of Chemical Education, Jagiellonian University, Krakow, Poland*

Secondary school students in classes with an extended Chemistry and Biology syllabus usually intend to follow a career in one of the branches of Medicine (Medicine, Dentistry, Pharmacy etc.) or Natural Sciences (Biology and Biotechnology, Chemistry, Environmental Protection, Environmental Sciences etc.). Chemistry and Biology teachers conducting such classes (who in Poland usually also act as the class tutor) must therefore ask themselves two key questions:

1. Will the students pass the '*matura*' graduation exam (final exam) and qualify for a place in higher education?
2. Do the students realise what kind of work their chosen career involves?

To get a positive answer to these two questions they must on the one hand teach the material in the syllabus and try to develop the students' interest and skills by involving them in extra activities, and on the other inform the students of the advantages and disadvantages of the professions they would like to enter after completing their studies (with the help of a careers consultant/advisor).

The 5th Upper Secondary School in Kraków (V LO) tries to promote the students' development by encouraging them to get involved in the school Chemistry or Biology club, attend lessons at Jagiellonian University's workshops (organised by the Kraków Young People's Society of Friends of Arts and Sciences – *Krakowskie Młodzieżowe Towarzystwo Przyjaciół Nauk i Sztuk*), workshops for Chemistry Olympiad future participants [1], lectures organised by the school given by academic staff from Jagiellonian University e.g. "Bread from Air" by Dr. hab. Andrzej Kotarba, or lectures by foreign academics such as that given by Dr. John Oversby (University of Reading, UK) etc. It also tries to stimulate the students' interest and motivation by organising week-long field trips (science camp), usually for students of the second year of that school (aged 18).

Organising trips for young people interested in a particular subject is by no means a new idea. This form of education is used to great effect by Petnica Science Center [2] for example. In Poland, as far as the author knows, only non-governmental organisations organise or have organised activities of this kind. For example, for many years the Polish Scouting and Guiding Association has organised science field trips (lasting 3 weeks) some of them Chemistry-related [3].

School field trips are organised by teaching staff and mainly financed by parents, which was also the case for the field trip described below.

The theme of this year's field trip to Zakopane (south part of Poland, Tatra Mountains) for class IIh of the 5th LO was Ecology and Environmental Protection. The program guidelines (aims) for the field trip included delivery of educational content contained in the syllabus for Chemistry, Biology as well as an interdisciplinary Ecology course (so called 'environmental pathway'); development of key skills such as groupwork, critical thinking, problem solving, decision-making, finding and processing information; and improvement of the image of Chemistry among students preferring Biology by showing them how it benefits people and the environment. Through the acquisition of critical thinking and skills of thoughtful decision-making students can develop active and responsible citizenship [4]. Education for citizenship requires awareness of the complexity derived from the relationships between science, technology, environment and society.

A location for the field trip was selected which would be relevant to the subject of the lessons and the trip's aims. The teaching program was structured in such a way as to prepare the students to take part in an educational game (role play game) held on the last day of the trip entitled: "A Sitting of the Commune Council of Zakopane". The game was structured in two parts. In the first part, students were given and shared a role-card, which outlines background and interests of a character they have to represent. They looked for the arguments to support their characters' point of view. A second group – the decision-makers – had to gather information about the controversial aspects of the issue and prepared the questions to the presenters. The final stage of the game involved creating an imaginary commune council and asking it to consider an application for building permission and establish building criteria for a new hotel, restaurant and sports complex on Droga do Białego St. in the periphery of Tatra National Park [5]. The debate ended with a verdict expressed by the decision-makers.

Suggested roles for participants in the open sitting of the Commune Council are:

- Mayor
- Director of the Department of Environmental Protection of the Municipal Council,
- the investor,
- a farmer,
- a forester, a representative of Tatra National Park,
- a local mountain guide,
- a resident of Droga do Białego St.,
- a shop owner,
- a doctor,
- an unemployed person,
- a representative of the Employment Office etc.

Necessary information was collected during field trip activities, which included:

a) theoretical background:

- review of multimedia presentations on water, air and soil protection and species preservation which the students had prepared at home,
- discussion of basic Ecology topics: population attributes, biocenosis profile, structure of the ecosystem, environmental laws, Biogeography,

– a viewing of the film “Quicksilver – Mercury” which concerns the toxicity of mercury, long term effect of pollution - Minamata Disease etc.

b) local conditions:

– a walk to Dolina Białego valley to survey the planned location for the project (investment),

– a visit to a biological sewage treatment plant (run by the SEWiK water and sewage company) to find out about sewage treatment methods and the potential (limitations) of the sewage treatment plant,

– a meeting with Krzysztof Owczarek, the Vice-mayor of Zakopane who is responsible for municipal utilities and the Head of the Department of Environmental Protection of the Municipal Council,

– a visit to the Tatra National Park Museum (to find out about the history of conservation in the Tatra Mountains and the surrounding area) and the Tatra Museum (to find out about the natural features of the land and the life and work of the local inhabitants),

– presentation of an alternative source of heating energy based on the example of Geotermia Podhalańska (an geothermal energy company).

Even the daylong excursion into the mountains (Dolina Pięciu Stawów Polskich – 1665m above sea level) had an educational purpose: not only was it intended to integrate the group and bring variety to the field trip by introducing a new kind of activity, but also to show the students the natural beauty of this potentially threatened environment and teach them about the regulations of the Tatra National Park.

Role-playing games on social-environmental controversial issues [6] propose a multidisciplinary approach to real problems. Participants of final discussion were asked to engage in a co-operative search for solutions, by exploring common needs and possible future scenarios.

Zakopane also provided us with the opportunity to investigate other topics from the school syllabus e.g. those related to the d-block elements, which the class had recently covered in their lessons. There was iron smelting and working, which has been practiced in Kuźnice near Zakopane since the XVIIIth century (its name is derived from 'kuźnia', the Polish word for forge), as well as in other parts of the Tatra Mountains and its surrounding areas e.g. Dolina Chochołowska valley. The history of these places and the working conditions of local inhabitants were illustrated by pictures and authentic exhibits in the Tatra Museum and in the Museum of Blacksmithery in the Krupówki pedestrian zone.

Another important element of field trips is usually research work. Although on this occasion it was not possible to conduct research for organisational reasons, the field trip staff, which included the biologist Ms Elżbieta Opozda-Zuchmańska, suggests that it should include:

- testing of the cleanliness of the air using lichen scale mapping,
- testing of the cleanliness of surface waters using biological indicators,
- chemical analysis of water, soil and vegetation.

Amateur environmental analysis has been growing in popularity in Poland since the 1990s and is already supported by a considerable body of reference material [7].

As part of our attempts to answer second key question (Do the students realise what kind of work their chosen career involves?) the students attended a talk given by the extraordinary Dr. Halszka Kostrzewa of the local casualty unit (Medical Emergency Service) on the realities of studying medicine and the work of a doctor. Dr. Kostrzewa spoke about responsibility, mental resilience, empathy, the complexities of running a health service in a new economic environment, and various areas of the medical profession and the demands they place on trainee medical professionals who would like to specialise in them. She also took the time to answer the students' many questions. As a result of this meeting a number of students were able to make preliminary choices regarding the areas they would like to specialise in, two of them choosing Immunology and three Pathology (stating fear of direct contact with patients and responsibility as the reason for their choice).

The above mentioned way of organization of science camp allowed us to use in our teaching and learning process such relation described in literature that: the more

- interfaces between various topics in one subject,
- interfaces between various subjects,
- references to students everyday life,

the better results will be achieved by students.

References

- [1] A.Reizer, K.Łopata, XLVII Zjazd PTChem i SITPChem Wrocław 2004, Materiały Zjazdowe, p. 1129.
- [2] WWW.psc.ac.yu; I.Maciejowska, N.Jevtic, Lj.Peric, M.Todorovic, V.D.Krsmanovic, , IV Yugoslav Symposium Chemistry and Environment Zrenjanin 2001 Proceedings, p. 452-454.
- [3] P.Górka, S.Kowalski, Zbiórka harcerska z ... chemią, HOW, Kraków 1987, I.Maciejowska, Zjazd PTChem i SITPChem, Toruń 1993, S10 P8; I. Maciejowska, Nietoperz, Poradnik metodyczny dla nauczycieli i instruktorów, Kraków 2001
- [4] J.Solomon, Teaching Science, Technology and Society, Milton Keynes Open University Press, 1996
- [5] I.Maciejowska: Jak uczniów klas humanistycznych można zainteresować chemią, Chemia w Szkole, 3 (2004) p. 23-27.
- [6] E. Camino, C. Calcagno, An interactive methodology for 'empowering' students to deal with controversial environmental problems. Env. Educ. Res., 1 (1995), p. 59-74.
- [7] M. Hafner, Ochrona Środowiska. Księga eko-testów do pracy w szkole i w domu, Polski Klub Ekologiczny, Kraków 1993; K. Łopata, Chemia a środowisko. Zbiór ciekawych doświadczeń, WSiP, Warszawa 1994; K. Łopata, I. Maciejowska, , Chemia w szkole, 5 (1994), p. 32 - 36

ENZYME-CATALYZED RESOLUTION OF 2,3-*O*-CYCLOHEXYLIDENE-1-PROPANOL

Maciej Maciejewski*, Janina Ewa Kamińska
*Institute of General Food Chemistry, Technical University of Łódź,
ul. Stefanowskiego 4/10, 90-924 Łódź*

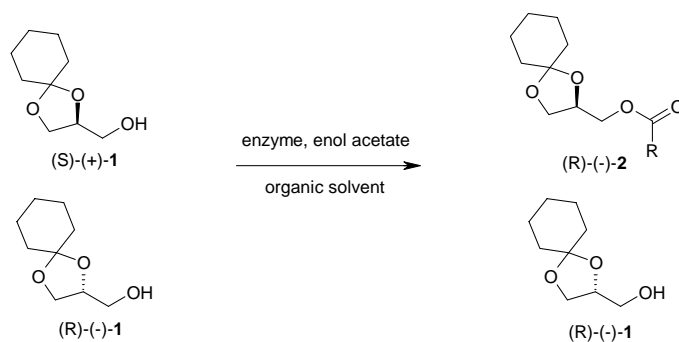
Abstract: The enzyme-catalyzed acetylation of *rac*-2,3-*O*-cyclohexylidene-1-propanol with enol acetates has been studied as a possible route to racemate resolution. We have found high enantioselectivities ($E \sim 200$) for some enzymes but only at low substrate conversion (2-4%). The best enantioselectivities compatible with good activity were found for non-commercial *Mucor racemosus* and *Mucor circinelloides* lipases (5.4 and 3.5 respectively).

Introduction

Glycerol derivatives containing hydroxyl group at C-2 are important substructures in many biologically active compounds and pharmaceuticals [1]. The majority of β -blockers with 3-aryloxy-2-propanol-1-amine structure consist the outstanding example. Chiral glycerol derivatives are regarded as convenient substrates for many syntheses [2]. Such building blocks are still rather expensive since their manufacturing requires chiral catalysts or enantiomerically pure starting materials [3-5]. Thus in recent years increasing interest in biotransformations as a method for pure enantiomers preparation is observed [6-9]. Numerous publications have appeared on resolution of racemic 2,3-*O*-substituted-1-propanols, especially 2,3-*O*-isopropylidene-1-propanol (solketal) [9-15] while 2,3-*O*-cyclohexylidene-1-propanol was investigated incidentally and low enantioselectivities were reported [16-19]. Here we describe our results on enzyme-catalyzed acetylation of 2,3-*O*-cyclohexylidene-1-propanol with enol acetates.

Results

We have studied enzyme-catalyzed acetylation of the substrate **1** in organic solvents with the aim of enantiomers resolution. Broad range of commercial, native and immobilized lipases, non-commercial *Mucor* species as well as acylase and proteinase were included in preliminary screening. Reactions were carried out in hydrophobic solvents – hexane, methylene chloride and *tert*-butyl methyl ether with vinyl acetate as acyl donor. All enzymes tested were found active and showed the same preference for faster acylation of (S)-enantiomer (see Scheme 1).



Scheme 1

However the reaction rate varied considerably with the solvent – the highest substrate conversion was observed in *tert*-butyl methyl ether and hexane while in methylene chloride only immobilized lipases retained high activity (see Table1). Unfortunately the high activity of these enzymes is connected with lack of enantioselectivity ($E \sim 1$).

Table 1. Activity and selectivity of enzymes with vinyl acetate as acyl donor.

Enzyme	Hexane, 40°C			CH ₂ Cl ₂ , 20°C			t-BuOMe, 20°C		
	c	ee _p	E	c	ee _p	E	c	ee _p	E
Lipase A	0.19	0.02	1.1	0.02	0.73	7	0.04	0.46	2.8
Lipase AY	0.41	0.13	1.4	-	-	-	-	-	-
Lipase PS	-	-	-	0.01	0.99	201	0.02	0.66	5.1
<i>Candida cylindracea</i> Lipase	0.51	0.14	1.5	0.03	0.60	4	0.16	0.24	1.7
<i>Candida rugosa</i> Lipase	0.33	0.15	1.4	0.02	0.79	9	0.06	0.31	1.9
Porcine Pancreatic Lipase	0.09	0.21	1.6	0.02	0.89	18	0.12	0.27	1.8
<i>Mucor circinelloides</i> Lipase	0.41	0.30	2.2	0.03	0.88	16	0.17	0.53	3.5
<i>Mucor racemosus</i> Lipase	0.10	0.54	3.5	0.03	0.83	11	0.08	0.28	1.8
Lipozyme RM [®]	0.99	0	1	0.34	0.26	2	0.73	0.09	1.4
Lipozyme TL [®]	0.99	0	1	-	-	-	-	-	-
Novozyme 435 [®]	-	-	-	1	0	1	0.63	0.03	1.1
Acylase	0.11	0.22	1.6	0.03	0.68	5	0.05	0.45	2.7
Papain	0.02	0.99	202	-	-	-	-	-	-

Enantioselectivity ratio ca. 200 was found for lipase PS in methylene chloride and for papain in hexane but only at very low conversion 1-2%.

Improvement of enantioselectivity in enzyme-catalyzed acetylation was frequently noted when vinyl acetate was replaced by more sterically hindered isopropenyl acetate as acyl donor [20]. In our case when substrate **1** was treated with isopropenyl acetate in hexane large decrease of activity (lower conversion) has been observed without significant change of enantioselectivity (see Table 2).

Table 2. Activity and selectivity of enzymes with isopropenyl acetate as acyl donor.

Enzyme	Hexane, 40°C			CH ₂ Cl ₂ , 40°C		
	c	ee _p	E	c	ee _p	E
Lipase A	0.04	0.39	2.3	0.02	0.94	24
Lipase AY	0.12	0.31	2.0	-	-	-
Lipase PS	-	-	-	0.02	0.99	202
<i>Candida cylindracea</i> Lipase	0.40	0.19	1.6	0.02	0.94	33
<i>Candida rugosa</i> Lipase	0.41	0.19	1.7	0.02	0.93	28
Porcine Pancreatic Lipase	0.02	0.99	203	0.03	0.99	205
<i>Mucor circinelloides</i> Lipase	0.23	0.26	1.8	0.03	0.65	4.8
<i>Mucor racemosus</i> Lipase	0.05	0.53	3.3	0.02	0.99	202
Lipozyme RM [®]	0.07	0.32	2.0	0.02	0.91	22
Lipozyme TL [®]	0.15	0.38	2.4	-	-	-
Novozyme 435 [®]	0.98	0.01	1.3	0.06	0.09	1.2
Acylase	0.05	0.45	2.6	0.02	0.92	25

On the other hand in methylene chloride decrease of conversion was not significant while increase in enantioselectivity could be observed. It is noteworthy that in the preliminary screening the best enantioselectivities compared with good activities were found for non-commercial lipases from *Mucor racemosus* and *Mucor circinelloides* used as whole mycelium.

Table 3. Solvent dependence of activity and selectivity of *Mucor* lipases.

Solvent	<i>M. racemosus</i>			<i>M. circinelloides</i>		
	c	ee _p	E	c	ee _p	E
Cyclohexane	0.13	0.50	3.2	0.27	0.40	2.7
Benzene	0.12	0.49	3.1	0.13	0.53	3.5
Toluene	0.19	0.35	2.2	0.38	0.28	2.1
Methylene chloride	0.10	0.36	2.2	0.15	0.47	3
Chloroform	0.08	0.54	3.5	0.22	0.47	3.1
1,2-Dichloroethane	0.10	0.44	2.7	0.004	0.99	200
Tetrahydrofuran	0.08	0.67	5.4	0.24	0.36	2.4
Ethyl acetate	0.23	0.35	2.3	0.32	0.31	2.2
Acetone	0.07	0.53	3.4	0.20	0.37	2.4
Acetonitrile	0.05	0.49	3	0.11	0.33	2.1

Therefore the activity and selectivity of these two lipases in acylation with vinyl acetate were determined for range of solvents varying in polarity and water miscibility (see Table 3). The best enantioselectivity compatible with good activity for *Mucor racemosus* was observed in tetrahydrofuran (E=5.4) while for *Mucor circinelloides* in benzene (E=3.5).

Conclusions

The results obtained in present study do not allow for preparative resolution of *rac*-2,3-*O*-cyclohexylidene-1-propanol. We are of the opinion that non-commercial lipases from *M. racemosus* and *M. circinelloides* are good candidates for search of enantioselectivity improvement by decreasing reaction temperature, changing the acyl donor or usage of chiral solvents. Nevertheless looking for new enzymes seems to be also necessary.

Materials and methods

Acylase, Lipase A, Lipase AY, Lipase PS were obtained from Amano, *Candida Cylindracea*, *Candida Rugosa*, Porcine Pancreas Lipases from Sigma, immobilized preparations Lipozyme RM[®] (*Rhizomucor miehei*), Lipozyme TL[®] (*Thermomyces lanuginosus*), Novozyme 435[®] (*Candida antarctica*) from Novozymes, and papain from Fluka. *Mucor racemosus* and *Mucor circinelloides* lipases (whole mycelium) were kindly donated by Prof. T. Antczak from Institute of Technical Biochemistry (Technical University of Łódź). *Rac*-2,3-*O*-cyclohexylidene-1-propanol (**1**) and its acetate (**2**) were prepared in our laboratory according to the following procedures.

Rac-2,3-*O*-cyclohexylidene-1-propanol (**1**): Glycerol (0.48 mol), cyclohexanone (0.4 mol), 100 mL toluene and a few drops of H₃PO₄ were refluxed under Dean-Stark apparatus for 6 hours. Then the mixture was poured into 100 mL of 5% aq. Na₂CO₃. The water layer was extracted with toluene, combined extracts washed with water and dried over MgSO₄. After solvent evaporation the crude product was distilled under reduced pressure (b.p. 100°C/1.5 Tr, n_D²⁰=1.4810, 70% yield). ¹H-NMR (250 MHz, CDCl₃), δ: 4.23 (ddt, J=6.4Hz, J=5.3Hz, J=4Hz, 1H); 4.03 (dd, J=8.2Hz, J=6.5Hz, 1H); 3.77 (dd, J=8.1Hz, J=6.4Hz, 1H); 3.72 (dd, J=11.6Hz, J=3.8Hz, 1H); 3.58 (dd, J=11.6Hz, J=5.2Hz, 1H); 2.42 (s, 1H); 1.65-1.54 (m, 8H); 1.49-1.36 (m, 2H). IR (film): 3450, 2950, 1460, 1370, 1120, 1070 cm⁻¹.

Rac-2,3-*O*-cyclohexylidene-1-propyl acetate (**2**): Acetic anhydride (0.036 mol) was added to the stirred solution of **1** (0.03 mol) and pyridine (0.042 mol) in 20 mL of dry methylene chloride at room temp. After 24 h the mixture was treated with 100 mL of 5% aq. NaHSO₄, and extracted with methylene chloride, washed with water and dried over MgSO₄. Then the solvent was evaporated and the crude product was distilled under

reduced pressure (b.p. 85°C/0.9 Tr, $n_D^{20}=1.4634$, 70% yield). $^1\text{H-NMR}$ (250 MHz, CDCl_3), δ : 4.34, 4.29 (2t, $J=6\text{Hz}$, 1H); 4.18-4.07 (m, 2H); 4.07 (dd, $J=8.4\text{Hz}$, $J=6.5\text{Hz}$); 3.74 (dd, $J=8.4\text{Hz}$, $J=6\text{Hz}$, 1H); 2.09 (s, 3H); 1.63-1.52 (m, 8H); 1.47-1.32 (m, 2H); IR (CHCl_3): 3000, 1760, 1380, 1240, 1110, 1050 cm^{-1} .

$^1\text{H-NMR}$ spectra were recorded on Bruker DPX 250 spectrometer and IR spectra on Shimadzu IR 408 apparatus.

Enzyme-catalyzed reactions were carried out as follows: to 1.5 mmol racemic **1** in 5 mL solvent, acyl donor (1.5 or 4.5 mmol), enzyme (50 mg) were added and the mixture placed in thermostated shaker for 24 h. Then enzyme was filtered and the solution analyzed by GC using chiral stationary phase CP-Chirasil-Dex CB (0,32mm x 0,25 μm x 25m) with temp. program 60 \rightarrow 195°C at 4°/min for evaluation of conversion and enantiomeric excesses. The order of enantiomers elution: (R)-**1** (28.8 min), (S)-**1** (28.9 min), (S)-**2** (30.4 min), (R)-**2** (30.6 min) was determined by separation of alcohol **1** and acetate **2** from enzymatic reaction and comparison of optical rotation with literature value [16].

Acknowledgements: This work was supported by European Social Fund and Polish State in “Mechanizm WIDDOK” programme (No Z/2.10/II/2.6/04/05/U/2/06).

References:

- [1] S.M. Brown, S.G. Davies, J.A.A. de Sousa, *Tetrahedron: Asymmetry*, 42 (1993) 447
- [2] R.M. Hanson, *Chem. Revs.*, 91 (1991) 437
- [3] F. Molinari, O. Brenna, M. Valenti, F. Aragozzini, *Enzym. Microb. Technol.*, 19 (1996) 551
- [4] S. Takano, H. Numata, K. Ogasawara, *Heterocycles*, 19 (1982) 327
- [5] G. Hirth, R. Barner, *Helv. Chim. Acta*, 65 (1982) 1059
- [6] W.E. Ladner, G.M. Whitesides, *J. Am. Chem. Soc.*, 106 (1984) 7250
- [7] B. Herradon, S. Cueto, A. Morcuende, S. Valverde, *Tetrahedron: Asymmetry*, 4 (1993) 845
- [8] N. Kasai, T. Suzuki, Y. Furukawa, *J. Mol. Catal. B: Enzymatic*, 4 (1998) 237
- [9] B.G. Davis, V. Boyer, *Nat. Prod. Reports.*, 18 (2001) 618
- [10] E. Vanttinen, L.T. Kanerva, *J. Chem. Soc. Perkin Trans.*, (1994) 3459
- [11] E. Vanttinen, L.T. Kanerva, *Tetrahedron: Asymmetry*, 8 (1997) 923
- [12] T. Sakai, T. Kishimoto, Y. Tanaka, T. Ema, M. Utaka, *Tetrahedron Lett.*, 39 (1998) 7881
- [13] F. Molinari, K. S. Cavenago, A. Romano, D. Romano, R. Gandolfi, *Tetrahedron: Asymmetry*, 15 (2004) 1945
- [14] D. Romano, F. Falcioni, D. Mora, F. Molinari, A. Buthe, M. Ansorge-Schumacher, *Tetrahedron: Asymmetry*, 16 (2005) 841
- [15] D. Romano, V. Ferrario, F. Molinari, L. Gardossi, J.M. Sanchez Montero, P. Torre, A. Converti, *J. Mol. Catal. B: Enzymatic*, 41 (2006) 71
- [16] M. Jungen, H-J. Gais, *Tetrahedron: Asymmetry*, 10 (1999) 3747
- [17] M. Pallavicini, E. Valoti, L. Villa, O. Piccolo, *J. Org. Chem.*, 59 (1994) 1751
- [18] V. Partali, A.G. Melbye, T. Alvik, T. Anthonsen, *Tetrahedron: Asymmetry*, 3 (1992) 65
- [19] E. Vanttinen, L.T. Kanerva, *Tetrahedron: Asymmetry*, 7 (1996) 3037
- [20] B.K. Pchelka, A. Loupy, J. Lenkiewicz, L. Blanco, *Tetrahedron: Asymmetry*, 11 (2000) 2719

ENZYME-CATALYZED RESOLUTION OF 2,3-*O*-CYCLOHEXYLIDENE-1-PROPANOL

Maciej Maciejewski*, Janina Ewa Kamińska
*Institute of General Food Chemistry, Technical University of Łódź,
ul. Stefanowskiego 4/10, 90-924 Łódź*

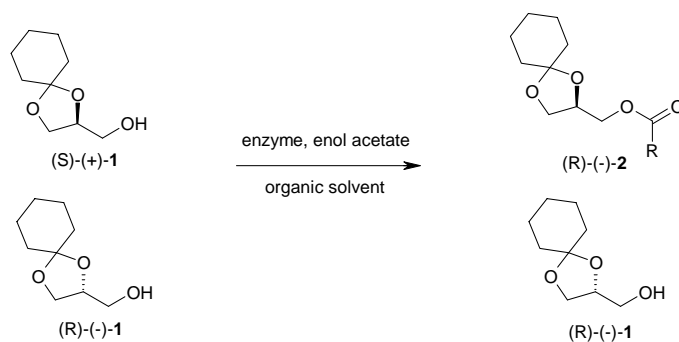
Abstract: The enzyme-catalyzed acetylation of *rac*-2,3-*O*-cyclohexylidene-1-propanol with enol acetates has been studied as a possible route to racemate resolution. We have found high enantioselectivities ($E \sim 200$) for some enzymes but only at low substrate conversion (2-4%). The best enantioselectivities compatible with good activity were found for non-commercial *Mucor racemosus* and *Mucor circinelloides* lipases (5.4 and 3.5 respectively).

Introduction

Glycerol derivatives containing hydroxyl group at C-2 are important substructures in many biologically active compounds and pharmaceuticals [1]. The majority of β -blockers with 3-aryloxy-2-propanol-1-amine structure consist the outstanding example. Chiral glycerol derivatives are regarded as convenient substrates for many syntheses [2]. Such building blocks are still rather expensive since their manufacturing requires chiral catalysts or enantiomerically pure starting materials [3-5]. Thus in recent years increasing interest in biotransformations as a method for pure enantiomers preparation is observed [6-9]. Numerous publications have appeared on resolution of racemic 2,3-*O*-substituted-1-propanols, especially 2,3-*O*-isopropylidene-1-propanol (solketal) [9-15] while 2,3-*O*-cyclohexylidene-1-propanol was investigated incidentally and low enantioselectivities were reported [16-19]. Here we describe our results on enzyme-catalyzed acetylation of 2,3-*O*-cyclohexylidene-1-propanol with enol acetates.

Results

We have studied enzyme-catalyzed acetylation of the substrate **1** in organic solvents with the aim of enantiomers resolution. Broad range of commercial, native and immobilized lipases, non-commercial *Mucor* species as well as acylase and proteinase were included in preliminary screening. Reactions were carried out in hydrophobic solvents – hexane, methylene chloride and *tert*-butyl methyl ether with vinyl acetate as acyl donor. All enzymes tested were found active and showed the same preference for faster acylation of (S)-enantiomer (see Scheme 1).



Scheme 1

However the reaction rate varied considerably with the solvent – the highest substrate conversion was observed in *tert*-butyl methyl ether and hexane while in methylene chloride only immobilized lipases retained high activity (see Table 1). Unfortunately the high activity of these enzymes is connected with lack of enantioselectivity ($E \sim 1$).

Table 1. Activity and selectivity of enzymes with vinyl acetate as acyl donor.

Enzyme	Hexane, 40°C			CH ₂ Cl ₂ , 20°C			t-BuOMe, 20°C		
	c	ee _p	E	c	ee _p	E	c	ee _p	E
Lipase A	0.19	0.02	1.1	0.02	0.73	7	0.04	0.46	2.8
Lipase AY	0.41	0.13	1.4	-	-	-	-	-	-
Lipase PS	-	-	-	0.01	0.99	201	0.02	0.66	5.1
<i>Candida cylindracea</i> Lipase	0.51	0.14	1.5	0.03	0.60	4	0.16	0.24	1.7
<i>Candida rugosa</i> Lipase	0.33	0.15	1.4	0.02	0.79	9	0.06	0.31	1.9
Porcine Pancreatic Lipase	0.09	0.21	1.6	0.02	0.89	18	0.12	0.27	1.8
<i>Mucor circinelloides</i> Lipase	0.41	0.30	2.2	0.03	0.88	16	0.17	0.53	3.5
<i>Mucor racemosus</i> Lipase	0.10	0.54	3.5	0.03	0.83	11	0.08	0.28	1.8
Lipozyme RM [®]	0.99	0	1	0.34	0.26	2	0.73	0.09	1.4
Lipozyme TL [®]	0.99	0	1	-	-	-	-	-	-
Novozyme 435 [®]	-	-	-	1	0	1	0.63	0.03	1.1
Acylase	0.11	0.22	1.6	0.03	0.68	5	0.05	0.45	2.7
Papain	0.02	0.99	202	-	-	-	-	-	-

Enantioselectivity ratio ca. 200 was found for lipase PS in methylene chloride and for papain in hexane but only at very low conversion 1-2%.

Improvement of enantioselectivity in enzyme-catalyzed acetylation was frequently noted when vinyl acetate was replaced by more sterically hindered isopropenyl acetate as acyl donor [20]. In our case when substrate **1** was treated with isopropenyl acetate in hexane large decrease of activity (lower conversion) has been observed without significant change of enantioselectivity (see Table 2).

Table 2. Activity and selectivity of enzymes with isopropenyl acetate as acyl donor.

Enzyme	Hexane, 40°C			CH ₂ Cl ₂ , 40°C		
	c	ee _p	E	c	ee _p	E
Lipase A	0.04	0.39	2.3	0.02	0.94	24
Lipase AY	0.12	0.31	2.0	-	-	-
Lipase PS	-	-	-	0.02	0.99	202
<i>Candida cylindracea</i> Lipase	0.40	0.19	1.6	0.02	0.94	33
<i>Candida rugosa</i> Lipase	0.41	0.19	1.7	0.02	0.93	28
Porcine Pancreatic Lipase	0.02	0.99	203	0.03	0.99	205
<i>Mucor circinelloides</i> Lipase	0.23	0.26	1.8	0.03	0.65	4.8
<i>Mucor racemosus</i> Lipase	0.05	0.53	3.3	0.02	0.99	202
Lipozyme RM [®]	0.07	0.32	2.0	0.02	0.91	22
Lipozyme TL [®]	0.15	0.38	2.4	-	-	-
Novozyme 435 [®]	0.98	0.01	1.3	0.06	0.09	1.2
Acylase	0.05	0.45	2.6	0.02	0.92	25

On the other hand in methylene chloride decrease of conversion was not significant while increase in enantioselectivity could be observed. It is noteworthy that in the preliminary screening the best enantioselectivities compared with good activities were found for non-commercial lipases from *Mucor racemosus* and *Mucor circinelloides* used as whole mycelium.

Table 3. Solvent dependence of activity and selectivity of *Mucor* lipases.

Solvent	<i>M. racemosus</i>			<i>M. circinelloides</i>		
	c	ee _p	E	c	ee _p	E
Cyclohexane	0.13	0.50	3.2	0.27	0.40	2.7
Benzene	0.12	0.49	3.1	0.13	0.53	3.5
Toluene	0.19	0.35	2.2	0.38	0.28	2.1
Methylene chloride	0.10	0.36	2.2	0.15	0.47	3
Chloroform	0.08	0.54	3.5	0.22	0.47	3.1
1,2-Dichloroethane	0.10	0.44	2.7	0.004	0.99	200
Tetrahydrofuran	0.08	0.67	5.4	0.24	0.36	2.4
Ethyl acetate	0.23	0.35	2.3	0.32	0.31	2.2
Acetone	0.07	0.53	3.4	0.20	0.37	2.4
Acetonitrile	0.05	0.49	3	0.11	0.33	2.1

Therefore the activity and selectivity of these two lipases in acylation with vinyl acetate were determined for range of solvents varying in polarity and water miscibility (see Table 3). The best enantioselectivity compatible with good activity for *Mucor racemosus* was observed in tetrahydrofuran (E=5.4) while for *Mucor circinelloides* in benzene (E=3.5).

Conclusions

The results obtained in present study do not allow for preparative resolution of *rac*-2,3-*O*-cyclohexylidene-1-propanol. We are of the opinion that non-commercial lipases from *M. racemosus* and *M. circinelloides* are good candidates for search of enantioselectivity improvement by decreasing reaction temperature, changing the acyl donor or usage of chiral solvents. Nevertheless looking for new enzymes seems to be also necessary.

Materials and methods

Acylase, Lipase A, Lipase AY, Lipase PS were obtained from Amano, *Candida Cylindracea*, *Candida Rugosa*, Porcine Pancreas Lipases from Sigma, immobilized preparations Lipozyme RM[®] (*Rhizomucor miehei*), Lipozyme TL[®] (*Thermomyces lanuginosus*), Novozyme 435[®] (*Candida antarctica*) from Novozymes, and papain from Fluka. *Mucor racemosus* and *Mucor circinelloides* lipases (whole mycelium) were kindly donated by Prof. T. Antczak from Institute of Technical Biochemistry (Technical University of Łódź). *Rac*-2,3-*O*-cyclohexylidene-1-propanol (**1**) and its acetate (**2**) were prepared in our laboratory according to the following procedures.

Rac-2,3-*O*-cyclohexylidene-1-propanol (**1**): Glycerol (0.48 mol), cyclohexanone (0.4 mol), 100 mL toluene and a few drops of H₃PO₄ were refluxed under Dean-Stark apparatus for 6 hours. Then the mixture was poured into 100 mL of 5% aq. Na₂CO₃. The water layer was extracted with toluene, combined extracts washed with water and dried over MgSO₄. After solvent evaporation the crude product was distilled under reduced pressure (b.p. 100°C/1.5 Tr, n_D²⁰=1.4810, 70% yield). ¹H-NMR (250 MHz, CDCl₃), δ: 4.23 (ddt, J=6.4Hz, J=5.3Hz, J=4Hz, 1H); 4.03 (dd, J=8.2Hz, J=6.5Hz, 1H); 3.77 (dd, J=8.1Hz, J=6.4Hz, 1H); 3.72 (dd, J=11.6Hz, J=3.8Hz, 1H); 3.58 (dd, J=11.6Hz, J=5.2Hz, 1H); 2.42 (s, 1H); 1.65-1.54 (m, 8H); 1.49-1.36 (m, 2H). IR (film): 3450, 2950, 1460, 1370, 1120, 1070 cm⁻¹.

Rac-2,3-*O*-cyclohexylidene-1-propyl acetate (**2**): Acetic anhydride (0.036 mol) was added to the stirred solution of **1** (0.03 mol) and pyridine (0.042 mol) in 20 mL of dry methylene chloride at room temp. After 24 h the mixture was treated with 100 mL of 5% aq. NaHSO₄, and extracted with methylene chloride, washed with water and dried over MgSO₄. Then the solvent was evaporated and the crude product was distilled under

reduced pressure (b.p. 85°C/0.9 Tr, $n_D^{20}=1.4634$, 70% yield). $^1\text{H-NMR}$ (250 MHz, CDCl_3), δ : 4.34, 4.29 (2t, $J=6\text{Hz}$, 1H); 4.18-4.07 (m, 2H); 4.07 (dd, $J=8.4\text{Hz}$, $J=6.5\text{Hz}$); 3.74 (dd, $J=8.4\text{Hz}$, $J=6\text{Hz}$, 1H); 2.09 (s, 3H); 1.63-1.52 (m, 8H); 1.47-1.32 (m, 2H); IR (CHCl_3): 3000, 1760, 1380, 1240, 1110, 1050 cm^{-1} .

$^1\text{H-NMR}$ spectra were recorded on Bruker DPX 250 spectrometer and IR spectra on Shimadzu IR 408 apparatus.

Enzyme-catalyzed reactions were carried out as follows: to 1.5 mmol racemic **1** in 5 mL solvent, acyl donor (1.5 or 4.5 mmol), enzyme (50 mg) were added and the mixture placed in thermostated shaker for 24 h. Then enzyme was filtered and the solution analyzed by GC using chiral stationary phase CP-Chirasil-Dex CB (0,32mm x 0,25 μm x 25m) with temp. program 60 \rightarrow 195°C at 4°/min for evaluation of conversion and enantiomeric excesses. The order of enantiomers elution: (R)-**1** (28.8 min), (S)-**1** (28.9 min), (S)-**2** (30.4 min), (R)-**2** (30.6 min) was determined by separation of alcohol **1** and acetate **2** from enzymatic reaction and comparison of optical rotation with literature value [16].

Acknowledgements: This work was supported by European Social Fund and Polish State in “Mechanizm WIDDOK” programme (No Z/2.10/II/2.6/04/05/U/2/06).

References:

- [1] S.M. Brown, S.G. Davies, J.A.A. de Sousa, *Tetrahedron: Asymmetry*, 42 (1993) 447
- [2] R.M. Hanson, *Chem. Revs.*, 91 (1991) 437
- [3] F. Molinari, O. Brenna, M. Valenti, F. Aragozzini, *Enzym. Microb. Technol.*, 19 (1996) 551
- [4] S. Takano, H. Numata, K. Ogasawara, *Heterocycles*, 19 (1982) 327
- [5] G. Hirth, R. Barner, *Helv. Chim. Acta*, 65 (1982) 1059
- [6] W.E. Ladner, G.M. Whitesides, *J. Am. Chem. Soc.*, 106 (1984) 7250
- [7] B. Herradon, S. Cueto, A. Morcuende, S. Valverde, *Tetrahedron: Asymmetry*, 4 (1993) 845
- [8] N. Kasai, T. Suzuki, Y. Furukawa, *J. Mol. Catal. B: Enzymatic*, 4 (1998) 237
- [9] B.G. Davis, V. Boyer, *Nat. Prod. Reports.*, 18 (2001) 618
- [10] E. Vanttinen, L.T. Kanerva, *J. Chem. Soc. Perkin Trans.*, (1994) 3459
- [11] E. Vanttinen, L.T. Kanerva, *Tetrahedron: Asymmetry*, 8 (1997) 923
- [12] T. Sakai, T. Kishimoto, Y. Tanaka, T. Ema, M. Utaka, *Tetrahedron Lett.*, 39 (1998) 7881
- [13] F. Molinari, K. S. Cavenago, A. Romano, D. Romano, R. Gandolfi, *Tetrahedron: Asymmetry*, 15 (2004) 1945
- [14] D. Romano, F. Falcioni, D. Mora, F. Molinari, A. Buthe, M. Ansorge-Schumacher, *Tetrahedron: Asymmetry*, 16 (2005) 841
- [15] D. Romano, V. Ferrario, F. Molinari, L. Gardossi, J.M. Sanchez Montero, P. Torre, A. Converti, *J. Mol. Catal. B: Enzymatic*, 41 (2006) 71
- [16] M. Jungen, H-J. Gais, *Tetrahedron: Asymmetry*, 10 (1999) 3747
- [17] M. Pallavicini, E. Valoti, L. Villa, O. Piccolo, *J. Org. Chem.*, 59 (1994) 1751
- [18] V. Partali, A.G. Melbye, T. Alvik, T. Anthonsen, *Tetrahedron: Asymmetry*, 3 (1992) 65
- [19] E. Vanttinen, L.T. Kanerva, *Tetrahedron: Asymmetry*, 7 (1996) 3037
- [20] B.K. Pchelka, A. Loupy, J. Lenkiewicz, L. Blanco, *Tetrahedron: Asymmetry*, 11 (2000) 2719

PHOTOCATALYTIC DEGRADATION OF TETRACYCLINE IN WATER SOLUTIONS

A. Makowski¹, G. Janikowska²

*Division of General and Inorganic Chemistry¹, Division of Analytical Chemistry²,
Department of General and Analytical Chemistry, Faculty of Pharmacy, Medical
University of Silesia,
41-200 Sosnowiec, Jagiellonska 4*

Introduction

Antibiotics are present in communal and hospital sewages, superficial waters and in ground soil or sediments of rivers and lakes [1, 2]. The presence of antibiotics in environment causes the bacterium resistance on these drugs [3].

Pharmaceutical substances are difficult to removals from sewages by the methods like biodegradation, coagulation, filtration or adsorption [4]. At present develops advanced oxygenations processes (AOP) rely on generating highreactive hydroxyl radicals during irradiations of solutions. Photocatalytic processes relying on irradiation of solutions with suspension of semi-conductor TiO₂ former were investigated under side of possibilities of their application to removing of antibiotics from sewages [5].

The aim of this work was examining of influence the metals ions: Fe³⁺, Cu²⁺, Mg²⁺ and Ca²⁺ on photocatalytic degradation rate constant of tetracycline and estimation of changes in content of total organic carbon (TOC) in course of investigated process.

Materials and methods

Degradation of tetracycline was carried out by irradiation of water solutions of initial concentration 0.1 mmol/l or solutions with ions of metals with UV radiation about wavelength of 366 nm and intensities of $8.76 \cdot 10^{-9}$ E/s cm². To preparing of solutions of metals ions were used of chlorides of iron, copper, magnesium and calcium (products of POCH laboratories).

Exactly 0.25g TiO₂ P-25 was added to 100 ml of every solution. Product of Degussa consisted of 80% anatase and 20% rutile had diameter of 21 nm and of specific surface of 50 m²/g were used. During irradiations the solutions were stirred and after definite time were centrifuged (30 minutes and 4000 rotations). Final concentration of tetracycline with method of HPLC (L-7100 pump and UV detector of Merck) was determined. The BDS Hypersil C18 column of 15 cm length and 2.1 mm diameter and 5 μm granulation were used.

To estimate the photocatalytic degradation rate constants of tetracycline, the relationship $\log C/C_0$ from time of duration of photocatalytic process were defined. Content of total organic carbon was investigated by automatic analyser of carbon Shimadzu 5000A.

Results

Figures 1-3 show relationship C/C_0 of tetracycline in the course of photocatalytic process. The constants of rate are given in table 1. The relationship TOC/TOC₀ vs. time of duration of photocatalytic process in solution of tetracycline and solution with ions of iron is introduced in figure 4 and comparison the changes of TOC/TOC₀ and C/C_0 for solution of tetracycline in fig. 5.

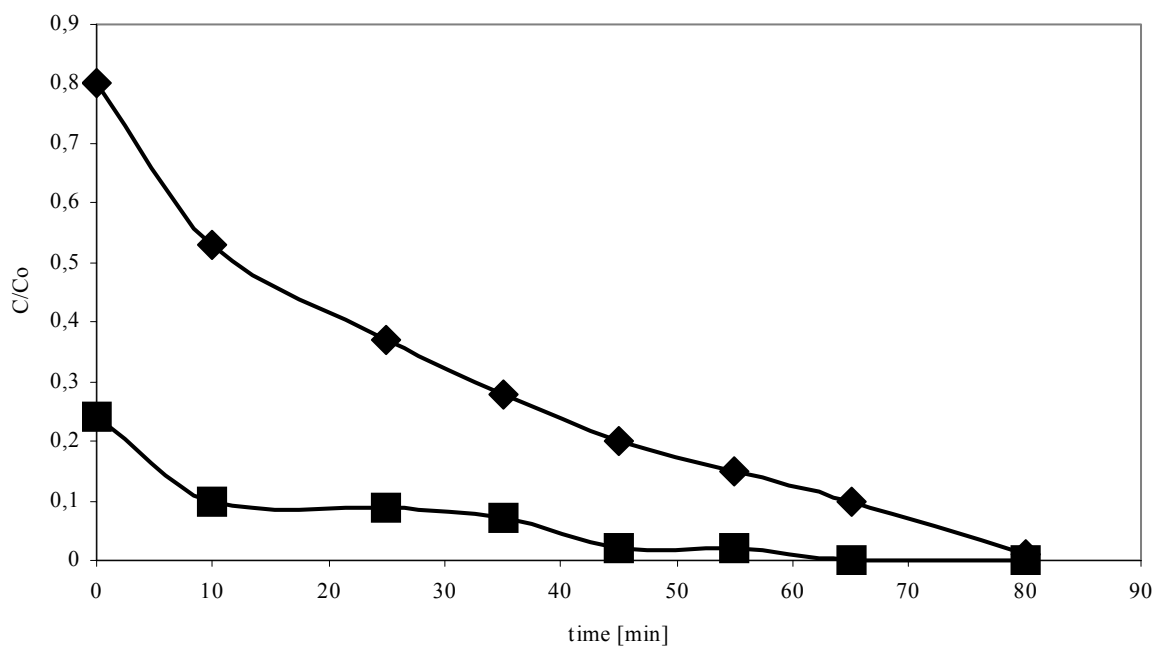


Fig.1. Tetracycline relationship of C/C_0 vs. time of duration of photocatalytic process in 0.1 mmol/l solution (\blacklozenge) and in presence of Fe^{3+} (\blacksquare); molar ratio of tetracycline and Fe^{3+} is equal 1.

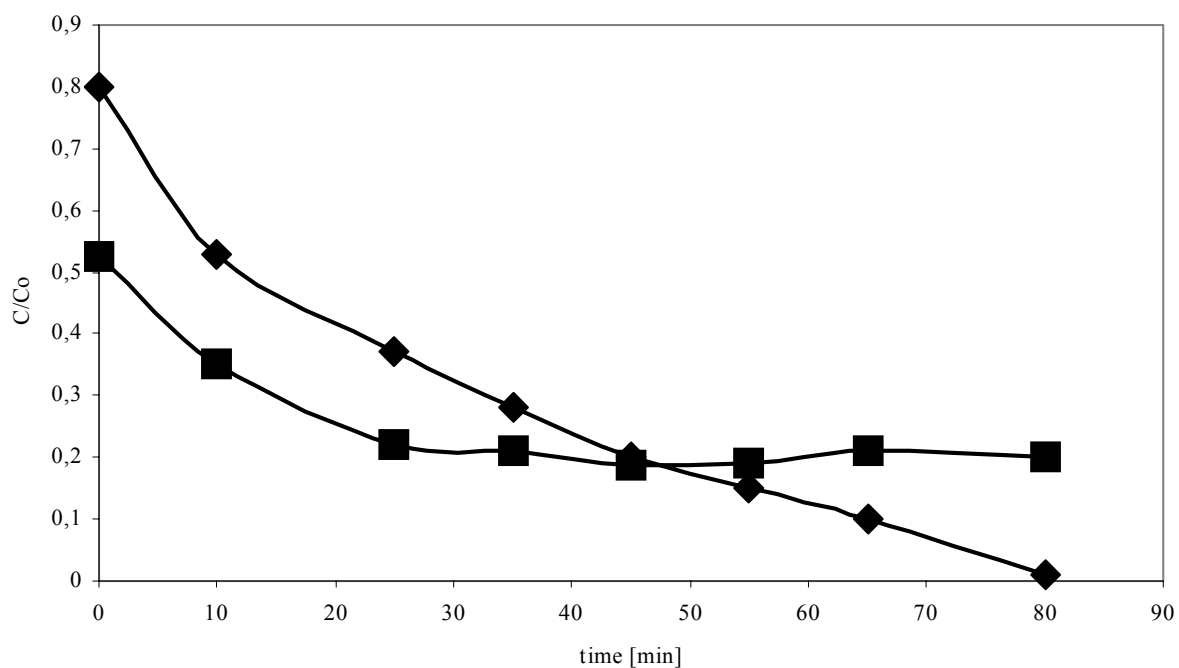


Fig.2. Tetracycline relationship C/C_0 vs. time of duration of photocatalytic process in 0.1 mmol/l solution (\blacklozenge) and in presence of Cu^{2+} (\blacksquare); molar ratio of tetracycline and Cu^{2+} is equal 1.

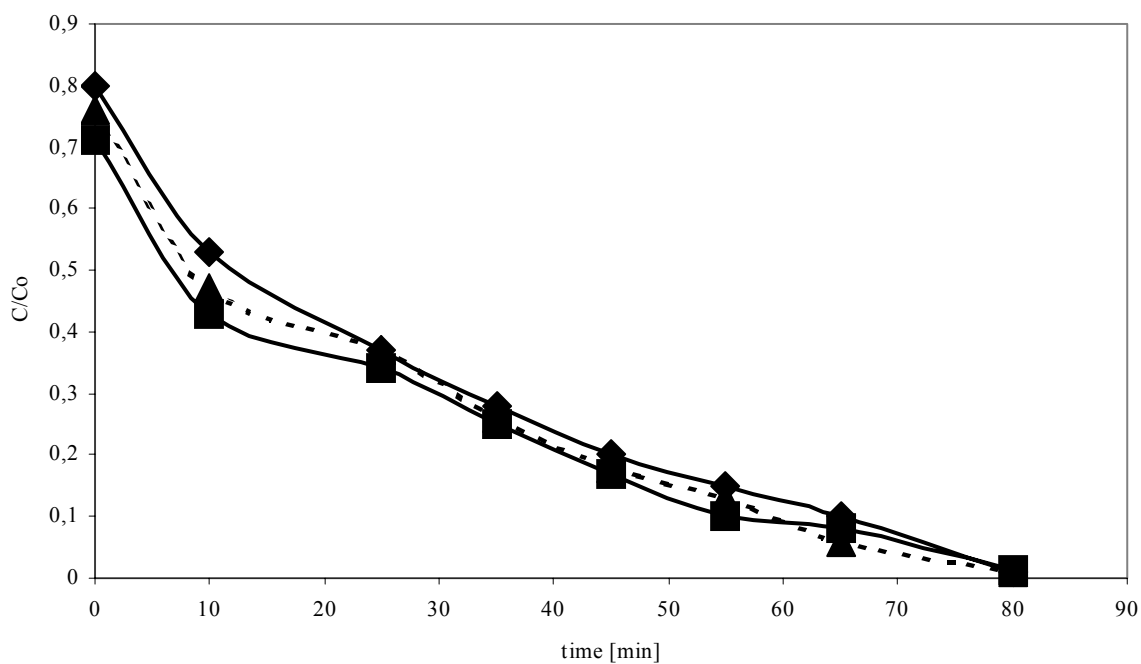


Fig.3. Tetracycline relationship C/C_0 vs time of duration of photocatalytic process in 0.1 mmol/l solution (♦) and in presence of Ca^{2+} (■) and Mg^{2+} (▲); molar ratio of tetracycline and metal ions is equal 1.

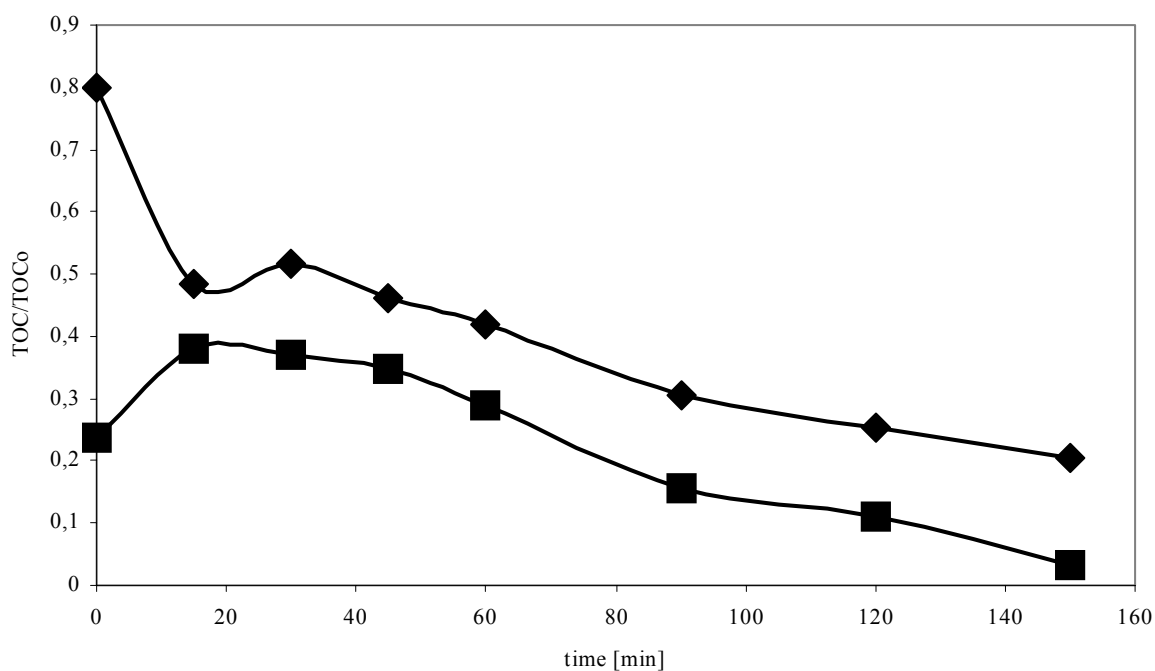


Fig.4. TOC/TOC₀ relationship vs time of duration of photocatalytic degradation of tetracycline in 0.1 mmol/l solution (♦) in presence of Fe^{3+} (■); molar ratio of tetracycline and Fe^{3+} is equal 1.

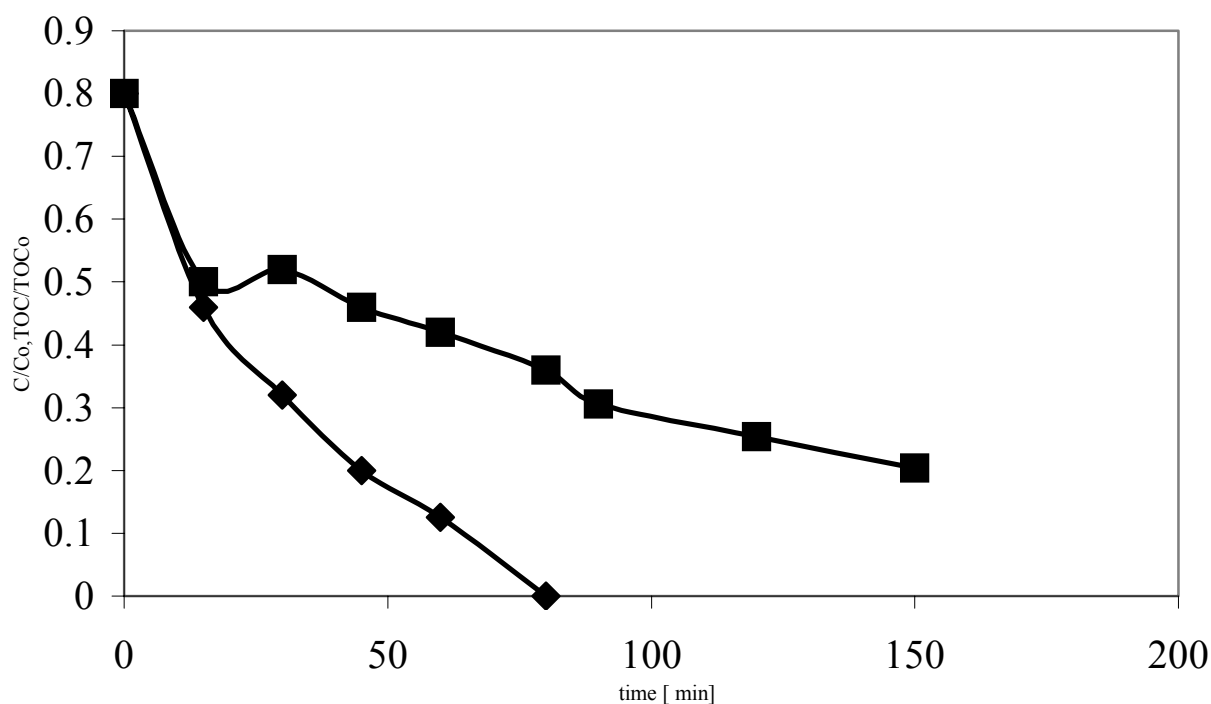


Fig.5. Comparison of the relationship C/C_0 (♦) and TOC/TOC_0 (■) vs time of duration of photocatalytic degradation of tetracycline in 0.1 mmol/l solution.

Table 1. Rate constants of tetracycline photocatalytic degradation

Initial concentration of tetracycline [mmol/l]	Metal ions	pH	Molar ratio antibiotic/metal ions	Rate constant [s^{-1}]
0.1	-	6.78	-	$9.14 \cdot 10^{-4}$
	Fe^{3+}	3.39	1	$1.40 \cdot 10^{-3}$
	Cu^{2+}	6.12	1	$1.88 \cdot 10^{-4}$
	Ca^{2+}	6.75	1	$9.01 \cdot 10^{-4}$
	Mg^{2+}	6.80	1	$8.77 \cdot 10^{-4}$

Discussion

The estimated rate constants of tetracycline photocatalytic degradation in water solutions testify that only presence of iron ions causes in their enlargement. Ions of this metal create sparingly soluble complexes with this antibiotic and perhaps this effect can be a cause of decreasing of tetracycline concentration in the first stage of reaction, what shown in figure 1. Degradation of this complex during irradiations can cause the increase of TOC/TOC_0 shown in fig. 4, what should however induce augmentation of value C/C_0 for solution of tetracycline with ions of iron (fig. 1). Appears probable that follows desorption the products of tetracycline degradation with metal from photocatalyst surface what can entail the observed increase of content of organic carbon in the first stage of reaction.

Mineralisation of tetracycline is process to slowly than process of its degradation what shown in figure 5 and more quickly runs in solutions with ions of iron than without

them (fig. 4). Decrease of tetracycline degradation in solutions with copper ions is caused with settling of metallic copper and poisoning of semi-conductor surface [5], what appears in course of relationship C/Co vs time in duration of photocatalytic process shown in fig. 2.

Ions of calcium and magnesium imperceptibly influence in rate of tetracycline photocatalytic degradation what became presented in fig. 3 and in table 1.

Conclusions

Ions of iron accelerate the photocatalytic process of degradation and mineralisation of tetracycline in water solutions.

Ions of copper moderate the photocatalytic process of tetracycline degradation in water solutions.

Ions of calcium and magnesium do not influence in essential manner on rate of tetracycline degradation in water solutions.

Acknowledgment. We extend our thanks to dr P. Hamera from Degussa Poland GmbH for the gift of photocatalyst P-25.

References

- [1]. B.Halling-Sørensen, Chemosphere, 40 (2000) 731
- [2]. B. Halling-Sørensen, S. Nielsen, P.F. Lanzky, F. Ingerslev, H.C. Holten-Lützhof, S.S. Jorgensen, Chemosphere, 36 (1999)
- [3]. A. Al-Ahmad, F.D. Daschner, K. Kümmerer, Arch. Environ. Cont. Toxicol., 3 (1999) 158
- [4]. T.A. Ternes, Wat. Res., 32 (1998) 3245
- [5]. A. Makowski, W. Wardas, W. Baran, Annals of Polish Chemical Society, (2003) 779
- [6]. V. Brezova, A. Blazkova, E. Borosova, M. Ceppan, R. Fiala, Journal of Molecular Catalysis A: Chemical, 98 (1995) 109

**ELEMENTS OF CHEMISTRY FOR ARCHAEOLOGISTS.
ORGANIZING CONSERVATION ARCHAEOLOGICAL
MONUMENTS CLASSES.**

Beata Miazga

Institute of Archaeology, Faculty of Historical and Pedagogical Sciences,

Wroclaw University

48 Szewska Rd, Wroclaw 50-139

Teaching the humanities students chemistry, including archaeology, has never been more necessary. There are several reasons for that, the most important is that the archaeology becomes the interdisciplinary science which is connected with variety of instruments taken from natural mathematical sciences. Mathematics with statistical elements, geology, biology, especially botany and zoology, as well as physics and chemistry are irreplaceable sciences necessary in doing archaeological research. The last mentioned ones are very important for archaeologists because they provide them plenty of modern physical-chemical methods, without which doing archaeological research seems to be unfeasible. Another important cause for teaching chemistry is restoration of archaeological monuments. Conservator works, which are currently carried out on historical legacy, to a large extent are based on chemical knowledge, which is first and foremost practical not only theoretical.

Consequently, it is not only important but also essential to include elements of chemistry in didactical process of teaching prospective archaeology students. The purpose of such education is not only to indicate analytical opportunities of various chemistry disciplines, but also systematizing chemical knowledge possessed by students and steering it on practical use while conservation works are being carried out.

Passing on knowledge connected with experience in creating and carrying out didactical classes in 'Conservation of Archaeological Monuments' is the essence of this research. Organizing such classes was preceded by an opinion pool performed in group of archaeologists. The first purpose of the pool was to characterize demand for particular elements of chemical knowledge which is necessary for restoration works. The second aim was to make an attempt to assess level of chemical knowledge possessed by students of archaeology. Gathered information, knowledge of current conservation works and analytical trends in archaeological researches were the basis for creating 'Conservation of Archaeological Monuments' laboratory classes curriculum. Further probing students' knowledge and skills was the reason for such form of conducting classes. Form of 30 lessons is opened, which means that students of all academic years may attend them, and lecturer has possibility of observing and modifying the applied methods of teaching.

Adjusting basic elements of chemistry to conservation processes of various archaeological monuments was the basis for selecting the chemical material and

knowledge for passing on during laboratory exercises [1]. As a result, teaching is divided on several blocks and the level of difficulty increases (table 1). The first block is preliminary for students, they have chance to familiarize with subject matter of classes and principles of work in a chemical laboratory. Knowing such rules guarantees safety of students and apparatus in the laboratory. In the second block, which working title is 'Organics', conservator works are conducted on monuments of organic origin. They were adapted to human needs, inter alia - tools and decorations of bones, anglers, wood, leather and textiles. The third block, named 'Inorganics', is devoted to conserving archaeological monuments made of mineral origin materials as ceramics, glass, and metal. The last, fourth, block named 'Complex Materials' deals with materials mixed of two different substances.

Table 1. Block division of 'Conservation of Archaeological Monuments' classes.

-1-	-2-	-3-	-4-	
Block	Working name	The scope of conservation works	Expectations	
			Knowledge - concepts	Skills
I	Introduction	Preliminary activities: -Health and safety-at-work legislation -Basic apparatus -Basic chemical calculations -Documentation of conservation works	Solution, percentage concentration, solubility, solution density	-Using laboratory glassware, basic chemical apparatus - calculation of concentration -preparing solution of specific concentration, with keeping proper sequence
II	Organics	Conservation of monuments made of: -bones and anglers -wood -leather and fabric	Polymers, acrylic resins, saccharose, polyethylene glycols, vegetable and animal fats	-Preparing polymeric solutions on the base of non-aqueous solvent -preparing of 'deironing' baths for leathers
III	Inorganics	Conservation of monuments made of: -ceramics -glass -metals	Extraction, acid-base indicator, metals corrosion, corrosion inhibitor, electrolysis, noble metals	-Testing reaction of solution, -determining of chloride content -Preparation of electrolytic purification of metals: selection of electrodes, electrolyte and conditions of current -Preparation of corrosion inhibitor solutions
IV	Complex Materials	Conservation of monuments made of complex material, for example iron knives with wooden handle, leather belts with bronze fastener	All concepts from blocks I-III	Ability of conserving various mixtures of different materials, as iron-wood, iron-wood-leather, leather-iron (bronze)

Such division of teaching according to material criteria is convenient for students because of raising expectations, level of knowledge and skills during the course. Skills gained in initial blocks of education are essential in the further ones. A shift of this sequence would extract the need of immediate learning by students all chemical procedures used for monuments conservation.

On the basis of such exercises division and teaching chemistry curriculum (for general as well as profiled and technical high-schools – basic educational level. Admission nr DKOS-4015-33/02) [2] the most important educational contents were chosen. The most important element taken into consideration while contents were selected, was that the classes can not be only chemistry oriented. Lessons should pass on the knowledge on practical use of chemistry elements in restoring works. ‘Conservation of Archaeological Monuments’ should not be based only on passing on concrete didactic contents. It should also shape proper conservator’s attitudes on grounds of students’ chemical knowledge.

Creation of syllabus was worked out as a broadening of block-division of lessons. Here, suitable teaching material was selected; moreover, a list of abilities and skills which students should possess during the course was prepared (see table 1, column 4).

The main goal of the first block is to pass on the chemical laboratory safety principles and practices. In the middle of participating the classes, learners gain skills of using basic laboratory glass and apparatus. They get to know rules of working with chemical reagents and order their knowledge of solutions, solubility, also of preparing solutions with specific concentration and their dilution. Next, students realize exercises from the block two and they do their first works on organic material. Protection of such monuments is usually based on preparing a thin coating (layer) which does not react with ground. And here, some elements of knowledge about polymers come out. They are not widely discussed during the elementary and high-school teaching curriculum; however, they are crucial for correct carrying on conservation works [3]. Conservation of bones as well as anglers, wood, and leathers requires substantial knowledge from students. They should know what polymers are and what are their properties and applications. It relates to not only the natural polymers (which are frequently used for conservation), but first and foremost to the polymers which were created by people and have a role in increasing durability of monuments, make protective coating and glues. Teaching such difficult thing requires using many simplifications, loose analogies to everyday life (as paints, lacquers, cosmetic products). Another chemical process of great importance, being used in conservation works is extraction. Fundamental purpose of the process is removing ions of iron and chlorine from objects (water extraction). Removing of iron from aqueous solution takes place by complexing by various complexing agents (as acids: citric, tartaric or EDTA). Making use of such chemical compounds and this method were not discussed during the earlier chemistry schooling. For this reason, it seems to be valuable to refer to the knowledge from school of reactions in water solution (methods of detecting and removing water from particular ions, inter alia iron and chlorides). Chloride ions, which are very destructive for metal monuments, have to be necessarily removed. A typical process, which is applied to restoring works is electrolytic ions removing. Even when the basic knowledge of metals, processes of oxidation-reduction, nobility of silver and gold, higher copper chemical resistance are well-known to students, they are not acquainted with essence of electrolysis and it is more difficult for them to understand. Here again, simplifications and portraying of

some similarities to well-known electrochemical processes, as charging batteries and accumulators are very helpful. Another very important element of chemistry, which is irreplaceable in restoring works, is ability of using pH-scale. Testing reaction of solutions during conducting conservation works is indispensable. Knowledge of pH-value, in which metals, leather and wood should be stored, as well as ability of making measurements of acid-base indicator, is necessary for archaeology students. In restoring processes carried out on metals, great chemical knowledge is being used. Starting with information about metal's origin, its receiving from ores, knowledge of its properties and behaviour during its exploitation, its occurring in earth layers (corrosion), through processes of chemical purifying exploited metal monuments, and finishing on their stabilisation (using corrosion inhibitors). However, restoring of complex archaeological monuments (see block IV) includes all knowledge and skills which had been developed during classes in previous blocks. Conservation of such monuments requires from students familiarity of applied methods and chemical-restoration procedures.

In the lessons, students are taught not only particular elements of chemistry which is used in restoring works. The major goal was skilful joining of chemical knowledge basics with restoration works rules that are imposed by proper restaurateurs-conservational practice and range of law legislations. However, this was not the only advantage of participating the classes, other important pieces of information were about physicochemical methods applied as research tools in archaeology. What can not be passed over, is making use by archaeologists of studies on radioactivity and its input into research on age of find, as well as various spectroscopic methods of testing composition, origin, and technology of monuments production. To such methods belong X-ray methods (XRF – X-ray fluorescence), spectroscopic examinations in Infrared Spectroscopy, and many other analytical techniques.

Summing up, the creation of school curriculum of laboratory classes on 'Conservation of Archaeological Monuments' was based on two assumptions. Firstly, students of archaeology have acquired substantial knowledge from previous stages of teaching (determined on the basis of curriculum analysis [2]). Secondly, it is necessary for students to gain knowledge and new skills in chemistry branches which were omitted in the humanities curriculum (basic teaching of subject), i.e. electrochemistry, polymers, analytical separation processes (extraction, complexometry). In the future, this task will be executed in two stages: within the confines of chosen monographic lecture and laboratory classes. Owing to possibility of choosing both forms of classes, various theories will have to be passed on during laboratory exercises. Complete success will be guaranteed if both forms of classes are obligatory.

References:

- [1] D.L. Hamilton: Methods of conserving archaeological material from underwater sites in: <http://nautarch.tamu.edu/class/anth605/File0.htm>
- [2] M.M. Poźniaczek, Z. Kluz, E. Odrowąż in: *Chemia. Poradnik dla nauczyciela i program nauczania w liceum ogólnokształcącym, liceum profilowanym i technikum*. WsiP, Warszawa, 2002.
- [3] J.Ciabach in: *Właściwości żywic sztucznych stosowanych w konserwacji zabytków*. Wydawnictwo Uniwersytetu Mikołaja Kopernika, Toruń, 2001.

CHEMISTRY in POLISH UNIVERSITIES 1783-1939

Roman Mierzecki

Polish Chemical Society, Section History of Chemistry

1. At the turn of XVIII c.

At the turn of XVIII c. three towns of the Polish Territory could be considered university centres: Cracow (Kraków), Wilno (now Vilnius in Lithuania) and Lwów (now Lviv in Ukraine). From 1783, lectures in chemistry were given in Kraków university (called „the Crown Main School”) in Polish by a physician, Jan Jaśkiewicz (1749-1809) and later by Franciszek Scheidt (1759-1807); in Wilno such lectures were presented from 1784 by an Italian, Joseph Sartoris in Latin. These scholars also organised small laboratories for their own studies. In 1772 the southern part of Poland was annexed by Austria, and Lwów became the capital of an Austrian province called Galicia. Here, the Austrian authorities opened a German university at which Joseph Markovičs (1755-1795), a Hungarian of Croatian origin, gave chemistry lectures in German. He conducted certain experimental studies on explosives and analysed crude oil from the nearby Carpatian sources.

Kraków and Wilno remained within the borders of the Polish state until 1795, when Poland as a whole lost the independence. The Austrian authorities tried to limit the activity of the old Kraków University, but chemistry lectures in Polish continued with minor interruptions. Although Wilno was incorporated into Russian Empire, the local University did not cease to be a Polish school. From 1797, chemistry was taught there in Polish by Jędrzej (Andrew) Śniadecki (1768-1838) and his student Ignacy Fonberg (1801-1891). Śniadecki was the author of the first Polish chemistry handbook in 1800, re-edited in enlarged form in 1806 and 1816. Together with Fonberg he developed the laboratory inherited from Sartoris.

2. Teaching of chemistry in Warsaw in XIX century

After the Vienna Congress in 1815 Warsaw became the capital of the Congress Polish Kingdom under Russian domination. The emperor of Russia Alexander I, as the king of Poland opened in 1816 the Royal University of Warsaw, where chemistry was taught by Adam Kitajewski (1789-1837). The Technical University also began to be organised in 1826 in Warsaw, but both these schools and the Wilno University have been closed by the Tsarist authorities in 1832 as a repression for November anti-Russian Uprising.

Twenty five years were in the Kingdom only primary and secondary Polish schools. In 1857 a Medico-Chirurgical Academy has been opened and in 1862 a Polish university named „the Warsaw Main School” that was active for seven years till 1869. Chemistry was lectured by Jakub Natanson (1832-1884), alumnus of Dorpat University. After 1869 the Russian authorities repressed any scientific movement in the Polish Kingdom (named then a Vistula District) and destroyed there all Polish centres of science. The Russian Emperor University of Warsaw was then opened. In 1898 the Russian Technical University was also opened in Warsaw.

Although the Russian authorities forbade the organisation of Polish societies, in 1875 certain Polish entrepreneurs as count Ludwik Krasieński, the owner of pyrite mine

in Spain and an asphalt plant in Italy, as well as certain scientists, including Jakub Natanson, were able to constitute a Warsaw Division of the Russian „Society for Promoting the Development of the Russian Commerce and Industry” which enjoyed the right to hold debates in Polish. The aim of the Division was to promote Polish businessmen. It organised lectures on different practical chemical topics held twice a month for twenty years. In 1875 the members of Warsaw Division organised a Museum of Industry and Agriculture, whose aims far surpassed those of a normal museum. To this Museum chemical laboratory was founded on a base of the small private laboratory of Napoleon Millicer (1842-1905). In 1882, the Museum moved to a new building, where five rooms were assigned to the chemical laboratory. It conducted analyses for the Polish entrepreneurs and farmers, but also instructed young people about the methods of chemical analysis. Here, many future Polish professors and scientists took their first steps in chemical analysis. They included Marya Skłodowska (later Mme Curie), who later, in Paris, applied the methods learned in this laboratory to analyse the pitchblende and in 1898 to separate the salts of the first radioactive elements: polonium and radium. Polish scientists have also organised in Warsaw a clandestine Polish university which held lectures, including chemistry, in ever-changing places, hence its name – the „Flying University”. After 1905, it became a private „Society of Scientific Courses” with laboratories attached, including a laboratory of colloidal chemistry and a radioactivity laboratory cared by Mme Curie from Paris.

4. The Jagiellonian University in Kraków and the liquefying of air

As it was mentioned above, lectures in chemistry were given at Kraków University in Polish almost without interruptions. For a certain period, the chair of chemistry was combined with the chair of pharmacy. An analysis of local water sources and those of Carpathian mineral waters remained one of the main aims of the University chemical laboratory. The most important achievement of the chemical and physical laboratories at Jagiellonian University during nineteenth century was the liquefying of air components in a static phase, achieved in 1883. At the very beginning of this year, Zygmunt Wróblewski (1845-1888), professor of physics at Jagiellonian University, returned from Paris, where he had been working for some length of time with Louis Paul Cailletet. Cailletet managed to liquefy air, but in a dynamic phase, only as a mist. Karol Olszewski (1846-1915), professor of chemistry in Kraków, proposed collaboration in attempts to liquefy oxygen and nitrogen. Olszewski was acquainted with the problem of liquefying certain gasses, as he demonstrated it during his lectures. He was as well a handy designer and maker of new instruments. He proposed and performed such modifications of the device brought from Paris, so that he could use the ethylene liquefied at reduced pressure as the cooling agent. In this way, achieved the temperature -136°C , lower than the critical temperature of oxygen. In February 1883, both scientists observed for the first time in the history of science the meniscus of the liquid oxygen and nitrogen, for the first time air was liquefied in a static phase.

After this joint success Olszewski continued to introduce new improvements, which permitted him to dispose with greater amounts of liquid gases. He thus could use liquid oxygen as a more effective cooling agent. He subsequently obtained a temperature of -213°C that enabled him to see hydrogen liquefied, but as a mist. Within ten years, Olszewski liquefied all gases known at that time, with the exception of helium and hydrogen, and solidified many of them. In 1894 he liquefied and solidified argon, sent him by W. Ramsay. At the turn of nineteenth century, the lowest

temperatures in the world were obtained in the Kraków laboratory, and liquefying laboratory devices constructed there were considered to be the best in the world and used in several European laboratories.

5. Lwów Universities, and the Petroleum and Nitrogen Industry

The strongest university centre on Polish lands in the nineteenth century, and specially in its last decade, was Lwów. During the whole century, the local university remained active with slight intervals, and in 1877 the Technical School opened in 1844, became a Technical University. Up to 1872 at these universities chemistry was taught in German, and then in Polish. Beginning from 1872, the head of the laboratory was the eminent Polish organic chemist, Bronisław Radziszewski (1838-1914), who suggested that sea flora and fauna formed the origin of the crude oil. As mentioned above, the Borysław-Drohobycz region, not far from Lwów was rich in crude oil, and many local chemists were interested in processing. In 1853, Ignacy Łukasiewicz, an alumnus of the Kraków and Vienna universities, working as a dispensing chemist in a large pharmacy of Piotr Mikolasch in Lwów, distilled the oil and extracted kerosene. In march 1853, a kerosene lamp, the first in the history of the world technology was lit in Lwów, in the window of the Mikolasch pharmacy. On the night of 31 July the same year, a patient underwent surgery in the light of kerosene lamps used in the Lwów hospital. During the next year Łukasiewicz built the first petroleum shaft, an in 1856 – the petroleum refinery first in the world, in Ulaszowice near Jasło, preceding the first American refinery Oil Creek by five years.

In the Technical School (Technical University), instructions focused more on technological problems and petroleum processing. In 1872-1880 the topic of lectures of Herman Günsberg was the petroleum and mineral wax industry as well as the production of lighting gas. In 1886 was inaugurated at the Technical University an Experimental Station for the Petroleum Industry, where petroleum of different origin and the best processing methods could be studied. It was directed by Bronisław Pawlewski (1852-1917) and from 1891 by Roman Załodziecki. After World War I, when Lwów became a part of independent Poland, from 1922 the world known specialist, Stanisław Pilat (1881-1941) presented lectures on „The Technology of Petroleum and Mineral Wax”. In 1924, he organised a new chair at the Chemical Faculty, dealing with „The Technology of Paraffin Oil and Gas Industry”.

Another member of the Chemistry Faculty staff of the Lwów Technical University, who played an important role in the development of the Polish fertilizer and nitrogen industry, was Ignacy Mościcki (1867-1946), from 1912 the head of the chair of the Chemical Physics and Technical Electrochemistry. During World War I, he constructed a factory of cyanic compounds in Borki near Jaworzno, where his invention of the circulating electric arc was applied. In 1922, leading a staff of Polish engineers directed by him returned to full production a great plant of massive synthetic ammonia, nitric acid and nitrogen fertilizers in Chorzów. In 1916, Mościcki organised in wartime in Lwów the METAN society to promote the Polish chemical industry. In 1922-26 this society was transferred to Warsaw, where it exists up to this day as the „Ignacy Mościcki’s Institute of Industrial Chemistry”.

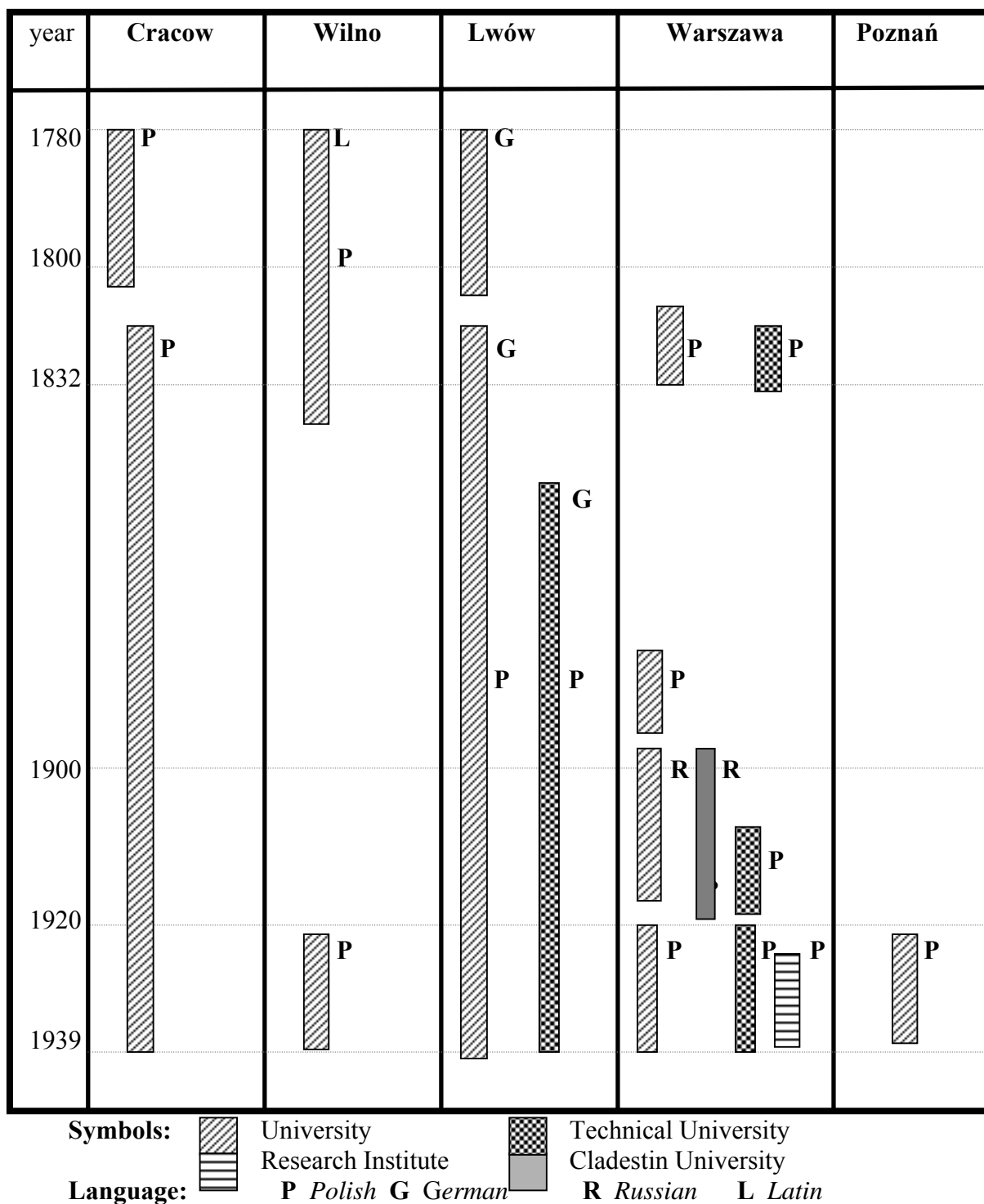
6. Other universities in the united Poland (1919-1939)

The regaining of the independence and the unification of the Polish territories after World War I created new needs and opportunities for Polish scientists. In 1915, a Polish University and Technical University were established in Warsaw. In Warsaw

Technical University, problems of sugar industry were studied by Kazimierz Smoleński. Wojciech Świątosławski developed the purification of organic substances by azeotropic methods.

Different branches of chemistry were developed in the newly opened University in Poznań and in the renowned University in Wilno.

Teaching of chemistry in Poland 1783 - 1939



INVESTIGATION OF THE PHASE TRANSITION IN POLYCRYSTALLINE $[\text{Ca}(\text{NH}_3)_6](\text{ClO}_4)_2$

Anna Migdał-Mikuli^a, Joanna Hetmańczyk^a, Łukasz Hetmańczyk^a

^a *Department of Chemical Physics, Faculty of Chemistry, Jagiellonian University, ul. Ingardena 3, 30-060 Kraków, Poland*

Abstract

$[\text{Ca}(\text{NH}_3)_6](\text{ClO}_4)_2$ has two solid phase between 95 and 295 K. The phase transition temperature at $T_C^h = 123.3$ K (on heating) and at $T_C^c = 122.0$ K (on cooling) was determined by means of differential scanning calorimetry (DSC), by extrapolating the T_{peak}^h and T_{peak}^c vs. rate of sample heating and cooling to the scanning rate value of $0 \text{ K}\cdot\text{min}^{-1}$, respectively. Room-temperature phase of this compound was analysed by means of X-ray powder diffraction. Heksaaminacalcium chlorate (VII) crystallizes in the cubic system ($\text{Fm}\bar{3}\text{m}$ space group) with cell parameter: $a = 11.685 \text{ \AA}$ and four molecules per unit cell. Fourier transform middle infrared (FT-MIR) spectra were measured in the temperature range of 20–290 K. One can observe appearing of a new band in the wavenumber range of $3100\text{--}3200 \text{ cm}^{-1}$ at the vicinity of T_C . This suggests that during the phase transition crystal structure change take place.

Introduction

Many hexaminametal(II) chlorates (e.g. Ni, Mg, Co, Cd) were investigated up to now [1-4]. All of them possess very interesting polymorphism. It was quite interesting to extend such investigations also for such complexes of metals from the second group of the periodic table. It was also interesting to compare results obtained for $[\text{Ca}(\text{NH}_3)_6](\text{ClO}_4)_2$ with previously studied $[\text{Mg}(\text{NH}_3)_6](\text{ClO}_4)_2$ compound. It was thought interesting to see whether a compound of the same type, but with different cation $[\text{Ca}(\text{NH}_3)_6](\text{ClO}_4)_2$ will possess a structure at room temperature and a phase situation similar to that of the magnesium compounds just mentioned.

Experimental

The examined compound was obtained from tetraaquacalcium chlorate(VII). The tetraaquacalcium chlorate(VII) complex placed in a quartz vessel and put in a glass tube, through which dry gaseous ammonia was blown, and the tube was placed in an oven, according to the method proposed by Smith and Koch [5]. First the tube was heated for several days up to about 400 K until all the water from $[\text{Ca}(\text{H}_2\text{O})_4](\text{ClO}_4)_2$ was lost and hexamine complex was composed. Then, after cooling the tube to room temperature, the obtained compound was put into a desiccator for several hours in order to get rid of ammonia excess.

The X-ray powder diffraction (XRPD) data, at the room temperature, were collected on a Philips X'Pert (PW1710) powder diffractometer, using graphite monochromatized $\text{CuK}\alpha$ radiation in the 2θ range of 5 to 80° , and scan step 0.02° .

The DSC measurements at 95-295 K were performed with a Perkin-Elmer PYRIS 1 DSC apparatus. The sample was placed in an aluminum vessel of mass ca. 12.70 mg and closed by compressing. Another empty aluminum vessel was used as a reference holder. Two characteristic temperatures of the DSC peaks obtained on heating and on cooling the sample were computed: temperature of the peak maximum (T_{peak}) and temperature calculated from a slope of the left-hand side of the peak (T_{onset}). These two temperatures differed by 2–4 K, what depended on the scanning rate of heating or cooling. The enthalpy change (ΔH) was calculated by numerical integration of the DSC curve under the anomaly peak after a linear background arbitrary subtraction. The entropy change (ΔS) was calculated using the formula $\Delta S = \Delta H/T_c$. For sharp peaks the values were calculated to a high accuracy (4 %), whereas for the diffuse peak they were estimations only. Other experimental details were the same as those published in our previous paper [6].

Fourier transform middle-infrared absorption measurements (FT-MIR) were performed using a Bruker EQUINOX-55 spectrometer. The temperature measurements of FT-MIR spectra at the frequency range 4000-500 cm^{-1} were carried out for the title compound for powdered sample mixed with Nujol and drifted on KBr pellet. In order to obtain the FT-MIR spectra at temperature range of 20–290 K a helium cryostats with controlled cooling rate and temperature stabilization within 0.2 K was used. The temperature of the “cold finger” was measured with an accuracy of ± 1 K, but the sample temperature could have been several Kelvin higher.

Results and discussion

Compound identification

Before the measurements were taken, the composition of the compound being studied was determined based on its calcium and ammonia content by titration using EDTA and HCl, respectively. Chemical analysis confirmed the presence of $[\text{Ca}(\text{NH}_3)_6](\text{ClO}_4)_2$. The average contents of calcium and NH_3 were found to be equal to the theoretical values within the error limit of ca. 1 % and 3%, respectively. In order to identify the synthesized compound further, the X-ray powder diffraction (XRPD) measurement was performed. The diffraction pattern obtained at room temperature can be indexed in regular system, space group No. 225 = $\text{Fm}\bar{3}\text{m} = O_h^5$, with lattice parameter $a = 11.685 \text{ \AA}$ and four formula units in the unit cell. Therefore, the results of X-ray diffraction are very similar to those obtained earlier for $[\text{Ni}(\text{NH}_3)_6](\text{ClO}_4)_2$ and especially $[\text{Mg}(\text{NH}_3)_6](\text{ClO}_4)_2$ [2, 7]. Additionally, the FT-RS and FT-MIR spectra, certified the purity of the investigated substance. Assignments of the bands of all spectra are with good agreement with literature data [8].

DSC examinations

The DSC measurements were performed both on heating and cooling a sample with a mass equal to 12.70 mg at constant rates of: 10, 20, 30 and 40 $\text{K}\cdot\text{min}^{-1}$. Fig. 1 shows the temperature dependencies of the heat flow (DSC curves) obtained while heating (upper curve) and while cooling (lower curve) of the $[\text{Ca}(\text{NH}_3)_6](\text{ClO}_4)_2$ sample at the scanning rate of 20 $\text{K}\cdot\text{min}^{-1}$. One anomaly on each of these DSC curves was registered at $T_c^h = 123.3 \text{ K}$ (on heating) and at $T_c^c = 122.0 \text{ K}$ (on cooling).

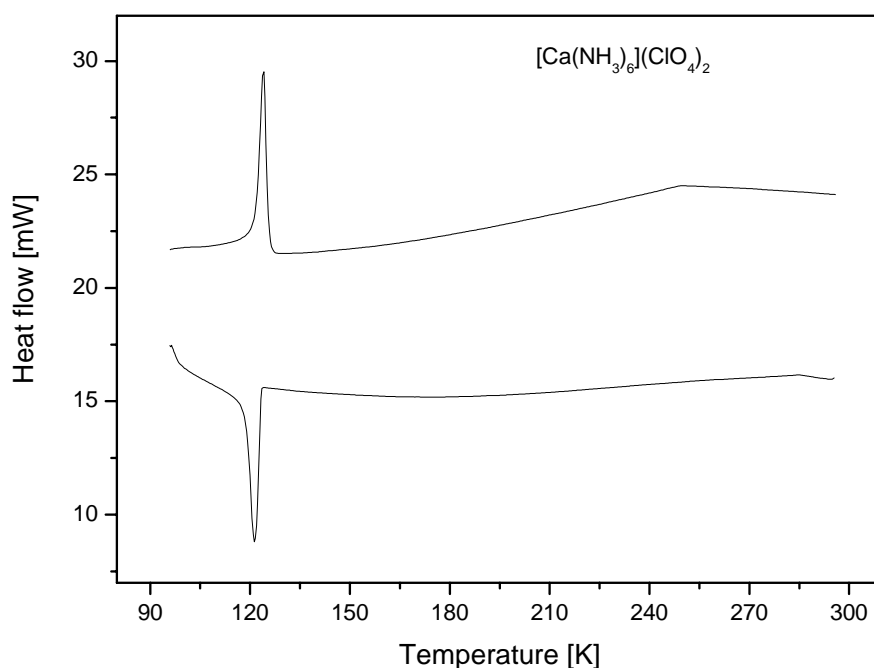


Fig. 1. DSC curves registered on heating and cooling of $[\text{Ca}(\text{NH}_3)_6](\text{ClO}_4)_2$ sample at a rate of $20 \text{ K} \cdot \text{min}^{-1}$ in the temperature range of 95 – 295 K

The presence of ca. 1.3 K hysteresis of the phase transition temperature at T_C and the heat flow anomaly sharpness suggest that the detected phase transition is a first-order one. The thermodynamic parameters of the detected phase transition are presented in Table 1.

Table 1. Thermodynamic parameters of the phase transitions of $[\text{Ca}(\text{NH}_3)_6](\text{ClO}_4)_2$

Parameters	T_c [K]	$\Delta H \pm \Delta\delta H$ [kJ/mol]	$\Delta S \pm \Delta\delta S$ [kJ/mol]
heating	123.3 ± 0.1	1.95 ± 0.22	15.8 ± 0.3
cooling	122.0 ± 0.1	1.79 ± 0.22	14.7 ± 0.3

Infrared absorption spectra vs. temperature examinations

The FT-MIR spectra were recorded during cooling of the sample at temperatures ranging from 290 to 20 K. Appearing of two new bands at the vicinity of 3200 cm^{-1} and 3100 cm^{-1} , respectively, can be noticed in the spectra in the region of the phase transition at $T_c^h = 123.3 \text{ K}$. Fig. 2. presents temperature dependencies of these two peaks positions. The appearing of these new bands suggests that the crystal symmetry is reduced.

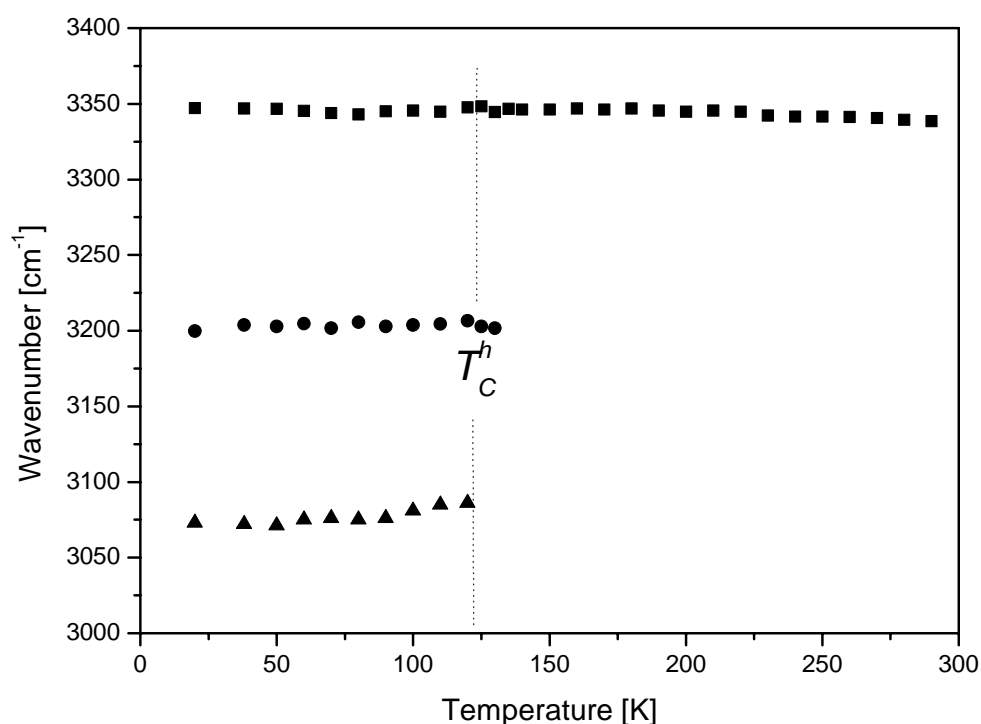


Fig. 2 . Temperature dependences of bands position in 3000–3400 cm^{-1} wavenumber range.

Concluding, at room temperature $[\text{Ca}(\text{NH}_3)_6](\text{ClO}_4)_2$ has a structure of cubic symmetry (space group: $\text{Fm}\bar{3}\text{m}$ No. 225) with four molecules in the unit cell and lattice parameter $a = 11.685 \text{ \AA}$. The crystal structure consist of octahedral $[\text{Ca}(\text{NH}_3)_6]^{2+}$ cations and tetrahedral ClO_4^- anions. $[\text{Ca}(\text{NH}_3)_6](\text{ClO}_4)_2$ is isostructural with the earlier studied $[\text{Mg}(\text{NH}_3)_6](\text{ClO}_4)_2$. The examined compound has one solid phase transition between 95 and 295 K at $T_C^h = 123.3 \text{ K}$ (on heating). Appearing of two new bands in TF-MIR spectra at the vicinity of 3200 cm^{-1} and 3100 cm^{-1} , respectively, suggests that during phase transition crystal structure changes.

References

- [1] M. Rachwalska, J.M. Janik, J.A. Janik, G. Pytasz, T. Waluta, *Phys. Stat. Sol. (a)* 16, (1973) K165.
- [2] A. Migdał-Mikuli, E. Mikuli, M. Rachwalska, S. Hodorowicz, *Phys. Stat. Sol. (a)* 47, (1978) 57.
- [3] A. Migdał-Mikuli, praca habilitacyjna, WCh UJ Kraków (1995).
- [4] A. Migdał-Mikuli, E. Mikuli, S. Wróbel, Ł. Hetmańczyk, *Z. Naturforsch.* 54(10-11), (1999) 590.
- [5] G. F. Smith, E.G. Koch, *Z. anorg. Chem.* 223, (1935) 17.
- [6] E. Mikuli, A. Migdał-Mikuli, S. Wróbel, *Z. Naturforsch.* 54a (1999) 225.
- [7] S. Hodorowicz, M. Ciechanowicz-Rutkowska, J.M. Janik, J.A. Janik, *Phys. Stat. Sol. (a)* 43, (1977) 53.
- [8] J. Fujita, K. Nakamoto, M. Kobayashi, *J. Am. Chem. Soc.* 78, (1956) 3295.

PREPARATION OF SUPPORT MATERIALS FOR SPECIALIST COURSES FOR CHEMISTRY STUDENTS

Anna Migdał-Mikuli, Paweł Bernard

The Department of Chemical Education, Jagiellonian University

Full-time chemistry courses at Jagiellonian University's Faculty of Chemistry currently take the form of uniform Masters courses. In the first two years of the course the students must attend a compulsory block of timetabled hours in core subjects and their selected majors; in the third year they choose a course profile from one of the available specialisation options; and in the fourth year they choose a group with a particular study profile within which they will prepare their Masters dissertation. They choose their specialisation courses on the basis of their selected study profile in consultation with the group in which they will be preparing their dissertation [1].

For the study profile “Physical Chemistry and Spectroscopy” students must attend lectures on “Phase Transitions in a Solid Body” (among others). These lectures are particularly important for students who would like to write a Masters dissertation in the Phase Transition Research Group in the fifth year. The option of writing a dissertation in this group and therefore enrolling in this course is also open to students of related subjects e.g. Biophysics, Environmental Protection, Material Engineering, as well as PhD students from Jagiellonian University and other institutions (AGH University of Science and Technology, Cracow University of Technology).

The course focuses on various methods of analysing phase transitions such as:

- adiabatic calorimetry,
- differential scanning calorimetry,
- Raman spectroscopy,
- IR spectroscopy,
- quasielastic neutron scattering,
- nuclear magnetic resonance,
- electron paramagnetic resonance,
- Mössbauer spectroscopy.

The students are expected to possess basic knowledge of these methods. For example, from the field of oscillation spectroscopy students should know the harmonic and anharmonic oscillator models and their mathematical descriptions and be able to analyse infrared spectrums on the basis of their shape and band arrangement. Due to the limited time available (30 teaching hours) only a brief recapping of these elementary topics is possible. New material introduced in lectures on infrared spectroscopy includes the concepts of correlation functions and correlation time and the form of graphs of reorientation correlation functions.

Students often have difficulty understanding the content of lectures (especially those studying non-chemistry subjects) due to a lack of basic knowledge. The considerable

differences in ability levels and the limited time available for recapping means that the material covered in the course is often considered too difficult or incomprehensible.

A questionnaire was conducted amongst course participants to gauge the students' knowledge of the topics in question and their opinions concerning their difficulty level and the level of detail of their presentation. The questionnaire below concerns topics associated with calorimetric methods for analysing phase transitions. It should be emphasised that calorimetric methods are among the most important research methods for analysing phase transitions in solid bodies, which is why they and the basic physics and chemistry they involve were dealt with in some detail during the course.

Topic	Previous knowledge of topic	Degree of difficulty of topic	Presentation of topic
1. System types and parameters	2.56	1.33	1.78
2. Basic thermodynamic functions	2.33	1.67	1.78
3. Principles of thermodynamics	2.11	2.00	1.89
4. Relationships between thermodynamic functions	1.89	2.33	1.56
5. The concept of molar heat capacity and its various types	2.22	1.89	1.78
6. Gibbs' phase rule	2.22	1.78	1.78
7. Forms of graphs for phase transitions described using various thermodynamic functions	1.56	3.00	2.00
8. Classification of phase transitions according to Ehrenfest	1.22	3.00	2.22
9. Types of polymorphism (enantiotropy, monotropy)	1.56	2.22	2.00
10. The contribution of various effects to specific heat	1.22	3.22	2.22
11. The concept of the phonon	1.56	2.56	2.00
12. Landau classification of phase transitions	1.33	3.33	2.22
13. The order parameter and its relationship to temperature	1.56	3.44	2.11
14. Pseudomorphism	1.33	2.56	2.11
15. Adiabatic calorimetry – the method	1.89	2.33	1.89
16. Adiabatic calorimetry – application	1.67	2.33	2.22
17. Scanning calorimetry – the method	1.67	2.89	2.33

Previous knowledge of topics:

1 – unknown

2 – known, recapping required

3 – known, recapping not required

Degree of difficulty of topics:

- 1 – very easy
- 2 – easy
- 3 – moderately difficult
- 4 – difficult
- 5 – very difficult

Presentation of topics:

- 1 – too detailed
- 2 – appropriate for the difficulty level
- 3 – insufficiently detailed

The results of the questionnaire showed that the students believed recapping to be necessary for all the topics except “System Types and Parameters”, which is introduced in secondary schools in classes with an extended chemistry profile. Many of the students rated the other topics as 'known, recapping required' (12 topics) or 'unknown' (4 topics). The way the students rated the difficulty level of the topics presented was also indicative of the state of their knowledge: out of the 13 topics rated 'known, recapping required' 8 were rated as being easy or very easy and 4 as being of medium difficulty. This demonstrates that the students are aware that they have shortcomings even in elementary topics. It should also be noted that, as was previously mentioned, detailed recapping of calorimetry topics was considered by the students to be necessary in view of the difficulty level of the topic, while in the case of topics rated 'unknown' by most students there were requests for even wider discussion.

In response to this clear lack of knowledge the Department of Chemical Education of Jagiellonian University in co-operation with the Phase Transition Research Group is preparing a multimedia programme to help students cope with the material covered in the course in question. The content of the programme has been divided into sections describing the various research methods presented during lectures. Each section is also divided into two subsections entitled:

- “What you should already know” – material which the students should be familiar with before attending lectures,
- The Lecture – material introduced in lectures, presented using various multimedia techniques.

The programme can therefore be used by students to prepare for lectures, which it is hoped will allow them to gain a better understanding of new material [2]. Of course an educational aid of this kind does not free the lecturer completely from the need to recap elementary material, but it should improve the productivity of lectures and allow more time to be spent on new or particularly challenging material.

Up till now because of the wide range of research methods introduced during the course students have had to make use of a large number of reference works. Also, because of the advanced level of the lectures the information they require is often contained in specialised monographic publications which can be extremely hard to find. Collecting

all the material in this single source will therefore allow the students much better access to the knowledge they need. The multimedia format of the programme also has many features designed to motivate the students to work independently and learn more effectively, using various forms of communication and illustrating topics via animation, films and moving models complete with audio commentary [3].

As well as the multimedia programme, which is designed for independent study, multimedia lectures are also being prepared. There are also plans to develop laboratory exercises, the instructions and required preparation for which will be included in the programme, as well as multimedia tests allowing students to assess their own progress and therefore better prepare themselves for exams or credit requirements.

Literature:

- [1] Informator ECTS, chemia, Uniwersytet Jagielloński, Kraków 2001
- [2] A. Migdał-Mikuli, P. Broś, in: Annals of the Polish Chemical Society Year 2005 vol. II, str. 504
- [3] A. Burewicz, H. Gulińska, Dydaktyka chemii, UAM Poznań 2002, str. 426

Application of La-2,2'-bipyridyl-bengal rose for preconcentration and determination of microelements in water

Barbara Mikula, Barbara Feist, Bożena Puzio

*Department of Analytical Chemistry, Institute of Chemistry, University of Silesia,
40-006 Katowice, 9 Szkolna Rd, Poland*

Preconcentration and separation methods are widely used in the analysis of trace ions prior to their determination by atomic spectrometry.

Co-precipitation is one of the most efficient separation methods for trace heavy metals ions. The main requirement for this technique is that collector should separate easily from matrix solution. This can be done by filtering, centrifuging and washing the precipitate.

The principle of co-precipitation is based on the precipitation of the analyte ions using inorganic or organic collectors. This technique has been widely applied in preconcentration procedure for determining trace heavy metals in water samples.

As co-precipitation collectors are used, for example: manganese dioxide [1-5], aluminum [6], cerium [7], gallium [8] or indium [9] hydroxide. As for organic carriers, the following have been used: copper diethyldithiocarbamate [10], sodium diethyldithiocarbamate [11, 12].

In the present study, La-2,2'-bipyridyl-bengal rose was used as co-precipitant in order to determine the traces of Cd, Cu, Pb, and Zn in various water samples by FAAS.

EXPERIMENTAL

Reagents and apparatus

All solvents and reagents were of analytical reagent-grade. Water was purified with an Elix 3 system (Millipore, USA).

Flame atomic absorption spectrometer (SOLAAR M6 TJA Solutions) was used for the determination of the analyte ions aqueous solutions. Analytical lines: Cd (228.8 nm), Co (240.6 nm), Cu (324.8nm), Ni (232.0 nm), Pb (217.0 nm), Zn (213.9 nm), measuring pipette 200-1000 μ L, 1-5 mL, 1-10 mL, LW-8 water bath (SWL Bytom), N-1570 pH - meter (Mera-Elwro, Wrocław) with a glass ESAGP-309 electrode, centrifuge MPW-350.

Preconcentration procedure

0,5 mg of lanthanum was added to the solution which contained a mixture of Cd, Cu, Pb, and Zn, then 2 mL of 2,2'-bipyridyl and erythrosine solution with concentration of 0,01 mol/L were added, then pH was determined due to appropriate buffer and the sample was completed with deionized water up to constant volume (50, 100 or 200 mL). The obtained samples were heated on the water bath for 20 min. in the temperature of 60 °C. Deposits formed under these conditions were centrifuged, the solution was decanted and the deposit of ion-association complexes was digested in 1 mL of ammonia solution with concentration 1+1 and it was completed with deionized water up to the volume of 10 mL. The obtained solutions were analysed by means of FAAS method, using the worked out programme of simultaneous determining Cd, Cu, Ni, and Zn, and taking into account correcting standards containing reagents' matrix.

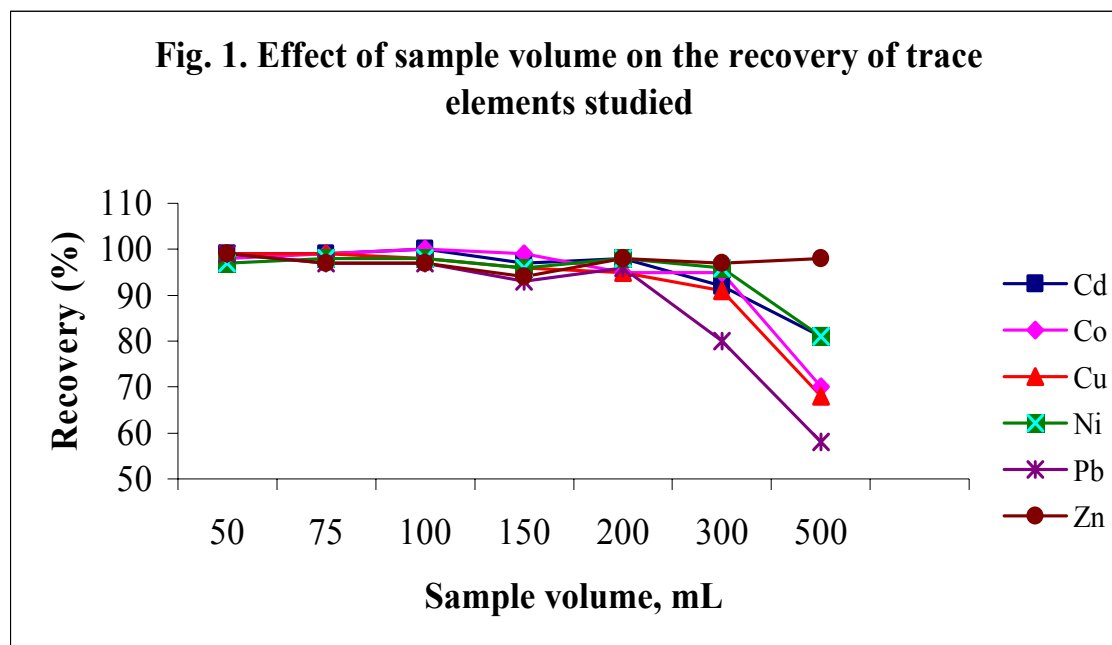
Water samples were preconcentrated from volume of 200 mL after filtration through paper filter.

RESULTS AND DISCUSSION

Optimization of the method

In order to optimize conditions for simultaneous preconcentration of Cd, Co, Cu, Ni, Pb, and Zn, the influence of such factors as pH, the molar ratio of 2,2'-bipyridyl to the bengal rose, the time and the temperature of deposit heating, the way of digesting of the ion-association complexes, and the sample volume on the recovery of the analytes was examined. The La-2,2'-bipyridyl-bengal rose ionic associate precipitates in acidified media. Influence of pH in the range of 2÷7 was examined. In the pH range of 3÷4,5 the analytes recoveries were of 95÷100 % range. At pH higher than 5.0, the precipitate does not form. pH=4 was chosen as an optimum value and it was applied in further studies. The amount of chelating agent and the dye necessary for preconcentrating appropriate metals, using the developed method, was tested by analysing the molar ratio of the reagents mentioned above. The molar ratio 1:1 turned out to be optimum for the tested system. Considering the effect of time and temperature on precipitating deposits, there is no clear influence of these factors on the determination results. Because of separating deposit through centrifuging, the deposit should undergo the process of ageing in the increased temperature, what makes its decantation easier.

The effect of sample volume on the recovery of the analytes was investigated, using different volumes (from 50 to 500 mL). The results of the recovery studies are given in Figure 1.



Basing on the obtained results, it was found that the analytes might be preconcentrated with a satisfactory recovery from volume of 300 mL, excluding Pb, which had a recovery of 80 % from this volume. Using volume of 500 mL, satisfactory result was obtained only for Zn.

The results of the recovery studies, detection limit and sensitivity are given in Table 1 and 2.

Table 1. Analytical characteristics of the F-AAS method

	Cd	Co	Cu	Ni	Pb	Zn
Concentration range [mg·L ⁻¹]	0.05-0.50	0.10-0.50	0.50-5.00	0.25-2.50	0.50-2.50	0.50-5.00
R	0.995	0.9926	0.9994	0.9994	0.9988	0.9978
LOD [mg·L ⁻¹]	0.0022	0.0012	0.0041	0.0016	0.0012	0.0094
Sensitive [mg·L ⁻¹]	0.0717	0.0192	0.0261	0.0180	0.0098	0.0690

LOD –detection limit, calculated as three times the standard deviation (3σ)

Table 2. Results of multi-elemental analysis F-AAS method after preconcentration using carrier. Sample volume: 200 mL, final volume: 10 mL. Added 2 µg Cd and Co, 10 µg Pb and Ni, 20 µg Cu and Zn; n = 10

	Cd	Co	Cu	Ni	Pb	Zn
Determined [µg]	1.99	2.01	19.62	9.83	9.70	19.50
Recovery %	100	100	98	98	97	97
RSD [%]	1.47	2.14	1.17	1.11	1.61	1.04
µ ₉₅ = X±t·s	1,47±0,025	2,01±0,036	19,62±0,19	9,83±0,09	9,70±0,13	19,50±0,17

APPLICATION

Co-precipitation method with La-2,2'-bipyridyl-bengal rose was applied to tap water from Katowice, snow water from an allotment garden in Katowice and river water (Rawa). Cd, Cu, Pb, and Zn were determined in the investigated samples. The results are given in Table 3.

Table 3. Results of determining Cd, Cu, Ni using F-AAS after preconcentration of waters (n = 8), p = 95 %

Samples	Added [µg/200 mL]				Measured [µg/200 mL]			
	Cd	Cu	Pb	Zn	Cd	Cu	Pb	Zn
tap water	0.50	4.00	1.00	-	0,69±0.03	8,95±0.13	0.99±0.07	9.44±0.89
snow	0.50	4.00	1.00	-	0,84±0.04	13.99±0.26	0.98±0.11	14.78±0.37
Rawa river	-	-	-	-	1.73±0.09	18.44±0.52	9.15±0.83	32.28±1.05

Co-precipitation with La-2,2'-bipyridyl-bengal rose has been successfully applied to the determination of trace amounts of Cd, Co, Cu, Ni, Pb, and Zn in water samples, with acceptable accuracy and precision. Recovery percentages of the analytes amount to more than 90%. The proposed method is inexpensive and fast.

REFERENCES

- [1] V. Umashankar, R. Radhamani, K. Ramadoss, D.S.R. Murty, *Talanta* 57 (2002) 1029.
- [2] K.M. Matthews, *Anal. Lett.* 16 (1983) 633.
- [3] G.A. Peck, J.D. Smith, *Anal. Chim. Acta*, 422 (2000) 113.
- [4] P.H. Towler, J.D. Smith, D.R. Dixon, *Anal. Chim. Acta*, 328 (1996) 53.
- [5] M.S. Bispo, M.G.A. Korn, A.C.S. Costa, E.S.B. Morte, L.S.G. Teixeira, M. Korn, *Spectrochim. Acta* 60B (2005) 653.
- [6] G. Doner, A. Ege, *Anal. Chim. Acta*, 547 (2005) 14.
- [7] U. Divrikli, L. Elci, *Anal. Chim. Acta*, 452 (2002) 231.
- [8] T. Akagi, H. Haraguchi, *Anal. Chem.* 62 (1990) 81.
- [9] U. Sahin, S. Tokahoglu, S. Kartal, A. Ulgen, *Chem. Anal. (Warsaw)* 50 (2005) 529.
- [10] H. Chen, J. Jin, Y. Wang, *Anal. Chim. Acta*, 353 (1997) 181.
- [11] D.M. Hopkins, *J. Geochem. Explor.* 41 (1991) 349.
- [12] D. Atanassova, V. Stefanova, E. Russeva, *Talanta*, 47 (1998) 1237.

‘...A PHARMACIST COMES TO A CHEMIST...’
– AN EXAMPLE OF CONTEXT BASED LEARNING

Jakub M. Milczarek¹, Iwona Maciejowska², Stanisław Walas¹

¹*Jagiellonian University, Faculty of Chemistry, Department of Analytical Chemistry*

²*Jagiellonian University, Faculty of Chemistry, Department of Chemical Education,
Ingardena 3, 30-060 Kraków, Poland*

Introduction

Curricula of chemistry thought at university level do not refer enough to authentic questions which inflame students and which they may meet in the professional life. On the contrary in Context - Based Learning (CBL) teachers choose real-life situations to show the application of chemistry. This rise motivation and enthusiasm of our students and provides a starting point of development for chemical concepts and competencies. Teaching chemistry within an applied context is gaining in popularity in many countries [1-4]. There is a vast number of possible contexts which can be used in chemistry teaching and learning process: environmental, industrial, forensic, analytical, and pharmaceutical.

CBL is included in wider conception called Problem Based Learning (PBL), which also takes into account that problems are encountered before all relevant knowledge has been acquired. Many studies have argued that problem – based learning makes students more engaged in learning because they feel they are empowered to have an impact on the outcome of the investigation. PBL offers students an obvious answer to the questions ‘why do we need to learn this?’ and ‘what does what I am doing in school have to do with anything in the real world?’[5].

PBL (and CBL) in analytical chemistry is not a new concept e.g. in the 1960s, Herbert Laitinen (USA) began focusing undergraduate analytical chemistry curriculum development on problem solving [6]. Recently, Simon Belt (UK) has developed problem solving case studies for students of analytical chemistry courses [7].

The problem

The course of Analytical Chemistry (Part Two – Instrumental Analysis) at Jagiellonian University, Faculty of Chemistry consists of 10 different exercises. Each of them concerns different analytical instrumental problem. The goal of one of these exercises is to acquaint students with basics of the electro analytical techniques and detection of titration equivalence point.

Usually this kind of exercise ‘brings no smile on students’ faces’ as they do not understand that in the simplicity and straightforward form of this kind of experiments lies the essential knowledge and practical skills needed to become a good chemist. In order to change that approach some innovation to the course should be introduced.

New approach

The quality of teachers' work can be always verified by the students' progress in understanding and solving given problems. Such approach involves constant research on new methods of teaching targeted at the maximization of this effect. These can be accomplished by formal, metrological, organisational or technical efforts. Unquestionably, one of the most vital elements of such work is usage of very widely understood students stimulating techniques, far from didactical conservatism, cognitive eclecticism or tiresome scholasticism.

Undoubtedly the simplest way of achieving this goal is to introduce the concept of solving a real-live scientific problems into academic courses. These problems must be characterized by probability so to induce genuine student involvement in planning its solving.

Exercise project

The new exercise plan consists of five stages, all described bellow and depicted on Fig.1.

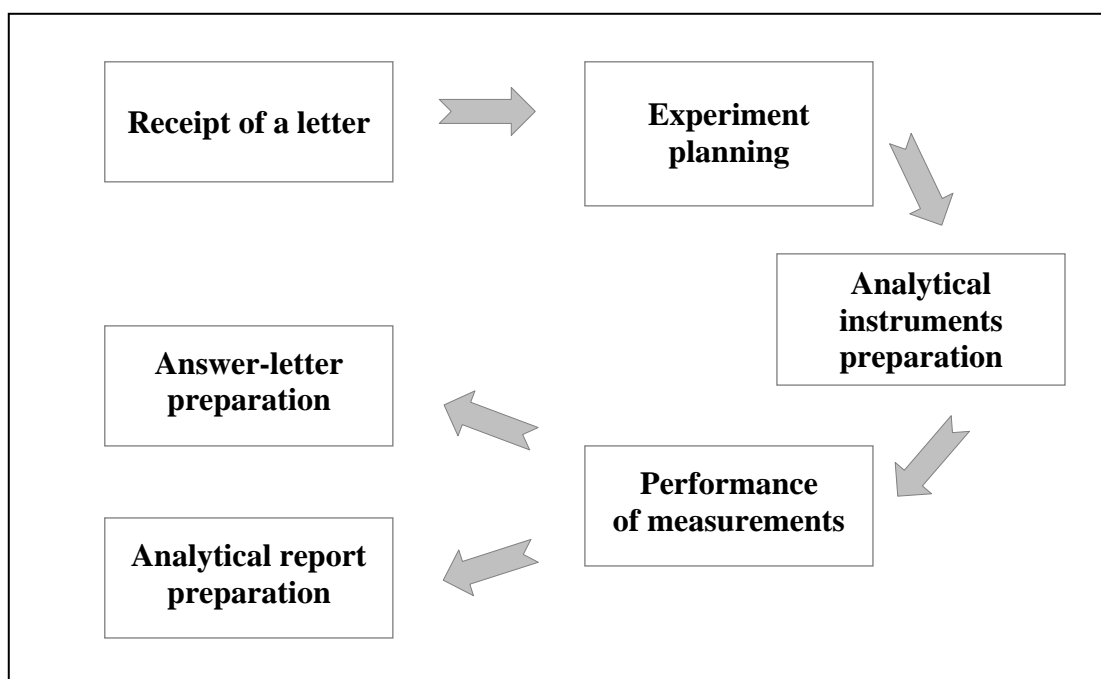


Fig. 1. Plan of the new approach

At the beginning of the exercise students receive a letter and a bottle of iodine tincture from a pharmacist for testing. In this letter they are asked to check the concentration of iodine in iodine tincture and juxtapose their results with provide current norm.

At the second stage students are asked to plan experiments. Firstly they need to check the available equipment in the laboratory which involves recognising different analytical instruments. Then, basing on their theoretical knowledge, they decide which techniques and tools should be used.

After that decision all automatic and semiautomatic devices must be checked in order to make any accident impossible and ensure that the operational principles are fully understood by all. Moreover, at this stage, students performing an exercise are asked to build a simple electrochemical devices based on electrical shames (Fig.2) from provided:

- battery (1);
- volt-meter (2);
- amperometer (3);
- electrodes (4);
- potentiometer;
- some cables with connectors.

The idea is similar to that of building Lego® constructions. From this elements more than three different devices can be assembled.

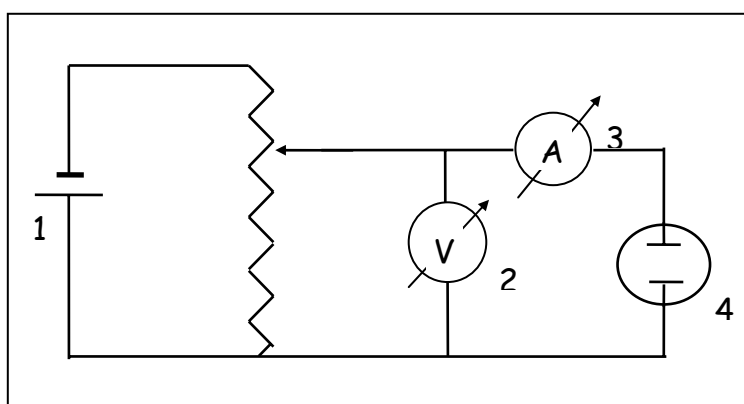


Fig. 2. An example an electrical shames

The next stage consists of performing exercise itself and collecting the vital data. That requires not only students' focused attention but also keep teacher alert as some small accidents may occur at this moment. Moreover it is important to ensure that all of the gain, printed or written information is properly labelled and described in the lab-book, so that no chaos is introduced and it is easier, for students, to write a proper and comprehensible analytical reports at home.

As a final stage students must write two documents. One of them is typical analytical report similar to the ones they are very familiar with (e.g. they came across it during inorganic chemistry or physical chemistry laboratories) and therefore it is a very common task. The second document is a letter. It should be an answer for the question given at the begging of the experiment. Because for most of the students it is a novelty, it intrigues them and gives opportunity to "show off".

Advantages and few disadvantages

Advantages:

- work conditions and tasks similar to real life problems;
- possibility of soft skills development;
- growth of (even poor) students attendance and interest during exercise;
- increase of cooperation within the student group;
- decrease of routine in teachers work.

Disadvantages:

- problems caused by performing different teaching method than cook-book chemistry;
- uncertainty that students dislike very much;
- poor communicational skills could be frustrating in putting everything together in the process of solving such problems.

Conclusions

Example of „Teaching and learning in context” described above is a verified in practice way to activate a group of students in order to solve not a trivial problem. This activity engages students’ ingeniousness, withdraws an excess of often abused didactics and employs elements of intellectual games.

The task given to the students is a mundane analytical chemistry problem consisting of instrumental measurement of concentration of iodine in pharmaceutical product such as iodine tincture. Methods used for solving given problem and ways of analysing collected data depends in great manner on student’ choice. That concerns for example students independence in constructing simple sets for electrochemical measurements based only on shames.

Not so typical, but nevertheless, very efficient element of this task is the need for students to write an answer to the letter given at the beginning of the classes. This, is a real life letter written by a pharmacist, owner of a drug store. The answer letter produced by students verifies their communication skills - formulating direct answers and proper conclusions about performed experiments and collected analytical data.

The above mentioned example is one of many that can be found when attending university courses such as the Analytical Chemistry (Part Two - Instrumental Analysis) at the Jagiellonian University, for instance: a coin composition analysis to prove its authenticity (ASA), soil composition analysis in order to detect pollution (ASA), drugs quality check (TLC) etc.

In one word all this effort is for students, to make links between different subject areas, do develop higher order thinking skills and so called key skills (team working, decision making, problem solving, communication, presentation etc.) and to strengthen self-directed learning.

References:

- [1] Eubanks L., Middlecamp C., Pienta N., Heltzel C., Weaver G., Chemistry in Context. Applying Chemistry to Society, 5th Ed., Mc Graw Hill, 2006
- [2] Hill, G., Holman, J. *Chemistry in Context*. Cheltenham: Nelson. (2000).
- [3] Demuth R., Gräsel C., Parchmann I, Ralle B. Chemie im Kontext, <http://www.chik.de/>
- [4] Salters Advanced Chemistry Project. *Chemical Storylines; Chemical Ideas; Activities and Assessment Pack*. Oxford: Heinemann Education. (1994)
- [5] Yuzhi W., Using problem-based learning in teaching Analytical Chemistry, *The China Papers*, July 2003, <http://science.uniserve.edu.au/pubs/china/vol2/wangyuzhi.pdf>
- [6] Wilson G. S., Anderson M., Lunte C. E Instrumental Analysis at the University of Kansas: An Experiment in Problem-based Learning. *Analytical Chemistry*, (1999), 71, 677A-681A
- [7] Belt S. T. , Evans, E. H. A problem based learning approach to analytical and applied chemistry, *University Chemistry Education*. (2002)

STUDIES OF THE REACTION OF N³-SUBSTITUTED AMIDRAZONES WITH PYRIDINE 2,3-DICARBOXYLIC ANHYDRID

Bożena Modzelewska-Banachiewicz^{a,b*}, Monika Prus^a

^a *Department of Organic Chemistry, Collegium Medicum, Nicolaus Copernicus University
M. Skłodowskiej-Curie 9, 85-094 Bydgoszcz, Poland*

^b *Department of Organic Chemistry, The Feliks Skubiszewski Medical University, Staszica 6.
20-081 Lublin, Poland*

*author to whom correspondence should be addressed

Abstract

The studies of the course of reaction of N³-substituted amidrazones with pyridine 2,3-dicarboxylic anhydrid demonstrated the influence of amidrazone substituents on the direction of the reaction.

Introduction

The amidrazones can be regarded as the reaction products of acidic thioamides with hydrazine and its derivatives. These compounds have basic character, which is attributed to the amide nitrogen atom [1]. Nitrogen atoms of amidrazone group are the potential site attack of the electrophilic agents.

In case of N³-substituted amidrazones, N¹ and then N³ nitrogen atoms are most susceptible for attack of electrophilic agents. At the same time carbon-nitrogen bonds are polarized and makes amidrazone carbon atom low electron density center. Such configuration enables those atoms for the reactions with nucleophilic agents.

Hindered synthesis, apparent in low yields and side reactions, is the major limitation of amidrazone use [2].

Most frequently amidrazones are used as substrates to synthesis of heterocyclic systems derivatives: five-membered [3, 4], six-membered [4, 5], seven-membered [6], and condensed systems [7].

Reactions carried out on N³-substituted amidrazones as free bases with: ammonium isothiocyanate [8], aliphatic and aromatic isothiocyanates [9, 10], N-arylsulfonyl- and iminodithiocarbonate acid dimethyl esters [11], acetylen dicarboxylic acid dimethyl ester [12], acids and chlorides [13] lead to formation of 1,2,4-triazole system derivatives. In those researches, the authors demonstrated the formation of by products from amidrazone decomposition. This decomposition depends on both reaction conditions and substituents on N¹ and N³ nitrogen atoms. In reaction of amidrazone and ammonium isothiocyanate e.g., there was proved the influence of amidrazone substituents on direction of the reaction:

- phenyl substituents – lead to formation thiosemicarbazide system, which cyclized in butanol to 1,2,4-triazole-5-thiol derivatives;
- substituent of basic character – the reaction occurred with 3,5-di-(2-pyridyl)-4-phenyl-1,2,4-triazole formation (which was formed from amidrazone decomposition).

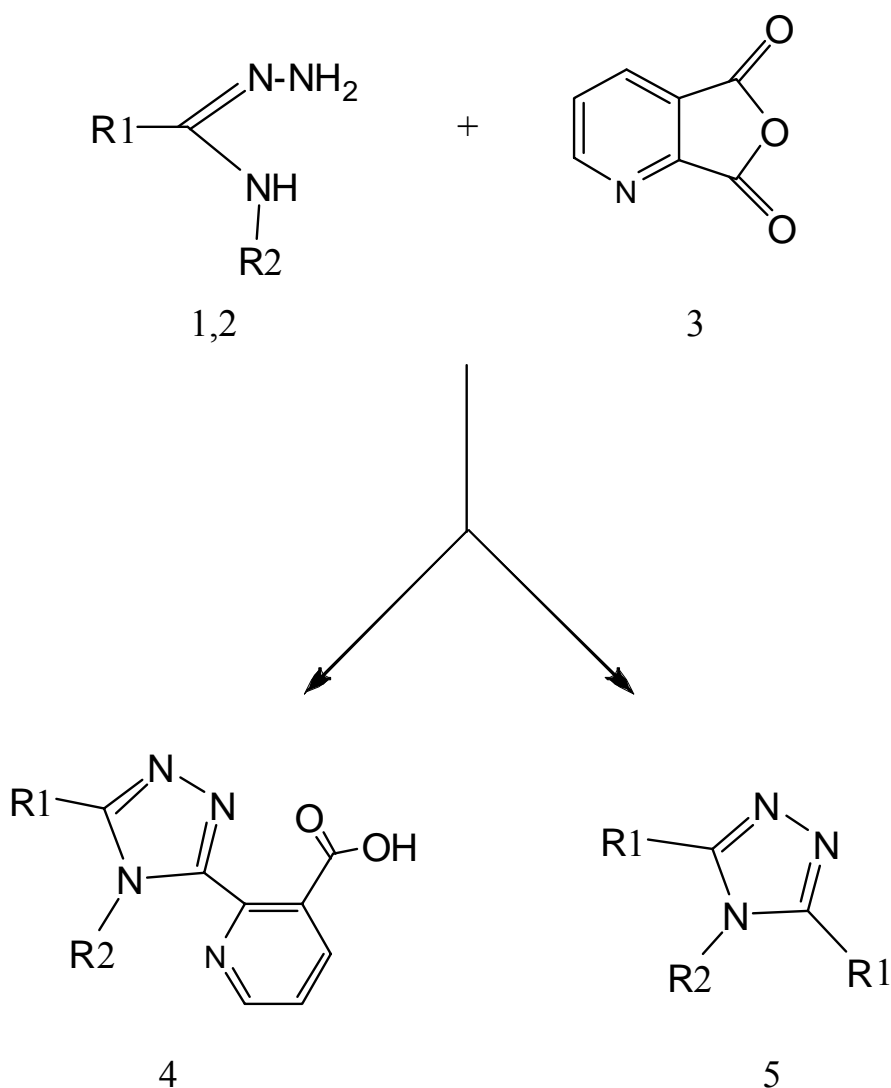
There were noted also the reactions of amidrazones with organic acids, where the influence of the environment on their course was remarkable. In the presence of acetic acid the reaction occurred in two directions. Aside from 3-(2-pyridyl)-4-phenyl-5-methyl-1,2,4-triazole, 2,3,5,6-tetrazine derivative was obtained as a product of amidrazone decomposition. The reaction of amidrazones with maleic anhydride lead to formation of Z 3-(2,4-diaryl-1,2,4-triazolo) propenoic acid [14]. The reaction occurred in one direction, in anhydrous diethyl

ether, in room temperature. The influence of amidrazone substituents was not observed.

The paper presents the reaction of N³-phenyl-(2-picolin)-amidrazone **1** and N³-(2-pyridil)-2-picolin amidrazone **2** with pyridine 2,3-dicarboxylic anhydride **3**. The reaction was carried out in anhydrous ether at the room temperature.

The structures of obtained compounds were confirmed by elementary and spectral analysis. In the IR spectra of compound **4** characteristic absorption bands for the C=O group in the range 1703 cm⁻¹ were observed.

In the ¹H NMR spectrum for compound **4** occurs wide signal of the protons of carboxyl group in the range 13.1 ppm. The signals in the range 7.0-8.8 ppm were attributed to aromatic protons.



	R1	R2
1,4	2-C ₅ H ₄ N	C ₆ H ₅
2,5	2-C ₅ H ₄ N	2-C ₅ H ₄ N

Experimental part.

Melting points were measured on a Boetius apparatus and are given uncorrected in Table 1. ^1H NMR spectra were recorded on a Tesla BS 567A (300 MHz) apparatus in D_6 -DMSO with TMS as an external standard. IR spectra were recorded on a Specord IR- 75 spectrometer. Results of elemental analysis for C, H, N by microanalysis method were in accordance with the calculated values: $\pm 0.7\%$ for C, 0.75% for N and 0.9% for H.

Synthesis of 3,4-diaryl-5-(3-carboxy-2-pyridyl)-1,2,4triazole **4**.

Amidrazone **1** (0,01 mole) was dissolved in 30cm^3 anhydrous diethyl ether. 0,01mole of pyridine 2,3-dicarboxylic anhydride **3** was added. The mixture was then left in room temperature for one week. The precipitated solid was then filtered and washed with diethyl ether and purified by crystallization from methanol. The product **4**, with melting point at $250\text{-}252^\circ\text{C}$, was obtained with 48% yield (1,6g).

Spectral analysis:

IR (KBr, cm^{-1}): 2970 arom, 1703 C=O

^1H NMR (D_6 -DMSO -, δ ppm): 13.1 (s, 1H, COOH), 7.0-8.8 (m, 12H, ar)

Filtrate after separation of **4** was evaporated under pressure and solid residue was then extracted with absolute ethanol. After concentration of extract pyridine 2,4-dicarboxylic acid (of melting point at 174°C) precipitated

Synthesis of 3,4,5-triarylo-1 ,2,4-triazole **5**.

Amidrazone **2** (0,01 mole) was dissolved in 30cm^3 anhydrous diethyl ether. 0,01 mole of pyridine-2,3-dicarboxylic anhydride **3** was added. The mixture was left in room temperature for one week. The precipitated solid was then filtered, washed with diethyl ether and mixed with 10cm^3 of 10% water solution of potassium hydrocarbonate. Solid, insoluble in solution of potassium hydrocarbonate, was filtered. The product compound **5**, with melting point at $198\text{-}200^\circ\text{C}$, was obtained with 49% yield (1,5g).

Spectral analysis:

IR (KBr, cm^{-1}): 3054 arom, 1616 C=N

^1H NMR (D_6 -DMSO, δ ppm): 7.2-9.2(m, 12H, ar)

References.

- [1] T. Bany, Polish J. Chem., 42 (1968) 247,
- [2] D. G. Nielson, R. Roger, J. W. M. Heatle, L. R. Newlands, Chem. Rev., 70 (1970) 171,
- [3] G. Cerioni, M. T. Cocco, C. Congiu, a. Maccioni, J. Heterocyclic Chem., 18 (1981) 1379,
- [4] K. N. Zelenin, O. Solod, w. Khrustaler, Khim. Geterostikl. Soedin, (1989) 827,
- [5] H. Neunhoeffer, B. Klein-Cullman, Justus Liebiges Ann. Chem., 12 (1992) 1271,
- [6] M. Takahashi, N. Sugawara, K. Yoshimuro, Bull. Soc. Jpn., 50 (1977) 957,
- [7] L. Strzemecka, Polish J. Chem., 64 (1990) 157,

- [8] B. Modzelewska, H. Szumiłło, *Acta Polon. Pharm.*, 53 (1996) 213,
- [9] B. Modzelewska, *Ann. UMCS Sec. AA* 41 (1986) 45,
- [10] B. Modzelewska, *Ann. UMCS Sec. AA* 41 (1986) 53,
- [11] B. Modzelewska-Banachiewicz, D. Matosiuk, *Pharmazie*, 54 (1999) 588,
- [12] B. Modzelewska, T. Kamińska, *Eur. J. Med. Chem.*, 36 (2001) 93,
- [13] B. Modzelewska, *Ann. UMCS Sec. AA* 48/49 (1993/1994) 171,
- [14] B. Modzelewska-Banachiewicz, J. Banachiewicz, A. Chodkowska,
E. Jagiełło-Wójtowicz, L. Mazur, *Eur. J. Med. Chem.*, 39 (2004) 873.

NUTRIENT COMPOUNDS IN ODRA RIVER

Możejko Janina

*Institute of Chemistry and Environmental Protection of Szczecin University of
Technology, Al. Piastow 42, 71-065 Szczecin*

Introduction

The concentrations of nitrogen and phosphorus compounds are well known to play a key role in determining the ecological status of aquatic system [1-5]. The present paper is concerned with time series analysis of nutrient compounds concentrations in the Odra River. This analysis has been increasing on examining the ratio in which these elements occur. The main aim of this study is to analyze trends in nutrient variables and their seasonal variations in Odra River. All analyses were performed using the computer software Statistica 6.1.

Data sets

Nutrient variables used in the study were obtained at the measuring point in Szczecin between 1996 and 1999. The data were collected every over week by the National Inspection Board for Environmental Protection in Szczecin. Total Kjeldahl nitrogen (N_{Kj}), nitrate ($N-NO_3$), nitrite ($N-NO_2$), total-nitrogen (N), total-phosphorus (P) and orto-phosphate (PO_4) concentrations were investigated in detail. From these measurements N_{Kj}/N , $N-NO_3/N$, $N-NO_2/N$, $P-PO_4/P$ fractions and of N/P , $N-NO_3/P-PO_4$ ratios were calculated. N/P and $N-NO_3/P-PO_4$ ratios were calculated using values based on mass. Figure 1 and 2 show plots of analyzed variables over time. All variables are characterized by strong seasonal fluctuations. From Fig.2 can be seen that total Kjeldahl nitrogen and nitrate fractions in total nitrate changed from 14 to 85 %, whereas $N-NO_2/N$ fractions are less then 2 %. Percentages of orto-phosphate in total phosphorus varied from 5 to 60 %. Large seasonal variations in N/P and $N-NO_3/P-PO_4$ ratios are observed as well (4.5 – 57 and 2.5-322 respectively).

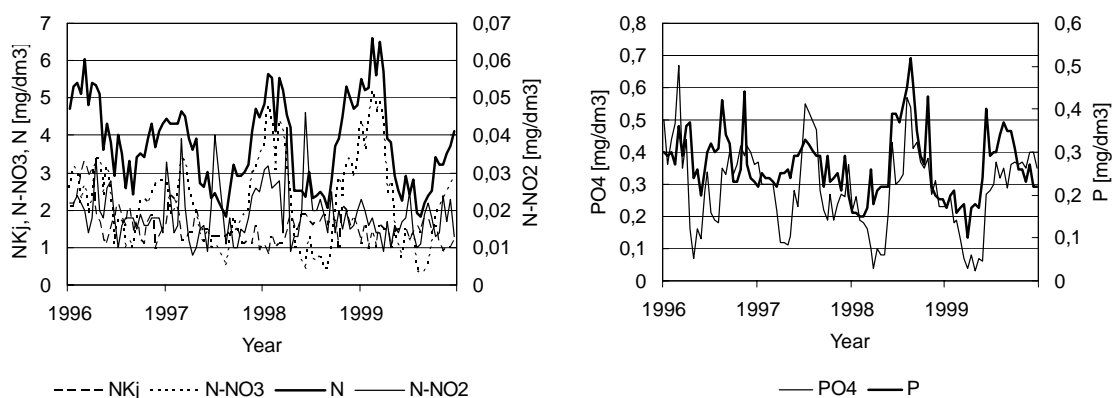


Fig.1. Nutrient concentrations in Odra River in the years 1996-1999

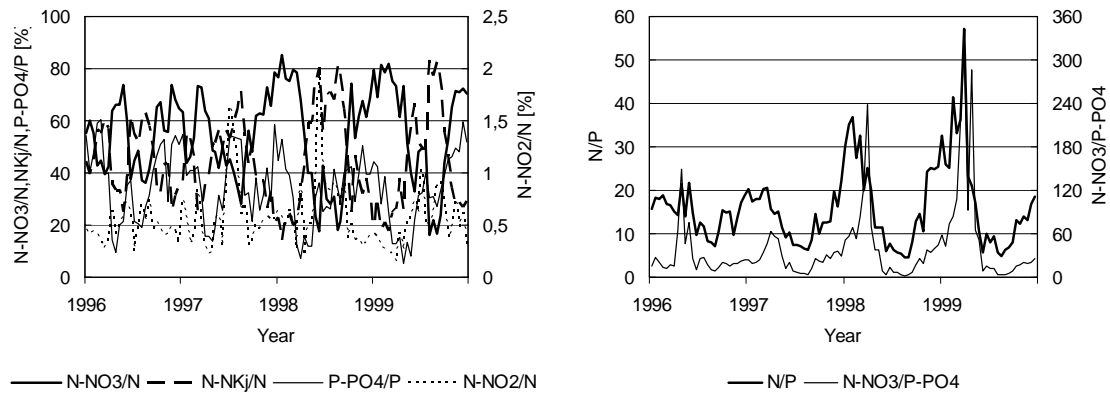


Fig. 2. N_{Kj}/N , $N-NO_3/N$, $N-NO_2/N$, $P-PO_4/P$ fractions and of N/P , $N-NO_3/P-PO_4$ ratios

Results and discussion

Spearman's rank correlation coefficient is used to detect monotonic trends in analyzed variables with time. It is a useful tool for exploratory data analysis in environmental investigation [6].

The Spearman rank correlation coefficient is a nonparametric technique for evaluating correlation between two independent variables. Because the technique operates on ranks of the data it is relatively insensitive to outliers and there is no requirement that the data be collected over regularly spaced intervals. It is calculated according to the following equation:

$$r_s = \frac{1 - 6 \sum_{i=1}^n d_i^2}{n^3 - n}$$

where d_i is difference between ranks for each x_i , y_i data pair and n is the number of data pairs.

Correlations are termed 'significant' when correlation coefficients indicate $p < 0.05$; where p is the probability that any random sample of uncorrelated experimental data points would yield an experimental correlation coefficient as large as or larger than the observed value of r . Results of correlation analysis are summarized in Table 1.

Table 1. Values of Spearman's correlation coefficients

Variable	r_s	p-value	Ratio	r_s	p-value
N_{Kj}	-0.3095	0.0014	$N-NO_3/N$	0.0548	0.5807
$N-NO_3$	-0.0821	0.4075	$N-NO_2/N$	0.0867	0.3817
$N-NO_2$	-0.1602	0.1042	N_{Kj}/N	-0.0571	0.5647
N	-0.2285	0.0196	$P-PO_4/P$	-0.0954	0.3355
PO_4	-0.1177	0.2340	N/P	-0.0586	0.5544
P	-0.1808	0.0663	$N-NO_3/P-PO_4$	-0.0092	0.9258

The significant negative trends were found only for total nitrogen and total Kjeldahl nitrogen. The strength of correlation was not very strong $|r| < 0.31$. The relative decrease in total Kjeldahl nitrogen is larger than the decrease in total-nitrogen.

The monthly means, standard deviations, ranges and median values for all variables were computed in order to establish seasonality. Data for N/P ratio are shown in table 2 as their represents.

Table 2. Monthly means, standard deviations, ranges and median values for N/P ratio

Month	Minimum	Maksimum	Mean	St. dev.	Median
1	15.7	35.2	23.7	7.4	20.2
2	16.8	41.4	25.3	9.4	22.1
3	15.1	57.1	27.9	13.4	20.6
4	11.4	25.2	18.2	4.5	17.8
5	9.0	21.6	13.3	4.2	11.4
6	5.6	14.7	9.0	2.9	8.7
7	5.8	12.5	8.5	2.3	8.1
8	4.5	7.9	6.1	1.1	6.0
9	4.5	15.3	9.7	3.9	8.7
10	8.1	15.1	12.4	2.4	12.7
11	9.8	25.1	16.4	5.8	13.8
12	13.0	25.4	19.3	4.1	18.7

During the dormant season (October to March) there is a wider range of N/P ratios, than during the growing season (April to September). Mean N/P ratios are higher than the corresponding median N/P ratios, which demonstrated that the ratios are skewed towards lower values, with a few high N/P ratios producing higher mean values (see Table 2).

Seasonal differences in monthly means for all variables are shown in Fig.3. A strong seasonality was found for nitrate, total nitrate and orto-phosphate concentrations. A maximum for orto-phosphate and phosphate occurred in summer months with peak maximum in August. In contrast during late summer total nitrogen and nitrate reach their minimum. Nitrate is a predominant form of nitrogen in winter. In summer most of dissolved nitrogen in the water is present as an organically bound form, as total Kjeldahl nitrogen. Orto – phosphate fraction in total phosphorus reaches its minimum in April.

During the dormant season monthly mean N/P and $N-NO_3/P-PO_4$ ratios reach as high as 57 and 111 respectively. A recurring minimum for these ratios occurred in September.

Detailed examination of N/P ratios has indicated conditions of potential phosphorus limitation for algal and other plant growth in Odra River, with period of nitrogen limitation, particularly in August.

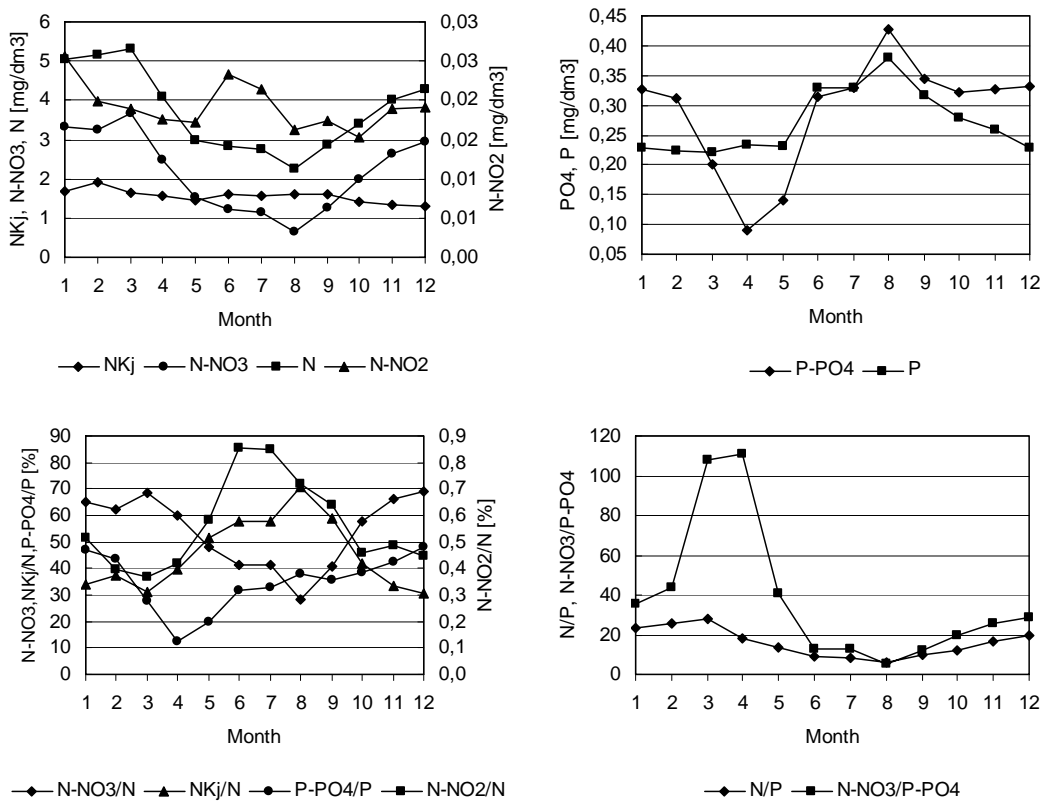


Fig.3. Seasonal variation of monthly means of nutrient concentrations and their ratios

References

- [1] A. Kontas, F. Kucuksezgin, O. Altay, E. Uluturhan, *Environ. Intern.*, (2004), 29, 1057-1062
- [2] H.P. Jarvie, B.A. Whitton, C. Neal, *Sci. Total Environ.*, (1998), 210/211, 79-109
- [3] P.H. Santischi, *Marine Environ. Res.*, 40 (1995), 337
- [4] G. Kowalewska, B. Wawrzyniak-Wydrowska, M. Szymczak-Zyla, *Marine Poll. Bull.*, (2004) 49, 148-153
- [5] R. Portielje, D.T. Van der Molen, *Wat. Sci. Tech.*, (1998), 37, 235-240
- [6] T.D. Douthier, *Environ. Forensics*, (2001), 2, 359-362

INVESTIGATIONS OF THE KINETICS OF THERMAL DECOMPOSITION OF MAGNESIUM HYDROXIDE CARBONATE

J. Możejko, M. Olszak-Humienik, B. Jakubowicz
*Institute of Chemistry and Environmental Protection,
Szczecin University of Technology, Szczecin, Poland*

The investigations of thermal decomposition of magnesium hydroxide carbonate are part of the studies of oxy-salts. The hydroxide carbonates represent an important group of salts. In literature there is little data on the subject of the thermal decomposition hydroxide carbonates of metals. There is nothing on the subject of the kinetics of thermal decomposition of magnesium hydroxide carbonate.

The thermal decomposition of magnesium hydroxide carbonate $3\text{MgCO}_3\cdot\text{Mg}(\text{OH})_2\cdot m\text{H}_2\text{O}$ was shown in [1] and was studied by S. Hiroyuki and coworkers [2]. The thermal instability of this is the result of the laminar structures of its crystals. Hydroxyl bonds are formed in hydrated oxy-salts. Hiroyuki suggested the exothermic process from the beginning of the DTA curves may be associated with magnesite crystallization, magnesite – CO_2 reaction, of magnesite crystallization process.

The authors of this paper studied the thermal decomposition of magnesium hydroxide carbonate under dynamic conditions in static air atmosphere, in the temperature range of 20 – 600°C at a heating rate of 4 – 10 K/min, with derivatograph MOM-PC. The sample mass was 20 mg. The samples were initially heated in a dryer at a temperature of about 250°C to constant mass. The final product of drying used in thermal decomposition had the formula $3\text{MgCO}_3\cdot\text{Mg}(\text{OH})_2\cdot 2\text{H}_2\text{O}$. The TG – curve at a heating rate - 8 K/min is shown in Fig.1. The DTA and DTG – curves at the same heating rate are presented in Fig.2.

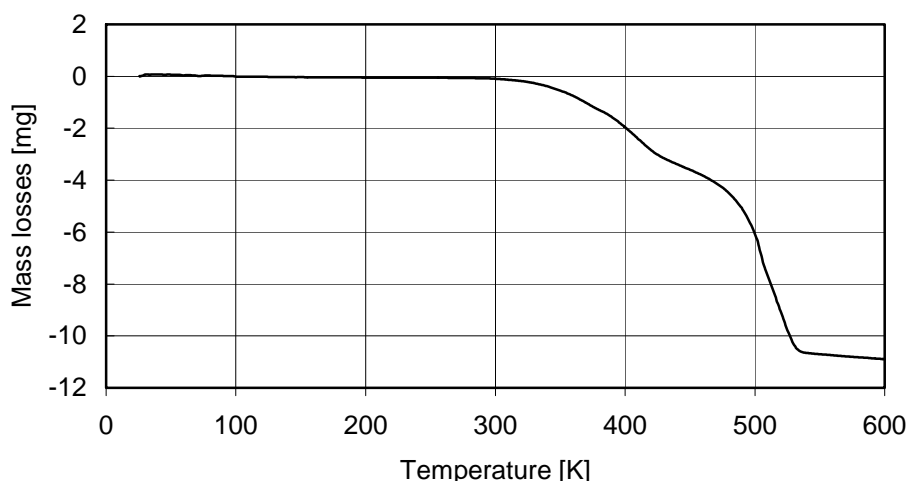


Fig.1 Thermal decomposition of magnesium hydroxide carbonate – 8 K/min

The thermal analysis curves of magnesium hydroxide carbonate (Fig.1 and 2) show that decomposition reaction is undoubtedly complex, involving several stages.

The removal of water under experimental conditions occurs in two steps, similar as the removal of carbon dioxide).

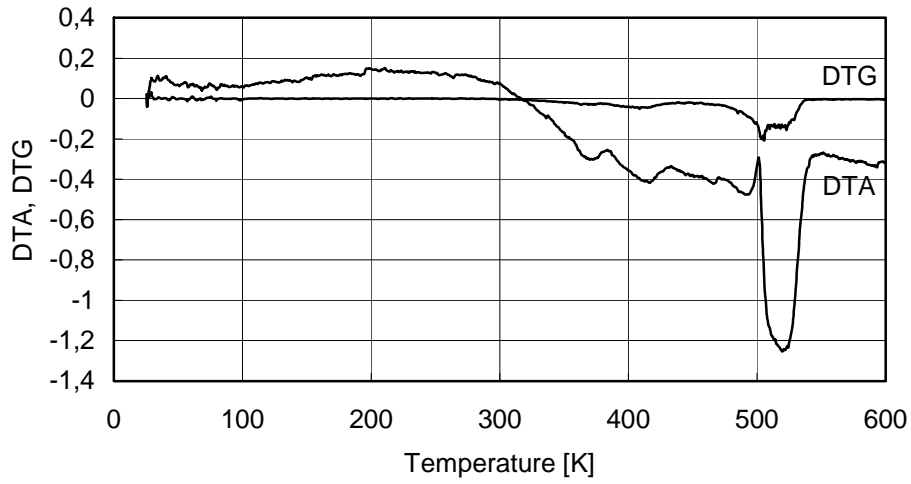
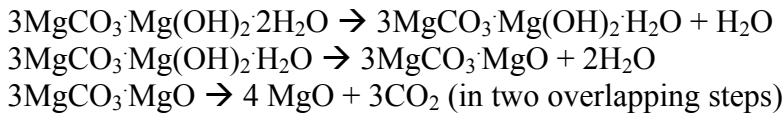


Fig.2. DTA and DTG curves for decomposition of magnesium hydroxide carbonate (heating rate -8 K/min)

On the basis of this study, we find that the following reactions occur in the course of the thermal decomposition of $3\text{MgCO}_3\cdot\text{Mg}(\text{OH})_2\cdot 2\text{H}_2\text{O}$:



The values of characteristics parameters of decomposition processes are presented in Table 1.

Table 1. Characteristic parameters of decomposition steps of $3\text{MgCO}_3\cdot\text{Mg}(\text{OH})_2\cdot 2\text{H}_2\text{O}$

Stage	Heating rate [K·min ⁻¹]	T _{range} [°C]	DTA peak temperature T _p [°C]
I	4	297 – 367	351
	6	285 – 378	364
	8	287 – 378	369
	10	295 – 383	374
II	4	367 - 463	427
	6	378 – 453	415
	8	380 – 430	416
	10	385 – 455	418
III	4	480 - 526	502
	6	475 - 533	516
	8	447 - 539	517
	10	450 - 546	522

The rate of the reaction - $d\alpha/dt$ under non-isothermal conditions has been expressed by the relation

$$\frac{d\alpha}{dt} = k(T) \cdot f(\alpha) = A \cdot e^{-\frac{E}{RT}} \cdot f(\alpha)$$

where: α is the fraction reacted, t - time [min], $k(T)$ is the constant rate as a function of absolute temperature T [K], $f(\alpha)$ is the conversion function dependent on the mechanism of the reaction, A is the preexponential factor [min^{-1}], E is the apparent activation energy [kJ/mol] and R is the gas constant [kJ/(mol·K)]. The general form of function $f(\alpha)$ is $f(\alpha) = (1 - \alpha)^n$, where n is the reaction order [3].

The kinetics parameters – the apparent activation energy E , preexponential factor A and the reaction order were obtained from the thermal characteristic of DTA peaks by Kissinger's method [4] and from the mass losses – temperature dependence observed in the TG-curves by Coats-Redfern's method [5, 6]. Fig.3 presents the dependence of fraction reacted on the temperature in the particular stages of decomposition at a heating rate of 8 K/min.

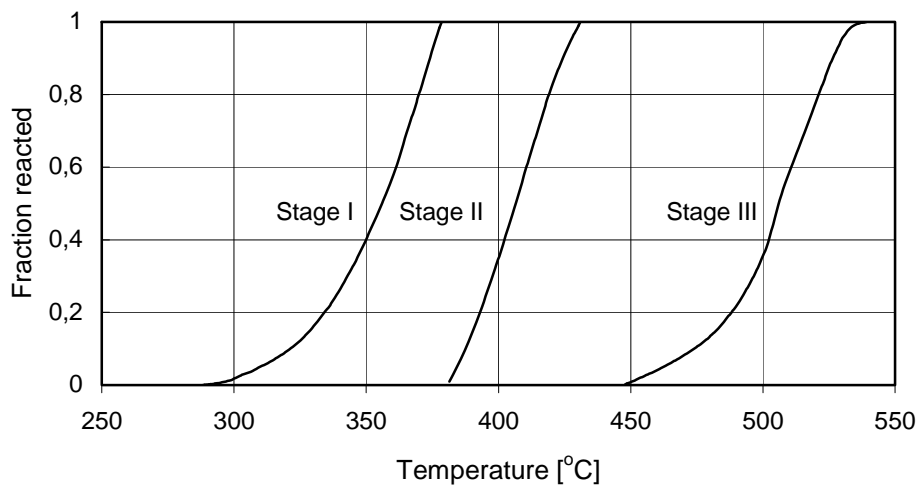


Fig.3. Dependence of transformation degree on a temperature for particular stages of decomposition of $3\text{MgCO}_3 \cdot \text{Mg}(\text{OH})_2 \cdot 2\text{H}_2\text{O}$ (at heating rate 8 K/min)

The water molecules in this compound are bonding with the various strengths. The first molecule of water is removed at temperatures from 297 to 383°C depending on the heating rate; with the maximum temperature T_p of DTA peak equals 351 – 374°C. The apparent activation energy of this step obtained by Kissinger's method is 121kJ/mol. The next two water molecules are removed in the second step simultaneously, at 367 – 455°C. In this instance the DTA peak is not acute and calculating the activation energy by Kissinger's method is difficult. The substitute kinetics parameters at this stage of decomposition were calculated from $\alpha(T)$

dependencies using Coats-Redfern's method and were equal: the apparent activation energy $E = 238$ kJ/mol and the preexponential factor $\ln A = 38.1$ for the reaction order equals 1. The form of function $f(\alpha)$ is $f(\alpha) = (1-\alpha)$

The DTA peak for the stage of carbon dioxide removal is not sharp-pointed. The DTG-curves results show that CO_2 evolution from $3\text{MgCO}_3\cdot\text{MgO}$ consists of two overlapping steps. The shape of the second part of DTG peak can be indicative of the reversibility of reaction in this stage. The substitute kinetics parameters of the stage of carbon dioxide evolution calculated by using Coats-Redfern's method were: $E = 310$ kJ/mol and $\ln A = 46.9$ for the reaction order equals 1.

References

1. Atlas of Thermoanalytical Curves, Akadémiai Kiadó, Budapest 1976.
2. S. Hiroyuki; O. Kouhei; O. Mototsune, Yonago Kogyo Koto Semmon Gakko Kenkyu Hokoku 11 (1975) 135-8 (Japan)
3. J. Straszko, M. Olszak-Humienik, J. Mozejko, Inż.Chem.Proc., 1 (1995) 45.
4. H. E.Kissiger, Anal.Chem., 29 (1957) 1702,
5. A..W.Coats, J.P.Redfern, Nature, 201 (1964) 68,
6. A..W.Coats, J.P.Redfern, Nature, 207 (1965) 290.

THE INFLUENCE OF SOLVENT ON THE YIELD OF REACTION AND COMPOSITION OF ISOMERS IN THE SYNTHESIS OF DISAZO PIGMENTS WITH EMPLOYMENT OF THE MV IRRADIATION

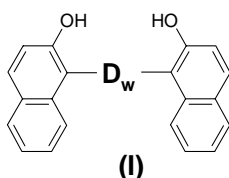
Z. Niewiadomski, K. Wojciechowski^{*)}

*Institute of Polymer and Dye Technology, Technical University of Łódź,
ul. Stefanowskiego 12/16, 90-924 Łódź*

^{)} Department of Environmental Engineering, Technical University of Łódź
Al. Politechniki 6, 90-924 Łódź*

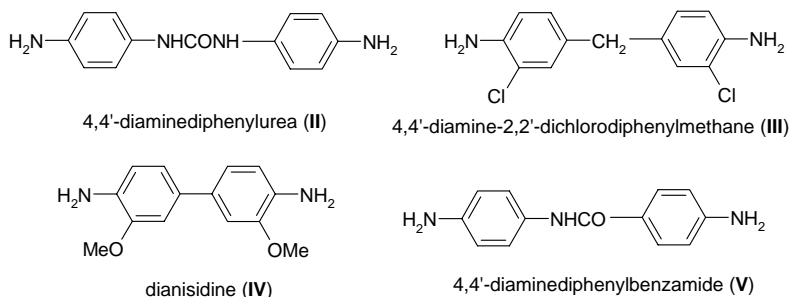
The preliminary researches on the synthesis of disazo pigments with the use of microwave irradiation (mw) in water as a medium of conversion, where aromatic diamines as diazo components were used, allowed us to obtain these products only with the very low yields [1].

In our researches we were interested in a possibility of synthesis of the azo pigments [I] with the use of microwave irradiation mv in organic solvents.



where D_w – diamine moiety

Results of researches on synthesis of diazo pigments (I) by means of microwave irradiation in organic solvents and their mixtures with water, and with the use of aromatic diamines as diazo components, are presented in the present work. As the diazo components (D_w) the following compounds were used,:



2-naphthol was applied as the coupling component. For our investigations we used the following organic solvents: N,N-dimethylformamide (DMF), N-methylpyrrolidone (NMP) and formamide (FM) as well as their 1:1 v/v mixtures with water.

The synthesis of pigments was carried out in described earlier manner [1-3], by means of microwave irradiation of frequency of 2.45 GHz and wavelength of 12.3 cm [4] (power 130 and 250W). Pigments obtained by means of a “classic” method, i.e. the method of diazotization and coupling reaction in water, were used as model pigments.

The spectrophotometric researches of pigments were carried out using solutions in DMF by means of the Perkin Elmer Lambda 40 spectrophotometer. A static analysis was done by means of the Microcal ORIGIN v.6.0 (Microcal Software, Inc.).

Results of the introduced researches are presented in a Table 1 and 2.

Table 1. Yields of reactions of obtained disazo pigments in pure solvents.

		Power [W]	130			250
Amine	Medium	t [min]	1	2	3	1
(II)	DMF	Yield	25.7	14.6	20.5	20.0
	NMP		14.7	13.3	12.1	9.5
	FM		30.1	29.0	26.2	22.0
(III)	DMF		31.4	26.3	20.7	31.5
	NMP		44.9	36.7	34.1	33.3
	FM		35.0	36.2	37.0	33.3
(IV)	DMF		17.3	16.0	10.1	11.5
	NPM		19.2	18.5	23.6	12.6
	FM		13.2	11.8	14.1	8.6
(V)	DMF		35.5	29.1	28.9	26.2
	NMP		23.0	24.6	25.1	16.6
	FM		24.8	23.1	23.8	19.3

Table 2. Increase of the yield of reaction of obtained disazo pigments (ΔW) in mixtures of H₂O/solvent (1:1 v/v).

		Power [W]	130			250
Amine	50% H ₂ O	t [min]	1	2	3	1
(II)	DMF	Yield	11.3	27.0	13.2	3.0
	NMP		23.2	26.4	28.0	10.1
	FM		14.3	17.9	26.9	22.5
(III)	DMF		16.2	24.5	28.9	20.7
	NMP		9.9	13.2	29.5	16.9
	FM		-9.0	-6.2	-2.3	-5.7
(IV)	DMF		---	---	---	---
	NMP		---	---	---	---
	FM		---	---	---	---
(V)	DMF		7.4	17.1	16.4	3.7
	NMP		15.1	14.0	14.6	21.3
	FM		8.6	11.5	14.7	12.7

An application of water as a medium [3] led to obtaining of contaminated products of not really high yields. Under such conditions, the reaction proceeds locally, within a wet part of the reactionary mixture. Thanks to the use of organic solvents the partial solubility of both substrates and reaction products is possible, while the application of their mixtures with water results in increase of polarity and it influences on the reaction yield (Table 2).

The pigments investigated by us can occur both in hydrazone (H) and azo (A) forms [5,6]. The hydrazone form H occurs in the form of dimers of the “sandwich” or “head-to-tail” type of shifted batho- or hypsochromic absorption bands in relation to unaggregated hydrazone form (Figure 1).

A compatibility parameter Φ , being a ratio of a surface area ΔS and oscillator strength under the absorption curve of pigment obtained by means of the S_{klas} “classic” method, determines differences resulting from aggregation of pigments or from existence of an $[A \leftrightarrow H]$ equilibrium. The accepted compatibility criterions are the same as those described earlier [2].

Most of the investigated pigments is obtained in a form similar to those obtained by means of the “classic” method ($\Phi \geq 0.9$) or with the average compatibility ($\Phi = 0.7 \div 0.9$). The low compatibility exists in the case of pigments, which are derivatives of **(IV)** in DMF and FM as well as pigments, derivatives of **(II)** in 50% NMP.

An analysis of composition of the A and H isomers was carried out for a range of absorption of A (420-430 nm) and in the case of the H form (in a form of monomer and two dimers) – in the range > 460 nm. The composition of mixture and equilibrium of forms $[A \leftrightarrow H]$ depends mostly on the type of the used amine. The **(V)** derivatives contain the most of the A form (60-70%) and the **(II-IV)** derivatives contain only 30-40% of the A form.

Reactions carried out in 50% water solutions of solvents result in increase of the H form in the mixture and this fact has an essential influence on increase of a light fastness of pigments.

The changes of ratio of monomer to dimer in the H form were investigated by means of a deconvolution method (Figure 1). The analysis of composition was carried out for the range > 460 nm. The results are presented in Table 3 and 4.

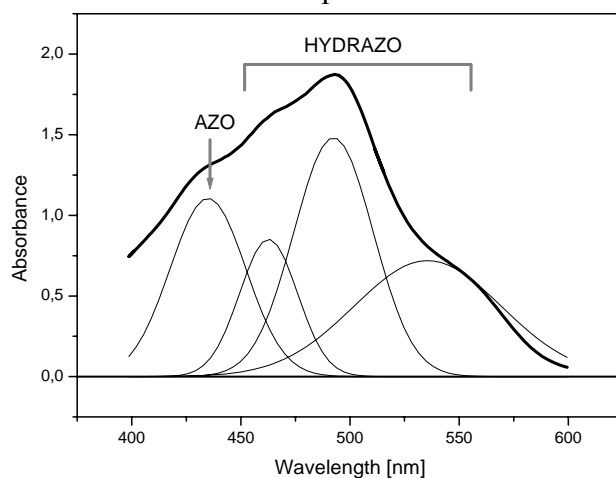


Figure 1. Example of deconvolution procedure of absorption spectrum (derivative of the **(II)** diamine) determined by means of analysis of the II derivative.

Table 3. The content of azo-isomer in the $[A \leftrightarrow H]$ mixture.

Amine	(II)	(III)	(IV)	(V)
*)	0.23	0.38	---	0.66
DMF	0.23	0.49	---	0.71
NMP	0.32	0.46	---	0.53
FM	0.23	0.34	---	0.68
50% H ₂ O/(DMF, NMP, FM)				
DMF	0.25	0.35	---	0.58
NMP	0.17	0.34	---	0.59
FM	0.18	0.36	---	0.59

*) The “classic” method of synthesis (model); analytical wavelengths [derivative of amine and nm]: **(II)** - 429, 462, 497, 558; **(III)** - 433, 488, 521; **(IV)** - 522, 588 and **(V)** - 427, 494, 520

Table 4. The content of unassociated hydrazo form in the [monomer \leftrightarrow dimer] mixture.

Amine	(II)	(III)	(IV)	(V)
*)	0.45	0.86	0.40	0.68
DMF	0.72	0.90	0.46	0.54
NMP	0.72	0.90	0.18	0.63
FM	0.38	0.90	0.25	0.73
50% H ₂ O/(DMF, NMP, FM)				
DMF	0.78	0.88	---	0.70
NMP	0.64	0.90	---	0.69
FM	0.64	0.90	---	0.69

(Description – Table 3.)

It was proved that pigments, which are derivatives of **(II)** and **(IV)** are the most aggregated (dominance of dimer) while derivatives of **(III)** and **(IV)** (65-85% of monomer) are the least aggregated pigments. In this case, it results in a high colouristic efficiency in application of pigments.

The aggregation ability of pigments results from their spatial structure. Both forms – the A form and the more probable H form [5,7] are not planar. It is evidenced thanks to calculations carried out by the AM1 method. Aromatic diamines, which structure influence on a shape of pigment molecules, play a basic role in this case.

Conclusions

Analysis of the obtained results leads to conclusions, which are similar as in the case of the described earlier syntheses [2]. The application of 50% mixtures of DMF, NMP and FM with water has beneficial influence on the yield of the reaction. It allows to get the increase of the yield up to 25%. The type of the applied organic solvent or its mixture with water determines the azo-hydrazo equilibrium. The aggregation of pigment molecules depends mainly on the type of diamine used for synthesis and, in the lower degree, on polarity of the applied solvent.

References

- [1] K. Wojciechowski, Z. Niewiadomski, A. Wyřębak, *Annal. Pol. Chem. Soc.* vol.3, PTChem, Wrocław 2004, str. 1367.
- [2] Z. Niewiadomski, A. Szymczak, K. Wojciechowski, *Annal. Pol. Chem. Soc.* vol.1, PTChem, Poznań 2005, str. 702.
- [3] J. Jin, Z. Wen, L. Wang, T. Motsuraq, J. Meng, *Synthetic Commun.* 30(5) (2000) 829.
- [4] D. M. Mingos, D. R. Baghurst, *Chem. Soc. Rev.* 20 (1991) 1.
- [5] L. M. Antonov „Theoretical Investigation of the Tautomerism of Some Phenylazonaphthols“, 31 UNESCO Course for Advances Research in Chemistry and Chemical Engineering, Tokyo Institute of Technology, 1996.
- [6] J. Jirman, A. Lycka, *Dyes and Pigments.* 8 (1987) 55.
- [7] *Colour Index, SDC 3^{ed}*, Bradford 1998.

SYNTHESIS AND PROPERTIES OF THE NEW ACYCLIC DERIVATIVE OF LUMINAROSINE

J. Nowak, J. Milecki, B. Skalski

*Faculty of Chemistry, A. Mickiewicz University,
Grunwaldzka 6, 60-780 Poznan, Poland*

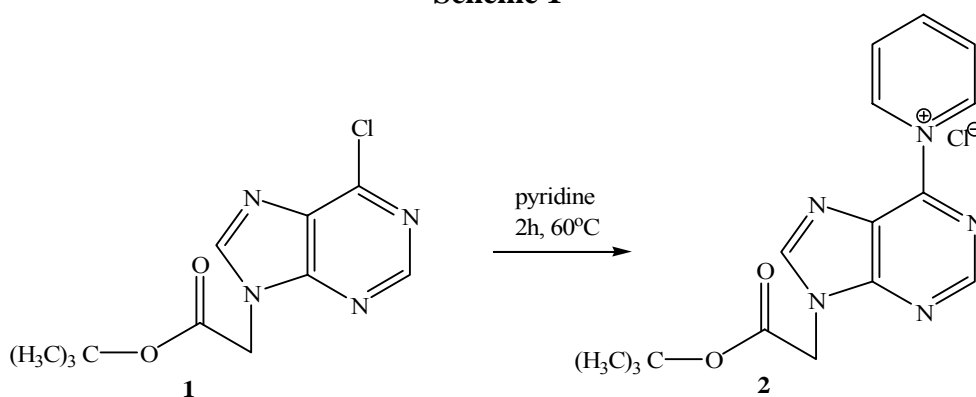
INTRODUCTION

Pyridinium derivatives of nucleosides are interesting objects of spectral, photophysical and photochemical research [1]. Pyridinium salt derived from 2',3', 5'-tri-O-acetyluracil, when irradiated with UV-light ($\lambda > 300\text{nm}$) undergoes transformation to 2',3', 5'-tri-O-acetyl-luminarosine- the strongly fluorescing nucleoside, being characterized with the long-wave absorption ($\lambda_{\text{max}}^{\text{A}} = 425\text{ nm}$) and the intensive fluorescence ($\lambda_{\text{max}}^{\text{F}} = 528\text{ nm}$) [2,3]. Because of its large chemical and photochemical stability and very profitable absorption-emission properties [4], 2',3', 5'-tri-O-acetyl-luminarosine and analogues can serve as fluorescent probes in biological system [5]. Luminarosine can also be used to fluorescent marking of oligonucleotides in the automatic synthesis on the solid support. But there is certain difficulty because of the high susceptibility of this nucleoside to spontaneous anomerisation leading in the final result to the mixture of oligonucleotides containing λ and β anomers of luminarosine [6]. Good alternative for luminarosine, as the fluorescent mark of DNA, can be its acyclonucleoside analogues, which don't undergo the anomerisation reaction. The attempt of the synthesis of such analogue, according to procedures worked out previously, basing on the photochemical transformation of the suitable N-(purin-6-yl)-pyridinium chloride is presented in this paper.

RESULTS AND DISCUSSION

1) Synthesis of the N[(9-tert-butoxycarbonylmethyl)purin-6-yl]pyridinium chloride (**2**).

Scheme 1



In the nucleophilic substitution of compound (**1**) - 6-chloro-9-(tert-butoxycarbonylmethyl)purine, according to the well-known procedure, consisting on the treatment of the chloroderivative of purine or nucleoside with the pyridine at 60°C during 2-5 hours, pyridium salt (**2**) has been obtained with 20% yield (**Scheme 1**).

The product **2** has UV spectrum characteristic for pyridinium salts (**Fig.1**) with two maximum of the absorption at $\lambda=272\text{nm}$ and $\lambda=295\text{ nm}$.

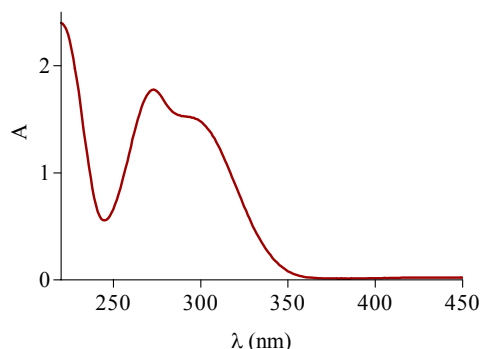
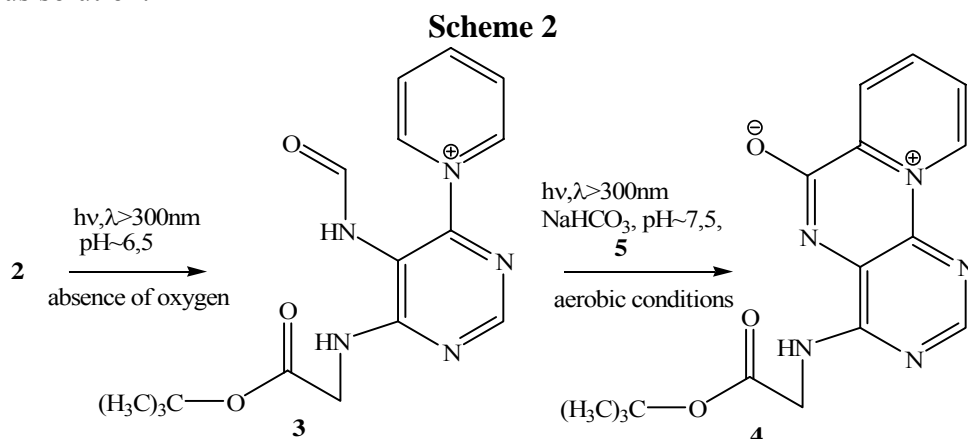


Figure 1. The spectrum of the absorption of compound **2**.

2) Synthesis of 9-N-(tert-butoxycarbonylmethyl)luminarine (**4**).

The obtained pyridinium salt (**2**) has been exposed to photochemical reaction in aqueous solution.



In the first step of reaction, deoxidized aqueous solution of the N-[(9-tert-butoxycarbonylmethyl)purin-6-yl]pyridinium chloride (**2**) was subjected to irradiation with near UV light ($\lambda > 300\text{ nm}$) using the reactor equipped with dip mercuric lamp TQ -150 Original Hanau stocked with the cylindrical pyrex filter. The course of the reaction was followed spectrophotometrically (**Fig. 2A**). The disappearance of pyridinium salt and the formation of the product with maximum of the absorption at $\lambda=242\text{ nm}$ was noted. The analysis of irradiated solution (**Fig. 2B and 2C**) showed the formation of the desirable intermediate product **3** in the synthesis of the acyclic derivative of luminarosine.

In the second step of reaction the aqueous solution of the compound **3** was alkalinized to $\text{pH} \sim 7,5$, 1,5 eq. of N-(9-methylpurin-6-yl)pyridium chloride (**5**) was added as the photosensitizer and mixture was exposed to sunlight in aerobic conditions. Based on analyses of the solution after the irradiation (**Fig. 3B and 3C**) and spectrophotometrical data (**Fig. 3A**) it was found that under this conditions of irradiation the compound **3** has been transformed into 9-N-(tert-butoxycarbonylmethyl)luminarine (**4**). The yield of the photochemical reaction was 18%. In order to isolate the product the aqueous solution of the compound **4** was extracted by CHCl_3 . Obtained product **4** shows band of absorption in the visible range with $\lambda_{\text{max}} = 426\text{ nm}$ characteristic for luminarosine.

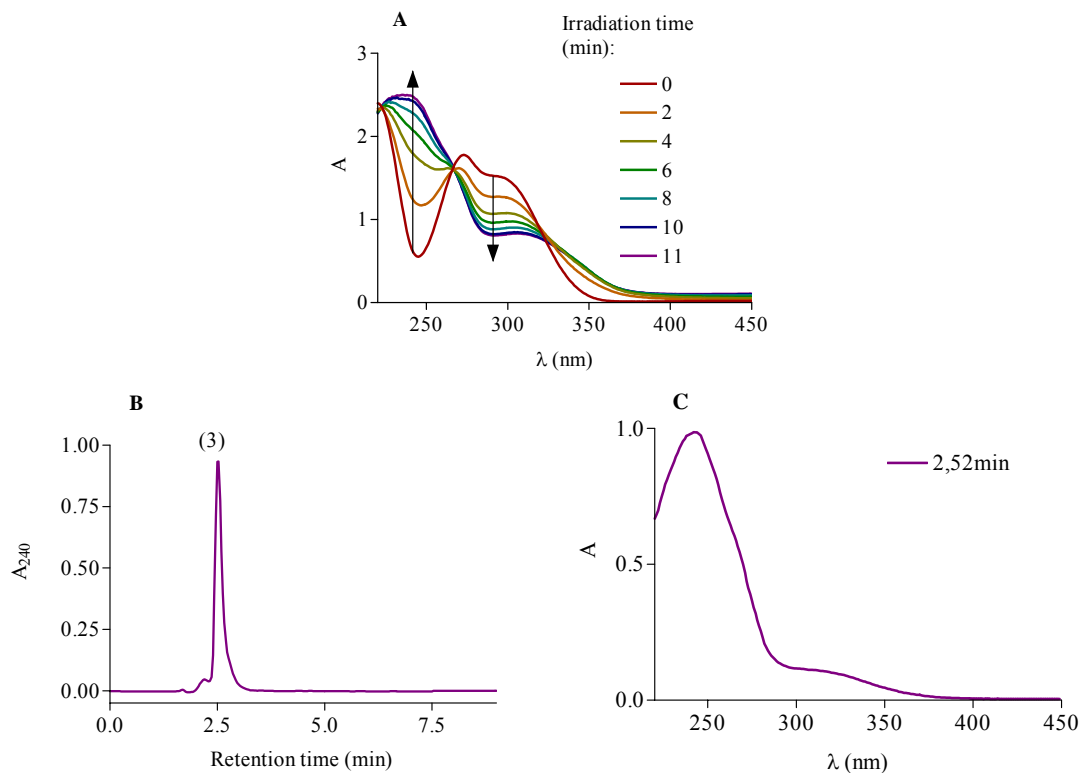


Figure 2. (A) Changes in the absorption spectra during the irradiation of deoxidized aqueous solution of the compound **1**, (B) the HPLC analysis of the solution after the irradiation and (C) the absorption spectrum of compound **3**.

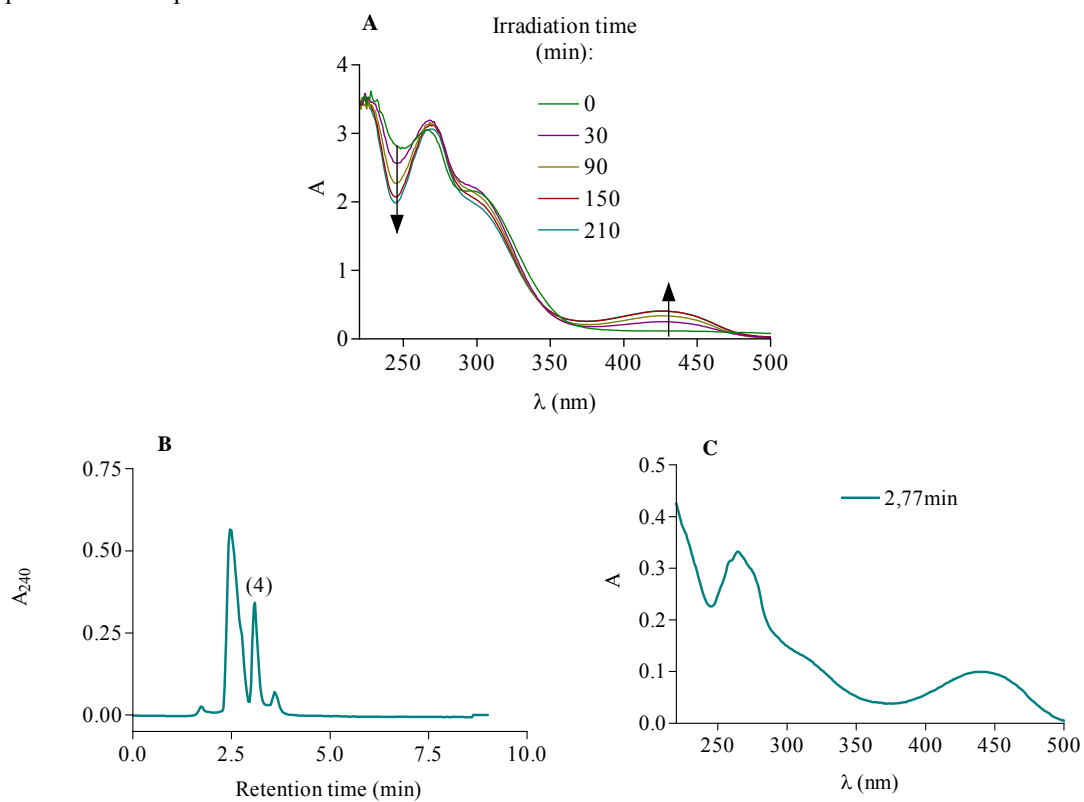
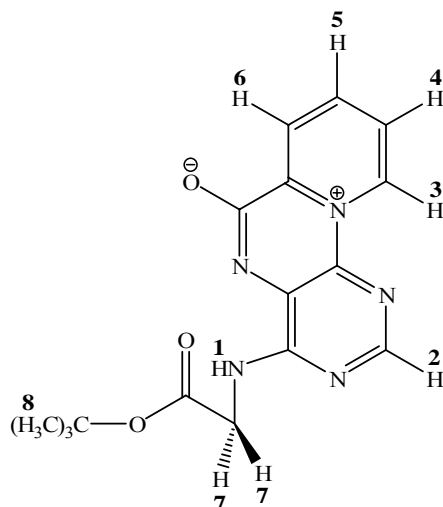


Figure 3. (A) Changes in the absorption spectra during the irradiation of aqueous solution of the compound **3**, (B) the HPLC analysis of the solution after the irradiation and (C) the absorption spectrum of compound **4**.

Structure of the compound was confirmed by H-NMR, ESI-MS and UV-VIS.



ESI MS m/z 328 ($M+H^+$), calculated m/z 327,13 for $C_{16}H_{17}N_5O_3$

UV-VIS λ_{max} (H_2O) 264 nm, 426 nm

1H NMR ($CDCl_3$), δ 1,48 (s, 9, H-8) 4,28 (d, $J=6,0$ Hz, 2, H-7), 7,62 (t, $J=6,0$ Hz, 1, H-1), 8,08 (m, $J=7,0$ Hz, 1, H-4), 8,26 (s, 1, H-2), 8,42 (m, $J=7,6$ Hz, 1, H-5), 9,10 (d, $J=8,0$ Hz, 1, H-6), 10,17 (d, $J=6,6$ Hz, 1, H-3)

CONCLUSION

The received new acyclic derivative of luminarosine - 9-N-(tert-butoxycarbonylmethyl)luminarine (**4**) after suitable modification of ester part can replace luminarosine and be used to the marking of any sequence of oligonucleotides on 3' or 5' end.

LITERATURE

- [1] B. Skalski, S. Paszyc, R. W. Adamiak, R. P. Steer, R. E. Verrall, Canadian Journal of Chemistry-*Revue Canadienne de Chimie*, 68 (1990) 2164.
- [2] B. Skalski, J. Bartoszewicz, S. Paszyc, Z Gdaniec, R. W. Adamiak, *Tetrahedron*, 43 (1987) 3955.
- [3] B. Skalski, R. P. Steer, R. E. Verrall, *J. Am. Chem. Soc.*, 113 (1991) 1756. B. Skalski, S. Paszyc, R. W. Adamiak, R. P. Steer, R. E. Verrall, *Journal of The Chemical Society-Perkin Transactions 2* (1989) 1691.
- [4] S. Jayaraman, L. Teitler, B. Skalski, A., S. Verkman, *American Journal of Physiology-Cell Physiology*, 277 (1999) C1008.
- [5] A. Burdzy, B. Skalski, S. Paszyc, M. Popenda, R. W. Adamiak, *Acta Biochim. Pol.*, 45 (1998) 941.
- [6] A. Burdzy, B. Skalski, S. Paszyc, Z Gdaniec, R. W. Adamiak, *Nucleosides Nucleotides*, 17 (1998) 143.

SYNTHESIS, STRUCTURE AND ANTIMICROBIAL ACTIVITY OF NEW DERIVATIVES OF (E)-CHALCONE

Zdzisława Nowakowska¹, Bogdan Kędzia²

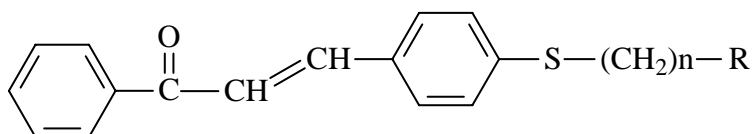
¹*Faculty of Chemistry, Adam Mickiewicz University, Grunwaldzka 6, 60-780 Poznań, Poland*

²*Institute of Medicinal Plants, Libelta 27, 61-707 Poznań, Poland*

Chalcones, considered as the precursors of flavonoids and isoflavonoids, are abundant in edible plants, and have also been shown to display a diverse array of pharmacological activities [1,2]. The oxygenated chalcones such as licochalcone A, have previously been described as a moderate potent antibacterial compounds with activity against Gram-positive bacteria. Additionally, enhanced selectivity and potency in the biological properties of chalcone with basic amino functions has been reported [3].

INTRODUCTION

The aim of this investigation is to procure (E)-4-aminoalkylthiochalcones **1-10**, from (E)-4-chalconethiols in the hope of obtaining new derivatives, which might show biological activity as antimicrobial and antifungal agents.



- | | | |
|-----------------------------|------------------------------|-------------------------------------|
| 1 R= piperazine n= 4 | 4 R= piperazine n= 10 | 7 R= 4-methylpiperidine n= 4 |
| 2 R= piperazine n= 5 | 5 R= piperidine n= 4 | 8 R= 4-methylpiperidine n= 6 |
| 3 R= piperazine n= 6 | 6 R= piperidine n= 6 | 9 R= morpholine n= 4 |
| | | 10 R= morpholine n= 6 |

(E)-4-chalconethiol was alkylated with dibromoalkanes (1,4-dibromobutane, 1,5-dibromopentane, 1,6-dibromohexane and 1,10-dibromodecane) at room temperature in DMF in the presence of triethylamine as a base. The obtained (E)-4-bromoalkylthiochalcones were reacted with 0.002 mole of morpholine, piperidine, 4-methylpiperidine or piperazine in 10 ml of DMF in the presence of 0.002 molar equivalents of triethylamine.

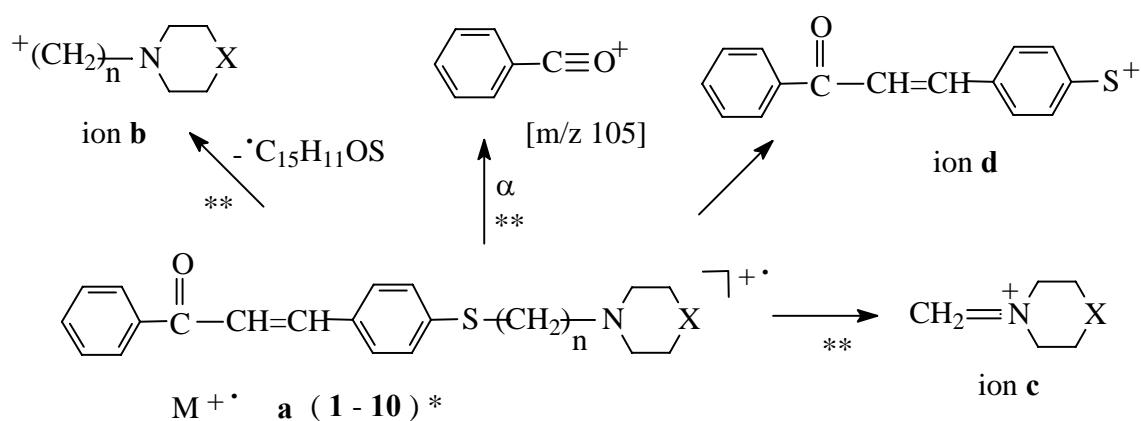
RESULTS

On the basis of low-resolution EI mass spectra, as well as B²/E linked-scan spectra the principal mass fragmentation routes of compounds **1-10** were interpreted as shown in Scheme 1 and Table 1. In all compounds studied the radical-site-induced α -cleavages of the C_{sp3}-C_{sp3} bond next to the heteroatom of the substituents proceed with the formation of the even-electron ions **b**, corresponding to the base peak in the mass spectra. For these compounds the elimination of \bullet C₁₅H₁₁OS-(CH₂)_{n-1} radical as the first step of the fragmentation is predominant. In this type of cleavage the positive charge of the ions **b**

is stabilized on the nitrogen atom of the piperazinomethylene **1-4**, piperidinomethylene **5, 6**, 4-methylpiperidinomethylene **7, 8**, or morpholinomethylene **9, 10** species. It ought to be pointed out that the annular nitrogen atom has extremely high ability to quaternization and charge acceptance. According to the B²/E linked scan spectra, the fragment ion **b** [CH₂=NC₄H₈X]⁺ is also formed from the even-electron fragment ion **d** *via* elimination of an olefin molecule by inductive cleavage. Decomposition of the molecular ions of **1-10** proceeds also by charge-site-initiated inductive cleavage of the S-C_{sp3} bond, providing even-electron ions **c**, observed in EI-MS spectra of the compounds studied.

TABLE 1. Selected mass spectral data (m/z and peak intensity in %) for **1 – 10**.

Ion	m/z, % Relative abundance									
	1	2	3	4	5	6	7	8	9	10
a	m/z380	m/z394	m/z408	m/z464	m/z379	m/z407	m/z393	m/z421	m/z381	m/z409
	17.8	11.5	13.8	18.1	11.2	6.8	15.5	8.5	9.1	12.6
b	m/z141	m/z155	m/z169	m/z225	m/z140	m/z168	m/z154	m/z182	m/z142	m/z170
	11.0	62.1	13.6	1.7	13.1	13.2	16.8	15.3	18.1	20.2
c	m/z99	m/z99	m/z99	m/z99	m/z98	m/z98	m/z112	m/z112	m/z100	m/z100
	100	100	100	100	100	100	100	100	100	100
d	m/z239	m/z239	m/z239	m/z239	m/z239	m/z239	m/z239	m/z239	m/z239	m/z239
	3.9	4.6	2.3	2.8	2.5	1.3	2.8	1.3	2.9	2.0
e	m/z105	m/z105	m/z105	m/z105	m/z105	m/z105	m/z105	m/z105	m/z105	m/z105
	17.4	31.9	18.4	20.9	9.2	5.7	9.9	5.9	8.8	7.5



* Transition checked by B/E spectra of compounds **1-10**.

** Transition checked by B²/E spectra of compounds **1, 5, 7** and **9**.

SCHEME 1. Fragmentation of the molecular ions of **1-10**.

For all compounds tested the ion **d** (m/z 239) with a small relative abundance in the range 1.3-4.6% was observed. The ion **e** (m/z 105) [C₇H₅O]⁺ is much abundant for **1-4** (17.4 – 31.8% r.a.), whereas for **5-10** it is low abundant (5.7-9.9% r.a.). The abundance of the remaining ions in the spectra of amine derivatives of chalcone is lower than 3.2%.

Assignments of the ¹H NMR and ¹³C NMR resonances of these compounds were deduced on the basis of signal multiplicities, and by the concerted application of the two-dimensional NMR technique (HETCOR).

The ¹H and ¹³C NMR data for **1-10** were nearly identical in the aromatic region of the spectra. The spectra of these compounds showed the two doublets at δ 7.48-7.50 ppm and δ 7.77-7.78 ppm (*J*= 15.6 Hz) integrating for one proton, assigned to the H-α and H-β protons, respectively. For **1-10** the ¹H NMR spectra showed the triplet at 2.22-2.89 ppm integrating for two protons ascribed to CH₂-N< protons and correlating in the HETCOR spectra with the carbon signal at 57.21-59.68 ppm. In the ¹H and ¹³C NMR spectra of **1-4** characteristic signals of piperazine ring at ~2.40 and ~2.90 ppm (45.9 and 54.0 ppm, respectively) were observed. The presence of a doublet assigned to protons from the methyl group in the range of 1.02-1.03 ppm in the ¹H NMR spectra of **7, 8** proves the occurrence of the 4-methylpiperidine ring in the molecules of these compounds. The ¹H NMR spectra of **9** and **10** in the range of 3.71-3.72 and 2.43-2.40 ppm showed two triplets of O<CH₂ and N<CH₂ protons of morpholine ring, correlating in the HETCOR spectra with the carbon signal at ~66.9 and ~53.8 ppm, respectively.

The potential antimicrobial activity of compounds **1-10** was estimated in vitro by determining the MIC (Table 2) against a wide spectrum of microorganisms: *Staphylococcus aureus* 209P FDA, *Escherichia coli* PZH 026 B6, *Candida albicans* PCM 1409 PZH, *Streptococcus faecalis* ATCC 8040, *Bacillus subtilis* ATCC 1633, *Klebsiella pneumoniae* 231, *Pseudomonas aeruginosa* SP1, *Aspergillus fumigatus* C1, and *Microsporium gypseum* K1.

TABLE 2. Antimicrobial activity of tested compounds.

Compd.	Minimum inhibitory concentration (MIC) ^a μM				
	<i>S. aureus</i>	<i>E. faecalis</i>	<i>B. subtilis</i>	<i>C. albicans</i>	<i>M. gypseum</i>
1	26	26	263	-	263
2	25	253	25	<253	190
3	24	24	245	<245	184
4	-	-	-	-	215
5	26	264	26	-	264
6	24	24	24	<246	<246
7	24	244	244	-	191
8	23	23	18	<237	<237
9	-	-	-	-	197
10	-	-	-	-	<244

^a MIC - the minimum inhibitory concentration it is the lowest value of concentration of the investigated compound which brakes the evolution of the microorganism.

The most pronounced antibacterial properties were found in the series of (E)-4-piperazinoalkylthiochalcones **1-3**, (E)-4-piperidinoalkylthiochalcones **5, 6** and (E)-4-(4-methyl)piperidinoalkylthiochalcones **7, 8**. The bacteriostatic effects of **1-3** and **5-8** were

shown by MICs of 18 to 264 μM for all Gram-positive bacteria tested, including *S. aureus*, *E. faecalis* and *B. subtilis*. However, they were not effective for Gram-negative bacteria tested. The data shown in Table 2 suggest that the piperidinoalkylthio, 4-methylpiperidinoalkylthio or piperazinoalkylthio, group at position 4 of the B ring of chalcone was essential for the activity, and that the length of alkyl chain influences the antimicrobial activity. The best activity is connected with the presence of five carbon atoms in alkyl chain. The antifungal studies show that **2**, **3**, **6** and **8** were active against the yeasts *Candida albicans* nor against the filamentous fungi *Asperillus fumigatus*. In contrast, the most sensitive species was *Microsporium gypseum*, growth of which was inhibited by concentrations 184-264 μM of **1-10**.

EXPERIMENTAL

The ^1H NMR and ^{13}C NMR spectra were recorded at room temperature on a Varian Mercury spectrometer operating at 75.46 MHz for ^{13}C and 300.07 MHz for ^1H . The spectra were measured in CDCl_3 . The HETCOR spectra were acquired with 2048 data points in the F_2 dimension and 256 increments in the F_1 dimension.

The low-resolution mass spectra were recorded on an AMD 402 two-sector mass spectrometer (AMD Intectra, Germany) of B/E geometry. Metastable ions were recorded on the same instrument using linked scans (B/E, B^2/E). The compounds were introduced into the mass spectrometer using a direct insertion probe in the EI mode (70 eV) with an accelerating voltage 8 kV, a source temperature of 200°C and an inlet temperature of 70-150°C.

General synthesis of (E)-4-aminoalkylthiochalcones 1-10.

To a solution of a given (E)-4-bromoalkylthiochalcone (0.001 mol) in 10 mL DMF, the following compounds: triethylamine (0.28 ml, 0.002 mol) and piperazine (0.172 g, 0.002 mol), piperidine (0.19 ml, 0.002 mol), 4-methylpiperidine (0.24 ml, 0.002 mol) or morpholine (0.17 ml, 0.002 mol) were added dropwise and the mixture was stirred for 3 days at room temperature. The solvent was evaporated to a syrop, which was added dropwise to cold water. The crystalline precipitate was isolated by filtration and the precipitated solid was purified by column chromatography. The isolated crude product was recrystallized from chloroform-ethanol 1:1.

Microbiology : Determination of minimum inhibitory concentration (MIC)

Compounds were dissolved using DMSO (Serva); concentration was 1000 $\mu\text{g}/\text{ml}$. The MIC values of the compounds were determined, with reference to standard microorganisms, by introducing 1ml of the corresponding solutions at various concentrations into a series of tubes (each 12x100 mm), then 0.1 ml of a standardized 1:1000 diluted suspension of a microorganism was added. The MIC values were determined after 18 h of incubation at 37°C. In each assay the bacterial culture sterility and standard bacteria growth were controlled. Sabouraud dextrise broth (Difco) was used as a test medium for fungi; MIC values were determined after 3-7 days of incubation at 25°C.

REFERENCES

- [1] J.R. Dimmock, D.W. Elias, M.A. Beazely, N.M. Kandepu, *Curr. Med. Chem.*, 6 (1999) 1125-1149.
- [2] M.L. Go, X. Wu, X.L. Liu, *Curr. Med. Chem.*, 12 (2005) 483-499.
- [3] X. Liu, M.-L. Go, *Bioorg. Med. Chem.*, 14 (2006) 153-163.

PHYSICO-CHEMICAL PROPERTIES OF ACTIVE CARBON ENRICHED IN NITROGEN

P. Nowicki, R. Pietrzak, H. Wachowska

*Laboratory of Coal Chemistry and Technology, Faculty of Chemistry
Adam Mickiewicz University, Grunwaldzka 6, 60-780 Poznań, Poland*

Abstract

The study was performed on the active carbon obtained from the coke coal from the Jas-Mos colliery, which was subjected to nitrogen enrichment in a reaction with a mixture of air and ammonia. The process of ammoxidation was performed at the stage of a precursor, carbonisate and active carbon. The carbon was activated at 700°C by KOH. The amount of nitrogen built into the carbon structure was found to depend on the ammoxidation temperature and the stage of carbon processing at which the ammoxidation was performed. It was shown that ammoxidation at different stages of carbon processing leads to obtaining products of different physico-chemical properties.

1. Introduction

Low cost of production, rich resources and significant chemical resistance make active carbon a much desired and demanded product. Active carbon is applied in many branches of industry and in new technologies developed to protect the natural environment. Recently much attention has been devoted to active carbon modified by introduction of all kinds of heteroatoms on their surface. Particularly interesting seems the active carbon enriched in nitrogen. Because of its specific physico-chemical properties such as the ion-exchange ability or strongly nucleophilic character it has been applied as adsorbents removing impurities from liquid and gas phase substances [1], as catalysts or catalyst supports, as electrode materials for electrochemical capacitors [2].

One of the possible processes leading to active carbon enrichment in nitrogen is ammoxidation [3]. It is a simultaneous oxidation and nitrogenation of active carbon leading to significant changes in its chemical structure that can be enhanced or reduced according to the temperature conditions of further treatment. The surface oxygen and nitrogen groups formed as a result of ammoxidation can, on further pyrolysis, evolve into the species strongly attached to the parent carbon structures or can be eliminated, which considerably changes the acid-base character of the material.

The aim of the study was to determine and compare the physico-chemical properties of carbon modified by ammoxidation at the stage precursor, carbonisate and active carbon.

2. Experimental

The material to be studied was the coking coal from the Jas-Mos colliery characterised in Table 1. The refined initial coal (S) of the grain size $\leq 0.2\text{mm}$ was demineralised by the Radmacher method [4].

Table 1. Elemental composition of the raw and demineralised coal (wt.%)

Sample	A ^d	C ^{daf}	H ^{daf}	N ^{daf}	S ^{daf}	O ^{daf*}
S	2.5	89.6	4.6	1.4	0.3	4.1
D	0.2	90.7	4.5	1.4	0.4	3.0

* by difference

A portion of the demineralised coal (D) was subjected to ammoxidation. This process was conducted at 300 (N₁) and 350°C (N₂) for 5 hours, by a mixture of ammonia and air at the ratio of 1:3. The products of ammoxidation (DN₁ and DN₂) together with the remaining part of the demineralised coal were subjected to carbonisation at 700°C in argon atmosphere for 1 hour. The carbonisate obtained (DK) was divided into two parts: one of them was subjected to ammoxidation under the same conditions as at the stage of the precursor, while the other was first subjected to activation. The process of activation was performed at 700°C, in argon atmosphere with KOH as an activiser. The carbonisate was mixed with the earlier ground KOH at the weight ratio of 1:4 and subjected to the thermal treatment for 45 minutes. The active carbon obtained (DKA) was then ammoxidised, in the same conditions as the precursor and carbonisate. The other carbonisates: DN₁K, DN₂K, DKN₁, DKN₂ were also subjected to activation.

The active carbon samples obtained were subjected to the studies aimed at determination of their porous structure (by the low-temperature nitrogen sorption method), chemical composition (elemental analysis), the content of the surface oxygen groups [5] and sorption capability (adsorption value of iodine) [6].

3. Results and discussion

According to the data collected in Table 2, the process of ammoxidation results in a significant increase in the content of nitrogen in the carbon material, which is a consequence of nitrogen building in the carbon structure.

Table 2. The elemental composition of the samples obtained (wt.%)

Sample	A ^d	C ^{daf}	H ^{daf}	N ^{daf}	S ^{daf}	O ^{daf*}
DN ₁	0.2	80.3	3.1	8.3	0.4	7.9
DN ₂	0.2	80.4	3.2	8.0	0.4	8.0
DN ₁ K	0.2	90.0	1.6	5.1	0.2	3.1
DN ₂ K	0.1	88.6	1.9	4.8	0.2	4.5
DN ₁ KA	0.4	91.4	0.6	1.6	0.0	6.4
DN ₂ KA	0.3	91.0	0.6	1.3	0.0	7.2
DK	0.4	94.1	1.8	1.2	0.3	2.6
DKN ₁	0.3	90.9	1.8	3.1	0.3	3.9
DKN ₂	0.3	89.7	1.6	3.9	0.3	4.5
DKN ₁ A	0.5	91.0	0.7	1.0	0.0	7.3
DKN ₂ A	0.7	91.1	0.6	1.3	0.0	7.0
DKA	0.7	91.3	0.6	0.6	0.0	7.5
DKAN ₁	0.4	87.6	0.6	5.2	0.0	6.6
DKAN ₂	0.3	85.4	0.7	7.2	0.0	6.7

* by difference

The greatest amount of nitrogen was built in the material in the process of ammoxidation of the demineralised coal (D), which testifies to its greatest reactivity with respect to the other samples. Much less nitrogen was introduced in the material when the ammoxidation was performed on the carbonisate (DK) and active carbon (DKA). It is a result of changes in the coal structure taking place on carbonisation and activation and hindering the nitrogen inclusion. The process of ammoxidation leads to a

decrease in the content of carbon, which the most pronounced when ammoxidation is applied at the stage of precursor. When ammoxidation is realised at the stage of precursor and carbonisate the content of oxygen increases, which is a result of oxidation in a reaction with a mixture of ammonium and air. However the decrease in the content of oxygen observed after ammoxidation of the active carbon is probably a result of nitrogen having been built into the coal structure via the oxygen groups. A considerable amount of nitrogen groups introduced on ammoxidation undergoes decomposition on carbonisation and activation, which indicates a low thermal stability of the built in nitrogen groups and their low resistance to alkalia.

Porous structures of the active carbon samples obtained were characterised on the basis of measurements of low-temperature nitrogen sorption. The results are given in Table 3.

Table 3. Structural parameters of the active carbon samples obtained.

Sample	Total surface area [m ² /g]	Micropore area [m ² /g]	Total pore volume [cm ³ /g]	Micropore volume [cm ³ /g]	Average pore diameter [nm]
DN ₁ KA	2021	1995	0.98	0.94	1.93
DN ₂ KA	2342	2307	1.13	1.08	1.94
DKN ₁ A	1661	1629	0.81	0.76	1.97
DKN ₂ A	1701	1668	0.84	0.78	1.97
DKA	1615	1586	0.79	0.75	1.96
DKAN ₁	1398	1372	0.68	0.64	1.96
DKAN ₂	1372	1344	0.67	0.63	1.97

Activation of nitrogen enriched carbon leads to microporous active carbon characterised by a much more developed surface area. The results have also shown a two-way effect of ammoxidation on the porous structure of active carbon. Ammoxidation of the precursor and carbonisate increases their reactivity favouring much better development of the porous structure, while ammoxidation of the active carbon leads to a deterioration of its porous structure. The best structural parameters of the active carbon can be obtained subjecting the material to the modifying processes in the sequence ammoxidation, carbonisation and activation.

In order to establish the acidic-basic properties of the active carbon samples obtained they were subjected to determination of the content of the surface oxygen functional groups. The results are given in Table 4.

The majority of the samples have acidic character of the surface, the exceptions are the samples ammoxidised after activation (DKAN) whose surface is acidic-basic. The greatest number of acidic groups and hence the lowest number of basic ones was found in the samples modified at the stage of precursor (DNKA). The number of the surface oxygen groups was also shown to be temperature dependent. The samples modified at 350°C contain a greater number of acidic groups than those ammoxidised at 300°C.

Table 4 presents also the adsorption value of iodine. The highest number was determined for the carbon samples ammoxidised at the stage of precursor (DNKA), characterised also by the largest surface area (Table 3). The lowest iodine adsorption numbers were found for the samples ammoxidised after activation (DKAN), showing

the smallest surface area. These results point to a correlation between the surface area of an active carbon sample and its sorption abilities.

Table 4. The content of the surface oxygen functional groups (mmol/g) and the adsorption value iodine (mg/g) obtained for the active carbon samples studied.

Sample	Acidic groups [mmol/g]	Basic groups [mmol/g]	Adsorption value of iodine [mg/g]
DN ₁ KA	1.42	0.60	1863
DN ₂ KA	1.56	0.58	1974
DKN ₁ A	1.28	0.62	1669
DKN ₂ A	1.41	0.57	1675
DKA	1.34	0.69	1672
DKAN ₁	0.86	0.99	1527
DKAN ₂	1.02	0.94	1410

4. Conclusions

The results obtained have shown that it is possible to obtain from coking coal a large gamut of active carbon samples characterised by different physico-chemical properties by applying the processes of ammoxidation, carbonisation and KOH activation. Depending on the sequence of the above mentioned processes the active carbon samples have a more or less acidic character of the surface and different sorptive properties towards substances of the molecules size close to 1nm. The development of the surface area significantly depends on the conditions and course of ammoxidation. The samples ammoxidised at the stage of demineralised coal (DNKA) have much greater surface area than those to which nitrogen has not been introduced (DKA). Ammoxidation performed after the activation of carbon (DKAN) causes a decrease in the surface area.

References

- [1] A. Bagreev, M.J. Angel, I. Dukhno, Y. Tarasenko, T. Bandoz, Carbon, 42 (2004) 469
- [2] K. Jurewicz, K. Babel, A. Ziolkowski, H. Wachowska, Journal of Physics and Chemistry of Solids, 65 (2004) 269
- [3] K. Jurewicz, K. Babel, A. Ziolkowski, H. Wachowska, M. Kozłowski, Fuel Processing Technology, 77-78 (2002) 191-198
- [4] W. Radmacher, O. Mohrhauer, Brennstof-Chemie, 37 (1956) 353
- [5] H.P. Boehm, Carbon, 32 (1994) 759
- [6] Polish Standards PN-83 C-97555.04

TOULUENE METHYL GROUP ALKYLATION. A DFT STUDY

Slawomir Ostrowski, Jan Cz. Dobrowolski*, Jacek Kijeński

Industrial Chemistry Research Institute, 8 Rydygiera Street, 01-793 Warsaw

E-mail: Jan.Dobrowolski@ichp.pl; Phone: +(22) 568 2421

Abstract:

Alkylation of the CH₃ group of toluene was modeled at the B3LYP/6-311++G** level. In presence of Na₂, the model basic catalyst, the CH₃ group is more active for the Na/H exchange than the aromatic H atoms and the reaction barrier equals ca. 35 kcal/mol. The PhCH₂Na molecule formed is next alkylated by ethane and, after 30 kcal/mol barrier is overcome, PhC₃H₆Na is formed. Finally, the Na/H exchange between PhC₃H₆Na and toluene proceeds through 18 kcal/mol barrier and ca. 10 kcal/mol is released. This study has confirmed the basic alkylation scheme proposed by Pines et al. over 50 years ago.

Introduction

Alkylation reactions are known since discovery of the Friedel Crafts reaction in 1877 [1]. Alkylation is carried out in presence of both acidic and basic catalysts [2]. Alkylation of alkyloaromatic compounds depends strongly on acid-base properties of a catalyst. The acidic catalysts direct the alkylation toward aromatic ring substitution, in agreement to Friedel Crafts mechanism [1], whereas superbasic catalysts, such as MgO/K α -Al₂O₃-K, favour elongation or branching of the side chain [3, 4]. The alkylation over superbasic catalysts has been also utilized in industrial technologies [5, 6].

The aim of this study is to understand why alkylation of toluene by ethane over a superbasic catalyst results in the side chain elongation. Such a reaction is assumed to proceed according to the scheme proposed by Pines et al. [3]. In this paper we consider the following steps of the reaction:

- (i) Toluene adsorption on a catalyst.
- (ii) Formation of PhCH₂Na: PhCH₃+BNa = PhCH₂Na+ BH, B - base, Ph- phenyl.
- (iii) Ethene insertion: PhCH₂Na+H₂C=CH₂ = PhCH₂CH₂CH₂Na.
- (iv) Na/H exchange: PhCH₂CH₂CH₂Na+PhCH₃ = PhCH₂CH₂CH₃ + PhCH₂Na.
- (v) Desorption of propylbenzene.

In the modeling performed, the Na₂ molecule was used as a model of the superbasic catalyst. To our best knowledge, the alkyloaromatics alkylation over superbasic catalysts has not been modeled by using quantum chemical calculations, so far.

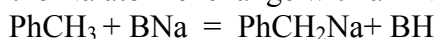
Calculations

The calculation were performed at the B3LYP/6-311++G** level as implemented in the Gaussian 03 program [7]. For each minimum energy structure all harmonic frequencies were positive, whereas for each transition states one imaginary frequency, corresponding to the reaction coordinate was detected. The TSs were found by applying the QST3 method [8]. For all TSs, the intrinsic reaction coordinate (IRC) routine [9] was additionally applied. The Gibbs free energies were also found [10]. It was assumed that the singlet state configuration is preserved throughout all reaction steps.

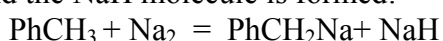
Results and Discussion

Toluene adsorption on a catalyst: The preliminary step of the alkylation reaction is adsorption of the reagent diffusing from bulk into the catalyst surface. Here, the catalyst is approximated by the Na₂ molecule. Thus, the adsorption is here equivalent to the formation of the toluene... Na₂ complex (R1, Fig. 1). At the B3LYP/6-311++G** level, such a process is barrierless and the complex formation is endoergic with Gibbs free energy (ΔG_{298}) equal to ca. 3. kcal/mol.

Formation of the PhCH₂Na molecule: According to Pines et al. [3], PhCH₂Na is formed by the Na atom exchange with a BNa molecule, where B is a base:



In this study it was assumed that the exchange occurs at the catalyst surface, i.e. the toluene H atom is replaced by the Na atom and the hydrogen is moved into the surface, and the NaH molecule is formed:



Because there are four possible sodium toluenates: substituted at o-, m-, p-, and CH₃ positions, it was first checked that the PhCH₂Na molecule more stable than the other three isomers by at least 7. kcal/mol Next, transition states for each of the Na/H exchange reactions were found and followed by the IRC. The barrier for the exchange towards PhCH₂Na was found to be ca 36 kcal/mol and to be smaller than the corresponding barriers towards o-, m-, and p- sodium toluenates by ca. 20 kcal/mol. Thus the PhCH₂Na molecule is not only more stable than the other sodium toluenates, but the barrier towards this compound is significantly smaller than towards the other isomers.

Ethene insertion: The next reaction step is the chain elongation that is ethene insertion into the C-Na bond. Two paths of such a reaction were studied: reaction of ethene with (i) the PhCH₂Na...HNa complex, and (ii) the PhCH₂Na molecule (after the PhCH₂Na...HNa system was dissociated):



The reaction barrier is equal to 30 and 15 kcal/mol for reaction (i) and (ii), respectively (Fig. 2). However, the reaction (ii) to occur requires 30 kcal/mol to be supplied first, to dissociate the PhCH₂Na...HNa complex (Fig. 2). For the two reaction paths, the IRC reaction profiles confirmed that the TSs found corresponds to the appropriate reactions.

The Na/H exchange and desorption: The following step of the basic alkylation of toluene is the Na/H exchange yielding propylbenzene. Again, two reaction paths were considered: (i) the Na/H exchange between sodium propylene benzenate and toluene, and (ii) the Na/H exchange between sodium propylene benzenate and the NaH molecule:

As for the PhCH₂Na...HNa complex, in the (i) reaction product, PhC₃H₆Na...HNa, the hydrogen atom of the NaH molecule is close to the intramolecular Na-H distance and the sodium atom of the NaH molecule interacts with the aromatic π -electron system stabilizing additionally the system (P2a, Fig. 1). On the other hand, the sodium propylene benzenate exhibits the side chain configuration allowing for the Na atom intramolecular interaction with the π -electron system (P2a, Fig. 1).

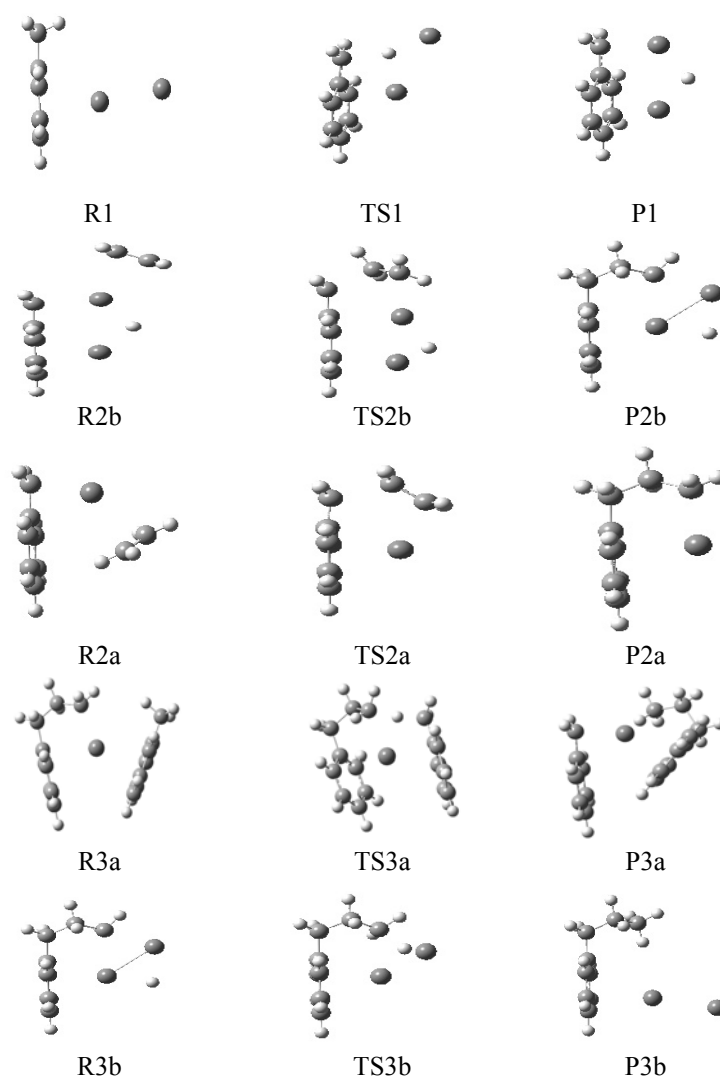


Fig 1. The B3LYP/6-311++G** optimized geometries of reactants, TSs, and products:

- (i) $\text{PhCH}_3 \dots \text{Na}_2 = \text{PhCH}_2\text{Na} \dots \text{NaH}$; ($\text{R1} \leftrightarrow \text{TS1} \leftrightarrow \text{P1}$)
- (ii) $\text{PhCH}_2\text{Na} \dots \text{NaH} + \text{C}_2\text{H}_2 = \text{PhCH}_2\text{CH}_2\text{CH}_2\text{Na} \dots \text{NaH}$; ($\text{R2a} \leftrightarrow \text{TS2a} \leftrightarrow \text{P2a}$)
- (iii) $\text{PhCH}_2\text{Na} + \text{C}_2\text{H}_2 = \text{PhCH}_2\text{CH}_2\text{CH}_2\text{Na}$; ($\text{R2b} \leftrightarrow \text{TS2b} \leftrightarrow \text{P2b}$)
- (iv) $\text{PhCH}_2\text{CH}_2\text{CH}_2\text{Na} + \text{PhCH}_3 = \text{PhCH}_2\text{CH}_2\text{CH}_2 + \text{PhCH}_3\text{Na}$; ($\text{R3a} \leftrightarrow \text{TS3a} \leftrightarrow \text{P3a}$)
- (v) $\text{PhCH}_2\text{CH}_2\text{CH}_2\text{Na} + \text{NaH} = \text{PhCH}_2\text{CH}_2\text{CH}_3 + \text{Na}_2$; ($\text{R3b} \leftrightarrow \text{TS3b} \leftrightarrow \text{P3b}$)

In the first reaction, postulated by Pines et al [3], desired propylbenzene is produced and PhCH_2Na is regenerated. In this case, the reaction barrier is equal to 18 kcal/mol and the reaction products are more stable than the reactants by ca. 9. kcal/mol (Fig. 2).

In the second reaction path, the hydrogen atom deposited at the surface, here the NaH molecule, returns to the organic molecule and metallic surface, here Na_2 , is regenerated. Then the molecule is desorbed from the surface: the $\text{PhCH}_2\text{CH}_2\text{CH}_3 \dots \text{Na}_2$ system dissociates. In such a case, more than 25 kcal/mol must be supplied to the system to overcome the reaction barrier (Fig. 1), and the product is more stable than the reactant complex by ca. 20 kcal/mol (Fig. 1).

- (i) $\text{PhCH}_2\text{CH}_2\text{CH}_2\text{Na} + \text{PhCH}_3 = \text{PhCH}_2\text{CH}_2\text{CH}_3 \dots \text{PhCH}_2\text{Na}$
- (ii) $\text{PhCH}_2\text{CH}_2\text{CH}_2\text{Na} \dots \text{HNa} = \text{PhCH}_2\text{CH}_2\text{CH}_3 \dots \text{Na}_2$

Finally, the $\text{PhC}_3\text{H}_7 \dots \text{Na}_2$ complex dissociation requires only ca. 3. kcal/mol to be supplied to the system.

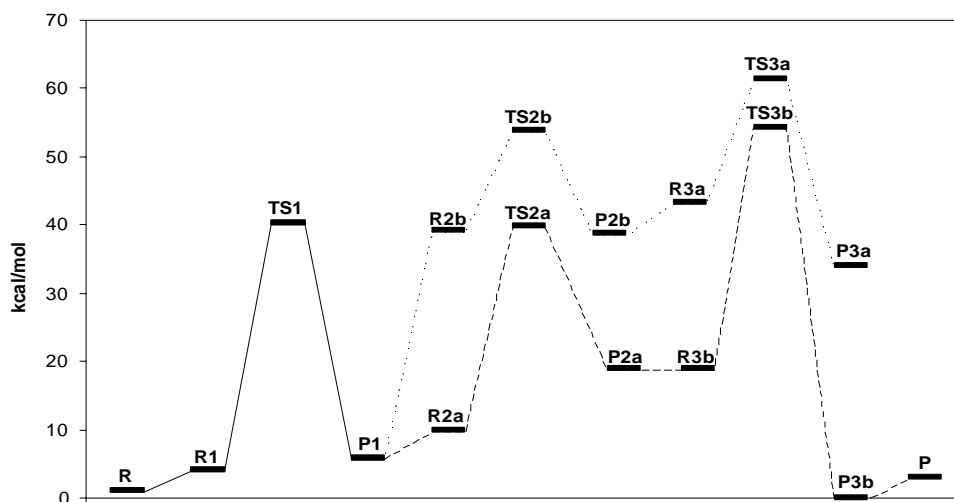


Fig. 2. The energetic scheme of the alkylation of toluene by ethane in presence of Na_2 molecule, as a basic catalyst, modeled at the B3LYP/6-311++G** level. R – all the reactants, P – products after dissociation of Na_2 molecule, the other symbols as in Fig. 1.

Conclusions

Alkylation of the methyl group of toluene over a model superbasic catalyst, the Na_2 molecule, was modeled at the B3LYP/6-311++G** level assuming that the singlet state configuration is preserved throughout all reaction steps. It was found that:

- In presence of the basic catalyst, Na_2 , the PhCH_2Na formation is preferred more than the formation of the isomeric o-, m-, and p- toluenates.
- The ethene insertion into the C-Na bond occurs seemingly easier for the free PhCH_2Na molecule, a matter of 15 kcal/mole, yet in fact this requires additional 30 kcal/mol to dissociate the $\text{PhCH}_2\text{Na}\dots\text{HNa}$ complex that has been formed in the previous step. Thus probably, the insertion to form $\text{PhCH}_2\text{CH}_2\text{CH}_2\text{Na}$ proceeds for the $\text{PhCH}_2\text{Na}\dots\text{HNa}$ reactant and goes through 30 kcal/mol barrier.
- The reaction ends by the Na/H exchange between $\text{PhC}_3\text{H}_7\text{Na}$ and toluene, and requires the 18 kcal/mol barrier to be overcome.

The study confirmed accuracy of the basic alkylation scheme over 50 years ago [3].

Acknowledgement

This work was supported by Grant for statutory activity of ICRI (Warsaw). The computational Grant G19-4 from the Interdisciplinary Center of Mathematical and Computer Modeling (ICM) at Warsaw University is gratefully acknowledged.

References

- [1] G. A. Olah, Friedel-Crafts and Related Reaction. Pp 1-24, New York, Wiley, 1963.
- [2] Ullmann's Encyclopedia of Industrial Chemistry, 7th Edition, Wiley, 2006.
- [3] H. Pines, J. A. Vesely, V. N. Ipatieff, J. Am. Chem. Soc., 77(1954)347.
- [4] J. Kijeński, P. Radomski, E. Fedoryńska, J. Catal., 203(2001)407.
- [5] W. F. Hölderich, in Proceedings of the 10th International Congress on Catalysis, Stud. Surf. Sci. Catal. 75 (1993) 127-163.
- [6] F. Kumata, T. Matsumoto, Mitsubishi Oil. Co., USP 5625102, 1997.
- [7] M. J. Frisch et al. Gaussian 03 (Revision C.02), Gaussian, Inc., 2004.
- [8] C. Peng, H. B. Schlegel, Israel J. Chem., 33(1993)449.
- [9] C. Gonzalez, H. B. Schlegel, J. Phys. Chem. 94(1990) 5523.
- [10] J. W. Ochterski, Thermochemistry in Gaussian, Gaussian, Inc., June 2, 2000.

MD SIMULATION OF CaCl₂ SOLUTION IN METHANOL-WATER MIXTURES.

Emilia Owczarek and Ewa Hawlicka

*Institute of Applied Radiation Chemistry, Department of Chemistry
Technical University, Zeromskiego 116, 90-924 Lodz, Poland*

Introduction:

The calcium ion plays a key role in many biological processes. It is decisive for the control of metabolism, muscle contraction and blood clotting in living bodies[1]. Hydration of Ca²⁺ ion affects a biological activity of many biochemically important polyelectrolytes (e.g. dextran and heparin). Thus our attention is focused on a hydration of calcium ion in water and water-alcohols mixtures.

MD simulation is an effective tool to investigate the structural and dynamical properties of such systems, especially if the experimental methods are not decisive[2].

Potentials and details of the simulation:

The effective potential of ion-ion and ion-solvent molecule interactions may be represented by the following form:

$$V_{ij}(r) = \sum_{j=1}^3 \left[\frac{Q_{ij}}{r_{ij}} + \frac{A_{ij}}{r_{ij}^{n_{ij}}} + B_{ij} \cdot \exp(-C_{ij} \cdot r_{ij}) \right] \quad (1)$$

where r_{ij} denotes distance between interacting sites. Q_{ij} terms represent the Coulomb interactions, which are defined by the ion charges and the partial charges of three sites of the PHH[3] methanol and BJH[4] water molecules. Parameters A_{ij} , B_{ij} and C_{ij} , which have no physical meaning, describe the non-Coulomb part of the potential energy. Interaction between Ca²⁺ and methanol molecule were represented by the recently derived effective potential [2] while for Ca²⁺ and water molecule by potential derived by Probst et al.[5]. The effective potentials reported by Marx et al.[6] and by Hawlicka et al.[7] respectively, were used for Cl⁻-methanol and Cl⁻-water molecules interactions. The ion-ion interactions were described by the effective potential elaborated by Probst et al.[5] and Dietz et al.[8]. All the potential parameters are given in Table 1.

Table 1. Parameters Q_{ij} , A_{ij} , B_{ij} and C_{ij} for interactions of ion-solvent and ion-ion.

i	α	$Q_{i\alpha}$ [kJ $\text{\AA}^n \text{mol}^{-1}$]	$A_{i\alpha}$ [kJ $\text{\AA}^n \text{mol}^{-1}$]	$B_{i\alpha}$ [kJ mol^{-1}]	$C_{i\alpha}$ [\AA^{-1}]	n	Reference
Ca	O _W	-1832.6	-1572.6	2.5970×10^5	3.4900	2	5
Ca	H _W	916.28	626.39	1.2022×10^5	6.7900	2	5
Ca	O _M	-1667.3	-1372.6	2.5970×10^5	3.4900	2	2
Ca	H _M	972.58	933.29	8.3273×10^2	0.9600	2	2
Ca	Me	694.70	-474.93	5.1660×10^4	2.7930	2	2
Cl	O _W	916.28	9.3400	1.1749×10^5	2.6727	2	7
Cl	H _W	-458.14	-68.270	9.0290×10^4	4.5420	2	7
Cl	O _M	833.61	127.00	1.4529×10^5	3.1999	2	6
Cl	H _M	-486.27	-193.37	2.5086×10^4	3.3082	2	6
Cl	Me	-347.34	6.7657	5.9250×10^5	3.2984	2	6
Ca	Ca	5557.6	-15198	2.6010×10^6	4.4870	6	2
Cl	Cl	1389.4	-28672	9.1704×10^5	3.3863	6	8
Ca	Cl	2778.8	-353.01	3.6608×10^5	3.0100	2	5

Two MD simulations were performed for standard NVE ensemble at 298K. The concentration of CaCl₂ was equal 0.52 and 0.50 M for mixtures containing 5 and 10 mol% of methanol in water, respectively. Thus the periodic cubes contained 400 solvent molecules, 4 cations and 8 anions. Their lengths were calculated from experimental densities at 298 K. Initial configurations were obtained by random placement of particles in the cubic box. Ewald summation was applied for Coulomb interactions, and the shifted force potential method was used for all non-Coulomb ones. The simulation time step was 0.25 fs. After about 5 ps of equilibration, simulations of systems were extended up to 150 ps. Velocities and coordinates of all sites were collected in 1 fs intervals for half of the total time and in 10 fs intervals for the rest of simulation. In both simulations the stability of the potential energy was better than 0.1%.

Results and discussion:

The nearest surrounding of the ions in methanol-water mixtures is described by 5 radial distribution functions (O_M, O_W, H_M, H_W, Me). The Ca²⁺O and Cl⁻O radial distribution function are depicted in Fig. 1 and 2, respectively. As seen from Fig.1 the Ca²⁺O_M and Ca²⁺O_W radial distribution function for methanol and water, respectively are completely different. The Ca²⁺O_W function exhibits a sharp peak at (0.240 ± 0.002) nm. Its position is the same in both systems, 5 and 10 mol% of methanol in water and is very close to that in aqueous CaCl₂ solution (0.237 ± 0.002) nm. For all systems the heights of these maxima are comparable. As seen from Fig. 1. the maximum for Ca²⁺O_M is not observed. This means that the methanol molecules do not enter the calcium ion coordination shell.

The Cl⁻O_M radial distribution function shows a sharp peak at (0.320 ± 0.002) nm. This distance is shorter than in methanolic CaCl₂ solution (0.327 ± 0.002) nm[2]. The height of Cl⁻O_M function in methanol-water CaCl₂ solution is almost three times as high as in the case of methanolic CaCl₂. As seen from Fig. 2. the Cl⁻O_W radial distribution function is worse pronounced. This maximum, located at about (0.320 ± 0.002) nm is significantly lower than in the case of Cl⁻O_M function in spite of much higher

concentration of water than methanol. That leads to the conclusion that methanol molecules in the Cl^- coordination shell are more fixed as compared with water ones. This is probably due to the hindered rotation.

The first coordination shell of calcium ion consists of 9 or 10 ($n_W=9.7$) water molecules but it does not contain methanol molecules. The first coordination shell of the chloride ion is completely different. Even in very diluted solution of methanol (5 mol%) the coordination shell of Cl^- contains a few ($n_M=1.6$) methanol molecules and about 6 water molecules. As the amount of methanol increases the number of methanol molecules in the Cl^- coordination shell doubles ($n_M=3.0$) whereas the number of water molecules decreases to about 4÷5 ($n_W=4.4$).

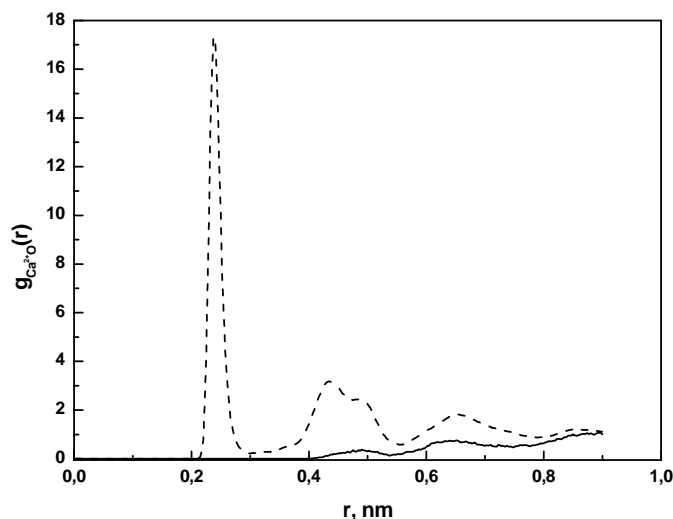


Fig. 1. Ca^{2+} -O radial distribution function for methanol (solid) and water (dashed) in 5 mol% methanol in water CaCl_2 solution.

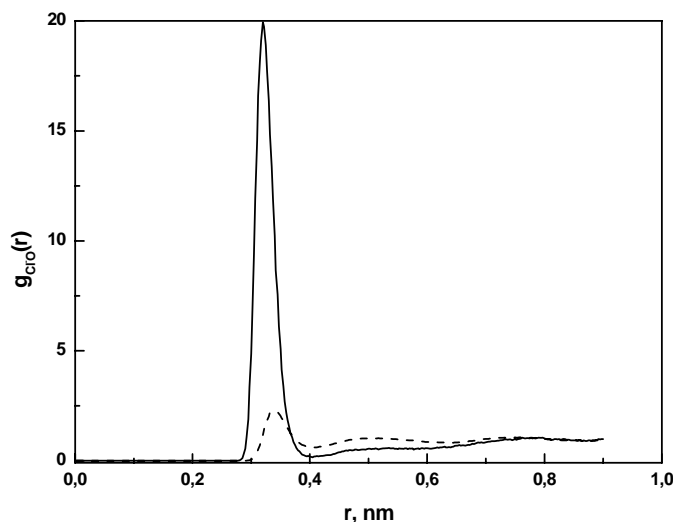


Fig. 2. Cl^- -O radial distribution function for methanol (solid) and water (dashed) in 5 mol% methanol in water CaCl_2 solution.

In order to investigate the hydrogen bonds network numbers and lifetime of the H-bonds were computed separately for whole system and for the ion coordination shells. A geometric criterion of the H-bond was used. That defines the distance between

oxygens of the nearest neighbours R_{OO} , the distance between the hydrogen and oxygen of the H-bond acceptor R_{OH} , and the angle φ between the OH intramolecular bond of the H-donor and the line connecting the oxygens [9].

In the simulated systems the number of H-bonds per one solvent molecule is independent of methanol concentration and is equal $\langle n_{HB} \rangle_M = 2$ and $\langle n_{HB} \rangle_W = 3$ for methanol and water, respectively. In calcium hydration shell the significant decrease of $\langle n_{HB} \rangle$ is observed. These values are 1.1 and 1.9 for 5 and 10 mol%, respectively. For the chloride ion coordination shell H-bond numbers are slightly lower than for the whole solutions. These results $\langle n_{HB} \rangle_M = 1.7$ and $\langle n_{HB} \rangle_W = 2.4$, for methanol and water, respectively are closer to the average HB-numbers, as compared with the results obtained for cation.

The average lifetime of H-bonds is equal (0.518 ± 0.002) ps and (0.412 ± 0.002) ps for 5 and 10 mol%, respectively. The calcium ion field probably hinders a rotation of water molecules causing a slight elongation of the H-bond lifetime. The lifetime of H-bonds in the chloride ion coordination shell is either comparable (for 5 mol%) or slightly shorter (for 10 mol%) than for whole system. Our results show that the addition of CaCl_2 stabilizes the hydrogen bonds network in methanol-water mixtures [9] and this effect is more observable in the case of 5 mol% solution.

Acknowledgement

Financial Support of calculations, done in Interdisciplinary Centre for Mathematical and Computational Modeling (ICM) of Warsaw University, Project Number G27-17, is gratefully acknowledged.

References:

- [1] G. L. Zubay, Biochemistry, Fourth ed., W.C. Brown Publishers, 1998
- [2] E. Owczarek, E. Hawlicka, J. Phys. Chem. B, in press
- [3] G. Palinkas, E. Hawlicka, K. Heinzinger, J. Phys. Chem., 91 (1987) 4334
- [4] P. Bopp, G. Jancso, K. Heinzinger, Chem. Phys. Lett., 98 (1983) 129
- [5] M. M. Probst, T. Radnai, K. Heinzinger, P. Bopp, B. M. Rode, J. Phys. Chem. 89 (1985) 753
- [6] D. Marx, K. Heinzinger, G. Palinkas, I. Bako, Z. Naturforsch. 46a (1991) 887
- [7] E. Hawlicka, D. Swiatla-Wojcik, Chem. Phys. 195 (1995) 221
- [8] W. Dietz, W. O. Riede, K. Heinzinger, Z. Naturforsch. 37a (1982) 1038
- [9] E. Hawlicka, D. Swiatla-Wojcik, Chem. Phys. 232 (1998) 361

complexes” comprises the simple, consecutive species and also the second heteroligand complex of MLL’ type, found in a corresponding solution under inert atmosphere [4,5]. Hence, after rearrangement:

$$[\text{active form}] = C_{\text{Co}} - 2C_{\text{Adduct}} \quad (3)$$

and finally, the oxygenation constant:

$$K_{\text{O}_2} = \frac{[C_{\text{Adduct}}]}{(C_{\text{Co}} - 2C_{\text{Adduct}})^2 [\text{O}_2]} \quad (4)$$

The equilibrium concentration of dioxygen, $[\text{O}_2]$, was calculated on the basis of the known oxygen solubility in water under the defined conditions.

Determination of K_{O_2} on the basis of the full mass balance

The mass balance equations for the metal, Co, amino acid, L, and imidazole, L’, lead to the non-linear equation system:

$$\begin{aligned} f_1([\text{Co}], [\text{L}], [\text{L}']) &= 0 \\ f_2([\text{Co}], [\text{L}], [\text{L}']) &= 0 \\ f_3([\text{Co}], [\text{L}], [\text{L}']) &= 0 \end{aligned} \quad (5)$$

where:

$$f_1 = C_{\text{Co}} - Y[\text{Co}] - [\text{Co}](\beta_1 [\text{L}] + \beta_2 [\text{L}]^2 + \beta_3 [\text{L}]^3) - [\text{Co}](\beta_{1\text{im}} [\text{L}'] + \beta_{2\text{im}} [\text{L}']^2 + \beta_{3\text{im}} [\text{L}']^3 + \beta_{4\text{im}} [\text{L}']^4 + \beta_{5\text{im}} [\text{L}']^5) - \beta_{111} [\text{Co}][\text{L}][\text{L}'] - \beta_{121} [\text{Co}][\text{L}]^2[\text{L}'] - 2 C_{\text{O}_2}$$

$$f_2 = C_{\text{L}} - Y_1[\text{L}] - [\text{Co}](\beta_1 [\text{L}] + 2\beta_2 [\text{L}]^2 + 3\beta_3 [\text{L}]^3) - \beta_{111} [\text{Co}][\text{L}][\text{L}'] - 2\beta_{121} [\text{Co}][\text{L}]^2[\text{L}'] - 4 C_{\text{O}_2}$$

$$f_3 = C_{\text{L}'} - Y_2[\text{L}'] - [\text{Co}](\beta_{1\text{im}} [\text{L}'] + 2\beta_{2\text{im}} [\text{L}']^2 + 3\beta_{3\text{im}} [\text{L}']^3 + 4\beta_{4\text{im}} [\text{L}']^4 + 5\beta_{5\text{im}} [\text{L}']^5) - \beta_{111} [\text{Co}][\text{L}][\text{L}'] - \beta_{121} [\text{Co}][\text{L}]^2[\text{L}'] - 2 C_{\text{O}_2}$$

The total concentrations and formation constants:

C_{Co} – total concentration of cobalt,

C_{L} – total concentration of ligand A, alanine,

$C_{\text{L}'}$ – total concentration of ligand B, imidazole,

C_{O_2} – total concentration of bound oxygen (also of the dimeric oxygen adduct),

$\beta_1, \beta_2, \beta_3$ – overall stability constants of binary Co(II)-alanine complexes

$\beta_{1\text{im}}, \beta_{2\text{im}}, \beta_{3\text{im}}, \beta_{4\text{im}}, \beta_{5\text{im}}$ – overall stability constants of binary Co(II)-imidazole complexes

β_{111}, β_{121} – summary stability constants of Co(II)-alanine-imidazole ternary complexes

The share of the hydrolyzed aquo-ion and the protonated forms of both the ligands was denoted by:

$$Y = 1 + (1/K_{\text{OH}}[\text{H}])$$

$$Y_1 = 1 + \beta_{1H}[H] + \beta_{2H}[H]^2$$

$$Y_2 = 1 + \beta_{1Him}[H]$$

where:

K_{OH} – hydrolysis constant of $Co(II)_{aq}$

β_{1H}, β_{2H} – summary protonation constants of alanine

β_{1Him} – protonation constant of imidazole N3

The equation system was solved numerically against $[Co]$, $[L]$ and $[L']$ by our own program based on the Newton procedure [7] and also by Mathcad 13 (Mathsoft Engineering&Education, Inc.).

Results and discussion

The measurements were carried out at the constant amounts of cobalt and imidazole (according to the experimental requirements) – 0.3 / 0.6 mmole at the sample volume of 30 cm³. Hence, the total concentration of cobalt equaled 0.01 mol dm⁻³. On the other hand, the excess of amino acid was variable.

Table 1 Results of numerical calculations in the cobalt(II) – L- α -alanine – imidazole – O₂ system. Temp. ~0 °C, $I = 0.5$ (KNO₃). Concentrations in mol dm⁻³.

Mmole ratio Co : Amac : Imid	[Co], [Amac], [Himid], log K_{O_2}	Newton procedure	Mathcad 13	Simplified method
0.3 : 0.375 : 0.3	[Co]	$1.224 \cdot 10^{-3}$	$1.224 \cdot 10^{-3}$	
	[Amac]	$4.884 \cdot 10^{-7}$	$4.884 \cdot 10^{-7}$	
	[Himid]	$1.678 \cdot 10^{-3}$	$1.678 \cdot 10^{-3}$	
	log K_{O_2}	16.920	16.920	5.030
0.3 : 0.5 : 0.3	[Co]	$5.714 \cdot 10^{-4}$	$5.713 \cdot 10^{-4}$	
	[Amac]	$3.743 \cdot 10^{-5}$	$3.744 \cdot 10^{-5}$	
	[Himid]	$1.188 \cdot 10^{-3}$	$1.188 \cdot 10^{-3}$	
	log K_{O_2}	10.455	10.455	5.669
0.3 : 0.6 : 0.3	[Co]	$6.701 \cdot 10^{-5}$	$6.701 \cdot 10^{-5}$	
	[Amac]	$3.272 \cdot 10^{-4}$	$3.272 \cdot 10^{-4}$	
	[Himid]	$7.893 \cdot 10^{-4}$	$7.893 \cdot 10^{-4}$	
	log K_{O_2}	8.954	8.954	6.301
0.3 : 0.75 : 0.3	[Co]	$1.570 \cdot 10^{-6}$	$1.570 \cdot 10^{-6}$	
	[Amac]	$1.588 \cdot 10^{-3}$	$1.588 \cdot 10^{-3}$	
	[Himid]	$2.689 \cdot 10^{-4}$	$2.689 \cdot 10^{-4}$	
	log K_{O_2}	10.441	10.441	7.460

As it follows from Table 1 the solutions of equation system (5), obtained by both numerical methods, were positive and almost identical at Amac : Co ratio from 1.25 : 1 up to 2.5 : 1. The free concentrations of cobalt decrease with the rising excess of amino acid. At the same time there is also an observable rise in free Amac concentrations and a relatively lower decrease in [Himid]. The log K_{O_2} values were distinctly different than the values resulting from the simplified method. Particularly at the lower amounts of Ala the differences reached many orders of magnitude. This effect may be explained by a relatively low degree of complexation under such conditions and also by the observed incomplete solubility of the $[Co(imid)_2]_n$ polymer at deficiency of the amino acid.

At the Amac : Co ratio not much less than 2 : 1 and higher, the log K_{O_2} based on full mass balance was similar to the one obtained by simplified calculations. The best consistence could be found at stoichiometric ratio 2 : 1 – the difference was only in two orders of magnitude. Such a difference is quite justifiable if the simplified balance does not take into account any other complex species in the solution except of the “active” complex and the complex equilibria are treated as entirely shifted towards formation of the oxygen dimer.

Conclusions

The approximate value of log K_{O_2} reported up to now for L- α -alanine, obtained at excess of the amino acid, amounted to 6.95 [3], which is a number comparable with our results shown in Table 1 for Amac : Co = 2 : 1 and 2.5 : 1. Thus, the higher values resulting from the full mass balance calculations may be evidently attributed to an essential share of other species, not active in the dioxygen uptake. Moreover, as the only accessible formation constants used in the mass balance referred to a higher temperature (25 °C), the final log K_{O_2} is rather an approximation of the exact value that could be found by applying the proper formation constants (determined at ~0 °C). Nevertheless, the method based on a full mass balance, described herein, seems to be a general method also for other mixed systems derived from the $[Co(imid)_2]_n$ polymer, involving all the accepted equilibria present in the inert solution.

Acknowledgment:

Financial support of this work by the Medical University of Łódź (project 503-3014-2) is acknowledged.

Literature:

- [1] B. Jeżowska-Trzebiatowska, A Vogt, P. Chmielewski, Zesz. Nauk. UJ, 731 (1985) 31
- [2] A. Kufelnicki, M. Pająk, Ann. Polish Chem. Soc., (2003), 467
- [3] A. Vogt, Ph.D. Thesis, Institute of Chemistry, University of Wrocław 1980, pp. 297, 156
- [4] A. Kufelnicki, M. Woźniczka, Ann. Polish Chem. Soc., 3 (2004), 692
- [5] M. Woźniczka, M. Pająk, A. Vogt, A. Kufelnicki, Polish J. Chem., in press
- [6] E. C. Niederhoffer, J.H. Timmons and A. E. Martell, Chem. Rev., 84 (1984) 137
- [7] K. Ebert, H. Ederer, Computeranwendungen in der Chemie, VCH, Weinheim 1985, p. 309

ENZYMATIC SYNTHESIS OF [2- ²H]-L-DOPA

Małgorzata Pająk, Marianna Kańska

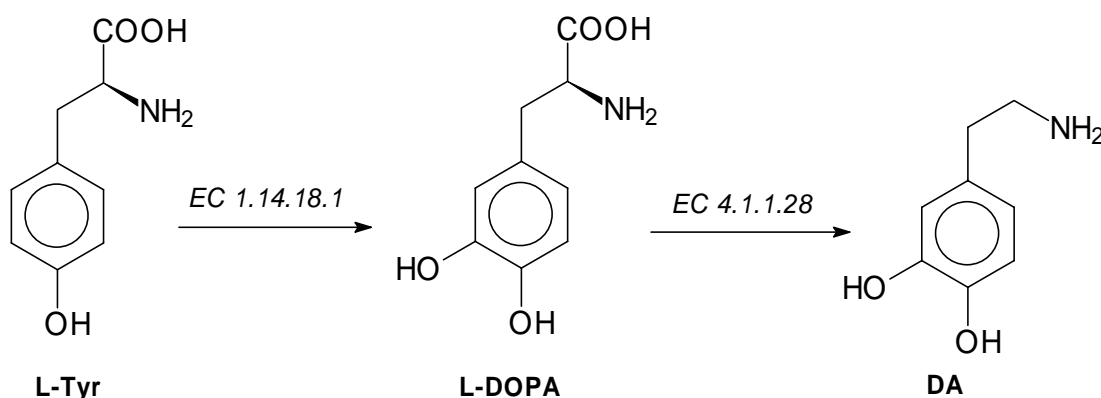
Department of Chemistry, University of Warsaw, Pasteur 1 Str., 02-093 Warsaw

Abstract

The synthesis of isotopomer of L-DOPA selectively labeled with deuterium, i. e., [2-²H]-L-DOPA, is reported. This compound was obtained in two step synthesis. In the first step by enzymatic introduction of deuterium into 2 position [2-²H]-L-tyrosine was afforded. In next step [2-²H]-L-tyrosine was converted to L-DOPA by enzymatic hydroxylation catalyzed by enzyme tyrosinase (EC 1.14.18.1) from mushrooms *Neurospora crassa*.

Introduction

L-DOPA (3',4'-dihydroxy-L-phenylalanine) plays a significant role in many metabolic processes [1-4]. It is precursor of biogenic amine dopamine, DA, a important neurotransmitter in the nervous system of mammals [5-7]. In the living cells L-DOPA is produced by enzymatic hydroxylation of L-tyrosine, L-Tyr, catalyzed by tyrosinase EC 1.14.18.1). Subsequently dopamine is formed in brain as a result of decarboxylation of L-DOPA catalyzed by enzyme Aromatic L-Amino Acid Decarboxylase (EC 4.1.1.28), [8-10], Scheme 1.



Scheme 1. Enzymatic conversion L-tyrosine into dopamine via L-DOPA

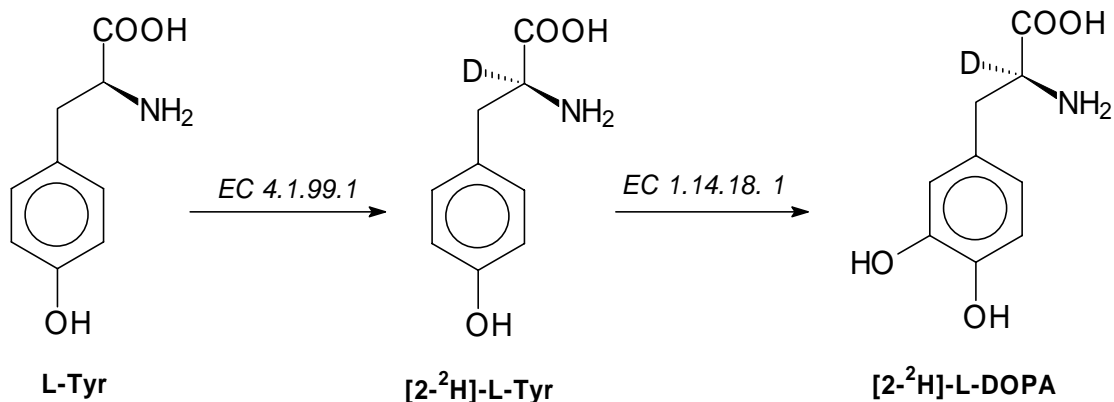
From the many years L-DOPA as a drug drew attention among biologists and medical doctors and researchers as a disorders in enzymatic decarboxylation of L-DOPA responsible for production of dopamine lead to disturbances of the brain functions and subsequently to many pathologies including also Parkinson disease [11-14].

The mechanisms of enzymatic hydroxylation of L-Tyr and decarboxylation of L-DOPA are not clear up to now, so it would be interesting to investigate this problem using kinetic isotope effect method, KIE. Determination of numerical values of KIE for these two reactions depicted in Scheme 1 allows to characterize the active complexes formed in transition step determining rate of reaction, find the bonds involved in formation of transition state, and elucidate other mechanism details [15]. For KIE

studies specifically labeled isotopomers of L-Tyr, L-DOPA and DA are needed. In this paper, a synthesis of specifically labeled with deuterium compounds [2-²H]-L-DOPA is presented.

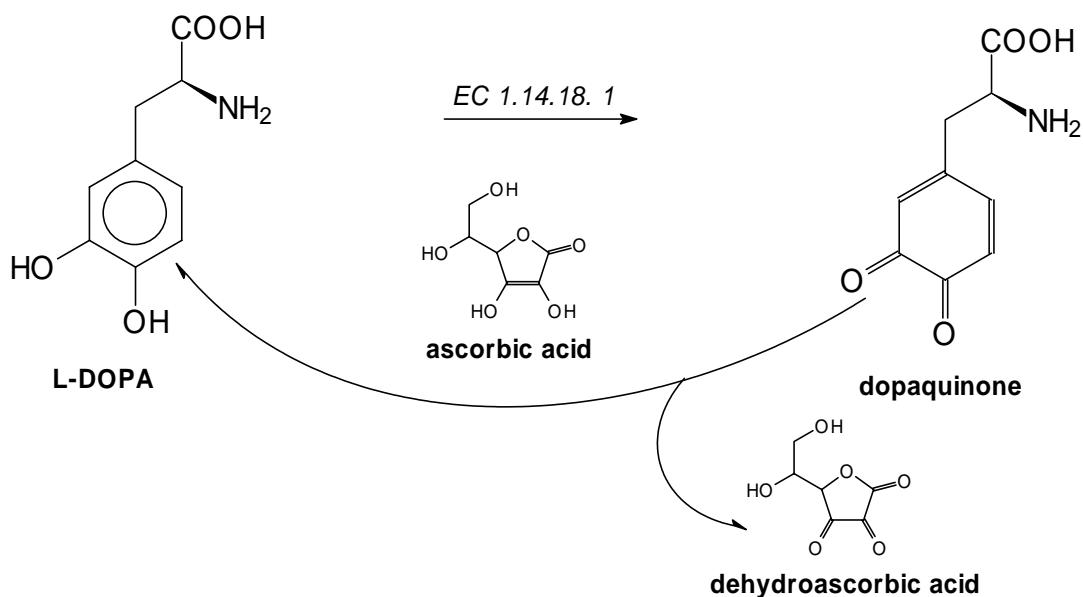
Result and discussion

The chosen synthetic path for obtain of [2-²H]-L-DOPA consists of two steps, Scheme 2.



Scheme 2. Enzymatic synthesis of [2-²H]-L-DOPA

In the first step the deuterium label was introduced into 2-position by enzymatic isotopic exchange between fully deuteriated incubation medium and L-Tyr catalyzed by enzyme tryptophanase (EC 4.1.99.1) from *E. coli*. In some conditions this enzyme causes labilization of hydrogen attached to α -carbon of many native L-amino acids and facilitates the H/D exchange with heavy water [16,17]. In the next step deuteriated [2-²H]-L-DOPA was afforded by enzymatic hydroxylation of intermediate [2-²H]-L-Tyr using enzyme tyrosinase (EC 1.14.18.1) isolated from mushrooms *Neurospora crassa* [18,19].



Scheme 3. Reversible reduction of dopaquinone by ascorbic acid

In the final step some precautions have been taken because tyrosinase immediately mediates the oxidation of L-DOPA to dopaquinone. Addition of ascorbic acid to incubation medium allows to reduce dopaquinone back to L-DOPA, and to afford a good yield in this step [20], Scheme 3. The degree and position of deuterium incorporation into L-Tyr and L-DOPA were determined by means of ^1H NMR spectra.

Experimental

1. *Synthesis of [2- ^2H]-L-tyrosine, 1.* A sample of 22.8 mg (0.126 mmol) of L-tyrosine was dissolved in 42.0 ml of fully deuteriated 0.05 M K_2DPO_4 buffer (pD 8.3), and next 1.1 mg of pyridoxal phosphate, PLP, and 300 U of enzyme tryptophanase from *E. coli* (EC 4.1.99.1) were added. The reaction mixture was incubated for 7 day in room temperature. After incubation the enzyme was removed by centrifugation, and the mixture was loaded on the chromatographic column (10 x 100 mm) filled with Amberlite IR-120 (H^+). First, the buffer salts were washed out with distilled water, and in next step **1** was eluted with 0.3 M $\text{NH}_3(\text{aq})$ and collected as 6 ml fractions. The fractions containing **1** were pooled and evaporated to dryness under reduced pressure. As a result 22.4 mg sample of **1** was obtained (98% yield). ^1H NMR analysis shown that the incorporation of deuterium at the $\alpha\text{-C}$ of **1** proceeds with nearly 100% yield. The purity of product was checked by TLC (silica gel; acetonitril: water = 4:1).
2. *Synthesis of [2- ^2H]-L-DOPA, 2.* A sample of 10 mg (0.055 mmol) of [2- ^2H]-L-tyrosine was dissolved in 10 ml of 0.1 M K_2HPO_4 buffer adjusted to pH 6.8 with solid ascorbic acid. To this solution 5000 U of enzyme tyrosinase from *Neurospora crassa* (EC 1.14.18.1) were added. This mixture was incubated for 24 h in room temperature. After incubation the enzyme was removed by centrifugation, and the residual solution was loaded on the chromatographic column (10 x 100 mm) filled with Al_2O_3 (chromatography active Brockmann, POCh Gliwice) equilibrated to pH 6.1 with 0.5 M ammonium acetate [3]. First, the unreacted **1** was washed out with 0.5 M ammonium acetate (pH 6.1), and in next step **2** was eluted with 0.5 M acetic acid and collected as 6 ml fractions. The presence of **2** in each fraction was checked with potassium iodide (KIO_3). Fractions containing **2** were pooled, acidified with conc. HCl to pH 1, and evaporated to dryness under reduced pressure. The residue was dissolved in 2 ml of water and once again loaded on the same column as above early washed with water. The residual ammonium acetate was washed out with water and product **2** was eluted with 0.5 M acetic acid. Fractions containing **2** were combined and evaporated under reduced pressure, and next evaporated to dryness under vacuum leaving 3.4 mg of **2** (yield 31%). Purity was checked by TLC as above.

Acknowledgements

This work was supported by grant BST-112123

References

- [1] L. Stryer, *Biochemistry*, Freeman, 3th Edition, New, York, 1988.
- [2] S. H. Pomerantz, *J. Biol. Chem.*, 228 (1963) 2351
- [3] S. H. Pomerantz, *Biochem. Biophys. Res. Comm.*, 16 (1964) 188
- [4] S. H. Pomerantz, M. C. Warner, *J. Biol. Chem.*, 242 (1967) 5308
- [5] M. M. Wick, G. Fitzgerald, *Chem. Biol. Interactions*, 38 (1981) 99

- [6] R. T. Premont, R. R. Gainetdinov, M. G. Caron, *Proc. Natl. Acad. Sci.*, 98 (2001) 9474
- [7] A. Nieoullon, A. Coquerel, *Curr. Opin. Neurol.*, 16 Suppl 2 (2003) 3
- [8] W. Lovenberg, H. Weissbach, S. Udenfriend, *J. Biol. Chem.*, 237 (1962) 89
- [9] C. Borri-Voltattorni, A. Minelli, P. Vecchini, A. Fiori, C. Turano, *Eur. J. Biochem.*, 93 (1979) 181
- [10] T. L. Sourkes, *Methods in enzymology*, Academic Press, New York, 147 (1987) 170
- [11] P. Bjurling, Y. Watanabe, S. Oka, T. Nagasawa, H. Yamada, B. Långström, *Acta Chem. Scand.*, 44 (1990) 183
- [12] R. Ceravolo, D. Volterrani, G. Gambaccini, S. Bernardini, C. Rossi, C. Logi, G. Tognoni, G. Manca, G. Mariani, U. Bonuccelli, L. Murri, *Neural. Transm.*, 111 (2004) 1065
- [13] J. Li, M. Zhu, A.B. Manning-Bog, D.A. Di Monte, A.L. Fink, *FASEB J.*, 18 (2004) 962
- [14] K. J. Lindner, P. Hartvig, J. Tedroff, A. Ljungström, P. Bjurling, B. Långström, *J. Pharmaceut. Biomed. Anal.*, 13 (1995) 361
- [15] F. Cook, *Enzyme mechanism from isotope effects*, CRS Press, Boca Raton, FL, USA, 1991.
- [16] K. D. Schnackerz, E. E. Snell, *J. Biol. Chem.*, 258 (1983) 4839
- [17] Y. Kawata, S. Tani, M. Sato, Y. Katsube, M. Tokushige, *FEBS*, 284 (1991) 270
- [18] H. Claus, H. Decker, *Syst. Appl. Microbiol.*, 29 (2006) 3
- [19] V. J. Hearing, T. M. Ekel, *Biochem. J.*, 157 (1976) 549
- [20] R. Ros, J. N. Rodríguez- López, F. García-Cánovas, *Biochem. J.*, 259 (1993) 309

ENZYMATIC SYNTHESIS OF ISOTOPOMERS OF TYRAMINE LABELED WITH DEUTERIUM AND tritium

Edyta Panufnik, Marianna Kańska*

Department of Chemistry, University of Warsaw, Pasteur 1 Str., 02-093 Warsaw

Summary

The combined chemical and enzymatic methods of synthesis of five isotopomers of L-tyrosine, L-Tyr, and their derivatives, i.e., corresponding isotopomers of tyramine, TA, labeled with deuterium and tritium have been reported. Two step synthesis consists with introduction of deuterium or tritium label into intermediate L-Tyr using isotope exchange followed by enzymatic decarboxylation using enzyme tyrosine decarboxylase (EC 4.1.1.25). This way five isotopomers of L-tyrosine, i.e. [2-²H]-L-, [2-³H]-L-, [2-²H/³H]-L-, [3',5'-²H₂]-L-, [3',5'-³H₂]-L-Tyr, and six isotopomers of tyramine i. e., [1S-²H]-, [1S-³H]-, [1S-²H/³H]-, [3',5'-²H₂]-, [3',5'-³H₂]-, [2',6'-²H₂]-tyramine were obtained.

Introduction

Tyramine, TA, a biogenic amine, found in plant cells and mammalian tissues and fluids, play an important role in very metabolic processes. It is one of the neurotransmitters in central nervous systems in human¹⁻³ and a substrate for enzymatic hydroxylation to other important neurotransmitter i.e., dopamine [4,5]. As a intermediate tyramine is responsible for generating the melanin in human and for browning fruits and vegetables.^{4,5} In the living cells tyramine is produced by enzymatic decarboxylation of L-tyrosine, L-Tyr, catalyzed by enzyme tyrosine decarboxylase (EC 4.1.1.25)⁶, Fig. 1.

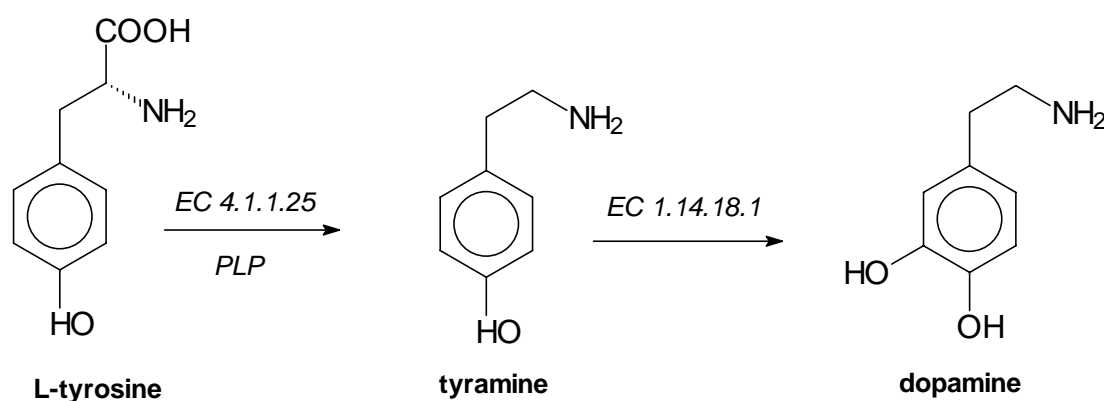


Fig.1. Enzymatic conversion of L-tyrosine into tyramine and dopamine

Despite many literature data the mechanisms of two above depicted reactions are not completely understood. It would be interesting to study these decarboxylation and hydroxylation reactions using isotope effects methods.⁷⁻¹⁰ Determination of numerical values for solvent isotope effects, SIE, and kinetic isotope effects, KIE, will be useful for distinguishing between the alternative intrinsic details, allows find the bonds involved in formation of active complex etc. For this kind of investigation the specifically labeled isotopomers of L-Tyr and TA are needed. In this paper the combined chemical and enzymatic methods of synthesis of ring and side chain labeled with deuterium and tritium five isotopomers of L-Tyr and six isotopomers of TA are described.

Result and discussion

For synthesis of labeled in 2-position of side chain L-Tyr, a substrate to obtaining a corresponding isotopomers of tyramine, we modified some methods early described.¹¹⁻¹⁷ The synthetic path depicted in Fig. 2 consists of using subsequently two enzymes; first of them, i.e., tryptophanase (EC. 4.1.99.1) introduces the label (deuterium or tritium into 2-position of L-Tyr, second one, i.e., tyrosine

In the first one using H/D isotope exchange method between heavy water and L-tyrosine a intermediate $[3',5'\text{-}^2\text{H}_2]\text{-L-Tyr-DCl}$, **8**, was achieved. In the acid catalyzed conditions the exchange between D_2O and L-Tyr, **1**, introduces deuterium exclusively into *ortho* position¹⁶ (respectively to ring hydroxyl group) in tyrosine yielding above mentioned isotopomer **8**. To avoid isotopic dilution the exchange was carried out in fully deuteriated medium ($\text{D}_2\text{O}/\text{DCl}$). The second step consists with enzymatic decarboxylation of deuteriated L-tyrosine, **8**, to desired product, **9**, catalyzed by enzyme tyrosine decarboxylase (EC 4.1.1.25) from *Streptococcus faecalis*. The same manner the commercial $[2',6'\text{-}^2\text{H}_2]\text{-L-Tyr}$ was decarboxylized to $[2',6'\text{-}^2\text{H}_2]\text{-TA}$, **10** isotopomer.¹³ The position and degree of incorporation of deuterium into aromatic ring of L-tyrosine and tyramine were determined using ^1H NMR spectra.

In the second direct synthetic route deuteriated $[3',5'\text{-}^2\text{H}_2]\text{-TA-DCl}$, **11**, as well as, tritiated $[3',5'\text{-}^3\text{H}_2]\text{-TA}$, **12**, were obtained in the course of acid catalyzed isotopic exchange²⁰ carried out between deuteriated or tritiated water and unlabeled tyramine, Fig. 5. In this case, as mentioned above, the deuterium is incorporated exclusively in 3 and 5 ring position of tyramine.

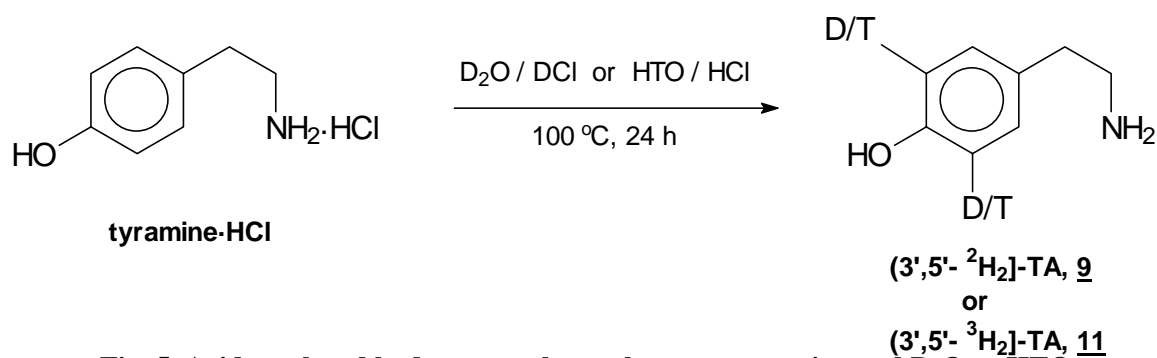


Fig. 5. Acid catalyzed hydrogen exchange between tyramine and D_2O or HTO

Experimental

Materials

Tritiated water was purchased from ICN Pharmaceutical Inc, Irvine Ca, USA. Deuteriated water (99.9 % deuterium), solutions of 37% $\text{DCl}/\text{D}_2\text{O}$, 83% $\text{D}_3\text{PO}_4/\text{D}_2\text{O}$, and 30% $\text{KOD}/\text{D}_2\text{O}$ needed for preparation of fully deuteriated phosphate buffer were obtained from Polatom (Poland). Deuteriated $[2',6'\text{-}^2\text{H}_2]\text{-L-tyrosine}$ was from Sigma. Scintillation cocktail was purchased from Rotiszint (Germany). TLC plates (*DC Plastikfolien Aluminiumoxid 60 F₂₅₆, neutral, type E*), and *Kieselgel 60* were from Merck. The enzymes: tryptophanase (EC 4.1.99.1) from *E. coli* and tyrosine decarboxylase (EC 4.1.1.25) from *Streptococcus faecalis*, and coenzyme pyridoxal 5-phosphate, PLP, were purchased from Sigma. L-Tyrosine and tyramine hydrochlorides, and other chemicals, needed for the enzymatic synthesis and control experiments, were obtained from Sigma.

Methods

The proton NMR spectra were recorded in DMSO-d_6 or D_2O using TMS as internal standard on Varian 200 MHz Unity-Plus spectrometer. The radioactivity of all samples was determined using liquid scintillation technique on automatic counter LISA LSC PW470 (Germany).

Synthesis

1. *Synthesis of $[2\text{-}^2\text{H}]\text{-L-tyrosine}$, **2**.* In incubation vial containing 42 ml of heavy water (99,8% atom D) were dissolved in turn: 27.3 mg (0.126 mmol) of L-tyrosine hydrochloride, **1**, 371 mg (2.13 mmol) of K_2HPO_4 , and 1.1 mg (4.5 μmol) of PLP. This reaction medium was adjusted to pH 8.3 with solid KH_2PO_4 , and about 1 U of enzyme tryptophanase isolated from *E. coli* (EC 4.1.99.1) was added. This reaction mixture was incubated for 7 days in room temperature. The exchange was quenched by immersing the vial in hot water for a few minutes. The precipitated proteins were separated by centrifugation, and the supernatant was loaded onto the column (Amberlite 120, H^+ ; 10×100 mm) and **2** was eluted with 0.3 M $\text{NH}_3(\text{aq})$. The presence of tyrosine in each eluted fraction was checked by TLC (silica gel, eluent: methanol - 25% $\text{NH}_3(\text{aq})$; v/v, visualization by ninhydrine). The fractions containing **2** were combined and solvent was evaporated under reduced pressure at 50°C. The precipitated crystals was washed with ethanol and ethyl ether, and dried under vacuum. As a result 22.2 mg (0.123 mmol) of **2** was obtained (97% yield). The ^1H NMR

- spectrum shown near 100% incorporation of deuterium into 2-position of **2**. ^1H NMR (200 MHz, DMSO- d_6): δ 3.03 (1H, β -H, d, 14.4 Hz), 3.18 (1H, β -H, d, 14.4 Hz), 6.89 (2H, ArH, d, 8.7 Hz), 7.18 (2H, ArH, d, 8.7 Hz). Signal from α -proton i.e., δ 3.93 (1H, α -H, dd, 5,7 Hz) disappeared.
- Synthesis of [2- ^3H]-L-tyrosine, **3**.** To 2.8 ml of 0.05 M potassium phosphate buffer (pH 8.3) was added in turn; 0.2 ml of tritiated water (total radioactivity of 55.6 GBq), 11.7 mg (54 μmol) of L-tyrosine hydrochloride, **1**, 1 μl of PLP, and 0.5 U of enzyme tryptophanase. The reaction mixture was incubated for 5 days at 30°C. The reaction was quenched by adding 40 μl of conc. HCl. Tritiated water was removed by lyophilisation, and a residue dissolved in small amount of water was loaded onto a column (Amberlite IR 120, H^+ , 10 \times 100 mm). The column was washed with water to remove the buffer salts and a rest of tritium from labile positions of tyrosine up to the moment when radioactivity of eluted fraction was close to background. Next, **3** was eluted with 0.3 M $\text{NH}_3(\text{aq})$ and collected as 5 ml fractions. From each fraction the 10 μl sample was taken for radioactivity assay. The fractions containing **3** were combined and treated as described in point 1. As a result a 9.5 mg (52.5 μmol) of **3** with total radioactivity of 1.94 MBq was obtained (97% radiochemical yield, specific activity – 3.7×10^7 Bq/mmol).
 - Synthesis of doubly labeled [2- ^2H / ^3H]-L-tyrosine, **4**.** A 4.3 mg (19.8 μmol) sample of L-tyrosine, **1**, was dissolved in 1.5 ml of fully deuteriated phosphate buffer (pD 8.3) prepared with 83% $\text{D}_3\text{PO}_4/\text{D}_2\text{O}$, 30% KOD/ D_2O and heavy water. To this solution were added in turn: 0.26 U of enzyme tryptophanase, 1 μmol PLP in D_2O , 10 μl of mercaptoethanol, and 0.3 ml of tritiated water with total radioactivity 58 GBq. The reaction mixture was incubated at 30°C for 7 days with constant stirring. The reaction was quenched by adding 40 μl of conc. HCl. The procedure of separation and purification of **4** was the same as described in points 1 and 2. As a result a 3.4 mg (18.8 μmol) sample of **4** with total radioactivity of 7.8×10^5 Bq was obtained (94% radiochemical yield, specific activity - 4.15×10^7 Bq/mmol).
 - Synthesis of [1S- ^2H]-tyramine, **5**.** To incubation vial containing 5 ml of 0.1 M phosphate buffer were added: 3.5 mg (19.3 μmol) sample of early obtained **2**, 1 μmol of PLP, and 1 mg (12.5 U) of enzyme tyrosine decarboxylase (EC 4.1.1.25) from *Streptococcus faecalis*. The reaction mixture was thermostated for 1 hour at 37°C. Next, the post reaction mixture was loaded onto the Kieselgel 60 (10 \times 100) column and eluted with solution: methanol: 25% $\text{NH}_3(\text{aq})$, (20:1, v/v), and collected as 1.5 ml fractions. The presence of tyramine in each eluted fractions was checked by TLC as described in point 1. The fractions containing tyramine were combined and evaporated under reduced pressure at 50°C. As a result 2.1 mg (15.3 μmol) sample of **5** was obtained with 80% chemical yield.
 - Synthesis of [1S- ^3H]-tyramine, **6**.** Decarboxylation of 3.5 mg sample of [1- ^3H]-L-tyrosine, **3**, (obtained as described in point 2) with total radioactivity 7.1×10^5 Bq was preceded the same manner as in the case of deuteriated one (see point 4). The presence of labeled compounds in eluted fractions was checked by radioassays as described in point 2. The fractions containing **6** were combined and evaporated under reduced pressure. The purity of product was checked by TLC as above. As a result 1.6 mg (11.6 μmol) sample of **6** with total radioactivity of 4.25×10^5 Bq was obtained (60% radiochemical yield, specific activity of 3.66×10^7 Bq/mmol).
 - Synthesis of doubly labeled [1S- ^2H / ^3H]-tyramine, **7**.** The synthesis of this isotopomer of tyramine was carried out as described in point 5. In decarboxylation procedure all sample of **4** (3,4 mg, total radioactivity of 7.8×10^5 Bq) was used. A 1.7 mg (12.5 μmol) sample of **7** was obtained with total radioactivity of 5.15×10^5 Bq (66% radiochemical yield, specific activity 4.1×10^7 Bq/mmol).
 - Synthesis of deuteriated [3',5'- $^2\text{H}_2$]-L-tyrosine-DCl, **8**.** A sample of 200 mg of L-tyrosine hydrochloride, **1**, was dissolved in 6 ml of 2 M deuteriochloric acid (5 ml of D_2O + 1 ml conc. DCl/ D_2O) and placed in glass ampoule. The ampoule was connected to vacuum apparatus, its contains frozen with liquid nitrogen, degassed under vacuum, and sealed. The ampoule was heated at 100°C for 24 h. Next, ampoule was cooled to room temperature, opened, and water with deuteriochloric acid were removed by lyophilisation under vacuum. As a result 197 mg of **8** was obtained (97% yield). The analysis of ^1H NMR spectrum (DMSO- d_6 , TMS, 200 MHz Unity plus spectrometer) shown near 100% deuterium incorporation into 3' and 5' position of **8**. ^1H NMR -: δ 3.03 (1H, β -H, d, 14.4 Hz), 3.18 (1H, β -H, d, 14.4 Hz), 3,93 (1H, α -H, dd, 5,7 Hz), 7.18 (2H, ArH,

d, 8.7 Hz). Signal from 3' and 5' of ring protons, i.e., δ 6.89 (2H, ArH, d, 8.7 Hz) disappeared. Purity of product checked by TLC shown negligible amount of impurities (silica gel, methanol:25% $\text{NH}_3(\text{aq})$, 20:1, v/v; visualization by ninhydrine). So, this crude product was taken for further enzymatic decarboxylation without purification.

8. *Synthesis of [3',5'- $^2\text{H}_2$]-tyramine, **9**.* To incubation vial containing 6 ml of 0.1 M phosphate buffer were added: 4.7 mg (19.3 μmol) of deuteriated L-Tyr·DCl, **8**, early obtained, 1 μmol of PLP and 12.5 U of enzyme tyrosine decarboxylase (EC 4.1.1.25) from *Streptococcus faecalis*. The incubation mixture was thermostated for 1 h at 37°C. Next, reaction mixture was loaded onto the Kiesegel (E. Merck) column (10x100 mm) and eluted with solution methanol:25% $\text{NH}_3(\text{aq})$, 20:1, v/v. The eluent was collected as 1.5 fractions. The presence of tyrosine and tyramine in each fraction was tested as above by TLC. The fractions contained **9** were combined, evaporated under reduced pressure at 50°C, and finally under vacuum. As a result 2.1 mg (15.3 μmol) of **9** was obtained with 80% yield. ^1H NMR (200 MHz, D_2O): δ 2.91 (2H, β -2H, t, 37 Hz), 3.23 (2H, α -2H, t, 37 Hz), 7.20 (2H, ArH, d, 20 Hz). Signal from 3' and 5' of ring-protons, i.e., δ 6.89 (2H, ArH, d, 21 Hz) disappeared.
9. *Synthesis of [2',6'- $^2\text{H}_2$]-tyramine, **10**.* This deuteriated isotopomer of tyramine was obtained by decarboxylation of commercial [2',6'- $^2\text{H}_2$]-L-tyrosine the same manner as described in point 8. For decarboxylation 3,5 mg (19.3 μmol) substrate were taken and as a result 2.1 mg (15.3 μmol) of **10** was obtained with 80% yield.
10. *Synthesis of [3',5'- $^2\text{H}_2$]-tyramine deuteriochloride **11**.* The isotopic H/D exchange between heavy water and tyramine was carried out similarly as described for synthesis of **8**. A sample of 201 mg of tyramine hydrochloride dissolved in 6 ml of 2 M deuteriochloric acid was heated at 130°C for 24 h. The further procedure was the same as in case of **8** (point 7). As a result 198 mg of **11** was isolated (near 99% yield). The ^1H NMR spectrum prove as in the of decarboxylation described in point 8 that incorporation of deuterium take also place exclusively in 3' and 5' ring position of tyramine.
11. *Synthesis of [3',5'- $^3\text{H}_2$]-tyramine, **12**.* Tritiated isotopomer **12** was obtained similarly as deuteriated one, i.e., **11**. To glass ampoule were added in turn: 200 mg (1.15 mmol) tyramine hydrochloride, 0.9 ml of water, 0.2 ml of conc. HCl, and 100 μl of tritiated water with total radioactivity 11.1 GBq. The ampoule was sealed under vacuum as in point 1a and heated at 130°C for 24 h. After opening the tritiated water was removed by lyophilisation, and residue was dissolved in small amount of water (1-2 ml) and loaded on column (10x100 mm) filled with Dowex WX-50 (H^+). The residual tritiated water and tritium with labile position of $-\text{NH}_2$ group were washed out with distilled water up to moment where radioactivity of eluent was close to background. Tritiated product, **12**, was eluted with 0.5 M $\text{NH}_3(\text{aq})$ and collected as 6 ml fractions. From each fraction 100 μl sample was taken for radioactivity assay on liquid scintillation counter. Fractions contained **12** were combined, evaporated under reduced pressure, and finally under vacuum. As a result 160 mg (0.92 mmol) of **12** was obtained (yield 74%) with total radioactivity 6.4×10^7 Bq (sp. activity – 6.9×10^7 Bq/mmol). The purity of product was verified by TLC.

Acknowledgment

This work was supported by grant KBN 1 T09A 029 30.

BIOGENIC SUBSTANCES VERSUS THE LEVEL OF GROUND WATERS IN CHOSEN WOODLAND ECOSYSTEMS OF SŁOWIŃSKI NATIONAL PARK

Agnieszka Parzych, Jan Trojanowski

*Department of Chemistry,
Institute of Biology and Environmental Protection,
Pomeranian Pedagogical University of Słupsk,*

1. Introduction

The location of Słowiński National Park (SNP) in the vicinity of big lakes and The Baltic Sea affects hydrological relations in the investigated woodland ecosystems in a significant way. Variations of the levels of ground waters in the examined soils show seasonal variability. Their level is mainly affected by precipitation as well as variations of water levels in adjacent lakes and The Baltic Sea. Seasonal variability of biogenic substances in the examined ground waters is influenced by the kind of soil as well as the type of woodland community [2]. The purpose of the work was to get to know and compare the dynamics of nitrogen and phosphorus compounds in ground waters of two different woodland communities.

2. Study area

The dynamics of ground waters in the area of SNP was examined in two different woodland communities in the years 2003-2005: *Vaccinio uliginosi – Betuletum pubescentis* (allotment I) covering proper podsol on mineral peat soil and *Empetro nigri – Pinetum Cladonietosum* (allotment II) on proper podsol. The examined woodland areas appear in the northern part of Gardnieńsko-Łebska Lowland combined with Słupska Plain and belong to the Protection District of Smołdziński Las. In the north they border Łebska Sandbar while in the south, with the zone of low peat-bogs they adjoin morainal height (Fig. 1) with quite a high, variable level of ground waters.

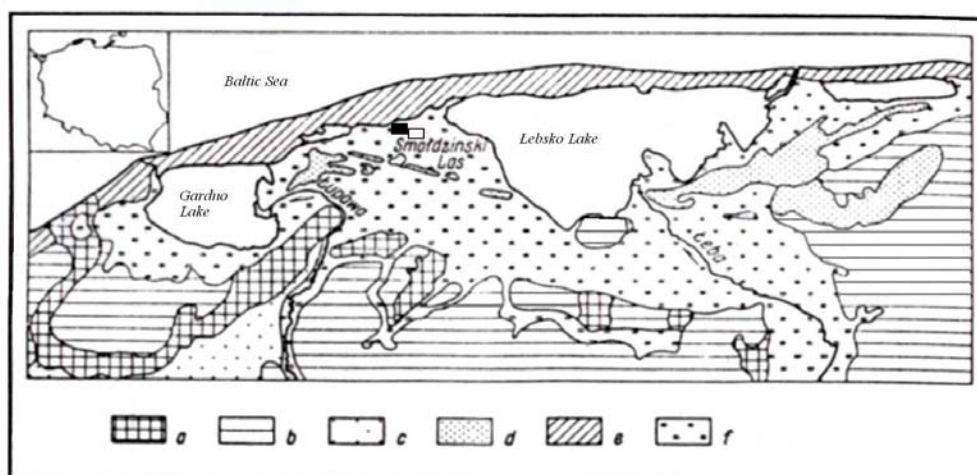


Fig. 1. Geomorphological picture of the Gardno-Łeba lowland: a - basal moraines, b - moraine upland, c - outwash plains, d - late-glacial eolic forms, e - holocenic eolic forms, f - forms on the organogenic and mineral accumulation in bottoms of valleys, urtals and depressions, □- Allotment I, ■-Allotment II.

3. Material and methods

In the period of three vegetation seasons, every 6 weeks on average, there were collected samples of ground waters from two small wells. The scope of research comprised examination of the content of nitrogen and phosphorus, pH reaction and dynamics of the level of ground waters (table 1).

Table 1. Methodology of determination according to [1].

Determination		Methodology of determination
General nitrogen	T-N	Kiejdahel's method ¹ , after mineralization in the mixture of H ₂ SO ₄ and H ₂ O ₂ .
Ammonia nitrogen	N-NH ₄	spectrophotometrically ² (with Nessler's reagent).
Nitrate nitrogen	N-NO ₃	spectrophotometrically ² (with sodium salicylate).
General phosphorus	T-P	spectrophotometrically ² (molybdate method, with ascorbic acid as reducing agent), after mineralization in the mixture of H ₂ SO ₄ and H ₂ O ₂ .
Phosphate phosphorus	P-PO ₄	spectrophotometrically ² (molybdate method, with ascorbic acid as reducing agent)
Reaction	pH	potentiometrically ³ .

¹ Parnas-Wagner apparatus

² Shimadzu spectrophotometer (UV-VIS 1202)

³ glass electrode: Eurosensor ESAGP-341W No 38

4. Results

In the examined woodland ecosystems the annual rhythm of level variations of ground waters was similar (Fig. 2). In the same periods there were observed minimums and maximums of the tables of ground waters. In the period of early spring the levels of ground waters were quite high due to spring thaws of snow cover as well as to poor consumption of water by plant roots in the early period of vegetation.

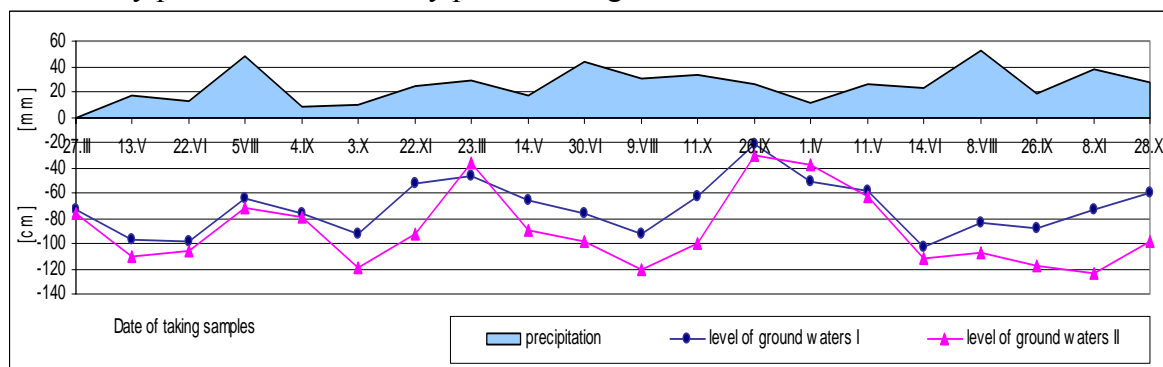


Fig. 2. Level changes of ground waters with regard to precipitation.

In all examined vegetation seasons there were observed higher amplitudes of variations of the water table of ground waters on allotment II (by 12 % on average).

The differences in the dynamics of ground waters on the allotments under investigation are the result of the differences in their soil profiles. Somewhat lower amplitudes (Table 2.) of ground water variations in the case of allotment I are the result of the presence of peat layer lying at the depth of about 80 cm in the soil profile of that allotment.

Table 2. Level variations of ground waters in the years 2003-2005.

	2003	2004	2005

	min	max	ampl.	min	max	ampl.	min	max	ampl.
Allotment I	-98	-53	45	-93	-21	72	-103	-51	52
Allotment II	-119	-72	47	-121	-31	90	-118	-38	80

The presence of peat profitably affects the retention of water due to strong absorption properties. Besides, it constitutes a rich source of biogenic compounds that are washed out from the organic layer by ground waters in the course of frequent washing and get into the solution. Thanks to the presence of peat in the genetic profile, the ground waters of allotment I are richer in nitrogen compounds by 35,65 % on average and phosphorus compounds by 26,61 % on average in relation to the ground waters on allotment II. The T-N and T-P dynamics in the examined ground waters is shown by the following diagrams (Fig. 3 and Fig. 4).

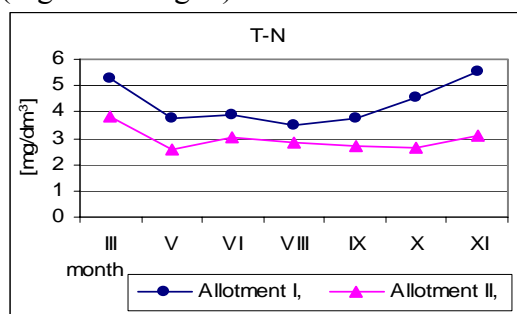


Fig. 3. Average monthly changes of general nitrogen content (T-N) in the examined ground waters.

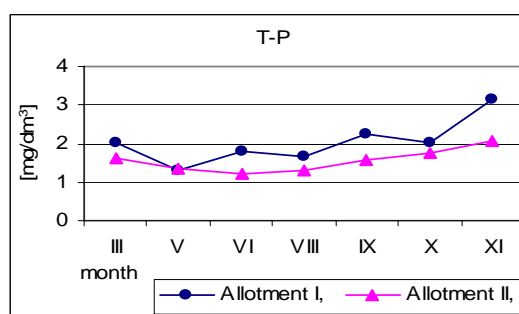


Fig. 4. Average monthly changes of general phosphorus content (T-P) in the examined ground waters.

Changes of mineral forms of nitrogen and phosphorus are inseparably connected with the changes of T-N and T-P. In the beginning period of vegetation season in the examined ground waters there was observed a decline of $N-NH_4$ and $N-NO_3$ contents caused by an intensive intake of mineral forms of nitrogen by plants.

In subsequent months there was observed a further decrease of ammonia form content and a gradual increase of nitrate nitrogen content that resulted from oxidation of ammonia form into nitrate form (Figs. 5 and 6) and, also, from ongoing processes of mineralization providing significantly bigger amounts of $N-NO_3$.

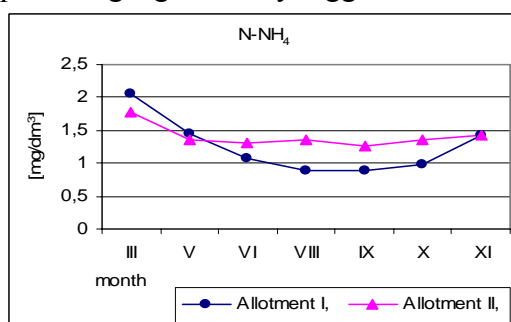


Fig. 5. Average monthly changes ammonia nitrogen content ($N-NH_4$) in the examined ground waters.

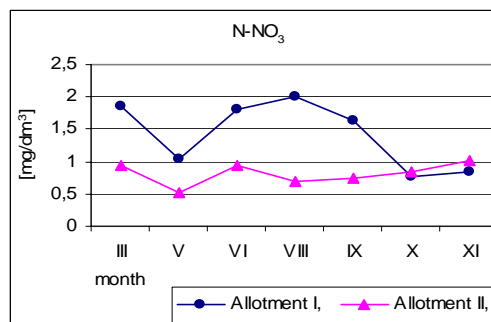


Fig. 6. Average monthly changes nitrate nitrogen content ($N-NO_3$) in the examined ground waters.

Also, the content of phosphate phosphorus in the examined ground waters undergoes significant changes. The loss of $P-PO_4$ in spring and summer months is the result of increased demand of plants for biogenic compounds while the increase of its content in the

period of autumn results from a poorer intake by plant roots as well as from ongoing processes of mineralization and precipitation (Fig. 7).

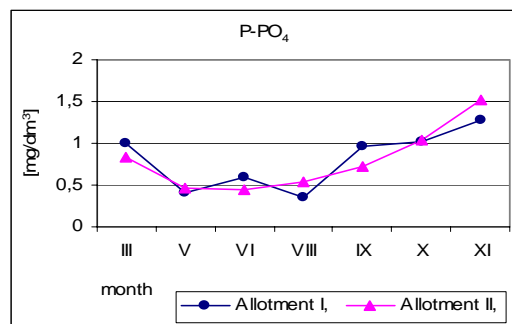


Fig. 7. Average monthly changes phosphate phosphorus content (P-PO₄) in the examined ground waters.

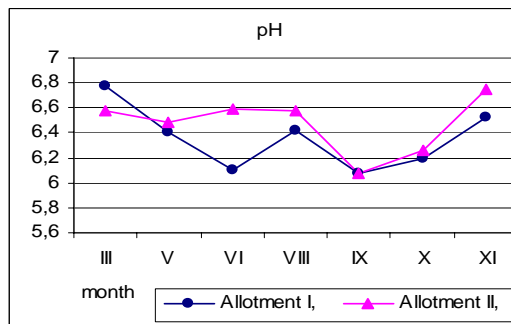


Fig. 8. Average monthly changes of reaction of the examined ground waters.

In the course of vegetation season there was observed a change in reaction of the examined ground waters (Fig. 8). In spring months there appeared an increase of acidity in ground waters connected with an intensive intake of basic cations by plants. The increase of pH value in summer and autumn may be explained on the grounds of intensive precipitation washing out basic cations into ground waters from higher levels of genetic soil profiles. The average values of pH during the period of three examined years remain on the level of 6,38 (allotment I), with standard deviation of $S_x=0,34$ and coefficient of variation of $C_v = 5,33 \%$ and 6,45 (allotment II), $S_x=0,52$, $C_v=8,05 \%$.

5. Conclusions

- the content of nitrogen and phosphorus compounds in ground waters is strictly connected with constitution of the soil profile as well as with the flora growing in that area.
- ground waters of allotment I are richer in nitrogen compounds by 35,65 % on average and phosphorus compounds by 26,61 % on average in relation to ground waters of allotment II;
- significantly higher amplitudes of level variations of ground waters exist in the case of allotment II (proper podsol);
- the biggest contents of T-N, T-P, N-NH₄ i P-PO₄ in the examined ground waters appear in spring and autumn, being accumulated as a result of ongoing processes of mineralization, while minimal values in summer months are caused by an intensive intake by plants;
- ground waters under investigation show a weak acid reaction. Average values of pH in the course of years under analysis remain on the level of 6,38 (allotment I) and 6,45 (allotment II).

6. References

- [1] Hermanowicz W., Dojlido J., Dożańska W., Kosiorowski B., Zerbe J.: Fizyczno-chemiczne badania wody i ścieków, Arkady, Warszawa 1999.
- [2] Kowalkowski A., Józwiak M., Chemizm wód gruntowych i powierzchniowych w mikrozewni, Świętokrzyski Park Narodowy: Przyroda, Gospodarka, Kultura, Bodzentyn - Kraków, 415-426, 2000

SYNTHESIS AND BIOLOGICAL PROPERTIES OF C-SUBSTITUTED ANALOGUES OF BENZISOSELENAZOLONES

M. Piętka-Ottlik^a, K. Kloc^a, E. Piasecki^b, J. Młochowski^a

^a*Institute of Organic Chemistry, Wrocław University of Technology,
Wyb. Wyspiańskiego 27, 50-375 Wrocław*

^b*Laboratory of Virology, Institute of Immunology and Experimental Therapy,
Polish Academy of Sciences, Weigla 12, 53-114 Wrocław*

Introduction

Research of the last twenty years have shown that selenaheterocyclic compounds are active immunostimulants, inhibitors of enzymes, antioxidants, anti-inflammatory, antitumor, antiviral and antimicrobial agents [1-5]. These findings started new trend in biology of selenoorganic compounds which are designed as drugs, mimetics and inhibitors of enzymes, immunomodifiers.

In this work we present two convenient methods of synthesis of C5-substituted analogues of benzenoselenazol-3(2H)-ones and results of biological studies carried out *in vitro* on three model viruses: HSV-1 (Herpes simplex virus type 1), EMCV (Encephalomyocarditis virus), VSV (Vesicular stomatitis virus).

Results and Discussion

Synthesis

The general strategies for synthesis of C5-substituted benzenoselenazol-3(2H)-ones **9**, presented in scheme 1, are based on the conversion of C5-substituted 2-chlorobenzoic acids **1**, **5** or 2-aminobenzoic acids **7** into C5-substituted 2-(chloroseleno)benzoyl chlorides **8** and finally on the tandem selenenylation-acylation of primary amines with this reagents.

*Synthesis of 5-nitro- and 5-(methylsulfonyl)-2,2'-diselenobisbenzoic acids **4a**, **4b***

Initially, acid chlorides **1**, **5** were converted to the *tert*-butyl esters **2**, **6** using 2-methylpropene in dry tetrahydrofuran in the presence of catalytic amounts of sulfuric acid. Before the next step, methylthio group of compound **6** was oxidized to methylsulfonyl group **2b** with hydrogen peroxide in the presence of sodium tungstate dihydrate as catalyst. In the next step, the chlorine atom in esters **2a** and **2b** were substituted with diselenide group in the reaction with freshly prepared dilithium diselenide in dry tetrahydrofuran and C5-substituted 2,2'-diselenobis(*tert*-butyl benzoates) **3a**, **3b** were obtained. Acid hydrolysis of esters **3a** and **3b** with methanesulfonic acid as hydrolyzing agent gave C5-substituted 2,2'-diselenobisbenzoic acids **4a**, **4b**.

*Synthesis of 5-methyl- and 5-chloro-2,2'-diselenobisbenzoic acids **4c**, **4d***

C5-substituted anthranilic acids **7c**, **7d** were diazotized and diazonium salts reacting with dilithium diselenide gave C5-substituted 2,2'-diselenobisbenzoic acids **4c**, **4d**.

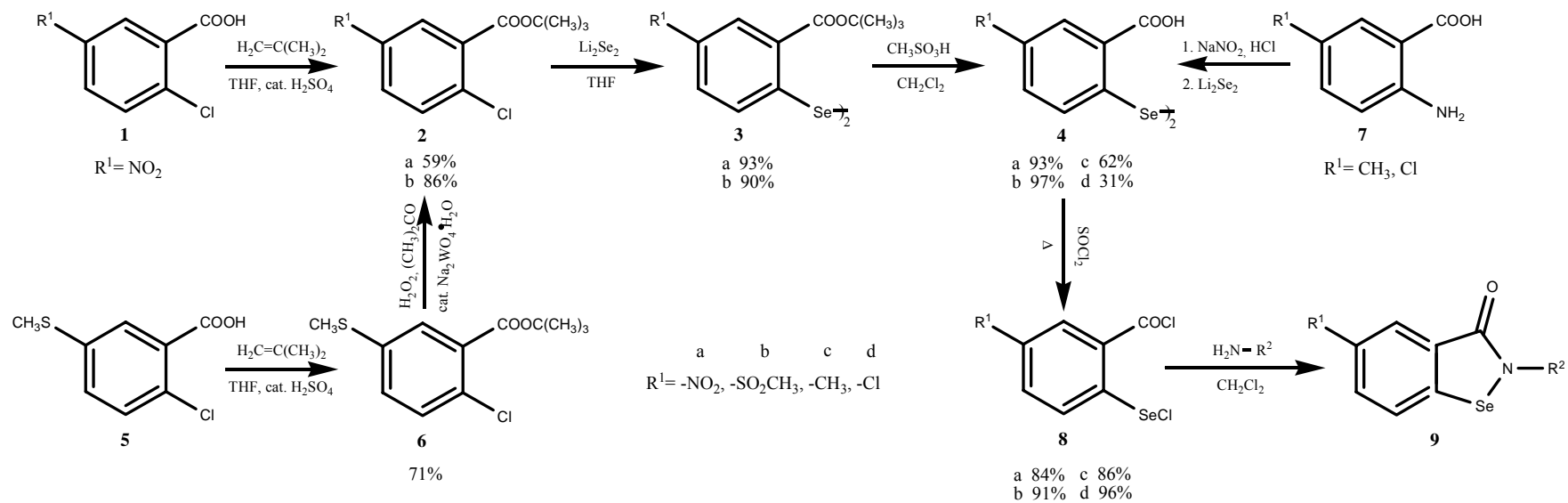


Table 1. Yield of C5-substituted benzisoselenazol-3(2H)-ones **9**.

$\text{R}^1 \backslash \text{R}^2$	H	Me	Pr	<i>t</i> -Bu	c.hexyl	Ph	4-Cl-Ph	2-Py	5-Cl-2-Py	N(Ph) ₂
NO ₂	82 %	86 %	85 %	81 %	82 %	81 %	83 %	82 %	70 %	57 %
SO ₂ CH ₃	83 %	84 %	82 %	86 %	82 %	83 %	92 %	71 %	88 %	46 %
CH ₃	82 %	70 %	75 %	81 %	77 %	77 %	80 %	77 %	59 %	45 %
Cl	70 %	79 %	76 %	78 %	79 %	62 %	73 %	68 %	76 %	48 %

Scheme 1 Synthesis of C5-substituted benzisoselenazol-3(2H)-ones.

Synthesis of C5-substituted benzisosenazol-3(2H)-ones **9a-d**

Acids **4a-d** were easily converted to 2-(chloroseleno)benzoyl chlorides **8a-d** with thionyl chloride, used in excess, in the presence of catalytic amounts of dimethylformamide. The reaction of dichlorides **8a-d** with ammonia, aliphatic or aromatic primary amines in dry dichloromethane produced corresponding 5-nitro-, 5-methylsulfonyl-, 5-methyl- and 5-chlorobenzisosenazol-3(2H)-ones **9a-d**. Since in the reaction hydrochloric acid was eliminated aliphatic amines were used in threefold excess or triethylamine was applied as a base in case of aromatic amines and cyclohexylamine. The structures of forty new compounds were confirmed by ¹H-NMR and IR spectra and elemental analysis.

Based on the reactions of dichlorides **8a-d** with primary amines we suppose that they can be convenient reagents for tandem selenenylation-acylation of primary amides, amino acids or other compounds, like these having active methylene groups, similarly as in case of 2-(chloroseleno)benzoyl chloride.

Antiviral activity

The compounds at various concentrations (1-1000 µg/ml) were incubated with following viruses: HSV-1 (herpes simplex virus type 1, Herpesviridae, enveloped virus), EMCV (encephalomyocarditis virus, Picornaviridae, non-enveloped virus) and VSV (vesicular stomatitis virus, Rhabdoviridae, enveloped virus). Viruses EMCV and VSV were used at the dose of 10⁵ TCID₅₀/ml, HSV-1 at the dose of 10⁴ TCID₅₀/ml. After 1 h incubation at room temperature, the virus titer was measured in human cell line A549 and minimal inhibitory concentration (MIC) was determined.

In the parallel experiment the cytotoxicity of compounds was determined in human lung adenocarcinoma cell line A549 (ATCC 185). The test was performed in 96-well microplates. The cells were treated with various doses of the compounds and cultivated for 48 h at 37 °C in the atmosphere of 5% CO₂ in air. Then the cultures were examined under microscope. The minimal concentration, which was toxic to approximately 50% of the cells was taken as TCCD₅₀ (tissue culture cytotoxic dose). Results are summarized in tables 2 and 3.

Table 2. Antiviral activity of C5-substituted benzisosenazol-3(2H)-ones **9**.

Substituents R ² \ R ¹	MIC for HSV-1					MIC for EMCV				
	CH ₃	CH ₃ SO ₂	NO ₂	Cl	H	CH ₃	CH ₃ SO ₂	NO ₂	Cl	H
H	2	20	6	4	8	6	60	80	10	4
Me	1	2	4	2	8	6	20	40	6	4
Pr	1	1	4	2	6	6	20	8	6	6
t-Bu	2	6	4	2	6	4	20	40	4	4
cyclohexyl	80	4	40	40	6	>1000	>1000	>1000	>1000	8
Ph	4	4	6	4	8	40	>1000	>1000	>1000	10
4-Cl-Ph	20	8	4	80	4	>1000	>1000	>1000	>1000	6
2-Py	4	40	>1000	>1000	4	>1000	>1000	>1000	>1000	>1000
5-Cl-2-Py	1000	>1000	>1000	>1000	>1000	>1000	>1000	>1000	>1000	>1000
N(Ph) ₂	8	4	40	6	-	>1000	>1000	>1000	>1000	-

MIC – minimal inhibitory concentration (µg/ml)

C5-substituted benzisosenazol-3(2H)-ones appeared to be very active against HSV-1. In most cases their anti-HSV-1 activity was higher than activity of benzisosenazol-3(2H)-ones non-substituted in C5 position. Loss of activity observed for compounds having 5-chloro-2-pyridyl group substituted on nitrogen atom probably was due to their low bioavailability connected with low solubility in medium used for cultivation.

Contrary to highly active benzisosenazol-3(2H)-ones, their C5-substituted analogues were found less active against EMCV. Anti-EMCV activity was observed only for alkyl derivatives, whereas analogues with aryl or cyclohexyl N-substituents were inactive.

All compounds were completely inactive against VSV (MIC>1000 µg/ml).

Table 3. Cytotoxicity of C5-substituted benzisosenazol-3(2H)-ones **9**.

Substituents		TCCD ₅₀ (µg/ml)				
R ² \ R ¹	CH ₃	CH ₃ SO ₂	NO ₂	Cl	H	
H	2,5	49	15,5	2,0	3,0	
Me	2,0	14,5	4,5	2,5	2,5	
Pr	5,0	7,5	5,5	3,5	3,5	
t-Bu	3,5	4,5	62	2,0	6,0	
cyclohexyl	156	7,5	58,5	14,5	3,0	
Ph	61	34	14,5	91	12	
4-Cl-Ph	78	73	10	>156	14,5	
2-Py	>156	6,0	>156	>156	117	
5-Cl-2-Py	>156	>156	18	>156	100	
N(Ph) ₂	>78	6,0	36,5	3,0	-	

Cytotoxicity of tested compounds was observed in a broad range, from highly (2-5 µg/ml) to weakly toxic (>156 µg/ml).

Chemotherapeutic indexes, defined as MIC/CYT, for antivirals against HSV-1 in most cases were lower than 1, which means that virus inhibiting concentration was lower than concentration causing cytotoxicity. Whereas, only few compounds exhibiting anti-EMCV activity had indexes below 1.

Conclusions

General strategies for synthesis of C5-substituted benzisosenazol-3(2H)-ones have been elaborated. Forty new C5-substituted analogues of benzisosenazol-3(2H)-ones have been designed and synthesized using these methods. All compounds have been tested against selected viruses as potential antiviral agents. Biological studies have demonstrated that discussed compounds exhibit high level of anti-HSV-1 (1-80 µg/ml) and anti-EMCV (4-80 µg/ml for alkyl derivatives) activity; however, they are completely inactive against VSV.

References:

- [1] G. Mugesh, WW. du Mont, H. Sies, *Chem. Rev.*, 101 (2001) 2125
- [2] G. Mugesh, B. Singh, *Chem. Soc. Rev.*, 29 (2000), 347
- [3] M. Soriano-Garcia, *Curr Med Chem.*, 11 (2004) 1657
- [4] H. Wójtowicz, M. Chojnacka, J. Młochowski, J. Palus, L. Syper, D. Hudecova, M. Uher, E. Piasecki, M. Rybka, *Farmaco*, 58(12) (2003) 1235
- [5] H. Wójtowicz, K. Kloc, I. Maliszewska, J. Młochowski, M. Piętka, E. Piasecki, *Farmaco*, 59(11) (2004) 863

This work was supported by PBZ-Min-015/P05/2004 grant.

THE EFFECT OF COALIFICATION DEGREE ON THE PROPERTIES AND STRUCTURE OF ACTIVE CARBON ENRICHED IN NITROGEN IN THE REACTION WITH UREA

R. Pietrzak, P. Nowicki, H. Wachowska, P. Puślecki

*Laboratory of Coal Chemistry and Technology, Faculty of Chemistry
Adam Mickiewicz University, Grunwaldzka 6, 60-780 Poznań, Poland*

Abstract:

The material studied was the Polish brown coal from the Konin colliery and gas-coking coal from the Sośnica colliery. These coals were used to obtain active carbon samples subjected to nitrogen enrichment in a reaction with urea at 350°C in oxidising atmosphere, performed at the stage of carbonisates obtained at 500-700°C, or at the stage of active carbons obtained from particular carbonisates. The samples were activated at 800°C by KOH in argon atmosphere. Irrespective of the type of the initial coal, the process composed of the stages: carbonisation → activation → reaction with urea was found to be an effective procedure for producing nitrogen enriched active carbon samples. The microporous active carbon samples were characterised by well-developed surface area and high content of nitrogen.

1. Introduction

Recently, much attention has been given to the nitrogen enriched active carbons. The introduction of nitrogen into the carbonaceous materials structure by ammonia and amines [1] have been known and used for many years, whereas a relatively new method is the introduction of nitrogen into the carbon structure by the reaction with urea.

This paper is a continuation of our earlier studies [2], and its main aim is determination of the effect of the coalification degree of the initial coal on the chemical structure and composition of active carbons enriched in nitrogen in the reaction with urea in oxidising conditions under atmospheric pressure.

2. Experimental

The material studied was the brown coal from the Konin colliery (B) and the gas-coke coal from the Sośnica colliery (S), characterised in Table 1. The demineralised coal was subjected to carbonisation at 500-700°C in argon atmosphere. The carbonisates obtained were divided into two parts – one of them was activated by KOH at the weight ratio of coal/KOH of 1:4, at 800°C, in argon atmosphere. The activates were further subjected to the reaction with urea at the weight ratio of coal/urea of 1:1, at 350°C, in the air flow of 100ml/min. The other part of the carbonisates was at first reacted with urea and then activated with KOH. All the samples obtained as a result of these processes were subjected to further examinations in order to determine their chemical structure and composition. Their elemental analysis was made and their surface area was established by the BET method. Porous structure parameters were determined by nitrogen adsorption-desorption in -196°C (ASAP 2010, manufactured by Micrometrics Instrument Corp. (USA)). Micropore volume and micropore area were calculated using t-plot method.

Table 1. Characteristic of demineralised coals [wt. %]

COAL	W ^a	A ^d	V ^{daf}	C ^{daf}	H ^{daf}	N ^{daf}	S ^{daf}	O ^{daf*}
B	0.0	0.2	50.2	62.3	5.4	0.6	1.4	30.3
S	0.0	0.8	31.8	82.6	2.9	1.3	1.0	12.2

* by difference

3. Results and discussion

As follows from the data characterising the carbonisates obtained, (Table 2), an increase in the carbonisation temperature leads to an increase in the content of carbon and a decrease in the oxygen content with respect to those in the initial coal, irrespective of the type of the initial coal (Table 1). Nitrogen content in carbonates does not change with increasing temperature of carbonisation which points to thermal stability of nitrogen-containing functional groups present in the structure of coal starting material.

Table 2. Characteristic of carbonisates [wt.%]

COAL	A ^d	C ^{daf}	H ^{daf}	N ^{daf}	S ^{daf}	O ^{daf*}
BK5	1.9	81.9	3.2	1.0	1.4	12.5
BK6	1.9	85.1	2.4	1.0	1.3	10.2
BK7	2.2	92.1	1.6	0.9	1.9	3.5
SK5	1.3	88.1	3.8	1.5	0.7	5.9
SK6	1.5	90.1	2.7	1.5	0.7	5.0
SK7	1.7	93.7	1.7	1.3	0.7	2.6

* by difference

Reaction of the carbonisates with urea in the oxidising conditions permits an introduction of considerable amounts of nitrogen in their structure (Table 3). All the samples obtained are characterised by a decreased content of carbon and increased content of oxygen with respect to those in the initial carbonisates, which is a consequence of the reaction conditions.

A comparison of the data obtained for particular carbonisates obtained at different temperatures from the coal of both types has shown that the greatest amount of nitrogen has built into the carbonisates obtained at 500°C (BK5M, SK5M) less to those obtained at 600°C (BK6M, SK6M) and the least to those obtained at 700°C (BK7M, SK7M). Moreover, analysis of the data in Tables 2 and 3 has indicated that when the carbonisates react with urea the amount of the nitrogen built into the carbon structure depends on the amount of oxygen in the initial sample.

The activation of the nitrogen-enriched carbonisates by KOH leads to an increase in the content of carbon and a decrease in the contents of the other elements in all active carbon samples such obtained relative to those in the samples before the activation. A drastic decrease in the content of nitrogen as a result of the activation of the nitrogen-enriched carbonisates is probably related to a low resistance of the nitrogen groups to the high temperature of the activation (800°C). The activation of the carbonisates (Table 2) results in an increase in the content of carbon and a significant decrease in the contents of hydrogen and sulphur (Table 4). Also the content of nitrogen is decreased as a consequence of a low resistance of nitrogen groups to the activating agent (KOH). As to the content of oxygen calculated from the difference, only the activation of the carbonisates obtained from brown coal at 500 and 600°C leads to its decrease. In all other samples the content of oxygen increases as a result of activation, and the greatest increase occurs as a result of activation of the carbonisates obtained at 700°C.

Table 3. Elemental analysis of nitrogen-enriched carbonisates and the active carbon samples obtained from them [wt.%]

COAL	A ^d	C ^{daf}	H ^{daf}	N ^{daf}	S ^{daf}	O ^{daf*}
BK5M	2.0	62.6	2.5	8.4	0.7	25.8
BK5MA	2.0	84.9	1.3	2.0	0.7	11.1
BK6M	3.9	73.9	2.1	6.3	0.6	17.1
BK6MA	1.0	93.5	0.4	0.6	0.1	5.4
BK7M	2.9	81.3	2.0	5.4	1.5	9.8
BK7MA	3.5	93.7	0.3	0.7	0.1	5.2
SK5M	0.7	82.6	3.3	6.4	0.6	7.1
SK5MA	0.9	91.7	0.5	1.0	0.3	6.5
SK6M	1.5	85.6	2.6	6.1	0.4	5.3
SK6MA	0.6	91.2	0.4	0.4	0.1	7.9
SK7M	1.3	88.3	1.6	4.9	0.4	4.8
SK7MA	0.0	92.7	0.3	0.2	0.2	6.6

* by difference

The reaction of the active carbon with urea brings about a decrease in the content of carbon in all samples and to a significant increase in the content of nitrogen. It should be mentioned that much less nitrogen can be introduced into the active carbon obtained from the brown coal from Konin (Table 4) than to the carbonisate obtained from this coal (Table 3). For the coal from Sośnica the situation is different: more nitrogen is built into the activate than to the carbonisate. The reaction of active carbons with urea leads to the differences in the content of oxygen depending on the type of coal from which the active carbon was obtained. According to the data from Table 4, the reaction of urea with the activate obtained from the brown coal from Konin leads to an increase in the content of oxygen in the nitrogen-enriched active carbon, while it leads to a decrease in the content of oxygen in the activate from the Sośnica coal. Analysis of the Table 4 data also reveals that the amount of nitrogen built into the active carbon depends on the content of oxygen in the initial sample.

Table 4. Results of the elemental analysis of the active carbon samples and nitrogen-enriched active carbon samples (in reaction with urea) [wt.%]

COAL	A ^d	C ^{daf}	H ^{daf}	N ^{daf}	S ^{daf}	O ^{daf*}
BK5A	0.9	94.3	0.3	0.4	0.5	4.5
BK5AM	1.5	87.9	0.5	4.8	0.2	6.6
BK6A	0.9	94.4	0.2	0.3	0.3	4.8
BK6AM	1.3	86.1	0.6	5.4	0.2	7.7
BK7A	1.0	94.0	0.2	0.2	0.4	5.2
BK7AM	0.5	86.6	0.6	5.6	0.2	7.0
SK5A	0.7	93.0	0.4	0.1	0.2	6.3
SK5AM	0.8	85.1	0.6	8.6	0.3	5.4
SK6A	0.7	93.3	0.3	0.1	0.2	6.1
SK6AM	0.5	85.6	0.6	8.4	0.1	5.3
SK7A	0.4	94.3	0.5	0.0	0.2	5.0
SK7AM	0.0	89.6	0.5	5.2	0.1	4.6

* by difference

Structural investigation (Table 5) has shown that both types of coal from Konin and Sośnica can be used to obtain in the process of activation with KOH microporous active

carbons of well-developed surface area. For both types of coal, the lower the temperature of carbonisate production the greater the surface area of the active carbon obtained. Further reaction of the active carbon samples with urea leads to a decrease in their surface area.

Activation of the nitrogen-enriched carbonisates also leads to microporous active carbons but has a different effect on the surface area of the activates obtained from different types of coal. For the coal from Konin the activation of nitrogen-enriched carbonisates obtained at 500 and 600°C gives the active carbons of the surface area smaller than that of the carbonisates not subjected to the reaction with urea. On the other hand, the activation of nitrogen-enriched carbonisate obtained at 700°C gives the microporous active carbon samples of much more developed surface area than the activation of carbonisates not enriched in nitrogen. For the activation of nitrogen-enriched carbonisates from Sośnica coal the analogous relations are the opposite.

Table 5. Surface area and pore volume of the active carbon samples and nitrogen-enriched active carbon samples obtained

COAL	Surface area BET [m ² /g]		Pore volume [cm ³ /g]	
	Total surface area	Micropore area	Total pore volume	Micropore volume
BK5A	3268	2915	1.86	1.52
BK6A	3122	2835	1.72	1.44
BK7A	2530	2446	1.24	1.15
BK5AM	3042	2739	1.72	1.42
BK6AM	2838	2613	1.54	1.32
BK7AM	2209	2135	1.08	1.00
BK5MA	2593	1582	1.80	0.92
BK6MA	1876	1274	1.26	0.75
BK7MA	3201	2913	1.73	1.44
SK5A	2932	2916	1.39	1.36
SK6A	2902	2876	1.51	1.45
SK7A	2126	2115	1.02	1.00
SK5AM	2322	2296	1.19	1.15
SK6AM	2448	2426	1.16	1.13
SK7AM	1787	1777	0.85	0.84
SK5MA	3195	3137	1.76	1.66
SK6MA	3013	2976	1.55	1.48
SK7MA	1937	1922	0.93	0.91

4. Conclusions

The above discussed results have shown that irrespective of the type of coal the most effective procedure leading to nitrogen-enriched active carbon is that applied in the following sequence of processes carbonisation → activation → reaction with urea. The final products are the active carbon samples of well-developed surface area and enriched in nitrogen.

Literature:

- [1] K. Jurewicz, K. Babeł, A. Ziółkowski, H. Wachowska, Journal of Physics and Chemistry of Solids, 65 (2004) 269
- [2] R. Pietrzak, H. Wachowska, P. Nowicki, Energy & Fuels, 20 (2006) 1275

SYNTHESIS OF POROUS MICROSPHERES OF 4,4'-DI (2-HYDROXY-3-METHACRYLOYLOXYPROPOXY) BENZOPHENONE –DIVINYLBENZENE FOR POTENTIAL HPLC PURPOSES

Beata Podkościelna, Małgorzata Maciejewska, Barbara Gawdzik,
Andrzej Bartnicki

*Faculty of Chemistry, MCS University, pl. Marii Curie-Skłodowskiej 5, 20-031 Lublin,
Poland, mmacieje@hermes.umcs.lublin.pl*

Porous polymers used in different chromatographic techniques as column packings differ in their chemical and porous structures. The chemical structure of porous polymers depends upon the chemical structure of the monomers used, whereas the porous structure is mainly dependent on the copolymerization conditions. The most popular are macroporous copolymers of styrene cross-linked with divinylbenzene (ST-DVB). Their surfaces are hydrophobic and in consequence have poor contact with most of mobile phases. Considering this fact it is crucial to incorporate polar functional groups into polymer skeleton. It can be done by employing monomers of more polar character.

In this work synthesis of a new aromatic tetrafunctional methacrylate monomer 4,4'-di(2-hydroxy-3-methacryloyloxypropoxy)benzophenone and its application in the synthesis of porous microspheres is presented. This new monomer was copolymerized with divinylbenzene using suspension-emulsion polymerization. The mixture of toluene and decane-1-ol was used as a pore-forming agent providing material of different porosities.

Preparation of 4,4'-di(2,3-epoxypropoxy)benzophenone (BEP-EP)

In a 500 cm³ round bottomed three-necked flask equipped with a mechanical stirrer, an azeotropic head and a radiator, 0.1 mole of 4,4'-dihydroxybenzophenone (21.4g) was placed together with sodium acetate (0.134g), 1 mole (92.5g) of 2-(chloromethyl)oxirane (92.5g + 56g were placed into an azeotropic head), and 10 ml p-xylene. Meanwhile, 11 g of NaOH was put into a mortar and grinded. The obtained powder was mixed with 25 ml of p-xylene in a beaker and added to the reactor in portions. This process was exothermic. The content of the flask was maintained at boiling. After adding all the mixture (NaOH + p-xylene) to the flask, the reaction was continued for 1 hour. During the reaction a yellow compound was formed. When the reaction was over, the content of the flask was placed into the dropper, and the organic layer was distilled at low pressure (1.6kPa) in order to remove the excess of 2-(chloromethyl)oxirane. The epoxide derivative of benzophenone was crystallized from p-xylene. The yield of the obtained product was about 88.5 %; its epoxide number was close to the theoretical value.

Preparation of 4,4'-di(2-hydroxy-3-methacryloyloxypropoxy)benzophenone (BEP-DM)

The reaction between the epoxide groups of 4,4'-di(2,3-epoxypropoxy)benzophenone and the carboxylic ones of 2-methacrylic acid went on at 80-100 °C. The synthesis was carried out in a 500 cm³ round bottomed flask equipped with a thermometer, a mechanical stirrer and a heater. In such a flask 0.5 mole (163g) of BEP-EP, 1 mole (86.09g) of 2-methacrylic acid, 2g of TEBA (a catalyst), and 0.02g hydroquinone (polymerization inhibitor) were added. The progress of the reaction was controlled by

determination of the acidic number. The acidic number determines the amount of KOH milligrams used to neutralize the free acids contained in 1g of substance. The reaction was considered to be over when the acidic number was below 5. Its rate is higher when carried out at higher temperatures but a considerable exothermic effect can result in losing control of the reaction and appearing of some products of darker colour. Chemical structure of the new monomer was confirmed by spectroscopic methods.

Copolymerization

Copolymerization with DVB was performed in the aqueous medium. In a typical experiment, 150 mL of redistilled water and 1.4 g of bis(2-ethylhexyl)sulfosuccinate sodium salt (surfactant) were stirred for 1 h at 80°C in a three-necked flask fitted with a stirrer, a water condenser, and a thermometer. Then the solution containing 10 g of BEP-DM and 3 g of DVB, 0.18 g of α, α' -azoisobisbutyronitrile (initiator), and the mixture of pore-forming diluents (toluene and decan-1-ol) were added while stirring to the aqueous medium. Copolymerization was performed for 18 h at 80°C. The obtained copolymers in the form of porous microspheres were washed with distilled water, filtered off, dried and extracted in a Soxhlet apparatus. Uniform particles (5-15 μm) used in further studies were isolated by sedimentation.

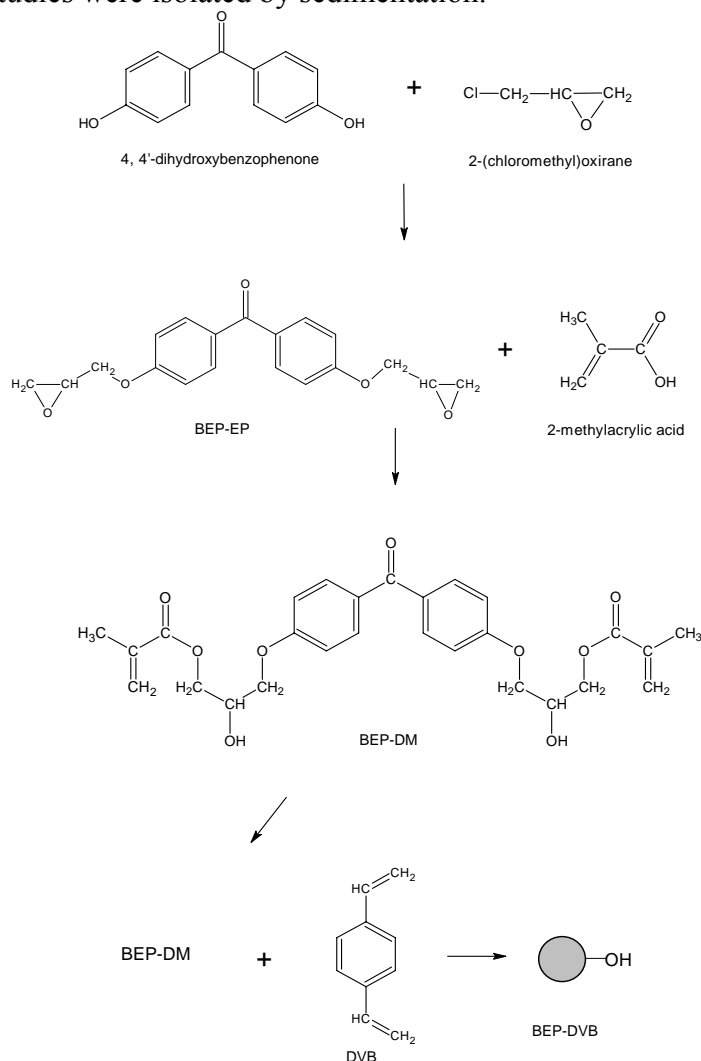


Fig.1 The scheme of synthesis and chemical structure of the compound used for copolymerization

Characterization of Porous Structure

Such parameters as specific surface areas, pore volumes, pore size distributions, and average pore diameters were determined by the method of nitrogen adsorption on the surface of the studied stationary phases in a dry state. The specific surface areas were calculated by the BET method, assuming that the area of a single nitrogen molecule is 16.2 \AA^2 . These determinations were made using an adsorption analyzer ASAP 2405 (Micrometrics Inc., USA). The measurements of the surface properties of the copolymers were preceded by activation of the samples at 200°C for 2 h. The beads were also examined using an atomic force microscope (AFM), AFM Nanoscope III (Digital Instruments, USA) operating in the contact mode (Fig.2). From this micrograph one can see that microspheres of obtained copolymer are characterized by a regular porous structure.

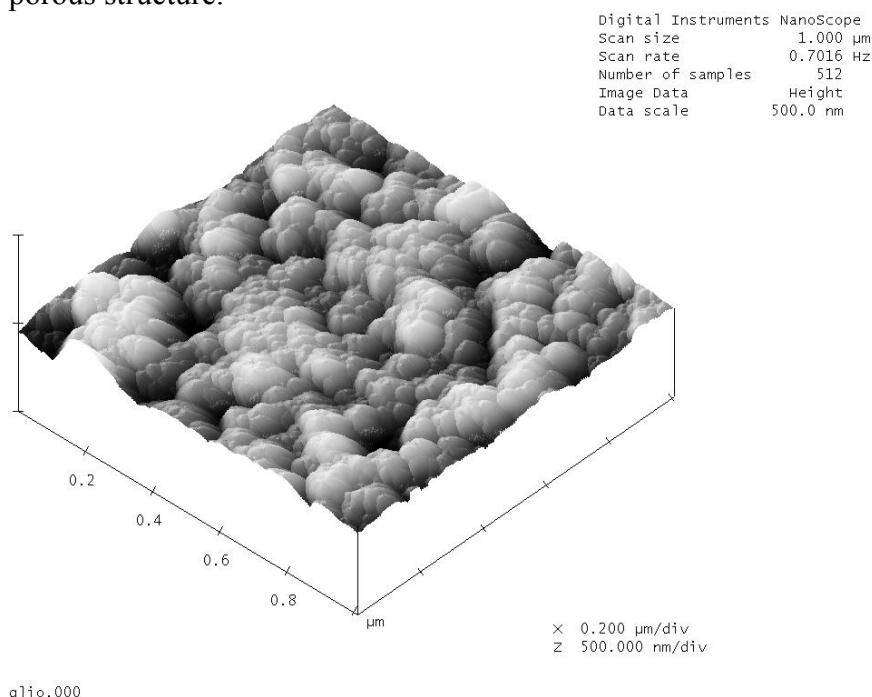


Fig.2 Contact-mode AFM images for BEP-DVB copolymer

In a swollen state the beads were characterized by the inverse exclusion chromatography (EC) technique introduced by Halász and Martin [1]. Table I contains information about the porous structure of copolymer

Table I. Parameters of the porous structure of the studied copolymer obtained from BET and EC methods

Method	Specific surface area(m^2/g)	Pore volume (cm^3/g)	Contribution of micropores (cm^3/g)	Most probable pore diameter (\AA)	Swelling propensity (SP factor)
BET	108	0.380	0	400	-
EC	-	0.607	0.047	20/520	0.70

The data given in Table I show, that dependently of the method used the pore volumes of the copolymer are not the same. Differences in their structures are also visible when volume of micropores and the most probable pore diameters are compared. In the swollen state contribution of micropores exceeds 7 %, while dry polymer doesn't reveal any micropores. The most probable pore diameters are also different. Changes of its porous structure in comparison to that of dry copolymer are caused by interactions of its net with THF. This good solvent swells the polymeric net. In consequence, some micropores become detectable. In a dry copolymer, micropores are not accessible for the nitrogen molecule, because their diameters are smaller than that of the nitrogen molecule. Materials used as packings in HPLC should have homogeneous mezo- or macroporous structure with minimum contribution of micropores which are responsible for site effects. Site effects, in consequence, lead to peak tailing. In porous structure of polymeric packing some micropores appear after swelling which was caused by contact with good solvents. The results from inverse exclusion chromatography, in which tetrahydrofuran was used as mobile phase, resemble the situation in real HPLC column. To investigate swelling behavior of these copolymers more precisely, the swellability coefficients in acetone, methanol, THF, dichloromethane and 1,4-dioxane were studied. The swellability coefficient, B , was determined using the centrifugation method. According to Tuncel [2] B can be expressed as:

$$B = \frac{V_s - V_d}{V_d} \times 100\%$$

where: V_s - the volume of the copolymer after swelling,
 V_d - the volume of the dry copolymer

Obtained results are summarized in Table II.

Table II Copolymer's swelling studies

Swellability coefficient, B (%)				
acetone	methanol	THF	dichloromethane	1,4-dioxane
10	6	15	8	10

Relatively small contribution of micropores in the internal structure of the copolymer and its small swellability coefficient cause that this material is interesting from chromatographic point of view. Results obtained from inverse exclusion chromatography suggest that 4,4'-di(2-hydroxy-3-methacryloyloxypropoxy) benzophenone – divinylbenzene porous microspheres can be applied in HPLC. To obtain column packings of better efficiencies, some work focused on optimization of their synthesis will be made.

References:

1. Nevejsans, F.; Verzele, M. J Chromatogr. 1985, 350, 145
2. Tuncel, A.; Pişkin, E. J. Appl. Polym. Sci. 1996, 62, 789

THE USE OF MICROWAVES IN THE SYNTHESIS OF BIODEGRADABLE ASPARTIC ACID COPOLYMERS

J. Polaczek, J. Pielichowski, M. Piątkowski

Cracow University of Technology

Department of Chemistry and Technology of Polymers

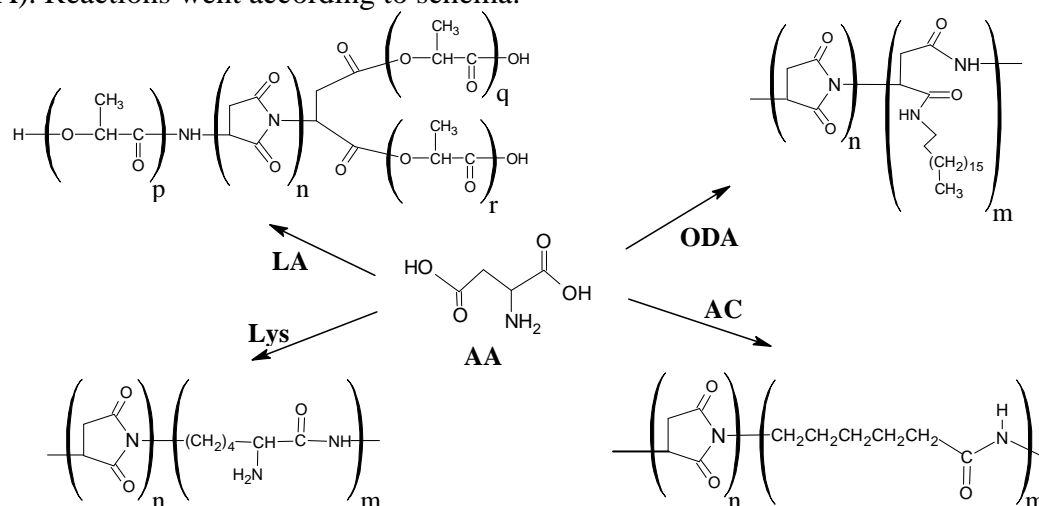
ul. Warszawska 24, 31-155 Kraków, Poland

Poly(aspartic acid) (PAA), which is a product of aspartic acid thermal polymerization, and its copolymers are biodegradable polyaminoacids which have found a wide application in different branches of industry. So far those polymers are used in e.g. household chemistry, cosmetics and food industry [1]. Non-toxicity and biocompatibility of poly(aspartic acid) and its copolymers enable their use in such areas like biomaterial engineering and pharmacy. Both polymers and products of their decomposition in human body are non-toxic, cause no inflammatory states or other immunological reactions.

All the so far known methods of obtaining those polymers take a long time (from few to a dozen hours) and need a catalyst like phosphoric acid or p-toluenesulphonic acid [2]. The use of catalyst eliminates a number of applications in pharmacy and biomaterial engineering. Recently, an original method of copolymers synthesis under microwave irradiation has been developed in the Department of Chemistry and Technology of Polymers at the Cracow University of Technology [3]. The use of microwave technique greatly reduces the reaction time and increases its yield. The most important advantage of this method is elimination of catalyst, so there is no need to separate it from final product.

The copolymerization of aspartic acid was performed to obtain new biocompatible polymers for biomedical applications. For instance, copolymerization of aspartic acid with long-chain amines yields thermoplastic polymer, thanks to internal plastification effect. Moreover, there is a possibility to obtain an amphiphilic copolymer by linking hydrophobic hydrocarbon chain from amine to hydrophilic chain of PAA.

One has performed copolymerization of aspartic acid (AA) with octadecylamine (ODA) [4], lysine hydrochloride (Lys), aminocaproic acid (AC) [5] and lactic acid (LA). Reactions went according to schema:



The obtained copolymers consist of cyclic imide's units formed during the polymerization of aspartic acid, combined with linear fragments of amines or amino- and hydroxyacids.

Experimental part.

Copolymerization has been carried out in a microwave reactor "Milestone", which has maximum power 1000 W and is equipped with magnetic stirrer and azeotropic column, in solvent (propylene carbonate), without catalyst. Depending on monomers used in copolymerization, process parameters were programmed: total reaction time, temperature, power of microwave irradiation and number of cycles needed to complete the synthesis.

In an experiment proper amount of monomers and solvent were added to the flask. The reaction was carried out until exudation of water was observed. After the reaction was completed, the obtained product was precipitated with methanol. In table below synthesis parameters of different copolymers are shown.

Copolymer	Molar ratio	Temperature [°C]	Time [min]	Power [W]	Yield [%]
AA/LA	1:1,38	125-200	52	200-300	26
AA/AC	3:1	130-230	38	300-400	55
AA/ODA	2,33 :1	176-230	41	380-440	66
AA/Lys	5,67 :1	176-226	42	380-440	68

In dependence of kind and composition of the used monomer, copolymers with different properties were obtained. All of them were powders with colours from bright yellow (with ODA) to bronze (with AC). They were insoluble in water, however soluble in DMF and DMSO, like poly(aspartic acid). Hydrolysis with the use of 25% NaOH causes "decomposition" of cyclic rings and an increase of soluble in water linear copolymers. For comparison, analogical reactions with use of 3 weight % H₃PO₄ as a catalysts have an increased yield for about 30%.

Results and Discussion

IR and H¹ NMR analyses of all obtained copolymers showed that they consist of cyclic imide units connected with linear fragments from amines or acids. It permits to suppose that the priority has a reaction of polymerisation of aspartic acid to cyclic imide and then linear fragments from other monomers are built in.

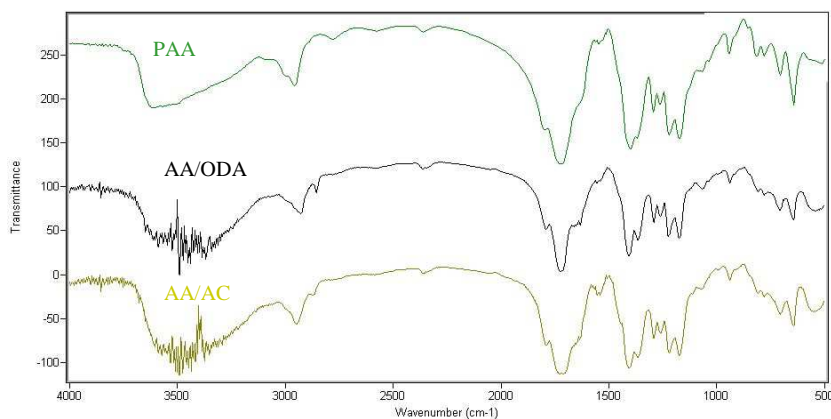


Fig.1.
IR spectra of pure PAA, AA/ODA and AA/AC copolymers

Thermogravimetric analysis (TG) of obtained copolymers confirms this assumption. It is known that cyclic poly(aspartic acid) (PSI) is thermally stable up to 340 °C. Insertion of linear fragments from $-\text{CH}_2-\text{CH}_2-$ bonds of aliphatic segments of used monomers into polymer chain cause a decrease of copolymer thermal stability.

Table 2. Thermal stability of aspartic acid copolymers.

Polymer	PAA	AA/Lys	AA/AC	AA/ODA	AA/LA
Initial temperature of degradation [°C]	340	300	280	250	200

It can be seen that an increase of molar share of e.g. ODA from 10 mol % to 30 mol % cause a decrease of copolymer thermal stability from 250 °C to 215 °C.

Degradation of aspartic acid copolymers.

PAA and its copolymers as biodegradable polymers undergo degradation during hydrolysis or by enzymes action. Hydrolytic degradations tests, which are one of the criterions for applicability of polymers in biomaterial engineering, were carried out. Change of pH of copolymers solutions in physiological salt (0,9 % water solution of NaCl), at temperature of 37 °C during 30 days was tested.

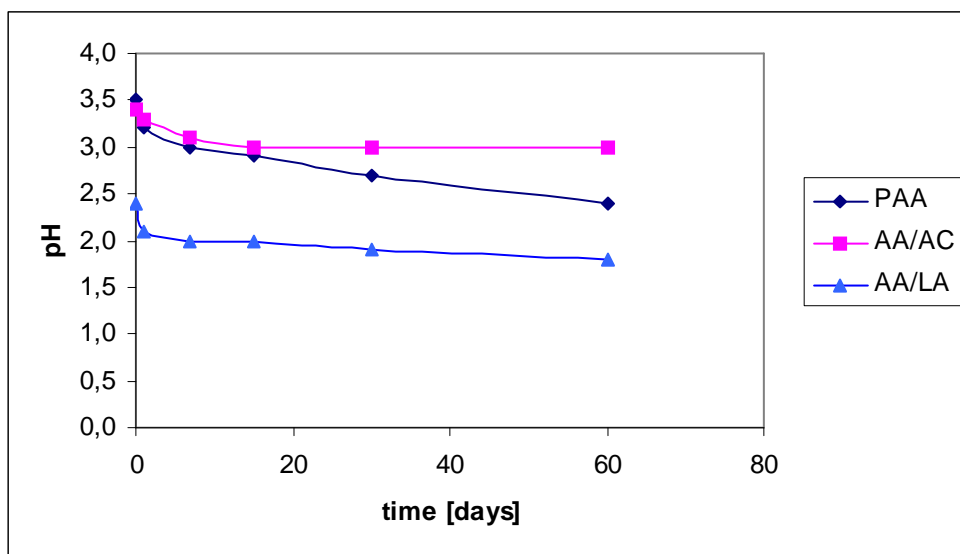


Fig. 2. Degradation curves

The most intensive degradation of PAA and its copolymers was found in first 24 hours. Moreover FT IR analyses showed that after 60 days poly(aspartic acid) degrades cyclic dimer. It was also observed that as a result of hydrolysis, soluble in water linear polymer goes to the solution and PAA with cyclic structure remains in precipitate. Analysis of degradation products confirmed literature reports that during hydrolysis PSI degrade into non-toxic aminoacids.

Conclusions

1. Application of the microwave irradiation permits shortening of the reaction time of copolymerization of aspartic acid with octadecylamine, lysine monohydrochloride, aminocaproic acid and lactic acid from a dozen hours to *ca.* 1 hour and enables to carry out the reaction without catalyst.
2. IR and H^1 NMR analyses confirmed that copolymers consist of cyclic and linear forms; with an increase of amine's molar ratio there are more linear fragments in copolymer, which causes a decrease of its thermal stability.
3. Degradation of copolymers was less intensive than for pure PAA.

References

- [1] Pat. USA 6 197 897 B1 (2001)
- [2] M. Tomida, T. Nakato, M. Kuramochi, *Polymer*, 1996, 19, 4435 – 4437.
- [3] J. Polaczek, J. Pielichowski, K. Pielichowski, E. Tylek, E. Dziki, *Polimery*, 2005, 50, 812-820
- [4] J. Polaczek, J. Pielichowski, J. Bachulska, 2nd International Seminar, *Modern Polymeric materials for Environmental Applications*, Kraków, 2006, vol. 2, 161-165
- [5] J. Pielichowski, E. Dziki, J. Polaczek, *Inżynieria Biomateriałów* 2003, 27, 6 – 9.

THE STUDY OF HUMIFICATION PROCESS IN SEDIMENT BOTTOM FROM GOCZAŁKOWICE DAM RESERVOIR (POLAND)

Justyna Polak, Anna Ziółkowska, Mariola Bartoszek, Maria Maślankiewicz, Wiesław W. Sułkowski

Department of Environmental Chemistry and Technology, Institute of Chemistry, University of Silesia, Szkolna 9, 40-006 Katowice, Poland, wsulkows@us.edu.pl

Introduction

The water reservoir at Goczałkowice has been exploited for 50 years. The main task of this dam reservoir is damming up of water for the purpose of water supplies of inhabitants of the Upper Silesia agglomeration. It is also the storage reservoir and it takes in the excess of water in periods of the flood threat. The studies of inflowing water indicate decrease of concentration of biogens. The observed over blooming of algae could be a result of the presence of large quantity of medium substances and nutrients in bottom sediments [1].

Substances, such as humic substances containing nitrogen, phosphorus and other compounds easily assimilable by the flora [2], are present in bottom sediments. These substances can be a medium for the water flora and they can cause blooming of algae in spite of the decrease of the concentration of biogens in waters flowing in the reservoir.

Therefore, the problem of the research of the eutrophication reasons is actual and important. This investigation can provide in the future to finding of the efficient method of the counteraction blooming of algae.

One of the possible explanation of the phenomenon observed in Goczałkowice dam reservoir is participation of humic substances in blooming of algae and humification processes having the influence on the oxygenic and anaerobic microflora.

Thereby the studies of humification processes of bottom sediments collected from various points of Goczałkowice dam were conducted.

Materials and methods

Sludge samples for studies were collected by workers of the (GPW) according to Polish standards from four places of Goczałkowice reservoir (Fig 1)[3].

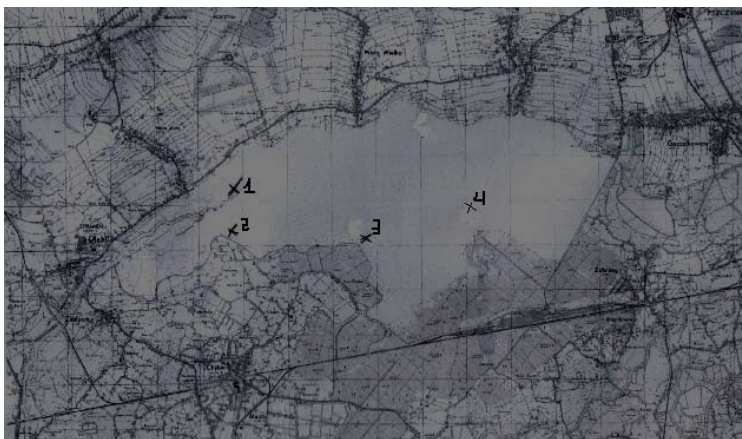


Fig. 1 The Goczałkowice reservoir with marked points of sampling.

Sediment bottom samples number (1) originated from the place situated at the river mouth Small Vistula from the coastal region (littoral) zone (Fig 1). Sediment bottom

samples number (2) and (3) were collected from place situated in coastal region (littoral) distant from the river mouth (Fig 1). Sediment bottom samples number (4) were collected from the deepest zone of the reservoir Goczałkowice called the profundal (Fig. 1).

Humic acid were extracted from sludge samples according to the method described before [4]. Electron paramagnetic resonance (EPR) spectra were obtained with Bruker EMX EPR spectrometer operating at X-band frequency at room temperature. The EPR was applied for both quantitative (free radicals concentration) and qualitative (g factor) analysis of humic acid extracted from sediment bottom at four place of Goczałkowice dam. Comparison of signal intensity of the main functional groups of humic acid was conducted by means of ^1H NMR techniques. The ^1H NMR spectra were obtained after dissolving 5 mg of humic acid in 0.3 M solution of NaOD in D_2O . All measurements were obtained with BRUKER 400 Ultra Shield spectrometer at room temperature. By integrating the field of a suitable range of chemical shifts the percentage of respective hydrogen was determined. The ratio of respective atoms was next calculated i.e. the integration field of the suitable range of chemical shifts was divided by the integration field of all signals on the spectra.

To determine the elementary composition changes in the extracted humic acid the percentage content of carbon, hydrogen, nitrogen and sulphur was determined by means of Series II CHNO/S 2400 PERKIN ELMER elementary analyser. Percentage concentration of oxygen was calculated by subtraction of the percentage content of carbon, hydrogen, nitrogen and sulphur from 100.

Results and discussion

Sediments bottom samples collected from various places of Goczałkowice reservoir differed with the consistency and percentage content of humic acids (Table 1).

The sediment bottom sampled from place (3) was sandy (Fig. 1). However the samples collected from places (1), (2), and (4) had consistency of silt which is characteristic for Goczałkowice dam which is eutrophic reservoir dam (the fertile reservoir with a lot of biogens).

Table 1. Percentage content of humic acid in sediment bottom and theirs colour

Nr próbki	Mass of humic acid extracted from 80g sediment bottom[g]	Percentage content of humic acid [%]	Colour of humic acid
1	1,91±0,39	2,39	dark brown
2	2,32±0,58	2,90	light brown
3	0,36±0,33	0,45	light brown
4	0,10±0,03	0,12	dark brown

The EPR spectroscopy results show that the humic acids extracted from sediment bottom taken from Goczałkowice dam reservoir have low free radical concentration (Table 2) [5].

The highest free radical concentration was obtained for humic acid extracted from sediment bottom (1) (Table 2). These sediments were characterized also with the relatively large content humic acid (Table 1).

It should be noticed that sediment collected from place (1) of dam reservoir is located in littoral zone (Fig.1). In this zone of Goczałkowice reservoir the greater content of humic acid than in another region occurs [6]. Moreover, the sediment bottom (1) were taken from the place situated at the river mouth Small Vistula what can also influence greater

content of humic acid and highest value of free radical concentration in the extracted humic acid (Table 2).

Table 2. The free radical concentration and g-factor obtained for humic acid extracted from sediment bottom from Goczałkowice reservoir.

Sample	Free radical concentration 10^{16}	g-factor
1	$6,19 \pm 0,66$	$2,0028 \pm 0,0001$
2	$3,01 \pm 0,12$	$2,0028 \pm 0,0001$
3	$1,79 \pm 0,81$	$2,0028 \pm 0,0001$
4	$4,90 \pm 1,28$	$2,0030 \pm 0,0001$

It is noteworthy, that to the river Small Vistula the raw and cleaned sewage is pipe away. The continuous inflow of sewage in this place can influence the course of humification process of bottom sediments [4,7]. The humic acid extracted from sediment bottom (2) and (3) are characterized with the considerably lower concentration of free radicals, although these sediments were also sampled from the coastal part of the reservoir (Fig 1). The percentage content of extracted humic acid is highest in the case of sediment bottom (2) and (1) (Table 1) what was expected because of location in coastal region (littoral) of the eutrophic reservoir [6]. However the distance of the place (2) from the river mouth Small Vistula, and the distance from the inflow of sewage, causes that humic acids extracted from sediment (2) have lower free radical concentration. This means that degree of humification of sediment bottom (2) is higher than sediment collected at the river mouth Small Vistula (1). The other situation can be observed for humic acid extracted from sediment bottom (3). The content of humic acid in sediment derived from this place is low (0.45%). Moreover the free radical concentration in the extracted humic acid is very low ($1.79 * 10^{16}$). It should be noticed that samples of sediment bottom (3) differ significantly from the other samples (1,2,4). Sediment bottom (3) was sandy what can evidence that the sample were collected from shallow region of reservoir where the humification processes proceed marginally. The sediment bottom (4) was collected from profundal zone which is the dipper region of the Goczałkowice dam reservoir (Fig.1). The percentage content of humic acid in this sediment (4) is also relatively low (0,12%). It is probably caused by decrease of dissolved oxygen along with deep of eutrophic dam and low activity of microorganism what organic matter transformation makes difficult [6]. It is difficult to explain why the free radical concentration of humic acid extracted from sediment bottom (4) is higher than free radical concentration of humic acid extracted from sediment bottom (2) from litoral zone.

Aromatisation of humic acid gives information about the course of humification process and age of sediment bottom [4,6-10]. The higher aromatisation of humic acid extracted from sediment indicates that humification process have been taken place longer and the sediment bottom is older [4,6-10].

In order to determine the aromatisation of humic acid extracted from sediment bottom the g-factor (Table 2) and the H/C atomic ratio were determine (Table 3). Moreover comparison of signal intensity of the aliphatic (H_{Ali}) and aromatic protons (H_{Ar}) of humic acid was conducted by means of 1H NMR techniques (Table 3).

Table 3. The H/C atomic ratio and percentage content of aromatic (H_{Ar}) and aliphatic protons (H_{Ali}) of humic acid extracted from sediment bottom.

Sample	Atomic ratio H/C	H_{Ar} [%]	H_{Ali} [%]
1	$1,68 \pm 0,27$	10,5	55,8
2	$1,76 \pm 0,06$	9,05	67,8
3	$2,67 \pm 1,29$	3,4	69,0
4	$1,46 \pm 0,17$	5,9	75,8

The values of g-factor of humic acid (Table 2) are very low when comparing with the usually obtained for semiquinone radicals [9] but there are typical for humic acid extracted from sediment bottom [10]. Such low g-factor values indicate the high aromatisation of humic acid extracted from sediment bottom. This fact is confirmed also by the H/C atomic ratio and high percentage content of aromatic protons (H_{Ar}) in humic acid extracted from sediment bottom. Percentage content of aromatic protons (H_{Ar}) in humic acid extracted from sewage sludge [9], which one considered strongly aromatized, amount to 6,91 % while for humic acid extracted from sediment bottom (Table 3) the percentage content of aromatic protons (H_{Ar}) amount as much as 10,5%. One may say that humic acid extracted from sediment bottom collected from Goczałkowice dam reservoir are high aromatised what would evidence the large age of sediments.

Conclusion

The spectroscopic and analytical studies of humic acid extracted from sediment bottom collected from Goczałkowice dam reservoir show that humic acid are high aromatised although the free radical concentration is low. This fact indicate the large age of sediments.

It was observed that Small Vistula river influences significantly on properties of sediment bottom. However, the depth from what the samples were collected and region of dam reservoir causes differences in properties of extracted humic acid.

References

- [1] A. Siudy, A. Bilnik, T. Świercz, Z. Szlęk, Materiały Konferencji Naukowo - Technicznej z okazji Jubileuszu 50-lecia budowy Zbiornika Wodnego na Małej Wiśle w Goczałkowicach, Pszczyna 2005. p. 10.
- [2] D. L. Sparks, in, Soil Physical Chemistry, Department of Plant and Soil Sciences, University of Delaware, CRC 1999.
- [3] PN-ISO 5667-15 (2004) Polish Standard (according to ISO 5667-15:1999).
- [4] J. Pajęczkowska, A. Sułkowska, W.W. Sułkowski, M. Jędrzejczyk, J. Mol. Struct. 651-653 (2003) 141.
- [5] A. Jezierski, F. Czechowski, M. Jerzykiewicz, Y. Chen, J. Drozd, Spectrochimica Acta, 56 (2000) 379.
- [6] A. Górniak, , Annales Universitatis Mariae Curie - Skłodowska, Lublin vol.42/43 (1988) 6.
- [7] J. Polak, W.W. Sułkowski, M. Bartoszek, W. Papież, J. Mol. Struct., 744-747 (2005) 983.
- [8] M. Jerzykiewicz, J. Drozd and A. Jezierski, Chemosphere, 39(2) (1999) 253.
- [9] J. Polak, F. Buhl, A. Kita, M. Bartoszek, W.W. Sułkowski, Acta Universitatis Latviensis 692 (2005) 115.
- [10] A. Busnot, F. Busnot, J. F. Le Querler, J. Yazbeck, Thermochemica Acta, 254 (1995) 319.

SYNTHESIS OF 2-(CHLOROMETHYL)BENZOYL CHLORIDE AND ITS REACTIONS WITH NUCLEOPHILES

P. Potaczek, M. Piętka-Ottlik, J. Młochowski
Institute of Organic Chemistry, Wrocław University of Technology,
Wyb. Wyspiańskiego 27, 50-375 Wrocław

Introduction

The chemistry and reactivity of the isoindolinone ring system are currently an area of interest for many research groups due to its biological activity. It has been recognized that *N*-substituted isoindolinones and their 3-substituted derivatives possess anxiolytic activity and are of interest as sedatives, hypnotics and muscle relaxants [1], including the anxiolytic [2] and the anxiolytic/anticonvulsant [3]. It was found that *N*-substituted isoindolinones (**11**) are constituents of antihypertensive [4], antiphlogistic [5] and analgesic [6] medicinal drugs and are substrates in the synthesis of different medicines [7] and natural products [8]. Other bioactive isoindolinones include the 5-HT antagonists [9] and the non-nucleosidic HIV-reverse transcriptase inhibitors [10].

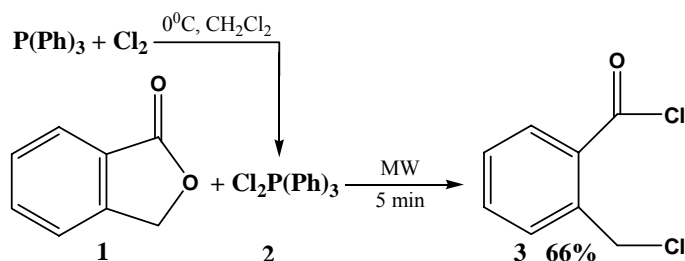
In this article we report results of our studies on the synthesis of 2-(chloromethyl)benzoyl chloride (**3**) and its reactions with primary aliphatic and aromatic amines, *CH*-acids and *S*-nucleophiles.

Results and Discussion

Synthesis of 2-(chloromethyl)benzoyl chloride (**3**)

2-(chloromethyl)benzoyl chloride (**3**) plays an important role in synthesis of many different organic compounds. In this work, we present alternative method for earlier known synthesis of this compound.

Our method is based on the reaction of 3*H*-isobenzofuran-1-one (**1**) with dichlorotriphenylphosphine (**2**) obtained from triphenylphosphine chlorinated with dry, gaseous chlorine in dry dichloromethane as shown in scheme 1. This reaction was carried out under cooling in the ice/salt bath until all substrate reacted. When the reaction was completed, dichloromethane was evaporated *in vacuo* and the reaction has been continued in the microwave (400 W) for 5 minutes. 2-(chloromethyl)benzoyl chloride (**3**) was distilled off *in vacuo* from the residue as colourless oil.



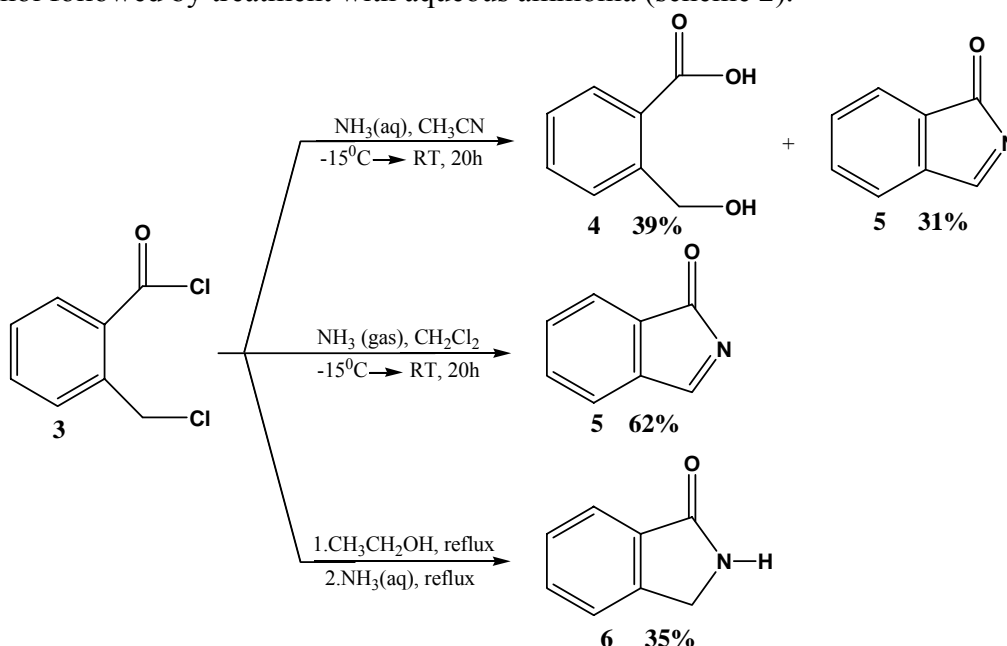
Scheme 1. Synthesis of 2-(chloromethyl)benzoyl chloride (**3**)

Reaction of 2-(chloromethyl)benzoyl chloride (3) with *N*-nucleophiles

2-(chloromethyl)benzoyl chloride (**3**) can act as *bis*-electrophile with one electrophilic center localized on the carbonyl atom and the second localized on the carbon. Both of these centers can compete toward nucleophile such as for example amine nitrogen, and finally give *N*-substituted isoindolinones (**11**).

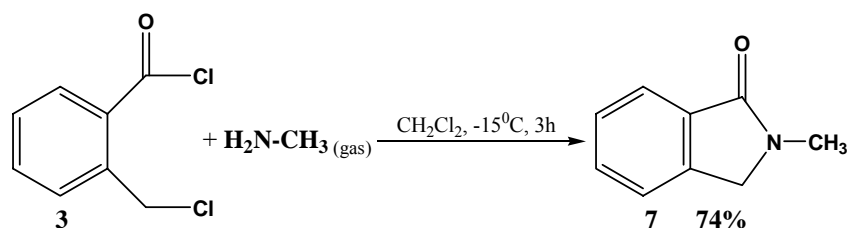
When a water solution of ammonia was a reagent, 2-(hydroxymethyl)benzoic acid (**4**) and benzisindolone (**5**) were produced. The compound **5** was obtained as a sole product, when vigorously stirred, cooled on ice/salt bath solution of 2-(chloromethyl)benzoyl chloride (**3**) in dry dichloromethane was saturated by dry, gaseous ammonia over 30 min.

Isoindolin-1-one (**6**) was obtained by heating of 2-(chloromethyl)benzoyl chloride (**3**) in ethanol followed by treatment with aqueous ammonia (scheme 2).



Scheme 2. Reaction of 2-(chloromethyl)benzoyl chloride (**3**) with ammonia

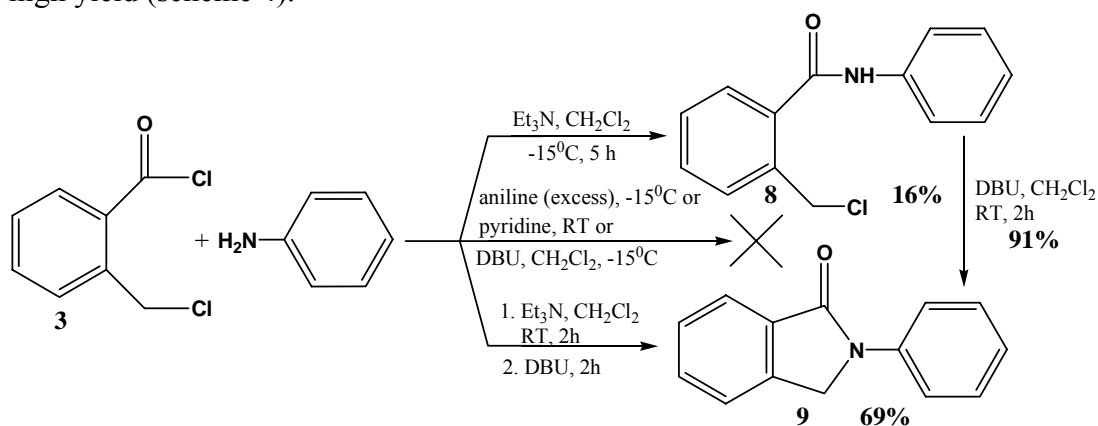
The reaction of dichloride (**3**) with methylamine gave 2-methylisoindolin-1-one (**7**) as shown in scheme 3, while the similar reaction with aniline in the presence of triethylamine led to 2-(chloromethyl)-*N*-phenylbenzamide (**8**). In the next step compound **8** treated with DBU gave stable *N*-phenylisoindolin-1-one (**9**) as final product.



Scheme 3. Reaction of 2-(chloromethyl)benzoyl chloride (**3**) with methylamine

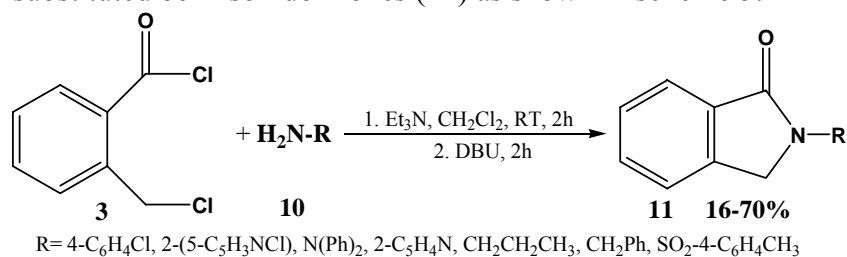
One observed, that aniline in the reaction with 2-(chloromethyl)benzoyl chloride (**3**) in excess aniline, pyridine or in attendance DBU gives mixtures of many unstable products.

Only two-step, one-pot reaction 2-(chloromethyl)benzoyl chloride (**3**) with aniline in the presence of triethylamine and then DBU gave *N*-phenylisoindolin-1-one (**9**) in a high yield (scheme 4).



Scheme 4. Reaction of 2-(chloromethyl)benzoyl chloride (**3**) with aniline

This method, having a general synthetic value, was applied for synthesis of several different *N*-substituted benzisoindolinones (**11**) as shown in scheme 5.



Scheme 5. Reaction of 2-(chloromethyl)benzoyl chloride (**3**) with amines (**10**)

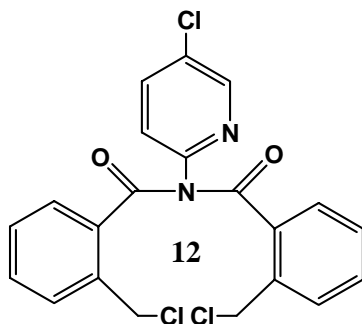


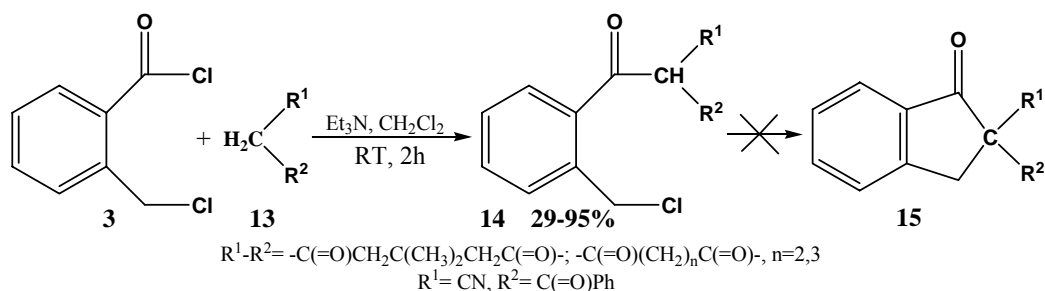
Figure 1.

When dichloride (**3**) was treated with 5-chloropyridin-2-amine, 2-(5-chloropyridin-2-yl)isoindolin-1-one (**11**) R=2-(5-Cl-C₅H₃N) and compound (**12**) (39%) were isolated on the silica gel column.

The urea, thiourea, ethane-1,2-diamine and acetamide in the reaction with 2-(chloromethyl)benzoyl chloride (**3**) give only complex mixtures of unstable products.

Reaction of 2-(chloromethyl)benzoyl chloride (**3**) with *CH*-acids (**13**)

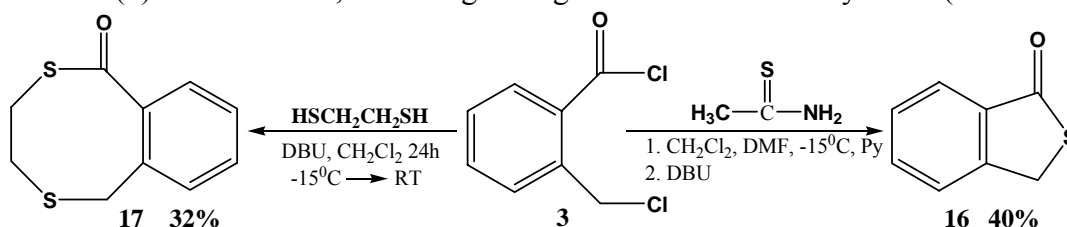
The compounds **13**, having methylene group activated by two electron-withdrawing substituents easily underwent acylation, and mono substituted 2-(chloromethyl)benzoyl chlorides (**14**), presented in scheme 6, were formed. The compounds **14** in the presence of bases such as Et₃N, DBU, K₂CO₃, NaH and LDA/CH₂Cl₂ did not undergo intramolecular alkylation. When compound **14** was treated with LDA in THF, *n*-butyl 2-(chloromethyl)benzoate was produced.



Scheme 6. Reaction of 2-(chloromethyl)benzoyl chloride (**3**) with *CH*-acids (**13**)

Reaction of 2-(chloromethyl)benzoyl chloride (3) with S-nucleophiles

Benzo[*c*]tiophen-1-(3*H*)-one (**16**) was obtained by the treatment of 2-(chloromethyl)benzoyl chloride (**3**) with ethanethioamide, but the reaction of the same dichloride (**3**) with ethane-1,2-dithiol gave eight-membered macrocycle **17** (scheme 7).



Scheme 7. Reaction of 2-(chloromethyl)benzoyl chloride (**3**) with *S*-nucleophiles

Biological tests

All *N*-substituted isoindolin-1-ones have been tested against selected viruses (HSV-1, EMCV, VSV) as control compounds for highly active group of benzisoselesazol-3(2*H*)-ones, same way as previously reported [11]. We hypothesized that antiviral activity of selenoorganic compounds was related to the presence of selenium. Thus, we designed compounds in which selenium has been replaced by methylene group and tested them in the same conditions as selenic compounds. As we suppose, isoindolin-1-ones didn't exhibit any antiviral activity what confirmed our hypothesis.

References:

- [1] H. P. Rang, et all, in Pharmacology, Churchill-livingstone, London, 1995
- [2] Z.-P. Zhuang, M.-P. Kung, M. Mu, H. F. Kung, J. Med. Chem., 41 (1998) 157
- [3] V. Gotor, et all Tetrahedron: Asymmetry, 8 (1997) 995
- [4] J.-M. Ferland, C. A. Demerson, L. G. Humber, Can. J. Chem., 63 (1985) 361
- [5] S. Li, et all Yiyano Gongye 16 (1985) 543; Chem. Abstr., 105 (1986) 6378
- [6] Laboratori Baldacci, S. P. A. Japanese Patent 5,946,268, (1984); Chem. Abstr., 101, (1984) 54922
- [7] P. Pigeon, B. Decroix, Tetrahedron Lett., 38 (1997) 2985
- [8] D. L. Boger, J. K. Lee, J. Goldberg, Q. Jin, J. Org. Chem., 65 (2000) 1467
- [9] Z. P. Zhuang, M. P. Kung, M. Mu, H. F. King, J. Med. Chem., 41 (1998) 157
- [10] E. De Clercq, J. Med. Chem., 38 (1995) 2491
- [11] H. Wójtowicz, et all, Farmaco, 59(11) (2004) 863

This work was supported by PBZ-Min-015/P05/2004 grant.

BIOCHEMISTRY IN SCHOOL CURRICULA – OPTIONAL COURSE FOR THE 4TH YEAR STUDENTS OF CHEMISTRY

Michał M. Poźniczek^{1,2}, Ewa Odrowąż^{1,3}

¹ Wydział Chemii UJ, ² III LO w Krakowie, ³ Gimnazjum nr 52 Ojców Pijarów w Krakowie

Biochemistry as a fairly new field of science gradually clears its way in the school curricula. It follows the path of other natural sciences which slowly and gradually spread to primary and high schools. At the present moment a significant part of the advanced chemistry courses involves elements of static biochemistry, and biology courses include elements of dynamic biochemistry. This fact may be confirmed by the following fragment of the current curriculum [1]

BIOLOGY

- Main nutrients (proteins, sugars, fats)
- Essential amino acids
- Vitamins, microelements and their sources
- Protein transcription and biosynthesis
- Photosynthesis
- Saving and realisation of genetic information (DNA)
- Enzymes and reactions occurring in cells

CHEMISTRY

- Amino acids
- Peptides and proteins
- Simple and complex fats
- Basic sugars and nucleic acids – occurrence, properties and importance in the lives of men

One should assume that the new faculties in educating students (biotechnology, biochemistry, biophysics) will expect former pupils to be able to take in certain contents and will soon force the change of teaching model and biochemistry will become a separate subject. In this situation a question rises: who will be qualified to teach this subject? One group will definitely consist in the graduates of the biochemical faculties, however, they will lack the didactic preparation. The other group will be formed by the graduates of the chemical faculties; these in turn will lack suitable factual knowledge. The students of chemistry do have basic biochemistry course, but it does not account for the needs of the schools. On the other hand, the students of environmental protection, who often become chemistry teachers, do not have those issues included in their curriculum. In order to prepare the future teachers to meet the challenge, for many years now courses in biochemistry have their permanent and established position at the postgraduate studies for chemistry teachers offered at the Faculty of Chemistry of the Jagiellonian University. A modified syllabus for these courses [2] was presented at the convention of the Polish Chemical Society. Another challenge for the Department of Didactics was to design a similar course for full-time university students who want to gain teaching qualifications. Here another question arises: why this course should be different from the one designed for post-graduate students? The answer to this question

is the number of hours. Post-graduate studies allot only 16 hours for biochemistry classes, and for full-time students a 30-hour course is organized. The course includes lectures and classes. The issues raised during the lectures are as follows:

1. Elements of the history of biochemistry – Polish contribution in the development of this field (the lecture discusses the lives of biochemists, but the main focus is on the factual issues connected with their studies)
2. Selected issues from cytology
3. Biological role of hydrocarbons
4. Isoprene lipids
5. Fats
6. Amino acids
7. Peptides and proteins
8. Nucleic acids
9. Protein biosynthesis process
10. Sugars and photosynthesis process

As mentioned before, the issues discussed in the lectures are accompanied by supplementary classes during which the students are given the opportunity to contact many simple experiments on their own. The experiments are selected so as they can be repeated in an average school laboratory. The classes comprise of three thematic parts: sugars, amino acids and proteins, and fats and other compounds.

SUGARS

Among natural organic compounds sugars definitely take the lead in the plant world in terms of numbers. The cellulose cell walls constitute the main ingredient of the plant biomass. Corn grains and tubers of many plants act as a deposit for starch, basic storage polysaccharide. In the animal world the main storage polysaccharide is glycogen whose large quantities are deposited in the liver and muscles. Sugars with simpler structures (simple sugars, disaccharides) exist mainly in the dissolved form and are the indirect or end products of certain metabolic pathways. Among simple sugars the most important ones are pentoses and hexoses.

During the classes the students conduct experiments which help to distinguish sugars from other substances and to identify specific sugars. Here are exemplary experiments:

1. Molisch's test
2. Bial's test
3. Selivanov's test
4. Fehling's test
5. Barfoed's test
6. Anthrone reaction
7. Obtaining osazone crystals

ANALYSIS OF AMINO ACIDS AND PROTEINS

Amino acids are compounds usually associated with proteins. It is true but only for around twenty amino acids called protein amino acids. The scientists isolated from the living organisms a significantly greater number of these compounds: the number of known natural amino acids amounts to several hundreds. During the classes we deal only with protein amino acids.

Experiments connected with these issues:

1. Ninhydrin reaction
2. Van Slyke's reaction
3. Reaction of amino acids and formaldehyde
4. Detecting sulphur amino acids
5. Detecting tryptophan
6. Detecting histidine
7. Detecting aromatic amino acids
8. Detecting proteins
9. Precipitation of poorly soluble proteinates
10. Showing the catalytic activity of catalase
11. Showing the catalytic activity of salivary amylase

FAT ANALYSIS

Due to their hydrophobe character fats are practically insoluble in water, however, they dissolve easily in so-called fat solvents, e.g. chloroform. This makes it difficult to analyse fats from biological material, because usually not only fats are extracted but also other fatty substances such as steroids (cholesterol).

Experiments:

1. Acid value determination in fats
2. Demonstration of the presence of unsaturated fatty acids in vegetable oils
3. Detecting cholesterol

In the 2005/06 academic year a course on the basis of this syllabus was conducted for the first time. The course ended with a mark and the requirements included positive partial marks for each of the following tasks:

1. laboratory test – e.g. in the test-tubes there are the following substance:
fructose, glycyn, glucose, maltose, ribose, saccharose, tryptophan, tyrosine, water.
On the basis of the known samples identify the substances..
2. written essay – e.g. “Mucopolysaccharides – aloes's secret weapon”
3. written test on the issues discussed during the lectures and classes.

Sample tasks

During the course students completed questionnaires which allow us to assess it. The answers will enable its modification especially in order to:

1. eliminate few issues that are familiar from other courses (e.g. physicochemical properties of sugars)
2. elaborate on the issues that were discussed rather cursorily due to the limited time

Modifications of didactic courses and introducing new courses have become common at the Faculty of Chemistry of the Jagiellonian University. Introduction of the above course in biochemistry is a sign of the Department of Didactics joining this trend.

Literatura.

- [1] Podstawa programowa Dz .U. Z 1999 roku Nr 14 poz.129
- [2] M. Poźniczek, Biochemia w programach studiów podyplomowych dla nauczycieli chemii, materiały zjazdowe, PTCh, Poznań 2005, S11, K6
- [4] L. Kłysztenko-Stefanowicz, Ćwiczenia z biochemii, PWN, Warszawa 1972
- [5] Z. Sikorski, B. Drozdowski, B. Samotus, M. Pałasiński, Chemia żywności, PWN, Warszawa 1988
- [6] A. Kozik, B. Turyna, Molekularne podstawy biologii, Wydawnictwo ZamKor, Kraków, 1996

SYNTHESIS AND PHYSICOCHEMICAL PROPERTIES OF NEW N-1 o-(m- and p-) BROMOBENZYL SUBSTITUTED DERIVATIVES OF 5- METHYLENEAMINOALKYLOCYTOSINE

Dorota Prukała

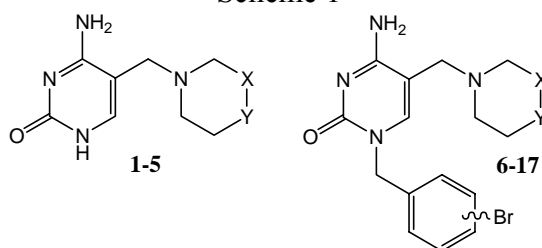
*Adam Mickiewicz University, Faculty of Chemistry
Grunwaldzka 6, 60-780 Poznań*

There has been increasing interest for many years in 5-substituted or/and 1,5-substituted cytosines as antiviral and anticancer agents.[1],[2],[3]

In view of above in this work presents a series of new compound having a structure of this type, wherein the cyclic amine is attached via methylene bridge to 5 position of cytosine (**1-5**). New derivatives having an ortho- (meta- and para-)bromobenzyl substituent at N-1 position of cytosine (**6-17**) are also presented.

The structures of compounds **1-5** and **6-17** are shown below:

Scheme 1



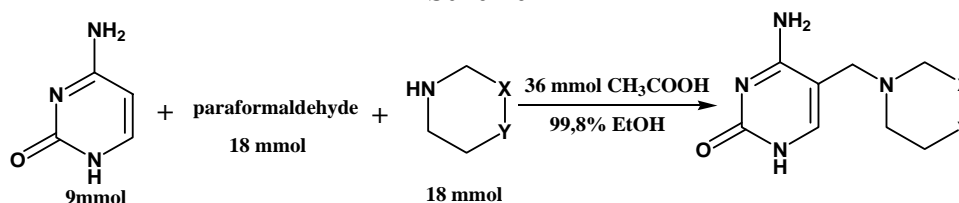
No	X	Y	Br	No	X	Y	Br	No	X	Y	Br
1	CH ₂	O	-	7	CH ₂	O	-m	13	CH ₂	CHCH ₃	-m
2	CH ₂	CH ₂	-	8	CH ₂	O	-p	14	CH ₂	CHCH ₃	-p
3	CH ₂	CHCH ₃	-	9	CH ₂	CH ₂	-o	15	CHCH ₃	CH ₂	-o
4	CHCH ₃	CH ₂	-	10	CH ₂	CH ₂	-m	16	CHCH ₃	CH ₂	-m
5	CH ₂	-	-	11	CH ₂	CH ₂	-p	17	CHCH ₃	CH ₂	-p
6	CH ₂	O	-o	12	CH ₂	CHCH ₃	-o				

Compounds **1-5** were synthesised via the Mannich reaction because it is known that other pyrimidines like uracil and 2-thiouracil under the Mannich reaction conditions give 5-substituted products.[4],[5]

However it is also known that the Mannich reaction of cytosine conducted in the conditions different than those described in this work (formalin, room temperature, THF as a solvent) give quite different products namely 1N,4N-substituted cytosines.[6]

The reaction for obtaining compounds **1-5** is presented as follows:

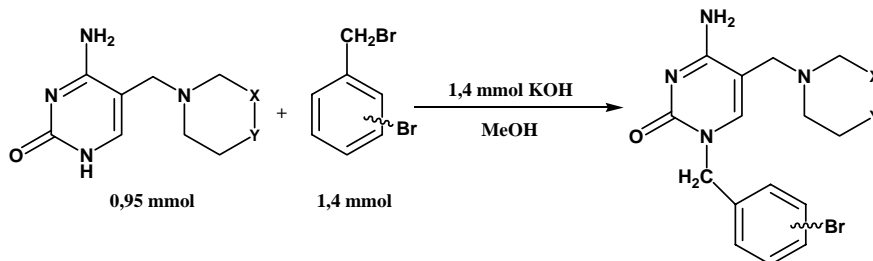
Scheme 2



This reaction was conducted in boiling ethanol solutions and usually carried out for 3,5-4 hours. The solids of **1-5** were isolated by precipitation and then they were purified by crystallisation from methanol. Yield of the product were in the order of 39-65%.

Compounds **6-17** were synthesised as follows:

Scheme 3



Fortunately this reaction was highly regioselective and no others products appeared, what was verified by TLC ($\text{CHCl}_3:\text{CH}_3\text{OH}$ 5:1/ SiO_2) and then by NMR methods. However it is known this simple alkylation method often suffers from the disadvantage that the ambient nature of the amide system leads to both O- and N-alkylation, and these O- and N-substituted derivatives of cytosine are difficult to separate [7].

Compounds **6-17** were synthesised by alkylation of appropriate **1-4** with o-(m- or p-) bromobenzyl bromide at room temperature in 20 ml of methanol in the presence of 1, 4 mmol of KOH. Reactions were carried out for 24 hours. After the reaction completion a half of the MeOH was evaporated and the water was added until the whole solid was precipitated. The solid was collected and washed with boiling ethyl ether. The compounds obtained were chromatographically pure (TLC) without further crystallisation what was checked by elemental analyses. Yields of the products (**6-17**) were in the order of 55-90%.

All compounds were characterised on the basis of spectral studies (^1H NMR, ^{13}C NMR and IR). Compounds **1-5** are low soluble in most of organic solvents, the only compounds **1**, **3** and **4** are sufficiently soluble in DMSO-d_6 for recording their ^1H NMR spectra in this solvent. These spectra are valuable because they confirm that the 1N and 4N atoms are not substituted by exhibition of two broad signals at 7,10ppm and 10,41 ppm assigned to the 4 NH_2 and 1 NH protons. The ^1H NMR spectra (DMSO-d_6) of **6-17** show only one broad signal in the range of 7.11-7.69 ppm assigned to the 4 NH_2 protons. For compounds **1-5** the ^1H NMR and ^{13}C NMR spectra were also recorded in TFA-d solutions. These ^1H NMR spectra show a characteristic singlet in the range 8,44-8,46 ppm assigned to the proton in 6 position in cytosine ring, but there are no signals of the proton in 5 position.

The signals of the same assignment (7.57-7.94 ppm) appear in the ^1H NMR spectra of compounds **6-17** but they are downfield shifted because of the solvent (DMSO-d_6). All signals in ^1H and ^{13}C NMR were confirmed by comparison with the spectra calculated using ACD/HNMR predictor and ACD/CNMR predictor. The spectra of all possible tautomers of compounds **1-17** were calculated and the tautomers in Scheme 1 are those giving the best fit with the calculated one.

The IR spectra of **1-17** (KBr disks) reveal two strong bands in the region 3670-3120 cm^{-1} which may be assigned to $\nu_{\text{as}}(\text{NH}_2)$ and $\nu_{\text{s}}(\text{NH}_2)$. In the 1682-1617 cm^{-1} range the intense bands of amine group scissoring vibrations α (NH_2) are observed adjacent to the carbonyl band stretching vibrations ν ($\text{C}=\text{O}$).

Characteristic spectral data for **1-17** are presented in Table 1 and in Table 2. The ^{13}C NMR signals of aromatic carbons are omitted

Table 1. The most important data from ¹H NMR spectra of compounds **1-17**

No	¹ H NMR (δ, ppm)
1	DMSO:morpholine-2.31-3.56 (8H); cytosineH6-7.26 (s,1H), NH ₂ 6.27 (br,2H), NH 10.46 (br,1H); N-CH ₂ -C ⁵ 3.15 (s,2H).
1	TFA:morpholine-3.58-4.40(8H); cytosineH6-8.46(s,1H); N-CH ₂ -C ⁵ 4.66 (s,2H).
2	DMSO:piperidine-1.48-2.49 (10H); cytosineH6-7.22 (s,1H), NH ₂ 7.10 (br,2H), NH 10.33 (br,1H); N-CH ₂ -C ⁵ 3.12 (s,2H).
2	TFA:piperidine-1.89-3.85(10H); cytosineH6-8.44(s,1H); N-CH ₂ -C ⁵ 4.51 (s,2H).
3	TFA:pyrrolidine-2.29-3.98(8H); cytosineH6-8.44 (s,2H); N-CH ₂ -C ⁵ 4.62 (s,2H).
4	DMSO:4-Mepiperidine-1.11-2.77(9H); CH ₃ 0.88(d,3H), cytosineH6-7.23 (s,1H), NH ₂ 7.07 (br,2H), NH 10.41 (br,1H), N-CH ₂ -C ⁵ 3.14 (s,2H).
4	TFA:4-Mepiperidine-1.59-3.85 (9H), CH ₃ 1.10 (d,2H); cytosineH6 8.44 (s,1H); N-CH ₂ -C ⁵ 4.51 (s,2H).
5	TFA:3-Mepiperidine-1.16-3.83 (9H), CH ₃ 1.09 (d,3H); cytosineH6- 8.44 (s,2H); N-CH ₂ -C ⁵ 4.51 (s,2H).
6	DMSO:Morpholine-2.93(m,4H),3.73(m,4H);cytosineH6-7.94(s,1H),4NH ₂ 7.57 (br.);N-CH ₂ -C ⁵ 3.39(s,2H);1N-CH ₂ -Ar 4.94(s,2H); Ar-H 7.05-7.68
7	DMSO:Morpholine-2.65(m,4H),3.65(m,4H);cytosineH6-7.90(s,1H),4NH ₂ 7.69(br.);N-CH ₂ -C ⁵ 3.50(s,2H);1N-CH ₂ -Ar 4.87(s,2H); Ar-H 7.29-7.49
8	DMSO:Morpholine-2.51(m,4H),3.55(m,4H);cytosineH6-7.67(s,1H),4NH ₂ 7.69(br.);N-CH ₂ -C ⁵ 3.15(s,2H);1N-CH ₂ -Ar 4.81(s,2H); Ar-H 7.21-7.54
9	DMSO:piperidine-1.39(m,2H),1.49(m,4H),2.30(m,4H);cytosineH6-7.58(s,1H); 4NH ₂ 7.18(br);N-CH ₂ -C ⁵ 3.15(s,2H);1N-CH ₂ -Ar 4.88(s,2H); Ar-H 6.90-7.66
10	DMSO:piperidine-1.39(m,2H),1.48(m,4H),2.29(m,4H);cytosineH6-7.68(s,1H); 4NH ₂ 7.12(br);N-CH ₂ -C ⁵ 3.15(s,2H);1N-CH ₂ -Ar 4.83(s,2H); Ar-H 7.28-7.48
11	DMSO:piperidine-1.39(m,2H),1.49(m,4H),2.30(m,4H);cytosineH6-7.69(s,1H); 4NH ₂ 7.20(br);N-CH ₂ -C ⁵ 3.15(s,2H);1N-CH ₂ -Ar 4.83(s,2H); Ar-H 7.22-7.55
12	DMSO:4-MePiperidine-0.88(d,CH ₃),1.11(m,2H),1.34(m,1H),1.59(m,2H),1.84 (m,2H)2.83(m,2H);cytosineH6-7.59(s,1H); 4NH ₂ 7.20(br);N-CH ₂ -C ⁵ 3.18(s,2H); 1N-CH ₂ -Ar 4.88(s,2H); Ar-H 6.91-7.66
13	DMSO:4-MePiperidine-0.88(d,CH ₃),1.11(m,2H),1.34(m,1H),1.59(m,2H),1.84 (m,2H)2.81(m,2H);cytosineH6-7.71(s,1H); 4NH ₂ 7.13(br);N-CH ₂ -C ⁵ 3.19(s,2H); 1N-CH ₂ -Ar 4.84(s,2H); Ar-H 7.26-7.49
14	DMSO:4-MePiperidine-0.89(d,CH ₃),1.11(m,2H),1.32(m,1H),1.59(m,2H),1.82 (m,2H)2.78(m,2H);cytosineH6-7.65(s,1H); 4NH ₂ 7.11(br);N-CH ₂ -C ⁵ 3.15(s,2H); 1N-CH ₂ -Ar 4.82(s,2H); Ar-H 7.22-7.55
15	DMSO:3-MePiperidine-0.83(d,CH ₃),1.41-1.79(m,7H),2.74(m,2H);cyt.H6-7.57(s, 1H); 4NH ₂ 7.11(br);N-CH ₂ -C ⁵ 3.15(s,2H); 1N-CH ₂ -Ar 4.82(s,2H); Ar-H 7.22-7.55
16	DMSO:3-MePiperidine-0.83(d,CH ₃),1.41-1.82(m,7H),2.72(m,2H);cyt.H6-7.69(s, 1H); 4NH ₂ 7.11(br);N-CH ₂ -C ⁵ 3.16(s,2H); 1N-CH ₂ -Ar 4.85(s,2H); Ar-H 7.24-7.49
17	DMSO:3-MePiperidine-0.81(d,CH ₃),1.38-1.82(m,7H),2.74(m,2H);cyt.H6-7.64(s, 1H); 4NH ₂ 7.11(br);N-CH ₂ -C ⁵ 3.13(s,2H); 1N-CH ₂ -Ar 4.81(s,2H); Ar-H 7.21-7.54

Table 2. The most important chemical shifts in ^{13}C NMR of compounds **1-17**

No	^{13}C NMR (δ , ppm)
1	TFA: morpholine -63.8 (C2,6), 51.9 (C3,5); cytosine - 94.4(C5), 148.1 (C2), 152.7 (C6), 159.9 (C4); N- CH₂-C⁵ - 51.8.
2	TFA: piperidine - 20.6 (C4), 22.9 (C3,5), 54.1 (C 2,6); cytosine -95.2 (C5), 148.2 (C2), 152.5 (C6), 159.9 (C4); N- CH₂-C⁵ 51.5.
3	TFA: pyrrolidine -22.1 (C3,4), 54.9 (C 2,5); cytosine - 96.8 (C5), 148.5 (2), 151.6 (C6), 159.6 (C4); N- CH₂-C⁵ 49.2.
4	TFA: 4-Mepiperidine -28.5 (C4), 30.9 (C3,5), 53.9 (C2,6), 19.1 (CH₃); cytosine - 95.3 (C5), 148.1 (C2), 152.5 (C6), 159.9 (C4); N- CH₂-C⁵ 51.3.
5	TFA: 3-Mepiperidine - 22.7 (C5), 29.5 (C3), 30.0 (C4), 53.4 (C6), 59.6 (C2), 16.7 (CH₃); cytosine - 95.5 (C5), 148.2 (C2), 152.6 (C6), 160.4 (C4); N- CH₂-C⁵ 51.6
6	DMSO: Morpholine -53.3(C2,6),64.3(C3,5); cytosine - 101.5(C5),144.0(C6),153.9 (C2),163.8(C4); N- CH₂-C⁵ 52.2; 1N- CH₂-Ar 51.2
7	DMSO: Morpholine -54.5(C2,6),65.1(C3,5); cytosine - 99.8(C5),147.5(C6),154.2 (C2),164.1(C4); N- CH₂-C⁵ 51.8; 1N- CH₂-Ar 50.9
8	DMSO: Morpholine -55.9(C2,6),66.1(C3,5); cytosine - 100.7(C5),144.9(C6),155.3 (C2),165.2(C4); N- CH₂-C⁵ 52.5; 1N- CH₂-Ar 50.7
9	DMSO: Piperidine -23.9(C4),25.6(C3,5),56.6(C2,6); cytosine - 101.5(C5),144.7 (C6),155.3(C2),165.5(C4), N- CH₂-C⁵ 53.3; 1N- CH₂-Ar 51.9
10	DMSO: Piperidine -23.9(C4),25.5(C3,5),56.5(C2,6); cytosine - 101.5(C5),144.5 (C6),155.3(C2),165.4(C4), N- CH₂-C⁵ 53.2; 1N- CH₂-Ar 50.7
11	DMSO: Piperidine -23.3(C4),25.6(C3,5),56.6(C2,6); cytosine - 101.5(C5),144.9 (C6),154.9(C2),164.9(C4), N- CH₂-C⁵ 52.4; 1N- CH₂-Ar 50.9
12	DMSO: 4-MePiperidine -30.2(C4),33.8(C3,5),56.1(C2,6),21,7(CH₃); cytosine - 101.5(C5),144.8 (C6),155.2(C2),165.4(C4), N- CH₂-C⁵ 52.5; 1N- CH₂-Ar 51.9
13	DMSO: 4-MePiperidine -30.1(C4),33.7(C3,5),56.1(C2,6),21,7(CH₃); cytosine - 101.6(C5),144.7 (C6),155.5(C2),165.5(C4), N- CH₂-C⁵ 52.5; 1N- CH₂-Ar 50.8
14	DMSO: 4-MePiperidine -30.3(C4),33.9(C3,5),56.2(C2,6),21,8(CH₃); cytosine - 101.5(C5),144.4 (C6),155.3(C2),165.3(C4), N- CH₂-C⁵ 52.7; 1N- CH₂-Ar 50.7
15	DMSO: 3-MePiperid. -24.9(C5),30.6(C3),32.4(C4),52.3(C6),60.5(C2),19.5(CH₃); cyt. -101.5(C5),144.7(C6),155.3(C2),165.5(C4),N- CH₂-C⁵ 52.8; 1N- CH₂-Ar 51.8
16	DMSO: 3-MePiperid. -24.9(C5),30.7(C3),32.5(C4),52.3(C6),60.4(C2),19.5(CH₃); cyt. 101.1(C5),144.5 (C6),155.4(C2),165.4(C4), N- CH₂-C⁵ 52.8; 1N- CH₂-Ar 50.7
17	DMSO: 3-MePiperid. -24.9(C5),30.7(C3),32.5(C4),52.3(C6),60.5(C2),19.5 (CH₃); cyt. 101.5(C5),144.5 (C6),155.4(C2),165.4(C4), N- CH₂-C⁵ 52.8; 1N- CH₂-Ar 50.7

References

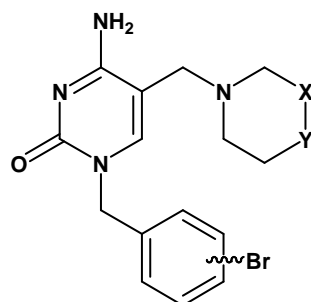
- [1]A.S. Jones, P. Serafinowski, R.T. Walker, Tetrahedron Lett., 28 (1977) 2459
- [2]A.C. Schroeder, R.G. Hughes Jr., A. Bloch, J.Med.Chem., 24 (1981) 1078
- [3]R.V. Joshi., Z.-Q. Xu, M.B. Ksebati, D. Kesler, J.Chem.Soc.Perkin Trans. 1, (1994) 1089
- [4]M.S. Motavia, P.T. Jørgensen, A. Kjøer, E.B. Pedersen, C.M. Nielsen, Monatsch.Chem., 124 (1993) 55
- [5]P. Kamalakannan, D. Vekappayya, T. Balasubramanian, J. Chem. Soc., Dalton Trans., (2002) 3381
- [6]K.B. Sloan, K.G. Siver, Tetrahedron, 40 (1984) 3997
- [7]D.M. Brown,C.M. Taylor, J.Chem.Soc.Perkin Trans.1, (1972) 2385

THE USE OF ESI MS METHODS FOR DIFFERENTIATION OF ISOMERIC o- (m- AND p-) BROMOBENZYL SUBSTITUTED DERIVATIVES OF 5- METHYLENEAMINOALKYLCYTOSINE

Dorota Prukała

Adam Mickiewicz University, Faculty of Chemistry
Grunwaldzka 6, 60-780 Poznań

This work reports the electrospray ionization (ESI) mass spectrometric behaviour of compound **1-12**.



1-12

1:X=CH₂, Y=O, o-Br; **2:**X=CH₂, Y=O, m-Br; **3:**X=CH₂, Y=O, p-Br; **4:**X=CH₂, Y=CH₂, o-Br; **5:**X=CH₂, Y=CH₂, m-Br; **6:**X=CH₂, Y=CH₂, p-Br; **7:**X=CH₂, Y=CHCH₃, o-Br; **8:**X=CH₂, Y=CHCH₃, m-Br; **9:**X=CH₂, Y=CHCH₃, p-Br; **10:**X=CHCH₃, Y=CH₂,o-Br; **11:**X=CHCH₃, Y=CH₂, m-Br; **12:**X=CHCH₃, Y=CH₂, p-Br.

The study was undertaken to check if it is possible to differentiate the isomeric 1N-ortho-(metha- or para-)bromobenzyl substituted derivatives of 5-methyleneaminoalkylcytosine using the ESI MS method. This method has been rarely used for this purpose. The compounds investigated are not described in literature (but presented in the Section 2-“Organic and Bioorganic Chemistry”) and may have important pharmaceutical properties, because the compounds of this class show a wide spectrum of antiviral and anticancer activity.

The ESI mass spectra of **1-12** were recorded in methanol solutions and cone voltages (CV) from 30 V through 60 V to 90 V. For the present study the positive ion mode was chosen.

The increase in CV causes the ions fragmentation/dissociation. The mass spectra recorded at higher values of CV show the daughter ions formed as a result of covalent bonds cleavages, but the ESI MS method does not allow tracing the detailed fragmentation pathways of particular fragment ions.

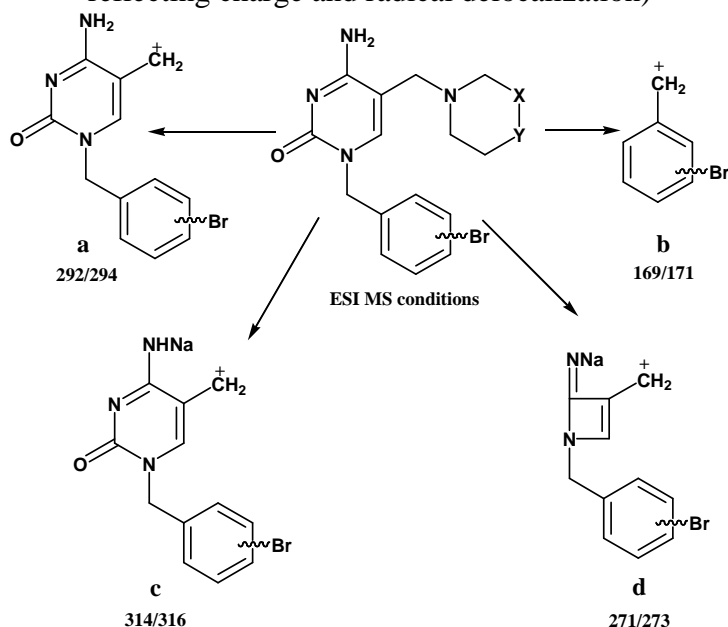
The plausible structures of the fragment ions formed in these processes are shown on *Scheme 1*. The elemental compositions of these ions were confirmed by checking of their isotopic compositions. (The elemental compositions and relative abundances of the most important ions are shown in *Table 1* where the low abundant ions are omitted). The ESI mass spectra of **1-12** show that with increasing CV the abundances of molecular ions [M+H]⁺ decrease; at the cone voltage 90V they are mostly low abundant, but ions [M+Na]⁺ were present in higher CV. This indicates that Na⁺ ions stabilize the structure of molecules of compounds **1-12** under the ESI MS conditions.

Ions **a** and **b** are formed by the rupture of the Csp³-N bonds. The fragment ion **a** is present even at CV 30 V; which means that the bond between CH₂ and N in the cyclic amine is very weak. The formation of ion **c** besides the cleavage of the C-N bond, needs also the exchange of the “acidic” hydrogen in the NH₂ group to the sodium atom; probably ion **c** is a daughter ion of ion **a**.

Ion **d** is formed by ejection of a neutral molecule of NH=C=O. The simplest way to formation of this ion is the ejection of this molecule from ion **c**, but there is no experimental proof for this process. It is worth of attention that this kind of ejection is very characteristic of cytosine and other pyrimidine bases under the EIMS condition and it is called “the retro Diels-Alder reaction”.

Scheme 1

The most abundant fragment ions formed under ESI MS conditions
(It is obvious that for each ion a number of plausible, resonance structures can be drawn reflecting charge and radical delocalization)



Differentiation of the isomers of the studied compounds is based on a comparison of the ratios of the relative abundances of ions **a** or **b** to those of [M+Na]⁺. These chosen ions appeared the most useful for this purpose. The ratios of the relative abundances of ions **a** or **b** to that of [M+Na]⁺ ions of particular isomers are presented in **Table 2**. As we can see in this table the differences between these ratios are significant which allows distinction of particular isomers of the compounds studied. It should be also mentioned that the differentiation is possible for CV from 30 V (the most convenient value of cone voltage) through 60 V to 90V.

In the series of compounds **1-3** it is possible to differentiate the position of Br according to the following sequences:

$$\frac{[a]^+}{[M+Na]^+} \text{ ortho} > \frac{[a]^+}{[M+Na]^+} \text{ metha} > \frac{[a]^+}{[M+Na]^+} \text{ para} \quad \text{CV 30V, 60V and 90V}$$

and

$$\frac{[b]^+}{[M+Na]^+} \text{ ortho} > \frac{[b]^+}{[M+Na]^+} \text{ metha} > \frac{[b]^+}{[M+Na]^+} \text{ para} \quad \text{CV 60V and 90V}$$

In the series of **4-6** it is possible to differentiate the position of the Br according to the following sequences:

$$\frac{[a]^+}{[M+Na]^+} \text{ ortho} < \frac{[a]^+}{[M+Na]^+} \text{ metha} < \frac{[a]^+}{[M+Na]^+} \text{ para} \quad \text{CV 30V, 60V and 90V}$$

and $\frac{[b]^+}{[M+Na]^+} \text{ ortho} < \frac{[b]^+}{[M+Na]^+} \text{ metha} < \frac{[b]^+}{[M+Na]^+} \text{ para} \quad \text{CV 60V and 90V}$

In the series of compounds **7-9** the values of these ratios also allow a differentiation of the isomers, as presented below:

$$\frac{[a]^+}{[M+Na]^+} \text{ ortho} > \frac{[a]^+}{[M+Na]^+} \text{ metha} > \frac{[a]^+}{[M+Na]^+} \text{ para} \quad \text{CV 30V, 60V and 90V}$$

and $\frac{[b]^+}{[M+Na]^+} \text{ ortho} > \frac{[b]^+}{[M+Na]^+} \text{ metha} > \frac{[b]^+}{[M+Na]^+} \text{ para} \quad \text{CV 60V and 90V}$

And for compounds **10-12**:

$$\frac{[a]^+}{[M+Na]^+} \text{ ortho} > \frac{[a]^+}{[M+Na]^+} \text{ metha} > \frac{[a]^+}{[M+Na]^+} \text{ para} \quad \text{CV 30V, 60V and 90V}$$

and $\frac{[b]^+}{[M+Na]^+} \text{ ortho} > \frac{[b]^+}{[M+Na]^+} \text{ metha} > \frac{[b]^+}{[M+Na]^+} \text{ para} \quad \text{CV 60V and 90V}$

The electrospray ionisation mass spectra were performed using a Waters/Micromass (Manchester, UK) ZQ mass spectrometer.

Table 1. The relative abundances of the most important ions in %, in cone voltage 30, 60 and 90V for compounds **1-12**

Cone voltage [V]	Ion	Compound /Rel.abundance			Cone voltage [V]	Ion	Compound /Rel.Abundance		
		1	2	3			4	5	6
30	[M+H] ⁺	58	100	97	30	[M+H] ⁺	100	100	100
	[M+Na] ⁺	24	24	61		[M+Na] ⁺	95	35	12
	a	15	7	14		a	15	9	14
60	[M+H] ⁺	76	100	15	60	[M+H] ⁺	20	46	100
	[M+Na] ⁺	3	71	100		[M+Na] ⁺	100	100	12
	a	62	69	12		a	15	21	39
	b	100	30	21		b	21	41	51
	c	-	3	3		c	3	3	-
d	3	4	4	d	9	3	-		
90	[M+H] ⁺	3	6	3	90	[M+H] ⁺	-	-	-
	[M+Na] ⁺	3	20	45		[M+Na] ⁺	41	20	3
	a	9	52	6		a	9	12	5
	b	100	100	100		b	100	100	100
	c	-	5	21		c	24	9	-
d	-	9	56	d	65	22	-		

Table 1. Continuation

Cone voltage [V]	Ion	Compound /Rel.abundance [%]			Cone voltage [V]	Ion	Compound /Rel.abundance [%]		
		7	8	9			10	11	12
30	[M+H] ⁺	100	100	36	30	[M+H] ⁺	100	46	100
	[M+Na] ⁺	57	48	35		[M+Na] ⁺	37	26	45
	a	12	7	3		a	15	7	10
60	[M+H] ⁺	100	100	24	60	[M+H] ⁺	15	18	30
	[M+Na] ⁺	27	42	100		[M+Na] ⁺	100	100	36
	a	43	31	6		a	15	18	13
	b	30	35	16		b	38	49	100
	c	-	3	3		c	3	6	3
d	3	4	6	d	8	8	3		
90	[M+H] ⁺	3	3	3	90	[M+H] ⁺	5	3	-
	[M+Na] ⁺	5	8	71		[M+Na] ⁺	52	25	6
	a	17	18	5		a	13	7	5
	b	100	100	82		b	100	100	100
	c	3	3	24		c	25	17	3
d	7	6	100	d	77	32	6		

Table 2. The values of ratios [a]⁺/[M+Na]⁺ and [b]⁺/[M+Na]⁺ calculated from ESI MS spectra in cone voltages 30, 60 and 90V.

No	Cone voltage [V]	[a] ⁺ /[M+Na] ⁺	[b] ⁺ /[M+Na] ⁺	No	Cone voltage [V]	[a] ⁺ /[M+Na] ⁺	[b] ⁺ /[M+Na] ⁺
1	30	0.63	-	7	30	0.21	-
	60	20.67	33.33		60	1.59	1.11
	90	3.00	33.33		90	3.40	20.00
2	30	0.29	-	8	30	0.15	-
	60	0.97	0.42		60	0.74	0.83
	90	2.60	5.00		90	2.25	12.50
3	30	0.23	-	9	30	0.09	-
	60	0.12	0.21		60	0.06	0.16
	90	0.13	2.22		90	0.05	1.15
4	30	0.16	-	10	30	0.41	-
	60	0.15	0.21		60	0.15	0.38
	90	0.22	2.43		90	0.25	1.92
5	30	0.26	-	11	30	0.27	-
	60	0.21	0.41		60	0.18	0.49
	90	0.60	5.00		90	0.28	4.00
6	30	1.17	-	12	30	0.30	-
	60	3.25	4.25		60	0.42	2.78
	90	1.67	33.33		90	1.00	16.67

PRECONCENTRATION OF Cd(II), Co(II), and Cu(II) BY SPE METHOD USING OCTYL GROUP COLUMNS

Bożena Puzio, Barbara Feist, Barbara Mięka
*Zakład Chemii Analitycznej, Instytut Chemii, Uniwersytet Śląski
ul. Szkolna 9, 40-006 Katowice*

Extraction to the solid phase is a method which has been promptly applied for initial sample preparation for analysis. Removal of usually interfering matrix components and preconcentration of trace quantities of the analytes are the most important application of SPE. The method has many advantages, for instance it is simple, it requires small solvent volumes and allows for working in an *on-line* system.

Metals may be separated and preconcentrated using SPE method, directly in the form of cations, however considerably more often they are transformed into chelate or ionic-association complexes. Amongst complexing agents, used for complexing of the investigated metals, the following may be named: 1,10-phenanthroline [1-4], ammonium pyrrolidine dithiocarbamate [5,6], 8-hydroxyquinoline [7-9], 1-(2-pyridylazo)2-naphthol [10], 4-(2-pyridylazo)resorcinol [11], neocuproine [12], EDTA [13] etc.

In this paper, 1,10-phenanthroline was used as a complexing agent for simultaneous separation and preconcentration of Cd (II), Co (II), Cu (II) by SPE method, using a column with an active octyl group C₈. Non-polar phase (the octyl group) requires the metals to be introduced on columns as non-ionogenic complexes. Therefore the analyzed metals were transformed into an ionic-association complex using 1,10-phenanthroline and chlorate(VII) ions, and then preconcentrated on columns filled with octyl phase.

EXPERIMENTAL

Reagents, solutions: Standard solutions of Cd(II), Cu(II), and Co(II) having concentration of 1 mg dm⁻³ (Merck); octyl (C₈) disposable extraction columns 3 ml (500 mg) (J.T. Baker); deionized water and analytical grade reagents were used for the preparation of all the solutions. 1,10-phenanthroline solution contained 2 % of ethanol. pH of the solutions was adjusted with 0.1 mol dm⁻³ hydrochloric acid or 0.1 mol dm⁻³ sodium hydroxide solutions.

Apparatus: BAKERBOND spe – 12G system; Spectroflame - ICP Model M (Spectro Analytical Instruments);

Procedure: A 2 cm³ portion of the complexing reagent (0.01 mol dm⁻³ 1,10-phenanthroline and 0.1 mol dm⁻³ NaClO₄ solutions) was added to a beaker with 50 cm³ of the model solution containing Cd(II), Cu(II), and Co(II). Then, the pH value of the solutions was fixed, depending on the eluent used for elution of the adsorbed metals. When 10 cm³ of 2.0 mol dm⁻³ hydrochloric acid solution were applied (after earlier washing of the column with the adsorbed metals with sodium hydroxide solution having concentration of 0.01 mol dm⁻³), pH value of the solution was fixed to 4. Whereas, when 10 cm³ of 0.1 mol dm⁻³ EDTA solution with pH ≈ 12 were used as eluent, pH value of the final solution was fixed to 3. The sample solutions were passed through the columns at a flow rate of 1.5÷2.0 cm³ min⁻¹ using a BAKERBOND spe system. Quantity of Cd(II), Cu(II), and Co(II) in the obtained solution was determined by the ICP-OES method using the program of simultaneous determination of these metals and correction standards containing the matrix (1,10-phenanthroline, NaClO₄, EDTA or HCl).

Preparation of the column for use: The columns were removed with 5 cm³ EtOH, 10 cm³ of 4 mol dm⁻³ HCl, and washed with deionized water until it was free from acid.

RESULTS AND DISCUSSION

It was proved experimentally that hydrochloric acid, EDTA, NaClO₄ and 1,10-phenanthroline slightly influence the simultaneous determination of Cu(II), Co(II), and Cd(II) by the ICP-OES method. That is why the calibration standards have contained reagents being a reagent matrix. The model standard curves (for the solutions containing the matrix reagents) are linear in the concentration range 0.1÷2.0 µg cm⁻³ for Cd, Co and 0.5÷3.0 µg cm⁻³ for Cu at the corresponding wavelengths: Cd – 226.50 nm, Co – 228.62 nm and Cu – 324.75 nm.

In order to obtain quantitative recoveries of the metal ions on the columns containing C8 as a functional group, the preconcentration procedure was optimized for the various analytical parameters such as sample preparation, pH of the sample solution, amount of complexing reagent, volume of sample and eluent, flow rates of sample and eluent.

The initial step of the research was selection of the elution agent for the metals adsorbed on octyl columns. Possibilities of application the following compounds: nitric acid, ethyl alcohol, chloroform, EDTA, EDTA with pH=12, NaOH with concentration of 0.01 mol dm⁻³, and hydrochloric acid were examined. Analyzing the results of these investigations, it was found that EDTA solution with concentration of 0.1 mol dm⁻³ and pH ≈ 12, and hydrochloric acid solution might be used as elution agents for the studied metals. It was also ascertained that while using a hydrochloric acid solution as the eluent, the columns containing the adsorbed metals should be washed with 0.01 mol dm⁻³ NaOH solution. Application of the acid only did not yield satisfactory recoveries.

Next, the influence of pH of the initial solution on efficiency of separation and preconcentration of Cu(II), Co(II), and Cd(II) on C8 columns was examined. The effect of pH on the separation of metal ions was studied in the range of 2÷8, keeping the other parameters constant. The optimum pH range for maximum recovery of each metal ion is shown in Figures 1 and 2. It was found that pH = 3 is optimal for group preconcentration of the studied metals when EDTA was used as eluent, and pH = 4 is optimal when hydrochloric acid was used as eluent.

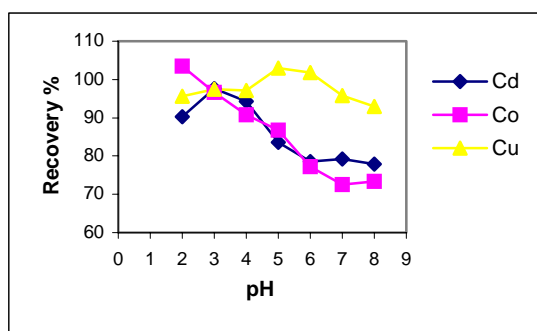


Figure 1. Influence of model solution pH value on metal recovery, using 0.1 mol dm⁻³ EDTA with pH=12 as eluent.

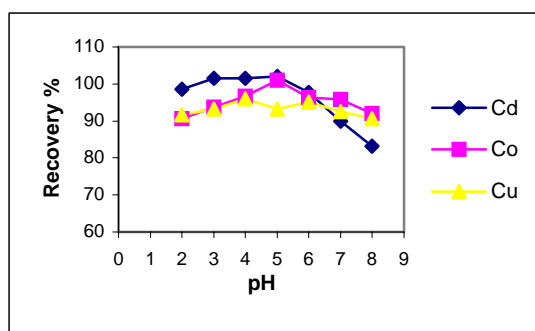


Figure 2. Influence of model solution pH value on metal recovery, using 2 mol dm⁻³ HCl as eluent.

During further investigations, the influence of hydrochloric acid concentration and pH value of EDTA applied on efficiency of elution of the studied metals was researched. The obtained results allowed to ascertain that after washing the columns (after the metals' preconcentration) with NaOH solutions having concentration of 0.01 mol dm^{-3} , 2 mol dm^{-3} hydrochloric acid would allow for an effective elution of the adsorbed metals (Figure 3). Whereas EDTA solution with concentration of 0.1 mol dm^{-3} should have $\text{pH} = 12$ (pH was fixed using sodium hydroxide solution with concentration of 0.1 mol dm^{-3}) (Figure 4).

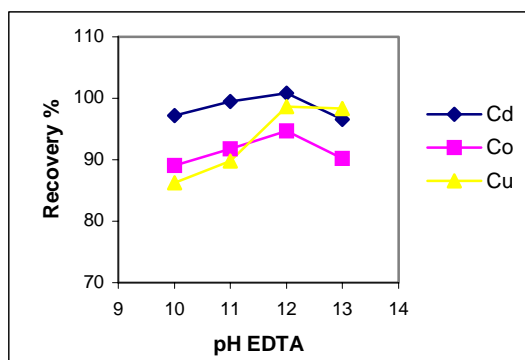


Figure 3. Influence of EDTA pH value as eluent on metal recovery.

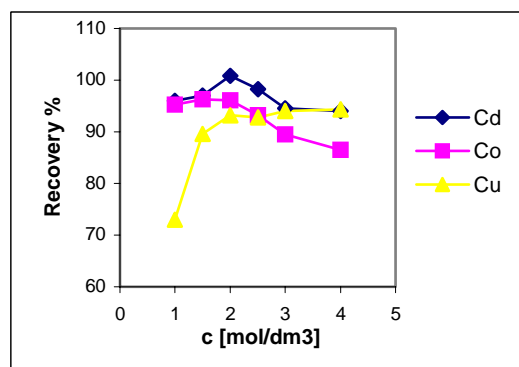


Figure 4. Influence of HCl concentration as eluent on metal recovery.

The sorption of the elements studied was examined in relation to the amounts of complexing agents (1,10-phenanthroline with concentration of 0.01 mol dm^{-3} , sodium chlorate(VII) with concentration of 0.1 mol dm^{-3}), which were varied from 1 to 3 cm^3 of the solution. Therefore, 2 cm^3 of the reagents was found to be optimum of all preconcentration purposes.

The influence of the flow rate in the range of $1.0 \div 3.0 \text{ cm}^3 \text{ min}^{-1}$ on the sorption of metals into SPE and elution were studied. The preconcentration and elution flow rate was quantitative for this range and hence the range of $1.5 \div 2.0 \text{ cm}^3 \text{ min}^{-1}$ was chosen for preconcentration and elution in the later studies.

It was found that the method may be used for determination of the metals in the concentrations from $0.016 \mu\text{g cm}^{-3}$ to $0.1 \mu\text{g cm}^{-3}$ in sample solution.

Table1. Results of determination of Cd(II), Co(II), and Cu(II) in the model solutions w by ICP-OES method, after preconcentration on C8 columns, using EDTA and HCl as eluent. 5 μg of the metals were introduced

Metal	Eluent EDTA			Eluent HCl		
	Recovery %	RSD %	$\mu_{95} = \bar{x}_{sr} \pm ts$ n=6	Recovery %	RSD %	$\mu_{95} = \bar{x}_{sr} \pm ts$ n=6
Cd	101.6	0.57	5.08 ± 0.025	100.6	1.33	5.04 ± 0.11
Co	95.2	1.07	4.76 ± 0.050	98.6	0.53	4.93 ± 0.025
Cu	98.0	1.39	4.90 ± 0.067	95.9	2.99	4.79 ± 0.13

In the Table 1., the results of group determination of Cd(II), Co(II), and Cu(II) using ICP-AES method, after separation and preconcentration on C18 columns in the form of ionic-association complexes for the model solutions. Basing on the obtained results, it was found that the developed method for preconcentration of heavy metals on octyl columns, with 1,10-phenanthroline and chlorate(VII) ions as complexing agents for the studied metals, characterized itself by good precision both when hydrochloric acid with concentration of 2.0 mol dm^{-3} , and EDTA with concentration of 0.1 mol dm^{-3} and pH=12 were used as eluents.

The limits of detection values (3s) are 8.4, 13.5 and $10.8 \text{ } \mu\text{g dm}^{-3}$ for Cd(II) Co(II) and Cu(II) respectively, and corresponding limit of quantification (6s) values are 16.8, 27.0 and $21.6 \text{ } \mu\text{g dm}^{-3}$ respectively, using EDTA with pH = 12 as eluent. Whereas, when 2 mol dm^{-3} hydrochloric acid has been used as eluent, the limits of detection values (3s) are 6.3, 19.2 and $9.9 \text{ } \mu\text{g dm}^{-3}$ for Cd(II) Co(II) and Cu(II) respectively, and corresponding limit of quantification (6s) values are 12.6, 38.4 and $19.8 \text{ } \mu\text{g dm}^{-3}$ respectively.

CONCLUSION

Basing on the obtained results one may ascertain that the examined octyl phase may be used for separation and preconcentration of Cd(II), Co(II), and Cu(II) after transforming the metals into ionic-association complex using 1,10-phenanthroline and chlorate(VII) ions. It has been also found that the adsorbed metals may be alternatively eluted using two eluents: EDTA with concentration of 0.1 mol dm^{-3} and pH=12 or hydrochloric acid with concentration of 2.0 mol dm^{-3} after earlier washing the columns with NaOH solution having concentration of 0.01 mol dm^{-3} . RSD values are in the range of $0.53 \div 3.0 \%$. The developed method may be applied successfully for separation and preconcentration of the metals studied.

References:

- [1] P. G. Krishna, K. S. Rao, V. M. Biju, T. P. Rao, G. R. K. Naidu, *Chemia Analityczna* (Warsaw, Poland), 49 (2004) 3
- [2] B. Mikuła, B. Puzio, *Ann. Polish Chem. Soc., Katowice* (2001) 239.
- [3] C.R. Lan, M.H. Yang, *Anal. Chim. Acta*, 287 (1994) 101.
- [4] M. T. P. O. Castro, N. Baccan, *Talanta*, 65 (2005) 1264
- [5] S. Saraçoğlu, L. Elçi, *Anal. Chim. Acta*, 452 (2002) 77
- [6] A. Ramesh, K.R. Mohan, K. Seshaiyah, *Talanta*, 57 (2002) 243
- [7] Z. S. Liu, S.D. Huang, *Anal. Chim. Acta*, 281 (1993) 185
- [8] Y. Yamini, A. Tamaddon, *Talanta*, 49 (1999) 119
- [9] S. Comber, *Analyst*, 118 (1993) 505
- [10] I. Narin, M. Soylak, *Talanta* 60 (2003) 215.
- [11] M.F. Molina, J.M. Bosque-Sendra, M. Nechar, R. El Bergmi, *Anal. Chim. Acta*, 389 (1999) 281
- [12] Z.S. Liu, S.D. Huang, *Anal. Chim. Acta*, 267 (1992) 31
- [13] C. Chang, Y. Ku, *Sep. Sci. Technol.*, 33 (1998) 483

APPLICATION OF GALLEIN AND BENZYLDIMETHYLDODECYLAMMONIUM BROMIDE FOR DETERMINATION OF TUNGSTEN IN MODEL SAMPLES OF STEEL

Katarzyna Pytlakowska, Wanda Winkler

Uniwersytet Śląski, Zakład Chemii Analitycznej, 40- 006 Katowice, ul. Szkolna 9

Gallein, a dye of the xanthen group, is rarely used as a spectrophotometric reagent. It could be explained by its instability in solutions of pH above 4. At pH>4 metal complexes are resolved because of the oxidation of the dye [1-3]. That is why gallein is used only for determination of small group of elements like: Bi(III), Zr(IV), In(III), Sn(IV) [4], Fe(III) [5], Th(IV) and La(III) [6], Mo(VI) [7] or W(VI) [8], which react with the dye in acid medium.

Spectrophotometric methods based on the binary complexes with gallein are low sensitive. In order to increase the sensitivity and contrast of these reactions long-chain surface active substances were introduced to the metal complex. These substances in the form of ion or non-ion cause many valuable analytical effects such as: a large increase of colour intensity, bathochromic shift of the absorption maximum of the system as well as hyperchromic effect. As three-component systems they could be useful for spectrophotometric determination.

The aim of this investigation was to study the conditions governing the formation of the tungsten (VI) chelate with gallein in the presence of benzyldimethyldodecylammonium bromide as surfactant and to apply this reaction for spectrophotometric determination of tungsten in model samples of steel.

EXPERIMENTAL

Apparatus

The absorbance was measured by using spectrophotometer V-530 (Jasco, Japan) in 1 cm cuvettes. pH measurements were performed by pH-meter CP-315 (Elmetron) with glass combined electrode.

Reagents

Tungsten (VI) solution ($1 \text{ mg}\cdot\text{mL}^{-1}$) was prepared by dissolving 0,63055 g of tungsten trioxide (WO_3) (Merck) in 6.5 mL of $2 \text{ mol}\cdot\text{L}^{-1}$ solution of sodium hydroxide. This solution was diluted with redistilled water in a volumetric flask to 500 mL. Working solutions were obtained by suitable dilution of the initial solution with redistilled water.

Gallein solution (Gal) ($1\cdot 10^{-3} \text{ mol}\cdot\text{L}^{-1}$) was obtained by dissolving 0.18215 g of gallein (Sigma - Aldrich Chemie GmbH) in methanol and dilution up to 500 mL with methanol.

Benzyldimethyldodecylammonium bromide solution (BDDA) ($1\cdot 10^{-1} \text{ mol}\cdot\text{L}^{-1}$) was obtained by dissolving 185 mL of Sterinol (Polfa) in water and dilution up to 500 mL.

EDTA, NaF, concentrated HCl, HNO_3

Glycin buffer solution pH = 1,5 [9]

Analysen-Testprobe No 95 (Deutsches Amt für Material- u. Warenprüfung der DDR Prüfdienststelle Magdeburg C1).

Procedure

Preparation of calibration graph by using of spectrophotometry

From 1 to 8 mL of $5 \mu\text{g}\cdot\text{mL}^{-1}$ solution of W (VI) was introduced into 25 mL volumetric flasks. To each sample 3 mL of $1\cdot 10^{-3} \text{ mol}\cdot\text{L}^{-1}$ solution of gallein (Gal), 3 mL of $1\cdot 10^{-1} \text{ mol}\cdot\text{L}^{-1}$ solution of BDDA and 8 mL of glycine buffer solution pH=1.5 were added. The samples were brought to the mark with redistilled water. Absorbance was measured at 589 nm, in 1 cm cells, against the reagent blank, and the calibration graph was plotted.

Preparation of model samples of steel

Analysen-Testprobe No 95 used to prepare synthetic samples of steel has the composition (in %): C-0,031, S-0,033, Mn-0,26, Cu-0,18, Si-<0,02, P-0,009, Cr-0,046, Ni-0,11.

0.25 g of Analysen-Testprobe No 95 were quantitatively transferred into 100 mL beakers. To each sample 10 μg , 25 μg , 50 μg , 100 μg , 250 μg , 500 μg or 1 mg of the standard solution of W and 20 mL of concentrate hydrochloric acid were added. Samples were heated on the electric plate at temperature 200-250 °C under cover until complete dissolution. Obtained solution was evaporated to dryness. To solid residue 20 mL of redistilled water was added and sample was heated under cover for 10 minutes. Insoluble parts were filtered off on a soft filter. pH of the filtrate was adjusted to 1.5, quantitative transferred into volumetric flask and filled up to the mark with $3\cdot 10^{-2} \text{ mol}\cdot\text{L}^{-1}$ HCl. If necessary samples were diluted in volumetric flasks before determination.

For determination of tungsten appropriate volume of solution was introduced into 25 mL volumetric flask. 1 mL of 0,5% NaF and 0.8 mL of $5\cdot 10^{-2} \text{ mol}\cdot\text{L}^{-1}$ EDTA were added and further procedure was the same as for preparation of calibration graph.

RESULTS AND DISCUSSION

Optimization of conditions of determination

Tungsten (VI) reacts with gallein (Gal) in the presence of benzyldimethyldodecylammonium bromide (BDDA) forming a coloured, water-soluble complex. The addition of BDDA into the system of tungsten - gallein in aqueous media changes location and intensity of the absorption band. The essential for analytical targets is a hyperchromic effect and a bathochromic shift ($\Delta\lambda=81 \text{ nm}$).

To establish the optimum conditions for the determination of tungsten with gallein in the presence of BDDA, the dependence of the absorbance of the pH, Gal, BDDA concentrations was examined. Complexation occurs in the slightly acidic medium with optimum pH at 1.5. In further experiments the glycine buffer pH at 1.5 was used. Experiments carried out at constant pH with different amounts of Gal showed that the minimal molar excess of Gal over W is 14. The absorbance of the complex using different amounts of BDDA showed that complete solubilization and clarity of solution is achieved when the minimal molar excess of BDDA over W is 1380. The highest absorbance was obtained when using the following order of reagents addition: W-Gal-BDDA- buffer. This order was applied for further studies. Absorbance of the ternary system is constant after 50 minute after preparing the chelate at room temperature and does not change for 1.5 hours.

Characteristic of the method

The calibration graph for determination of tungsten was obtained under the optimum conditions. The Beer's law is obeyed over W concentration range 0.2-1.6 $\mu\text{g}\cdot\text{mL}^{-1}$. Molar absorptivity at 589 nm is $\varepsilon = 3.70\cdot 10^4 \text{ L}\cdot\text{mol}^{-1}\cdot\text{cm}^{-1}$. The statistical evaluation of the method was carried out for ten determination using 10 μg of W and following results were obtained: standard deviation 0.056, confidence interval $10.07\pm 0.04 \mu\text{g W}$. Spectrophotometric characteristic of the method is shown in Table 1.

Table 1. Spectrophotometric characteristic of the proposed method

parameter	value
Molar absorptivity, ε [$\text{L}\cdot\text{mol}^{-1}\cdot\text{cm}^{-1}$]	$(3.70\pm 0.13)\cdot 10^4$
Specific absorptivity, a [$\text{mL}\cdot\text{g}^{-1}\cdot\text{cm}^{-1}$]	(0.20 ± 0.01)
Sandell's sensitivity, S [$\mu\text{g}\cdot\text{mL}^{-2}$]	$(4.98\pm 0.16)\cdot 10^{-3}$
Detection limit [$\mu\text{g}\cdot\text{mL}^{-1}$]	0.02
Limit of quantification [$\mu\text{g}\cdot\text{mL}^{-1}$]	0.04
Beer's law [$\mu\text{g}\cdot\text{mL}^{-1}$]	0.20-1.40
Regression equation: $y=a\cdot x + b$, y-absorbance, x-analyte concentration [$\mu\text{g}\cdot\text{mL}^{-1}$], intercept, b	0.0054
slope, a	0.0077
correlation coefficient, r	0.9996
RSD%, n = 10	0.56

The composition of the examined complex was established by Job's method. It was found that stoichiometry of the chelate W-Gal is 2:3 in the presence of BDDA at the optimum conditions.

Interferences

Solutions containing $0.80 \mu\text{g}\cdot\text{mL}^{-1}$ of W(VI) and varying amounts of other ions were prepared and W(VI) content was determined according to the procedure developed. Concentration of the interferent that caused a deviation in absorbance $\geq \pm 5\%$ in the estimation of W ions was considered to be causing interference. Results obtained are given in Table 2.

Table 2. Influence of foreign ions on determination of W-Gal-BDDA

weight ratio, W:X	foreign ions, X
1:1000 and below	Na^+ , K^+ , NO_3^- , SO_4^{2-} , PO_4^{3-} , F^- , NH_4^+
1:500 and below	Mg^{2+} , Ca^{2+} , Zn^{2+} , Pb^{2+} , Ni^{2+} , Co^{2+} ,
1:100 and below	CH_3COO^-
1:10 and below	Cd^{2+} , citrate, EDTA
1:1 and below	Fe^{3+} , Bi^{3+} , oxalate, tartrate
1:0,1 and below	Al^{3+} , Cr^{3+}
1:0.01 and below	Sn^{2+} , Ge^{4+} , Sb^{3+} , Mo^{6+}

The developed method was tested by determining tungsten in model samples of steel. The results of analyses were collected in Table 3.

Tablica 3. Results of tungsten determination in model samples of steel
($\lambda = 589 \text{ nm}$, $l = 1 \text{ cm}$, $n = 10$)

No sample	Content of W in synthetic sample [%]	Content of W determined spectrophotometrically [%]
1.	0,40	0,42 \pm 0,02
2.	0,20	0,19 \pm 0,03
3.	0,10	0,094 \pm 0,007
4.	0,040	0,041 \pm 0,003
5.	0,020	0,019 \pm 0,002
6.	0,010	0,010 \pm 0,002
7.	0,004	0,0039 \pm 0,0003

Application of surface-active substance creates better conditions for the determination of tungsten by means of gallein. In the presence of BDDA hyperchromic and bathochromic effect is observed. The proposed method is simple and accurate. The molar absorptivity is $\varepsilon = 3.70 \cdot 10^4 \text{ L} \cdot \text{mol}^{-1} \cdot \text{cm}^{-1}$. Beer's law is obeyed in the range of 0.20 to 1.40 $\mu\text{g W} \cdot \text{mL}^{-1}$. The detection limit of the method is 0.04 $\mu\text{g W} \cdot \text{mL}^{-1}$. The statistical evaluation of the method have shown good reproducibility.

The studies carried out prove that the elaborated method could be used for direct determination of tungsten in steel. The obtained results are satisfactory.

References:

- [1] S.T. Orłowski, P.P.Kish, Ukr. Khim. Zh., 687 (1961), 27
- [2] J. Minczewski, Z. Skorko-Trybuła, M. Krzyżanowska, Chem. Anal. (Warsaw), 20 (1975), 339
- [3] V.P. Antonovich, G.I. Ibragimov, I.M. Grekova, V.A. Nazarenko, Zh. Anal. Khim., 32 (1977), 876
- [4] A. Hulanicki, S. Głab, G. Ackermann, Pure and Appl. Chem, 55 (1983), 1137
- [5] I. Mori, Y. Fujita, K. Ikuta, Y. Nakahashi, K. Kato, K. Tamura, M. Ohji, Fresenius'Z. Anal. Chem., 334 (1989), 49
- [6] I. Mori Y. Fujita, K. Fujita, T. Tanaka, Y. Koshiyama, H. Kawabe, Chem. Pharm. Bull., 34 (1986), 4836
- [7] J. Hernandez-Mendez, B. Moreno-Cordero, L. Gutierrez-Davila, Analyst (London), 112 (1987), 1507
- [8] V.A. Nazarenko, G.I. Ibragimov, E.N. Poluektova, G.G. Shitareva, Zh. Anal. Khim., 33 (1978), 938
- [9] J. Lurie, in: Handbook of analytical chemistry; Mir Publishers: Moscow, 1975

DETERMINATION OF TUNGSTEN IN MODEL SAMPLES OF STEEL BY USING OF BROMOPYROGALLOL RED AND BENZYLDIMETHYLDODECYLAMMONIUM BROMIDE

Katarzyna Pytlakowska, Wanda Winkler

Uniwersytet Śląski, Zakład Chemii Analitycznej, 40- 006 Katowice, ul. Szkolna 9

Tungsten is a refractory metallic element used principally as an alloying agent in steel, cast iron, and super alloys to enhance harden ability, strength, toughness, wear and corrosion resistance. To achieve desired metallurgical properties, tungsten is frequently used in combination with or added to molybdenum, chromium, niobium, manganese, nickel, or other alloy metals. The versatility of tungsten in enhancing a variety of alloy properties has ensured it a significant role in contemporary industrial technology, which increasingly requires materials that are serviceable under high stress, expanded temperature ranges, and resistant highly corrosive environments.

Xanthen dyes like phenylfluorone and its derivatives [1-4], bromopyrogallol red [5-6] or gallein [7] are often used as chromogenic reagents in many spectrophotometric methods for determination of tungsten. The great progress in sensitivity of spectrophotometric methods has been done by using multicomponent systems, especially ternary and quaternary systems in which an important role play surface-active substances. The addition of surfactant to the metal complex usually leads to: increase of sensitivity of multicomponent system in comparison with dual complexes; decrease of the pH interval at which an analytically useful chelate is formed. This effect provides the increase of selectivity of the method; shorten the time required to establish equilibrium and enhance the stability of the coloured system. Bathochromic effect of the spectra position of the peak of multicomponent systems in comparison to dual complexes is also observed.

The aim of this investigation was to study the conditions governing the formation of the tungsten (VI) chelate with bromopyrogallol red in the presence of benzyldimethyldodecylammonium bromide as surfactant and to use this reaction for spectrophotometric determination of tungsten in model samples of steel.

EXPERIMENTAL

Apparatus

The absorbance was measured by using spectrophotometer V-530 (Jasco, Japan) in 1 cm cuvettes. pH measurements were performed by pH-meter CP-315 (Elmetron) with glass combined electrode.

Reagents

Tungsten (VI) solution ($1 \text{ mg}\cdot\text{mL}^{-1}$) was prepared by dissolving 0,63055 g of tungsten trioxide (WO_3) (Merck) in 6.5 mL of $2 \text{ mol}\cdot\text{L}^{-1}$ solution of sodium hydroxide. This solution was diluted with redistilled water in a volumetric flask to 500 mL. Working solutions were obtained by suitable dilution of the initial solution with redistilled water.

Bromopyrogallol red solution (BPR) ($1\cdot 10^{-3} \text{ mol}\cdot\text{L}^{-1}$) was obtained by dissolving 0,2881 g of bromopyrogallol red (Lachema, Brno) in mixed water-methanol solution (1+1) and dilution up to 500 mL with solution containing methanol and water (1+1).

Benzyltrimethylammonium bromide solution (BDDA) ($2 \cdot 10^{-1} \text{ mol} \cdot \text{L}^{-1}$) was obtained by dissolving 370 mL of Sterinol (Polfa) in redistilled water and dilution up to 500 mL.

Glycin buffer solution pH = 2.0 [8]

Analysen-Testprobe No 95 (Deutsches Amt für Material-u. Warenprüfung der DDR Prüfdienststelle Magdeburg C1)

EDTA, NaF, concentrated HCl, HNO_3

Procedure

Preparation of calibration graph by using of spectrophotometry

From 1 to 7 mL of $5 \mu\text{g} \cdot \text{mL}^{-1}$ solution of W (VI) were introduced into 25 mL volumetric flasks. To each sample 9 mL of glycin buffer solution pH=2, 0.9 mL of $1 \cdot 10^{-3} \text{ mol} \cdot \text{L}^{-1}$ solution of bromopyrogallol red (BPR) and 5 mL of $2 \cdot 10^{-1} \text{ mol} \cdot \text{L}^{-1}$ solution of BDDA were added. The samples were filled to the mark with redistilled water. Absorbance was measured at 589 nm, in 1 cm cells, against the reagent blank, and the calibration graph was plotted.

Preparation of synthetic samples

Analysen-Testprobe No 95 used to prepare synthetic samples has the composition (in %): C-0.031, S-0.033, Mn-0.26, Cu-0.18, Si-<0.02, P-0.009, Cr-0.046, Ni-0.11.

0.25 g of Analysen-Testprobe No 95 were quantitatively transferred into 100 mL bakers. To each sample 10 μg , 25 μg , 50 μg , 100 μg , 250 μg , 500 μg or 1 mg of the standard solution of W and 20 mL of concentrate hydrochloric acid were added. Samples were heated on the electric plate at temperature 200-250 °C under cover until complete dissolution. Obtained solution was evaporated to dryness. To solid residue 20 mL redistilled water was added and sample was heated under cover for 10 minutes. Insoluble parts were filtered off on a soft filter. pH of the filtrate was adjusted to 2, quantitative transferred into volumetric flask and filled up to the mark with $1 \cdot 10^{-2} \text{ mol} \cdot \text{L}^{-1}$ HCl. If necessary samples were diluted before determination.

For determination of tungsten appropriate volume of solution was introduced into 25 ml volumetric flask. 1 mL of 0,5% NaF and 0.8 mL of $5 \cdot 10^{-2} \text{ mol} \cdot \text{L}^{-1}$ EDTA were added and further procedure was the same as for preparation of calibration graph.

RESULTS AND DISCUSSION

Optimization of conditions of determination

Tungsten (VI) reacts with bromopyrogallol red (BPR) in the presence of benzyltrimethylammonium bromide (BDDA) forming a coloured, water-soluble complex. The addition of BDDA to the binary complex W-BPR creates better conditions for the determination of tungsten because of hyperchromic and bathochromic effects ($\Delta\lambda=89 \text{ nm}$).

To establish the optimum conditions for the determination of tungsten with bromopyrogallol red in the presence of BDDA, the dependence of the absorbance of the pH, BPR, BDDA concentrations was examined. Complexation occurs in the slightly acidic medium with optimum pH at 2. In further experiments the glycin buffer pH at 2 was used. Experiments carried out at constant pH with different amounts of BPR showed that the minimal molar excess of BPR over W is 4.7. The absorbance of the complex using different amounts of BDDA showed that complete solubilization and clarity of solution is achieved when the minimal molar excess of BDDA over W is 5256. The highest absorbance was obtained when using the following order of reagents

addition: W-buffer-BPR-BDDA. This order was applied for further studies. Absorbance of the ternary system is constant after 10 minute after preparing the chelate at room temperature and does not change for 1.5 hours.

Characteristic of the method

The calibration graph for determination of tungsten was obtained under the optimum conditions. The Beer's law is obeyed over W concentration range 0.2-1.4 $\mu\text{g}\cdot\text{mL}^{-1}$. Molar absorptivity at 589 nm is $\varepsilon=5.60\cdot 10^4 \text{ L}\cdot\text{mol}^{-1}\cdot\text{cm}^{-1}$. The statistical evaluation of the method was carried out for ten determination using 10 μg W and following results were obtained: standard deviation 0.070, confidence interval $10.05\pm 0.05 \mu\text{g}$ W. Spectrophotometric characteristic of the method is shown in Table 1.

Table 1. Spectrophotometric characteristic of the proposed method

parameter	value
Molar absorptivity, ε [$\text{L}\cdot\text{mol}^{-1}\cdot\text{cm}^{-1}$]	$(5.60\pm 0.28)\cdot 10^4$
Specific absorptivity, a [$\text{mL}\cdot\text{g}^{-1}\cdot\text{cm}^{-1}$]	(0.30 ± 0.01)
Sandell's sensitivity, S [$\mu\text{g}\cdot\text{mL}^{-2}$]	$(3.30\pm 0.16)\cdot 10^{-3}$
Detection limit [$\mu\text{g}\cdot\text{mL}^{-1}$]	0.02
Limit of quantification [$\mu\text{g}\cdot\text{mL}^{-1}$]	0.04
Beer's law [$\mu\text{g}\cdot\text{mL}^{-1}$]	0.20-1.40
Regression equation: $y=a\cdot x + b$, y-absorbance, x-analyte concentration [$\mu\text{g}\cdot\text{mL}^{-1}$], intercept, b	0.0166
slope, a	0.0111
correlation coefficient, r	0.9991
RSD%, n = 10	0.70

Interferences

Solutions containing $0.60 \mu\text{g}\cdot\text{mL}^{-1}$ of W(VI) and varying amounts of other ions were prepared and W(VI) content was determined according to the procedure developed. Concentration of the interferent that caused a deviation in absorbance $\geq \pm 5\%$ in the estimation of W ions was considered to be causing interference. Results obtained are given in Table 2.

Table 2. Influence of foreign ions on determination of W-BPR-BDDA

weight ratio, W:X	foreign ions, X
1:1000 and below	Na^+ , K^+ , NO_3^- , SO_4^{2-} , PO_4^{3-} , F^- , NH_4^+
1:500 and below	Mg^{2+} , Ca^{2+} , Zn^{2+} , Pb^{2+} , Ni^{2+} , Co^{2+} ,
1:100 and below	CH_3COO^-
1:10 and below	Cd^{2+} , citrate, EDTA
1:1 and below	Fe^{3+} , Bi^{3+} , oxalate, tartrate
1:0,1 and below	Al^{3+} , Cr^{3+}
1:0.01 and below	Sn^{2+} , Ge^{4+} , Sb^{3+} , Mo^{6+}

The composition of the examined complex was established by Job's method. It was found that stoichiometry of the chelate W-BPR is 2:3 in the presence of BDDA at the optimum conditions.

The developed method was tested by determining tungsten in model samples of steel. The results of analyses were collected in Table 3.

Tablica 3. Results of tungsten determination in model samples of steel
($\lambda = 589 \text{ nm}$, $l = 1 \text{ cm}$, $n = 10$)

Nr sample	Content of W in synthetic sample [%]	Content of W determined spectrophotometrically [%]
1.	0,40	0,39 ± 0,02
2.	0,20	0,21 ± 0,02
3.	0,10	0,11 ± 0,01
4.	0,040	0,041 ± 0,001
5.	0,020	0,021 ± 0,003
6.	0,010	0,011 ± 0,001
7.	0,004	0,0038 ± 0,0003

The proposed spectrophotometric method for determination of tungsten by means of bromopyrogallol red in the presence of benzyldimethyldodecylammonium bromide is simple, sensitive and accurate. The addition of BDDA to the binary complex W-BPR creates better conditions for the determination of tungsten because of hyperchromic and bathochromic effects. The molar absorptivity of the studied system W-BPR-BDDA is $\epsilon = 5.60 \cdot 10^4 \text{ L} \cdot \text{mol}^{-1} \cdot \text{cm}^{-1}$. Beer's law is obeyed in the range of 0.20 to 1.40 $\mu\text{g W} \cdot \text{mL}^{-1}$. The detection limit of the method is 0.04 $\mu\text{g W} \cdot \text{mL}^{-1}$. The statistical evaluation of the method have shown good reproducibility.

The studies carried out prove that the elaborated method could be used for direct determination of tungsten in steel. The obtained results are accurate and satisfactory.

References:

- [1] V.P. Antonovich et al., Zh. Anal. Khim., 37 (1982) 2197
- [2] V.A. Nazarenko et al., Zh. Anal. Khim., 39 (1984) 2151
- [3] V.A. Nazarenko, V.P. Antonovich, N.A. Verschikova, Talanta, 34 (1987) 215
- [4] I.F. Ivanova, L.L. Klimkovich, L.I. Ganago, Zh. Anal. Khim., 39 (1984) 1259
- [5] I.Yu. Andreeva, L.I. Lebedeva, E.A. Flotskaya, Zh. Anal. Khim., 37 (1982) 454
- [6] I.Yu. Andreeva, L.I. Lebedeva, G.L. Kavelina, Zh. Anal. Khim., 37 (1982), 2202
- [7] V.A. Nazarenko, G.I. Ibragimov, E.N. Poluektova, G.G. Shitareva, Zh. Anal. Khim., 33(1978) 938
- [8] J. Lurie, in: Handbook of analytical chemistry; Mir Publishers: Moscow, 1975

APPLICATION OF SOME BIOINDICATORS FOR STUDIES OF RADIOACTIVE AND TOXIC FALLOUT ACCUMULATION

Marek Reszka, Aneta Wołoszyn

Maria Curie-Skłodowska University, Department of Radiochemistry and Colloid Chemistry, Pl. M. C. Skłodowskiej 3, 20-031 Lublin, Poland

Due to their commonness, availability, permanent contact with environment and relatively short generation time plants seem to be excellent material for studying consequences of environment contamination. Vast variety of species enables selection of organisms particularly vulnerable to specific toxins.

For studying concentration of heavy metals and gamma radioactive isotopes in plant samples the species selected were especially liable to suffer such contaminants due to their anatomy or its nutritional way. The plant samples were collected from areas of various emission levels of toxic gas and dusts. Radionuclide and heavy metal concentrations were compared to those of surface soil samples from respective sites. Concentration of heavy metals and main gamma radioactive isotopes both natural and anthropogenic origin (post Chernobyl ^{137}Cs) were measured using AAS and gamma spectrometric methods, respectively.

Sample collection sites

The material was collected late autumn 2004 at territory of Eastern Poland in extensive forest of similar kind of species in following sites: Zemborzyce near Lublin, Obojna (Puszcza Sandomierska-Wilderness), Łomnica (Poleski National Park). These sites represent various contamination levels.

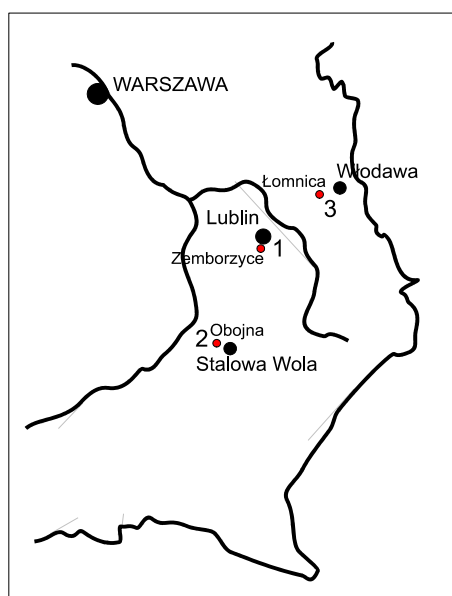


Fig.1 Location of sampling points.

Point 1 was located about 5 km from the center of a big town - Lublin. In previous years a heavy industry factories were in operation (foundry, car factory). Nowadays the only working factory that may emit contaminations to atmosphere is heat and power station „Wrotków” using hard coal. The town is surrounded by farmlands of low agriculture level;

Point 2 was located at wilderness Puszcza Sandomierska. This region is known as one of the most unpolluted in Poland but not far away (7 km) there are potentially dangerous points for environment. There is a town of Stalowa Wola with coal powered heat and power station and until 1993 sulfur strip mine worked in Tarnobrzeg, a town nearby. Surrounding farmlands are also of low level.

Point 3 was selected in borders of Poleski National Park. Due to lack of industry this region seemed to be relatively clean potentially threatened only by develop of Bogdanka coal mine located in vicinity as well as fertilizers and herbicides used in agriculture.

Collection and preparation of samples

Samples of lichens were picked up from tree trunks at height 1-2 meters. The bedding was removed and lichens were air dried in laboratory. Mosses were collected in exposed clearings and air dried after removing of leaves and soil particles. Coniferous needles were collected from young pine-trees. Surface bark of older trees was removed with knife and after cleaning from lichens was grinded and air dried. Faded leaves of various trees was collected from clearings and dried. To avoid problems with collection of mushrooms of the same type an arboreal type fungus - polyphore (*Fomes fomentarius*) was chosen.

Radioactivity measurements

Air dried material was grinded and weighted to standard 500cm³ Marinelli vessel. The concentration of gamma isotopes was measured with Silena/Canberra spectrometer equipped with HPGe detector. Identification of isotopes and calculation of their concentration was made with Genie 2000 (Canberra) software.

Results

The level of radioactivity of the most important gamma isotopes in plant and soil samples was similar to their concentration in the samples of the same type measured in previous years and is much lower than values measured soon after explosion of Chernobyl power plant [1]. In studied samples of lichens, mosses and mushrooms the concentration of ¹³⁷Cs was much higher than in other samples collected in the same sites. The highest concentration was noticed for Obojna that was in agreement with previous measurements [2].

Natural isotopes concentrations are much lower than measured for ¹³⁷Cs. Sometimes even below detection limit of the spectrometer. An exception is ²¹⁰Pb which beside ⁴⁰K and ¹³⁷Cs has greatest share in gamma radioactivity of the all samples. Such as for cesium the higher concentration of ²¹⁰Pb was observed in lichens and mosses. For these samples collected in Łomnica also the concentration of natural isotopes was relatively high. It was probably caused by intense dusting from surrounding fields.

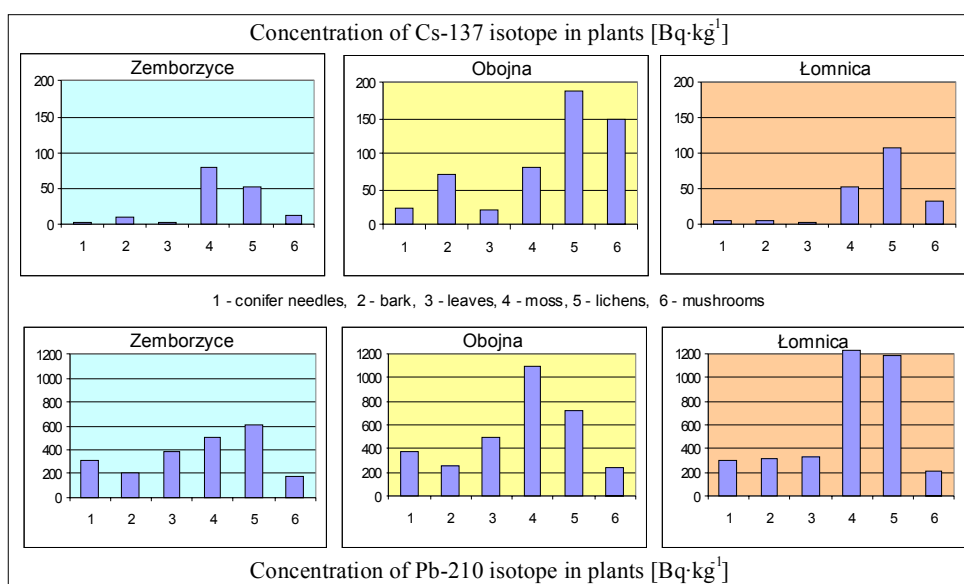


Fig 2. Concentration of main gamma isotopes in plant samples

Table 1. Concentration of main natural gamma isotopes in soil samples

Site	Zemborzyce		Obojna		Łomnica	
	Radioactivity [Bq·kg ⁻¹]	Error [Bq·kg ⁻¹]	Radioactivity [Bq·kg ⁻¹]	Error [Bq·kg ⁻¹]	Radioactivity [Bq·kg ⁻¹]	Error [Bq·kg ⁻¹]
K-40	272.08	6.31	220.38	5.62	252.20	5.82
Cs-137	0.12	0.37	3.14	0.97	6.12	0.21
Pb-210	3.72	1.41	5.44	2.04	1.41	0.53
Bi-212	0.86	0.51	6.07	0.56	9.53	0.48
Pb-212	1.68	1.08	1.10	0.93	1.65	1.07
Bi-214	1.16	0.38	1.07	0.36	1.14	0.32
Pb-214	1.13	0.98	1.04	0.90	1.12	0.91

Heavy metal concentration measurements

Concentration of some heavy metals in the samples was measured with Spectr AA880 Varian spectrometer. Considering results of similar measurements in Poland one may state that obtained values are on the level obtained for non-polluted areas. [3,4] The concentration of selected heavy metals in soils ranges considerably (20-3000 $\mu\text{g}\cdot\text{g}^{-1}$) and is much higher than in plants (from 0.2 to 1200 $\mu\text{g}\cdot\text{g}^{-1}$). The higher concentration in mushrooms results from their ability to cumulate zinc, copper, iron and manganese from soil. Slightly lower concentration of these metals may be noticed also in mosses and lichens. The lowest concentration of these elements was noticed in leaves and needles. Because similar concentration was measured in the bark samples one may state that there no emission of contaminating dusts nor compounds was in the last years.

Table 2. Concentration of main heavy metals in plant and soil samples [$\mu\text{g}\cdot\text{g}^{-1}$]

Sample	Site	Zn	Mn	Cu	Cd	Fe	Cr	Ni	Pb
conifer needles	1	43.2	0.43	2.5	0.43	453	0.7	0.4	2.2
	2	42.2	0.8	4.8	0.68	612	2.8	0.6	11.8
	3	35.1	1.36	3.4	0.21	438	1.2	0.4	10.6
bark	1	62.7	0.43	6.5	0.53	453	2.7	1.4	14.2
	2	64.3	0.8	8.8	0.66	612	3.5	1.6	18.1
	3	46.5	1.36	7.4	0.51	438	2.2	1.4	10.6
leaves	1	13.3	0.46	3.78	0.21	461.4	0.61	0.3	6.08
	2	18.2	1.14	4.65	0.3	467.8	0.48	0.5	7.07
	3	13.1	0.17	2.71	0.31	491.4	0.71	0.2	3.78
moss	1	39.6	12.5	15.8	0.36	870	0.2	0.53	14.2
	2	43.8	18.9	16.5	0.52	1151	4.9	2.11	22.7
	3	22.6	6.8	4.2	0.32	387	2.35	1.34	16.8
lichens	1	25.3	17.6	15.4	0.14	356	2.6	3.16	40.3
	2	74.7	32	22.9	0.25	740	2.9	4.43	122.3
	3	48.4	28.3	11.6	0.11	271	2.8	1.88	12.23
mushrooms	1	72.2	55.4	24.4	1.67	410	7.5	5.1	17.9
	2	124.1	78.8	67.4	2.8	1220	11.4	6.4	40.6
	3	64.4	43.2	66.2	0.94	1108	9.8	1.3	28.5
soil	1	75.2	112.4	24	22.9	2100	92.1	71.9	130.2
	2	86.4	135.6	28.3	24.8	3368	96.9	83.8	179.8
	3	63.7	11.6	23.5	22.3	1698	76.8	58.9	122.4

Conclusions

Lichens, mosses and mushrooms, accumulating in their tissues radioisotopes and heavy metals are very sensitive indicators of environment pollution. However, quantitative measurements demands consideration of many factors connected with biological diversity of these plants and climate fluctuation. Obtained data may inform of the contamination level of studied areas and warn us against hazardous situations.

References

1. J. Jagielak, M. Biernacka, D. Grabowski, J. Hensche. Zmiany sytuacji radiologicznej środowiska Polski w okresie 10 lat po awarii w Czarnobylu. Państwowa Inspekcja Ochrony Środowiska, Warszawa 1996.
2. W. Fołtynowicz. Wykorzystanie porostów do oceny powietrza. Centrum Edukacji Ekologicznej Wsi, Krosno 1995.
3. K. Grodziska i in. Ocena skażenia środowiska Polski metalami ciężkimi przy użyciu mechów jako biowskaźników. Państwowa Inspekcja Ochrony Środowiska, Warszawa 1997.
4. E. Panek. Metale śladowe w glebach i wybranych gatunkach roślin obszaru polskiej części Karpat. IGSMiE PAN, Kraków 2000.

COMPUTER MODELING OF BIOCHEMICAL PROCESSES BY POWERPOINT

Milada Roštejnská, Helena Klímová.

Charles University in Prague - Faculty of Science

Department of Teaching and Didactics of Chemistry, Albertov 3, 128 40 Praha 2

Introduction

We encounter a negative approach to the teaching of biochemistry from both students and many teachers at high schools. That leads to an effort in creating new didactic instruments, which should help in ameliorating the biochemistry classes of high schools. These didactic instruments could be educational presentations made in PowerPoint application aimed on high school teachers of chemistry. The simplification of teaching while using PowerPoint presentations consists in several aspects, as are e.g. simple manipulation with prepared presentations, possible distribution via the Internet, increased motivation of students or possibility to concretize the course of biochemical processes with the aid of animated pictures.

Software application Microsoft PowerPoint

The software application Microsoft PowerPoint is a part of the Microsoft Office package. It is an easy-to-handle tool for creation of presentations. This application enables to create eye-catching presentations with graphic, animations and multimedia.

Advantages and disadvantages of using Microsoft PowerPoint in teaching Biochemistry

Advantages:

1. *Easy availability of the PowerPoint software*
PowerPoint software is a part of the Microsoft Office package.
2. *Easy creation of presentations:*
The PowerPoint application is easy-to-handle and enables creating time scanty presentations.
3. *Inserting notes:*
The teacher can insert own didactical notes in the presentations.
4. *Easy handling with prepared presentations:*
The prepared presentations can be taken from one computer to another.
5. *Distribution via the Internet:*
The presentations can be saved on Internet pages and can be easily distributed e.g. via e-mails
6. *Enhancing motivation of students for teaching biochemistry:*
The presentations enable insertion of interesting biochemical pictures, video and sound or creating animations which dynamics should attract the viewers and make the teaching process more efficient.
7. *Explanation and the possibility to concretize the course of biochemical processes using animated pictures:*
The presentations make understanding the subject matter easier.

Disadvantages:

1. *The Microsoft PowerPoint versions are not unified:*

Not all computers have installed the same version of Microsoft Office. When transferring a presentation from one computer to another there can occur unwanted changes in the presentation (e.g. some animation need not be functional, there can be changes in writing or colors etc.)

2. *School equipment:*

Some schools need not have available a classroom with a dataprojector

3. *Students can be overdosed with information:*

Teachers can want to use inadequate number of pictures during a lesson with the explanation that the students will have the presentations at home available and will be able to have a look at them one more time. The teacher should choose adequate number of pictures and not overload his/her students with excessive and mostly irrelevant information

4. *Possibility of using excessive information:*

Excessive use of animations routes attention of students away from the subject mater. Students cannot be concentrated sufficiently on the subject mater.

PowerPoint presentations for teaching biochemistry

In 2004 we started to develop on-line courses in the Moodle environment. Moodle (*Modular Object-Oriented Dynamic Learning Environment*) is a software pack designed for creation of educational systems and electronical courses on the Internet.

The courses are called: „Education in biochemistry I - Metabolism“ and „Education in biochemistry II - The Cell and Nucleic Acids“. These two on-line courses were created for teaching biochemistry at the Faculty of Science, Charles University in Prague.

First course is focused on teaching metabolical processes in human body. It is divided into twelve parts and includes six explanatory presentations (Digestion, General Metabolism, Metabolism of Proteins, Metabolism of Sugars, Metabolism of Lipids, Citric Acid Cycle and The Electron Transport Chain), two presentations with biochemical tests (Biochemical Tests 1-Digestion, Biochemical Tests 2-Metabolism) and three multiple-choice tests.

The second course is focused on knowledge concerning the cell and nucleic acids. The course is divided into eleven parts and includes six explanatory presentations (The Cell, Nucleic Acids, The Chromosome, Replication, Transcription, Translation) and five presentations for verification of student's knowledge (The Cell-Test, Biochemical Tests 3-Nucleic Acids and The Chromosome, Biochemical Tests 4-Replication, Biochemical Tests 5-Transcription, Biochemical Test 6-Translation).

Both courses are designated for students of Teaching of Chemistry at the Faculty of Science, Charles University in Prague and for further education of teachers.

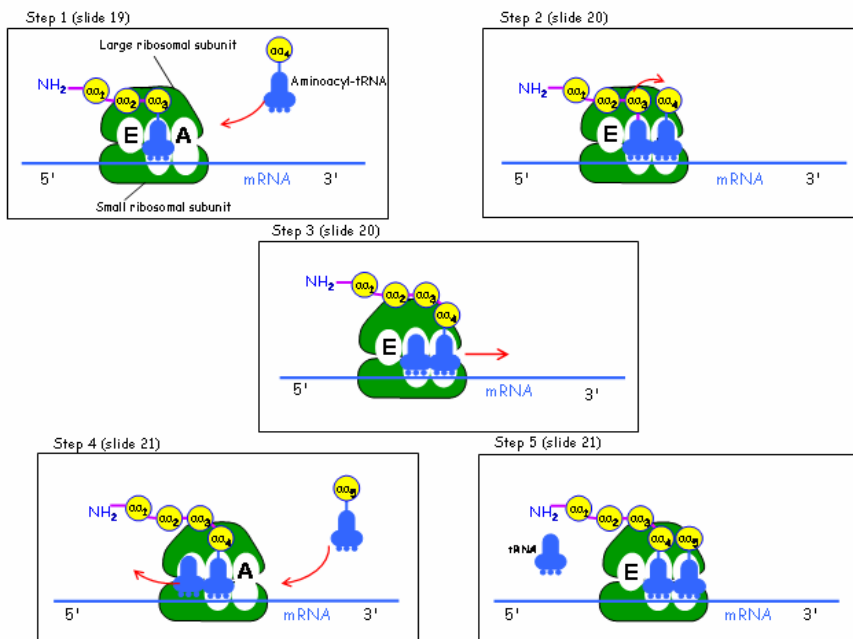
These presentations contain a number of animations, which should help students to master important biochemical notions, reactions, cycles etc. The principle lies in the use of fistful of appealing pictures and schemes, which should absorb students and raise the efficiency of the teching process with their dynamism.

In the process of creation PowerPoint presentations I drew from variety of biochemical and biological books [1, 2, 3, 4, 7, 8, 9, 12, 13, 14, 17, 18, 19, 20, 22, 24, 27], high-school textbooks [6, 11, 15, 16, 23, 26] and encyclopedies [5, 25].

The Cell – Test and Biochemical tests 1-6 are also created in the form of PowerPoint presentations. In the construction of tests we came from the content of the explanatory presentations and used literature [10, 21]. We can find following types of

test elements in the tests: assignment tasks, tasks with the choice of response (only one response is correct, tasks with the choice of response (possibly more correct answers) and tasks with brief answer.

Figure 1: Elongation of Translation (from presentation „Translation“)



In the figure 1 there are represented animated steps of three slides (19-21) illustrating the elongation of translation.

In the first step is the aminoacyl-tRNA bound to the ribosome in the A site. The second step is peptide bond formation between the A site amino acid and the growing peptide chain. The third step involves translocation. The ribosome is moved along the mRNA. The uncharged P site tRNA is released from the ribosome and the tRNA bearing the growing peptide chain moves into the P site (step 4). The next aminoacyl-tRNA is bound to the ribosome in the A site (step 5).

In multiple-choice tests (test A, B and C) is always composed of 10 or 11 test elements. In majority of cases these are tasks with the choice of response, in which student chooses from two or three alternatives, where only one alternative is correct.

Summary

Using PowerPoint presentations offers a variety of compelling opportunities, which could lead to better efficiency of the biochemistry teaching at high schools. These presentations could be an interesting tool for teachers, who could use them during explanation of new subject matter or in repeating the subject matter already explained.

Both educational courses mentioned above are currently available at the Internet address <http://dl.cuni.cz/> under the category „Chemické“. Courses are designated for students of Teaching of Chemistry at the Faculty of Science, Charles University in Prague and for further education of teachers.

Literature

1. B. Alberts a kol., *Základy buněčné biologie*, Espero Publishing, Ústí nad Labem 1997.
2. S. Alters, *Biology – Understanding Life*, Mosby-Year Book, Inc. St. Luis, 1996.
3. E. Baldwin, *Co je biochemie*, Orbis, Praha 1968.
4. M. Bloomfield, *Chemistry and the Living Organism*, John Wiley & Sons, Inc., Canada 1992.
5. D. Burnie, *Stručná encyklopedie lidského těla (The Consise Encyklopedia of the Human Body)*. Talentum, 1996.
6. N. Cibis, H. J. Dobler, V. Lauer, R. Meyer, E. Schmale, H. Strecker, *Člověk*, Scientia, Praha 1996.
7. P. Dostál, Z. Řeháček, V. Ducháč, *Kapitoly z obecné biologie*, SPN, Praha 1994.
8. S. L. Engel-Arieli, *Jak pracuje lidské tělo*, UNIS, Brno 1995.
9. K. M. Van De Graaf, S. I. Fox, *Concepts of human anatomy & physiology (fifth edition)*, The McGraw-Hill Companies, 1999.
10. J. Gunnell, E. Jenkins: *Structured Questions in “A” Level Chemistry*, Oliver and Boyd. Edinburgh 1973.
11. H. Hančová, M. Vlková, *Biologie I v kostce*, Fragment, Havlíčkův Brod 1999.
12. J. R. Holum, *Elements of General and Biological Chemistry*, John Wiley & Sons, Inc., 1975.
13. P. Karlson, *Základy biochemie*, Academia, Praha 1981.
14. P. Karlson, W. Gerok, W. Gross, *Pathobiochemie*, Academia, Praha 1987.
15. K. Kolář, M. Kodíček, J. Pospíšil, *Chemie II (organická a biochemie) pro gymnázia*, SPN, Praha 1997.
16. B. Kotlík, K. Růžičková, *Chemie II. V kostce*, Fragment, Havlíčkův Brod 1997.
17. V. Kubišta, *Buněčné základy životních dějů*, Scientia, Praha 1998.
18. B. Löwe, *Biochemie*, C.C. Buchners Verlag, Bamberg 1989.
19. T. McKee, J. R. McKee, *Biochemistry: An Introduction (Second Edition)*, The McGraw-Hill Companies, United States of America 1999.
20. O. Nečas a kol. *Obecná biologie pro lékařské fakulty*, Nakladatelství H&H, Jinočany 2000.
21. M. M. L. Oblitas, *Certificate Chemistry: Multiple Choice Questions*, Heinemann Educational Books, London 1976.
22. J. Pacák, *Jak porozumět organické chemii*, Karolinum, Praha 1997.
23. P. Pokorný, D. Hlásná, *Chemie 3 – Biochemie pro 2. ročník středních průmyslových škol chemických, potravinářských a střední školy pro pracující*, SNTL, Praha 1983.
24. D. Sofrová, M. Tichá a kol., *Biochemie – základní kurz*, skripta UK, Praha 1993.
25. C. Stockleyová, Ch. Oxlade, J. Wertheimová, *Velká ilustrovaná encyklopedie*, Fragment, Havlíčkův Brod 1997.
26. J. Vacík, J. Barthová, J. Pacák, B. Strauch, M. Svobodová, F. Zemánek, *Přehled středoškolské chemie*, SPN, Praha 1995.
27. D. Voe, J. G. Voetová, *Biochemie*. Victoria Publishing, Praha 1995.

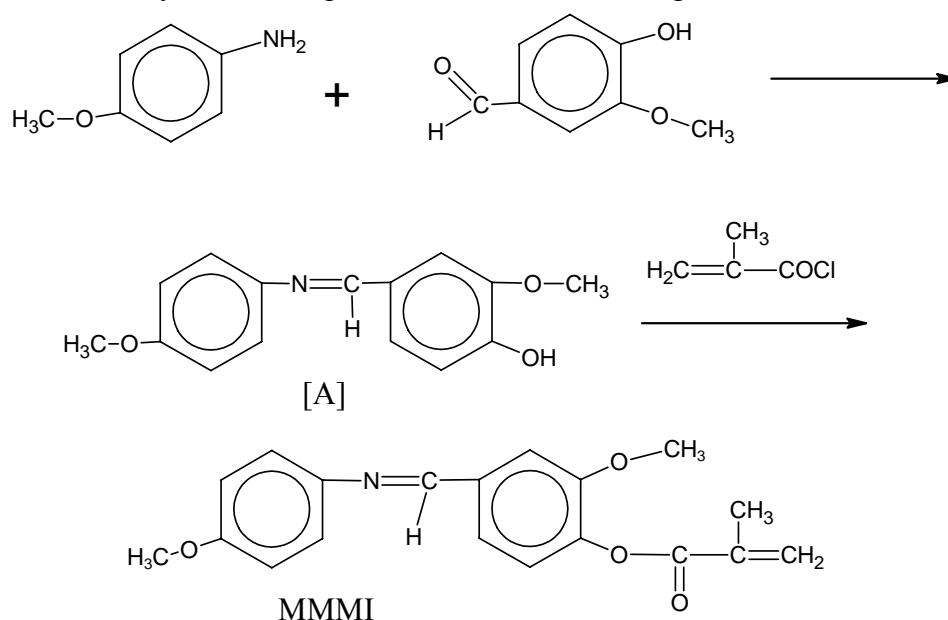
SYNTHESIS OF 4-METHOXYPHENYL-3-METHOXY-4-METHACRYLOYLPHENYLIMINE AND ITS APPLICATION FOR POLYMERIZATION

Wiesław Rudź and Władysław Charmas

Department of Organic Chemistry and Technology, Maria Curie-Skłodowska University, 20-614 Lublin, Gliniana 33

The aim of this work was to prepare a new stereoregular [1] vinyl monomer. The title compound appeared only once in chemical literature but the authors did not obtain it in the pure state and did not determine its structure and properties. In this work this compound was obtained in a pure form and then used for preparation of a polymer containing the mesogenic group attached to the backbone chain.

The synthesis of 4-methoxyphenyl-3-methoxy-4-methacryloylphenylimine (MMMI) can be described by the two-step reaction shown in the diagram



Schiff's base [A] was obtained by 4h refluxing of methanol solution of 30.42g vaniline and 24.64g(0.2mol) p-anisidine. The precipitated sediment of Schiff's base [A] was filtered and crystallized with methanol. The yield of [A] was 39g (75.5%), the melting point 132-134° C. The second step of MMMI synthesis was the reaction of 6.46g (0.025mol) of [A] with 3.14g (0.03mol) newly obtained methacryloyl chloride. Methacryloyl chloride was added dropwise to the acetone solution of [A] at 0°C for 1h. The crude product was crystallized from methanol. Its melting point was 68.5-69.5°C measured using Boëtius apparatus while the result from the DSC analysis is 73.8 ° C. (The yield 43%).

MMMI was characterized by:

a) elemental analysis (Perkin-Elmer CHN-2400)

Its results are as follows; C calculated 70.14%, found 70.35%; H calc. 5.89%, found 5.82%; N calc. 4.31%, found 4.35%

b) IR analysis (Perkin-Elmer-1725)

In the IR spectrum the bands are as follows: 2973-2840 cm^{-1} C-H of CH_3 , 2841 cm^{-1} C-H of CH_2 , 1737 cm^{-1} C=O of alkene, 1630 cm^{-1} C=N of imine, 1240 cm^{-1} C-O of ester and 1130 cm^{-1} O-C of $-\text{OCH}_3$, 1626 cm^{-1} ; 1604 cm^{-1} and 1452 cm^{-1} C=C in aromatic ring

c) $^1\text{H-NMR}$ analysis (Brucker-300)

The spectrum shows the following signals: 8.4 (1H of $\text{CH}=\text{N}$), 7.1-7.7ppm (7 aromatic protons), 5.8 and 6.4 ppm (2H of vinyl group), 3.9ppm (6H of OCH_3) and 2.1ppm (3H of CH_3).

d) $^{13}\text{C-NMR}$ (Brucker-300MHz)

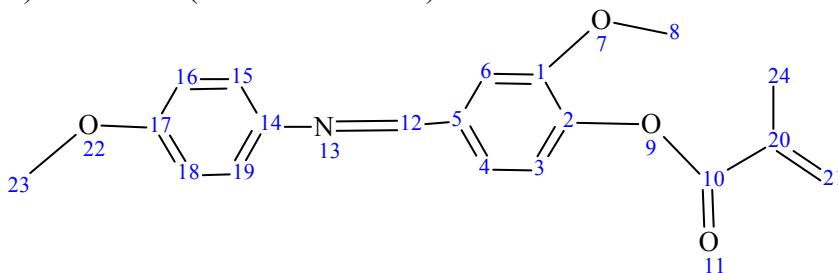


Table 1. Results of $^{13}\text{C-NMR}$ analysis

Chemical shift ppm	No of carbon	Group	Chemical shift ppm	No of carbon	Group
18.4	24	C aliphatic- CH_3	142.4	2	ring- ester group
55.4	8	O- CH_3 ring B	144.7	14	C-N=CH
56.0	23	O- CH_3 ring A	151.8	1	Ring B- OCH_3
110.5	6	CH ring B	157.8	17	Ring A- OCH_3
114.4	16; 18	CH ring A	158.3	12	N=CH
122.2	3	CH ring A	165.1	10	C=O
123.0	4	CH ring B	122.8	15; 19	CH ring A
127.5	21	= CH_2	135.5	20	C(CH_3)= CH_2
135.4	5	Ring- $\text{CH}=\text{N}$			

The results of these analyses confirmed the structure of MIMI. As follows from the studies of MIMI solubility at 25 °C (calculated to 1g of MIMI/ x ml of solvent), it is well soluble in methanol, (1g/3ml) ethanol (1g/5ml) and acetone (1g/2ml), poorly in hexane (1g/20ml), cyclohexane (1g/15ml) and toluene (1g/11). MIMI is insoluble in water. Thermal properties of MIMI were studied by means of differential scanning calorimeter (NETZSCH DSC200). The DSC plot of MIMI shows that the melting point occurs below 74.3°C. This is the point of the minimum of the endothermic signal. During the second heating in the range from 0°C to 300°C, no changes were observed. Using the polarization microscope, the existence of mesophase in the narrow range of temperatures 68°C-74 °C was observed.

The next stage of this work was the free radical polymerization. Polymerization of MIMI solutions in the closed ampoules was carried out at 65°C in the presence of AIBN as an initiator. At first the influence of the solvent kind on the yield and the reduced viscosity of polymers was investigated. The four solvents: tetrahydrofuran (THF), N,N-dimethylacetamide (DMAc), ethyl methyl ketone (EMK) and N,N-dimethylformamide (DMF) were used for polymerization. The polymerization

conditions were as follows: volume of solvent 5cm³, quantity of monomer 1.22g (0.00375mol), and quantity of AIBN 0.0164g (100ppm), time of reaction 1440min. The obtained results are shown in Table 2.

Table 2. Influence of solvent kind on the yield and reduced viscosity of polymers

Sample	Kind of solvent	Quantity of solvent	Yield [%]	Reduced viscosity[dL/g]
1HMB	THF	5	84	0.131
2HMB	DMF	5	92	0.191
3HMB	DMAc	5	89	0.245
4HMB	EMK	5	90	insoluble

From the data in Table 2 one can see that the best results were achieved when DMAc was used. In the case of EMK the insoluble product was obtained. That is why reduced viscosity was not measured. In the next experiments, the two solvents DMAc and EMK were chosen. Then the influence of polymerization time on the yield and reduced viscosity was determined. The results are summarized in Table 3.

Table 3 Influence of reaction time on the yield and reduced viscosity of polymers

Sample	Time of reaction [min]	Kind of solvent	Quantity of solvent [cm ³]	Yield [%]	Reduced viscosity [dL/g]
3HMB	1440	DMAc	5	89	0.245
4HMB	1440	EMK	5	90	insoluble
7HMB	720	DMAc	5	91	0.214
6HMB	720	EMK	5	84	0.198
8HMB	360	DMAc	5	87	0.239
5HMB	360	EMK	5	72	0.156

Taking into consideration the data in Table 3, DMAc was used in further investigations. The influence of quantity of DMAc on the yield and reduced viscosity of polymers was determined. Polymerization was carried out till significant density increase of ampoules content was achieved. The results are shown in Table 4

Table 4. Influence of DMAc quantity on the yield and reduced viscosity of polymers

Sample	Quantity of DMAc [cm ³]	Polymerization time [min]	Yield [%]	Reduced viscosity [dL/g]
9HMB	10	360	87	0.182
8HMB	5	360	87	0.239
12HMB	3.75	240	81	0.330
11HMB	3.75	120	86	0.301
10HMB	2.5	120	90	0.406
13HMB	1.5	105	69	0.681

From the data presented in Table 4, one can see that the decrease of quantity of solvent results in an increase of reduced viscosity. It means that macromolecular weight also increases but the yield changes insignificantly. The polymerization time was shortened because the product was almost gelled. Prolonged time of polymerization led to gelation. In the next step the influence of AIBN quantity on polymerization was studied. The data of these polymerizations are presented in Table 5

Table 5. Influence of AIBN quantity on the yield and reduced viscosity of polymers

Sample	Quantity of AIBN [ppm]	Reaction time [min]	Quantity of solvent [cm ³]	Yield [%]	Reduced viscosity [dL/g]
14HMB	50	120	2.5	51	0.490
10HMB	100	120	2.5	88	0.406
15HMB	200	120	2.5	91	0.282
16HMB	225	90	4.5	77	0.950

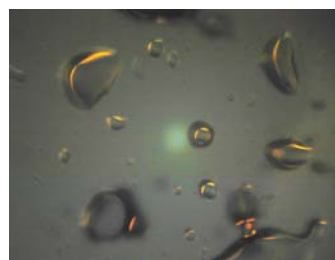
From these data one can see that 50ppm of AIBN are the most effective if the reduced viscosity is taken into consideration but the yield is distinctly lower than in the case of using 100ppm of AIBN. For this reason in the case of 16HMB sample, the quantity of AIBN was 75ppm per 0.00375 mol of MMMI. Polymerization of 3 times as large portion of polymer was carried out under the following conditions: 3.66g (0.01125 mol) of MMMI, 4.5 cm³ DMAc, 225ppm of AIBN, the reaction time 90 min, the temperature 65°C. For the 16HMB polymer sample (Table 5) solubility was examined. Chloroform (1g/16ml), DMF (1g/24ml EMK 1g/28ml and THF (1g/36ml), acetone (1g/55ml) are poor solvents, the sample is insoluble in benzene, toluene, xylene, ethanol and methanol.

The results of its elemental analysis are as follows: C calculated 70.19%, found 69.62%; H calc.5.84%, found 5.66%; N calc.4.30%, found 3.98%.

The ¹H-NMR spectrum of 16HMB shows the signals at 2.3 and 2.7ppm which confirms the presence of protons of -CH₂- group. The spectrum did not show the signals at 5.8 and 6.4 ppm characteristic of vinyl group protons. Thermal properties of 16HMB sample were tested by the use of DSC and derivatograph (Paulik-Erdey MOM) instruments. During the DSC measurements the 16HMB sample was heated to 250°C, cooled to 20°C and then heated again to 450°C. The first heating curve shows glass transition at 110 and 140° C, on the second heating curve there are two endothermic signals at 256 and 270°C and a large one at 342°C. The last signal refers to the destruction point but in the range from 256 to 270°C there is probably a mesophase which was confirmed by the polarization microscope observation.



MMMI



16HMB

Almost regular circles with yellow orange banks can be observed under microscope at a temperature about 262°C Their regular shape and the fact that monomer is stereoregular indicate that this polymer can form disc (cholesterol mesophase)

References:

- [1] Kazuo Sugijama, Tadeo Nakaya; Makromol. Chem. **178** (1977) 271-275

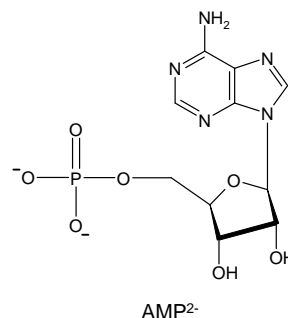
POLYAZACYCLOPHANE DERIVATIVES AS THE AMP NUCLEOTIDE RECEPTORS

Piotr Seliger, Grzegorz Andrijewski

*University of Łódź, Faculty of Physics and Chemistry,
Department of General and Inorganic Chemistry,
90-136 Łódź, Narutowicza 68, Poland*

Introduction

According to the fact that the large number of substances engaged in biological processes are anions, the increasing interest in the research of anions as well as the processes of their complexation, has been noticed [1, 2]. Among the anions which play important role in biological processes, especially in energy storage and transfer in living organisms, there is nucleotide adenosino-5'-monophosphate AMP.



One of the groups of compounds that is considered as the receptors of this kind of species are cyclophane derivatives. Polyazacyclophanes are versatile ligands able to complex either inorganic or organic molecules or ions [3]. The presence of nitrogen donor atoms provides a place to bind or interact with metal cations, but on the other hand when we have protonated form of the ligands they are able to interact strongly with anions.

The main goal of our investigation was to check the ability of the binding of AMP anion by the chosen receptors and the influence of the cavity size and the different side arms of the ligands on the stability constants of the formed complexes. The investigated ligands - polyazacyclophane derivatives with pyridine unit incorporated in macrocyclic ring possessed different size of the macrocyclic cavity as well as the different side arm attached to the ring. The phenyl substituents were chosen to check the possibility of additional binding of the investigated anion through the π - π interaction between phenyl ring and the aromatic moiety of the nucleotide.

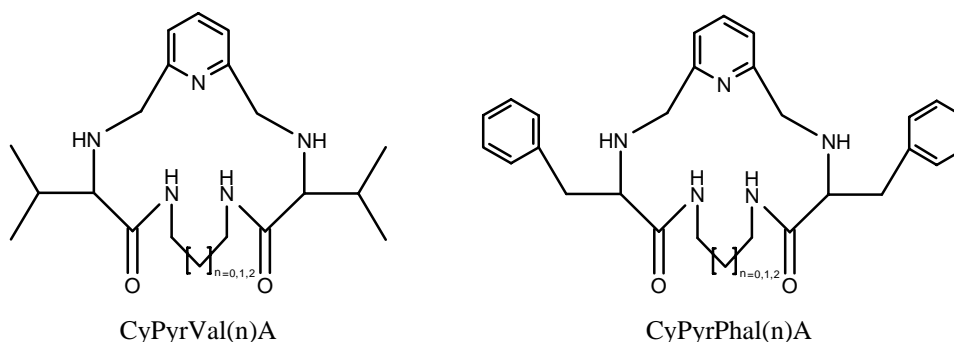


Fig.1. The investigated receptors

Experimental

Materials

Synthesis of receptors CyPyrVal(n)A and CyPyrPhal(n)A has been accomplished as previously described [4]. All compounds were purified and characterised by elemental analysis and spectroscopic measurements

The sodium salt of AMP was from Aldrich with purity greater than 98% and was used without further purification.

NaCl, used as supporting electrolyte was a POCh Gliwice product of analytical grade.

EMF measurements

The measuring equipment consists of automatic burette controlled by the computer, magnetic stirrer and potentiometric cell. The acquisition of the experimental data was used by computer program that was dedicated to the automatic burette.

The potentiometric titration were carried out at $298 \pm 1\text{K}$ in $\text{NaCl } 0.15 \text{ mol}\cdot\text{dm}^{-3}$

The glass electrode in water solutions was calibrated as a hydrogen-ion concentration probe by titration of previously standardised amounts of HCl with NaOH solution and determining the equivalent point by the Gran's method [5]

In methanol-water mixture ($x=0.1$) the glass electrode was modified - by using the saturated solution of NaCl in methanol-water mixture ($x=0.1$) in the reference electrode compartment. The electrode was calibrated similarly as in water.

The concentrations of the anion as well as investigated receptors ranged from 1×10^{-3} to $5 \times 10^{-3} \text{ mol}\cdot\text{dm}^{-3}$.

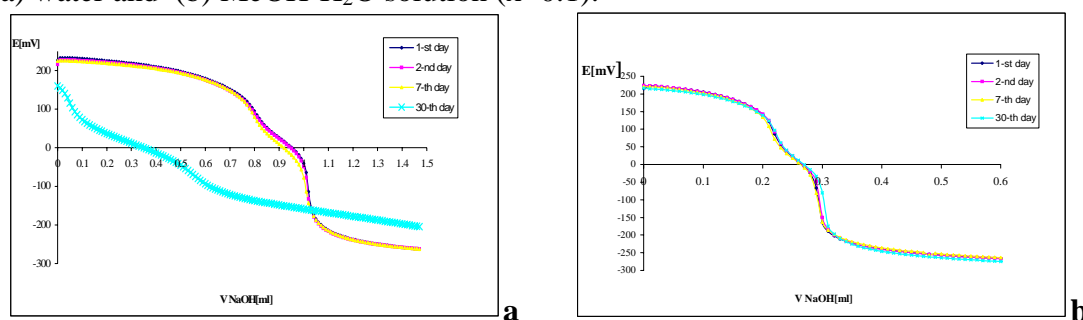
Three titration curves were done (at least 100 experimental points) for each of the investigated systems

To calculate the protonation as well as stability constants the computer program HYPERQUAD was used [6].

Results and discussion

Due to the relative low stability of the AMP nucleotide in water solutions we decided to use methanol to stabilise the system. As can be noticed (Fig.2) the small addition of methanol to the investigated mixture stabilise the nucleotide - giving the similar results even after period of one month.

Fig.2. Titration curves of protonated form of AMP^{2-} at 298 K in $0.15 \text{ mol}\cdot\text{dm}^{-3}$ NaCl in (a) water and (b) MeOH- H_2O solution ($x=0.1$).



The protonation constants of the AMP nucleotide were determined in water and in methanol-water mixture ($x=0.1$) - the calculated values are presented in table 1.

Table 1. The calculated protonation constant of AMP at 298 K in $0.15 \text{ mol}\cdot\text{dm}^{-3}$ NaCl in water and MeOH- H_2O solution ($x=0.1$).

solvent	$\log K_1$	$\log K_2$
H_2O	6.39 ± 0.01	3.96 ± 0.02
MeOH- H_2O ($x=0.1$)	6.93 ± 0.01	4.10 ± 0.01

As could be predicted, the first as well as the second protonation constant of the nucleotide AMP in MeOH-H₂O mixture are higher than in water, what is the typical trend observed after changing the solvent from water to methanol-water systems [7].

To check the ability of AMP nucleotide binding by cyclophane derivatives the protonation constants of the ligand were determined. The calculated values of the protonation constants determined at 298 K in 0.15 mol·dm⁻³ NaCl in MeOH-H₂O solution (x=0.1) are presented in table 2.

Table 2. The protonation constants of the investigated polyazacyclophane derivatives complexes determined at 298 K in 0.15 mol·dm ⁻³ NaCl in MeOH-H ₂ O solution (x=0.1)		log K ₁	log K ₂
		CyPyrVal2A	6.34±0.02
	CyPyrVal3A	6.49±0.01	5.37±0.01
	CyPyrVal4A	6.45±0.01	5.13±0.02
	CyPyrPhal2A	5.84±0.02	4.41±0.02
	CyPyrPhal3A	6.07±0.01	5.05±0.02
	CyPyrPhal4A	5.96±0.01	4.65±0.02

As can be seen from table 2 first and the second protonation constant are lower for the ligands that possess phenyl rings attached to the macrocyclic ring. Electron acceptor character of these substituents makes the withdrawal of the electrons from macrocyclic ring through inductive effect. Due to the spacer (-CH₂- group) this effect isn't strong, so the observed differences between the protonation constants values are not very large. Very interesting is the fact that in case of the both groups of macrocycles the highest values of protonation constants possess the ones that has three methylene groups between amide nitrogen atoms.

In table 3 there are cumulative formation constants for the interaction of macrocycles (L) with the nucleotide AMP determined in 0.15 mol·dm⁻³ NaCl in MeOH-H₂O solution (x=0.1).

Table 3. The cumulative stability constants of AMP-L complexes determined at 298 K in 0.15 mol·dm⁻³ NaCl in MeOH-H₂O solution (x=0.1) (A=AMP²⁻)

	CyPyr Val2A	CyPyr Val3A	CyPyr Val4A	CyPyr Phal2A	CyPyr Phal3A	CyPyr Phal4A
L + A ⇌ LA ^a	3,88	3,95	3,93	3,01	3,66	3,63
L + H + A ⇌ HLA	10.68	10.89	10.87	9.92	10.42	10.37
L + 2H + A ⇌ H ₂ LA	16.62	17.08	17.01	15.71	16.30	16.15
L + 3H + A ⇌ H ₃ LA	22.06	22.53	22.26	20.87	21.47	21.15

^a charges omitted for clarity,

the standard deviations for the calculated constants do not exceed the 0.03 value

As can be seen from table 3, there is a trend to form more stable complexes of AMP nucleotide with ligands without phenyl rings attached to the macrocycle (predominant higher values of cumulative stability constants for CyPyrVal(n)A derivatives). Such results suggest that there is no additional stabilisation by participation of phenyl substituents in π -stacking interaction with adenine moiety.

In table 4 there are representative stability constants for all investigated systems L-AMP.

Table 4. Representative stability constants for the systems L-AMP (where A=AMP²⁻, L=macrocycle) determined at 298 K in 0.15 mol·dm⁻³ NaCl

	CyPyr Val2A	CyPyr Val3A	CyPyr Val4A	CyPyr Phal2A	CyPyr Phal3A	CyPyr Phal4A
L + A ⇌ LA ^a	3,88	3,95	3,93	3,01	3,66	3,63
HL + A ⇌ HLA	4,34	4,40	4,42	4,08	4,35	4,41
HL + HA ⇌ H ₂ LA	3,39	3,66	3,63	2,94	3,30	3,26
H ₂ L + A ⇌ H ₂ LA	5,00	5,22	5,43	5,46	5,18	5,54
H ₂ L + HA ⇌ H ₃ LA	3,47	3,74	3,75	3,69	3,42	3,61
HL + H ₂ A ⇌ H ₃ LA	4,69	5,01	4,78	4,00	4,37	4,16

^a charges omitted for clarity

From the analysis of the representative stability constants we can noticed that the highest value is observed for the equilibrium in which the double protonated ligand binds unprotonated nucleotide anion AMP²⁻. In case of this equilibrium there are not significant differences between the ligands with different substituents. This fact, as well as that predominant trend in forming more stable complexes with CyPyrVal(n)A derivatives suggest that there isn't any additional binding of the investigated anion through π -stacking interaction.

Conclusions

The methanol-water mixture (x=0.1) due to the stabilisation of the AMP anion and the repeatability of the measurements, in contrast with the water solution, seems to be a good medium for conducting the experiments with this nucleotide

Comparing the stability constants values versus the size of the macrocyclic ring we couldn't observed any significant diversification, what makes us draw the conclusion that in case of the investigated ligands, such small differences between the macrocyclic cavity sizes do not have any influence on the AMP²⁻ binding. The introduction of the phenyl ring as the side arm doesn't show the expected additional binding by the π - π stacking interactions.

References

- ¹ A.Bianchi, K.Bowman-James, E. Garcia-Espana, eds., *Supramolecular Chemistry of Anions*, Wiley-VCH, New York, 1997
- ² J.M.Llinares, D.Powell, K.Bowman-James, *Coord.Chem.Rev.*, 240 (2003),57
- ³ (a)M. T. Albelda, J. C. Frias, E. Garcia-Espana and S. V. Luis, *Org. Biomol. Chem.*, 4 (2004), 816;
(b) M. I. Burguete, B. Escuder, J.C. Frias, E. Garcia-Espana, S.V.Luis, J.F.Miravet, *J. Org. Chem.*, 63 (1998), 1810;
(c) M.A. Bernardo, F. Pina, E. Garcia-Espana, J. Latorre, S.V. Luis, J.M. Llinares, J.A. Ramirez and C.Soriano, *Inorg. Chem.*, 37 (1998), 3935;
(d) C. Bazzicalupi, A. Bencini, A. Bianchi, V. Fusi, C. Giorgi, P. Paoletti and B. Valtancoli, *J. Chem. Soc., Dalton Trans.*, (1997), 3535;
- ⁴ I. Alfonso, .I. Burguete, S.V. Luis, J.F. Miravet, P. Seliger, E. Tomal, *Org. Biomol. Chem.*, 4 (2006), 853–859
- ⁵ (a) G.Gran, *Analyst* 77 (1952) 881, (b) F.J.Rossotti, H.Rossotti, *J. Chem. Educ.* 42 (1965) 375
- ⁶ P.Gans, A.Sabatini, A.Vacca *Talanta*, 43 (1996), 1739
- ⁷ M. Rose's, F. Rived, E. Bosch, *J. Chrom. A*, 867 (2000), 45–56

APPLICATION OF AOP TO UTYLIZATION OF MTBE IN SALINITY WASTEWATER

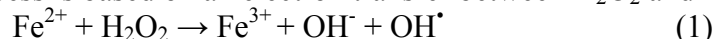
Ewa Maria Siedlecka, Anna Januszewska, Piotr Glamowski

*Department of Environmental Engineering, Faculty of Chemistry, University of Gdańsk,
ul. Sobieskiego 18, 80-952 Gdańsk*

INTRODUCTION

There is a growing concern about the problem of waste elimination. Among the various types of methods which can be used for treating waste water, oxidation processes seem to be very attractive. Advanced oxidation processes (AOP) are based on the generation the hydroxyl radicals $\text{OH}\cdot$ to initiate oxidation. Frequently, the main aim of the AOP's when applied to biorecalcitrant compounds is often not mineralize the compounds but rather to convert them to byproducts which are readily biodegradable in conventional biological treatment system.

Fenton oxidative system belongs to the group of homogenous AOPs, involving a mixture of ferrous ion and H_2O_2 that generates hydroxyl radicals at room temperature [1]. The process is based on an electron transfer between H_2O_2 and Fe^{2+} :



It is the major advantage of Fenton process that highly complicated instrumentation or pressurized systems are not required and reagent components are safe to handle.

MTBE is a compound that is used in relatively large amounts as gasoline additive. As a results of this frequency of its detection in ground water has increased, and it has also become one of the leading environmental contaminants. Studies published concerning the presence of MTBE in environmental water report concentration levels that can change considerably from environmental background levels (in the low $\mu\text{g}/\text{l}$ range) to sites affected by point sources (high mg/l levels). For example average MTBE concentration of 8,8 mg/l was measured at marines and areas used intensively for recreational boating [2,3]. One treatment approach is the use of free radical based processes. Several applications of advanced oxidation processes (AOPs) have reported promising results [4,5]. $\text{Fe}^{2+}/\text{H}_2\text{O}_2$ system as well as $\text{Fe}^{3+}/\text{H}_2\text{O}_2$ system were used for the treatment of petroleum-contaminated in soil and groundwater [6].

However, contaminated waters usually contain not only MTBE, but also substantial concentrations of inorganic anions (chloride, phosphate, carbonate, sulfate, nitrate). Chloride ion concentration in saline wastewater can vary from 0,1 to 100 mM. In this study the effect of chlorides on the degradation of MTBE using $\text{Fe}^{2+}/\text{H}_2\text{O}_2$ and $\text{Fe}^{3+}/\text{H}_2\text{O}_2$ systems were examined.

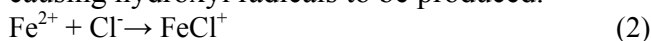
MATERIALS AND METHODS

Oxidation of MTBE has been conducted in dilute aqueous solution of MTBE (5×10^{-4} M). The initial concentration of hydrogen peroxide was 7.5×10^{-3} M and ferric (or ferrous) ions was 1×10^{-3} M. Chloride concentrations were adjusted to 0.05, 0.1, and 1 M with NaCl and $\text{pH}=2,8$.

Experiments were conducted in a well stirred and thermostated batch reactor at $25 \pm 1^\circ\text{C}$. Reactions were carried out in darkness. The reaction was started by the addition of H_2O_2 . During the experiment, samples were collected after various reaction times and immediately quenched with $0,01\text{M Na}_2\text{S}_2\text{O}_3$. MTBE was analyzed directly on a gas chromatograph (Perkin Elmer Clarus 500). Hydrogen peroxide was determined iodometrically ($[\text{H}_2\text{O}_2] > 10^{-3}\text{M}$) or spectrophotometrically using TiCl_4 method ($[\text{H}_2\text{O}_2] < 10^{-3}\text{M}$) [7]. UV/Visible spectra of Fe(III) and Fe(II) solutions have been measured with a UV-VIS Perkin Elmer Lambda 18 under various experimental conditions at $\text{pH}=2,8$.

RESULTS AND DISCUSSION

The presence of chloride ions in salinity wastewater can inhibit Fenton's reaction through complexation or radical scavenging [8,9]. Chloride ions may undergo a complex reaction with ferrous and ferric ions, which impedes the Fenton reaction, causing hydroxyl radicals to be produced.



The data presented in Figure 1 demonstrated the UV-VIS absorption spectra of Fe(II) and Fe(III) solutions in the absence and in the presence of chloride.

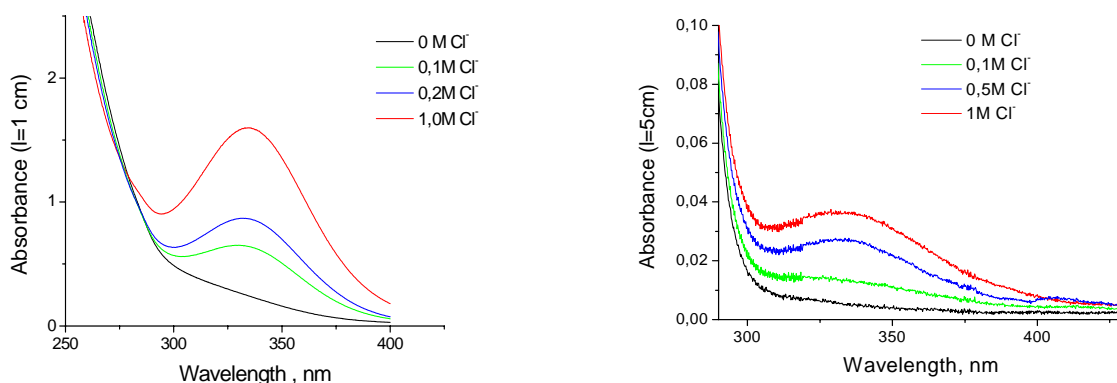


Figure 1. Absorption spectra of Fe(III) a) and Fe (II) b) solutions in the absence and in the presence of different concentrations of chloride.

(Experimental conditions: $\text{Fe(II)}_0 = \text{Fe(III)}_0 = 1 \times 10^{-3}\text{M}$, $\text{pH}=2,8$, $T=25 \pm 1^\circ\text{C}$)

The addition of increasing concentration of NaCl ($0-1\text{M}$) to solution of Fe^{3+} as well as to solution of Fe^{2+} ($[\text{Fe}^{3+}] = [\text{Fe}^{2+}] = 1\text{mM}$, $\text{pH}=2,8$) leads to increase of the absorbance within $300-400\text{nm}$ (fig.1a,b) wavelength range. The increased of the absorbance in this region with increasing chloride concentration reflects the formation of chlorocomplexes: FeCl^{2+} and FeCl_2^+ for Fe(III) or FeCl^+ for Fe(II). Distribution curve of ferrous and ferric species in Figure 2 show that iron(III)-chlorocomplexes (FeCl^{2+} , FeCl_2^+) represent the predominant Fe(III) species at $[\text{Cl}^-] > 0,125\text{M}$. In the same conditions the concentration of iron(II)-chlorocomplexes (FeCl^+) is lower than concentration of Fe^{2+} .

The chlorocomplexes of Fe^{2+} have the same reactivity as the free ferrous ions for the overall reaction with H_2O_2 [8].

As it can be seen at Figure 3, the effect of decomposition of H_2O_2 by Fe(III) species decreased significantly when the chloride ions concentration increased in range 0,01M-0,1M. It indicated that in contrast to ferrous complexes, the ferric complexes with chloride ions cannot react with hydrogen peroxide to produce hydroxyl radicals as effectively as their free ions.

A comparison was made between MTBE degradation by $\text{Fe}^{2+}/\text{H}_2\text{O}_2$ and MTBE degradation by $\text{Fe}^{3+}/\text{H}_2\text{O}_2$ (Figure 4). The rate of MTBE degradation in the absence and in the presence of chloride by $\text{Fe}^{2+}/\text{H}_2\text{O}_2$ was faster than MTBE degradation by $\text{Fe}^{3+}/\text{H}_2\text{O}_2$. However, the effectiveness of MTBE degradation in both systems was similar. In the absence of chloride ions, after 90 min of reaction the degradation of MTBE was 97%-98%. In the presence of 0.05 – 0.1M of chloride ions, the effectiveness of MTBE degradation was 85-87%. With a 1M concentration of chloride ions the decomposition of MTBE after 90 min. of reaction dropped to 68% and 59% respectively for $\text{Fe}^{2+}/\text{H}_2\text{O}_2$ and $\text{Fe}^{3+}/\text{H}_2\text{O}_2$ system.

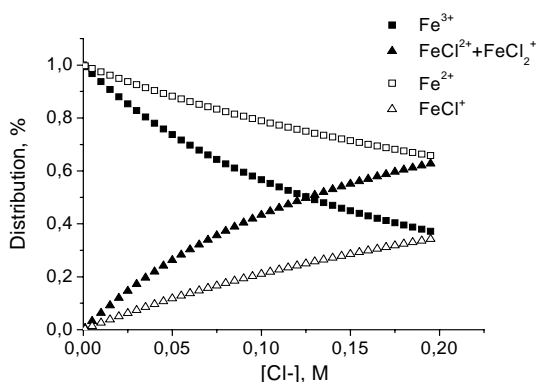


Figure 2. Distribution of Fe(II) and Fe(III) species as a function of the concentration of chloride (computed simulation).

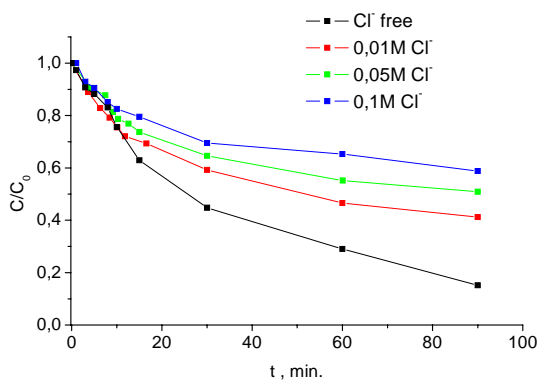


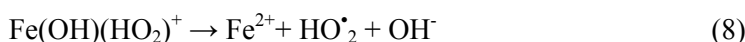
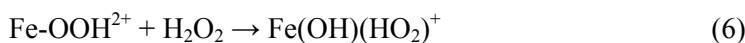
Figure 3. Decomposition of H_2O_2 by Fe (III).

Experimental conditions: $[\text{Fe}^{2+}]_0 = 1 \times 10^{-3} \text{M}$ or $[\text{Fe}^{3+}]_0 = 1 \times 10^{-3} \text{M}$, $[\text{H}_2\text{O}_2] = 7,5 \times 10^{-3} \text{M}$, $\text{pH} = 2,8$, $T = 25 \pm 1^\circ\text{C}$, $I = 0,1$.

The experimental results obtained in the present study demonstrated that the decrease the efficiency of oxidation of MTBE in both $\text{Fe}^{2+}/\text{H}_2\text{O}_2$ and $\text{Fe}^{3+}/\text{H}_2\text{O}_2$

process in presence of chloride ions are attributed to the formation of iron(III)-chlorocomplexes.

The Fenton process consists of two phases: the $\text{Fe}^{2+}/\text{H}_2\text{O}_2$ and $\text{Fe}^{3+}/\text{H}_2\text{O}_2$ stages. In our experiments, where $[\text{H}_2\text{O}_2] > [\text{Fe}^{2+}]$, the first phase of the $\text{Fe}^{2+}/\text{H}_2\text{O}_2$ process was likely to be predominant ($\text{Fe}^{3+}/\text{H}_2\text{O}_2$), since Fe^{2+} is rapidly oxidized. In $\text{Fe}^{3+}/\text{H}_2\text{O}_2$ stage (according to Fig.1. and Fig 2.), it was found that most ferric ions formed chlorocomplexes reducing the rate of ferric ions to reproducing ferrous ions as shown in reaction 5-8.



Therefore, at this stage, the oxidation rate of MTBE decreased as the chloride ion concentration increased.

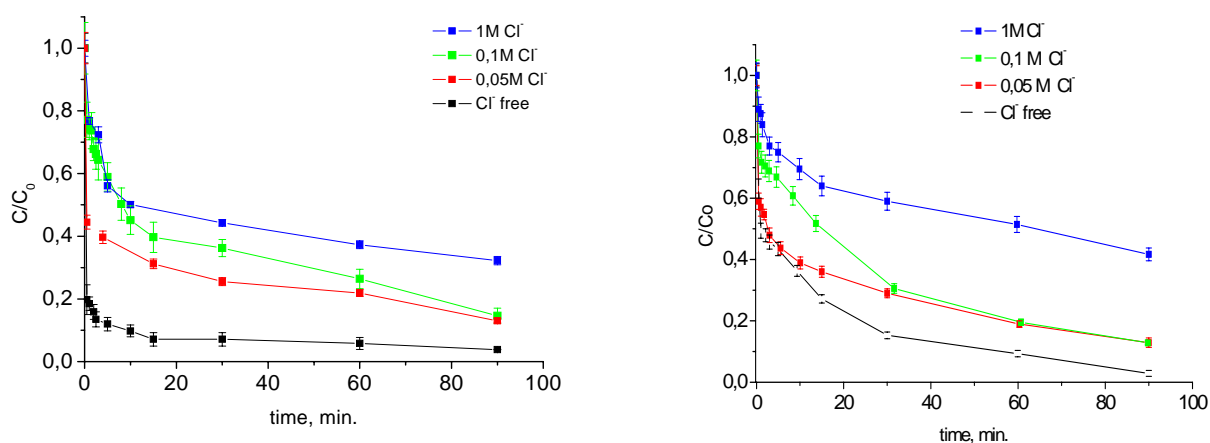


Figure 4. Influence of the concentration of chloride on MTBE degradation by $\text{Fe}^{2+}/\text{H}_2\text{O}_2$ - a) or $\text{Fe}^{3+}/\text{H}_2\text{O}_2$ -b)

Experimental conditions: $[\text{MTBE}] = 1 \times 10^{-3} \text{ mol/l}$, $[\text{Fe}^{2+}]_0 = 1 \times 10^{-3} \text{ mol/l}$, $[\text{Fe}^{3+}]_0 = 1 \times 10^{-3} \text{ mol/l}$, $[\text{H}_2\text{O}_2] = 7,5 \times 10^{-3} \text{ mol/l}$, $\text{pH} = 2,8$, $T = 25 \pm 1^\circ\text{C}$.

In $\text{Fe}^{3+}/\text{H}_2\text{O}_2$ process the formation of iron(III)-chlorocomplexes lead to a decreased of the rate of MTBE oxidation because the generation of Fe(II) was inhibited. It caused that in presence of chloride hydroxyl radicals were produced in lower concentration (in reaction 1) and the inhibition effect was more significant than for $\text{Fe}^{2+}/\text{H}_2\text{O}_2$ system.

The formation and the reactivity of $\text{Cl}_2^{\bullet-}$ have a role in the inhibition of rate of MTBE degradation too. Therefore the mechanism of decomposition of H_2O_2 and organic matter in Fenton process is very complicated in presence of chloride.

Acknowledgements

Financial support was provided by the Polish Ministry of Education and Research under grants: DS 8270-4-0093-6 and BW 8000-5-0192-4. The authors want to extend thanks to Małgorzata Pietrzak to take part in experimental works.

REFERENCES

- [1] I. Casero, D. Sicilia, S. Rubio, D. Perez-Bendito, *Wat. Res.*, 31 (1997) 1985.
- [2] M. Mezcuca, A. Aquera, M.D. Hernando, L. Piedra, A.R. Fernandez-Alba, *Journal of Chromatography A* 999 (2003) 81-90,
- [3] J.M. Davidson, D.N. Creek, *Environmental Forensics* (2000) 1, 31-36
- [4] J. Jacobs, C. Guertin, Herron, *MTBE: Effects on Soil and Groundwater Resource*,
- [5] P.J. Squillance, J.S. Zagorski, W.G. Wilber, C.V. Price, *Environ. Sci. Technol.* 30 (1996) 1721 Lewis Publishers; Boca Raton, 2001.
- [6] R.J. Watts, D.R. Haller, A.P. Jonem, A.L. Teel. *Journal of Hazardous Materials B76* (2000) 73-89
- [7] G.M. Eisenberg, *Ind. and Eng. Chem.* 15 (1943) 327
- [8] G.L. Truong, J. De Laat, B. Legube, *Water Res.* 38 (2004) 2383
- [9] E.M. Siedlecka, P. Stepnowski, A. Więckowska, in: J. Hupka, R. Aranowski (Eds.), *Proceedings of 4th International Conference „Oils and Environment”*, Gdansk University of Technology, Gdansk, 2005, 384

EFFECT OF SULFATE IONS ON THE OXIDATION OF MTBE BY FENTON'S REAGENT

Ewa Maria Siedlecka, Anna Januszewska, Piotr Glamowski

*Department of Environmental Engineering, Faculty of Chemistry, University of Gdańsk,
ul. Sobieskiego 18, 80-952 Gdańsk*

INTRODUCTION

$\text{Fe}^{2+}/\text{H}_2\text{O}_2$, commonly known as Fenton's reagent, and $\text{Fe}^{3+}/\text{H}_2\text{O}_2$ can be used to oxidize organic pollutants present in industrial wastewater. The mechanisms and kinetics of the decomposition of H_2O_2 by $\text{Fe}(\text{II})$ and $\text{Fe}(\text{III})$ in homogenous aqueous solution have been the subject of numerous studies [1,2]. Depending on the nature of the ligands, pH and solvents, different reactive species are supposed to be formed: free and bound hydroxyl radicals, iron complexes. Kinetic model assumes the formation of hydroxyl radicals by the reaction of H_2O_2 with ferrous ions (reaction 1 in Fig. 1) and the regeneration of ferrous ion from $\text{Fe}(\text{III})$ -hydroperoxo complexes (reaction 2 and 3 in Figure 1).

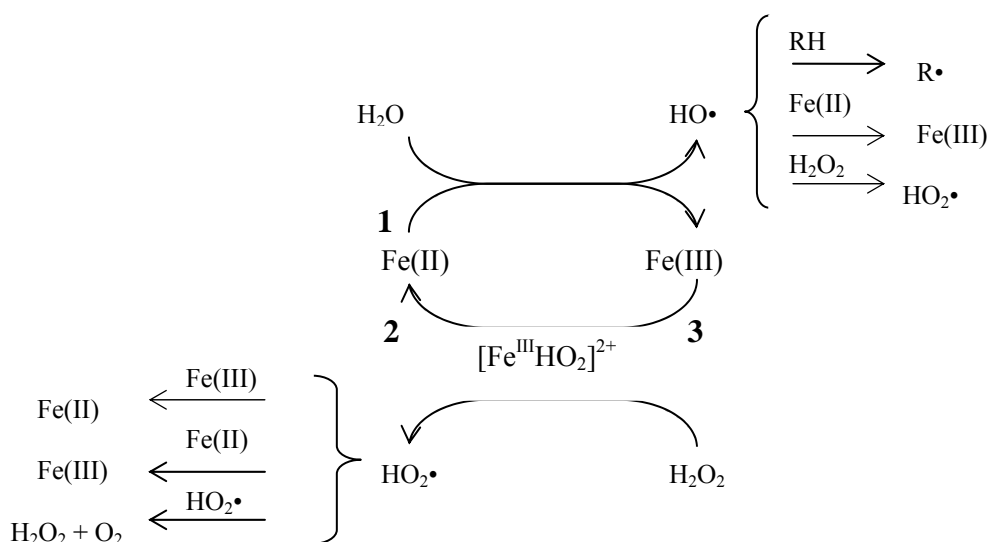
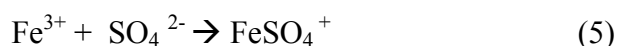
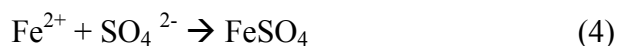


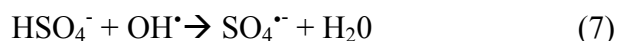
Figure 1. Simplified reaction scheme for Fenton's reaction at acidic pH [3].

Recently most of the studies concerning the oxidation of organic pollutants by Fenton's reaction are carried out in the presence of inorganic anions [4,5,6]. They may be present in the solution to be treated or introduced in the solution with a reactants. Inorganic anions may have a significant effect on the overall reaction rates. Sulfate ions was found to decrease the rates of oxidation of chloro- and nitro-phenols, direct dyes, methyl t-butyl ether (MTBE) [5,6,7]. The possible effects of sulfate ions are complexation reactions with ferric and ferrous ions (reaction 4-6)





and scavenging of hydroxyl radicals (reactions 7).



Recently, we undertook a preliminary examination of the effect of selected inorganic anions on the effectiveness of the Fenton advanced oxidative treatment ($\text{Fe}^{2+}/\text{H}_2\text{O}_2$) of waters contaminated with methyl t-butyl ether [4,7]. With respect to chloride, inhibition of oxidation was clearly in evidence, whereas the addition of sulfates rates to a much lesser extent. The present study was undertaken in order to compare the influence of sulfate anions on the degradation rates of MTBE in $\text{Fe}^{2+}/\text{H}_2\text{O}_2$ and $\text{Fe}^{3+}/\text{H}_2\text{O}_2$ systems.

MATERIALS AND METHODS

The initial concentration of MTBE was 5×10^{-4} M, that of hydrogen peroxide was 7.5×10^{-3} M. Sulfate concentrations were adjusted to 3.3×10^{-2} M and 6.6×10^{-2} M with Na_2SO_4 . The reactions were carried out in a batch reactor ($V=0.25$ L). The oxidation experiments were performed in darkness at $25 \pm 1^\circ\text{C}$. Reaction mixtures were obtained by taking the appropriate aliquot of MTBE stock solution, adding Fe^{2+} (or Fe^{3+}), and adjusting the pH with perchloric acid to $\text{pH} = 2.8$. The reaction was started by the addition of H_2O_2 . During the experiment, samples were collected after various reaction times and immediately quenched with $20 \mu\text{l}$ of 0.01 N $\text{Na}_2\text{S}_2\text{O}_3$. The degradation of MTBE was stopped after 90 min.

Hydrogen peroxide was determined iodometrically ($[\text{H}_2\text{O}_2] > 10^{-3}$ M) or spectrophotometrically using TiCl_4 method ($[\text{H}_2\text{O}_2] < 10^{-3}$ M) [8]. MTBE were analyzed directly on a gas chromatograph (Perkin Elmer Clarus 500) coupled to a flame ionization detector (FID) (Perkin Elmer Elite Series PE).

RESULTS AND DISCUSSION

Fig.2 illustrates the effect of sulfate ions on the degradation of MTBE in the $\text{Fe}^{2+}/\text{H}_2\text{O}_2$ and $\text{Fe}^{3+}/\text{H}_2\text{O}_2$ systems in excess hydrogen peroxide ($[\text{Fe}]:[\text{H}_2\text{O}_2]=1:7,5$). As can be seen from Figure 2 the presence of sulfate ions in system influences this process in different way. In the case of $\text{Fe}^{3+}/\text{H}_2\text{O}_2$ system used, distinctive inhibition of oxidation can be seen, whereas addition of sulfates to $\text{Fe}^{2+}/\text{H}_2\text{O}_2$ system influence these rates to much smaller extend. Effectiveness of degradation change significantly too. In presence of 6.6×10^{-3} M SO_4^{2-} after 90 min. of reaction MTBE is degraded down to 3% of the initial concentration in $\text{Fe}^{2+}/\text{H}_2\text{O}_2$ system whereas in $\text{Fe}^{3+}/\text{H}_2\text{O}_2$ to 46% of the initial concentration.

As previously observed Pignatello [2], the presence of sulfate ions drastically decreased the rate of decomposition of H_2O_2 by $\text{Fe}(\text{III})$. As shown in the data in Figure 3, under our experimental conditions ($[\text{Fe}^{3+}]=1 \times 10^{-3}$ M, $\text{pH}=2,8$, $I=0,2$) concentration of sulfate 6.6×10^{-3} M can lead to a 10 times reduction of kinetic constant (k_{obs}).

Absorption spectra of $\text{Fe}(\text{III})$ solutions have been measured in order to show the effect of sulfate concentration on the speciation of $\text{Fe}(\text{III})$ (Fig 4). The addition of sulfate to solution of $\text{Fe}(\text{III})$ in concentration 1×10^{-3} M leads to an increase of absorbance band close to 304 nm (Fig.3) This is attributed to the formation of iron(III)

sulfatocomplexes: FeSO_4^+ and $\text{Fe}(\text{SO}_4)_2^-$. The sulfatocomplexes of Fe^{2+} (FeSO_4) have the higher reactivity as the free ferrous ions for the overall reaction with H_2O_2 [9,10].

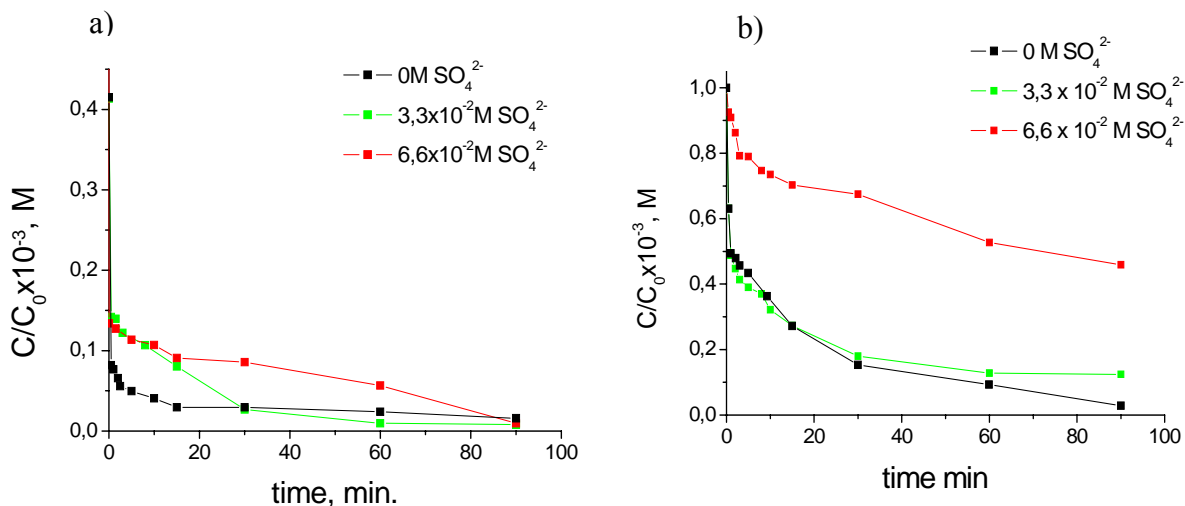


Figure 2. Influence of the concentration of sulfate on MTBE degradation by $\text{Fe}^{2+}/\text{H}_2\text{O}_2$ - A) or $\text{Fe}^{3+}/\text{H}_2\text{O}_2$ -B)

Experimental conditions: $[\text{MTBE}] = 1 \times 10^{-3}$ mol/l, $[\text{Fe}^{2+}]_0 = 1 \times 10^{-3}$ mol/l, $[\text{Fe}^{3+}]_0 = 1 \times 10^{-3}$ mol/l, $[\text{H}_2\text{O}_2] = 7.5 \times 10^{-3}$ mol/l, pH=2,8, $T = 25 \pm 1^\circ\text{C}$.

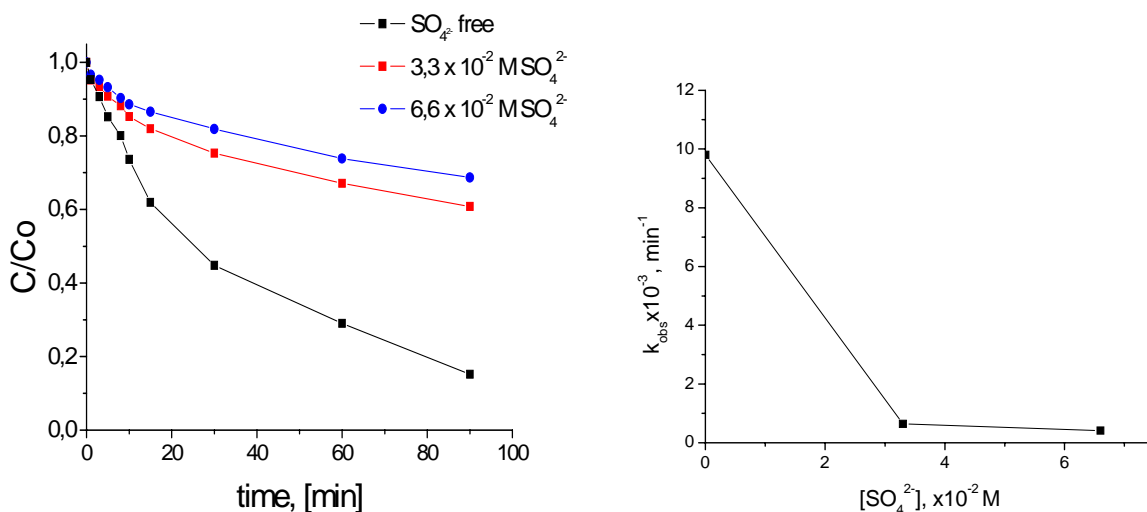


Figure 3. Decomposition of H_2O_2 by $\text{Fe}(\text{III})$ and first-order rate constant in the presence of sulfate. (Experimental condition: $[\text{Fe}^{3+}]_0 = 1 \times 10^{-3}$ mol/l, pH=2,8).

Therefore, under the conditions used in the present study, the extend and rate of mineralization of MTBE was dependent on formation of $\text{Fe}(\text{III})$ -sulfatocomplexes. Based on the discussion above $\text{Fe}(\text{III})$ -sulfocomplexes in contrast to $\text{Fe}(\text{II})$ -sulfocomplexes

inhibit the generation of hydroxyl radicals because they are non or less reactive than free ferric ions to decomposition of H_2O_2 .

The Fenton reaction under conditions of excess peroxide, may be predominantly the Fe^{3+}/H_2O_2 process, since Fe^{2+} is rapidly oxidized. However, as shown in Fig. 3a, in Fe^{2+}/H_2O_2 system the concentration of hydroxyl radicals were enough to mineralization of MTBE in 97% independent on concentration of sulfate in solution. Substituting Fe^{2+} for Fe^{3+} (Fig.3b) caused significant decreased of rate and effectiveness of MTBE decomposition. This indicates that sulfates retards the reaction by complexation of Fe^{3+} at initial stage, when the ferrous ions is generated from ferric ions. Sulfates ions create competition between hydrogen peroxide and ferric ions leading to the inhibition of hydroxyl radicals generation.

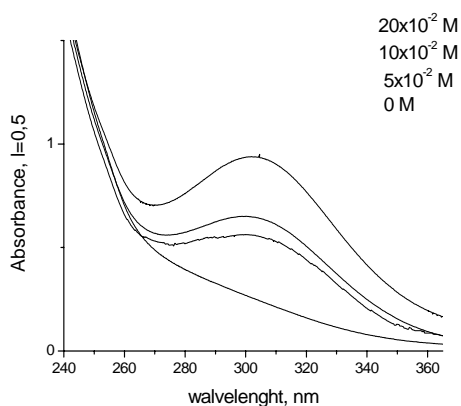


Figure4. Absorption spectra of Fe(III) solution in the absence and in the presence of different concentration of sulfate (Experimental conditions: $Fe(III)_0=1 \times 10^{-3}$, $pH=2,8$, $T = 25 \pm 1^\circ C$).

Acknowledgements

Financial support was provided by the Polish Ministry of Education and Research under grants: DS 8270-4-0093-6 and BW 8000-5-0192-4. The authors want to extend thanks to Joanna Piotrowska to take part in experimental works.

REFERENCES

- [1] M.I. Kremer, J.Phys.Chem.A.(2003),107,1734
- [2] J. Pignatello, L. Di, P. Huston, Environ.Sci.Technol (1999) 33, 1832
- [3] De Laat J. Le G.T. Legube B, Chemosphere (2004) 55, 715
- [4] E.Siedlecka, P. Stepnowski, Separation and Purification Technology (2006) 52,317
- [5] E. Lipczyńska-Kochany, G. Sprah, S.Harms, Chemosphere (1995) 30, 9
- [6] J. Kiwi , A. Lopez, V. Nadtochenko, Environ.Sci.Technol. (2000) 34, 2162
- [7] E.M. Siedlecka, P. Stepnowski, A. Więckowska, in: J.Hupka, R. Aranowski (Eds.), Proceedings of 4th International Conference „Oils and Environment”, Gdansk University of Technology, Gdansk, 2005, 384
- [8] G.M. Eisenberg, Ind. and Eng. Chem. 15 (1943) 327
- [9] G.L. Truong, J. De Laat, B. Legube, Water Res. 38 (2004) 2383
- [10] De Laat J., Le G.T., Environ.Sci.Technol, 39 (2005) 1811

ELECTRO-OXIDATION OF METHYLATED NAPHTHALENES

Roman Edmund Sioda, Jan Dąbrowski, Grzegorz Męcza and Magdalena Kwak

*Department of Analytical Chemistry and Electrochemistry, Institute of Chemistry,
University of Podlasie, ul.3 Maja 54, 08-110 Siedlce, Poland; e-mail:
romsioda@ap.siedlce.pl*

Alkylated benzenes were oxidized by oxidants, like e.g. thallium tris-(trifluoroacetate) [1-3]. The primary products obtained were radical cations, which reacted further to form dehydrodimers. A similar mechanism was postulated for oxidations of alkylated naphthalenes. Radical cationic species ArH^+ , dimers $(\text{ArH})_2^+$ and dehydrodimers $(\text{Ar-Ar})^+$ were detected in CH_2Cl_2 at -60°C using ESR [4-7]. It is plausible that a radical cation is attracted to a neutral aromatic hydrocarbon molecule, behaving as a soft base. The charge of two radical cations is transferred to two protons in formation of a dehydrodimer. Such dehydrodimers were the main stable products, although of unspecified yields and selectivities [1-7].

Anodic oxidations require solvents, which dissociate conductive salts and dissolve non-polar substrates, like aromatic hydrocarbons. Earlier, we employed a mixture of water and *dipolar aprotic solvent* acetone [8]. In presence of water it was difficult, to observe radical cations, because water, a hard base and a *nucleophile*, reacted with the radical cations [9].

The techniques for investigating electro-oxidations are cyclic voltammetry (CV) and a preparative electrolysis [4, 8-13]. The peak potentials, E_p , determined by CV are a measure of an energy required to promote the reaction at the electrode. E_p may be correlated with the calculated energy of the *highest occupied molecular orbital* (HOMO), i.e. this orbital from which an electron is removed in oxidations.

The purpose of the present paper is to show how similar calculations may help to interpret results obtained by electro-oxidations of naphthalene derivatives.

Experimental

CV was performed using Auto-Lab PGST12 potentiostat (Eco-Cell, Holland), and a glassy carbon disc (3.0 mm dia.) working electrode. The supporting electrolyte solution was 0.1 M $(\text{CH}_3)_4\text{N}(\text{BF}_4)$ in a 1:1 (v/v) mixture of distilled water and acetone. Preparative electrolyses were performed galvanostatically in a cell shown at [14], and experimental conditions described in [8]. The working electrode was a Pt-grid of *c.* 27 cm^2 area, submerged in a 50 ml of electrolyzed solution [15], containing 0.1 M Na_2SO_4 conductive salt in the mixed solvent. Naphthalene derivatives, acenaphthene, and $(\text{CH}_3)_4\text{N}(\text{BF}_4)$ were bought from Aldrich and Fluka. CV was conducted at room temperature (22°C), while the electrolyzed solutions were cooled to *c.* 30°C . GC-MS measurements used Hewlett-Packard instrument consisting of an HP 5890 II gas chromatograph with HP-SM5 capillary column and MSD 5972A mass-sensitive detector, and NMR spectra were measured with 400 MHz Varian instrument.

Characteristics of a mixture of dimethyl-1,1'-binaphthyls ($\text{C}_{22}\text{H}_{18}$) produced by electrolysis of 2-methylnaphthalene.

White solid. TLC: $R_f = 0.62$ (SiO_2 , eluent: n-hexane-ethyl acetate, 4 : 1). GC-MS: 4 GC peaks of the relative intensity ratios: 20 : 10 : 1.5 : 1, decreasing toward longer retention

times, which formed the relative ratios: 1.000 : 1.017 : 1.034 : 1.048. All 4 isomers had practically identical MS spectra, as shown below.

2,2'-dimethyl-1,1'-binaphthyl ^1H NMR (400 MHz, CDCl_3), δ (ppm): 2.03 (s, 6H: 2-Me, 2'-Me), 7.04 (dd, $J=8.4, 1.0$ Hz; 2H: H8/H8'), 7.20 (ddd, $J=8.4, 6.8, 1.2$ Hz; 2H: H7/H7'), 7.39 (ddd, $J=8.2, 6.8, 1.2$ Hz; 2H: H6/H6'), 7.50 (d, $J=8.5$ Hz; 2H: H3/H3'), 7.88 (bt, $J=8.3$ Hz, 4H: H4/H4'; H5/H5') [16]. MS: m/e (relative intensity, %): 283 ($M^+ + 1$, 24), 282 (M^+ , 100), 268 (9), 267 (40), 266 (19), 265 (33), 264 (7), 263 (13), 253 (11), 252 (30), 239 (8), 133 (13), 132 (16), 126 (21).

MOPAC calculated dihedral angle between naphthyl planes: $87^\circ 4^m$.

2,7'-dimethyl-1,1'-binaphthyl ^1H NMR (400 MHz, CDCl_3), δ (ppm): 2.11 (s, 3H: 2-Me), 2.27 (s, 3H: 7'-Me), aromatic protons could not be resolved.

MOPAC calculated dihedral angle between naphthyl planes: $82^\circ 55^m$.

Results and discussion

The measured CV parameters of the studied compounds are presented in the Table 1, below. The "current function" (CF) of the fourth column is derived from the Randles-Ševčík equation [17]:

$$I_p = (2.69 \times 10^5) n^{3/2} A D^{1/2} \nu^{1/2} c \quad (1)$$

where I_p is the diffusional peak current [A], n is the number of electrons transferred per molecule of substrate, A is the electrode surface area [cm^2], D is the diffusion coefficient of substrate [cm^2/s], ν is the voltage sweep rate [V/s], and c is the concentration of substrate [mol/cm^3]. CF is equal to:

$$CF = (I_p / A c \nu^{1/2})^{2/3} = (4.18 \times 10^3) n D^{1/3} = k' \cdot n \quad (2)$$

where k' is a *constant* for compounds having similar diffusion coefficients. CF can be determined experimentally, and from it n can be estimated, provided that k' is determined first. We have determined k' , as in [8], by calculating CF for 1,2-benzenediol from its CV oxidation curve, where n was known to be 2 [18]. Table 1 contains also the respective energies of HOMO orbital of the investigated compounds calculated by the WinMOPAC 2.0 program [19].

The use of solvent containing high content of water precludes observing radical ions, because of their high reactivity. However, the initial formation of radical cations can be *indirectly* inferred from the dependence of the measured peak potentials, E_p , on the energies of the HOMO orbital. The dependence is linear, and - according to the *least squares* method - is described by the following straight line:

$$E_p [\text{V}] = -0.7781 \cdot E_{\text{HOMO}} [\text{eV}] - 5.1588 \text{ V} \quad (3)$$

which has a coefficient of correlation, $r = 0.9540$ (E_{HOMO} - the energy of HOMO orbital). The line (3) shows that the electrical energy necessary to promote the initial oxidation reaction at the electrode is linearly dependent on the energy of HOMO orbital. According to a cited work, E_p of 1-methylnaphthalene, 1,4-dimethylnaphthalene and acenaphthene are, respectively, equal to: 1.58, 1.49 and 1.32 V vs. NHE, measured in CH_2Cl_2 as solvent at a gold working electrode [4]. Further, E_p , of 1-methylnaphthalene and 1,4-dimethylnaphthalene were measured as equal to 1.74 and 1.63 V vs. Ag/AgCl in CH_2Cl_2 , respectively [5]. Those values are similar to the values measured in this paper on glassy carbon electrode, equal to: 1.58, 1.49 and 1.39 V vs. Ag/AgCl, respectively for 1-methylnaphthalene, 1,4-dimethylnaphthalene and acenaphthene (Table 1). Clearly, the measured values are similar despite of the different solvents and electrodes used.

Table 1. Cyclic voltammetry and molecular orbital parameters for the compounds studied.

No.	Compound	E_p [V]	Current function, CF , eq. (2)	n , number of electrons transferred	E_{HOMO} [eV]
1	1-Methylnaphthalene*	1.58 1.88 2.15	188 ** **	1.8	-8.584
2	1-Naphthalenemethanol	1.62 1.85	139 177***	1.3 1.7***	-8.778
3	1-Naphthalenaldehyde	1.87	196	1.9	-9.046
4	1-Acetylnaphthalene	1.80	162	1.6	-8.890
5	2-Methylnaphthalene*	1.52 2.00	189 **	1.8	-8.633
6	1,4-Dimethylnaphthalene	1.49 1.80	235 216***	2.3 2.2***	-8.456
7	4-methyl-1-Naphthalenaldehyde	1.83	171	1.6	-8.917
8	Acenaphthene****	1.39 1.60 1.79	167 206***	1.6 2.0***	-8.495
9	1-Acenaphthenol****	1.58 1.87	146 136	1.4 1.3	-8.733
10	1-Acenaphthenone	1.85	208	2.0	-9.011
11	1,2-Benzenediol*****	0.17	204	2.0	-8.796

* - Remeasured in respect to ref. [8]. ** - Barely visible. *** - Summary value for all peaks. **** - Taken from ref. [20]. ***** - Experimental data according to [18].

Thus, the solvents are not as decisive, as is the energy of the HOMO orbital, i.e. radical cations are the probable initial electro-oxidation products.

Further, it follows that the solvation (hydration) of the radical cations initially formed is a relatively slow process. If the radical cations would be hydrated immediately when formed, then the values of E_p should depend on the solvents used. Consequently, E_p values should appreciably differ between our results and those of the earlier two papers, but it is not the actual case. Thus, the solvation (hydration) must be a relatively slow process, e.g.:

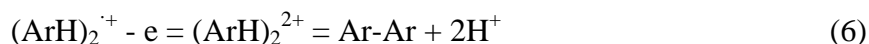


where ArH is an aromatic hydrocarbon and $\text{ArH}^{\cdot+}$ - its radical cation [8, 21].

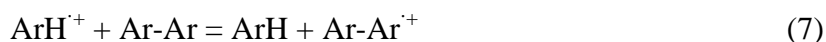
In solvents of low *nucleophilicity*, e.g. CH_2Cl_2 , at low temperatures (190-200 K), and in the presence of strong acids, like 5% trifluoroacetic acid, to suppress trace nucleophiles [4], radical cations are present as face-to-face π -dimers, observable by ESR spectra [1-7]:



The π -dimers may be oxidized to a dication, which can form a dehydrodimer by σ -coupling of nuclei:



Dehydrodimers are oxidized easier than the monomers, and their radical cations are formed immediately:



observable by ESR [7]. Alternatively, the monomeric radical cations are observed by ESR in case of 1,4- and 1,5-dimethylnaphthalenes, which are sterically blocked. to make π -dimers possible.

It is further possible that hydrocarbons are present as face-to-face π -dimers in solutions, and are oxidized in a dimeric form:



It may be especially true for naphthalene and 1-methylnaphthalene, which are not sufficiently blocked sterically to prohibit the formation of π -dimers, while the binding energy comes from a π -electron interaction of two face-to-face naphthalene nuclei [4]. The above discussion may explain the ease of formation of dimethylbinaphthyls (DMBN) during the electro-oxidation of 2-methylnaphthalene [8]. It followed from GC-MS analysis that a mixture of 4 isomers of DMBN was formed. The measured NMR spectrum allowed to assign to the two most abundant isomers the structures of: 2,2'-dimethyl- and 2,7'-dimethyl-1,1'- binaphthalenes, respectively, in the order of decreasing yield [22]. The DMBN are examples of *atropoisomerism*, i.e. an axial chirality due to the hindered rotation around the biaryl axis (σ -coupling bond) [23].

Acknowledgment

The author is grateful to Mr. M. Olejnik, M.Sc. for performing GC-MS determinations and to Mr. A. Koprowski, M.Sc. for obtaining NMR spectra.

References

- [1] I.H. Elson, J.K. Kochi, J. Am. Chem. Soc., 95 (1973) 5060
- [2] J.K. Kochi, R.T. Tang, T. Bernath, J. Am. Chem. Soc., 95 (1973) 7115
- [3] A. McKillop, A.G. Turrell, D.W. Young, E.C. Taylor, J. Am. Chem. Soc., 102 (1980), 6504
- [4] A. Terahara, H. Ohya-Nishiguchi, N. Hirota, A. Oku, J. Phys. Chem., 90 (1986) 1564
- [5] L. Ebersson, M.P. Hartshorn, O. Persson, J. Chem. Soc. Perkin Trans. 2, (1995) 409
- [6] L. Ebersson, M.P. Hartshorn, O. Persson, J. Chem. Soc. Perkin Trans. 2, (1995) 1735
- [7] L. Ebersson, M.P. Hartshorn, O. Persson, Acta Chim. Scand., 49 (1995) 640
- [8] R.E. Sioda, B. Frankowska, J. Electroanal. Chem., 568 (2004) 365
- [9] R.E. Sioda, J. Phys. Chem., 72 (1968) 2322
- [10] D. Nematollahi, M. Hesari, J. Electroanal. Chem., 577 (2005) 197
- [11] N.B. Salah, F. Matoussi, J. Electroanal. Chem., 583 (2005) 1
- [12] R.N. Goyal, A. Sangal, Electrochim. Acta, 50 (2005) 2135
- [13] O. Onomura, Y. Kanda, M. Imai, Y. Matsumura, Electrochim. Acta, 50 (2005) 4926
- [14] R.E. Sioda, T.Z. Fahidy, J. Appl. Electrochem., 35 (2005) 97
- [15] R.E. Sioda, B. Frankowska, A. Łobuzińska, T.Z. Fahidy, Polish J. Chem., 78 (2004) 1567
- [16] T. Ooi, M. Kameda, K. Maruoka, J. Am. Chem. Soc., 125 (2003) 5139
- [17] A.J. Bard, L.R. Faulkner, Electrochemical Methods: Fundamentals and Applications, Wiley, New York, 1980, pp. 218-220
- [18] D. Nematollahi, R.A. Rahchamani, J. Electroanal. Chem., 520 (2002) 145
- [19] J.J.P. Stewart, WinMOPAC 2.0 User Manual, Fujitsu Limited, Tokyo, Japan, 1998
- [20] R.E. Sioda, B. Frankowska, Annals Polish Chem. Soc., 3 (2004) 891
- [21] J. Matsui, H. Park, K. Otsuka, M. Oyama, J. Electroanal. Chem., 528 (2003) 49
- [22] H. Millauer, Ger. Pat. DE 4342282 (14 June 1995)
- [23] G. Bringmann, A.J.P. Mortimer, P.A. Keller, M.J. Gresser, J. Garner, M. Breuning, Angew. Chem. Int. Ed., 44 (2005) 5384

SYNTHESIS OF NEW 1,2,4-TRIAZOLES

Agata Siwek^a, Irena Wawrzycka-Gorczyca^b, Monika Wujec^a, Monika Pitucha^a, Maria Dobosz^a, Dariusz Maciej Pisklak^c

^a Department of Organic Chemistry, Faculty of Pharmacy, Medical University,
6 Staszica Str., 20-081 Lublin, Poland

^b Department of Crystallography, Faculty of Chemistry,
Maria Curie-Skłodowska University, 20-031 Lublin, Poland

^c Department of Physical Chemistry, Faculty of Pharmacy, Medical University,
02-097 Warszawa, 1 S. Banacha Str.

Abstract

New 4-aryl-3-(indol-2-yl)- Δ^2 -1,2,4-triazoline-5-thiones **2** were synthesized by intramolecular dehydrative cyclization of 4-aryl-1-[(indol-2-yl)-carbonyl]thiosemicarbazides **1** in alkaline medium. For **2** calculations using HyperChem7 by the MM⁺ force field were carried out to predict more favorable tautomeric form. Molecular structure proposed for 1,2,4-triazoles **2** was confirmed by X-ray structure analysis of **2a**.

The cyclodehydration of acylthiosemicarbazides in an alkaline medium affords 3,4-disubstituted- Δ^2 -1,2,4-triazoline-5-thiones which can exist in two tautomeric forms i.e. thione or thiol (Fig. 1) [1,2].

This report tries to predict which tautomeric form seems to be more favorable for new synthesized 1,2,4-triazoles. To this end, analysis of IR, ¹H NMR spectra and DFT calculations using Gaussian 98 were performed.

The molecular structure proposed for **2** was confirmed by X-ray structure analysis of **2a**.

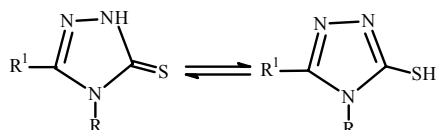


Fig. 1. 5-Thiol/thione forms of 3,4-disubstituted- Δ^2 -1,2,4-triazoline-5-thiol/thione

EXPERIMENTAL

All chemicals were purchased from Merck Co. or Lancaster and used without further purification. Melting points were determined in a Fischer-Johns block and are uncorrected. IR spectra (ν , cm^{-1}) were recorded in KBr using a Specord IR-75 spectrophotometer. ¹H NMR spectra (δ , ppm) were recorded on a Bruker Avance 300 in DMSO-*d*₆ with TMS as internal standard.

4-Aryl-1-[(indol-2-yl)-carbonyl]thiosemicarbazides **1**

The compounds **1** were prepared by a previously reported procedure [2].

4-(2-Fluorophenyl)-1-[(indol-2-yl)-carbonyl]thiosemicarbazide (**1a**)

C₁₆H₁₃FN₄OS *M_w*: 328.365. *M.p.* 210–212°C. *Yield*: 90%. *IR*: 3299, 3215 (NH), 1595, 1503, 1458, 744 (CH_{Ar}), 1664 (C=O), 1532, 1200 (C=S). ¹H NMR: 7.02–7.66 m, 9H (4×CH_{Ar}, 5×CH_{indole}), 9.69, 9.92, 10.62, 11.74 4s, 4H (4×NH).

1-[(indol-2-yl)-carbonyl]-4-(4-Methylphenyl)-thiosemicarbazide (1b)

C₁₇H₁₆FN₄OS *M_w*: 324.401. *M.p.* 213–215°C. *Yield*: 92%. *IR*: 3284 (NH), 2956, 1578, 1424, 810 (CH_{Ar}), 1667 (C=O), 1530, 1226 (C=S). ¹H NMR: 2.28 s, 3H (CH₃), 6.98–7.66 m, 9H (4×CH_{Ar}, 5×CH_{indole}), 9.68, 9.80, 10.51, 11.72 4s, 4H (4×NH).

4-Aryl-3-(indol-2-yl)-Δ²-1,2,4-triazoline-5-thione 2

The compounds **2** were prepared by a previously reported procedure [2].

4-(2-Fluorophenyl)-3-(indol-2-yl)-Δ²-1,2,4-triazoline-5-thione (2a)

C₁₆H₁₁FN₄S *M_w*: 310.350. *M.p.* 272–274°C. *Yield*: 66%. *IR*: 3285 (NH), 1591, 1502, 746 (CH_{Ar}), 1300 (C=S). ¹H NMR: 5.70–7.69 m, 9H (4×CH_{Ar}, 5×CH_{indole}), 11.98, 14.36 2s, 2H (2×NH).

X-ray crystallography for 2a:

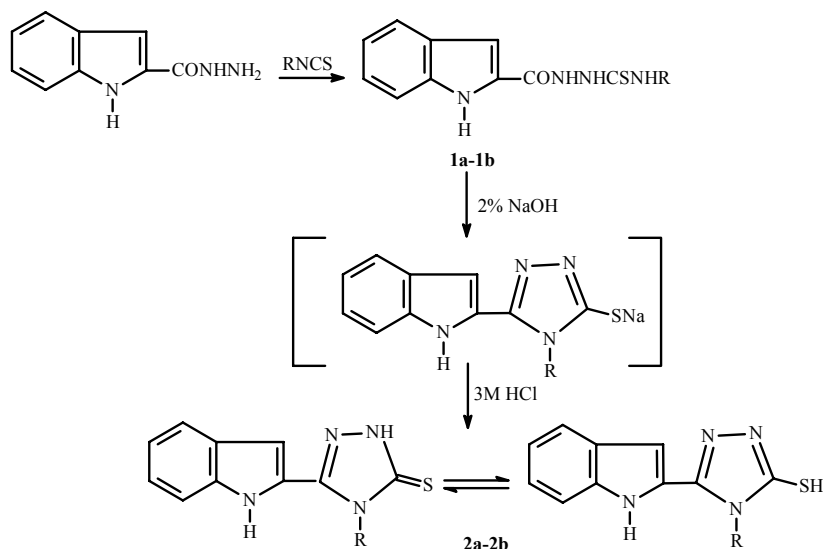
Diffraction data were collected on a KUMA KM4 diffractometer (T = 293 K, CuKα: λ = 1.54178 Å). Up to θ_{max} = 75.3°, 3059 reflections were collected. The data set was corrected for absorption effect (μ = 2.122 mm⁻¹). Crystal structure was solved by direct methods (SHELXS-97 [3]) and refined by full-matrix least-squares on F² using the program SHELXL-97 [4]. The non-hydrogen atoms were refined anisotropically. The H atoms bonded to the N atoms were located by difference Fourier synthesis, while other H atoms were positioned geometrically. Final discrepancy factors for I > 2σ(I) are: R1 = 0.0527, wR2 = 0.1614.

4-(4-Methylphenyl)-3-(indol-2-yl)-Δ²-1,2,4-triazoline-5-thione (2b)

C₁₇H₁₄N₄S *M_w*: 306.386. *M.p.* 109–111°C. *Yield*: 69%. *IR*: 3287 (NH), 1500, 812 (CH_{Ar}), 1305 (C=S). ¹H NMR: 2.46 s, 3H, (CH₃), 5.58–7.84 m, 9H (4×CH_{Ar}, 5×CH_{indole}), 11.88, 14.18 2s, 2H (2×NH).

Calculations

For two tautomers of the compounds **2a** and **2b** quantum chemical calculations were performed. Geometry was optimized with B3LYP [5] hybrid DFT potential using 6-31G** basis set. Calculation of IR frequencies showed that obtained geometry is an energy minimum and allowed to determine the correction for zero point vibrational energy (ZPE). All of the quantum chemical calculations were accomplished by Gaussian 98 package [6].



Scheme 1

RESULTS AND DISCUSSION

The synthesis of new compounds **1**, **2** are illustrated in the Scheme 1. Indole-2-carboxylic acid hydrazide was converted to corresponding thiosemicarbazide derivatives **1** by condensing with the appropriate isothiocyanate in the melt for 10 h. Subsequently, in an attempt to prepare the corresponding 4-aryl-3-(indol-2-yl)- Δ^2 -1,2,4-triazoline-5-thiones **2**, compounds **1** were refluxed with 2% NaOH and, after cooling, acidified with 3M HCl.

The characterization of **1** and **2** is based on the elementary analysis, whose results for C, H, and N were within the acceptable error limits, IR and ^1H NMR spectra. The ^1H NMR spectra of the cyclic compounds **2** gave proton signal typical for C(=S)-NH group in the range 14.18-14.36 ppm. The predominance of thione group was observed also in IR. The infrared spectra of **2** showed an absorption in the region 3287-3285 cm^{-1} attributed to NH and at 1305-1300 cm^{-1} attributed to C=S. The molecular structure proposed for **2** was confirmed by the X-ray crystal structure analysis of **2a**.

A perspective view of **2a**, including the atomic numbering scheme, is shown in Fig. 2. All rings in molecule are planar. 2-Fluorophenyl ring is disordered over two orientations. The dihedral angle between the fluorophenyl ring and triazole-indole system is 83.6(3) $^\circ$.

The crystal is monoclinic, with the space group $P2_1/c$ [unit cell parameters: $a = 9.024(2)$, $b = 21.738(4)$, $c = 7.601(2)$ Å $\beta = 90.74(3)^\circ$] and **2a**:H₂O ratio of 1:0.5. Molecules form centrosymmetric dimers in which N1-H \cdots S1 (triazole \cdots S=C) hydrogen bonds are formed, Fig. 3. Moreover, the observed hydrogen bonds are: (i) N5-H \cdots O1w (indole \cdots water), (ii) O1w-H \cdots N2 (water \cdots triazole) and (iii) C7/10-H \cdots F1 (indole \cdots fluorophenyl).

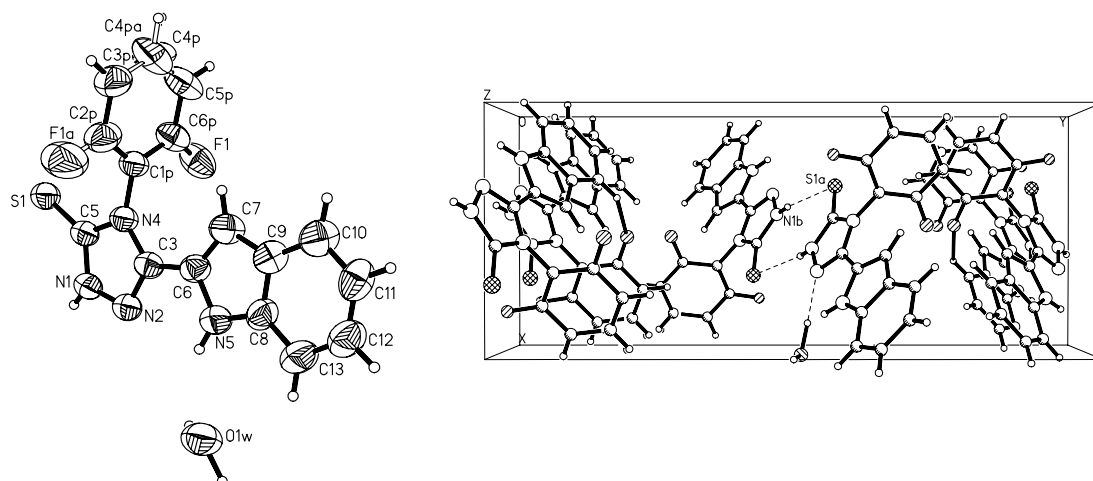


Fig. 2. The molecular structure of **Fig. 3.** The crystal structure; the view is along the **2a** hemihydrate. 2-Fluorophenyl fragment was found to be disordered with an occupation ratio 0.8:0.2.

Theoretical calculations showed that for both molecules (**2a** and **2b**) lower energy was obtained always for the thione forms, and the differences in energy between both tautomers were within 9-10 kcal/mol.

REFERENCES

- [1] I. Wawrzycka-Gorczyca, A. Siwek, M. Dobosz, *Acta Crystallographica*, E62, (2006) o128
- [2] M. Dobosz, A. Siwek, *Annals of the Polish Chemical Society*, Vol II, Part I, (2003) 26
- [3] G.M. Sheldrick: SHELXS-97. Program for crystal structure solution, University of Göttingen, Germany 1997
- [4] G.M. Sheldrick: SHELXL-97. Program for the refinement of crystal structures from diffraction data, University of Göttingen, Germany 1997
- [5] A. D. Becke, *J. Chem. Phys.* 98 (1993) 5648
- [6] Gaussian 98, Revision A.7, M. J. Frisch, G. W. Trucks, H. B. Schlegel, G. E. Scuseria, M. A. Robb, J. R. Cheeseman, V. G. Zakrzewski, J. A. Montgomery, Jr., R. E. Stratmann, J. C. Burant, S. Dapprich, J. M. Millam, A. D. Daniels, K. N. Kudin, M. C. Strain, O. Farkas, J. Tomasi, V. Barone, M. Cossi, R. Cammi, B. Mennucci, C. Pomelli, C. Adamo, S. Clifford, J. Ochterski, G. A. Petersson, P. Y. Ayala, Q. Cui, K. Morokuma, D. K. Malick, A. D. Rabuck, K. Raghavachari, J. B. Foresman, J. Cioslowski, J. V. Ortiz, A. G. Baboul, B. B. Stefanov, G. Liu, A. Liashenko, P. Piskorz, I. Komaromi, R. Gomperts, R. L. Martin, D. J. Fox, T. Keith, M. A. Al-Laham, C. Y. Peng, A. Nanayakkara, C. Gonzalez, M. Challacombe, P. M. W. Gill, B. Johnson, W. Chen, M. W. Wong, J. L. Andres, C. Gonzalez, M. Head-Gordon, E. S. Replogle, and J. A. Pople, Gaussian, Inc., Pittsburgh PA, 1998

SOLVENT ISOTOPE EFFECT IN ENZYMIC REDUCTION OF PHENYLPYRUVIC ACID

Katarzyna Skowera, Dorota Hertel, Marianna Kańska

Department of Chemistry, University of Warsaw, Pasteur 1 Str., 02-093 Warsaw

Abstract

Deuterium solvent isotope effect in enzymatic reduction of phenylpyruvic acid to L-phenylolactid acid catalyzed by enzyme *L-Lactic Acid Dehydrogenase* (EC 1.1.1.27) was determined.

Introduction

Enzyme *L-Lactic Acid Dehydrogenase*, LDH, (EC 1.1.1.27) catalyses very important metabolic reaction of reduction of pyruvic acid to L-lactic acid [1,3]. Under some condition this enzyme is also converting phenylpyruvic acid into L-phenylolactic acid, Fig. 1. Catalytic action of LDH is dependent from cofactor NADH (nicotinamide-adenine dinucleotide), which is oxidized to NAD⁺ in the course of reaction [2,4,5].

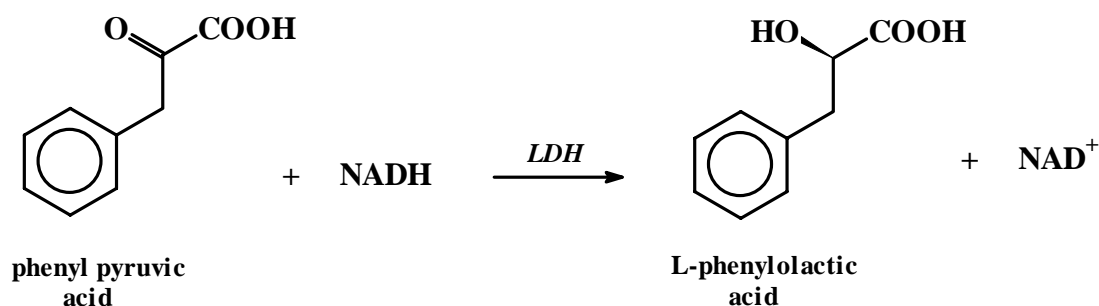


Fig. 1. Reduction of phenylpyruvic acid by enzyme LDH

In literature there are many reports concerning enzymatic reduction α -ketoacids to α -hydroxyacids [2,6,7,8]. Mechanism of action of LDH was investigated using different methods including isotope technique also [9]. In this paper we report the kinetic data obtained in course of measurements of parameters in Michaelis equation.

$$K_m = S \left[\frac{V_{max}}{v} - 1 \right]$$

Where K_m is Michaelis constant, S is concentration of substrate ($S \gg$ concentration of enzyme), v is reaction rate at concentration S , V_{max} is maximum reaction rate. These data are needed to calculate deuterium solvent isotope effect, SIE, in reaction depicted in Fig. 1. For determining SIE in reduction of phenylpyruvic acid noncompetitive method

was chosen. The parameters in Michaelis equation i.e., K_m and V_{max} , were determined separately for normal and deuteriated incubation medium. The progress of reduction of phenylpyruvic acid was determined indirectly by spectrophotometric measurements the decrease of absorbance of NADH ($\lambda = 340 \text{ nm}$, molar extinction coefficient for NADH, $\varepsilon = 6.22 \text{ mM}^{-1}\text{cm}^{-1}$). The numerical values of SIE were calculated by dividing kinetics parameters obtained in phosphate buffer by the ones obtained in fully deuteriated buffer.

Results

The kinetic data needed to calculate of Michaelis constant, K_m , and maximal reaction rate, V_{max} , were obtained from measurements of absorbance vs. time for a dozen independent runs of enzymatic reduction phenylpyruvic acid. The composition of incubation medium was the same for each run, excluding the starting concentration of substrate, which was changing in range between 0.032 M to 0.192 M. The typical dependence of decreasing of absorbance of NADH in the progress of reaction are shown in Fig. 2.

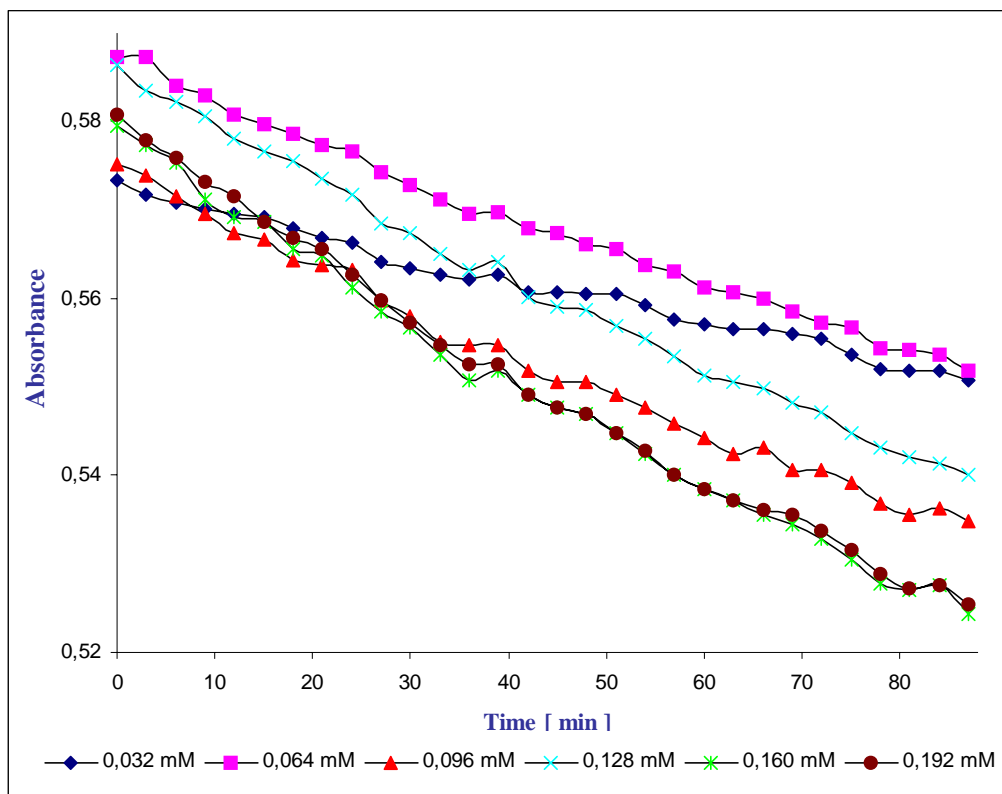


Fig. 2. Decreasing of absorbance of NADH in the course of reaction

The constant K_m and reaction rate V_{max} for reduction carried out in water buffer and fully deuteriated one were calculated using software Enzfitter 1.05 and presented in Fig. 3 and listed in Table 1.

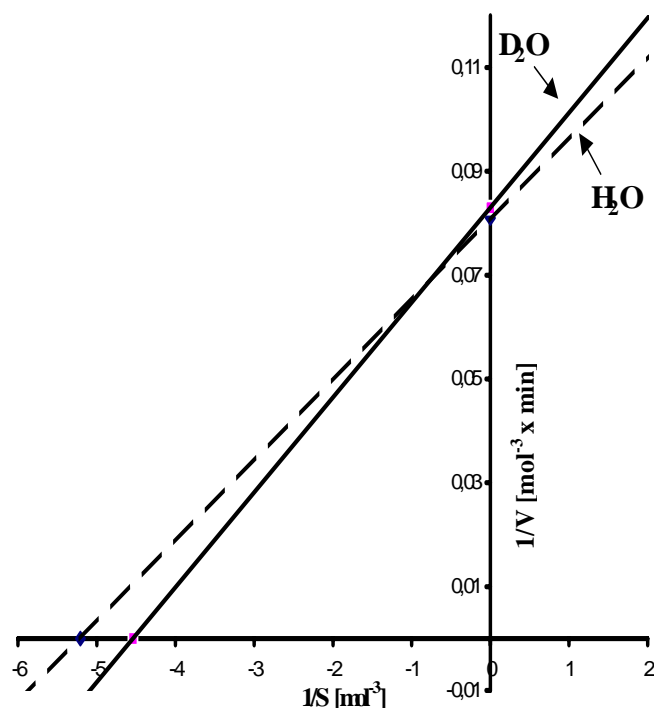


Fig. 3. Lineweaver-Burk's plots for enzymatic reduction of phenylpyruvic acid in H₂O and D₂O

Solvent	V_{max} [mM min ⁻¹]	K_m [mM]
H ₂ O	12.378 ± 0.17	0.192 ± 0.16
D ₂ O	12.068 ± 0.004	0.220 ± 0.004

Table 1. Average values of V_{max} and K_m for enzymatic reduction of phenylpyruvic acid

Solvent isotope effects on V_{max} and K_m were calculated by dividing the data obtained in water buffer by those ones measured in fully deuteriated buffer. Solvent isotope effects, SIE, on V_{max} and V_{max}/K_m are equal 1.026 ± 0.12 and 1.18 ± 0.14 respectively. The experimental errors were calculated using Student's equation with 0.95 confidence level.

Experimental

Each kinetic run was carried out in incubation medium of following constant composition: in 3,2 ml volume of 0.1 M phosphate buffer (pH 8) 2 mM of cofactor NADH and 271 U enzyme L-Lactic Acid Dehydrogenase (EC 1.1.1.27) were dissolved. The starting concentration of phenylpyruvic acid varied in the range 0.032 to 0.192

mM. Fully deuteriated 0.1 M phosphate buffer was prepared by dissolving in heavy water calculated amounts of 83% D₃PO₄/D₂O and 30% KOD/D₂O, and adjusting resulted buffer to pD 8 with 0.5 M solution of KOD/D₂O. The decreasing of absorbance vs. time was registered on spectrophotometer UV-VIS at 340 nm.

Acknowledgment

This work was supported by grant BST-1121-12000023

References:

- [1] H. Umeyama, S. Nakagawa, T. Nomoto, Chem Pharm Bull, 28 (1980) 2874.
- [2] R. A. Stinson, H. Gutfreund, J Biochem, 121 (1971) 235
- [3] H. U. Bergmeyer, J. Bergmeyer, Methods of Enzymatic Analysis, vol.6, Verlag Chemie, Weinheim, 1984 pp. 582-588
- [4] H.U. Bergmeyer, Methods of Enzymatic Analysis, vol.3, Verlag Chemie, Weinheim, 1974, pp. 1464-1468
- [5] C. N. Sarkissian, C. R. Scriver, O.A. Mamer OA, Anal Biochem, 280, (2000) 242
- [6] C. Shyh-Hang, L. Hwei-Jen, C. Gu-Gang, J Biochem, 267 (1990) 51
- [7] S. McClendon, N. Zhadin, R. Callender, Biophysical J, 89 (2005) 202
- [8] C. Gu-Gang, H. Shih-Ming, C. Shyh-Horng, Arch Biochem Biophys, 284 (1991) 285
- [9] R. Ropchan, J. R. Barrio, J. Nucl Med, 25 (1984) 887

NEW CALIX[4]ARENE SILICA GEL BONDED STATIONARY PHASES. CHARACTERIZATION AND APPLICATION TO HPLC.

Magdalena Śliwka-Kaszyńska, Sebastian Demkowicz

*Department of Organic Chemistry, Gdansk University of Technology
Narutowicza 11/12, 80- 952 Gdańsk, Poland, e-mail kaszynski@interia.pl*

INTRODUCTION

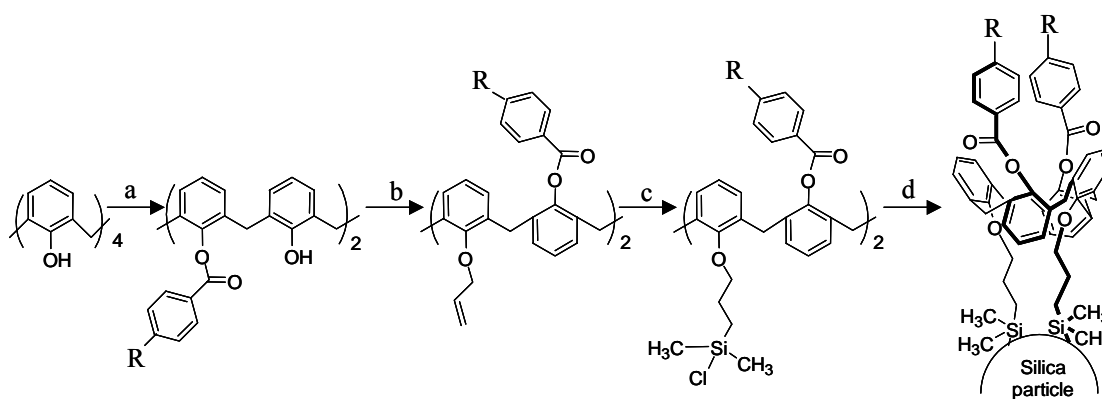
The ability to form complexes with other molecules of suitable size and hydrophobicity makes the calixarenes a useful class of stationary phases. The potential of these macrocyclic compounds for applications in gas chromatography [1-2], capillary electrophoresis [3-4], solid phase extraction [5] and high-performance liquid chromatography [6-10] has been shown in last years. Calixarene-bonded stationary phases in a cone conformation are excellent in reversed-phase chromatography. Recently, we have reported synthesis of three calix[4]arene-bonded silica gel stationary phases in *1,3-alternate* conformation (*1,3-Alt* CalixPr, *1,3-Alt* CalixBn, *1,3-Alt* CalixBz) and we have confirmed that these phases possess high selectivity toward selected analytes [13-14]. In this paper we described the synthesis of two novel *1,3-alternate* 25,27-bis-[*p*-*tert*butylobenzoyloxy]-26,28-bis-[3-propyloxy]-calix[4]arene (Calix *t*Bu) and *1,3-alternate* 25,27-bis-[*p*-methoxybenzoyloxy]-26,28-bis-[3-propyloxy]-calix[4]arene (Calix OMe) bonded silica gel stationary phases and their application to resolution of aromatic positional isomers, purine and pyrimidine bases as well as water soluble vitamins. The efficiency and selectivity comparison of these phases has been investigated.

EXPERIMENTAL SECTION

The synthesis of new calix[4]arene stationary phases is shown in Scheme 1. Elemental analyses of modified silica gels gave 19.86 %C, 2.04 %H (coverage density of the gel 0.344 mmol g⁻¹) for Calix *t*Bu and 18.33%C, 2.31 %H (coverage density of the gel 0.352 mmol g⁻¹) for Calix OMe. Stainless steel columns (150 x 4.6 mm I.D.) were packed with modified calix[4]arene-silica gels according to a slurry packing procedure. The column efficiency of about 30 000 plates/meter was determined with a commercially available test mixture.

Chromatographic procedure:

Liquid chromatograph HP Series 1090 (Hewlett-Packard Inc.) equipped with quaternary pump, autosampler, thermostated column compartment and diode-array detector was used. Analytes were dissolved in MeOH/H₂O (1:1 v/v) mixture at the concentration in range of 0.25 to 0.5 mg ml⁻¹ and 5 µl of the solution were injected onto the chromatographic column. A mixture of MeOH in water or in 0.01 mol l⁻¹ water solution of phosphate buffer was used as a mobile phase at flow rate of 1.0 ml min⁻¹. Diode array detector was operated in single wavelength mode. All analyses were carried out at 30° C.



Scheme 1. Synthesis of the *1,3-alternate* Calix *t*Bu and Calix OMe silica gel stationary phases; (a) *p*-substituted benzoyl chloride, ACN, K₂CO₃, reflux for 24 h; (b) allyl iodide, Cs₂CO₃, ACN, reflux for 72 h; (c) (CH₃)₂SiHCl, H₂PtCl₆, CHCl₃, reflux for 4 h; (d) activated silica gel, pyridine, shaking for 4 days at room temperature. Substituents R: *tert*-butyl or methoxyl.

RESULTS AND DISCUSSION

Both novel stationary phases exhibit strong retention power and selectivity toward analytes of very similar structure. A variety of aromatic positional isomers, representing compound with acidic, basic and neutral character, were well resolved. Retention capacity factors (*k*) and separation factors (α) of these isomers at the best, individually optimized, chromatographic conditions are given in Table 1.

Table 1. Retention and separation factors for benzene positional isomers on Calix *t*Bu and Calix OMe stationary phases.

Analytes	Isomers	Calix <i>t</i> Bu		Calix OMe	
		<i>k</i>	α	<i>k</i>	α
Hydroxypyridine ^A	<i>para</i>	0,05	9,98	0,09	4,60
	<i>ortho</i>	0,50	2,71	0,42	1,11
	<i>meta</i>	1,35		0,88	
Aminobenzhydrazide ^A	<i>para</i>	0,32	2,78	1,06	1,07
	<i>meta</i>	0,90	1,35	1,14	1,69
	<i>ortho</i>	1,20		1,92	
Hydroxybenzyl alcohol ^B	<i>para</i>	1,43	1,43	1,47	1,23
	<i>meta</i>	2,04	1,45	1,80	1,22
	<i>ortho</i>	2,96		2,20	
Aminophenol ^B	<i>para</i>	0,74	1,44	0,99	1,10
	<i>meta</i>	1,07	1,82	1,08	1,41
	<i>ortho</i>	1,94		1,61	
Nitroaniline ^C	<i>para</i>	2,99	1,13	2,65	1,02
	<i>meta</i>	3,39	1,48	2,69	1,48
	<i>ortho</i>	5,01		4,01	
Hydroxybenzoic acid ^D	<i>ortho</i>	4,08	1,09	1,18	1,06
	<i>meta</i>	4,45	1,51	1,26	2,07
	<i>para</i>	6,72		2,60	
Chlorobenzoic acid ^D	<i>ortho</i>	0,25	9,41	1,03	3,19
	<i>meta</i>	2,34	1,08	3,28	1,06
	<i>para</i>	2,54		3,47	
Nitrobenzoic acid ^E	<i>ortho</i>	1,22	5,71	1,81	5,75
	<i>meta</i>	6,95	1,05	10,43	1,17
	<i>para</i>	7,33		12,22	

Mobile phases: A- H₂O/MeOH (9:1 v/v); B- H₂O/MeOH (8:2 v/v); C- H₂O/MeOH (6:4 v/v); D- 10mM phosphate buffer at pH 3.5/MeOH (9:1 v/v); E-10mM phosphate buffer at pH 3.5/MeOH (3:7 v/v)

As can be seen, compounds possessing nitro substituents in the phenyl ring have higher retention times in comparison to the rest of investigated analytes. This may be explained by π -electron transfer interaction resulting from the electron-withdrawing effect of the nitro groups of analytes and π -electron system of the *para*-substituted benzoiloxo groups of calixarene. The elution order of positional isomers of the investigated compounds on calixarene columns strongly depends on their chemical nature. Polar neutral, basic and weak acidic compounds (for example dinitrobenzene, nitroaniline and nitrophenol) were eluted on both columns in order: *para* < *meta* < *ortho*, which may be associated to guest-host interactions of the calixarene cavity and the analyte molecule. Only *ortho*-hydroxypyridine was eluted before *meta* isomer (*para*>*ortho*>*meta*). It can be explained by ability of *ortho* and *para* isomers of hydroxypyridine to exist in tautomeric form of pyridin-(1H)-one. The elution order of the substituted benzoic acid isomers was opposite (*ortho*>*meta*>*para*) and follows pK_a values order of these acids. Capacity factor values of the most separated isomers are greater on Calix OMe column than on Calix *t*Bu phase. It may be due to stronger electro donating properties of methoxyl substituents present in aromatic ring of calixarene molecules at *para* position. Moreover, hydrogen bond interaction between the methoxyl group and hydrogen-donor (OH, NH₂) isomers can play additional role in the discrimination process.

The chromatographic performance of Calix OMe and Calix *t*Bu stationary phases was also evaluated using nucleobases and water-soluble vitamins separation. Figures 2 and 3 show typical chromatograms of above-mentioned analytes.

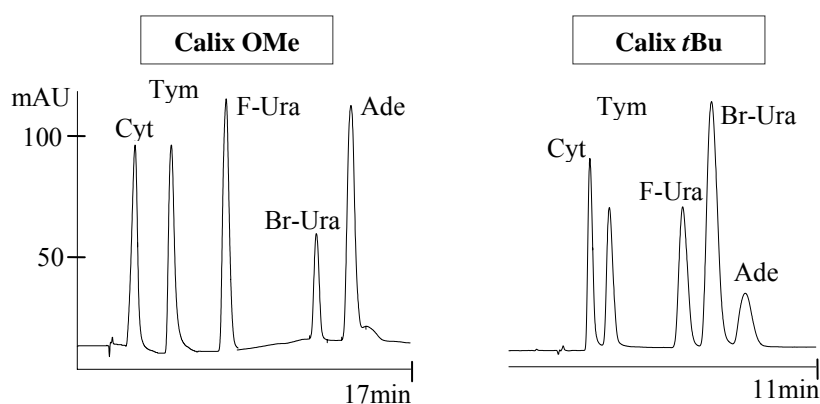


Figure 2. Separation of purine and pyrimidine bases. Mobile phase: methanol-10mM phosphate buffer at pH= 6 (1:9 v/v), flow 1ml min⁻¹, UV 254 nm, T=25°C.

Mixture of five bases was separated completely on both calixarene columns (Fig.2). Elution order of the analytes was the same however, solutes are a little more retained on Calix OMe and peaks are sharper.

The separation of seven water-soluble vitamins (Fig.3) can be achieved in isocratic mode within 16 minutes. It must be noted that such results is very difficult to achieve on ODS column, where retention mechanism based only on hydrophobicity of the analytes.

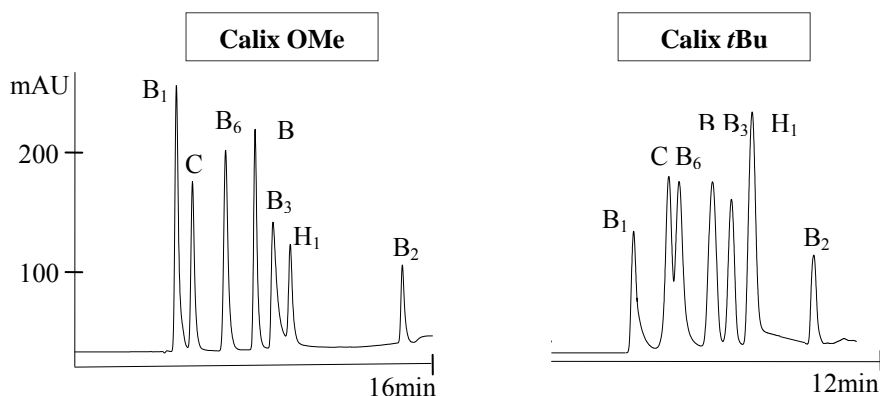


Figure 3. Separation of water-soluble vitamins. Mobile phase: with methanol-phosphate buffer at pH=3.5 (10:90 v/v), flow 1 ml min⁻¹, UV 254 nm, T=25°C.

Better separation of vitamins was observed on Calix OMe, which exhibited stronger retention power and better resolution toward the analytes. Separation of vitamins C and B₆ were not complete on Calix *t*Bu.

CONCLUSION

Screening evaluation of *1,3*-alternate Calix *t*Bu and Calix OMe revealed that the new stationary phases are chemically stable and can be successfully used for separation of positional isomers of aromatic compounds. The applicability of the novel chromatographic columns to analysis of selected biologically vital compounds was also demonstrated. Investigation of surface properties of calixarene stationary phase and retention mechanism is in progress.

Acknowledgements

The authors gratefully acknowledge financial support for this work from the State Committee for Scientific Research (KBN 3 T09 A, Project No. 13829).

REFERENCES:

- [1] Mnuk P., Feltl L. and Schurig V., *J. Chromatogr. A*, **732** (1996) 63.
- [2] Lin L., Wu C.Y., Yan Z.Q., Yan X.Q., Su X.L., *Chromatographia*, **47** (1998) 689.
- [3] Sun S., Sepaniak M.J., Wang J.S. and Gutsche C.D., *Anal. Chem.*, **69** (1997) 344.
- [4] Zhao T., Hu X., Cheng J. and Lu X., *Anal. Chim. Acta*, **358** (1998) 263.
- [5] Hutchinson S., Kearney G.A., Glennon J.D., *Anal. Chim. Acta*, **291** (1994) 269.
- [6] Bridle R., Albert K., Harris S.J., Glennon J.D., *J. Chromatogr. A*, **731** (1996) 47.
- [7] Gebauer S., Friebe S., Gübitz G., *J. Chromatogr. Sci.*, **36** (1998) 383.
- [8] Li L.S., Da S.L., Feng Y.Q. and Liu M., *Talanta*, **64** (2004) 373.
- [9] Li L.S., Liu M., Da S.L. and Feng Y.Q., *Talanta*, **62** (2004) 643.
- [10] Sokoließ T., Menyes U., Roth U. and Jira T., *J. Chromatogr. A*, **948** (2002) 309.
- [11] Śliwka-Kaszyńska M., Jaszczolt K., Witt D. and Rachoń J., *J. Chromatogr. A*, **1055** (2004) 21.
- [12] M. Śliwka-Kaszyńska, K. Jaszczolt, A. Kołodziejczyk, J. Rachoń, *Talanta*, **68** (2006) 1560.
- [13] M. Śliwka-Kaszyńska, K. Jaszczolt, A. Hoczyk, J. Rachoń, *Chem. Anal.*, **51** (2006) 123.

DETERMINATION OF HAFNIUM IN ZIRCONIUM COMPOUNDS USING INDUCTIVELY COUPLED PLASMA ATOMIC EMISSION SPECTROMETRY

M. Smolik*, A. JakóbiK – Kolon*, M. Porański**

**Department of Inorganic Chemistry and Technology, Faculty of Chemistry, Silesian University of Technology, 44-100 Gliwice, Poland*

***Power Research & Testing Company „Energopomiar” Ltd, PO BOX 402, 44-101 Gliwice, Poland*

Introduction

Hafnium occurs in Zr ores in the range of 2 – 3%. Separation of these elements is however very difficult because of the large similarity of chemical properties and analytical problems, which grow up when the content of the analyte (Hf) (in relation to Zr) approaches to the level of 100 ppm [1].

Technique of inductively coupled plasma atomic emission spectrometry is, beside radiometric and neutron activation analysis, one of the most often used techniques of hafnium determination in zirconium ores during attempts of their separation [2, 3].

The aim of our study was to settle the conditions of hafnium determination in various zirconium compounds by means of ICP – AES and adaptation of the method to the determination of this element in two phases of aqueous biphasic system (ABS) containing saturated solutions of salts (eg. sodium sulfate, sodium citrate (Na₃Cit)) and aqueous solution of polyethylene glycol (PEG).

Experimental

Reagents and solutions

High purity zirconium dichloride oxide octahydrate 99.9% metal basis (~ 100 ppm Hf), hafnium dichloride oxide octahydrate 98+% were obtained from Alfa Aesar and used as received. Reagent grade anhydrous sodium sulphate, trisodium citrate dihydrate, hydrochloric acid, sulfuric acid and “pure” zirconium dichloride oxide octahydrate (~ 2 % Hf), zirconium sulphate tetrahydrate (~ 2 % Hf) all from POCh (Gliwice, Poland) was used without further purification. “Pure” zirconium nitrate pentahydrate were obtained from International Enzymes Limited (Windsor, Berkshire, England). Polyethylene glycol 2000 (PEG 2000) was purchased from Fluka and used as received. Water was distilled and purified using a Millipore Elix 10 system.

Concentrated solutions of studied metals (~ 0.15 g of metal/ml) were prepared and stored in 2M HCl (except of Zr(SO₄)₂*4H₂O in 0.5M H₂SO₄ and Zr(NO₃)₄*5H₂O in 1M HNO₃). The solutions were standardized by gravimetric procedure utilizing mandelic acid [4].

Apparatus

IRIS II ADVANTAGE RAD HR (serial no 7063) Thermo Jarrell Ash (USA) inductively coupled plasma emission spectrometer was used. The conditions for determination of Hf by ICP-AES are presented in Table 1.

Tab.1. Operation conditions for determination of Hf by ICP-AES

Rf [MHz]	27.12
RF power [W]	1150
Argon coolant flow rate [l/min]	14
Argon carrier pressure [PSI]	32
Integration time [s]	low WL 10
	high WL 10
Resolution [nm]	<0.005 at 200 nm
	<0.01 at 400 nm
	<0.02 at 600 nm
Peristaltic pump flow rate [ml/min]	1.85
Wavelength [nm]	196.4; 227.7; 232.2; 235.1
Low WL range [nm]	175 - 275
High WL range [nm]	210 – 800

Determination of Hf by flame atomic absorption spectrometry (FAAS) was performed using Perkin-Elmer 3300 spectrometer with hollow cathode Hf lamp (PHOTRON PERKIN ELMER). Following conditions were used: wavelength 286.6 nm; slit 0.2 nm; current intensity 25 mA; flame C₂H₂ – N₂O.

Procedure

Four Hf emission lines (196.4; 227.7; 232.2; 235.1 nm) of relatively high sensitivity and free from coincidence with emission lines of Zr were selected. Standard curves containing two different concentrations of matrix: 0.1 and 1% Zr in the range 0 – 0.7 µgHf/ml and 0 – 7 µgHf/ml, respectively were prepared threefold. Thanks to proper processing of signal (background correction and matching of peak width) very high correlation coefficients ($r^2 \sim 0.999$) were obtained. Standard additions method was utilized to determine hafnium in zirconium matrix at 100 ppm level (Tab. 2.). ICP – AES was also used for determination of hafnium in various zirconium compounds (ZrOCl₂·8H₂O, Zr(SO₄)₂·4H₂O, Zr(NO₃)₄·5H₂O) at 2 – 4% level. Standard curves method was employed in this case (Tab. 3.). Additionally, the effect of some substances utilized in aqueous biphasic systems (ABS) (polyethylene glycol (PEG), sodium sulfate, sodium citrate (Na₃Cit)) on results of Hf determination was investigated to adapt the method for determination of Hf in both phases after extraction in ABS (Tab. 5.).

Flame atomic absorption spectrometry was used as comparative method of Hf(IV) determination applying solutions containing 1% HF and 0.1% Al in the presence of 1% ZrOCl₂ matrix.

Results and Discussion

Table 2. shows contents of hafnium in high purity zirconium dichloride oxide. Obtained averages for each series do not differ significantly, what has been confirmed by T- Student test. Therefore it is possible to calculate mean value of hafnium contents using results of three series (n = 15). Mean values obtained in such a way for 0.1 and 1% Zr matrix do not differ essentially, what allows to compute average of all 30 values presented in Table 2.

Tab.2. Contents of hafnium in high purity ZrOCl₂ [ppm Hf in relation to Zr] determined by ICP-AES using standard additions and 0.1 or 1% Zr matrix (n = 3).

λ [nm]	0.1% Zr matrix			1% Zr matrix		
	196.423	192	187	257	185	204
227.716	140	135	170	137	153	164
227.716	150	167	171	145	166	169
232.247	207	229	208	170	187	156
235.122	177	223	229	177	196	233
average	173 ± 35	188 ± 48	207 ± 47	163 ± 26	181 ± 26	190 ± 47
average (n=15)	189 ± 31			178 ± 25		
average (n=30)	184 ± 12					

During determination of higher contents of hafnium (Tab. 3.) a decrease of scatter of the results is observed in comparison with the latter determination of Hf at 10⁻²% level, which does not depend on kind of zirconium salt.

Tab.3. Contents of hafnium in zirconium compounds [% Hf in relation to Zr] determined by ICP – AES using standard curves for various wavelength (n = 2).

λ [nm]	ZrOCl ₂ ·8H ₂ O		Zr(SO ₄) ₂ ·4H ₂ O		Zr(NO ₃) ₄ ·5H ₂ O	
	196.423	2.50	2.50	2.65	2.66	3.14
227.716	2.49	2.50	2.66	2.65	3.16	3.16
227.716	2.50	2.51	2.65	2.66	3.17	3.15
232.247	2.49	2.49	2.65	2.65	3.16	3.17
235.122	2.49	2.50	2.66	2.65	3.20	3.18
average (n=10)	2.50 ± 0.01		2.65 ± 0.01		3.17 ± 0.02	

Accuracy of the investigated method was verified by the addition of precise amounts of hafnium and its determination, employing ICP – AES and FAAS methods. The results presented in tab. 4. show that ICP – AES method is characterized by high accuracy and better precision than FAAS.

Tab.4. Contents of hafnium in zirconium dichloride oxide [% Hf in relation to Zr] determined by ICP – AES and FAAS methods, n = 5.

added Hf [%]	found Hf [%]	
	ICP – AES	FAAS
0.388	0.388 ± 0.005	0.388 ± 0.035
1.94	1.98 ± 0.04	1.87 ± 0.04

The results presented in tab. 5. indicate that after taking into account proper corrections, ICP – AES method can be utilized for Hf determination in phases after extraction in ABS. Polyethylene glycol affects emission intensity (decrease of signal by about 30%). Presence of sodium sulfate results in slight increase and sodium citrate slight decrease of emission intensity.

Tab.5. Effect of some substances on Hf determination in Zr matrix using ICP – AES.

λ [nm]	227.7	227.7	232.2	235.1	
	found [% of Hf addition]				$\bar{x} \pm \frac{t \cdot s}{\sqrt{n}}$
PEG 2.5%	82.2	83.0	81.8	83.8	82.7 ± 1.4
PEG 5%	72.0	72.0	72.1	74.5	72.7 ± 2.0
Na ₂ SO ₄ 1.5%	106.5	105.2	106.4	105.2	105.8 ± 1.1
Na ₃ Cit 4%	93.0	92.0	92.7	92.3	92.5 ± 0.7

Conclusions

The presented method permits with large accuracy and precision to determine the content of Hf in various compounds of zirconium (dichloride oxide, nitrate and sulfate) at 0.4 – 3.2% level and to estimate its content at 10⁻²% level (in relation to Zr).

The presence of polyethylene glycol causes approximately 30% decrease in the emission intensity, Na₃Cit (4%) – approximately 7.5%, while the presence of Na₂SO₄ results in 5.8 % increasing in the signal. Taking into account constant and stable influence of these phase components on the emission intensity, the ICP – AES method can be used in the direct analysis of phases from the extraction in aqueous biphasic systems, after prior introduction of corrections.

Literature

- [1] N. Z. Baluch, K. Anwar, S. M. Ifzal, Journal of Radioanalytical and Nuclear Chemistry, Articles, 141(2) (1990) 417
- [2] X. J. Yang, A. G. Fane, C. Pin, Chemical Engineering Journal, 88 (2002) 37
- [3] X. J. Yang, A. G. Fane, C. Pin, Analytica Chimica Acta, 360 (1998) 17
- [4] M. Taddia, P. Modesti, A. Albertazzi, Journal of Nuclear Materials, 336 (2005) 173

SYNTHESIS OF 2'-DEOXYURIDINE DERIVATIVES MODIFIED WITH AMINO ACID RESIDUES ON THE NUCLEOBASE MOIETY

Damian Smuga, Beata Stanisławczyk, Elżbieta Sochacka

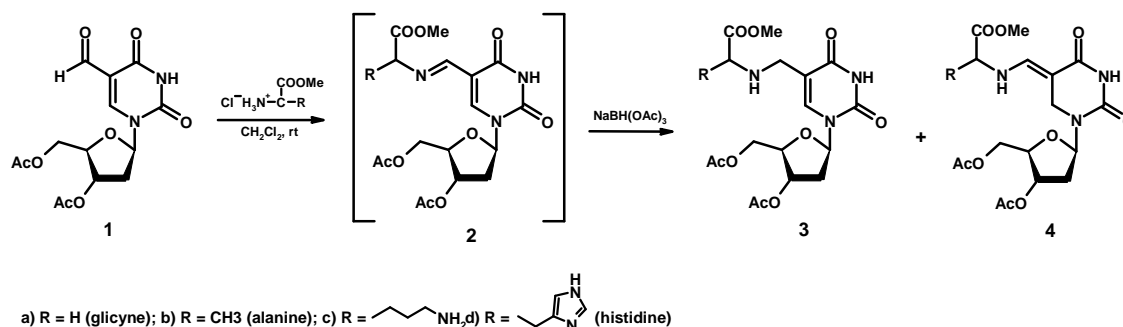
*Institute of Organic Chemistry, Technical University of Lodz, Zeromskiego 116,
90-924 Lodz, Poland*

Introduction

Recently much attention has been focused on the development of modified nucleosides suitable for structure – function elucidation of catalytically active nucleic acids [1,2]. Modification of nucleic acid enzymes (ribozymes, deoxyribozymes) by introduction of protein-like functionality gives a chance for enhancing their catalytic diversity and activity [1-5]. The incorporation of extra functional groups into nucleic acid enzymes may be achieved by employing suitably modified analogues of nucleoside 5'-triphosphates in place of their natural counterparts during SELEX process [3-6], or by chemical synthesis of modified nucleosides and their incorporation into deoxyribozyme sequences by solid support oligonucleotide synthesis [5,7].

Results and discussion

In our studies on the structure – function relationships of deoxyribozyme “10-23” by employing the model synthetic oligonucleotides we are interested in site specific incorporation of modified nucleosides bearing amino acids functionality on heterocyclic base moieties [8,9]. Herein, we report the results of our work on the synthesis of 2'-deoxyuridine derivatives modified with the glycine (**3a**), alanine (**3b**), lysine (**3c**) and histidine (**3d**) residues at the 5 position of uracil ring. To obtain nucleosides **3a-d** a reductive amination of 3',5'-di-*O*-acetyl-5-formyl-2'-deoxyuridine (**1**) [10] with appropriate amino acid components and NaBH(OAc)₃ as the reducing agent has been chosen (Scheme 1).



Scheme 1. Reductive amination of 3',5'-di-*O*-acetyl-5-formyl-2'-deoxyuridine with amino acid methyl ester hydrochlorides and NaBH(OAc)₃ as the reducing agent

Recently the procedures of reductive amination of nucleosides containing aldehyde function have found important application in the synthesis of various nucleic acid conjugates [11], in the formation of direct crosslinks between oligonucleotides containing 5-formyl-2'-deoxyuridine and proteins [12] as well as in the synthesis of several 5-aminomodified nucleosides [13-16].

In our preliminary experiment performed according to the protocol of a direct reductive amination 3',5'-di-*O*-acetyl-5-formyl-2'-deoxyuridine (**1**) was treated with 1.2 molar equivalents of glycine methyl ester hydrochloride, triethylamine and NaBH(OAc)₃, and the reaction was left at room temperature for 2 hours. The desired secondary amine derivative **3a** was isolated in very good yield (82%) along with a small amount of by-product **4a** (yield 8%) as a result of unwanted 1,4 reduction of intermediate Schiff base. When the same conditions were applied to the reaction of aldehyde **1** with optically pure L-alanine methyl ester the product with secondary amine structure **3b** was also obtained in good yield (73%). However, the analysis of its ¹H NMR spectrum indicated the presence of two singlets with 7:3 integration ratio belonging to H6 proton of uracil moiety (Fig 1a). The same integration ratio was observed for two singlets of methyl ester protons of **3b**. These data suggested that diastereoisomeric mixture of **3b** was formed probably due to the partial racemization of amino acid residue *via* tautomerization and non selective reduction of the isomerized Schiff base intermediate (Scheme 2) [17]. The reaction of aldehyde **1** with D,L-alanine methyl ester fully confirmed the above assumptions. In ¹H NMR spectrum of **3b** modified with racemic amino acid residue the integration ratio of H6 singlets was as 1:1 (Fig. 1b).

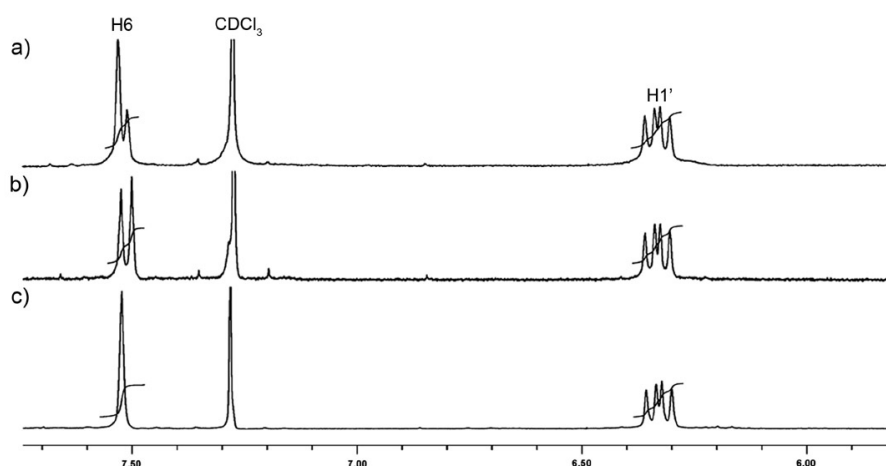
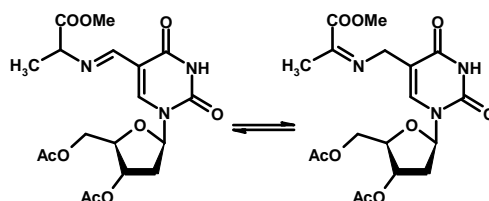


Figure 1. ¹H NMR spectra of H6 and H1' regions of **3b**;

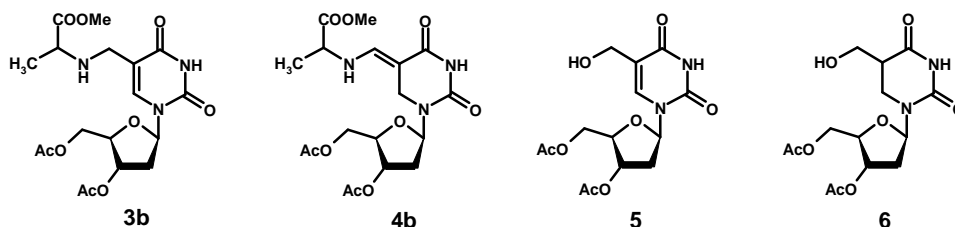


Scheme 2. Tautomerization of Schiff base intermediate

As only modified nucleosides bearing natural L-amino acid residues were interesting for our further structure - function study of deoxyribozyme "10-23" and more detailed investigations on the reductive amination of aldehyde **1** were undertaken. Several experiments were performed according to the direct and indirect (stepwise) preparative procedures of reductive amination using free L-alanine methyl ester or its hydrochloride as a model amino acid component. The borohydrides with different

activity: NaBH₄, NaBH₃CN, NaBH(OAc)₃ were applied as reducing agents. The results of experiments are summarized in Table 1.

Table 1. Reductive amination of 3',5'-di-*O*-acetyl-5-formyl-2'-deoxyuridine (**1**) with hydrochloride of alanine methyl ester under various conditions



Reaction conditions ¹				Yield of products [%]			
entry	Et ₃ N	reducing agent	temp.	3b (ratio of diastereoisomers) ²	4b	5	6
Direct reductive amination							
1	+	NaBH ₄	rt	45 (1:0)	-	20	35
2	+	NaBH ₄	0 °C	55 (1:0)	<5	20	20
3	+	NaBH ₃ CN	rt	75 (3:1)	15	<5	<5
4	+	NaBH(OAc) ₃	rt	75 (7:3)	20	<5	-
5	-	NaBH ₄	0 °C	30 (1:0)	15	35	20
6	-	NaBH ₃ CN	rt	25 (1:0)	25	25	20
7	-	NaBH(OAc) ₃	rt	50 (1:0)	35	15	-
Indirect reductive amination							
8	+	NaBH ₄	0 °C	80 (3:2)	-	<5	15
9	+	NaBH ₃ CN	rt	70 (1:1)	20	<5	<5
10	+	NaBH(OAc) ₃	rt	75 (1:1)	20	<5	-
11	-	NaBH ₄	0 °C	50 (1:0)	15	10	25
12	-	NaBH ₃ CN	rt	50 (1:0)	20	<5	20
13	-	NaBH(OAc) ₃	rt	60 (1:0)	35	<5	-

¹All experiments were performed in 0.2 mmol scale with 1.2 molar excess of amino acid component over aldehyde **1** in anhydrous methylene chloride as a solvent. Free L-alanine methyl ester was obtained *in situ* by the treatment of its hydrochloride with equimolar amount of triethylamine. Direct reductive amination was carried out for 2 hr. Experiments of indirect reductive amination were performed for 1 hr of intermediate Schiff base formation and 30 min of reduction step.

²The ratio of diastereoisomers of **3b** was determined on the basis of ¹H NMR spectra by comparison of H6 and methyl ester protons integration for each isomer.

Our results indicate that reductive amination of aldehyde **1** with free L-alanine methyl ester (formed *in situ* from its hydrochloride by triethylamine treatment) let to obtain the desired product **3b** in a good yield, but with significant epimerization at α -carbon atom of incorporated amino acid residue (Table 1, entry 3,4,8-10). In the experiments with free amino acid ester the non-epimerized nucleoside **3b** was formed

when more active NaBH₄ was used under conditions of direct reductive amination (entry 1,2). However, in this case the competitive reduction of starting aldehyde took place and unwanted products **5**, **6** were obtained in large amount.

The application of hydrochloride of L-alanine methyl ester as the amine component in direct as well as in the stepwise reductive amination allowed to synthesize nucleoside **3b** without change in natural chirality of amino acid residue (entry 5-7 and 11-13). The better yields of desired **3b** were obtained by indirect procedure (entry 11-13). The indirect syntheses performed with NaBH₄ or NaBH₃CN resulted in more complicated reaction mixtures containing undesirable products of starting aldehyde reduction (entry 11,12). The application of milder NaBH(OAc)₃ allowed us to obtain **3b** in good yield (entry 13) accompanying with only one main by-product **4b** – 5,6-dihydrouridine derivative modified with 5-*exo*-methylidene group at the base moiety. It is worth to note that compound **4b** as a novel dihydrouridine derivative may serve as an interesting modified nucleoside for further investigation of its bioactivity.

Conclusions

To obtain 2'-deoxyuridines bearing natural L-amino acid residues at 5-position of uracil by the reductive amination of 5-formyl nucleoside **1** it is crucial to use hydrochlorides of L-amino acid methyl esters as the amine components. Additionally, the application of very mild NaBH(OAc)₃ as the reducing agent under the conditions of indirect reductive amination allowed to suppress undesirable reduction of the starting nucleoside aldehyde.

The conditions described above were successfully applied for the synthesis of 2'-deoxyuridines modified with L-alanine **3b** (¹H NMR spectrum, Fig.1c), L-lysine **3c** and L-histidine **3d** residues for their further incorporation into model oligonucleotides with the sequences of deoxyribozyme "10-23".

Acknowledgements

This work was supported by Technical University of Lodz (Grant D.S. I-18/15).

References

- [1] G. M. Emilsson, R. R. Breaker, *Cell. Mol. Life Sci.*, 59 (2002) 596
- [2] J. Kurreck, *Eur. J. Biochem.*, 270 (2003) 1628
- [3] D.M. Perrin, T. Garestier, C. Helene, *J. Am. Chem. Soc.*, 123 (2001) 1556
- [4] A.V. Sidorov, J.A. Grasby, D.M. Williams, *Nucleic Acids Res.*, 32 (2004) 1591
- [5] S.W. Santoro, G.F. Joyce, K. Sakthivel, S.Gramatikova, C.F. Barbas III, *J. Am. Chem. Soc.*, 122, (2000) 2433
- [6] M. Kuwahara, K. Hanahawa, K. Ohsawa, R. Kitagata, H. Ozaki, H. Sawai, *Bioorg. Med. Chem.*, 14 (2006) 2518
- [7] L. Lermer, J. Hobbs, D.M. Perrin, *Nucleos., Nucleot. & Nucl. Acids*, 21 (2002) 651
- [8] E. Sochacka, D. Smuga, I. Frątczak, *Coll. Czech. Com. Symp. Ser.*, 7, (2005) 471
- [9] E. Sochacka; G. Leszczynska, I. Frątczak, D. Smuga, *Ann. Pol. Chem. Soc.*, 3, (2004) 652
- [10] A. Ono, T. Okamoto, M. Inada, H. Nara, A. Matsuda, *Chem. Pharm. Bull.*, 42, (1994), 2231
- [11] T.S., Zatsepin, D.A. Stetsenko, M.J. Gait, T.S. Oretskaya, *Bioconjugate Chem.* 16 (2005), 471
- [12] T. Sugiyama, A. Kittaka, M. Y. Ida, *Bioorg. Med. Chem. Lett.*, 13 (2003) 2847
- [13] T. Takeda, K. Ikeda, Y. Mizuno, T. Ueda, *Chem. Pharm. Bull.* 35 (1987) 3558
- [14] P. Godzina, W.T. Markiewicz, *Collect. Czech. Chem. Com., Symp. Ser.* 2 (1999) 79
- [15] A. Kittaka, Ch. Horii, T. Kuze, T. Asakura, K. Ito, T. Miyasaka, J. Inoue, *Synlett.* (1999) 869
- [16] B. Catalanotti, A. Galeone, L. Mayol, G. Oliviero, M. Vara, *Nucleos. Nucleot. Nucl. Acids*, 10&11 (2001) 1831
- [17] S.T. Cheung, N.L. Benoiton, *Can. J. Chem.*, 55 (1977) 916

THE EFFECT OF CULTURE CONDITIONS ON TOXICITY OF 6-MERCAPTOPYRINE TO *CHLORELLA VULGARIS*

J. Sochacka, W. Wardas

Department of General and Analytical Chemistry, Medical University of Silesia,
Faculty of Pharmacy, Jagiellonska 4, 41-200, Sosnowiec, Poland
e-mail: jsochacka@slam.katowice.pl

INTRODUCTION

The thiopurine antimetabolite 6-Mercaptopurine (6-MP) is an analogue of the purine base hypoxanthine and is indicated for remission induction and maintenance therapy of acute lymphatic leukemia. The active metabolites of 6-MP alter cellular metabolism in a number of ways, including inhibition of purine biosynthesis *de novo* and incorporation into cellular RNA and DNA [1].

6-MP is practically insoluble in water, it dissolves in dilute solutions of alkali hydroxides and hydrochloric acid. The ionization constants, pK , for anion formation is 7.7 (in pyrimidine ring) and 11.8 (in imidazole ring) and for cation formation < 2.5 (in imidazole ring) [2]. The partition coefficient octanol-water, $\log P_{ow}$, is -0.19 [3]. 6-MP can exist in six tautomeric forms because of the protropic tautomerism of the imidazole ring and thione-thiol tautomerism of the pyrimidine ring. 6-MP in aqueous solution may exist in the equilibrium of tautomeric forms, but in alkaline medium is practically completely in anionic form (Fig. 1).

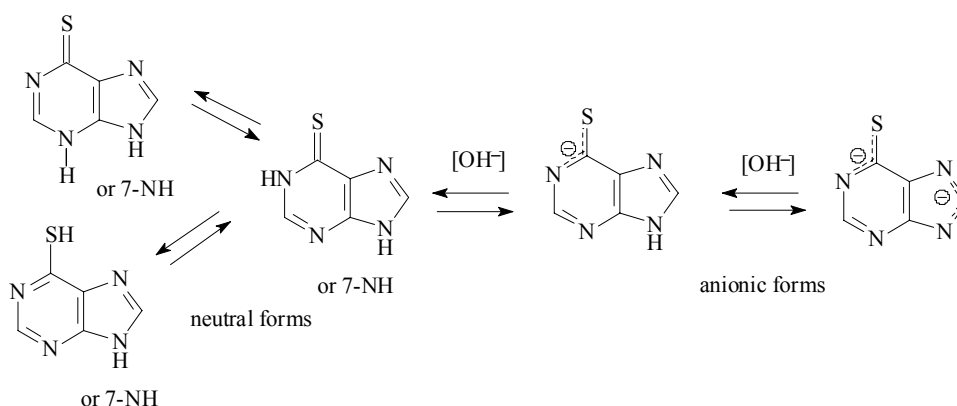


Figure 1. Structures of the neutral and anionic forms of 6-Mercaptopurine.

An adsorption and distribution of the drug are determined by its physicochemical properties e.g. its ionization and a partition coefficient between lipid and aqueous phases corresponding to drug lipophilicity. Non-ionized form of the drug is most often preferably dissolved in lipids and thus is easily transported through lipid membranes.

In recent studies about toxicity of new synthesized purine thioderivatives relative to *Chlorella vulgaris*, in which 6-MP was treated as reference compound, cultures were processed in culture media with pH of 6.7 – 7.0 [4, 5]. However *C. vulgaris* exhibit high resistance to pH changes of culture medium (even to 11.0). In this work the effect of increased pH on 6-MP toxicity was examined.

EXPERIMENTAL

Experiments were carried out with unicellular green alga *Chlorella vulgaris*, Beij., strain 264, Boehm and Borns 1972/1 CCALA (Czechoslovak Academy of Science). The cultures were conducted in 250 ml Erlenmeyer flasks with 50 ml of modified Kuehl-Lorenzen [6] liquid medium (enriched with 4% CO₂ and 3.85 mmol/l HCO₃⁻) at 24 ± 2°C and with continuous mixing using a magnetic stirrer. The cultures were synchronized by light-dark cycles (12-h light and 12-h dark period). The 6-Mercaptopurine (Sigma Aldrich) was added to algal medium as a solution in DMSO or 0.1 mol/l NaOH to obtain the required concentration (48.0, 96.0 and 144.0 mg/l). The final concentration of DMSO and NaOH did not inhibit nor stimulated the growth of *C. vulgaris*. The initial pH of the liquid medium was 6.7, 7.7 or 9.0. The tested cultures and control cultures (without the 6-MP) were conducted in parallel. Three replicates of each examined concentration and six replicates of the controls were examined. A growth of the cultures was monitored after 24 and 48 hs by measuring spectrophotometrically the optical density of the cell suspension at 680 nm. Growth inhibition and EC₅₀ were calculated according to ISO 8692 [7].

The distribution coefficient, $\log D$, which is a function of both its lipophilicity when non-ionized and the degree of ionization and is defined as the effective lipophilicity of a compound at a given pH, was calculated using eq. (1) [8]:

$$\log (P/D) - 1 = pK - \text{pH} \quad (1)$$

where: $pK = 7.72$ [5], $\log P = 0.62$ is the value calculated for neutral form of 6-MP from experimental values obtained with RPTLC method [9].

The amount (%), of 6-MP ionized form were calculated using the eq. (2) [10]:

$$\% \text{ ionized} = 100/[1 + 10^{(pK - \text{pH})}] \quad (2)$$

Absorption spectra of the 6-MP in standard solutions of pH 5.0 – 13.0 and in liquid media (after the end of the cycle) were recorded between 220 and 380 nm using Jasco (V-530) UV VIS Spectrophotometer.

RESULTS

The calculated distribution coefficient ($\log D$) and the percentage of 6-MP ionized form in solutions of pH range 5.0 – 9.0 are presented in Table 1. The presented results show that effective lipophilicity of 6-MP is depended to solution pH and will decrease if pH and amount of ionized form increases.

Table 1. The effect of pH on the physicochemical properties of 6-MP

	pH											
	5.0	5.5	6.0	6.5	6.7	7.0	7.5	7.7	8.0	8.5	9.0	13.0
% ionized	0.2	0.6	1.9	5.7	8.7	16.0	37.6	49.0	65.5	85.6	95.0	-
$\log D$	0.61	0.61	0.60	0.58	0.57	0.53	0.40	0.32	0.15	-0.24	-0.69	-
λ_{max}	321.8	-	-	-	-	319.5	-	-	-	-	313.1	308.6

The λ_{max} values of 6-MP standard solutions in a pH range of 5.0 – 13.0 determined according to UV spectra calibration curves (ultraviolet spectra) are also presented in Table 1. The changes of UV maximum absorption and hypsochromic shift of λ_{max} of about 13 nm for 6-MP solutions are related to formation of monoanionic form from neutral one and dianionic form from monoanionic one.

The characteristic of *C. vulgaris* culture growth is presented in Table 2 as percentage of growth inhibition related to control culture. In the same table the λ_{\max} values determined for 6-MP in a culture media are presented that confirms various ionization state of this compound. The determined values of 6-MP toxic concentration related to *C. vulgaris* are expressed as EC50 (mg/l). These results indicate that toxicity of 6-MP is depended to pH of culture media. The EC50 value for culture media of pH 9.0 was twice higher than one determined for culture media of pH 6.7.

Table 2. EC50 values characterizing toxicity of 6-MP to *C. vulgaris* cultured in media of various pH

6-MP concentration in a culture (mg/l)	Type of the culture tested					
	DMSO, pH 6.7		NaOH, pH 7.7		NaOH, pH 9.0	
	% inhibition ^a					
	λ_{\max} [nm] of 6-MP in the liquid medium					
48.0	33.3	λ 321.6	4.5	λ 317.8	5.5	λ 314.4
96.0	49.3	λ 321.4	33.5	λ 316.4	16.2	λ 313.4
144.0	66.2	λ 321.6	46.2	λ 316.4	45.3	λ 312.5
EC50 (mg/l)	88.3		140.7		171.7	

^a inhibition percentage related to the control culture

DISCUSSION

Obtained results indicate that pH of culture media influences the toxicity of 6-MP and the ionized forms of 6-MP were significantly less toxic for *C. vulgaris*. This phenomenon may be caused by decreased lipophilicity of anionic form relative to neutral one. Lipophilicity is an important property affecting the bioactivity of drugs and increasing lipophilicity usually correlates with increasing biological activity. The transport rate and the amount of transported substance into the cell is positively correlated with a partition coefficient $\log P$. The $\log P$ depends on pH and degree of dissociation, which directly corresponds to the amount of dissociated form. Non-ionized and lipophilic substance is easily transported into the cell because the cell membrane is a selectively permeable lipid bilayer. However, it has only a very low permeability to ionic molecules and thus their concentration inside the cell will be lower.

The other cause of decreased toxicity of dissociated 6-MP might be its impaired interaction with DNA. 6-MP is an antimetabolite of natural purine base and may be incorporated into DNA as deoxy-6-thioguanosine (S6G) instead of guanine and thus modify structural properties of DNA duplex.

Bohon J. [11] and Somerville L. [12] have shown, that active metabolite S6G (in keto form) was incorporated into DNA. This required formation of weakened Watson-Crick hydrogen bonds which led to S6G-C and S6G-T pairs (Fig. 2). However, S6G-C is highly favoured because of triple hydrogen-bond.

It can be concluded, that 6-MP monoanionic form generated during N(1)-H dissociation at pH 7.7 and 9.0 may not combine with natural base by forming Watson-Crick hydrogen bonds. This is a reason why this form S6G does not incorporate into DNA duplex and, in consequence, does not show cytotoxic activity to *C. vulgaris*.

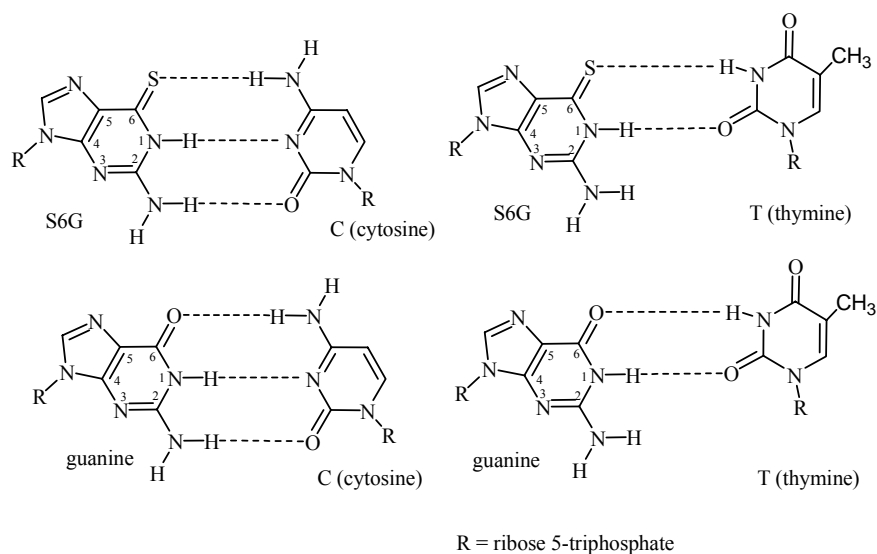


Figure 2. Base pair configuration for S6G-C, S6G-T and G-T and canonical G-C [11].

REFERENCES

- [1] J.E. Polifka, J.M. Friedman, *Teratology*, 65 (2002) 240.
- [2] D.J. Brown, S.F. Mason, *J. Chem. Soc.*, (1957) 682.
- [3] P.N. Craig, in: *Comprehensive Medicinal Chemistry*, C. Hansch (ed.), vol. 6, Pergamon Press, Oxford 1990, p. 897.
- [4] A. Kowalska, J. Sochacka, *Acta Polon. Pharm – Drug Res.*, 60 (2003) 144.
- [5] J. Sochacka, A. Kowalska, *Ann. Pol. Chem. Soc.*, 3(2) (2004) 735.
- [6] A. Kuehl, H. Lorenzen, in: *Methods and Cell Physiology*, D. M. Prescott (ed.), N. Y. and London 1964, p. 152.
- [7] ISO 8692, International Organization for Standardization, Geneva Switzerland 1989.
- [8] B. Malawska, K. Kulig, M. Wiśniewska, *J. Planar Chromatogr.*, 13 (2000) 187.
- [9] J. Sochacka, A. Kowalska, *J. Planar Chromatogr.*, 19 (2006) 320.
- [10] A. Albert, E.P. Serjant, *The Determination of Ionization Constants*, 3rd edn, Chapman and Hall, New York 1984, p. 203.
- [11] J. Bohon, C. Santos, *Nucl. Acids Res.*, 31 (2003) 1331.
- [12] L. Somerville, E. Krynecki, *J. Biol. Chem.*, 278 (2003) 1005.

INVESTIGATIONS OF THE PALLADIUM – 4-VINYLPYRIDINE AND PALLADIUM – POLY(4-VINYLPYRIDINE) SYSTEMS WITH THE METHODS OF COMPUTATIONAL CHEMISTRY

Joanna Stawowska, Witold M. Bartczak

*Institute of Applied Radiation Chemistry, Technical University of Łódź,
Wróblewskiego 15, Łódź, Poland*

The research project is devoted to computer modelling of the structure and electron properties of the Pd atoms bound to a poly(4-vinylpyridine) support. P4VP is an important functional polymer. The pyridine ring contains tertiary nitrogen atom which endows this polymer with distinct features. For instance P4VP, due to its adsorption on the metal surface, is a corrosion inhibitor of mild steel in HCl. The electric conductivity of P4VP is also of interest and causes its application in modern batteries and electric charge sources.

The quantum calculations of the present work have been performed using the DFT method (Gaussian 98 code). The hybrid, gradient-corrected B3P86 functional for the exchange and correlation and the LANL2DZ basis set have been used in our calculations. The basis set (the Dunning-Huzinaga DZ basis plus the core potentials for the elements beyond the first row, see e.g. Gaussian 98 help files) has been extensively applied in the calculations involving transition elements. The preliminary calculations performed up to now include:

(1) The DFT calculations of the 4-vinylpyridine molecule and its dimer. The optimisation runs resulted in full information about the structure, electronic properties, charge distribution, etc., for the molecules. As an example of the results, the structure of the 4-VP dimer is shown in Figure 1. It is worth noting that the Mulliken charge on the nitrogen atoms is negligible, $-0.01 e$.

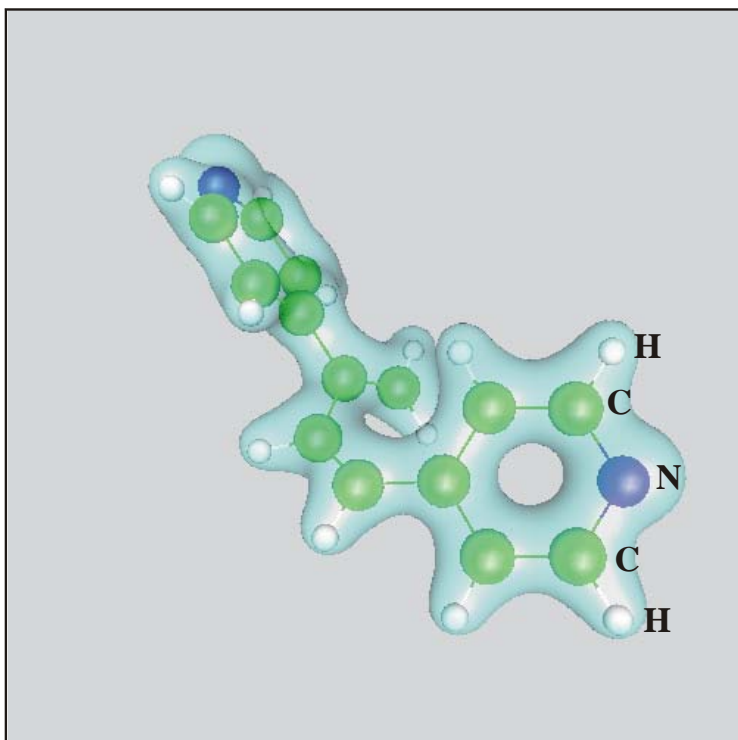


Fig. 1. *The structure of the 4-VP dimer from the DFT calculations.*

The spheres show the positions of the C, N and H atoms, as labelled in the figure. The isosurfaces of the electron density drawn at $\rho=0.08 e/\text{\AA}$ are shown in the figure.

(2) The DFT calculations of one or two Pd atoms interacting with 4-VP and its dimer. The purpose of the calculations was to find favourable sites for the Pd binding to the polymer and investigate the influence of the Pd atom on the electronic properties of the 4-VP monomer and dimer.

An extended series of calculations have been performed: single VP with 1 Pd atom at different positions, VP with 2 Pd atoms and 3 Pd atoms, VP dimer with 2 Pd atoms at different positions. The results (for single VP and 1 Pd atom) indicate that the favourable site for the Pd binding is in the vicinity of the N atom, the binding energy is -1.04 eV. For the case of the Pd position above the center of the C-C bond the binding energy is -0.79 eV. The Mulliken charge on the Pd atom is -0.088 e and +0.073 e , respectively. For the case of a single VP and 2 Pd atoms, one of the Pd atoms is bound to the N atom and the other Pd can be bound to a C atom. The binding energy for different structures are: -2.24 eV, -2.32 eV, -1.86 eV, per two atoms.

More interesting structures appear when 2 Pd atoms interact with the VP dimer. The structure with the Pd atoms in the vicinity of the N atoms is shown in Figure 2 A. The charges are -0.085 e , the binding energy is -2.07 eV per two Pd.

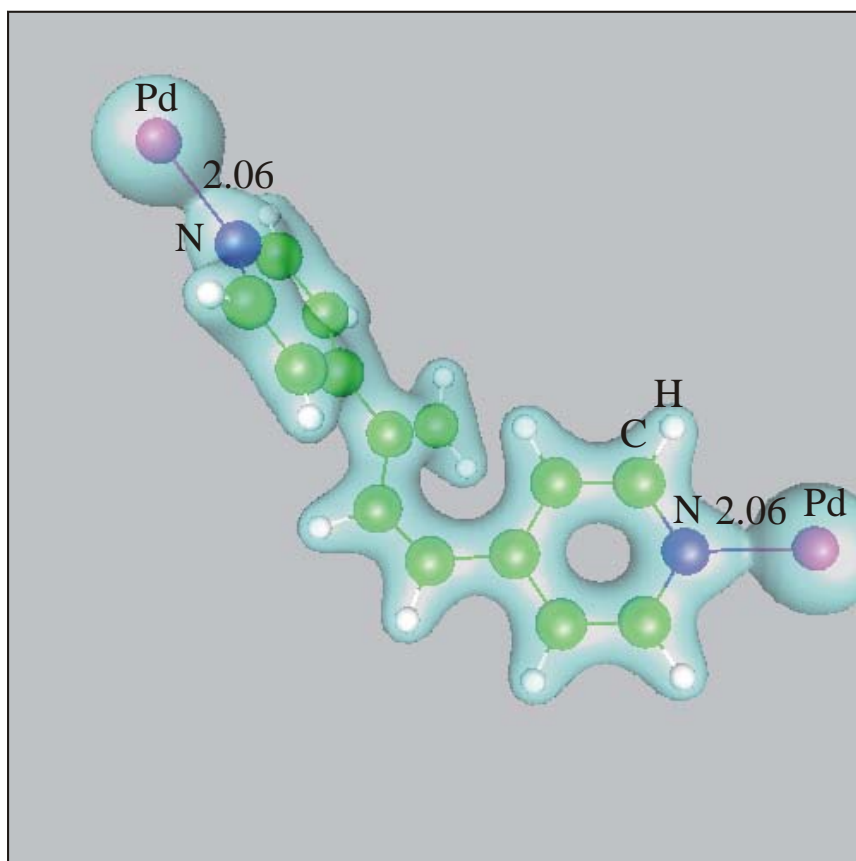


Fig. 2A. The structure of the 4-VP dimer with 2 Pd atoms bound at the nitrogen sites obtained from the DFT calculations. The bond lengths are given in Å. The spheres show the positions of the C, N, Pd and H atoms, as labelled in the figure. The isosurfaces of the electron density are drawn at $\rho=0.08 e/\text{Å}$.

The structure with the Pd atoms above the centres of the C-C bonds (in the rings) is shown in Figure 2 B. The charges are very close to 0, the binding energy is -2.08 eV per two Pd, almost identical with the former structure.

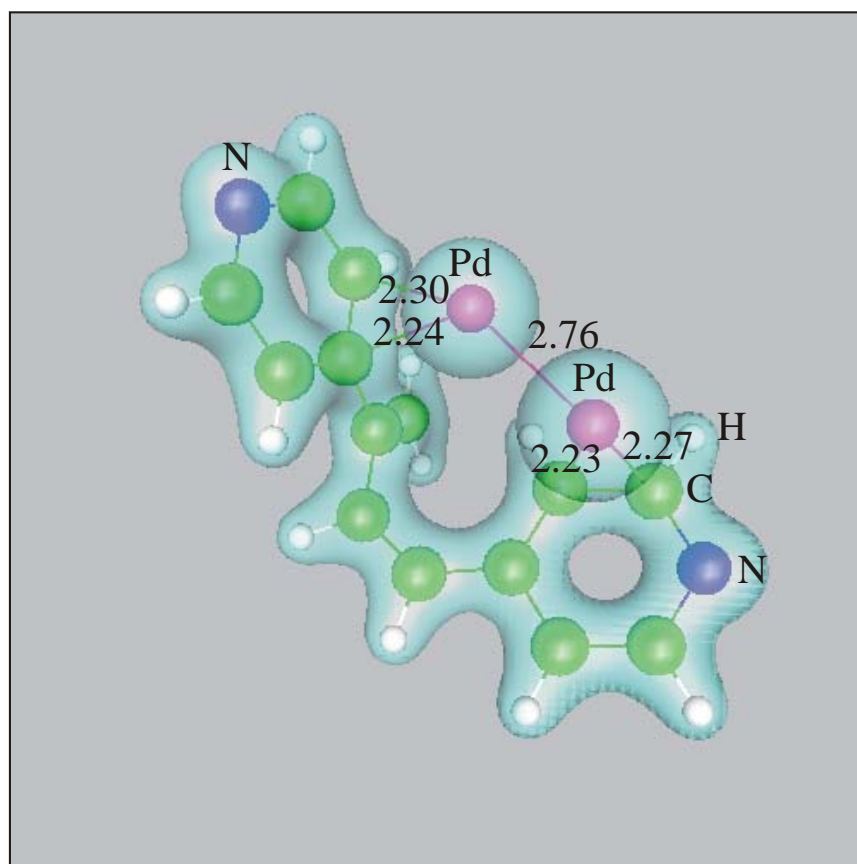


Fig. 2B. The structure of the 4-VP dimer with 2 Pd atoms placed above the centers of the C-C bonds. The bond lengths are given in Å.

(3) The DFT calculations of the interaction of Pd-4VP, 2Pd-4VP, Pd-(4VP)₂, 2Pd-(4VP)₂ systems with additional atoms and small molecules: H, Cl, 2Cl, Cl₂, 2H, H₂, HCl, Cl+H, etc., adsorbed on the polymer units.

The calculations indicate that the Pd atoms bound to polymer units make very powerful reactive sites. For all the cases the atoms and molecules added to Pd - 4 VP complexes migrated to the vicinity of the Pd atoms and were trapped at these centers - such structures have the lowest total energy. On account of a large number of the valence electrons the Pd atom plays a role of an electron pool. An example of the structure obtained as a result of optimization of Cl₂ molecule added to 2Pd-(4VP)₂ complex is given in Figure 3. The Cl₂ molecule dissociates and the Cl atoms migrate until they are bound to the Pd atoms of the complex. The chlorine atoms have the charge -0.32 e, the Pd atoms become slightly positive +0.12 e. The binding energy of Cl atoms (with respect to a free Cl₂ molecule) is very high, -4.73 eV. The Pd-N bond is only slightly stretched by the presence of the Cl atom: from 2.06 Å to 2.09 Å. We found similar behaviour of all the atoms and molecules listed above.

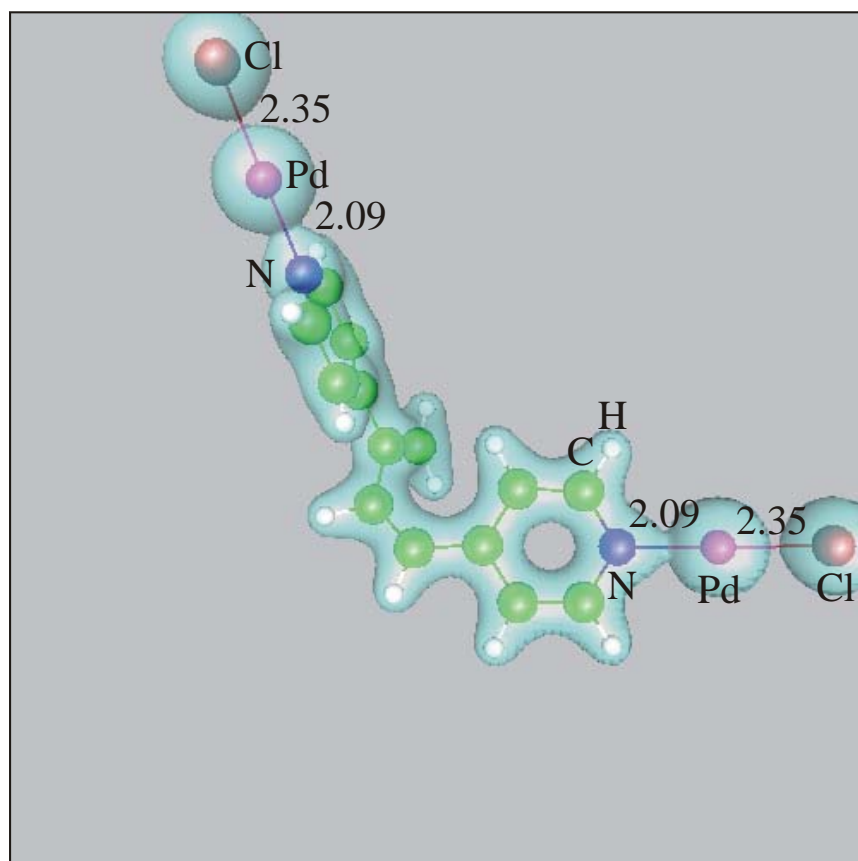


Fig. 3. The structure of the $2\text{Pd}-(4\text{VP})_2$ complex (see Fig. 2A) after addition of the Cl_2 molecule and optimization of the molecular system. The bond lengths are given in Å. The isosurfaces of the electron density are drawn at $\rho=0.08 \text{ e}/\text{Å}$.

Acknowledgments: The present work was supported by the grant PBZ-KBN-116-T09/2004. The authors wish to thank Professor Alicja Drelinkiewicz for helpful suggestions concerning the present project.

INVESTIGATIONS OF THE DIHYDROGEN DISSOCIATION
IN CONTACT WITH PALLADIUM CLUSTERS
BY THE QUANTUM MOLECULAR DYNAMICS.
THE ADMP CALCULATIONS PERFORMED ON THE DFT LEVEL

Joanna Stawowska, Witold M. Bartczak

*Institute of Applied Radiation Chemistry, Technical University of Łódź,
Wróblewskiego 15, Łódź, Poland*

Introduction and methods

An important model of catalysis is represented by the behaviour of the simplest molecule, H_2 , dissociating at the surfaces of the transition and noble metals and their alloys. Subsequent migration of atomic hydrogen over the metal surface and its reactions with atoms or molecules adsorbed on the surface form principal parts of mechanism of numerous catalytic processes.

In the present work the quantum calculations of interaction of the molecular hydrogen with Pd clusters have been performed. Two kinds of the calculations have been performed: 1) the static quantum chemistry calculations, and 2) the quantum molecular dynamics simulation.

The calculations have been based on the gradient-corrected methods of the Density Functional Theory with the hybrid functionals B3P86, B3LYP, B3PW91. For all the calculations reported here the LANL2DZ double-zeta basis set was used. The calculations have been performed using the Gaussian 2003 code.

Potential energy surface calculations

The calculations of the potential energy surface (PES) for the hydrogen molecule placed over the Pd_5 clusters with the planar structure of the Pd elementary cell have been performed (see Figure 1). It was found that the H_2 molecule which is parallel to the metal plane dissociates (in principle without activation barrier) in contact with metal and its H atoms are bound to the cluster. There is a small potential barrier for rotation in the plane and very small barrier for rotation from horizontal to vertical position of H_2 . The rotation barriers do not exceed 1 – 2 kcal/mol.

Figure 1 shows the PES for the B3P86 model. The H_2 molecule is parallel to the Pd plane with H-H bond oriented along the diagonal of the Pd-Pd bonds. The configuration coordinates are: d_{HH} – the internuclear distance in the H_2 molecule, and Z – the distance of the centre of the H-H bond to the Pd plane. The PES was sampled to the following ranges of the coordinates: $0 \leq d_{HH} \leq 3.89 \text{ \AA}$, $0 \leq Z \leq 3.0 \text{ \AA}$. The energy surface is plotted for the difference between energy of the H_2Pd_5 cluster and energy of the separate Pd_5 cluster and H_2 molecule. The figure shows only the part of the PES for negative energy.

The PES shows clearly the activationless dissociation process. The dissociation path is marked by the white line with crosses. The dissociation path is better visualized in the Figure 2 as a function of the d_{HH} distance. The adsorption energy of the H_2 molecule with bond length 0.74 \AA is about -0.6 eV . The increase of the bond length leads initially to a slight decrease of energy but above $d_{HH}=1.2 \text{ \AA}$, when the H-H bond breaks, the energy rapidly decreases. The stable positions of the H atoms are near the edges of the cell, for d_{HH} about 3.5 \AA . The total energy of adsorption and dissociation of a H_2 molecule is -1.77 eV (40.8 kcal/mol) with respect to energy of isolated H_2 i Pd_5 .

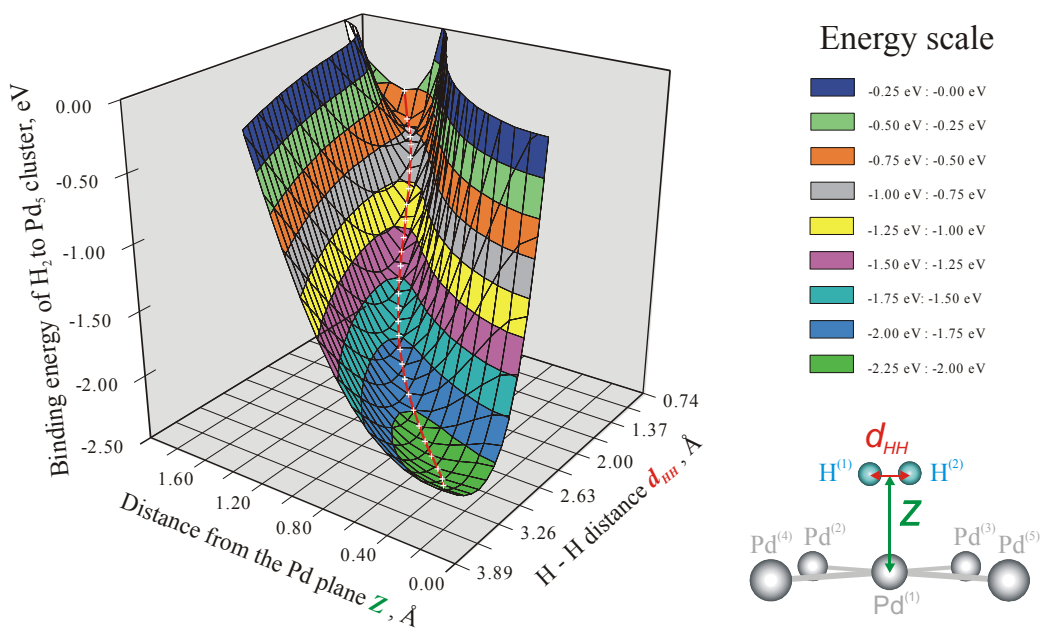


Fig. 1. Potential Energy Surface for H_2 molecule bound to the planar Pd_5 cluster (DFT/B3P86).

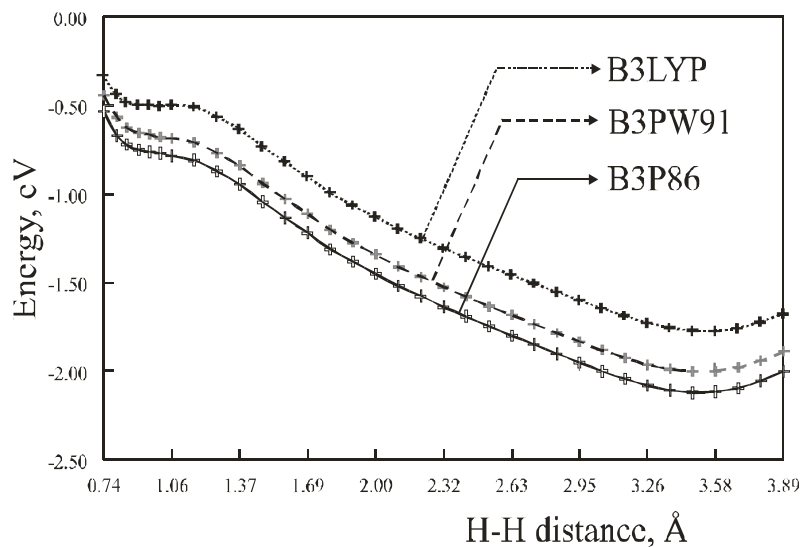


Fig. 2. Energy of the H_2 - Pd_5 cluster along the dissociation path of the H_2 molecule. The calculations were performed for three hybrid functionals as marked in the figure.

It is interesting to note that while the calculations based on the B3P86 and B3PW91 functionals predict the activationless dissociation of H_2 , the B3LYP calculation results in a very small activation barrier, of the order of 0.01 eV.

Quantum Molecular Dynamics calculations

The dynamic calculations of the H₂ molecule in contact with the clusters cut from the (100) Pd surface have been performed using the ADMP method [1,2]. This method performs a classical trajectory calculation using the Atom Centered Density Matrix Propagation molecular dynamics model. ADMP belongs to the extended Lagrangian approach to molecular dynamics using Gaussian basis function and propagating the density matrix. The best known method of this type is Car-Parrinello (CP) molecular dynamics, in which the Kohn-Sham molecular orbitals, ψ_i , are chosen as the dynamical variables to represent the electronic degrees of freedom in the system.

The simulations list: (1) two cases of H₂ dissociation in contact with the planar Pd₅ cluster shown in Fig. 1. In the first case the H₂ molecule was positioned directly above the Pd-Pd bond centre, in the second case the H₂ was on top of the central Pd atom, initially at a distance of 1.5 Å. (2) H₂ dissociation in contact with the planar Pd₇ cluster with the structure described as two square cells joined together by the central Pd atom. (3) H₂ dissociation in contact with the nonplanar Pd₉ cluster with the structure of Pd₇ plus two Pd atoms from the subsurface layer placed below the centers of the square cells. In the latter cases the H₂ was on top of the central Pd atom, initially at a distance of 1.5 Å.

Figure 3 shows the geometry and electron density distribution of the H₂ - Pd₉ system at selected times: 2.8 fs, 7.6 fs, 14.0 fs, 20.6 fs and 36.8 fs. The H-H distance d , which is the parameter monitoring the degree of the H₂ dissociation, is given for each structure.

Figure 4 shows the evolution of the energy of the systems (with respect to the energy of isolated H₂ i Pd_n) as a function of time. The simulations were performed with the timestep of 0.2 fs. The lower figure shows the H₂ - Pd₉ system, the upper right figure the H₂ - Pd₇ system and the upper left figure H₂ - Pd₅ system. The system temperatures varied from 77 K to as much as 3000 K. The H₂ - Pd₇ evolution shown in the figure corresponds to 773 K, the remaining two cases correspond to 3000 K.

The plots of the figure show that the typical time necessary to complete the H₂ dissociation process is about 20 fs if we define the time window from the first negative binding energy to the onset of the energy fluctuations around the stabilized value. However, the real time of the process is usually much longer (by factor of 2-3) because for most of the initial H₂ configurations the energy is positive and we frequently observe the escape of the hydrogen molecule. This is due to the rotation energy barriers mentioned in the PES part of the calculations. The longer time window (of about 40 fs) was shown for H₂ - Pd₉ system in the upper figure. It is necessary to underline that each simulation course gives different energy evolution curve, mostly in the initial part but also in the fluctuation stage and the 20 fs value corresponds to an average.

References

- [1] D. L. Thompson, in: Encyclopedia of Computational Chemistry, P. v. R. Schleyer, N. L. Allinger, P. A. Kollman, T. Clark, H. F. Schaefer III, J. Gasteiger, and P. R. Schreiner (eds), Wiley, Chichester, 1998. p. 3506.
- [2] H. B. Schlegel, S. S. Iyengar, X. Li, J. M. Millam, G. A. Voth, G. E. Scuseria, and M. J. Frisch, *J. Chem. Phys.* 117 (2002) 8694.

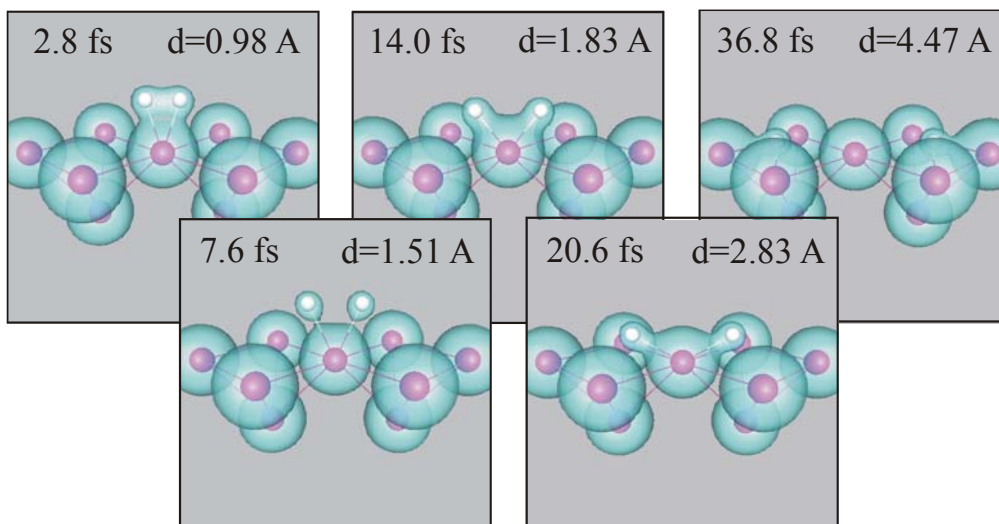


Fig. 3. A series of transitory structures appearing in the course of the dissociation of H_2 in contact with Pd_9 cluster. The color of the spheres marks the Pd atoms (mauve) and the H atoms (white). Isosurfaces of the electron density ($\rho=0.08 e/\text{\AA}^3$) are shown with cyan color. The time from the start of the simulation and actual H-H distance are given in for each figure.

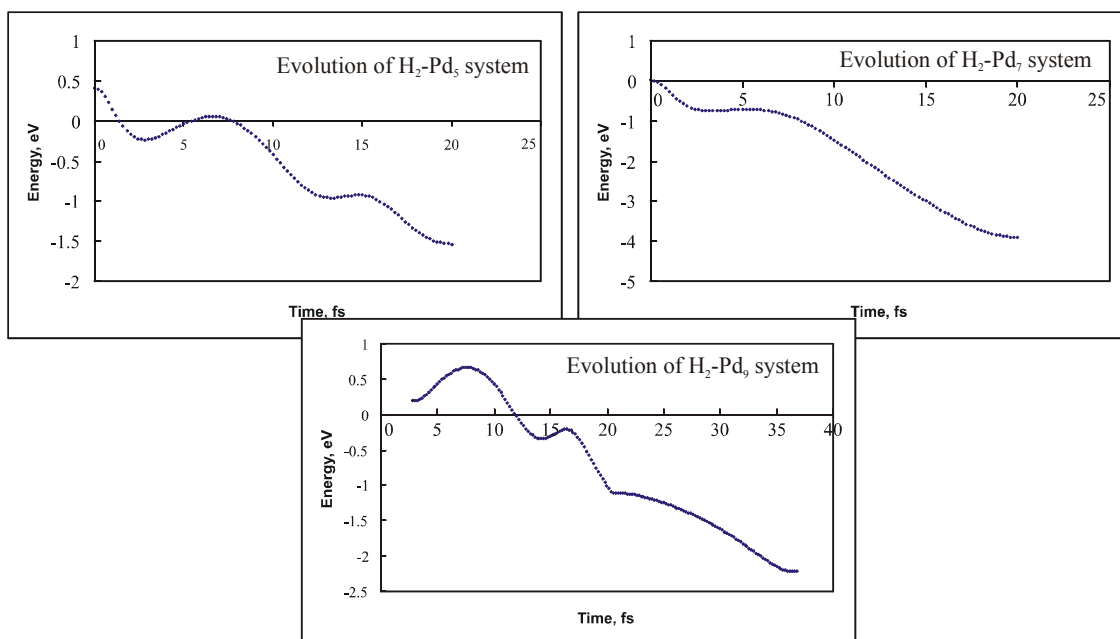


Fig. 4. Evolution of energy of the $H_2 - Pd_n$ systems (with respect to the energy of isolated H_2 i Pd_n) as a function of time obtained from the ADMP quantum simulations. The lower figure shows the $H_2 - Pd_9$ system, the upper right figure the $H_2 - Pd_7$ and the upper left $H_2 - Pd_5$ system.

INVESTIGATIONS OF THE PALLADIUM – POLYANILINE SYSTEM WITH THE METHODS OF COMPUTATIONAL CHEMISTRY

Joanna Stawowska, Witold M. Bartczak

Institute of Applied Radiation Chemistry, Technical University of Łódź,

Wróblewskiego 15, Łódź, Poland

The research project is devoted to computer modelling of the structure and electron properties of the Pd clusters on a polyaniline (PANI) support. The system is considered as a model of the metal catalyst on a conducting polymer support.

PANI doped with Pd has been applied as a heterogeneous catalyst for hydrogenation of nitrobenzene and of the C≡C bond in hexine. Recently, the role of the catalyst in hydrogenation of 2-ethylantrachinone in liquid phase has been investigated [1].

Polyaniline is usually a combination of the oxidized and reduced forms. The 50 % combination, emeraldine, is stable in natural conditions. For the modelling purpose it is assumed that the periodically repeated structure is composed of four aromatic rings and four nitrogen atoms.

The project applies advanced methods of quantum chemistry (the methods based on the density functional theory in the gradient-corrected version). The calculations have been performed using the Gaussian 98 code, the B3LYP hybrid correlation-exchange functional and the standard Lanl2DZ basis set have been selected for the calculations.

The oxidized, reduced and mixed forms of the polyaniline rings have been taken into account in the calculations which included the geometrical structure optimization, the electron density distributions, the distribution of the partial electrostatic charges. At the present stage, particular attention has been paid to the interaction of PANI with Pd atoms and with HCl molecules.

The parts of the project completed up to now list:

(1) The calculations of the structure of polyaniline support. The calculations have been performed for the aniline monomer, dimers, trimers and tetramers (the latter either in the form of a single chain or two interacting dimers) with or without hydrogen atoms at the N sites. The calculations were analyzed in order to find the evolution of the structure and electronic properties of aniline unit while the number of units is increased. The polyaniline forms the twisted chain, the planes of the neighbouring rings are twisted by about 42°.

(2) The calculations of a single Pd atom and small clusters of Pd atoms interacting with aniline and its dimers, trimers and tetramers. A series of the energy optimisation runs have been performed for the Pd/aniline systems. The purpose of the calculations was to find favourable sites for the Pd adsorption on the polymer. An example of the optimum structure of the trimer with a single Pd atom adsorbed is shown in Figure 1. Two favourable trapping sites with the lowest energy have been found: a) the Pd atom is adsorbed over the centers of the C-C bonds of the aniline rings with the distance of 2.19 Å from the C atoms and b) the Pd atom is bound to the bridge nitrogen atom with the distance of 2.06 Å between Pd and N atom. The structures of the Pd sites, together with the electron density distributions, are given in Figure 2.

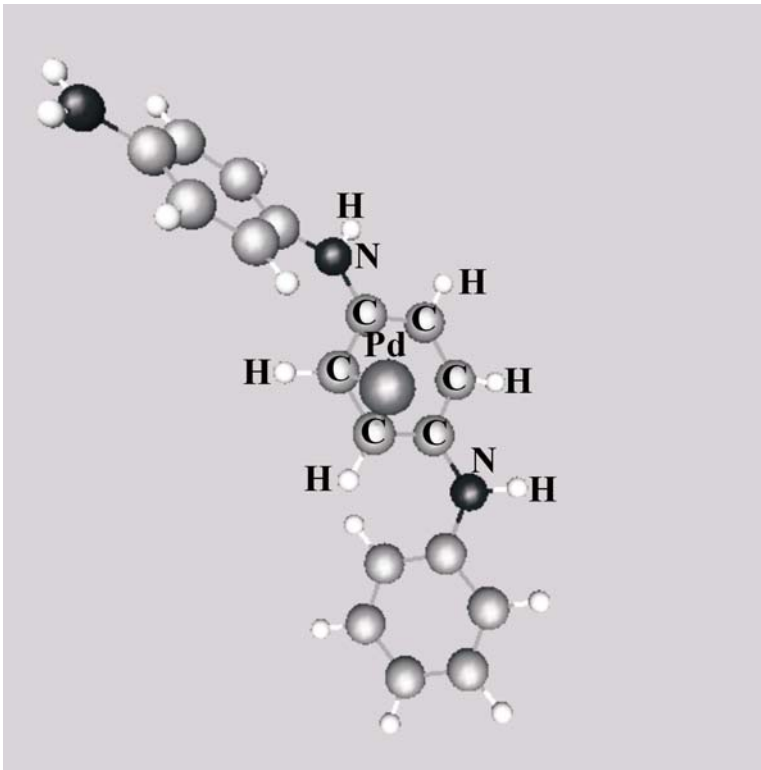


Fig. 1. The structure of the aniline trimer with the Pd atom adsorbed at the central ring obtained from the calculations.

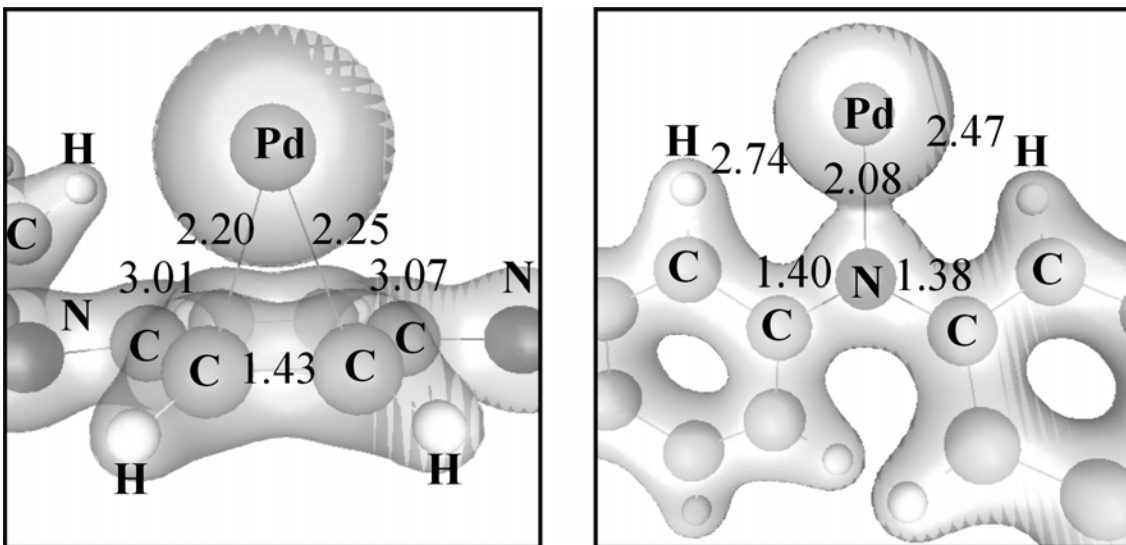


Fig 2. Geometric structure of the Pd trapping sites on the polyaniline chain and the isosurfaces of the electron density drawn at $\rho=0.08 \text{ e}/\text{Å}$. The interatomic distances are given in Å.

Left: the Pd site at the center of the edge of the aniline ring. Right: the Pd site at the nitrogen atom.

Optimization of the system composed of 3 Pd atoms and aniline dimer results in the structure shown in Figure 3. The interatomic distances between the Pd atoms are 2.77 and 2.76 Å and resemble the nearest neighbourhood distance 2.75 Å in the Pd crystal. The Pd-Pd-Pd angle is 132.64°. The first Pd atom is bound to the C atom (bond length 2.15 Å), the second Pd with the aniline bridge N atom (bond length 2.14 Å) and the third one again with the C atom (bond length 2.19 Å). The Mulliken charges are respectively 0.055 e (Pd1), -0.071 e (Pd2) and 0.038 e (Pd3), the total binding energy of the Pd atoms is -3.75 eV which makes -1.25 eV on the average.

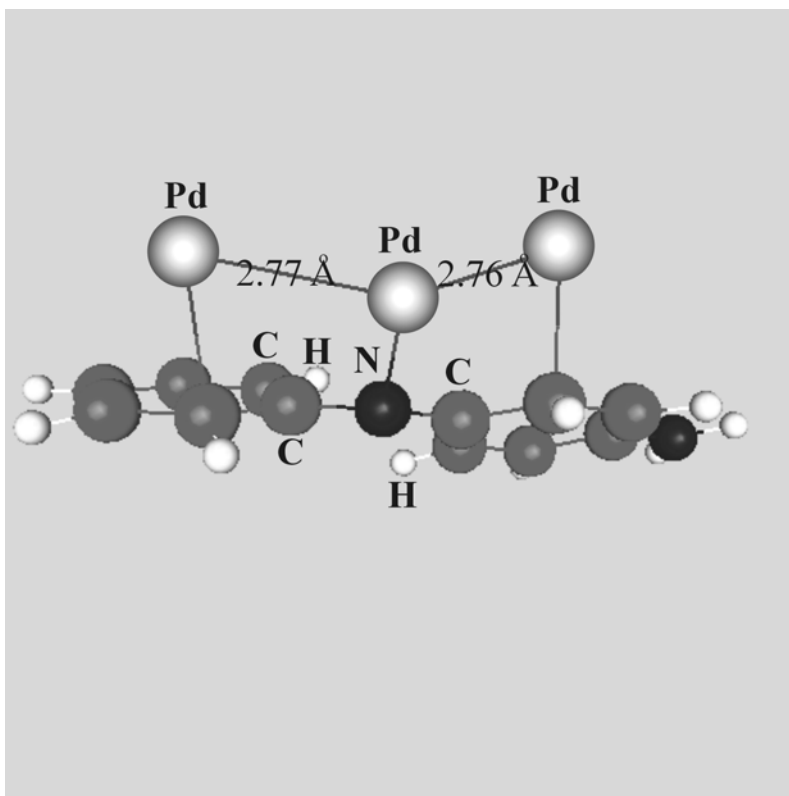


Fig. 3. The structure of the aniline dimer with 3 Pd atoms adsorbed.

Another structure calculated for 3 Pd atoms interacting with the aniline trimer represents the Pd atoms positioned over the C atoms and the Pd - Pd distances are 2.82 Å and 2.73 Å, total binding energy slightly lower: -3.62 eV and very small charges on the Pd atoms. Optimization of the 3 Pd plus aniline trimer system with additional H atoms bound to the N atoms of the aniline molecule (reduced form) gives a structure which is more distorted with respect to the trimer without palladium than it was in the case of the oxidized form. The Pd - Pd distances are 2.82 Å and 2.78 Å, total binding energy is now significantly lower: -3.29 eV and the charges on the Pd atoms are also very small.

The results of the calculations indicate the possibility of the Pd adsorption along the polyaniline chain as an almost regular array with the Pd-Pd distances very close to the Pd-Pd distance in the Pd crystal. We however found another stable configuration of the Pd polyaniline system. The optimization of two dimers results in a structure with the dimers bound together by the Pd atom in the N-Pd-N configuration. The Pd-N bond

length is 2.01 Å for the both nitrogen atoms, the Mulliken charge on Pd is 0.13 *e* while on the N atoms is -0.40 *e*. The binding energy of the Pd atom is very high: -2.85 eV.

(3) The next part of the project concerns the interaction of small molecules with polyaniline and Pd-doped polyaniline. As a preliminary approach to this part we started the calculations with the optimization of a series of the structures of HCl plus aniline tetramer. All the structures represent predissociation state of HCl. In the first case the HCl molecule was placed in the vicinity of the nitrogen atom connecting the third and fourth aniline ring (the reduced form). After optimization the H atom becomes attached to the nitrogen (the bond length 1.1 Å) while the distance between the H atom and the Cl atom is increased to 1.84Å. The HCl binding energy is -1.12 eV. The second case corresponds to the HCl molecule in the vicinity of the N atom connecting the second and the third ring. The N-H distance is 1.11Å, the H-Cl distance is 1.82Å, the HCl binding energy is -1.09 eV. Another optimization run corresponds to the geometry of the first case but the aniline tetramer is now in fully oxidized form. The N-H distance is 1.11Å, the H-Cl distance is 1.82Å, the binding energy is -1.02 eV. The last case of the series represents the tetramer with the single N atom in oxidized form. The N-H distance is now 1.09Å, the H-Cl distance is 1.89Å, and the binding energy is relatively high -1.30 eV.

The calculations concerned also two HCl molecules interacting with the 50 % oxidized tetramer. The binding energy per two molecules is -1.99 eV.

The calculations which include the Pd-atom bound to aniline clusters and HCl molecule are currently performed in our laboratory.

[1] A. Drelinkiewicz, J. Stejskal, A. Waksmundzka, J. W. Sobczak, Synth. Met. 140 (2004) 233.

Acknowledgments: The present work was supported by the grant PBZ-KBN-116-T09/2004. The authors wish to thank Professor Alicja Drelinkiewicz for helpful suggestions concerning the present project.

INTERACTION OF SELECTED FREON MOLECULES WITH PALLADIUM SURFACE. A DFT STUDY

Joanna Stawowska, Witold M. Bartczak

Institute of Applied Radiation Chemistry, Technical University of Łódź,

Wróblewskiego 15, 93-590 Łódź, Poland

The report presents the preliminary calculations of the adsorption, activation and dissociation of freon molecules: CCl_2F_2 and $\text{C}_2\text{Cl}_2\text{F}_2$ on the surface of palladium catalysts.

Freons represent the class of organic compounds which are very difficult to remove from environment. Their aggressive interaction with the atmospheric ozone layer has very serious consequences. The organic molecules containing halogen atoms, particularly chlorine, are usually toxic, carcinogenic and much effort has been directed towards neutralization of these compounds. Catalytic hydrodechlorination represents very important method of transformation of the chlorine compounds towards less aggressive molecules. The catalysts for this process are still investigated but it is already known that palladium makes the catalysts of very high activity and selectivity in the processes which remove the chlorine atoms from the freon molecules [1,2]

Methodology of the Calculations

The quantum calculations of the present work have been performed using the DFT method (Gaussian 98 code). The hybrid, gradient-corrected B3P86 functional for the exchange and correlation and the LANL2DZ basis set have been used in our calculations. The basis set (the Dunning-Huzinaga DZ basis plus the core potentials for the elements beyond the first row, see e.g. Gaussian 98 help files) has been extensively applied in the calculations involving transition elements.

A series of the optimisation runs have been performed for CCl_2F_2 and $\text{C}_2\text{Cl}_2\text{F}_2$ molecules in contact with the metal cluster. However, we want the metal part of the system to simulate the (100) surface of the fcc Pd crystal, therefore the metal positions have been frozen during the optimization. In this way we ignore the metal surface relaxation but if the restraints are released, the Pd positions shift to such an extent that the cluster structure does not resemble the surface structure any more. The optimized structures of freon molecules, in most cases representing the dissociated or predissociated molecule, have been obtained and the isosurfaces of the electron density have been plotted.

Results and Discussion

Interaction of CCl_2F_2 molecule with metal clusters

The extensive calculations have been performed for the CCl_2F_2 molecule in different orientations with respect to the Pd_7 cluster. The molecule with the F atoms pointing down towards the metal cluster is only weakly adsorbed (this is a local energy minimum and the configuration is stable) but its forced reorientation to the position with the Cl atoms down and F atoms up leads to strong adsorption. The CCl_2F_2 molecule dissociates then to CF_2 and two Cl atoms. The process proceeds without activation barrier. Figure 1 shows a series of structures appearing in the course of optimization. The electron density distribution is shown together with the geometrical structures. The

lower right figure shows the energy evolution in the course of dissociation from CCl_2F_2 to $\text{CF}_2 + 2\text{Cl}$.

The CF_2 radical has stretched bonds (1.39 and 1.40 Å). The C atom is placed over the center of the Pd-Pd bond with the C-Pd distances 1.98 and 1.97 Å. The structure, together with the electron density, is shown in Fig. 2 A. The binding energy of CCl_2F_2 after dissociation is -8.55 eV .

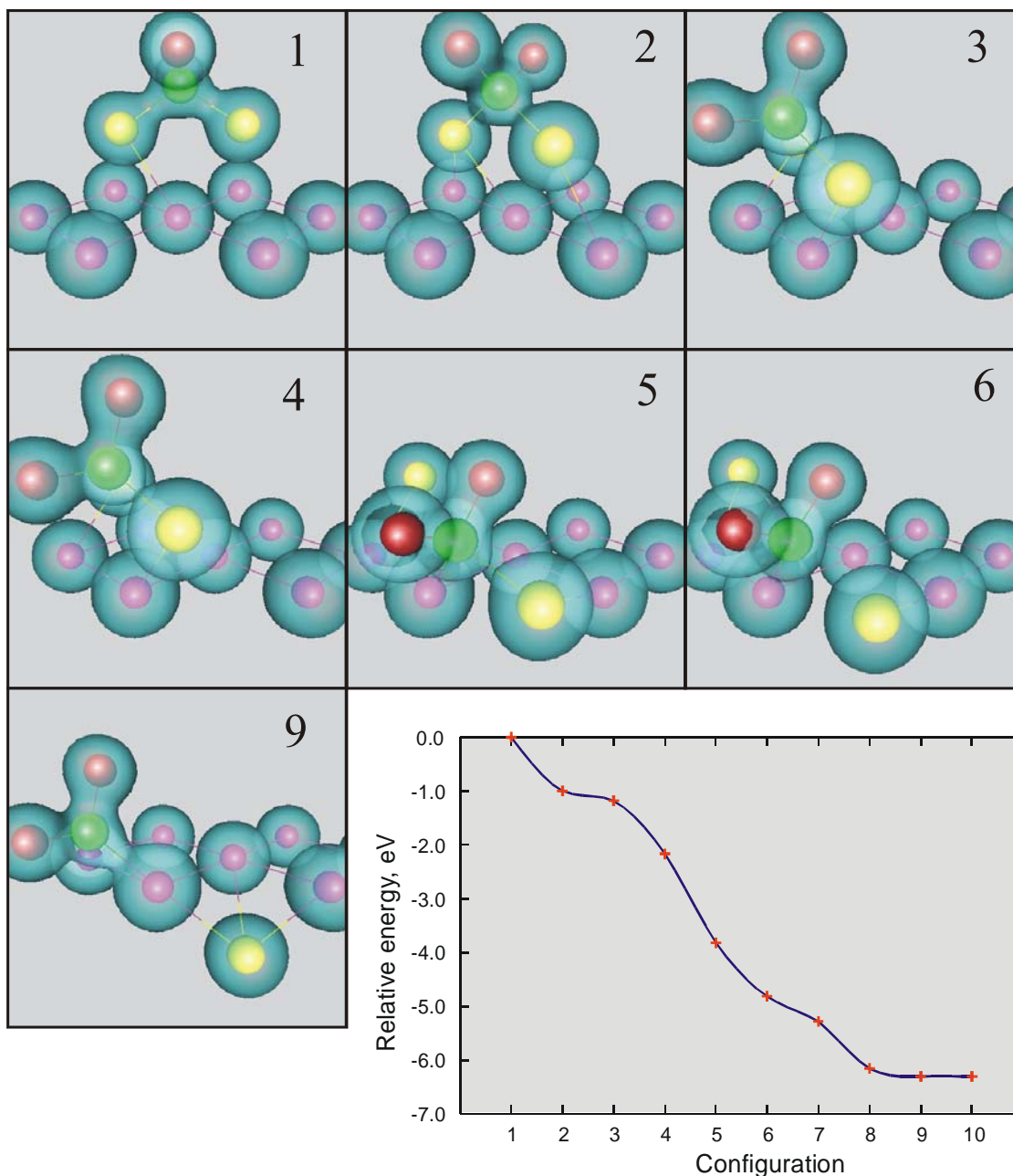


Fig. 1. A series of transitory structures appearing in the course of the dissociation of CCl_2F_2 in contact with Pd cluster to $\text{CF}_2 + 2\text{Cl}$. The color of the spheres marks the following atoms: Pd - mauve, C - green, F - red, Cl - yellow. Isosurfaces of the electron density ($\rho=0.10\text{ e}/\text{\AA}^2$) are shown with cyan color. In the lower right part of the figure the plot of the energy (relative to the energy of the initial configuration) for consecutive configurations is shown.

Further (activated) dissociation of CF_2 leads to a stable CF radical and isolated F atom. We found the transition state shown in Fig. 2 B, with energy -3.68 eV which should be compared with -4.62 eV (the binding energy of the adsorbed CF_2) and resulting activation energy is 0.94 eV. The energy gain in the dissociation process is rather large -5.55 eV. The CF group is localized between Pd atoms in the hollow site and the carbon atom is equidistant from the Pd atoms: 2.02 , 2.04 , 2.08 , 2.04 Å, respectively.

The final dissociation to isolated C and F atoms adsorbed on Pd cluster proceeds with an activation barrier and energy gain of -0.9 eV. The final structure is shown in Fig. 2 C.

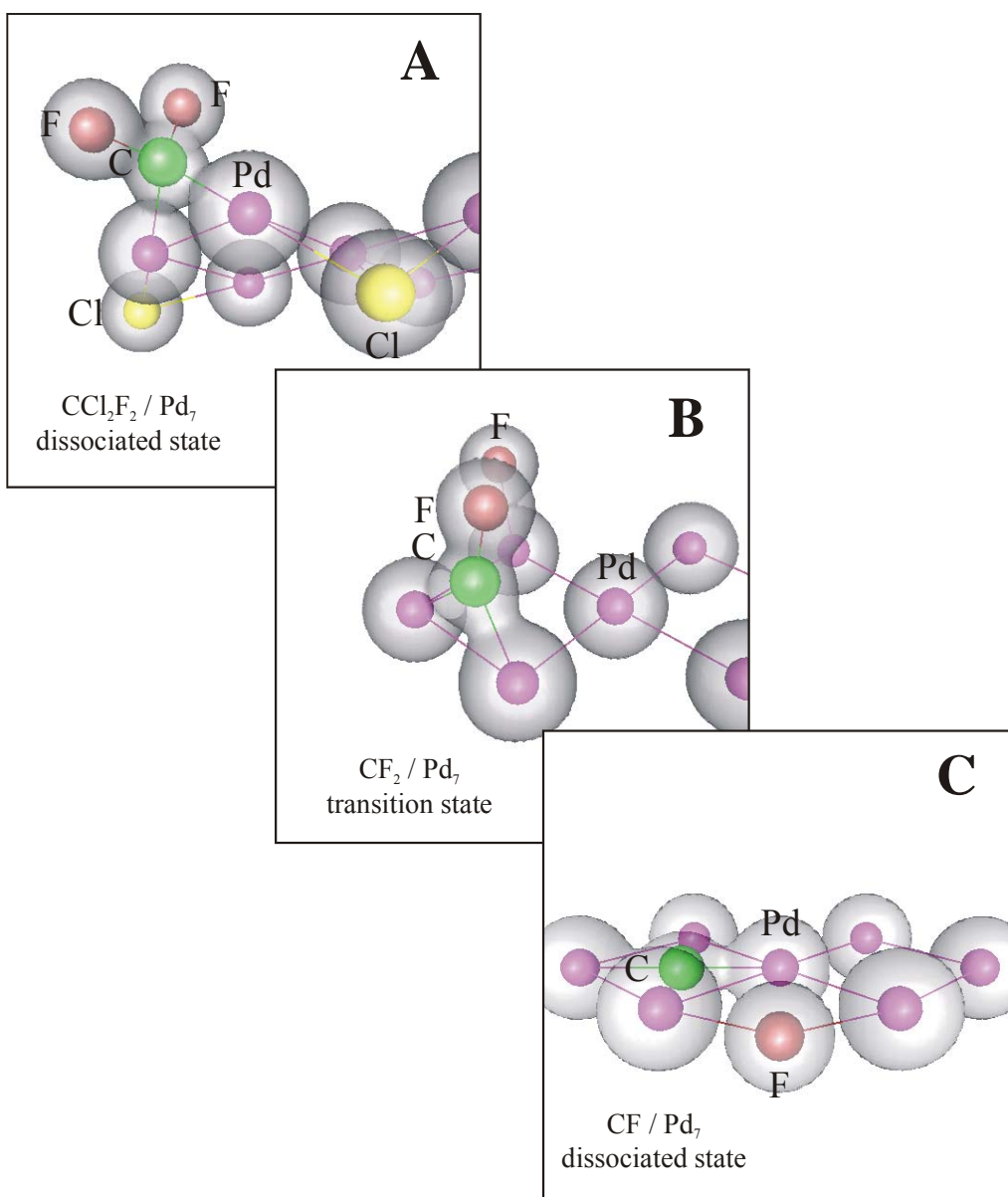


Fig. 2. Isosurfaces of the electron density ($\rho=0.10 \text{ e}/\text{\AA}^2$, marked with light gray color): (A) Dissociation of the CCl_2F_2 molecule in contact with the Pd_7 cluster, (B) Transition state of the CF_2 radical, (C) Dissociation and final structure of the CF radical in contact with the Pd_7 cluster.

Interaction of C₂Cl₂F₂ molecule with metal clusters

The next series of the calculations concern the C₂Cl₂F₂ molecule in contact with the Pd₇ cluster. The calculations have been performed for the C₂Cl₂F₂ molecule parallel to the planar Pd cluster (Fig. 3). After energy optimisation the adsorbed molecule exhibits significantly stretched C-Cl bonds (1.91 and 1.97 Å) which suggest the further dissociation towards the isolated Cl atoms (this is verified by lower energy of the C₂F₂ plus two isolated adsorbed Cl atoms). The C-C bond length is increased from 1.34 to 1.53 Å. The C-F bonds are stretched to 1.42 and 1.44 Å. The adsorption energy with respect to the isolated C₂Cl₂F₂ and metal cluster is -1.46 eV. The dissociation of the C-Cl bonds in C₂Cl₂F₂ is expected due to the similarity with the smaller CCl₂F₂ molecule. However, while in the case of the smaller molecule a simple rotation could start the dissociation, in the case of C₂Cl₂F₂ one can expect a transition state with a small activation barrier.

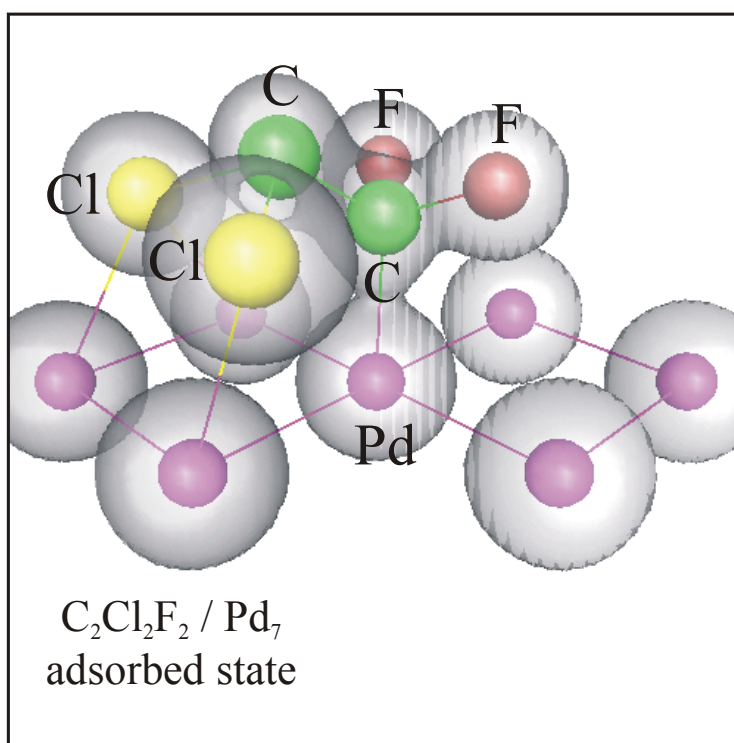


Fig. 3. Molecular geometry and the isosurfaces of the electron density ($\rho=0.10 e/\text{\AA}^3$, marked with light gray color) for the adsorbed state of the C₂Cl₂F₂ molecule in contact with the Pd₇ cluster.

References

- [1] M. Bonarowska, B. Burda, W. Juszczyk, J. Pielaszek, Z. Kowalczyk, Z. Karpiński, Appl. Catal. B: Environ., 35 (2001) 13
- [2] M. Bonarowska, J. Pielaszek, V.A. Semikolenov, Z. Karpiński, J. Catal. 209 (2002) 528

Acknowledgments: *The present work was supported by the grant PBZ-KBN-116/T09/2004. The authors wish to thank Professor Zbigniew Karpiński for his suggestions which resulted in the present research project.*

COMPARISON OF SELECTED THERMOGRAVIMETRIC ANALYSIS METHODS OF POLYMERS

Dawid Stawski, Zbigniew Draczyński

Department of Physical Chemistry of Polymers, Technical University of Łódź

Fundamental and representative methods used for determining kinetic parameters of thermal polymer decomposition process on the basis of thermogravimetric data were characterised. Assumed mathematical hypotheses, simplifications and theoretical conditions were discussed. Specific methods were analysed as far as application, limitation and difficulties in their usage are concerned.

General thermal analyses techniques can be divided into three basic groups: Differential Scanning Calorimetry (DSC), Differential Thermal Analysis (DTA) and Thermogravimetry (TG). The last technique is used specially to evaluate thermal stability of polymer materials as well as it can help to obtain various valuable technical information. With the use of thermobalance not only dependence of sample mass loss on temperature with determined heating velocity can be obtained, but also one can determine temperature (T) or time derivative (t). Thermogravimetric analysis has a number of advantages especially when compared to isothermic methods.

As the cognition of the dependence between thermal resistance and chemical composition of compounds used in high temperatures is essential it is important to determine the thermal decomposition parameters as activation energy (E), reaction order (n), frequency coefficient (A).

These parameters are of vital importance for mechanism of polymer degradation determination [1,2] and its thermal stability [3].

There are a number of methods used to determine the kinetic pyrolysis parameters. They vary not only in the kind of data analysis and assumed hypotheses but also in the way of mathematical elaboration. However even the most modern methods using complicated calculation schemes make use of original basic theories [4-8].

Two basic groups of kinetic analysis methods of pyrolysis process are distinguished.

Derivative methods are based on the dependence:

$$d\alpha/(1-\alpha)^n = (A/\beta) \exp(-E/RT) dT \quad (1)$$

where α is the transformation degree, β heating velocity, R universal gas constant and T is temperature.

Determination of initial parameters as $\alpha = 0$, $T = T_0$ (room temperature 25 °C), and integrating the equation (1) gives the dependence used in so called integration methods

$$\int_0^\alpha d\alpha/(1-\alpha)^n = A/\beta \int_{T_0}^T \exp(-E/RT) dT \quad (2)$$

Kissinger Method [9]

The basic assumption made by the author is that the reaction order in most cases does not undergo any change during pyrolysis. As the heating temperature goes up the mass loss velocity increases up to the maximum value T_m .

After inserting this value the author obtains

$$\frac{E\beta}{RT_m^2} = An(1-\alpha)_m^{n-1} \exp\left(-\frac{E}{RT_m}\right) \quad (3)$$

Kissinger method was next often modified and after the assumption that kinetic parameters are not affected by heating velocity the most commonly used equation was obtained [10]:

$$\frac{d(\ln(\beta / T_m^2))}{d(1/T_m)} = \left(\frac{-E}{R}\right) \quad (4)$$

In this equation reaction order does not appear. The above mentioned equation allows, plotting $\ln(\beta/T_m^2) = f(1/T_m)$, to calculate from the tilting angle activation energy for simple processes with the reaction order from 0 to 1.

This method requires that several thermograms are made but demands little work as far as calculations are concerned. Having thermograms done for several heating velocities it is sufficient to determine T_m .

The application of this method was proved for brucite, calcite, halloysite, magnesite and kaolinite [9], and for polymer compounds such as cellulose, starch, sizal fibres and their mixtures and composites [11].

Freeman and Carrol Method [1, 12]

The starting point for consideration for the authors are the following equation (5)

$$\Delta \log(d\alpha/dT) = n\Delta \log(1-\alpha) - (E/2,303R)\Delta(1/T) \quad (5)$$

From equation (5) it can be concluded that the values E and n can be calculated using only one thermogram. The left side of (5) should be a linear function $\Delta \log(1-\alpha)$ with constant $\Delta(1/T)$. The slope of the linear dependence should give the reaction order and the cutting point the activation energy. Despite the simplicity of mathematical basis this method is far more complicated than Kissinger method from the applicational point of view. The first stage is to accept the right step value $1/T$ in the analysed range. The determination of sufficiently small value of this coefficient makes the calculations more exact but also makes it necessary to introduce more data. One should read the temperatures for the given $1/T$ section and next the increment value $\log d\alpha/dT$ and $\log(1-\alpha)$. This process requires a lot of work. Obtaining the linear character of the plot $\Delta \log(d\alpha/dT) = f(\Delta \log(1-\alpha))$ in the measuring scope means that the method can be used for the analysed data. This method can be used for polyethylene and poly(tetrafluoroethylene) [1].

Coats and Redfern Method [13]

The authors use integration method. They obtain the following equation (6)

$$\ln\left(\frac{\alpha}{T^2}\right) = \ln\frac{AR}{\beta E} \left(1 - \frac{2RT}{E}\right) - \frac{E}{RT} \quad (6)$$

Plotting $\ln\left(\frac{\alpha}{T^2}\right) = f(1/T)$ E value can be calculated. It must be remembered that the equation is only true for zero reaction order, which results from the former simplifications. The results obtained by this method are true for low α , but they can be generalized for the whole of the process assuming that the reaction mechanism does not change during reaction duration. From the practical point of view this method is moderately laborious. It requires taking the α values from the thermogram and doing the necessary calculations for obtaining the plot. The authors use this method among others to investigate poly (tetrafluoroethylene) [13], poly (3-dimethyloacryloyloxyethyl) ammonium propanosulfate [14], obtaining the results corresponding to the results obtained from other calculating methods.

Reich Method [15]

In this method one should compare sample mass changes in sufficiently small temperature distances ΔT . If we choose sufficiently small temperature section ΔT then for all reaction orders except $n = 1$ can be written:

$$\ln\left[\frac{1}{(n-1)}\left(\frac{\alpha^{n-1} - \alpha_i^{n-1}}{\alpha^{n-1} \times \alpha_i^{n-1}}\right)\right] = -\frac{E}{RT} + \ln\left[\frac{A\Delta T}{\beta}\right] \quad (7)$$

where $\Delta T = \text{const.} = (T - T_i)$,

α and α_i – mass loss in temperatures T and T_i respectively.

For special cases of reaction orders one can obtain the following equations:

$$\text{For } n=1 \quad \ln\left[\ln\left(\frac{\alpha}{\alpha_i}\right)\right] = -\frac{E}{RT} + \ln\left[\frac{A\Delta T}{\beta}\right] \quad (8)$$

$$\text{And for } n=0 \quad \ln(\alpha - \alpha_i) = -\frac{E}{RT} + \ln\left[\frac{A\Delta T}{\beta}\right] \quad (9)$$

One can observed if this method is to give satisfactory results one should assume the reaction order beforehand to apply the necessary equations. Then one should note the adequate relations α and α_i in the assumed section ΔT and plot the dependences of the left side of the equation (7-9 dependent on the reaction order) on inverted temperature. From such plot one can read activation energies values and coefficient A . When the reaction order is not known one can evaluate it comparing the linearity of the plots (7-9). The method is experimentally quite laborious especially when assuming small section ΔT . The authors obtain satisfactory results for poli (tetrafluoroethylene) among others.

Ozawa Method [16]

The author starts with the equation (10):

$$\int_{T_0}^T \exp(-E/RT) dT = \int_0^T \exp(-E/RT) dT \quad (10)$$

The value of the write side of the above mentioned equation was determined and shown in a table Doyle [17] as the function p so one can have

$$\frac{E}{R} p\left(\frac{E}{RT}\right) = \int_0^T \exp(-E/RT) dT \quad (11)$$

If E/RT is smaller than 20 then the value $p(E/RT)$ can be approximated using the following equation [18]:

$$\log p\left(\frac{E}{RT}\right) = -2,315 - 0,4567 \frac{E}{RT} \quad (12)$$

For the given values of change degree the left side of the equation (12) is constant not dependant on β . So for the assumed α , T and β are given and one can have

$$\frac{AE}{\beta_1 R} p\left(\frac{E}{RT_1}\right) = \frac{AE}{\beta_2 R} p\left(\frac{E}{RT_2}\right) = \dots \quad (13)$$

Plotting $\log \beta$ in the function of temperature inversion one should obtained the straight line the tilting of which can give activation energy value.

The Ozawa method from the experimental point of view is very simple but requires thermograms made with various heating velocities. From these thermogrames one should only take the T values with the given change degree. However one should remember the assumption of the author that the activation energy does not depend on the heating velocity. Data obtained from a number of thermogrames makes it possible to

obtain more exact measurement. Data obtained with the various change degrees should be averaged out so it is necessary to make the calculations for a number of change degrees. Too big results dispersion depending on the change degree can indicate that this method is inadequate for the measured sample. This method was used for do polyamide, calcium oxalate [13], starch and cellulose [11] giving the results largely dispersed dependent on the change degree however the average values were similar to those obtained from other methods.

Conclusions

The methods presented in this work give the survey of the various approaches to the problem of determining the kinetic parameters of pyrolysis process. In order to choose the most appropriate method first of all one should consider the theoretical assumptions and simplifications present in mathematical calculations. One should choose the right method for the particular polymer compounds supported by literature and choose the correct reference method. Next it is essential to analyse the experimental data what influences the time dedicated to obtaining the results. This publication should make it easier to choose the right method for the sample investigated.

Generally and individual approach should be taken to each of the sample analysed and the method should be decided upon every single time if we deal with the comparative analysis. Ozawa method and modified Kissinger method assume a difficult hypothesis that the heating velocity does not affect the kinetic parameters values. Whereas Coats and Redfern calculate the activation energy values for low α , assuming the generalization of results for the whole of the process. Often used Reich method requires the beforehand assumption of reaction order and can give false results when fractional values of n. For the analysis of new products the Freeman - Carrol method is the safest, which is quite laborious but gives the certainty of getting the correct results.

LITERATURE

1. Bikales N.: Characterization of Polymers, Wiley Interscience, New York 1971
2. Levi D., Reich L., Lee H.: *Polymer Eng. Sci.*, 1965, **5**, 135
3. Reich L., Levi D.: *Makromol. Chem.* 1963, **66**, 102
4. Brown M., Maciejewski M., Vyazovkin S., Nomen R., Sempere J., Burnham A., Opfermann J., Strey R., Anderson H., Kemmler A., Keuleers R., Janssens J., Desseyn H., Li C., Tang T., Roduit B., Malek J., Mitsuhashi T.: *Thermochim. Acta*, 2000 **355**, 125
5. Maciejewski M.: *Thermochim. Acta*, 2000 **355** 145
6. Vyazovkin S.: *Thermochim. Acta*, 2000 **355** 155
7. Burnham A.: *Thermochim. Acta*, 2000 **355** 165
8. Roduit B.: *Thermochim. Acta*, 2000 **355** 171
9. Kissinger H.: *Anal. Chem.*, 1957, **29**, 1702
10. Murray P., White J.: *Trans. Brit. Ceram. Soc.*, 1955, **54**, 204
11. Alvarez V., Vázquez A.: *Polym. Deg. Stab.*, 2004, **84**, 14
12. Freeman E., Carroll B.: *J. Phys. Soc.*, 1958, **62**, 394
13. Coats A., Redfern J.: *J. Polym. Sci., Polym. Lett. Ed.*, 1965, **3**, 917
14. Lee W.: *J. Appl. Polym. Sci.*, 1989, **37**, 3263
15. Reich L.: *J. Polym. Sci., Polym. Lett. Ed.*, **3**, 231 (1965)
16. Ozawa T.: *Bull. Chem.*, 1965, **38**, 1881
17. Doyle C.: *J. Appl. Polym. Sci.*, 196, **15**, 285
18. Doyle C.: *J. Appl. Polym. Sci.*, 1962, **6**, 639

LACTIC ACID SOLUTION INFLUENCE ON POLYAMIDE/POLYETHYLENE LAMINATES PROPERTIES

I. Steinka¹, M. Morawska²

*Gdynia Maritime University,
Department of Commodity and Cargo Science¹,
Department of Chemistry and Industrial Commodity Science²,
83 Morska Str., 81-225 Gdynia, Poland
izas@am.gdynia.pl, mmoraw@am.gdynia.pl*

Introduction

Plastics have been present in the market of packaging since the twenties of the last century, when the foil made of regenerated cellulose named cellophane was first introduced [1]. The next years brought further development of plastic packaging including the packaging of food.

The food packaging performs a number of important functions. The most obvious is protection of the packed product. The food product is protected against external agents, such as moisture, oxygen, dust, micro-organisms. It is also protected against mechanical damages and the loss of volatile components.

The present-day development of the physics and chemistry of polymers has provided opportunities for producing plastics that reveal properties adapted to individual products. One of the most important advances in this field has been the development of multilayer packaging materials. These materials are made up of several layers adhered together, and they were designed to provide new material revealing properties which are required for the packed product.

A laminate composed of polyamide and polyethylene is one of multilayer film packaging.

High-pressure polyethylene LDPE is obtained by ethylene polymerisation, conducted under high pressure in the presence of oxygen or free-radical catalysers. It reveals high purity, and good transparency, flexibility and elasticity. It is permeable for gases such as oxygen, carbon dioxide and sulphur dioxide. It softens in the temperature above 80°C – 90°C, and can be easily pressure welded. It is resistant to the action of acids, alkalies, and organic solvents (except hydrocarbons and fats).

Polyamides are obtained by polycondensation of amino acids or lactams. Their advantage is high mechanical strength, good thermal properties, flexibility and resistance to the action of organic solvents, alkalise and weak acids. Low barrier level towards steam is the reason why the polyamides are more and more frequently used in multi-layer laminates [2].

A composition of those two polymers allows producing the material that reveals better barrier properties towards light, steam, oxygen, and improved mechanical properties of the packaging.

PA/PE laminates are most often used for vacuum packing of meat and its products, dairy products, smoked fish products, ready-to-serve dishes, vegetables [3].

Lactic acid cheese is one of dairy products which until recently was only packed in pergamin paper. Now the consumers have it more and more often delivered in vacuum packaging made of PA/PE laminate. This packaging considerably prolongs the storage time, but is connected with the risk of migration of packaging components into the packed product.

An overview of the subject leads to the conclusion that the problem of lactic acid cheese - packaging interaction has been never discussed in the available literature. Moreover, model liquids and food simulants cannot be used in case of lactic acid cheese [4].

The cottage cheese is an untypical food product due to high number of ingredients composing its mass. Along with protein and water, it contains fat, lactic acid and lactic acid bacteria. All those components can unfavourably act on the packaging material. Whey, the liquid part of the cottage cheese, can penetrate between the layers of the laminate, which may result in the migration of low-molecular compounds used in the process of polymerisation or lamination [5,6,7].

Prolongation of lactic acid cheese storage time increases the exposure of the packaging to the action of bacteria and their metabolites which are present in the product.

The aim of this paper was the evaluation of the influence of lactic acid solution on mechanical properties of the packaging material.

Materials and methods

Materials: The PA/PE laminate bags received from “Pakmar” were selected for investigations.

Bags of PA/PE were filled with water solution of lactic acid prepared by volume in an analytical balance to pH 4,7 (according to pH of the lactic acid cheese). After 2, 4, 7, 14, 21 days of storage at 4°C, the bags were taken out from refrigerator, washed with distilled water and dried at room temperature. The changes in weight (one side contact), tensile strength and surface morphology of PA/PE samples were tested before and after storage.

Weight changes was determined using a Gibertini E42s electronic balance. The changes of lactic acid solution absorbability of polyamide/polyethylene material were studied by weight determination. For this purpose, squares of total area 25 cm² were cut off from PA/PE bags and then weighed (m_a) with accuracy to 0,0001g. Blank sample was a sample dried at 50±2°C (m_o). The average of 5 samples was the final result of the investigation.

$$\text{Weight changes [\%]} = (m_a - m_o) / m_o * 100\%$$

Tensile strength was measured at room temperature by means of a Tensile Tester Type Fu 1000e. Tensile testing was performed before and after storage using rectangular strips of investigated polymer films (PA/PE 20mm x 150mm x 0.08mm,) in accordance with PN-EN ISO Standard [8]. Tensile strength was calculated as tensile force [N] to cross-sectional area [mm²]. The results for three specimens were averaged for each value determined.

Microscopic observations of polymer samples surface were analyzed with optical microscope ALPHAPHOT-2YS2-H linked to a Nikon F90X camera. The surface was analyzed before and after 2, 4, 7, 14, 21 days of storage.

Results

Figure 1 shows weight changes of PA/PE samples after one-side contact with lactic acid solution. The weight changes of PA/PE after storage with lactic acid solution increased

during the first 14 days. On about Day 21 the absorbability slightly decreases which may be caused free flow of the liquid out from between particular layers caused by the relaxation of the structure of the laminate.

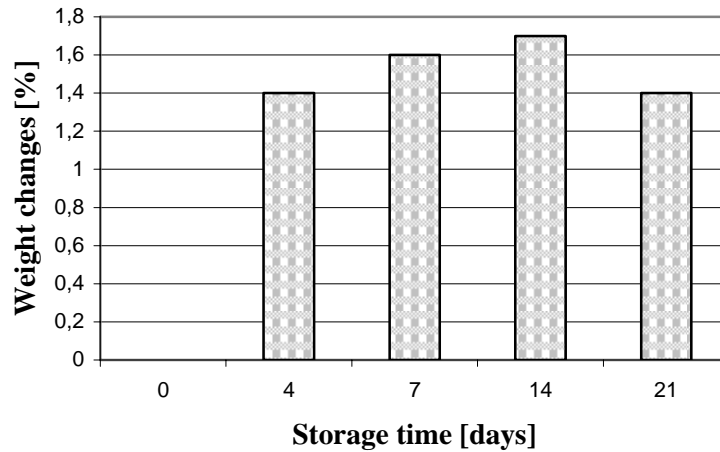


Fig.1 The weight changes of polyamide/polyethylene laminates after storage with lactic acid solution

The tensile strength increased after storage with lactic acid solution (Fig.2). It can be speculated that the penetration of lactic acid solution into the structure of the laminate may facilitate orientation of polymer chains, during the measurement of the tensile strength.

Since Day 7, lactic acid solution could wash out low molecular compounds of laminate (additives, adhesives) resulted in weakness of the structure of the packaging.

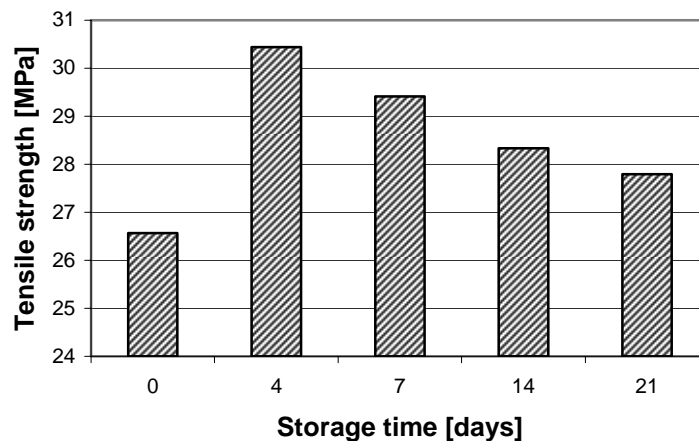


Fig. 2 The tensile strength of polyamide/polyethylene laminates after storage with lactic acid solution

The microscopic observation of polyamide/polyethylene samples after storage with lactic acid solution did not reveal very significant changes [Fig.3].

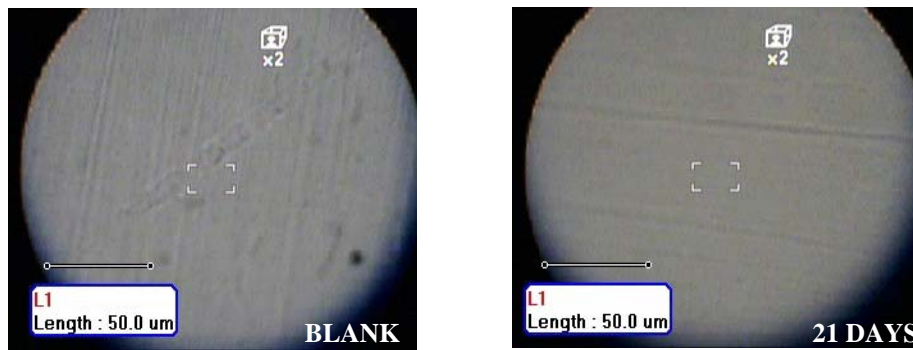


Fig.3. Microscopic observations of PA/PE

Conclusions

The obtained results revealed that the some physical properties as weight changes and tensile strength of packaging material made of PA/PE laminate are changed after the contact with lactic acid solution. Lactic acid is one of components of lactic acid cheese which trickles from cheese during storage.

It is possible that liquid components of the cottage cheese penetrate into the structure of the laminate and may cause the migration of low-molecular compounds of PA/PE laminate.

References

1. Czerniawski B., *Opakowania żywności*, Agro Food Technology, Czeladź, 1998, 199
2. Gruin I., *Materiały polimerowe*, Wydawnictwa Naukowe PWN, Warszawa, 2003, 151
3. Cichoń Z., *Nowoczesne opakowalnictwo żywności*, Zakład Narodowy im. Ossolińskich, Wrocław, 1996, 118
4. Hernandez-Munoz P., Atala R., Gavara R., Simple method for the selection of the appropriate food simulat for the evaluation of a specific food/packaging interaction, *Food Additives and Contaminants*, 2002, 19, 192-200
5. Grob K., Biedermann M., Artho A, Egli J., Food contamination by hydrocarbons from packaging materials determined by coupled LC-GC, *European Food Research and Technology*, 1991, 193(3), 213-219
6. Fordham P.J., Gramshaw J.W., Castle L., 2001, Analysis for organic residues from aids to polymerization used to make plastics intended for food contact, *Food Additives and Contaminants*, 18(5), 461-471,
7. Nerin C., Acosta D., Rubio C., 20002, Potential migration release of volatile compounds from plastic containers destined for food use in microwave ovens, *Food additives and Contaminants*, 19, 594-601
8. PN-EN ISO 527-1,2,3: 1998, *Plastics – determination of tensile properties*

ACRYLAMIDE-QUENCHING OF HARMANE IN ORGANIC SOLVENTS

Agnieszka Stobiecka and Joanna Jabłońska

*Faculty of Biotechnology and Food Science, Technical University of Łódź
Institute of General Food Chemistry, ul. Stefanowskiego 4/10, 90-924 Łódź, Poland*

INTRODUCTION

Harmane (or 1-methyl-9*H*-pyrido[3,4-*b*]indole), a β -carboline derivative, belongs to the class of alkaloids which attract much attention because of their interesting biological and pharmacological properties [1]. Supposedly, those properties can be related to the specific structure of the β -carboline ring, which confers the ability to interact with various biological receptors, macromolecules or enzymes. As a consequence of the biological significance the complexing ability of β -carbolines has stimulated many experimental (particularly spectroscopic) and theoretical studies in the last years [2]. Results of these studies indicate that organic compounds may bind to the β -carboline molecule by different modes, e.g. by van der Waals forces, charge-transfer forces or hydrogen-bonding interactions.

The aim of the present study was to investigate the nature of intermolecular interactions between harmane and acrylamide in various organic solvents. The existence of specific (e.g. hydrogen-bonding) interactions between the carbonyl group of acrylamide and the pyrrolic nitrogen atom of harmane could not be excluded. Therefore, to verify this possibility the absorption as well as the steady-state and time-resolved fluorescence measurements have been performed in protic (i.e., methanol) and aprotic medium (i.e. 1,4-dioxane and acetonitrile).

EXPERIMENTAL METHODS

Harmane, acrylamide (AA) and organic solvents were purchased from Sigma-Aldrich (Poznań, Poland). All chemicals were of spectroscopic grade and were used without further purification. Solutions of β -carboline were prepared by setting the concentration at $\sim 10^{-5}$ M. In titration experiments aliquots of acrylamide stock solution were added directly to the sample at small steps. Absorption and fluorescence spectra were additionally corrected for dilution by the titrant. Absorption spectra were recorded in a Nicolet Evolution 300 (Thermo Electron Corporation) UV-VIS spectrophotometer. The steady-state fluorescence measurements were performed with a FluoroMax2 (Jobin Yvon Spex) spectrofluorimeter and the fluorescence lifetime measurements were carried out with a FL900CDT time-correlated single photon counting fluorimeter from Edinburgh Analytical Instruments. For all fluorescence experiments the excitation wavelength was set to 340 nm. Time-resolved data acquisition and analysis were performed as described elsewhere [3]. All measurements were performed at room temperature ($25 \pm 1^\circ\text{C}$).

RESULTS AND DISCUSSION

Titration with AA in organic solvents under study caused no significant change in absorption spectrum of harmane (results not shown). On the contrary, the [AA] increase was followed by a pronounced change of fluorescence intensity of β -carboline dissolved

in apolar and aprotic solvents. As shown in Fig. 1, the fluorescence intensity monitored at the dual fluorescence maximum of harmane was progressively decreased without changing the shape of spectrum.

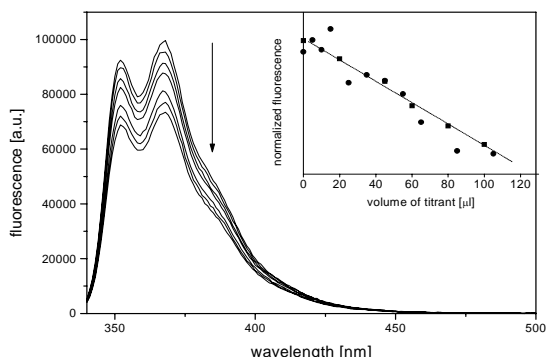


Figure 1. Changes in the steady-state fluorescence spectra of harmane dissolved in 1,4-dioxane upon addition of AA. Inset shows results of fluorimetric titration of harmane performed with methanolic AA stock solution (●) and with pure methanol (■). Concentration of AA in organic solvents was varied from 0 M to 0.05 M.

In contrast to 1,4-dioxane and acetonitrile, titration with AA performed in methanol did not accelerate significant changes in the steady-state fluorescence spectrum of harmane (for comparison see inset in Fig. 1), suggesting that the intermolecular interactions between alkaloid and quencher might operate only in aprotic solvents. Therefore, to obtain more information on the fluorescence quenching mechanism in 1,4-dioxane and acetonitrile the time-resolved measurements were performed. The time-resolved data were analyzed in terms of a multi-exponential decay law shown below:

$$I(t) = \sum_{i=1}^n \alpha_i \exp(-t / \tau_i) \quad (1)$$

where α_i and τ_i are the preexponential factor and decay lifetime of component i , respectively. The goodness of fit of fluorescence curves was judged by the reduced χ^2 value. According to the results of deconvolution of experimental data, the fluorescence decay of harmane in pure 1,4-dioxane as well as in pure acetonitrile was best described by a mono-exponential function with fluorescence lifetime equal to $\tau_0 = 2.93 \pm 0.004$ ns ($\chi^2 = 0.998$) and $\tau_0 = 2.83 \pm 0.004$ ns ($\chi^2 = 0.992$), respectively. The time-resolved data collected for harmane plus AA have been fitted to a bi- or tri-exponential functions but due to the relatively high value of reduced χ^2 parameter both models were immediately rejected and the mono-exponential fitting was considered as the best theoretical model. Since the increase of AA concentration was followed by the decrease in both the fluorescence lifetime (for comparison see Table 1) and fluorescence intensity, the possibility of dynamic or dynamic and static mechanism of fluorescence quenching of harmane by AA was taken into account. In order to estimate the value of dynamic quenching constant the time-resolved data were analyzed using the Stern-Volmer equation:

$$\frac{\tau_0}{\tau} = 1 + K_D[AA] = 1 + k_q\tau_0[AA] \quad (2)$$

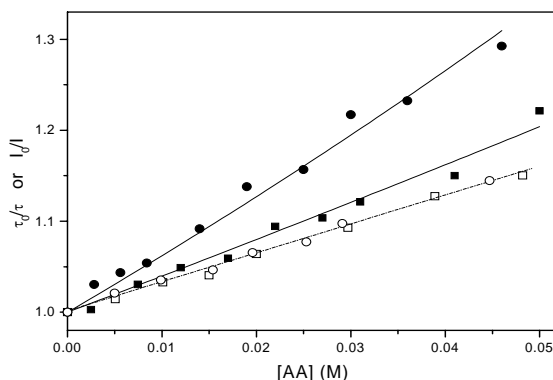
where τ_0 and τ are the fluorescence lifetimes in the absence and in the presence of AA, respectively. K_D and k_q are the Stern-Volmer quenching constant and the rate constant for quenching process, respectively. The plot of τ_0/τ vs. $[AA]$ was linear irrespective of the solvent used (Fig. 2). The calculated values of dynamic quenching constants for 1,4-

dioxane and acetonitrile were equal to $3.18 \pm 0.09 \text{ M}^{-1}$ and $3.20 \pm 0.08 \text{ M}^{-1}$, respectively. The corresponding bimolecular rate quenching constants were equal to $1.09 \times 10^9 \text{ M}^{-1}\text{s}^{-1}$ and $1.13 \times 10^9 \text{ M}^{-1}\text{s}^{-1}$, respectively.

Table 1. Fluorescence lifetimes of harmane at different AA concentrations. The time-resolved fluorescence of harmane in 1,4-dioxane and acetonitrile was monitored at 368 nm and 367 nm, respectively. The values in parentheses are the standard deviations of the lifetimes.

1,4-dioxane			acetonitrile		
[AA] $\times 10^2$ (M)	τ (ns)	χ^2	[AA] $\times 10^2$ (M)	τ (ns)	χ^2
0.49	2.87 (± 0.004)	0.998	0.51	2.79 (± 0.004)	0.993
0.99	2.83 (± 0.004)	0.984	1.01	2.74 (± 0.003)	0.995
1.54	2.80 (± 0.004)	1.168	1.50	2.72 (± 0.003)	1.048
1.96	2.75 (± 0.003)	1.052	2.00	2.66 (± 0.003)	0.992
2.53	2.72 (± 0.004)	1.270	2.97	2.59 (± 0.003)	1.108
2.91	2.67 (± 0.003)	1.065	3.89	2.51 (± 0.004)	0.987
4.47	2.56 (± 0.003)	1.341	4.82	2.46 (± 0.003)	0.982

Figure 2. Stern-Volmer plots for acrylamide-quenching of harmane dissolved in 1,4-dioxane (●) or acetonitrile (■). Solid and open symbols correspond to the data obtained from the steady-state and time-resolved measurements, respectively. The solid lines represent least-squares fit to Eq. 4, while the dashed line represents fit of experimental data to Eq. 2.



The Stern-Volmer plots obtained from the steady-state measurements showed deviation from linearity. As shown in Fig. 2, the quenching curves tend towards the y-axis at higher concentrations of AA which might indicate presence of static component in the quenching mechanism. Thus, taking into account the above observations, the static quenching constants, K_S , were estimated using two different methods based on the modified Stern-Volmer equations [4]:

$$\frac{I_0/I}{\tau_0/\tau} = 1 + K_S[AA] \quad (3)$$

and

$$\frac{I_0}{I} = (1 + K_D[AA]) \exp(K_S[AA]) \quad (4)$$

Direct fitting of the steady-state and time-resolved data to Eq. 3 resulted in linear plots with the correlation coefficient well above 0.99 and the intercept equal to unity. The K_S values determined from the slopes of these plots were equal to $K_S = 2.73 \pm 0.10 \text{ M}^{-1}$ and

$K_s = 0.83 \pm 0.08 \text{ M}^{-1}$ for 1,4-dioxane and acetonitrile, respectively. Furthermore, the values of static quenching constants for 1,4-dioxane and acetonitrile calculated according to Eq. 4 (with K_D estimated from Eq. 2) were in good agreement with those obtained from Eq. 3 and were equal to $K_s = 2.89 \pm 0.14 \text{ M}^{-1}$ and $K_s = 0.74 \pm 0.09 \text{ M}^{-1}$, respectively. The results of fitting the experimental data to Eq. 4 are shown in Fig. 2.

CONCLUSIONS

The present study shows that acrylamide is able to quench the fluorescence of harmaline dissolved in 1,4-dioxane and acetonitrile by a complex mechanism. Particularly in the case of the former solvent, the presence of static component in the quenching mechanism may imply the existence of specific ground-state interactions between AA and alkaloid. It should be stressed that in 1,4-dioxane the radius of so-called 'sphere of action' [4] estimated from the K_s value was greater than the distance of closer approach between the quencher and harmaline (i.e., $\sim 10 \text{ \AA}$ vs. $\sim 6 \text{ \AA}$). In contrast, in acetonitrile the sphere radius and the sum of the radii of the interacting molecules are comparable suggesting that the fluorescence quenching occurs immediately and the formation of intermolecular complex is less likely. Nevertheless, assuming that the calculated static quenching constant, K_s , may be related to the association constant of the ground-state complex, it might be concluded that the strength of interaction between AA and alkaloid is dependent on the solvent nature and is strongly weakened by increased polarity of the medium. Importantly, in methanol (a polar and hydrogen-bonding solvent) there was no evidence of intermolecular interactions either in the ground or in the excited state. On the contrary, formation of the ground-state complex between β -carboline and quencher seems to occur in nondipolar and aprotic solvent ($K_s^{1,4\text{-dioxane}} \gg K_s^{\text{acetonitrile}}$). Furthermore, since the solvation process strongly affects the nature of intermolecular interactions in the harmaline / AA / organic solvent system the existence of specific (e.g. hydrogen-bonding) interactions between AA and β -carboline should be taken into account.

REFERENCES

- [1] (a) R.H.F. Manske, in: *The Alkaloids*, R.H.F. Manske (ed.), vol. VIII, Academic Press, New York, 1965, p. 47; (b) W.E. Muller, K.J. Fehske, H.O. Borbe, U. Wollert, C. Nanz, H. Rommelspacher, *Pharm. Biochem. Behav.*, 14 (1981) 693; (c) M.M. Airaksinen, I. Kari, *Med. Biol.*, 59 (1981) 21; (d) E. Ruiz-Durantez, J.A. Ruiz-Ortega, J. Pineda, L. Ugedo, *Neurosci. Lett.*, 308 (2001) 197
- [2] (a) M.A. Muñoz, C. Carmona, J. Hidalgo, P. Guardado, M. Balón, *Bioorg. Med. Chem.*, 3 (1995) 41; (b) M. Balón, M.A. Muñoz, C. Carmona, P. Guardado, M. Galán, *Biophys. Chem.* 80 (1999) 41; (c) M.A. Muñoz, P. Guardado, M. Galán, C. Carmona, M. Balón, *Biophys. Chem.*, 83 (2000) 101; (d) L. Martín, A. Leon, M.A. Martín, B. del Castillo, J.C. Mendez, *J. Pharm. Biomed. Anal.*, 32 (2003) 991
- [3] A. Stobiecka, *J. Photochem. Photobiol. B*, 80 (2005) 9
- [4] J.R. Lakowicz, in: *Principles of Fluorescence Spectroscopy*, J.R. Lakowicz (ed.), Plenum Press, New York, 1999, p. 238

ACKNOWLEDGEMENTS

Financial support from the State Committee for Scientific Research, Grant No. 3T08E06327 (Poland) is gratefully acknowledged.

PROBING THE PROTOTROPIC AND HYDROGEN-BONDING EQUILIBRIA OF HARMANE IN THE PRE-POLYMERISATION SYSTEM USING SPECTROSCOPIC METHODS

Agnieszka Stobiecka

*Faculty of Biotechnology and Food Science, Technical University of Łódź
Institute of General Food Chemistry, ul. Stefanowskiego 4/10, 90-924 Łódź, Poland*

INTRODUCTION

β -Carbolines (pyridoindoles) constitute a class of compounds of great importance in pharmacology and clinical chemistry. They are present in medicinal plants as well as in mammalian tissues and body fluids [1,2]. β -Carbolines in solution may exist in neutral, monoprotonated, anionic and zwitterionic forms. Furthermore, the presence of the pyrrolic and pyridinic sites in the heteroaromatic ring makes them a suitable ligand for binding various organic compounds that possess hydrogen acceptor/donor properties. In the current study changes in the photophysical properties of harmane (1-methyl-9H-pyrido[3,4-*b*]indole, HN), a fully aromatic β -carboline alkaloid, were used for qualitative and quantitative determination of the intermolecular interactions which may occur between biological molecule and functional monomer during the synthesis of molecularly imprinted polymer (MIP). It should be noted that the presence of specific intermolecular interactions between the imprinted molecule (analyte) and the functional monomer(s) is frequently used to produce the MIP by the non-covalent method. Importantly, the type and strength of those intermolecular interactions that may develop during the pre-polymerisation step have a big influence on the performance of MIP as a selective matrix [3].

EXPERIMENTAL METHODS

Spectroscopic grade chemicals were purchased from Sigma-Aldrich (Poznań, Poland) and were used without further purification. Absorption spectra were recorded in a Nicolet Evolution 300 (Thermo Electron Corporation) UV-VIS spectrophotometer. The steady-state fluorescence measurements were performed with a FluoroMax2 (Jobin Yvon Spex) spectrofluorimeter and the fluorescence lifetime measurements were carried out with a FL900CDT time-correlated single photon counting fluorimeter from Edinburgh Analytical Instruments. Time-resolved data acquisition and analysis were performed using software provided by EAI. All measurements were performed at room temperature ($25 \pm 2^\circ\text{C}$). The value of the ground-state association constant was estimated using the Benesi-Hildebrand method. For 1:1 stoichiometry, the association constant for complex formation, K_b , may be calculated from the absorption data using the following equation:

$$\frac{1}{(A - A_0)} = \frac{1}{(\varepsilon_b - \varepsilon_{HN})[HN]} + \frac{1}{K_b(\varepsilon_b - \varepsilon_{HN})[HN]} \times \frac{1}{[MAA]} \quad (1)$$

where A and A_0 are the absorbance of the HN solution with and without MAA, respectively; ε_b and ε_{HN} denote the molar absorption coefficient of HN/MAA complex and free HN, respectively.

RESULTS AND DISCUSSION

Spectroscopic properties of harmane in the binary system consisting of toluene and methacrylic acid (MAA) mixture have been studied at the wide MAA concentration range using UV-VIS and fluorescence spectroscopy. In order to monitor the possible intermolecular interactions, the absorption and fluorescence spectra of HN have been recorded up to MAA concentration of about 6×10^{-1} M and 6 M, respectively. As can be seen from Fig. 1A, absorption changes observed in the system under study strongly depended on the functional monomer concentration. At low [MAA] (from 0 to $\sim 6 \times 10^{-2}$ M) the absorption signal monitored at dual absorption maximum of neutral form of HN (N) decreased and only small red shift of absorption band was recorded. The presence of isosbestic points at 332 nm and 344 nm established the existence of equilibrium between two different forms of HN. However, with a further increase of [MAA], a continuous bathochromic shift of spectra and an appearance of another isosbestic point at 346 nm were observed suggesting the formation of new ground-state species. In both cases the growth of absorption shoulder at $\lambda \geq 350$ nm was observed. Finally, at high [MAA] (above 3×10^{-1} M) a shoulder above 360 nm was developed indicating protonation of the pyridinic nitrogen atom of HN and formation of the cationic form (C) of β -carboline [4]. Recalling a hydrogen donor / acceptor properties of both the HN and MAA molecules it might be assumed, that the absorption changes observed at $\lambda \sim 350$ nm were accelerated by the intermolecular hydrogen-bonding interactions. The profile of the Benesi-Hildebrand plot (Eq. 1) suggested the stepwise formation of different hydrogen-bonded HN/MAA complexes in the ground state. Thus, based on the above results, the presence of H-bonded assemblies with different stoichiometry, i.e. 1:1 and 1:2 (or higher) should be taken into account. The estimated association constant for 1:1 HN/MAA complex formed at low [MAA] was equal to $K_b = 245 \pm 51 \text{ M}^{-1}$. On the other hand, the analysis of multiple equilibria at elevated [MAA] was complicated due to the strong overlapping of the H-bonded and cationic species absorption (Fig. 1B).

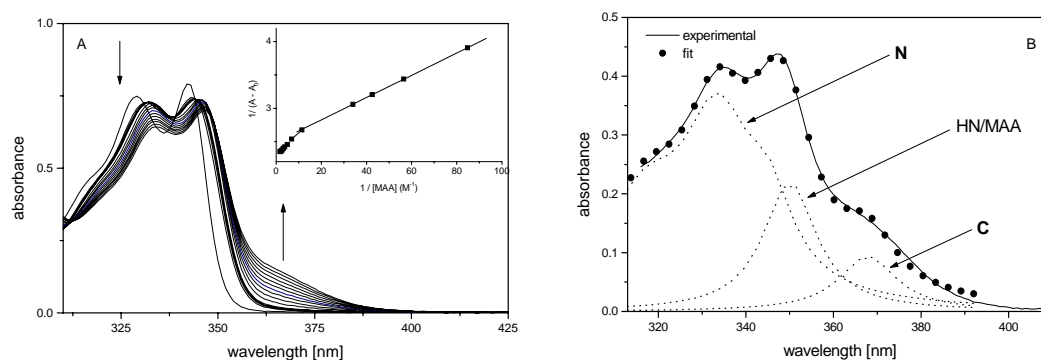


Figure 1: (A): Changes in the absorption spectrum of HN upon increasing MAA concentration. Inset: The Benesi-Hildebrand plot for H-bonded complexes equilibrium monitored at 350 nm. Concentration of functional monomer was increased from 0 M to 0.6 M as indicated by arrows. (B): Bands characteristic of neutral (N), H-bonded (HN/MAA) and cationic (C) form of HN in the MAA/ toluene solution.

The steady-state fluorescence spectra of HN in MAA/toluene system were monitored at excitation wavelengths characteristic for the absorption of neutral and cationic form of HN, i.e. at 340 nm and 370 nm, respectively. Exciting at 340 nm, the fluorescence intensity of HN decreased with the increased [MAA] (Fig. 2A). Similar to the

absorption spectrum, the fluorescence spectrum of HN in the presence of MAA was red shifted and broadened in comparison to the emission of the neutral form but, additionally, the lost of vibrational structure was also observed. The above results may suggest that the fluorescence monitored at the wavelength range between 350 nm and 400 nm may correspond to the emission of H-bonded complexes formed both in the ground as well as in the excited state. Furthermore, even at relatively low [MAA], a structureless fluorescence band appeared near 510 nm which corresponded to the HN zwitterion (Z) emission [5]. It should be also noted that at the long wavelength range i.e., at $\lambda_{em} > 400$ nm, beside the Z emission the fluorescence of HN cation was also observed. Analysis of the steady-state fluorescence spectra collected at different excitation wavelengths indicated that the Z species developed prior to the C (for comparison see Figs. 2A and 2B). The above observation was in accordance with the time-resolved data collected in Table 1.

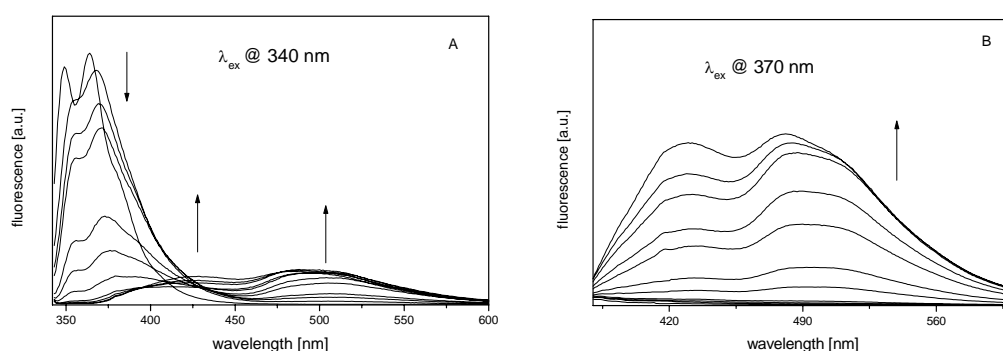


Figure 2: Changes in the fluorescence spectrum of HN upon increasing MAA concentration. The pre-polymerisation mixture was excited at 340 nm (**A**) and at 370 nm (**B**), respectively; concentrations of MAA were: 0, 0.010, 0.029, 0.059, 0.29, 0.56, 1.18, 2.36, 3.54, 4.72, 5.90 M.

The appearance of Z emission clearly indicates the presence of the excited state proton transfer reactions in the system under study. According to the results from the time-resolved measurements, at $[MAA] \geq 0.1$ M the fluorescence decay ascribed to HN/MAA^* emissions monitored at 360 nm was monoexponential and was decreased with functional monomer concentration. On the contrary, the fluorescence decay monitored at 450 nm and 510 nm was a biexponential at medium [MAA] and became a triple-exponential at elevated [MAA]. Importantly, in the biexponential decay monitored at 510 nm the pre-exponentials, a_i , were similar but were of different sign. From the comparison of decay parameters obtained at 360 nm and 510 nm it may be concluded that the shorter decay time (appearing as a risetime at Z emission band) may correspond to the emission of the ground-state H-bonded precursor of Z whereas the longer component with $\tau_2 \approx 9$ ns may be associated with Z emission. The latter result is in good agreement with the 11 ns value measured in cyclohexane [5]. At elevated [MAA], when the Z and C species emit simultaneously (for comparison see Fig. 2B) a more complex kinetics was observed. However, since the shortest and medium lifetimes found in the triexponential decay at 510 nm were characterized by the pre-exponential factors with a similar magnitude and opposite sign they were ascribed to the complexed and zwitterionic form of HN. The longest decay component with lifetime τ_3 was associated with C emission since the relative contribution of this component, f_3 , to the fluorescence decay monitored at 450 nm was increased with MAA concentration.

Table 1: Fluorescence decay parameters for HN in MAA / toluene system ($\lambda_{\text{ex}} = 340 \text{ nm}$).

[MAA] (M)	$\lambda_{\text{em}}=360 \text{ nm}^{a,d}$	$\lambda_{\text{em}} = 450 \text{ nm}^d$						$\lambda_{\text{em}} = 510 \text{ nm}^d$					
	τ (ns)	τ_1 (ns)	f_1 (%) ^c	τ_2 (ns)	f_2 (%)	τ_3 (ns)	f_3 (%)	τ_1 (ns)	a_1	τ_2 (ns)	a_2	τ_3 (ns)	a_3
0.117	2.10	2.43	77	11.49	23	—	—	2.35	- 0.107	9.45	0.106	—	—
0.399	1.27	1.60	53	9.37	28	17.33	19	1.23	- 0.065	8.92	0.078	15.37	0.004
0.561	0.89	1.32	45	9.59	32	17.87	23	1.07	- 0.058	9.06	0.071	15.00	0.007
2.948	n.d. ^b	0.78	27	6.75	25	16.15	48	0.39	- 0.079	7.26	0.075	16.67	0.005

^a the τ value recorded at [MAA] = 0 M was 2.74 ns ($\chi^2 = 1.130$); ^b not determined due to low fluorescence signal; ^c the relative contribution of component i , f_i , was calculated from the relationship: $f_i = (\alpha_i \tau_i / \sum_{i=1}^n \alpha_i \tau_i) \times 100 \%$; ^d χ^2 value for each fit was equal or lower than 1.2.

CONCLUSIONS

The results of absorption measurements performed in the above study suggest that the HN molecule is able to form hydrogen-bonded complexes with different stoichiometries as well as the monocation, depending on the functional monomer concentration. However, at a short [MAA] range, i.e. at the condition mimicking a pre-polymerisation mixture, the presence of one hydrogen-bonding equilibrium in the ground state is observed. The association constant for 1:1 H-bonded HN/MAA complex may be estimated basing on the spectral change of absorption data. At the same experimental conditions, in the S_1 state a new equilibrium in the HN/MAA/toluene system is established and the HN zwitterion with decay lifetime of ~ 9 ns is formed. The exact mechanism of the above process is not clear yet. Taking into account results obtained in this study it may be assumed that the Z species are formed in the excited state from the 1:1 complex which undergoes a double proton transfer reaction or from another ground-state precursor (most probably the 1:2 complex) through a proton transfer with one MAA molecule. This hypothesis may be further supported by the fact that the value of lifetime recovered for the Z form in the HN/MAA/toluene system reminisces the lifetime assigned for HN zwitterionic phototautomers with stoichiometry equal or higher than 1:3 [5].

REFERENCES

[1] J.R.F. Allen, B.R. Holmstedt, *Phytochemistry*, 19 (1980) 1573; [2] M.M. Airaksinen, I. Kari, *Med. Biol.*, 59 (1981) 21; [3] I.A. Nicholls, K. Adbo, H.S. Andersson *et al.*, *Anal. Chim. Acta.*, 435 (2001) 9; [4] A. Dias, A.P. Varela, M. da G. Miguel *et al.*, *J. Phys. Chem.*, 96 (1992) 10290; [5] C. Carmona, M. Galán, G. Angulo *et al.*, *Phys. Chem. Chem. Phys.*, 2 (2000) 5076

ACKNOWLEDGEMENTS: A financial support from the State Committee for Scientific Research, Grant No. 3T08E06327 (Poland) is gratefully acknowledged.

THERMAL CHARACTERISTICS AND MORPHOLOGY OF PA6 NANOCOMPOSITES AND PA6/TPU BLENDS CONTAINING ORGANICALLY MODIFIED MONTMORILLONITE

Michał Strankowski^{1*}, Józef Tadeusz Haponiuk¹, Maria Gazda²,
Grzegorz Nowaczyk³

¹Department of Polymer Technology, Chemical Faculty,

²Faculty of Applied Physics and Mathematics, Gdańsk University of Technology,
G. Narutowicza Str. 11/12, 80-952 Gdańsk,

³Department of Macromolecular Physics UAM, Umultowska Str. 85, 61-614 Poznań.

* [Corresponding author. Tel.: +48 58 3472434; fax: +48 58 3472134; E-mail address:
mic@urethan.chem.pg.gda.pl (M. Strankowski)]

Introduction

Polymer composites modified with nanoparticles are inorganic-organic hybrid materials which attract great scientific and technological interest. Polymer layered-silicate nanocomposites represent advantageous alternative to conventional composites due to the large surface area and high aspect ratio of the incorporated layered silicates. It causes improvement of physical, mechanical and thermal properties at low nanoparticle content. Therefore these systems are expected to replace some polymers, polymer blends and traditional composites in products obtained by melt processing techniques [1-5] and simultaneously they are promising candidates for use in other applications. PA6 nanocomposites were the first one used in commercial products [6] and initiated a great development in the field of polymeric nanocomposites in the last two decades. Recently we have reported on synthesis of a new class of PA6 nanocomposite blends. Here we present studies about morphology, x-ray analysis and thermal properties.

Experimental

Materials: Montmorillonites modified with a quaternary ammonium salt (OMMT) (Cloisite[®] 10A and Cloisite[®] 20A) were purchased from Southern Clay Products Inc., Texas, USA.

All nanocomposite systems were obtained using a twin screw extruder from:

- commercial grade polyamide 6 (Tarnamid T-27 MS);
- polyurethanes (TPU) synthesized in our laboratory from poly(ethylene, butylene)adipate (PEBA) (commercial product Poles 55/20), 4,4'-methylenebis(phenyl isocyanate) (MDI) and 1,4-butanediol;
- appropriate montmorillonite.

Samples for the measurements were moulded by injection.

Methods: Thermal analysis (TG) was performed using Perkin-Elmer Thermogravimetric Analyzer TGA Pyris 1 at a heating rate of 20°C/min under nitrogen flow and heating program 50–600°C. The X-ray patterns of the crystalline residues were recorded in a X'Pert Philips diffractometer (source radiation: CuK_{α1}, λ = 0.1546 nm, 40 kV, 30 mA). In the 0,5÷10° 2θ range and at scanning rate 0.25°/s. Rheology of obtained systems were investigated using ARES (Advanced Rheometric Expansion System), in the 0,1÷100 rad/s frequency range and at the temperature 235°C. Morphology was

studied using Atomic Force Microscopy (AFM) - Digital Instruments (USA) NanoScope III in tapping mode (Silicon tips, model RTESP from Veeco).

Table 1. Samples designation and formulations.

Design.	Composition	Parts (wt%)	Design.	Composition	Parts (wt%)
PA6	PA6	100	NC-III	PA6/Cloisite 20A	98/2
NC-I	PA6/Cloisite 10A	98/2	NC-IV	PA6/Cloisite 20A	96/4
NC-II	PA6/Cloisite 10A	96/4	NCB-IV	PA6/TPU/Cloisite 20A	96/2/2
NCB-I	PA6/TPU/Cloisite 10A	96/2/2	NCB-V	PA6/TPU/Cloisite 20A	92.5/5.5/2
NCB-II	PA6/TPU/Cloisite 10A	92.5/5.5/2	NCB-VI	PA6/TPU/Cloisite 20A	90.5/5.5/4
NCB-III	PA6/TPU/Cloisite 10A	90.5/5.5/4			

Results and discussion

X-ray diffraction analysis was used to confirm formation of the PA6/OMMT nanocomposites and PA6/TPU/OMMT nanocomposite blends. The X-ray diffraction patterns are shown in the Figure 1.

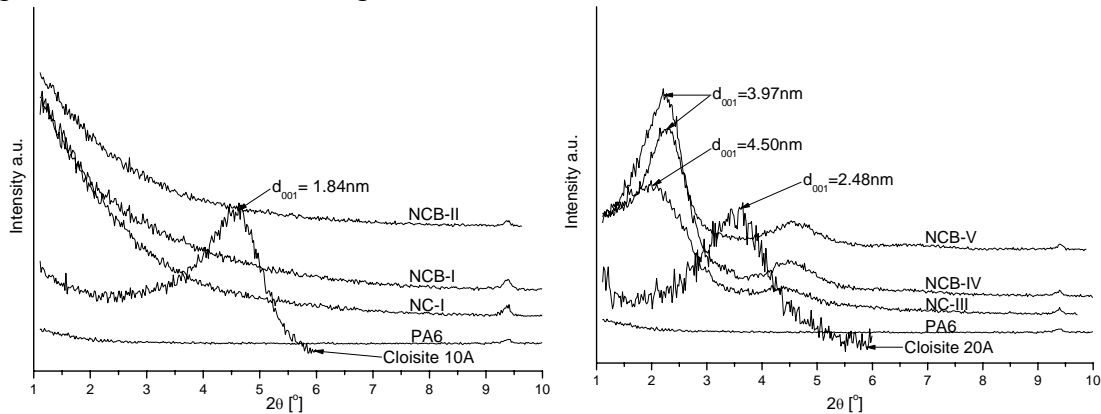


Fig. 1. X-ray diffraction patterns of OMMT (Cloisite 10A and Cloisite 20A), nanocomposites (NC) and nanocomposites blends (NCB) containing 2 wt% OMMT.

For nanocomposites containing aromatically modified Cloisite 10A exfoliated structure may be presumed since in the x-ray diffraction patterns (Fig. 1) there is no diffraction maxima of the montmorillonite present. This assumption was confirmed also by the TEM investigations. For the nanocomposites containing aliphatically modified Cloisite 20A in the x-ray diffraction patterns one can observe maxima at lower 2θ values. Therefore after recalculation the intergallery spacing was estimated as wide as about 1.5–2.0 nm and the structure of nanocomposites can be designated as intercalated.

Figure 2 shows the thermogravimetric (TG) curves for the virgin PA6 and the nanocomposites. Polyamide 6 nanocomposites obtained using either Cloisite 10A or Cloisite 20A exhibit better thermal stability comparing with the virgin polyamide. At low nanoparticle loading improvement of the stability was observed up to 2 wt% of the montmorillonite.

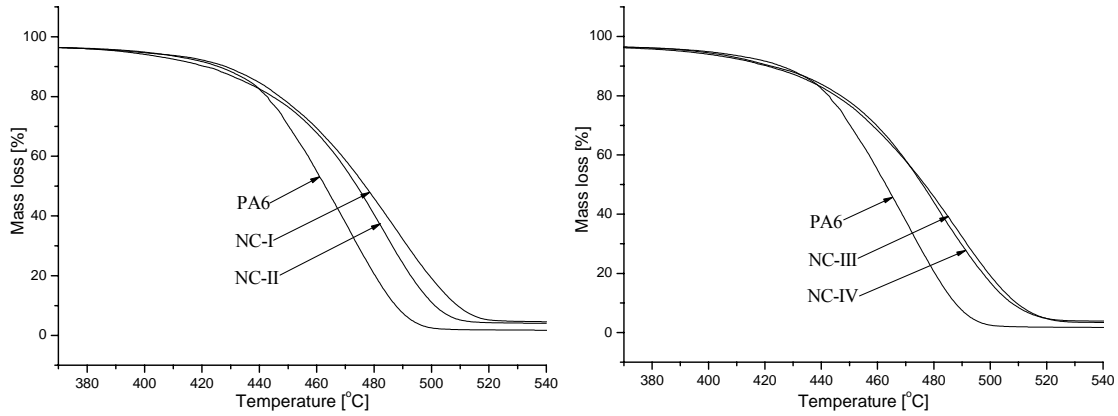


Fig. 2. TG curves for virgin PA6 and PA6 nanocomposites with different type and loading of OMMT.

The structure of nanocomposites strongly influences the rheological behavior, especially in the low frequency range [7]. Polymer nanocomposites with 2-D layered silicates exhibit pronounced shear-thinning behavior. Received nanocomposites have higher absolute viscosity in comparison to the unmodified polyamide 6. At low shear rates nanocomposite blends have higher absolute viscosity, especially for NCB-VI nanocomposite blend. The addition of thermoplastic polyurethane and organically modified montmorillonite caused increase of absolute viscosity.

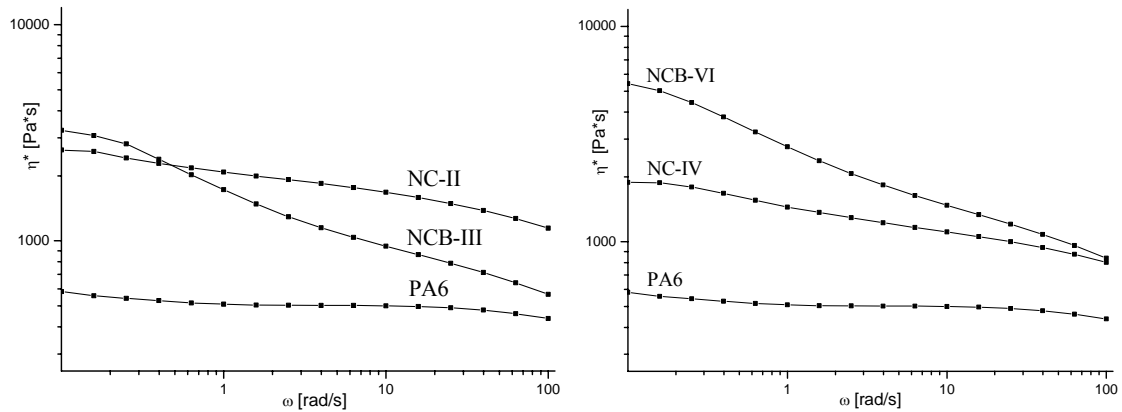


Fig. 3. Absolute viscosity vs. frequency for virgin PA6 and nanocomposite blends containing 4% organically modified montmorillonite.

The morphology was verified using Atomic force microscopy (AFM). Micrographs obtained in tapping-mode are presented in figure 4. Dark regions (Fig. 4a) represent amorphous phase, while the bright regions are the picture of crystalline forms. Addition of nanoclay caused increase in rigidity, what is represented by the greater content of bright regions (Fig. 4b, 4c).

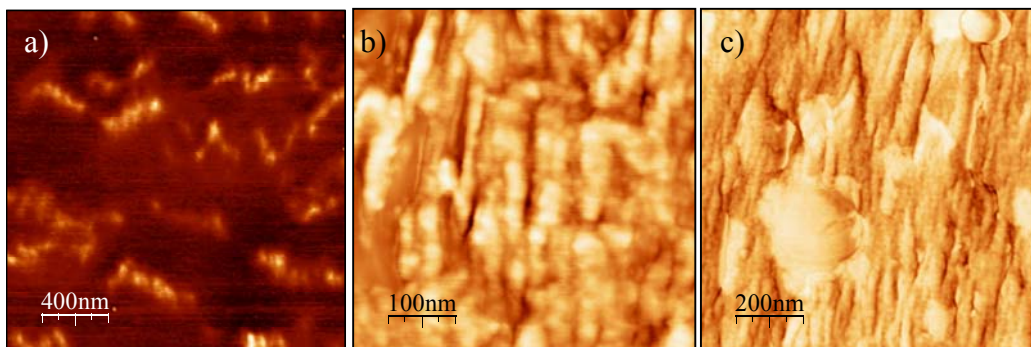


Fig. 4. AFM micrographs for virgin PA6 (a) and nanocomposites containing 2% (b) and 4% (c) of Cloisite 10A.

Conclusions

Structure and properties of PA6/OMMT nanocomposites and PA6/TPU/OMMT nanocomposite blends were investigated using two kinds of aromatically modified and aliphatically modified montmorillonites. Undertaken research confirmed the formation of exfoliated and intercalated structures respectively. PA6/TPU blends were advantageously modified by the nanofiller and exhibited at the same time improvement in yield stress, elasticity, tensile and barrier properties. In all cases improvement of viscosity and thermal properties was also observed. The morphology of these systems was additionally confirmed by AFM surface analysis.

Acknowledgements

We are thankful for the financial support from the Ministry of Scientific Research and Information Technology (Grant No. 3 T09B 109 28).

References

- [1] Ch. Ding, B. Guo, H. He, D. Jia, H. Hong, *Eur. Polym. J.* **41** (2005) 1781-1786.
- [2] T.J. Pinnavaia, G.W. Beall, *Polymer-Clay Nanocomposites*, Chichester, Wiley 2000.
- [3] G.H. Michler, F.J. Balta-Calleja, *Mechanical Properties of Polymer Based on Nanostructure and Morphology*, Taylor & Francis 2005.
- [4] S. Sinha Ray, M. Okamoto, *Progr. Polym. Sci.*, **28** (2003) 1593-1641.
- [5] L. Chazeau, C. Gauthier, G. Vigier, J.Y. Cavaille, *Handbook of Organic-Inorganic Hybrid Materials and Nanocomposites, Vol 2: Nanocomposites*, American Scientific Publ. 2003.
- [6] US patent 4,739,007; 1988.
- [7] H. S. Nalwa, *Handbook of Organic-Inorganic Hybrid Materials and Nanocomposites*, American Scientific Publishers, USA, 2003.

SYNTHESIS OF NEW DERIVATIVES OF 4-AMINO-10-OXA-4-AZATRICYCLO[5.2.1.0^{2,6}]DEC-8-ENE-3,5-DIONE

Jerzy Kossakowski¹, Marta Struga¹, Barbara Mirosław², Anna E. Koziol²

¹*The Medical University, Department of Medical Chemistry, 3 Oczki Str.,*

02-007 Warsaw

²*Faculty of Chemistry, Maria Curie-Skłodowska University, 20-031 Lublin, Poland*

10-Oxo-4-azatricyclo[5.2.1.0^{2,6}]dec-8-ene-3,5-dione derivatives are characterized by various pharmacological actions [1-4].

Imide (**a**) or anhydride (**b**) obtained in Diels-Alder reaction was used as a starting material [5]. Compounds (**a**) or (**b**) in reaction with hydrazine (80% aqueous solution) gave compound **1** [6]. Afterwards the compound **1** was subjected to the reaction with phenyl, 4-methoxyphenyl, ethyl isothiocyanate to be transformed into the corresponding thiourea derivatives. 4-Amino-10-oxa-tricyclo[5.2.1.0^{2,6}]dec-8-ene-3,5-dione (**1**) was used to the reaction with ethyl chloroformate, ethyl bromoacetate and acetic anhydride. Obtained esters (**2** and **5**) were transformed into the corresponding amides.

All final compounds were characterized by ¹H NMR spectra which corresponded with the proposed structures. The structure of obtained product (**4**) was confirmed by the X-ray crystallography.

A general synthesis pathway is given in Scheme 1.

Experimental

Chemistry.

Melting points were determined in a Kofler's apparatus and are uncorrected. The ¹H NMR spectra were recorded on a Bruker AVANCE DMX400 spectrometer, operating at 400.13 MHz. The chemical shift values are expressed in ppm relative to TMS as an internal standard. Elemental analyses were recorded with a CHN model 2400 Perkin-Elmer. Flash chromatography was performed on Merck silica gel 60 (200-400 mesh) using chloroform/methanol (19:1 vol.) mixture as eluent. Analytical TLC was carried out on silica gel F₂₅₄ (Merck) plates (0.25 mm thickness).

The diffraction data were collected at 275 K on a KM-4 diffractometer using the crystal of dimensions 0.22 × 0.15 × 0.11 mm and CuK α radiation. Within the θ range of 5.3 to 72.2°, 2445 reflections were collected. The structure was solved by direct methods and refined by full-matrix least-squares on F^2 (programs SHELXS97 and SHELXL97 [7,8]). The refinement of 175 parameters converged at final R indices: $R_1 = 0.0311$, $wR_2 = 0.0889$ (for 1039 observed reflections, $I > 2\sigma(I)$) and $R_1 = 0.1377$, $wR_2 = 0.1188$ (all data), and $Goof = 0.996$. The extinction coefficient was 0.0032(3), residual electron density $\Delta\rho(max) = 0.20$ and $\Delta\rho(min) = -0.18$ e \AA^{-3} .

4-Amino-10-oxa-tricyclo[5.2.1.0^{2,6}]dec-8-ene-3,5-dione (**1**) has been synthesized as described previously [6].

(3,5-Dioxo-10-oxa-4-aza-tricyclo[5.2.1.0^{2,6}]dec-8-en-4-yl)-carbamic acid ethyl ester (**2**), (3,5-dioxo-10-oxa-4-aza-tricyclo[5.2.1.0^{2,6}]dec-8-en-4-ylamino)-acetic acid ethyl ester (**5**), *N*-acetyl-*N*-(3,5-dioxo-10-oxa-4-aza-tricyclo[5.2.1.0^{2,6}]dec-4-yl)-acetamide (**4**).

0.01Mole (1.8g) of the compound **1** 3g of K₂CO₃ and 0.011 mole of ethyl chloroformate (1.1g) or ethyl bromoacetate (1.68g) or acetic anhydride (1.1g) in 100cm³ acetone were refluxed for 6h. The reaction mixture was filtered and the solvent was removed under a reduced pressure. The residue was crystallized from ethanol. Next it was purified by column chromatography (silica gel) using chloroform/methanol (19:1) as eluent.

2: m.p. 140-141°C. ¹H NMR (CDCl₃) δ (ppm): 1.22 (t, 3H, CH₃); 3.1 (s, 2H, CH-C=O); 4.15 (q, 2H, CH₂); 5.17 (s, 2H, CH-O); 6.06 (s, 2H, CH=). For C₁₁H₁₂N₂O₅ (252.22) calculated: 52.83 % C, 4.8 % H, 11.11 % N; found: 52.92 % C, 5.16 % H, 10.72 % N.

5: m.p. 144-145 °C. ¹H NMR (CDCl₃) δ (ppm): 1.22 (t, 3H, CH₃); 3.02 (s, 2H, CH-C=O); 4.15 (q, 2H, CH₂); 4.16 (s, 2H, CH₂); 5.17 (s, 2H, CH-O); 6.06 (s, 2H, CH=). For C₁₂H₁₄N₂O₅ (266.24) calculated: 54.13 % C, 5.3 % H, 10.52 % N; found: 54.26 % C, 5.32 % H, 10.62 % N.

4: m.p. 128°C. ¹H NMR (CDCl₃) δ (ppm): 1.68 (m, 2H, CH₂); 1.93 (m, 2H, CH₂); 2.11 (s, 3H, CH₃); 2.59 (s, 3H, CH₃); 3.1 (s, 2H, CH-C=O); 4.96 (s, 2H, CH-O). For C₁₂H₁₄N₂O₅ (266.25) calculated: 54.13 % C, 5.30 % H, 10.52 % N; found: 54.18 % C, 45.32 % H, 10.72 % N.

Crystal data for (**4**): C₁₂H₁₄N₂O₅, *M.W.* = 266.25, crystal system orthorhombic, space group *Pbca* with unit cell dimensions *a* = 6.977(1), *b* = 16.658(3), *c* = 21.361(4) Å and *V* = 2482.6(7) Å³; *Z* = 8, *d(calc)* = 1.425 g cm⁻³, *μ* = 0.952 mm⁻¹, *F*(000) = 1120.

(3,5-Dioxo-10-oxa-4-aza-tricyclo[5.2.1.0^{2,6}]dec-8-en-4-yl)-urea (**3**), 2-(3,5-dioxo-10-oxa-4-aza-tricyclo[5.2.1.0^{2,6}]dec-8-en-4-ylamino)-acetamide (**6**).

100cm³ of a 25% aqueous ammonia solution was added to a tightly closed vessel containing 0.01 mole of compound **2** (2.5g) or **5** (2.6g). The reaction mixture was kept for one week at room temperature. The obtained products **3** or **6** were collected by filtration and recrystallised from ethanol – water solution (1:1).

3: m.p. 170°C. ¹H NMR (CDCl₃) δ (ppm): 3.1 (s, 2H, CH-C=O); 4.20 (s, 2H, NN₂); 5.08 (s, 2H, CH-O); 6.06 (s, 2H, CH=). For C₉H₉N₃O₄ (223.18) calculated: 48.43 % C, 4.06 % H, 18.83 % N; found: 48.72 % C, 4.16 % H, 18.72 % N.

6: m.p. 182°C. ¹H NMR (CDCl₃) δ (ppm): 3.02 (s, 2H, CH-C=O); 4.16 (s, 2H, CH₂); 4.82 (s, 2H, NH₂); 5.17 (s, 2H, CH-O); 6.06 (s, 2H, CH=). For C₁₂H₁₄N₂O₅ (266.24) calculated: 54.13 % C, 5.3 % H, 10.52 % N; found: 54.26 % C, 5.32 % H, 10.62 % N.

1-(3,5-Dioxo-10-oxa-4-aza-tricyclo[5.2.1.0%2,6&]dec-8-en-4-yl)-3-(phenyl)-thiourea (**7**), 1-(3,5-Dioxo-10-oxa-4-aza-tricyclo[5.2.1.0%2,6&]dec-8-en-4-yl)-3-(4-methoxyphenyl)-thiourea (**8**), 1-(3,5-Dioxo-10-oxa-4-aza-tricyclo[5.2.1.0%2,6&]dec-8-en-4-yl)-3-(ethyl)-thiourea (**9**).

A solution of compound **1** (0.01 mole; 1.8g) in acetonitrile (6 cm³) was treated with phenyl, 4-methoxyphenyl, ethyl isothiocyanate (0.011mol) and the mixture was refluxed for 6h. The precipitate was filtered and then washed with ether to give compounds **7** - **9**. Next it was purified by column chromatography (silica gel) using chloroform/methanol (19:1) as eluent.

7: m.p. 167-168°C. ¹H NMR (CDCl₃) δ (ppm): 3.0 (s, 2H, CH-C=O); 5.21 (s, 2H, CH-O); 6.58 (s, 2H, CH=); 7.2-7.36 (m, 5H, CH_{arom.}); 9.93 (s, 1H, NH); 10.34 (s, 1H, NH). For C₁₅H₁₃N₃O₃S (315.33) calculated: 57.13 % C, 4.16 % H, 13.33 % N; found: 57.24 % C, 4.16 % H, 13.24 % N.

8: m.p. 178°C. ¹H NMR (CDCl₃) δ (ppm): 3.83 (s, 2H, CH-C=O); 3.79 (s, 3H, OCH₃); 5.21 (s, 2H, CH-O); 6.51 (s, 2H, CH=); 6.81-7.45 (m, 5H, CH_{arom.}); 8.31 (s, 1H, NH);

8.5 (s, 1H, NH). For $C_{16}H_{15}N_3O_4S$ (345.37) calculated: 55.64 % C, 4.83 % H, 12.12 % N; found: 55.82 % C, 4.48 % H, 12.16 % N.

9: m.p. 165°C. 1H NMR ($CDCl_3$) δ (ppm): 1.74 (t, 3H, CH_3); 2.13 (q, 2H, CH_2); 3.96 (s, 2H, $CH-C=O$); 5.15 (s, 2H, $CH-O$); 6.56 (s, 2H, $CH=$). For $C_{11}H_{13}N_3O_3S$ (267.3) calculated: 49.43 % C, 4.9 % H, 15.72 % N; found: 49.64 % C, 4.92 % H, 15.78 % N.

References

[1] J. Kossakowski, A. Raszkievicz, R. Bugno, A.J. Bojarski: *Pol. J. Pharmacol.*, 56 (2004) 843-848.

[2] C.H. Grogan, L.M. Rice: US Patent, (1963) 2,784,199.

[3] J. Kossakowski, M. Struga, M.E. Maciąg, B.J. Starościak: *Acta Pol. Pharm.*, 62 (2004) 289-294.

[4] J. Kossakowski, M. Struga, B.J. Starościak, I.E. Maciąg: *Acta Pol. Pharm.*, 61 (2004) 367-371.

[5] H. Kwart, J. Burchuk: *J. Am. Chem. Soc.*, 74 (1952) 3094-3097.

[6] M. Struga, B. Mirosław, I. Wawrzycka-Gorczyca, J. Kossakowski, A.E. Koziół: *Polish J. Chem.*, 81 (2007) 3-9.

[7] G.M. Sheldrick, SHELXS-93: Program for crystal structure solution; University of Göttingen, Germany, (1993).

[8] G.M. Sheldrick, SHELXL-97: Program for the refinement of crystal structures from diffraction data; University of Göttingen, Germany, (1997).

Scheme 1.

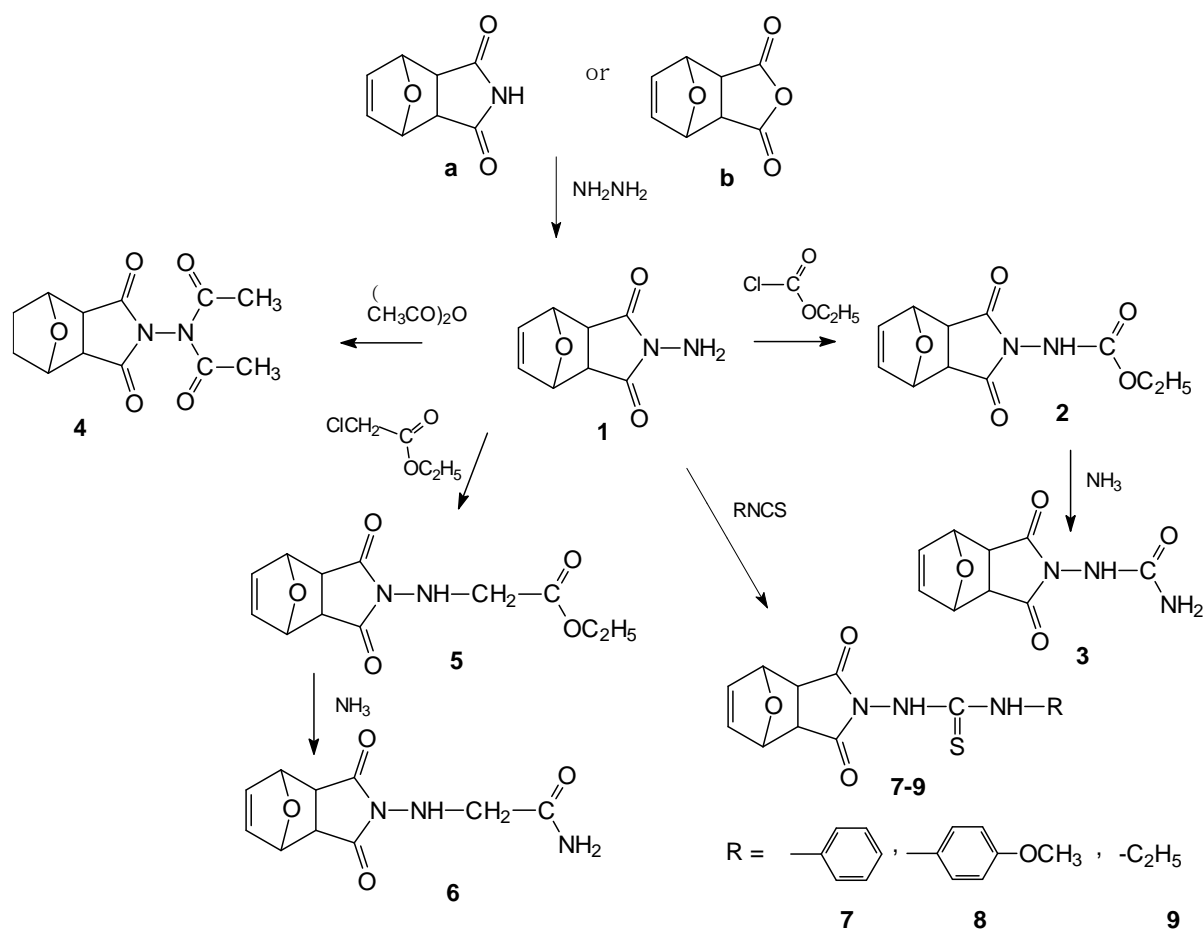


Fig. 1. Perspective view of molecular structure of compound **4**. *Cis, exo* configuration at the ring junction (C3–C8); the N,N-diacetyl fragment is planar with perpendicular orientation to the imid ring plane; the C=O bonds of acetyl groups are *anti*.

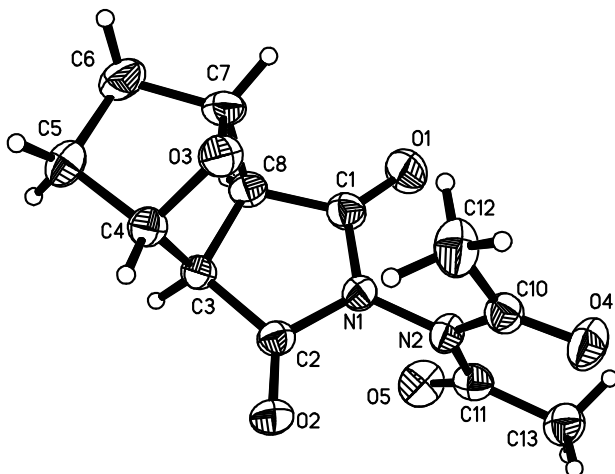


Table 1. Bond lengths (Å).

N(1)-N(2)	1.383(2)	C(3)-C(4)	1.525(3)
N(1)-C(1)	1.393(3)	C(3)-C(8)	1.542(3)
N(1)-C(2)	1.396(3)	C(4)-C(5)	1.529(3)
N(2)-C(10)	1.416(2)	C(5)-C(6)	1.537(3)
N(2)-C(11)	1.420(3)	C(6)-C(7)	1.521(3)
O(1)-C(1)	1.205(3)	C(7)-C(8)	1.542(3)
O(2)-C(2)	1.201(2)	C(10)-C(12)	1.490(3)
O(3)-C(4)	1.440(2)	C(11)-C(13)	1.486(3)
O(3)-C(7)	1.442(3)	N(2)-N(1)-C(1)	122.5(2)
O(4)-C(10)	1.198(2)	N(2)-N(1)-C(2)	123.2(2)
O(5)-C(11)	1.199(2)	C(1)-N(1)-C(2)	114.0(2)
C(1)-C(8)	1.489(3)	C(1)-N(1)-N(2)-C(10)	93.2(2)
C(2)-C(3)	1.508(2)	C(2)-N(1)-N(2)-C(11)	90.6(2)

INFLUENCE OF HUMAN SERUM ALBUMIN ON PHOTOCHEMICAL PROPERTIES OF CHLORIN E₆

Edyta Sulak¹, Marian Wolszczak¹, Jerzy Kroh¹, Cezary Peszyński-Drewny²

¹*Institute of Applied Radiation Chemistry, Technical University of Lodz,*

Wroblewskiego 15, 93-590 Lodz

²*Laser Diagnostics and Therapy Centre of the Technical University of Lodz*

Wolczanska 215, 93-005 Lodz

INTRODUCTION

Photolon® (*Fig.1*) is a photosensitizer successfully used in photodynamic therapy of tumors (PDT) in Russia and Belarus. In this therapy the photosensitizing and tumor-localized chemical is activated with a specific wavelength of non-ionizing electromagnetic radiation to produce cytotoxic species.

These cytotoxic species are generated in the tissue by the triplet state of photosensitizer via two possible photooxidation pathways. Type I – involving radical intermediates and Type II – with singlet oxygen as an intermediate [1-3]. The main cause of photodamage of a living tissue is ascribed to singlet oxygen. However, the relative importance of these two main pathways continues to be a matter for experiments and discussion. In both cases, the most readily modified targets are some sulfur containing or aromatic and heterocyclic amino acid residues, unsaturated lipids and steroids [4].

Since proteins, next to water, are the most abundant constituents of cells and extracellular fluids by weight, the probability of their interaction with cytotoxic species is higher than for other biomolecules. Upon photosensitizer administration in the bloodstream drug first encounters plasma proteins. Affinity of photosensitizer to plasma proteins thus plays an important role in drug distribution and photodynamic outcome.

For our studies human serum albumin (HSA) was chosen as the most abundant protein in human blood plasma. The present work is aimed to study the influence of HSA on photochemical properties of photosensitizer.

EXPERIMENTAL

Photolon® was obtained from JSC Belmedpreparaty, Minsk, Belarus, and Chle₆ was purchased from Porphyrin Products, UK. HSA was obtained from Sigma-Aldrich.

Transient triplet-triplet absorption spectra were recorded using a Lambda-Physik COMPex 201 XeCl excimer laser. Experimental details were described earlier [5]. Fluorescence polarization was measured on Fluoromax-2 spectrofluorimeter (Jobin Yvon Co., excitation 658 nm, emission 668 nm). In all measurements 1/15 M KH₂PO₄/Na₂HPO₄ buffer – pH: 8.6 ÷ 8.8 – was used as a solvent.

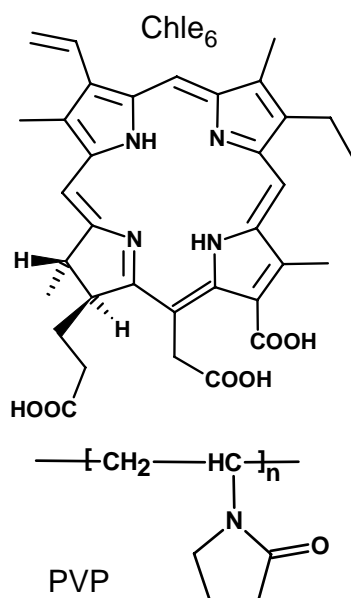


Fig.1 Photolon® represents a pharmaceutical composition of chlorin e₆ (Chle₆) and polyvinylpyrrolidone (PVP).

RESULTS AND DISCUSSION

The absorption spectrum of the buffer solution of Photolon® comprises of an intense near-UV Soret band and four weaker Q-bands. The presence of PVP does not significantly influence spectral properties of Chle₆ [6]. The Soret band located at 401 nm in the absorption spectrum of buffer solution undergoes a red shift to 408 nm upon addition of HSA. A more prominent red shift is observed for the most intensive Q-band, from 655 nm to 664 nm, with 33% increase in the intensity of this band (Fig.2).

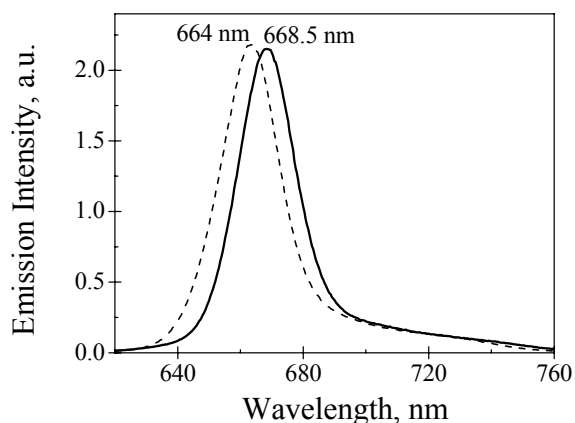
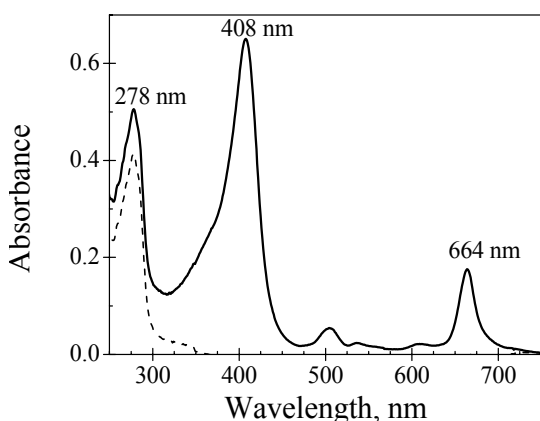


Fig.2 Absorption spectrum of 12 μM HSA (dash line) and absorption spectrum of 12.6 μM Chle₆ (dash line) and the same 12 μM HSA with 13.5 μM Photolon® (solid line). Fig.3 Fluorescence emission spectra of system containing also 12 μM HSA (solid line). $\lambda_{exc}=419$ nm.

The steady-state fluorescence spectrum of Photolon® and Chle₆ exhibits less marked response to the addition of HSA (Fig.3). The fluorescence band undergoes a small shift in the presence of HSA and the fluorescence intensity decreases negligibly, indicating the absence of fluorescence quenching of excited singlet state of Chle₆ molecule by constituents of the HSA backbone. The inefficient singlet state quenching is attributed to its short lifetime, of the order a few ns.

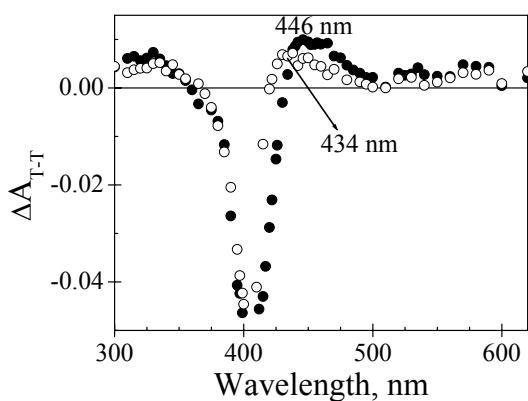


Fig.4 Transient difference triplet-triplet absorption spectra of 13.5 μM Photolon® (black circle) upon addition of 12 μM HSA (open circle) recorded 300 ns after pulse of light.

The triplet excited state of Chle₆ molecule, which can be monitored by laser flash photolysis, absorbs intensely around 440 nm. Upon excitation with a 350 nm laser pulse the triplet-triplet absorption, originating from the lowest excited triplet state of Chle₆, increases, and a rapid onset of bleaching of the ground state absorption in the region of the Soret band is observed. For the buffer solution of Photolon®, the triplet – triplet absorption maximum is at 434 nm. On addition of HSA the triplet – triplet absorption band maximum shifts to 446 nm with 1.5-fold increase in the absorbance (Fig. 4). Flash photolysis studies indicate that after decay of the triplet state no long-lived transient species

are present that might arise from electron transfer between the triplet and amino acids of HSA.

The triplet-triplet absorption decays obey first-order kinetics with rate constants $k_{T-T} \sim 10^4 \div 10^6 \text{ s}^{-1}$ depending on oxygen concentration (*Fig. 5, transient 1 and 3*). The kinetic profiles of the decay of the triplet – triplet transient absorption, probed at 436 nm, and the recovery of the bleached signal, probed at 400 nm, are presented in *Fig. 5* and *Fig.6*, respectively. Temporal evolution of the transient triplet-triplet absorption band is correlated with evolution of the bleached band located at 400 nm.

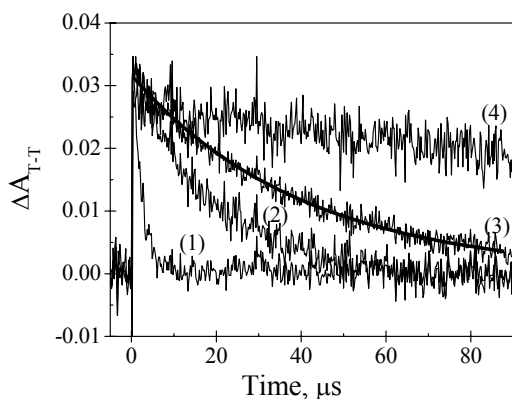


Fig5. Time profiles of the absorbance recorded at 436 nm after laser pulse irradiation of 13.7 μM Photolon® at 0.27 mM (1) and 0 mM (3) oxygen concentration [7] and in the presence of 12.3 μM HSA at 0.27mM (2) and 0 mM (4) oxygen concentration. The initial value of absorbance is normalized to 0.0346.

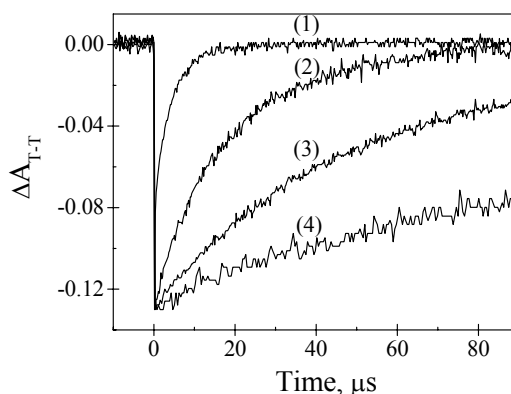


Fig6. Time profiles of the absorbance recorded at 400 nm after laser pulse irradiation of 13.7 μM Photolon® at 0 mM oxygen concentration (3) and upon addition of 12.3 μM HSA at 1.27 mM (1) 0.27mM (2) and 0 mM (4) oxygen concentration [7]. The initial value of absorbance is normalized to -0.13.

The monoexponential decay of the triplet absorbance indicates that Chle₆ could be complexed at a single binding site among many different subdomains of HSA which are capable to trap a variety of agents such as drugs, fatty acids or metabolites in the bloodstream.

The triplet state of Chle₆ generated in the buffer solution of Photolon® is efficiently quenched by molecular oxygen (as observed for Photolon® in earlier studies [6]). The triplet-triplet absorption lifetime (t_{T-T}) decreases over eighty-fold on going from the oxygen saturated to the oxygen free solution. The estimated rate constant for oxygen quenching (k_{O_2}) is greater than $10^9 \text{ M}^{-1}\text{s}^{-1}$ and is controlled by the diffusion of oxygen. In the presence of HSA the value of k_{O_2} decreases to $\sim 10^8 \text{ M}^{-1}\text{s}^{-1}$. The Chle₆ is bound to HSA in a form that permits dynamic quenching by molecular oxygen, but the rate of quenching is ten times slower than that measured for the noncomplexed photosensitizer. The addition of HSA causes an increase in the t_{T-T} up to a maximum value of 180 μs under oxygen free conditions (*Fig. 5, transient 2 and 4*). In the same conditions the t_{T-T} for the buffer solution of Photolon® is 40 μs. Increase in the t_{T-T} in the presence of HSA indicates the Chle₆ molecules get incorporated in the HSA assemblies. Such incorporation causes the Chle₆ molecules to drift apart from oxygen molecules thereby

causing that the triplet state is stable under oxygen free conditions, with the lifetime greater than 150 μ s. In this term, we have observed protective effect of HSA.

Similar effect we have observed in the studies of the interaction of Chle₆ with hydrated electron generated by pulse radiolysis.

The following *Table 1* summarises the polarization measurements. By monitoring the degree of fluorescence polarization of the photosensitizer one can detect significant changes in its mobility, and hence conclude about interaction or binding of Chle₆ molecule with other molecules present in its vicinity. High degree of fluorescence polarization of photosensitizer molecule in the presence of HSA indicates the low mobility of the Chle₆ within the binding site of HSA and suggesting that photosensitizer is buried deeply inside the protein where is protected against a variety of agents such as hydrated electron, radicals or oxygen molecules. In the presence of PVP, likewise in the presence of proteins but to a smaller extent, Chle₆ molecules can be fixed in the hydrophobic cavities of the polymer.

SYSTEM	Chle ₆	Chle ₆ /PVP	Chle ₆ /HSA	Photolon®	Photolon®/HSA
<i>P</i> _{668 nm}	0.042	0.119	0.344	0.076	0.326 (669 nm)

Table 1. The degrees of fluorescence polarization of 16.7 μ M Chle₆ and 13.6 μ M Photolon® solutions before and after addition of 11.5 μ M HSA or 72 μ M (per monomer unit) PVP.

Studies of the influence of HSA on photochemical properties of Chle₆ indicate that photosensitizer binds to HSA and independently of the presence of polymer Chle₆ molecules are located in the same protein domain. On the basis of obtained results it can be also affirmed that the triplet excited states of a photosensitizer can be used as probes for the microenvironments experienced within the binding sites of transport proteins. These probes are not employed as substitutes for singlet state probes but deliver additional information that is not easily accessible with fluorescent probes.

Acknowledgements. The authors thanks the Ministry of Science and Information Society Technologies, grant no. 3 T09A 112 28, for financial support. This work was partially supported under Ministry's subsidy project (138/E-370/SPB/COST/KN/DWM 103) in the framework of COST P9 Action.

LITERATURE:

- [1] B. W. Henderson, T. J. Dougherty, in: *Photodynamic Therapy. Basic Principles and Clinical Applications, Part 1*, Marcel Dekker (ed.), New York, 1992
- [2] R. Bonnett, *J. Heterocyclic Chem.*, 39 (2002) 455
- [3] D.E.J.G.J. Dolmans, D. Fukumura, R. K. Jain, *Nature*, 3 (2003) 380
- [4] G. Jori, J. D. Spikes, in: *Topics in Photomedicine*, K. C. Smith (ed), Plenum Press, New York, 1984
- [5] M. Wolszczak, E. Grzesiak, D. Kowalczyk and R. Ostaszewski, *Proc. SPIE*, 4749 (2002) 259
- [6] E. Sulak, M. Wolszczak, J. Kroh, C. Peszyński-Drews, *Annals of the Polish Chemical Society*, 1 (2005) 684
- [7] S. L. Murov, I. Carmichael, G. L. Hug, in: *Handbook of Photochemistry Second Edition Revised and Expanded*, Marcel Dekker (ed.), New York, 1993, p.293

DFT CALCULATION OF STRUCTURE AND VIBRATIONAL SPECTRUM OF β -4-HYDROXY-1-METHYL-PIPERIDINE BETAININE HYDROCHLORIDE

M. Szafran¹, Z. Dega-Szafran¹, J. Koput¹, E. Dulewicz¹, W.B. Person², K. Szczepaniak²

¹Faculty of Chemistry, Adam Mickiewicz University, 60-780 Poznań, Grunwaldzka 6, Poland

²Department of Chemistry, University of Florida, P O Box 117200 Gainesville, Florida 32611, USA

Two polymorphic crystals (α and β) of 4-hydroxy-1-methylpiperidine betaine hydrochloride, HO-MPBH⁺·Cl⁻ have been synthesized and their structures solved by the X-ray diffraction method [1]. The piperidine ring adopts a chair conformation and the hydroxy group at C(4) in the α -polymorph is in the axial position, while in the β -polymorph it is in the equatorial one. In both polymorphs the CH₂COOH is in equatorial position, while the CH₃ group in axial one. In α -HO-MPBH⁺·Cl⁻ the molecules are linked by COOH...Cl and Cl...HOC(4) hydrogen bonds of 2.988(2) and 3.158(3) Å into infinite chains antiparallel to each other. In β -HO-MPBH⁺·Cl⁻ there are two non-equivalent chains in the unit cell, formed by $\beta(1)$ and $\beta(2)$ molecules, containing COOH...Cl and Cl...HOC(4) hydrogen bonds of lengths: 2.974(2) and 3.147(3) Å in $\beta(1)$ and 3.011(2) and 3.147(3) Å in $\beta(2)$. These chains are linked by C-H...Cl and van der Waals contacts into polar ribbons.

The aim of the present work is to predict the structure and vibrational FTIR spectrum of β -HO-MPBH⁺·Cl⁻ using the B3LYP/6-31G(d,p) level of theory [2-4]. The optimized structures of $\beta(1)$ and $\beta(2)$ molecules have identical energies (-1055.12865 a.u.), dipole moments (11.33 D) and geometries. Most of the calculated bond lengths and angles are slightly greater than those in the crystal. The predicted COOH...Cl hydrogen bond distance is 2.982 Å, which is shorter than that found in the crystal (2.974(2)). In the optimized structure the C(4)OH group is not engaged in H-bond (Fig. 1)

The optimized structure of β -HO-MPBH⁺·Cl⁻ is shown in Fig. 1. β -HO-MPBH⁺·Cl⁻ is insoluble in aprotic organic solvents and its vapour pressure is very low, thus the IR spectrum was measured in the solid state and is shown in Fig. 2.

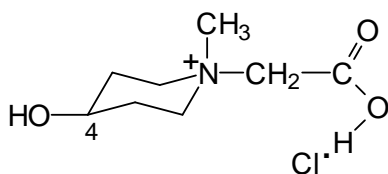


Fig. 1.
Structure of β -HO-MPBH⁺·Cl⁻

The local symmetry coordinates were defined in terms of the internal valence coordinates, following the IUPAC recommendation [6]. The force fields so determined were used to calculate the wavenumbers and vibrational PED (potential energy distribution) among the normal coordinates. PED is defined as recommended by Keresztury and Jalsovszky [7] and calculated with program PACK. Table lists the calculated harmonic frequencies, intensities and PED.

The observed frequencies of the C(4)OH group are at: 3336 cm⁻¹ (ν OH) and 1200 cm⁻¹ (δ OH), and on deuteration they shift to 2777 and 912 cm⁻¹, respectively. In the optimized molecules the OH group is not engaged in H-bond and the calculated frequencies are at much higher wavenumbers (3738 cm⁻¹). The broad absorption in the 2900-2400 cm⁻¹ region (Fig. 2) arises from the ν OH vibration of the COOH...Cl group. A similar absorption is present in the FTIR spectrum of 1-methylpiperidine betaine hydrochloride, MPBH⁺·Cl⁻ [5]. On deuteration the ν OD appears at 2200-1900 cm⁻¹ region. The in-plane deformation bands are at 1403 cm⁻¹ (δ OH) and 942 cm⁻¹ (δ OD). The strong band at 1755 cm⁻¹ arises from the ν C=O vibration.

Table. Observed and calculated (B3LYP/6-31G(d,p)) vibrational frequencies (cm^{-1}), absolute intensities (A, km/mol) and potential energy distribution (PED, %) for β -4-hydroxy-1-methylpiperidinium betaine hydrochloride, β -HO-MPBH-Cl

	ν_{obs}	ν_{cal}	$\nu_{\text{scal}}^{\text{b}}$	A	Assign.	PED
Q1	3336s	3814	3738	24.6	ν_{OH}	(100-)
Q2		3211	3147	5.2	$\nu_{\text{as}}\text{CH}_3$	(88+)
Q3		3166	3104	28.1	$\nu_{\text{as}}\text{CH}_3$ $\nu_{\text{s}}\text{CH}_3$	(72+) (19+)
Q4		3160	3097	6.6	$\nu_{\text{as}}\text{CH}_2$ $\nu_{\text{s}}\text{CH}_2$	(80-) (14+)
Q5	3079 ^a	3150	3088	16.9	$\nu_{\text{as}}\text{CH}_2$	(88-)
Q6	3069 ^a	3131	3069	12.0	$\nu_{\text{as}}\text{CH}_2$	(93-)
Q7		3119	3057	15.2	$\nu_{\text{as}}\text{CH}_2$	(95-)
Q8		3195	3044	16.1	$\nu_{\text{as}}\text{CH}_2$	(86-)
Q9	3018 ^a	3082	3021	26.6	$\nu_{\text{s}}\text{CH}_2$ $\nu_{\text{as}}\text{CH}_2$	(67-) (12-)
Q10		3075	3014	19.8	$\nu_{\text{s}}\text{CH}_2$	(87+)
Q11	3008 ^a	3071	3010	35.0	$\nu_{\text{s}}\text{CH}_2$ $\nu_{\text{s}}\text{CH}_2$	(67-) (11+)
Q12	2985 ^a	3059	2999	119	$\nu_{\text{s}}\text{CH}_2$ $\nu_{\text{s}}\text{CH}_2$ $\nu_{\text{s}}\text{CH}_2$	(64+) (15-) (11-)
Q13		3057	2997	10.3	$\nu_{\text{s}}\text{CH}_2$	(77-)
Q14	2974 ^a	3037	2977	83.1	$\nu_{\text{s}}\text{CH}_3$ $\nu_{\text{as}}\text{CH}_3$	(73+) (14-)
Q15	2919 ^a	2962	2904	44.6	ν_{CH}	(99+)
Q16	2900- 2400br	2805	2749	1323	$\nu(\text{OHCl})$ ν_{OH}	(55+) (42+)
Q17	1755vs	1825	1789	352	ν_{CO}	(78-)
Q18		1544	1514	25.0	β_{Me2} β_{Me4}	(54-) (21+)
Q19		1535	1505	7.2	β_{Me4} CH_2 sciss	(39+) (19+)
Q20		1528	1498	2.5	CH_2 sciss CH_2 sciss CH_2 sciss β_{Me2}	(23+) (20-) (13+) (11-)
Q21	1484w	1513	1483	6.0	CH_2 sciss CH_2 sciss	(48-) (35-)
Q22	1467w	1510	1480	14.0	CH_2 sciss CH_2 sciss β_{Me2} CH_2 sciss	(48+) (18+) (15+) (11-)
Q23		1495	1466	2.4	CH_2 sciss CH_2 sciss CH_2 sciss	(32+) (27-) (12-)
Q47	1026m	1039	1019	16.1	ν_{CC}	(46+)
Q48	1005w	1027	1007	16.2	CH_2 rock	(33-)
Q49		1005	985	37.6	δ ring $\nu_{\text{C-O}}$ ν_{CN}	(18-) (11-) (11-)
Q24	1459w	1491	1461	6.5	CH_2 sciss β_{Me1} CH_2 sciss β_{Me4}	(30+) (15+) (15-) (11-)
Q25	1445vw	1471	1442	33.3	CH_2 sciss β_{Me1}	(44+) (28-)
Q26	1436w	1461	1432	48.8	CH_2 wag β_{Me1}	(26+) (24+)
Q27	1421m	1450	1422	35.4	γ_{CH} $\delta_{\text{s}}(\text{OHCl})$ β_{Me1}	(26+) (14+) (10-)
Q28	1403w	1439	1410	235	δ_{OH} (OHCl)	(41-) (14+)
Q29	1398w	1430	1402	12.4	CH_2 wag	(38-)
Q30	1383m	1407	1380	6.6	δ_{CH} CH_2 wag γ_{CH}	(25+) (24-) (11+)
Q31	1360vw	1395	1367	5.1	CH_2 wag δ_{CH} CH_2 wag	(31+) (13+) (11-)
Q32		1386	1359	1.1	CH_2 twist CH_2 wag CH_2 twist	(36-) (22+) (12-)
Q33	1340w	1357	1330	12.7	CH_2 wag CH_2 twist	(45-) (11-)
Q34	1332w	1342	1315	5.7	CH_2 wag CH_2 twist γ_{CH}	(26-) (11-) (11-)
Q35		1320	1294	14.1	CH_2 twist CH_2 wag CH_2 wag	(14-) (12+) (10+)
Q36	1309w	1306	1280	23.9	ν_{CO} CH_2 wag	(33-) (21-)
Q37	1274w	1299	1273	3.5	CH_2 twist CH_2 twist γ_{CH}	(30-) (17+) (11-)
Q38	1253w	1268	1242	3.4	CH_2 twist β_{Me3} CH_2 twist	(18+) (16+) (13-)
Q39	1200vs	1259	1234	40.3	δ_{OH} CH_2 twist	(20-) (11+)
Q40		1223	1199	1.4	β_{Me3}	(41-)
Q41	1198m	1208	1184	11.6	CH_2 twist β_{Me5}	(27-) (19-)
Q42	1154w	1168	1145	5.9	β_{Me5} CH_2 twist	(16+) (15-)
Q43		1162	1139	3.5	CH_2 rock TCO CH_2 twist	(13-) (12-) (10+)
Q44		1123	1101	51.2	$\nu_{\text{C-O}}$ δ ring	(57-) (11+)
Q45	1088m	1091	1069	44.9	ν_{CC} $\delta_{\text{s}}(\text{OHCl})$ ν_{CC}	(23+) (19+) (15-)
Q46	1042w	1051	1031	9.8	ν_{CC} β_{Me5} ν_{CN}	(34-) (13-) (12+)
Q65	442w	454	445	6.0	τ_{CN} τ_{CN} δ_{CN}	(18-) (18-) (12+)
Q66		439	430	1.3	δ_{CN}	(41-) (14+)
Q67		412	404	4.2	τ_{CN} τ ring	(27+) (16+)

					CH ₂ rock	(11+)
Q50	974vw	982	963	7.2	CH ₂ rock vCN	(18+) (16+)
Q51	949w	952	933	12.3	CH ₂ rock CH ₂ rock	(17-) (12-)
Q52	940w	940	921	4.8	vCC vCN vCO	(23-+) (20+) (10-)
Q53	907w	932	914	73.5	γ(OHCl) γOH δ(OHCl)	(40+) (24-) (24+)
Q54	883m	904	886	13.4	vCN vCN vCC CH ₂ rock	(21+) (16-) (12-) (10-)
Q55	863m	875	858	10.3	vCN vCC	(20-) (18+)
Q56	832w	825	809	4.8	vCC vCC CH ₂ rock vCN	(22+) (20+) (13-) (12-)
Q57	799w	805	789	4.0	CH ₂ rock CH ₂ rock CH ₂ rock vCN	(21-) (20+) (14+) (10-)
Q58	773vw 735w	776	761	16.5	vCN τCO τCO δCN	(17+) (17-) (13+) (12-)
Q59	667w	695	667	2.2	vCN vCN vCN	(24-) (19-) (16-)
Q60	648w	656	643	3.2	δCO ₂ δ ring δCO ₂	(27+) (17+) (11+)
Q61	623w	587	576	10.2	δCO ₂ δ ring τCO vCN	(15+) (13-) (11+) (11+)
Q62	518w	513	503	6.6	δ ring δCO	(39+) (11-)
Q63		489	480	14.2	δCO ₂ τCO δ ring τCN	(16+) (13+) (12-) (10-)
Q64		470	461	2.6	τ ring δ ring τCO δ ring τCN	(17+) (16-) (16-) (12+) (12-)

Q68		352	345	0.3	τCN	(83+)
Q69		340	333	6.6	δCO δ ring δCN	(51+) (26+) (11-)
Q70		306	300	30.0	δ ring γOH τCN τCN	(36-) (13+) (11-) (11-)
Q71		300	294	93.7	γOH	(81+)
Q72		291	285	4.3	τ ring τCO τCN	(39+) (12+) (11+)
Q73		257	252	8.4	δCN	(21+)
Q74		239	234	5.4	τ ring τCN	(77+) (10-)
Q75		201	197	33.5	vOH v(OHCl)	(42+) (41-)
Q76		192	189	7.8	δCN γOHCl γOH δOH	(26-) (23-) (10-) (10+)
Q77		156	153	24.9	δ(OHCl) δCN δOH δCN	(29-) (17-) (16-) (14+)
Q78		99	97	3.1	γOH τCN δCN	(42-) (13-) (11+)
Q79		86	84	10.2	τ ring γOH	(69-) (28-)
Q80		68	67	0.2	τCO τCO τCN	(48+) (40+) (15+)
Q81		49	48	6.1	τCN τCO	(61+) (17-)

^a Band cover by the broad intense absorption due to the vOH vibration. Their wavenumbers were estimated from the second derivative spectrum; ^b Wavenumbers scaled by 0.98

Inspection of the calculated and experimental data in Table shows that the differences between the experimental wavenumbers and calculated harmonic scaled by 0.98 factor are in the range between -47 and $+34$ cm^{-1} . The largest difference is for the vOH vibration of the hydroxyl group at C(4) atom. In the crystal the C(4)OH group is engaged in the hydrogen bond of length 3.147(3) Å with a neighbouring Cl⁻ anions.

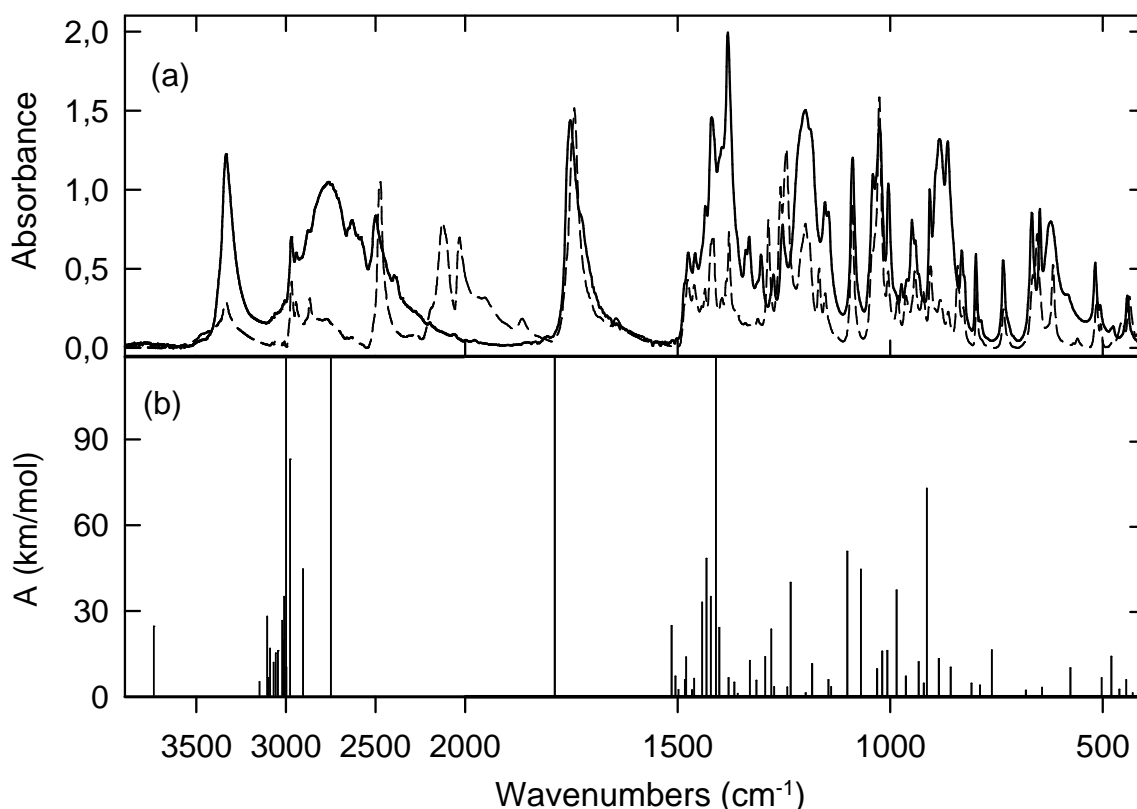


Fig. 2. Comparison of the spectra of β -HO-MPBH⁺·Cl⁻: (a) FTIR spectrum in Nujol and Fluorolube emulsions; β -DO-MPBD⁺·Cl⁻ dotted line and (b) the spectrum calculated at the B3LYP/6-31G(d,p) level of theory and scaled by 0.98 factor.

The IR spectrum of β -DO-MPBD⁺·Cl⁻ has been used to reexamine the question of vibrational assignments. PED contributions are the same for 45 normal modes. For the other vibrations one more or one less PED contribution is observed. A similar situation was observed for pyridine [8], pyridine betaine [9] and formamide [10].

Acknowledgement.

Calculations were performed at the Poznań Supercomputing and Networking Centre

References

- [1] Z. Dega-Szafran, E. Dulewicz, G. Dutkiewicz, Z. Kosturkiewicz, M. Szafran, *J. Mol. Struct.*, 751 (2005) 139
- [2] D.A. Becke, *Phys. Rev.*, A38 (1988) 3098
- [3] D.A. Becke, *J. Chem. Phys.*, 98 (1993) 5648
- [4] C. Lee, W. Yang, R.G. Par, *Phys. Rev.*, B37 (1988) 785
- [5] Z. Dega Szafran, M. Szafran, E. Dulewicz, A. Addlagatta, M. Jaskólski, *J. Mol. Struct.*, 654 (2003) 71
- [6] P. Pulay, G. Fogarasi, F. Pang J.E. Boggs, *J. Am. Chem. Soc.*, 101 (1979) 2550
- [7] G. Keresztury, G. Jalsovszky, *J. Mol. Struct.*, 10 (1971) 304
- [8] (a) K.B. Wiberg, V.A. Walters, K.N Wong, S.D. Colson, *J. Phys. Chem.*, 88 (1984) 6067; (b) M. Szafran, J. Koput, *J. Mol. Struct.*, 565-566 (2001) 439
- [9] M. Szafran, J. Koput, *J. Mol. Struct.*, 381 (1996) 157
- [10] A. Mortensen, O.F. Nielsen, *Spectrochim. Acta A*, 51 (1995) 1345.

APPLICATION OF SUBLATION AND TWO PHASE TITRATION METHODS FOR ANALYTICAL OF SURFACTANTS IN AFFF FIRE-FIGHTING FOAMS

Łukasz Szewczulak^{*}, Jan Hupka^{*}, Dominik Kuziemski^{*}, Sebastian
Pastewski^{**}

^{*}Department of Chemical Technology, ^{**}Department of Fat and Detergents Technology
Chemical Faculty, Gdansk University of Technology
Narutowicza Str. 11/12, 80-952 Gdansk, Poland
luke@chem.pg.gda.pl

INTRODUCTION

Firefighting foams, most commonly produced with fluorosurfactants, have found a wide application for extinguishing fires of flammable liquids such as oil, gasoline, and jet fuel [1,2]. Because of unique property of forming an aqueous film on the hydrocarbon surface they are designated by the term *Aqueous Film Forming Foams* AFFF [3]. AFFF blanket and cool the burning fuel surface, and are recognized as the most efficient substances in use today for fighting of fuel fires in both civilian and military situations [4]. AFFF solutions blended with fuels being extinguished and with the combustion products cause problems in treatment and disposal of wastes. Foams can interfere with the operation of oil-water separators and flotation units [5,6]. The extinguishing wastewater-based emulsions are very stable - also due to the presence of fluorosurfactants. Typical AFFF surfactant components comprise anionic alkyl sulfates, amphoteric fluoroalkylamide and anionic fluoroalkyl sulfonates. Prediction and monitoring of AFFF pollution control are not possible without appropriate easy analytical methods for measuring AFFF components concentration [7-9]. One of the most important method for measuring of total concentration of anionic surfactants is the two phase titration method [10,11]. The preliminary step before the analysis was a preconcentration of surfactants using the solvent sublation process based on the transport of surfactants from water phase to organic solvent phase by gas bubble [12].

EXPERIMENTAL

The solvent sublation and two phase titration methods are dedicated to determine of total concentration of anionic surfactants in the environmental samples.

The objective of the research was to examine the usefulness of these techniques for analysis of fluorinated and non-fluorinated anionic surfactants in AFFF fire-fighting foams.

A pair of perfluorocarbon (Tricosfluorododecanoic Acid /C₁₁F₂₃CO₂H/) /SIGMA/ and hydrocarbon (Lauric Acid Sodium Salt /C₁₁H₂₃CO₂Na/) /FLUKA/ surfactants imitating composition and surface properties of AFFF were selected. The surfactant solutions and mixtures based on them in range of concentrations (100 to 300 mg/dm³) were prepared. Using the sublation and two phase titration techniques the surfactants (molar ratio 1:1) were isolated from the mixtures and their total concentration before and after sublation were measured. The procedure has been done also in the presence of oil phase imitating a real fuel in fire-fighting wastewater as gasoline and diesel oil in wide range of concentrations

(100 to 1000 mg/dm³).

For surfactants separation and their preconcentration a solvent sublation technique was used. The apparatus for solvent sublation consisted of 60 mm diameter and 505 mm length glass column, fitted at the bottom with a sintered-glass sparger, used to disperse the gas bubbles (Fig. 1). The column was filled with 1 dm³ of sample. To obtain high surfactants recovery 100 g NaCl and 5 g NaHCO₃ were added to the sample. On the top of the aqueous phase 100 cm³ of ethyl acetate was poured. The air flow rate was kept at 1 dm³/min. Sublation was continued for 10 min. Then, the process was repeated with the second 100 cm³ layer of ethyl acetate. Combined ethyl acetate solution was evaporated. The surfactant remained as a film residue in the flask and was dissolved in methanol and transferred to a 100 cm³ flask, which afterwards was filled with water.

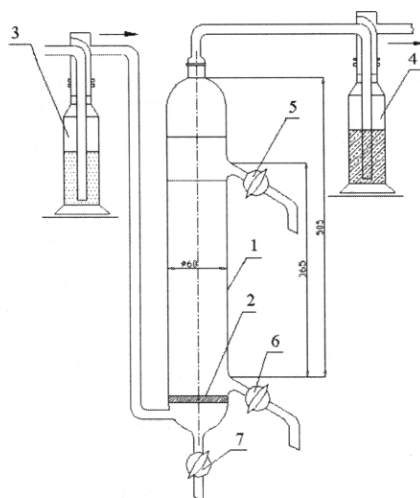


Fig. 1 Scheme of Wickebold's sublation column:

1 – glass column 1000 cm³; 2 –Shott's sintered-glass sparger G1; 3 – absorption bulb filled with ethyl acetate 250 cm³; 4 – absorption bulb filled with active carbon 250 cm³; 5, 6, 7 – drain valves.

In the next step, 300 cm³ conical flask was filled with 10 cm³ of sample and 25 cm³ of methylene blue, 20 cm³ of water and 20 cm³ of chloroform were added to the one. The mixture was stirred and titration of sample using cationic surfactant Hyamine 1622 was carried out to equalize the colour of phases.

RESULTS AND CONCLUSIONS

In Figures 2-9, the results of fluorinated and non-fluorinated anionic surfactants concentration in mixture are presented. All experimental results revealed that the sublation and two phase titration methods are suitable and useful for surfactant separation and determination of total concentration with reference to surfactants and surfactant mixtures imitating AFFF composition. With increasing surfactant and oil phase concentration the accuracy and precision of measurement are invariable. The comparison of concentration values for selected surfactants and commercial AFFF agents before and after isolation in next step of the tests will be investigated. The positive application results of the separation and analytical techniques mentioned above are expected.

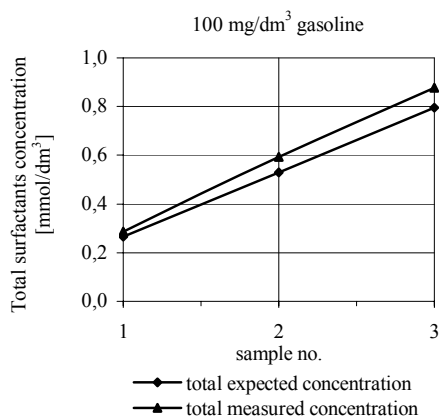


Fig. 2. Total surfactants concentration in presence of 100 mg/dm³ gasoline

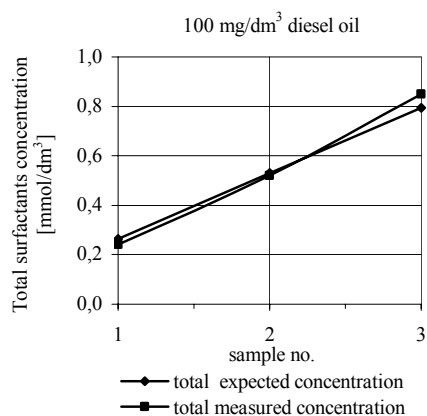


Fig. 3. Total surfactants concentration in presence of 100 mg/dm³ diesel oil

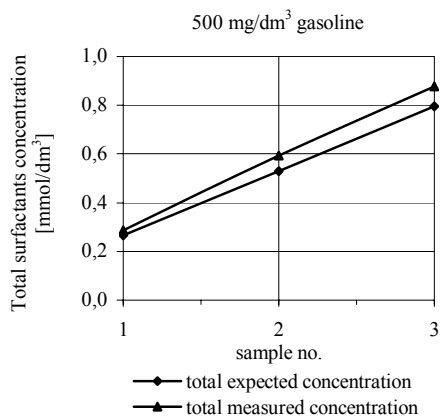


Fig. 4. Total surfactants concentration in presence of 500 mg/dm³ gasoline

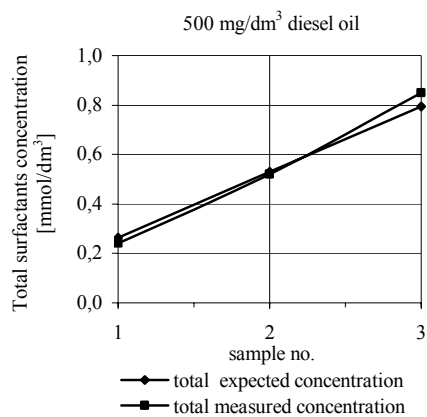


Fig. 5. Total surfactants concentration in presence of 500 mg/dm³ diesel oil

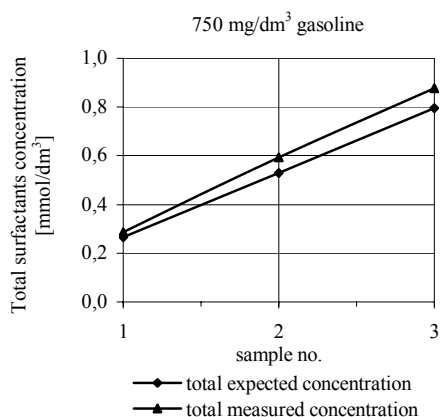


Fig. 6. Total surfactants concentration in presence of 750 mg/dm³ gasoline

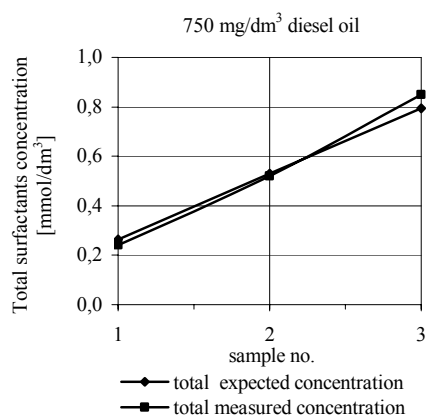


Fig. 7. Total surfactants concentration in presence of 750 mg/dm³ diesel oil

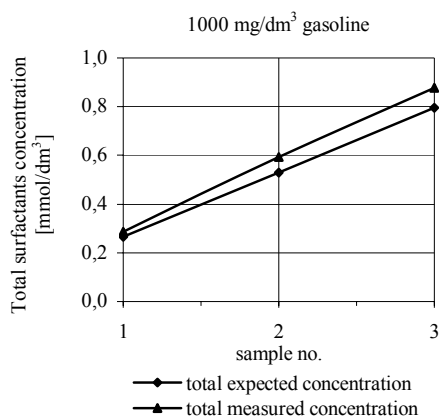


Fig. 8. Total surfactants concentration in presence of 1000 mg/dm³ gasoline

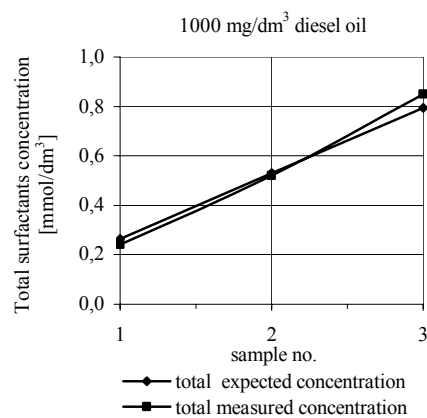


Fig. 9. Total surfactants concentration in presence of 1000 mg/dm³ diesel oil

REFERENCES

- [1] Howell R.D., Turcker E.E., *American Laboratory News Edition*, 28 (6), 1996, 10.
- [2] Norman E.D., Hanauska C.P., *NFPA Journal*, May/June 1995.
- [3] Shinoda K., Nomura T., *J. Phys. Chem.*, 84 (4) 1980.
- [4] Allison M.C., *Fluorochemical Surfactants*, The Proceedings of a Symposium "Industrial Applications of Surfactants", Karsa D.R. ed., University of Salford, Great Britain, 15-17 April 1996.
- [5] Pintens J., Joos P., *J. Colloid Interface Sci.*, 60 (3) 1977.
- [6] Moody C.A., Field J.A., *Environ. Sci. Technol.*, 34 (18), 2000, 3864.
- [7] Martin. J.W., Kwan W.C., Muir D.C.G, Mabury S.A., *Anal. Chem.*, 73 (10), 2001, 2200.
- [8] Martin. J.W., Kwan W.C., Muir D.C.G, Mabury S.A., *Environ. Sci. Technol.*, 36 (4), 2002, 545.
- [9] Elliott D.E., Chiesa P.J., *Fire Technol.*, February 1990.
- [10] Epton S.R., *Trans. Faraday Soc.*, 44, 1948, 226.
- [11] Reid V.W., Longman G.F., Heinerth E., *Tenside*, 4, 1967, 292.
- [12] Polish Norm PN-EN 903.

THE INVESTIGATIONS OF EFFECTIVENESS OF SUSPENSION SEDIMENTATION

Dariusz Szychowski, Anna Dorota Klepańska, Jakub Gęsiarz
*Warsaw University of Technology, Institute of Chemistry,
09-400 Plock, Lukaszewicza 17*

Introduction

In many processes of chemical industry suspensions of solids in liquid occur. Separation of solids from a liquid by the use of filtration can often be too expensive. Sedimentation is a one of the basic processes used for water purification, to remove settling particles having higher density than water. Depending on the type of suspension, settling of granular or flocculent particles can be marked out, depending on hydraulic condition there is free settling or condensed settling. Free settling of spherical particles is well explained and the mathematical description of this process is used in practice, also in the processes of water purification. Mathematical model of settling of flocculent particles is more complicated. It is related to the connections in the particle-liquid system and changing parameters such as mass, volume and shape of settling flocculent suspensions. In order to determine the parameters of sedimentation of these suspensions laboratory studies are necessary. Basing on these studies, employing for instance a sedimentation scale, a curve of sedimentation can be drawn for a suspension. Many authors point out the necessity of carrying out such studies. In the presented work the investigations of effectiveness of the suspension removal from the after-rinse waters obtained from rinsing of the filtering beds in pressure filters working in the side filtering stations in cooling open recirculating circuits are presented. In the studies on sedimentation two methods were used: based on the measurement of turbidity and weight method. The use of a laboratory turbidimeter Hach AN2100 allowed measurement of the turbidity of studied after-rinse waters and its changes in time. Turbidity is an important indicator of the level of water pollution, allowing the evaluation of the concentration of particles suspended in studied sample. Turbidity measurement is based on the estimation of the intensity of light scattered by the sample, which is proportional to the concentration of scattering light substance particles. Weight method, employing the Krüss K100 tensiometer, was used to measure the mass of flocculent suspension settling on the surface of measuring component, recording the increase of mass as a function of time. Measuring component of the shape of an inverted umbrella is attached to the scale and immersed in studied sample of water. Settling of impurities on the surface of measuring element causes the increase of its mass, recorded as a function of time. The depth of immersion, total time of measurement and number of measurement points is controlled.

Sedimentation is carried out in settlers. After-rinse water is introduced at the axle of the settler. Sediment settles down at the bottom, where it is periodically removed along with a part of the liquid. Cleared water overflows the upper edge of the settler into a gutter and is led away for further utilization.

In the presented work the after-rinse water was collected from two parallel settlers, from cell 1 (cleared water), cell 2 (sedimentation in the settler) and cell 3 (inflow from filters after rinsing).

Measurements of turbidity – results

Selected results of turbidity measurements for water collected from cells 1, 2 and 3 of the settler, carried out in 60 minutes are presented in charts (Figure 1). Comparatively, turbidity was also measured after the time of 24 hours and longer. In Table 1 the analysis of the results of the sedimentation studies is presented, showing the high level of after-rinse waters turbidity reduction. The clear water cell (cell 1) fulfills its task collecting water of lowest turbidity, carried out from the settler for further utilization.

Table 1. The results of studies on sedimentation – turbidity measurements

	Cell 1	Cell 2	Cell 3
Reduction of turbidity after 60 min	30 %	43 %	47 %
Turbidity after 24 h	10- 12 NTU		
Reduction of turbidity after 24h	ca. 80%		
Turbidity after 72h	< 3 NTU		
Reduction of turbidity after 72h	> 90%		

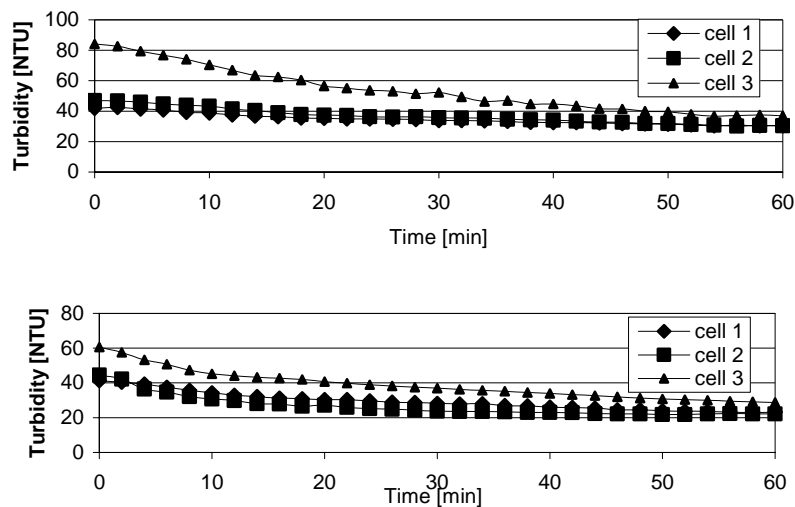
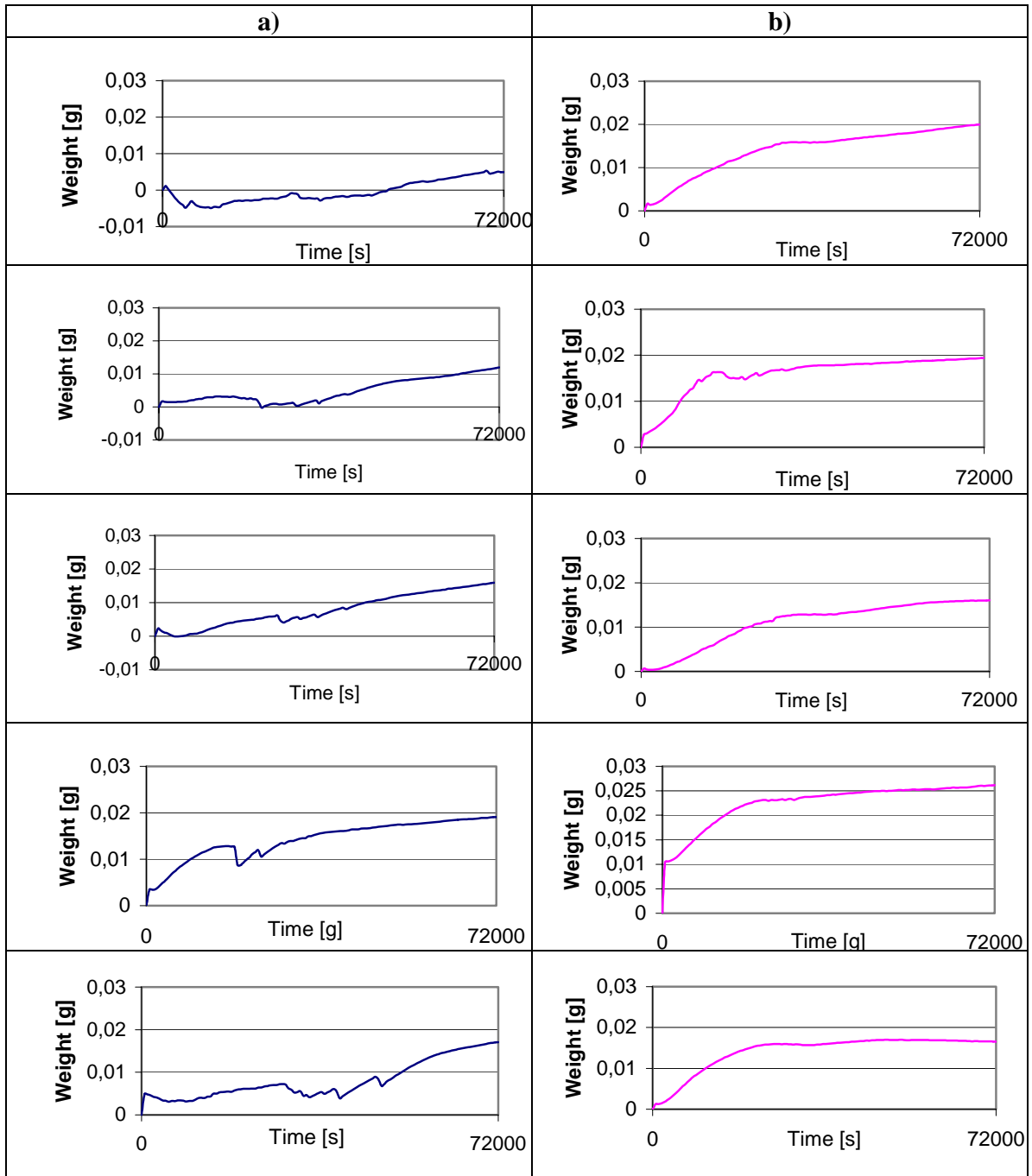


Fig. 1. Sedimentation of impurities in after-rinse water

Weight method – results

The mass of settling impurities in after-rinse water in 20 hours was measured. Measurements were carried out directly after collecting the sample from cell 2 of the settler (reference sample) and after 48 hours from the time of collection (Figure 2).



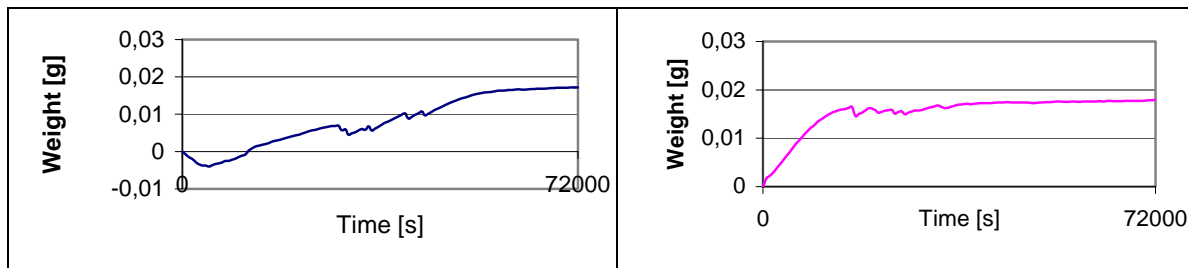


Fig. 2. Sedimentation of the impurities in after-rinse water
a) reference sample, b) sample after 48 hours

The results of sedimentation studies obtained with the use of weight method give the possibility to compare the after-rinse water directly after being collected from the settler and water after 48 hours. During the time of measurement of the mass of settling particles, going on for 20 hours, small bubbles of air on the lower surface of measuring element, escaping the reference sample, were observed. The presence of air in the sample can be related to the use of air during the cycle of filtration bed rinsing. Its exhaling from the sample of studied water can be related to the increase of temperature of water during measurement compared to the temperature of water collected directly from the settler. The increase of sample temperature causes the decrease of air solubility in water. In the weight method measurements, the appearance of air bubbles on measuring element gave negative values of sediment mass, where the mass of the measuring element, recorded by the scale at the beginning of the measurement was assumed as zero. This phenomenon was not observed in case of samples studied after 48 hours from the time of collection from the settler. It can indicate unfavourable for after-rinse waters purification, transport of flocky particles from the washed out sediment to the water surface in the settler by air exhaling from studied sample.

Conclusions

Methodology of studies on the process of sedimentation of after-rinse waters collected from pressure filters in the cycle of rinsing, proposed in this work, using the measurements of turbidity changes and mass of settling flocky particles, gives the possibility to formulate conclusions relating to the possibility of purifying of after-rinse waters with the use of sedimentation.

Results discussed in a presented work confirm the necessity of carrying out of investigations on the sedimentation character of studied waters, containing impurities mostly in the form of flocky particles. The need to carry out such studies is pointed out by many authors investigating the conformity of results obtained in model studies of the process of sedimentation with the results obtained in real systems.

NEW COPPER(I) CARBOXYLATES COMPOUNDS WITH VINYLTRIALKYLSILANES AS CVD PRECURSORS

Iwona Barbara Szymańska*

Faculty of Chemistry, Nicolaus Copernicus University, ul. Gagarina 7, 87-100 Toruń, Poland, Tel.: +48-56-6114317; Fax: +48-56-6542477; e-mail: pola@chem.uni.torun.pl

Abstract

Copper(I) carboxylates compounds with vinyltrialkylsilanes are di- or trimeric species with bridging carboxylates. In MS spectra the metallated fragments were detected. The highest signal intensity for $[\text{Cu}_2(\text{RCOO})]^+$ and $[\text{Cu}_2(\text{RCOO})_2]^+$ ions were noted, which analogues can be the metal carriers in the CVD process. The vaporization temperature of metallated fragments was lower for $[\text{Cu}(\text{C}_2\text{F}_5\text{COO})(\text{L})]$ than $[\text{Cu}(\text{CF}_3\text{COO})(\text{L})]$ compounds. The $[\text{Cu}(\text{C}_2\text{F}_5\text{COO})(\text{L})]$, L = VTMS (**1**), VTES (**2**) were useful for the metallic, bimetallic and mixed layers preparation.

Key words: copper(I), vinyltrialkylsilane, perfluorinated carboxylates, MS, CVD

Introduction

Synthesis and characterization of copper coordination compounds as new precursors for Chemical Vapor Deposition (CVD) of metallic thin layers and mixed materials is an area of extensive research. Fabrication of metals thin films using CVD techniques is a matter of interest, due to its advantages coming out, among others, from kinetically controlled processes of deposition. The unique structural, optical and electrical properties of this metal resulted in its wide applications in microelectronic and optoelectronic devices [1,2,3,4], and components of high-temperature superconducting materials [5]. The most frequently used for copper CVD is the commercially available compound $[\text{Cu}(\text{hfac})(\text{VTMS})]$ (copper(I) 1,1,1,5,5,5-hexafluoro-2,4-pentadionate vinyltrimethylsilane) [6,7,8,9].

In the presented paper, the studies of $[\text{Cu}(\text{RCOO})(\text{L})]$ (R = CF_3 , C_2F_5 ; L = VTMS, VTES, VTMOs) and the selection of compounds suitable for CVD will be reported.

Experimental

Materials

Vinyltrimethylsilane (VTMS) (97%), vinyltriethylsilane (VTES) (97%), vinyltrimethoxysilane (VTMOs) (98%), copper powder (99%) and CF_3COOH (99%), $\text{C}_2\text{F}_5\text{COOH}$ (97%) were purchased from Aldrich, whereas $\text{CuCO}_3 \cdot \text{Cu}(\text{OH})_2 \cdot n\text{H}_2\text{O}$, from POCh (Poland) and were used as received. $(\text{C}_2\text{F}_5\text{COO})_2\text{Cu}$, $(\text{CF}_3\text{COO})_2\text{Cu}$ and sodium salts were prepared in similar manner as reported [10]. As solvent was used CH_3CN (Aldrich; 99.93%; dried and deoxygenated by standard methods).

Instrumentation

Mass spectra were detected with a Finnigan MAT 95 mass spectrometer, using EI ionization method in the temperature range 303–573K. IR spectra were measured with a Perkin-Elmer Spectrum-2000 FT-IR spectrometer, using KBr (400–4000 cm^{-1}) and polyethylene discs (100–400 cm^{-1}). Temperature-variable IR spectra were measured with a SPECAC cell (20–250°C), at dynamic vacuum $p = 10^{-2}$ mbar using the same instrument. The amount of Cu was determined with a Carl-Zeiss Jena AAS spectrophotometer. Thermal studies (TGA/DTA) were performed on SDT 2960 TA analyzer (dry N_2 ; the heating rate – 2.5° min^{-1} , for (**1**) – 1° min^{-1} ; sample mass 12–18 mg). Gaseous products of the thermal decomposition were detected by a FT IR BioRad Excalibur spectrophotometer equipped with a thermal connector

($T_L = 150^\circ\text{C}$) for gases. Powder X-ray diffraction data for the residues from thermal analysis were obtained with a Philips X'PERT diffractometer using CuK_α radiation. The deposition experiments were carried out using horizontal *hot-wall* CVD reactor as described [11].

Synthesis

Syntheses were carried out using standard Schlenk technique in argon atmosphere, according to methods described in our earlier reports [10,12,13,14,15,16]. Yields were in the range 70-80%.

[Cu(C₂F₅COO)(VTMS)](1) EI-MS $T = 489\text{ K}$ (m/z, RI %) ([VTMS]⁺ – 100, 19; [Cu₂(C₂F₅COO)]⁺ 289, 100; [Cu₂(C₂F₅COO)₂]⁺ 452, 57; [Cu₃(C₂F₅COO)₂]⁺ 517, 2), IR (KBr, 1682, 1413, 1028, 933; PE 541, 289, 243 cm^{-1})

[Cu(C₂F₅COO)(VTES)](2) EI-MS $T = 441\text{ K}$ (m/z, RI %) ([Cu₂(C₂F₅COO)]⁺ 289, 100; [Cu₂(C₂F₅COO)₂]⁺ 452, 78; [Cu₃(C₂F₅COO)₂]⁺ 517, 3; [Cu₂(C₂F₅COO){VTES}]⁺ 431, <1), IR (KBr, 1690, 1412, 1031, 931; PE 540, 279, 253 cm^{-1})

[Cu(CF₃COO)(VTMS)](3) EI-MS $T = 506\text{ K}$ (m/z, RI %) ([VTMS]⁺ – 100, 26; [Cu₂(CF₃COO)]⁺ 239, 98; [Cu₂(CF₃COO)₂]⁺ 352, 46; [Cu₂(CF₃COO)₂(VTMS)]⁺ 452, 2), IR (KBr, 1684, 1438, 1032, 942; PE 523, 280, 247 cm^{-1})

[Cu(CF₃COO)(VTES)](4) EI-MS $T = 508\text{ K}$ (m/z, RI %) ([Cu₂(CF₃COO)]⁺ 239, 98; [Cu₂(CF₃COO)₂]⁺ 352, 46), IR (KBr, 1681, 1433, 1035; PE 524, 279, 247 cm^{-1})

[Cu(C₂F₅COO)(VTMOS)](5) EI-MS $T = 415\text{ K}$ (m/z, RI %) ([Cu₂(C₂F₅COO)]⁺ 289, 100; [Cu₂(C₂F₅COO)₂]⁺ 452, 34; [Cu₂(C₂F₅COO)(VTMOS)(C₂F₅)]⁺ 553, ~1), IR (KBr, 1688, 1410, 1031, 973; PE 543, 299, 227 cm^{-1})

Results and Discussion

The obtained compounds (1-4) were dark brown, fine-crystalline powders, stable in the inert atmosphere. The derivative (5) with VTMOs was the brown oil, highly air and moisture sensitive that depreciated it as CVD precursor. The thermal analysis data point on the multistage, endothermic decomposition of studied compounds with metallic copper formation in the range 537-548K. Unfortunately for (5) process finished at higher temperature – 823K. Moreover, in the case of (3) and (5) the decomposition final product was impured by carbon that is not promised for potential CVD precursors. Therefore the most promising results revealed complexes (1) and (2).

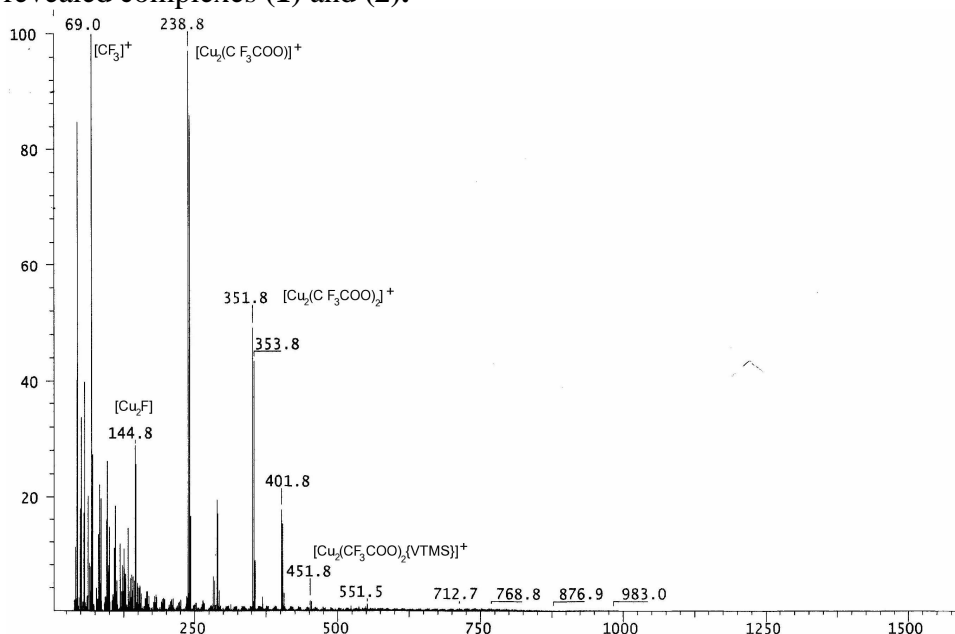


Figure 1 EI-MS spectra of [Cu(CF₃COO)(VTMS)](3).

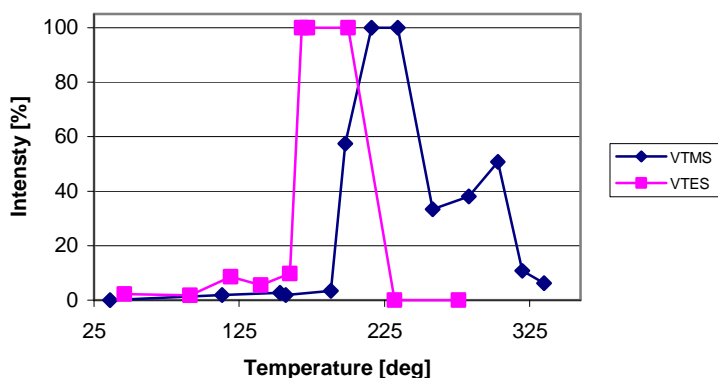


Figure 2 Temperature dependence of the $[\text{Cu}_2(\text{RCOO})]^+$ (289 m/e) signal intensity for (1) and (2).

In EI-MS spectra of all synthesized compounds $[\text{Cu}(\text{RCOO})(\text{L})]$ the metallated fragments were detected. The lack of monometallic fragments and detection of following multinuclear ions types: $[\text{Cu}_3(\text{RCOO})_2]^+$, $[\text{Cu}_2(\text{RCOO})_2]^+$, $[\text{Cu}_2(\text{RCOO})]^+$, $[\text{Cu}_2(\text{RCOO})_2(\text{L}')^+]$ and $[\text{Cu}_2(\text{RCOO})(\text{L}')^+]$, where $\text{L}' = \text{vinyltrialkylsilane}$ or its fragments suggests di- or trimeric structure of studied compounds with bridging carboxylates (Figure 1). The highest signal intensity for carboxylate dicopper species $[\text{Cu}_2(\text{RCOO})]^+$ and $[\text{Cu}_2(\text{RCOO})_2]^+$ ions were noted, which analogues can be the metal carrier in the CVD process. The onset vaporization temperature of these metallated fragments was lower in the case of pentafluoropropionates $[\text{Cu}(\text{C}_2\text{F}_5\text{COO})(\text{L})]$ 443–463K than for trifluoroacetates $[\text{Cu}(\text{CF}_3\text{COO})(\text{L})]$ 533–553K. Summarizing analysis of thermal and MS data compounds (1) and (2) were chosen as potential Cu CVD precursors.

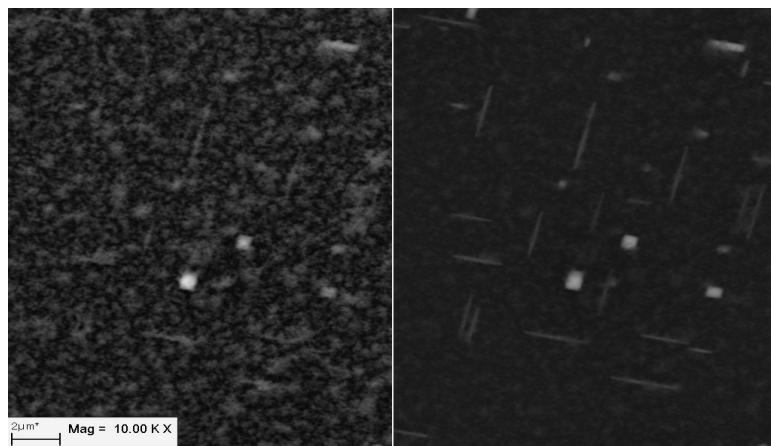


Figure 3 SEM microphotographs of cluster layers deposited using $[\text{Cu}\{\text{VTES}\}(\text{C}_2\text{F}_5\text{COO})]$, $T_V=573\text{K}$, $T_D=773\text{--}793\text{K}$, Si(111).

Copper thin layers (clusters or continuous) were deposited on Si(111) and glass substrates by CVD method using $[\text{Cu}(\text{C}_2\text{F}_5\text{COO})(\text{L})]$ ($\text{L} = \text{VTMS}$ (1), VTES (2)) as precursors (Figure 3). Application of a multistage deposition of Cu films on glass surfaces resulted in metallic membrane formation. Moreover, bimetallic Ag/Cu (Figure 4) and mixed materials TiO_2/Cu were obtained using two respective precursors in one CVD process.

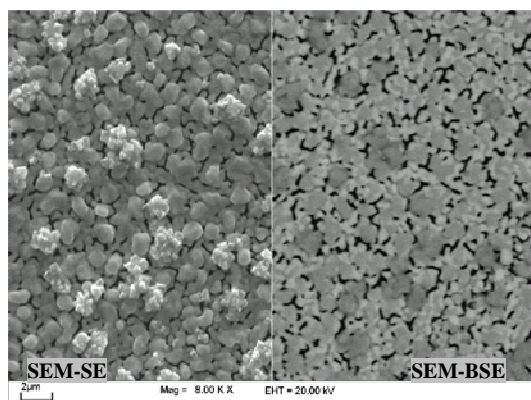


Figure 4 SEM microphotographs of the bimetallic Ag/Cu membrane obtained using $[\text{Cu}(\text{C}_2\text{F}_5\text{COO})(\text{VTMS})]$ (**1**) and $[\text{Ag}(\text{EtC}(\text{CH}_3)_2\text{COO})(\text{PMe}_3)]$, ($T_V = 220^\circ\text{C}$, $T_D = 440^\circ\text{C}$, $p = 1,0 \text{ mbar}$, $t = 3 \text{ h}$)

Conclusions

Copper(I) carboxylates compounds with vinyltrialkylsilanes $[\text{Cu}(\text{RCOO})(\text{L})]_n$ ($\text{R} = \text{CF}_3$, C_2F_5 ; $\text{L} = \text{VTMS}$, VTES , VTMOS) are di- or trimeric species with bridging carboxylates. The $[\text{Cu}(\text{C}_2\text{F}_5\text{COO})(\text{L})]$, $\text{L} = \text{VTMS}$ (**1**), VTES (**2**) complexes were stable at room temperature in Ar atmosphere. Moreover, they are a source of species, which volatility was sufficient for the transport in vapours and decomposed to metallic films under mild thermal CVD conditions, therefore were useful for the metallic, bimetallic and mixed layers fabrication.

Acknowledgements

The author wish to acknowledge MNiSzW for financial support grant no. PBZ-KBN-118/T09/2004.

References:

- [1] T.T. Kodas, M.J. Hampden-Smith, in: *The Chemistry of Metal CVD*, VCH, Weinheim 1994, pp. 20-30, 175, 239.
- [2] M. Hoshino, K. Kasai, J. Komeno, *Jpn. J. Appl. Phys.* 31 (1992) 4403.
- [3] S.P. Murarka, *Mater. Sci. Eng.*, 19 (1997) 76.
- [4] A. Grodzicki, I. Łakomska, P. Piszczek, I. Szymańska, E. Szłyk, *Coord. Chem. Rev.*, 249 (2005) 2232.
- [5] R. Kalyanaraman, S. Oktyabrsky, J. Narayan., *J. Appl. Phys.*, 85 (1999) 6636.
- [6] J.A.T. Norman, B.A. Muratore, P.N. Dyer, D.A. Roberts, A.K. Hochberg, *J. Phys. IV* 1 (1991) C2–271.
- [7] P. Doppelt, *Coord. Chem. Rev.*, 178-180 (1998) 1785.
- [8] M.L.H. ter Heerdt, J.J. Overdijk, P.J. van der Put, J. Schoonman, *Chem. Mat.*, 11 (1999) 3470.
- [9] M.L.H. ter Heerdt, P.J. van der Put, J. Schoonman, *Chem. Mater.*, 11 (1999) 3470.
- [10] E. Szłyk, I. Szymańska, *Polyhedron*, 18 (1999) 2941.
- [11] E. Szłyk, P. Piszczek, I. Łakomska, A. Grodzicki, J. Szatkowski, T. Błaszczyk, *Chem. Vap. Dep.*, 6 (2000) 105.
- [12] E. Szłyk, R. Kucharek, I. Szymańska, *J. Coord. Chem.*, 53, 55 (2001).
- [13] E. Szłyk, R. Kucharek, I. Szymańska, *Pol. J. Chem.*, 75, 337 (2001).
- [14] E. Szłyk, R. Kucharek, I. Szymańska, L. Pazderski, *Polyhedron*, 22, 3389 (2003).
- [15] I. Szymańska, L. Pazderski, R. Kucharek, E. Szłyk, *Pol. J. Chem.*, 79, (2005) 1705.
- [16] E. Szłyk, R. Kucharek, I. Szymańska, *Materials Science-Poland*, 21 (2003) 245.

CHEMICAL FORMS OF HEAVY METALS IN SOME TYPE OF SOILS

Świerk Katarzyna, Bielicka Aleksandra, Bojanowska Irena,
Lempart Mirosława, Maćkiewicz Zbigniew

*Department of Environmental Engineering, Faculty of Chemistry, University of Gdansk,
18 J. Sobieskiego St., 80 - 852 Gdańsk, Poland*

Pollution of environment appears in increase of metals contents in soils, water and plants. Soil is a basic constituent of the natural environment and a basic link of the biological chain involving soil – plant – animal and the man. Heavy metals pollution is an important ecological problem [1-3].

The concentration of heavy metals in the soil solution is believed to depend on the equilibrium between the soil solution and solid phase, with pH playing the decisive role. Apart from pH, other soil properties, such as cation exchange capacity, organic matter content, quantity and type of clay minerals, the content of the oxides of iron, aluminium, and manganese, and the redox potential determine the soil's ability to retain and immobilize heavy metals [4-6].

The fate of heavy metals in a contaminated soil is controlled by the chemical forms in which the metals exist in the soil, and it is essential to have an understanding of the metal distribution in each soil fraction. Metals are distributed throughout soil components and are associated with them in various ways including ion exchange, adsorption, precipitation, and complexation. Sequential extraction to fractionate metals in soils into several groups of different leachability is widely employed to determine the distribution of metals in different phases [6-8].

The aim of this work was to identify different metals (copper, nickel, lead and zinc) fractions in three type of soils (sandy, arable and loamy) by the sequential extraction method according to the modified procedure of Tessier et al [9-12].

Investigations were performed for air-dry weight of the soils samples having mass 1g and homogenized in a mortar. Characterization of selected properties of soils is presented in Table 1.

Table 1. Some properties of investigated soils

Type of soil	Sandy soil		Arable soil		Loamy soil	
Parameters						
pH (H ₂ O)	6.9		7.7		7.9	
Organic matter [%]	0.73		12.18		2.96	
Water content [%]	0.1		3.3		1.0	
Total metal content [mgMe/kg d.w.]	Cu	2.91±1.5	Cu	13.8±5.7	Cu	5.89±3.9
	Ni	12.24±7.0	Ni	28.2±14	Ni	20.52±18
	Pb	253.0±33	Pb	243.6±66	Pb	243.7±34
	Fe	2082.1±196	Fe	17597±2486	Fe	11219±1856
	Zn	34.9±27	Zn	218.8±25	Zn	59.56±33.7

A five - step sequential extraction separated the heavy metals into the following species: FI – exchangeable, F II – bound to carbonate, F III – bound to Fe/Mn oxides, F IV- bound to organic matter and F V – residuals.

The sequential extraction of Cu, Ni, Fe, Zn and Pb from the studied soils was carried out on three parallel samples. Between each successive extraction, separation was affected by centrifuging at 10 000 rpm for 15 minutes. The supernatant was removed with a pipette and analyzed for metals quantity whereas the residue was subjected to the next extraction step. Metal concentrations in supernatants were determined by using Atomic Absorption Spectroscopy Method, AAS model 30 of the Karl Zeiss Jena Company.

The percent contributions of heavy metals in particular fractions in investigated soils were presented in Figures 1-3.

The highest contribution of particular metal form in sandy soil was: Cu – F IV, Ni – F V, Pb – F V, Fe – F V, Zn - FII (Fig.1).

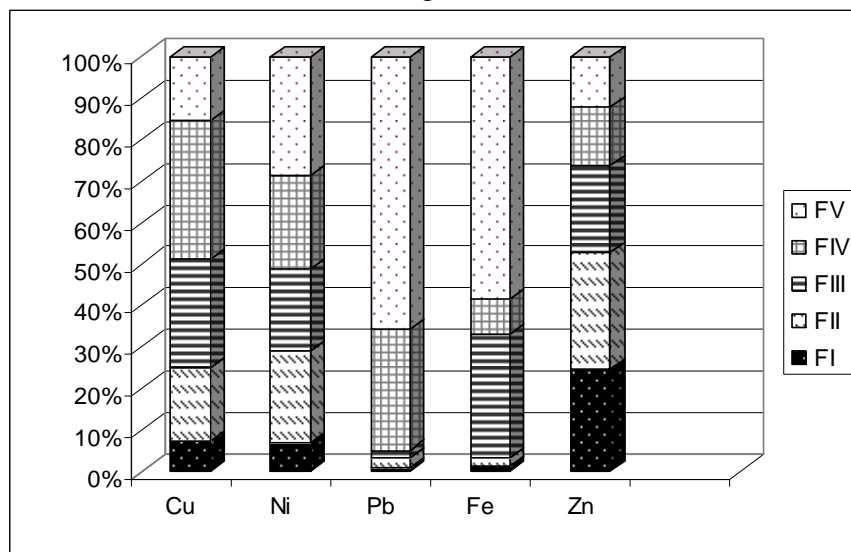


Fig. 1. Percent contribution of heavy metals in particular fractions in the total metals content in sandy soil.

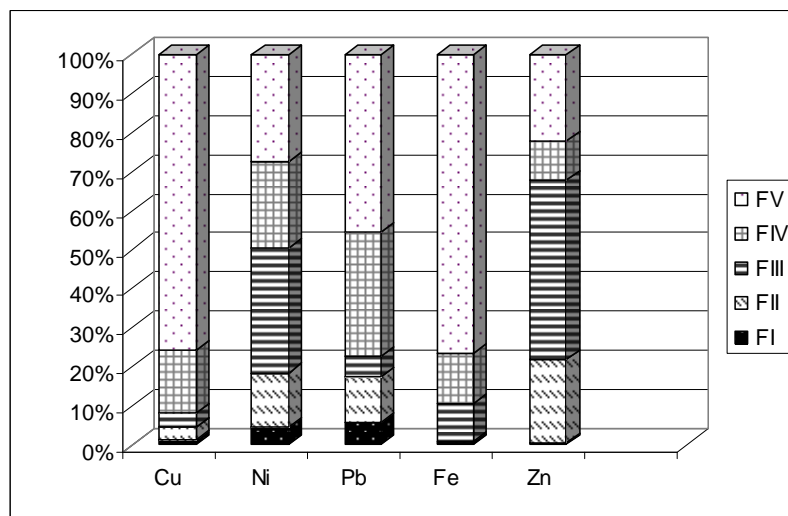


Fig. 2. Percent contribution of heavy metals in particular fractions in the total metals content in arable soil.

The highest content of Cu, Pb and Fe in arable soil were in the residual fraction - FV, while Ni, Zn were in the organic matter fraction – FIII (Fig.2.). In loamy soil the same trend was observed in Cu, Pb and Fe (Fig.3).

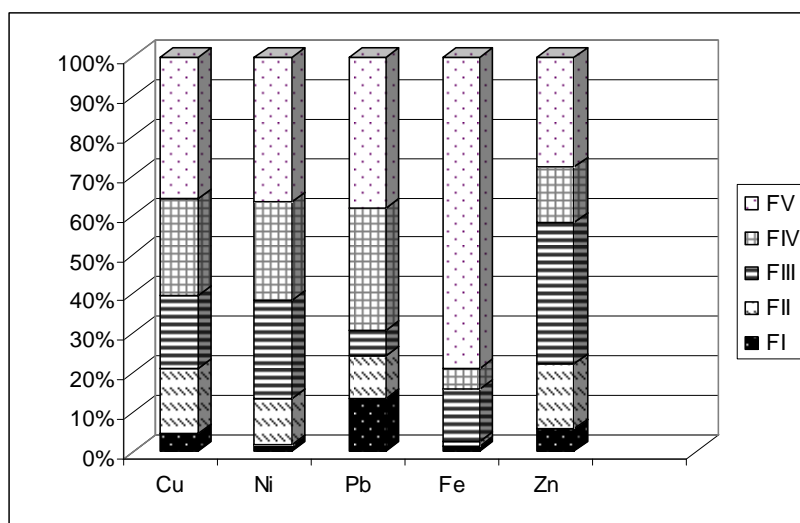


Fig. 3. Percent contribution of heavy metals in particular fractions in the total metals content in loamy soil.

In the all tree soils the highest concentration of Pb and Fe were in the residual fraction.

The metals forms occurred in fractions F I – F IV can be released to the environment under changeable conditions. The metals forms occurring in the residual fraction FV are permanently immobilized.

Financial support by the University of Gdansk, projects DS/8270-4-0093-6 and BW/8000-5-0279-6 are gratefully acknowledged.

References:

- [1] B.Gworek, M. Borowiak, E. Malborczyk, Rekultywacja gleb zanieczyszczonych metalami ciężkimi, Materiały II Międzynarodowej Konferencji Naukowo-Technicznej Obieg Pierwiastków w Przyrodzie, Warszawa 1997, 173-179
- [2] J. Kalambkiewicz, L. Filar, Oznaczenie zawartości miedzi i molibdenu w glebach, Zeszyty Naukowe Komitetu „Człowiek i Środowisko” 14 (1996),60-66
- [3] T. Kowalkowski, B. Buszewski, Polish J. Environ. Stud., 2 (2002) 135-139
- [4] C. Aydinalp, S. Marinova, Polish J. Environ. Stud., 5 (2003) 629
- [5] M. Kaasalainen, M. Yli-Halla, Environ. Pollut., 126 (2003) 225
- [6] M. Piantar-Kallio, S. Reinikainen, M. Oksanen, Anal. Chim. Acta, 439 (2001) 9
- [7] I. M.-C. Lo, X.-Y. Yang, Wast. Manag., 18 (1998) 1
- [8] J. Siepak, Analiza specjacyjna metali w próbkach wód i osadów dennych, UAM, Poznań 1998, str. 67
- [9] A. Bielicka, I. Bojanowska, K. Świerk, Ann. Polish Chem. Soc.,3 (2004) 1183
- [10] A. Bielicka, I. Bojanowska, K. Świerk, J. Kowalczyk, Ann. Polish Chem. Soc., 2 (2005) 114
- [11] A. Kot, J. Namieśnik, Trends Anal. Chem., 19 (2000) 69
- [12] A. Bielicka, I. Bojanowska, A. Wiśniewski, Polish J. Environ. Stud., 2 (2005) 145

INFLUENCE OF THE URETHANE - ISOCYANATES ON PROPERTIES OF UV CURABLE THE URETHANE-EPOKSY METHACRYLATES

Bogdan Tarasiuk, Andrzej Bartnicki, Władysław Charmas
*Department of Organic Chemistry and Technology, Faculty of Chemistry,
Maria Curie-Skłodowska University, ul. Gliniana 33, 20-031 Lublin, Poland*

INTRODUCTION

The use of high-intensity radiation, especially ultraviolet, in the process of polymerization and curing of various types of monomers and oligomers produced a quantitative increase in the range of their application in many important technological branches of industry during the last twenty years. It is connected with the economizing of both the energy and the production area, the rent ability of production and especially with almost 100% decrease in the emission of solvents, a very significant consideration for environmental protection. Urethane-acrylates, epoxy acrylates oligomers containing the highly reactive acrylates groups undergo in a very short time a reaction of polyaddition under the influence of ultraviolet irradiation. Used as typical no-solvent lacquer systems are used as protective coatings for metal, plastic materials, wood, and optical fibers as the materials in electrotechnics and lithography.

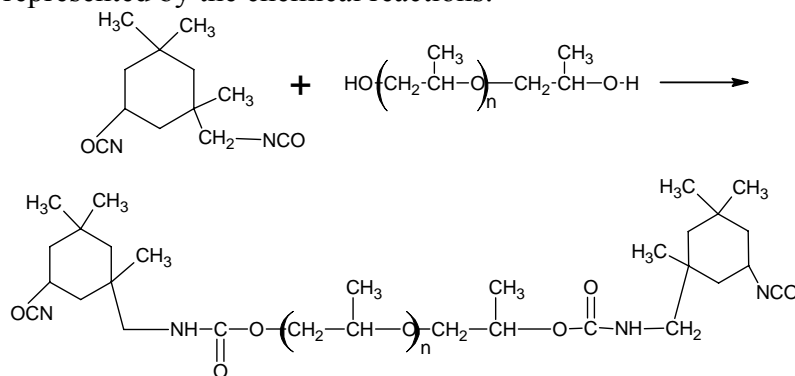
Since a many years our investigation has been directed to the synthesis and checking of the application of urethane-acrylates, epoxy-acrylates as the main components of lacquer compositions, hardened with the ultra-violet radiation, for protective coatings of various materials, especially the glass fibres [1 – 4].

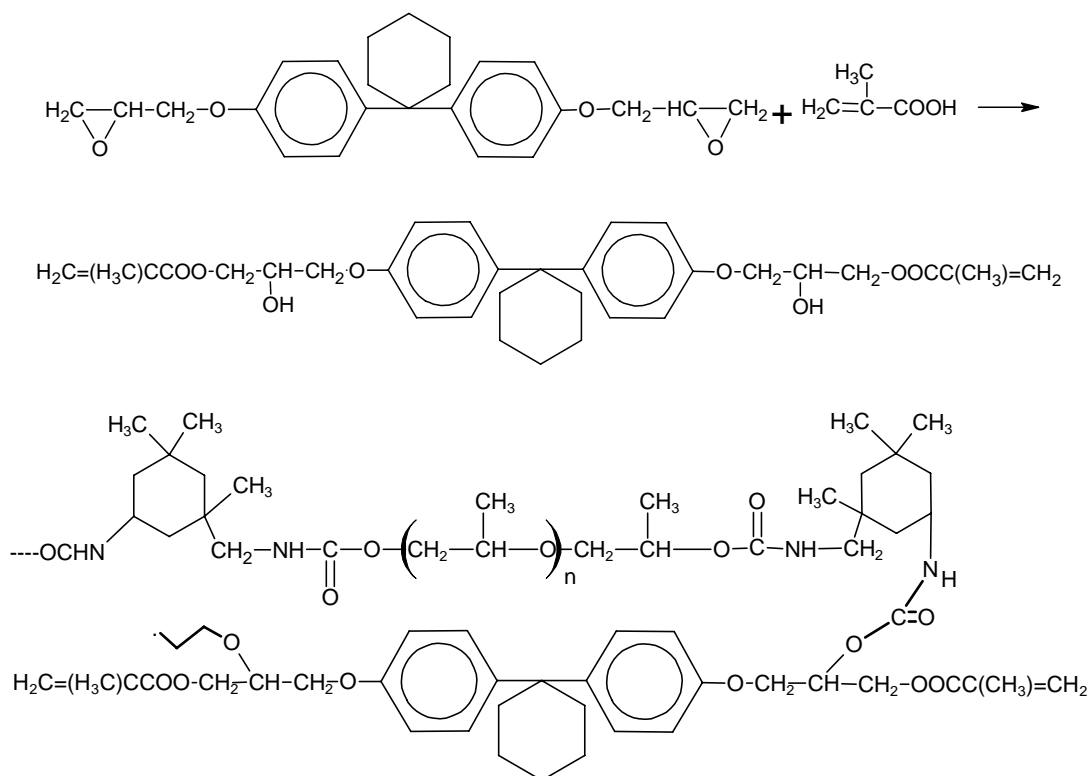
Lately, it has concentrated on the research related to the synthesis of determine the influence of the kind and amount of urethane-isocyanates subtracts on the properties of the urethane-epoxy methacrylates oligomers, before and after their hardening with the ultra-violet light.

EXPERIMENTAL PART

Materials: isophorone diisocyanate (IPDI) (Hüls AG), polypropylene glycol (PPG) of an average molecular weight of 2000 ("Rokita" Brzeg Dolny), epoxy resin from Epidian C (Epx C) [1], methacrylic acid (MA) (Aldrich), butyl acrylates (BA) (Aldrich).

A general scheme of preparation of the urethane-epoxy methacrylates (UEM) oligomers is represented by the chemical reactions.





Urethane-epoxy methacrylic (UEM) macromonomers were synthesized by condensation of epoxy methacrylic resin with urethane-isocyanate prepolymer. Epoxy methacrylate and urethane-isocyanate prepolymer were prepared from Epidian C and methacrylic acid, isophorone diisocyanate and polypropylene glycol of molecular weight 2000. Then the reaction was carried out until all NCO groups disappeared which was confirmed with spectra FTIR (no peak at 2270 cm^{-1}).

In order to confirm the structure of the urethane-epoxy methacrylate, epoxy methacrylate and urethane-isocyanate prepolymer an elemental analysis was carried out as well as the FTIR analysis (spectrophotometer Perkin Elmer model 1725X; film).

The received oligomer was mixed with active diluents in amount of 5 - 16%. Active solvent decreases the viscosity as desired in accordance with the expectations and take part in the photo polymerization process of urethane-methacrylate compositions. The following active diluents were applied butyl acrylate. This way, the composition UEM was obtained. The urethane-epoxy methacrylates composition are presented in Table 1.

Lacquer compositions, after the determination of their physicochemical properties, with addition of the photo initiator – Irgacure 651 (2,2-dimethoxy-2-phenylacetophenone), were hardened with the ultra-violet radiation. They were poured out on the glass plates of the UEM compositions, the samples were exposed to the light of a Hg lamp (400 W, wavelength 320-380 nm) at a distance of 30 cm during 5 min. in non-oxygen atmosphere. The mechanical properties of the received polymeric films were investigated (Table 2).

Table 1. Urethane-epoxy methacrylate compositions.

No UEM	IPDI [g]	PPG [g]	HEM [g]	Epx C [g]	MA [g]	BA [g]
1	44.4	200.0	26	-	-	13.5
2	27.1	122.0	-	19	8.6	8.8
3	20.0	90.3	-	19	8.6	6.9
4	31.0	139.8	-	38	17.2	11.3
5	22.1	99.4	-	38	17.2	8.8
6	15.6	70.1	-	38	17.2	7.0
7	17.7	79.7	-	57	25.8	9.0
8	17.1	77.3	-	76	34.4	10.2
9	10.4	47.1	-	76	34.4	8.4
10	12.9	58.3	-	152	68.8	14.6
11	-	-	-	76	34.4	22.1

Table 2. Mechanical properties of the poly(urethane-epoxy methacrylate)s.

No PUEM	Properties					
	Gel content [%]	Hardness Shore's [A; D*]	Young's Modulus [MPa]	Breaking stress [MPa]	Relative elongation at break [%]	Glass transition temp. [°C]
1	93.0	57; 12*	10.3	3.4	54.0	- 56
2	96.2	60; 11*	3.7	0.3	7.6	- 41
3	98.0	83; 22*	20.1	2.1	31.7	- 54
4	99.0	86; 29*	146	9.7	28.9	- 22
5	99.5	91; 35*	197	10.8	21.4	- 20
6	99.6	97; 43*	470	12.5	17.7	- 55; -1
7	99.5	98; 45*	540	15.9	11.8	- 13
8	99.5	97; 38*	510	17.8	11.9	- 52; -1
9	100	98; 49*	694	18.3	3.7	-52; +1
10	100	99; 74*	870	24.9	3.5	-52; +2
11	100	99; 78*	1880	63.2	2.8	+35

RESULTS AND DISCUSSION

By using isophorone diisocyanate and polypropylene glycol with molecular weights 2000 g/mol and epoxy methacrylate resins, the components lacquer for protective coatings were obtained. The structure of the synthesized molecules of urethane-epoxy methacrylates confirms a very good agreement of the results of elemental analysis and the calculated contents of the atoms of N and the presence of the characteristic peaks of the absorption bands in the spectra in Fourier transform infrared spectrophotometer. Important absorption peaks observed in the urethane-epoxy methacrylates oligomers spectra included the peaks corresponding to the stretching vibration of carbonyl group at 1728 - 1700 cm^{-1} , 3620 cm^{-1} stretching vibration of OH groups, aromatic ring stretching vibration at 3087 - 3030 cm^{-1} , CH, CH₂, CH₃ stretching vibrations at 2930 - 2897 cm^{-1} , stretching vibrations of the NH at 3300 and 1530 cm^{-1} , stretching vibrations of the C - O - C ethers and ether - urethanes at 1230 cm^{-1} and 1060 cm^{-1} , and no observed the peaks of NCO group at 2270 cm^{-1} .

One observed a distinct influence of the amount of the urethane-isocyanate component on the properties of the poly(urethane-epoxy methacrylate)s. The polypropylene glycol influence on the elasticity and flexibility of polymers. Addition of the hard segments – phenyl, urethane, ester and methacrylate groups, causes the hardness and mechanical resistance of the segment polymers obtained. A considerable content of the stiff segments results in a larger elasticity modulus, larger hardness and mechanical resistance. The soft segments (the propylene and ether bonds) make the urethane-epoxy methacrylates chain more flexible, they lengthen it until it breaks and they are resistant at a low temperature. The received poly(urethane-epoxy methacrylate)s contain 17 - 71% of soft segments, and the ratio of the flexible segments to the stiff ones makes that the received have a desired flexibility as well as good mechanical resistance and hardness. As it results the contents of gel in the hardened PUEM was about 93 – 100%. It means a high degree of polymerisation. As for the mechanical values the following ones merit a special attention: hardness 11 - 78 (Shore's scale D), Young's modulus 3.7 - 1880 MPa and a large range of lengthening until breaking: 3 – 54 %. Results from the analysis of the thermal resistance data state that the initial decomposition temperature and the temperature corresponding to the maximum decomposition rate are within 215 – 240 °C and 345 – 370 °C. This means that they show a relatively good thermal durability.

Poly(urethane-epoxy methacrylate)s coatings show the properties typical for soft, hard and intermediate protective coating, depending on kind and amount of urethane-isocyanates.

These lacquer compositions perfectly and fast hardened on the metals, glass, plastic materials and optical glass fibres.

Literature:

- [1] W. Podkościelny, A. Bartnicki, *Molecular Crystals&Liquid Crystals*, 353 (2000) 35
- [2] B. Tarasiuk, *Polish Journal of Chemical Technology*, 5(4) (2003) 11
- [3] B. Tarasiuk, *Annals of the Polish Chemical Society*, 3 (2004) 1074
- [4] B. Tarasiuk, A. Bartnicki, in: *Modyfikacja polimerów*, D. Żuchowska, R. Steller (ed), Oficyna Wydawnicza Politechniki Wrocławskiej. Wrocław 2005, pp273

PHYSICO-CHEMICAL AND CATALYTIC PROPERTIES OF POLYPYRROLE-PLATINUM COMPOSITES

Wincenty Turek¹, Agnieszka Śniechota¹, Magdalena Hasik², Anna Nyczyk²

¹*Department of Chemistry, Silesian Technical University, Gliwice, Poland,*

²*Faculty of Materials Science and Ceramics, AGH University of Science
and Technology, Kraków, Poland*

Introduction

Polypyrrole (PPy) is one of conjugated polymers whose unique electronic properties allow to incorporate various chemical species via the so-called doping reaction [1]. Therefore PPy is often applied as the support for various heterogeneous catalysts. Due to relatively high electronic conductivity, PPy is a particularly attractive matrix for redox catalysts. In the present work PPy-Pt composites have been obtained and characterized. Their physico-chemical and catalytic properties have been studied.

Experimental methods

Preparation of the catalysts

In the catalysts studied metallic platinum particles have been dispersed within polypyrrole matrix. As the matrix, polypyrrole doped with chloride ions (PPyCl) has been used. This polymer has been prepared by oxidative polymerization of pyrrole using ammonium peroxodisulphate as the oxidizing agent and hydrochloric acid as the reaction medium. Metallic platinum particles have been incorporated into PPyCl by three methods:

A) a two-step procedure

In this method platinum ions have been introduced into the polymer first. This has been achieved by polymer doping in the PtCl₄ aqueous solution. Then the incorporated platinum ions have been reduced in the NaBH₄ aqueous solution;

B) by reduction of platinum ions from PtCl₄ aqueous solution using NaBH₄ as the reducing agent carried out in the presence of PPyCl;

C) using metallic platinum aqueous sol

In this method platinum sol has been prepared separately according to [2]. The sol has been obtained at the temperature of 140 °C by reduction of Pt⁴⁺ ions originating from PtCl₄ with sodium citrate in an aqueous solution. The ions remaining in the resulting sol have been removed by ion exchange (Amberlite MB-1, Aldrich has been applied). Transmission electron microscope (TEM) investigations have shown that the size of platinum particles present in the sol has been in the range of 8-10 nm. Then into the platinum sol obtained in the described way PPyCl powder has been added. From such suspension water has been evaporated by heating during vigorous stirring. The resulting PPyCl-Pt powder has been additionally dried in dynamic vacuum.

All the PPy-Pt composites obtained have been in the form of powders insoluble in the studied catalytic reaction media.

Physico-chemical properties

Physico-chemical properties of the catalysts have been investigated using wide angle X-ray diffraction (XRD).

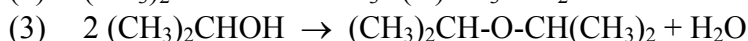
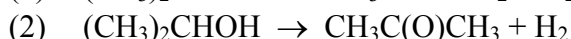
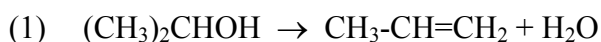
Catalytic properties

Catalytic properties of PPy-Pt nanocomposites obtained have been investigated using isopropyl alcohol conversion and phenol oxidation as the test reactions.

a) isopropyl alcohol conversion

Isopropyl alcohol conversion has been carried out in the presence of the PPy-Pt systems obtained in order to test their redox properties [1,3]. In this popular test reaction the alcohol is dehydrated to propene (1) on the acidic centers of the catalyst and dehydrogenated to acetone (2) on the redox (at high rate) or basic (at high temperatures) centers of the catalyst.

Formation of diisopropyl ether due to intermolecular dehydration of two isopropyl alcohol molecules (3) proceeding on acidic (mainly Lewis type) centers has been also observed in the presence of some catalysts.



Catalytic tests have been performed in the flow of nitrogen in the temperature range of 80 – 160 °C. Alcohol conversion has not exceeded 15%. Catalytic reaction products have been analyzed by gas chromatography.

b) phenol oxidation

Phenol can be easily oxidized using even weak oxidizing agents.

The first stage of the reaction results in the formation of phenoxyl radical due to elimination of hydrogen from phenol hydroxyl group. Such radical is relatively stable since it is stabilized by delocalization of the single electron over the aromatic ring.

Oxidation of phenol with hydrogen peroxide has been carried out at the temperature of 80 °C [4] in the presence of the most active catalysts B and C as well as without a catalyst.

¹H NMR spectra have been recorded using UNITY/NOVA 300 MHz (Varian) spectrometer. The samples have been analyzed in DMSO solutions with TMS as the chemical shift standard.

Results and discussion

Physico-chemical properties

It has been established that in all the samples metallic platinum has been present. Metallic Pt has been visible in the XRD patterns of the composites obtained (characteristic reflections of various intensities at $2\theta = 40^\circ$ and $47,5^\circ$, $\text{CuK}\alpha$ radiation). Results of XRD studies are presented in Figures 1 and 2.

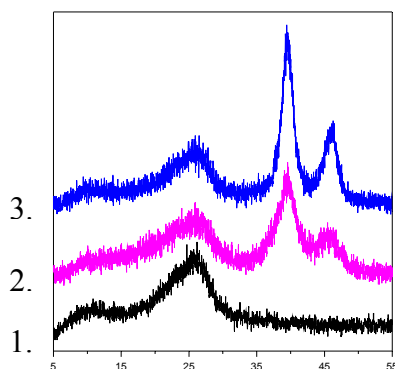


Fig. 1. XRD patterns (CuK α radiation):
 1. PPyCl
 2. PPyCl-Pt composite obtained by method (C)
 3. PPy-Pt composite obtained by method (B)

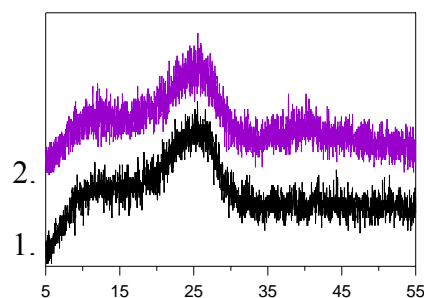


Fig. 2. XRD patterns (CuK α radiation):
 1. PPyCl doped with platinum ions
 2. PPyCl-Pt composite obtained by method (A)

It should be noted that all the catalysts have contained 7 wt. % of Pt.

Catalytic properties

a) isopropyl alcohol conversion

Based on the kinetic measurements it can be concluded that the catalysts obtained by methods B and C show very high and similar activity in the redox dehydrogenation reaction leading to acetone. These catalysts are significantly more active than the one prepared by method A.

In order to compare activity in the redox reaction (dehydrogenation to acetone) of catalysts B and C, its absolute specific rates have been calculated for both catalysts (Table 1).

Table 1. Absolute specific rate of the redox reaction proceeding in the presence of catalysts B and C

Catalyst	Absolute specific rate $\times 10^9$ [mol/g·s]	
	373 K	385 K
B	43,44	70,98
C	24,85	54,70

Table 2. Selectivity and activation energy of propene and acetone formation during isopropyl alcohol conversion in the presence of studied catalysts

Catalyst	Selectivity [%]				Activation energy [kJ/mol]	
	380 K		400 K		Propene	Acetone
	Propene	Acetone	Propene	Acetone		
A	82,11	17,89	64,71	35,29	75,08	136,07
B	1,13	98,87	0,85	99,15	30,79	48,69
C	1,01	98,99	0,68	99,32	18,90	43,90

b) phenol oxidation

Examination of ^1H NMR spectra has shown that catalytic phenol oxidation carried out in the presence of catalysts B and C leads to the formation of low molecular weight acids and aldehydes. In both cases the following products have been identified: formaldehyde (s, $\delta = 9,52$ ppm), acetaldehyde (d, $\delta = 2,14$ ppm; q, $\delta = 9,65$ ppm) and acetic acid (s, $\delta = 1,93$ ppm). The signal in the range characteristic for aldehyde protons (s, $\delta = 10,36$ ppm) may also indicate the presence of glyoxal or glyoxalic acid. Additionally, formic acid (s, $\delta = 8,15$ ppm) has been identified in the products of reaction carried out using catalyst B. No signals which could be ascribed to the intermediate products, such as *o*- and *p*-benzoquinone, hydroquinone, catechol, maleic acid, fumaric acid, muconic acid or aldehyde have been observed in the case of catalysts B and C.

Conclusions

1. Based on the kinetic measurements it can be concluded that the catalysts obtained by methods B and C show very high and similar activity in the redox isopropyl alcohol dehydrogenation reaction leading to acetone. These catalysts are significantly more active than the catalyst prepared by method A.

Higher activity of catalyst B with respect to that of C can be explained by smaller sizes of Pt crystallites in catalyst B than those in catalyst C. Smaller crystallites at the same Pt content lead to higher specific surface area of the active phase. This results in the increase of the total rate of the catalytic reaction as has been also observed in the case of electrochemically prepared PPy-Pt samples [5, 6].

2. Low intensities of the reflections corresponding to metallic Pt in the XRD pattern of sample A indicate that Pt ions incorporated into the PPyCl matrix have been reduced only to a small extent in this case. This may be the reason for low catalytic activity of this sample. Low activity of PPy-Pt systems containing ionic platinum acting as catalysts in methanol electrooxidation has been also observed in [6].

3. Phenol oxidation studies show that in the presence of the catalyst containing smaller Pt crystallites (catalyst B) which is more active in the redox reaction (the highest absolute specific rate of dehydrogenation reaction) the products of deep destructive oxidation (formic acid) are formed to higher extent.

References

- [1] W. Turek, E. Stochmal-Pomarzanska, A. Pron, J. Haber, *J. Catal.*, 189, 297 (2000)
- [2] D. N. Furlong, A. Laukonis, W. H. F. Sasse, *J. Chem. Soc. Faraday Trans. I*, 80 (1984) 571
- [3] W. Turek, J. Haber, A. Krowiak, *Appl. Surf. Sci.*, 252, (2005) 823
- [4] R. Liou, S. Chen, M. Hung, C. Hsu, *Chemosphere*, 59, (2005) 117-125
- [5] K. Rajeshwar, C.S.C. Bose, US 5 334 292 (1994)
- [6] K. Bouzek, K.-M. Mangold, K. Jüttner, *J. Appl. Electrochem.* 31 (2001) 501

Acknowledgment

The work was financially supported by Polish Ministry of Scientific Research and Information Technology grant No T09A 003 26.

INFRALINE GRAPHIC - MULTIFUNCTIONAL DATA COLLECTION INSTRUMENT FOR PHYSICAL CHEMISTRY EDUCATION

Eva Stratilová Urválková, Petr Šmejkal, Hana Čtrnáctová

Charles University in Prague - Faculty of Science

Department of Teaching and Didactics of Chemistry, Albertov 3, Prague 2, 128 43

Introduction

Experiment is a very important part of educational process in chemistry. It is a source of knowledge and experience and it helps students to adapt new routines and skills. The experiment must be as visual as possible; it is important to indicate distinct trends, for example precipitation, change of color, pH or conductivity of a solution. The experiments carried out with scientific measurement devices and along with Personal Computer (PC) or supported by PC can be useful in education with high impact. Advantages are direct visualization of a studied problem, immediate feedback, excellent clearness, employment of PC is attractive for students etc. In addition to that, the treatment of experimental data is easy, which allows students to focus on a studied problem. Experiment made or supported by PC also makes possible simultaneous theoretical and practical illustration of taught themes and leads to a better understanding of studied phenomena. Further important point to employ the measurement devices along with PC is that students of technically and technologically specialized schools have to master philosophy and control of these devices to be fully prepared for their profession or study at universities and other schools.

Utilization of experiments supported and/or provided by PC in the Czech Republic is not newcomer [1, 2], nevertheless, there is a lot of obstacles complicating this tendency, such as dimension, weight, know-how, money. Therefore, the perfect and suitable “high-school device” should be designed with respect to specific conditions and requirements of the high school laboratories and classes and, accordingly, requirements for a suitable measurement device for a high school slightly differ from the needs for a scientific one. The device should provide relatively exact and comfortable measurements (perfect accuracy, sensitivity and a variety of functions are not the most important parameters). The attention has to be also focused on mobility, easy and user-friendly control (software, manipulation, simple assembling and disassembling etc.), easy and cheap maintenance, robustness, reasonable dimensions, possibility to make experiments with or without PC, modularity (ability to provide more types of experiments from various fields of chemistry, biology, physics with one device) etc..

Infraline Graphic by Pierron Education

An instrument available at the Czech market, which is designed to fulfill the mentioned requirements, is Infraline Graphic by Pierron Education (Fig. 1). It is small and mobile device allowing connection of various sensors (even simultaneously) [3] and can operate with (through programme DidexPro by Pierron Education) as well as without PC. Its design allows measurement either in laboratory or outside the laboratory.

Fig. 1 Infraline Graphic

Objectives

Our contribution is focused on laboratory and demonstrational experiments potentially suitable for high schools and universities; the experiments are performed by Infraline Graphic. Particularly,

we have focused our attention on experiments in physical chemistry, because the physical chemistry is not favorite part of chemistry for most of the students in the Czech Republic. A reason is that some principles, concepts and definitions are rather abstract and complex to understand and they need supporting materials which help to visualize the studied problems. Therefore the experiments are important and integral part of the supporting materials.

Results and discussion

This contribution should be a summary of the two-year work with the instrument Infraline Graphic. It is impossible to concretize all the experiments; we show just two examples of our whole work. The testing of the Infraline Graphic has shown that the device is suitable for laboratory experiments at high schools and universities, especially due to its user-friendly and easy control through PC and multifunctional possibilities. Sensitivity and accuracy of tested sensors were acceptable and sufficient for a variety of experiments. Communication and operation along with PC was smooth and showed that experiments supported by PC can additionally improve quality of the experiment and simplify its treatment. It leads to better understanding of studied phenomena and improves and makes education more effective.

On the basis of the preliminary testing, there was proposed, tested and evaluated a set of 24 laboratory and demonstrational experiments, which were divided into four groups according to the used sensor:

Thermochemistry and calorimetry (temperature sensor)	
The heat capacity of a calorimeter	Dependence of released heat on the amount of the reactant
The temperature of heated copper wire	Heat of neutralization
Conductometry (conductometric sensor)	
Conductivity of distilled, tap and mineral water	pK_a of weak acid (conductometric measurement)
Conductivity dependence on solution concentration	Conductometric titration of a weak diprotic acid
Precipitation titration of NaCl by AgNO ₃ with equivalence point indication by measuring the solution conductivity	Acid-base titration of acid by base with equivalence point indication by measuring the solution conductivity
Conductivity of acids and bases aqueous solutions	
Potentiometry and pH measurements (glass electrode)	
pK_a of phosphoric acid by potentiometric acid-base titration	pH dependence on concentration of CO ₂ in solution
Colour-change interval for acid-base indicator: thymol blue	Acid-base titration with potentiometric indication of equivalence point
Colour-change interval for acid-base indicator: bromphenol blue	Colour-change interval for acid-base indicator : methyl orange
Colour-change interval for acid-base indicator : phenolphthalein	
VIS Spectrometry (photometric sensor)	
Determination of unknown concentration in a sample using calibrating curve method: (for Ni(NO ₃) ₂ , NiSO ₄ , CoCl ₂ , Co(NO ₃) ₂ , K ₃ [Fe(CN) ₆], AlluraAC red)	

Experiments with two or more sensors	
Acid-base titration of weak acid (simultaneous equivalence point indication by measurement of pH and conductivity of the solution)	Acid-base titration (simultaneous equivalence point indication by measurement of pH and conductivity of the solution)
The pH dependence on temperature	Mineral water – pH and conductivity
Analysis of water (pH, conductivity, Cl^- , NO_2^- , acidity, alkalinity)	

The most important advantage of PC utilization is visualization. It can be perfectly seen during the titration, indicated with potentiometric and/or conductometric sensor (using the software DidexPro provided by manufacturer). In Fig. 2 is shown a graph, which is continuously recorded and displayed while measuring. Fig. 2 is a graph of acid-base titration: HCl ($0.1232 \text{ mol.L}^{-1}$) was titrated with 0.195 mol.L^{-1} NaOH (previously standardized with oxalic/ethanedioic acid). The solution of HCl with stirrer put on mixing vessel is titrated with micropipette: the NaOH titrant (0.3 ml) is added every 10 seconds after measured value, which provides consequent stirring. Potentiometric and conductometric curve are logged at once in one graph, the table of values is also exhibited on the screen. The equivalence point can be read right from these curves (the inflection point at potentiometric curve, the minimum at conductometric curve), or there can be worked out a first derivation, where can be read an exact value of equivalence point (Fig. 3). In this example the equivalence point is at time 240 sec for potentiometric sensor (230 sec for conductometric sensor), it means 23 (22) addition, because the starting addition is after first 10 seconds. The volume of the titrant is therefore $23 \times 0.3 \text{ ml} = 6.9 \text{ ml}$ ($22 \times 0.3 \text{ ml} = 6.6 \text{ ml}$). With this volume we can get the unknown concentration of acid, which is in this example $0.1345 \text{ mol.L}^{-1}$ for potentiometric sensor and $0.1287 \text{ mol.L}^{-1}$

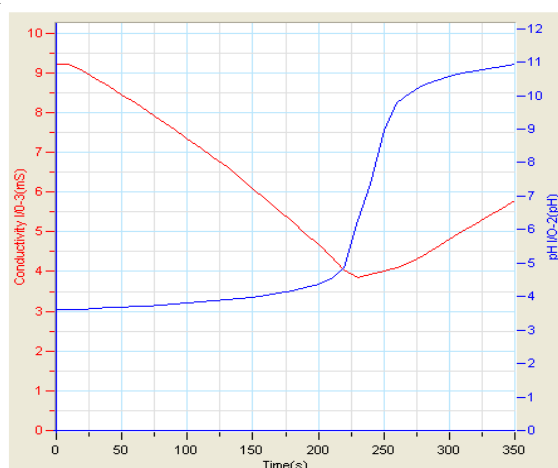


Fig. 2 Titration curves: potentiometric (blue) and conductometric (red)

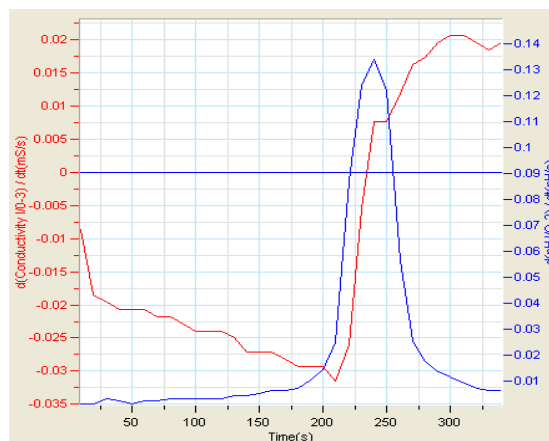


Fig. 3 Derivation of the titration curves

for conductometric sensor ($0.1316 \text{ mol.L}^{-1}$ at the average). Error 6.8 % is receivable.

Secondly we would like to focus on VIS spectrometric sensor. Its principle and construction are simple [4]. Light emitting diode (LED) acts as a light source. The corresponding wavelength is specified by a suitable filter which absorbs remaining wavelengths emitted by the source. The light passes through a solution of a sample

where a part of light intensity is absorbed by the sample. The light which is not absorbed is detected by photo-sensitive diode. The sensor is cheaper than similar scientific devices, so there was a question, whether the sensor works. To test the sensor, we made a set of comparative measurements with scientific spectrometer USB-2000 (OceanOptics, Netherlands). We observed that measured values with VIS spectrometric sensor are well comparable with those obtained with USB-2000 spectrometer. We designed a set of experiments based on determination of unknown concentration in a sample by calibrating curve method (for $\text{Ni}(\text{NO}_3)_2$, NiSO_4 , CoCl_2 , $\text{Co}(\text{NO}_3)_2$, $\text{K}_3[\text{Fe}(\text{CN})_6]$, AlluraAC red, nitrite in water). Especially, the determination of AlluraAC red (E-129, food-dye) concentration in sweets or drinks can be attractive for students. We obtained a fair calibration curve (line) with reasonable square coefficient of determination R^2 ($R^2 = 0.9884$) suitable for determination the unknown concentration of AlluraAC red in a sample by mentioned method. Similarly, another attractive experiment, determination of nitrite ion concentration in a sample of fresh water, was also successful. For the VIS spectrometry sensor is suitable for experiments demonstrating absorption of light by a sample and the calibrating curve method.

Conclusion

The device has shown to be suitable especially due to its user-friendly and easy control through PC and multifunctional possibilities. The principal advantage of the experiments practiced with the Infraline Graphic is a direct visualization of the experiments results on the screen of the device and/or PC and the possibility for immediate treatment of acquired data. The set of experiments using Pierron Infraline Graphic has been proposed, tested and evaluated. 22 experiments seem to be suitable for utilization at high schools and in early courses at universities. In the case of two unsuccessfully tested experiments, the sensitivity of corresponding sensor was not sufficient (Determination of pK_a of weak acid by conductometric measurements and Conductometric titration of weak diprotic acid). The worksheets will be published on a website. The work sheets for the experiments have been designed for teachers (containing important notes to the experiments, calculations, possible results etc.) as well as for students allowing easy editing to adapt the experiment for teacher needs (.doc format). The proposed laboratory experiments can be easily performed in laboratory as well as demonstrational experiments and cover some important phenomena and principles of physical chemistry, in particular parts of Thermometry and Calorimetry, Potentiometry, VIS Spectrometry and Conductometry.

References

- [1] BÍLEK, M. et al.: *Výuka chemie s počítačem*. Hradec Králové: Gaudeamus, 1997. 134 s. ISBN 80-7041-769-2
- [2] BÍLEK, Martin: *Školní chemický experiment s využitím počítače*. Chem. Listy 91, 1074, 1997.
- [3] PIERRON PRAHA: *Infraline Graphic- Uživatelská příručka*. Praha: Pierron.
- [4] PIERRON Education: *Capteur Colorimètre – user manual*. Sarreguemines CEDEX: Pierron.
- [5] ČERMÁKOVÁ, L. et al.: *Analytická chemie 2 – Instrumentální analýza*. 2. vydání. Praha: SNTL, 1987, 320 s. ISBN 04-616-87.
- [6] OPEKAR, Fr. et al.: *Základní analytická chemie*. Praha: Karolinum, 2003. 200 s. ISBN 80-246-0553-8.

THE REACTIONS OF HYDRAZIDE (4-NITROIMIDAZOL-1-YL) ACETIC ACID WITH ISOTHIOCYANATES

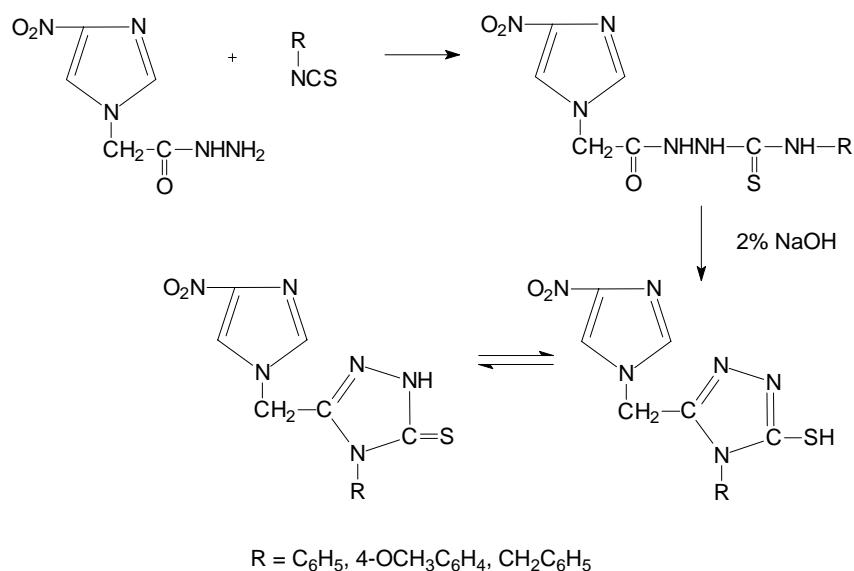
Monika Wujec^a, Maciej Pisklak^b, Monika Pitucha^a, Maria Dobosz^a, Agata Siwek^a

^a Department of Organic Chemistry, Faculty of Pharmacy, Medical University, Lublin, 6 Staszica Str., monika.wujec@am.lublin.pl

^b Department of Physical Chemistry, Faculty of Pharmacy, Medical University, Warszawa, 1 Banacha Str.

The biological activities of various triazoles [1-11] and imidazoles [12-13] have been extensively studied. We observed from the literature that combination of two heterocyclic moieties can enhance these activities [14]. In continuation of our work on the synthesis of heterocycles of pharmaceutical interest [15-16] we report here synthesis and characterisation of new derivatives of 3-[(4-nitroimidazol-1-yl) methyl]-1,2,4-triazoline-5-thione.

The new obtained compounds can exist in two tautomeric forms: thione or thiole.



Experimental

Melting points were determined in a Fisher-Johns block without corrections. The ¹H NMR spectra were recorded on a Bruker Avance 300 in DMSO-d₆ with TMS as internal standard. TLC was performed on commercial Merck SiO₂ 60 F₂₅₄ plates with chloroform-ethanol (10:1) eluent system, visualization: UV light λ 254 nm. Elemental analyses were performed on a Perkin-Elmer analyzer and were in the range of ± 0.4%

for each element analyzed (C, H, N). Chemicals were purchased from Merck Co. or Lancaster and used without purification.

(4-nitroimidazol-1-yl) acetic acid hydrazide (**I**)

Methyl (4-nitroimidazol-1-yl) acetate (0.01 mole), dry ethanol (5 cm³) and hydrazine hydrate (80%, 0.02 mole) were mixed and kept for 24 h in room temperature. The product was filtered, dried and crystallized from 95% ethanol.

C₅H₇N₅O₃ *M_w*: 185.14. *M.p.*: 110-1°C. *Yield* 86%.

Thiosemicarbazide derivatives of (4-nitroimidazol-1-yl) acetic acid (**IIa-IIIc**)

Hydrazide I (0.01 mole) and isothiocyanates (0.01 mole) were mixed carefully and then placed in a round bottom flask, and heated on oil bath at 70°C for 8 h. The reaction product was washed with diethyl ether in order to remove the unreacted isothiocyanate and then with water to remove the unreacted hydrazide. Next, the product was filtered, dried and crystallized from 95% ethanol.

4-Phenyl-1-[(4-nitroimidazol-1-yl)acetyl]thiosemicarbazide (**IIa**)

C₁₂H₁₂N₆O₃S *M_w*: 320.33. *M.p.*: 140-2°C. *Yield* 88%. ¹H NMR (δ, d₆); 4.99 (s, 1H, CH₂); 6.90-7.43 (m, 5H, arom. benzene); 7.52 (s, 1H, CH); 8.24 (s, 1H, CH); 9.57, 9.88, 10.34 (3s, 3H, 3NH).

4-(4-Methoxyphenyl)- 1-[(4-nitroimidazol-1-yl)acetyl]thiosemicarbazide (**IIb**)

C₁₃H₁₄N₆O₄S *M_w*: 350.36. *M.p.*: 192-4 °C. *Yield* 93%. ¹H NMR (δ, d₆); 3.75 (s, 3H, CH₃); 4.94 (s, 1H, CH₂); 6.88-7.40 (m, 4H, arom. benzene); 7.80 (s, 1H, CH); 8.31 (s, 1H, CH); 9.56, 9.65, 10.44 (3s, 3H, 3NH).

4-Benzyl-1-[(4-nitroimidazol-1-yl)acetyl]thiosemicarbazide (**IIc**)

C₁₃H₁₄N₆O₃S *M_w*: 334.36. *M.p.*: 149-150°C. *Yield* 90%. ¹H NMR (δ, d₆); 4.78 (s, 1H, CH₂); 4.91 (s, 1H, CH₂); 7.21-7.36 (m, 5H, arom. benzene); 7.80 (s, 1H, CH); 8.30 (s, 1H, CH); 8.59, 8.61, 10.33 (3s, 3H, 3NH).

3-[(4-Nitroimidazol-1-yl)methyl]-4-substituted-1,2,4-triazoline-5-thione (**IIIa-IIIc**):

thiosemicarbazide IIa-IIc (0.01 mole) and sodium hydroxide (2%, 20 cm³) were boiled for 2 h. after cooling, the solution was neutralized with diluted hydrochloric acid. The precipitate was filtered and then crystallized from 95% ethanol.

3-[(4-Nitroimidazol-1-yl)methyl]-4-phenyl-1,2,4-triazoline-5-thione (**IIIa**)

C₁₂H₁₀N₆O₂S *M_w*: 302.31. *M.p.*: 309-310°C. *Yield* 89%. ¹H NMR (δ, d₆); 5.33 (s, 1H, CH₂); 7.40-7.59 (m, 5H, arom. benzene); 7.49 (s, 1H, CH); 8.16 (s, 1H, CH); 14.02 (s, 1H, NH).

4-(4-Methoxyphenyl)-3-[(4-nitroimidazol-1-yl) methyl]-1,2,4-triazoline-5-thione (**IIIb**)

C₁₃H₁₂N₆O₃S *M_w*: 332.34. *M.p.*: 148-150°C. *Yield* 88%. ¹H NMR (δ, d₆); 3.83 (s, 3H, CH₃); 4.95 (s, 1H, CH₂); 7.38-7.64 (m, 4H, arom. benzene); 7.76 (s, 1H, CH); 7.93 (s, 1H, CH); 13.85 (s, 1H, NH).

4-Benzyl-3-[(4-nitroimidazol-1-yl) methyl]-1,2,4-triazoline-5-thione (**IIIc**)

C₁₃H₁₂N₆O₂S *M_w*: 316.34. *M.p.*: 120-2°C. *Yield* 78%. ¹H NMR (δ, d₆); 5.35 (s, 1H, CH₂); 5.57 (s, 1H, CH₂); 7.07-7.48 (m, 5H, arom. benzene); 7.84 (s, 1H, CH); 8.19 (s, 1H, CH); 14.05 (s, 1H, NH).

Calculation

Theoretical quantum chemical calculations were performed for the thiole and thione form of compounds **IIIb** and **IIIc**.

The molecular geometries were optimized by semi-empirical PM3 quantum chemical method. Finally, B3LYP hybrid DFT potential with the 6-31G** functional base was used to gain the single-point electronic energies. All of the quantum chemical calculations were accomplished by Gaussian 98 package [17].

The results of calculations evidenced that the thione forms are more favourable for both compounds. However, the energy difference between both tautomers is significantly higher for compounds with the benzyl substituent **IIIc** (18.7 kcal/mol) than for **IIIb** (14.7 kcal/mol).

References

1. Abdeal A. M.; Gineinah M. M.; Nasar M. N.: *Bull. Chim. Farm.* 137, 372 (1998).
2. Shivarama H. B.; Sooryanarayana R. B.; Shridhara K.; Akberali P. M.: *Farmaco* 55, 338 (2000).
3. Udupi R. H.; Bhat A. R.: *Indian I. Heterocycl. Chem.* 6, 41 (1996).
4. Pasenko O.; Shevchenko I.; Samura B.; Bakumenko M.; Toryanik O.; Knish E.: *Farm. Zh.* 3, 44 (1999).
5. Patil S. A.; Badiger B. M.; Kudari S. M.; Kulkarni V. H.: *J. Indian. Chem. Soc.* 61, 713 (1984).
6. Talawar M. B.; Laddi U. V.; Somannavar Y. S.; Bennur R. S.; Bennur S. C.: *Indian I. Heterocycl. Chem.* 4, 297 (1995).
7. Pourmorad F.; Shafice A.: *I. Sci. Islamic Repub. Iran* 9, 30 (1998).
8. Sharma R.; Bahel S.: *I. Indian Chem. Soc.* 59, 877 (1982).
9. Budeanu C.; Iorga T.; Rusan M.: *Rev. Chim.* 34, 791 (1983).
10. Goswami B.; Katakya I.; Boruah I.; Nath S.; Bordoloi D.: *I. Indian Chem. Soc.* 61, 530 (1984).
11. Mishra R.; Teari R.; Srivastava S.; Bahel S.: *I. Indian. Chem. Soc.* 68, 110 (1991).
12. Iradyan M.A., Iradyan N.S., Stepanyan G.M., Arsenyan F.G., Paronikyan G.M., Darbinyan G.A., Kaaryan E.V., Garibdzhanyan B.T.: *Pharmaceutical Chemistry Journal* 37 (2003).
13. Antolini M., Bozzoli A., Ghiron Ch., Kennedy G., Rossi T., Ursini A.: *Bioorganic&Medicinal Chemistry Letters*, 9, 7 (1999).
14. Sztanke K., Fidecka S., Kędzierska E., Karczmarzyk Z., Philaja K., Matosiuk D.: *Eur. J. Med. Chem.*, 40 (2005).
15. M. Dobosz, A. Siwek, A. Chodkowska, E. Jagiełło–Wójtowicz : *Acta Polon. Pharm.* 61, Supplement, 5–7 (2004).
16. Wujec M., Pitucha M., Dobosz M., Kosikowska U., Malm A.: *Acta Pharm.*, 54 (2004).
17. Gaussian 98, Revision A.7, M. J. Frisch, G. W. Trucks, H. B. Schlegel, G. E. Scuseria, M. A. Robb, J. R. Cheeseman, V. G. Zakrzewski, J. A. Montgomery, Jr., R. E. Stratmann, J. C. Burant, S. Dapprich, J. M. Millam, A. D. Daniels, K. N. Kudin, M. C. Strain, O. Farkas, J. Tomasi, V. Barone, M. Cossi, R. Cammi, B. Mennucci, C. Pomelli, C. Adamo, S. Clifford, J. Ochterski, G. A. Petersson, P. Y. Ayala, Q. Cui, K. Morokuma, D. K. Malick, A. D. Rabuck, K. Raghavachari, J. B. Foresman, J. Cioslowski, J. V. Ortiz, A. G. Baboul, B. B. Stefanov, G. Liu, A. Liashenko, P. Piskorz, I. Komaromi, R. Gomperts, R. L. Martin, D. J. Fox, T. Keith, M. A. Al-Laham, C. Y. Peng, A. Nanayakkara, C. Gonzalez, M. Challacombe, P. M. W. Gill, B. Johnson, W. Chen, M. W. Wong, J. L. Andres, C. Gonzalez, M. Head-Gordon, E. S. Replogle, and J. A. Pople, Gaussian, Inc., Pittsburgh PA, 1998.

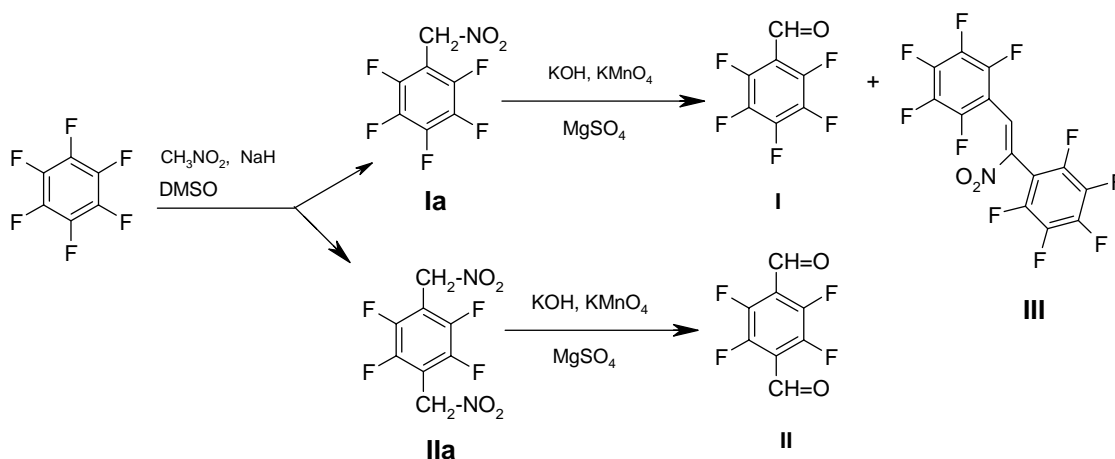
NEW SYNTHESIS AND SYNTHETIC UTILISATION OF PENTAFLUOROBENZALDEHYDE AND TETRAFLUOROTEREPTHALIC ALDEHYDE AS BUILDING BLOCS FOR NOVEL OPTO-ELECTRONIC MATERIALS

Daniel VÉGH^a, Tomáš SOLČÁN^a, Katarína HRNČARIKOVÁ^a
and Jozef KOŽÍŠEK^b

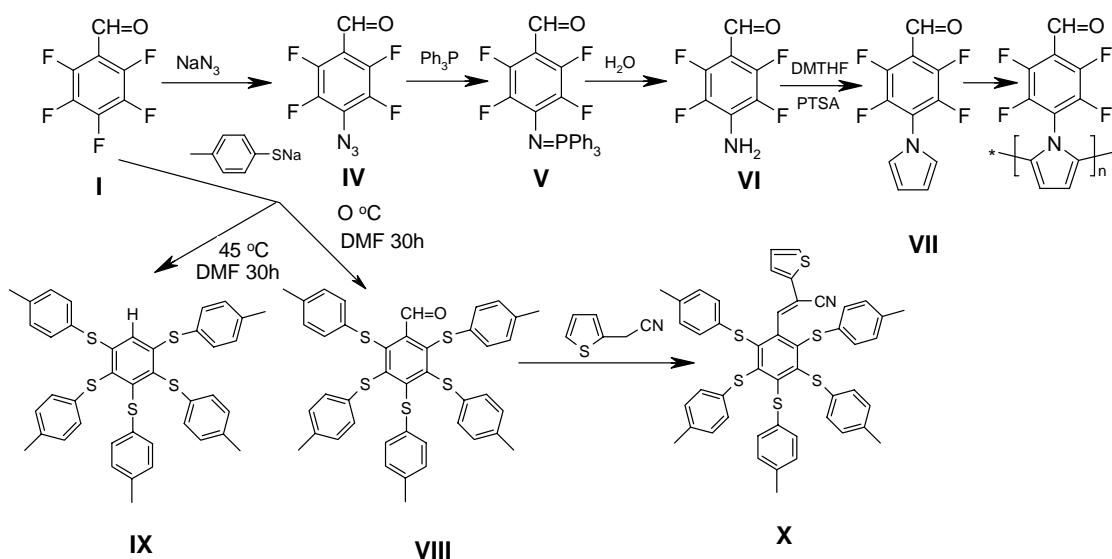
^a*Institute of Organic Chemistry, Catalysis and Petrochemistry,* ^b*Institute of Physical Chemistry and Chemical Physics, Slovak University of Technology, Radlinského street 9, SK-812 37 Bratislava, Slovakia, email: daniel.vegh@stuba.sk*

The utilization of perfluoroaromatics for molecular recognition has in recent years been an intensely studied topic. The pentafluorobenzaldehyde (PFBA) (**I**) and tetrafluoroterephthalic aldehyde (TFTA) (**II**), both important starting materials for the above mentioned research have so far been hardly investigated. With the sole exception of the reduction of pentafluorobenzonitrile[1] to pentafluorobenzaldehyde (yield 64%) all the known methods for the synthesis of PFBA [2-9] and TFTA [10,11] involve multi-step processes with low overall yields and starting from rather inaccessible raw materials.

In the course of our search for alternative cheap and accessible starting materials for the preparation of PFBA and TFTA we were intrigued by the possible deployment of the pentafluorobenzene and hexafluorobenzene for this purpose. However, given the electron-deficient nature of pentafluorobenzene standard formylation methods [12] are not plausible. Bearing in mind that Nef [13] reaction would be a straightforward pathway to achieve this transformation through an S_NAr reaction under mild and controlled conditions. The nitromethyl derivatives obtained were readily transformed into the corresponding aryl aldehyde **I**, **II** overall as an equivalent process of nucleophilic formylation in which nitromethane serves as the synthon for formyl anion. Hexafluorobenzene reacted readily with nitromethane in the presence of NaH in DMFA or DMSO at room temperature. This nitromethylation proceeded well with hexafluorobenzene. Nucleophilic displacement of a single fluorine atom in hexafluorobenzene by nitromethane affords 1,2,3,4,5-pentafluoro-6-nitromethylbenzene (**Ia**) replacement of another fluorine affords then 1,2,4,5-tetrafluoro-3,6-bis-nitromethyl-benzene (**Ib**) a compounds easily undergoing the Nef reaction when treated with KOH and KMnO₄ with good yields. The procedure represents a novel, as yet unpublished synthesis (scheme 1.) of PFBA (**I**) and TFTA (**II**). The formation of the by product **III** also detected during the preparation of **I**.



We investigated the reactivity of fluorine substituents in PFBA (**I**) towards nucleophiles (e.g. azide anion, 4-methylphenylthiolate anion) as well as that of carbonyl group in PFBA towards 2-thenylacetonitrile. The target compounds **VI-X** can be used as building blocks for novel materials with optoelectronic properties and supramolecular structure in solid state.



General procedure for the preparation of Ia and IIa Nitromethane (300 mmol) in DMSO (100 mL) was dropped into the suspension of NaH (300 mmol) in 100 mL of dry DMSO with stirring.
 a/ **Ia**, After the bubbling subsided, hexafluorobenzene (100 mmol) was added; the mixture was stirred at r.t. 5h, 100°C 1h and 150°C 1h and then poured into ice-water; acidified with 6 N HCl, then extracted with ethyl acetate. The organic

extraction was washed with water and brine and dried over anhydrous MgSO₄. Evaporation of the solvent in vacuum gave a residue, which was separated by column chromatography on glass columns packed with silica gel Merck60 using toluene as eluant to afford **Ia** 49% and a small amount of **IIa**.

b/ **Ia** and **IIa** After the bubbling subsided, hexafluorobenzene (50 mmol) was added; the mixture was stirred at r.t. 5h, 100°C 5h and 150°C 1h and then poured into ice-water; acidified with 6 N HCl, then extracted with ethyl acetate. The organic extraction was washed with water and brine and dried over anhydrous MgSO₄. Evaporation of the solvent in vacuum gave a residue, which was separated by column chromatography on glass columns packed with silica gel Merck60 using toluene as eluant to afford **Ia** 44% and **Ib** 25%.

Ia. Yellow oil (R_f=0.7 – toluene) ¹H NMR (300 MHz, CDCl₃) 4.50 (s, CH₂)

IIa. M.p. 149-152 °C, (R_f=0.5 – toluene) ¹H NMR (300 MHz, CDCl₃) 4.52 (s, CH₂)

General procedure of the preparation of I and II: A stirred suspension of **Ia** or **IIa** (20 mmol) in methanol (140 mL) was cooled to -10 °C to 5 °C and then a freshly prepared solution of KOH (60 mmol) in methanol (200 mL) was added dropwise. After stirring for an additional 30 min, a solution of KMnO₄ (15 mmol) and MgSO₄ (60 mmol) in water (600 mL) was added dropwise with vigorous stirring. When the reaction was complete, the mixture was filtered over a thin layer of *Celite*. The filtrate was extracted with CH₂Cl₂ and the extract was washed with saturated Na₂CO₃, water, and brine successively and then dried over MgSO₄. Removal of the solvent in vacuum gave a residue which was separated by column chromatography on glass columns packed with silica gel Merck60 using toluene as eluant to afford **I** in 64% yield b.p. 55°C/2.4 kPa and **II** in 60% yield as light yellow crystals m.p.132 °C (chloroform) lit. [10,11] 131-132 °C.

4-Azido-2,3,5,6-tetrafluorobenzaldehyde (IV). A mixture of NaN₃ (60 mmol) and **I** (50 mmol) in 100 ml acetone and 40ml water was refluxed for 10 h. The mixture was cooled, diluted with 200 ml water and extracted by ether. The extract was dried and evaporated to leave 95% **IV** m.p. 44-45°C. ¹H NMR (300 MHz, CDCl₃) 10.23 (1H, CHO) IR (film) ν_{max}/cm⁻¹: 2125 (N₃). The ether solution of **IV** with equivalent of triphenylphosphine resulted quantitatively **V** m.p. 139-141°C. ¹H NMR (300 MHz, CDCl₃) 10.07(1H, CHO), 7.28-7.36 (m,15H, H_{Ar}).

4-Amino-2,3,5,6-tetrafluorobenzaldehyde (VI) Prepared by hydrolysis of **V** in THF-H₂O 1:1, 20h, 65°C in 90% yield m.p. 110-111°C. lit[14] 110-111°C.

4-N-pyrrolo--2,3,5,6-tetrafluorobenzaldehyde (VII). Prepared by *Paal-Knorr* pyrrole synthesis [15] in 85% yield m.p. 60-61 °C. ¹H NMR (300 MHz, CDCl₃), 10.31(1H, CHO), 6.47-6.42 (2H, H_{Ar}), 7.01-7.10 (2H, H_{Ar}), ¹⁹F-NMR(C₆F₆): -5,67 (q), -10,30(q).

Preparation of VIII a IX The synthesis of **VIII** were carried out using the *MacNicol*[16] reaction. The 7 eqv. of sodium 4-methylphenylthiolate species generated in situ by treating the thiol with potassium hydroxide, were reacted with **I** in DMFA in various temperature producing the pentasubstituted benzenes **VIII** in 44% yield and **IX** in 37% yield. The moderate yield of analytically pure material **VIII** probably result from the presence of the products of lower degrees of substitution and the potassium hydroxide present in the potassium 4-methylbenzenethiolate effects a

haloform cleavage product **IX**.

VIII. m.p. 119-120°C. ¹H NMR (300 MHz, CDCl₃) 9.75 (1H, CHO), 6.87-6.95 (m, 20H, H_{Ar}), 2.27 (s, 15H, CH₃), ¹⁹F-NMR(C₆F₆): δ = Ø

IX m.p. 107-110°C. ¹H NMR (300 MHz, CDCl₃) 6.80-7.08 (m, 21H, H_{Ar}), 2.23 (s, 15H, CH₃), ¹⁹F-NMR(C₆F₆): δ = Ø

Preparation of X. By heating of **I** with 2-thienylacetonitrile in ethanol and 2 drops of 50% NaOH in 64% yield, m.p. 167-169 °C, ¹H NMR (300 MHz, CDCl₃) 6.72-7.18 (m, 23H, H_{Ar}), 6.41 (s, 1H, CH=C), 2.22 (s, 15H, CH₃),

Structures of target compounds **I-X** were proved by IR, UV, ¹H NMR, ¹³C NMR and ¹⁹F NMR spectral methods, and **IIb** by X-ray analysis [17].

This work was financially supported by grants from the Ministry of Education of the Slovak Republic No. 1/1379/04 1/2449/05 and the Science and Technology Assistance Agency (No. APVT-20- 007304).

REFERENCES

- [1]. N.B. Chapman, K. Clarke, R.M. Pinder, S.N. Shavney: J.Chem. Soc.C., (1967) 293
- [2]. E. Nield, R. Stephens, J.C. Tatlow: J.Chem.Soc., (1959) 166
- [3]. A.K. Barbour, M.W. Buxton, P.L. Coe, R. Stephens, J.C. Tatlow: J.Chem.Soc., (1961) 808
- [4]. P.L. Coe, R. Stephens, J.C. Tatlow: J.Chem.Soc., (1962) 3227
- [5]. N.N. Vorozhotsov, V.A. Barkash, N.G. Ivanova: Dokl.Akad.Nauk.SSSR, 159, (1964) 125
- [6]. J.M. Birchall, R.N. Haszeldine, M.E. Jones: J.Chem.Soc.C, (1971) 1343
- [7]. N.I. Petrenko : Izv.Akad.Nauk SSSR, Ser.Khim., (1984) 1378
- [8]. G.G. Furin, A.O. Miller, Yu.V. Gatilov: J.Fluorine Chem., 28, (1985) 23
- [9]. M. Julliard, M. Chanon: Bull.Soc.Chim.Fr., 3, (1992) 242
- [10]. C.F. Krebs, T Jensen.: J. Fluorine Chem., 120, (2003) 77
- [11]. Sh. Zhu, J. Zhao, X. Cai.: J. Fluorine Chem. 125, (2004) 451
- [12]. L. Kurti, B. Czakó,: *in book* Synthetic Applications of Named Reactions in Organic Synthesis, Elsevier Academic Press. 2005 p. 242
- [13]. L. Kurti, B. Czakó,: *in book* Synthetic Applications of Named Reactions in Organic Synthesis, Elsevier Academic Press. 2005 p. 308
- [14]. K. Kanakarajan, K. Haider, A.W. Czarnik.: Synthesis (1988) 566
- [15]. L. Kurti, B. Czakó,: *in book* Synthetic Applications of Named Reactions in Organic Synthesis, Elsevier Academic Press. 2005 p. 328
- [16]. D.D. MacNicol, P.R. Mallinson, A. Murphy, G.J. Sym: Tetrahedron Lett., 23, (1982) 4131
- [17]. L. Perašinová, I. Svoboda, D. Végh, T. Solčán, J. Kožíšek: Acta Cryst Sect E62, (2006) 1689

KINETICS AND MECHANISM OF REDUCTION REACTION OF μ -OXO-BIS [AQUATETRACHLORORUTHENATE (IV)] WITH IRON(II) IN ACIDIC MEDIUM

Dorota Wawrzak¹, Bogdan Banaś²

¹*Institute of Chemistry and Environmental Protection,
J. Długoż University of Częstochowa,
42-200 Częstochowa, Al. Armii Krajowej 13/15*

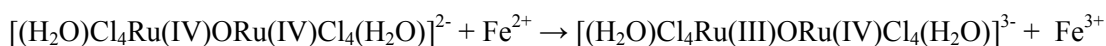
²*Faculty of Chemistry, University of Wrocław,
50-383 Wrocław, F. Joliot – Curie 14*

INTRODUCTION

Dinuclear ruthenium (III,IV) complexes, $[\text{Cl}_5\text{RuORuCl}_5]^{n-}$ ($n = 4, 5$), and their aquated derivatives, belong to the group of well – defined ruthenium dimers and oligomers [1- 4] where the link between the metal sites is a μ -oxo bridged ligand. Small structural differences between the oxidized and reduced forms, together with the specific contribution of the oxygen bridges to the electron transfer processes, create favourable conditions to the fast and reversible redox chemistry [5].

In our previous paper [6] we have reported on the kinetics of the reduction of μ -oxo-bis[aquatetrachlororuthenate (IV)] ion with ascorbic acid in acidic solution. Formation of mixed oxidation state complex with a linear Ru(III)-O-Ru(IV) core and dehydroascorbic acid as a reaction products has been observed.

In this paper the kinetics and mechanism of the one-electron reduction of μ -oxo-bis[aquatetrachlororuthenate (IV)] with iron (II) in water-HCl solution are presented:



It is generally accepted that binuclear electron transfer reactions proceed via a sequence of elementary steps: formation of the precursor complex, intramolecular electron transfer within the precursor complex, and dissociation of the successor complex. For outer-sphere reactions, the precursor and successor complexes are ion pairs or outer-sphere complexes. For inner-sphere reactions, the precursor and successor complexes are binuclear complexes in which a bridging ligand connects the two metal centers [7, 8].

EXPERIMENTAL

$\text{K}_4[\text{Ru}_2\text{OCl}_{10}] \cdot \text{H}_2\text{O}$ was prepared and analysed as described in [9]. $[\text{Ru}_2\text{OCl}_8(\text{H}_2\text{O})_2]^{2-}$ was obtained during four hours lasting aquation process of $[\text{Ru}_2\text{OCl}_{10}]^{4-}$ in 0.1 mol dm^{-3} HCl solution [2]. After this time more than 99.8% of the complex was in the form of $[(\text{H}_2\text{O})\text{Cl}_4\text{RuORuCl}_4(\text{H}_2\text{O})]^{2-}$. Iron (II) perchlorate solution was prepared by dissolving analytical grade iron wire in an excess of previously deaerated perchloric acid. Iron (II) concentration was determined by titrating with permanganate, and excess of acid by potentiometric titration with alkali in absence of oxygen. The ionic strength was adjusted by introducing suitable quantities

of 1.0 mol dm⁻³ NaCl solution into the solution to be investigated. HCl and NaCl were an AR grade samples and were used without further purification.

Kinetic measurements were performed under pseudo-first order conditions, with Fe(II) and hydrogen ions concentration in an excess over the ruthenium complex concentration. Electronic absorption spectra, as well as kinetic measurements, were made on Specord UV-Vis spectrophotometer. Reaction was monitored at 470 nm ($\epsilon = 5120$ [2]) and the observed first order rate constant, k_{exp} , was calculated by linear least-squares fitting of $\log(A_t - A_\infty)$ to time t . A_t and A_∞ are the absorbance of the solution at time t and after 8-10 half-lives. Each kinetic run was repeated 3 to 4 times.

RESULTS AND DISCUSSION

Reaction rate measurements in a broad range of reagents concentration and pH revealed first order kinetics with respect to the ruthenium complex and zero order kinetics with respect to hydrogen ion concentration. The reaction order with respect to $[\text{Fe}^{2+}]$ depends on reductor concentration and changes from 1 to 0 with $[\text{Fe}^{2+}]$ increase (Table 1).

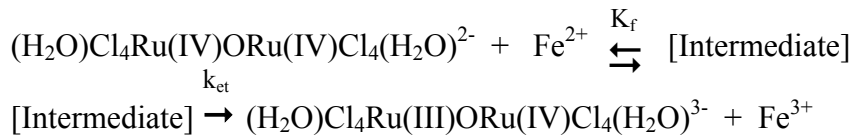
Table 1. Kinetic data for the reduction of $[\text{Ru}_2\text{OCl}_8(\text{H}_2\text{O})_2]^{2-}$ by Fe^{2+}

$10^5[\text{Ru}_2\text{OCl}_8(\text{H}_2\text{O})_2]^{2-}$ (mol dm ⁻³)	$10^3[\text{Fe}^{2+}]$ (mol dm ⁻³)	[HCl] (mol dm ⁻³)	[NaCl] (mol dm ⁻³)	10^2k_{exp} (s ⁻¹)
8.01	0.25	0.10	—	0.563
8.65	0.50	0.10	—	0.691
7.70	1.0	0.10	—	1.23
8.65	2.0	0.10	—	1.57
8.10	3.0	0.10	—	2.07
8.53	6.0	0.10	—	2.27
4.23	6.0	0.10	—	2.31
16.10	6.0	0.10	—	2.23
31.40	6.0	0.10	—	2.26
8.18	1.0	0.10	0.10	1.75
8.07	1.0	0.10	0.20	2.03
8.18	1.0	0.10	0.40	2.83
9.31	1.0	0.10	0.80	2.96
9.81	1.0	0.20	0.70	2.89
11.10	1.0	0.40	0.50	2.95
10.90	1.0	0.90	—	2.41

$k_{\text{et}} = 2.20 \times 10^{-2} \text{ s}^{-1}$, $K_f = 1.26 \times 10^3 \text{ mol}^{-1} \text{ dm}^3$
temp. = 25°C (correlation coefficient $r = 0.9674$)

At a sufficient excess of the reductor concentration over the ruthenium complex, the reaction display saturation kinetics [4] and a limiting rate is observed. The observed saturation in the reaction rate at higher reductor concentration can be interpreted by the mechanism involving ion pair formation between the highly and oppositely charged reactants, or inner-sphere complex, where two metal ions are bridged by the chloride ion.

The kinetic data together with previous findings for the reduction reaction of μ -oxo-bis[aquatetrachlororuthenate (IV)] ion by ascorbic acid [6] allow to propose the following reaction mechanism (all iron ions are hydrated species) :



where [Intermediate] = $[(\text{H}_2\text{O})\text{Cl}_4\text{RuORuCl}_4(\text{H}_2\text{O})^{2-} \parallel \text{Fe}^{2+}]$
or $[(\text{H}_2\text{O})\text{Cl}_4\text{RuORuCl}_4(\text{H}_2\text{O})\text{Fe}]$

The rate law of the investigated process is given by the kinetic equation :

$$-\frac{d[\text{Ru}_2\text{OCl}_8(\text{H}_2\text{O})_2^{2-}]}{dt} = \frac{k_{et} K_f [\text{Ru}_2\text{OCl}_8(\text{H}_2\text{O})_2^{2-}][\text{Fe}^{2+}]}{1 + K_f [\text{Fe}^{2+}]} \quad (1)$$

where: k_{et} - rate constant of electron transfer
 K_f - formation constant of intermediate complex

At the pseudo-first order conditions:

$$k_{exp} = \frac{k_{et} K_f [\text{Fe}^{2+}]}{1 + K_f [\text{Fe}^{2+}]} \quad (2)$$

The equation (2) in its inverse form:

$$\frac{1}{k_{exp}} = \frac{1}{k_{et}} + \frac{1}{k_{et} K_f [\text{Fe}^{2+}]} \quad (3)$$

provides useful way of determining of k_{et} and K_f from the intercept and slope of the linear plot of $1/k_{\text{exp}}$ against $1/[\text{Fe}^{2+}]$ (Fig. 1).

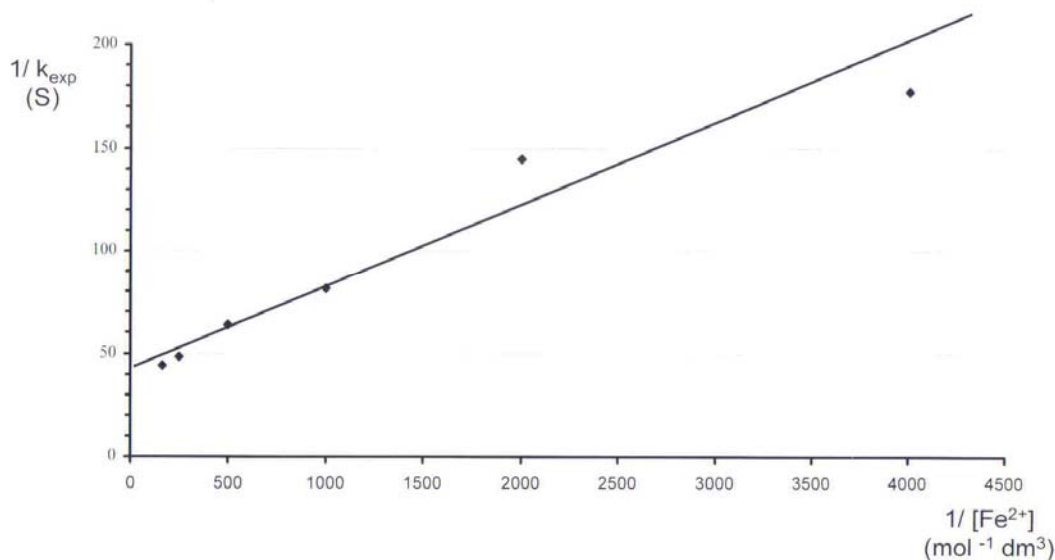


Fig. 1. Plot of $1/k_{\text{exp}}$ versus $1/[\text{Fe}^{2+}]$ for the reduction reaction of $[\text{Ru}_2\text{OCl}_8(\text{H}_2\text{O})_2]^{2-}$ by Fe^{2+} (test of eq. (3)). Reaction conditions as in Table 1.

Kinetic data for the reduction of $[\text{Ru}_2\text{OCl}_8(\text{H}_2\text{O})_2]^{2-}$ with Fe^{2+} in water-HCl solutions are presented in Table 1.

The positive salt effect is not in agreement with that expected for the reaction between oppositely charged ions. Increase of the rate constant with NaCl concentration increase suggests that electron transfer process proceeds through formation of an chloride bridged intermediate rather than by ion pair formation. Inner sphere electron transfer mechanism has been suggested also for the reduction process of this complex with ascorbic acid [6].

References:

1. N.K. Pshenicyn, N.A. Jezerskaya, Zhur. Neorg. Khim., 5 (1960) 1068
2. N.G. Maksimov, O.K. Shpigunova, T.T. Babanakova, N.M. Sinicyn, E.D. Korniec, V.E. Volkov, I.D. Danilov, Zhur. Neorg. Khim., 34 (1989) 419
3. J.A. Baumann, T.J. Meyer, Inorg. Chem., 19 (1980) 345
4. B. Banaś, Polish J. Chem., 74 (2000) 1911
5. B. Banaś, M. Nahorska, J. Mroziński, Bull. Pol. Acad. Sci., Chem., 49 (2001) 203
6. B. Banaś, D. Wawrzak, Annals Polish Chem. Soc., 2 (2003) 490
7. A. Haim, Accounts of Chemical Research, 8 (1975) 264
8. A.J. Miralles, R.E. Armstrong, A. Haim, J. Am. Chem. Soc., 99 (1977) 1416
9. B. Jezowska-Trzebiatowska, R. Grobelny, W. Wojciechowski, Bull. Pol. Acad. Sci., Chem., 12 (1964) 827

THE USE OF SURFACTANTS FOR THE SPECTROPHOTOMETRIC DETERMINATION OF ZINC BASING ON COMPLEXES WITH AZO DYES.

Wanda Winkler, Katarzyna Pytlakowska, Agata Arenhövel-Pacufa
*Department of Analytical Chemistry, Institute of Chemistry, University of Silesia,
Szkolna 9, 40-006 Katowice, Poland*

ABSTRACT. A simple and direct spectrophotometric methods for determination of zinc are based on reaction with azo dyes: 1-(2-pyridylazo)-2-naphtol (PAN) and Chromothrop 2B in the presence benzyldimethyldodecylammonium bromide (BDDABr) have been developed. Optimum concentrations of PAN, Chromothrop 2B, BDDABr and pH ensuring maximum absorbance were defined. The effect of foreign ions was elucidated. The complex Zn-PAN-BDDABr shows maximum absorbance at 597nm with the molar absorptivity value $8.55 \cdot 10^4 \text{ L mol}^{-1} \text{ cm}^{-1}$, and complex Zn-Chromothrop 2B-BDDABr has maximum absorbance at 595nm with the molar absorptivity value $4.26 \cdot 10^4 \text{ L mol}^{-1} \text{ cm}^{-1}$. The Beer's law is obeyed for zinc concentrations in the range $0.24\text{-}0.80 \mu\text{g mL}^{-1}$ for the complex Zn-Chromothrop 2B-BDDABr and $0.36\text{-}0.80 \mu\text{g mL}^{-1}$ for the complex Zn-PAN-BDDABr. The method basing on the complex Zn-PAN-BDDABr has been applied for the determination of zinc in milk, milk substituting preparations, insulin and blood serum.

INTRODUCTION. The very sensitive and selectivity methods for the spectrophotometric determination of many metals and also zinc are based on the reaction with azo-dyes [1-3]. The most popular of these chromogenic reagents are 1-(2-pyridylazo)-2-naphtol (PAN) and Chromothrop 2B. PAN belongs to group of pyridylazo dyes and Chromothrop 2B is example of o-hydroxyarylaazo compounds. Metal-PAN complex does not dissolve in aqueous solution, so it is necessary to do a solvent extraction. This complex had been extracted with non-polar solvents such as chloroform or benzene, which was found to be carcinogenic. Application of surface active substances, which play the role of a protective colloids gives possibility to increase solubility of a Zn-PAN and Zn-Chromothrop 2B complexes and creates better conditions for determination [4-7]. The harmful organic solvents used in the extraction-spectrophotometric methods have been eliminated. An advantage of these methods is a direct spectrophotometric measurement of absorbance of analysed solution.. Application of three component systems, and also more often use of four-component systems, causes the spectrophotometric methods to exhibit high sensitivity-molar absorptivity usually larger than $1 \cdot 10^5 \text{ L mol}^{-1} \text{ cm}^{-1}$ and can compete with other extraction-spectrophotometric and spectrophotometric methods [8-13].

EXPERIMENTAL. Reagents. All the reagents were of analytical grade and were used without further purification. Double-distilled water was used in all experiments.

Zinc stock solution (1 mg mL^{-1}) was prepared by dissolving 0.43987 g of $\text{ZnSO}_4 \cdot 7\text{H}_2\text{O}$ (PPH"POCh" S.A.) in water with addition of 0.5 mL of concentrated H_2SO_4 and dilution up to 100 mL. Working solutions of $10 \mu\text{g mL}^{-1}$ and $20 \mu\text{g mL}^{-1}$ were obtained by diluting the stock solution. 1-(2-pyridylazo)-2-naphtol (PAN) solution in methanol

($1 \cdot 10^{-3} \text{ mol L}^{-1}$) was obtained by dissolving 0.0250 g of PAN (PPH"POCh" S.A.) in methanol and dilution up to 100 mL.

Chromothrop 2B solution ($1 \cdot 10^{-3} \text{ mol L}^{-1}$) was obtained by dissolving 0.12835 g of Chromothrop 2B (PPH"POCh" S.A.) in water and dilution up to 250 mL. Triton X-100 ($1 \cdot 10^{-2} \text{ mol L}^{-1}$) was obtained by dissolving 3.2343 g of Triton X-100 (BDH) in water and dilution up to 500 mL. Benzyldimethyldodecylammonium bromide (BDDABr) solution ($1 \cdot 10^{-1} \text{ mol L}^{-1}$) was obtained by dissolving 3.8445 g of BDDABr (Fluka) in water and dilution up to 100 mL. Borate buffer pH=8, pH=7.6 [14]. Control of blood serum Cormay HP and samples of human blood serum (Medical Laboratory). Insulin Actrapid, Mixtard (Polfa, Tarchomin, Poland) Milk Nan 1 (Nestle) and milk substituting preparations Isomil (Abbot Laboratories B.V.), Nutrison (Ovita Nutricia).

Apparatus. An Jasco (Japan) model V-530 spectrophotometer UV-VIS was used for all absorbance measurements with a 10 mm glass cell. An Elwro (Poland) model N-517 pHmeter was used for pH measurements. The spectrometer ICP-OES made by Spectro Analytical Instruments (Germany) was used with the following parameters: 27.12 MHz, power 1.1 kW, nebulizer-concentric Meinhard. Mineralization was conducted in a Uni-Clever BM-1z microwave mineralizer, Plasmotronika (Poland).

Procedure. Zn-PAN-BDDABr: To the flask of 25 mL capacity were introduced 2 mL of the BDDABr solution, 1.3 mL PAN solution, 3.5 mL borate buffer (pH=7.6) and 5-20 μg zinc. The flasks were filled up with water to the same volume. After 30 min, absorbance was measured at 597 nm in 10 mm cuvettes, against the blank and the calibration graph was plotted.

Zn-Chromothrop 2B-BDDABr: To the flask of 25 mL capacity were introduced 2.5 mL of the Chromothrop 2B solution, 4 mL borate buffer (pH=8), 2-20 μg zinc and 1 mL BDDABr solution. The flasks were filled up with water to the same volume. After 15 min, absorbance was measured at 595 nm in 10 mm cuvettes, against the blank and the calibration graph was plotted.

RESULTS AND DISCUSSIN. Absorption spectrum and effect of surfactants. Zinc reacts with PAN forming of an orange coloured water-insoluble neutral chelate. The application cationic surface active agent – benzyldimethyldodecylammonium bromide or nonionic surfactant – Triton X-100 gives possibility to increase to solubility of the Zn-PAN complex and improves conditions for its determination.

Figure 1 presents the absorption spectra for the zinc chelate with PAN in the presence of BDDABr and Triton X-100. The complexes Zn-PAN-BDDABr and Zn-PAN-BDDABr Tritoin X-100 show the absorption maximum at the same wavelength $\lambda_{\text{max}}=597 \text{ nm}$ (curve 1,2), and the ternary Zn-PAN-Triton X-100 system at 555 nm (curve 3) A large bathochromic effect of maximum absorption of studied system (curve 1) comparing with the complex Zn-PAN-Triton X-100 (curve 3, $\Delta\lambda=42 \text{ nm}$) was observed. In the presence BDDABr there is a significant hyperchromic effect. Introduction of Triton X-100 to Zn-PAN-BDDABr system distinctly lowers of absorbance. In consideration of more intensity of absorption of complex wavelength $\lambda=597 \text{ nm}$ was choosen. Figure 2 presents the absorption spectra for the zinc complex with Chromothrop 2B in the presence of surfactants.

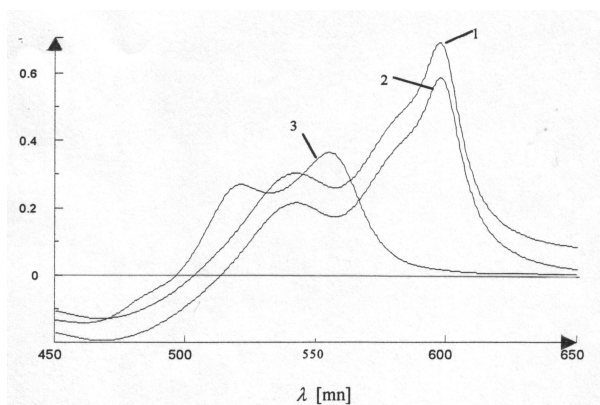


Fig.1 Absorption spectra, pH=7.6, l=1cm

1. Zn-PAN-BDDABr complex measured against blank $\lambda=597\text{nm}$
2. Zn-PAN-BDDABr-Triton X-100 complex measured against blank $\lambda=597\text{nm}$
3. Zn-PAN-Triton X-100 complex measured against blank $\lambda=555\text{nm}$

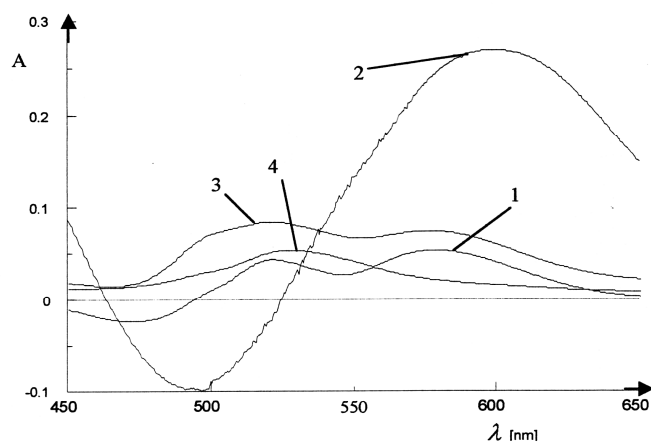


Fig.2 Absorption spectra, pH=8, l=1cm

1. Zn-Chromothrop 2B complex measured against blank $\lambda=515\text{nm}$, $\lambda=580\text{nm}$
2. Zn-Chromothrop 2B-BDDABr complex measured against blank $\lambda=595\text{nm}$
3. Zn-Chromothrop 2B-Triton X-100 complex measured against blank $\lambda=519\text{nm}$, $\lambda=585\text{nm}$
4. Zn-Chromothrop 2B-BDDABr-Triton X-100 complex measured against blank $\lambda=528\text{nm}$

Media and the reaction time. The complexation occurs in a weak alkaline medium with the optimum at pH=7.6 for the Zn-PAN-BDDABr complex and with the optimum at pH=8 for the Zn-Chromothrop 2B-BDDABr complex. In both cases in further experiments the borate buffer of these value pH was used. Absorbance of the complexes is constant after 30 min (Zn-PAN-BDDABr) and 15 min (Zn-Chromothrop 2B-BDDABr) at room temperature and remains constant for 1.5 h. Optimum concentrations of PAN, Chromothrop 2B, BDDABr and order of reagents addition were defined. The conditions required for the studied systems are given in Table 1.

Table1. The conditions of determination of the studied complexes.

System	λ [nm]	pH	Time [min]	Order of reagent addition	Molar excess		
					PAN	Chr.2B	BDDABr
Zn-PAN-BDDABr	597	7.6	30	BDDABr-PAN- buffer-Zn	8	-	130
Zn-Chr2B-BDDABr	595	8.0	15	Chr.2B-buffer-Zn- BDDABr	-	7	31

Composition of the complexes. The continuous variation method was used to establish the stoichiometry of the investigated complexes. This method requires the measurement of the absorbance or other physical quantity in the series of solutions containing different amounts of two reacting components, yet the total sum of their moles is kept constant. It was found that in the presence BDDABr, PAN and Chromothrop 2B bound to Zn in the molar ratio 2:1.

Characteristic of the methods. Under the optimum conditions the calibration plot for zinc determination was obtained. The Beer's law was obeyed over the Zn concentration range 0.36-0.80 $\mu\text{g mL}^{-1}$ for the system with PAN in the presence BDDABr and 0.24-0.80 $\mu\text{g mL}^{-1}$ for the system with Chromothrop 2B with BDDABr. Molar absorptivity for the complex Zn-PAN-BDDABr at 597 nm is $8.55 \cdot 10^4 \text{ L mol}^{-1} \text{ cm}^{-1}$ and the correlation coefficient $r=0.9998$. For the complex Zn-Chromothrop 2B-BDDABr molar absorptivity at 595 nm is $4.26 \cdot 10^4 \text{ L mol}^{-1} \text{ cm}^{-1}$ and the correlation coefficient $r=0.9967$.

Interference from coexisting ions. The studies of the effect of foreign ions on the determination of zinc with PAN in the presence BDDABr show that the selectivity of the method is rather poor. The cations Na^+ , NH_4^+ , K^+ , Mg^{2+} , Ca^{2+} and anions Cl^- , Br^- , NO_3^- , SO_4^{2-} , PO_4^{3-} , CH_3COO^- (examined in the 1000-fold molar excess over zinc) do not affect the determination. All cations forming complexes with PAN have an interfering effect. It was found that ions F^- , I^- may be present in 50-fold molar excess over Zn and Mn^{2+} , Co^{2+} in 10-fold molar excess over Zn and Fe^{3+} 7-fold molar excess over Zn. Cation Pb^{2+} presents at the twenty times lower concentration than the Zn concentration and Mo^{2+} , Ni^{2+} , Cd^{2+} , Cu^{2+} present at the ten times lower concentration than the Zn negatively influenced the determination results. Ions CN^- and EDTA forming permanent complexes with zinc, interfered. Cation Al^{3+} also affects determination because hydrolyzes.

Analytical application. The most sensitive of the elaborated methods (Zn-PAN-BDDABr) was applied to the determination of zinc ions in blood serum samples, insulin samples as well as milk samples and milk substituting preparations.

Before the determination was carried out, the samples of milk were mineralized in the microwave mineralized with concentrated HNO_3 .

Blood serum samples were subjected to the deproteinization process. A 1+1 mixture of 20% solutions of sulfuric and nitric acids was used [11]. It was also found that copper present in the serum was eliminated efficiently by complexation with tartrates.

Determination of zinc.

Milk samples and milk substituting preparations. In order to prepare the samples for analysis, 1 g of milk sample (NAN) and milk substituting preparations (ISOMIL, NUTRISON) were transferred to microwave mineralizer and mineralized using 6 mL of concentrated nitric acid. When mineralization was completed, the samples were quantitatively transferred to the flasks and volumes were made up to 25 mL with redistilled water. Then, to 5 mL aliquot of each sample the appropriate amount of the saturated NaOH solution was added to obtain pH of about 7.6. Next to 25 mL flasks the following reagents were added: 2 mL of BDDABr, 1.3 mL of PAN, 3.5 mL of borate buffer (pH=7.6) and prepared after mineralization of the milk solution. This was filled to 25 mL with redistilled water. Absorbance was measured after 30 min at 597 nm, relative to a blank test as standard solution. The zinc concentration was read from the standard curve obtained in the presence of all reagents used for the milk analysis.

Blood serum. In order to prepare the sample for analysis 1 mL of serum (standard serum HP and human blood serum) was poured into a test tube and centrifuged; then 1 mL of redistilled water and 0.5 mL of deproteinizing mixture (1+1 20 % HNO_3 +20 %

H₂SO₄ [11]) were added. After mixing, the sample was heated in boiling water for 3-5 min, cooled down and centrifuged at 3000 turns min⁻¹. The sediment was filtered off and washed twice in 2 mL of redistilled water. Next to the solution an amount of saturated NaOH was added to final pH of 7.6. To a 25 mL flask was added: 2 mL of BDDABr, 1.3 mL of PAN, 3.5 mL of borate buffer (pH=7.6), prepared after deproteinization of the serum solution and 0.5 mL of sodium tartrate in order to mask copper present in the sample. This was filled to 25 mL with redistilled water. After 30 min equilibration time the absorbance of solutions was measured at 597 nm against the blank.

Insulin. Samples of 1.5 mL of insulin were transferred to a 10 mL standard flasks and dilute the samples with redistilled water to the mark. If MIXTARD insulin samples are analysed, before diluting the samples acidify them with hydrochloric acid (1·10⁻¹ mol L⁻¹) to obtain clear solution. In order to prepare the samples of MIXTARD insulin for analysis to the 5 mL of insulin solution an amount of saturated NaOH was added to pH 7.6. Zinc in ACTRAPID insulin was determination directly from sample. Than to each 25 mL flasks was added: 2 mL of BDDABr, 1.3 mL of PAN, 3.5 mL of borate buffer (pH=7.6) and 5 mL of insulin solution. This was filled to 25 mL with redistilled water. Absorbance was measured after 30 min at 597 nm against a blank solution.

The all results of Zn determination in the studied samples and statistical evaluation of the results are given in Table 2. In order to compare the results obtained with the use of the elaborated method the comparative ICP-OES method was also applied.

Table 2. Results of the determination of the content of zinc in milk samples, blood serum and insulin preparations by the developed method and the reference method ICP-OES.

Sample	Method	Average result of determination [µg mL ⁻¹]	Standard deviation SD n=3	µ ₉₅ =x±t×SD [µg mL ⁻¹]
ISOMIL	BDDABr-PAN-Zn	1.871	0.02	1.871±0.08
	ICP-OES	1.884	0.02	1.884±0.03
NUTRISON	BDDABr-PAN-Zn	1.342	0.04	1.342±0.05
	ICP-OES	1.363	0.01	1.363±0.01
NAN	BDDABr-PAN-Zn	1.099	0.02	1.099±0.03
	ICP-AES	1.130	0.04	1.130±0.05
SERUM CORMAY HP	BDDABr-PAN-Zn	0.159	0.02	0.159±0.05
	ICP-OES	0.169	0.01	0.169±0.04
BLOOD SERUM 1	BDDABr-PAN-Zn	0.185	0.04	0.185±0.10
	ICP-OES	0.188	0.03	0.188±0.08
BLOOD SERUM 2	BDDABr-PAN-Zn	0.167	0.04	0.167±0.09
	ICP-OES	0.178	0.01	0.178±0.04
INSULIN ACTRAPID	BDDABr-PAN-Zn	2.760	0.05	2.760±0.13
	ICP-OES	2.766	0.06	2.766±0.15
INSULIN MIXTARD	BDDABr-PAN-Zn	3.645	0.03	3.645±0.09
	ICP-OES	3.676	0.05	3.676±0.13

CONCLUSION. The developed spectrophotometric methods for determination of zinc by means of PAN and Chromothrop 2B in the presence of benzyldimethyldodecylammonium bromide consist in the direct measurement of absorbance of the analysed solution. Therefore determined methods are simple, faster and safer compared to the know extraction-spectrophotometric methods. The harmful

organic solvents used in the extraction-spectrophotometric methods have been eliminated.

The application of surfactant, which acts as protective colloid, gives the possibility to increase the solubility of the Zn-PAN and Zn-Chromothrop 2B complexes in the analysed solutions and improves conditions for determination. The proposed method of determination of Zn in the form of its complex with PAN and BDDABr is precise and sensitive. The molar absorptivity of the complex is $8.55 \cdot 10^4 \text{ L mol}^{-1} \text{ cm}^{-1}$ and the Beer's law is obeyed for zinc concentrations in the range $0.36 - 0.80 \mu\text{g mL}^{-1}$. The studies carried out prove that method based on the complex Zn-PAN-BDDABr can be used for the determination of zinc in blood serum, insulin and various milk samples.

REFERENCES

- [1] G.Ackerman, J.Kothel, *Talanta* 26 (1979) 693.
- [2] A.Cygański, *Spectroscopic Methods in Analytical Chemistry*, WNT, Warsaw, 1993.
- [3] Z.Marczenko, M.Balcerzak, *Spectrophotometric Methods in Inorganic Analysis*, PWN, Warsaw, 1998.
- [4] C.S.Feldkamp, R.Watkins, E.S.Baginski, B.Zak, *Microchem. J.*, 22 (1977) 347.
- [5] J.Kobyłecka, E.Skiba, *Chem. Anal.(Warsaw)* 38 (1993) 599.
- [6] A.Cygański, J.Krystek, *Chem. Anal.(Warsaw)* 37 (1992) 377.
- [7] W.B.Oi, *Talanta* 32 (1985) 1013.
- [8] Y.P.Huang, K.M.Yan, H.S.Zhang, *Fenxi-Shiyanshi* 19 (2000) 43.
- [9] N.K.Agnihotri, S.Ratnani, V.K.Singh, H.B.Singh, *Anal. Sci.*, 20 (2004) 955.
- [10] I.Mori, *Talanta*, 41 (1996) 25.
- [11] A.Cygański, J.Krystek, *Chem. Anal.(Warsaw)*, 36 (1991) 769.
- [12] W.Winkler, A.Arenhövel-Pacufa, *Talanta* 53 (2000) 277.
- [13] W.Winkler, F.Buhl, A.Arenhövel-Pacufa, U.Hachuła, *Bioanal. and Anal. Chem.*, 376 (2003) 934.
- [14] J.Ciba, *Chemist Analyst Hand-book*, WNT, Warsaw, 1989.

SILVER(I) COMPLEXES WITH 2-MERCAPTO-1-METHYLIMIDAZOLE (THIAMAZOLE)

Marek Z. Wiśniewski

Institute of Chemistry, Świętokrzyska Academy, 25-020 Kielce, Chęcińska 5, Poland

The silver(I) complex with 2-mercapto-1-methylimidazole (thiamazole, TMZ) of the formula $\text{Ag}(\text{TMZ})_2\text{NO}_3$ has been obtained. The new compound has been identified by elemental analysis, derivatography, IR spectroscopy, X-ray diffraction and conductivity measurements. The stability constants of TMZ with Ag(I) have been determined by the potentiometric method. The gravimetric method of determining 2-mercapto-1-methylimidazole has also been worked out.

1,3- diazole derivatives have found widespread use in therapy [1-3]. Also many compounds with imidazole ring have found on form stable coordination compounds with transition metal ions, their formation being frequently accompanied by interesting structural phenomena [4-9]. Thus it seemed worthwhile to develop a gravimetric method for the determination of thiamazole, a known drug used for treatment of thyroid malfunctions, by utilizing its complexation capability of the silver(I) ion.

EXPERIMENTAL

Reagents. 2-mercapto-1-methylimidazole was purchased from Aldrich-Europe (Belgium). After crystallization from double distilled water the compound melted at 114°C. Silver(I) nitrate (POCH, Gliwice, Poland) was determined both titrimetrically and gravimetrically [10,11].

Physical measurements. Elemental composition of the complex was determined on a Model 240 CHN Perkin Elmer analyzer. X-ray powder patterns were taken on a DRON-4 (Russia) instrument equipped with a scintillation counter within the 4-90° range of the angles on the 2θ scale. Monochromatic Cu-K_α radiation was used and a nickel filter.

Thermogravimetric measurements were run over the temperature range 20-1000°C in the air atmosphere, under normal pressure, on a MOM (Hungary) derivatograph. The IR spectra over the range 4000-250cm⁻¹ were recorded on a Model 4240 Beckman spectrophotometer in KBr pellets. The far-IR spectra (500-100cm⁻¹) were taken on DIGILAB FTS-14 spectrophotometer. A suspension of the compound in acetone was applied onto the polyethylene window of the instrument. The melting points were measured on a Boetius apparatus.

Potentiometric measurements were carried out using a PHM-64 pH meter (Radiometer, Denmark). Ag-101 silver electrodes (Energopomiar- Gliwice) were used. Potentiometric measurements were taken in a water thermostat maintaining the temperature of 298K [3].

Synthesis. A sample of TMZ (0.05-0.1G) was dissolved in 50-100cm³ of water. The solution was then cooled to 5°C and, under stirring, the calculated volume of a 0.1 M AgNO₃ solution was added with a 2-5 cm³ excess of the reagent. A white precipitate which fell out was filtered off on a fritted glass filter G-4, washed first with a small volume of cold (5°C) 0.01 M HNO₃ and then with double distilled water, and dried at 105°C to constant weight.

RESULTS AND DISCUSSION

To check the composition of the compound, its carbon, nitrogen, hydrogen and metal contents were determined. The results were as follows: calc.: C 24.1, H 3.0, N 17.6, Ag 27.1%. Found: C 24.4, H 3.0, N 17.6, Ag 27.3%, M.p. 193°C, λ_M 96.1 cm² dm⁻¹ mol⁻¹.

Both the indexation and determination of unit cell dimensions of the complex were accomplished by using a DICVOL program [12]. The results of the measurements were pooled by using an XDATA program and further processed by a XRAYAN program [13]. The X-ray powder patterns revealed that the Ag(TMZ)₂NO₃ complex is orthorhombic with the following unit cell patterns: a(Å) 3.643 ± 0.025, b(Å) 13.326 ± 0.041, c(Å) 3.715 ± 0.014; V (Å³) 675.27.

The DTA trace of the complex shows that it is stable up to 180°C, where a small endothermic peak is observed probably associated with rotation of the nitrate ion. On the other hand, a large endothermic peak at 193°C is due to the melting and simultaneous degradation of the complex. At 300°C probably the decomposition of Ag₂O (71% loss in weight) takes place. At higher temperatures a series of endothermic effects is noted at 330, 375, 415 and 460°C, as well as a very strong exothermic peak at 595°C due to complete decomposition of the complex.

X-ray powder patterns reveal that over the temperature range 595-855°C Ag₂SO₄ occurs together with silver metal, whereas above 855°C (76% loss in weight) silver is the sole degradation product.

In the IR spectra of both TMZ and its Ag(I) complex, remarkable are broad absorption bands (2500-3200cm⁻¹) due to stretching vibrations of the -NH group. On the other hand, a band at 2470cm⁻¹ assignable to the -SH group is weak in the spectrum of TMZ and is missing in the spectrum of the complex. This suggests the preponderance of the thiocarbonyl form over the thiol one of TMZ, as demonstrated also by a fairly strong 1020 cm⁻¹ band ascribable to the vibrations of the =C=S group [14,15]. It can also be concluded that the complexation causes only a slight displacement (by 10-20cm⁻¹) of the absorption bands relative to those of the free TMZ. The spectrum of the complex exhibits also a 1430cm⁻¹ band assigned to the NO₃⁻ ion. The band at 265cm⁻¹ can be assigned to the vibrations of the Ag-S dative bond [16,17].

To determine the stability constants of Ag(I) complexes with TMZ, the SEM cells were measured: (-) Ag/solution A+(B)/ 0.5m³dm⁻³ KNO₃/solution A/Ag⁺.

Solution A of the composition: a mol³dm⁻³ AgNO₃, (0,5-a) mol³dm⁻³ KNO₃ was titrated with solution B containing X mol³dm⁻³ the ligand, a mol³dm⁻³ AgNO₃ and (0,5-a) mol³dm⁻³ KNO₃. To calculate the ratio of $C_{Ag^+}/[Ag^+]$, the dependence: $\Delta E = 59.16 \log C_{Ag^+}/[Ag^+]$ was used. The stability constants $\log_{\beta 1}=7.69$, $\log_{\beta 2}=9.39$, $\log_{\beta 3}=12.48$ were calculated by the Leden method, just like in the previous paper [18]. The interaction of soft acid (Ag⁺) and soft base (S), according to the HSAB theory [19], can account for considerable stability of the present complexes.

A test of gravimetric determination of thiamazole as the complex with Ag(I). Six TMZ determinations were carried out according to the description given when the synthesis of the complex was discussed.

Results of the statistical treatment are as follows: $\bar{x}=0.0988$; $R=0.0011$; $a_r=0.40$; $\bar{x}+R \cdot a_r=0.0988 \pm 0.0004$, where \bar{x} is the arithmetic mean of the results; R is the range ($R= x_n-x_1$); a_r is the confidence coefficient of the range for the probability level 0.95 (for the number of experiments $n=6$) [20]. The results show a high precision of the determinations.

CONCLUSION

The paper provides information on the stability of complexes obtained in aqueous solution and on the composition of the complex, its properties and the way of fixing the cation by means of the organic ligand in stable state. A simple way of determining the content of TMZ in medicinal preparations is presented in the paper.

REFERENCES

- [1]. A. Zejc, M. Gorczyca, *Chemia Leków*, PZWL, Warszawa, 1999
- [2]. E. Pawelczyk, *Chemia Leków*, PZWL, Warszawa, 1986
- [3]. B. Lenarcik, M. Wiśniewski, *Polish J. Chem.*, **57** (1983) 735
- [4]. M. Wiśniewski, W. Surga, B. Lenarcik, *Trans. Met. Chem.*, **15** (1990) 63
- [5]. K. Kurdziel, T. Głowiak, *Polish J. Chem.*, **72** (1998) 2182
- [6]. K. Kurdziel, T. Głowiak, *Polyhedron*, **19** (2001) 2183
- [7]. T. Głowiak, K. Kurdziel, *J. Mol. Struct.*, **516** (2000)
- [8]. M.Z. Wiśniewski, J. Wietrzyk, A. Opolski, *Archiv. Immuno. Ther. Exp.* **48** (2000) 51
- [9]. M. Z. Wiśniewski, T. Głowiak, A. Opolski, J. Wietrzyk, *Metal Based Drugs*, **8** (2001) 189
- [10]. E. Merck, *Complexometric Assay Methods with Titriplex*, Darmstadt (1980)
- [11]. M. Struszyński, *Analiza ilościowa i techniczna*, PWT, Warszawa 1954
- [12]. D. Lauer, *Laboratoire de Cristalochimie Université de Rennes, France*, MS DOS/PS DOS version adapted to PC by Z. Gałdecki, Institute of General Chemistry, Technical University, Łódź, Poland, 1992
- [13]. H. Marciniak, R. Diduszko, *X-Ray Phase Analysis, Version 2,81*, Copyright © HM and RD (1992). This Copy is licenced to: Institute of Chemistry Pedagogical School, Kielce, Poland
- [14]. M. Wiśniewski, W. Surga, *Polish J. Chem.* **67** (1993) 2143
- [15]. S. Zaidi, D. Varshney, K. Siddigi, Z. Siddigi, V. Islam, *Acta. Chim. Acad. Sci. Hung.*, **95**: (1977) 383
- [16]. M. Gabryszewski, *Polish J. Chem.*, **70** (1996) 1220
- [17]. M. Gabryszewski, *Spectr. Lett.*, **33** (2000) 23
- [18]. B. Lenarcik, M. Wiśniewski, *Roczniki Chem.*, **51** (1977) 1625
- [19]. R. Pearson, *J. Am. Chem. Soc.*, **85** (1963) 3533
- [20]. A. Rokosz, *Wiadomości Chem.*, **12** (1956) 635

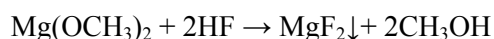
SOL-GEL SYNTHESIS OF MgF₂ GELS AND THEIR CHARACTERIZATION

Maria Wojciechowska, Anita Wajnert, Nadia Krawczyńska,
Michał Zieliński
*Adam Mickiewicz University, Faculty of Chemistry,
Grunwaldzka 6, 60-780 Poznań*

The sol-gel synthesis is a modern technique applied to produce a different materials of specific structural properties, i.e. high surface area, narrow pore size distribution and well-developed mesoporous structure. The high-surface area materials obtained hitherto by the sol-gel synthesis include: silica dioxide [1], mesoporous titanium oxide [2], monolithic barium titanate gel [3] and metal fluorides with aluminium fluoride, zinc fluoride and magnesium fluoride among them [4,5].

Recently, increasing interest is observed in the application of MgF₂ in catalysis as a support of the active phase [6]. The commercial magnesium fluoride made by Aldrich has the surface area of only 0.4 m²/g. However the surface area of MgF₂ obtained in the reaction of magnesium carbonate with a water solution of hydrofluoric acid reaches 45 m²/g [7]. So far MgF₂ gels were synthesized in two steps with process of fluorination with gaseous HF in second stage [8,9]. In view of the above, attempts have been made to develop a single-stage method of MgF₂ preparation that would ensure getting much higher surface area at the same time retaining the properties of a good support.

This paper reports results on obtaining magnesium fluoride in the reaction of magnesium methoxide and hydrofluoric acid in methanol as a solvent, according to the equation below:



The synthesis was performed for different molar ratios of Mg/F. The magnesium methanol solution was introduced dropwise by a peristaltic pump into the solution of hydrofluoric acid in methanol in the nitrogen atmosphere over the time of 2h. The dense xerogels obtained were aged in ambient conditions, dried at 80⁰C and calcined at 400⁰C and 500⁰C. The products obtained were labelled as MgF₂-MeX/4 and MgF₂-MeX/5, where Me stands for the precursor – magnesium methanol, X is the molar ratio of Mg/F, and the numbers 4 and 5 refer to the temperature of calcination (400 and 500⁰C, respectively).

Table 1 gives characterisation of the MgF₂ samples obtained. The effect of the preparation conditions, i.e. the Mg/F molar ratio and calcination temperature, on the size of the surface area was tested by the low-temperature nitrogen adsorption (the surface area was established by the BET method, while the pore size by the BJH method from the desorptive branch of the isotherm). The highest surface area of 218 m²/g was found for the MgF₂-Me2.0 sample obtained for the stoichiometric Mg/F ratio. The surface areas of the samples MgF₂-Me2.4/4, MgF₂-Me2.7/4, MgF₂-Me3.0/4 and MgF₂-Me3.3/4, decreased with increasing Mg/F molar ratio. The lowest surface area from this group of samples was determined for the sample MgF₂-Me3.3/4 (110 m²/g). The samples

calcined at 500°C (MgF₂-Me2.4/5 i MgF₂-Me3.0/5) were characterised by lower surface area than those calcined at 400 oC, which was explained by the sintering of fine pores. The magnesium fluoride sample obtained from magnesium carbonate, labelled as MgF₂-W/4 (calcined at 400°C) had the surface area of 40 m²/g but after calcination at 500°C it decreased to only 23 m²/g. Hence, the surface areas of the samples obtained by the sol-gel method were much higher than that of the sample obtained from magnesium carbonate.

Table 1 . Characterisation of the MgF₂ samples obtained by the sol-gel method.

SYMBOL	MOLAR RATIO Mg/F	CALCINATION TEMPERATURE [°C]	SURFACE AREA [m ² /g]	TOTAL PORE VOLUME (p/p ₀ =0.99) [cm ³ /g]	AVERAGE PORE RADIOUS (BET) [nm]
MgF ₂ -Me2.0/4	1:2.0	400	218	0.330	3.0
MgF ₂ -Me2.4/4	1:2.4	400	198	0.361	3.5
MgF ₂ -Me2.4/5	1:2.4	500	152	0.337	4.5
MgF ₂ -Me2.7/4	1:2.7	400	176	0.389	4.5
MgF ₂ -Me3.0/4	1:3.0	400	124	0.336	5.5
MgF ₂ -Me3.0/5	1:3.0	500	81	0.332	8.0
MgF ₂ -Me3.3/4	1:3.3	400	110	0.266	5.0
MgF ₂ -W/4	1:2.0	400	40	0.180	9.0
MgF ₂ -W/5	1:2.0	500	23	0.182	14.5

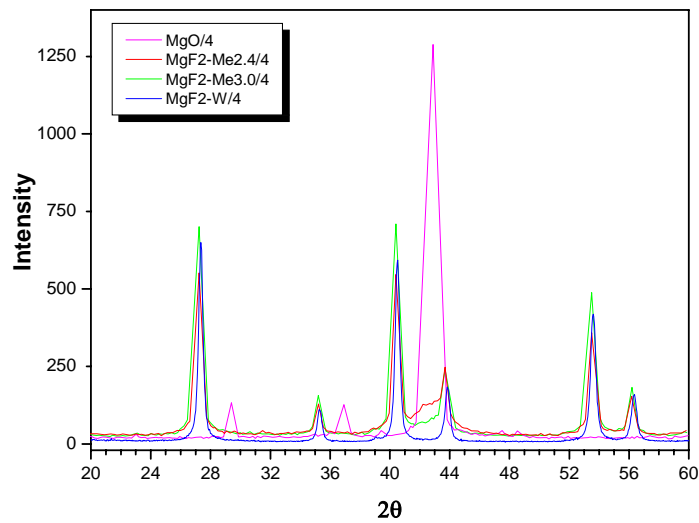


Figure 1. XRD diffraction of magnesium oxide and magnesium fluoride prepared by different methods.

In order to determine the purity of the samples obtained by the sol-gel method, the samples were subjected to the XRD study for 2θ in the range 20-60, (Fig. 1.). In the samples calcined at 400°C trace amounts of MgO were detected. In the sample obtained from magnesium carbonate no MgO was found. Therefore, MgO could be a product of decomposition of magnesium hydroxide from hydrolyzed magnesium methoxide. Magnesium hydroxide could be formed during the synthesis as a result of the reagents contact with steam from the air. The presence of MgO was confirmed by FT-IR results

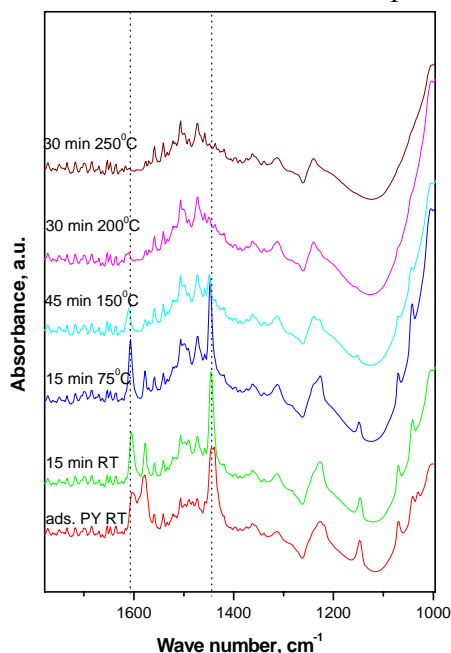


Figure 2. IR spectra of $MgF_2-Me_{3.3/4}$ after adsorption of pyridine.

In order to get the information on the character of the surface of the MgF_2 samples obtained, they were subjected to adsorption of pyridine and after desorption their IR spectra were taken at different temperatures from the range 25-250°C. The results are presented as difference spectra obtained after subtraction of the fundamental spectrum. After pyridine adsorption at room temperature the spectra revealed a characteristic band at 1450 cm^{-1} , indicating the presence of the Lewis type acidic centres. As a result of desorption at 150°C, the intensity of the bands assigned to the adsorbed pyridine considerably decreased indicating the weakness of these centres.

At the next step the possibility of use of the magnesium fluoride samples obtained as support of an active phase was tested. Ruthenium from $RuCl_3 \cdot 3H_2O$ as a precursor was supported on the samples in the amount of 1% wt. The systems Ru/MgF_2 were prepared using the conventional method of impregnation. The catalysts were activated in a mixture of 50% H_2S/He and their activity was tested in the reaction of thiophene hydrodesulfurisation. The catalytic properties of Ru/MgF_2 were compared with those of Ru/Al_2O_3 and $CoMo/Al_2O_3$ - the commercial catalyst of hydrodesulfurisation (Fig. 3).

The activity of the ruthenium phase depended significantly on the type of the support used. The most active proved the sample $Ru/MgF_2-Me_{3.3/4}$, then $Ru/MgF_2W/4$. These catalyst were much more active than the commercially used ones Ru/Al_2O_3 and $CoMo/Al_2O_3$.

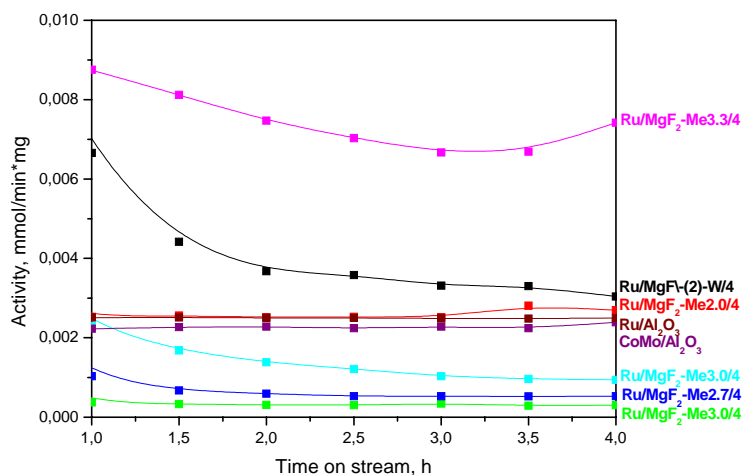


Figure 3. Activity of Ru/MgF₂, Ru/Al₂O₃ and CoMo/Al₂O₃ catalyst in thiophene hydrodesulfurisation for 1mg of metal.

In conclusion, the magnesium fluoride samples obtained by the method of the sol-gel synthesis were characterised by the surface area a few times greater than that of the MgF₂ prepared by the conventional methods. The effect of the mode of MgF₂ preparation, in particular the Mg/F molar fraction, on the porous structure of the final samples was observed. The mode of MgF₂ preparation also influenced the activity of the ruthenium phase supported. The most active in the reaction of thiophene hydrodesulfurisation was the catalyst Ru/MgF₂-Me_{3.3}/4, obtained for Mg/F molar ratio of 1:3.3. It is supposed that the high activity of this catalyst is related to the specific structure of ruthenium sulphide, as established earlier for the ruthenium catalysts supported on MgF₂ obtained from magnesium carbonate [10,11].

1. W. L. Huang, K. M. Liang, S. H. Cui, S. Ren Gu, *J. Colloid Interface Sci.*, **231** (2000)152-157.
2. H. Hirashima, H. Imai, V. Balek, *J. Non-Cryst. Solids*, **285** (2001) 96-100.
3. J.-H. Cho, M. Kuwabara, *J. Eur. Ceram. Soc.*, **24** (2004) 2959-2968.
4. U. Groß, S. Rüdiger, M. Feist, H. A. Prescott, S. Ch. Shekar, S. I. Troyanow, E. Kemnitz, *J. Mater. Chem.*, **15** (2005) 588-597.
5. WO PCT 2004/060806 (*Method for the preparation of high surface area metal fluorides*, inventors: E. Kemnitz, U. Groß, S. Rüdiger).
6. M. Wojciechowska, M. Zieliński, W. Przystajko, M. Pietrowski, *Catal. Today*, **119** (2007) 44-47.
7. M. Wojciechowska, M. Zieliński, M. Pietrowski *J. Fluorine Chem.*, **120** (2003)1-11.
8. J. Krishna, U. Groß, S. Rüdiger, E. Kemnitz, J. M. Winfield, *J. Solid State Chem.*, **179** (2006) 739-746.
9. H. A. Prescott, Z.-J. Li, E. Kemnitz, J. Deutsch, H. Lieske, *J. Mater. Chem.*, **15** (2005) 4616-4628.
10. M. Wojciechowska, M. Pietrowski, S. Łomnicki, *J. Chem. Soc., Chem. Commun.*, **5** (1999) 463.
11. M. Wojciechowska, M. Pietrowski, B. Czajka, S. Łomnicki, *Catal. Lett.*, **87** (2003) 153.

ANALYSIS OF C.I. ACID BLUE 193 STRUCTURE BY MEANS OF QUANTUM-CHEMICAL METHODS

Krzysztof Wojciechowski, Lucjan Szuster^{a)}, Maciej Urbaniak^{b)}

Department of Environmental Engineering, Technical University of Łódź, 90-924 Łódź

^{a)}Institute of Dyes & Organic Product, ul. Chemików 2/4, 95-100 Zgierz

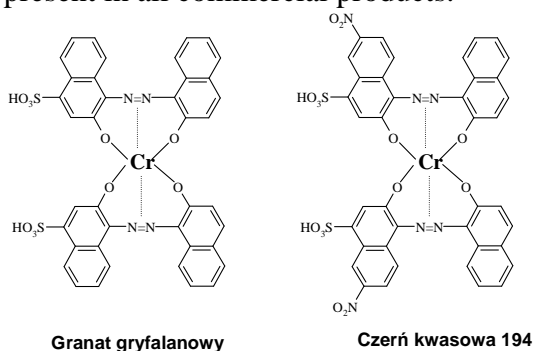
^{b)}Institute of Leather Industry, u. Zgierska 73, 91-462 Łódź

During researches on synthesis of metal-complex dyes it was stated, that processes of azo dyes metallizing often goes with formation of mixture of dyes. This is clearly seen on the basis of such dyes as Acid Blue 193 (C.I. 15705) and Acid Black 194 (C.I. 14645). These dyes are synthesized in many countries, among others in Poland too.

These dyes are of great importance for the sake of their application properties, low cost and shades which are difficult to obtain in acid group of dyes. Despite of their common application and production, from the beginning of the 20th century, their structure are not precisely known.

Acid Blue 193 is a chromium complex 1:2 of monoazo dyes obtained as a product of coupling of 1,2-diazoxynaphthalene-4-sulfonic acid with 2-naphthol.

All above mentioned commercial products show the presence at least three components about different R_F values and different shades. These components are present in all commercial products.



For the research it was used a commercial product – Acid Blue 193 (“Organica-Zachem” in Bydgoszcz). The process of separation of dye isomers was performed on preparative plates DC-Fertigplatten Kieselgel 60. According to Polish Standard BN-90/6041-58 polyamide fabric was dyed. Dyed fabrics were submitted under colorimetric measurements.

Figure 1a points on the differences in the course of curves testifying about differences in shades. The confirmation is a diagram in the CIELab system (fig. 1b)

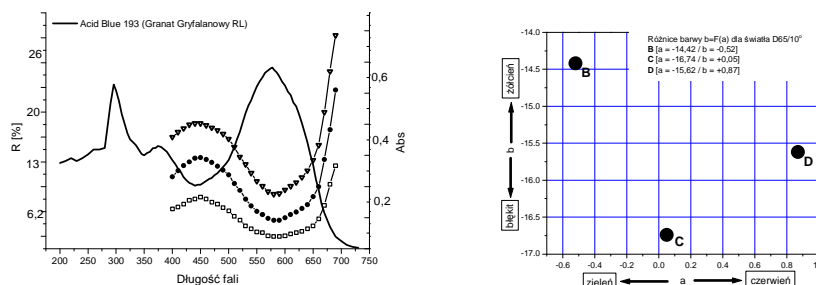


Fig. 1. a) Spectrum of Acid Blue 193 (in water —) and remission spectra of three isomers (on polyamide fabric —∇—, —○—, —□—...) in function of wavelength λ ; b) colour co-ordinates of three isomers of Acid Blue 193 on the a-b plane of CIELab 1976 system

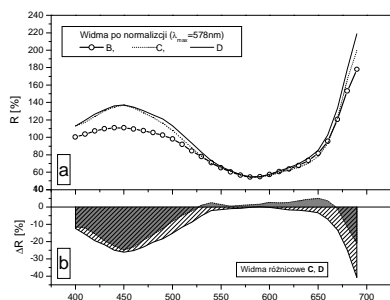


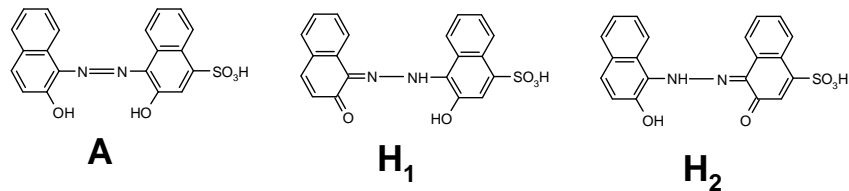
Fig. 2. a) Remission spectra **B**, **C**, **D** forms after the normalization (on polyamide fabric) and b) differential spectrum of **C** and **D** form in relation to form **B** ($\Delta S = \Delta S_B - \Delta S_{i(C,D)}$)

From the colorimetric analysis results that colour of tested components (**B**, **C**, **D**) depend on the composition of isomers mixture. By means of II-derivative analysis of UV-VIS spectra it can be stated, that each of isomers consist of, at least, 4 components which absorption maxima should be in ranges: 460, 530, 578 and 624nm (maxima at 530 and 624nm are shown as inflexion points on absorption curves). The presence of groups about anionic character ($-\text{SO}_3^-$) and anionic character of complex (which results from the charge of the central chromium atom) could make aggregates of tested dyes difficult for creation [2]. Experimental data confirm the creation of the mixture of metal-complex dyes, but as to their structure exist a few hypothesis applying the kind of isomerism of created structures. It is a possibility, for 1:2 complex, a creation of 11 spatial structures (nine complexes of Pfeffla-Shelly and two of Drew-Pfitznera) [1,3-6] (fig. 2). Zollinger proposed that could form so-called N_α and N_β isomers [1].

Up till now, tautomerism [$A \leftrightarrow H$] of Acid Blue 193 was not considered as a factor which could have an influence on coloured and fastness properties. The latest literature reports take note of the role of spatial configuration in similar complexes (type 1:2), not combining such phenomenon with the existence of dye in azo or hydrazone form [9].

Quantum-chemical calculations for Acid Blue 193

To begin with molecule of dye in azo form (**A**) and two hydrazone forms (**H₁** and **H₂**) was optimized. Calculations of molecule geometries in a gaseous phase are sufficient for many analyses, however they don't correctly characterize the state of tautomeric equilibrium of dyes in solutions [7]. In our research optimization of dye structure was performed for molecule in gaseous phase. Taking into consideration the presence of water molecules causes a decrease of difference of H-A energy and it conduces the stronger stabilization of H form [10]. A helpful parameter is so-called hardness η of the molecule - a value determining a probability of existence of A or H form, depending on the kind of presented substituents.



		$-\text{SO}_3\text{H}$			$-\text{SO}_3^-$	
	H	$\alpha[^\circ]$	η	H	$\alpha[^\circ]$	η
A	-59,827	62,3	3,257	-106,952	76,2	2,921
H₁	-54,175	101,2	2,896	-103,289	32,8	2,968
H₂	-51,682	-6,4	3,167	-97,277	-49,8	2,516

Table 1. Calculated values of heat of formation **H** [kcal/mol] of forms: **A**, **H₁** and **H₂** (in neutral and ionized form of dye), angles (α) of twist of aromatic rings planes and hardness (η)

Ionization ($-\text{SO}_3^-$) of the molecule causes that in the ground state HOMO the biggest changes result from the presence of electronegative substituent, $-\text{SO}_3^-$ group. In our research, calculations were performed for non-solvated molecules and total energies of obtained 1:2 complexes of dyes were compared.

Table 2. Examples of calculated of heat of formation values of 1:2 complexes for neutral ($-\text{SO}_3\text{H}$) and ionized molecule of dye ($-\text{SO}_3^-$)

	$-\text{SO}_3\text{H}$	$-\text{SO}_3^-$	
	$\mathbf{A_1A_1} (\alpha\alpha)$	-17771,6	-17470,2
	$\mathbf{A_1A_2} (\alpha\beta)$	-17772,9	-17468,8
	$\mathbf{A_2A_2} (\beta\beta)$	-17772,9	-17467,5

The most probable form is form $\mathbf{A_1A_1}$ – i.e. such form in which the bond is formed between nitrogen atoms N_α . Hydrazone forms could form only these complexes in which the dye exist in $\mathbf{H_1}$ or $\mathbf{H_2}$ form.

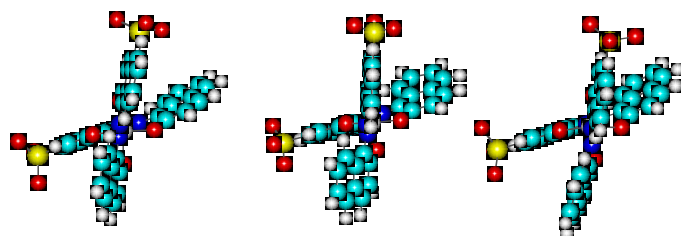
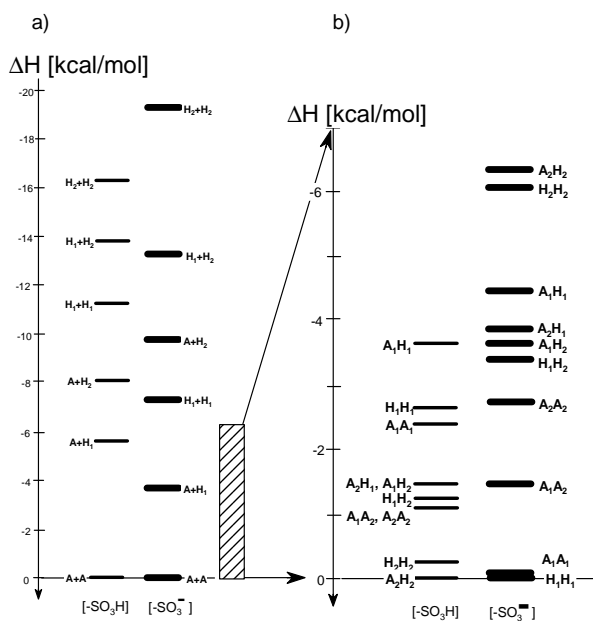


Fig. 3. Example of spatial structure of complexes with anionic azo form of dye (adequately: $\mathbf{A_2A_2}$, $\mathbf{A_1A_2}$, $\mathbf{A_1A_1}$)

Fig. 4. Differences of heat of formation $\Delta\mathbf{H}$ [kcal/mol] of Acid Blue 193 isomers in azo and hydrazone form; a) differences of component energies of monoazo dyes (it was marked the range of changes of metal-complex dye energy – fig. 4b), b) differences of energies of metal-complex dyes 1:2 after optimization by means of ZINDO1



Differences of energy are so insignificant, that in the condition of carrying a reaction of metallizing ($>80^\circ\text{C}$) it is possible the conversion one form to second, hence it is observed as a product the mixture of few products colour distinguishing. Until now, no of proposed methods of synthesis, despite of their significant diversity, don't result in obtaining chromatographically pure and homogeneous products (as regards application properties).

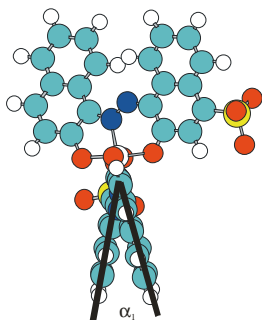


Fig. 5. Example analysis of changes of angles of twist of naphthalene rings planes in metal-complex dye Cr (A_1A_1)

Characteristic is the spatial structure of examined dyes. In each case there are formed complexes in which both parts of dye (monoazo dyes) are twisted with respect to themselves of angle similar to about 60° (chromium atom play a role of bridging group), fig. 3.

As a result of metallizing are formed isomers, in which the distribution of electron density is in significant extent balanced and similar to distribution of electron density in azo form. Not large changes in electron density on chromium atom support for its dominant role in complex formation. Observed position of absorption bands of a dye, both in water solution and on polyamide dyeings (II derivative analysis, fig. 1a), could be the result of existence of complex of examined dye, in azo (A_1 , A_2) as well as hydrazone form (H_1) (calculated values of energy indicate on that).

The process of metallizing with chromium insignificantly influences on absorption bands position, it only influences on their relative intensity [11]. For the possible formation of complex of hydrazone form of dye (H_1H_1) support the fact of high hardness η of H_1 form and its high stability in water solution, in conditions of solvation with solvent molecules [8].

References.

1. H.Zollinger "Colour Chemistry", VCH Weinheim 1991
2. L.Antonov, G.Gergov, V.Petrov, M.Kubista, J.Nygren, *Talanta* **49**(1999)99
3. G.Schetty, *Helv.Chim.Acta* **53**(1970)1437
4. J.Shore "Colorant and Auxiliaries. Organic Chemistry and Application Properties", wyd. Society of Dyes and Colourists 1999, t.I, str.196
5. E.Coates, B.Rigg, *J.Soc,Dyesrs Colourists*, **78**(1962)612
6. K.Venkataraman "The Chemistry of Synthetic Dyes", t.III, str.167 (tłum. rosyjskie)
7. L.Antonov, St.Stoyanov, *Dyes and Pigments* **28**(1995)31
8. L.M.Antonov, 31 UNESCO Course for Advances Research in Chemistry and chemical Engineering, Tokyo Institute of Technology 1996
9. A.Lyčka, J.Holeček, *Dyes and Pigments* **57**(2003)115
10. L.Antonov, S.Kawauchi, M.Satoh, J.Komijama, *Dyes and Pigments* **40**(1999)163
11. L.Szuster (unpublished data)

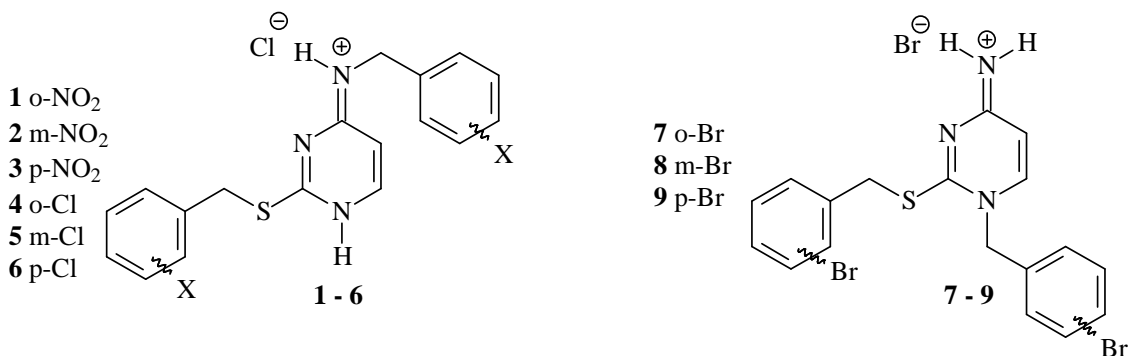
APPLICATION OF ESI-MS AND FAB-MS IN THE
DIFFERENTIATION OF THE ISOMERIC HYDROHALIDES
OF 1,2- AND 2,4-DIBENZYL SUBSTITUTED DERIVATIVES
OF 2-THIOCYTOSINE

Elżbieta Wyrzykiewicz and Tomasz Pospieszny

Faculty of Chemistry, Adam Mickiewicz University, Grunwaldzka 6, 60-780 Poznań

The modified derivatives of 2-thiocytosines are of interest because of their biological and pharmacological activities [1-4]. Recently, we have reported on the synthesis and physicochemical properties of new fluorescents 2-o-(m- and p-)chloro-(bromo-)benzylthio-N-phenylcytosines and 6-methylcytosines [1], as well as new isomeric hydrohalides of 1,2- and 2,4-dibenzyl substituted derivatives of 2-thiocytosine [2]. The EIMS spectra of these compounds have been analyzed to check the possibility to distinguish between the S- and N-1, as well as S- and N-4 disubstituted isomers of hydrohalides of 2-thiocytosine. As a continuation of our previous studies it seemed reasonable to extend our investigation to ESI and FAB mass spectra of three 1,2-o-(m- and p-)bromobenzyl substituted hydrobromides of 2-thiocytosine (7-9) and six 2,4-o-(m- and p-)nitro(chloro)benzyl substituted hydrochlorides of 2-thiocytosine (1-6). The choice of experimental methods was dictated by the necessity to distinguish between the purely mass spectrometric reaction of fragmentation and the corresponding thermally induced process. FAB spectra may be more advantageous for studying mass fragmentations of hydrohalides of disubstituted derivatives of 2-thiocytosine, because samples are ionized at ambient temperatures precluding thermal decomposition. The purpose of this investigation is the elucidation of the ESI ionization and FAB ionization mass fragmentation of (1-9). This investigation was also undertaken to discover whether it is possible to differentiate isomeric o-(m- and p-)NO₂ (Br and Cl) benzyl substituted hydrohalides of 2-thiocytosines (1-9). These compounds were obtained and their structures confirmed according to the literature methods [2]. The ESI mass spectra were recorded on a Waters/micromass Manchester UK/ZQ mass spectrometer equipped with a Harvard Apparatus syringe pump. The sample solutions were prepared in methanol.

The ESI source potentials were 3 kV and cone voltage 30 V. The source and desolvation temperatures were 120 and 300 °C, respectively. Nitrogen was used as nebulizing and desolvation gas. The FAB spectra were produced by LSIMS ionization (Cs^+ ions bombardment) using 3-nitrobenzyl alcohol (NBA) as liquid matrix. These spectra were recorded on an AMD – Intectra GmbH – Harpstedt D-27243 Model 402 two-sector mass spectrometer.



Results and conclusions.

We found that the compounds (1-6) gave strong positive-ion ESI mass spectra but in the positive-ion ESI mass spectra of (7-9) only M-X^+ and X^+ even-electron-ions were observed (Table 1).

Table 1. Relative abundances of characteristic ion peaks in the positive-ion ESI mass spectra of (1-9)

Comp	$\text{M}^+ \text{A}^+$ m/z (%)	$\text{M-X}^+ \text{B}^+$ m/z (%)	C^+ m/z (%)	C+Na^+ m/z (%)	D^+ m/z (%)
1	-	398 (5) $\text{C}_{18}\text{H}_{16}\text{N}_5\text{O}_4\text{S}$	263 (95) $\text{C}_{11}\text{H}_{11}\text{N}_4\text{O}_2\text{S}$	285 (15) $\text{C}_{11}\text{H}_{11}\text{N}_4\text{O}_2\text{SNa}$	125 (100) $\text{C}_4\text{H}_5\text{N}_3\text{S}$
2	-	398 (48) $\text{C}_{18}\text{H}_{16}\text{N}_5\text{O}_4\text{S}$	263 (100) $\text{C}_{11}\text{H}_{11}\text{N}_4\text{O}_2\text{S}$	285 (15) $\text{C}_{11}\text{H}_{11}\text{N}_4\text{O}_2\text{SNa}$	-
3	433 (8) $\text{C}_{18}\text{H}_{16}\text{N}_5\text{O}_4\text{SCl}$	398 (100) $\text{C}_{18}\text{H}_{16}\text{N}_5\text{O}_4\text{S}$	263 (68) $\text{C}_{11}\text{H}_{11}\text{N}_4\text{O}_2\text{S}$	-	-
4	-	376 (100) $\text{C}_{18}\text{H}_{16}\text{N}_5\text{O}_4\text{SCl}_2$	252 (5) $\text{C}_{11}\text{H}_{11}\text{N}_3\text{SCl}$	-	125 (5) $\text{C}_7\text{H}_6\text{Cl}$
5	-	376 (100) $\text{C}_{18}\text{H}_{16}\text{N}_5\text{O}_4\text{SCl}_2$	252 (20) $\text{C}_{11}\text{H}_{11}\text{N}_3\text{SCl}$	-	125 (8) $\text{C}_7\text{H}_6\text{Cl}$
6	-	376 (100) $\text{C}_{18}\text{H}_{16}\text{N}_5\text{O}_4\text{SCl}_2$	252 (10) $\text{C}_{11}\text{H}_{11}\text{N}_3\text{SCl}$	-	125 (12) $\text{C}_7\text{H}_6\text{Cl}$
7	-	466 (100) $\text{C}_{18}\text{H}_{16}\text{N}_3\text{SBr}_2$	-	-	169/171(7) $\text{C}_7\text{H}_6\text{Br}$
8	-	466 (100) $\text{C}_{18}\text{H}_{16}\text{N}_3\text{SBr}_2$	-	-	169/171(8) $\text{C}_7\text{H}_6\text{Br}$
9	-	466 (100) $\text{C}_{18}\text{H}_{16}\text{N}_3\text{SBr}_2$	-	-	169/171(7) $\text{C}_7\text{H}_6\text{Br}$

In the fragmentation of the $M-X^+$ even-electron ions of compounds (1-6) simple cleavages of Csp^3-S bonds of o-(m- and p-)nitro(chloro)benzyl substituents gave C^+ [$M-C_7H_5X$] $^+$ ions. In the cases of the ESI fragmentation of (7-9) the positive charge is also stabilized on the $C_7H_5X+H^+$ species. The differences in the fragmentation within two sets of isomeric compounds (1-3; 4-6) were expressed quantitatively by comparing the calculated values of the coefficient μ i.e. % rel. int. C^+ / % rel. int. B^+ (Table 2). The differences between these values may be sufficient to differentiate among the isomeric o-(m- and p-)nitro(chloro) substituted isomers (1-6).

Table 2. The values of calculated coefficients μ determined for the ESI mass spectra of (1-6).

Comp.						
	1	2	3	4	5	6
μ	19.00	2.08	0.68	0.05	0.20	0.10

The FAB LSIMS spectra of (1-9) produced in the positive-ion mode by LSIMS ionization (Cs^+ ions bombardment) using 3-nitrobenzyl alcohol (NBA) as liquid matrix, show strong fragmentation (Table 4). The relative abundances of $M-X^+$, $M-2X^+$, $M-C_7H_6^+$ and $C_7H_6X^+$ fragment ions clearly differ between o-(m- and p-)nitro(chloro and bromo) substituted isomers. Generally speaking the main fragment ion compositions correspond to those formed under the ESI conditions. These diagnostic ions are produced by splitting of the Csp^3-S bonds of o-(m- and p-)nitro(chloro and bromo)benzyl substituent. The differences in the fragmentation within three sets of isomeric compounds (1-3, 4-6, 7-9) were expressed quantitatively by comparing the calculated values of μ_1 and μ_2 (% rel. int. $C_7H_6X^+$ / % rel. int. [$M-X^+$]) and % rel. int. [$M-C_7H_6X^+$] / % rel. int. [$M-X^+$]) respectively (Table 3). The differences between these values may be sufficient to differentiate among the isomeric o-(m- and p-)nitro(chloro and bromo) substituted isomers.

Table 3. The values of calculated coefficients μ_1 and μ_2 determined for the FAB /LSIMS mass spectra of (1-9).

Comp.									
	1	2	3	4	5	6	7	8	9
μ_1	1.48	1.62	0.45	0.39	0.71	0.98	0.24	0.35	0.44
μ_2	2.22	0.92	1.90	0.18	1.21	0.69	0.07	0.08	0.05

Table 4. Relative abundances of characteristic ion peaks in the FAB /LSIMS mass spectra of (1-9).

Comp	[M-Cl]⁺ A m/z (%)	[M-Cl-2X+H]⁺ B m/z (%)	[M-Cl- C₇H₆X+H]⁺ C m/z (%)	C₇H₅X+H]⁺ D m/z (%)	NBA+1⁺ E m/z (%)
1	398 (45) C ₁₈ H ₁₆ N ₅ O ₄ S	307 (9) C ₁₈ H ₁₇ N ₃ S	263 (100) C ₁₁ H ₁₁ N ₄ O ₂ S	136 (67) C ₇ H ₆ NO ₂	154 (56) C ₇ H ₈ NO ₃
2	398 (536) C ₁₈ H ₁₆ N ₅ O ₄ S	307 (18) C ₁₈ H ₁₇ N ₃ S	263 (49) C ₁₁ H ₁₁ N ₄ O ₂ S	136 (86) C ₇ H ₆ NO ₂	154 (100) C ₇ H ₈ NO ₃
3	398 (20) C ₁₈ H ₁₆ N ₅ O ₄ S	307 (27) C ₁₈ H ₁₇ N ₃ S	263 (88) C ₁₁ H ₁₁ N ₄ O ₂ S	136 (69) C ₇ H ₆ NO ₂	154 (100) C ₇ H ₈ NO ₃
4	376 (100) C ₁₈ H ₁₆ N ₃ SCl ₂	307 (4) C ₁₈ H ₁₇ N ₃ S	252 (18) C ₁₁ H ₁₁ N ₃ SCl	125 (39) C ₇ H ₆ Cl	154 (23) C ₇ H ₈ NO ₃
5	376 (182) C ₁₈ H ₁₆ N ₃ SCl ₂	307 (4) C ₁₈ H ₁₇ N ₃ S	252 (100) C ₁₁ H ₁₁ N ₃ SCl	125 (59) C ₇ H ₆ Cl	154 (56) C ₇ H ₈ NO ₃
6	376 (100) C ₁₈ H ₁₆ N ₃ SCl ₂	307 (9) C ₁₈ H ₁₇ N ₃ S	252 (69) C ₁₁ H ₁₁ N ₃ SCl	125 (98) C ₇ H ₆ Cl	154 (41) C ₇ H ₈ NO ₃
7	466 (100) C ₁₈ H ₁₆ N ₃ SBr ₂	307 (23) C ₁₈ H ₁₇ N ₃ S	296/298 (6/7) C ₁₁ H ₁₁ N ₃ SBr	169/171(24/23) C ₇ H ₆ Br	154 (76) C ₇ H ₈ NO ₃
8	466 (100) C ₁₈ H ₁₆ N ₃ SBr ₂	307 (10) C ₁₈ H ₁₇ N ₃ S	296/298 (8/9) C ₁₁ H ₁₁ N ₃ SBr	169/171(35/34) C ₇ H ₆ Br	154 (78) C ₇ H ₈ NO ₃
9	466 (100) C ₁₈ H ₁₆ N ₃ SBr ₂	307 (12) C ₁₈ H ₁₇ N ₃ S	296/298 (5/6) C ₁₁ H ₁₁ N ₃ SBr	169/171(49/48) C ₇ H ₆ Br	154 (65) C ₇ H ₈ NO ₃

The analytical ions which have been selected from the positive-ion ESI and positive-ion FAB/LSIMS mass spectra of (1-9) may be useful in the mass fragmentography.

References:

- [1] E. Wyrzykiewicz, Z. Nowakowska, Na pograniczu chemii i biologii, Wydawnictwo Naukowe UAM, tom III, 1999, str. 187
- [2] E. Wyrzykiewicz, T. Pospieszny, S. Mielcarek, Phosphorous, Sulfur, Silicon and Related Elements, 2005, 180 (2005) 2051;
- [3] E. Wyrzykiewicz, T. Pospieszny, A. Barłóg, Rapid Commun. in Mass Spectrometry, 19 (2005) 580
- [4] E. Wyrzykiewicz, T. Pospieszny, M. Sobolewska, Rapid Commun. in Mass Spectrometry, 20 (2006) 713

MALTOL VERSUS THIOMALTOL. THEORETICAL COMPARISON OF SELECTED PROPERTIES.

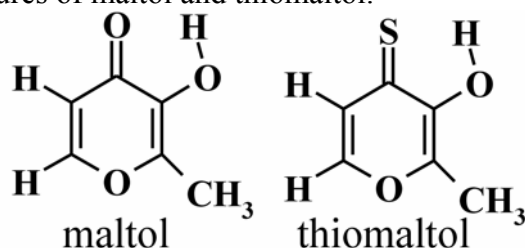
Krzysztof Bolechała^a, Krzysztof Zborowski^a,
Leonard M. Proniewicz^{a,b}

^a*Faculty of Chemistry, Jagiellonian University, 3 Ingardena Str., 30-060 Kraków,
Poland*

^b*Regional Laboratory of Physicochemical Analysis and Structural Research,
Jagiellonian University, 3 Ingardena Str., 30-060 Kraków, Poland*

Derivatives of the pyromeconic acid (3-hydroxy-4H-pyran-4-one) are family of the ligands widely used in coordination chemistry. Among them, the importance of maltol (3-hydroxy-2-methyl-4H-pyran-4-one) as the most important member of this class of compounds must be underlined [1]. Maltol complexes with different metal ions possess strong biological activity and are tested as new medicines in diabetes and anaemia therapy as well as new radiopharmaceutical agents. In order to obtain new useful ligands several modifications of the hydroxypyronone system have been attempted. From several years, thiomaltol, ligand in which oxygen atom from the keto group is replaced by sulphur (see Fig. 1) is widely investigated [2]. Such mixed oxygen – sulphur ligands can be for example useful as efficient scavengers of lead ions, a serious contaminant [3].

Fig.1. Molecular structures of maltol and thiomaltol.



Ligands investigations are of crucial importance for prediction and interpretation of the properties of their complexes with metal ions. In this study geometries of tautomeric structures, equilibrium constants among them and aromaticity properties of the most stable tautomers are presented. Data for both, neutral and charged forms (anion and cation, created by deprotonation or protonation, respectively) of thiomaltol are included. Thiomaltol properties are compared with those reported previously for maltol (tautomeric equilibria [4], heteroaromaticity in the pyran rings [5], and π -electron delocalisation in the OCCO molecular fragment [6]). Studying the SCCO molecular fragment properties is very important because this group is responsible for metal ions binding in the studied ligand.

All quantum-chemical calculations have been executed at the B1LYP[7]/6-3111++G(d,p)[8] level as implemented in the GAUSSIAN-03 package [9]. In order to select the most probable conformations of studied thiomaltol species their potential energy surfaces have been scanned and the lowest minimum has been located for every tautomer. These lowest energy conformations have been fully optimized and the nature (minimum or saddle point) of them have been checked by frequency calculations at the

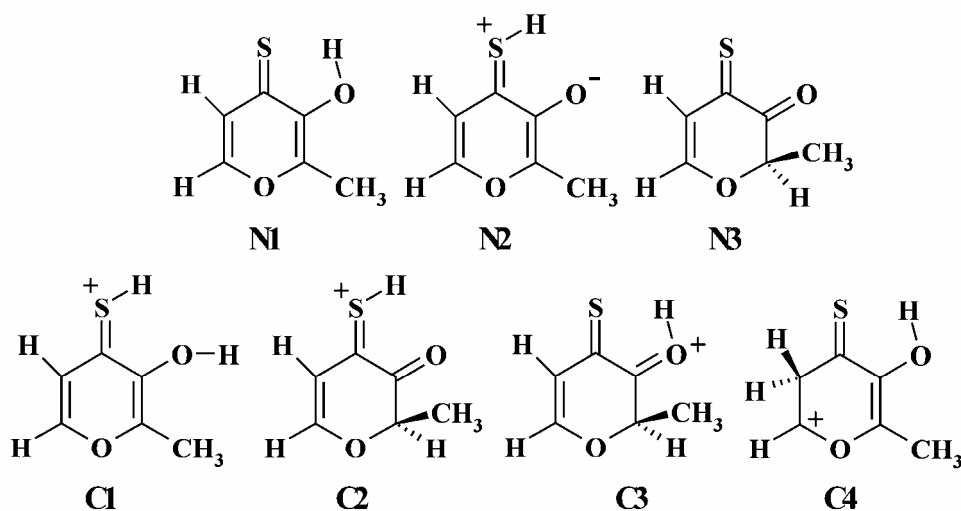
same computational level. All molecular energies have been corrected by the zero point energies (ZPE) of vibrational motions.

Statistical thermodynamic treatment has been used for tautomeric equilibrium constants determination [10]. In this method equilibrium constant (K_T) is related to the standard change of the Gibbs energy, ΔG^0 , by the following equation: $\Delta G^0 = -RT \ln K_T$. ΔG^0 values have been estimated by GAUSSIAN from the total partition function given as a product of translational, rotational and vibrational partition functions evaluated within the rigid motor – harmonic oscillator – ideal gas approximation.

HOMA (Harmonic Oscillator Model of Aromaticity) and NICS (Nuclear Independent Chemical Shift) indices have been employed to determine aromaticity/ π -electron delocalization properties of studied compounds. HOMA [11] is a geometry-based index calculated on the base of bond lengths of the potential aromatic system using the equation: $HOMA = 1 - [\alpha/N \sum (R_{opt} - R_i)^2]$. R_{opt} and R_i are optimal bond lengths and bond lengths in the real system, respectively. Empirical factor, α , sets the HOMA value equal to 0 for the Kekule structure of benzene and 1 for real benzene structure. N is the number of bonds in the studied system. The HOMA index was splitted i two parts, GEO and EN [12]. $HOMA = 1 - \alpha(R_{opt} - R_{ave})^2 - \alpha/N \sum (R_{ave} - R_i)^2 = 1 - EN - GEO$. GEO and EN are two effects that can decrease the aromaticity of the molecular system, namely: bond lengths alternation (GEO) and bond elongation (EN). The NICS index was originally defined as the negative value of the magnetic shielding computed at the aromatic ring center or at another point of the molecule[13]. From that time other NICS technics were introduced. Two of them are employed in this work. The NICS(1) index is the negative magnetic shielding calculated 1 Å above the ring (or another point) center [14] while NICS(1)_{zz} is the out of plane component of the NICS(1) magnetic tensor [15]. Highly negative NICS values denote aromaticity whereas systems with positive values are antiaromatic.

A lot of tautomeric structures are possible for neutral thiomaltol and its cation. Tautomerism cannot occur for the anion, due to the lack of labile proton (the labile proton of the hydroxyl group dissociates during the anion formation). In this work only the most stable types of tautomers (determined previously for pyromeconic acid, maltol, and ethylmaltol [4] and kojic acids family [16]) are considered. Their structures are presented in Fig. 2.

Fig. 2. Studied neutral and cationic tautomers.



Relative energies and equilibrium constants of neutral and protonated thiomaltol tautomers are collected in Table 1 (for comparison maltol data are also presented). Only two neutral thiomaltol tautomers (N1 and N3) are stable. In the case of N2 tautomer, during geometry optimization procedure, proton from the –SH group migrates toward exocyclic oxygen. As a result, tautomer N2 transforms into N1. Like in maltol the N1 structure is the most stable neutral form. The energy gap between N1 and N2 for thiomaltol and corresponding tautomeric equilibrium constant are similar to their maltol counterparts. In the case of the thiomaltol cation protonation occurs in the same place as for native maltol molecule (protonation on the sulphur atom of the thioketo group in thiomaltol and protonation of the oxygen atom of the keto group in maltol). But in contrary, the energy gap between the tautomer with the lowest energy, C1, and others is much more lower, see Table1. Because of that, C2 and C3 maltol cation tautomers are much less possible than the same types of tautomers in the case of thiomaltol. Tautomer C4 possess one imaginary frequency and all attempts to obtain a minimum have not given satisfactory results.

Table 1. Relative Energies (kJ/mol, ZPE included) and tautomeric equilibrium constants (B1LYP/6-311++G(d,p) calculations).

Tautomers	Maltol [4]		Thiomaltol	
	Relative Energy	K_T	Relative Energy	K_T
Neutral molecules				
N1 ↔ N2	49.53	$3.46 \cdot 10^{-9}$	-----	-----
N1 ↔ N3	62.23	$4.27 \cdot 10^{-11}$	68.23	$7,31 \cdot 10^{-13}$
Cations				
C1 ↔ C2	230.70	$3.83 \cdot 10^{-41}$	77.38	$3.17 \cdot 10^{-14}$
C1 ↔ C3	310.92	$3.37 \cdot 10^{-55}$	130.08	$1.17 \cdot 10^{-23}$
C1 ↔ C4	266.55	$2.00 \cdot 10^{-47}$	-----	-----

Aromaticity data for thiomaltol and maltol are presented in Table 2 (heterocyclic pyran ring) and 3 (XCCO group). The HOMA index predicts a bit stronger aromatic character of thiomaltol than maltol. This is true for both, the XCCO molecular fragment and for the heterocyclic pyran ring. The same (except aromaticity of the cation in the pyran ring) is true for the NICS(1) index. In contrary, behaviour of the NICS(0) is different. Here, maltol structures are slightly more aromatic. In general differences between maltol and thiomaltol are not big and for these three indices mentioned above the aromaticity order determined previously for maltol and other hydroxypyrones (aromaticity of cation > aromaticity of neutral molecule > aromaticity of anion) is still valid. Different results are obtained for the NICS(1)_{zz}. In this case the aromaticity order is different in every case, i.e. one aromaticity order is observed for heterocyclic ring in maltol, another one for heterocyclic ring in thiomaltol, etc. The reason, why the results provided by the NICS(1)_{zz} method are so different than data from other indices is unknown so far. This problem will be studied in the future for the biggest set of hydroxypyrones and thiohydroxypyrones. In general, weights of GEO and EN sub-indices calculated for thiomaltol are similar to those determined for maltol.

Authors thank the Warsaw University Interdisciplinary Centre for Mathematical and Computational Modelling “ICM” for allowing us to use their computers (project number G17-8).

Table 2. Aromaticity indices values for various maltol and thiomaltol species – heterocyclic pyran rings.

	HOMA	GEO	EN	NICS(0)	NICS(1)	NICS(1) _{zz}
Maltol [5]						
Neutral	0.02	0.68	0.30	-2.63	-4.58	-9.02
Cation	0.55	0.40	0.06	-7.15	-7.84	-17.14
Anion	-0.46	0.70	0.76	-1.38	-3.81	-8.62
Thiomaltol						
Neutral	0.27	0.50	0.23	-1.93	-4.63	-9.10
Cation	0.62	0.26	0.12	-5.79	-7.36	-15.97
Anion	-0.03	0.46	0.57	-0.79	-3.89	-9.40

Table 3. Aromaticity indices values for various maltol and thiomaltol species – XCCO group. (X=O maltol, X=S thiomaltol)

	HOMA	GEO	EN	NICS(0)	NICS(1)	NICS(1) _{zz}
Maltol [6]						
Neutral	0.05	0.55	0.40	-4.37	-3.20	-3.96
Cation	0.45	0.07	0.48	-7.83	-3.38	-2.65
Anion	-0.40	1.12	0.28	-0.54	-2.04	-2.19
Thiomaltol						
Neutral	0.36	0.21	0.43	-3.86	-3.90	-5.09
Cation	0.49	0.06	0.45	-7.00	-3.88	-3.50
Anion	0.05	0.63	0.32	0.73	-2.76	-3.78

References:

1. KH. Thompson, C. Orvig, *Coord. Chem. Rev.*, 219 (2001) 1033
2. JA. Levis, DT. Puerta, SM. Cohen, *Inorg. Chem.*, 42 (2003) 7455
3. JA. Levis, SM. Cohen, *Inorg. Chem.*, 43 (2004) 6534
4. K. Zborowski, R. Gryboś, LM. Proniewicz, *J. Mol. Struct. (THEOCHEM)*, 639 (2003) 87
5. K. Zborowski, R. Gryboś, LM. Proniewicz, *J. Phys. Org. Chem.*, 18 (2005) 250
6. K. Zborowski, LM. Proniewicz, submitted for publication
7. C. Adamo, V. Barone, *Chem. Phys. Lett.*, 274 (1997) 242
8. R. Krishnan, JS. Binkley, R. Seeger, JA. Pople, *J. Chem. Phys.*, 72 (1980) 650
9. MJ. Frisch et al., GAUSSIAN-03, Gaussian Inc., Wallingford, CT 2003.
10. P. Hobza, J. Sponer, *Chem. Rev.*, 99 (1999) 3247
11. TM. Krygowski, *J. Chem. Inf. Comput. Sci.*, 33 (1993) 70
12. TM. Krygowski, MK. Cyrański, *Tetrahedron*, 52 (1996) 10255
13. PvR. Schleyer C. Maerker, A. Dransfeld, H. Jiao, NJR. Eikema Hommes, *J. Am. Chem. Soc.*, 118 (1996) 6317
14. PvR. Schleyer, M. Monohar, Z. Wang, B. Kiran, H. Jiao, R. Puchta, *NJR Hommes, Org. Lett.*, 3 (2001) 2465
15. C. Corminboeuf, T. Heine, G. Seifert, PvR. Schleyer, J. Weber, *Phys. Chem. Chem. Phys.*, 6 (2004) 273
16. K. Zborowski, A. Korenova, M. Uher, *J. Mol. Struct. (THEOCHEM)*, 683 (2004) 15

FT-IR STUDY OF Cu-O/MgF₂, Co-O/MgF₂ AND Cu-Co-O/MgF₂ CATALYSTS IN NO+C₃H₆+O₂ REACTION

Michał Zieliński¹, Maria Wojciechowska¹, Sławomir Łomnicki²

¹ Faculty of Chemistry, A. Mickiewicz University, ul. Grunwaldzka 6, 60-780 Poznań, Poland, e-mail: mardok@amu.edu.pl

² Chemistry Department, Louisiana State University, USA

The aim of this work is to bring about new evidence on possible reaction mechanism of NO reduction by propene over copper-cobalt oxides catalysts supported on an unconventional support - MgF₂ [1,2]. Such systems have been studied earlier and have shown activity and selectivity in purification of fuel combustion products from nitrogen oxides [3]. We used in situ IR adsorption experiments of NO, O₂ and C₃H₆ on CuO/MgF₂, CoO_x/MgF₂ and CuO-CoO_x/MgF₂ catalysts.

The Cu/MgF₂ and Co/MgF₂ catalysts were obtained by impregnation from aqueous solutions of Cu(NO₃)₂·3H₂O and Co(NO₃)₂·6H₂O of known concentrations onto MgF₂ powder of 0.25-0.50 mm grain size (preheated at 400°C for 4h). The suspension was then evaporated until dry. Thus, all copper nitrate and cobalt nitrate was introduced into the microporous MgF₂ particles. The CuCo/MgF₂ catalysts were prepared by the conventional co-impregnation method from the aqueous solutions of Cu(NO₃)₂·3H₂O and Co(NO₃)₂·6H₂O, then dried in air at 120°C for 24h and then calcined at 400°C.

The samples were marked with a symbol MFCu₂, MFCo₄, MFCu₂Co₄, where "2 and 4" stands for the content of metallic copper or cobalt in wt %, F-MgF₂.

IR spectra were taken on a spectrometer Bio-Rad, model Excalibur 3000 with Fourier Transform (FT-IR). The catalysts were pressed into tablets (~4 mg/cm²) under a pressure of 20 MPa, and placed in a vacuum cell with windows made of KRS5. The samples were annealed at 150°C, degassed under 10⁻⁴ Torr for 1,5 hour and then cooled to RT at which the spectrum was taken. Then the gases adsorbed (NO, C₃H₆ and O₂) were subsequently introduced into the cell and the spectra were taken again. The results are presented as difference spectra obtained after subtraction of the fundamental spectrum.

Adsorption of propene as the first reagent on **MFCu₂** catalyst (Fig. 1a) is manifested as the appearance of bands in the range 1660-1633cm⁻¹ and 1500-1345cm⁻¹ assigned to the C-H and C-C bonds in the adsorbed C₃H₆ and a band at 1605cm⁻¹ assigned to the adsorbed species containing C=O or COO⁻ groups [4]. Other bands, characteristic of -CH₃ group appear at 1463, 1442, 1365cm⁻¹. After adsorption of oxygen the intensity of the bands at 1605 and 1447cm⁻¹ increase, indicating the oxidation of propene to carboxyl compounds. There is also a band at 1341cm⁻¹ assigned to the -CH groups of the adsorbed carboxyl groups [4,5]. Adsorption of nitrogen oxide on the earlier adsorbed propene and oxygen is reflected by the appearance of bands assigned to the gas NO – a triplet at 1905, 1875 and 1860 cm⁻¹, to N₂O adsorbed at Cu²⁺ centres – at 2195, and the bands at 1633, 1429 and 1047cm⁻¹ assigned to nitrates III)/(V) adsorbed at the Cu²⁺ centres [6]. The intensity of the bands at 1499 and 1341cm⁻¹, assigned to the Cu²⁺NO₂ groups also increases [7].

The reversed sequence of gas introduction (Fig. 1b), i.e. the adsorption of nitrogen oxide as the first, leads to the appearance of bands at 2195cm^{-1} and in the range $1600\text{-}1660\text{cm}^{-1}$ assigned to N_2O and NO adsorbed at the Cu^{2+} centres [6,8]. The bands appearing below $\sim 1350\text{cm}^{-1}$ correspond to the NO_3^- and NO_2^- groups adsorbed at the Cu^{2+} centres. There is also an intense band at 1447cm^{-1} , assigned to the NO_2 adsorbed on the surface of the catalyst [8].

Adsorption of O_2 on the earlier adsorbed nitrogen oxide leads to an increase in the

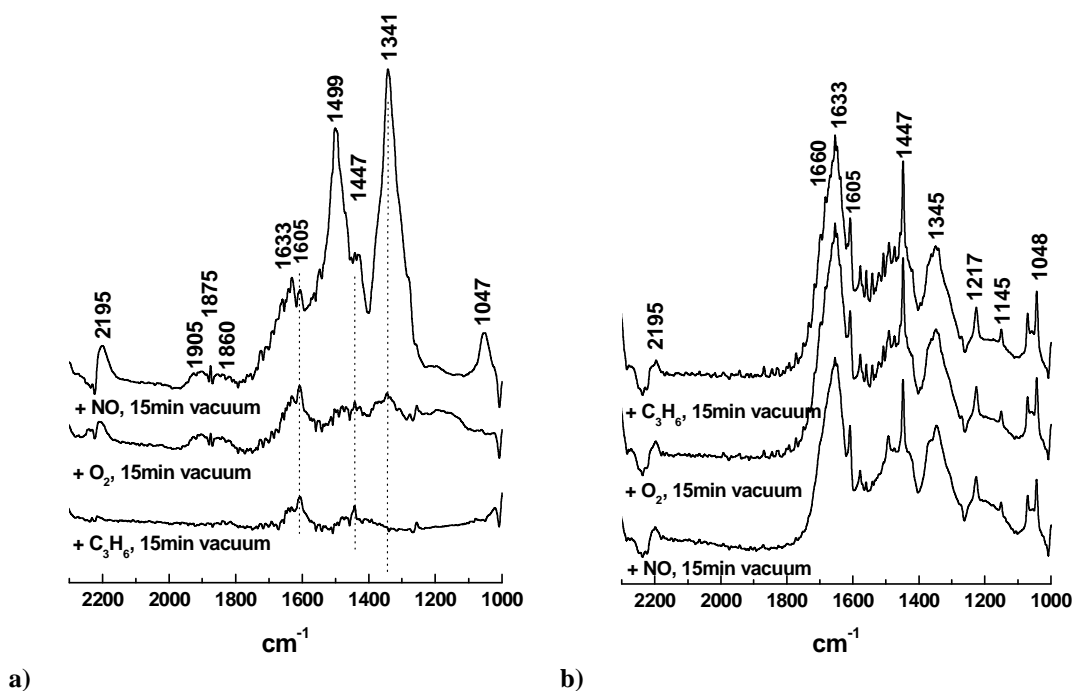


Fig. 1. IR spectra after adsorption a) C_3H_6 , O_2 , NO and b) NO , O_2 , C_3H_6 on MFCu_2 taken at 80°C . intensity of the signal at 1447cm^{-1} assigned to NO_2 formed as a result of the surface reaction of the adsorbed $\text{NO}^* + \text{O}_2^*$.

Adsorption of propene as the first reagent on the MFCo_4 catalyst (Fig. 2a) brings the appearance of characteristic bands assigned to acetate ions at 1610 , 1581 and 1442cm^{-1} [4]. Their intensity significantly increases after addition of oxygen, which means that propene is further oxidised to carboxyls. Adsorption of nitrogen oxide on the catalyst with the earlier adsorbed propene and oxygen leads to an increased intensity of the bands at 1695 and 1660cm^{-1} assigned to the interactions C-H, C-C propene and nitrates (III)/(V) adsorbed at Co^{2+} centres.

It should be emphasised that as a result of adsorption of C_3H_6 on a cobalt catalyst the FT-IR spectra reveal the bands indicating the presence of carboxyl groups, in particular after oxygen has been introduced into the system. It suggests that the presence of cobalt ions on the catalyst surface favours the oxidation of propene. This conclusion is confirmed by the earlier obtained results on the high activity of the cobalt catalysts in the process of $\text{NO} + \text{C}_3\text{H}_6 + \text{O}_2$. Adsorption of C_3H_6 occurs as a result of the interaction of the surface Co^{2+} ions with the double bond of propene leading to breaking of this bond.

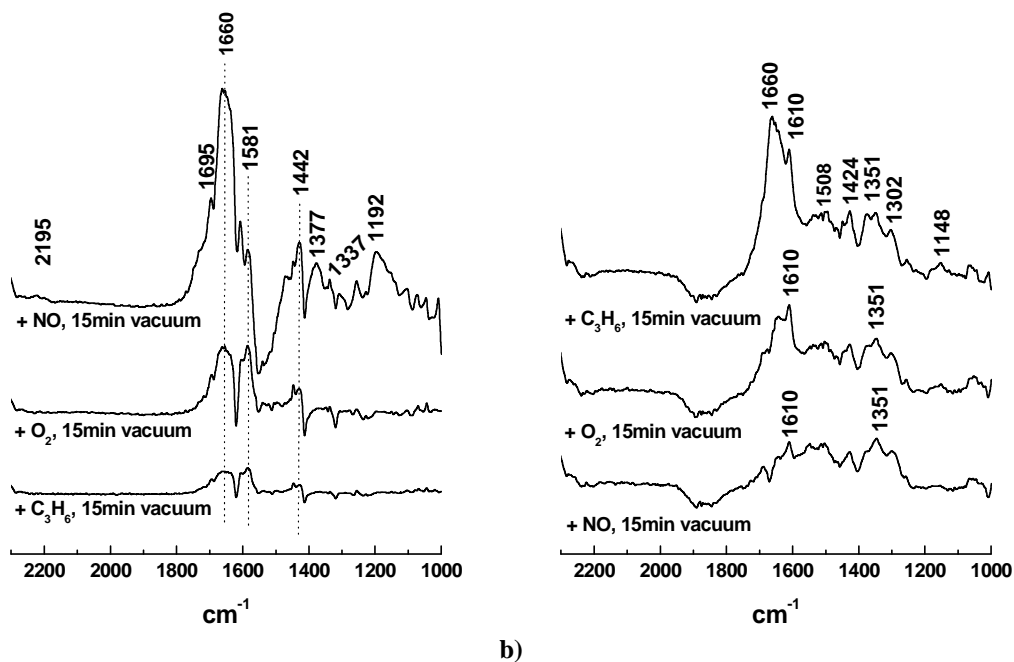


Fig. 2. IR spectra after adsorption a) C_3H_6 , O_2 , NO and b) NO , O_2 , C_3H_6 on MFCo_4 taken at 80°C .

Good oxidising properties of MFCo_4 are also confirmed by the presence of strong bands assigned to the adsorbed nitrates (the bands below 1400cm^{-1} , particularly well seen when the first reagent adsorbed is nitrogen oxide, Fig. 2b). In contrast to the copper catalyst, the adsorption of propene on the earlier adsorbed NO and O_2 does not lead to considerable changes in the spectrum.

Fig. 3 presents IR results for a mixture of copper and cobalt oxides supported on MgF_2 . When propene is introduced as the first reagent on MFCu_2Co_4 (Fig. 3a) the IR spectra show the band corresponding to the oxidised species C_3H_6 at 1633cm^{-1} . This

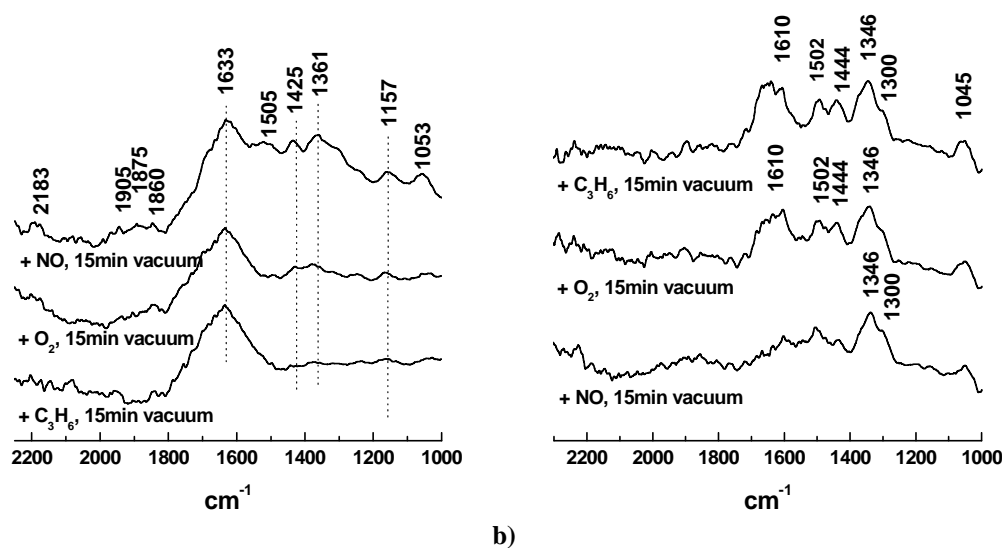


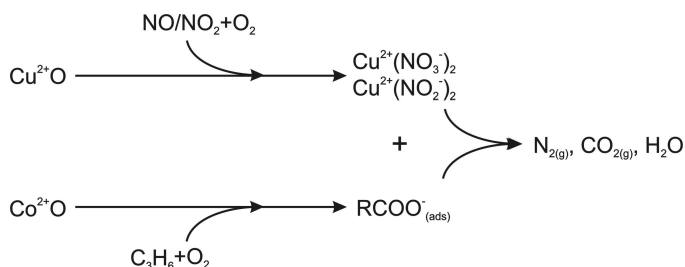
Fig. 3. IR spectra after adsorption a) C_3H_6 , O_2 , NO and b) NO , O_2 , C_3H_6 on MFCu_2Co_4 taken at 80°C .

band's intensity increases after introduction of oxygen. There is also an additional band at 1361cm^{-1} corresponding to COO^- . Adsorption of NO on the earlier adsorbed propene and oxygen gives an increased intensity of the band at 1361cm^{-1} , which can point to a further oxidation of propene to carboxylic compounds. The other bands that appear are at 1053cm^{-1} – assigned to the C-O and C-C bonds and at 1157 and 1053cm^{-1} assigned to nitrates (III)/(V) adsorbed at the Cu^{2+} or Co^{2+} centres.

The reversed sequence of the introduction of gases (Fig. 3b), with nitrogen oxide as the first reagent, brings the appearance of the bands assigned to NO_3^- and NO_2^- at 1346 and 1300cm^{-1} , respectively. After adsorption of O_2 there is a signal at 1444cm^{-1} corresponding to NO_2 formed as a result of the surface reaction of $\text{NO}^* + \text{O}_2^*$. After adsorption of propene the intensity of the bands at $1620\text{-}1550\text{cm}^{-1}$ increases, which indicates the oxidation of the propene adsorbed and the formation of the COO^- species [6,8].

The results of the study of nitrogen oxide, propene and oxygen adsorption on the catalysts MFCu_2 , MFCo_4 and MFCu_2Co_4 allowed us to propose a mechanism of the reaction $\text{NO} + \text{C}_3\text{H}_6 + \text{O}_2$ taking place on the copper-cobalt oxide catalyst supported on MgF_2 , Scheme 1. At the first stage of the reaction NO is adsorbed on Cu^{2+} ions. In the presence of oxygen the adsorbed nitrogen oxide is oxidised to nitrates (III) and/or nitrates (V). The adsorption of propene leads to a breaking up of the double bond. The key stage of the reaction seems to be that between the adsorbed NO_2^- and NO_3^- groups and the adsorbed hydrocarbon leading to formation of carboxyl groups, which, as a result of further oxidation, are transformed into CO_2 .

Because the catalyst surface is capable of oxidation of the hydrocarbon owing to the presence of cobalt oxides, the reaction of propene oxidation being competitive to the reduction of NO will also take place on the catalyst. When the oxidation of propene to CO_2 dominates, the nitrates (III) and nitrates (V) present on the catalyst surface will block the active sites of the catalyst inhibiting its activity.



Scheme 1. Possible reaction pathways.

ACKNOWLEDGEMENTS

We acknowledge a support from the Polish Committee for Scientific Research (grant 3 T09A 174 28). Michał Zieliński expresses his gratitude to the Foundation of Polish Science for fellowship.

- [1] M. Wojciechowska; M. Zieliński; M. Pietrowski, J. Fluorine Chem., 120 (2003) 1
- [2] M. Wojciechowska; M. Zieliński; J. Goslar; B. Czajka, Mol. Phys. Reports, 34/2 (2001) 171
- [3] M. Wojciechowska; M. Zieliński; A. Malczewska, W. Przystawko, M. Pietrowski, Appl. Catal. A, 298 (2006) 225
- [4] G. Busca, Catal. Today, 27 (1996) 457
- [5] Y. Chi, S.S.C. Chuang, Catal. Today, 62 (2000) 303
- [6] K. Hadjiivanov, D. Klissurski, G. Ramis, G. Busca, Appl. Catal. B, 7 (1996) 251
- [7] M. Sirilumpen, R. T. Yang, N. Tharapiwattananon, J. Mol. Catal. A, 137 (1999) 273
- [8] S. Park, V. Kurshev, Z. Luan, C. W. Lee, L. Kevan, Micro. and Mesoporous Mat., 38 (2000) 255

THE COURSE OF ELECTROCRYSTALLISATION AND ELECTRO-OXIDATION PROCESSES OF A BINARY COBALT-MOLYBDENUM ALLOY IN CONSTANT MAGNETIC FIELD

M. Zieliński, E. Miękoś

*Department of General and Inorganic Chemistry, University of Lodz,
Narutowicza str. 68, 90-136 Lodz, Poland*

Introduction

Electrocrystallisation is the process of electrolytic deposition of metals and alloys, including the phenomena occurring during incorporation of metal atoms into the crystal lattice of the surface of the resulting alloy. A binary alloy is a substance with metallic properties, consisting of two elements, at least one of which is a metal. Research into alloys is conducted mainly for the possibility of obtaining new materials, as well as for the need to predict the properties and composition of alloys. co-deposition of cobalt and molybdenum is the so-called induced co-deposition. The cation which induces the co-deposition process is cobalt. The role of hydrogen release in the deposition processes of such alloys as Co-Mo is also taken into consideration [1,2].

Molybdate (VI) ions are transformed in the cathode area to the form of oxide, which is adsorbed onto the cathode surface:



Subsequently, molybdenum (VI) trioxide becomes electroreduced to oxides at lower oxidation state:



Reduction of oxides, which would lead to reduction of pure molybdenum, ceases to occur. Introduction of ions of another metal, in this case Co(II), to the electrolyte solution containing molybdate (VI) results in the following course of reaction:



Ions of a metal which co-deposits with molybdenum occur in the electrolyte in the ionic form at lower oxidation state [Co(II)] and are invariable. The ionic radiuses of Mo and Co are similar and that is why atoms of metals which inhibit the process of alloy deposition may easily be placed within the crystal lattice of molybdenum. The properties of Co-Mo alloys include: high strength, good ductility, high corrosion resistance, as well as very good electrical conduction. This is determined by the appropriate standards of electrical and mechanical requirements for such materials (e.g. high temperature-sparking) [3,4]. As was proved in the course of X-ray structure analysis, electrolytic coatings of the Co-Mo alloy do not have crystal structure. However, the possibility that a major part of the crystal component of the alloy coating is constituted by cobalt or solid solution of molybdenum in cobalt is not excluded [5,6,7]. Structure of the Co-Mo alloy deposited onto copper, graphite and glass-carbon cathodes was studied by Gomez E. et al [8,9,10]. They also studied the magnetic properties (magnetisation) of the obtained alloys in an applied magnetic field. The effects of constant magnetic field on electrochemical redox reactions were investigated by Bund A. et al [11]. They studied the following systems: Cu^{2+}/Cu , Ni^{2+}/Ni , $[\text{IrCl}_6]^{2-}/[\text{IrCl}_6]^{3-}$ referring to previous solutions. Such alloys as Ni-Cu or Ni-Fe were also deposited electrolytically in a

magnetic field ($B = 0,1 \text{ T}$) [12,13]. The structure of these alloys and coating thickness were observed with the help of an AFM.

Experimental

The cyclic voltammetry (CV) method was employed in the study. It was used for analysing the kinetics of the processes of electrocrystallisation and electrooxidation of the Co-Mo alloy. The experiments were performed on polycrystalline golden disk electrodes with the area of approx. $0,1 \text{ cm}^2$. Magnetic induction values (B) used for the experiments ranged from 0 to 1200 mT. Tests were performed for different directions of magnetic induction (B): $N \rightarrow S$ and $S \leftarrow N$, where the direction of each was parallel to the surface of the working electrode (gold). The study solution consisted of: $0,1 \text{ mol/dm}^3 \text{ CoSO}_4$, $0,01 \text{ mol/dm}^3 \text{ Na}_2\text{MoO}_4$, $0,2 \text{ mol/dm}^3 \text{ Na}_3\text{C}_6\text{H}_5\text{O}_7$ and $0,01 \text{ mol/dm}^3 \text{ H}_2\text{SO}_4$. Electrochemical redox processes of the Co-Mo alloy were conducted within the potential range of $(-1,5\text{V}; +0,5\text{V})$ at the rate of 100 mV/s . On the basis of kinetic tests from the obtained voltammetry diagrams it was determined that the potential at which Co-Mo alloys were deposited was 1250 mV (in reference to the calomel electrode). The alloys were deposited with and without the application of constant magnetic field for the time $t = 1000 \text{ s}$.

Results and Discussion

The current and voltage parameters were read from the CVC curves, obtained using the cyclic voltammetry method: cathode current density (j_k), anode current density (j_a), cathode potential (U_k), anode potential (U_a). Example CVC curves for the reactions of electroreduction and electrooxidation of Co-Mo alloy, for different values of magnetic induction (B), are shown in Figures 1. As may be observed, the values of anode and cathode peaks decrease under the influence of constant magnetic field.

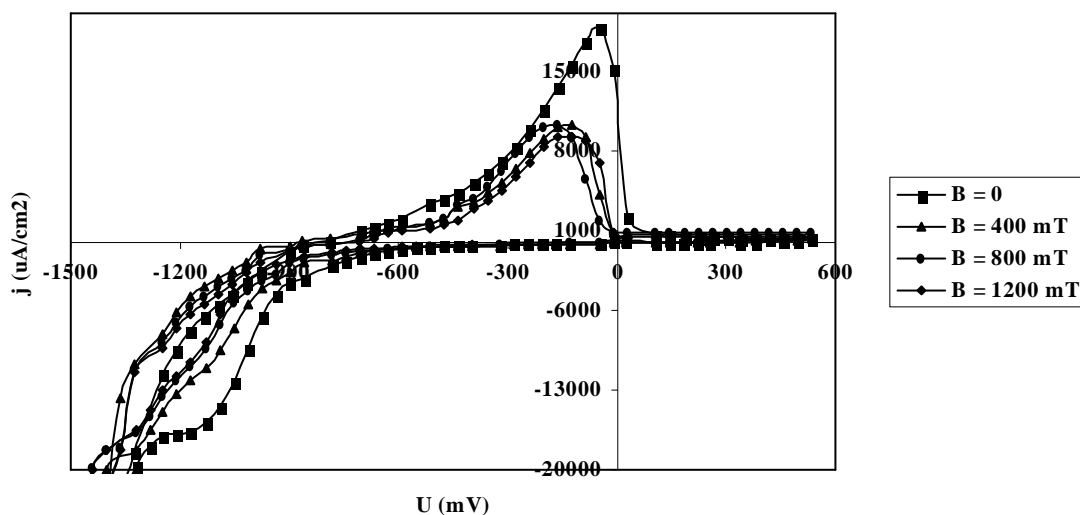


Fig. 1. CVC curves in the process of electroreduction and electrooxidation of Co-Mo alloy, with the application of constant magnetic field with different magnetic induction values B and direction $N - S$.

On the basis of the analysis of current and voltage parameters, dependence graphs were drawn: $j_{kB}/j_{k0} = f(B)$ and $j_{aB}/j_{a0} = f(B)$, where: j_{kB} , j_{aB} – average cathode and anode current density in constant magnetic field with magnetic induction value (B), j_{k0} , j_{a0} – average cathode and anode current density without the field. The dependencies are presented in Figures 2 and 3. On the basis of Figures 2 and 3, conclusions were drawn

that both electroreduction and electrooxidation processes are modified depending on the magnetic induction value (\mathbf{B}). Figure 2 shows that changes in cathode current density (j_k) are larger for the (S \leftarrow N) direction setting of \mathbf{B} (solid line): $\Delta j_k \approx 12\%$ at $B = 400$ mT, than for the (N \rightarrow S) direction of \mathbf{B} (broken line): $\Delta j_k \approx 5\%$ at $B = 500$ mT. Figure 3 shows that changes in anode current density (j_a) are larger for the (N \rightarrow S) direction setting of \mathbf{B} (broken line): $\Delta j_a \approx 28\%$ at $B = 500$ mT, than for the (S \leftarrow N) direction of \mathbf{B} (solid line): $\Delta j_a \approx 25\%$ at $B = 700$ mT.

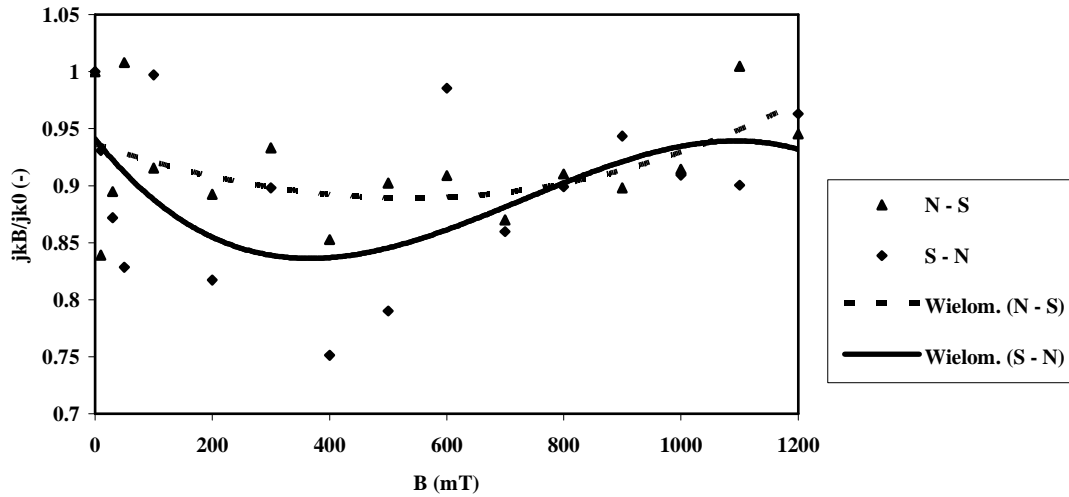


Fig. 2. Dependence of the quotient of average cathode current density in constant magnetic field (j_{kB}) and without the field (j_{k0}) on the value of magnetic induction B , in the electroreduction of Co-Mo alloy, with the direction of B : N - S and S - N.

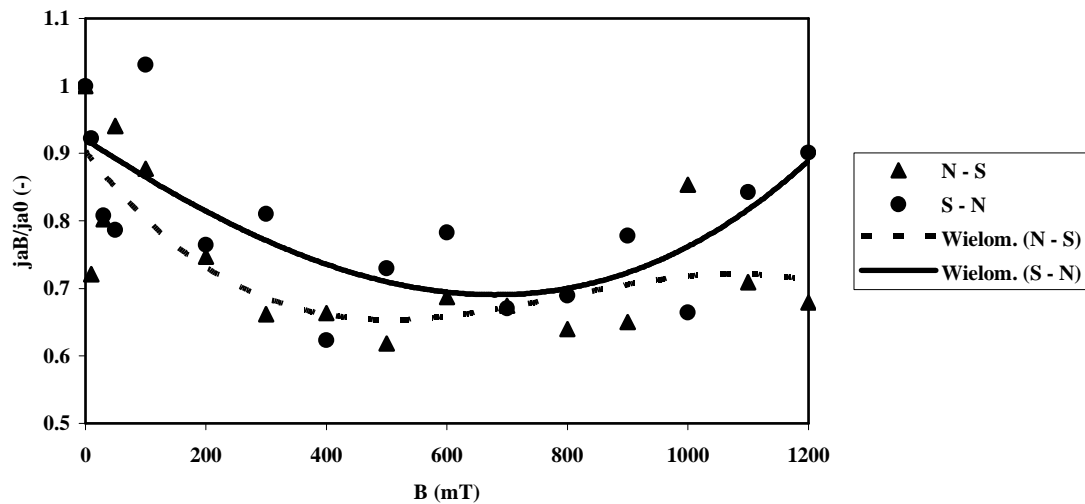


Fig. 3. Dependence of the quotient of average anode current density in constant magnetic field (j_{aB}) and without the field (j_{a0}) on the value of magnetic induction B , in the electrooxidation of Co-Mo alloy, with the direction of B : N - S and S - N.

This is consistent with the previous knowledge [11,14,15], according to which forces \mathbf{F}_B originating in the solution as a result of the action of constant magnetic field (in other words: MHD forces – magnetohydrodynamic), where:

$$\mathbf{F}_B = Q_+ \cdot \mathbf{v} \cdot \mathbf{B} \cdot \sin \alpha \quad (5)$$

Q_+ - positive charge of the entity (ion),

\mathbf{v} – velocity vector of the entity (ion),

\mathbf{B} – magnetic induction vector,

α - angle between vectors \mathbf{B} and \mathbf{v} ,

have opposite directions in the reactions of electroreduction and electrooxidation. This can be observed in diagrams e.g. for the electroreduction process (Fig. 4).

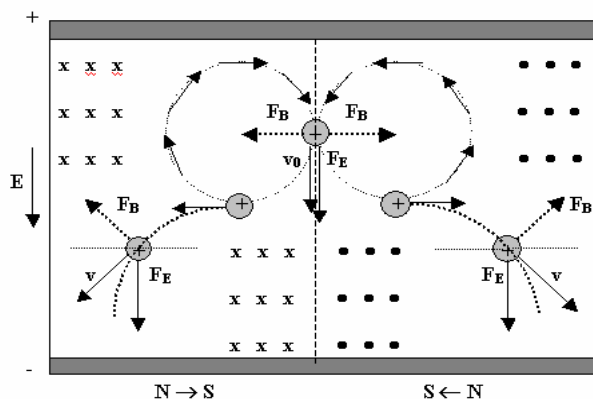


Fig. 4. Diagrams of the origination of force \mathbf{F}_B as a result of the action of constant magnetic field in the process of electroreduction of a paramagnetic positive ion, at the settings of magnetic induction direction \mathbf{B} : ($N \rightarrow S$) and ($S \leftarrow N$).

The characteristic points in the diagrams (Fig. 2 and 3) are those for $B = 800$ mT, where the direction of magnetic induction \mathbf{B} : ($N \rightarrow S$) and ($S \leftarrow N$) seems not to have any importance for this particular process. Below these points, the largest changes in current density occurred in constant magnetic field, whereas above these points the changes decreased. According to the Lorentz formula [14,15], the total force \mathbf{F} originating as a result of action of both electric fields (\mathbf{F}_E) and magnetic fields (\mathbf{F}_B) was:

$$\mathbf{F} = \mathbf{F}_E + \mathbf{F}_B = (Q_+ \cdot \mathbf{E}) + (Q_+ \cdot \mathbf{v} \cdot \mathbf{B} \cdot \sin \alpha) \quad (6)$$

\mathbf{E} – electric field intensity.

References

- [1] H.J. Seim, M.L. Holt, J. Electrochem.Soc. (1949)96, 206-213.
- [2] R.F. Mc Elwee, M.L. Holt, (1952)99, 48-52.
- [3] J. Socha, Pokrycia stykowe, Konf. Nauk.-Techn., Bydgoszcz, 1972.
- [4] J. Francyk, T. Źołnierczyk, Powłoki Ochronne 7(1979)5, 59-65.
- [5] T. Źak, J. Socha, S. Safarzyński, Powłoki Ochronne 7(1979)4/5, 2-10.
- [6] J. Socha, T. Źak, S. Safarzyński, Metalloberflasche 34, (1979)12, 540-545.
- [7] J. Lampe, E. Gazicka, Unpublished study (1979).
- [8] E. Gomez, E. Pellicer, E. Valles, J. Electroanal.Chem. 517:109, (2001).
- [9] E. Gomez, E. Pellicer, E. Valles, J. Electroanal.Chem. 556:137, (2003).
- [10] E. Gomez, E. Pellicer, X. Alcobé, E. Valles, J. Solid State Electrochem., 8,(2004).
- [11] A. Bund, S. Koehler, H.H. Kuehnlein, W. Plieth, Electrochimica Acta 49(2003).
- [12] J. Tabakovic, S. Riemer, M. Sun, V.A. Vaško, M.T. Kief, Journal of The Electrochemical Society 152(12) C851-C860 (2005).
- [13] J. Tabakovic, S. Riemer, V.A. Vaško, V. Sapozhnikov, M.T. Kief, Journal of The Electrochemical Society 150(9) C635-C640 (2003).
- [14] M. Zieliński, Thesis, University of Lodz (2001).
- [15] R. Resnick, D. Halliday, Fizyka, PWN, Warsaw (1999).

GENETIC ALGORITHM IN ESTIMATION RHEOLOGICAL PARAMETERS OF MACROMOLECULES

A. Zalewska, M. Górecki

Department of Inorganic and Analytical Chemistry, K. Marcinkowski University of Medical Sciences, Grunwaldzka 6, 60-780 Poznań, POLAND

Non-newtonian systems make a group of drugs and auxiliary substances used in pharmaceutical therapy, occurring in certain forms. They have been studied, among others by rheological methods, recently significantly developed. At present it is assumed that rheology is an interdisciplinary science dealing with different aspects of deformation of physical bodies under the effect of external stress.

In view of the above, in search of a complex method of assessment of pharmaceutical systems an attempt was undertaken to apply rheological methods, in particular rheometric analysis, which enables a quantitative description of physical properties on the basis of mathematical models

To determine the values of the rheological parameters have been used the genetic algorithm.

The activity of the genetic algorithm begins with the creation of a random population of genomes, then, new populations are created by choosing the best genomes from the previous generation and modifying them by genetic operators: crossing and mutation, so that the new population, on average, has better properties.

In the studied case, the problem of obtainment of the least differences between results from the rheological model and the result received in experimental way has been solved. Quality of fitting, (also called the target of function), has been measured by adding up differences the result of absolute values of the shear stress received from the models and experiment in all measuring points. The estimation was negative, what meant, that the smaller was the target of function the nearer was model, to the experimental result.

Investigation has done by simulating the population of models with the use of a computer. A single model is an equivalent of genom, while rheological parameters of the model are represented by genes [1-6]

The algorithm used:

1. **Selection of population**
2. **The proper algorithm(Iteration)** - consists of:
 - a) An estimation of individuals in the population
 - b) Creations of a new population through crossing of individuals of the preceding population. The new one has to have the same size as the old one
 - c) A mutation individuals of the newly received population

Materials and methods

Substances studied: sodium salt of carboxymethylcellulose - Hoechst AG; sodium alginate – Fluka Chemie AG. in concentration of 0,50% - 2,00%. Apparatus: rotational viscometer Rheotest2 – Medingen, with a system of coaxial cylinders SS1, aligned with a recording attachment. The shear rate was varied from $3,0^{s^{-1}}$ to $1312^{s^{-1}}$. Rheometrics Rotation Fluid Spectrometer RFS II (cone –plate) .The water solutions of the high-molecular compounds of the concentrations 0,50%, 1,00%, 1,50%, 2,00% were prepared. Further characteristic of the substances studied was made on the basis of the

mathematical equation described by the Szulman model. The values of the shear stress (τ_M) were calculated from the rheological equation, and then, with the use of the genetic algorithm, which finds local minimum of a difference ($\tau_M - \tau_D$), the rheological parameters of the models τ_y , η_p , n , m were determined. The calculations were based on 18 types of algorithms. About 2000 iterations were proposed to each of algorithms (Tab. 1 and 2).

Tab.1. The example of different types of algorithms for Szulman model

Algorithm	IV	V	XVII	XVIII
Population	10000	10000	10000	10000
Population cross methods	Best Random	Best Random	Best Random	Best Random
Genom cross methods	One by one	One by one	One by one	One by one
Parents %	80	80	80	80
Parents family	2	2	2	2
Population member mute %	40	40	40	40
Gen mute %	20	20	60	20
Mute strength	2	4	2	1
Parent alive %	20	20	20	20

Tab.2. The example of different types of algorithms for Szulman model

Algorithm	VI	VII	VIII	IX	X
Population	1000	5000	10000	10000	10000
Population cross methods	Best Random	Best Random	Best Random	Best Random	Best Random
Genom cross methods	One by one	One by one	One by one	One by one	One by one
Parents %	80	80	80	80	50
Parents family	2	2	2	2	2
Population member mute %	40	40	40	40	40
Gen mute %	20	20	20	20	20
Mute strength	2	2	6	10	10
Parent alive %	20	20	20	20	20

The mathematic equation for model analyzed

$$\tau^n = \tau^n + (\eta_n \cdot D)^m \quad (\text{eq. 1) Szulman model}$$

Discussion

An example of comparison of different types of genetic algorithms for Szulman model for CMC-Na and ALG-Na

When comparing of the algorithm XVIII, IV, V, VIII and IX for the Szulman model, it was stated that the best description of behaviour of 0,50% and 1,00%

CMC-Na has algorithm VIII and IX. For the 1,50% and 2,00% concentration of CMC-Na the algorithm IV and XVIII is better (Tab. 3).

It is expected that a further increase of the of mutation can only to speed up to strive for improvements, the algorithm attains local minimum quicker, but if the straight of mutation is to big, the algorithm can skip the local minimum so, it does not necessarily mean that the result will be better. Large value of the strength of mutation causes significant fluctuation of the value of gens therefore it causes difficulty in receiving the best result.

In further stage of investigations an estimation of influence of the strength of mutation on quality of the result obtained is proposed.

Tab.3. The values of the target function for different types of algorithms for CMC-Na (strength of mutation)

Concentration	Algorithm				
	V	IV	XVIII	VIII	IX
0,50%	98,09	43,19	133,92	41,83	44,54
1,00%	4447,21	4629,15	6022,56	1156,94	86,01
1,50%	8070,60	4978,58	4783,93	7513,155	6691,97
2,00%	31005,32	4742,43	33825,92	22115,40	9115,34

When comparing the algorithm IV, VI and VII it was showing that algorithm IV give a more accurate description which means that for a population containing more individuals an algorithm attains better results. Too few genoms stop an algorithm in local minimum where poor solution dominates over all population giving the worse result. From the other point of view too large number of population decreases the speed of activity of the algorithm. (Tab.4).

Tab.4. The values of the target function for different types of algorithms for CMC-Na (population size)

Concentration	Algorithm		
	IV	VI	VII
0,50%	43,19	195186,20	51,43
1,00%	4629,15	4882,01	4748,01
1,50%	4978,58	6981,76	7950,55
2,00%	4742,43	5738,83	5113,37

From the investigations it was chose the best algorithm, consisting from many parameters of algorithms (Tab.5)

Tab. 5. The example of algorithm for 0,50% CMC-Na – Szulman model

Algorithm	Algorithm parameters
Population IV	10000
Genom cross methods IV	One by one
Parents alive % IV	20%
Parents % X	50%
Strength of mutation	6
Population member mute % IV	40%
Gen mute % XVII	60%

Comparing the values of the sum of squares from differences between theoretical shear stress and experimental obtained from genetic algorithms and with the using of solver application, it was stated that both of methods are good. It was received good approximation of behavior the studied fluids.

Statistical analysis showed however, that values of rheological parameters counted with the use of algorithms are more repetitive (Tab. 6.)

Tab.6. The value of standard deviation and coefficient of variance for 1,50% CMC-Na Szulman model

	Solver		Genetic algorithm	
	τ_v	η_p	τ_v	η_p
Standard deviation	5,70	779,13	0,004	6,08
Coefficient of variance	173,20	90,58	108,10	50,30

Conclusions

1. A comparative analysis of different kinds of genetic algorithms showed, that most of them describe experimental flow curve very well. This fitting is, however, different depending on type of algorithm, for example from the straight of mutation, the numbers of population, and parents alive and etc. It was stated that the results obtained from genetic algorithm are similar to the process found in nature.
2. Assessment of the physical properties of macromolecules by the mathematical models is of the great importance for drug designing of certain desired physical and chemical as well as biopharmaceutical properties.
3. The application of mathematical models and determination of rheological parameters from them, with the use of method of the genetic algorithm and Solver allows predicting the physical properties of the systems studied [3].

References

1. Franco J.M. in: J. Colloid Interface Sci. 4 (1999) 288
2. Goldberg D. in: W.N.T., W-wa 1995
3. Górecki M., Zalewska A : Int. J. App. Mech.& Eng.; 10 (2005) 165
4. Riberio C.P., Cafio Andrade M.M. in: J. Food Eng. 53 (2002) 1
5. Rutkowska D., Piliński M.in: W.N. PWN, 1997
6. Stokes J.R. in: J. Rheol. 45 (2001) 1173

NETWORK OF HYDROGEN BONDS IN METHANOL – WATER MIXTURES WITH LOW WATER CONTENT. COMPUTER SIMULATION STUDIES

Witold M. Bartczak, Joanna Stawowska
*Institute of Radiation Chemistry, Technical University of Łódź,
Wróblewskiego 15, 93-590 Łódź, Poland*

The structure of the network of hydrogen bonds in alcohol is dramatically changed by addition of even small amount of water. A single alcohol molecule can take part in two hydrogen bonds, one as a donor and one as an acceptor, and therefore the bulk structure of alcohol is composed of isolated, linear and cyclic clusters of molecules. Addition of water molecules which can form up to four hydrogen bonds results in transformation of the hydrogen-bond structure towards global network by linking the alcohol clusters.

From the knowledge of the percolation phenomena [1] it is expected that the change of the network character is of an abrupt type and the network becomes suddenly global after the water content has exceeded a threshold value.

The change of the hydrogen-bond network has far-reaching consequences for all the phenomena connected with energy dissipation in the medium: the relaxation of the electronic excitation energy, the vibrational relaxation, the excess electron localization and, in general, the exothermic chemical reactions. In the global network the excess energy is dissipated out of a reaction site via the hydrogen bonds and the reaction is completed much easier than in the case of nonlinked local clusters. The changes in the reaction rate caused by small changes of the water content in alcohol are more profound at low temperatures.

In the first stage of the project we performed the simulation of the rise of the global network by adding small amounts of the four-functional monomers (representing water molecules) to the system of bi-functional monomers (alcohol molecules). The simulations assumed the system of 64000 monomers arranged in the cubic lattice. A series of calculations were performed for different concentrations of four-functional monomers, from C=1 % to 5 %. The results indicate that the global network of hydrogen bonds appears when the critical concentration C_0 of 1.6 – 1.7 % is exceeded.

In the second part of the project we performed quantum-chemical calculations of a series of the methanol clusters and mixed methanol-water clusters: 1) the clusters $(\text{CH}_3\text{OH})_n$ for $n=2$ to 6; 2) the clusters $(\text{CH}_3\text{OH})_{n-1}(\text{H}_2\text{O})$ for $n=2$ to 6; 3) selected clusters $(\text{CH}_3\text{OH})_{n-2}(\text{H}_2\text{O})_2$; 4) the clusters of water molecules $(\text{H}_2\text{O})_n$ for $n=2$ to 6.

The calculations have been performed using the gradient-corrected version of the density functional theory (DFT) with the hybrid exchange – correlation functional B3LYP and with the DZ-type basis set. The optimization runs produced the cluster geometry, hydrogen – bond energy, vibrational frequencies and the electron density isosurfaces.

The series of the calculations started with three bimolecular clusters: $(\text{H}_2\text{O})_2$, $(\text{CH}_3\text{OH})_2$ and $(\text{H}_2\text{O})(\text{CH}_3\text{OH})$. The geometrical structures have been obtained as a result of the energy optimization runs. The hydrogen bond angle for water dimer is close to 180° , the angles for methanol dimer and water-methanol bond are by about 10° smaller. The bond lengths are almost identical for all three cases: 0.99 Å for the OH

bond in the parent molecule and 1.75 Å for the other bond. The energy of the hydrogen bond was calculated as the difference of energy of the dimer and energy of the separated molecules. For (H₂O)₂ dimer the hydrogen bond energy is -0.414 eV, it is slightly lower for (CH₃OH)₂ dimer: -0.384 eV. It is interesting to note that the H-bond energy for water-methanol bond is -0.415 eV, the same as for the water dimer.

Figure 1 shows the hydrogen bonded n=3 clusters: (A) (H₂O)₃, (B) (H₂O)₂(CH₃OH), (C) (H₂O)₁(CH₃OH)₂, and (D) (CH₃OH)₃. The oxygen atoms in all the cases form nearly equilateral triangles. The length of the hydrogen bond is slightly shorter for the water trimer (A), about 1.68 Å, and with the increase of the number of methanol molecules in the cluster it gradually increases up to 1.71 Å and 1.73 Å. The binding energy of the cluster was calculated as the difference of the cluster energy minus the energy of the separated molecules and it was recalculated per single bond.

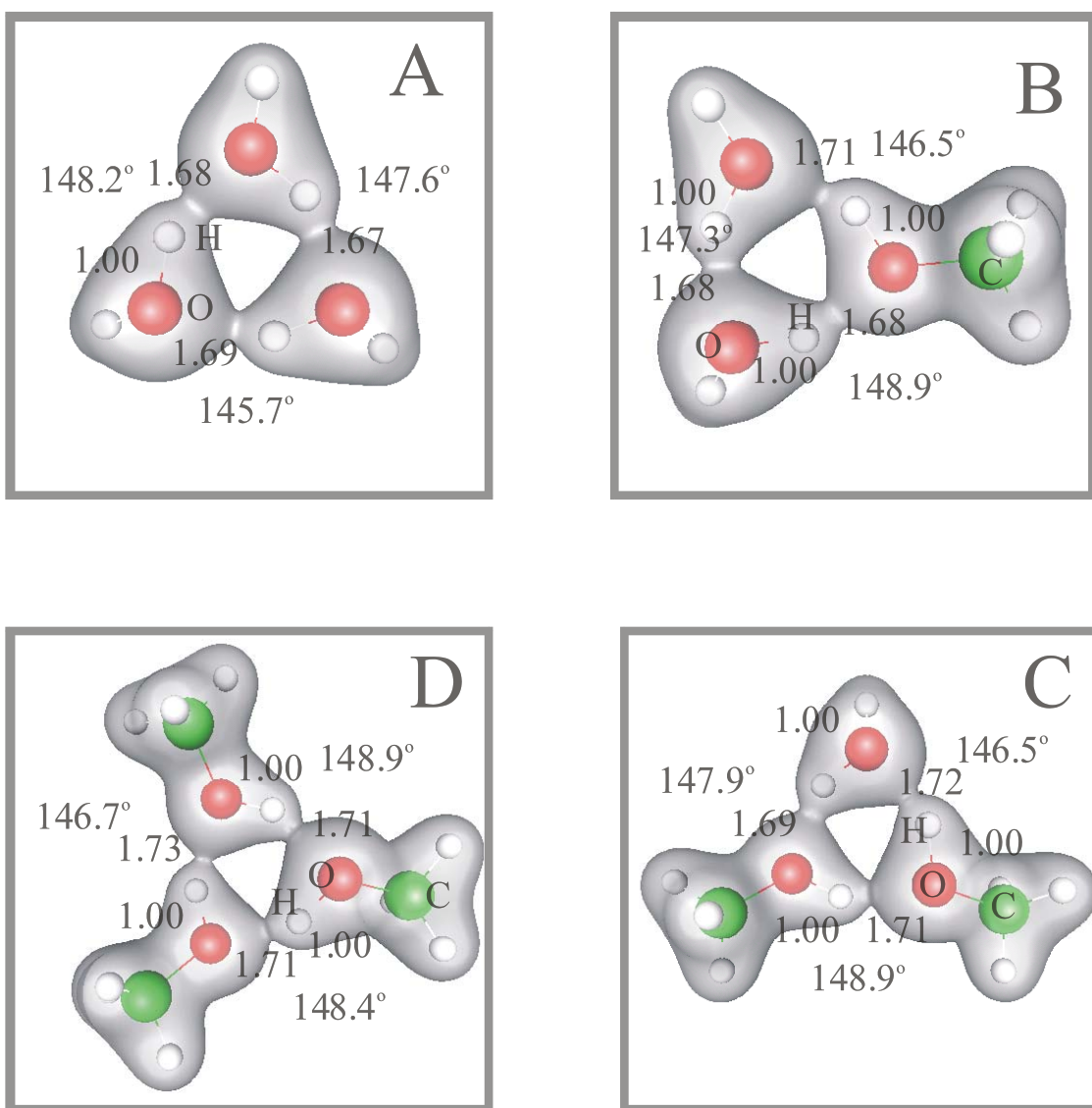


Fig. 1. Isosurfaces of the electron density for the following n=3 clusters: (A) (H₂O)₃, (B) (H₂O)₂(CH₃OH), (C) (H₂O)₁(CH₃OH)₂, and (D) (CH₃OH)₃. The density $\rho=0.04$ e/Å². The lengths of the OH bonds (in Å) and the O-H-O angles for the H-bridge are given in the figure.

The binding energy for the water trimer (A) is the highest, -0.446 eV, and it is also slightly higher than the $(\text{H}_2\text{O})_2$ binding energy. Exchanging water molecule by methanol (B) slightly lowers the average binding energy to -0.430 eV, further exchange (C) results in -0.413 eV and, finally, in methanol trimer the binding energy per single bond is -0.396 eV. We can conclude that addition of water to methanol cluster leads to slightly stronger hydrogen bonds. The angles O-H-O are significantly smaller for the trimer case (about 148°) as compared to the dimer angles between 170° and 180° .

Two $n=4$ clusters, $(\text{H}_2\text{O})_4$ and $(\text{CH}_3\text{OH})_4$ are shown in Fig. 2. The oxygen atoms viewed from above form the square - the planar angles O-O-O are very close to 90° . However the figures are nonplanar: the distortion measured as the O-O-O-O angle is about 8.6° in the case of methanol and 9.3° in the case of water tetramer.

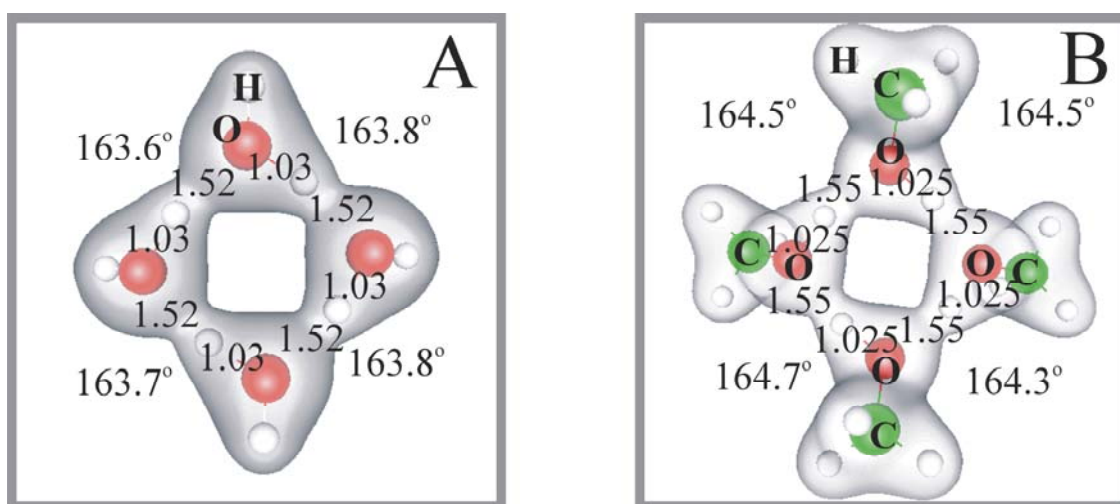


Fig. 2. Isosurfaces of the electron density for the following $n=4$ clusters: (A) $(\text{H}_2\text{O})_4$, (B) $(\text{CH}_3\text{OH})_4$. The density $\rho=0.04 \text{ e}/\text{\AA}^2$. The lengths of the OH bonds (in \AA) and the O-H-O angles for the H-bridge are given in the figure.

Figure 3 presents examples of the larger clusters, $n=5$, after the structure optimization towards the lowest energy. The clusters are of the cyclic type, with 5 hydrogen bonds, all of the pentagons are nonplanar. The deviation from the plane is relatively small in the water pentamer (A) and the methanol pentamer (B) but for the mixed structure $(\text{H}_2\text{O})_1(\text{CH}_3\text{OH})_4$ (C) it is easily seen that one of the methanol molecules is placed above the plane formed by the remaining four molecules. The binding energies (recalculated per single bond) are significantly higher than the corresponding energies for smaller clusters. The binding energy is -0.653 eV for $(\text{H}_2\text{O})_5$, it is somewhat lower for the methanol pentamer: -0.581 eV and still lower for the mixed cluster $(\text{H}_2\text{O})_1(\text{CH}_3\text{OH})_4$, -0.531 eV.

The calculations for larger clusters are under way but we still consider the results of optimizations as pilot results due to huge number of possible initial structures. For instance, the clusters for $n=3$ are final results of optimizations for 11 different initial structures. The number of the structures for higher n grows by an order of magnitude.

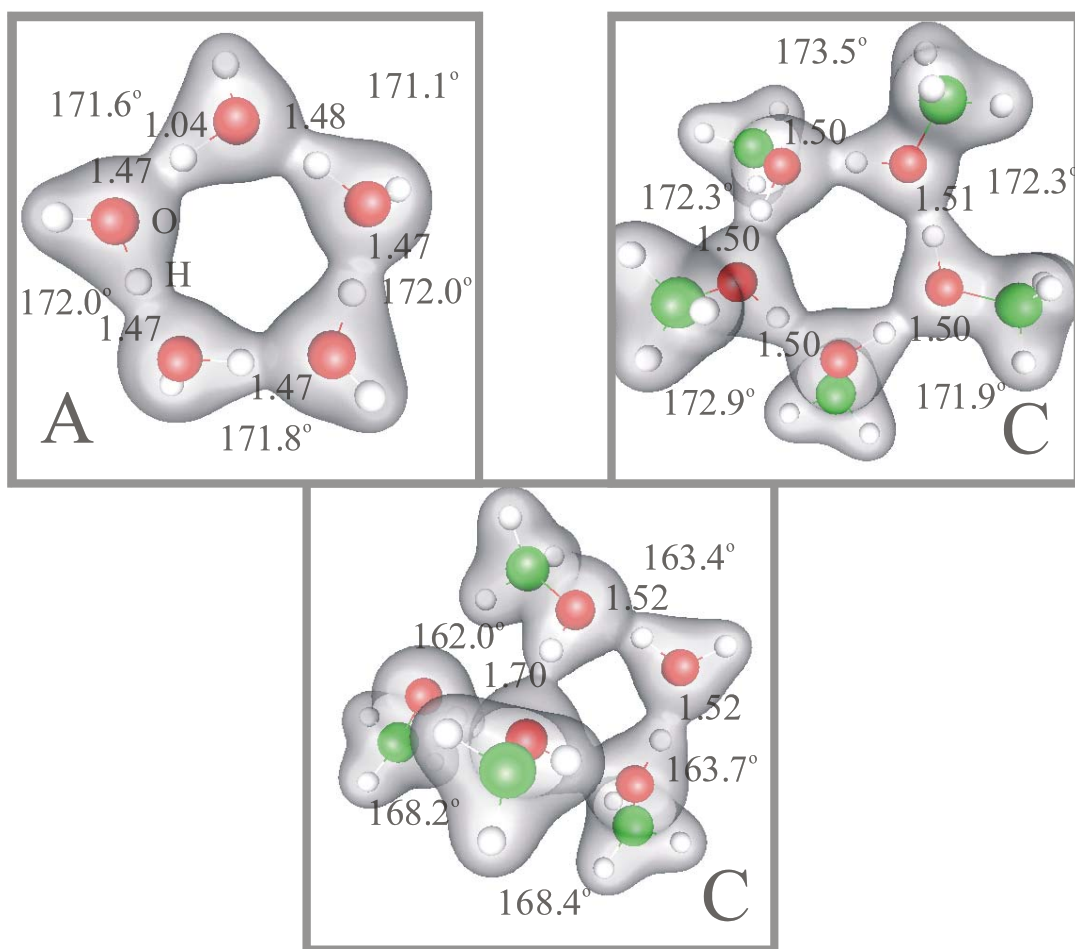


Fig. 3. Isosurfaces of the electron density for the following $n=5$ clusters: (A) $(\text{H}_2\text{O})_5$, (B) $(\text{CH}_3\text{OH})_5$, and (C) $(\text{H}_2\text{O})_1(\text{CH}_3\text{OH})_4$. The density $\rho=0.04 \text{ e}/\text{\AA}^2$. The lengths of the OH bonds (in \AA) and the O-H-O angles for the H-bridges are given in the figure.

[1] G. Grimmett, *Percolation*, 2nd ed., Springer, Berlin, 1999.

Acknowledgment: The present work was supported by the KBN grant nr. 4 T09A 048 25.